

GEOTECHNICAL FRAMEWORK, NORTHEAST GULF OF ALASKA

by

**Homa J. Lee
William C. Schwab**

**U . S. Department of the Interior
Geological Survey**

**Final Report
Outer Continental Shelf Environmental Assessment Program
Research Unit 589**

1983

TABLE OF CONTENTS

List of Figures	99
List of Tables*	105
INTRODUCTION*	107
SETTING	107
Geologic Setting	107
Offshore Geologic Hazards	108
Morphology of Submarine Slides and Flows	109
GEOTECHNICAL APPROACH	111
General Methodology	111
Cyclic Strength Degradation and Test Type Effects	112
Summary of NSP Strength Determination	113
Quantitative Evaluation of Offshore Stability	114
TEST PROCEDURES	115
Shipboard Sampling and Testing	115
In Place Testing	115
Shore Laboratory Testing	116
RESULTS	118
Study Areas and Core Locations	118
Organization of Laboratory Test Data Presentation	118
In Place Test Data	119
SYNTHESIS AND DISCUSSION	119
Analysis of Parameters	119
Undrained Strength to Consolidation Stress Ratio for Normal Consolidation, S_{nc}	120
Test Type Correction Factor, AC	120
Cyclic Strength Degradation Factor, AD	121
Degree of Consolidation, U, Overconsolidation Ratio., OCR, and Normalized Strength Exponent, Δ_o	122
Ratio of Submerged to Total Unit Weight, γ'/γ	122
Validity of NSP Approach, Vane Shear Tests and Type (a) Triaxial Tests	123
Evaluation of Consolidation State Using Field Strength Results and Gibson's Theory	123
Critical Acceleration Calculation	124
Regional Variations	125
SUMMARY AND CONCLUSIONS	126
ACKNOWLEDGEMENTS*	127
REFERENCES	128

TABLE OF CONTENTS (Continued)

TABLES	*.....*	133
FIGURES		149
APPENDIX A: METHANE IN SEDIMENTS OF THE EASTERN GULF OF ALASKA by Marge Golan-Bat and Keith A. Kvenvolden		217
APPENDIX B: RELATIVE IMPORTANCE OF SEISMIC AND STORM WAVE LOADING		223
APPENDIX C: INDEX PROPERTY PROFILES		227. . . .
Copper River Study Area		231
Kayak Trough Study Area		239
Bering Trough Study Area		249
Icy Bay-Malaspina Study Area		251
Icy Bay Study Area		297
Yakutat Bay Study Area		301
Yakutat Study Area		305
Alsek River Study Area		325
Other		343
APPENDIX D: CONSOLIDATION AND TRIAXIAL TEST RESULTS - LAW ENGINEERING AND TESTING COMPANY (1977 Cores)		349
APPENDIX E: CONSOLIDATION AND TRIAXIAL TEST RESULTS - GEOTECHNICAL ENGINEERS, INC. (1977 Cores)		363
APPENDIX F: CONSOLIDATION AND TRIAXIAL TEST RESULTS - LAW ENGINEERING AND TESTING COMPANY (1980 Cores)		395
APPENDIX G: CONSOLIDATION AND TRIAXIAL TEST RESULTS - USGS (1980 AND 1981 Cores)		415

LIST OF FIGURES

- Figure 1. Distribution of four continental shelf surface sedimentary units between Cross Sound and Prince William Sound (Molnia and Carlson, 1980).
- Figure 2. Simplified geologic setting of the northern Gulf of Alaska, showing general trends of Mesozoic and Cenozoic rocks (modified from Bruns, 1979). Onshore geology is from Plafker (1967), and Beikman (1974, 1975). Relative convergence vector between Pacific and North American plates (large arrow) is from Minster and Jordon (1978).
- Figure 3. Holocene sedimentation rates (mm/yr) in the northeast Gulf of Alaska (Molnia and Carlson, 1980).
- Figure 4. Location map of seafloor flows and slumps west of Kayak Island (Carlson and Schwab, 1982).
- Figure 5. High resolution seismic reflection record of the sediment slide off the Copper River.
- Figure 6. High resolution seismic reflection record of the submarine slide located in Kayak Trough (Hampton and others, 1978).
- Figure 7. Location map of seafloor geologic hazards east of Icy Bay, Gulf of Alaska (modified from Carlson and others, 1980).
- Figure 8. High resolution seismic reflection record of the Icy Bay-Malaspina Slump (Carlson, 1978).
- Figure 9. High resolution seismic reflection record of the Yakutat Slump.
- Figure 10. High resolution seismic reflection data and side scan sonographs depicting a water-column gas plume southeast of the Dangerous River delta (Carlson and others, 1980).
- Figure 11. Side-scan sonograph example of small slides and linear flows on the Alsek River prodelta (Molnia and Rappeport, 1980). Onshore direction is toward the top of the figure.
- Figure 12. Side-scan sonograph depicting a massive, lobate slide toe and a series of smaller slide toes on the Alsek River prodelta (Molnia and Rappeport, 1980). Onshore direction is toward the top of the figure.
- Figure 13. Side-scan sonograph depicting multiple flows, slumps, and slides on the Alsek River prodelta (Molnia and Rappeport, 1980).

- Figure 14. Locations of study areas.
- Figure 15. Core locations-Copper River Study Area (group to west) and Kayak Trough Study Area (group to east).
- Figure 16. Core locations-Bering Trough and Icy Bay Study areas.
- Figure 17. Core locations-Icy Bay-Malaspina Study Area (Cruise DCI-77-EG).
- Figure 18. Core and in-place test locations-Icy Bay-Malaspina Study Area (Cruises S8-77-EG, DC2-80-EG, and DCI-81-EG).
- Figure 19. Core and in-place test locations-Yakutat Study Area.
- Figure 20. Core and in-place test locations-Alsek River Study Area.
- Figure 21. Core locations-Yakutat Bay Study Area and "other."
- Figure 22. Results of field vane shear test MV-1 (Alsek River Study Area) compared with normalized strength parameter (NSP) estimate of undrained strength from triaxial tests.
- Figure 23. Results of field vane shear test MV-2 (Yakutat Study Area) compared with laboratory vane shear strengths and NSP estimates from triaxial tests. CIU and UU tests represent triaxial tests with consolidation to near the overburden stress and to nearly no stress, respectively.
- Figure 24. Results of field vane shear test MV-3 (Yakutat Study Area). Arrows indicate locations where the capacity of the field vane torque cell was reached.
- Figure 25. Results of field vane shear test MV-4 (Icy Bay-Malaspina Study Area) compared with laboratory vane shear strengths and NSP estimates from triaxial tests. CIU and UU tests represent triaxial tests consolidated to near the overburden stress and to nearly no stress, respectively.
- Figure 26. Results of field vane shear test MV-5 (eastern part of Icy Bay-Malaspina Study Area) compared with laboratory vane shear strengths and NSP estimates from triaxial tests. CIU and UU tests represent triaxial tests consolidated to near the overburden stress and to nearly no stress, respectively.
- Figure 27. Results of in-place cone penetration test MP-2 (off the mouth of the Dangerous River). Stratigraphy of nearby core is given at right.
- Figure 28. Results of in-place cone penetration test MP-3 (Alsek River Study Area). Stratigraphy of nearby core is given at right.

- Figure 29. Results of in-place cone penetration test MP-4 (Yakutat Study Area). Stratigraphy of nearby core is given at right.
- Figure 30. Results of in-place cone penetration test MP-5 (Yakutat Study Area). Stratigraphy of nearby core is given at right.
- Figure 31. Results of in-place cone penetration test MP-6 and MP-7 (Alsek River Study Area). Stratigraphy of nearby core is given at right.
- Figure 32. Results of in-place cone penetration test MP-8 (Quaternary glacial deposits off Dangerous River Delta). Stratigraphy of nearby core is given at right.
- Figure 33. Results of in-place cone penetration test MP-9 (Icy Bay-Malaspina Study Area). Stratigraphy of nearby core is given at right.
- Figure 34. Results of in-place cone penetration test MP-10 (eastern part of Icy Bay-Malaspina Study Area). Stratigraphy of nearby core is given at right.
- Figure 35. Correlation of ratio of undrained shearing strength, S_u , to vertical consolidation stress, σ'_{vc} , with natural water content; all type (c) static triaxial tests. Circled data points represent anisotropic consolidation. Solid line is a fit of the isotropic consolidation data points (uncircled dots). Dashed line represents 0.8 times the solid line and roughly follows anisotropic data points.
- Figure 36. Relative cyclic stress level versus number of cycles to failure: Core 4G (Copper River Study Area).
- Figure 37. Relative cyclic stress level versus number of cycles to failure: Cores 8G and 11G (Copper River and Kayak Trough Study Areas).
- Figure 38. Relative cyclic stress level versus number of cycles to failure: Core 28G (Icy Bay-Malaspina Study Area).
- Figure 39. Relative cyclic stress level versus number of cycles to failure: Core 33G (Icy Bay-Malaspina Study Area).
- Figure 40. Relative cyclic stress level versus number of cycles to failure: Alsek River Study Area, Method I.
- Figure 41. Relative cyclic stress level versus number of cycles to failure: Alsek River Study Area, Method II.
- Figure 42. Relative cyclic stress level versus number of cycles to failure: Alsek River Study Area, Method III.

- Figure 43. Relative cyclic stress level versus number of cycles to failure: Yakutat Study Area, Method I.
- Figure 44. Relative cyclic stress level versus number of cycles to failure: Yakutat Study Area, Method II.
- Figure 45. Relative cyclic stress level versus number of cycles to failure: Yakutat Study Area, Method III.
- Figure 46. Relative cyclic stress level versus number of cycles to failure: Icy Bay-Malaspina Study Area (USGS testing), Method I.
- Figure 47. Relative cyclic stress level versus number of cycles to failure: Icy Bay-Malaspina Study Area (USGS testing), Method II.
- Figure 48. Relative cyclic stress level versus number of cycles to failure: Icy Bay-Malaspina Study Area (USGS testing), Method III.
- Figure 49. Relative cyclic stress level for failure in 10 cycles versus natural water content, Method I.
- Figure 50. Relative cyclic stress level for failure in 10 cycles versus natural water content, Method II.
- Figure 51. Relative cyclic stress level for failure in 10 cycles versus natural water content, Method III.
- Figure 52. Predicted degree of consolidation (U) at the base of a sediment column that has been deposited at a steady rate, m , for t years (after Gibson, 1958).
- Figure 53. Correlation between coefficient of consolidation (c_v) and liquid limit (after Lambe and Whitman, 1969, p. 412).
- Figure 54. Solid lines represent constant degrees of consolidation, U , predicted by the Gibson (1958) technique. Selected locations in the eastern Gulf of Alaska for which the required parameters were available are shown as data points. Bars indicate a larger segment over which the sedimentation rate varies.
- Figure 55. Estimate of critical earthquake acceleration, k , versus natural water content.
- Figure 56. Locations of core samples within the Icy Bay-Malaspina Study Area relative to the observed slump feature. Numbers near the core locations represent the percentage of the core that has a water content in the critical 35% to 45% range.

- Figure 57. Locations of core samples within the Yakutat Study Area relative to the observed slump feature. Numbers near the core locations represent the percentage of the core that has a water content in the critical 35% to 45% range.
- Figure 58. Locations of core samples within the Alsek River Study Area relative to the observed slump feature. Numbers near the core locations represent the percentage of the core that has a water content in the critical 35% to 45% range. All cores are thought to be in the failed zone.
- Figure 59. Plasticity chart for Copper River and Icy Bay Study areas with least squares regression fits of the data.
- Figure 60. Plasticity chart for Kayak Trough Study Area and Yakutat Sea Valley (SE portion of Icy Bay-Malaspina Study Area) with least squares regression fits of the data.
- Figure 61. Plasticity chart for Bering Trough and Yakutat Bay Study Areas with least squares regression fits of the data.
- Figure 62. Plasticity chart for Icy Bay-Malaspina Study Area with least squares regression fits of the data (not including Cruise DCI-77-EG data).
- Figure 63. Plasticity chart for Yakutat Study Area with least squares regression fits of the data.
- Figure 64. Plasticity chart for Alsek River Study Area with least squares regression fits of the data.
- Figure 65. Summary of linear regression fits of plasticity data for the various study areas.

LIST OF TABLES

- Table 1. Core and in-place test locations organized by study area.
- Table 2. Consolidation Test results.
- Table 3. Static Triaxial Test results.
- Table 4. Cyclic Triaxial Test results.
- Table 5. Calculation of NSP exponent, Λ_0 .

INTRODUCTION

The U.S. Geological Survey began a systematic study of sediment distribution, depositional environments, and shallow structure of the northeast Gulf of Alaska in 1974. The objective of the study was primarily to evaluate seafloor hazards on a regional basis in preparation for possible offshore petroleum development. The study was extended to include an extensive sediment sampling program in 1975 when approximately 400 samples of continental shelf sediments were collected (Carlson and others, 1977). Systematic measurement of geotechnical properties was started in 1977 (Carlson and others, 1978).

Detailed geologic study of seismic reflection records and sediment samples in areas of sediment instability, although valuable for specifying the types and extents of different past hazardous conditions, leave unanswered questions. For example, they often do not specify causes of failures, provide information on the safety of apparently unfailed areas, suggest whether existing slide bodies will fail again or enlarge, or predict the implications of certain earthquake or storm events.

The quantitative methods of geotechnology have the potential for answering some of these questions. A vast amount of previously unpublished geotechnical data, primarily derived from tests on core samples but supplemented with a few in situ tests, has been accumulated on the continental shelf between Montague Island and Cross Sound (Fig. 1). The primary objective of this report is to make these data available with a consistent format. A secondary objective is to provide preliminary quantitative analyses of some of the geologic hazards.

SETTING

Geologic Setting. Glaciation is the most important process contributing sediment to the northeast Gulf of Alaska continental shelf. In Miocene time, glaciation was restricted to the onshore area but by early to middle Pleistocene, a large ice sheet had spread across the continental shelf (Molnia and Carlson, 1978; Molnia and Sangrey, 1979; Carlson and others, 1982). Today glaciers in the Gulf of Alaska region are restricted to the onshore areas (Fig. 1). As recently as 75 years ago, however, a glacier filled Icy Bay and extended 5 km or 6 km onto the continental shelf (Molnia, 1979).

The complex Quaternary history of the northeast Gulf of Alaska has generated a variety of sedimentary deposits. Four major sedimentary units (Fig. 1) are defined on the basis of seismic reflection and sedimentologic data (Carlson and Molnia, 1975; Molnia and Carlson, 1975, 1980; Carlson and others, 1977, Molnia and Sangrey, 1979; Molnia and Carlson, 1980). These units are: A. Holocene glacial-marine sediment; B. Holocene end moraine deposits; C. Quaternary glacial deposits; and D. Pleistocene and older lithified sedimentary rocks. Holocene end moraine deposits, Quaternary glacial-marine sediment, and Pleistocene and older lithified sedimentary rocks are predominantly dense and hard, reflecting diagenesis or glacial ice loading. These compacted deposits are probably not susceptible to instability on the continental shelf (Lee and Schwab, 1982). Therefore, Geotechnical studies have been directed almost exclusively toward investigating Holocene glacial-marine sediment.

Fine sand and clayey silt of the Holocene glacial-marine unit cover most of the inner shelf, reaching a maximum thickness of about 350 m seaward of the Copper River, about 200 m seaward of Icy Bay (Carlson and Molnia, 1975), and about 260 m seaward of the Alsek River. This sediment is glacially derived from the Gulf of Alaska Tertiary province and bordering rocks of Mesozoic and older age, then fluvially transported to the gulf as rock flour (Molnia and Carlson, 1980). The Mesozoic and older age rocks are highly deformed, locally metamorphosed sedimentary and volcanic rocks that are commonly intruded by igneous plutons, whereas the Tertiary Province is a compound continental margin basin made up almost entirely of terrigenous elastic rocks with minor coal. For a summary of the onshore geology of the Gulf of Alaska the reader is referred to Plafker (1971), Bruns (1979), and Bruns and Plafker (1982).

West of Kayak Island, the Copper River is the primary source of Holocene sediment, carrying a sediment load of 107×10^9 kg/yr (Reimnitz, 1966). East of Kayak Island, major sediment sources are streams draining the larger ice fields (Malaspina and Bering Glaciers) and the Alsek River. Accumulation rates of the Holocene glacial-marine unit on the continental shelf range from 0 to 29 mm/yr (Molnia and others, 1980). Accumulation rates of Holocene glacial-marine sediment in coastal embayments are thought to be as high as 2 to 3.75 m/yr (Molnia, 1979).

The largest deposits of sand in the Holocene glacial-marine unit occur along the barrier islands at the mouth of the Copper River, along the nearshore zone both adjacent to and west of the Malaspina Glacier (Carlson and others, 1977), and along the nearshore zone between the Alsek River and Yakutat Bay (Fig. 1). The moderately well sorted, mineralogically immature sand (containing about equal parts of quartz and metamorphic rock fragments) is mostly found in water depths less than 50 m indicating an environment subject to high wave and current energy. Storm waves and longshore currents resuspend the fine silt and clay particles or maintain them in suspension and the Alaska Current transports them offshore and westward (Molnia and Carlson, 1980).

Large deposits of Holocene glacial-marine clayey silt occur seaward of the Copper River and seaward of the Malaspina and Bering Glaciers (Carlson and others, 1977). The mean grain size of Gulf of Alaska Holocene glacial-marine sediment generally decreases with distance from shore and is largely glacial rock flour which is dominated by the silt fraction (Carlson and others, 1977).

Offshore Geologic Hazards. Seafloor geologic hazards in the northeast Gulf of Alaska are summarized by Carlson and Schwab (1982) and have been described by Carlson and others (1975), Carlson and Molnia (1977), Molnia and others (1977), Carlson (1978), and Carlson and others (1980). The hazards include shallow faults, buried channels, gas-charged sediment, and submarine slides and flows.

Active faulting is well documented using conventional geophysical techniques (Bruns 1979; 1982; Bruns and Schwab, 1982; Carlson and Schwab, 1982). Buried channels involve sediment and sedimentary rocks that are too deeply buried to be sampled with conventional coring equipment and therefore have not been studied except with geophysical profiling.

Bubble phase gas charging, although present in the northeastern Gulf of Alaska, is not widespread. Of the hydrocarbon gases, only methane is present in concentrations that may exceed the saturation of interstitial water (Appendix A). Anomalously high concentrations of methane suggesting the presence of bubble phase gas in place and potentially unstable sediment, were found in only two areas: a fault zone southeast of Kayak Island (sample concentration of 14,000 $\mu\text{l/l}$), and an area east of Dry Bay (sample concentration of 32,800 $\mu\text{l/l}$). Other locations had significant amounts of methane but the amounts measured in samples were insufficient to indicate that the sediment in situ was, indeed, charged with bubble-phase gas. No correlation between the occurrence of **seismic** reflection anomalies and the presence of gas-charged sediment is apparent, except for the sediment southeast of Kayak Island. The sampling and analytical techniques needed to quantitatively assess gas-charged sediment as a geologic hazard have not been fully developed.

Geotechnical studies have been directed almost exclusively toward investigating slides and flows in the Holocene glacial-marine sediment. Holocene morainal sediments, Quaternary glacial-marine sediment and Pleistocene and older lithified sedimentary rocks are predominantly dense and hard, reflecting diagenesis or glacial ice loading. These compacted deposits are probably not susceptible to sliding on the continental shelf. In contrast, the Holocene glacial marine sediment is weak. In this area of frequent earthquakes and large storm waves, the Holocene glacial marine sediment is susceptible to slope failure under cyclic loading (Lee and Schwab, **1982**).

Morphology of Submarine Slides and Flows. Numerous slides and slumps have been identified from seismic profiles of an 8 by 100 km area seaward of the mouth of the Copper River (Hampton and others, **1978**; Carlson and Schwab, **1982**) (Fig. 4). Some disrupted reflectors on a few of the profiles may indicate the presence of gas-charged sediment (Fig. 5). The disrupted reflectors occur beneath a slope of about **0.5°** and appear to outline individual slump "blocks" that range in height from 1 m to 5 m and in length from 0.3 km to 1.0 km. The slump structures appear to be developed to a depth in the sediment of 20 m to 40 m in water depths of 40 m to 125 m.

A spectacular example of a large submarine slide is located in Kayak Trough (Carlson and Molnia, **1977**; Molnia and others, 1977; Hampton and others, **1978**) (Fig. 4). This slide has a length of 17 km, a maximum width of 12 km, and a maximum thickness of 115 m (estimated volume is approximately 5.9 km^3). The slide occurred on a **1°** slope. Seismic profiles over the Kayak Trough slide typically show disrupted internal reflectors and irregular surface morphology. This slide has a fairly well-preserved pull-apart scarp with a relief of about 10 m and a well-developed toe that is 20 m thick about 2 km from the distal end (Fig. 6). Apparently there was enough momentum to carry the toe of the slide past the thalweg of the trough (Carlson and Molnia, 1977).

The largest known slide on the continental shelf east of Kayak Island is the Icy Bay-Malaspina slump (Carlson, 1978, located seaward of the Malaspina Glacier (Slide A, Fig. 7). Here a process of en echelon slumping of Holocene clayey silt is taking place in water depths of 70 m to 150 m on a slope of less than **0.5°** (Fig. 8). These slump structures extend over an area of about

1080 km². The slump blocks are about 0.5 km long and have reliefs of 2 m to 5 m. The slip surfaces extend to a depth of 15 m to 40 m beneath the sea floor. The volume of the entire slump is about 32 km³.

Four smaller slides have been mapped in the nearshore zone east of the Icy Bay-Malaspina slump, all of which begin in water shallower than 100 m (Carlson and others, 1980) (Slide B, Fig. 7). One slide southwest of Yakutat Bay begins on the north wall of Yakutat Sea valley and extends across most of the valley floor. This slide covers an area of 350 km² and incorporates the upper few meters of clayey silt. This slide appears to fit into Varnes (1978) classification as a mudflow that failed due to lateral spreading (Carlson and others, 1980).

The second of the four smaller slides, the Yakutat slide, begins 4 km seaward of the coastline between Yakutat Bay and the Dangerous River. It is about 40 km in width, and about 260 km² in area (Carlson and others, 1980) (Slide C, Fig. 7). The slope of the upper part of the slide is about 1° and decreases to about 0.5° at the seaward edge of the slide. This slide mass is characterized by a series of clayey silt blocks undergoing rotational slump movement. The steplike surfaces of the blocks have a tread length of about 100 m and a riser height of 3 to 4 m (Fig. 9). The slip surfaces extend 10 m below the sea floor and the volume of slumped material is nearly 3 km³.

The third smaller slide is located southeast of the Dangerous River in clayey silt (Carlson and others, 1980) (Slide D, Fig. 7). This slide begins about 2 km offshore in water depths less than 20 m. This area of seafloor instability is thought to be associated with gas-charged sediment interpreted from acoustic anomalies in high resolution seismic profiles, and water column gas plumes visible on side-scan sonographs (Carlson and others, 1980) (Fig. 10).

The fourth of the smaller slides is just seaward of the Alsek River (Alsek River Prodelta) (Slide E, Fig. 7) and has an area of 150 km². The shoreward edge of the slide is in sand and sandy mud less than 2 km offshore. Water depths are around 35 m and the slope is about 0.5°. This slide is thought to have moved down the headwall of the Alsek Sea Valley (1.3° slope) possibly as far offshore as the floor of the valley (Slide F, Fig. 7) where it offsets the clayey silt to a depth of 10 m to 20 m (Carlson and others, 1980). A detailed picture of the sea floor in a 10 x 2 km area within the Alsek River prodelta was made by assembling 21 speed corrected, digitally processed, side-scan sonographs (Molnia and Rapoport, 1980). Typical side-scan sonographs of the Alsek River slide are presented in Figures 11, 12, and 13. Molnia and Rapoport (1980) suggest that the principal factor for causing the Alsek Prodelta slope failures is saturation of the sediment by biogenic methane gas. Carlson and others (1980) also mapped this failure as an area of gas-charged sediment.

In addition to the slides and flows in the nearshore zone, other slides have been mapped within the Yakutat and Alsek Sea Valleys (Carlson and others, 1980) (Fig. 7). These slides all appear to be mud flows affecting the upper 10 m to 20 m of clayey silt.

Numerous areas of slides and slumps have been mapped on the continental slope (Fig. 7) (Carlson and others, 1980). Although most of these slides are

immediatly seaward of the valleys, sliding appears to be a common mechanism for transporting sediment down the continental slope in the entire Gulf of Alaska (Hampton and others, 1978; Carlson, 1979). Many of these slides are longer than 5 km and occur on slopes with gradients of 3° to 6° . The slides range from discrete mudflows, thinner than 50 m, to complex zones of mass transport several hundred meters thick consisting of multiple slides, such as in the area southeast of Yakobi Sea Valley (Carlson and others 1980; Carlson and Schwab, 1982). The sediment contained in these slides is primarily a pebbly mud that was deposited by glaciers on the shelf during parts of the Pleistocene (Carlson and others, 1980).

GEOTECHNICAL APPROACH

General Methodology. The critical sediment geotechnical property measured for use in geologic hazards evaluations is the shearing strength. It must be exceeded by environmental loads for most types of failure to occur. Index properties (grain size, water content, bulk density, Atterberg limits and grain density) are measured as well because they aid in classifying the sediment and can be correlated with both strength parameters and sedimentary processes. Also, they are not strongly affected by coring disturbance. Compression or consolidation properties are measured because the consolidation state (relative degree of compaction) correlates well with relative shearing strength (Ladd and Foott, 1974), and reflects earlier geologic events (for example preloading by glaciers or erosion of overburden).

The usefulness of most of our geotechnical data are limited by the short length of cores (typically 7 m to 10 m) and by core disturbance. Because many failure features have basal shearing planes that are much deeper (50 m or more) than conventional coring devices penetrate, the sediment involved in failure may not have the same properties as that sampled. Coring disturbance, generated by the thick walled samplers that are commonly used, alters the engineering properties of the sampled sediment from the properties of the sediment in place. Both of these limitations, core shortness and disturbance, are serious and capable of greatly reducing the validity of any geotechnical study.

A methodology for partially overcoming these limitations is provided by the normalized soil parameter (NSP) approach (Ladd and Foott, 1974, Mayne, 1980). The NSP approach is based on empirical results that show certain engineering properties of certain sediments to be constant if normalized by appropriate consolidation stresses. For example, in a normally consolidated sediment profile (one in which no removal of sediment or preloading has occurred), the ratio of undrained shearing strength to overburden effective stress is often constant. If this ratio is known, a strength profile can be constructed by multiplying the ratio by values of overburden effective stress (sub-bottom depth times the average submerged density). If the sediment is overconsolidated, that is, if it has been preloaded by glaciers or other sediment that has since been eroded, a different ratio of strength to overburden stress will result. This ratio of strength to overburden stress is constant as long as the degree of overconsolidation, expressed as the overconsolidation ratio (OCR), is constant. The ratio of strength to overburden stress typically varies with the OCR raised to the power Λ_o , where h_o is a sediment constant (Mayne, 1980). If the variation of OCR with depth in the sediment column is known, a prediction of the strength variation can be

made. If the sediment is normally or underconsolidated, as the Holocene glacial-marine sediment appears to be in **most** locations, the value of λ_o is irrelevant.

One advantage of the NSP approach lies in its ability to provide parameters that are independent of consolidation stress and depth in the sediment column. In a sense, therefore, the limitation imposed by short samples is at least partially removed, particularly in large depositional environments where the type of sediment being deposited at a given location is fairly constant over a long period of **time** (i.e., to a significant depth). The northeast Gulf of Alaska is probably such a large depositional environment. A second advantage of the NSP approach is that normalized parameters can be made somewhat-independent of coring disturbance by conducting all strength tests at greatly increased consolidation stresses (Ladd and Foott, 1974). That is, a disturbed sample and a nearly undisturbed sample would produce almost the same normalized strength parameters if both are consolidated (in a triaxial or direct simple shear cell) to a high stress level before testing for shear. Once the normalized strength parameters have been measured at the high stress levels, they can be applied to any stress level including the low level that the sample originally experienced in place.

The NSP approach cannot handle all offshore geotechnical conditions. Ladd and Foott (**1974**) warn against applying it in cases of naturally cemented clays. Offshore sediments often display "psuedo-overconsolidation"; that is, most aspects (low surface strength, no obvious hiatus, steady increase of strength with depth) point to normal consolidation but consolidation tests indicate a moderate degree of overconsolidation. If "psuedo-overconsolidation" results from a form of interparticle cementation, the NSP approach would predict strengths that are too low.

The presence of significantly different sediment below the level of sampling or the presence of undetermined environmental factors that might alter the consolidation state also cannot be handled by the NSP approach. Bubble phase gas might be an example of the latter. Highly varied or stratified sediment might also produce complications.

Cyclic Strength Degradation and Test Type Effects. Excess pore water pressures that develop during episodes of cyclic loading from earthquakes or storm waves effectively reduce the ability of the sediment to resist shear. This effect on shearing resistance can be expressed as a strength degradation factor, A_D . If this factor is multiplied by the static shearing strength obtained by the NSP approach, an estimate of the strength remaining in the sediment after dynamic loading will result. The degradation factor, A_D , varies with the type and magnitude of cyclic loading. If the loading is wave induced and the sediment is fairly pervious, an effective stress approach with allowance for partial pore pressure dissipation **may** be required for accurate modeling. For this situation a worst case (lower bound of strength) model can be provided by using a strength degradation parameter, A_D corresponding to no drainage. For earthquakes the duration of cyclic loading is short and a simple, undrained approach can be taken.

Another factor affecting measured sediment strength is the type of strength test performed. A reported value of shearing strength is not independent of test type because of initial consolidation conditions, shearing

rate, stress inhomogeneities, variations in stress orientations and many other potential differences. A parameter that relates the strength corresponding to the mode and rate of stress application that would exist during failure in the field to the strength of the same material measured in a field or laboratory test is needed. In the present studies most strengths were obtained through isotropically consolidated triaxial shear tests. Because field consolidation conditions are typically anisotropic, a correction factor, A_c , is applied to correct strength values for these consolidation effects.

Summary of NSP Strength Determination. A summary of the normalized soil parameter approach as it has been applied in the northeastern Gulf of Alaska is given by the following equation:

$$S_u / \sigma_v' = A_c A_D (OCR)^{\lambda} s_{nc} \dots \dots \dots (1) \dots \dots$$

Where S_u = **The** undrained shearing strength applicable to the mode of failure under consideration

σ_v' = overburden effective stress = $\gamma' z$

U = degree of consolidation

= 1 for complete normal or over-consolidation

γ' = average submerged density

z = sub-bottom depth

A_c = Test type correction factor

A_D = Cyclic strength degradation factor

OCR = Overconsolidation ratio

= σ_{vm}' / σ_v'

σ_{vm}' = **Maximum past** effective stress

λ = A normalized strength exponent that is constant for a given sediment

s_{nc} = the ratio of static undrained shearing strength to isotropic consolidation stress for normally consolidated conditions.

A program that involves a family of triaxial test types has been developed to obtain the parameters needed to evaluate Equation 1. **The** specific procedures are described under TEST PROCEDURES. Not that all of these properties relate to undrained conditions. For earthquake loading and wave loading of relatively impervious sediment, the undrained assumption is valid. For long term gravitational loading and wave loading of pervious sediment, a drained or partially drained analysis would be required.

Other shearing strength tests have been conducted that do not follow the NSP methodology directly. These include laboratory vane shear, field vane shear and static cone penetration, and certain types of triaxial shearing tests. The field tests were conducted to establish a level of ground truth -and provide a basis for judging the quality of subsequent laboratory data. Also, **some** field penetration tests were conducted in sandy deposits and provide the **only** reliable geotechnical data for these deposits. Laboratory vane tests were conducted onboard **the** ship immediately following sample recovery. They typically provide a lower bound estimate of the in place undrained shearing strength (Lee, 1979). The triaxial tests that did not follow the NSP methodology involved samples consolidated to the in situ effective overburden stress or lower. These types of tests typically produce an upper bound estimate of the in place undrained shearing strength (Ladd and Lambe, 1963).

Quantitative Evaluation of Offshore Stability. of these geotechnical results can be readily used to evaluate geologic hazards or provide a means of mapping relative stability. offshore downslope driving forces are gravity, earthquake shaking and storm wave loading. By writing a simplified equation for each driving force and setting it equal to the estimated, in place undrained shearing strength, we can determine the level of force needed to achieve failure. For example, it can be shown (Lee and others, that the approximate shearing stress developed under combined earthquake and gravitational loading is given by the simplified equation:

$$\tau = \gamma'z \sin\alpha + k\gamma z \dots\dots\dots (2)$$

Where: τ = mobilized shearing stress at depth z
 α = slope angle
 k = horizontal pseudo-static earthquake acceleration (in g's)
 γ = average total density of sediment (unit weight in air)

This relation was derived from Morgenstern's (1967) infinite-slope pseudo-static, earthquake-influenced slope stability analysis. It is valid only for small slope angles (α less than about 10°). The pseudo-static approach assumes that an earthquake can modeled by a constant horizontal acceleration. The infinite slope approach assumes that the seafloor is and has the slope over a large area. Failure occurs on a plane parallel to the surface of the slope and movement takes the form of a sliding sheet. At failure the driving force will equal the resisting force. Substituting τ from Equation 2 for S_u in Equation 1 and solving for k yields:

$$k = (\gamma/\gamma')U A_C A_D^A (OCR)^\circ S_{nc} - (\gamma'/\gamma)\sin\alpha \dots\dots\dots (3)$$

The resulting critical acceleration, k , derived from Equation 3 is the pseudo-static acceleration needed to induce failure given all of the conditions and assumptions present in the derivation. It is a function of sediment and site parameters. Lower values of the critical acceleration would correspond to areas that are vulnerable to induced sliding, given a uniform degree of the region being investigated. **The** value of this approach is increased if known failures are sampled. Critical accelerations from a known failure area indicate the level of shaking required to cause failure and provide a value by which the significance of other measured critical accelerations can be judged.

A similar approach could be followed to evaluate relative stability with respect to wave-induced shearing stresses. However, as shown in Appendix B, the magnitude of peak wave-induced stresses exceeds that of peak earthquake-induced stresses only in relatively shallow water (water depth less than 35 to 76 m). In these depths the sediment is primarily sand which might allow nearly full dissipation of excess pore water pressures during If full dissipation did not occur, a condition similar to liquefaction might develop under certain combinations of density, wave height and permeability (**Clukey and others, 1980**). This situation is unlikely and not considered in this report. For other conditions, earthquake loading dominates and Equation (3) can serve as the critical equilibrium relation.

TEST PROCEDURES

Geotechnical testing was conducted in conjunction with four cruises to the Gulf of Alaska: three from the R/V DISCOVERER in 1977, **1980** and **1981** (**DC1-77-EG**, **DC2-80-EG** and **DC1-81-EG**) and one from the R/V SEA SOUNDER in **1977** (**S8-77-EG**). Many different USGS individuals were involved in planning and conducting these tests in-house, and three outside laboratories conducted additional tests on four separate contracts (Geotechnical Engineers, Incorporated (**GEI**), **1977** cores, University of California, Berkeley, **1977** cores and Law Engineering Testing Company (**LETCO**), **1977** cores and **1980** cores). As a result, not all of the procedures followed in determining each property were identical throughout the test program. In the following discussion, major differences in procedure are listed whenever significant.

Shipboard Sampling and Testing. Most core samples were taken with gravity corers weighing between 2 and 10 **kNt**. A few samples were obtained with piston samplers or a vibratory corer similar to the Alpine Vibracore sampler described by Tirey (**1972**). All cores were contained within a plastic liner. Once aboard ship the core liners were sectioned into 1 or 1.5 m lengths. At **most** sites replicate cores were obtained; one was split, described and subsampled on shipboard (stratigraphy-sedimentology core), while the other was sealed with cheesecloth and microcrystalline wax and preserved under refrigeration for shore laboratory testing (geotechnical core). One of the split core sections was subsampled for water content determination.

Most **vane** shear testing was conducted on split cores sections. A miniature four-bladed vane (typically **1.22 x 1.22 cm**) was inserted perpendicular to the split face so that it was at least 1.2 cm below the surface. The vane was rotated by a motor-driven device through a calibrated spring on the **1977** cruises and through a torque cell on the **1980** and **1981** cruises. The top of the torque cell **or** spring rotated at **90°/minute**, a rate relayed directly to the vane by the stiff torque cell. With the more flexible springs, the true vane rotation rate was less than **90°/minute** before failure and greater after failure. The peak torque was measured and used to calculate the sample undrained shearing strength (ASTM, **1982** standard D 2573-72).

In Place Testing. In place vane shear and cone penetration tests were conducted during the **1980** cruise. **The** Multi-purpose in situ testing system (**MITS**) was leased from Woodward-Clyde Consultants, Plymouth Meeting, PA, and deployed at seven locations in the eastern Gulf of Alaska. **The** device is a tethered, bottom-supported platform capable of conducting static cone penetration and vane shear tests to a depth of 6 m below the seafloor. **The** device weighs 27 **kNt** (2.7 metric tons) in water. The ultimate cone penetration depth at a few locations was limited because of insufficient reaction force. The static cone penetrometer tip has a standard **10 cm²** base area and a **60°** tip angle. The load on the cone was measured **by** a full-bridge strain gage load cell mounted directly above the cone. The shear vane sensor consisted of a torque cell mounted above the vane blade. The vane was rotated by a pressure compensated electric motor at a rate of **60°/min** and the shearing strength was calculated from the **same** formula as that used for laboratory vane shear measurements. Both the cone and the vane were driven into the seafloor by a sliding drive head coupled to a drill rod. The drive head was moved at 1 m/minute by **an electric motor** and a chain and sprocket assembly. **The sub-**

bottom depth to the cone or vane was measured by a **360°** potentiometer connected to the sprocket assembly. A tilt indicator mounted on the base sensed the attitude of the frame to determine whether the maximum deadweight reaction was exceeded or if lateral loads on the tether line were pulling the device over. All electrical signals were carried to shipboard recorders through a shielded cable.

The MITS **system** was deployed from the R/V DISCOVERER from a two-point mooring. Typically the **system** was assembled in the cone penetrometer mode on its first deployment at a site. After a penetrometer record was obtained, the device was returned to the ship and rigged to perform a vane shear test. The size of vane and torque cell as well as sub-bottom locations for vane shear tests were selected based on the cone penetration resistance. **The** device was redeployed and the vane was driven in to the predetermined depths. At each depth the vane was rotated to obtain a peak torque and thus a measure of in place undrained shearing strength. At **some** depths the vane was rotated in the opposite direction (following an initial undisturbed strength determination) to obtain a measure of the remolded strength and the sediment sensitivity.

Shore Laboratory Testing. Water contents were obtained using drying and weighing techniques (ASTM, 1982 standard **D2216-80**). A correction was made to the weights to account for dried salts (assuming a salinity of 35 ppt).

Atterberg **limits** were obtained using ASTM standards (**D 423-66**, **D 424-59** and wet preparation technique, **D 2217-66**) with the exception that the Casagrande grooving tool was used instead of the ASTM tool. Salt corrections identical to those described above were applied to both the liquid and plastic limits. The grain density was obtained using a Beckman air comparison pycnometer at the USGS laboratory and by ASTM Standard **D 854-58** for the **tests** conducted **by** contractors. Grain size distributions and parameters were obtained using pipette analysis (Carver, 1971) at the USGS and by the hydrometer technique (ASTM Standard **D 422-63**) at the contractor laboratories.

Consolidation testing followed ASTM Standard **D 2435-70** with these exceptions:

- (a) In two early **contracts** (**GEI** and **LET**CO testing of 1977 cores), calculated and plotted void ratios corresponded to the end of a stress increment **time** period. In later testing the plotted void ratios corresponded to 100% consolidation.
- (b) In all contracted tests the coefficient of consolidation (**c_v**) was calculated using the square root of time method. For the tests conducted at the USGS, **c_v** was obtained using the **log of time** method.
- (c) In the **LET**CO testing of 1980 samples, about half of the tests were conducted with a pneumatically controlled **Anteus** consolidometer while the remainder were conducted with a dead weight oedometer.
- (d) **Some** of the tests conducted by the USGS on 1980 and 1981 samples were performed in a back pressured triaxial cell using the constant rate of strain technique (Wissa and others, 1971).

In all cases the results were used to estimate the maximum past vertical stress, σ'_{vm} , using the Casagrande (1936) construction and to obtain other consolidation parameters.

static triaxial testing roughly followed the procedures given by Bishop and Henkel (1957). Cylindrical samples (3.6 cm in diameter by about 9 cm in height) were hand-trimmed from larger core sections extruded from the plastic liner. Filter strips were attached and the sample was enclosed in a thin rubber/latex membrane in a triaxial cell. Differential pressures between cell and sample fluids were applied and full drainage was allowed. These consolidation stresses were applied in increments until a final value was reached. In some tests conducted by the USGS and LETCO on 1980 and 1981 samples, final consolidation was set to a level of about four times the maximum past stress. This was followed by a reduction in differential pressure and full drainage. In this way, an induced state of overconsolidation with a known value of OCR was generated. A few samples were consolidated anisotropically with the horizontal consolidation stress equal to about 0.5 times the vertical consolidation stress.

Most samples were sheared without drainage by increasing the axial load at a constant rate of strain, typically 0.03% to 0.16% per hour. Some of the LETCO testing of 1977 cores involved constant rate of **stress** application. Excess pore water **pressures** developed in the samples during undrained shear were measured using electronic pressure transducers. Axial loads were measured with strain gage type load cells and axial deformations were obtained with linearly variable differential transformers (**LVDT's**). Testing was continued until about 20% axial strain was obtained. Stresses and strains were calculated using standard procedures but without membrane or filter strip corrections. The static undrained shearing strength was obtained from the peak axial load measured over the full 20% axial strain range of the test.

Three types of static triaxial tests were performed:

- (a) Consolidation to a stress level less than three times the estimated maximum past stress without rebound.
- (b) Consolidation to a stress level greater than three times the estimated maximum past stress with a subsequent rebound to a lower final consolidation stress. A known induced overconsolidation ratio is obtained.
- (c) Consolidation to a stress level greater than three times the estimated maximum past stress without rebound.

Type (a) tests produce strength values that may be less than, equal to or greater than the in place shearing strength, depending on the details of the consolidation stresses. The approach does not provide parameters that can be used in the NSP approach. The value of this type of test would be in obtaining upper and lower bound values of strength and in studying naturally cemented sediment for which the NSP approach is not applicable.

Type (b) and (c) tests yield strength values for use in the NSP approach. Type (c) is used to obtain the ratio of strength to consolidation stress for normal consolidation, S_{nc}' , while type (b) yields the parameter Λ_o required for Equation 1.

Specimens for cyclic triaxial tests were prepared and consolidated in the same way as specimens for static tests (b) and (c) above. Because the static test for each consolidation condition was performed first on an adjacent sample, an estimate of the static strength of the cyclic specimen could be

made. Cyclic stresses less than the estimated static strength were then applied and the number of cycles needed to cause a predetermined **one-directional** strain was measured. Nearly full stress reversal (tensile and compressive stresses approximately equal) was developed. Loading was sinusoidal with a frequency of 0.1 Hz. The results were graphed on a plot of relative stress level (maximum average one-directional cyclic stress/estimated static strength) versus the log of number of cycles to 20% one-directional strain. A straight line connecting the data points was drawn and the stress level required for failure in 10 cycles was estimated by interpolation or extrapolation. Because 10 cycles is a characteristic number of significant **cycles** for a **major** earthquake (Seed and Peacock, 1971), this stress level was used for AD in Equations 1 and 3 for earthquake analysis. **The** parameter AD for storm-wave-induced instability would correspond to a larger number of cycles.

RESULTS

Study Areas and Core Locations. To simplify locating core sample and in place data, the region has been divided into eight study areas. Many of the study areas are associated with the major failure features discussed previously. Proceeding from west to east the eight study areas are (Figure 14):

- (A) Copper River
- (B) Kayak Trough
- (C) Bering Trough
- (D) **Icy Bay**
- (E) Icy Bay-Malaspina
- (F) Yakutat Bay
- (G) Yakutat
- (H) Alsek River

A ninth category, "other", includes a few sampling and in place stations that fall outside the regular areas.

Core and in place test location maps for each study area are given in Figures 15 through 21. The coordinates for these locations are given in Table 1.

Organization of Laboratory Test Data Presentation. All of the index property data are provided on summary plots in Appendix C. These data include water content, Atterberg **limits**, vane shear, grain size and grain density. **Downcore** locations of samples on which consolidation and triaxial tests were performed are also shown. The nature of these tests is indicated by a coded test number. **The** code for the test numbering **system is** as follows:

First two letters:

- (a) OE - **Oedometer** test
- (b) CE - Constant rate of strain (**CRS**) consolidation test
- (c) TE - Static triaxial test
- (d) TC - or D - Cyclic triaxial test

Trailing characters:

- (a) No trailing characters - test performed by the USGS

- (b) L1 - Test of 1977 core sample by Law Engineering and Testing Company
- (c) G - Test of 1977 sample by Geotechnical Engineers, Incorporated
- (d) B - Test of 1977 sample by University of California, Berkeley
- (e) L2 - Test of 1980 sample by Law Engineering and Testing Company

Critical sediment geotechnical parameters from each test are summarized in Tables 2 (consolidation), 3 (static triaxial) and 4 (cyclic triaxial). Graphical presentations of the results of each test are given in Appendices D (Law Engineering testing of 1977 cores), E (Geotechnical Engineers, Incorporated testing), F (Law Engineering testing at 1980 cores) and G (USGS testing of 1980 and 1981 cores). The appendices are grouped according to the organization performing the test because of a variation in the formats followed in graphically presenting the data. Each appendix is subdivided according to test type (consolidation, static triaxial or cyclic triaxial).

For the consolidation tests, a standard plot of void ratio, e , versus vertical effective stress, σ_v' , is given. These plots were used to obtain the slopes of the virgin compression and rebound curves (C_c and C_r) and the maximum past stresses, σ_{vm}' , all of which are tabulated in Table 2. For some of the testing organizations, a plot is also given of the calculated coefficient of consolidation, c_v , versus the vertical effective stress.

For the static triaxial tests, plots are given of the shearing or deviatoric stress, q , versus the mean normal effective stress, p . These stress paths provide a definition of the failure envelope and indicate whether sediment behavior is of a collapsing (bend to the left) or dilatative (bend to the right) nature. Also given are plots of shearing or deviatoric stress and pore pressure change versus axial stress.

The cyclic triaxial test plots include shearing stress-axial strain curves (hysteresis loops) and shearing stress-average normal effective stress (stress path) plots for selected cycles. The stress path plots indicate roughly the failure envelope applicable for cyclic loading and the rapidity with which pore pressures develop as a result of cyclic loading. The hysteresis loops indicate damping (proportional to relative area of each loop) and degrading stiffness (proportional to average slope through each loop). For the USGS tests these results are further presented on four additional plots that show pore pressure developed, damping, stiffness (modulus) and peak strain developed as a function of cycle number.

In Place Test Data. The results of in place vane shear testing are given in Figures 22 through 26 and cone penetrometer records appear in Figures 27 through 34. The vane shear results are plots of calculated undrained shearing strength versus sub-bottom depth. The cone results are continuous plots of cone pressure versus depth. Additional information plotted on the figures is discussed in a later section.

SYNTHESIS AND DISCUSSION

Analysis of Parameters. A major goal of the geotechnical testing was to provide parameters that could be inserted into Equation 3 so that a **stability-**related parameter, the critical acceleration, k , could be calculated. These parameters are:

- (a) S_{nc} - ratio of undrained strength to consolidation stress for normal consolidation
- (b) A_c - test type correction factor
- (c) A_D - cyclic strength degradation factor
- (d) U - degree of consolidation
- (e) OCR - overconsolidation ratio
- (f) h_o - normalized strength exponent
- (g) γ/γ' - ratio of submerged unit weight to total unit weight
- (h) α - slope angle

The next few sections discuss several of these parameters and how they were obtained from the basic engineering properties given in Tables 2 through 4 and in the appendices. Most of these parameters are correlated with sediment water content. In these correlations the water content is used as an index property that is representative of more basic sediment characteristics such as clay mineralogy, grain size and plasticity. The water content is used in place of these other parameters because it is the only parameter that was measured in conjunction with every other test. Also, because more water contents were measured than any other property, correlations can be applied to any location where a water content measurement was made. The influence of in place consolidation on reducing the water content with sub-bottom depth is ignored because of the shortness of the cores and the relative incompressibility of the silty sediment. The significant down-core fluctuations in water content in many of the cores appear to be related to basic lithologic changes.

Undrained Strength to Consolidation Stress Ratio for Normal Consolidation, S_{nc} . The type (c) tests listed in Table 3 were used to obtain values of S_{nc} . The criterion used to distinguish type (c) tests was that the final consolidation stress applied in the triaxial cell needed to exceed the natural maximum past stress by at least a factor of 3. Any lower consolidation stresses, in conjunction with disturbance effects, might produce a sample with some characteristics of overconsolidation (Ladd and Foott, 1974). The ratios of strength to overburden pressure for all of the type (c) tests were obtained and are plotted versus water content in Figure 35. The correlation is fairly good, given the scatter typically involved in geotechnical measurements, and shows a trend toward decreasing S_{nc} with increasing water content. A solid line follows the trend of the tests for which the initial consolidation was isotropic. The tests for which initial consolidation was anisotropic (lateral stress about one-half of the vertical stress) are shown with circled dots. Although a limitation in the number of these points prevents the construction of a line as complete as that for isotropic consolidation, a line with values of S_{nc} that are 0.8 times the isotropic values seems to fit the data fairly well.

Test Type Correction Factor, A_c . The factor A_c ideally should relate strength under laboratory test rate, test mode and consolidation stress conditions to the strength effective in the field under natural loading conditions. Most aspects cannot be considered without a major increase in the scope of investigation. The relation between strength under laboratory consolidation (predominately isotropic) and field consolidation (predominately anisotropic) condition is straightforward and represented by the difference between the two lines in Figures 35. Because a ratio of 0.8 appeared to account for most of the variation, this value will be used for A_c . The value

is similar to that obtained in an earlier study of sediment from offshore northern California. (Lee and others, 1981).

Cyclic Strength Degradation Factor, A_D . Results of cyclic triaxial tests on fine **grained** sediment are typically presented on a plot of cyclic stress level (as a percent of static strength) versus number of cycles to failure (Lee and Focht, 1976). Such a presentation is dependent upon knowledge of a static strength that can be used for normalization. In the University of California, Berkeley tests, the static strength of a third sample cut from the same increment as two cyclic test samples was determined. Normalizing the cyclic stress levels by this static strength is legitimate because the cyclic samples probably would have had the same strength if failed statically. For the USGS and Law Engineering tests, however, a static strength was measured on a sample from the same core but a different depth increment from that of the cyclic tests. One method (Method I) of normalizing the cyclic stress is to divide the cyclic stress level by this measured static strength. In some cores, however, there were lithologic changes **downcore** and the static and cyclic tests were not run on the same material type. This problem was solved partially by estimating a static strength from the water content and consolidation stress of the cyclic sample and an estimate of the ratio of static strength to consolidation stress from Figure 35. This approach to obtaining the static strength is termed Method II. A third method of handling this problem is to eliminate the need for static strength estimation by evaluating the product $A_D S_{nc}$ rather than its components. Because A_D is a cyclic shear stress, τ_c , divided by a static strength, S_u , and S_{nc} is S_u divided by a **consolidation** stress, σ_{vc}' , the product is τ_c/σ_{vc}' . This ratio can be obtained from a cyclic test alone without any static test results. The use of the ratio τ_c/σ_{vc}' is termed Method III.

Plots of relative cyclic stress levels versus number of cycles to failure are given in Figures 36 through 48. Separate figures corresponding to the three methods of analysis are given for the USGS/Law Engineering test results. The lines shown in the figures connect two or more cyclic test results and have been extended when necessary to cover the 10 cycles to failure zone. For methods I and II, the relative stress level corresponding to 10 cycles to failure was taken as A_D . For method III this value was taken as $A_D S_{nc}$ or τ_c/σ_{vc}' . Plots of relative stress level for failure in 10 cycles versus representative water content for the three methods of analysis are given in figures 49 through 51. **Method II** (Figure 50) shows a somewhat closer correlation than Method I (Figure 49); a solid line fit of the data shows an acceptable level of scatter (Figure 50). **The** trend shows an increase in A_D with increasing water content. That is, the lower water content coarse silts and sands are more susceptible to cyclic strength degradation than are the higher water content fine silts and clays. The product of the solid line fits for S_{nc} (Figure 35) and A_D (Figure 50) yields a solid line fit for $S_{NC} AD$ versus water content (Method III, Figure 51).

Some of the University of California, Berkeley, tests were performed with a static bias (Figures 36 through 39). That is, following nearly isotropic consolidation but before cyclic shear, a static shearing stress was applied. The sinusoidal cyclic stress was then applied relative to the static bias. The level of principal stress rotation (alternating compressive and tensile stresses) is reduced as the static bias is increased. **Herrmann** and Houston

(1976) show that the greater the level of principal stress rotation the greater is the extent of cyclic strength degradation. In cyclic earthquake loading of nearly horizontal sediment deposits, there is considerable rotation of principal stresses with each major cycle of loading (Seed and Peacock, 1971). Therefore, the case of no static bias or full stress rotation is more realistic as well as more conservative. The tests with a significant static bias give an intermediate level of cyclic strength degradation.

Degree of Consolidation, U , Overconsolidation Ratio (OCR) and Normalized Strength Exponent, Λ_o . A critical concern in evaluating offshore stability is the relative **consolidation** state of the sediment. Table 2 provides some information on consolidation state in the form of two parameters: σ_e' and $\sigma_{vm}'/\gamma'z$. The parameter, σ_e' is the difference between the maximum past stress, σ_{vm}' and the **submerged** weight per unit area of overlying material, $\gamma'z$. The parameter is negative for underconsolidated sediment (not all submerged overburden carried by interparticle stress), zero for normal consolidation and greater than 1 for overconsolidation. The ratio $\sigma_{vm}'/\gamma'z$ is the degree of consolidation, U , for values of σ_e' less than or equal to 1 and the overconsolidation ratio (OCR) for values greater than or equal to 1. As may be seen, scattered values of both parameters were obtained with apparently underconsolidated, normally consolidated and overconsolidated sediment all present. There is little consistency among the values, however, and in only about 10% of the tests is the absolute value of σ_e' greater than 50 kPa. Because of inaccuracies present in the Casagrande procedure and coring disturbance, these small deviations from normal consolidation are probably insignificant. In later sections additional in place data and theoretical information is used to further evaluate the consolidation state of these sediments. Based on Table 2 alone, it appears that the best estimate for both U and OCR for most of the cores is 1.0 (normal consolidation).

In anticipation of at least some of the cores being overconsolidated, a few static triaxial tests of the type (b) variety (induced overconsolidation ratio) were performed. These were used to obtain estimates of the parameter Λ_o needed for **Equations** 7 and 3. To obtain Λ_o , one first obtains the ratio of **undrained** strength to consolidation stress for a specimen that has an induced overconsolidation ratio (OCR known). This ratio is divided by the ratio of strength to consolidation stress for normal consolidation, S_{nc} to obtain a shear strength that has been normalized twice. Again, S_{nc} may be obtained from a test on a different sample from the same core or estimated from Figure 35 (if the initial water content of the induced OCR sample is known). These methods are termed I and II, respectively, and are similar to Methods I and II for normalizing cyclic triaxial test data discussed previously. The parameter Λ_o is obtained by dividing the log of the twice normalized shear strength by **the** log of the induced OCR (Mayne, 1980). Values of Λ_o (by both Methods I and II) and the intermediate parameters required to calculate them are given in Table 5. There is considerable scatter and a few values exceed 1.0 (not physically reasonable; probably indicative of experimental error at some level). Also, there is no correlation between Λ_o and water content. The average value of 0.9 would be appropriate for overconsolidated sediment. However, in the present study, all Holocene glacial-marine silty clays tested appear to be **under-** or normally consolidated.

Ratio of Submerged to **Total** Unit Weight, γ'/γ . The ratio of submerged to total unit weight can be calculated directly from the water content by

assuming 100% saturation and using the average measured grain density, 2.8 g/cm³.

Validity of NSP Approach, Vane Shear Tests and Type (a) Triaxial Tests. One purpose of performing in place strength tests was to provide a ground truth check on values obtained in the laboratory. The locations where both in place vane shear tests were performed and cores were taken for shore geotechnical analysis offer an opportunity to check the quality of laboratory strength determination procedures. Strengths were measured in the laboratory using the miniature vane, type (a) static triaxial tests (consolidation to a low value, often near the estimated in situ overburden stress) and normalized soil property (NSP) oriented tests (types (b) and (c)). These laboratory strength determinations are shown on the same figures as the field vane shear results (Figures 22 through 26). In these comparisons the laboratory vane shear results are consistently lower than the field results. The laboratory values range between about 50 and 80% of the field values. These findings are thus in line with a value of 60% obtained for a low plasticity (PI=15%) southern California sediment (Lee, 1979). The type (a) static triaxial tests consistently yielded strengths 150 to 250% higher than the field values.

The NSP values were obtained by using measured core water contents to obtain ratios of static strength to overburden effective stresses (S_{nc}) from Figure 34. The overburden effective stresses were obtained from $\gamma'z$ (average submerged unit weight times depth) and multiplied by the S_{nc} estimates to obtain an estimated shear strength profile. An implicit assumption of normal consolidation was made. These estimated shear strength values ranged between about 60% and 140% of the measured field values for the depth range sampled (excluding the upper 1 m). Below the level of sampling, a range of estimated strengths is given, corresponding to the range of water contents measured in the core. In this deeper unsampled sediment the NSP estimated shearing strengths were about 80 to 140% of the field values.

The NSP approach appears to provide the best estimate of the in place shearing strength values while the type (a) static triaxial test (consolidation to a low stress level with no normalization) appears to provide the poorest estimate and has the lowest correlation with the in place results. The simple laboratory vane shear test is nearly as accurate as the NSP approach if measured strengths are multiplied by a correction factor of about 1.7 (1/0.6) to account for disturbance. The laboratory vane test is not suitable for extrapolation below the level of sampling or evaluating cyclic strength degradation, however.

Evaluation of Consolidation State Using Field Strength Results and Gibson's Theory. Laboratory consolidation tests showed little indication of underconsolidation but the results were fairly scattered. Another means of judging consolidation state is to compare field vane strengths with NSP generated strengths. Such a comparison (Figures 22 through 26) shows no indication of overconsolidation except possibly for the upper 3.5 m of field test MV-1. That is, the field strengths do not greatly exceed the NSP strengths calculated by assuming normal consolidation. With field test MV-1 the high field strengths are probably a result of layered sand observed in nearby vibratory cores rather than true overconsolidation.

Field tests MV-4 (Figure 25) and, to a lesser extent MV-5 (Figure 26) suggest that a state of underconsolidation exists in the sediment in the eastern portion of the Icy Bay-Malaspina study area. The field strengths are 60 to 80% of the NSP generated strengths for normal consolidation. **Excluding** any other errors or opportunities for variability, these values correspond directly to the degree of consolidation.

To further evaluate the potential for underconsolidation in the northeast Gulf of Alaska, we performed a simplified theoretical analysis using the method of Gibson (1958). Gibson modeled a layer of sediment deposited at a steady and continuing sedimentation rate, m , that began to be deposited at a time, t , in the past. The degree of consolidation at the base of the sediment column can be predicted (Figure 52) as a function of the dimensionless parameter, m^2t/c_v , where c_v is the coefficient of consolidation. The degree of consolidation at **shallower** levels is somewhat lower.

values of c_v were measured in this study but are fairly scattered and inconsistent (Table 2). To reduce the scatter, a simplified correlation between c_v and liquid limit (Figure 53) from Lambe and Whitman (1969, p. 412) was used along with average liquid limit values for several locations. Sedimentation rates were taken from Figure 3.

By combining the results of Figures 52 and 53, we constructed lines of constant degree of consolidation on a plot of liquid limit versus m^2t (Figure 54). Using measured results, locations within the eastern Gulf of Alaska were plotted on the same figure. The position of these data points relative to the lines of constant degree of consolidation indicates the theoretical degree of consolidation of the sites. Most of the sites fall to the left of the 90% consolidation line indicating a degree of consolidation approaching 100%. All of the field vane shear tests except MV-4 (eastern Icy Bay-Malaspina study area) correspond to sites that fall in this range. **The eastern Icy Bay-Malaspina study area has a theoretical degree of consolidation of about 85%,** somewhat greater than the discrepancy between NSP and field strengths (Figures 25 and 26), but in the same range. Therefore, several lines of evidence (field versus NSP strength, theory and consolidation test results) suggest a degree of underconsolidation (60 to 85% of normal consolidation) of the sediment in the eastern Icy Bay-Malaspina study area. As indicated on Figure 54, the eastern portion of the Alsek **prodelta** study area and Kayak Trough may also display a similar underconsolidation level. Two of the embayments, Icy Bay and Yakutat Bay, appear to be highly underconsolidated, having degrees of consolidation of 30 and near **15%**, respectively. The remainder of the Holocene glacial-marine sediment sites appear to be normally consolidated.

Critical Acceleration Calculation. **The** critical acceleration, k , is calculated from Equation 3. If we assume normal consolidation ($U=OCR=1$) and horizontal surfaces ($\alpha=0$), then all of the remaining parameters have been obtained as a function of water content in the sections above. Note that with a value of OCR equal to 1.0, the value of λ_o is irrelevant. Also, with OCR equal to 1.0, the solution for k is independent of sub-bottom depth. By combining the best fits of the data using Equation 3, a plot of critical acceleration versus water content can be drawn (Figure 55). **The** resulting values of the critical acceleration have a broad-based minimum between water contents of 35% and 45%. On either side of this zone the acceleration increases rapidly. The existence of this minimum range indicates that certain

types of sediment found in the eastern Gulf of Alaska are more susceptible to earthquake loading than others. If we assume that each location within the region has the **same** potential ground shaking intensity and that underconsolidation and slope effects can be ignored initially, then locations that have more of the susceptible material should have failed **more** often. Within the Icy Bay-Malaspina study area (Figure **56**), this appears to be the case. The portion of each core with a water content between 35% and 45% has been calculated and listed by the location of the core. It appears that those cores within the observed failure feature typically have more of the susceptible sediment than do those outside the feature. The correlation is not exact but is consistent. **Thus** mapping of vulnerable material according to surface core water content may **be** viable even though the extent of underconsolidation, steepness of slope, variations in seismicity and variations in **seismic** response have not been considered.

The distribution of susceptible **material** in the Yakutat study area is shown in Figure 57. The correlation of susceptible material with the slump zone is not as good as for the Icy Bay-Malaspina area. The higher level of underconsolidation in the Icy Bay-Malaspina area **may** contribute to the greater extent of failure. Also, the boundaries of the Yakutat slump are poorly defined acoustically.

In the Alsek study area (Figure **58**), all cores were collected within the failure zone. The majority of samples appear to consist of susceptible sediment.

Regional Variations. Most of the geotechnical properties discussed above have been tied together through a seismic-induced instability analysis. A correlation of parameters with water content has shown **some** consistent trends and has helped to identify a susceptible sediment type. The water content, in turn, typically increases offshore, although not consistently. **Downcore** variations in water content are large.

No consistent variations in the correlations of geotechnical parameters with water content were found that could be related to study area. Indeed, the differences between study areas appear to be of the **same** order as variations within study **areas**. **Some** differences in landslide morphology were noted in the geologic framework discussion that cannot be explained by these basic correlations. For example, the multiple, complex flows of the Alsek **prodelta** contrast with the **massive** but simple rotational slumps of the Icy Bay-Malaspina study area. One possible explanation of these morphology differences is that fundamental sedimentological parameters contribute to variations in post failure behavior. **That** is, certain geotechnical properties that correlate well with water content **may** determine the point of initial failure. Movement after failure **may** be controlled by other characteristics that are not properly evaluated in triaxial testing.

An example of at least one characteristic that appears to vary consistently among the study areas is plasticity. All of the Atterberg limits measurements, grouped according to geographic area, are plotted on a series of plasticity charts (plasticity index versus liquid limit, **Lambe** and Whitman, 1969, p. 35) in Figures 59 through 64. Least squares regression fits of each set of data were developed and displayed fairly good correlation coefficients. Figure 65 presents **a summary of all** of the linear regression

lines. All plot above the "A-line" and fall near or within the zone generally occupied by glacial clays (**Lambe, 1951**, p. 27). Most sediment classifies as CL ("inorganic clays of low to medium plasticity, gravelly clays, sandy clays, silty clays, lean clays"). The regression lines are nearly parallel to each other and to the "A-line." The continental shelf study areas (Alsek prodelta, Yakutat, Icy Bay-Malaspina, Copper River) show a progressively greater distance from the "A-line" as one progresses toward the west. The Alsek **prodelta** slide, which has the **most** unusual morphology, provides data that plot closest to the "A-line." The embayments (Icy Bay, Yakutat Bay) and troughs (Bering, Kayak) show the greatest distance from the "A-line". **This** behavior probably relates to changes in clay mineral activity. The unusual morphology of the Alsek **prodelta** slides and flows **may** relate to these changes in index properties.

SUMMARY AND CONCLUSIONS

1. Previous studies have shown the **major** seafloor geologic hazards in the eastern Gulf of Alaska to be slides and flows, shallow faults, **gas** charged sediment and buried channels. Excluding shallow faulting, these hazards on the continental shelf are associated with Holocene glacial-marine sediment. This sediment consists primarily of sand and muddy sand in water depth less than 50 m and clayey silt at greater depths. The Holocene glacial-marine sediment is a typical glacial rock flour produced by intense mechanical weathering. Massive failure features have been identified acoustically on slopes of **0.5°** to **1.3°** on the continental shelf. Sediment volumes of up to 32 **km³** are involved.
2. Both underconsolidation (Hampton and others, **1978**; **Carlson** and others, **1978**; Molnia and Sangrey, **1979**) and bubble-phase gas charging (**Carlson** and others, **1980**; Hampton and others, **1978**; Molnia and Rapoport, **1980**) have been suggested as principal causative factors for sediment instability in the region. The present study indicated that both features are present but that their occurrence is uncommon.
3. Cyclic loading by **storm waves** and particularly earthquakes appears sufficient to cause the observed failure features. Gas charging and underconsolidation may facilitate failure in a few locations. Major wave induced shearing stresses exceed major earthquake induced stresses only in relatively shallow water (less than 35 to 76 m),
4. As noted by Ladd and Foott (**1974**), the normalized soil parameter (**NSP**) approach appears capable of partially overcoming the problems of coring disturbance and core shortness in obtaining valid geotechnical properties. This is illustrated in this study by good comparisons between NSP generated strength profiles and those measured with an in place vane shear device. One comparison that is not as good can be explained by underconsolidation predicted by Gibson's (1958) analysis.
5. Laboratory vane shear tests produce shearing strengths that are consistently lower than the field strengths. Triaxial specimens consolidated to near the in place overburden stress produce strengths that are erratically higher to much higher than the field strengths.

6. There is little evidence for overconsolidation in the Holocene glacial-marine sediment tested.

7. Many of the geotechnical parameters correlate well with water content, which is probably representative of more basic sediment characteristics such as clay mineralogy, grain size, and plasticity. According to laboratory tests, sediment with a water content between 35% and 45% is most susceptible to earthquake loading. Cores that contain more of this susceptible material roughly correlate with the locations of failure features.

8. Differences in failure morphology are difficult to relate to advanced geotechnical parameters but may relate to observed variations in plasticity.

ACKNOWLEDGEMENTS

These studies were supported by the U.S. Geological Survey and the Bureau of Land Management through an interagency agreement with the National Oceanic and Atmospheric Administration, under which a multiyear program responding to needs of petroleum development of the Alaskan continental shelf is managed by the Outer Continental Shelf Environmental Assessment Program (OCSEAP) office.

We wish to thank Bill Levy, Ed Clukey, Charles Fitts, Dwight Sangrey, Arnold Bouma, Bruce Molnia and Paul Carlson for their effort in acquiring the early geotechnical data presented in this report. We also wish to thank Dan Bright, Pat Spragge, Kris Johnson and Mike Torresan for performing the later geotechnical tests. Finally, we thank Monty Hampton, Bill Winters and Jim Booth for their thoughtful and helpful reviews of this manuscript.

REFERENCES

- American Society for Testing and Materials (ASTM), **1982, 1982** annual book of ASTM Standards, part **19**, Natural Building Stones; Soil and Rock, ASTM, Philadelphia, 710 pp.
- Bea, R.G., 1976**, Earthquake criteria for platforms in the Gulf of Alaska: Proceedings of the 8th Offshore Technology Conference, Houston, vol. **2.**, p. 657-679.
- Beikman, Helen, **1974**, Preliminary geologic map of the southeast quadrant of Alaska: U.S. Geological Survey Miscellaneous Field Studies Map MF-612, Scale **1:1,000,000**.
- Beikmann, Helen, 1975, Preliminary geologic map of southeastern Alaska: U.S. Geological Survey Miscellaneous Field Studies Map MF-673, Scale **1:1,000,000**.
- Bishop, A.W. and Henkel, D.J., **1957**, The measurement of soil properties in the triaxial test, Edward Arnold, Ltd, **London**, 227 p.
- Bruns, T.R., 1979, Late Cenozoic structure of the continental margin, northern Gulf of Alaska, in Sisson, Alexander, ed., The relationship of plate tectonics to **Alaskan** geology and resources: Alaska Geological Society 1977 Symposium Proceedings, p. **11-130**.
- Bruns, T.R., **1982**, Structure and petroleum potential of the continental margin between Cross Sound and Icy Bay, northern Gulf of Alaska: U.S. Geological Survey Open-File Report 82-929, 63 p.
- Bruns, T.R. and Plafker, George, **1982, Geology**, structure, and petroleum potential of the southeastern Alaska and northern Gulf of Alaska continental margins, in Bruns, T.R., ed., Hydrocarbon resource report for proposed O.C.S. **Lease Sale 88**: Southeastern Alaska, Northern Gulf of Alaska, Cook Inlet, and Shelikof Strait, Alaska, p. **11-52**.
- Bruns, T.R., and Schwab, W.C., **1982**, Structure maps and **seismic** stratigraphy of the Yakataga segment of the continental margin, northern Gulf of Alaska: U.S. Geological Survey Miscellaneous Field Studies Map MF-1424, 2 sheets and 25 p., scale **1:250,000** (in press).
- Carlson, P.R., 1978**, Holocene slump on continental margin off Malaspina Glacier, Gulf of Alaska: American Association of Petroleum Geologists, Bulletin, vol. 62, no. 12, p. **2412-2426**.
- Carlson, P.R., 1979**, Extensive sliding of continental slope sediments, eastern Gulf of Alaska (**abs.**): Geol. **Soc.** of America, Abstracts with Program, vol. **11**, p. 398.
- Carlson, P.R., Bruns, T.R., and Molnia, B.F., 1975**, Submarine slides and near surface faults, northern Gulf of Alaska: U.S. Geological Survey Open-File Report 75-505, **1** map.

- Carlson, P.R.,** Bruns, T.R., Molnia, B.F., and Schwab, W.C., **1982**, Submarine valleys in the northeastern Gulf of Alaska: Characteristics and probable origin: Marine Geology, vol. 47, p. 217-242.
- Carlson, P.R.,** Levy, W.P., Molnia, B.F. and Hampson, J.C., 1978, Geotechnical properties of sediments from the continental shelf south of Icy Bay, northeastern Gulf of Alaska: U.S. Geological Survey Open-File Report 78-**1071**, **29** p.
- Carlson, P.R.,** and Molnia, B.F., **1975**, Preliminary isopach map of Holocene sediments, northern Gulf of Alaska: U.S. Geological Survey Open-File Report 75-507.
- Carlson, P.R.,** and Molnia, B.F., 1977, Submarine faults and slides on the continental shelf, northern Gulf of Alaska: Marine Geotechnology vol. 2, p. 275-280.
- Carlson, P.R.,** Molnia, B.F., Kittelson, S.C., and Hampson, J.C., Jr., **1977**, Distribution of bottom sediments on the continental shelf, northern Gulf of Alaska: U.S. Geological Survey Miscellaneous Field Studies Map MF-876, 2 sheets and 13 p., scale **1:500,000**.
- Carlson, P. R.,** Molnia, B. F., and Wheeler, M. C., **1980**, Seafloor geologic hazards in O.C.S. lease area 55, eastern Gulf of Alaska: Proceedings of the 12th Offshore Technology Conference, Houston, **v. 1**, p. 563-603.
- Carlson, P. R.,** and Schwab, W. C., 1982, **Northern** Gulf of Alaska environmental **geology**, in Bruns, T. R., ed., Hydrocarbon resource report for proposed OCS lease sale 88: southeastern Alaska, northern Gulf of Alaska, Cook Inlet, and Shelikof Strait, Alaska: U.S. Geological Survey Open-File Report 82-928, p. 73-86.
- Carver, R. E., **1971**, Procedures in sedimentary petrology: Wiley-Interscience, New York.
- Casagrande, Arthur, 1936, The determination of the pre-consolidation load and its practical significance: Proceedings, 1st International Conference of Soil Mechanics and Foundation Engineering, p. 60.
- Clukey, E. C., Cacchione, D. A., and Nelson, C. H., **1980**, Liquefaction potential of the Yukon Prodelta, Bering Sea: Proceedings of the 12th Annual Offshore Technology Conference, Houston, vol. **1**, p. 315-325.
- Gibson, R. E., 1958, The progress of consolidation in a clay layer increasing **in** thickness with time: Geotechnique, vol. 8, p. 71-182.
- Hampton, M. A., Bouma, A. H., **Carlson, P. R.,** Molnia, B. F., Clukey, **E. C.,** and Sangrey, D. A., **1978**, Quantitative study of slope instability in the Gulf of Alaska: Proceedings of the 10th offshore Technology Conference, Houston, vol. 4, p. **2307-2318**
- Herrmann, H. G., and Houston, W. N., **1976**, Response of seafloor soils to combined static and cyclic loading: Proceedings of the Eighth Offshore Technology Conference, paper number OTC 2428.

- Ladd, C. **C.**, and Foott, Roger, 1974, New design procedure for stability of soft clays: American Society of Civil **Engineers**, Journal of the Geotechnical Engineering Division, vol. 100, no. GT7, **p.** 763-786.
- Ladd, C. **C.**, and **Lambe**, T. W., **1963**, The strength of "undisturbed" clay determined from undrained tests: American Society for Testing and Materials, Standard Technical Publication **361**, **p.** **342-371**.
- Lambe**, T. W., **1951**, Soil testing for engineers, J. Wiley and Sons, New York, **165 p.**
- Lambe**, T. W. and Whitman, R. V., 1969, Soil Mechanics, J. Wiley and Sons, New York, 533 p.
- Lee, H. J., 1979, Offshore soil sampling and geotechnical parameter determination: Proceedings of the 11th annual offshore Technology conference, paper number OTC 3524.
- Lee, H. J., Edwards, B. D., and Field, **M. E.**, **1981**, Geotechnical analysis of a submarine slump, Eureka, California: Proceedings of the 13th annual Offshore Technology Conference, paper number OTC **4121**.
- Lee, H. J., and Schwab, W. C., 1982, **Geotechnical** investigations related to geologic hazards: northern Gulf of Alaska, *in*, Bruns, ed, Hydrocarbon resource report for proposed O.C.S. Lease Sale 88: **southeastern** Alaska, northern Gulf of Alaska, Cook Inlet, and Shelikof Strait, Alaska: U.S. Geological Survey Open-File Report 82-928, **p.** 87-94.
- Lee, K. L., and Focht, J. A., **1976**, Strength of clay subjected to cyclic loading: Marine Geotechnolgy, vol. **1**, no. 3, **p.** **165-186**.
- Mayne, Paul, **1980**, Cam-clay prediction of undrained strength: American Society of Civil Engineers, Journal of the Geotechnical Engineering Division, vol. **106**, **p.** **1219-1242**.
- Minster, J. B., and Jordon, T. H., **1978**, Present day plate motions: Journal of Geophysical Research, vol. **83**, no. B11, **p.** 5331-5354.
- Molnia, B. F., **1979**, Sedimentation in coastal embayments, northeastern Gulf of Alaska: Proceedings of the 11th Annual Offshore Technology Conference, Houston, vol. **2**, **p.** 665-676.
- Molnia, B. F., and **Carlson**, P. R., 1975, Surface sediment distribution, northern Gulf of Alaska: U.S. Geological Survey Open-File Report 75-505, 1 sheet.
- Molnia, B. F., and **Carlson**, P. R., **1978**, Surface sedimentary units of northern Gulf of Alaska continental shelf: American Association of Petroleum Geologists Bulletin, vol. 62, no. 4, **p.** 633-643.

- Molnia, B. F., and **Carlson, P. R., 1980**, Quaternary sedimentary **facies** on the continental shelf of the northeastern Gulf of Alaska, in Field, M. E., **Bouma, A., and Colburn, I., ed.**, Quaternary **depositional environment** of the U.S. Pacific **continental margin**: Society of Economic Paleontologists and Mineralogists Symposium, Pacific Section, Bakersfield, p. **157-168**.
- Molnia, B. F., **Carlson, P. R.**, and Bruns, T. R., **1977**, Large submarine slide in Kayak Trough, Gulf of Alaska, in Coates, D. R., ed., Landslides: Reviews in Engineering Geology, **vol. 3**, Geological Society of America, p. **137-148**.
- Molnia, B. F., Levy, W. P., and **Carlson, P. R., 1980**, Map showing sedimentation rates in the northeastern Gulf of Alaska: U.S. Geological Survey Miscellaneous field studies Map, MF-1170 **1** sheet.
- Molnia, B. F., and Rapoport, M. L., 1980, Seafloor mosaic of the Alsek pockmark, slump, and sediment failure area, northeast Gulf of Alaska (**Abs.**): Geol. Soc. Amer., abstracts with programs, Atlanta, p. 436.
- Molnia, B. F., and Sangrey, D. A., **1979**, Glacially derived sediments in the Gulf of Alaska; geology and engineering characteristics: Proceedings of the **1979** Offshore Technology Conference, Houston, vol. 1, p. 647-655.
- Morgenstern, N. **M., 1967**, Submarine slumping and the initiation of turbidity currents: in Marine Geotechnique, A. F. Richards (**ed.**), University of Illinois **Press**, p. **189-220**.
- Plafker, George, 1967, **Geologic map** of the Gulf of Alaska Tertiary province, Alaska: U.S. **Geological** Survey Miscellaneous Geologic Investigations Map I-484, scale **1:500,000**.
- Plafker, George, **1971**, Pacific margin Tertiary basin, in Future petroleum provinces of North America: American Association of Petroleum Geologists Memoir 15, p. **120-125**.
- Reimnitz, Erk, 1966, Late Quaternary history and sedimentation of the Copper River delta and vicinity, Alaska: University of California, San Diego, Ph.D. thesis (**unpub.**), **160** p.
- Seed, H. **B.**, and Peacock, W. H., **1971**, Procedures for measuring soil liquefaction characteristics: American Society of Civil Engineers, Journal of the Soil Mechanics and Foundation Engineering Division, vol. **97**, no. **SM8**, p. **1099-1119**.
- Seed, H. B., and Rahman, M. S., 1978, Wave-induced pore pressure in relation to ocean floor stability of cohesionless soils: Marine Geotechnology, vol. 3, no. 2, p. **123-150**.
- Stephens, C. D., and Page, R. A., **1982**, **Seismic activity** in the northern Gulf of Alaska since 1974, in, Bruns, T. R., Hydrocarbon resource report for proposed O.C.S. Lease **Sale 88**: Southeastern Alaska, Northern Gulf of Alaska, Cook Inlet, and Shelikof Strait, Alaska, p. **115-121**.

- Tirey, **G. B.**, 1972, Recent trends in underwater soil sampling methods:
American Society for Testing and Materials, Standard Technical Publication
501, p. 42-54.
- Varnes, D. J., **1978**, Slope movement types and processes, in Schuster, R. L.,
ed., Landslides, analysis and **control**: National **Research** Council,
Transportation Research Board Special Report **176**, p. **12-23**.
- Wissa, A.E.Z., Christian, J. T., Davis, E. H., and Heiberg, Sigurd, 1971,
Consolidation at constant rate of strain, American Society of Civil
Engineers, Journal of the Soil Mechanics and Foundation Division, vol. 97,
no. **SM10**, p. **1393-1413**.

TABLES

Table 1. Core and in place test locations organized by study area

Study Area	Cruise	Core or In Place Test Number	Latitude		Longitude	
Copper River	S8-77-EG	4G	60°	15.18' N	145°	45.91' W
		6G	60°	12.94' N	145°	44.87' W
		7G	60°	12.93' N	145°	44.79' W
		8G	60°	10.64' N	145°	45.13' W
		9G	60°	10.64' N	145°	45.13' W
Kayak Trough	S8-77-EG	10G	60°	06.59' N	144°	39.06' W
		11G	60°	06.59' N	144°	39.06' W
		13G	60°	05.12' N	144°	40.44' W
		14G	60°	05.12' N	144°	40.44' W
		15G	60°	00.44' N	144°	34.55' W
		16G	60°	00.93' N	144°	40.16' W
		17G	60°	01.15' N	144°	40.7' W
		18G	59°	56.05' N	144°	39.14' W
		19G	59°	56.22' N	144°	39.24' W
		20G	59°	56.35' N	144°	39.34' W
		21G	59°	56.43' N	144°	38.27' W
Bering Trough	S8-77-EG	34G	59°	56.53' N	143°	32.36' W
		36G	59°	56.64' N	143°	35.75' W
		38G	59°	58.05' N	143°	38.00' W
Icy Bay-Malaspina	S8-77-EG	25G	59°	34.86' N	141°	58.20' W
		26G	59°	45.29' N	141°	57.17' W
		27G	59°	49.38' N	141°	55.61' W
		28G	59°	30.98' N	141°	20.73' W
		29G	59°	31.13' N	141°	20.90' W
		31G	59°	34.30' N	141°	21.04' W
		32G	59°	34.43' N	141°	20.96' W
		33G	59°	37.45' N	141°	20.18' W
	DC2-80-EG	95G	59°	36.60' N	141°	23.40' W
		96G	59°	36.60' N	141°	23.30' W
		173G	59°	38.05' N	141°	22.75' W
		175G	59°	37.25' N	141°	23.35' W
		176G	59°	37.25' N	141°	23.15' W
		178G	59°	36.10' N	141°	23.50' W
		179G	59°	36.00' N	141°	23.40' W
		181G	59°	35.30' N	141°	24.60' W
		182G	59°	35.20' N	141°	24.50' W
		184G	59°	34.40' N	141°	25.30' W
		185G	59°	34.40' N	141°	25.30' W
		187G	59°	33.30' N	141°	25.80' W
		188G	59°	33.30' N	141°	25.80' W
		190G	59°	32.50' N	141°	26.30' W
		191G	59°	32.50' N	141°	26.30' W
		193G	59°	31.20' N	141°	26.6' W
		194G	59°	31.30' N	141°	26.20' W

Table 1. Core and in place test locations organized by study area (continued)

Study Area	Cruise	Core or In Place Test Number	Latitude		Longitude	
Icy Bay-Malaspina	DC2-80-EG	196G	59°	36.50' N	141°	19.10' W
		197G	59°	36.50' N	141°	19.10' W
		MP9	59°	36.6' N	141°	23.4' W
		MP10	59°	36.5' N	140°	19.1' W
		MV4	59°	36.6' N	141°	23.4' W
		MV5	59°	36.5' N	140°	19.1' W
	DC1-81-EG	626G3	59°	35.00' N	140°	33.60' W
		627G1	59°	36.30' N	140°	45.20' W
		627G2	59°	36.35' N	140°	44.80' W
		628G2	59°	37.60' N	140°	57.00' W
		628G3	59°	37.50' N	140°	56.90' W
		630A1	59°	41.90' N	141°	20.10' W
		630A2	59°	41.70' N	141°	20.20' W
		632G1	59°	35.50' N	141°	09.50' W
		632G2	59°	35.50' N	141°	09.50' W
		633G1	59°	32.40' N	141°	06.00' W
		633G2	59°	32.40' N	141°	06.00' W
		634G1	59°	30.20' N	141°	00.00' W
		634G2	59°	30.20' N	141°	00.00' W
	DC1-77-EG	635A2	59°	39.81' N	141°	09.15' W
		709B	59°	34.30' N	141°	51.45' W
		709C	59°	34.30' N	141°	51.45' W
		710B	59°	41.50' N	141°	40.50' W
		710C	59°	41.40' N	141°	40.40' W
		711B	59°	42.60' N	141°	39.85' W
		715B	59°	36.45' N	141°	47.45' W
		715C	59°	36.45' N	141°	47.45' W
		717B	59°	39.30' N	141°	42.20' W
		717C	59°	39.30' N	141°	42.20' W
		718B	59°	38.45' N	142°	07.30' W
		719B	59°	42.60' N	142°	01.85' W
		720B	59°	45.65' N	141°	57.85' W
		721C	59°	47.00' N	141°	52.85' W
		721D	59°	48.00' N	141°	52.85' W
Icy Bay	S8-77EG	39G	60°	04.16' N	141°	23.42' W
		40G	60°	03.56' N	141°	22.27' W
		41G	60°	01.71' N	141°	21.06' W
		42G	60°	01.05' N	141°	21.31' W
		43G	59°	56.99' N	141°	26.49' W
		44G	59°	59.03' N	141°	27.94' W
Yakutat Bay	S8-77-EG	45G	59°	52.15' N	139°	41.85' W
		46G	59°	52.21' N	139°	41.81' W
		47G	59°	43.93' N	139°	42.08' W
		48G	59°	38.22' N	139°	47.93' W
Yakutat	DC2-80-EG	61G	59°	28.45' N	139°	48.16' W
		64G	59°	28.23' N	139°	48.83' W

Table 1. Core and in place test locations organized by study area (continued)

Study Area	Cruise	Core or In Place Test Number	Latitude	Longitude
Yakutat	DC2-80-EG	65G	59° 28.22' N	139° 48.97' W
		66G	59° 28.20' N	139° 48.88' W
		69G	59° 28.13' N	139° 49.38' W
		72G	59° 27.83' N	139° 49.59' W
		83G	59° 28.21' N	139° 48.00' W
		84G	59° 28.21' N	139° 48.40' W
		85G	59° 27.71' N	139° 50.06' W
		87G	59° 27.49' N	139° 50.58' W
		88G	59° 27.50' N	139° 50.64' W
		MP4	59° 28.21' N	139° 48.40' W
		MP5	59° 28.63' N	139° 48.14' W
		MV2	59° 28.21' N	139° 48.40' W
		MV3	59° 28.63' N	139° 48.15' W
	DC1-81-EG	616A2	59° 28.80' N	139° 48.10' W
		617G1	59° 22.70' N	139° 48.90' W
		617G2	59° 22.90' N	139° 48.80' W
		618G1	59° 23.19' N	139° 48.45' W
		618G2	59° 23.34' N	139° 48.44' W
		619G1	59° 24.45' N	139° 48.19' W
		620G1	59° 25.59' N	139° 48.09' W
		620G2	59° 26.03' N	139° 48.20' W
		621G1	59° 26.58' N	139° 47.31' W
		621G2	59° 27.04' N	139° 47.34' W
		623A1	59° 28.70' N	139° 49.70' W
		624A1	59° 28.70' N	139° 49.10' W
		624A2	59° 28.70' N	139° 48.70' W
		625A1	59° 28.70' N	139° 47.90' W
		625A2	59° 28.50' N	139° 48.20' W
Alsek River	DC2-80-EG	MC3-22	59° 06.99' N	138° 44.31' W
		23G	59° 06.99' N	138° 44.31' W
		26G	59° 07.09' N	138° 44.19' W
		28G	59° 06.99' N	138° 43.97' W
		29G	59° 06.93' N	138° 43.85' W
		31G	59° 06.89' N	138° 43.72' W
		32G	59° 06.99' N	138° 43.72' W
		35G	59° 06.99' N	138° 43.39' W
		36G	59° 06.94' N	138° 43.44' W
		38G	59° 06.94' N	138° 43.17' W
		43G	59° 06.94' N	138° 43.09' W
		46G	59° 06.91' N	138° 42.85' W
		47G	59° 06.94' N	138° 42.79' W
		49G	59° 06.92' N	138° 42.63' W
		50G	59° 06.92' N	138° 42.67' W
		52G	59° 06.93' N	138° 42.58' W
		55G	59° 06.93' N	138° 42.10' W
		56G	59° 06.88' N	138° 42.11' W
		MP3	59° 07.00' N	138° 44.29' W
		MP6	59° 07.74' N	138° 43.85' W

Table 1. Core and in place test locations organized by study area (continued)

Study Area	Cruise	Core or In Place Test Number	Latitude	Longitude
Alsek River	DC2-80-EG	MP7	59° 07.74' N	138° 43.85' W
		MV1	59° 07.00' N	138° 44.31' W
	DC1-81-EG	601G2	59° 06.60' N	138° 42.20' W
		602G3	59° 06.18' N	138° 40.25' W
		603G1	59° 06.16' N	138° 39.25' W
		604G3	59° 06.02' N	138° 39.42' W
		604G4	59° 06.09' N	138° 39.57' W
		605G1	59° 05.47' N	138° 38.01' W
		605G2	59° 05.49' N	138° 38.09' W
		606G1	59° 05.50' N	138° 36.80' W
		606G2	59° 05.27' N	138° 37.13' W
		607A1	59° 07.60' N	138° 44.60' W
		607A2	59° 07.50' N	138° 44.60' W
		608A2	59° 06.90' N	138° 45.40' W
		609A1	59° 05.70' N	138° 39.60' W
		610A2	59° 05.50' N	138° 37.70' W
		611G1	59° 04.90' N	138° 38.60' W
		611G2	59° 05.10' N	138° 39.10' W
		G12G1	59° 05.60' N	138° 40.50' W
		G13G2	59° 06.20' N	138° 43.70' W
		G14G2	59° 07.00' N	138° 46.10' W
Other	S8-77-EG	1G	60° 02.21' N	147° 11.28' W
		2G	60° 02.21' N	147° 11.28' W
	DC2-80-EG	23G	59° 50.75' N	144° 24.26' W
		92G	59° 00.15' N	139° 54.03' W
	DC1-81-EG	MP2	59° 18.81' N	139° 18.59' W
		MP8	59° 00.16' N	139° 54.01' W
	DC1-77-EG	615A1	58° 18.80' N	139° 19.20' W
		700B	59° 42.15' N	142° 41.80' W
		704B	59° 55.10' N	142° 31.05' W

Core or test number code

G, B, C, or D - Gravity or piston core

A - Vibratory core

MP - In place cone penetration test

MV - In place vane shear test

Table 2. Consolidation Test Results

Cruise Core #	Depth in Core, z, cm	Test Number	Study Area	$\gamma'z, \text{kPa}^a$	$\sigma_{vm}', \text{kPa}^b$	σ_e', kPa^c	$\frac{\sigma_{vm}'}{\gamma'z}^d$	C_c^e	C_s^f	$\frac{C_v}{\gamma'z}^g$ (cm^2/sec) [$\times 10^{-3}$]	Initial Water Content, %
S8-77-BG											
1G	80-90	OE1L1	Other	6.5	7	0.5	1.08	0.20	0.015	0.5-2	45.8
	230-235	OE2L1	Other	17.8	17	-0.8	0.96	0.15	0.020	0.5-3	37.5
4G	90-100	OE1G	Copper River	7	13	6	1.86	0.13	0.027	0.8-4	47.5
	190-200	OE2G	Copper River	13	12	-1	0.92	0.20	0.023	1.1-4.4	45.3
	310-320	OE3G	Copper River	23	14(?)	-9	0.61	0.25	0.038	2.0-4.1	39.2
	400-410	OE4G	Copper River	31	40	9	1.29	0.24	0.020	4.5-5.8	36.0
	605-610	OE5G	Copper River	49	29(?)	-20	0.73	0.23	0.032	4.0-5.0	40.1
6G	30-40	OE6G	Copper River	3	10	7	3.33	0.41	0.032	0.4-2.5	61.9
	100-107	OE7G	Copper River	6	8	2	1.33	0.48	0.053	0.6-2.4	60.5
7G	850-860	OE8G	Copper River	66	39(?)	-27	0.59	0.36	0.045	2.0-3.3	45.1
8G	200-210	OE9G	Copper River	12	11	-1	0.92	0.49	0.061	0.5-1.4	73.6
	350-360	OE10G	Copper River	22	20	-2	0.91	0.41	0.041	2.0-3.1	55.9
	410-420	OE11G	Copper River	26	26	0	1.00	0.71?	0.105?	1.5-3.3	58.0
	660-670	OE12G	Copper River	45	68	23	1.51	0.42	0.062	2.5-3.1	52.3
	730-740	OE13G	Copper River	51	56	5	1.10	0.37	0.039	3.8-4.8	41.7
	800-810	OE14G	Copper River	58	58	0	1.00	0.30	0.033	3.5-4.8	42.0
	860-870	OE15G	Copper River	63	56	-7	0.89	0.33	0.033	3.9-4.9	43.8
9G	85-100	OE16G	Copper River	5	11	6	2.20	0.48	0.048	1.0-3.0	77.7
	290-300	OE17G	Copper River	20	18	-2	0.90	0.25?	0.034	2.1-4.1	45.2
10G	190-200	OE3L1	Kayak Trough	13.9	27	13.1	1.94	0.17	0.015	?-2	38.9
11G	115-125	OE4L1	Kayak Trough	1.8	?	?	?	0.17	0.02	0.2-2	28.4
	240-250	OE5L1	Kayak Trough	19.8	15	-4.8	0.76	0.15	0.015	2.6-3.5	35.7
	390-400	OE6L1	Kayak Trough	31.9	60	28.1	1.88	0.20	0.02	1-3	39.9
	545-555	OE7L1	Kayak Trough	44.2	45	0.8	1.02	0.20	0.03	2.5-8	41.2
14G	100-110	OE8L1	Kayak Trough	6.3	10	3.7	1.59	0.23	0.02	0.4-1.5	42.0
16G	10-15	OE9L1	Kayak Trough	1.1	6	4.9	5.45	0.31	0.015	?	53.9
	102-107	OE10L1	Kayak Trough	9.2	12	2.8	1.30	0.13	0.02	1-2	30.0
	190-195	OE11L1	Kayak Trough	16.9	24	7.1	1.42	0.32	0.03	0.7-1.3	50.3
18G	30-40	OE12L1	Kayak Trough	2.2	?	?	?	0.30	0.02	0.2-0.5	63.8
	180-190	OE13L1	Kayak Trough	14	7	-7	0.50	0.21	0.03	?	47.7
	250-260	OE14L1	Kayak Trough	18.2	44	25.8	2.41	0.24	0.03	1-2.5	52.5
19G	65-75	OE15L1	Kayak Trough	4.6	8	3.4	1.74	0.24	0.015	?	53.9
	160-170	OE16L1	Kayak Trough	10.9	17	6.1	1.56	0.38	0.04	0.7-1.5	57.3
	260-270	OE17L1	Kayak Trough	17.5	15	-2.5	0.86	0.20	0.03	0.5-1.8	42.3
21G	280-300	OE18L1	Kayak Trough	13.8	14	0.2	1.01	0.30	0.04	0.5-2.0	43.1
	400-410	OE19L1	Kayak Trough	19.3	35	15.7	1.81	0.25	0.02	0.03-2.5	49.7
23G	100-110	OE20L1	Other	8.6	11	2.4	1.28	0.09	0.01	1-5	29.0
25G	80-90	OE18G	Icy Bay-Malaspina	6	9	3	1.50	0.21	0.026	1.0-3.1	58.4
	290-300	OE19G	Icy Bay-Malaspina	21	44	23	2.10	0.40	0.050	0.9-2.6	53.4
26G	100-110	OE20G	Icy Bay-Malaspina	9	12	3	1.33	0.17	0.02	2.5-3.3	36.9
	200-210	OE21G	Icy Bay-Malaspina	19	14	-5	0.74	0.18	0.029	2.1-4.0	34.5
27G	190-200	OE22G	Icy Bay-Malaspina	18	37	19	2.06	0.07	0.010	2.9-5.6	26.7
29G	105-115	OE23G	Icy Bay-Malaspina	9	14	5	1.56	0.23	0.021	2.1-4.5	39.4
	185-195	OE24G	Icy Bay-Malaspina	16	14	-2	0.88	0.25	0.027	2.0-4.1	44.6

Table 2. Consolidation Test Results (continued)

Cruise Core #	Depth in Core, z, cm	Test Number	Study Area	$\gamma'z, \text{kPa}^a$	$\sigma_{vm}', \text{kPa}^b$	σ_e', kPa^c	$\frac{\sigma_{vm}'}{\gamma'z}, ^d$	C_c^e	C_s^f	C_s^g (cm^2/sec) ($\times 10^{-3}$)	Initial Water Content
88-77-EG											
29G	290-300	OE25G	Icy Bay-Malaspina	26	20	-6	0.77	0.19	0.020	2.9-4.8	35.3
31G	90-100	OE26G	Icy Bay-Malaspina	9	15	6	1.67	0.16	0.019	4.6-6.1	34.0
	180-190	OE27G	Icy Bay-Malaspina	17	12	-5	0.71	0.17	0.017	2.0-5.5	33.1
	273-283	OE28G	Icy Bay-Malaspina	21	26	5	1.24	0.18	0.028	2.1-4.2	30.5
33G	22-30	OE29G	Icy Bay-Malaspina	2	13	11	6.50	0.24	0.025	1.0-5.7	35.5
	90-100	OE30G	Icy Bay-Malaspina	9	33	24	3.67	0.13	0.019	2.8-6.1	33.1
	205-216	OE31G	Icy Bay-Malaspina	19	16	-3	0.84	0.13	0.018	2.7-5.0	29.0
	361-371	OE32G	Icy Bay-Malaspina	32	25	-7	0.78	0.21	0.025	2.3-4.9	31.6
	500-510	OE33G	Icy Bay-Malaspina	48	25	-23	0.52	0.22	0.029	2.9-4.8	34.2
	675-685	OE34G	Icy Bay-Malaspina	62	66	4	1.06	0.18	0.023	2.9-5.3	30.2
	790-800	OE35G	Icy Bay-Malaspina	73	35(?)	-38	0.48	0.16	0.024	3.8-5.1	29.7
34G	60-70	OE21L1	Bering Trough	7	6	-1	0.86	0.05	0.008	1-2.5	23.0
38G	27-37	OE22L1	Bering Trough	3	6	3	2.00	0.20	0.020	0.9-1.6	46.9
40G	306-316	OE36G	Icy Bay	22	12	-8	0.55	0.020	0.23	0.3-2.0	46.4
	506-516	OE37G	Icy Bay	44	23	-21	0.52	0.43	0.081	1.8-3.2	60.4
42G	110-120	OE38G	Icy Bay	8	8	0	1.00	0.34	0.039	0.3-1.6	37.7
	270-280	OE39G	Icy Bay	20	13	-7	0.65	0.29	0.050	1.0-2.8	43.9
47G	100-110	OE23L1	Yakutat Bay	7.7	11	3.3	1.43	0.18	0.020	?	43.8
	250-260	OE24L1	Yakutat Bay	18.8	10	-8.8	0.53	0.18	0.025	0.5-3.5	41.1
DC2-80-EG											
MC3-22	86-92	OE1L2	Alsek River	7.6	22	14.4	2.89	0.20	0.023	3-28	43.0
28G	37-39	CE11	Alsek River	3.8	80	76.2	20.9	0.09	0.014	---	26.7
35G	10-13	CE7	Alsek River	1.0	19(?)	18.0	19.3	---	---	---	34.7
	40-44	CE8	Alsek River	3.2	47	43.8	14.6	0.22	0.02	---	46.4
38G	68-74	OE2L2	Alsek River	6	22	16	3.67	0.20	0.021	6-17	31.6
43G	4-8	CE4	Alsek River	.5	11(?)	10.5	23.0	0.08	0.01	---	30.0
	38-41	CE5	Alsek River	3.6	17(?)	13.4	4.7	0.09	0.01	---	31.9
46G	4-7	CE10	Alsek River	.5	42	41.5	79.6	0.12	---	---	35.8
	41-44	CE9	Alsek River	3.8	51	47.2	13.5	0.15	0.02	---	36.1
49G	64-77	OE3L2	Alsek River	5.6	30	24.4	5.4	0.16	0.037	2.6-14	41.4
55G	74-80	OE4L2	Alsek River	6.2	28	21.8	4.5	0.27	0.028	5.3-15.6	53.1
84G	14-21	OE5L2	Yakutat	1.6	12	11.4	7.5	0.18	0.035	1.5-8	37.4
	76-84	OE6L2	Yakutat	5.6	20	14.4	3.6	0.22	0.030	---	44.0
	200-210	OE7L2	Yakutat	14.4	50	35.6	3.5	0.10	0.016	5.7-23	23.8
87G	146-148	CE26	Yakutat	11.8	50	38.2	4.2	0.17	---	20-80	41.1
96G	86-96	OE8L2	Icy Bay-Malaspina	7.4	10	2.6	1.4	0.17	0.053	1.8-15.3	39.3
	263-271	OE9L2	Icy Bay-Malaspina	27.0	120	93.0	4.4	0.13	0.015	19-28	28.6
	354-261	OE10L2	Icy Bay-Malaspina	30.8	31	0.2	1.0	0.17	0.022	1.5-7.9	32.7
	374-381	OE11L2	Icy Bay-Malaspina	33.4	40	6.6	1.2	0.14	0.037	3.0-12.3	38.0
181G	33-35	CE3	Icy Bay-Malaspina	2.7	11	9.3	4.1	0.22	---	---	40.0
	116-118	CE1	Icy Bay-Malaspina	9.4	22	12.6	2.3	0.21	---	---	41.3
	196-198	CE2	Icy Bay-Malaspina	15.8	13	-2.8	0.8	0.26	---	---	44.0
190G	30-38	OE12L2	Icy Bay-Malaspina	3.2	70	65.8	21.9	0.16	0.017	19-26	31.5
	227-234	OE13L2	Icy Bay-Malaspina	18.8	45	26.2	2.4	0.21	0.028	2.1-9.3	40.7

Table 2. Consolidation Test Results (continued)

Cruise Core #	Depth in Core	Test Number	Study Area	$\gamma'z, \text{kPa}^a$	$\sigma_{vm}', \text{kPa}^b$	σ_e', kPa^c	$\frac{\sigma_{vm}'}{\gamma'z}, ^d$	C_c^e	C_s^f	C_v^g (cm ² /sec) ($\times 10^{-3}$)	Initial Water Content
DC2-80-EG											
190G	281-289	OE14L2	Icy Bay-Malaspina	23.2	50	26.8	2.2	0.21	0.054	2.1-6.7	38.0
196G	142-148	OE15L2	Icy Bay-Malaspina	14.2	23	8.8	1.6	0.10	0.031	10.2-34.8	28.6
	248-255	OE16L2	Icy Bay-Malaspina	25.2	140	114.8	5.6	0.12	0.021	14.7-21.7	25.7
	435-439	OE17L2	Icy Bay-Malaspina	45.8	120	74.2	2.6	0.11	0.027	8.6-17.8	21.9
DC1-81-EG											
604-G3	142	OE44	Alsek River	11.6	280(?)	268.4	24.1	0.13	0.009	10-20	32.2
605G2	70	OE46	Alsek River	5.0	70	65	14.0	0.25	0.017	2-11	52.8
	154	CE25	Alsek River	11.0	50	39	4.5	0.25	---	6-22	46.9
	198	OE45	Alsek River	16.4	42	25.6	2.6	0.17	0.012	2.5-9	40.2
618G2	62-64	CE22	Yakutat	5	31	26	6.2	0.25	---	6-25	49.7
	106-108	OE41	Yakutat	10	250(?)	240	25.0	0.16	0.007	9-12	31.3
	110-115	CE17	Yakutat	11	14	3	1.3	0.14	0.014	3-40	30.0
	166-168	CE29	Yakutat	13.4	32	18.6	2.4	0.25	---	5-22	44.8
	190-195	CE18	Yakutat	16.4	22	5.6	1.3	?	---	3-30	39.0
620G2	71-73	CE23	Yakutat	5.8	28	22	4.3	0.26	---	5-22	43.0
624A1	152-157	CE33	Yakutat	15.7	570	554	36.3	0.03	---	2000	27.6 sand
	210-212	CE27	Yakutat	19.5	8.4to105	-11to85	.4to5.4	0.12	---	2-40	33.6
627G2	26-28	CE16	Icy Bay-Malaspina	2	22	20	11.0	0.21	---	3.5-15	44.2
	32-34	CE14	Icy Bay-Malaspina	2.6	82	80	31.6	0.21	---	10-25	41.1
	116-118	CE13	Icy Bay-Malaspina	9.4	28	18.6	3.0	0.27	0.025	4-22	40.1
	122-124	OE40	Icy Bay-Malaspina	9	15	6	1.7	0.24	0.017	0.9-10	48.1
	222-224	CE15	Icy Bay-Malaspina	18	28	10	1.6	0.20	---	2-10	38.7
630A2	210	CE32	Icy Bay-Malaspina	21	1050	1029	49.3	?	---	?	26.2 Sand
632G1	77	CE31	Icy Bay-Malaspina	7	90	83	12.9	0.16	---	5-30	33.9
634G2	47-49	CE24	Icy Bay-Malaspina	3	12	9	4.0	0.33	---	2-12	56.7

a - Sediment submerged unit weight times embedment depth, equal to in situ overburden stress for normal- and over-consolidation

b - Maximum past stress obtained by Casagrande technique

c - Difference between σ_{vm}' and $\gamma'z$; negative values correspond to under-consolidation, near zero values to normal consolidation and positive values to overconsolidation

d - This parameter is the overconsolidation ratio for normally or overconsolidated sediment and the degree of consolidation for normally or underconsolidated sediment

e - Slope of the laboratory virgin compression curve

f - Slope of the laboratory rebound curve

g - Coefficient of consolidation for stresses greater than σ_{vm}'

Table 3. Static Triaxial Test Results

Core #	Depth in core, z, cm	Test Number	Study Area	$\gamma'z, \text{kPa}^a$	$\sigma'_{vm}, \text{kPa}^b$	$\sigma'_{vc}, \text{kPa}^c$	$\sigma'_{hc}, \text{kPa}^d$	Test Type ^e	Induced OCR ^f	$q_r(Su), \text{kPa}^g$	$S_u/\sigma'_{vc}{}^h$	$\phi^i, \text{degrees}$	Initial Water Content,
8-77-BG	117-130	TE1L1	Other	9.5	9.1	10		a		16.5	1.65		47.4
	140-150	TE4L1	Other	11.2	10.7	7		a		27.5	3.93		44.6
	163-177	TE2L1	Other	13.1	12.6	20		a		17	0.85		44.7
	190-202	TE3L1	Other	15.1	14.5	40		a		29.5	0.74		42.4
	202-214	TE7L1	Other	16.0	15.4	50		c	1	34.3	0.69	34.3	38.4
	214-225	TE6L1	Other	16.9	16.2	30		a		25.5	0.85		41.1
	225-235	TE5L1	Other	17.7	17.0	20		a		29.7	1.49		38.4
	210-220	TE1G	Copper River	17.1	14	15		a		16.5	1.10		42.0
	220-230	TE2G	Copper River	17.9	14.5	29		a		21.0	0.72		45.7
	230-240	TE3G	Copper River	18.7	15.0	59		c	1	35.5	0.60	36.0	41.9
	240-250	TE4G	Copper River	19.5	15.5	10	5	a		15.0	1.50		41.6
	630-640	TE5G	Copper River	50.4	29.5	34		a		39.5	1.16		39.2
	640-650	TE6G	Copper River	51.2	30.0	69		a		53.5	0.78		36.9
	650-660	TE7G	Copper River	52.0	30.5	139		c	1	63.0	0.46	34.5	43.6
	660-670	TE8G	Copper River	52.8	30.5	25	12.5	a		55.0	2.20		36.0
	670-680	TE9G	Copper River	53.6	31.0	75		a		40.5	0.54		40.5
	680-690	TE10G	Copper River	54.4	31.5	200		c	1	93.0	0.47	36.5	37.6
	690-700	TE11G	Copper River	55.2	32.0	125		c	1	76.0	0.61	34.8	36.5
	780-790	TE12G	Copper River	60.8	35	40		a		22	0.55		47.7
	790-800	TE13G	Copper River	61.5	36	80		a		39	0.49		46.6
8G	800-810	TE14G	Copper River	62.3	36	30	15	a		27	0.90		46.6
	810-820	TE15G	Copper River	63.1	37	160		c	1	73	0.46	34.8	45.9
	230-240	TE16G	Copper River	16.2	11	15		a		9	0.60		61.3
	240-250	TE17G	Copper River	16.9	12	30		a		16	0.53		67.8
	250-260	TE18G	Copper River	17.6	11	10	5	a		9	0.90		66.0
	260-270	TE19G	Copper River	18.3	14	23		a		23	1.00		63.3
	650-660	TE20G	Copper River	45.3	49	50		a		23	0.47		58.4
	670-680	TE21G	Copper River	46.6	51	90		a		46	0.51		50.3
	680-690	TE22G	Copper River	47.3	52	140		a		51	0.36		53.7
	790-800	TE23G	Copper River	54.9	62	160		a		80	0.50		45.4
	810-820	TE24G	Copper River	56.3	64	40		a		36	0.90		45.7
	820-830	TE25G	Copper River	57.0	64.5	80		a		54	0.68		44.3
	830-840	TE26G	Copper River	57.7	65.5	30	15	a		41	1.37		---
	260-270	TE27G	Copper River	18.4	17	30		a		11.5	0.38		63.3
	270-280	TE28G	Copper River	19.1	17.5	15		a		10.5	0.70		48.7
	270-280	TE29G	Copper River	19.1	17.5	60		c	1	24	0.40	32.4	50.8
	280-290	TE30G	Copper River	19.8	18	10		a		11	1.10		59.5
	120-137	TE8L1	Kayak Trough	9.2	17.8	10		a		6	0.60		46.4
11G	137-150	TE9L1 [†]	Kayak Trough	10.3	20.0	20		a		9.5	0.48		45.0
	150-162	TE10L1	Kayak Trough	11.1	21.5	30		a		11.5	0.38		49.2
	162-174	TE11L1 [†]	Kayak Trough	12.0	23.3	7		a		14.7	2.10		41.6
	270-284	TE12L1	Kayak Trough	22.4	27.3	35		a		21.3	0.61		38.3
	300-314	TE13L1	Kayak Trough	24.8	30.3	60		a		50.1	0.84		36.3
	354-368	TE14L1	Kayak Trough	29.2	35.6	90		a		38.2	0.42		35.8
	555-568	TE17L1	Kayak Trough	45.4	55.4	120		a		30.0	0.25		40.3

Table 3. Static Triaxial Test Results (continued)

Cruise Core #	Depth in core, z, cm	Test Number	Study Area	$\gamma'z, \text{kPa}^a$	$\sigma'_{vm}, \text{kPa}^b$	$\sigma'_{vc}, \text{kPa}^c$	$\sigma'_{hc}, \text{kPa}^d$	Test Type ^e	Induced OCR ^f	$q_f(S_u),^g$ kPa	$S_u/\sigma'_{vc},^h$	$\phi',^i$ degrees	Initi Water Conte
88-77-EG													
141	11G	582-592	TE18L1 ^j	Kayak Trough	47.4	57.8	21	a		13.8	0.66		42.
		642-655	TE16L1 ^j	Kayak Trough	52.4	63.9	60	a		19.3	0.32		35.
		662-675	TE15L1 ^j	Kayak Trough	54.0	65.9	30	a		16.8	0.56		34.
	14G	41-54	TE19L1 ^j	Kayak Trough	2.9	4.6	10	a		9	0.90		70.
		54-68	TE20L1 ^j	Kayak Trough	3.7	5.9	20	a		4.7	0.24		60.
		84-98	TE21L1	Kayak Trough	5.5	8.7	40	c	1	20	0.50	33.7	55.
	16G	120-132	TE22L1	Kayak Trough	11.1	15.2	13	a		13	1.00		29.
		132-144	TE24L1	Kayak Trough	12.2	16.6	54	c	1	19.8	0.37	31.5	35.
		144-156	TE25L1	Kayak Trough	12.9	17.9	7	a		20	2.86		43.
		167-180	TE23L1	Kayak Trough	15.3	20.8	20	a		30	1.50		30.
141	19G	80-94	TE26L1 ^j	Kayak Trough	5.8	8.0	10	a		11.5	2.00		52.
		94-108	TE27L1 ^j	Kayak Trough	6.7	9.3	20	a		14.3	2.13		53.
		108-122	TE28L1 ^j	Kayak Trough	7.6	10.5	40	a		17.0	2.23		53.
	21G	140-160	TE29L1	Kayak Trough	10.2	14.4	20	a		11.7	0.59		56.
		195-210	TE30L1	Kayak Trough	13.7	19.3	35	a		26.3	0.75		50.
		210-225	TE31L1	Kayak Trough	14.8	20.9	60	c	1	25.8	0.43	34.7	45.
	23G	42-56	TE33L1	Other	4.0	6.4	20	c	1	24	1.20	33.5	31.
		56-70	TE34L1 ^j	Other	5.1	7.5	40	c	1	37	0.93	40.5	34.
		70-84	TE35L1 ^j	Other	6.3	8.9	7	a		11.3	1.61		36.
		84-108	TE32L1 ^j	Other	7.8	11.0	10	a		18.8	1.88		34.
141	25G	240-250	TE31G	Icy Bay-Malaspina	18.0	35.5	15	a		11	0.73		54.
		260-270	TE32G	Icy Bay-Malaspina	19.5	39	60	a		25.5	0.43		54.
		270-280	TE33G	Icy Bay-Malaspina	20.2	41	10	a		7	0.70		55.
		280-290	TE34G	Icy Bay-Malaspina	20.9	43	30	a		15.5	0.52		49.
	26G	90-100	TE35G	Icy Bay-Malaspina	8.5	11	10	a		11	1.10		37.
		160-170	TE36G	Icy Bay-Malaspina	14.8	13	20	a		17.5	0.88		37.
		170-180	TE37G	Icy Bay-Malaspina	15.7	13	40	c	1	38.5	0.96	38.5	32.
		180-190	TE38G	Icy Bay-Malaspina	16.6	13.5	10	a		19	1.90		31.
	27G	50-60	TE39G	Icy Bay-Malaspina	4.9	29	10	a		6	0.60		52.
		60-70	TE40G	Icy Bay-Malaspina	5.8	30	30	a		13.5	0.45		51.
141		80-90	TE41G	Icy Bay-Malaspina	7.6	31	20	a		10.5	0.53		39.
		90-100	TE42G	Icy Bay-Malaspina	8.5	31.5	10	a		12	1.20		34.
		140-150	TE43G	Icy Bay-Malaspina	13.0	34	25	a		23	0.92		34.
		150-160	TE44G	Icy Bay-Malaspina	13.9	35	15	a		14.5	0.97		40.
		180-190	TE45G	Icy Bay-Malaspina	16.5	36	40	a		25	0.63		37.
	29G	135-145	TE46G	Icy Bay-Malaspina	12.1	14	15	a		10.5	0.70		47.
		145-155	TE47G	Icy Bay-Malaspina	13.0	14	25	a		12	0.48		43.
		155-165	TE48G	Icy Bay-Malaspina	13.9	14.5	40	a		10	0.25		39.
		250-260	TE49G	Icy Bay-Malaspina	22.1	18	15	a		8.5	0.57		45.
		330-340	TE50G	Icy Bay-Malaspina	29.0	21	10	a		11.5	1.15		35.
141		340-350	TE51G	Icy Bay-Malaspina	29.9	21.5	60	a		29	0.48		41.
		350-360	TE52G	Icy Bay-Malaspina	30.8	22	30	a		23.5	0.78		35.
	31G	150-160	TE53G	Icy Bay-Malaspina	14.4	15.5	10	a		10	1.0		33
		160-170	TE54G	Icy Bay-Malaspina	15.4	16	10	a		12.5	1.25		35
		170-180	TE55G	Icy Bay-Malaspina	16.3	17	20	a		27	1.35		33

Table 3. Static Triaxial Test Results (continued)

Cruise Core #	Depth in core, z, cm	Test Number	Study Area	$\gamma'z, \text{kPa}^a$	$\sigma'_{vm}, \text{kPa}^b$	$\sigma'_{vc}, \text{kPa}^c$	$\sigma'_{hc}, \text{kPa}^d$	Test ^e Type	Induced ^f OCR	$q_f(Su),^g$ kPa	$s_u/\sigma'_{vc}{}^h$	ϕ'^i , Initial degrees Water Content, %
88-77-EG												
31G	190-200	TE56G	Icy Bay-Malaspina	18.2	18	40		a		32.5	0.81	34
33G	290-300	TE57G	Icy Bay-Malaspina	27.4	21	10	5	a		18.5	1.85	32.4
	321-331	TE58G	Icy Bay-Malaspina	30.2	22	10	5	a		13.5	1.35	37.2
	331-341	TE59G	Icy Bay-Malaspina	31.2	22	15		a		10	0.66	31.0
	341-351	TE60G	Icy Bay-Malaspina	32.1	22.5	30		a		25	0.83	36.0
	351-361	TE61G	Icy Bay-Malaspina	33.0	23	60		a		46.5	0.78	33.3
	470-480	TE62G	Icy Bay-Malaspina	44.0	26.5	45		a		30	0.67	37.5
	480-490	TE63G	Icy Bay-Malaspina	45.0	27	75		a		33	0.44	43.8
	490-500	TE64G	Icy Bay-Malaspina	45.9	27	98		c	1	41	0.42	30.5
36G	46-60	TE37L1	Bering Trough	4.7	---	40		a		39	0.98	37.9
	60-75	TE36L1	Bering Trough	5.9	---	10		a		13.3	1.33	27.0
38G	90-110	TE38L1	Bering Trough	9.5	19	10		a		24.5	2.45	25.9
40G	340-350	TE65G	Icy Bay	23.7	14	40		a		19	0.48	49.3
	350-360	TE66G	Icy Bay	24.4	14.5	80		c	1	26.5	0.33	25.8
42G	231-245	TE67G	Icy Bay	17.9	12	20		a		18.5	0.93	41.6
	245-258	TE68G	Icy Bay	18.9	12	39		c	1	22.5	0.58	30.0
	258-270	TE69G	Icy Bay	19.9	12.5	10	5	a		13.5	1.35	42
47G	133-147	TE41L1	Yakutat Bay	10.3	12.4	50		a		58.8	1.18	42.3
	189-202	TE39L1	Yakutat Bay	14.4	14.4	20		a		24.0	1.20	42.8
	239-250	TE40L1	Yakutat Bay	18.0	?	30		a		70.5	1.45	48.6
DC2-80-EG												
MC3-22	3-13	TE1L2	Alsek River	0.5	22	1.4		a		13	9.27	35.0
	47-62	TE6L2	Alsek River	4.8	22	3.4		a		58	17.06	25.0
	62-76	TE4L2	Alsek River	6.1	22	27.6		b	3	124.4	4.51	29.4
28G	6-14	TE64	Alsek River	0.8	80	328.5	136.8	c	1	159.4	0.48	39.6
	25-34	TE63	Alsek River	2.6	80	56.9		b	5.7	227.1	3.99	36.2
	26-35	TE62	Alsek River	2.6	80	310.7		c	1	268.8	0.87	38.2
31G	4-11	TE65	Alsek River	0.7	60	3		a		27.2	9.08	28.7
	4-11	TE66	Alsek River	0.7	60	223.2		c	1	215.0	0.96	38.2
	11-19	TE67	Alsek River	1.4	60	251.2	126.1	c	1	146.1	0.58	33.5
35G	14-23	TE56	Alsek River	1.6	40	154.8		c	1	80.8	0.52	36.3
	14-23	TE57	Alsek River	1.5	40	24.7		b	6.2	58.4	2.36	40.4
	25-32	TE58	Alsek River	2.3	40	137.6	68.5	c	1	60.3	0.44	34.8
38G	52-64	TE3L2	Alsek River	5.4	22	27.6		b	6	86.1	3.12	31.6
43G	8-17	TE27	Alsek River	1.1	14(?)	6.5		b	5	37.4	5.74	33.9
	18-27	TE34	Alsek River	2.0	14(?)	31.3		a		79.9	2.55	32.5
	18-27	TE35	Alsek River	2.0	14(?)	31.1		a		73.9	2.38	32.9
46G	18-27	TE59	Alsek River	2.1	45	203.1		c	1	222.4	1.10	35.8
	28-37	TE60	Alsek River	2.0	45	35.7		b	6.2	166.0	4.66	33.9
	28-37	TE61	Alsek River	2.2	45	0.7		a		23.4	33.46	29.8
49G	18-28	TE5L2	Alsek River	2.24	30	169.2	61.93	c	1	89.5	0.53	40.5
	28-40	TE2L2	Alsek River	3.19	30	120.6		c	1	87.7	0.73	38.3
84G	21-33	TE11L2	Yakutat	2.45	15	103.4		c	1	64.4	0.62	36.9
	63-76	TE8L2	Yakutat	6.06	20	3.4		b	6	27.8	8.17	35.7

Table 3. Static Triaxial Test Results (continued)

Cruise Core #	Depth in core, z, cm	Test Number	Study Area	$\gamma'z, \text{kPa}^a$	$\sigma'_{vm}, \text{kPa}^b$	$\sigma'_{vc}, \text{kPa}^c$	$\sigma'_{hc}, \text{kPa}^d$	Test ^e Type	Induced ^f OCR	$q_t(Su),^g$ kPa	$S_u/\sigma'_{vc},^h$	$\phi^i,$ degrees	Initial Water Content
DC2-80-EG													
84G	100-112	TE7L2	Yakutat	9.26	20	20.7		c	1	14.6	0.70	36.9	33.
	160-172	TE10L2	Yakutat	15.78	33	1.4		a		34.9	24.93		24.
	176-190	TE9L2	Yakutat	17.97	35	17.2		a		78.2	4.54		21.
87G	150-158	TE84	Yakutat	13.04	50	203.1		c	1	122.8	0.61	35.7	38.
96G	108-124	TE17L2	Icy Bay-Malaspina	11.17	95(?)	379.3	165.8	c	1	135.8	0.36	37.3	36.
	155-170	TE12L2	Icy Bay-Malaspina	15.27	30	1.4		a		12.1	8.71		34.
	173-183	TE13L2	Icy Bay-Malaspina	16.74	30	35.1		a		30.1	0.85		38.
	198-212	TE16L2	Icy Bay-Malaspina	19.28	30	30.3		b	3	61.3	2.02		32.
	343-356	TE15L2	Icy Bay-Malaspina	34.51	35	34.8		b	4	70.4	2.02		33.
	361-374	TE14L2	Icy Bay-Malaspina	36.11	35	139.9		c	1	71.8	0.51	31.7	34.
	5-15	TE15	Icy Bay-Malaspina	0.84	15	277.7		c	1	131.5	0.47	35.9	39.
	5-15	TE16	Icy Bay-Malaspina	0.84	15	45.0		b	6.1	105.6	2.35		39.
	71-81	TE18	Icy Bay-Malaspina	6.16	15	39.9		c	1	23.7	0.59	39.8	42.
	71-81	TE19	Icy Bay-Malaspina	6.16	15	5.3		b	7.3	19.0	3.57		41.
181G	100-110	TE20	Icy Bay-Malaspina	8.04	15	39.4	20.3	c	1	17.6	0.45	33.6	46.
	100-110	TE21	Icy Bay-Malaspina	8.04	15	13.1		b	3	17.4	1.33		46.
	120-130	TE22	Icy Bay-Malaspina	11.00	15	0.5		a		8.7	18.49		36.
	120-130	TE23	Icy Bay-Malaspina	11.00	15	9.7		a		20.9	2.15		35.
	80-94	TE20L2	Icy Bay-Malaspina	7.86	50	48.2		b	6	97.8	2.03		31.
	101-114	TE18L2	Icy Bay-Malaspina	10.38	50	62.0		a		36.1	0.58	39.8	38.
	114-125	TE19L2	Icy Bay-Malaspina	11.44	50	96.5		b	3	80.7	0.84		42.
	175-188	TE21L2	Icy Bay-Malaspina	17.70	50	230.6	96.4	c	1	82.6	0.36	39.0	41.
	201-214	TE22L2	Icy Bay-Malaspina	19.74	50	1.4		a		11.0	7.86		39.
	214-227	TE23L2	Icy Bay-Malaspina	20.6	50	16.5		a		12.7	0.77		42.
196G	160-173	TE24L2	Icy Bay-Malaspina	17.0	100	165.2	82.8	a		99.3	0.60		32.
	234-246	TE28L2	Icy Bay-Malaspina	24.8	100	48.2		a		48.6	1.01		30.
	274-286	TE25L2	Icy Bay-Malaspina	29.0	100	172.3		b	3	251.8	1.46		25.
	286-298	TE26L2	Icy Bay-Malaspina	30.3	100	1.4		a		42.4	30.29		25.
	355-365	TE29L2	Icy Bay-Malaspina	37.6	100	55.1		b	6	184.3	3.34		26.
	367-377	TE30L2	Icy Bay-Malaspina	38.8	100	248.1		c	1	265.9	1.07	37.2	24.
	381-400	TE27L2	Icy Bay-Malaspina	42.0	100	320.4		c	1	256.4	0.80	37.2	25.
DC1-81-EG													
604G3	120-127	TE114	Alsek River	11.0	280(?)	293.4		a		176.6	0.60		34.
605G2	44-52	TE113	Alsek River	4.3	55	222.2		c	1	163.8	0.74	38.1	34.
	141-149	TE116	Alsek River	11.1	55	0.3		a		8.4	28.07		46.
	156-164	TE111	Alsek River	13.6	55	216.1		c	1	127.9	0.59	37.0	38.
	156-164	TE112	Alsek River	13.6	55	35.3		b	6.2	87.6	2.48		38.
	176-184	TE115	Alsek River	14.8	55	227.9	102.9	c	1	114.2	0.50	39.9	40.
	186-194	TE117	Alsek River	15.4	55	71.3		b	3.1	91.0	1.28		42.
	127-132	TE87	Yakutat	10.2	35	184.7		c	1	95.6	0.52	34.2	44.
	127-132	TE88	Yakutat	10.2	35	231.5	113.6	c	1	157.8	0.68	44.2	43.
	149-158	TE74	Yakutat	11.9	35	0.5		a		4.6	9.28		45.
	149-158	TE75	Yakutat	11.9	35	12.1		a		15.6	1.29		46.
620G2	90-99	TE82	Yakutat	7.1	28	120.8		c	1	53.2	0.44	32.5	48.

Table 3. Static Triaxial Test Results (continued)

Cruise Core #	Depth in core, z, cm	Test Number	Study Area	$\gamma'z, \text{kPa}^a$	$\sigma'_{vm}, \text{kPa}^b$	$\sigma'_{vc}, \text{kPa}^c$	$\sigma'_{hc}, \text{kPa}^d$	Test Type ^e	Induced ^f OCR	$q_f(S_u),^g$ kPa	$S_u/\sigma'_{vc},^h$	$\phi',^i$ degrees	Initial Water Content, %
DC1-81-EG													
624A1	141-150	TE91	Yakutat	14.7	100to500	333.1		c?	1?	401.25	1.21	38.0	29.0
	141-150	TE93 ^k	Yakutat	14.7	100to500	341.5		c?	1?	440.27?		34.3?	37.0
625A1	170-180	TE118	Yakutat	18.0	?	293.3		c?	1?	889.0	3.03	39.8	25.3
627G2	71-78	TE72	Icy Bay-Malaspina	6.0	25	18.6		b	5.5	44.7	2.40		42.2
	71-78	TE73	Icy Bay-Malaspina	6.0	25	31.0		b	3.1	45.9	1.48		46.4
	82-90	TE70	Icy Bay-Malaspina	7.0	25	104.7	48.7	c	1	44.4	0.42	37.1	42.3
	82-90	TE71	Icy Bay-Malaspina	7.0	25	100.1		c	1	53.2	0.53	36.1	40.7
	104-112	TE68	Icy Bay-Malaspina	8.5	25	1.6		a		2.1	1.31		45.1
	104-112	TE69	Icy Bay-Malaspina	8.5	25	10.4		a		10.4	0.99		43.4
630A2	220-229	TE89	Icy Bay-Malaspina	23.1	1050	299.9		a		561.98	1.87		24.3
	220-229	TE90 ^k	Icy Bay-Malaspina	23.1	1050	295.5		a		631.95		42.9	25.9
632G1	80-89	TE92	Icy Bay-Malaspina	7.8	90	362.8		c	1	208.4	0.57	36.4	32.4
634G2	73-80	TE83	Icy Bay-Malaspina	5.3	12	57.9		c	1	23.9	0.41	33.7	56.0

a - Sediment submerged unit weight times sub-bottom depth, equal to in place overburden stress for normal - and over-consolidation

b - Sediment natural maximum past stress, interpolated or extrapolated from adjacent consolidation tests

c - final vertical consolidation stress

d - final horizontal consolidation stress, blank if same as vertical stress

e - Type (a) test has a final vertical consolidation stress less than three times the maximum past stress without rebound. Type (b) test has a maximum triaxial vertical consolidation stress greater than three times the natural maximum past stress. The sample was subsequently rebounded to a lower consolidation stress inducing a known overconsolidation ratio. Type (c) test has a final vertical consolidation stress greater than three times the maximum past stress without rebound.

f - Blank indicates a type (a) test: final level of overconsolidation is unknown. Value greater than 1 indicates a type (b) test: value given is known induced overconsolidation ratio. Value of 1 indicates a type (c) test: sample has been forced to be normally consolidated.

g - maximum shear stress over 15 or 20% strain: assumed equal to undrained shear strength, S_u .

h - Ratio of undrained shear strength to vertical consolidation stress

i - Effective friction angle assuming no cohesion intercept: given for type (c) or drained tests only

j - Stress control test

k - Drained test

Table 4. Cyclic Triaxial Test Results

Cruise Core #	Depth in Core, z, cm	Test Number	Study Area	σ_{vc} , kPa ^a	σ_{hc} , kPa ^b	Induced ^c OCR	(q_f Static) ^d I	(q_f Static) ^e II	Static ^f Bias, kPa	Peak ^g Cyclic Stress, τ_c , kPa	$\frac{\tau_c}{q_f \text{ static}}$ (I)	$\frac{\tau_c}{q_f \text{ static}}$ (II)	$\frac{\tau_c}{\sigma_{vc}}$ (III)	# of ^k Cycles to failure	Strain at ^l failure, %	Initial Water Content %
S8-77-BG																
4G	485	TC1B	Copper River	34.3	29.4		27.0		11.9	18.9	0.70		0.55	5000	5	39.9
	485	TC2B	Copper River	34.3	29.4		27.0		11.9	27.5	1.02		0.80	13	12	41.5
	485	TC3B ^m	Copper River	33.3	29.4		36.8		15.5	28.0	0.76		0.84	403	11	41.5
	500	TC4B	Copper River	34.3	29.4		25.0		10.5	17.5	0.70		0.51	5000	6	42.3
	500	TC5B	Copper River	34.3	29.4		25.0		10.8	23.5	0.94		0.69	45	12	43.3
	500	TC6B ^m	Copper River	33.3	29.4		31.9		13.7	23.3	0.73		0.70	4583	8.8	43.3
	510	TC7B	Copper River	34.3	29.4		25.5		10.7	19.9	0.78		0.58	5000	7.4	44.3
	520	TC8B	Copper River	211.8	196.1	1	107.8		8.6	34.5	0.32		0.16	2493	1.4	35.6
	520	TC9B	Copper River	212.7	196.1	1	107.8		3.2	67.9	0.63		0.32	30	-8.8	38.2
	530	TC10B	Copper River	216.7	196.1	1	100.5		42.2	94.5	0.94		0.44	37	12	42.7
	545	TC11B	Copper River	217.6	196.1	1	92.6		38.0	80.6	0.87		0.37	150	12	40.7
	555	TC12B	Copper River	217.6	196.1	1	108.8		38.1	74.0	0.68		0.34	935	12	39.3
	575	TC13B	Copper River	217.6	196.1	1	93.1		37.2	70.8	0.76		0.33	5000	10	40.8
8G	495	TC14B	Copper River	216.7	196.1	1	100.0		19.0	63.0	0.63		0.29	87	12	41.4
	530	TC15B	Copper River	215.7	196.1	1	96.1		16.3	53.8	0.56		0.25	500	12	40.8
11G	420	TC16B	Kayak Trough	32.4	29.4		18.1		0.7	11.2	0.62		0.35	71	12	46.7
	450	TC17B	Kayak Trough	32.4	29.4		24.0		2.4	9.1	0.38		0.28	3994	12	39.6
	450	TC18B	Kayak Trough	32.4	29.4		24.0		2.4	10.3	0.43		0.32	2679	12	40.6
	470	TC19B	Kayak Trough	32.4	29.4		19.6		2.0	11.8	0.60		0.36	243	12	42.7
	470	TC20B	Kayak Trough	32.4	29.4		19.6		2.0	12.5	0.64		0.39	152	12	43.6
	485	TC21B	Kayak Trough	32.4	29.4		20.6		1.6	14.4	0.70		0.44	74	12	45.0
	485	TC22B	Kayak Trough	32.4	29.4		20.6		1.6	16.5	0.80		0.51	13	12	44.8
	515	TC23B	Kayak Trough	32.4	29.4		24.0		8.4	19.7	0.82		0.61	200	12	39.8
	515	TC24B	Kayak Trough	32.4	29.4		24.0		8.1	20.4	0.85		0.63	15	12	41.9
28G	20	TC25B	Icy Bay-Malaspina	32.4	29.4		27.9		0.5	10.3	0.37		0.32	391	12	35.4
	40	TC26B	Icy Bay-Malaspina	32.4	29.4		20.6		1.4	12.2	0.59		0.38	35	12	40.7
33G	550	TC27B	Icy Bay-Malaspina	32.4	29.4		26.5		9.0	16.7	0.63		0.51	5000	5.1	33.9
	550	TC28B	Icy Bay-Malaspina	32.4	29.4		26.5		8.2	20.7	0.78		0.64	175	12	35.6
	560	TC29B	Icy Bay-Malaspina	33.3	29.4		56.4		18.6	28.2	0.50		0.85	5000	4.3	26.6
	560	TC30B	Icy Bay-Malaspina	23.3	29.4		56.4		18.6	33.8	0.60		1.02	537	11	26.1
	585	TC31B	Icy Bay-Malaspina	217.6	196.1	1	98.0		16.7	61.7	0.63		0.28	21	12	33.6
	600	TC32B	Icy Bay-Malaspina	215.7	196.1	1	103.9		12.5	63.4	0.61		0.29	2	-12	34.3
	610	TC33B	Icy Bay-Malaspina	217.6	196.1	1	87.7		29.8	78.1	0.89		0.36	55	12	39.6
	620	TC34B	Icy Bay-Malaspina	217.6	196.1	1	100.5		19.1	68.3	0.68		0.31	29	12	34.8
	630	TC35B	Icy Bay-Malaspina	216.7	196.1	1	104.4		18.8	60.6	0.58		0.28	500	12	32.6
DC2-80-BG																
MC3-22	35-47	TC1L2	Alsek River	27.6		6	84.6		-23.7		0.28			35	-15	28.1
28G	15-22	TC24	Alsek River	302.6		1	268.9	226.9	115.6		0.43	0.51	0.38	4	-20	31.8
	15-22	TC25	Alsek River	297.9		1	268.9	226.9	21		0.08	0.09	0.07	1100	-20	31.8
35G	32-39	TC18	Alsek River	160.3		1	80.8	83.4	54.9		0.68	0.66	0.34	7	20	41.2
	32-39	TC19	Alsek River	154.6		1	80.8	75.8	51.6		0.64	0.68	0.33	20	20	44.8
38G	1-15	TC2L2	Alsek River	27.6		6	86.4		-38.0		0.44			3	-15	40.7
	27-38	TC3L2	Alsek River	120.6		1	88.9	63.9	-24.9		0.28	0.39	0.21	8	-15	40.9

Table 4. Cyclic Triaxial Test Results (continued)

ruise ore #	Depth in Core, z, cm	Test Number	Study Area	σ_{vc} ^a , kPa	σ_{hc} ^b , kPa	Induced ^c OCR	(q _f Static) ^d I	(q _f Static) ^e II	Static ^f Bias, kPa	Peak ^g Cyclic Stress, τ_c , kPa	$\frac{\tau_c}{q_{fstatic}}$ ^h (I)	$\frac{\tau_c}{q_{fstatic}}$ ⁱ (II)	$\frac{\tau_c}{\sigma_{vc}}$ ^j (III)	# of ^k Cycles to failure	Strain at ^l failure, %	Wat ^l Con %
C2-80-BG																
38G	40-52	TC4L2	Alsek River	120.6		1	87.4	74.8	-33.2	0.38	0.44	0.28	10	-15	36.	
43G	27-35	TC20	Alsek River	28.3			73.9		43.2	0.59			8	20	33.	
	27-35	TC21	Alsek River	27.2			73.9		43.2	0.62			8	20	32.	
46G	7-15	TC22	Alsek River	196.2		1	222.4	141.3	-42.4	0.19	0.30	0.22	94	20	33.	
	7-15	TC23	Alsek River	192.6		1	222.4	138.7	79	0.36	0.57	0.41	15	20	33.	
49G	6-17	TC5L2	Alsek River	120.6		1	87.1	71.2	-65.3	0.75	0.92	0.54	0.5	-15	37.	
84G	33-48	TC6L2	Yakutat	103.3		1	64.6	108.5	-23.9	0.37	0.22	0.23	80	-15	25.	
	48-63	TC7L2	Yakutat	103.3		1	64.1	72.3	-31.4	0.49	0.43	0.30	6	-15	33.	
87G	161-172	TC52	Yakutat	200.9		1	122.8	148.7	-106.3	0.87	0.71	0.53	4	-20	32.	
87G	161-169	TC53	Yakutat	194.3		1	122.8	147.7	-45.5	0.37	0.31	0.23	82	-20	31.	
96G	145-155	TC11L2	Icy Bay-Malaspina	34.5		4	70		-39.2	0.56			2	-15	35.	
	226-237	TC8L2	Icy Bay-Malaspina	137.8		1	71	107.5	-34.1	0.48	0.32	0.25	33	-15	31.	
	286-300	TC10L2	Icy Bay-Malaspina	35.1		4	70		-16.1	0.23			60	-15	35.	
	331-343	TC9L2	Icy Bay-Malaspina	137.8		1	78.7	96.5	-59.8	0.76	0.62	0.43	8	-15	33.	
181G	61-68	TC30	Icy Bay-Malaspina	30.3		1	23.7	14.5	-25	1.06	1.72	0.83	59	20	46.	
	61-68	TC31	Icy Bay-Malaspina	24.2		1	23.7	11.4	-24	1.00	2.11	0.99	12	20	46.	
	85-95	TC32	Icy Bay-Malaspina	10.4		3.5	19.0		-15	0.79			20	20	44.	
	85-95	TC33	Icy Bay-Malaspina	2.5		14.4	19.0		-15.9	0.84			10	20	47.	
190G	66-80	TC12L2	Icy Bay-Malaspina	151.6		1	88.4	86.4	-61.9	0.70	0.72	0.41	1	-15	38.	
	80-97	TC13L2	Icy Bay-Malaspina	151.6		1	87.8	87.9	-40.4	0.46	0.46	0.27	4	-15	37.	
	160-175	TC14L2 ⁿ	Icy Bay-Malaspina	232	96.5	1	89.4		67.8	89.6	1.00		300	1.3	42.	
196G	197-213	TC15L2 ⁿ	Icy Bay-Malaspina	166.5	83.3	1	99.3		41.6	96.8	0.97		300	0.9	26.	
	312-326	TC16L2	Icy Bay-Malaspina	53.4		6	182.1		-51.0	0.28			16	-15	23.	
	326-340	TC17L2	Icy Bay-Malaspina	53.4		6	187.7		-41.3	0.22			24	-15	25.	
	400-414	TC18L2	Icy Bay-Malaspina	320.2		1	257.0	256	-187.6	0.73	0.73	0.59	0.5	-15	24.	
	414-428	TC19L2	Icy Bay-Malaspina	320.2		1	255.5	256	-92	0.36	0.36	0.29	10	-15	24.	
C1-81-BG																
604G3	130-137	TC99	Alsek River	297.1		1	176.6	175.3	61.5	0.35	0.35	0.21	35	-20	37.	
	130-137	D102	Alsek River	290.4		1	176.6	174.2	86.5	0.49	0.50	0.30	28	20	36.	
605G2	55-62	TC92	Alsek River	215.9		1	163.8	127.4	-55.7	0.34	0.44	0.26	26	-20	37.	
	55-62	TC93	Alsek River	204.8		1	163.8	120.8	-84.1	0.51	0.70	0.41	5	-20	37.	
	166-173	TC87	Alsek River	215.1		1	127.9	133.4	-41.8	0.33	0.31	0.15	78	-20	35.	
	166-173	TC86	Alsek River	216.3		1	127.9	125.5	-66.5	0.52	0.53	0.31	5	-20	35.	
618G2	138-145	TC58	Yakutat	184.8		1	95.6	92.4	56.2	0.59	0.61	0.30	17	-20	43.	
	138-145	TC59	Yakutat	183.9		1	95.6	86.4	44.6	0.47	0.52	0.24	42	-20	46.	
620G2	100-148	TC46	Yakutat	121.8		1	53.2	67.0	31.0	0.58	0.46	0.25	58	20	39.	
	100-108	TC47	Yakutat	117.6		1	53.2	65.9	46.1	0.87	0.70	0.39	14	20	38.	
624A1	172-179	TC60	Yakutat	338.9		1	401.3	186.4	206.6	0.51	1.11	0.61	1	-20	39.	
	172-179	TC61	Yakutat	344.7		1	401.3	186.1	-134.6	0.54	0.72	0.39	7	-20	39.	
627G2	60-71	TC36	Icy Bay-Malaspina	18.3		5.4	44.7		21.5	0.48			42	20	46.	
	60-67	TC37	Icy Bay-Malaspina	17.3		5.7	44.7		34.7	0.78			8	20	46.	
	93-104	TC34	Icy Bay-Malaspina	100.7		1	53.2	47.3	-39.4	0.74	0.83	0.39	5	20	47.	
	93-100	TC35	Icy Bay-Malaspina	99.5		1	53.2	48.8	-26.4	0.50	0.54	0.26	280	-20	44.	

Table 4. Cyclic Triaxial Test Results (continued)

Cruise Core #	Depth in Core, z, cm	Test Number	Study Area	σ_{vc}' , kPa ^a	σ_{hc}' , kPa ^b	Induced ^c OCR	(q_f Static) ^d I	(q_f Static) ^e II	Static ^f Bias, kPa	Peak ^g Cyclic Stress, τ_c , kPa	$\frac{\tau_c^h}{q_f \text{ static}}$ (I)	$\frac{\tau_c^i}{q_f \text{ static}}$ (II)	$\frac{\tau_c^j}{\sigma_{vc}'}$ (III)	# of ^k Cycles to failure	Strain at ^l failure, %	Initial Water Content %
DC1-81-EG																
630A2	153-161	TC57	Icy Bay-Malaspina	297.9		1	562	259.2		162.9	0.29	0.63	0.55	>27	-20	29.3
	153-161	TC56	Icy Bay-Malaspina	301.0		1	562	295.0		120.2	0.21	0.41	0.40	>37	-20	27.4
634G2	61-69	TC48	Icy Bay-Malaspina	60.3		1	23.9	25.3		-40.6	1.70	1.60	0.67	2	-20	56.4
	61-68	TC49	Icy Bay-Malaspina	58.1		1	23.9	24.4		-31.8	1.33	1.30	0.55	6	-20	59.0
	72-79	TC54	Icy Bay-Malaspina	61.9		1	23.9	27.9		17.6	0.74	0.63	0.28	158	20	48.9
	73-80	TC55	Icy Bay-Malaspina	59.3		1	23.9	26.7		22.2	0.93	0.83	0.37	37	20	50.3

a - Final vertical consolidation stress

b - Final horizontal consolidation stress, blank if same as vertical stress

c - Induced OCR defined in Table 3.

d - Static shear strength obtained from test on sample from the same core (Method I)

e - Static shear strength obtained from water content, consolidation stress and Figure 35 (Method II)

f - A static shear stress applied under undrained conditions prior to cyclic testing. The cyclic shear stress is symmetrical about this bias level.

g - The maximum shear stress level applied during cyclic loading (may include some static bias in addition to cyclic component - negative sign indicates tension)

h - Ratio of maximum cyclic shear stress to static shearing strength estimated using Method I.

i - Ratio of maximum cyclic shear stress to static shearing strength estimated using Method II

j - Ratio of maximum cyclic shear stress to vertical consolidation stress (termed method III)

k - Number of cycles required to reach strain given in next column

l - Strain level defined as failure or strain level at which test was halted (if less than 10%)

m - Reconsolidated sample

n - Cyclic loading in compression only

Table 5. Calculation of NSP exponent, Λ_o

Cruise Core #	Depth in Core, z, cm	Test Number	Study Area	Induced ^a OCR	(S_{nc}) ^b _I	(S_{nc}) ^c _{II}	q_f/σ_{vc} ^d	(Λ_o) ^e _I	(Λ_o) ^f _{II}	Initial Water content, %
DC2-80-EG										
MC3-22	62-76	TE4L2	Alsek River	3	----	0.86	4.51	----	1.51	29.4
28	25-34	TE63	Alsek River	5.7	0.87	0.62	3.99	0.88	1.07	36.2
35	14-23	TE57	Alsek River	6.2	0.52	0.53	2.36	0.83	0.82	40.4
38	18-28	TE3L2	Alsek River	6	----	0.76	3.12	----	0.79	31.6
43	8-17	TE27	Alsek River	5	----	0.67	5.74	----	1.33	33.9
46	28-37	TE60	Alsek River	6.2	1.10	0.67	4.66	0.82	1.06	33.9
84	63-76	TE8L2	Yakutat	6	0.70	0.63	8.17	1.37	1.43	35.7
96	198-212	TE16L2	Icy Bay-Malaspina	3	0.51	0.72	2.02	1.25	0.74	32.8
	343-356	TE15L2	Icy Bay-Malaspina	4	0.51	0.70	2.02	0.99	0.76	33.3
181	5-15	TE16	Icy Bay-Malaspina	6.1	0.47	0.55	2.35	0.89	0.80	39.2
	71-81	TE19	Icy Bay-Malaspina	7.3	0.47	0.52	3.57	1.02	0.97	41.9
	100-110	TE21	Icy Bay-Malaspina	3	0.47	0.48	1.33	0.95	0.93	46.2
190	80-94	TE20L2	Icy Bay-Malaspina	6	0.58	0.75	2.03	0.70	0.91	31.9
	114-125	TE19L2	Icy Bay-Malaspina	3	0.58	0.50	0.84	0.34	0.47	42.6
196	274-286	TE25L2	Icy Bay-Malaspina	3	0.93	1.06	1.46	0.41	0.29	25.9
	355-365	TE29L2	Icy Bay-Malaspina	6	0.93	1.06	3.34	0.71	0.64	26.0
DC1-81-EG										
605G2	186-194	TE112	Alsek River	3.1	0.59	0.51	1.28	0.68	0.81	42.0
	156-164	TE117	Alsek River	6.2	0.59	0.57	2.48	0.79	0.81	38.4
627G2	71-78	TE72	Icy Bay-Malaspina	5.5	0.53	0.51	2.40	0.89	0.91	42.6
	71-78	TE73	Icy Bay-Malaspina	3.1	0.53	0.47	1.48	0.91	1.01	46.4

a - Induced OCR defined in Table 3

b - Ratio of undrained shear strength, S_u , to vertical consolidation stress, σ_{vc} , for normal consolidation obtained from test on sample from the same core (Method I)

c - Ratio of undrained shear strength, S_u , to vertical consolidation stress, σ_{vc} , for normal consolidation obtained from initial water content and Figure 35 (Method II)

d - Ratio of measured undrained shear strength to vertical consolidation stress

e - The NSP exponent, Λ_o , calculated using S_{nc} from Method I.

f - The NSP exponent, Λ_o , calculated using S_{nc} from Method II

FIGURES

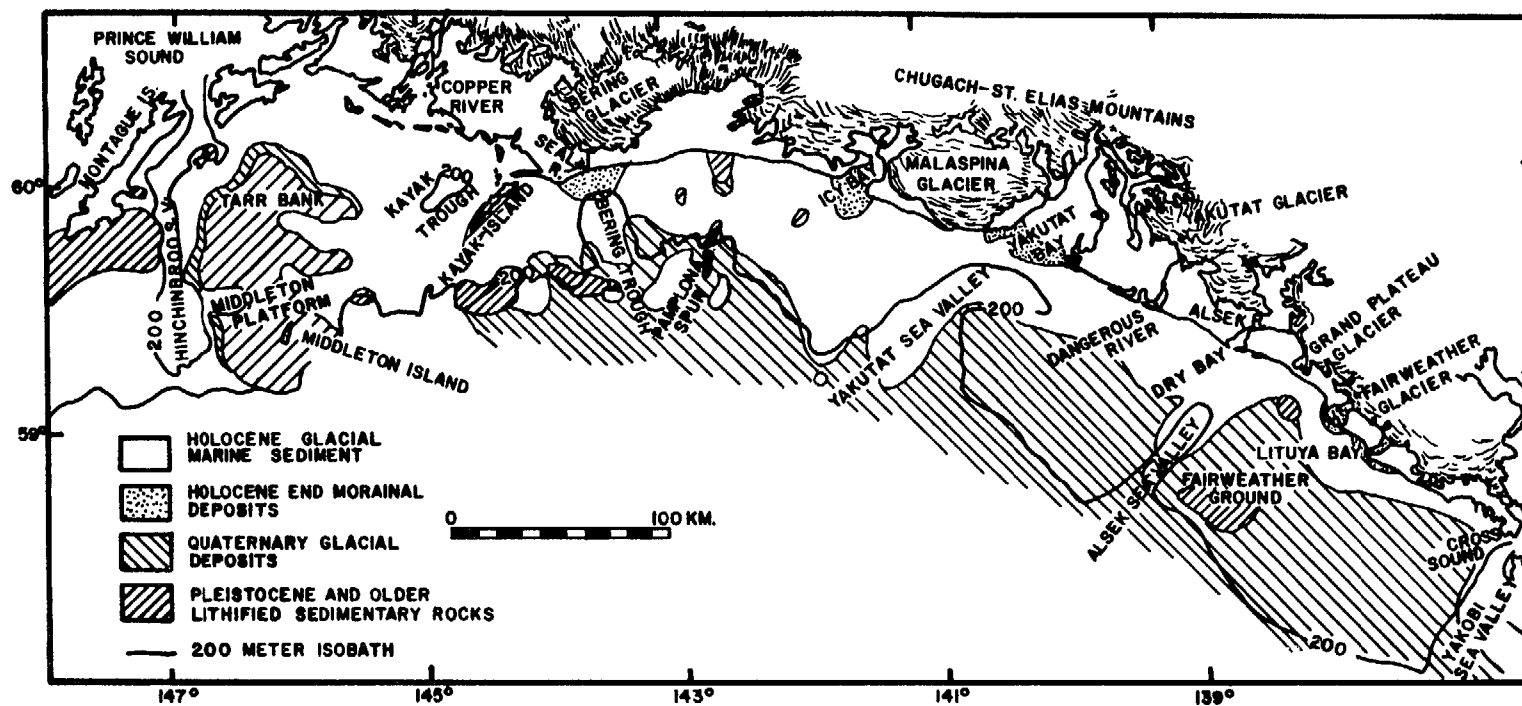


Figure 1. Distribution of four continental shelf surface sedimentary units between Cross Sound and Prince William Sound (Molnia and Carlson, 1980)

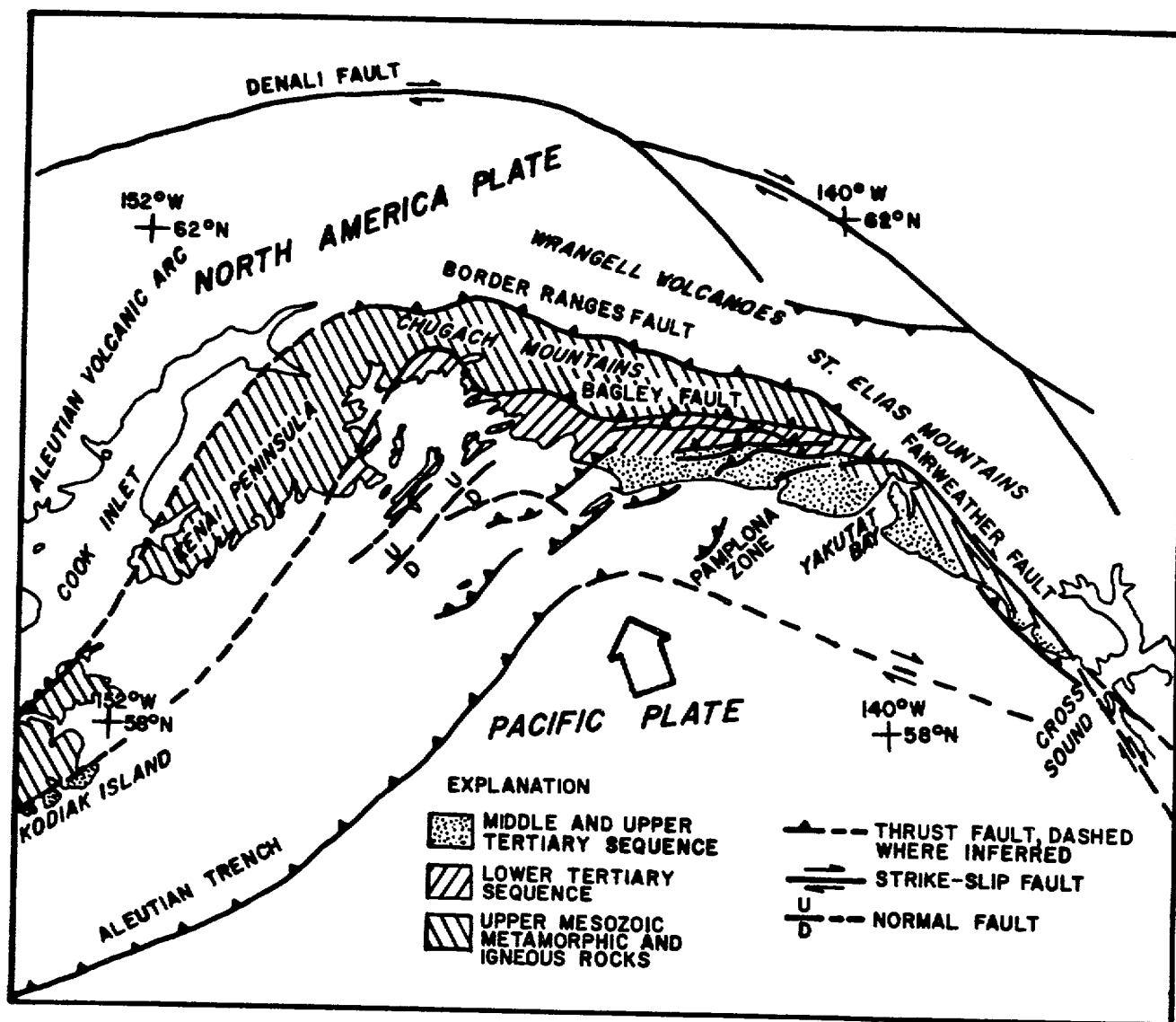


Figure 2. Simplified geologic setting of the northern Gulf of Alaska, showing general trends of Mesozoic and Cenozoic rocks (modified from Bruns, 1979). Onshore geology is from Plafker (1967), and Beikman (1974,1975). Relative convergence vector between Pacific and North American plates (large arrow) is from Minster and Jordon (1978)

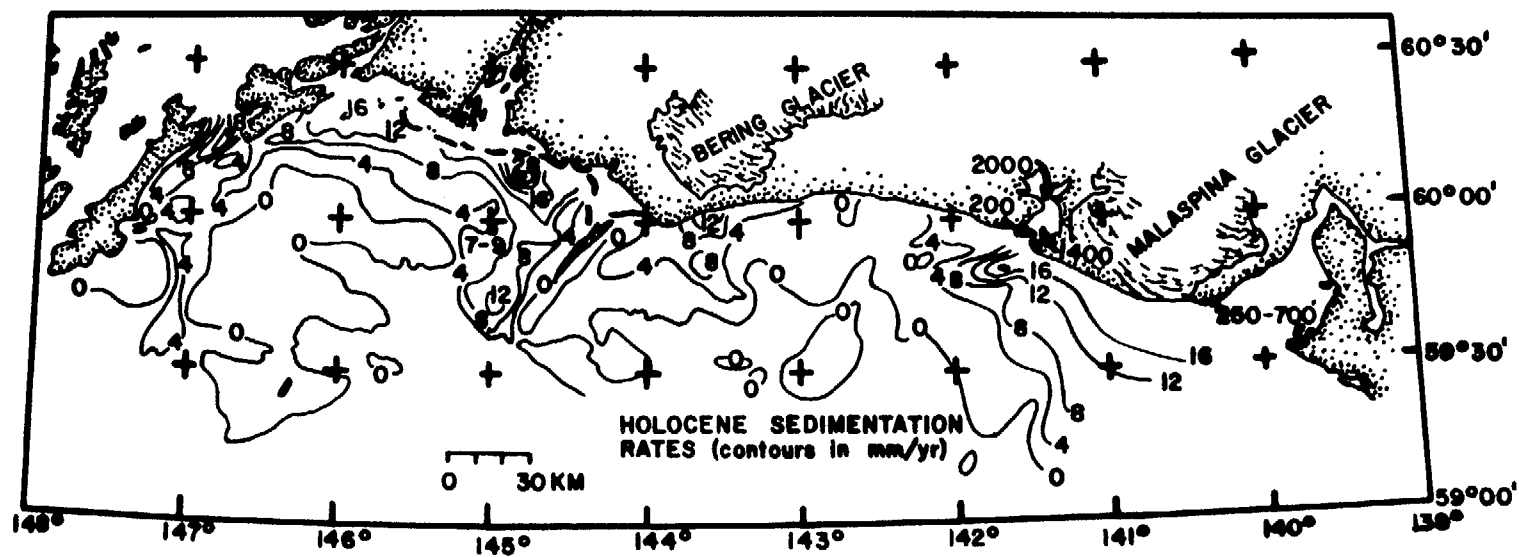


Figure 3. Holocene sedimentation rates (mm/yr) in the northeast Gulf of Alaska (Molnia and Carlson, 1980)

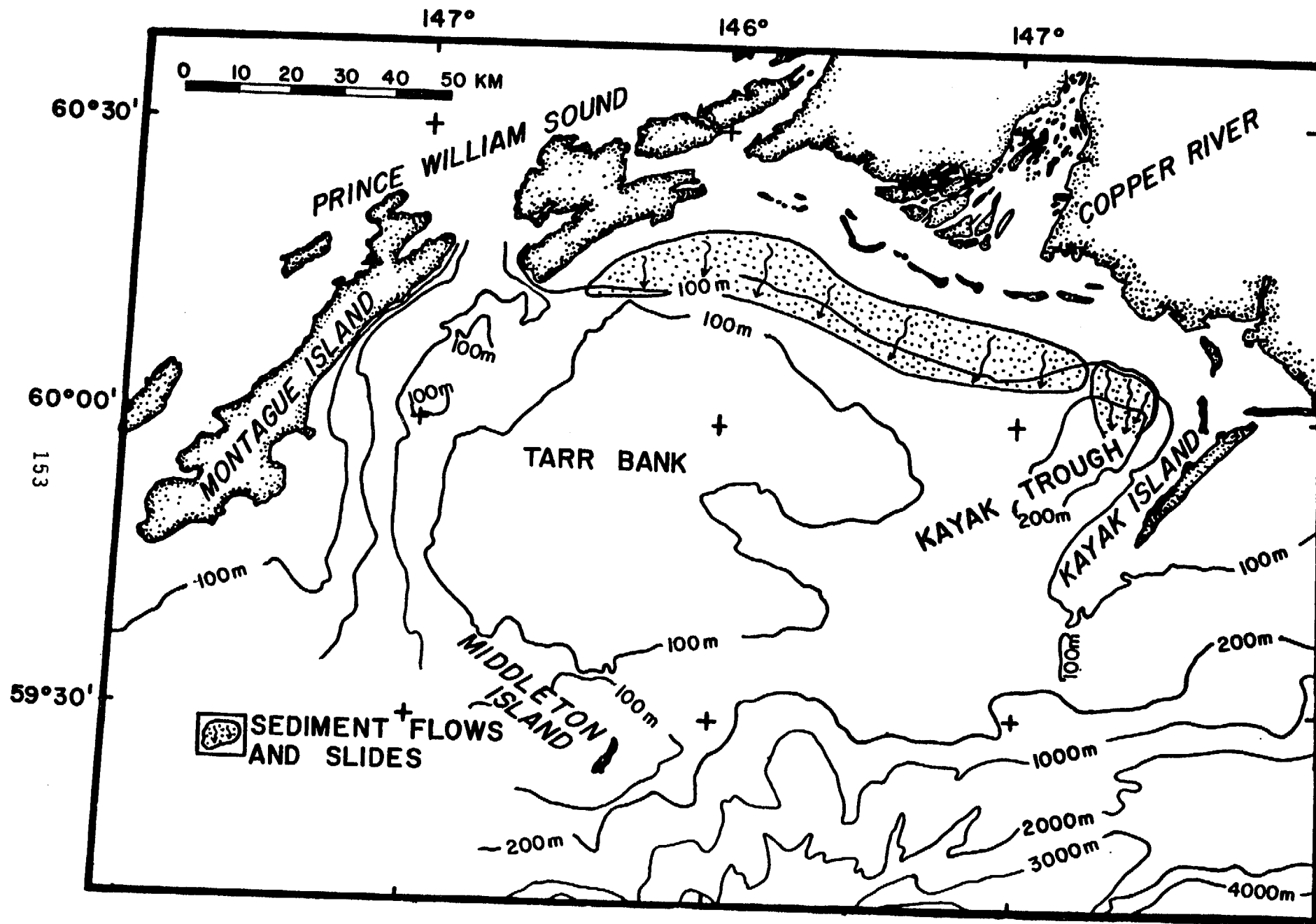


Figure 4. Location map of seafloor flows and slumps west of Kayak Island (Carlson and Schwab, 1982)

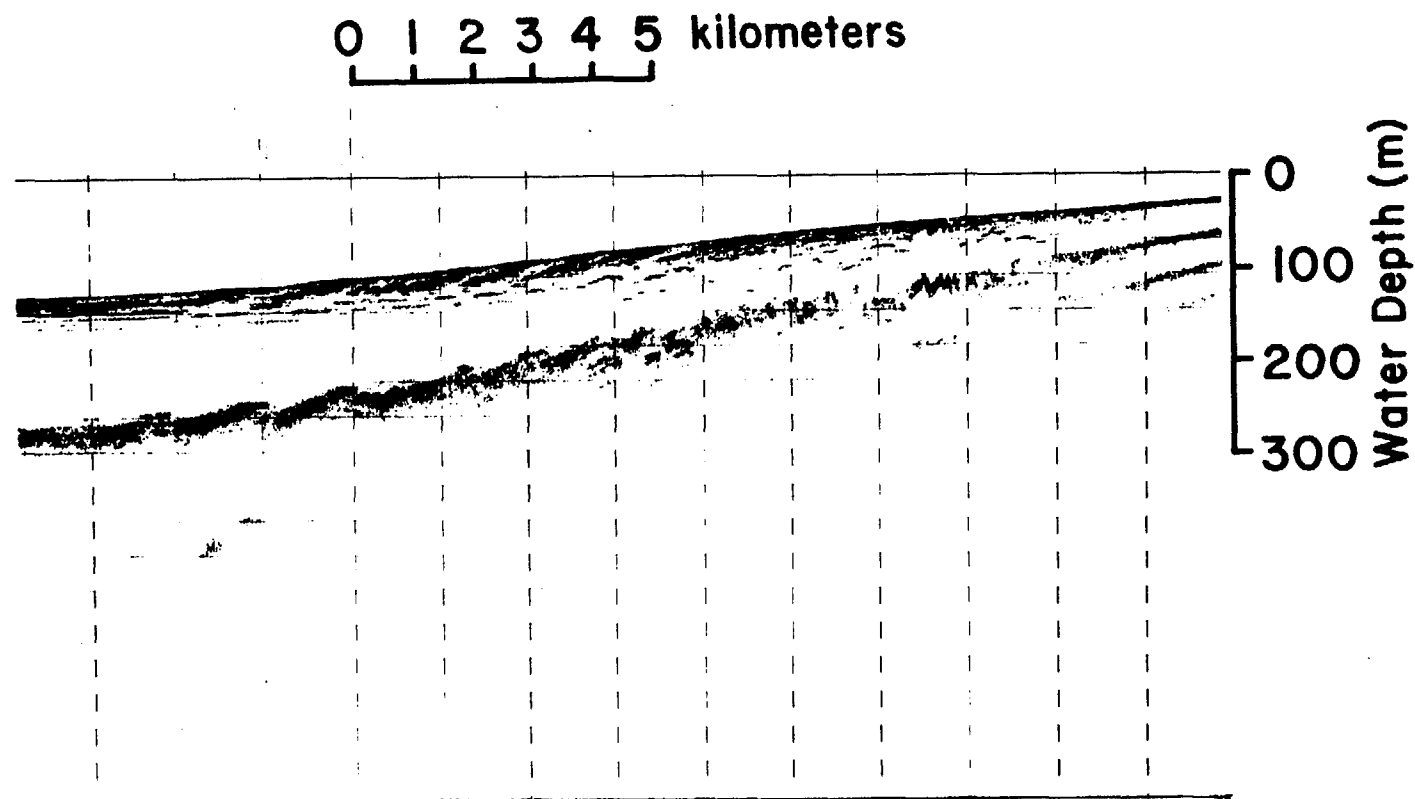


Figure 5. High resolution seismic reflection record of the sediment slide off the Copper River.

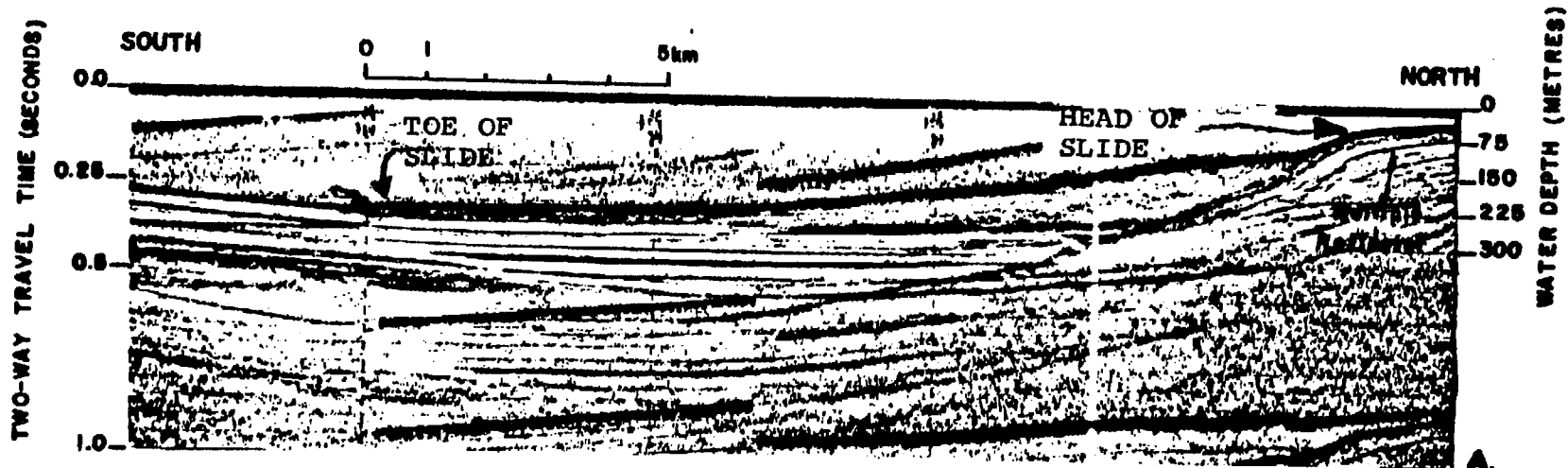


Figure 6. High resolution seismic reflection record of the submarine slide located in Kayak Trough (Hampton and others, 1978).

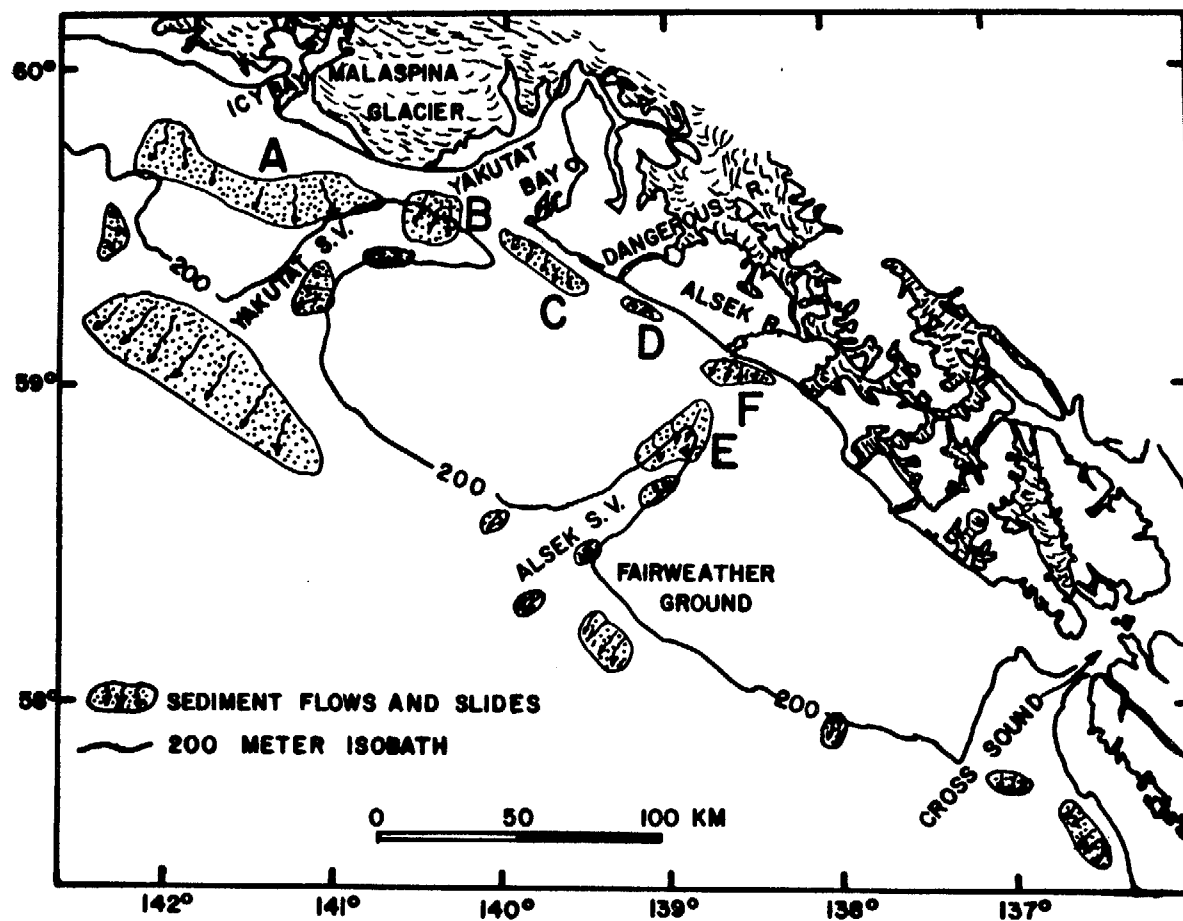


Figure 7. Location map of seafloor geologic hazards east of Icy Bay, Gulf of Alaska (modified from Carlson and others, 1980).

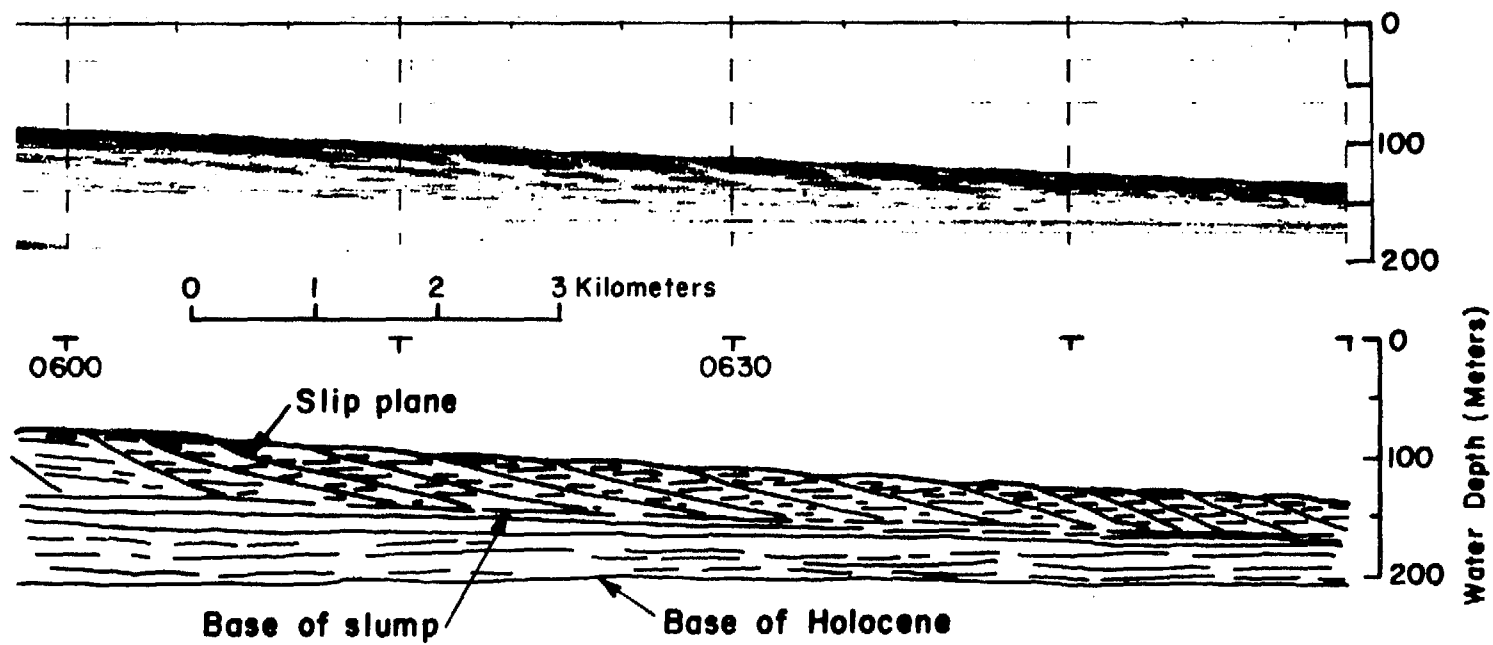


Figure 8. High resolution seismic reflection record of the Icy Bay-Malaspina Slump (Carlson, 1978).

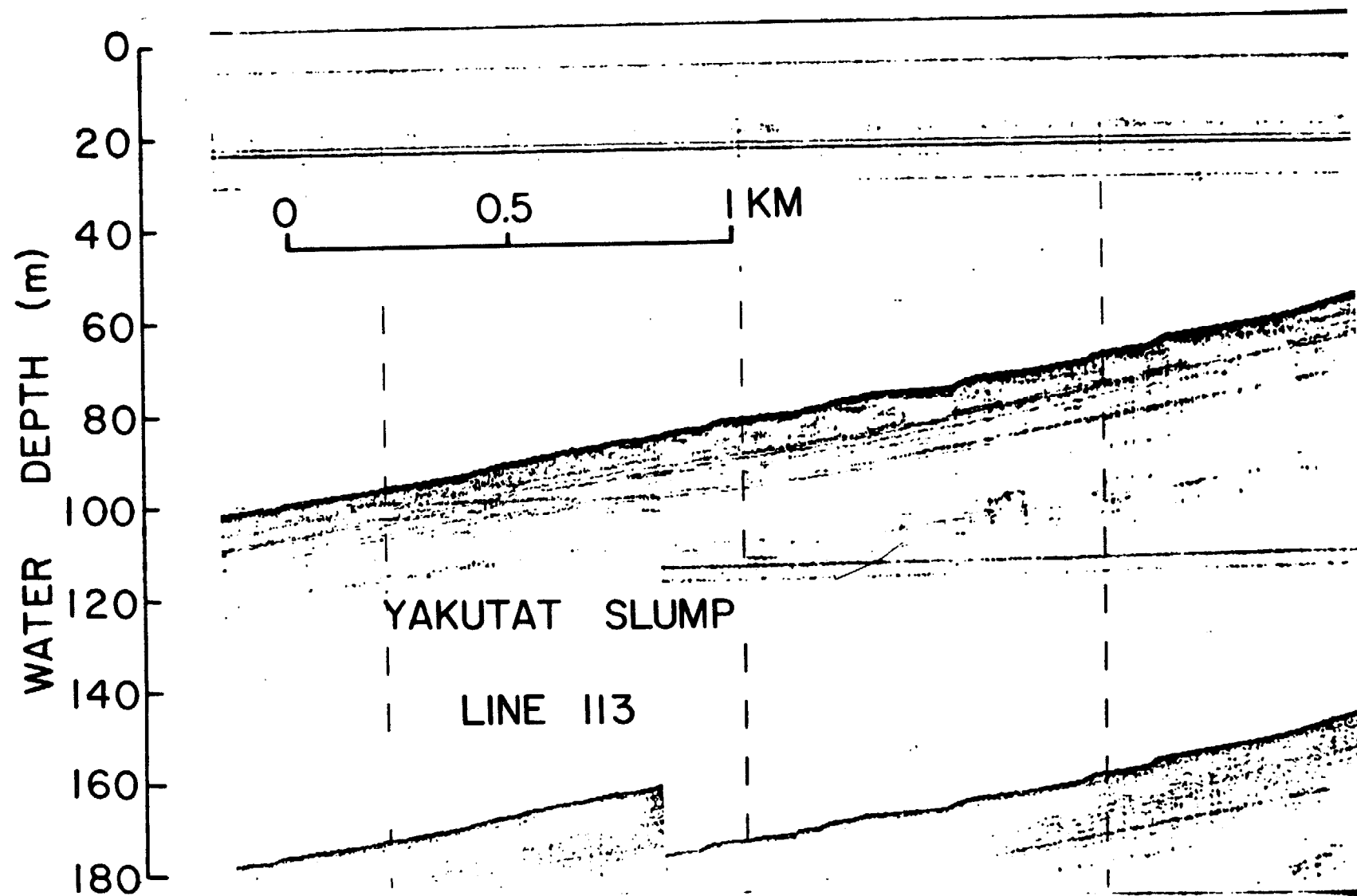


Figure 9. High resolution seismic reflection record of the Yakutat Slump.

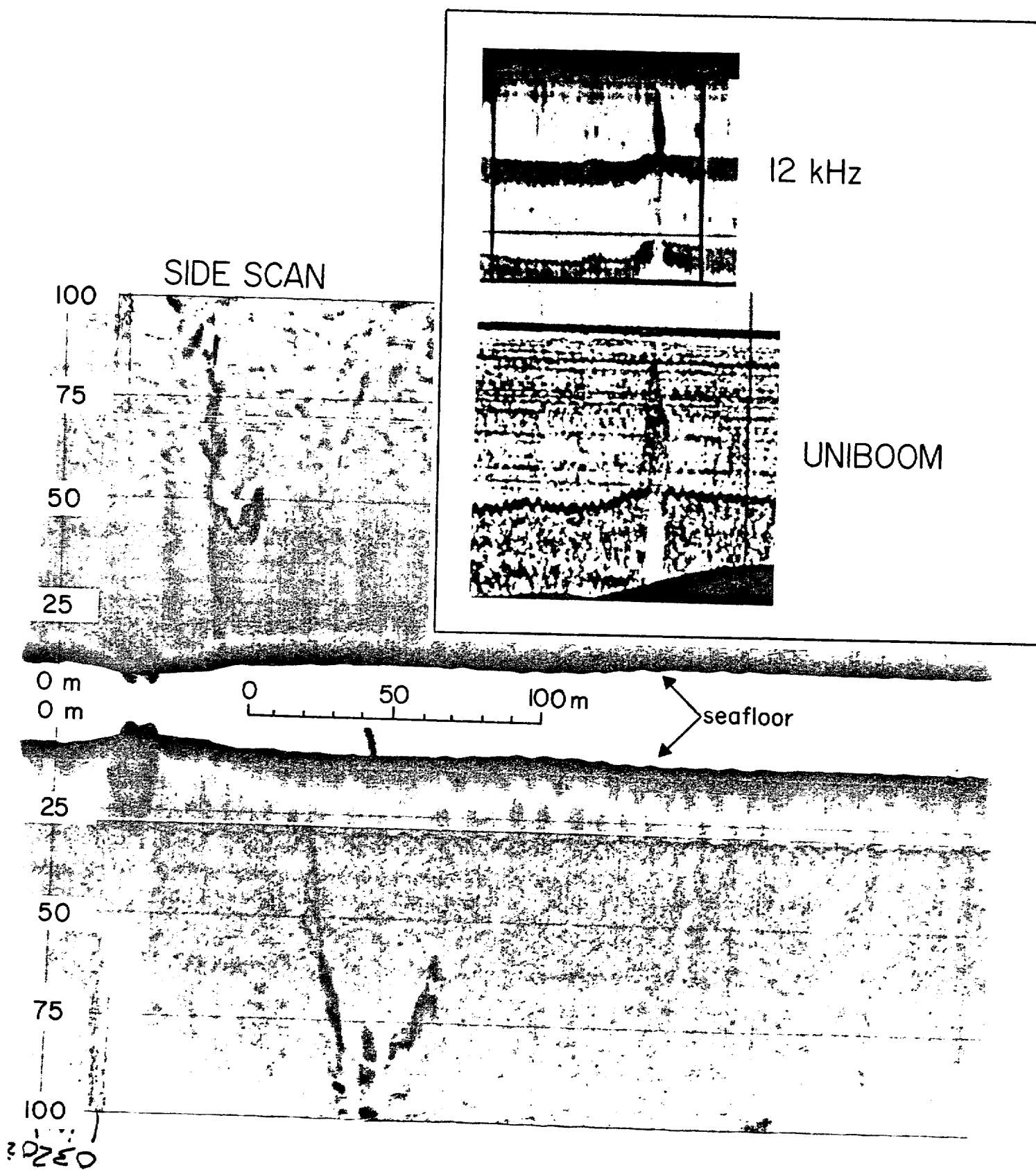


Figure 10. High resolution seismic reflection data and side scan sonographs depicting a water column gas plume southeast of the Dangerous River delta (Carlson and others, 1980).

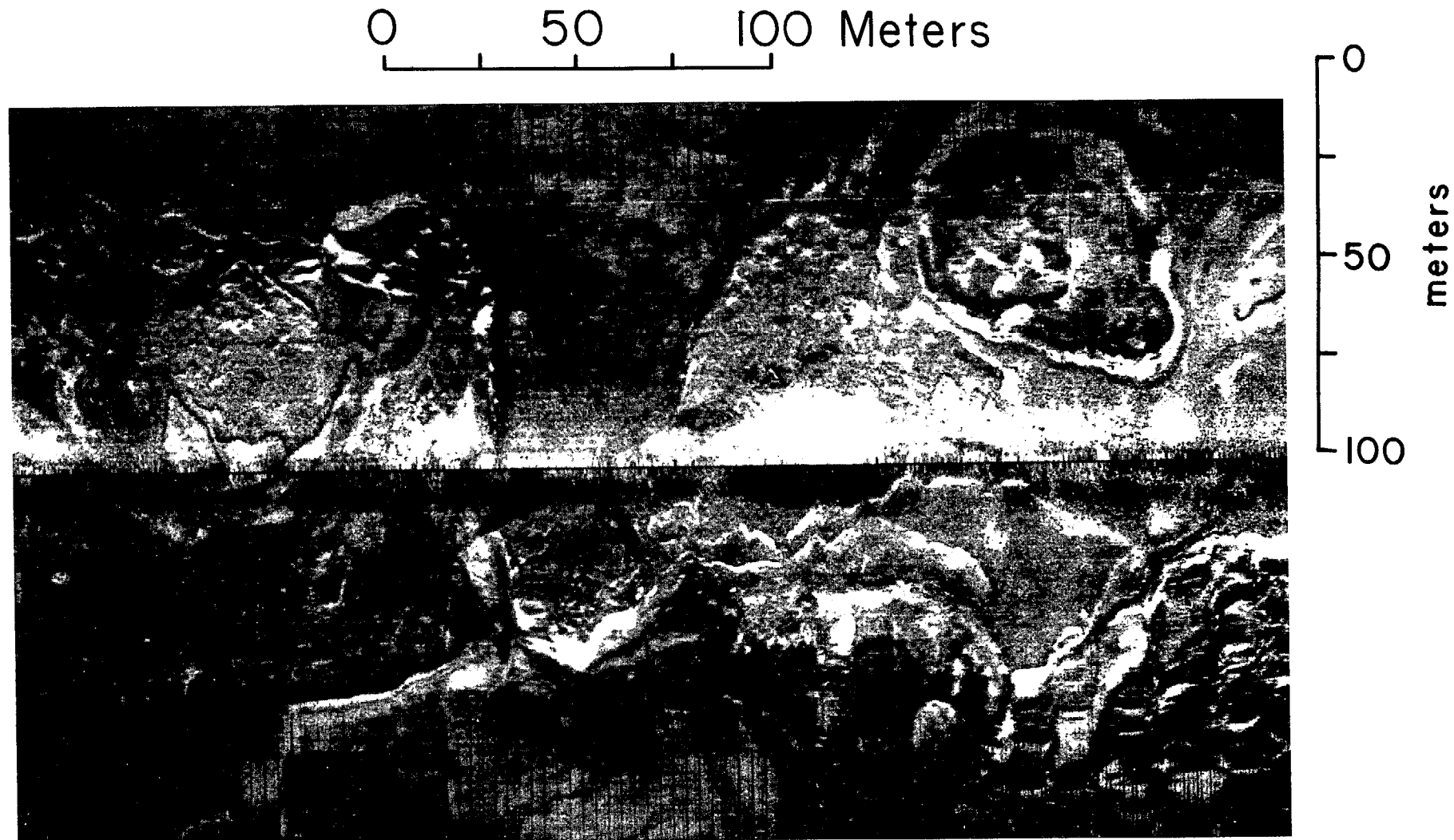


Figure 11. Side scan sonograph example of small slides and linear flows on the Alsek River prodelta (Molnia and Rapoport, 1980). Onshore direction is toward the top of the figure.

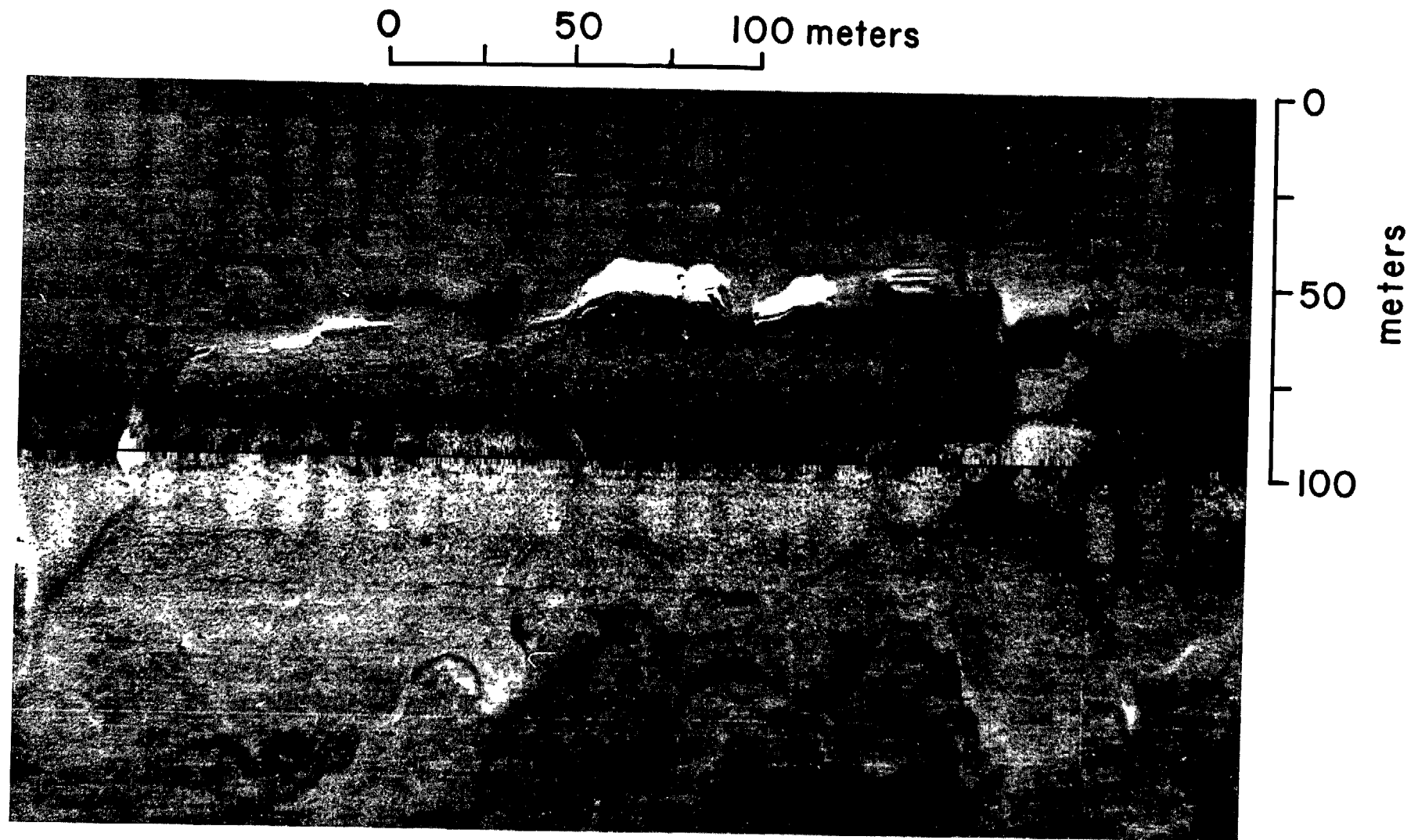


Figure 12. Side scan sonograph depicting a massive, lobate slide toe and a series of smaller slide toes on the Alsek River prodelta (Molnia and Rapoport, 1980). Onshore direction is toward the top of the figure.

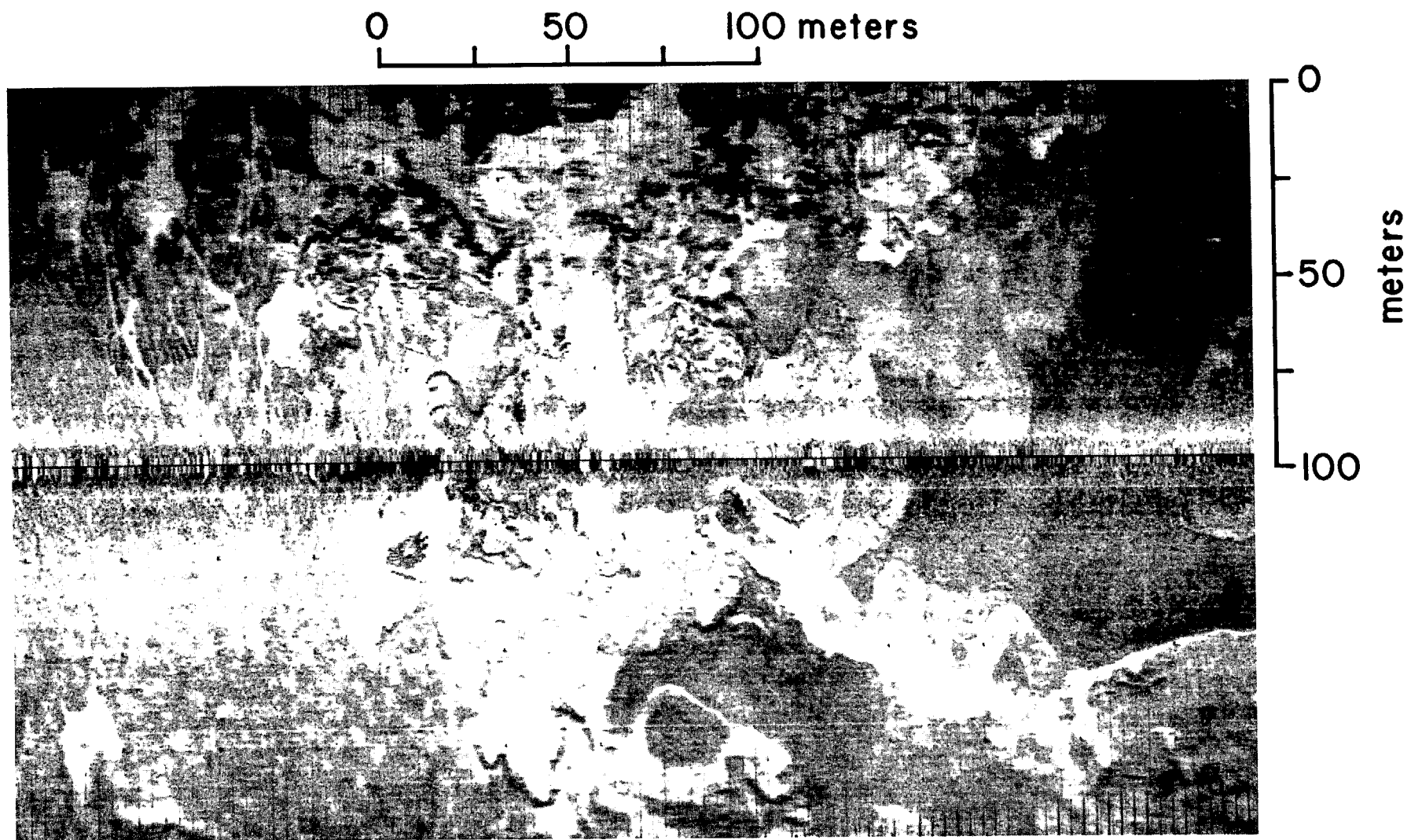


Figure 13. Side scan sonograph depicting multiple flows, slumps and slides on the Alsek River prodelta (Molnia and Rapoport, 1980).

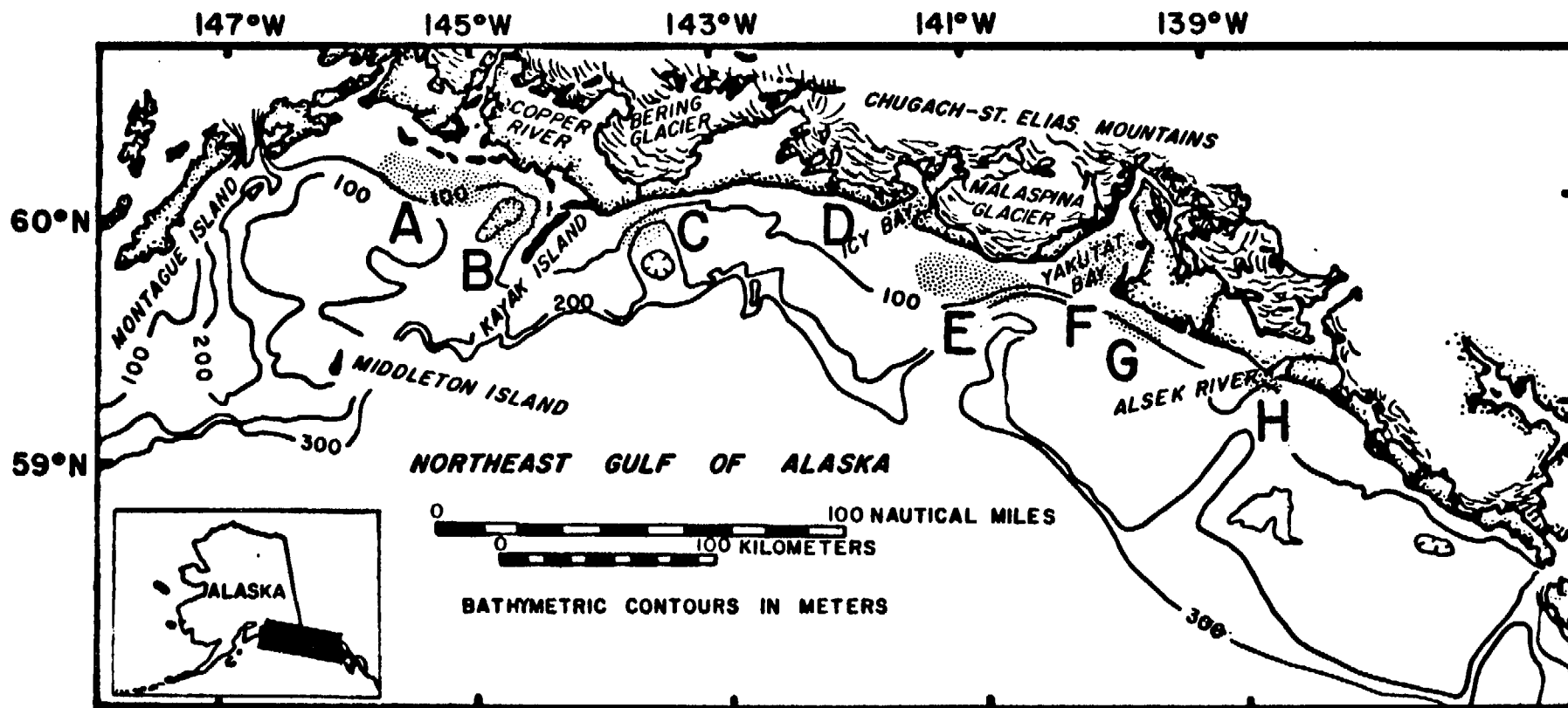


Figure 14. Locations of study areas.

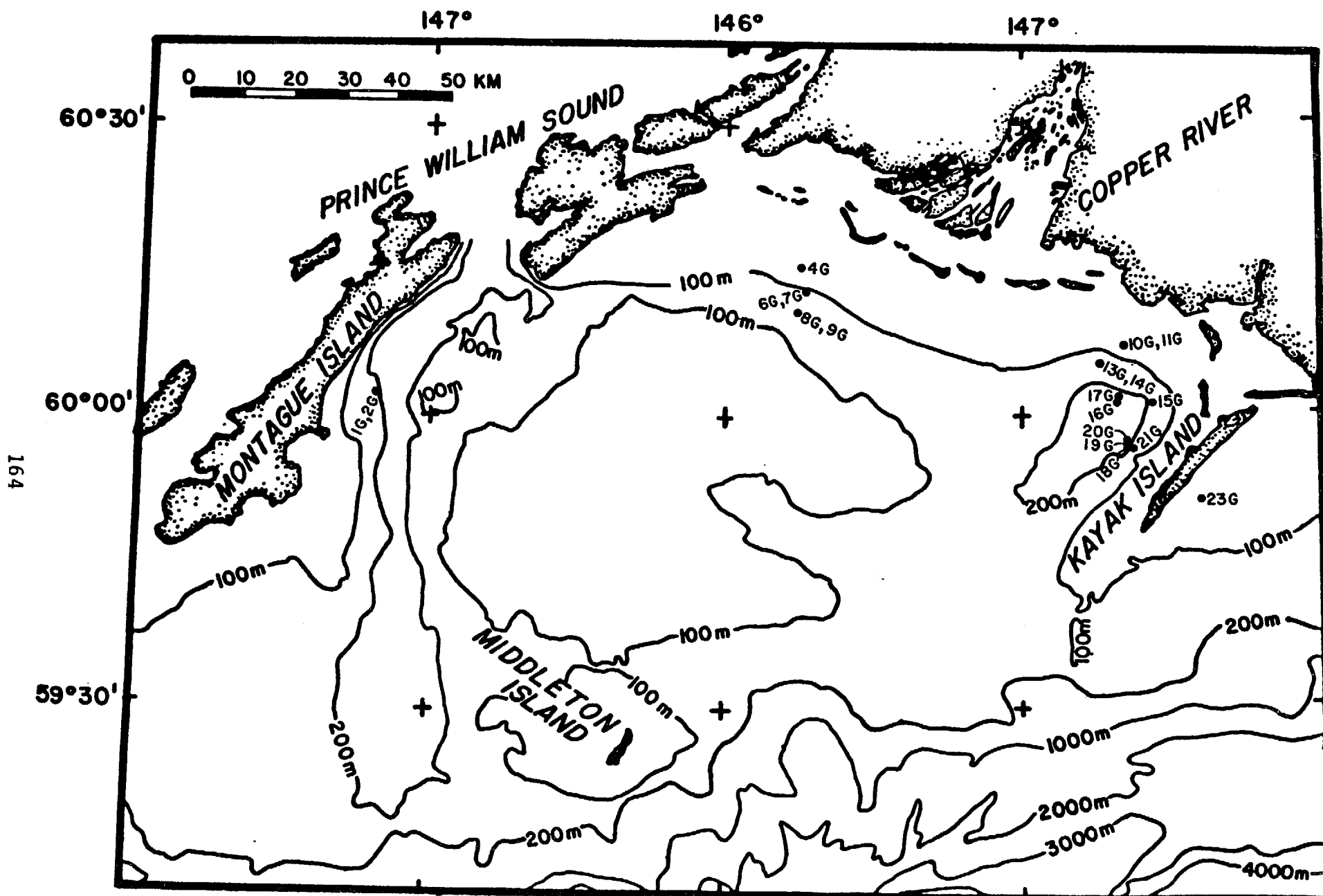


Figure 15. Core locations-Copper River Study Area (group to east) and Kayak Trench Study Area (group to east)

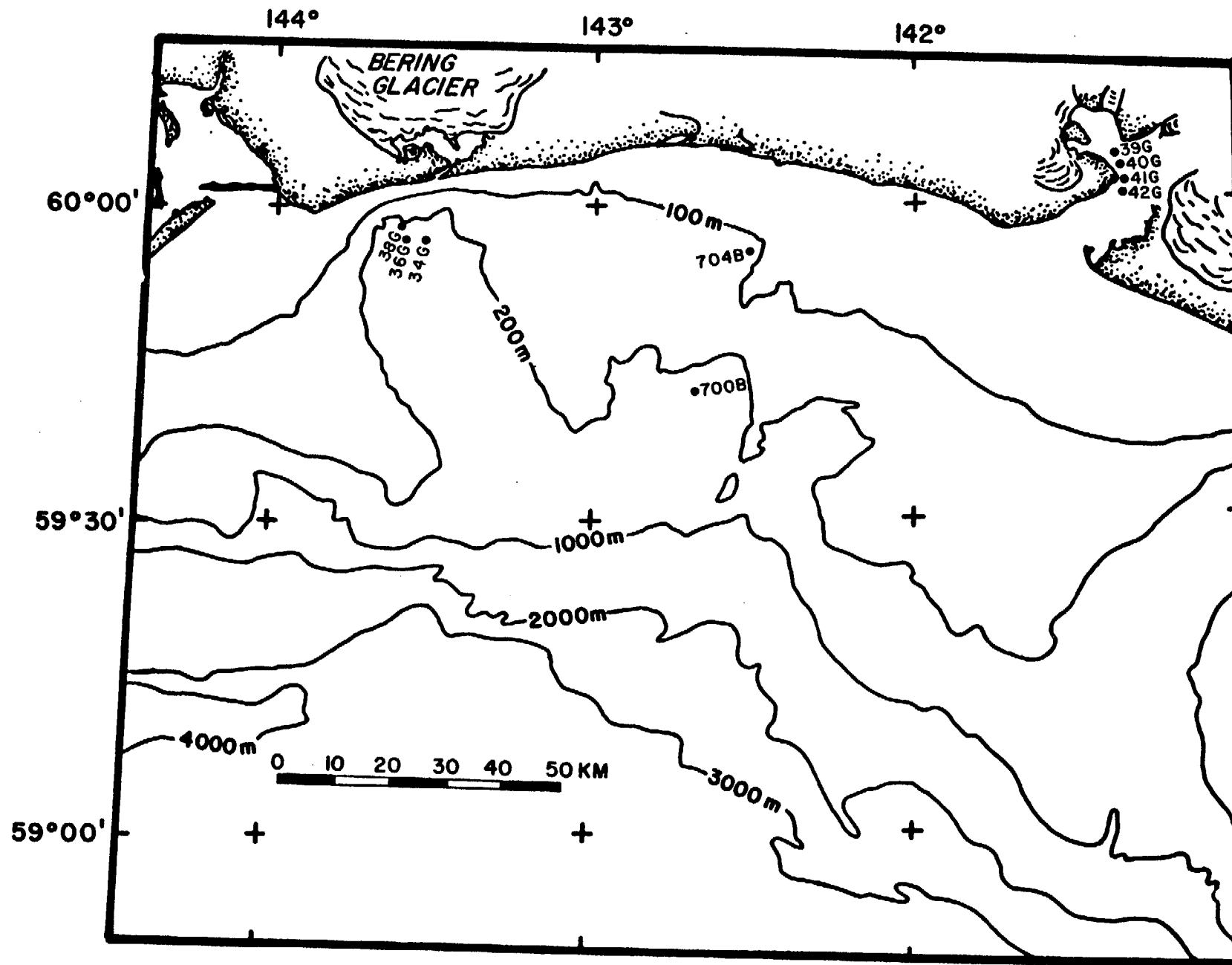


Figure 16. Core locations-Bering Trough and Icy Bay Study Areas.

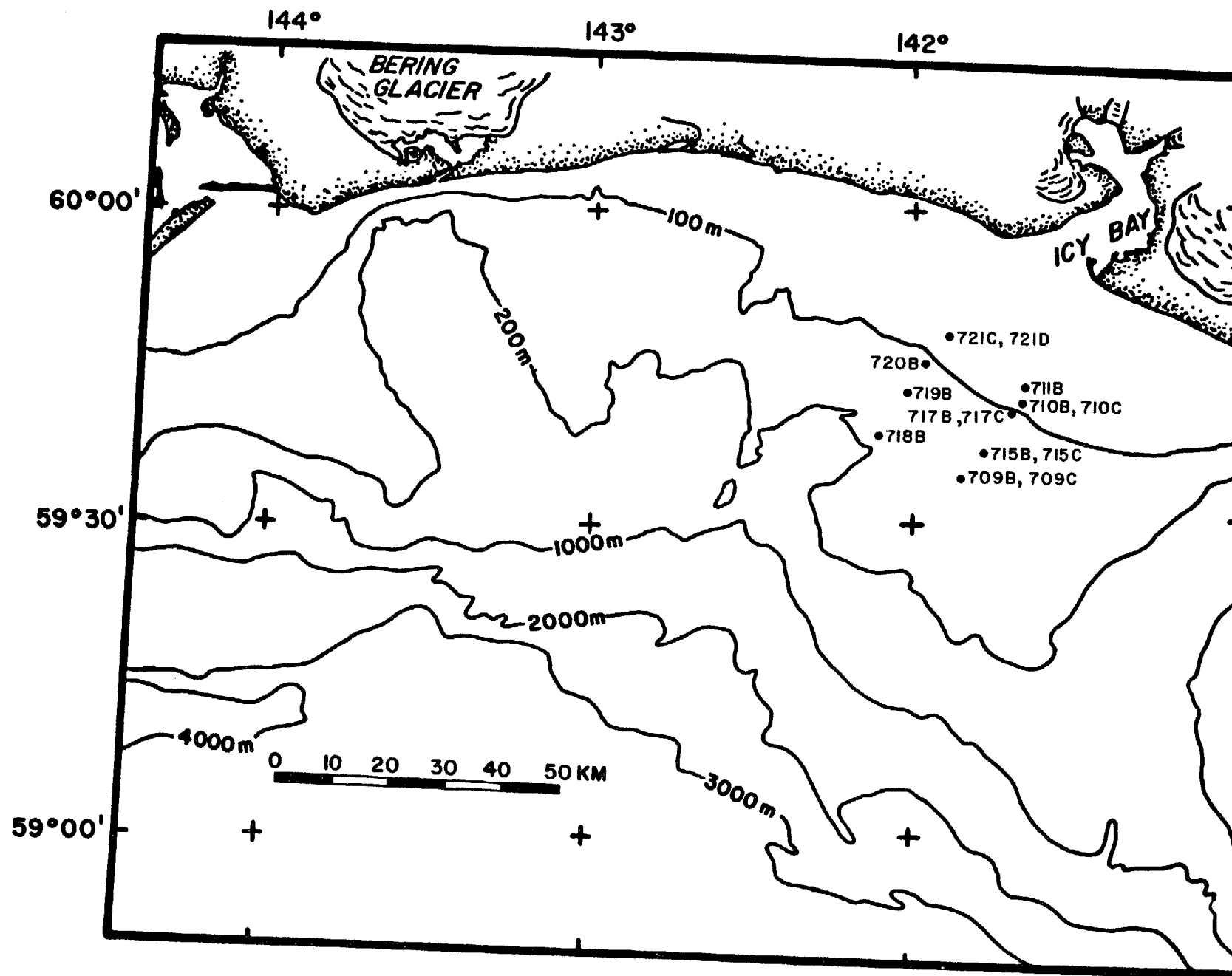


Figure 17. Core locations-Icy Bay-Malaspina Study Area (Cruise DCI-77-EG)

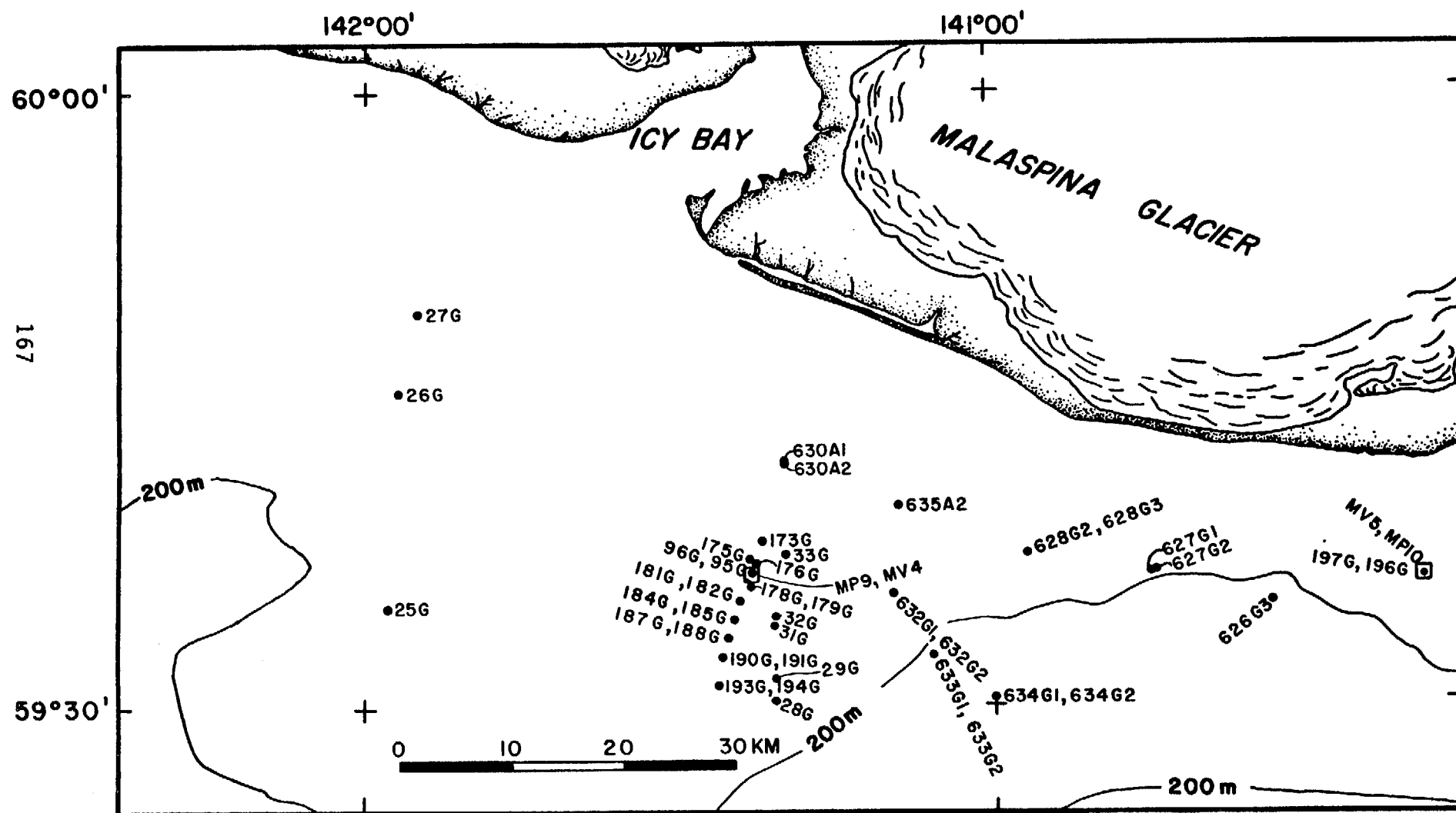


Figure 18. Core and in place test locations-Icy Bay-Malaspina Study Area (Cruises S8-77-EG, DC2-80-EG and DC1-81-EG).

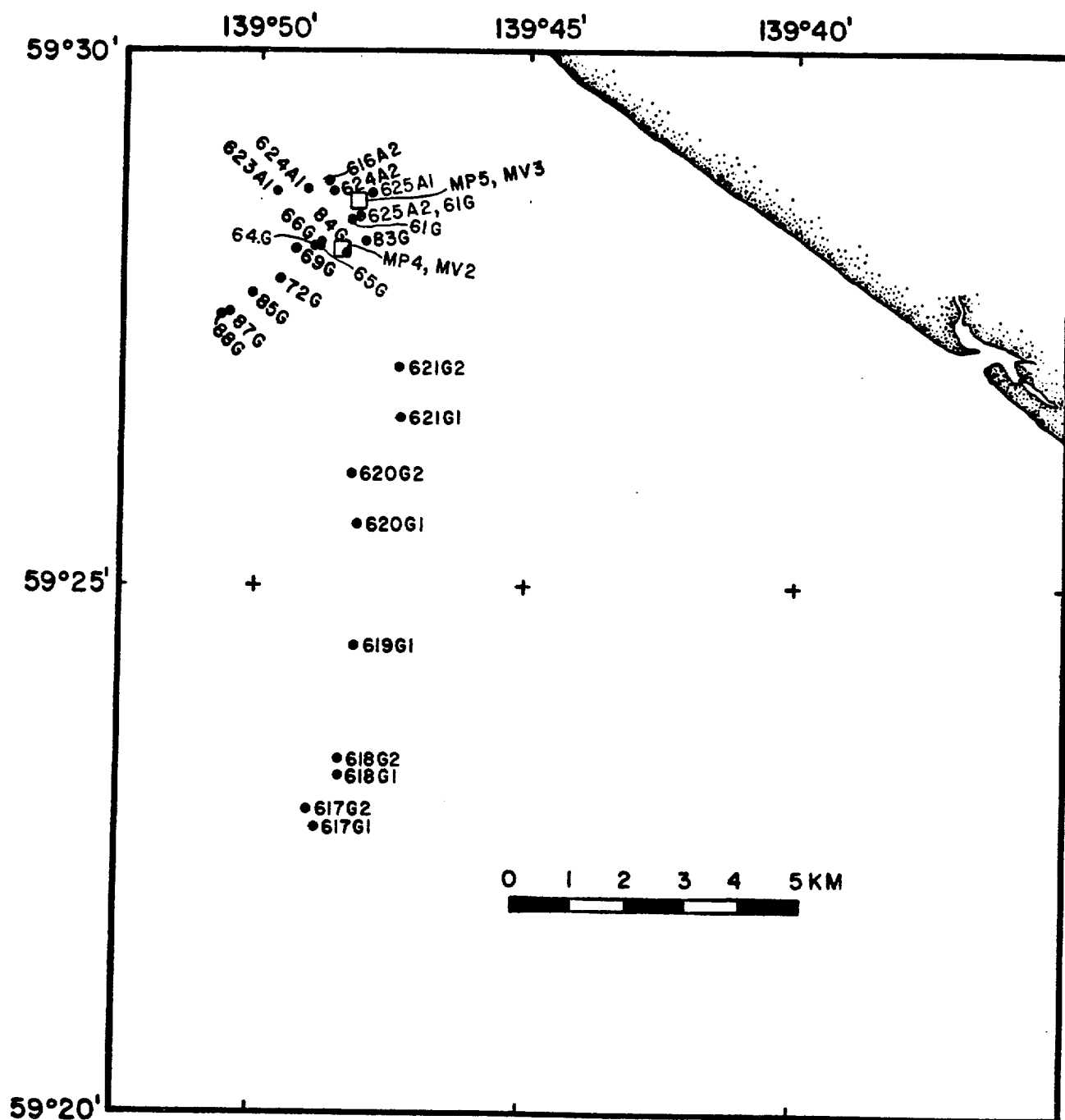


Figure 19. Core and in place rest locations-Yakutat Study Area.

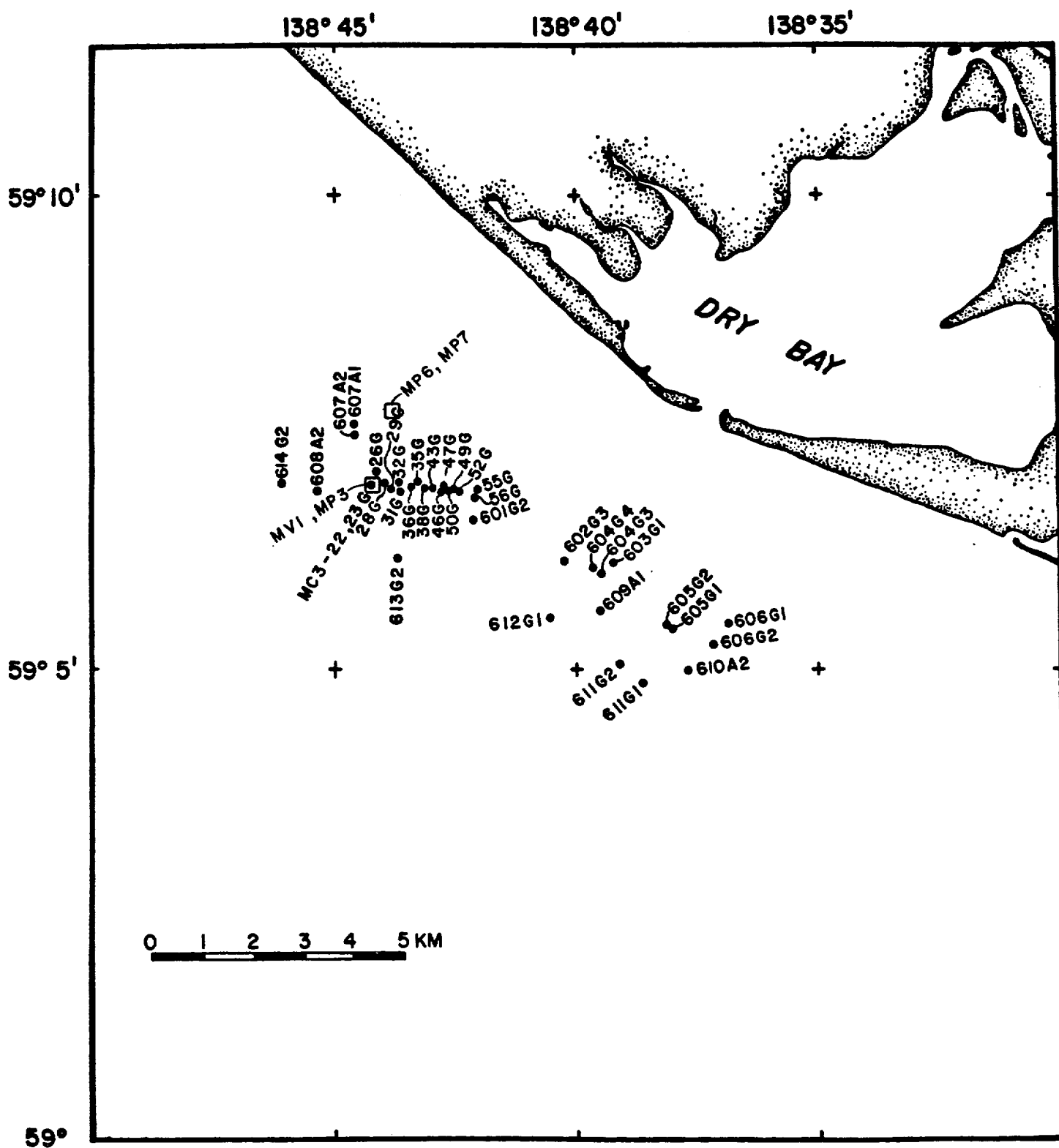


Figure 20. Core and in place test locations-Alsek River Study Area.

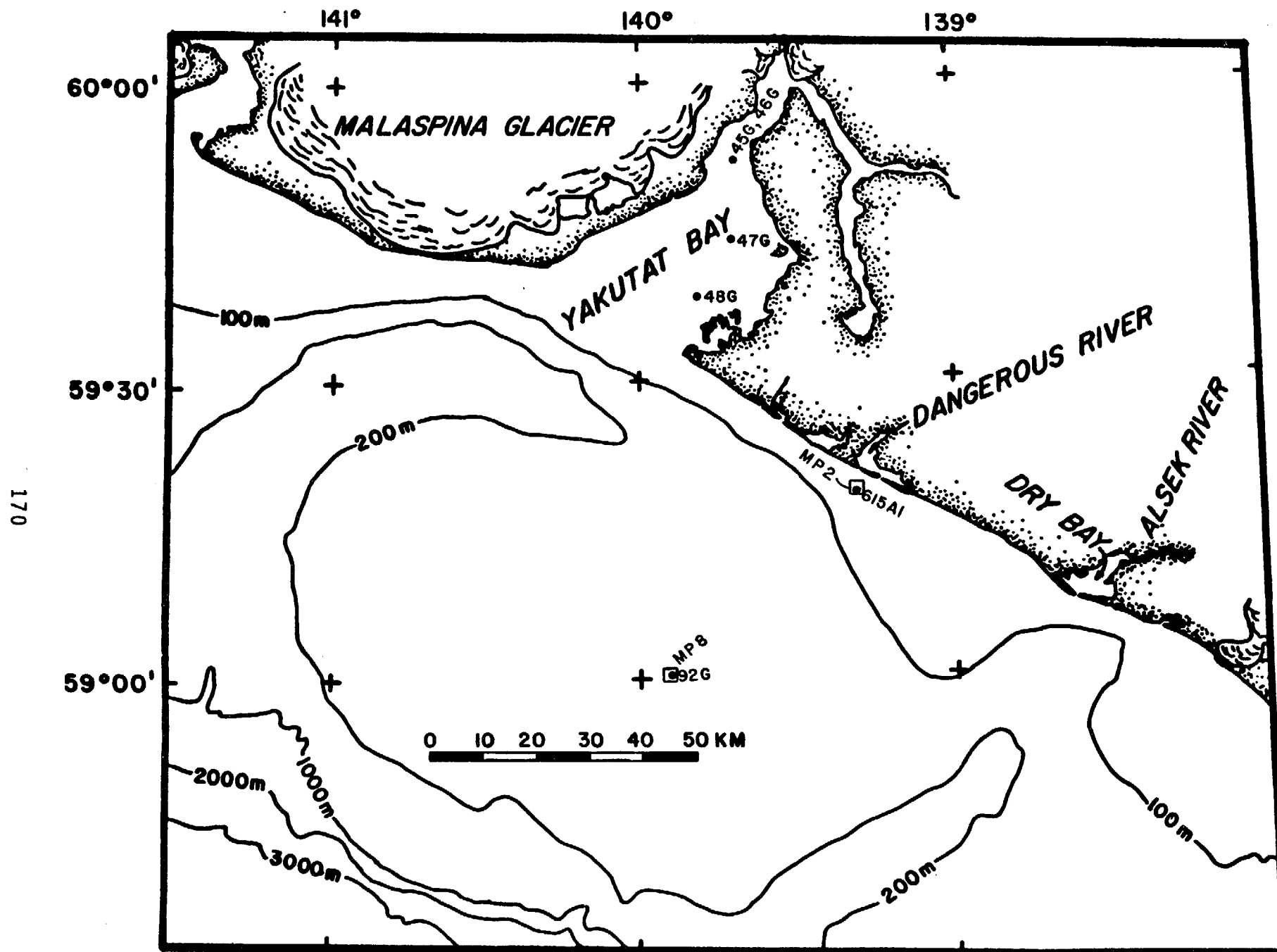


Figure 21. Core locations-Yakutat Bay Study Area and "other"

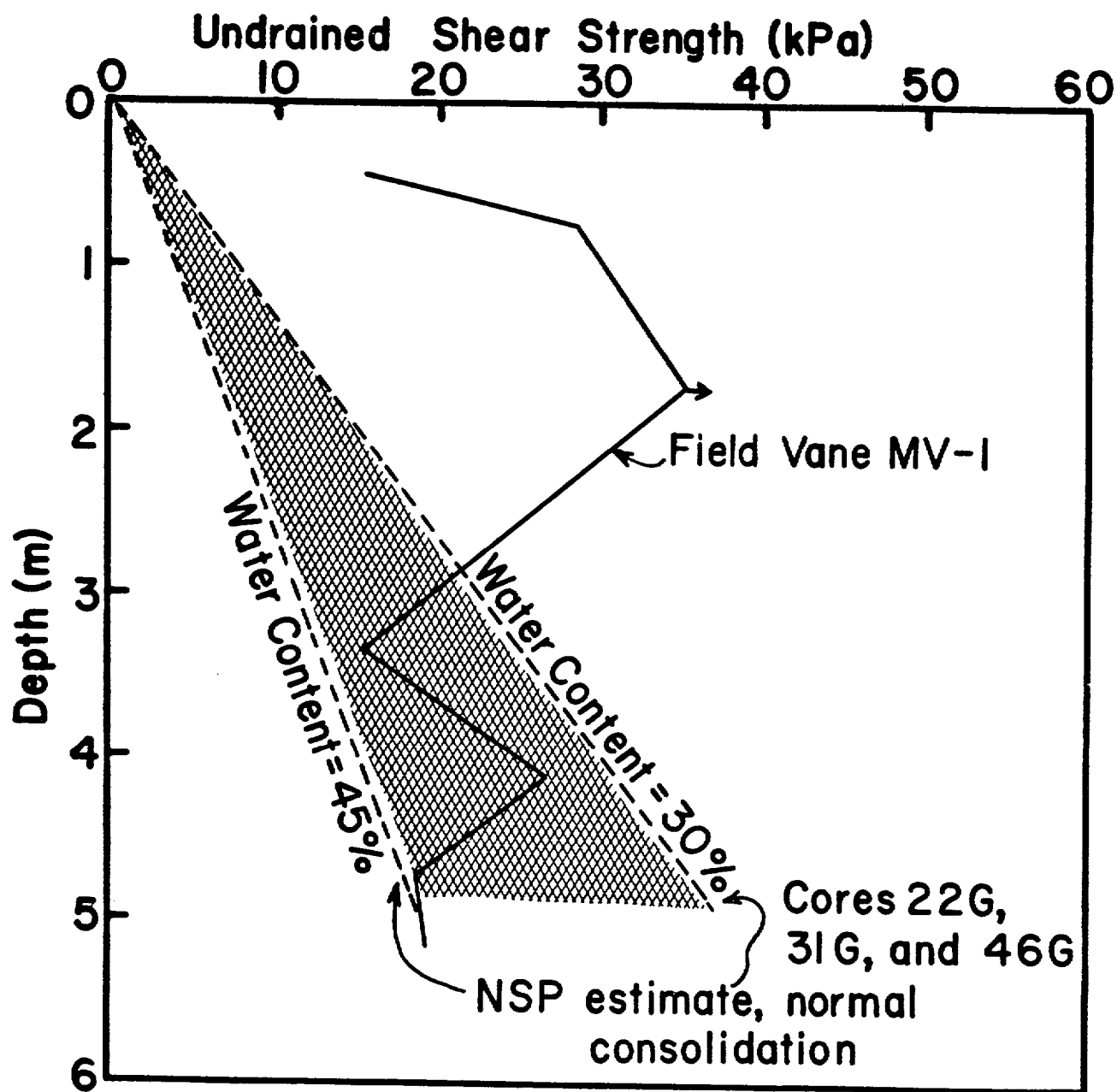


Figure 22. Results of field vane shear test MV-1 (Alsek River Study Area) compared with normalized strength parameter (NSP) estimate of undrained strength from triaxial tests.

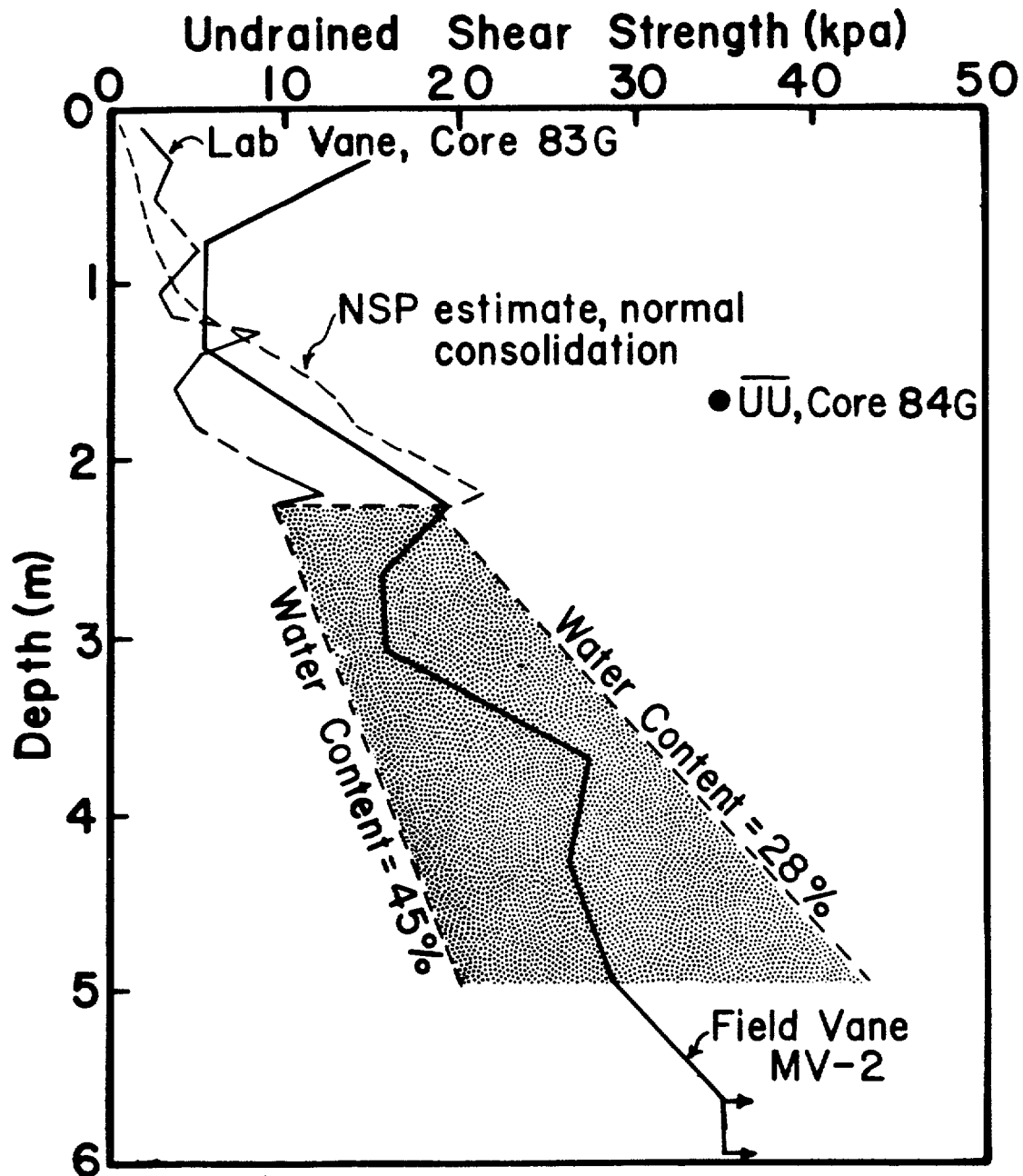


Figure 23. Results of field vane shear test MV-2 (Yakutat Study Area) compared with laboratory vane shear strengths and NSP estimates from triaxial tests. CIU and UU tests represent triaxial tests with consolidation to near the overburden stress and to nearly no stress, respectively.

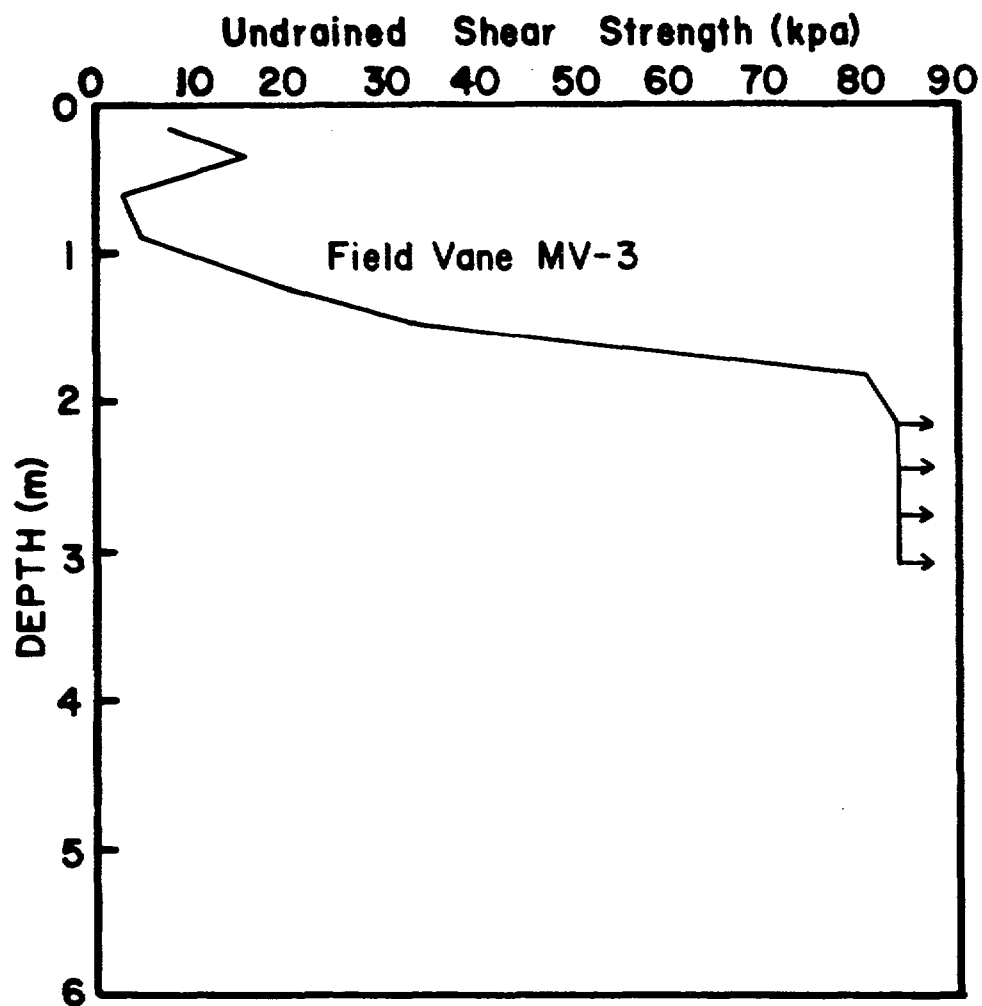


Figure 24. Results of field vane shear test MV-3 (Yakutat Study Area). Arrows indicate locations where the capacity of the field vane torque cell was reached.

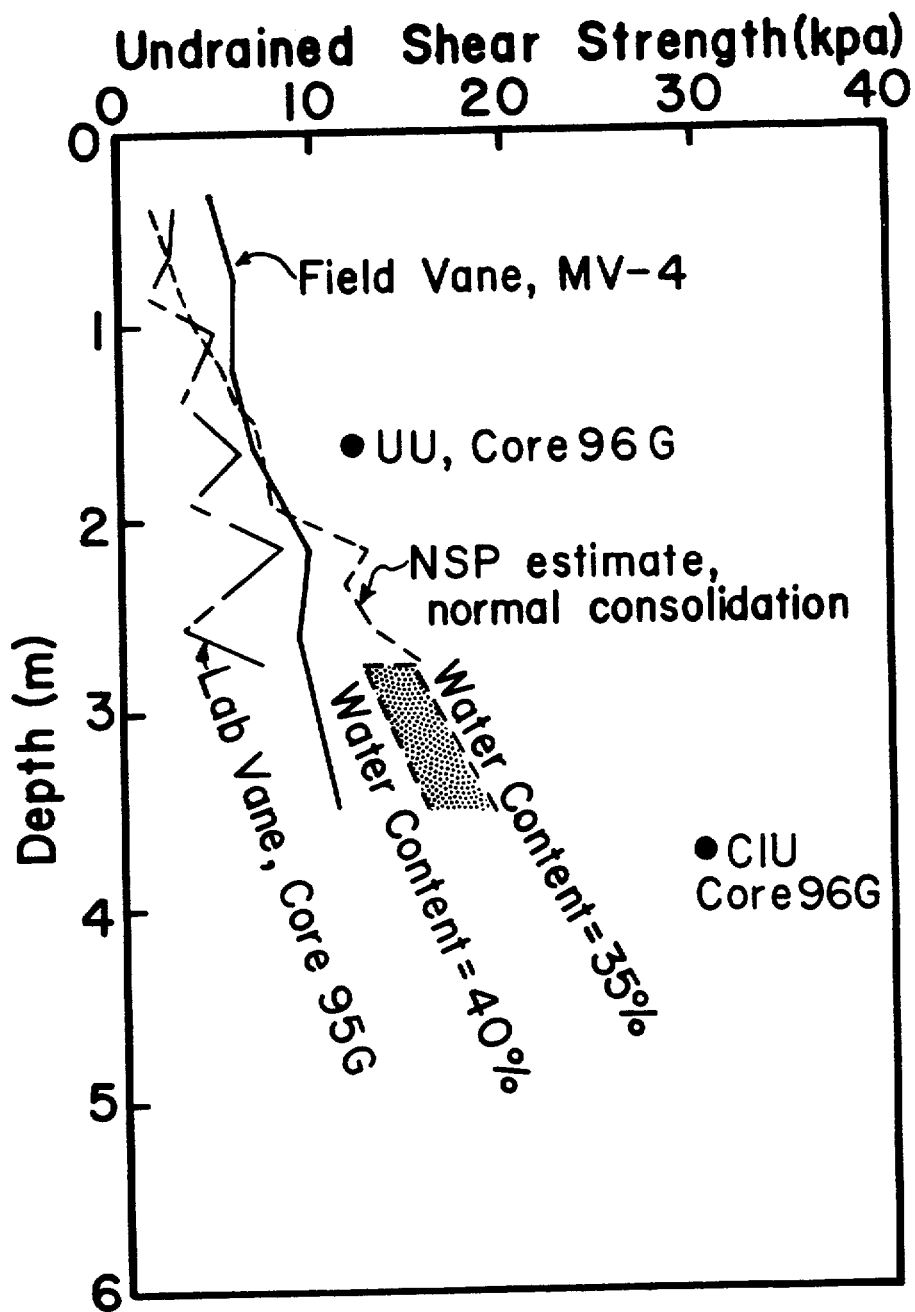


Figure 25. Results of field vane shear test MV-4 (Icy Bay-Malaspina Study Area) compared with laboratory vane shear strengths and NSP estimates from triaxial tests. CIU and UU tests represent triaxial tests consolidated to near the overburden stress and to nearly no stress, respectively.

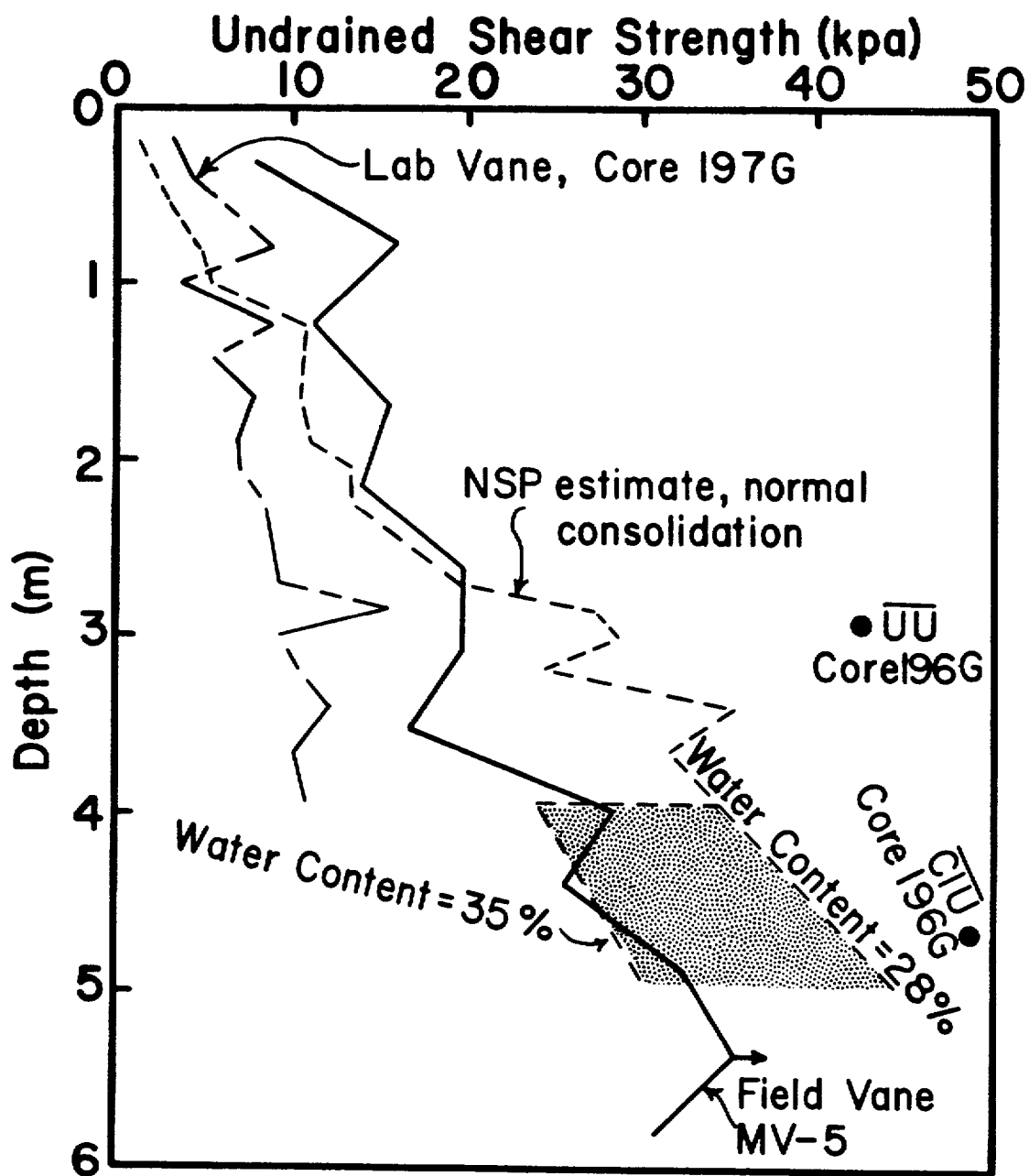


Figure 26. Results of field vane shear test MV-5 (eastern part of Icy Bay-Malaspina Study Area) compared with laboratory vane shear strengths and NSP estimates from triaxial tests. CIU and UU tests represent triaxial tests to near the overburden stress and to nearly no stress, respectively.

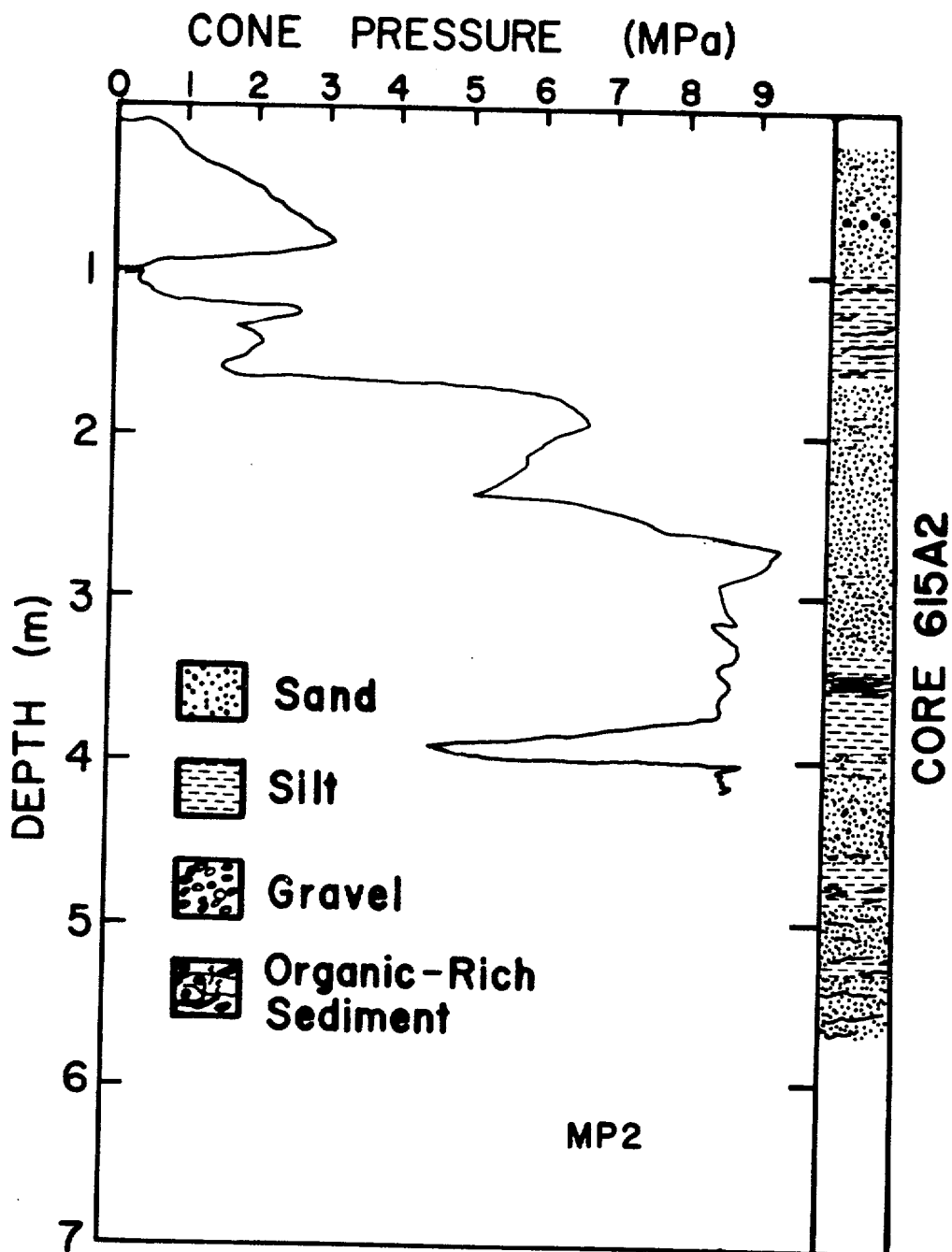


Figure 27. Results of in place cone penetration test MP-2 (off the mouth of the Dangerous River). Stratigraphy of nearby core is given at right.

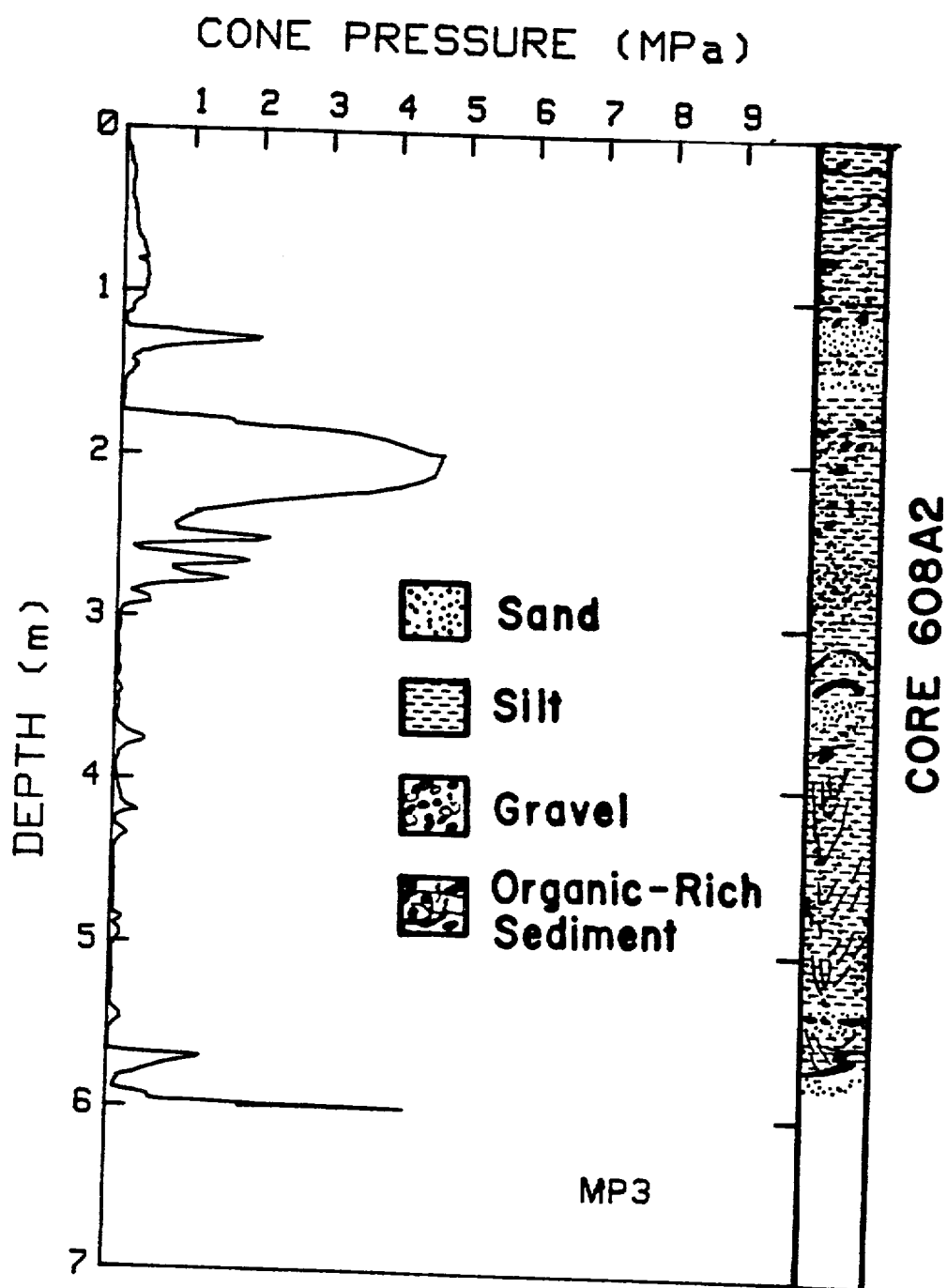


Figure 28. Results of in place cone penetration test MP-3. (Alsek River Study Area). Stratigraphy of nearby core is given at right.

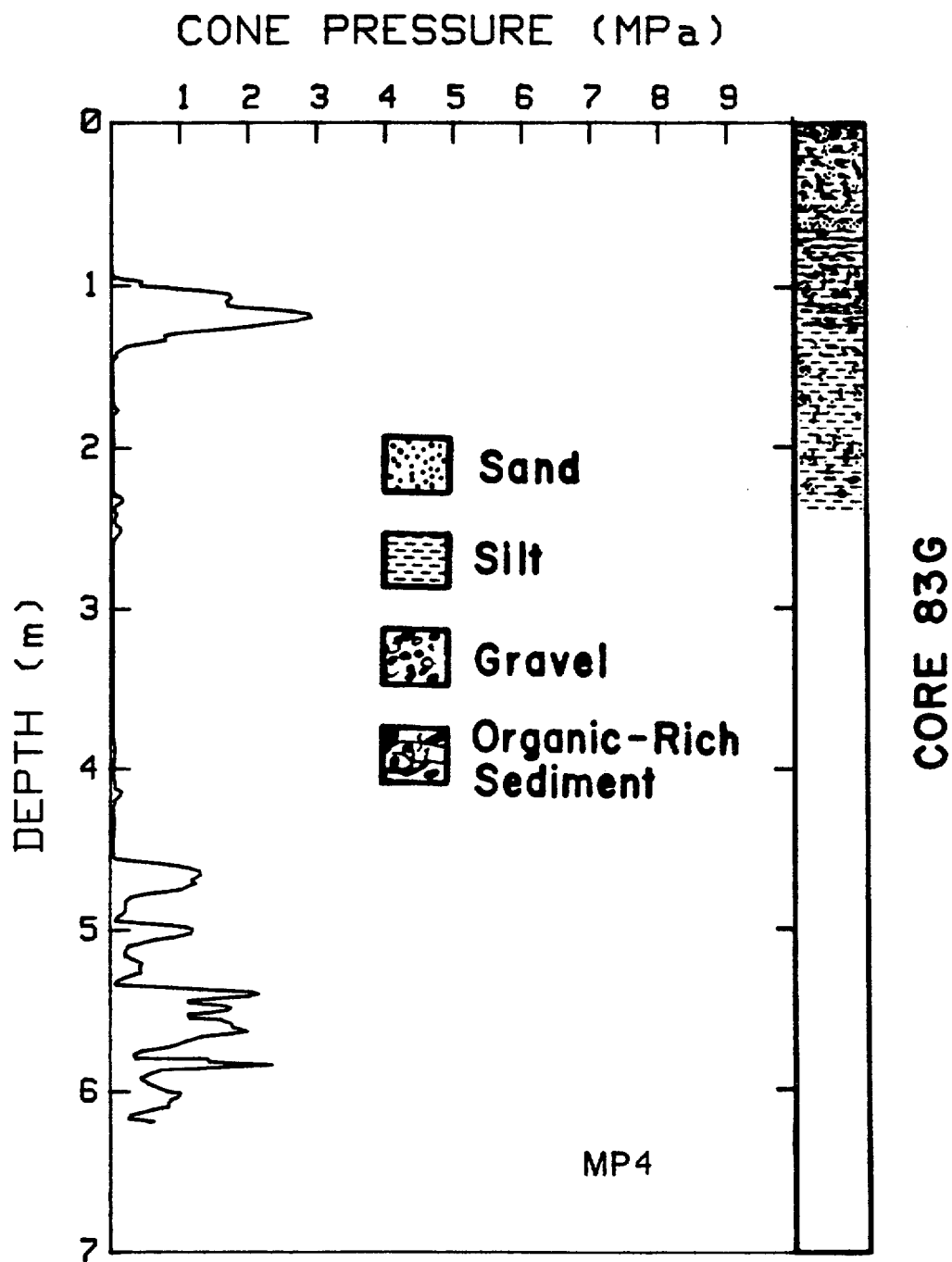


Figure 29. Results of in place cone penetration test MP-4 (Yakutat Study Area). Stratigraphy of nearby core is given at right.

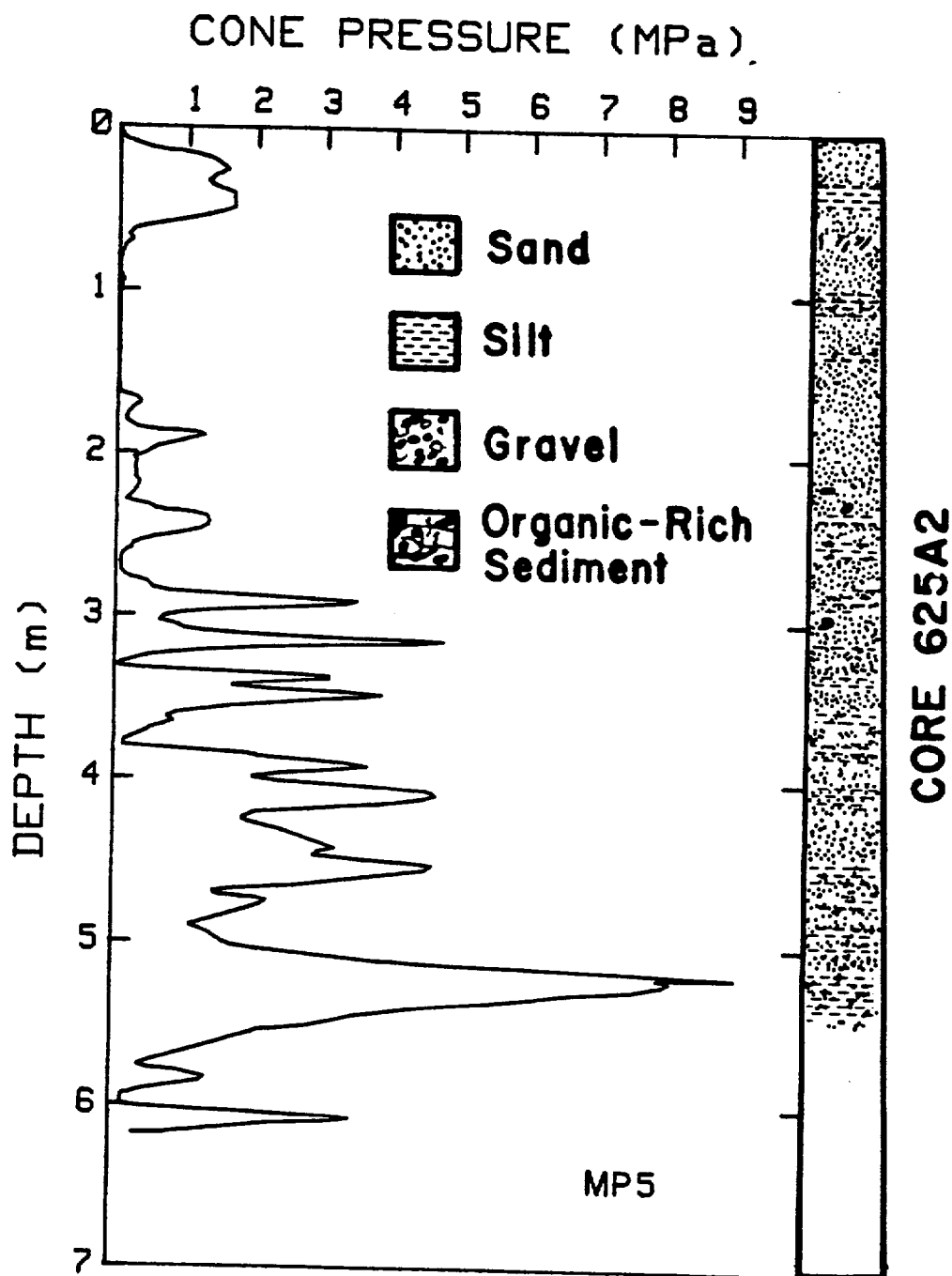


Figure 30. Results of in place cone penetration test MP-5 (Yakutat Study Area). Stratigraphy of nearby core is given at right.

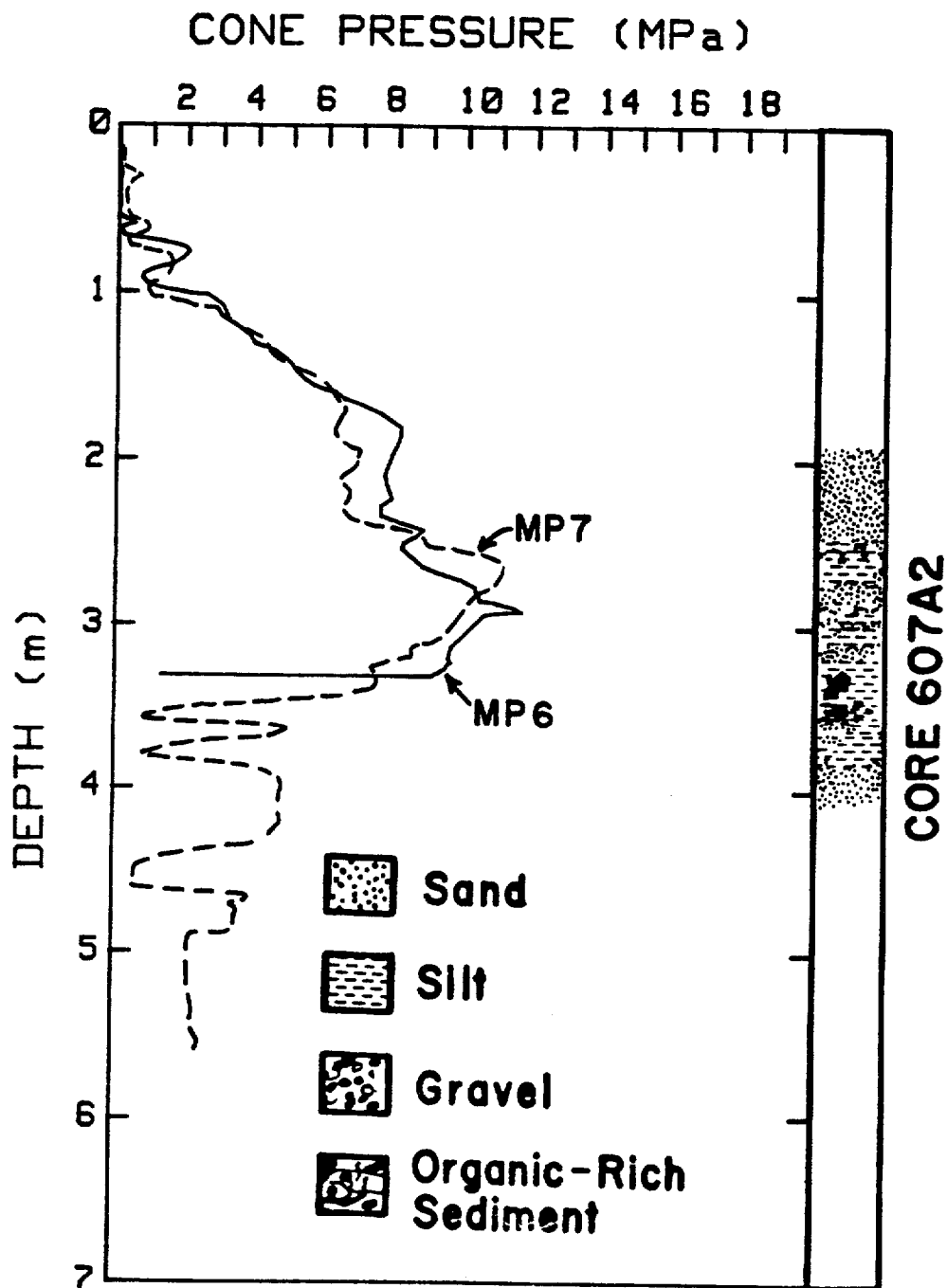


Figure 31. Results of in place cone penetration tests MP-6 and MP-7 (Alsek River Study Area). Stratigraphy of nearby core is given at right.

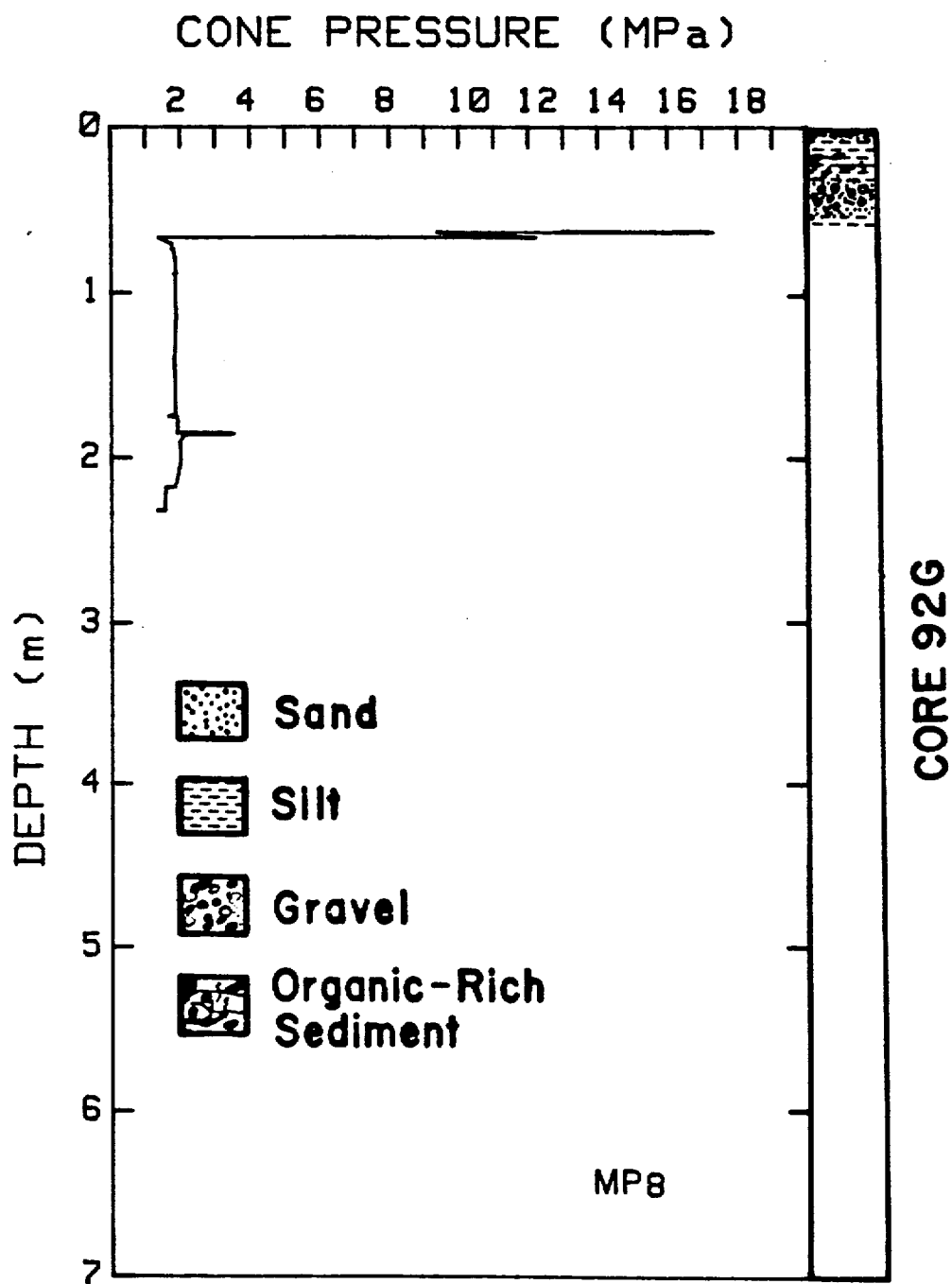


Figure 32. Results of in place cone penetration test MP-8 (Quaternary glacial deposits off Dangerous River Delta). Stratigraphy of nearby core is given at right.

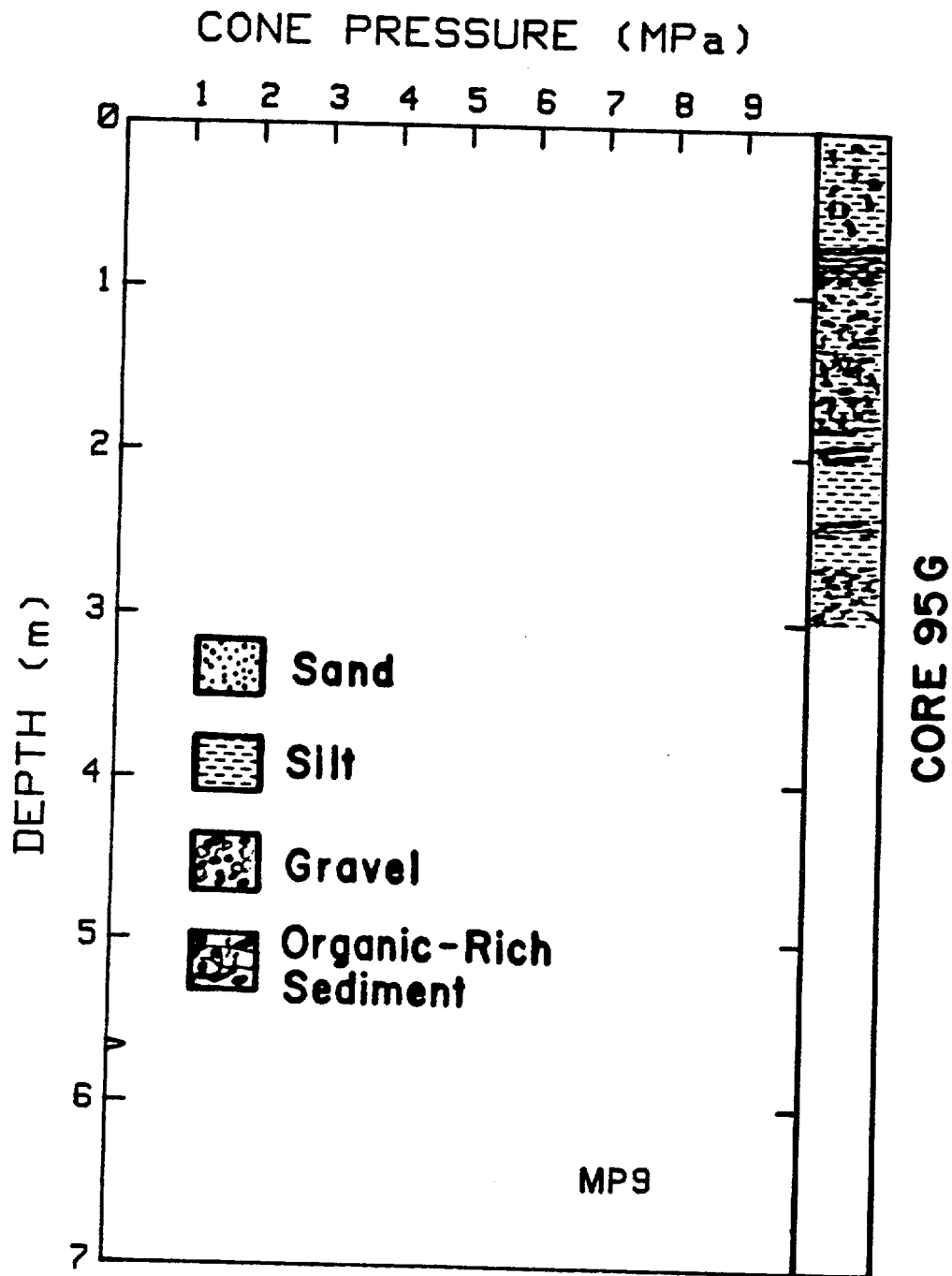


Figure 33. Results of in place cone penetration test MP-9 (Icy Bay-Malaspina Study Area). Stratigraphy of nearby core is given at right.

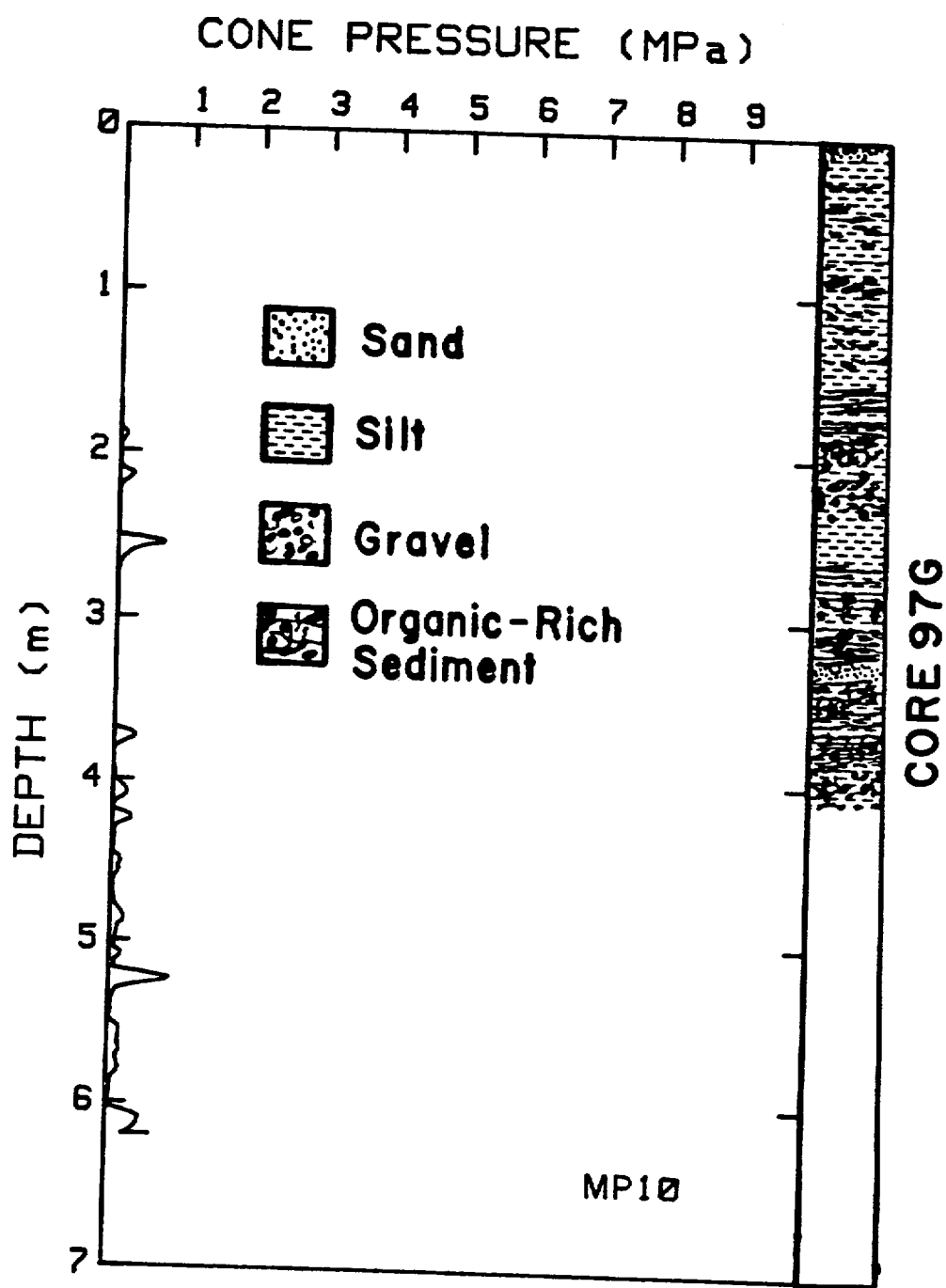


Figure 34. Results of in place cone penetration test MP-10 (eastern part of Icy Bay-Malaspina Study Area). Stratigraphy of nearby core is given at right.

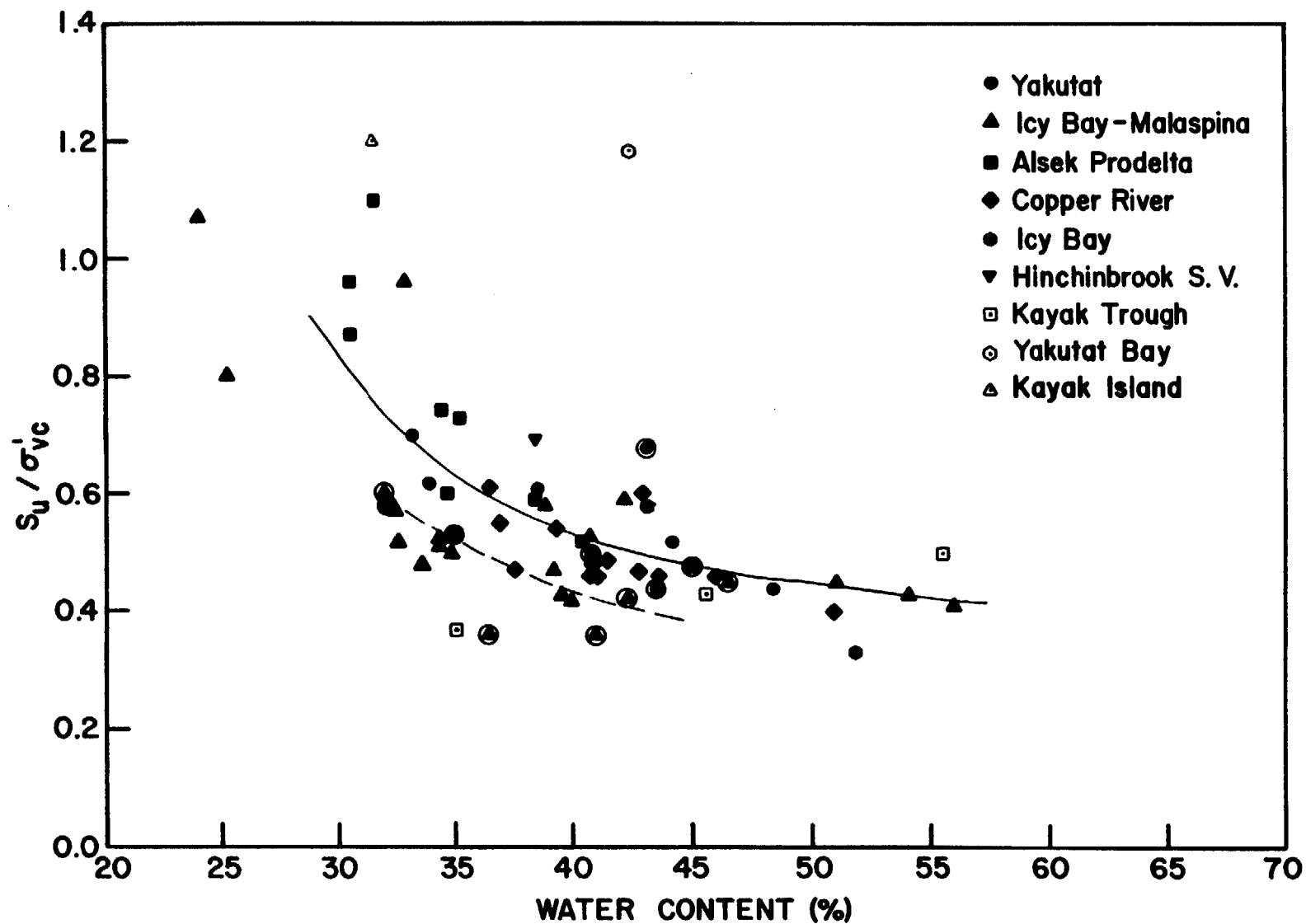


Figure 35. Correlation of ratio of undrained shearing strength, S_u , to vertical consolidation stress, σ'_{vc} , with natural water content; all type (c) static triaxial tests. Circled data points represent anisotropic consolidation. Solid line is a fit of the isotropic consolidation data points (uncircled dots). Dashed line represents 0.8 times the solid line and roughly follows anisotropic data points.

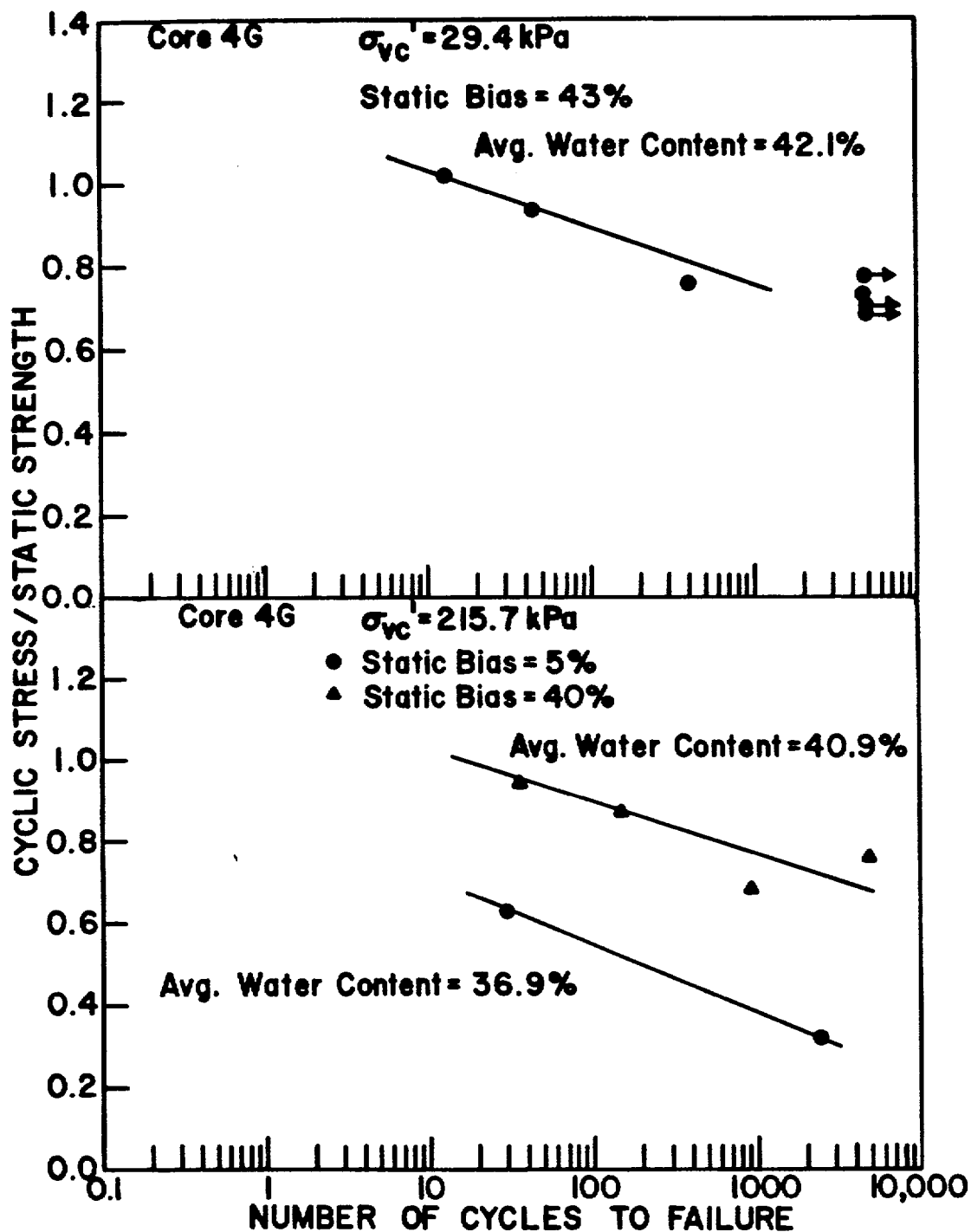


Figure 36. Relative cyclic stress level versus number of cycles to failure: Core 4G (Copper River Study area).

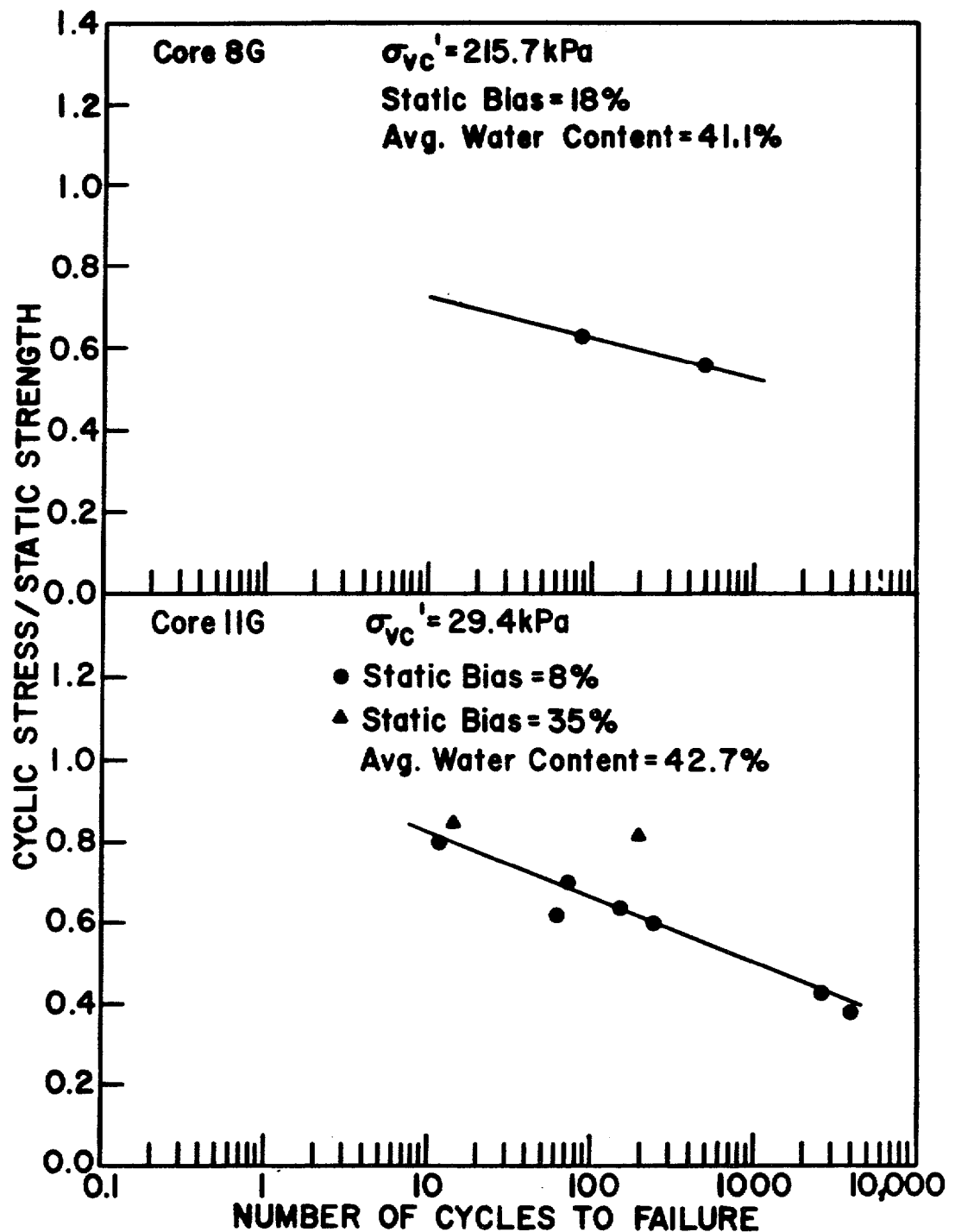


Figure 37. Relative cyclic stress level versus number of cycles to failure: Cores 8G and 11G (Copper River and Kayak Trough Study Areas).

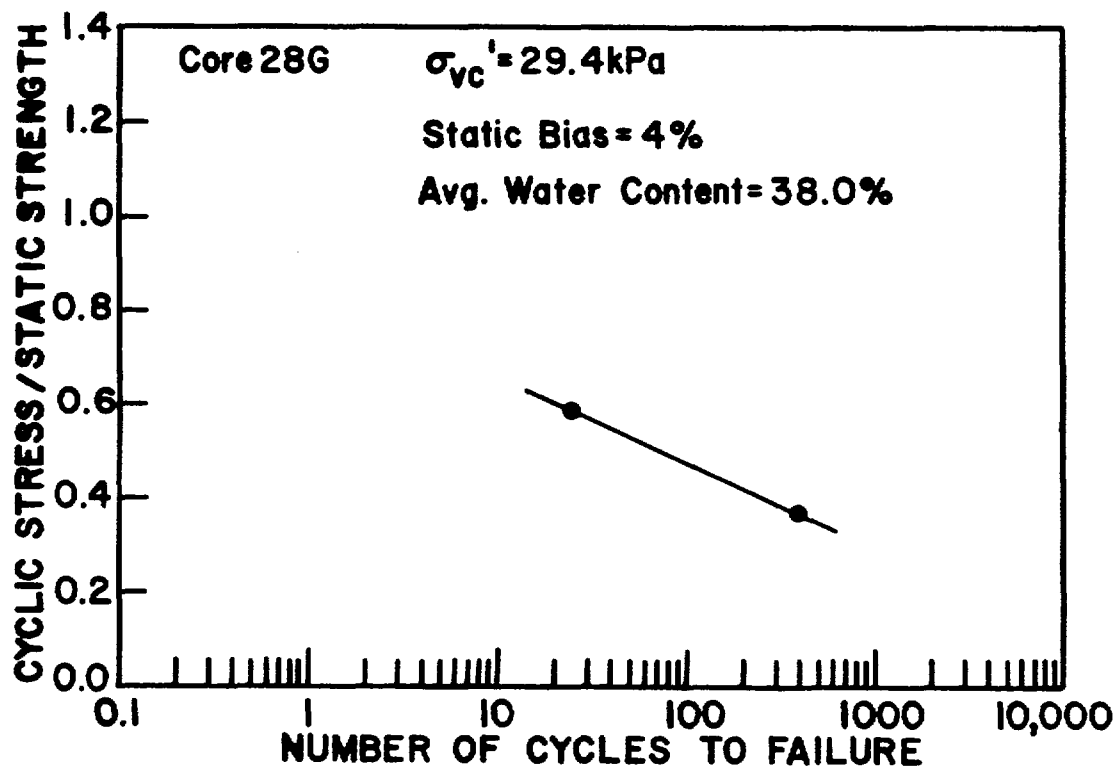


Figure 38. Relative cyclic stress level versus number of cycles to failure: Core 28G (Icy Bay-Malaspina Study Area).

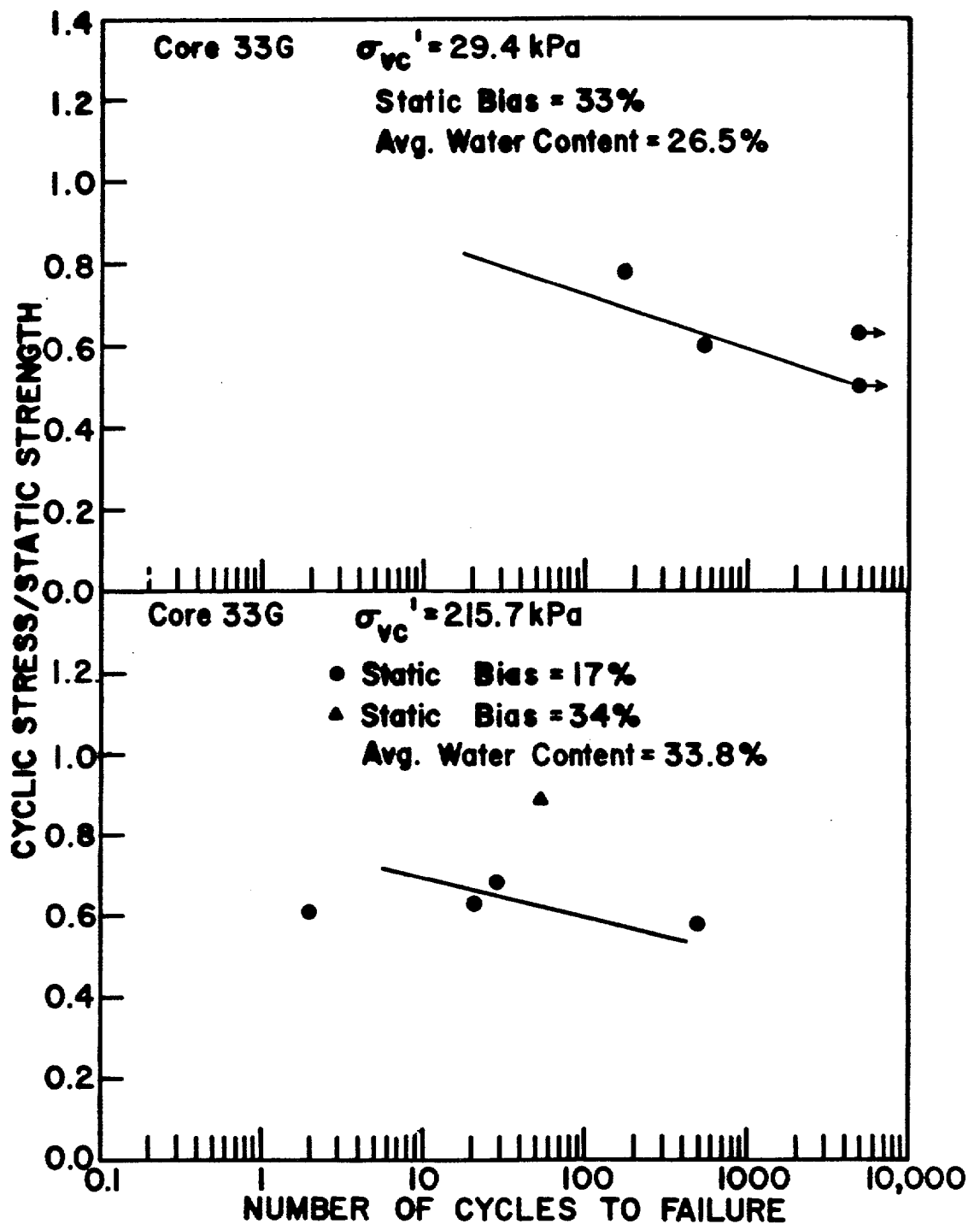


Figure 39. Relative cyclic stress level versus number of cycles to failure: Core 33G (Icy Bay-Malaspina Study Area).

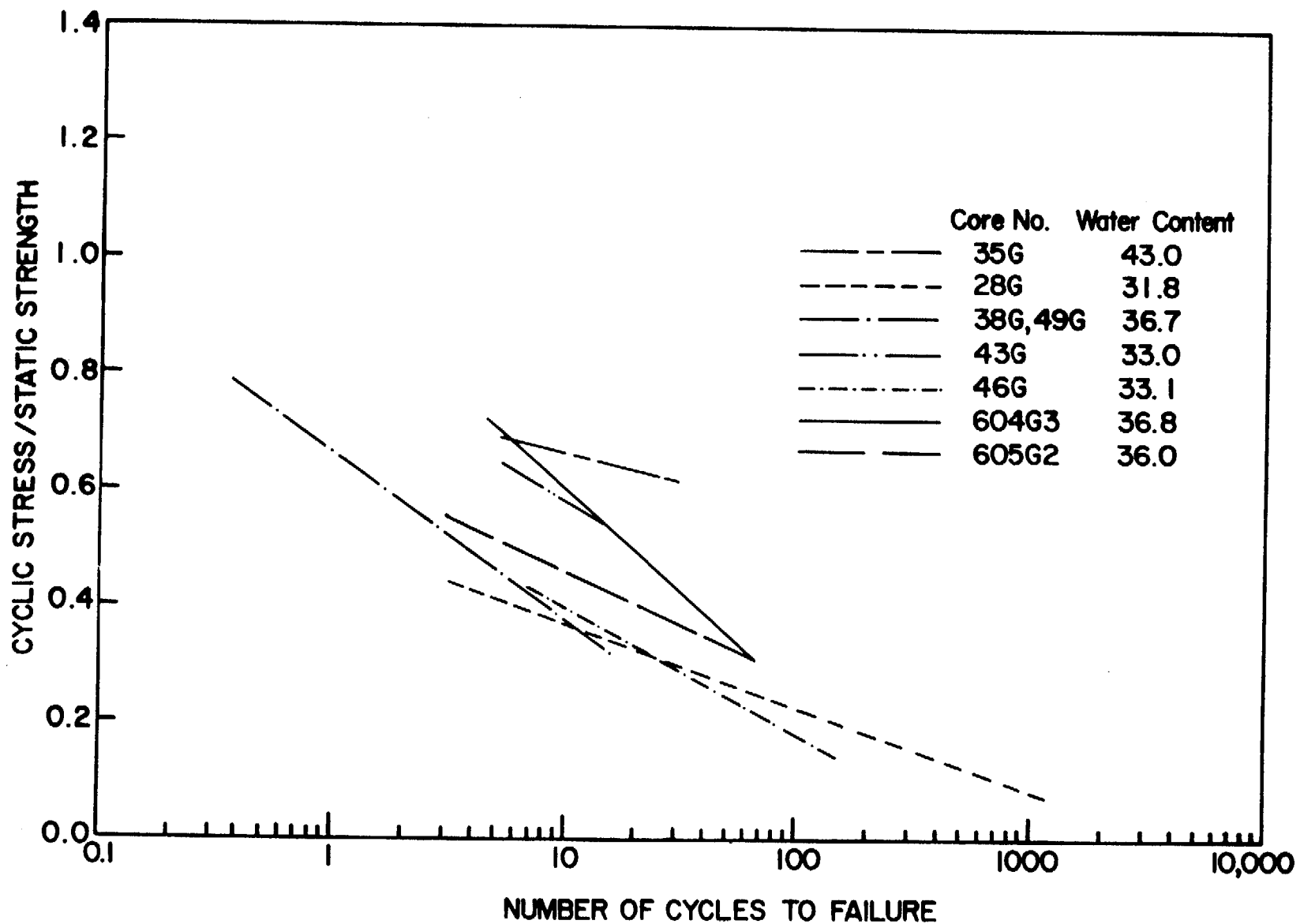


Figure 40. Relative cyclic stress level versus number of cycles to failure: Alsek River Study Area, Method I.

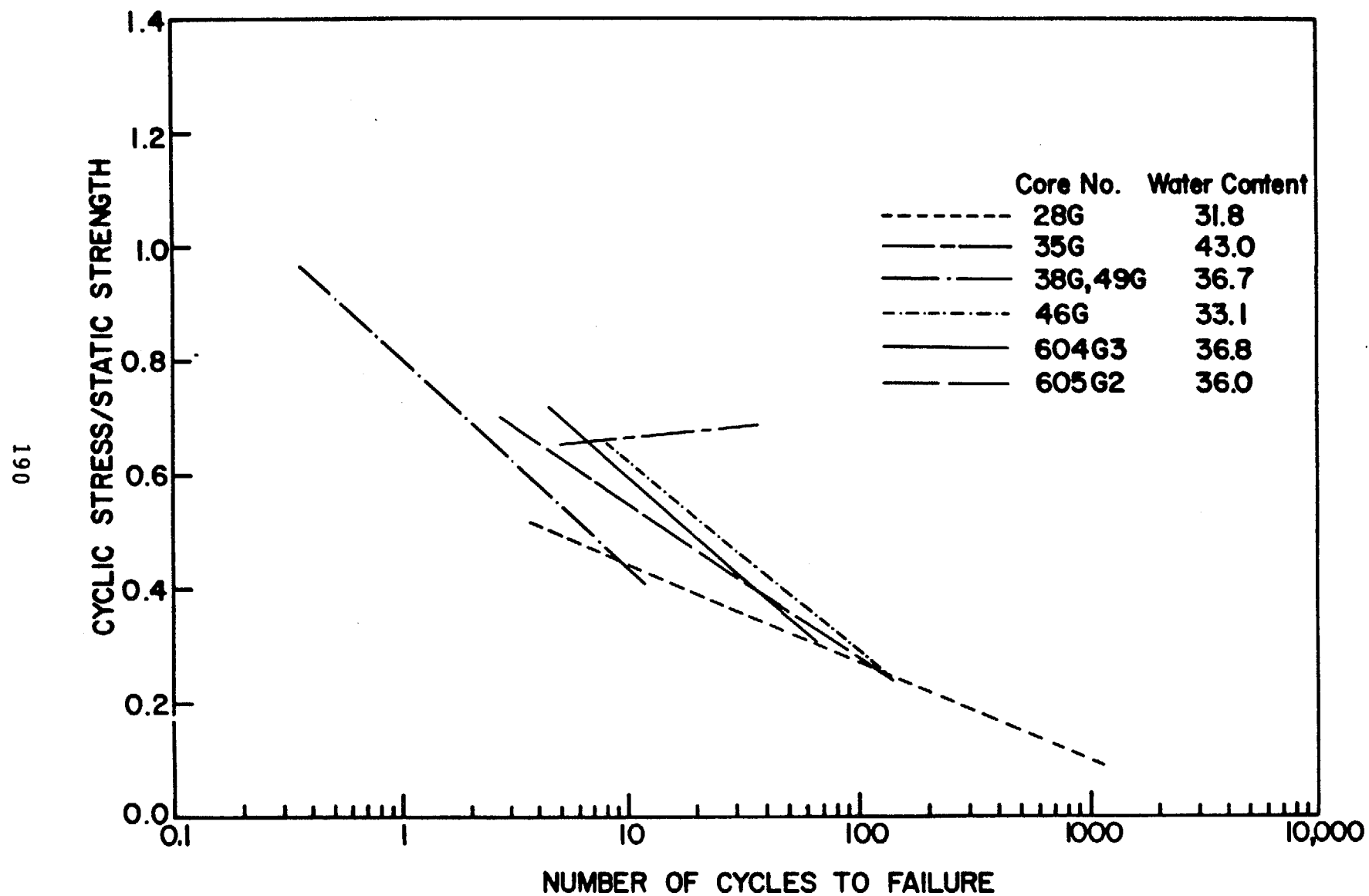


Figure 4I. Relative cyclic stress level versus number of cycles to failure: Alsek River Study Area, Method II.

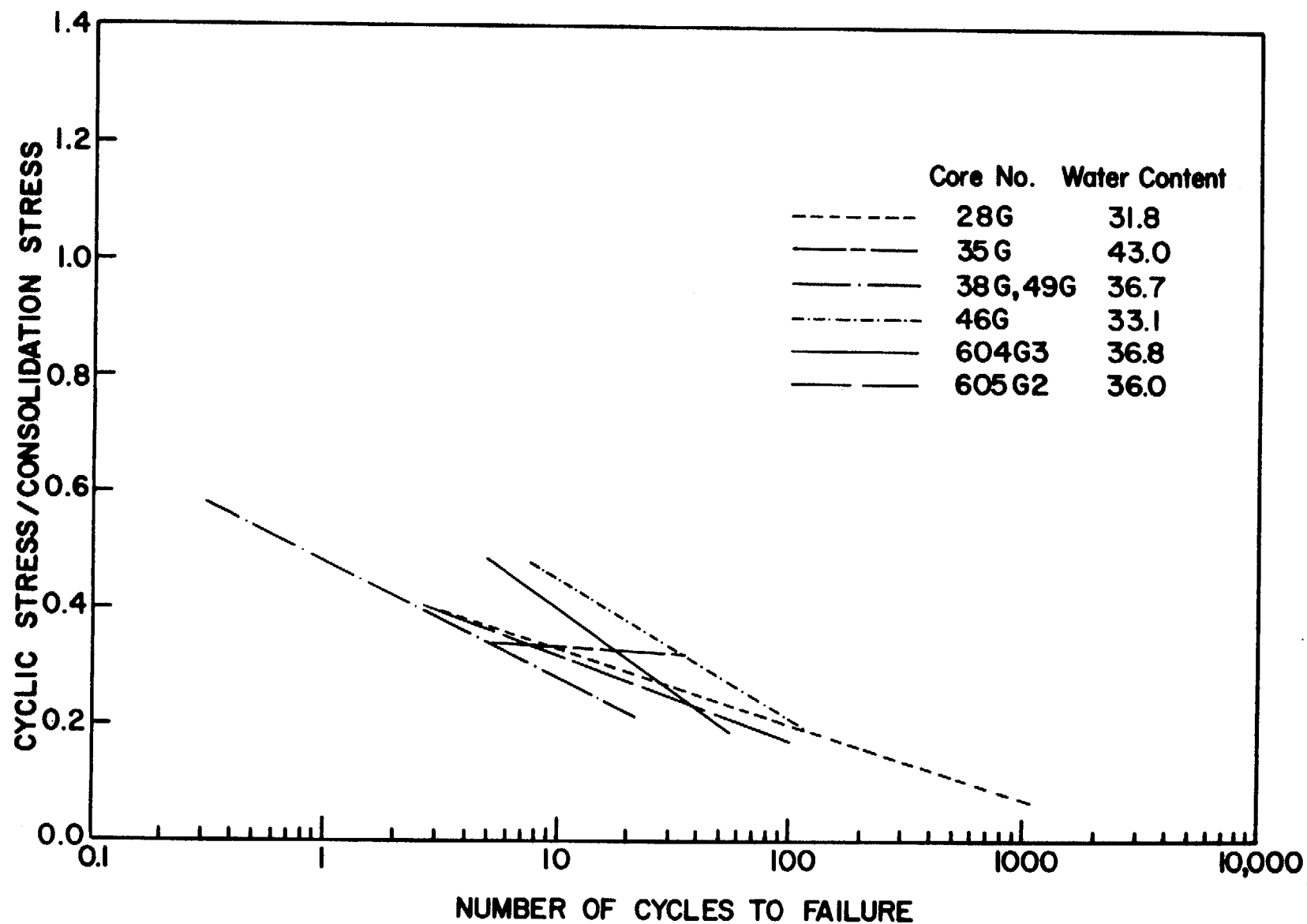


Figure 42. Relative cyclic stress level versus number of cycles to failure: Alsek River Study Area, Method III.

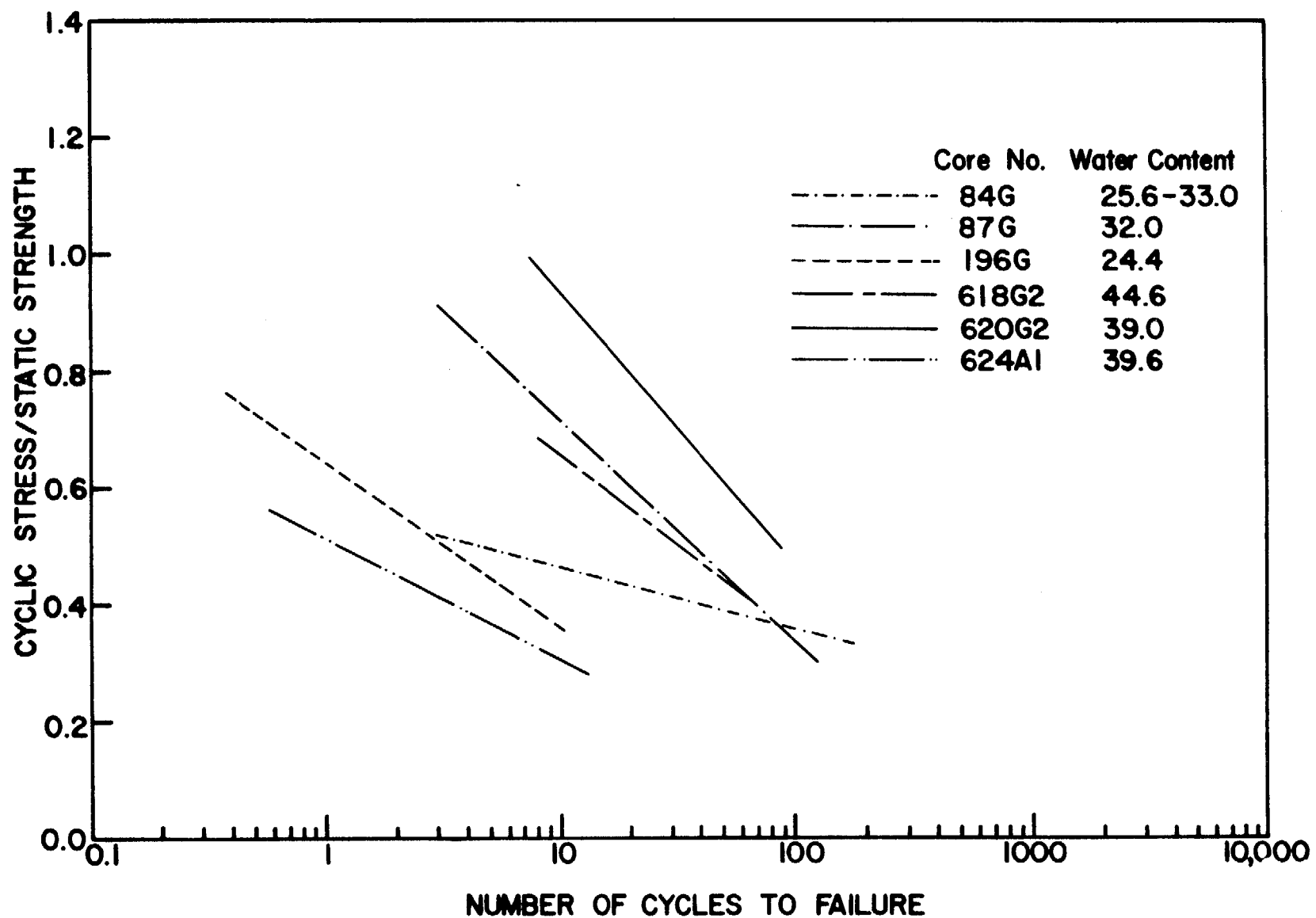


Figure 43. Relative cyclic stress level versus number of cycles to failure: Yakutat Study Area, Method I.

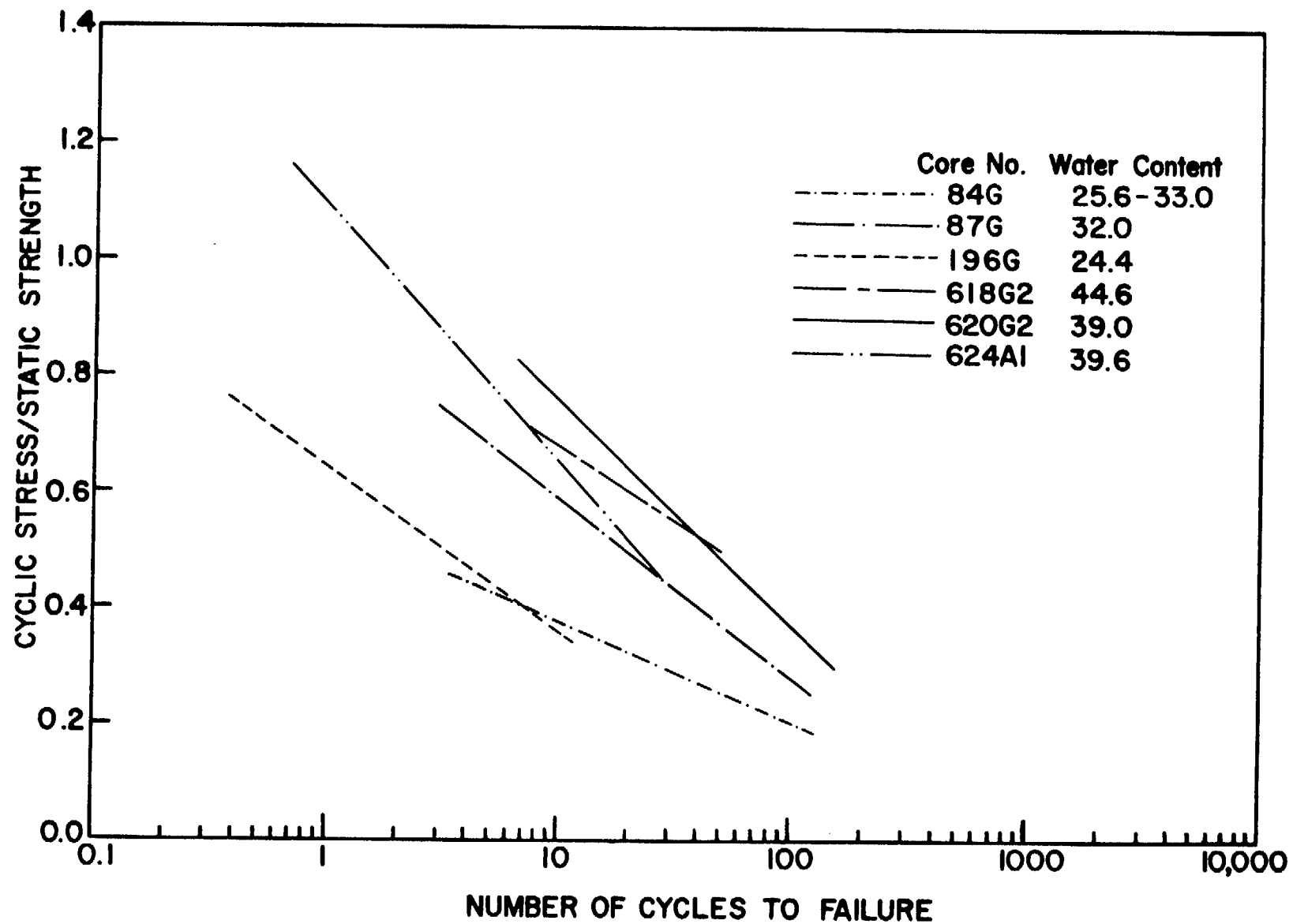


Figure 44. Relative cyclic stress level versus number of cycles to failure: Yakutat Study Area, Method II.

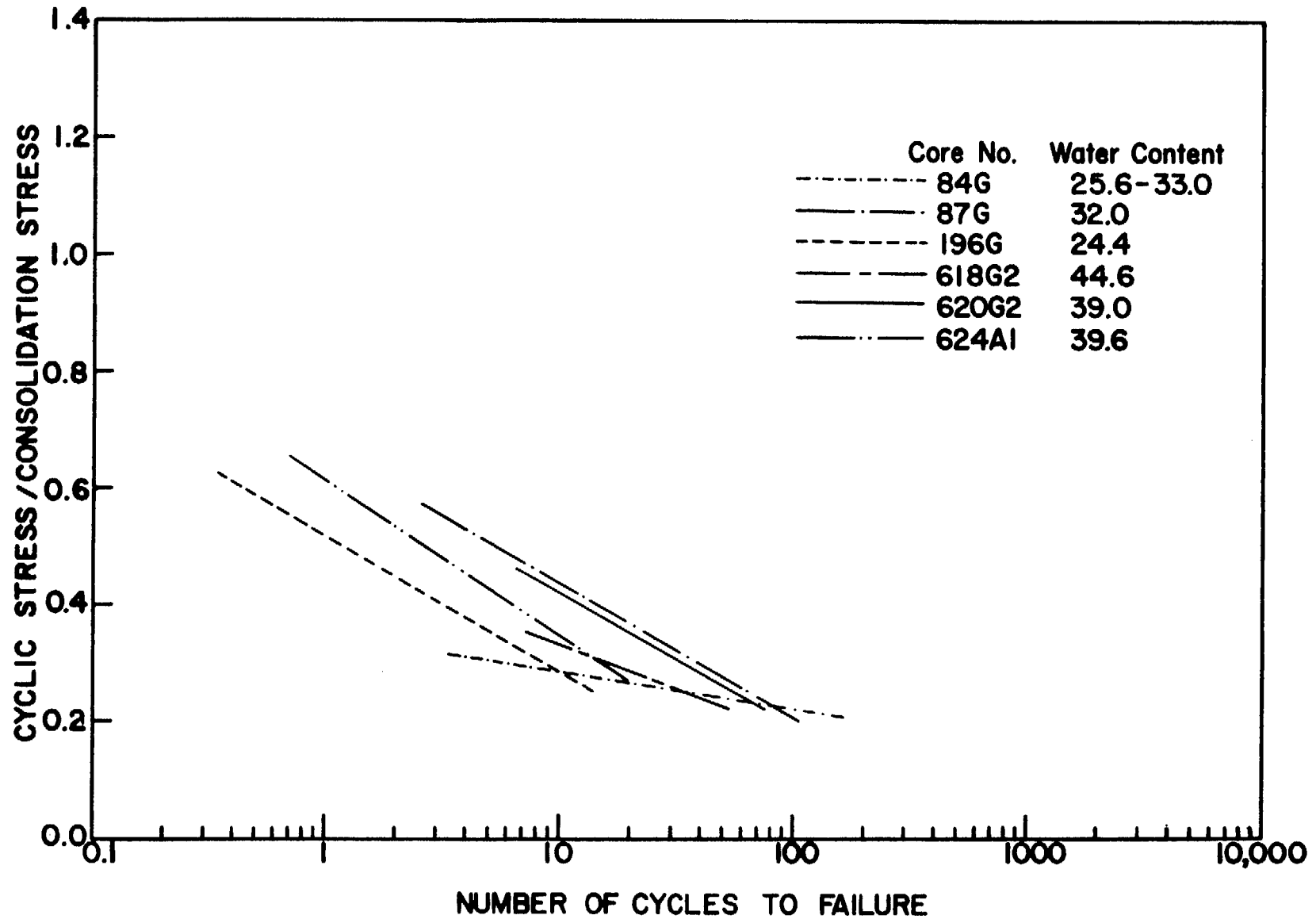


Figure 45. Relative cyclic stress level versus number of cycles to failure: Yakutat Study Area, Method III.

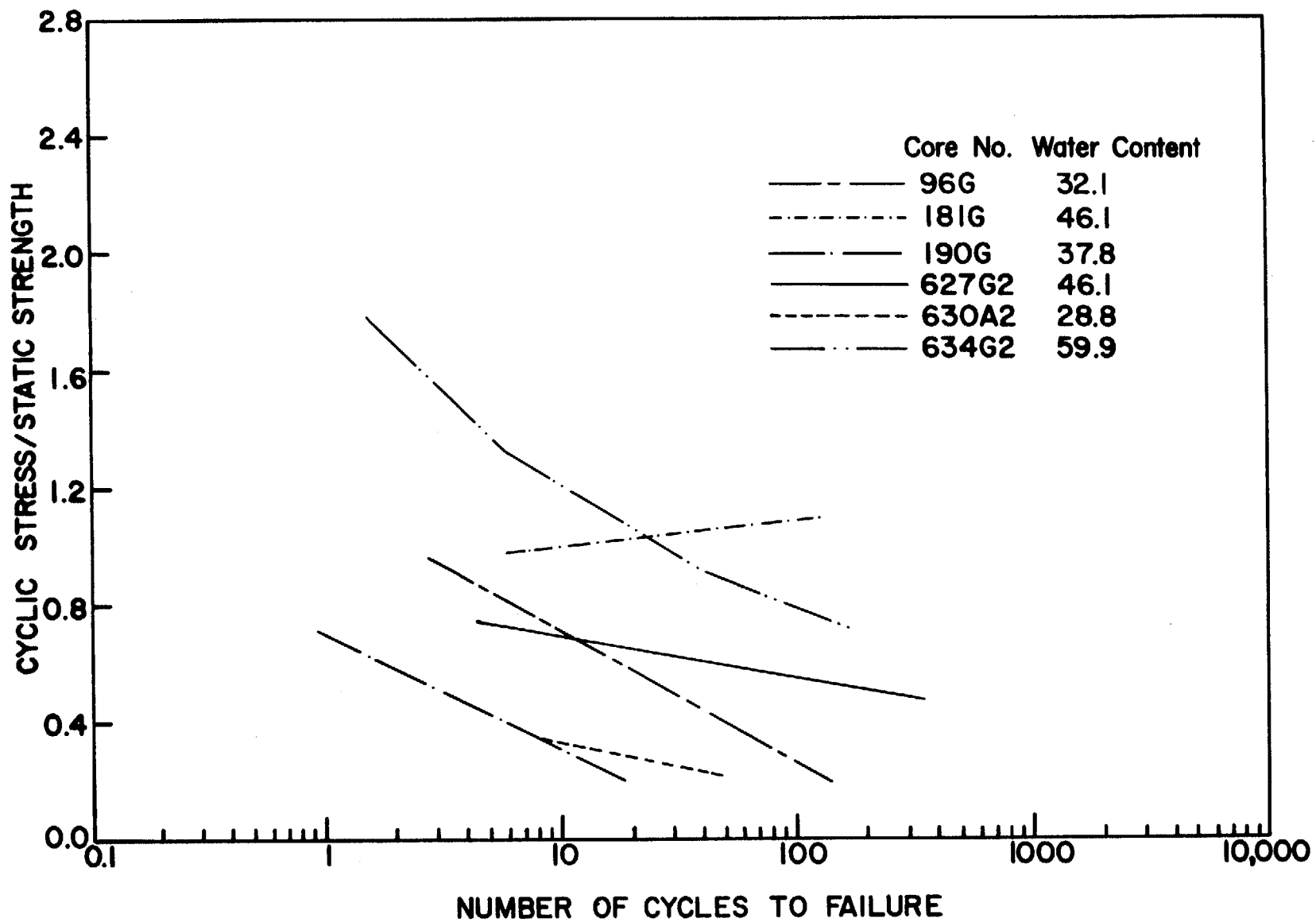


Figure 46. Relative cyclic stress level versus number of cycles to failure: Icy Bay-Malaspina Study Area (USGS testing), Method I.

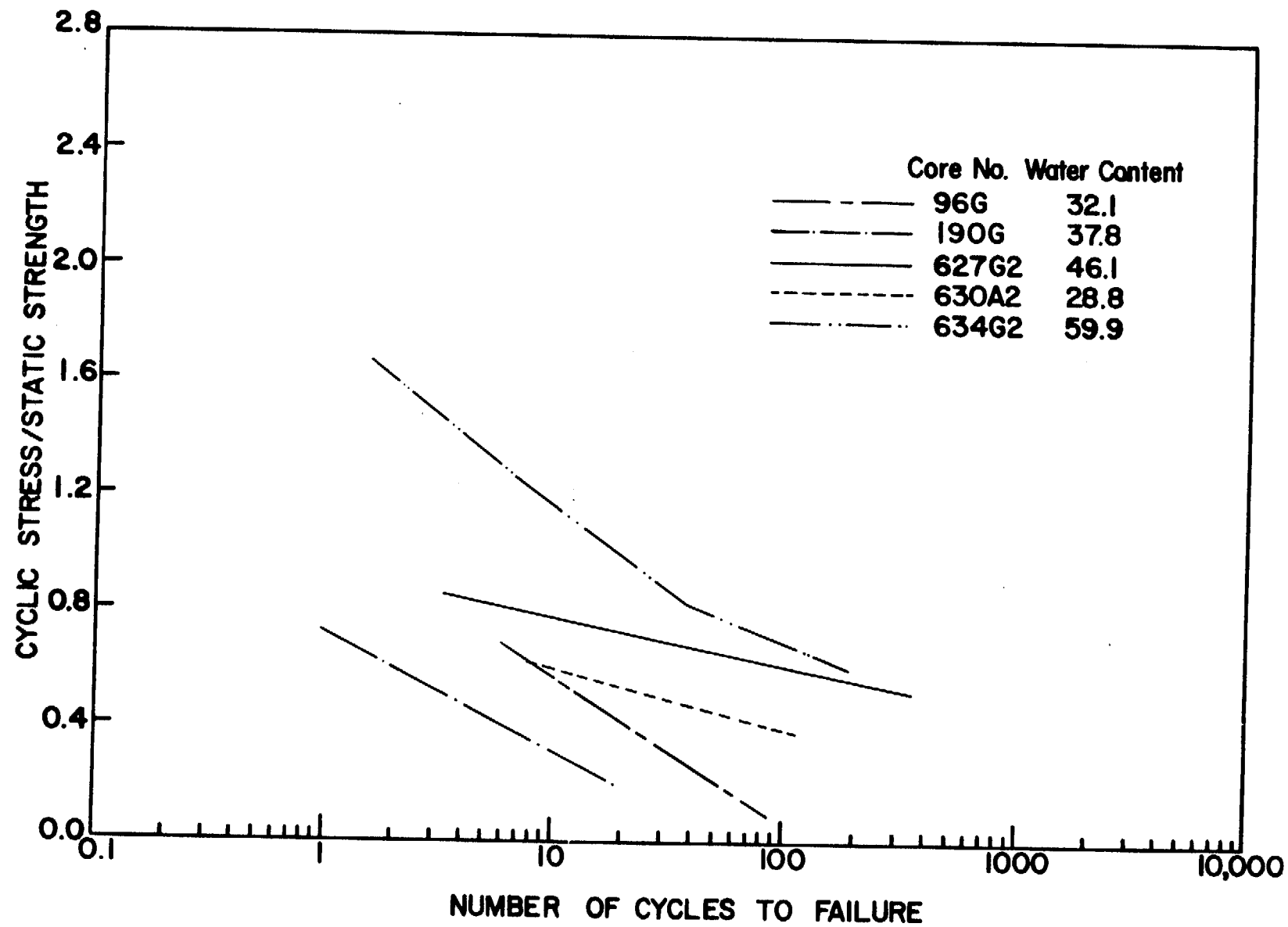


Figure 47. Relative cyclic stress level versus number of cycles to failure: Icy Bay-Malaspina Study Area (USGS testing), Method II.

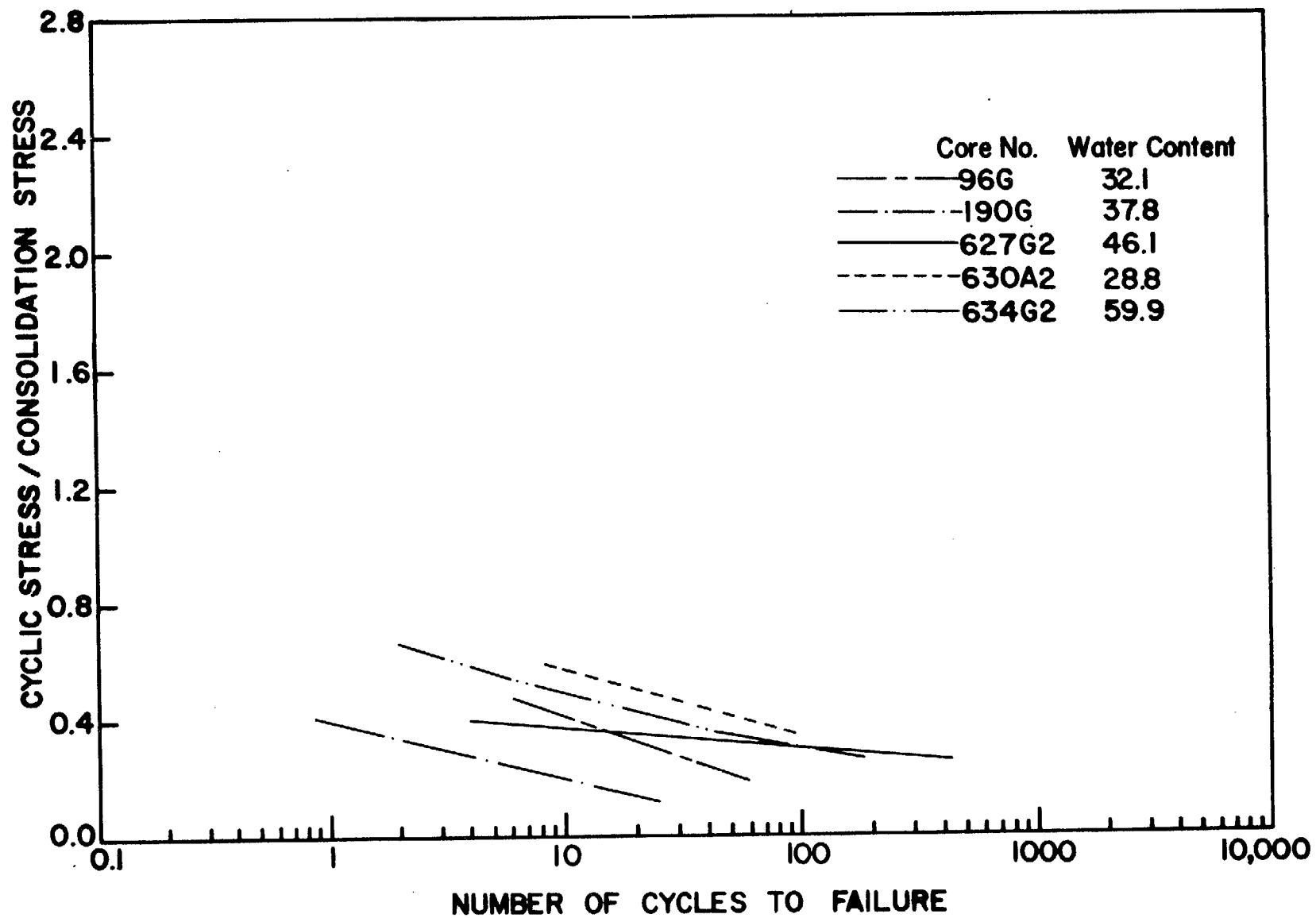


Figure 48. Relative cyclic stress level versus number of cycles to failure: Icy Bay-Malaspina Study Area (USGS testing), Method III.

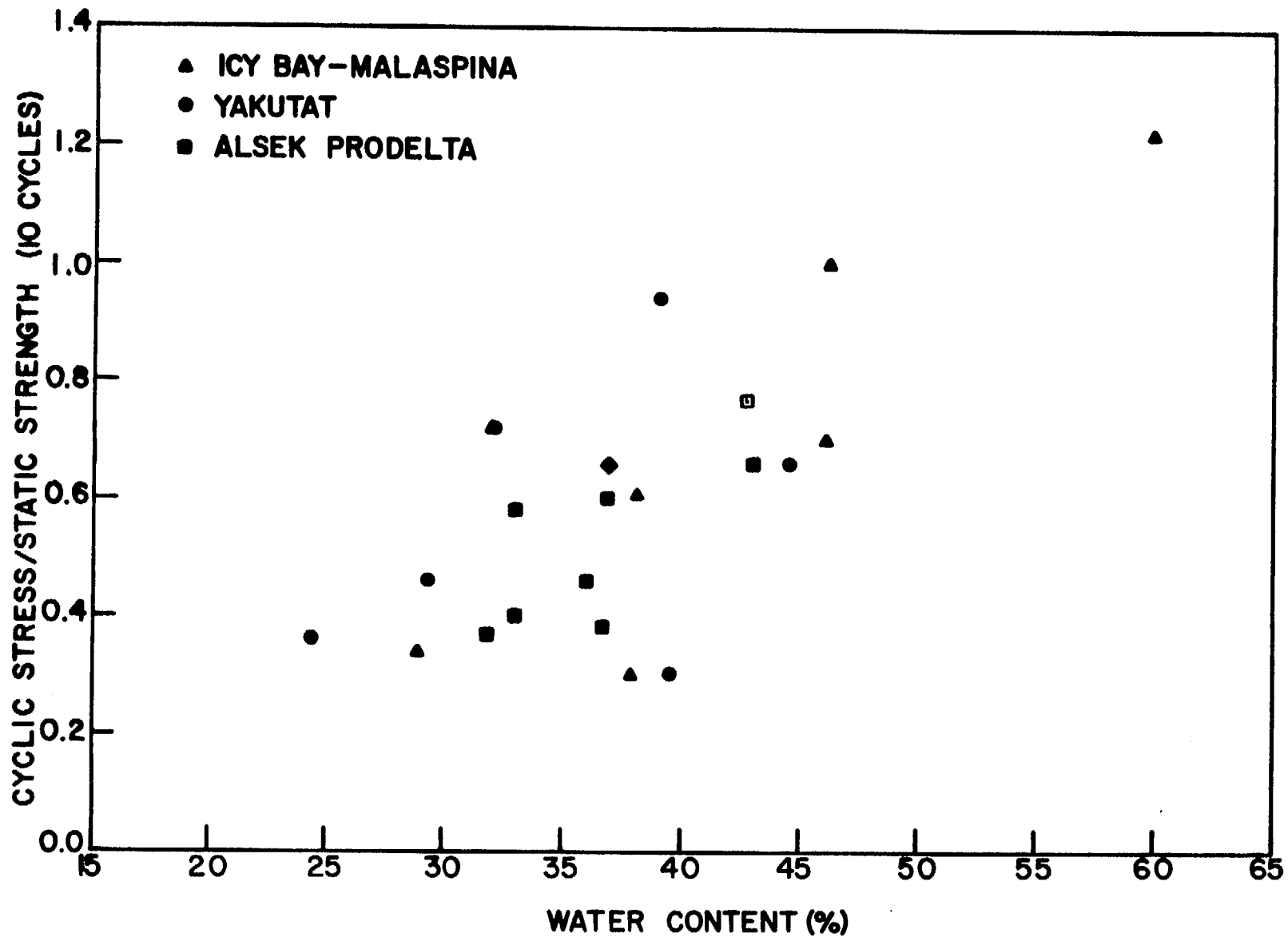


Figure 49. Relative cyclic stress level for failure in 10 cycles versus natural water content, Method I.

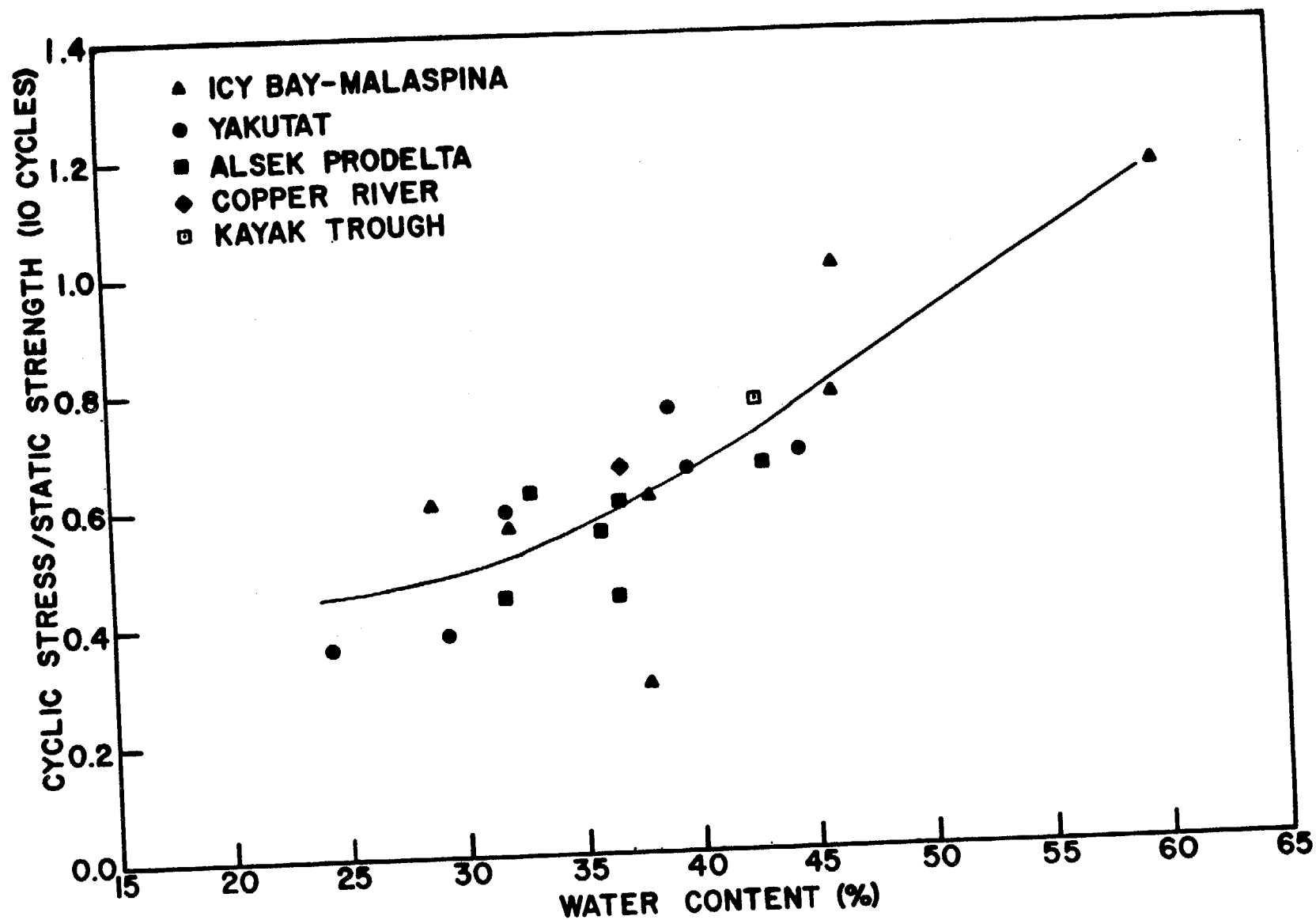


Figure 50. Relative cyclic stress level for failure in 10 cycles versus natural water content, Method II.

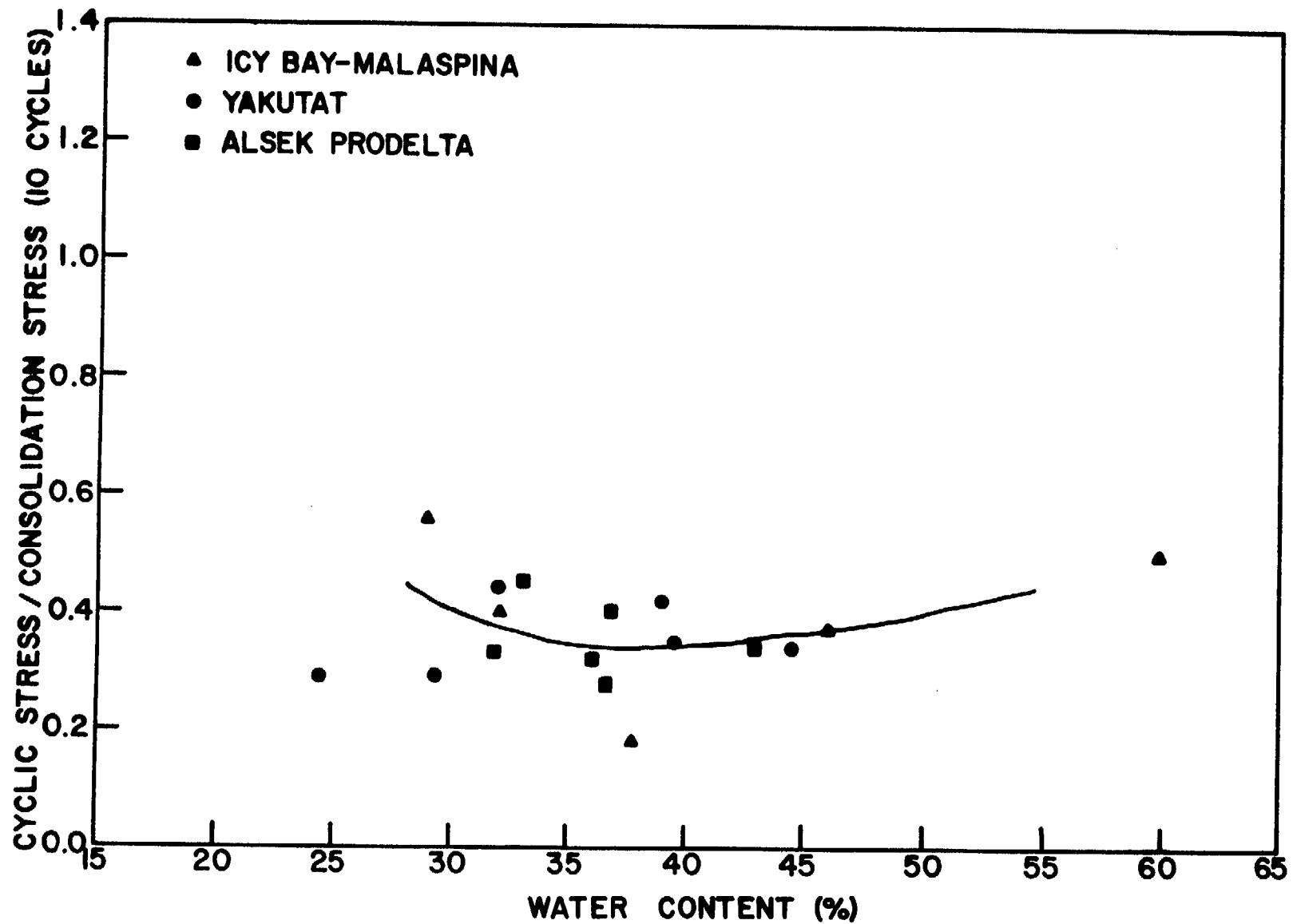


Figure 51. Relative cyclic stress level for failure in 10 cycles versus natural water content, Method III.

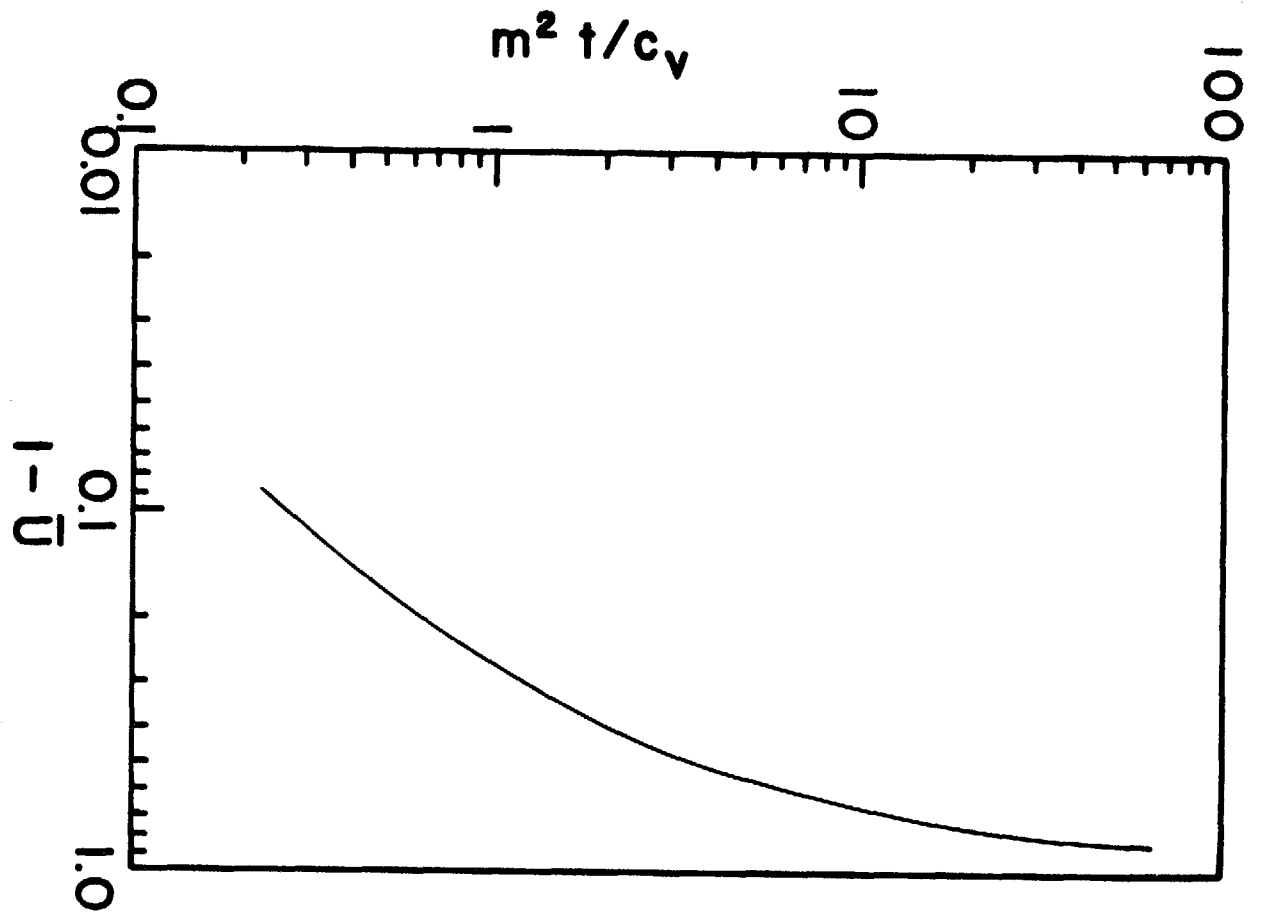


Figure 52. Predicted degree of consolidation (U) at the base of a sediment column that has been deposited at a steady rate, m , for t years (after Gibson, 1958).

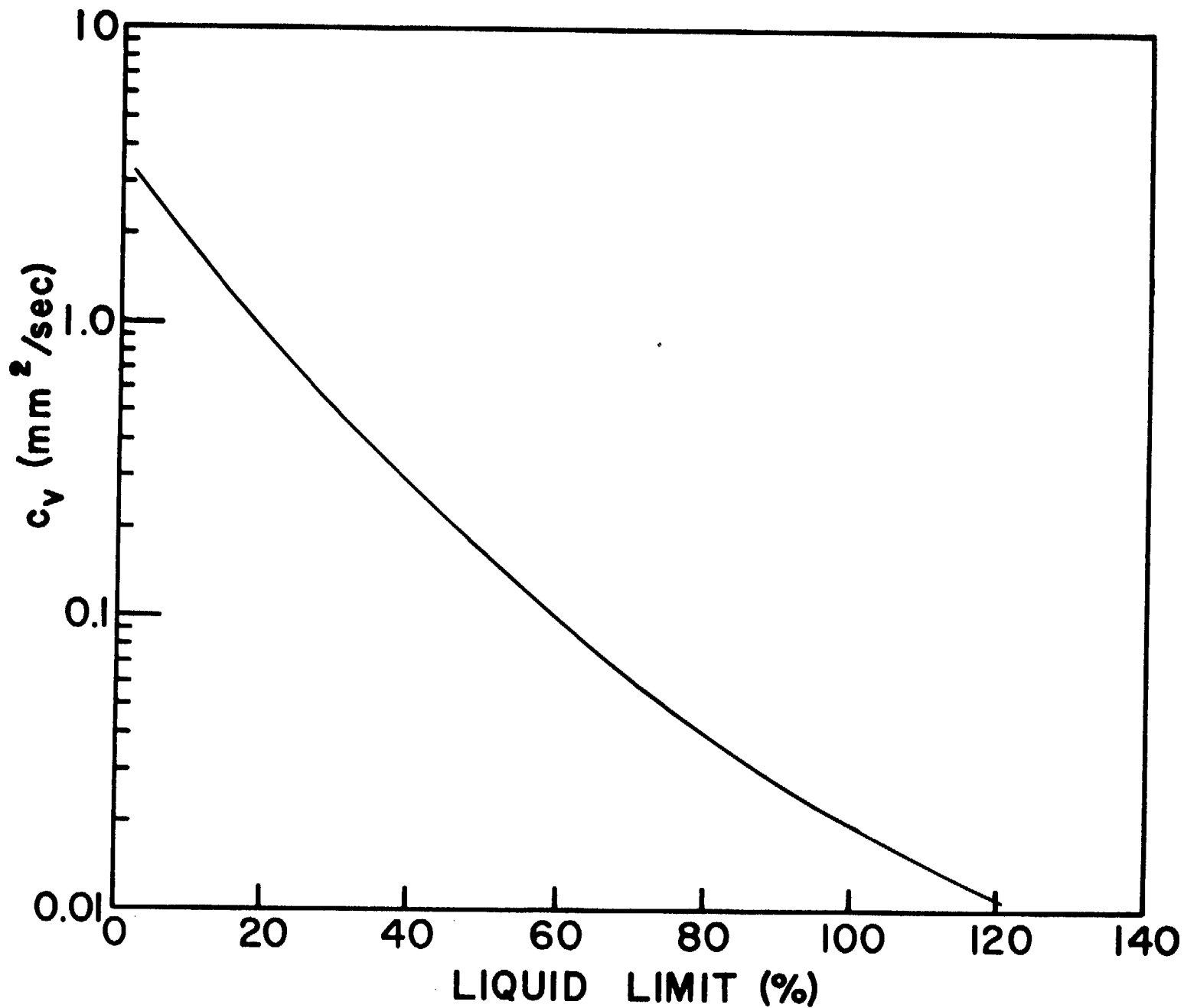


Figure 53. Correlation between coefficient of consolidation (c_v) and liquid limit (after Lambe and Whitman, 1969, p. 412).

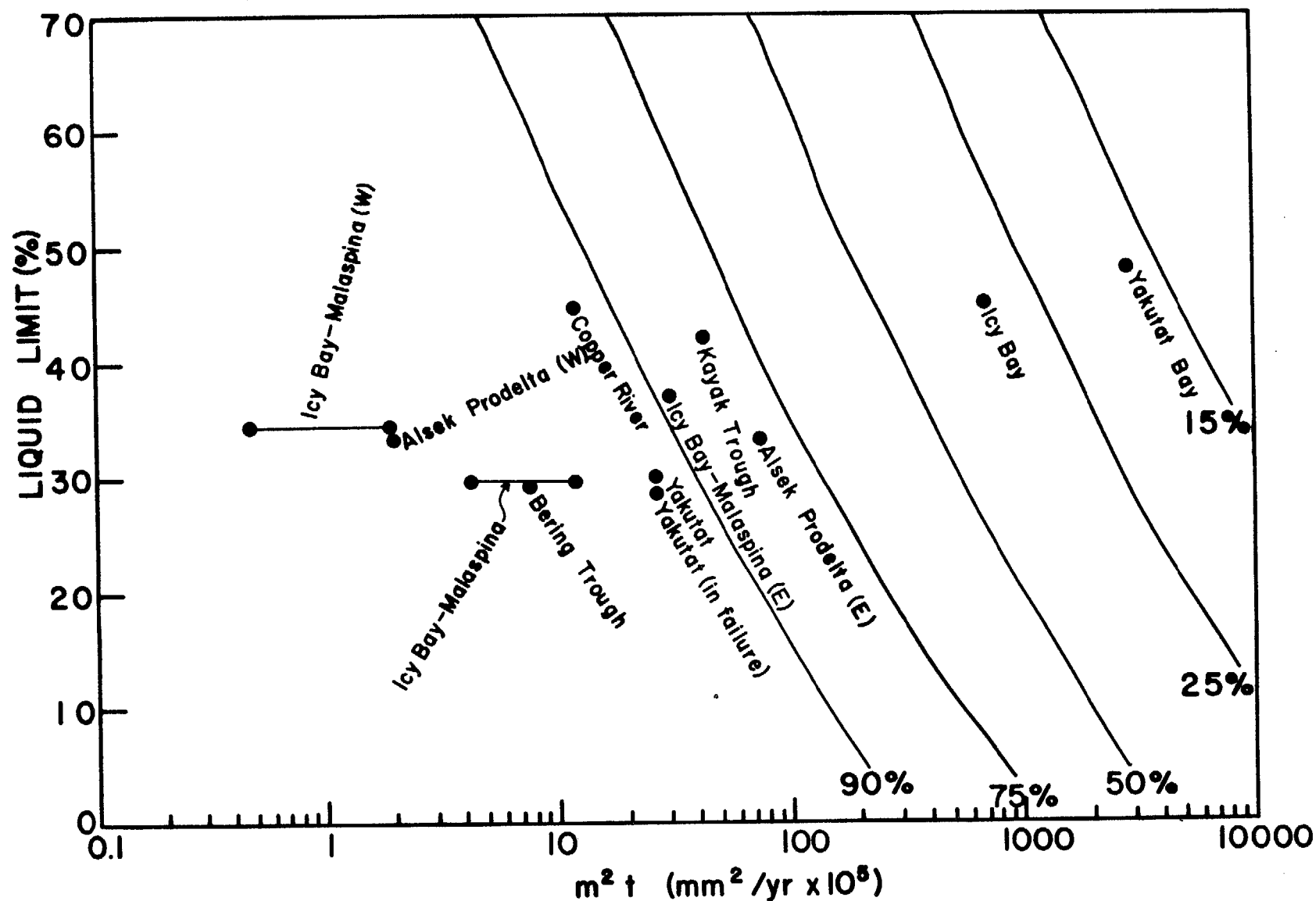


Figure 54. Solid lines represent constant degrees of consolidation, U , predicted by the Gibson (1958) technique. Selected locations in the eastern Gulf of Alaska for which the required parameters were available are shown as data points. Bars indicate a larger segment over which the sedimentation rate varies.

Malaspina and Yakutat

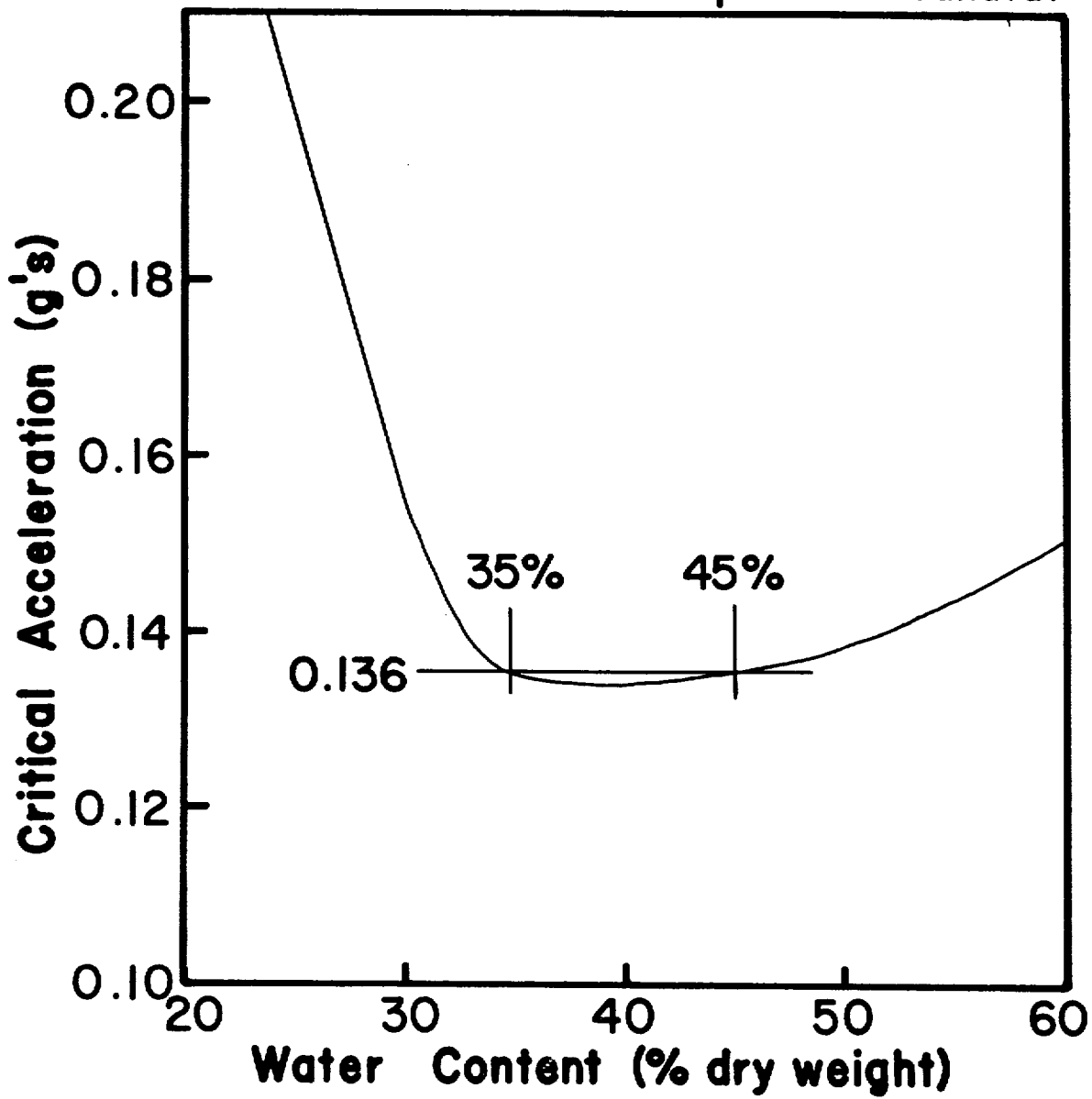


Figure 55. Estimate of critical earthquake acceleration, k , versus natural water content.

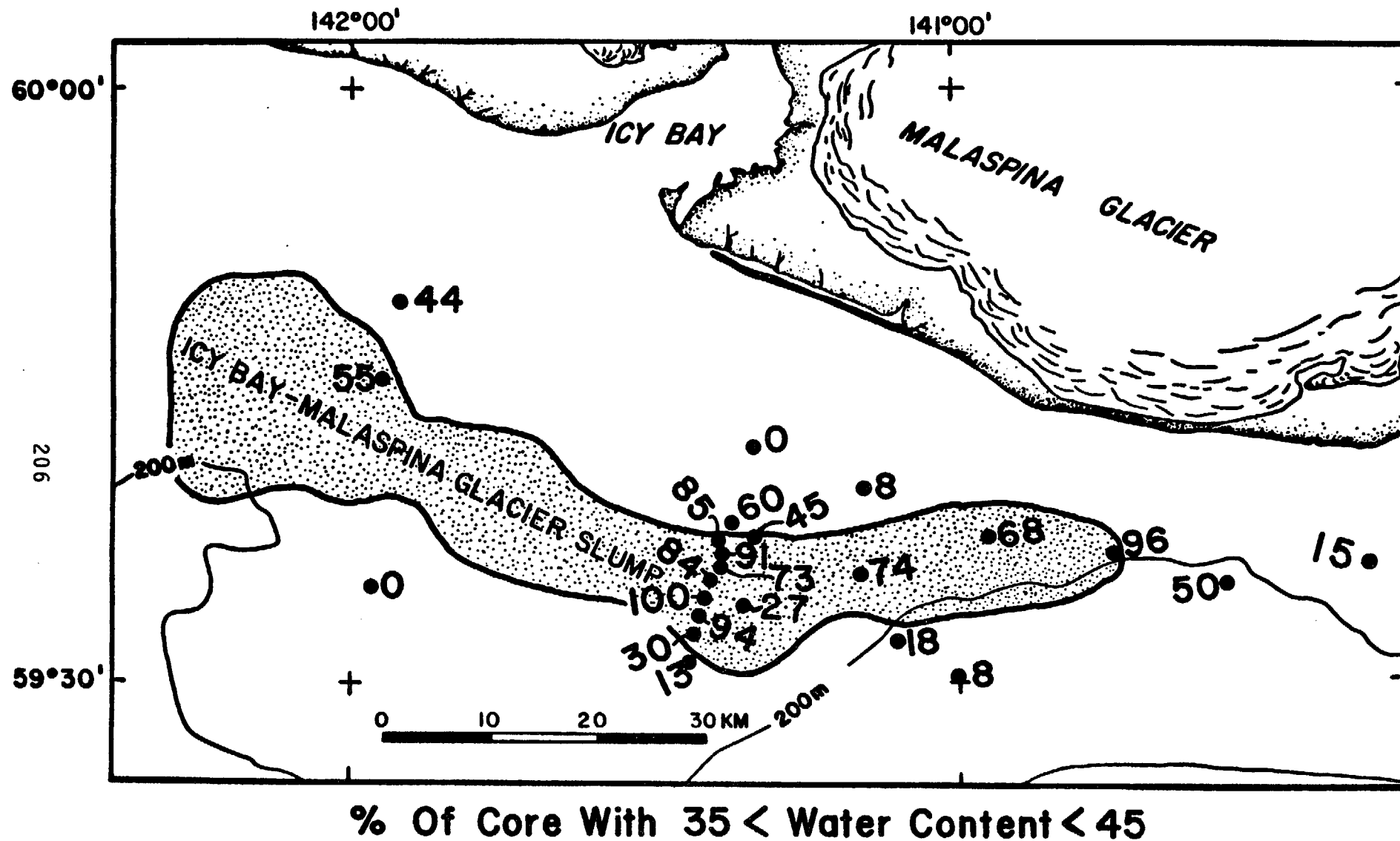
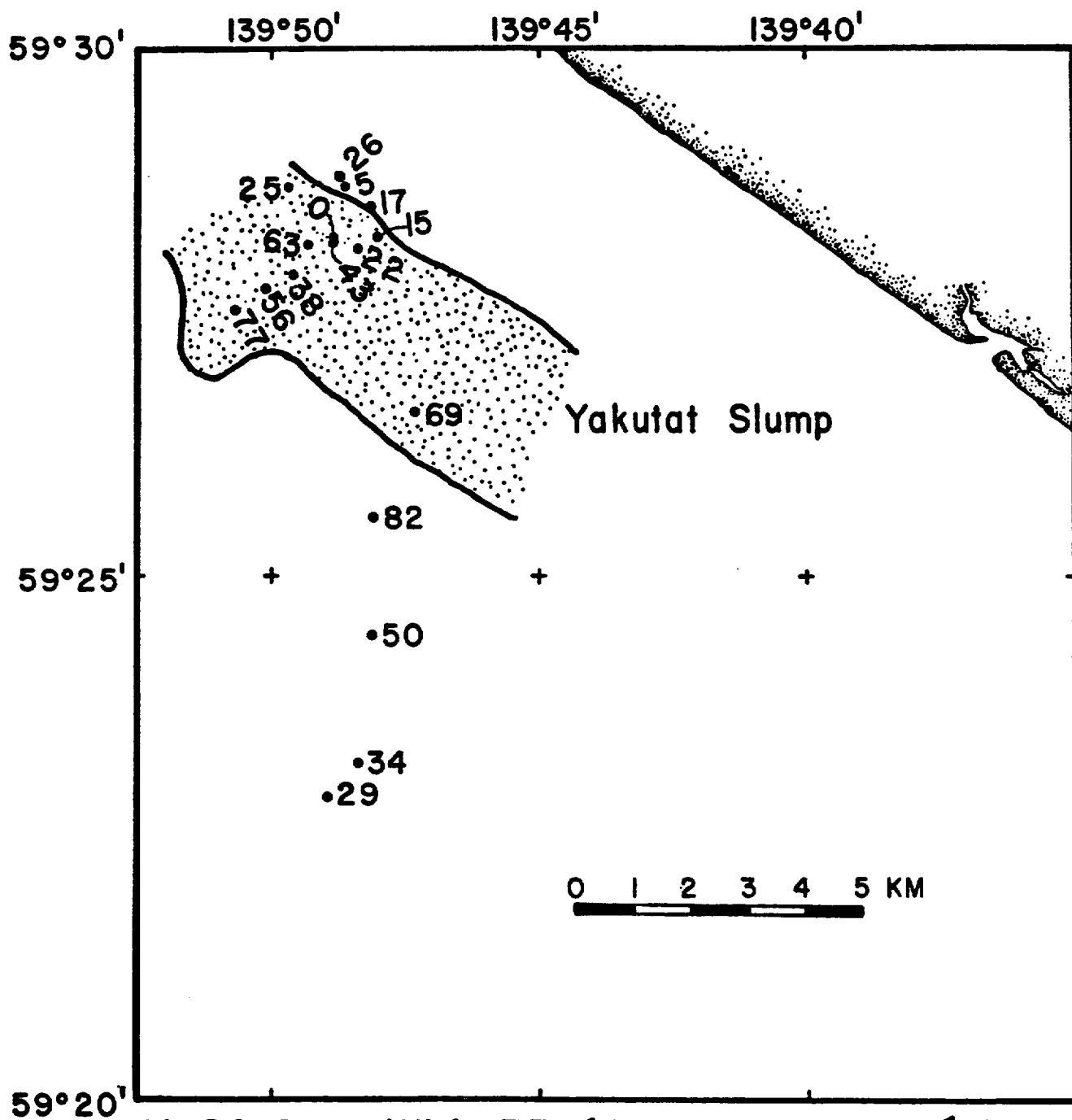


Figure 56. Locations of core samples within the Icy Bay-Malaspina Study Area relative to the observed slump feature. Numbers near the core locations represent the percentage of the core that has a water content in the critical 35% to 45% range.



% Of Core With $35 < \text{Water Content} < 45$

Figure 57. Locations of core samples within the Yakutat Study Area relative to the observed slump feature. Numbers near the core locations represent the percentage of the core that has a water content in the critical 35% to 45% range.

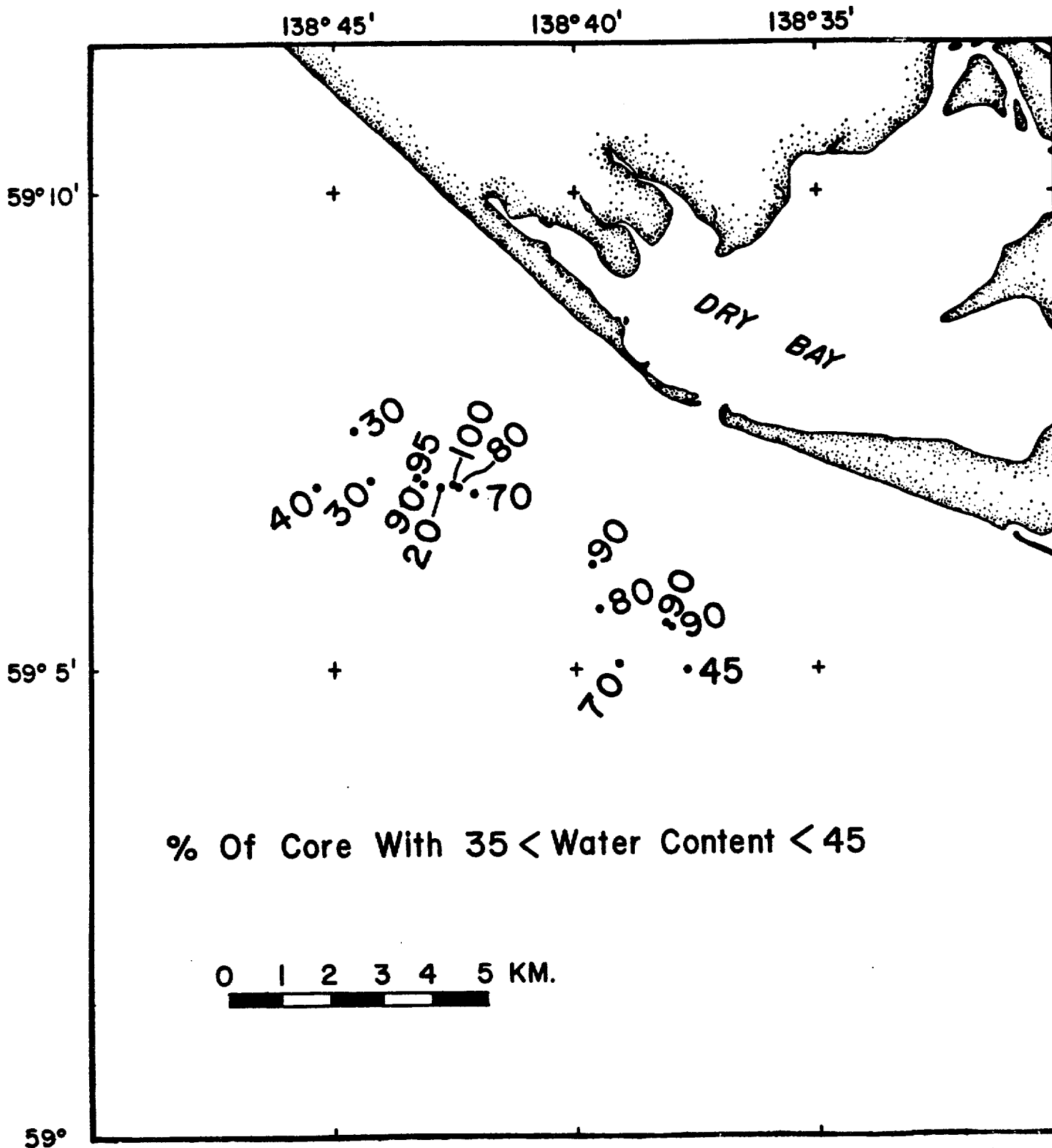


Figure 58. Locations of core samples within the Alsek River Study Area. Numbers near the core locations represent the percentage of the core that has a water content in the critical 35% to 45% range. All cores are thought to be in the failed zone.

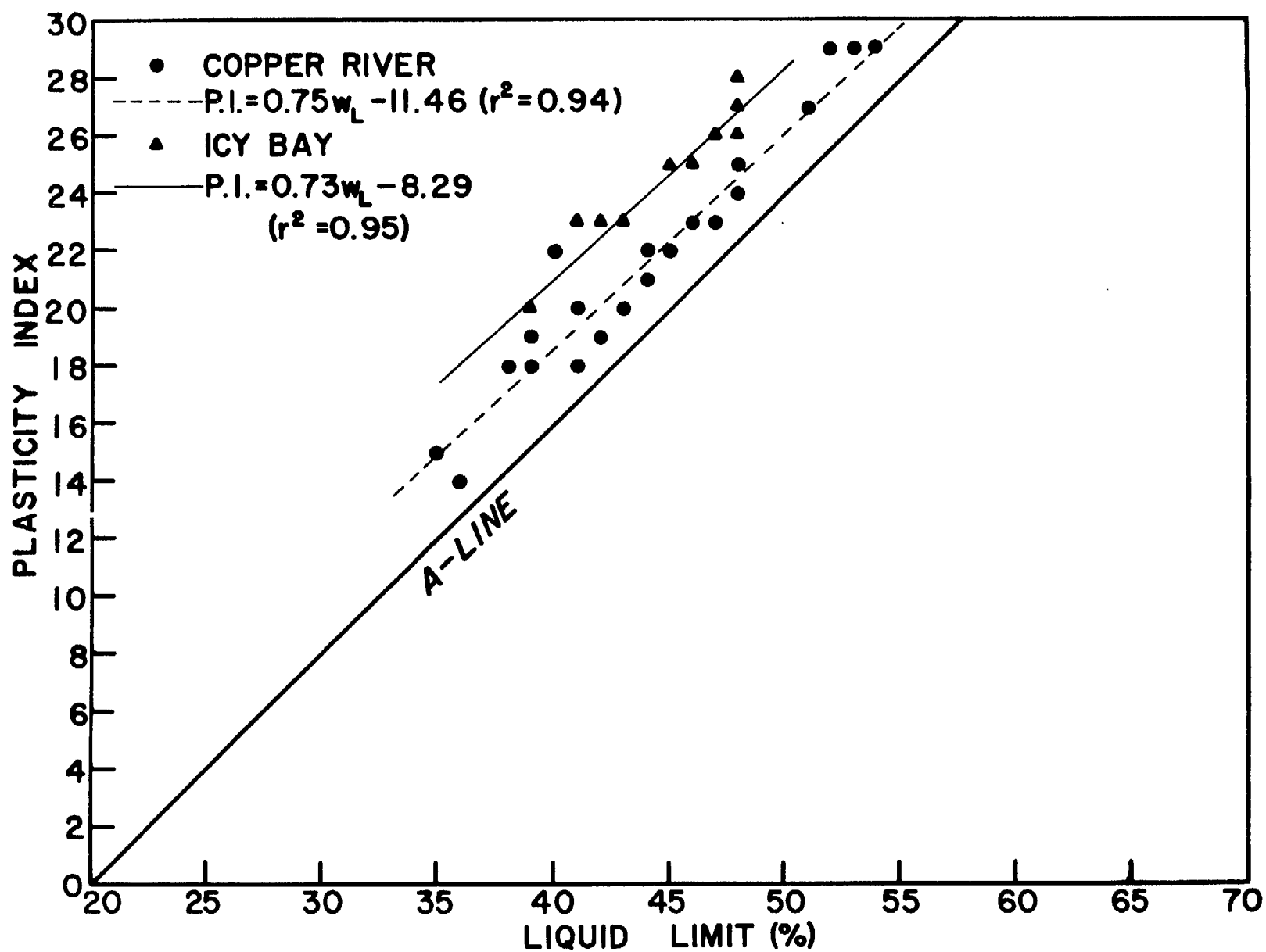


Figure 59. Plasticity chart for Copper River and Icy Bay Study Areas with least squares regression fits of the data.

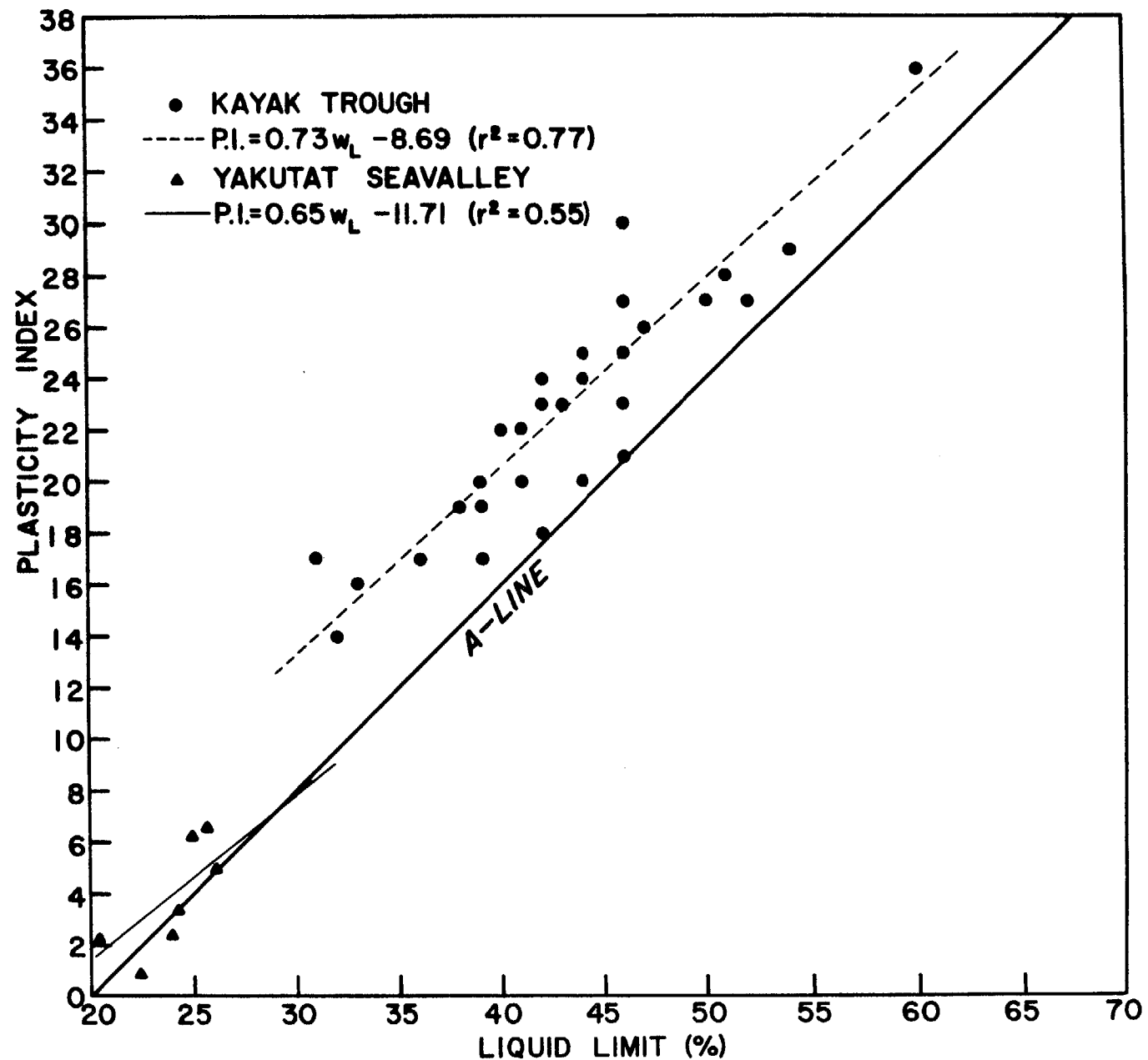


Figure 60. Plasticity chart for Kayak Trough Study Area and Yakutat Sea Valley (SE portion of Icy Bay-Melaspina Study Area) with least squares

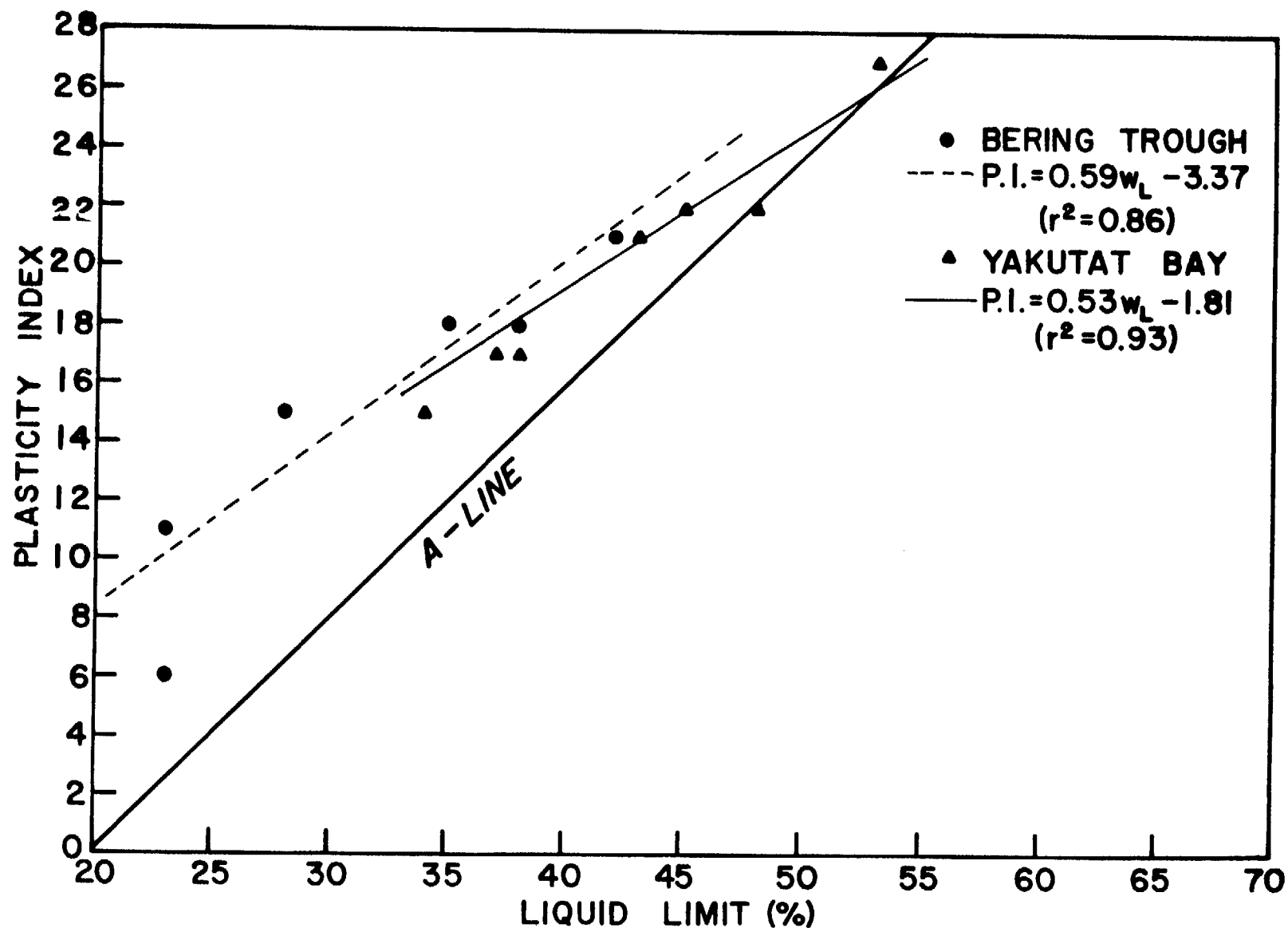


Figure 61. Plasticity chart for Bering Trough and Yakutat Bay Study Areas with least squares regression fits of data.

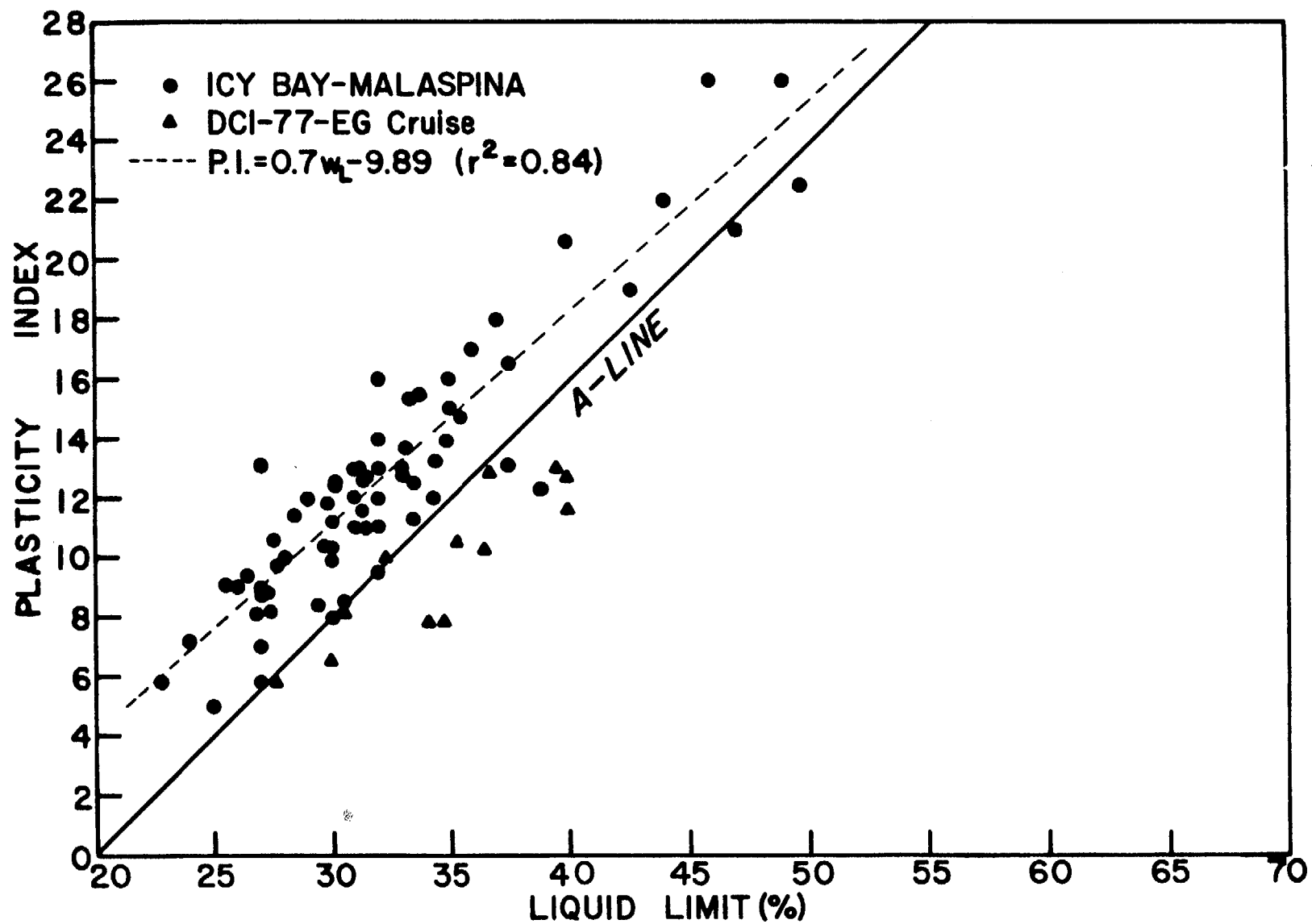


Figure 62. Plasticity chart for Icy Bay-Malaspina Study Area with least squares regression fit of the data (not including Cruise DCI-77-EG data).

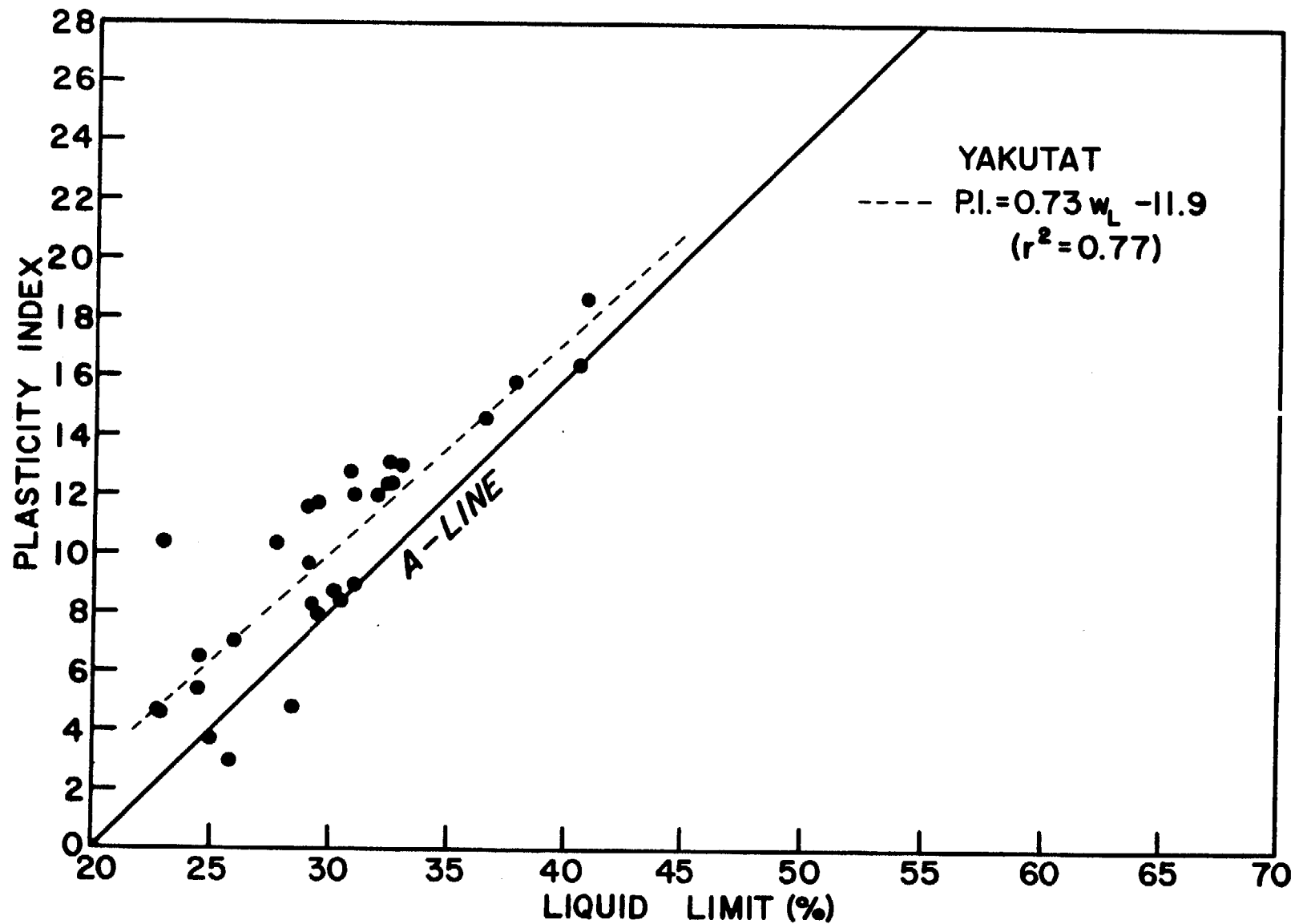


Figure 63. Plasticity chart for Yakutat Study Area with least squares regression fit of data.

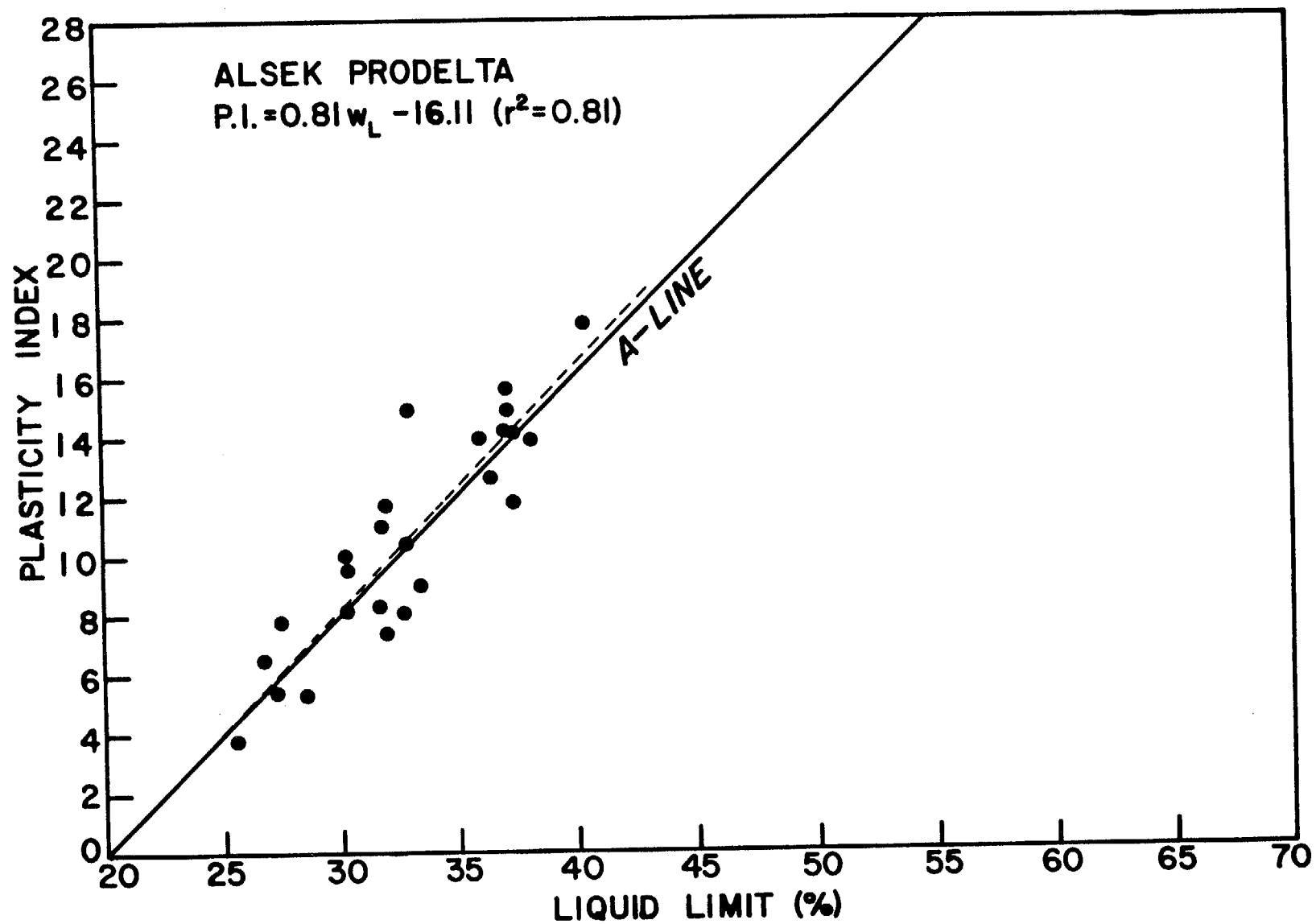


Figure 64. Plasticity chart for Alsek River Study Area with least squares regression fit of data.

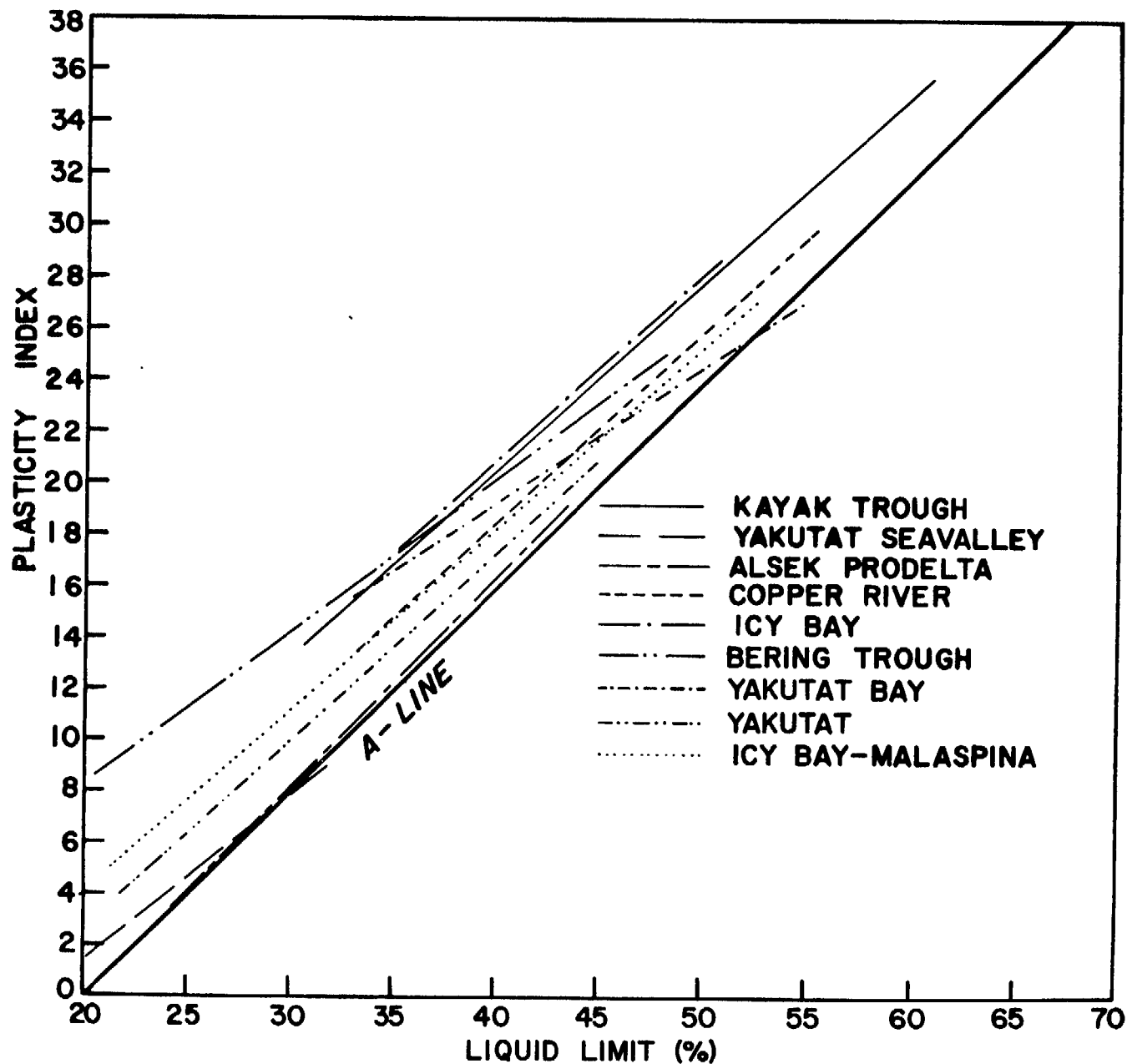


Figure 65. Summary of linear regression fits of plasticity data for the various study areas.

APPENDIX A

METHANE IN SEDIMENTS OF THE EASTERN GULF OF ALASKA

by

Marge Golan-Bat
Keith A. Kvenvolden

Because the presence of interstitial gas may have a significant effect on the stability of sediment, analysis of gas contents can be an important part of an overall hazards evaluation of an area. Accordingly, hydrocarbon gas data from four cruises in the eastern Gulf of Alaska (**S1-76-EG**, **S8-77-EG**, **S6-78-EG**, and **S11-79-EG**) may be applied to this investigation. Although the gases methane, ethane, ethene, propane, propene, **iso-butane**, and n-butane were analyzed, this discussion is limited to the concentrations and distributions of methane. It is the only hydrocarbon gas present in concentrations that may exceed its saturation level in the interstitial water.

During the **S1-76-EG** cruise, 15 samples from 12 stations were taken from Van Veen samples and gravity cores that covered a large area of the eastern Gulf of Alaska, from off the western end of the Copper River Delta to the western end of **Palma** Bay (geographic locations shown in Fig. 1 of the main text). Methane values ranged from the detection level to approximately 60 $\mu\text{l/l}$ wet sediment. Note that these and other gas concentration values reported in this appendix are sample concentrations. The actual gas concentrations in place are probably higher. The highest concentration was found at Station 665 near the mouth of the Copper River. The next highest concentrations (approximately 30 and 40 $\mu\text{l/l}$) were at stations 658 and 659 respectively, east of the southern end of Kayak Island. Discontinuous seismic reflectors and turbid seismic returns were found in this area, suggesting that the sediments are gas-charged. The gas concentrations, although among the highest measured during this cruise, are well below saturation level (which is about 40,000 $\mu\text{l/l}$ at atmospheric pressure): free gas is probably not present in the sediment. During the 1977 cruise, samples taken near these stations measured much higher concentrations of methane as discussed below. At Station 661 in the Kayak Trough Slump the methane concentration was approximately 30 $\mu\text{l/l}$. All other samples from the 1976 cruise had methane concentrations less than 10 $\mu\text{l/l}$.

The **S8-77-EG** cruise concentrated on recovering samples from specific geologic features located in an area from off the east coast of Montague Island to Yakutat Bay. The specific areas involved, from west to east, were: the Hinchinbrook Sea Valley, east of Montague Island; a slump in the Egg Island Trough, southwest of the Copper River Delta; a slump mass in the Kayak Trough, southeast of the Copper River Delta; a zone of faulting southeast of Kayak Island; the Bering trough, off the Bering Glacier; a large slump southwest of Icy Bay; Icy Bay; a slump off the western edge of Malaspina Glacier; Yakutat Bay. Sixty samples from 23 stations were obtained from gravity, piston and hydroplastic cores. Methane values ranged from 0.8 to 19,000 $\mu\text{l/l}$ wet sediment. Most concentrations were equal to or exceeded by a factor of 2 the four highest concentrations measured during the 1976 cruise. Core 14G in the Kayak Trough Slump and Cores 36G and 38G from the Bering Trough had higher concentrations (180, 380. and 180 $\mu\text{l/l}$, respectively) than other cores in this particular area. The concentrations of methane from these samples were not high enough to indicate gas-charged sediment in place, however. At these stations the sediment may have larger concentrations of methane at depth. Core 23G from the zone of faulting southeast of Kayak Island had anomalously high concentrations of methane. This core was taken in the same area as those cores from stations 658 and 659 from the **S1-76-EG** cruise. However, the concentrations obtained from Core 23G were 2,100 $\mu\text{l/l}$ at the surface and 14,000 $\mu\text{l/l}$ at the 100 cm depth. The latter concentration

begins to approach the solubility of methane in water at atmospheric conditions. Because these laboratory values represent a lower bound for the in place concentrations, the concentration of methane at this station in place may in fact have reached or exceeded its solubility. These anomalously high methane values correlate with acoustic anomalies attributed to gas-charged sediments; the presence of gas may affect the stability of the sediment southeast of Kayak Island.

The **S6-78-EG** cruise recovered 17 samples from Van Veen samplers and gravity cores. The area covered included 5 main localities: Icy Bay and a slump off the western edge of the Malaspina Glacier, both areas covered during the **S8-79-EG** cruise; off the Dangerous River and just east of Dry Bay, both areas which were later covered during the **S11-79-EG** cruise; and an area beyond the 200 m bathymetric contour situated southwest of Lituya Bay, that was not sampled during any other cruise. These methane values ranged from about 1 to 48 $\mu\text{l/l}$ wet sediment from sediments up to a depth of 296 cm. Core 13A in Icy Bay represents the upper limit of this range and is similar to the concentrations obtained in 1977. Four cores (8A, 8B, 9B, and 12B) from off the western edge of Malaspina Glacier ranged from 21 to 40 $\mu\text{l/l}$ wet sediment, which is also similar to the concentrations obtained in the 1977 cruise. Three cores off the Dangerous River (3, 4, and 5) had low concentrations of methane, averaging 1.4 $\mu\text{l/l}$ wet sediment. The **S11-79-EG** cruise the next year confirmed these low concentration levels in 4 cores (3, 5, 6, and 26) which averaged 7.0 $\mu\text{l/l}$ wet sediment. Core 1 just east of Dry Bay indicated a very low concentration of methane (1.4 $\mu\text{l/l}$) similar to 7 of 8 cores taken in that area on the **S11-79-EG** cruise. The concentrations averaged 12 $\mu\text{l/l}$ wet sediment. Two cores (10A and 11A) were taken beyond the 200 m bathymetric level southwest of Lituya Bay and averaged 3.0 $\mu\text{l/l}$ wet sediment.

The **S11-79-EG** cruise concentrated on 3 main localities: off the Dangerous River, off Dry Bay and just east of Dry Bay. Thirty-seven samples were obtained from 17 vibracores and gravity cores. Methane concentrations ranged from just detectable to 33,000 $\mu\text{l/l}$. In eight cores (1, 2, 11, 16, 20, 21, 26 and 30) the amount of methane was greater than 10 but less than 64 $\mu\text{l/l}$, a range of values similar to those observed on the **S1-76-EG** and **S6-78-EG** cruises. Except for one core the methane concentrations at the other stations were less than 10 $\mu\text{l/l}$. Core 14 at a site just east of Dry Bay was anomalous. At the 80-90 cm depth interval, the concentration of methane was approximately 32,800 $\mu\text{l/l}$ wet sediment, a value which nearly equals the solubility of methane in the interstitial water at atmospheric conditions. This high concentration of methane may indicate gas-charging which would affect the stability of the sediments.

Anomalously high concentrations of methane suggesting the presence of gas-charged and, therefore, unstable sediments, were found in only two areas: a fault zone southeast of Kayak Island and east of Dry Bay. Sediments from near the mouth of the Copper River, from the Kayak Trough, and from east of Kayak Island had significant amounts of methane, but the amount measured was insufficient to indicate that the sediments in place were, indeed, gas-charged. Deeper sediments in the area may be gas-charged, however. There appears to be no good correlation between the occurrence of seismic anomalies and the possible presence of sampled gas-charged sediment except for the sediment southwest of Kayak Island.

Methane in Sediments of the Eastern Gulf of Alaska-Sample Locations.

<u>Cruise</u>	<u>Sample or station</u>	<u>Latitude</u>	<u>Longitude</u>
S1-76-EG	658B	59°47.19'N	144°28.83'W
	659B	59°49.40'N	144°28.03'W
	661	60°06.20'N	144°40.30'W
	665	60°08.20'N	145°00.00'W
S8-77-EG	14G	60°05.12'N	144°40.44'W
	23G	59°50.75'N	144°24.26'W
	36G	59°56.64'N	143°35.75'W
	38G	59°58.05'N	143°38.00'W
S6-78-EG	1	59°02.70'N	138°22.80'W
	3	59°17.70'N	139°16.60'W
	4	59°17.35'N	139°15.90'W
	5	59°16.95'N	139°14.30'W
	8A	59°36.50'N	140°55.50'W
	8B	59°36.20'N	140°56.00'W
	9B	59°37.40'N	140°55.70'W
	10A	57°55.01'N	138°04.89'W
	11A	57°55.36'N	138°04.19'W
	12B	59°36.80'N	140°55.80'W
	13A	59°55.97'N	141°32.27'W
S11-79-EG	1	59°06.08'N	138°42.36'W
	2	59°06.00'N	138°42.17'W
	3	59°16.33'N	139°12.29'W
	5	59°17.49'N	139°16.10'W
	6	59°17.74'N	139°17.31'W
	11	59°03.53'N	138°25.32'W
	14	59°02.21'N	138°25.50'W
	16	59°05.95'N	138°38.97'W
	20	59°05.81'N	138°42.01'W
	21	59°02.45'N	138°25.38'W
	26	59°17.27'N	139°16.03'W
	30	58°59.84'N	138°43.51'W

APPENDIX B

RELATIVE IMPORTANCE OF SEISMIC AND STORM WAVE LOADING

The Gulf of Alaska is susceptible to both high seismicity (Stephens and Page, 1982) and large storm waves (Bea, 1976). This appendix provides a brief discussion of the factors influencing cyclic loading dominance and develops a quantitative estimate of the water depth separating storm wave and earthquake control.

One way of separating earthquake and wave control is to determine the water depth at which the shearing stresses developed by peak storm waves equal the shearing stresses developed by a critical earthquake. Modifying Equation (2) from the main text for a horizontal bottom, we obtain:

$$\tau/\sigma_v' = k\gamma/\gamma' \dots\dots\dots (B-1)$$

where τ is the shearing stress generated by an earthquake with a critical acceleration, k .

As shown in the main text, the critical acceleration corresponding to many of the failure features (including the Icy Say-Malaspina slump in water depths ranging from 75 to 175 m) is **0.136g** (Figure 55). Assuming that failures in relative deep water are earthquake induced, this critical value of k can be used to estimate a representative level of shearing stress developed by major earthquakes in the area. For typical sediment densities ($\gamma=1.8 \text{ g/cm}^3$ and $\gamma'=0.8 \text{ g/cm}^3$), Equation (B-1) yields $\tau/\sigma_v'=0.306$ for major earthquakes.

Seed and Rahman (1978) provide the following equation for shearing stresses near the seafloor surface produced by large storm waves:

$$\tau/\sigma_v' = [\pi\gamma_w H] / [\cosh(2\pi d/L)\gamma' L] \dots\dots\dots (P-2)$$

where γ_w =unit weight of water
 d =water depth
 H =wave height
 L =wave length

The maximum probable storm wave for the area (Bea, 1976) is 37 m, corresponding to a very limited number of waves. For a longer series of waves, we assumed 30 m as a more realistic maximum wave height. Because the solution is fairly independent of wave length, any reasonable choice of wave length is satisfactory. We assumed a representative value of 300 m. Inserting these values into Equation B-2 and solving for the water depth, d , necessary to produce shearing stresses comparable to those produced by earthquakes ($\tau/\sigma_v'=0.306$ from Fig. 35 in the main text) yields a critical water depth of 35 m. Therefore, in water depths shallower than 35 m, major storms would **produce** shearing stresses greater than major earthquakes would induce. In greater water depths earthquakes would produce the greater stresses.

Equating stress levels does not completely determine the level at which the influence of major earthquakes and waves is equal. Waves produce a much larger number of critical cycles than earthquakes and would cause a greater level of strength degradation under completely undrained conditions. That is, waves might cause the same damage at a lower stress level than that produced

by an earthquake. Judging by the extensive data base of Lee and Focht (1976), the strength degradation factor, AU, might be reduced by up to 50% if 1000 cycles were considered rather than 10. Under fully undrained conditions and a major storm with 1000 cycles, the stress level required to cause the same damage as the representative major earthquake for the area would be only one-half as much as that induced by the earthquake. **That** is, a value of $\tau/\sigma_v' = (0.5)(0.306) = 0.153$ would be needed. The water depth at which earthquakes and waves would cause the same level of damage would drop to 76 m, as calculated from Equation (B-2).

The 76 m level is the deepest for which storm waves and earthquakes could be equivalent. The water depth at which earthquakes and waves would cause the same level of failure is probably shallower because some drainage of pore pressures during a storm would be expected (Seed and Rahman, 1978). If enough drainage were to occur, the level of equivalence could even be shallower than the 35 m calculated for equivalent stresses. Because the glacial marine sediment is silty and drains fairly easily, the 35 m level is probably a good estimate of the depth of equivalent damage; the depth could drop to as deep as 76 m under special circumstances.

APPENDIX C

INDEX PROPERTIES

APPENDIX C. INDEX PROPERTIES

This Appendix presents **downcore** profiles of all the index property measurements. The profiles are organized by study area ordered from west to east. Within study areas the profiles are ordered by core number. **The** measurements include laboratory original and remolded vane shear strength, natural water content, liquid and plastic limits, grain density, and grain size (as percent sand, silt, and clay). Also shown are locations of consolidation or triaxial tests. **The** identification number indicates the type of test and the testing organization. The nature of these tests is indicated by a coded test number. **The** code for the test numbering system is as follows:

First two letters:

- (a) OE - Oedometer test
- (b) CE - Constant rate of strain (**CRS**) consolidation test
- (c) TE - Static triaxial test
- (d) TC - or D - Cyclic triaxial test

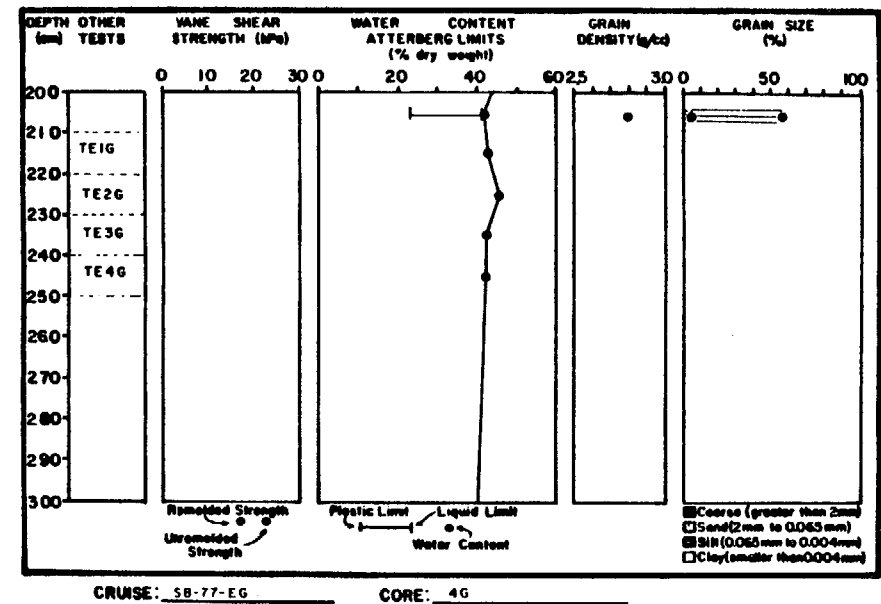
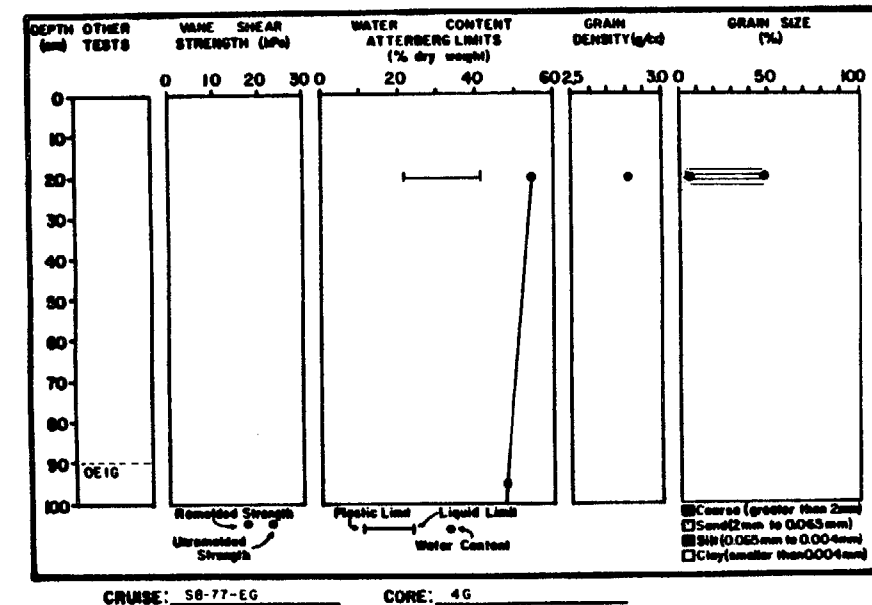
Trailing characters:

- (a) No trailing characters - test performed by the USGS
- (b) L1 - Test of 1977 core sample by Law **Engineering** and Tasting Company
- (c) G - Test of 1977 sample by Geotechnical Engineers, Incorporated
- (d) B - Test of 1977 sample by University of California, Berkeley
- (e) L2 - Test of 1980 sample by Law Engineering and Testing Company

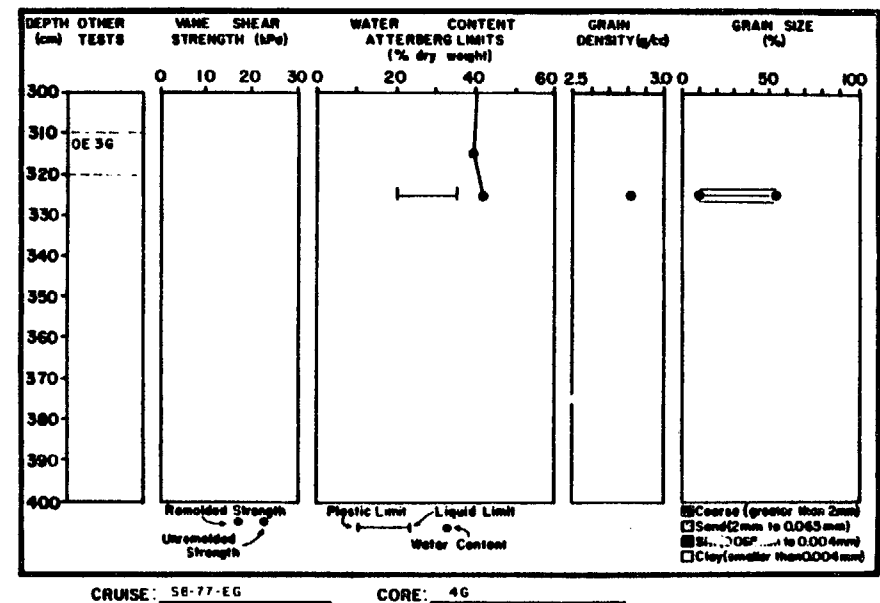
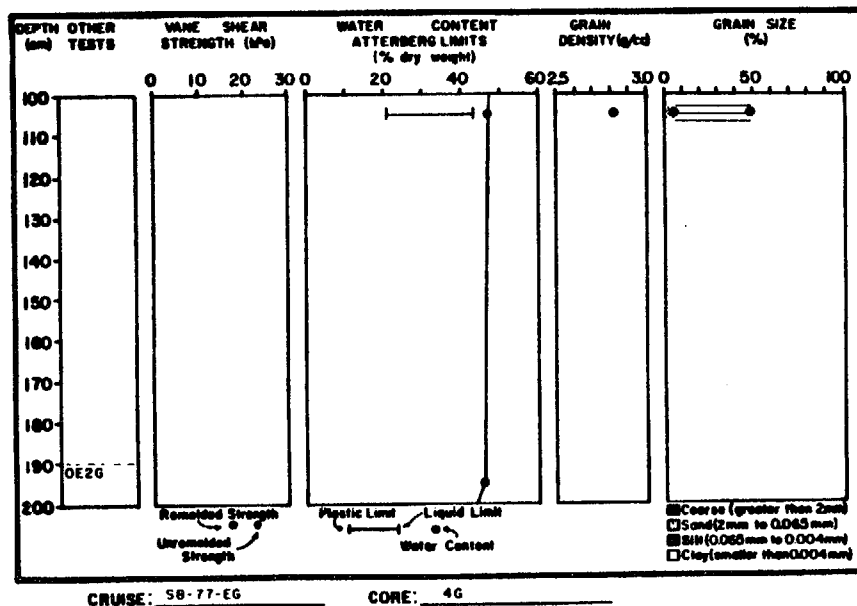
These consolidation and triaxial test results are presented in Appendices D through G and are grouped according to the organization performing the test.

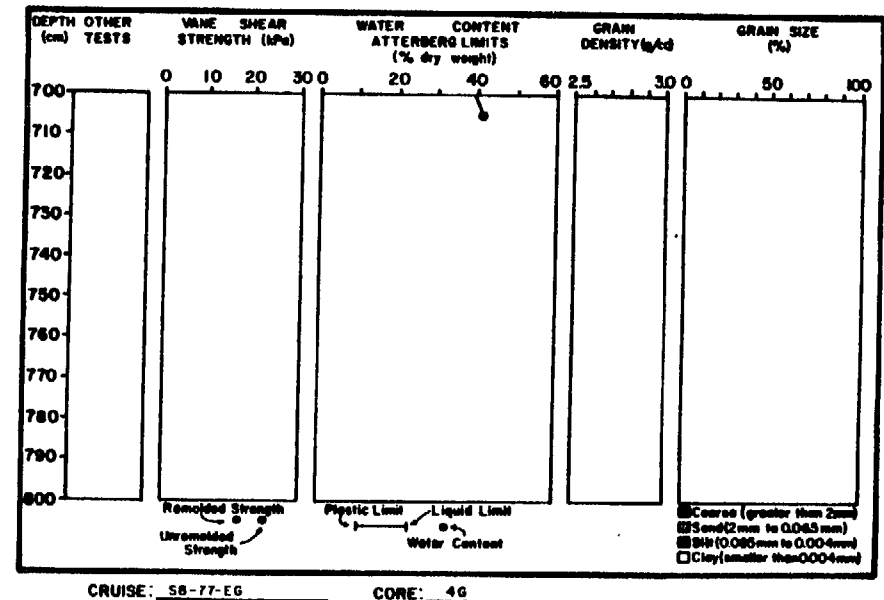
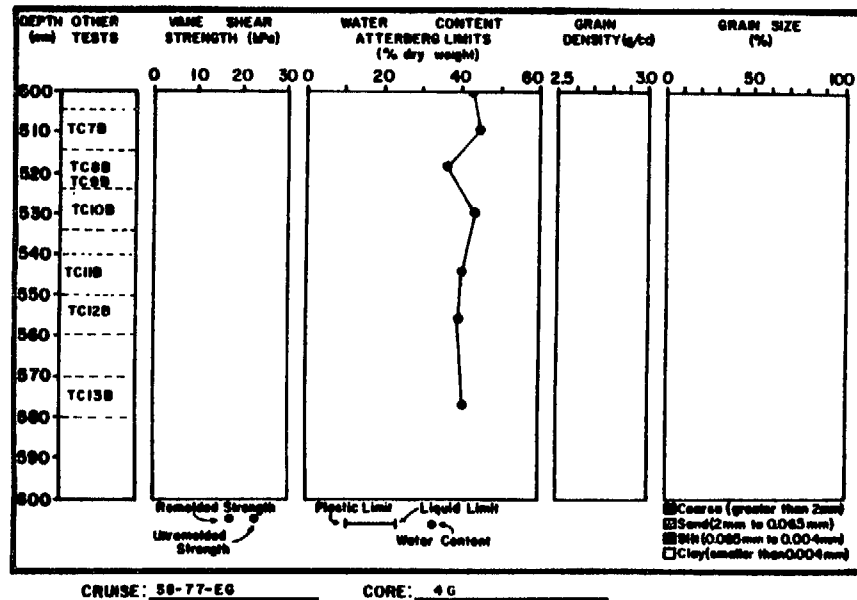
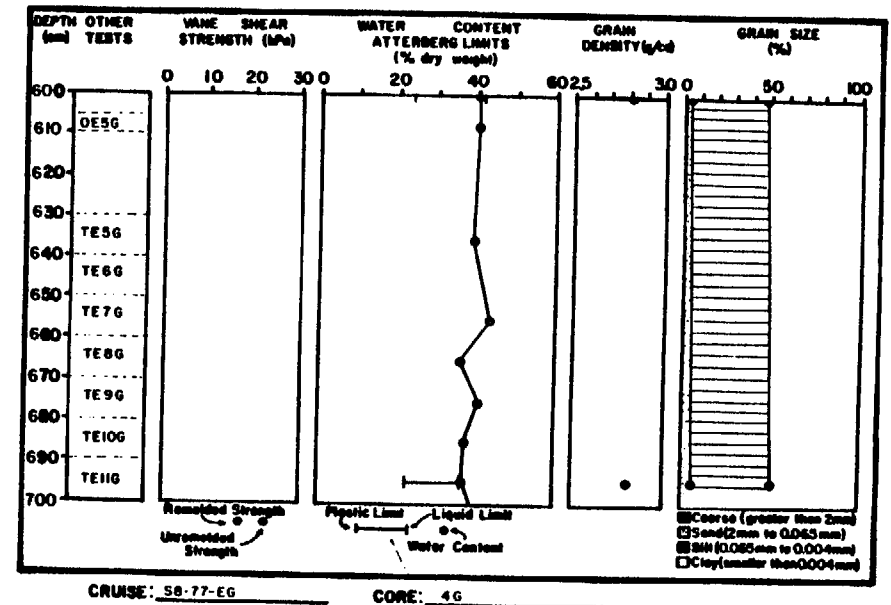
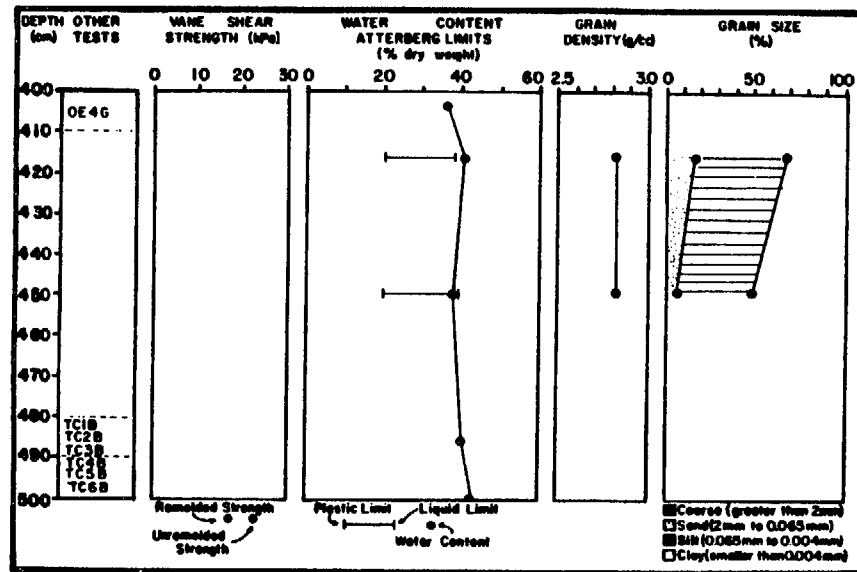
The water contents from **Cruise DC1-77-EG (Carlson and others, 1978)** appear to have been calculated incorrectly, possibly through a faulty computer program. The error is indicated in Figure 62 in which the Atterberg limits for **DC1-77-EG** plot in a distinctly different section of the plasticity chart from that in which the results of tests from other cruises to the same area plot. Because of this discrepancy, water contents from **DC1-77-EG** were not shown in Figure 56.

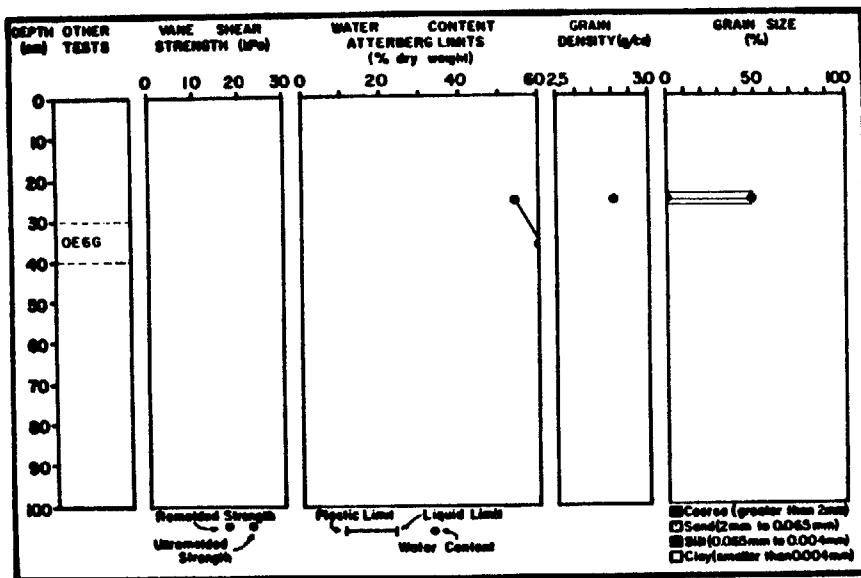
COPPER RIVER STUDY AREA



232

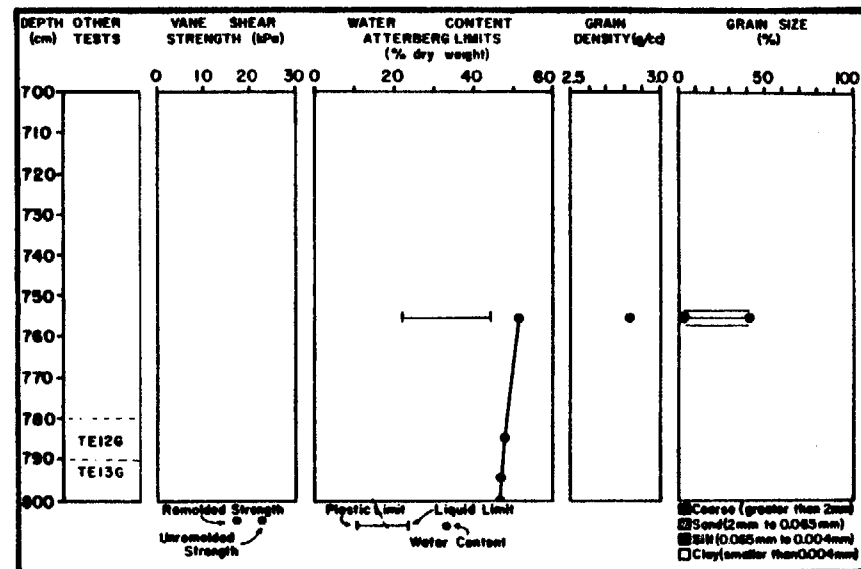






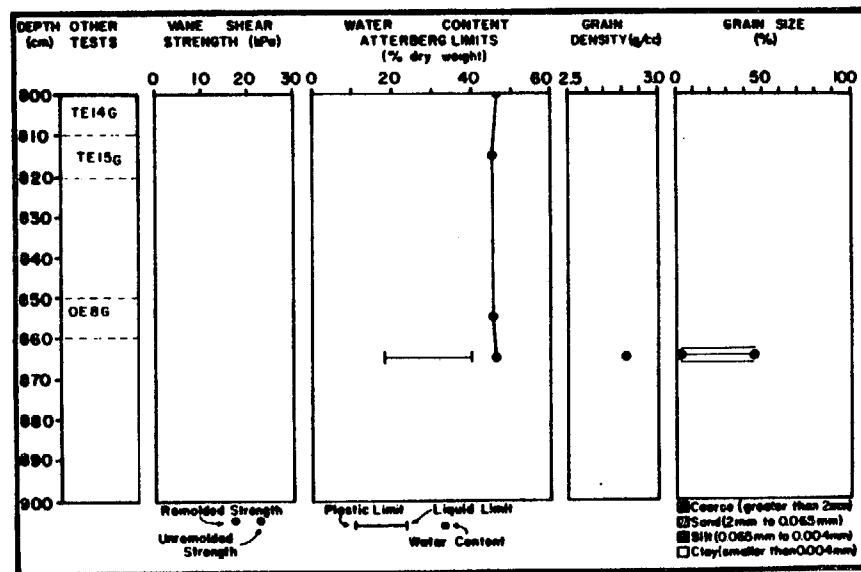
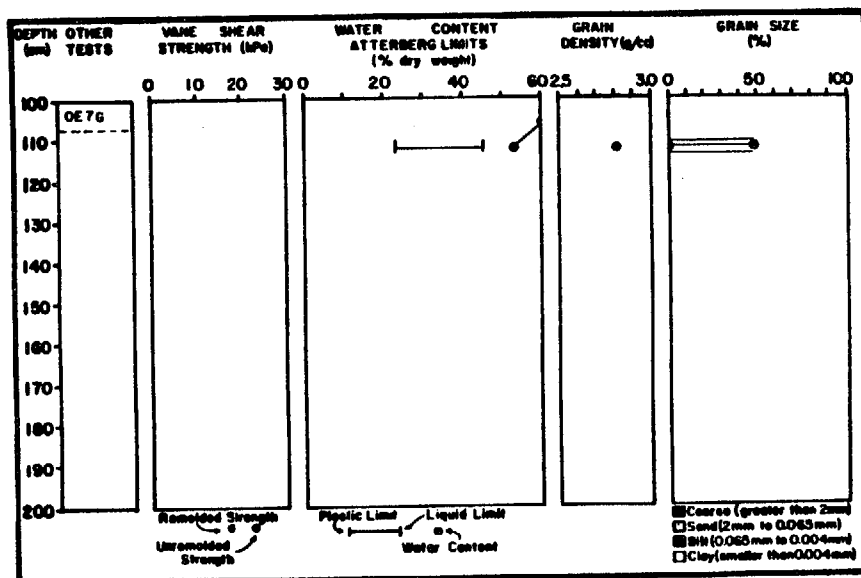
CRUISE: 58-77-EG

CORE: 6G



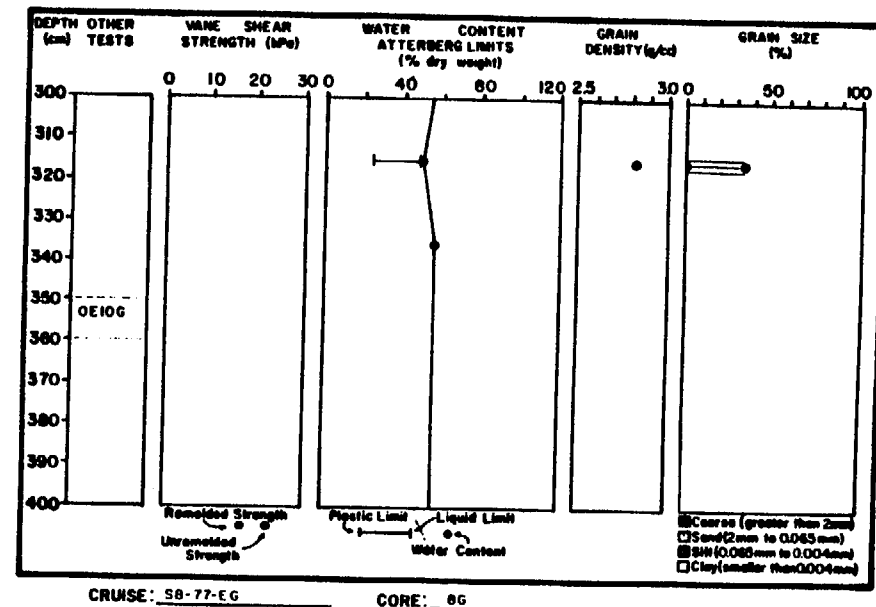
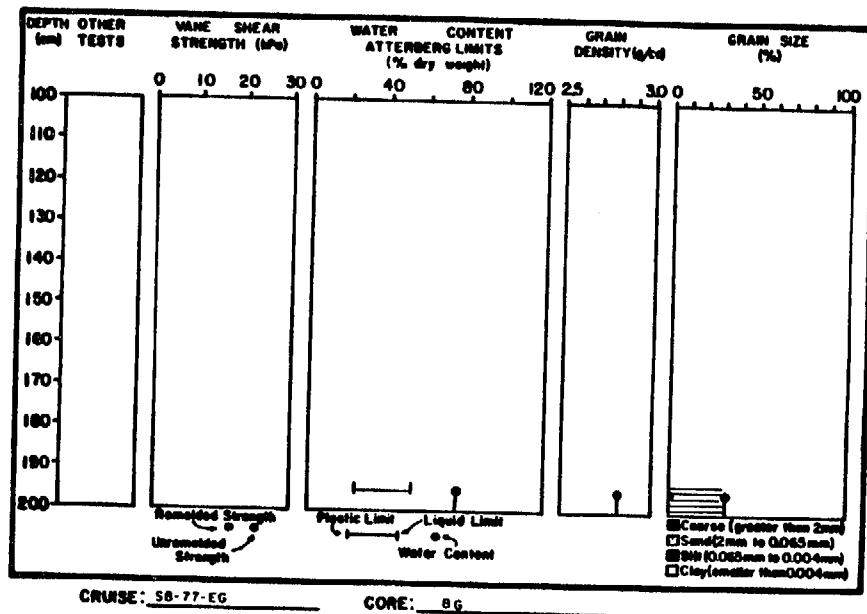
CRUISE: 58-77-EG

CORE: 7G

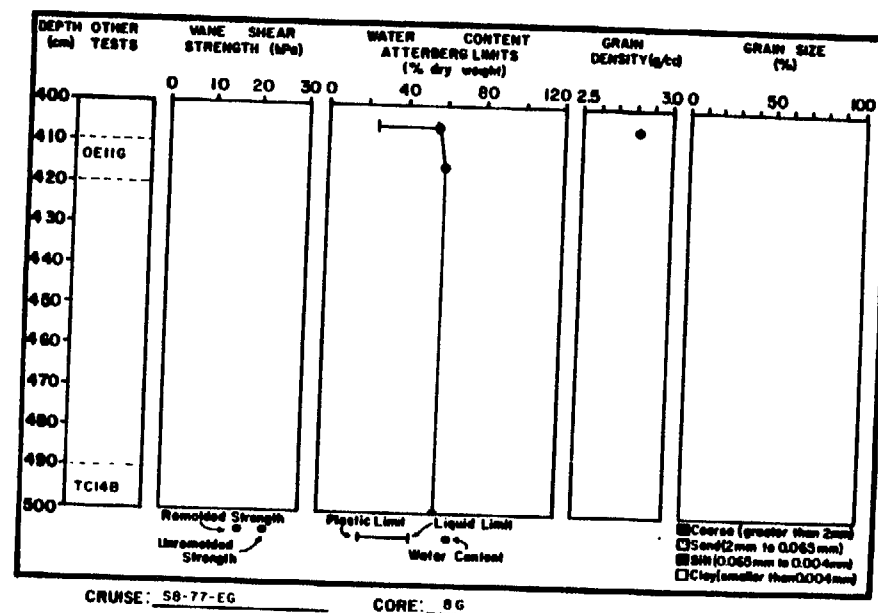
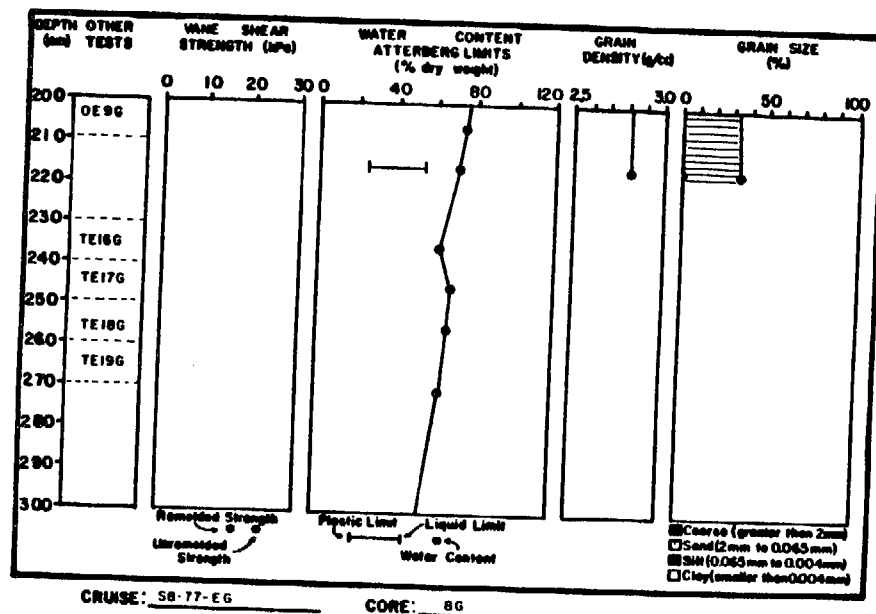


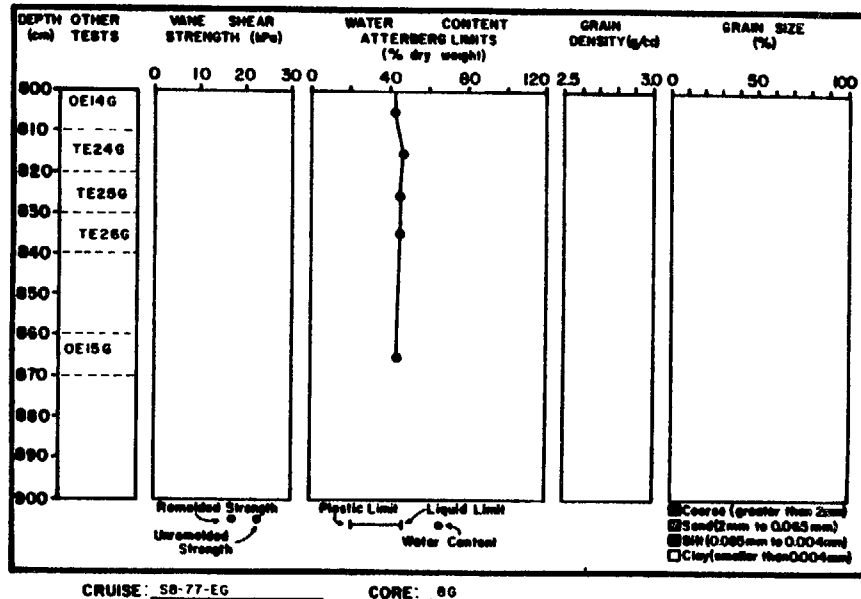
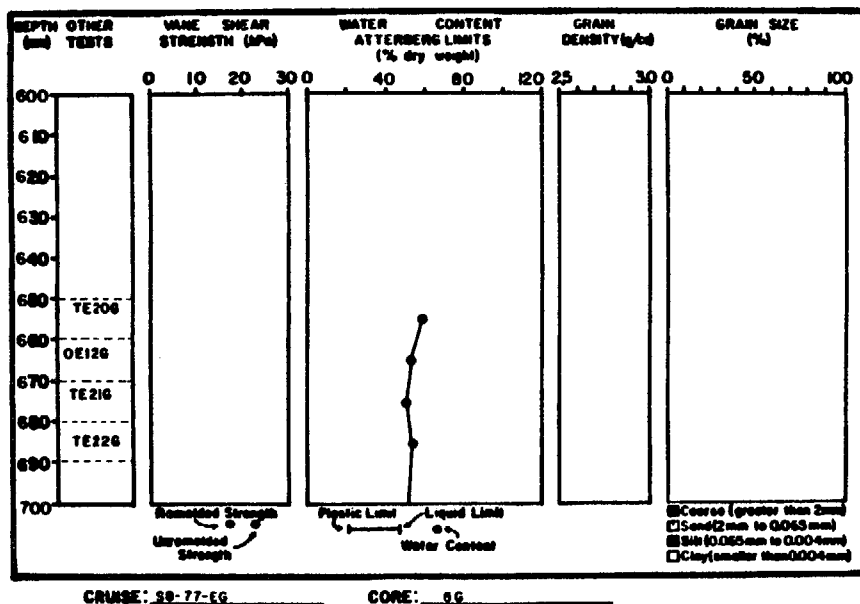
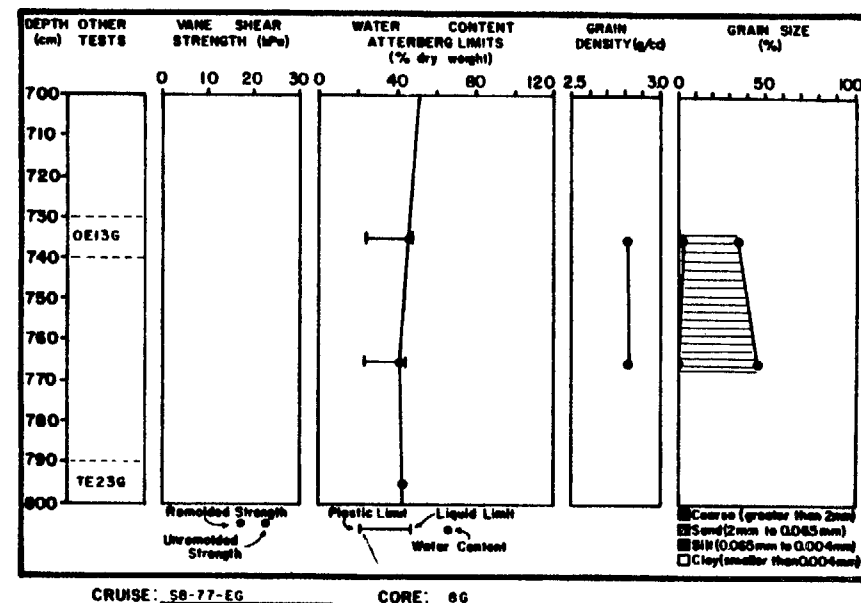
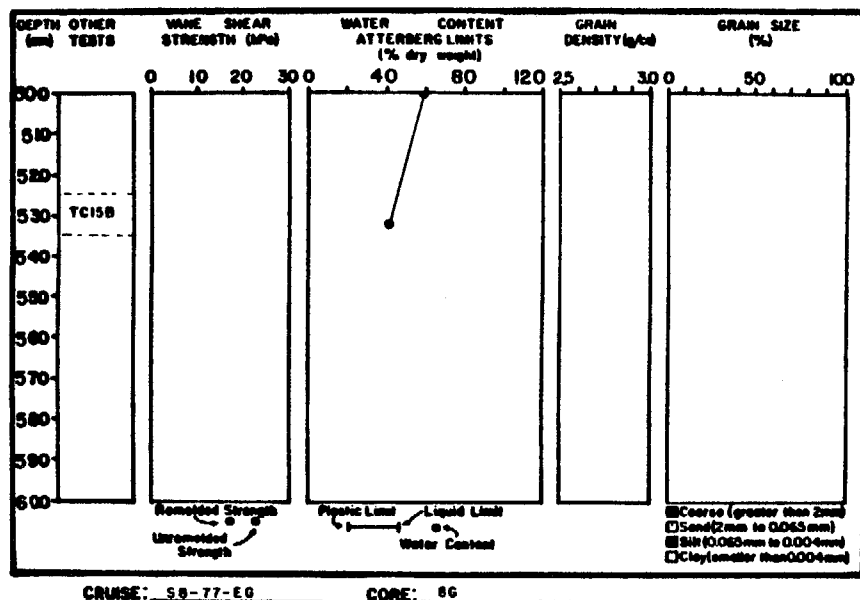
CRUISE: 58-77-EG

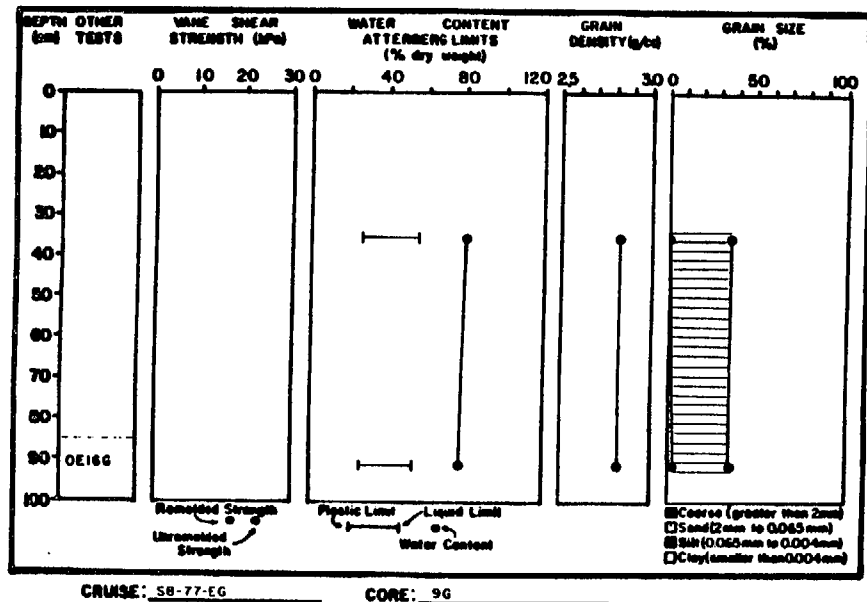
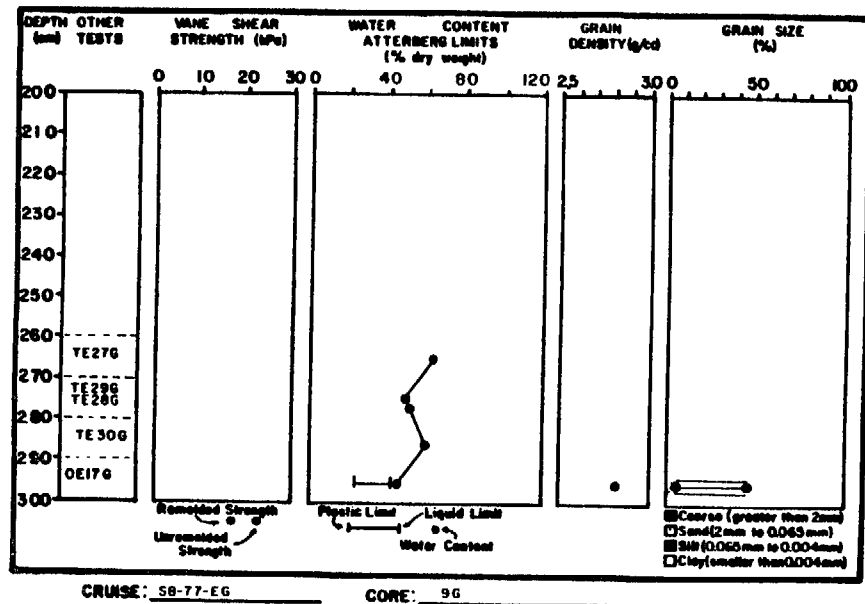
CORE: 7G



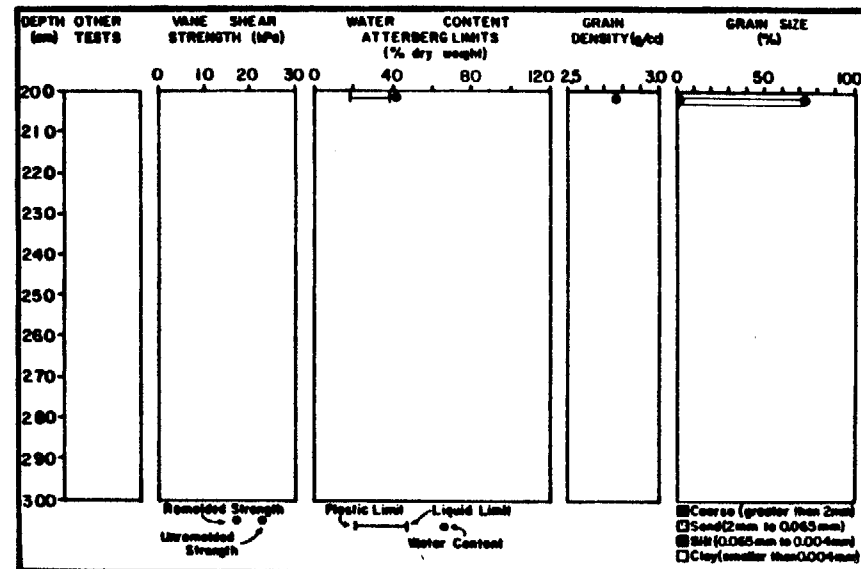
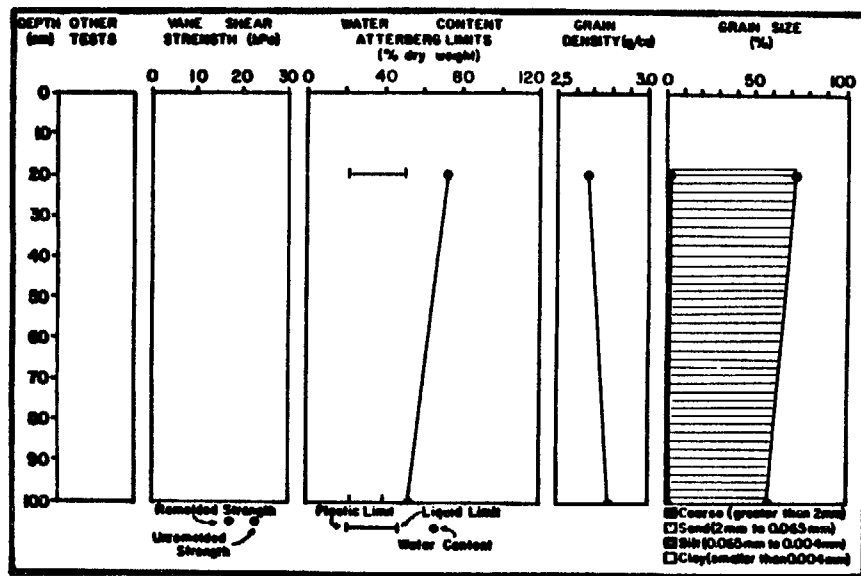
235



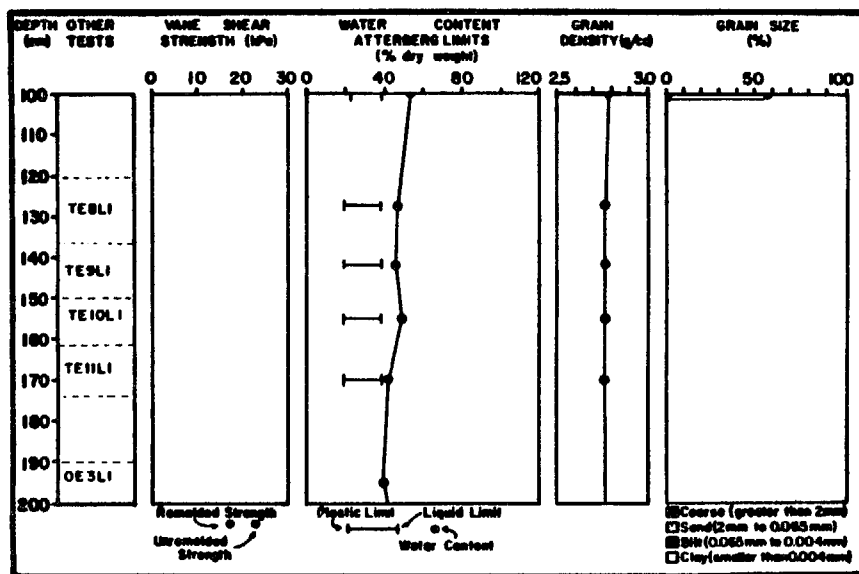


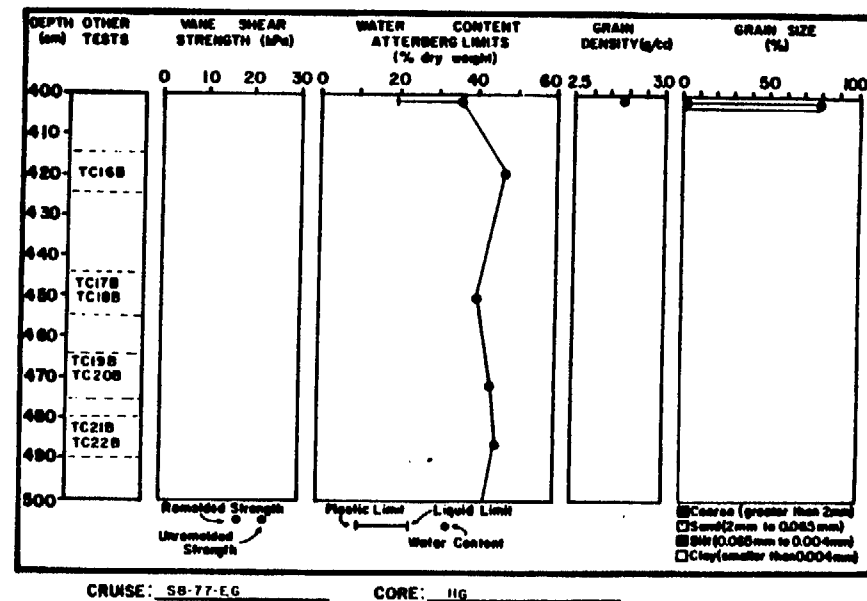
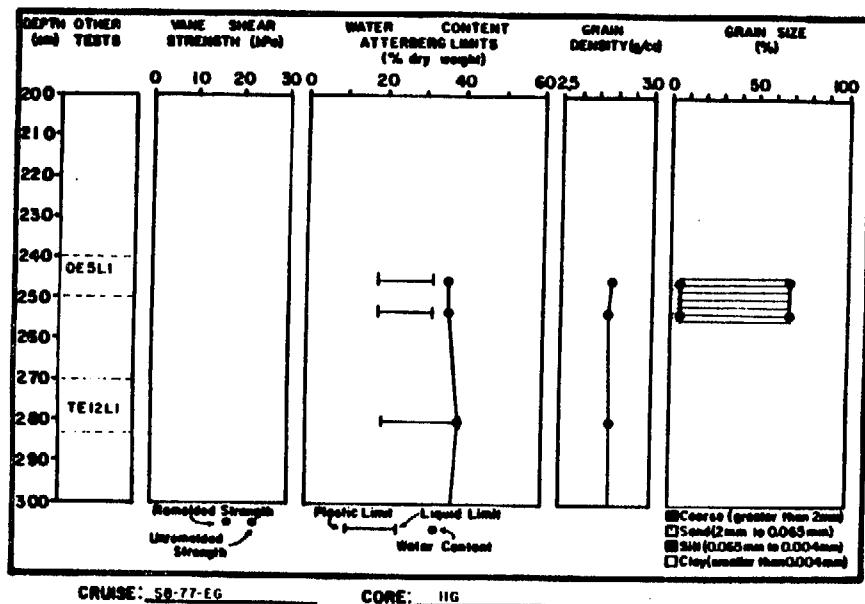
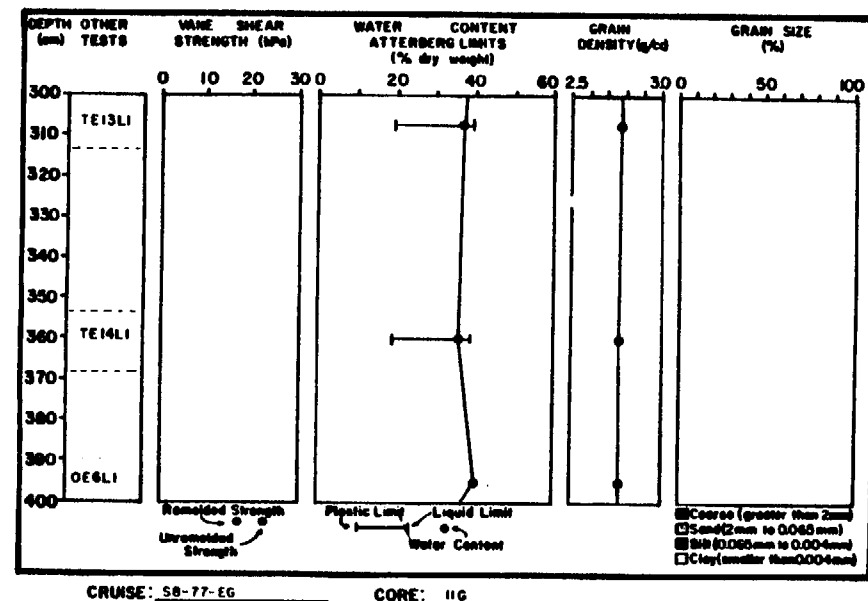
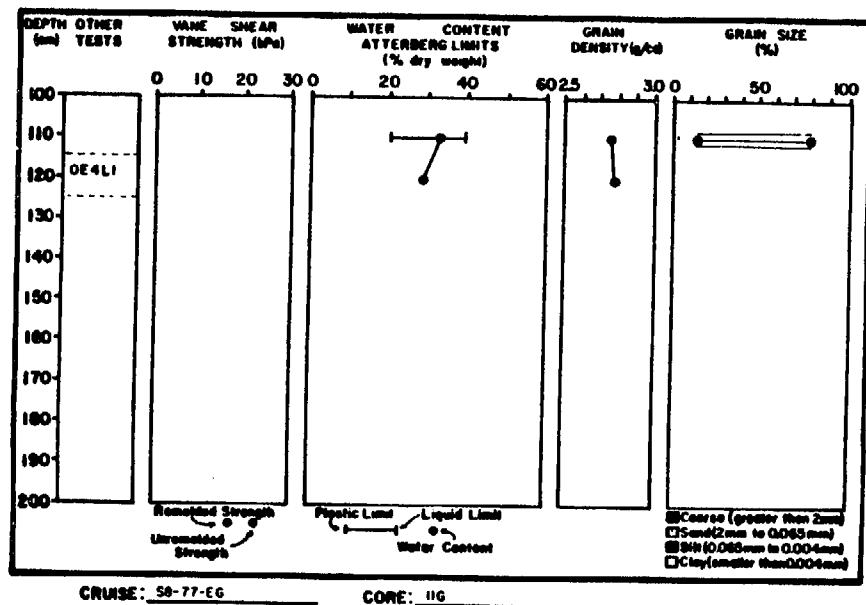


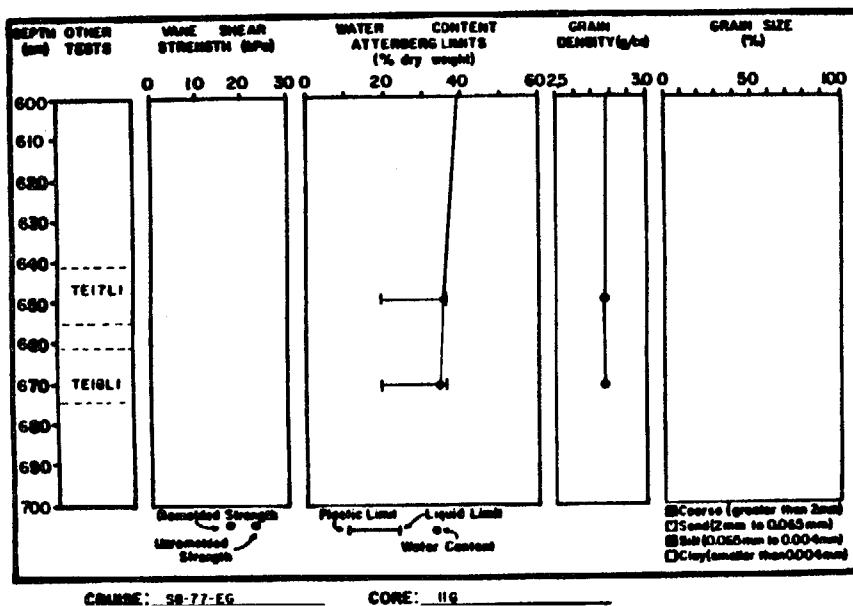
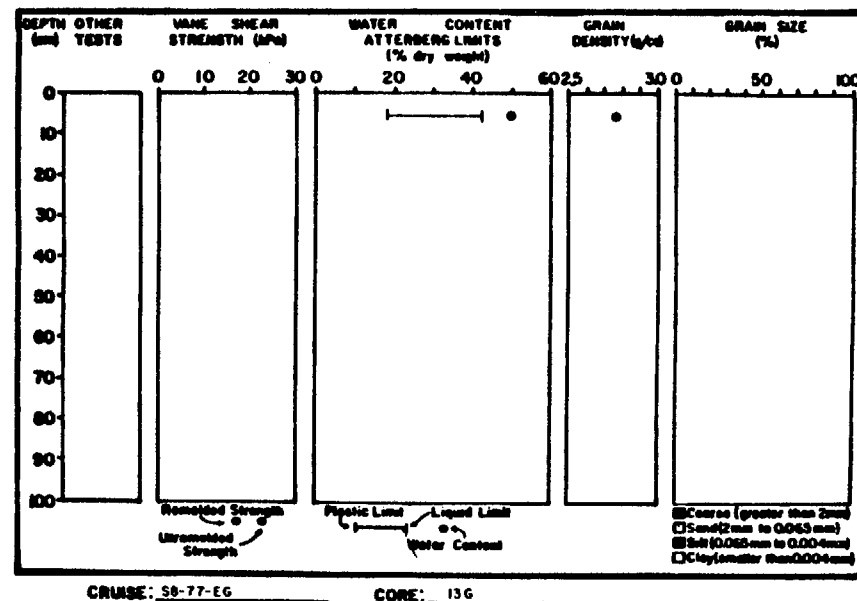
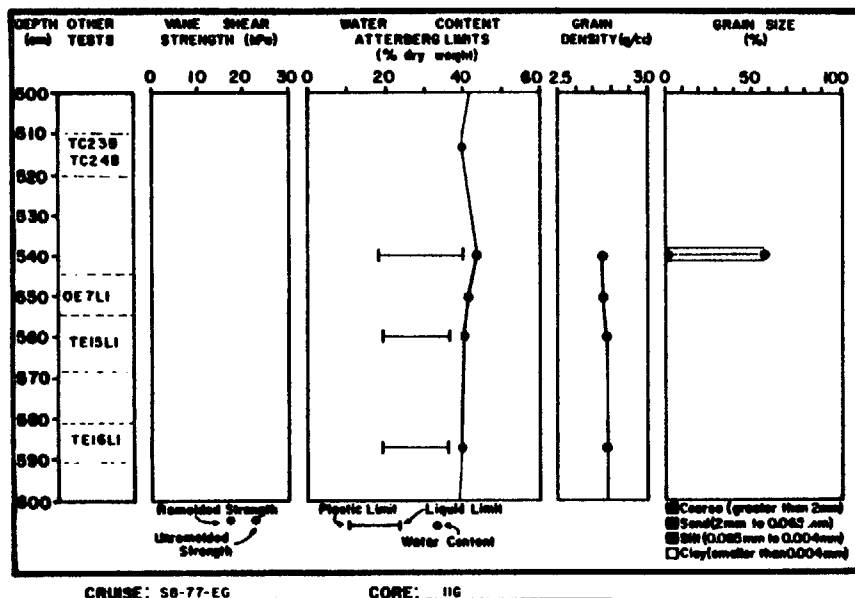
KAYAK TROUGH STUDY AREA

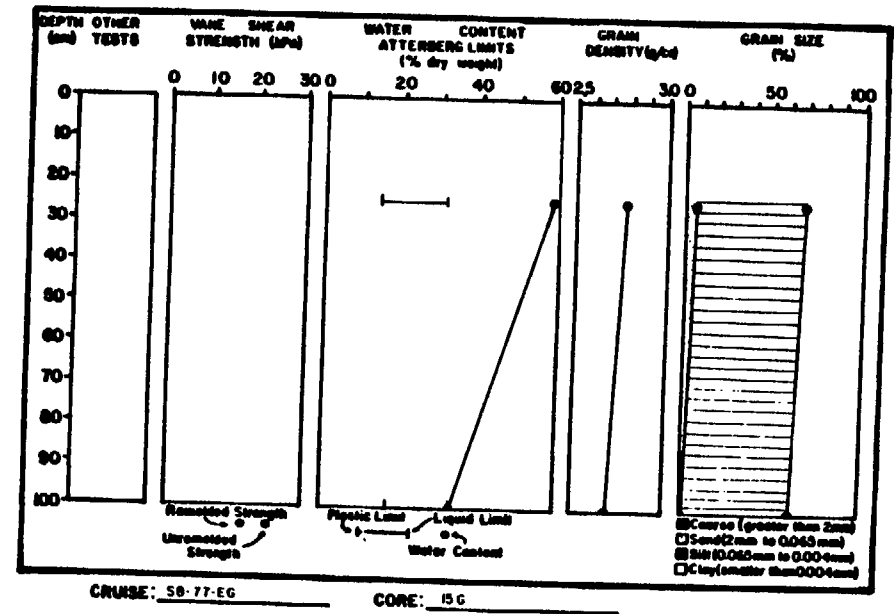
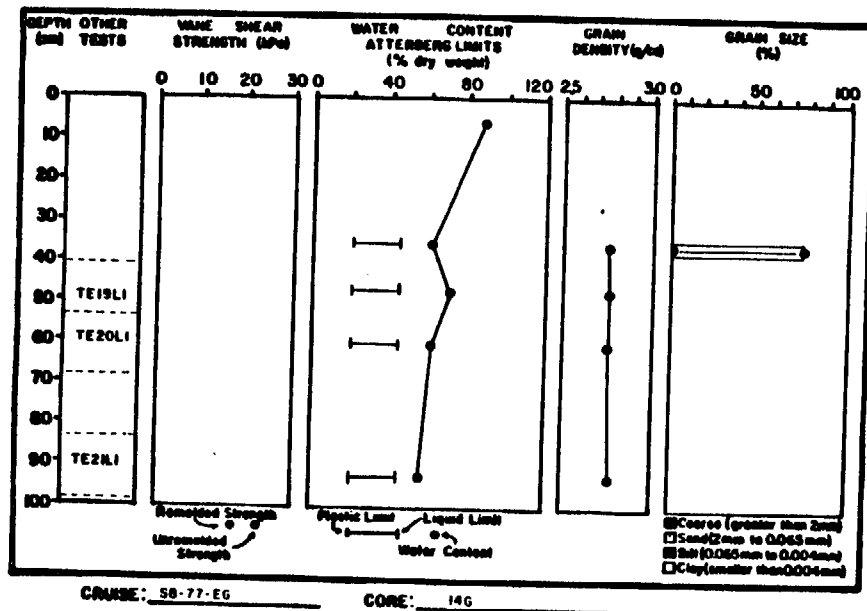


240

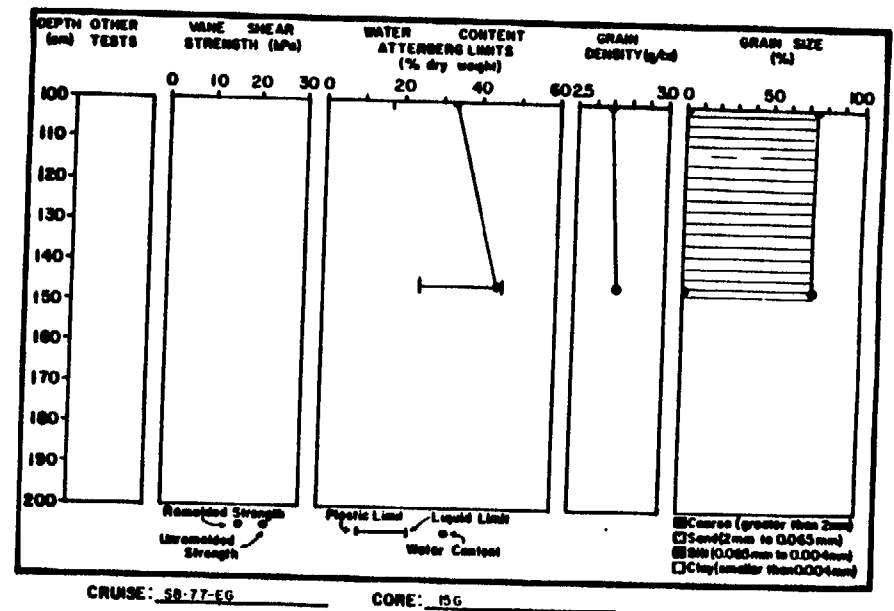
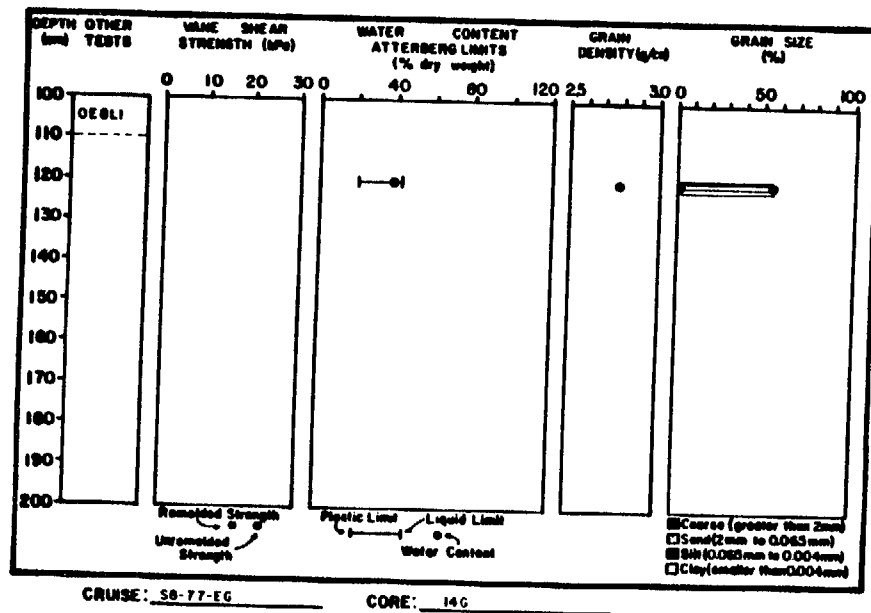


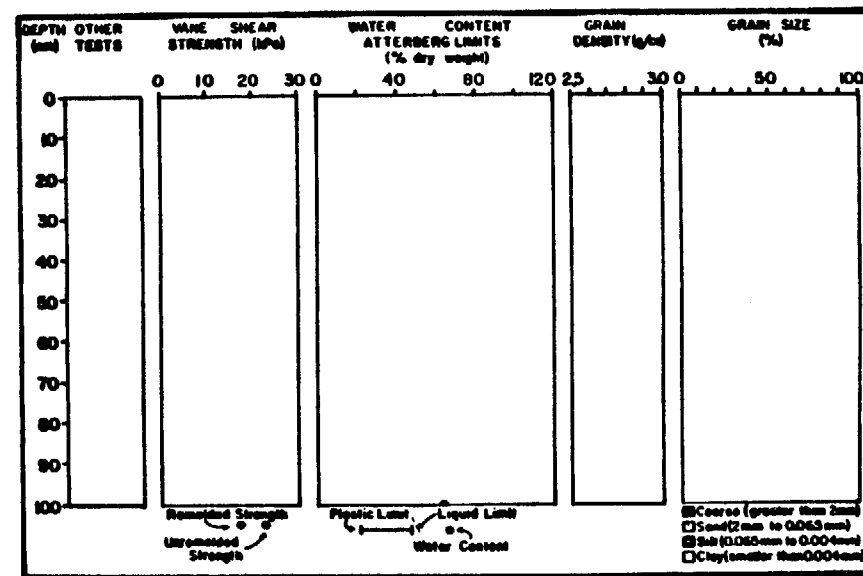
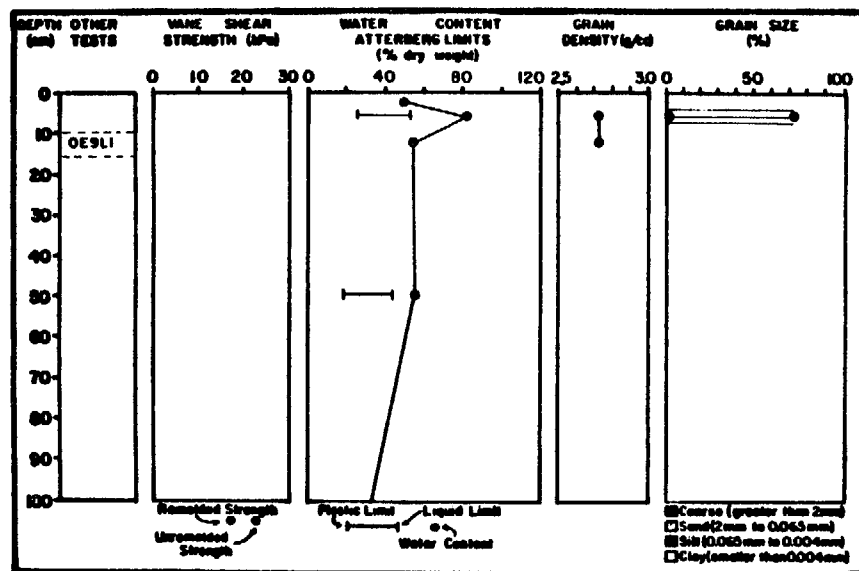




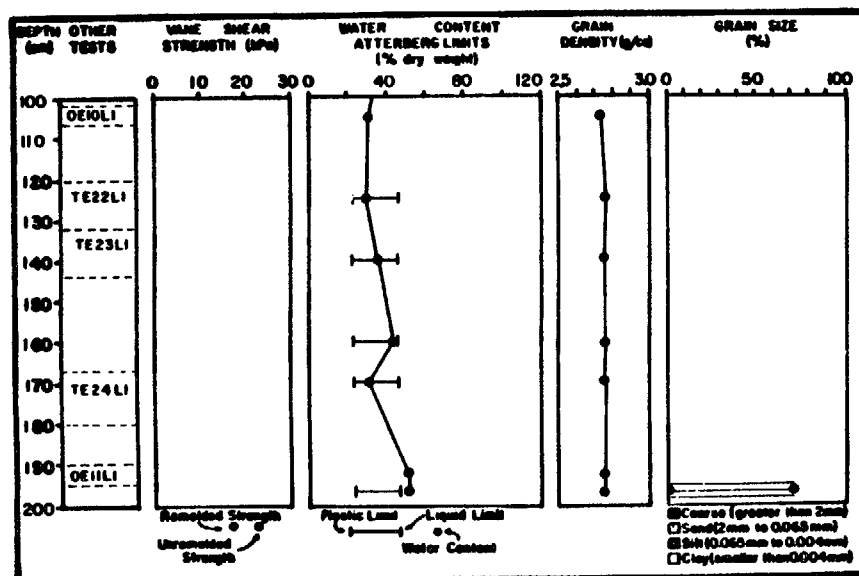


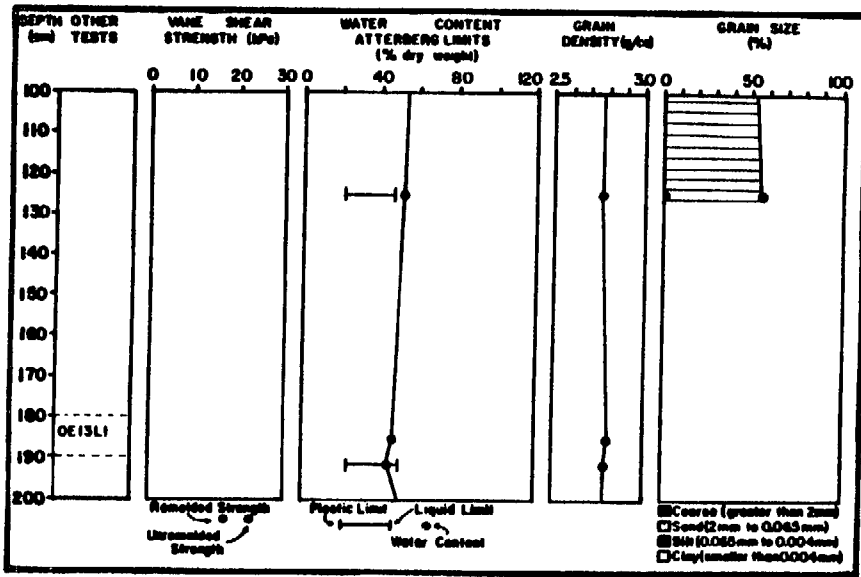
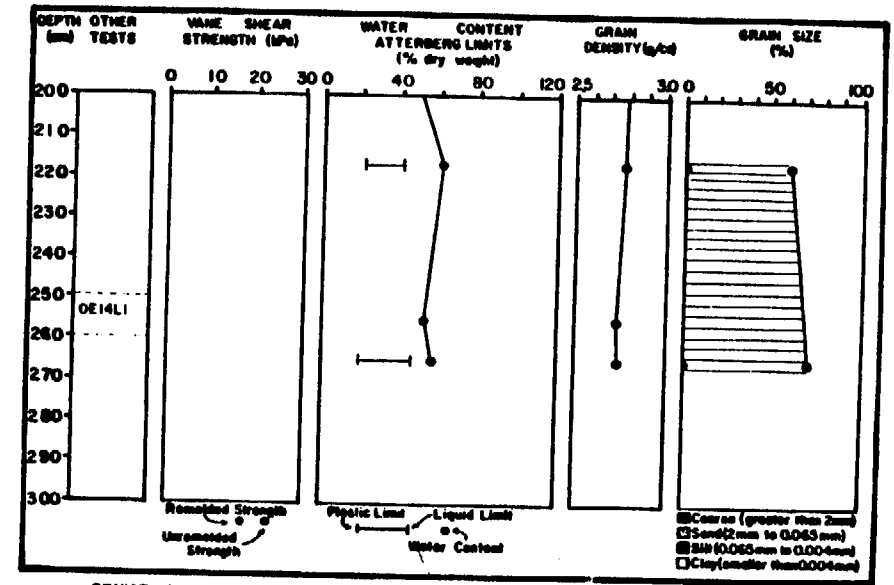
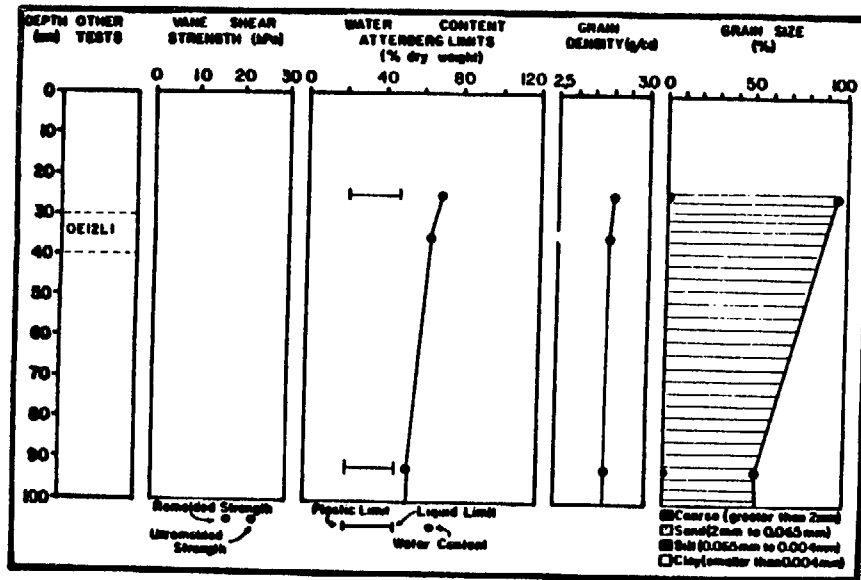
243

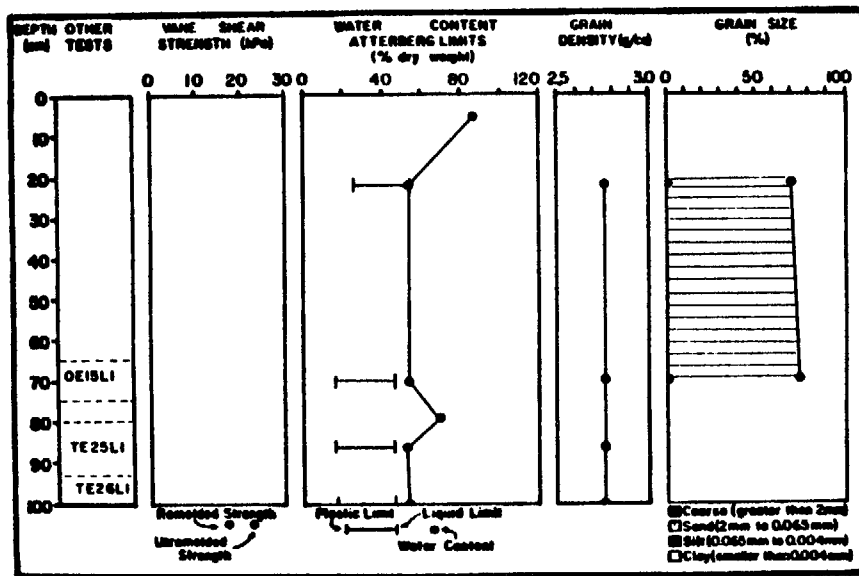




244

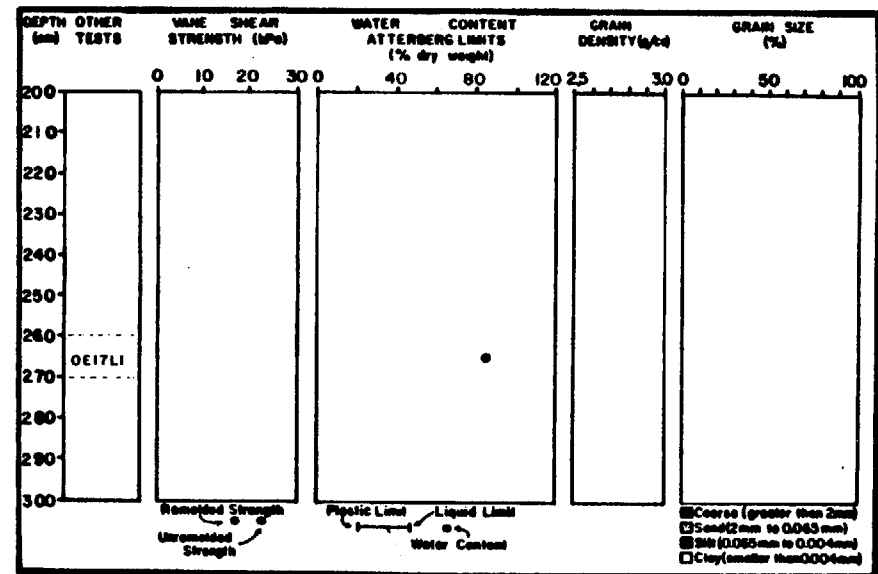






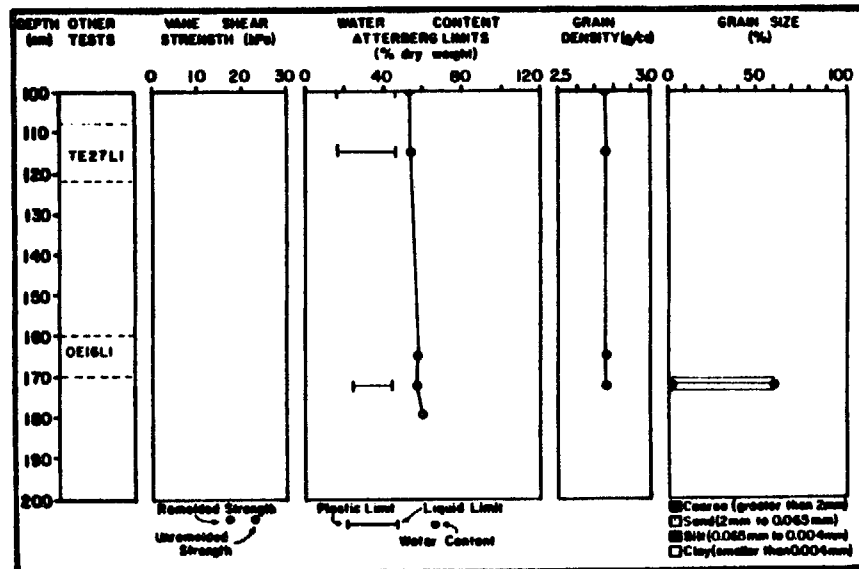
CRUISE: 58-77-EG

CORE: 19G



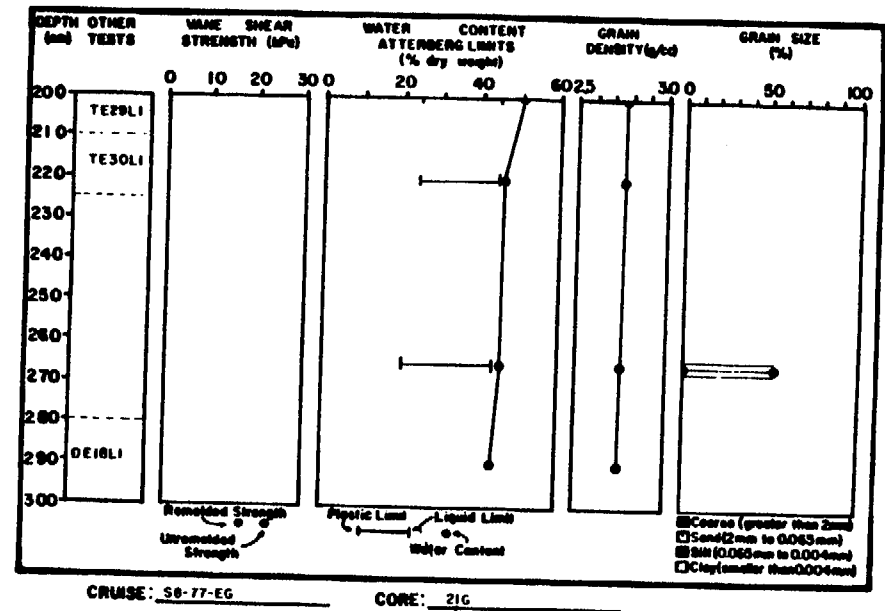
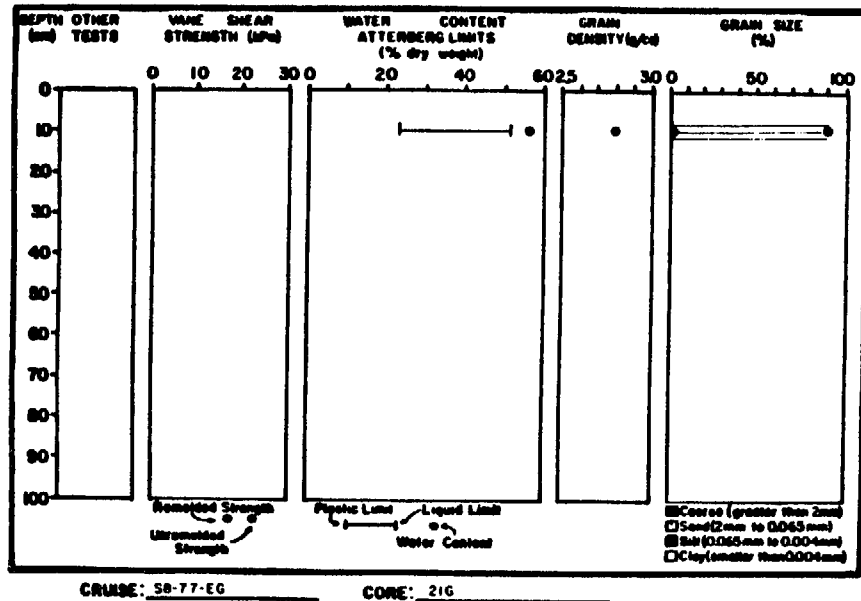
CRUISE: 58-77-EG

CORE: 19G

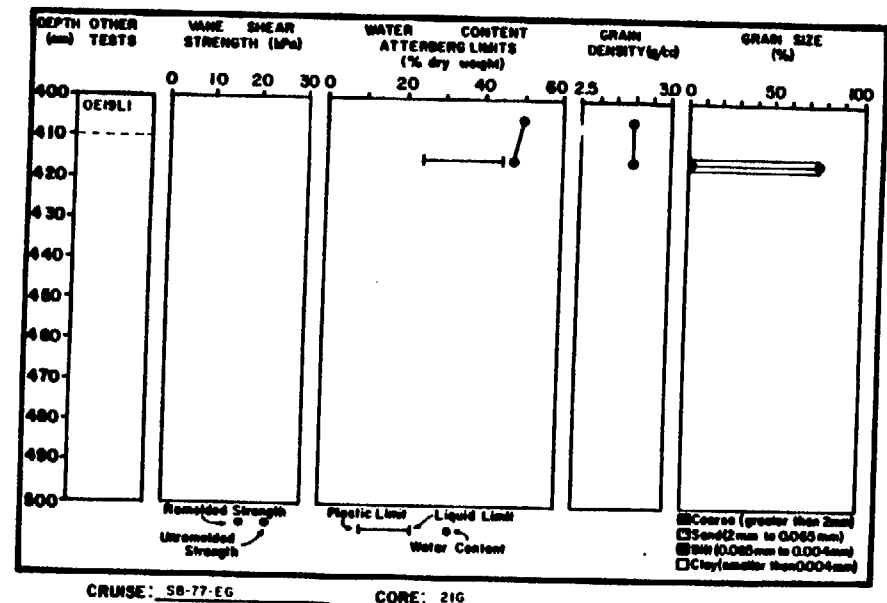
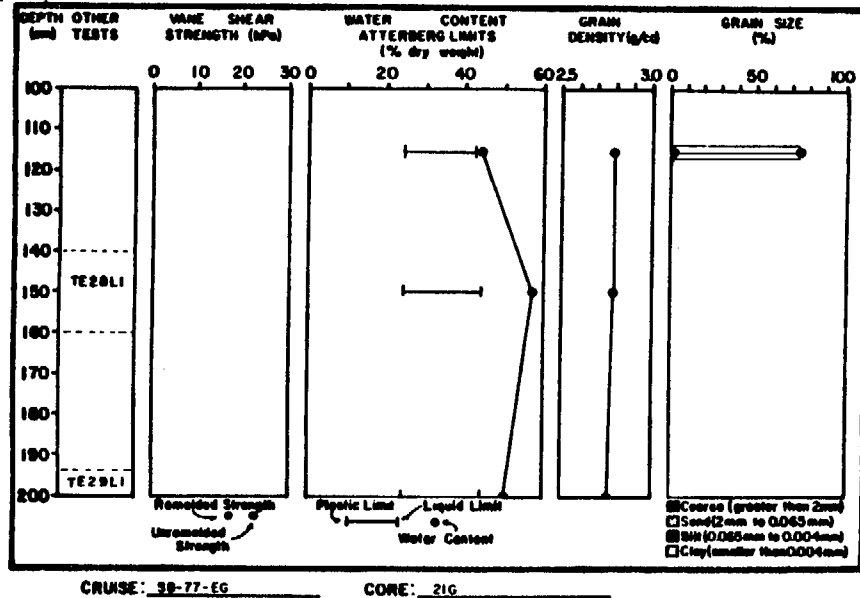


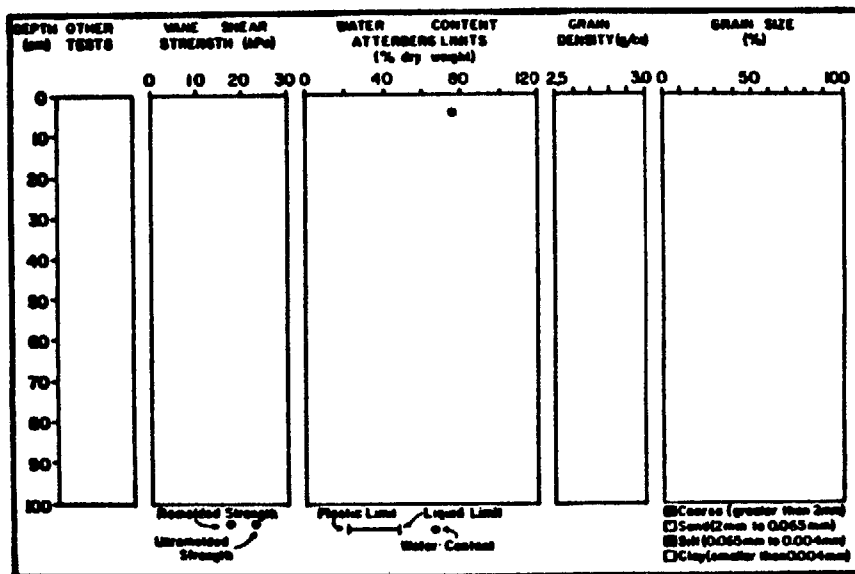
CRUISE: 58-77-EG

CORE: 19G

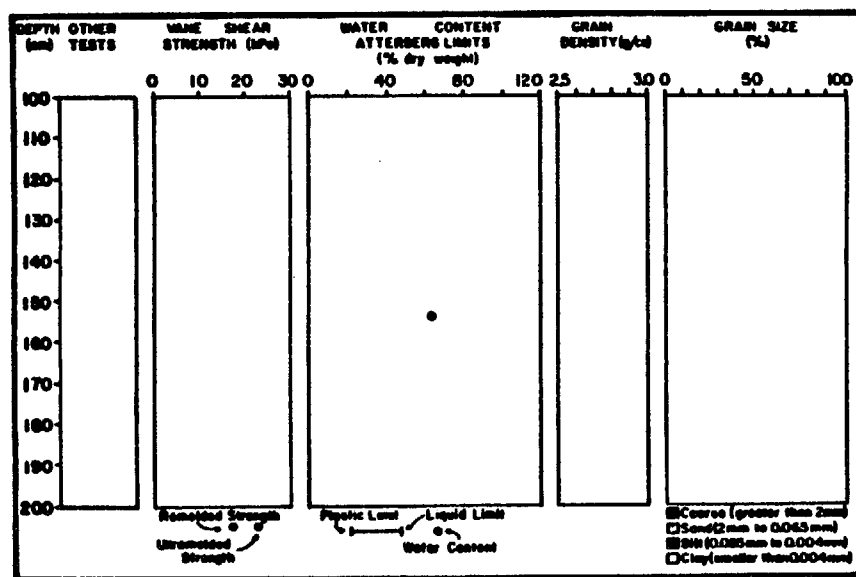


247



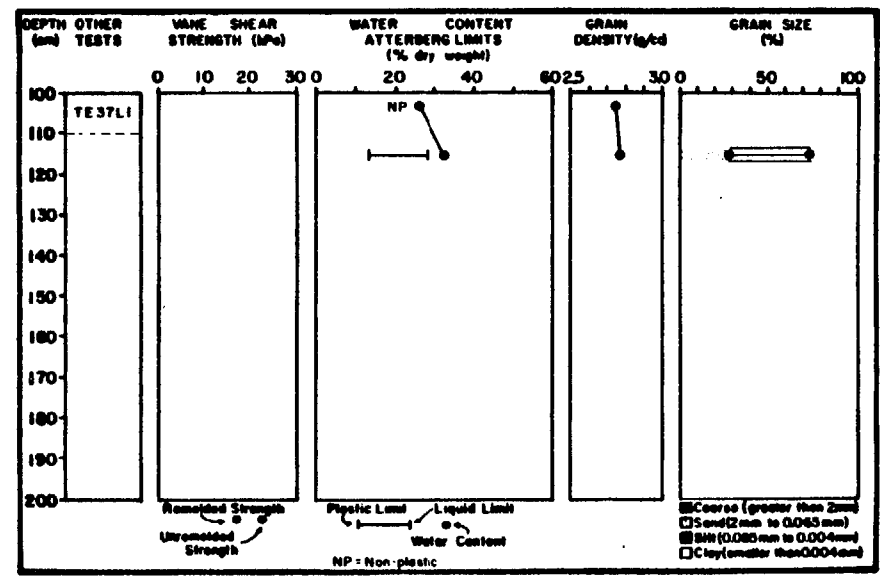
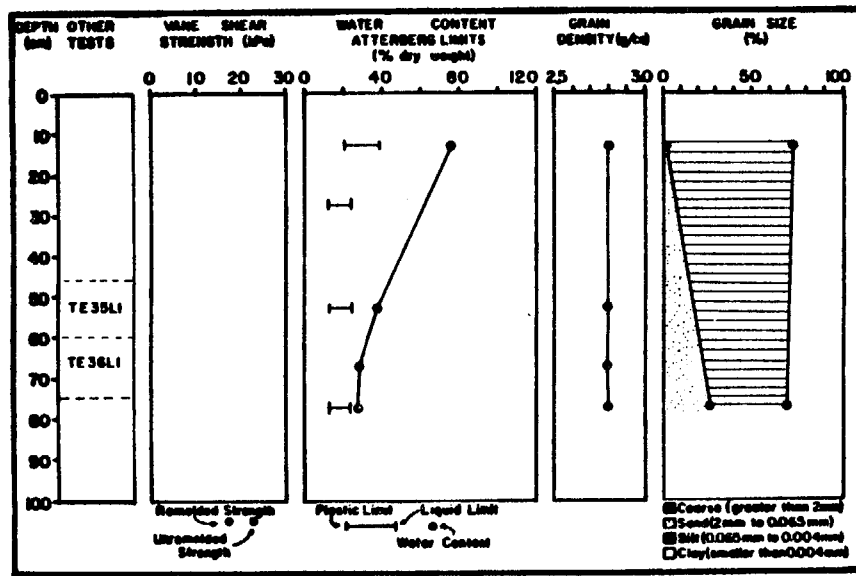
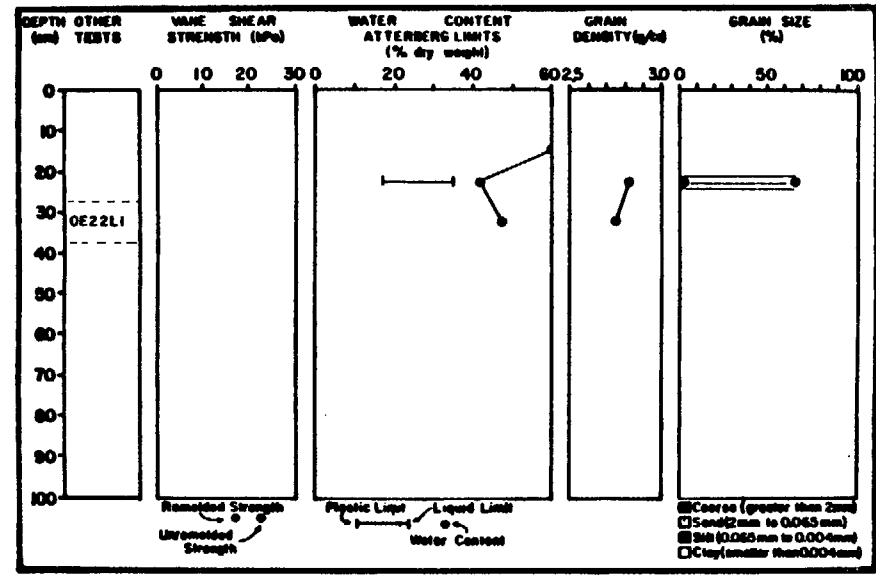
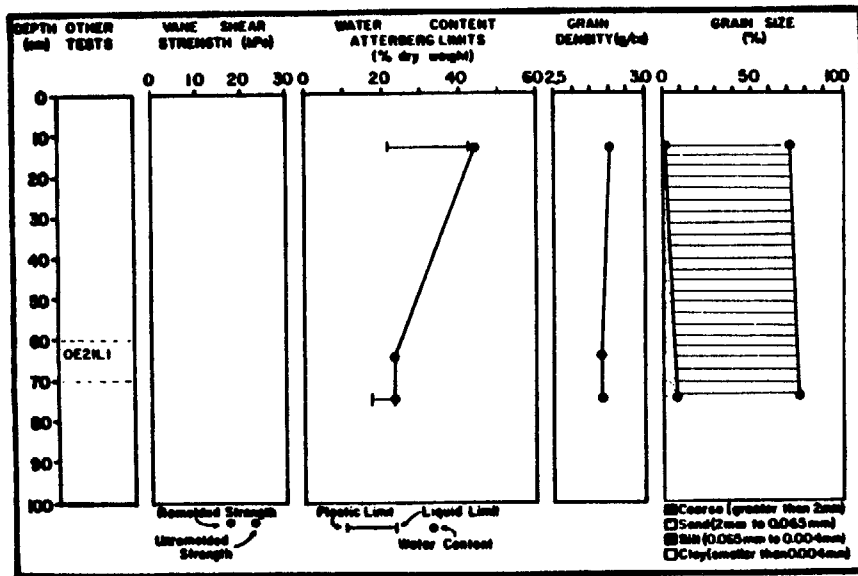


CRUISE: 58-77-EG CORE: 206

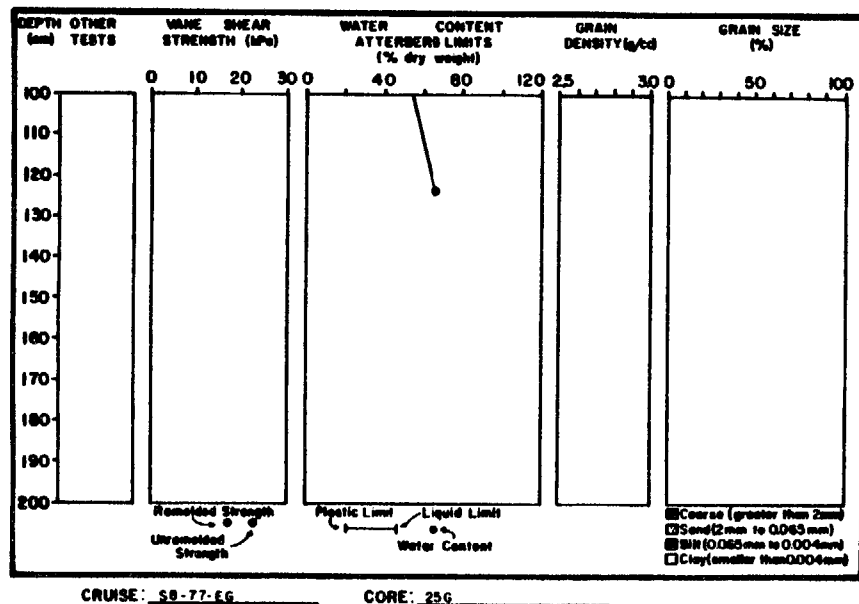
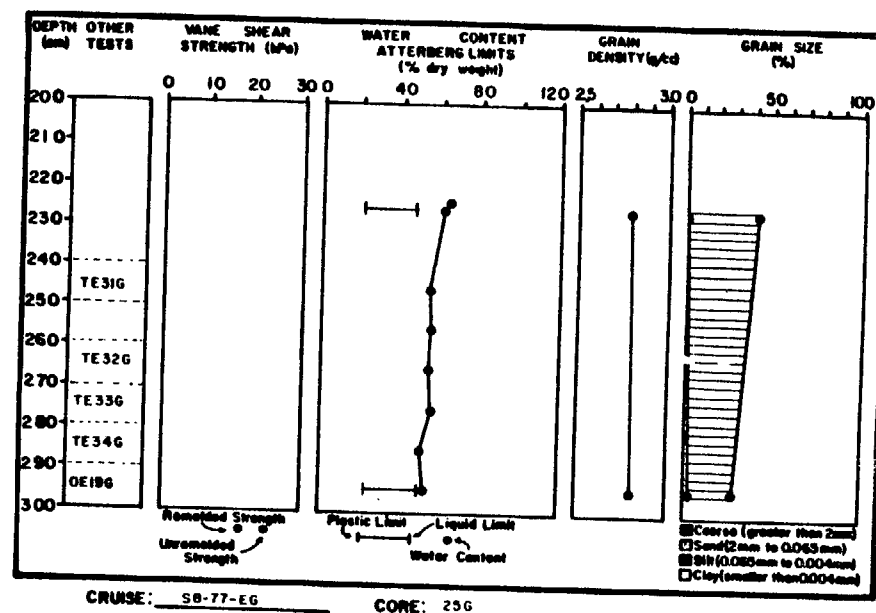
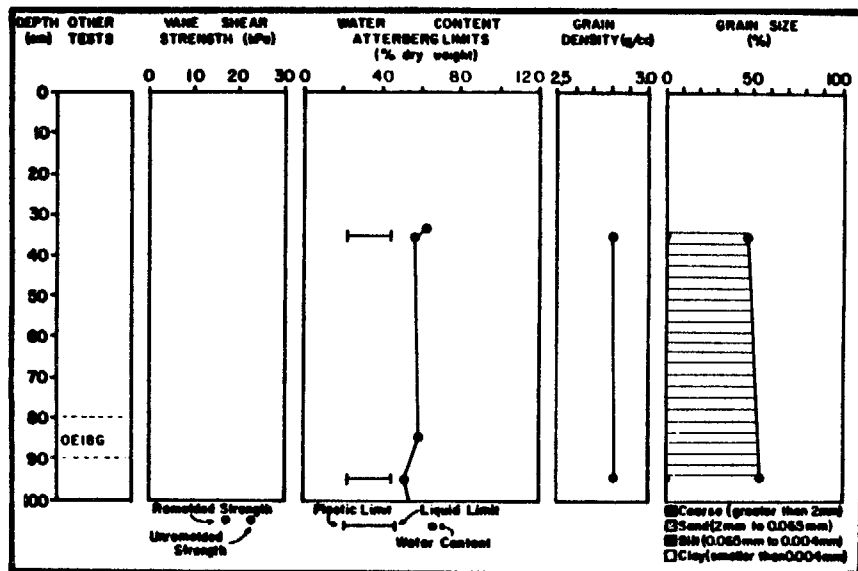


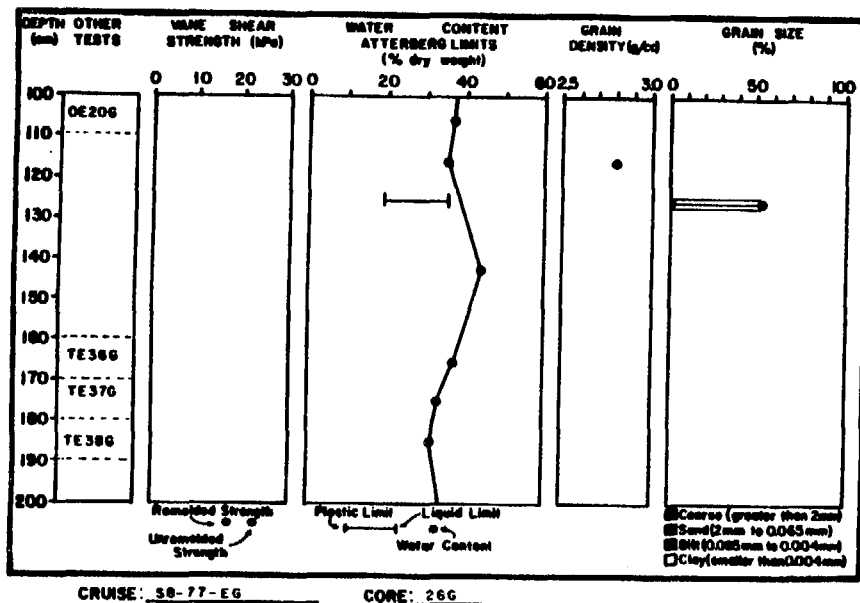
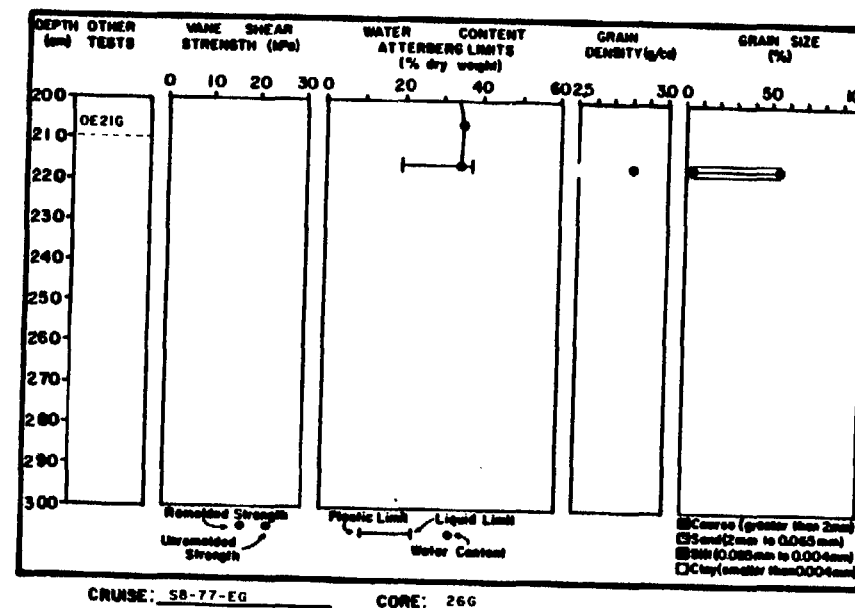
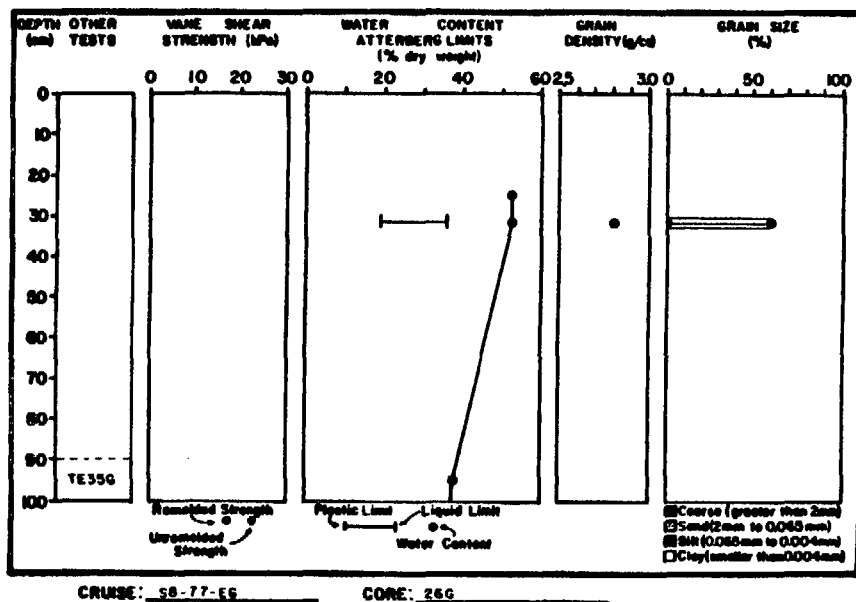
CRUISE: 58-77-EG CORE: 206

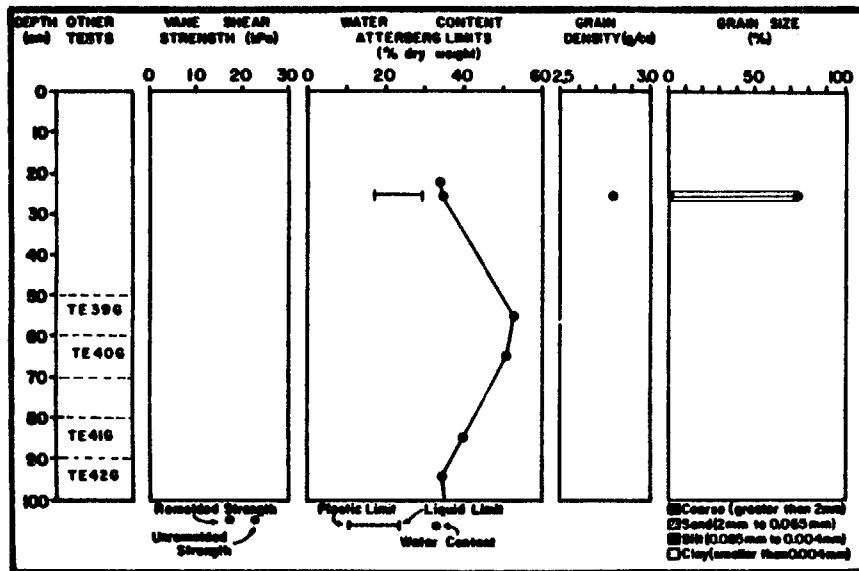
BERING TROUGH STUDY AREA



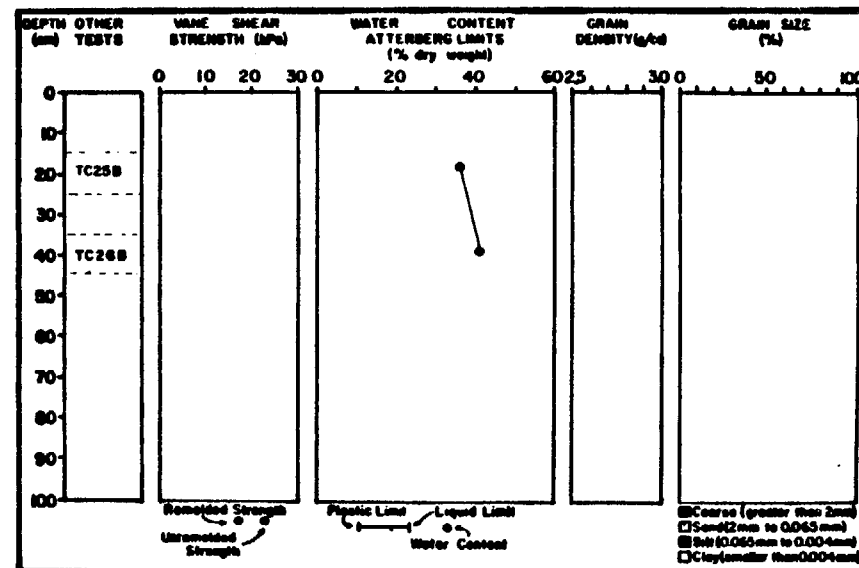
ICY BAY-MALASPINA STUDY AREA



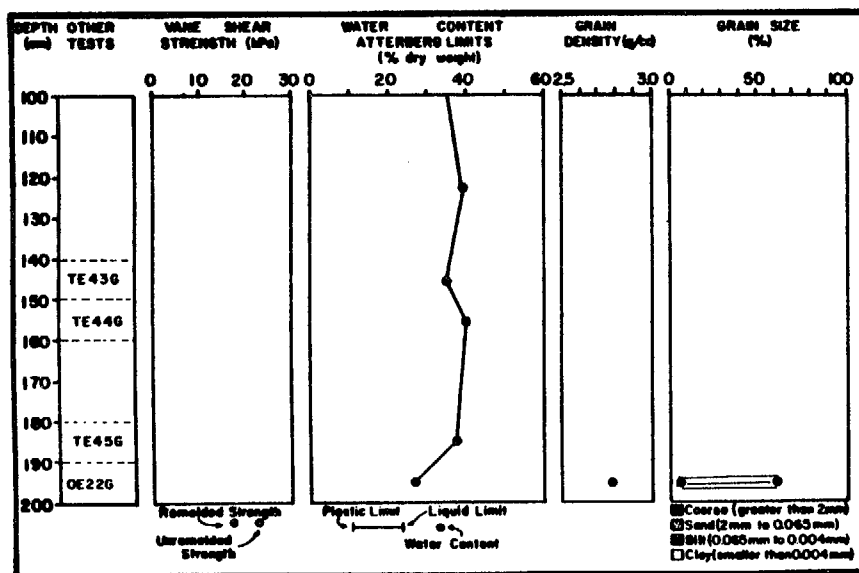




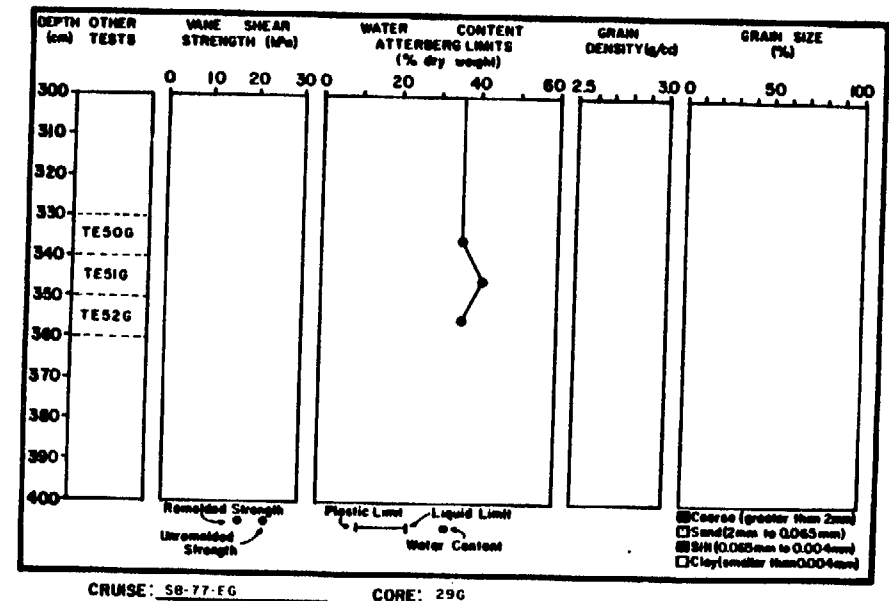
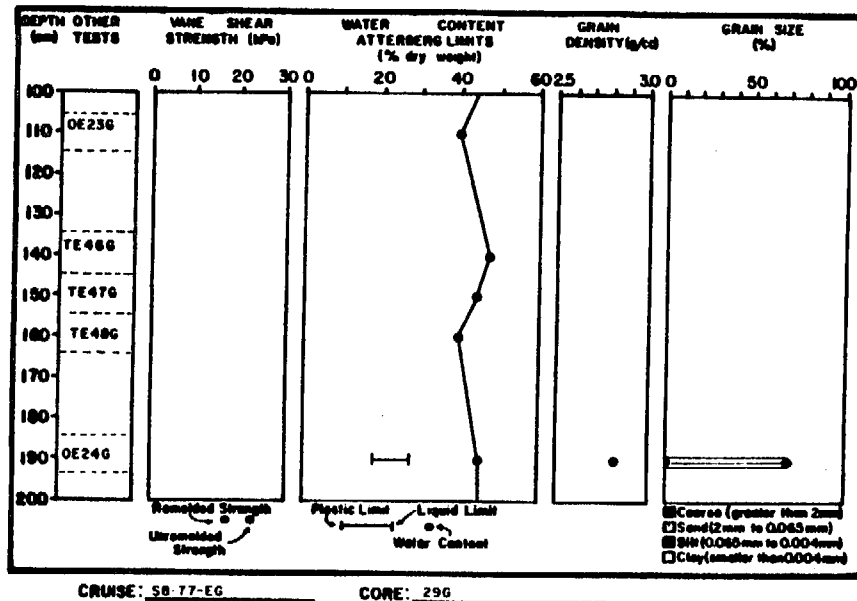
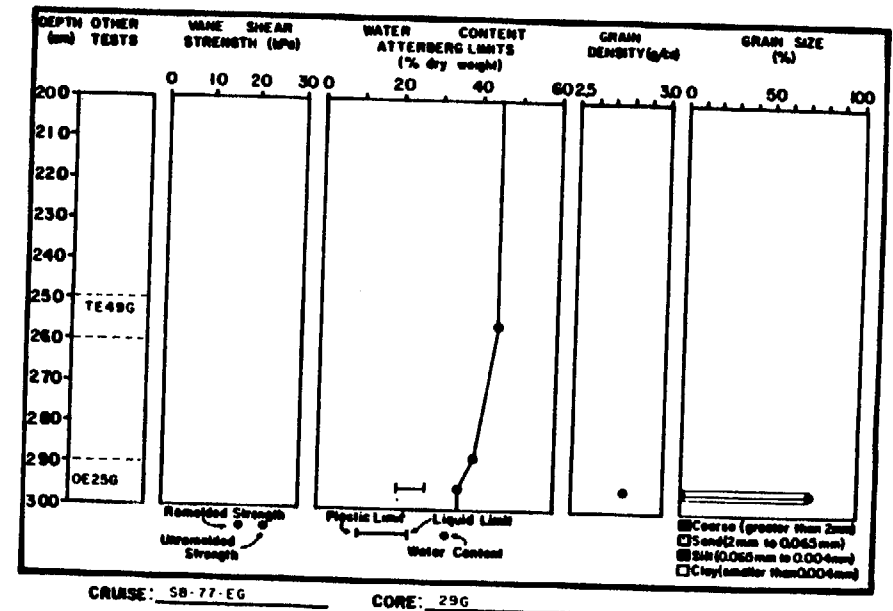
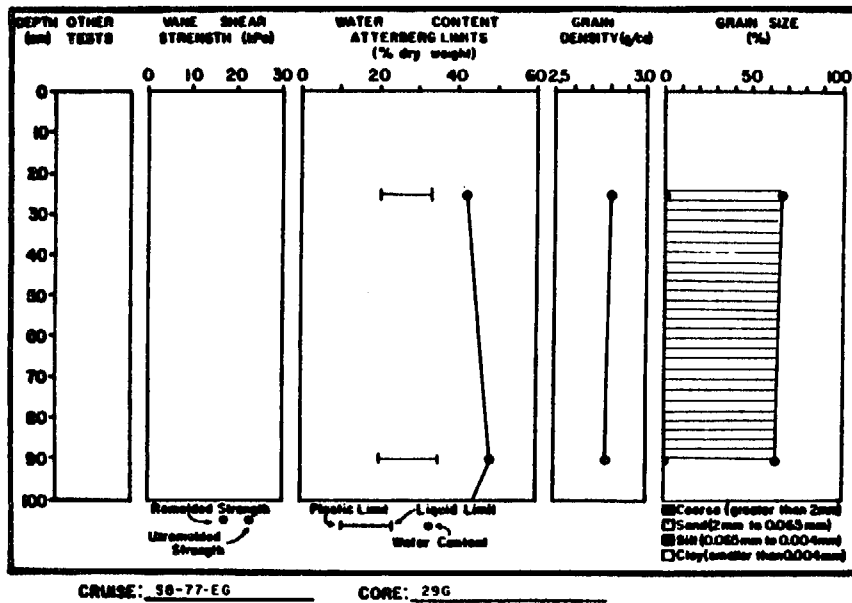
CRUISE: 58-77-EG CORE: 276

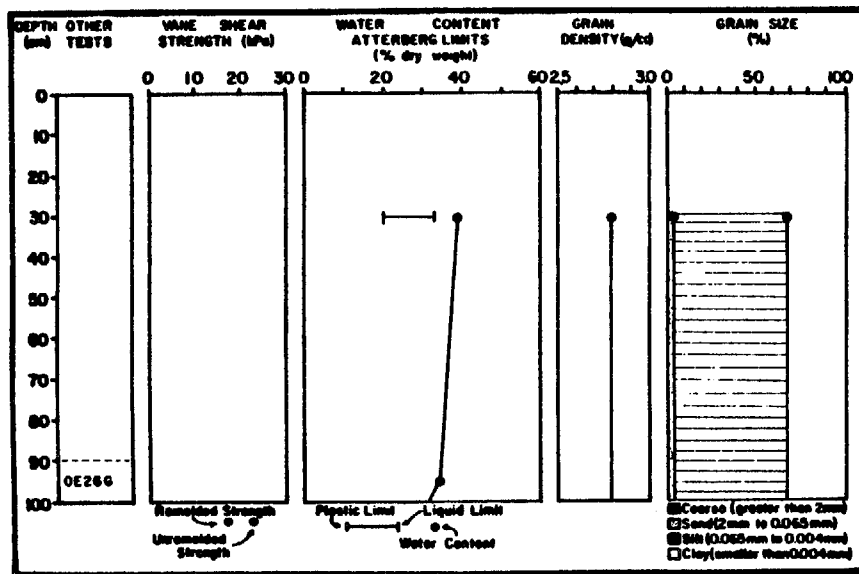


CRUISE: 58-77-EG CORE: 286

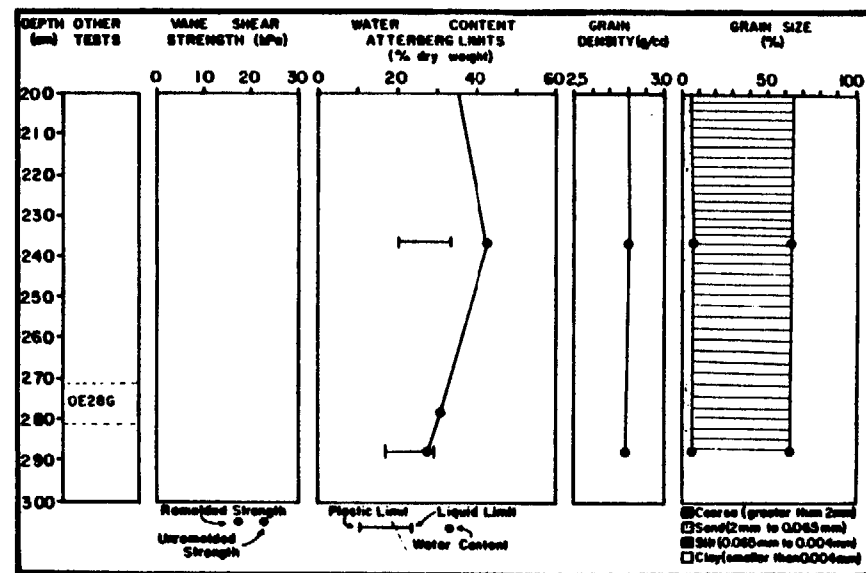


CRUISE: 58-77-EG CORE: 276

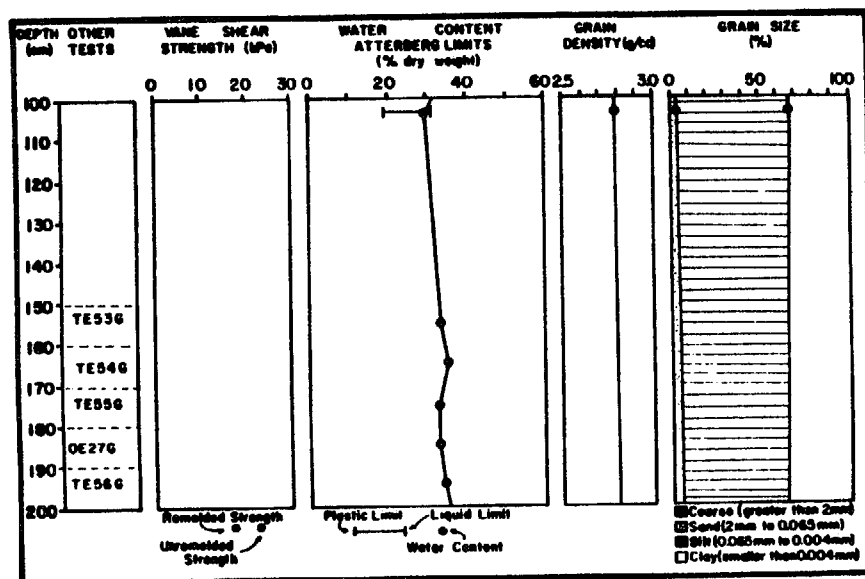




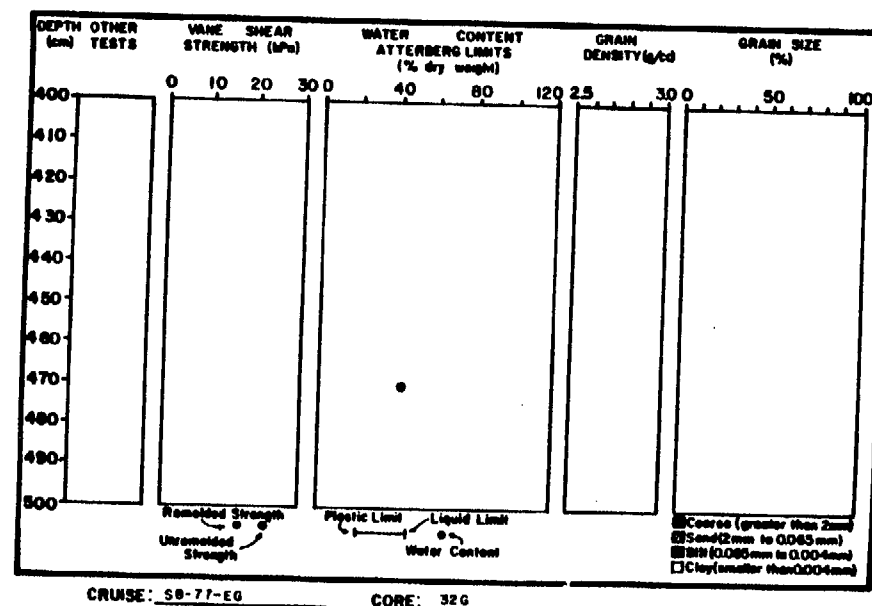
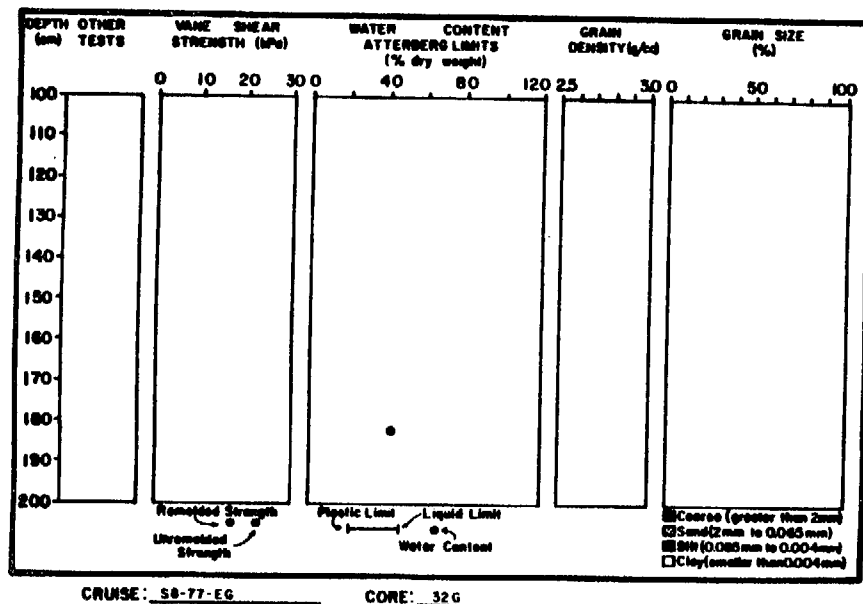
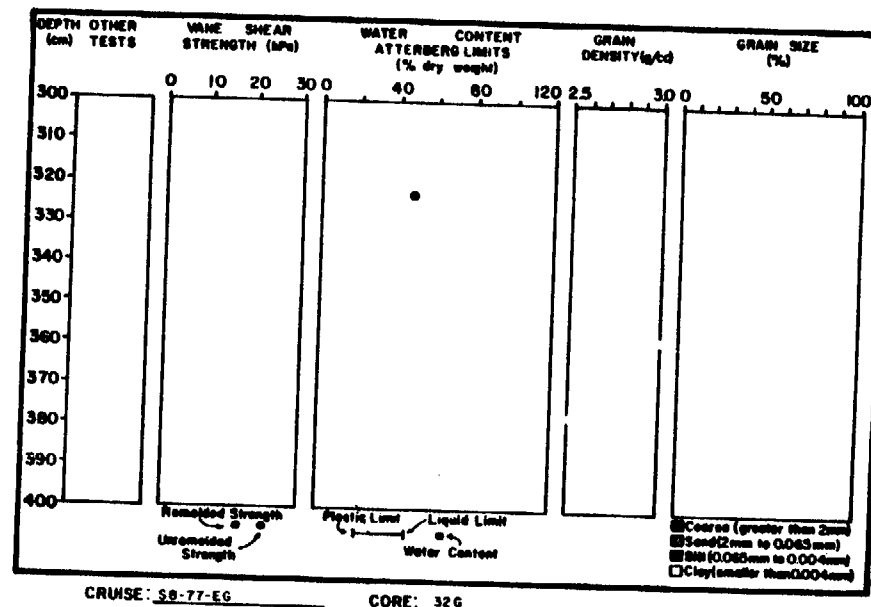
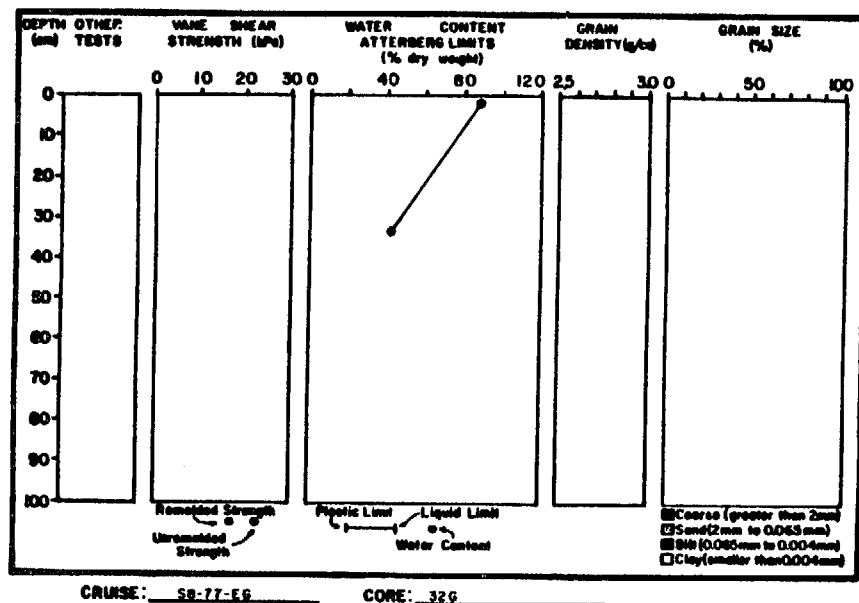
CRUISE: 58-77-EG CORE: 31G

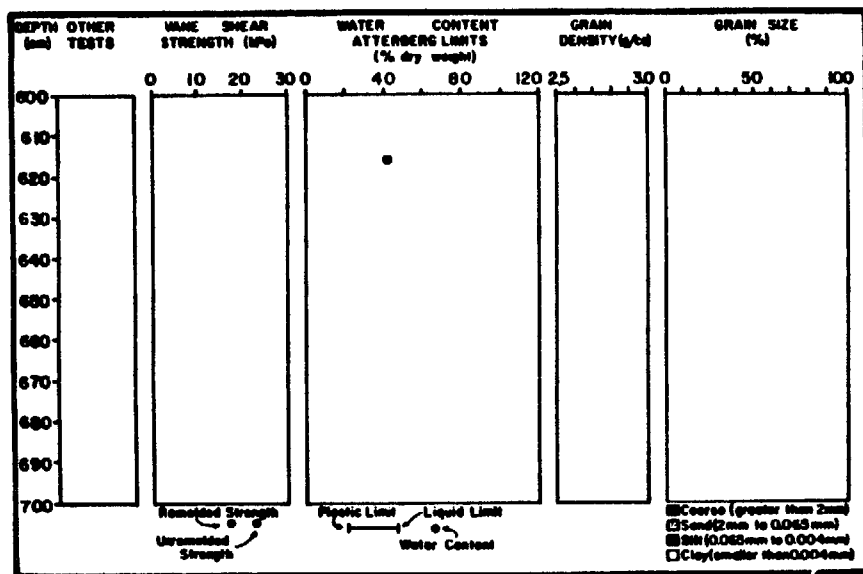


CRUISE: 58-77-EG CORE: 31G



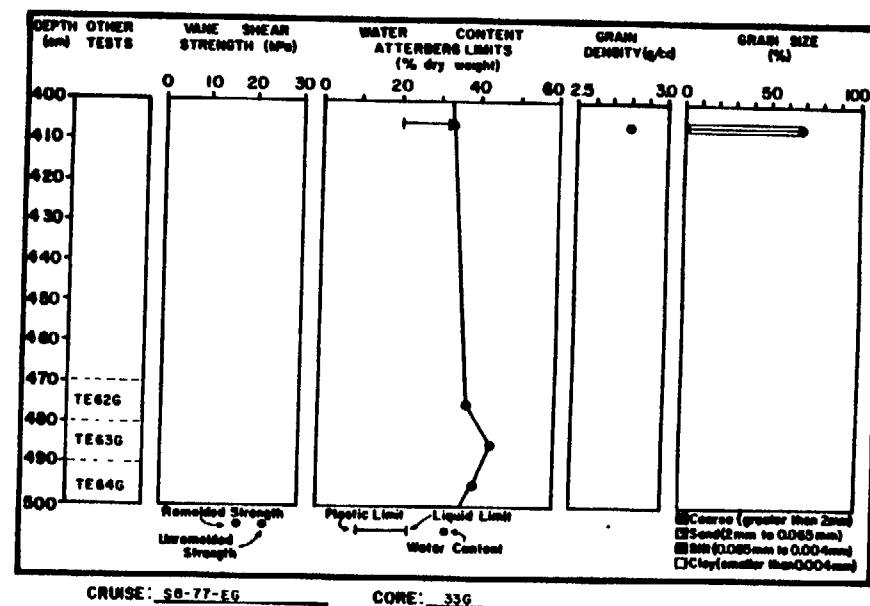
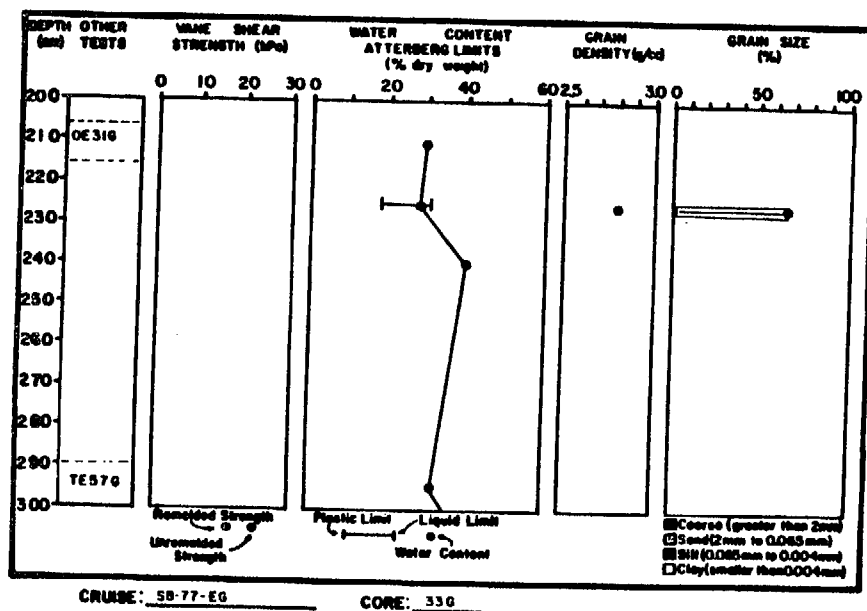
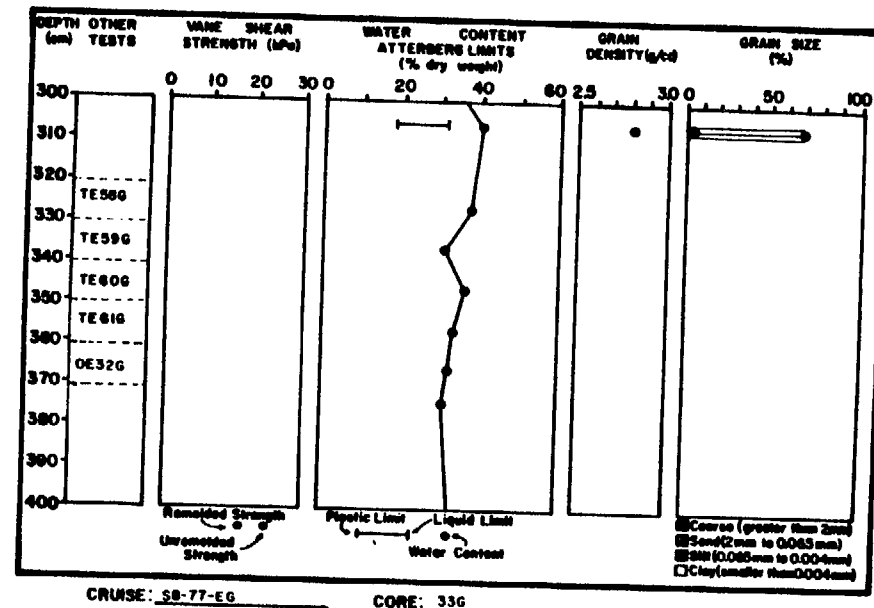
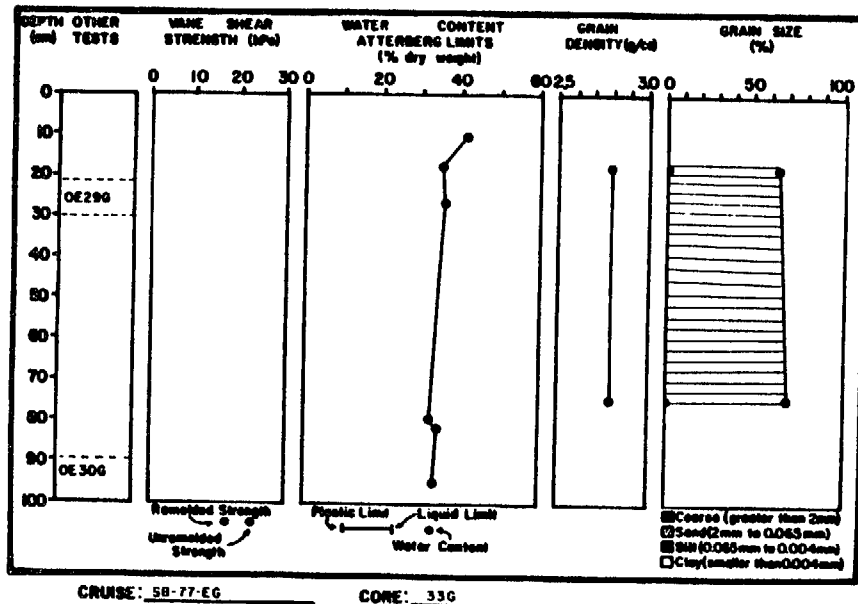
CRUISE: 58-77-EG CORE: 31G

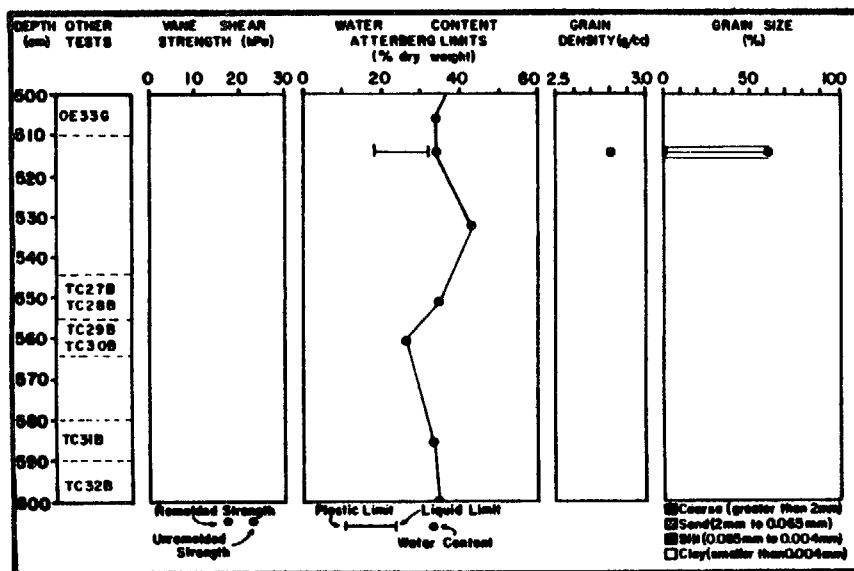




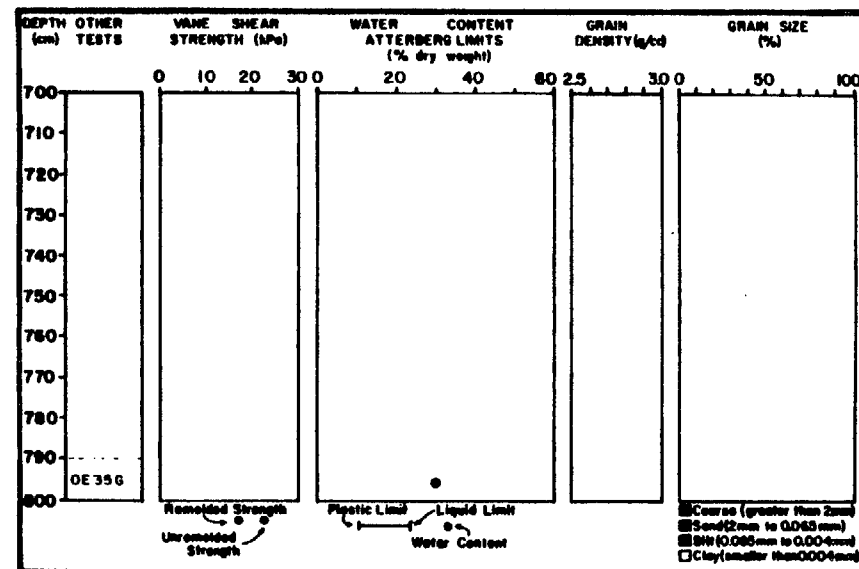
CRUISE: 58-77-EG

CORE: 32G

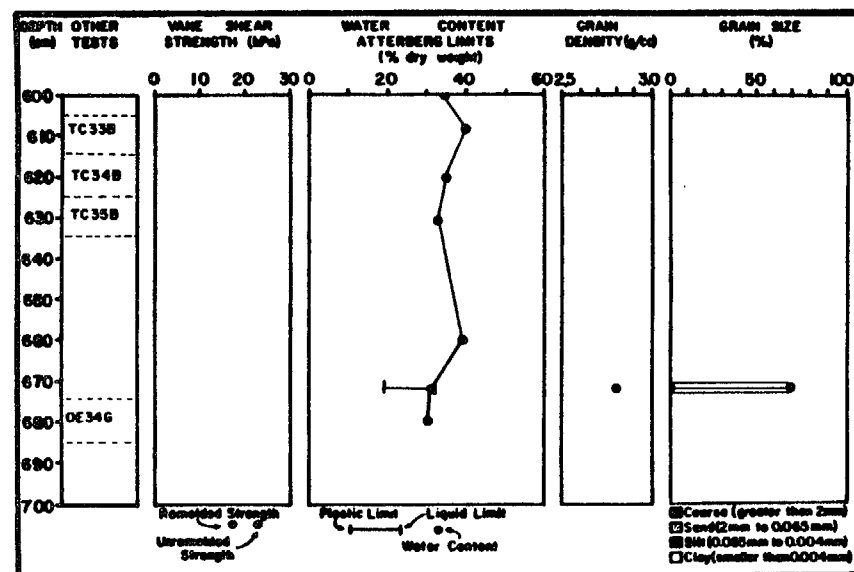




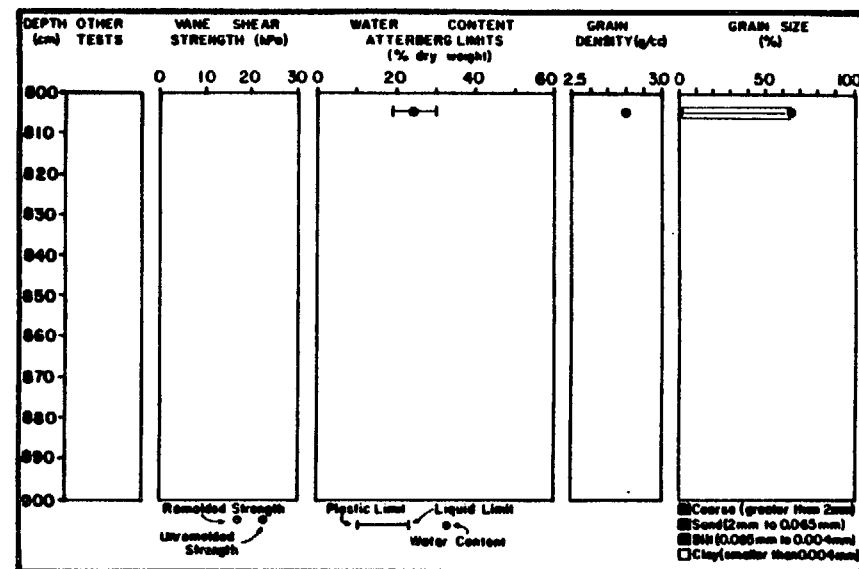
CRUISE: SB-77-EG CORE: 33G



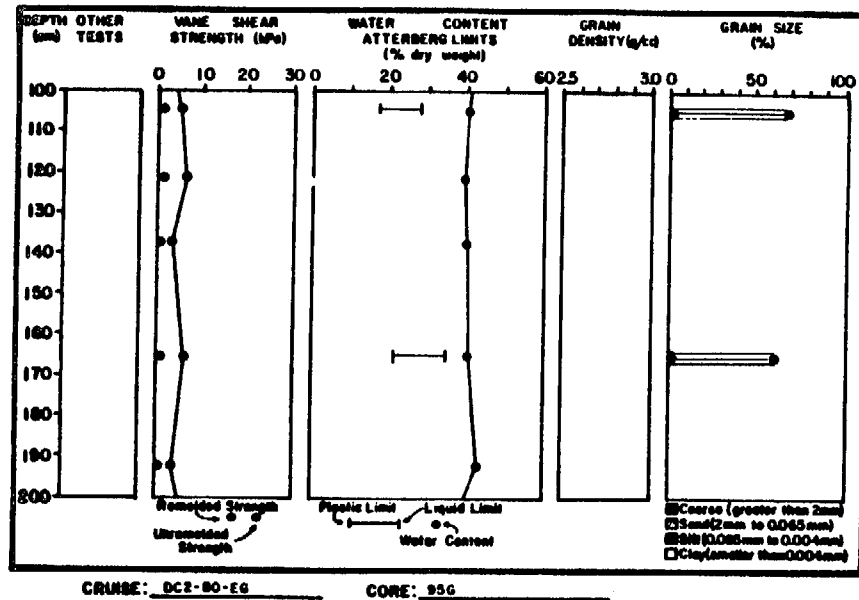
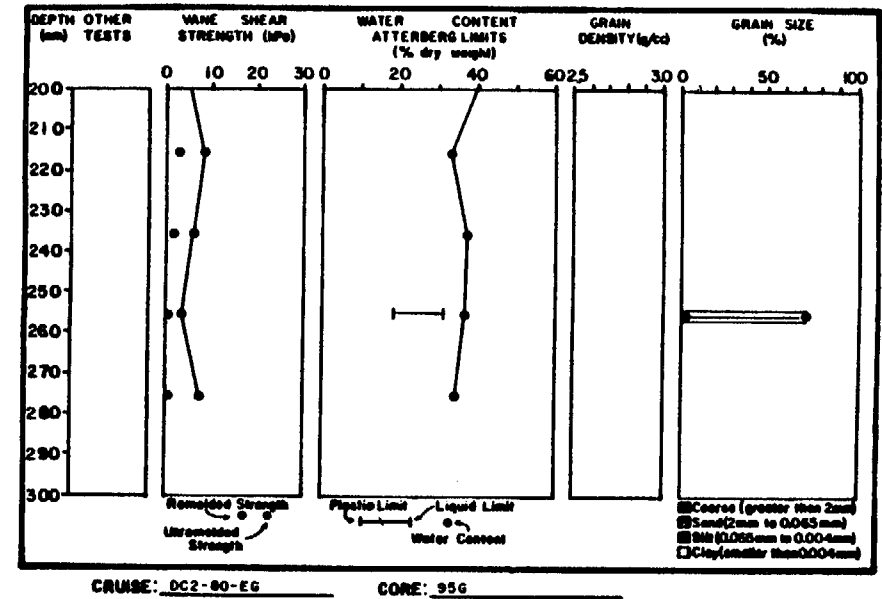
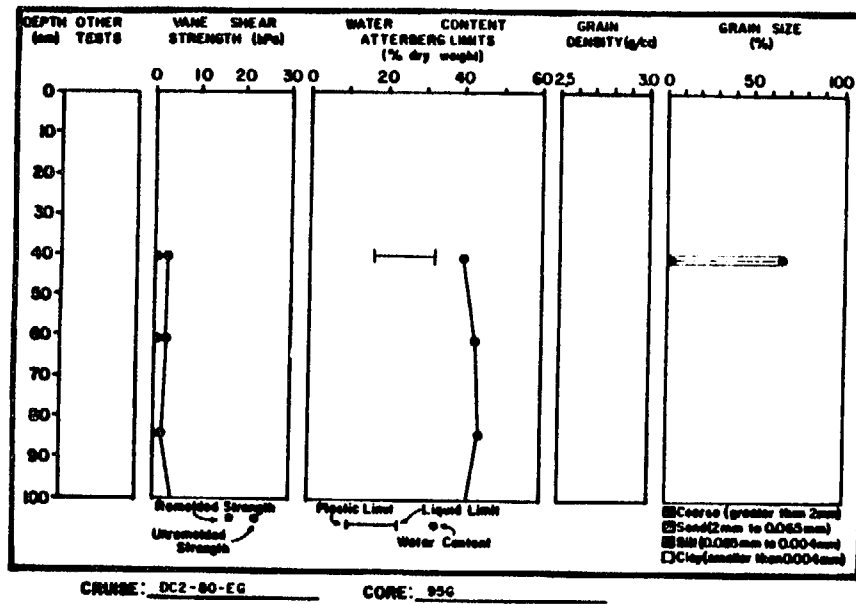
CRUISE: SB-77-EG CORE: 33G

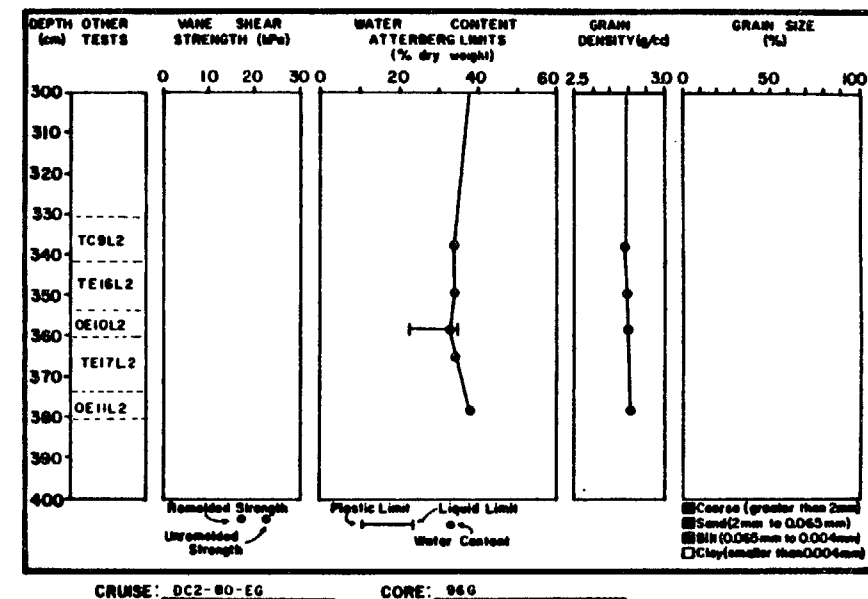
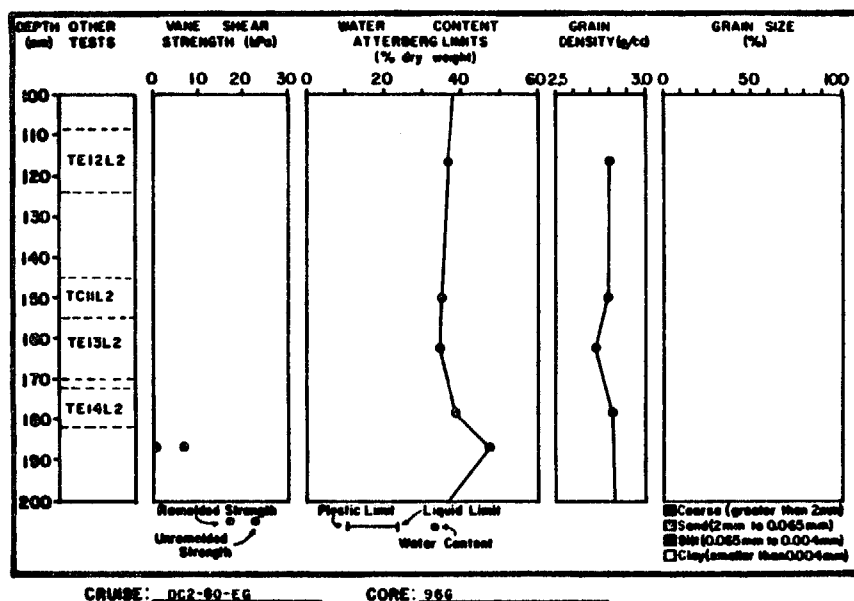
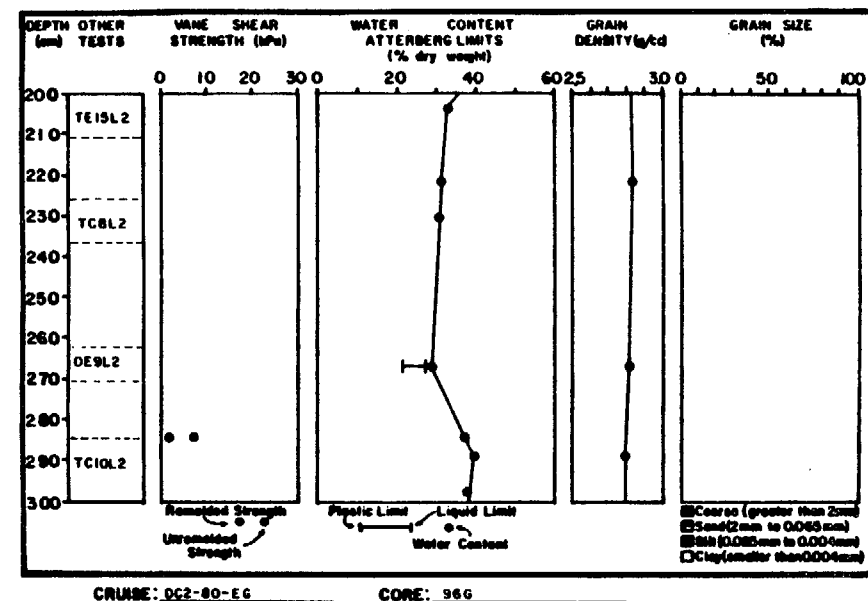
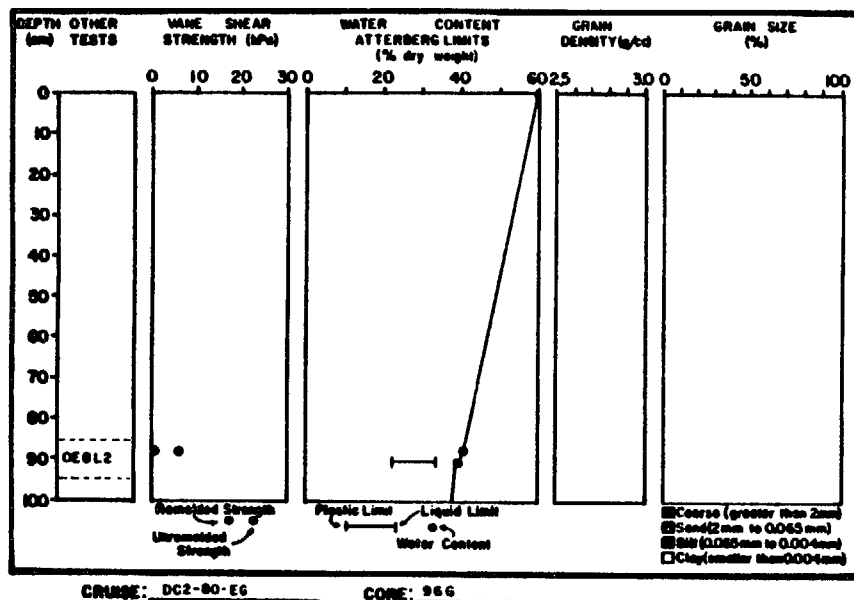


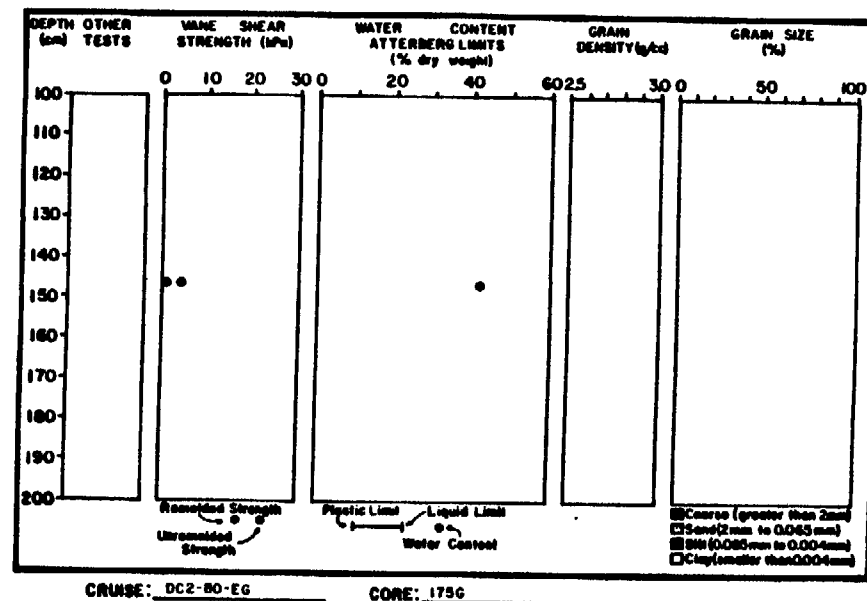
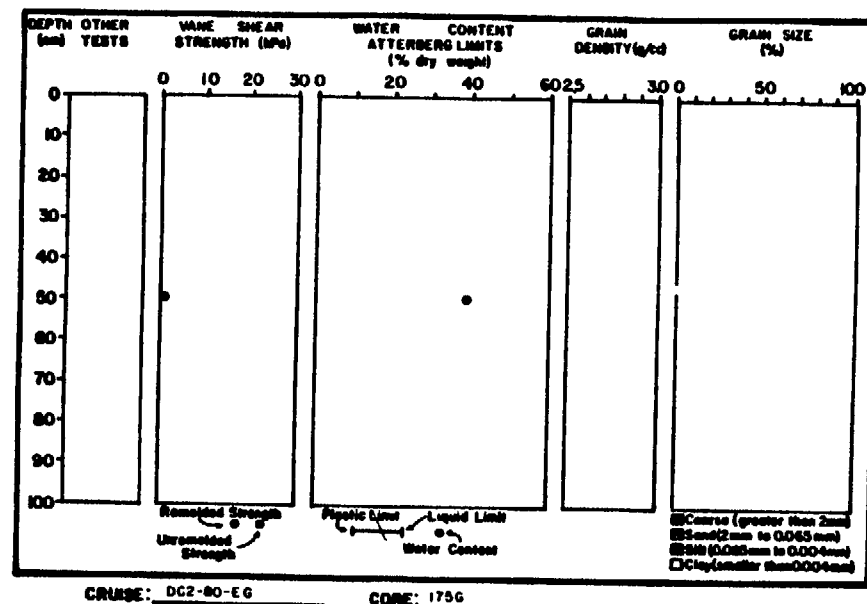
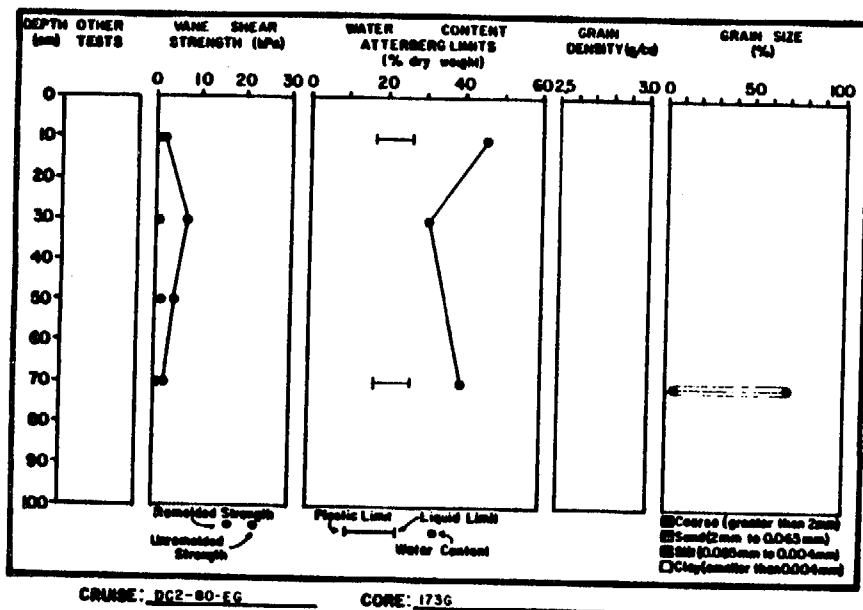
CRUISE: SB-77-EG CORE: 33G

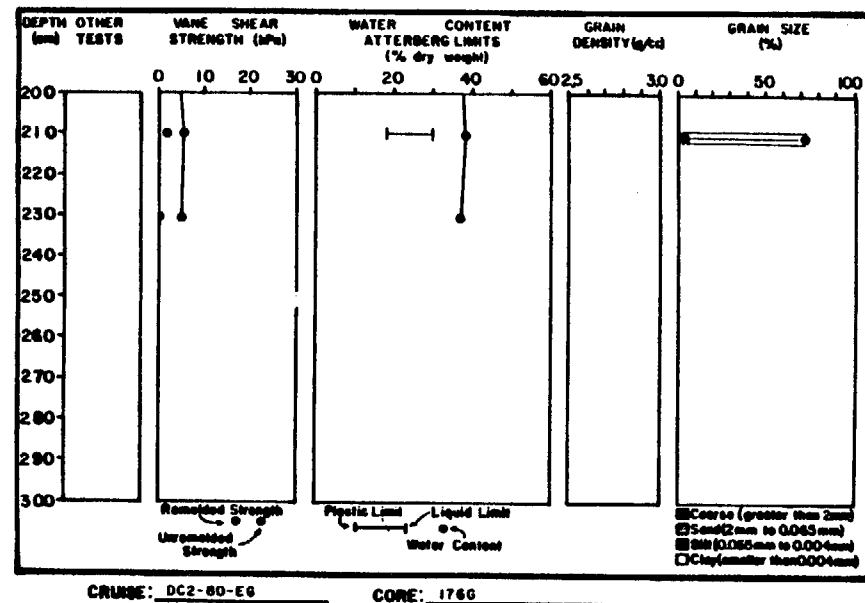
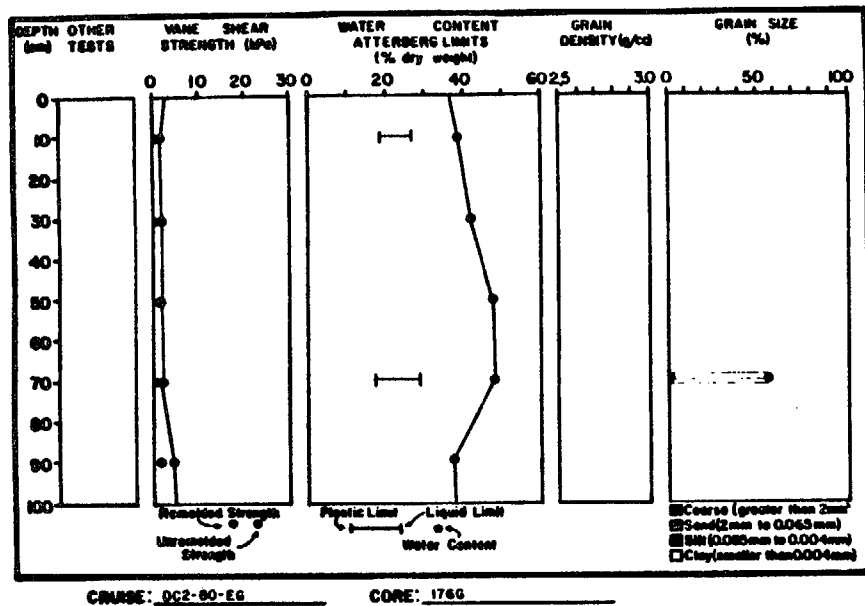


CRUISE: SB-77-EG CORE: 33G

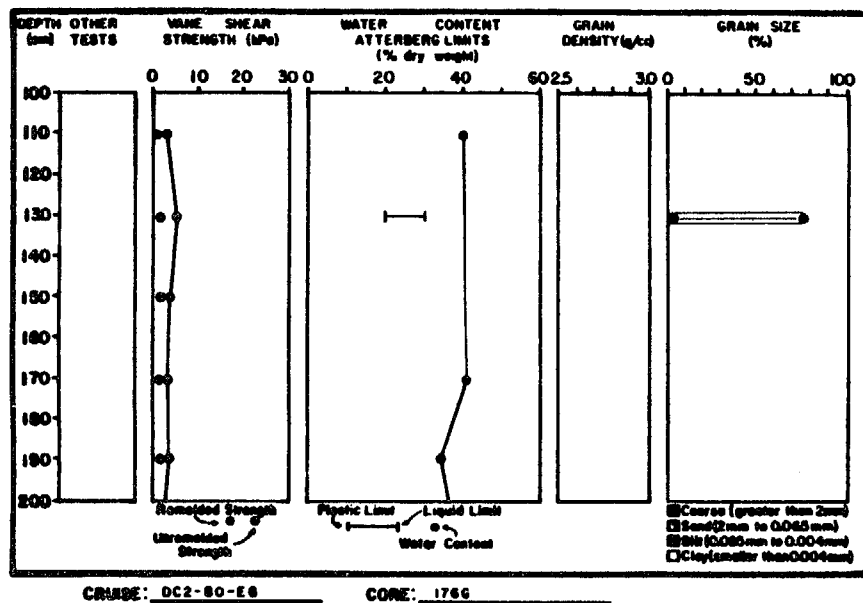


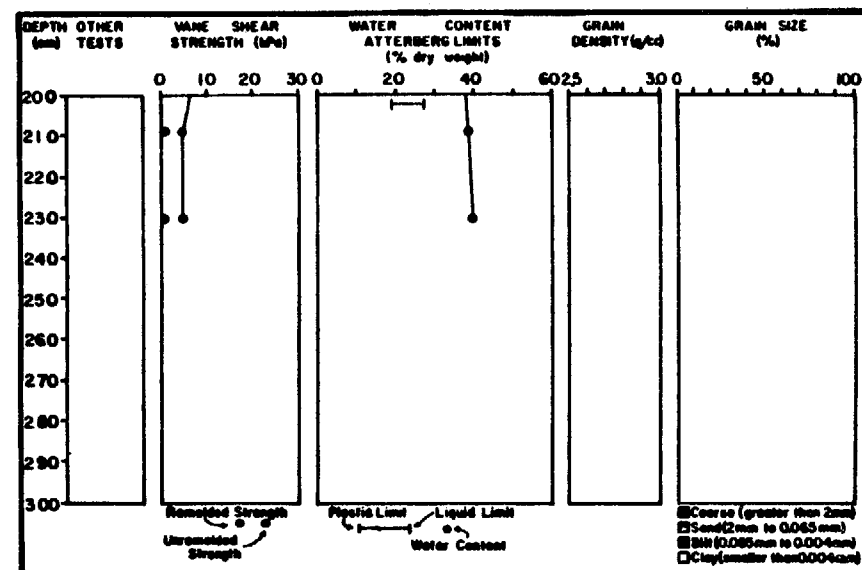
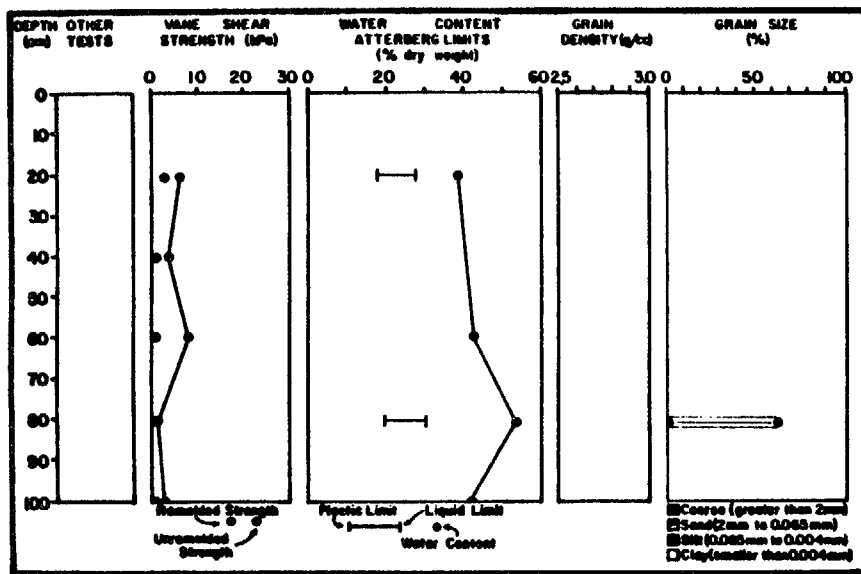




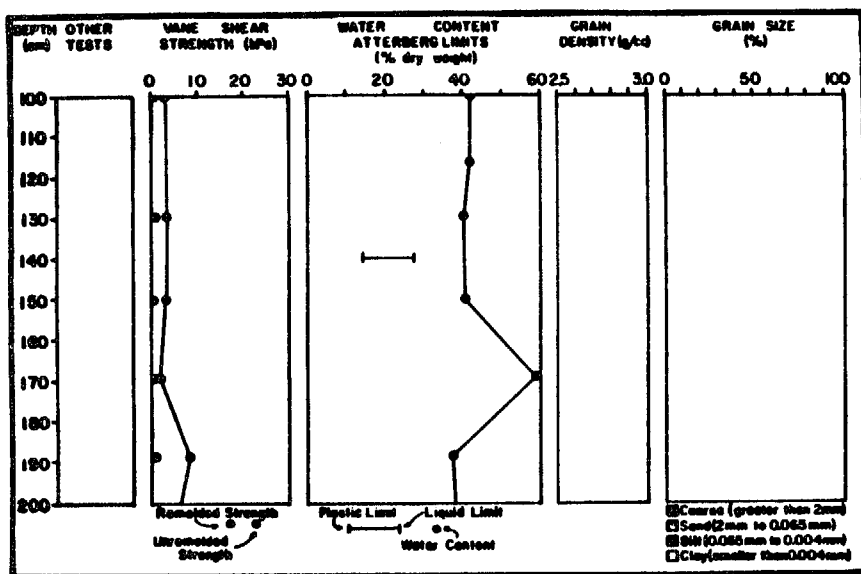


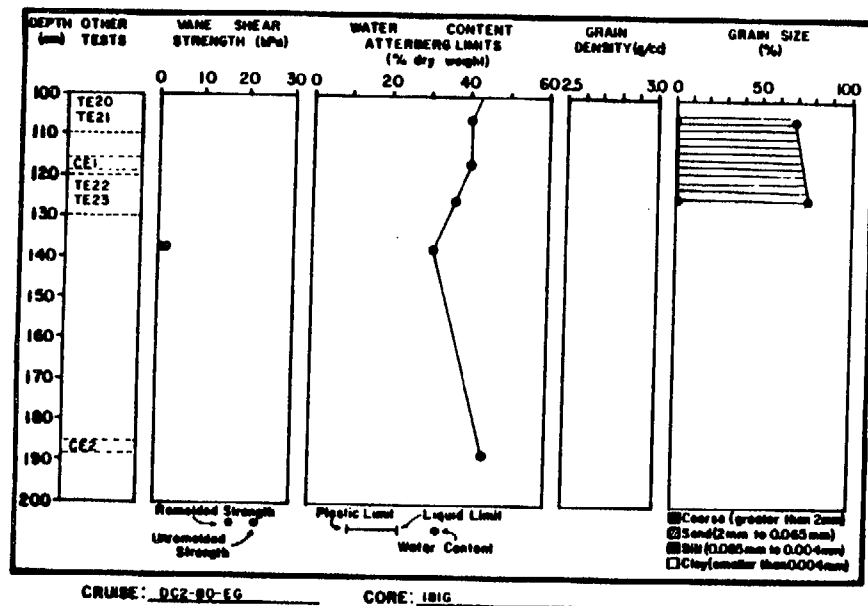
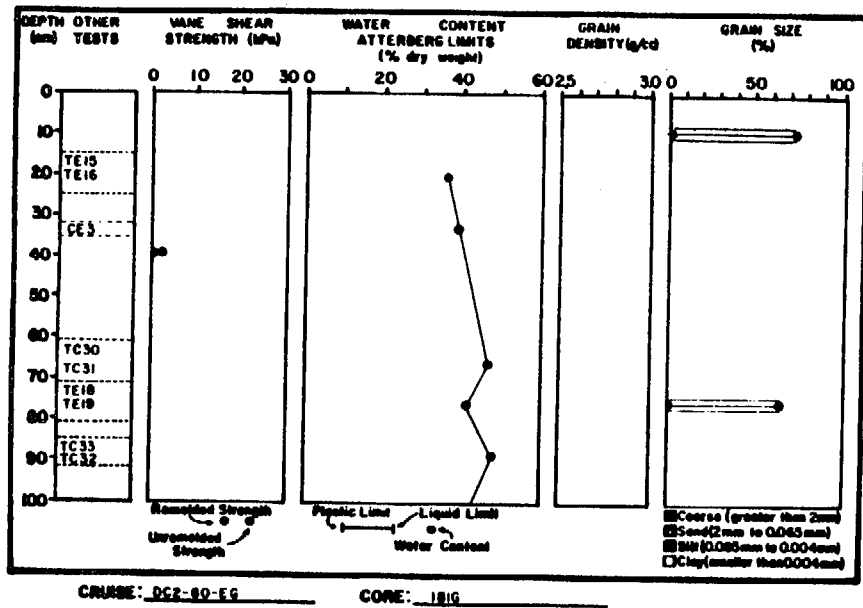
264

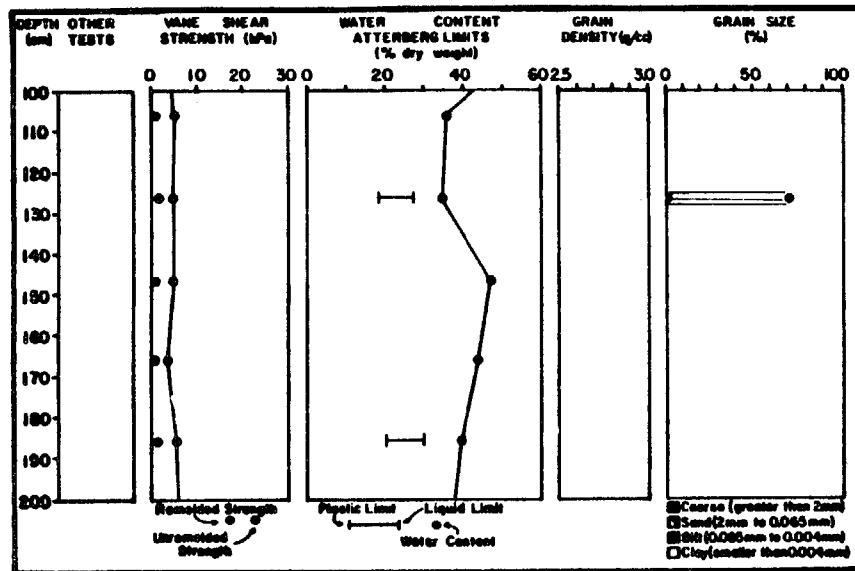
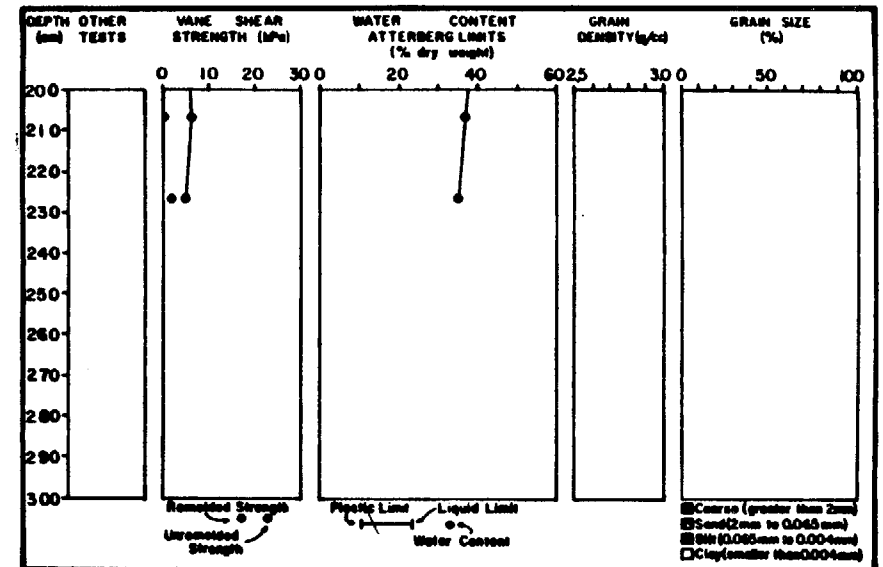
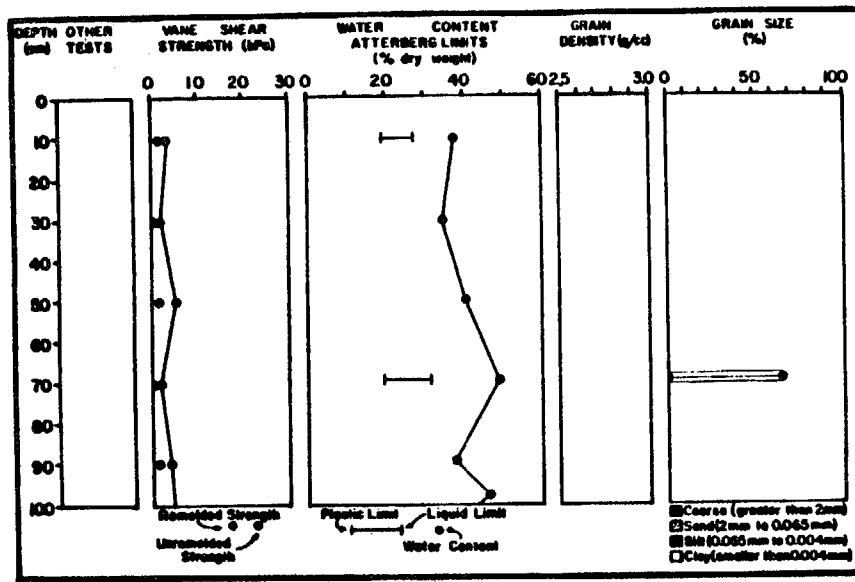


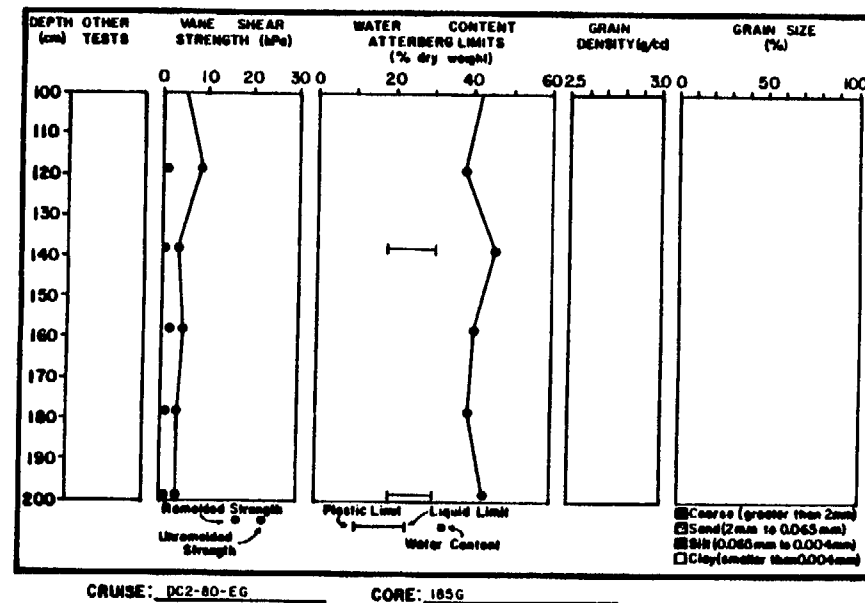
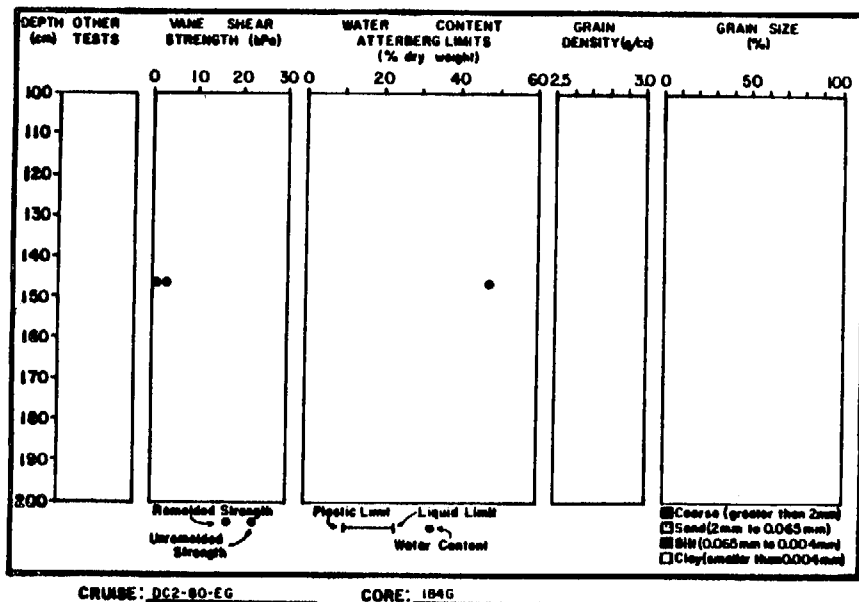
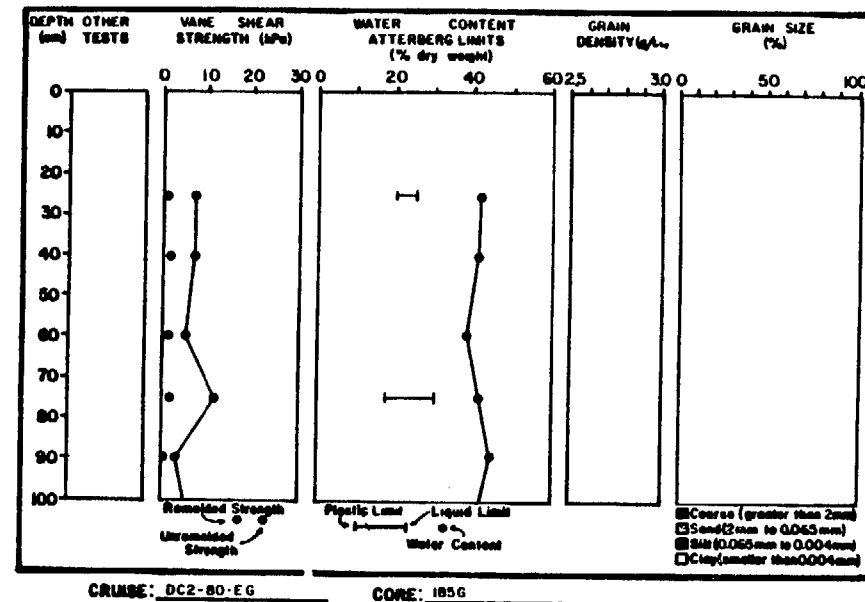
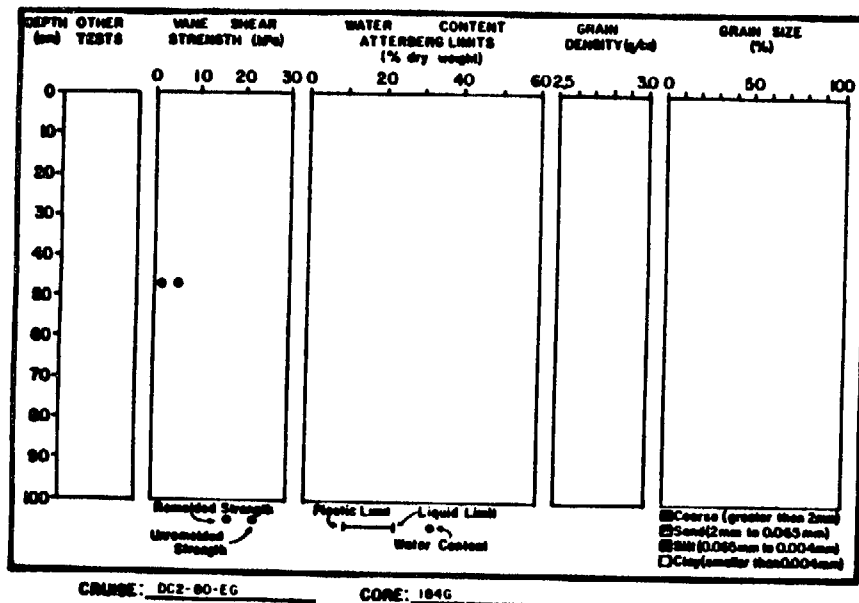


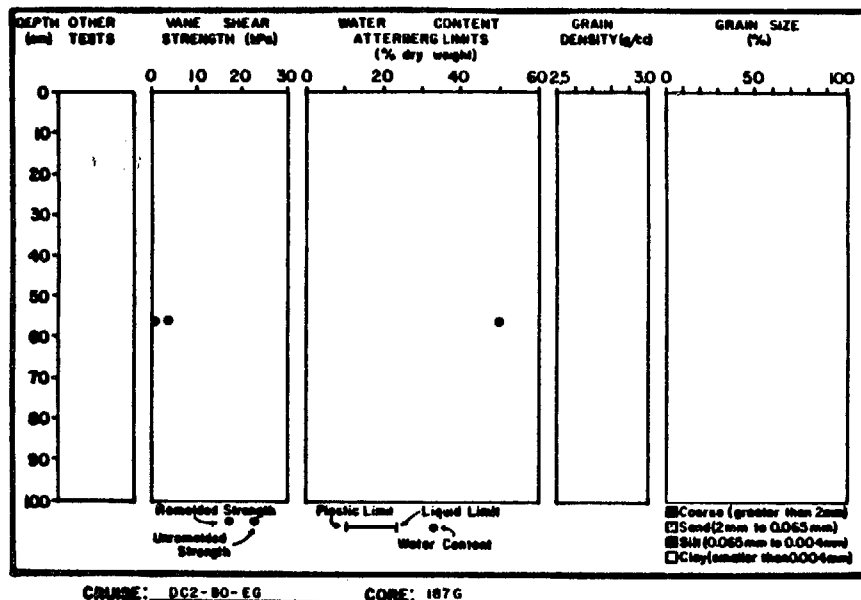
266



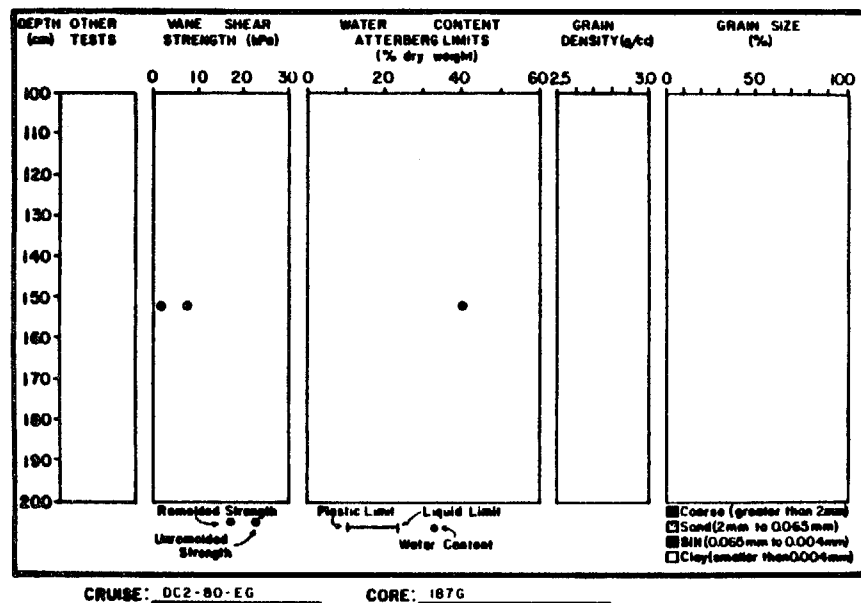


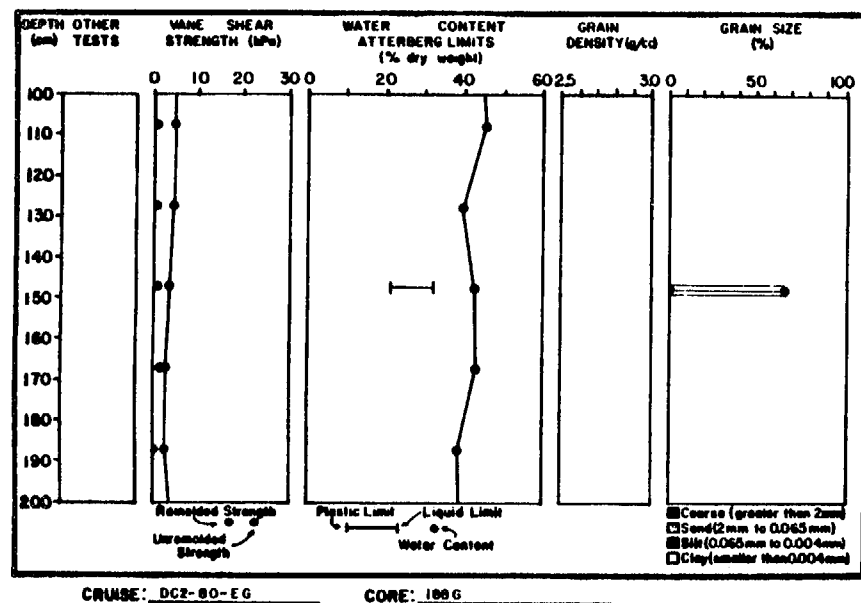
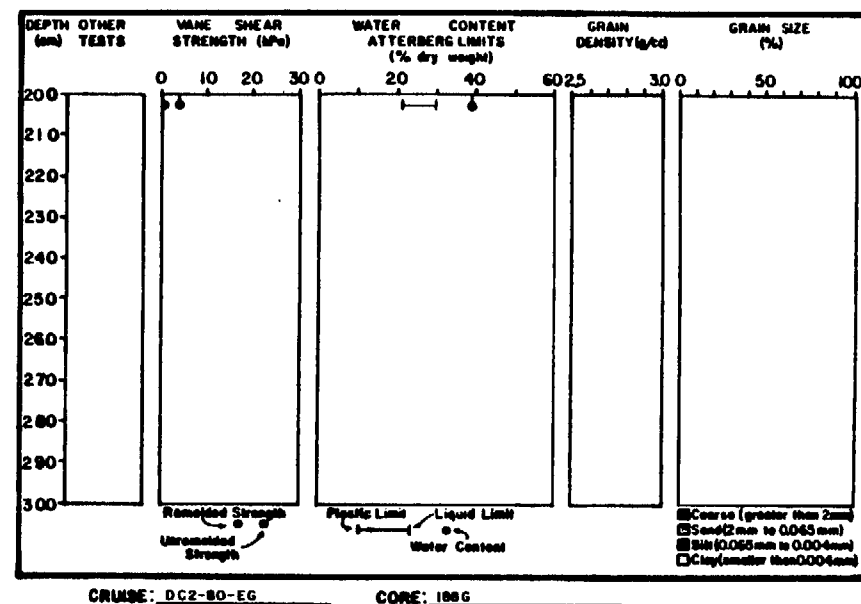
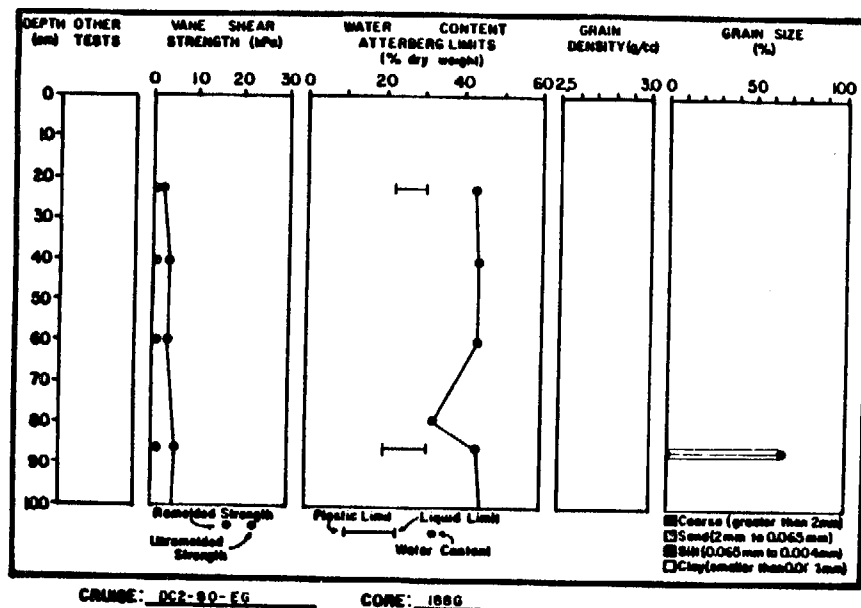


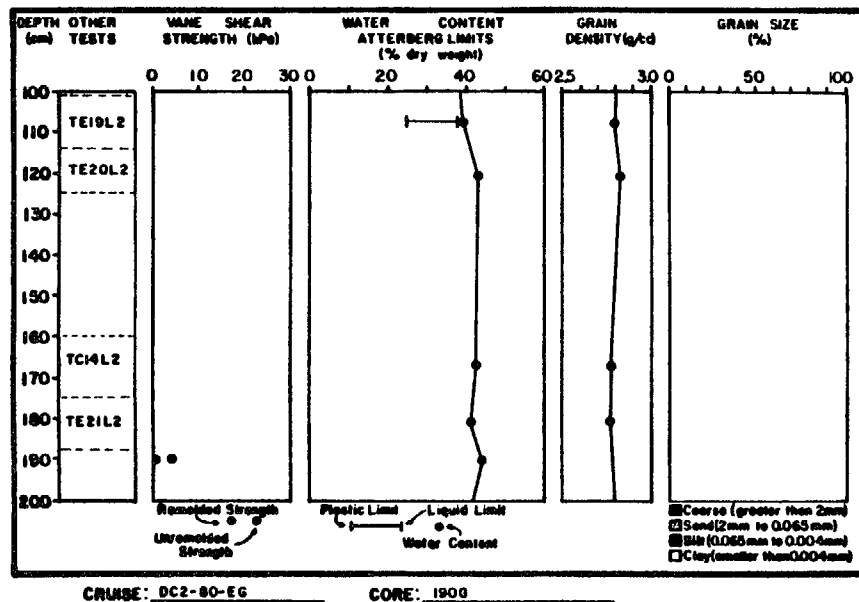
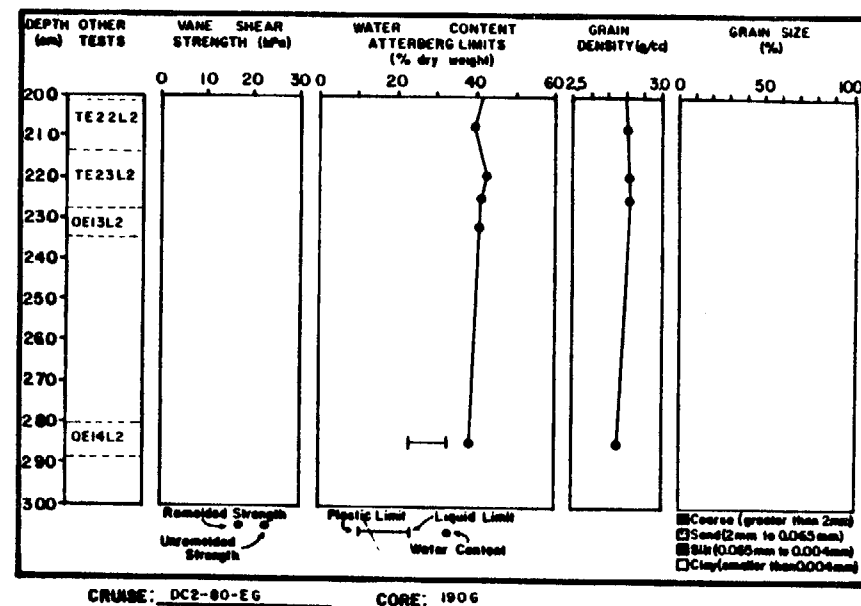
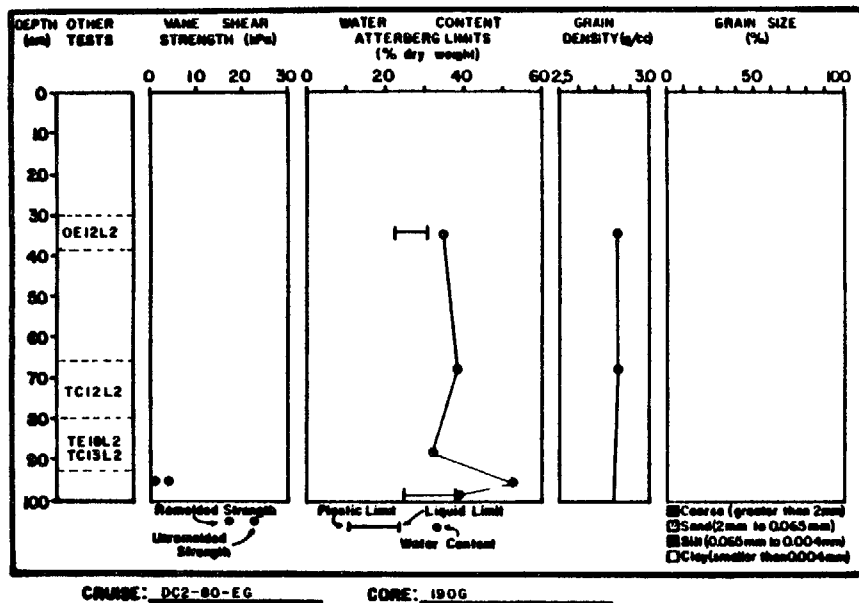


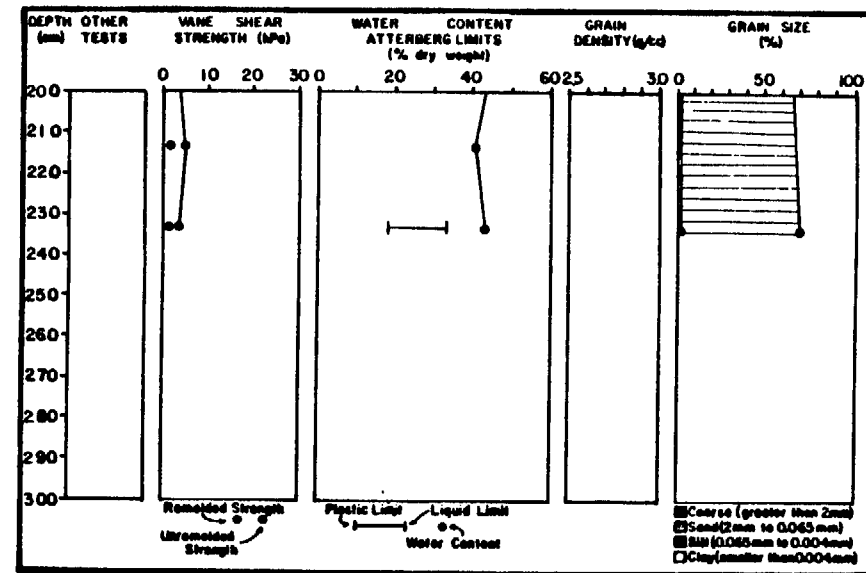
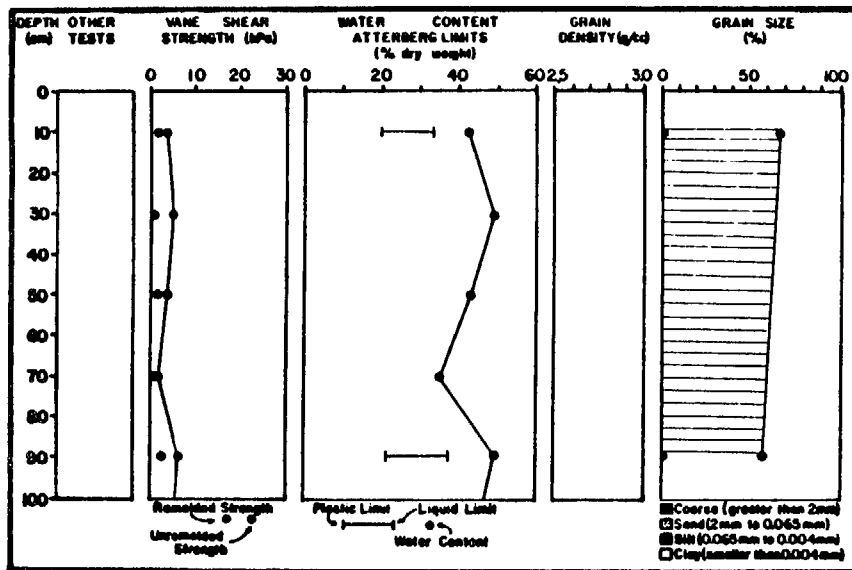


270

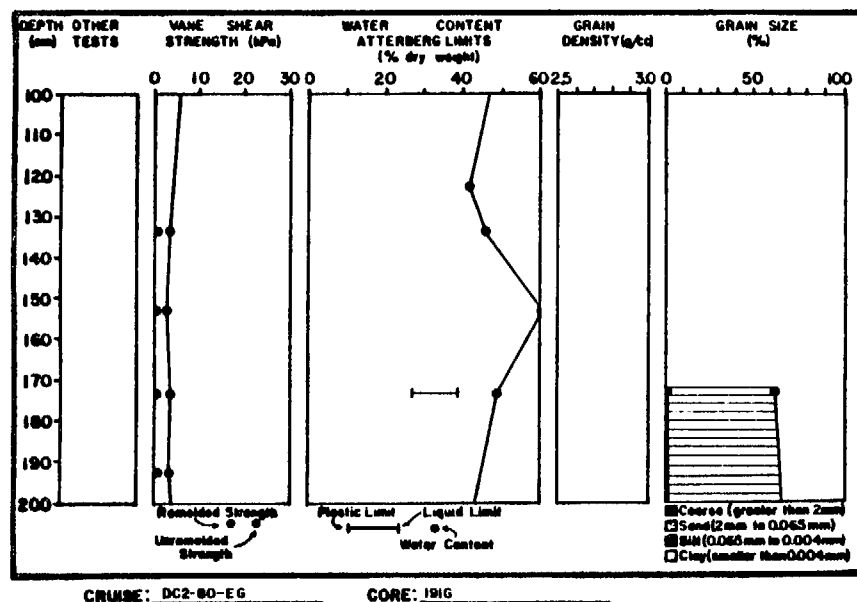


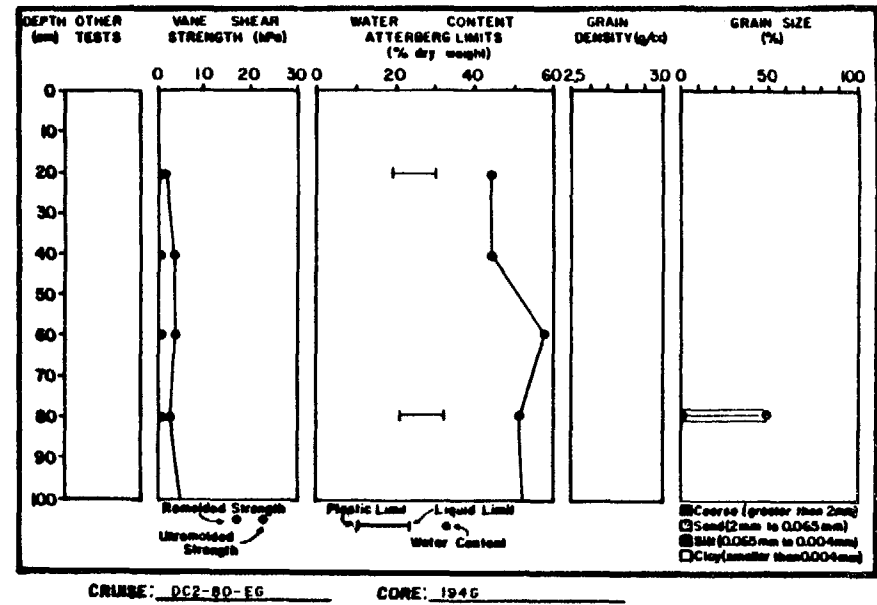
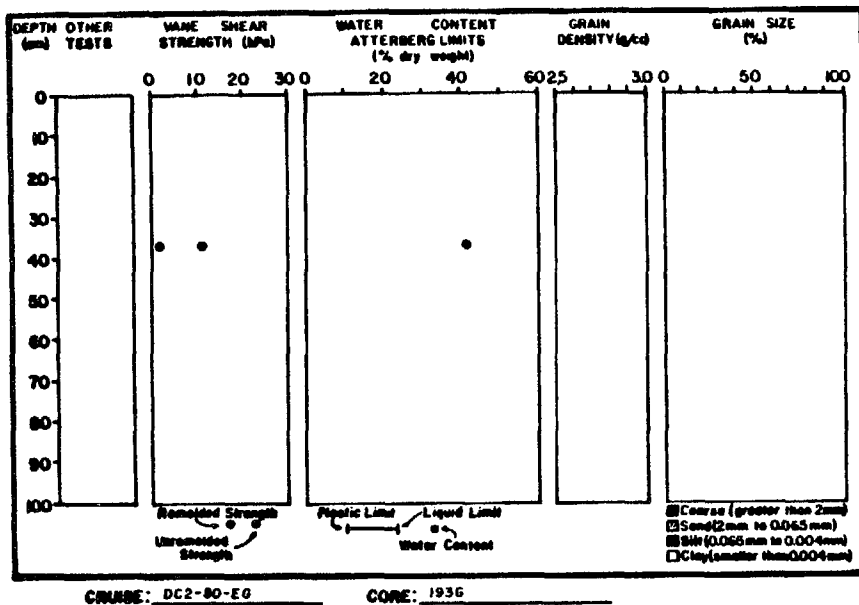




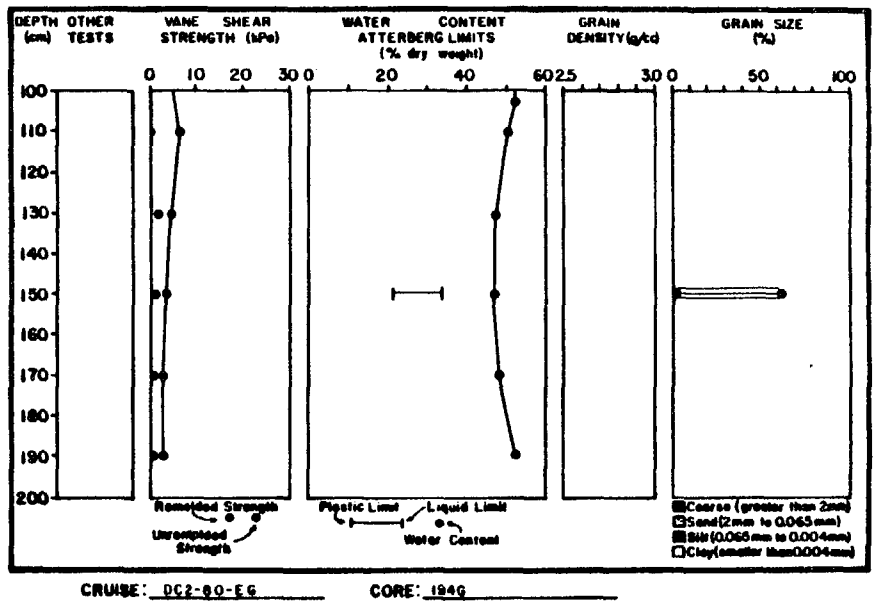
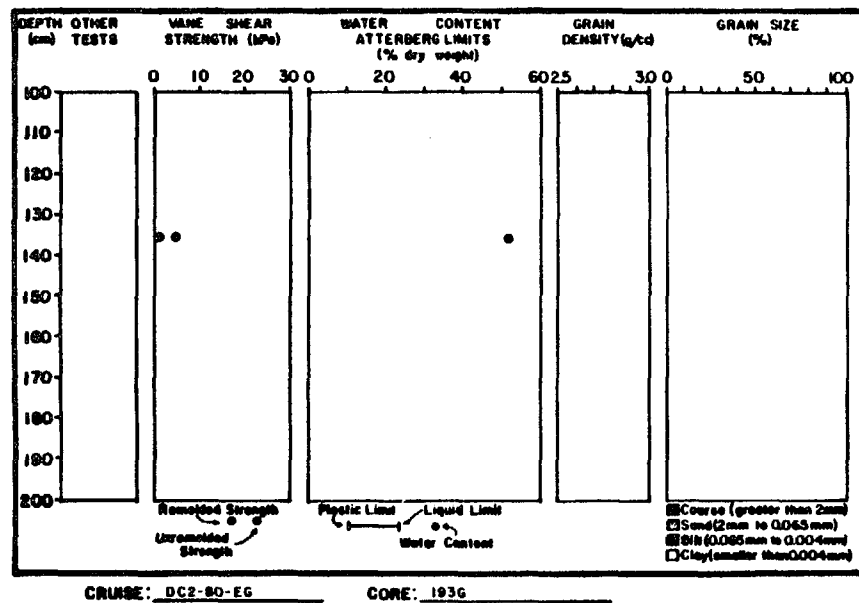


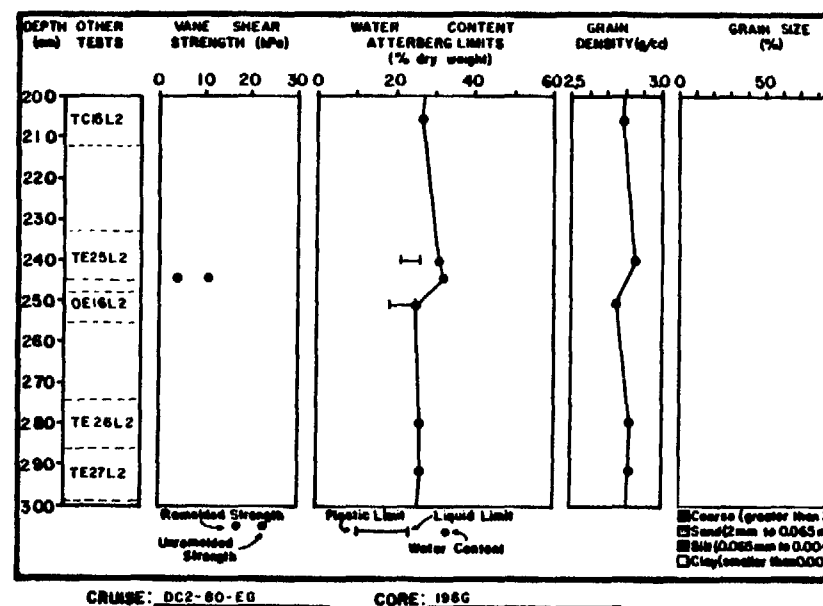
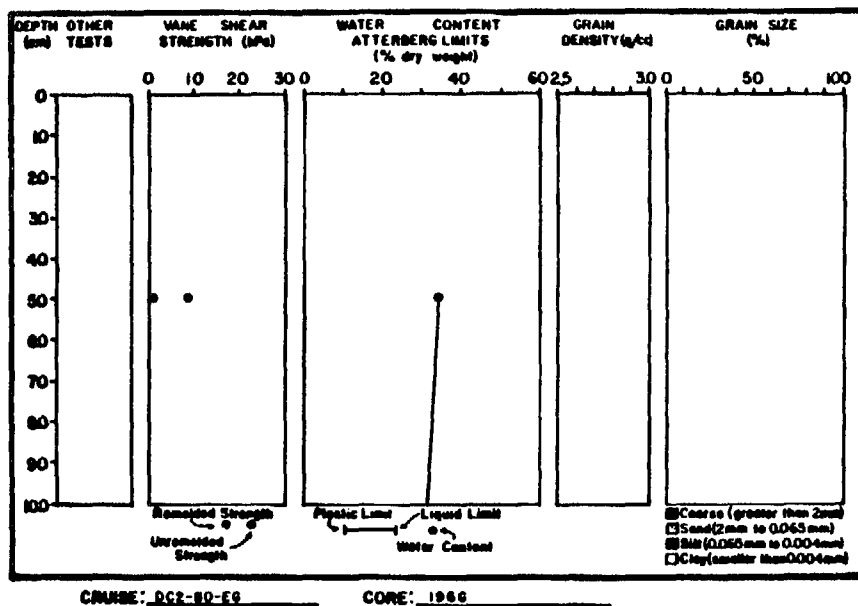
273



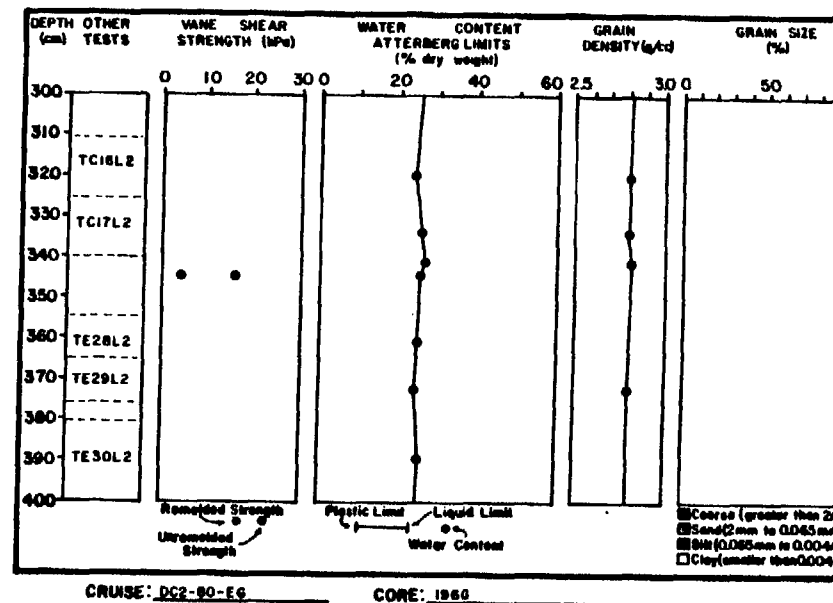
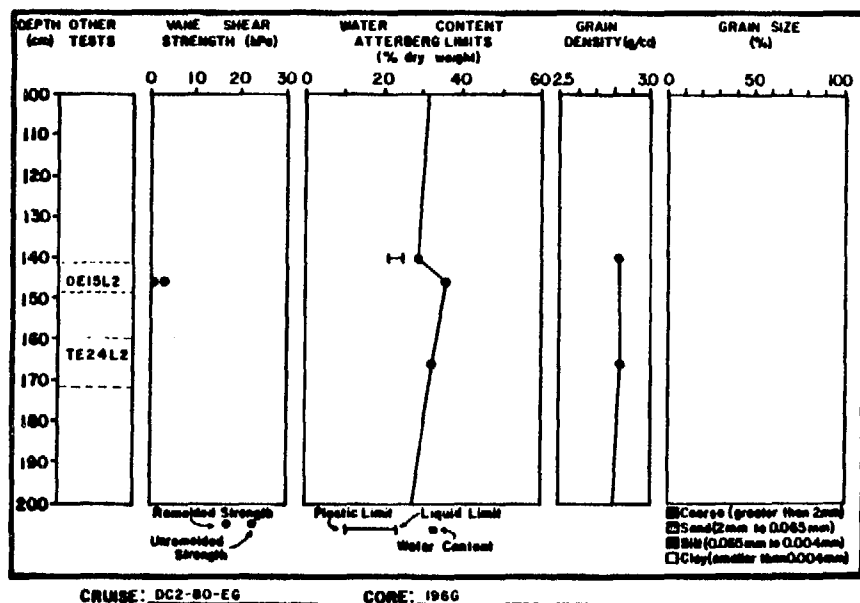


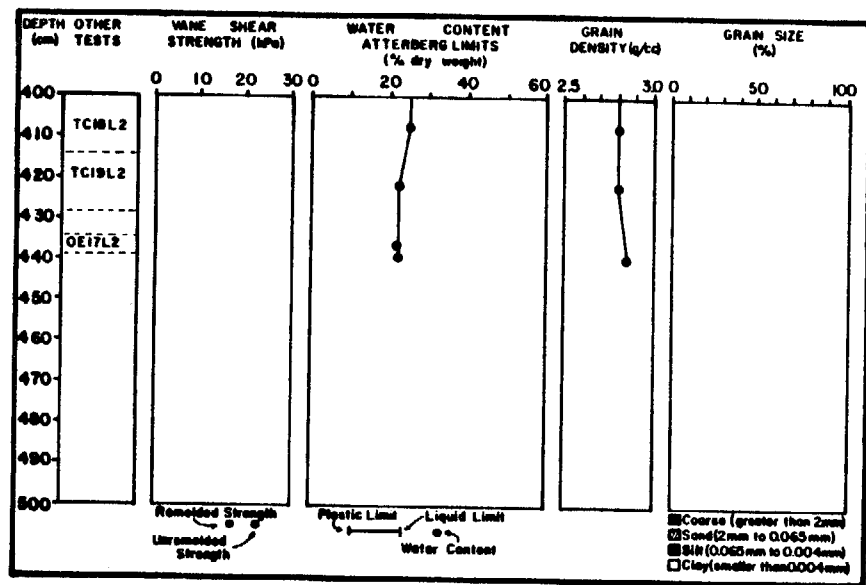
274





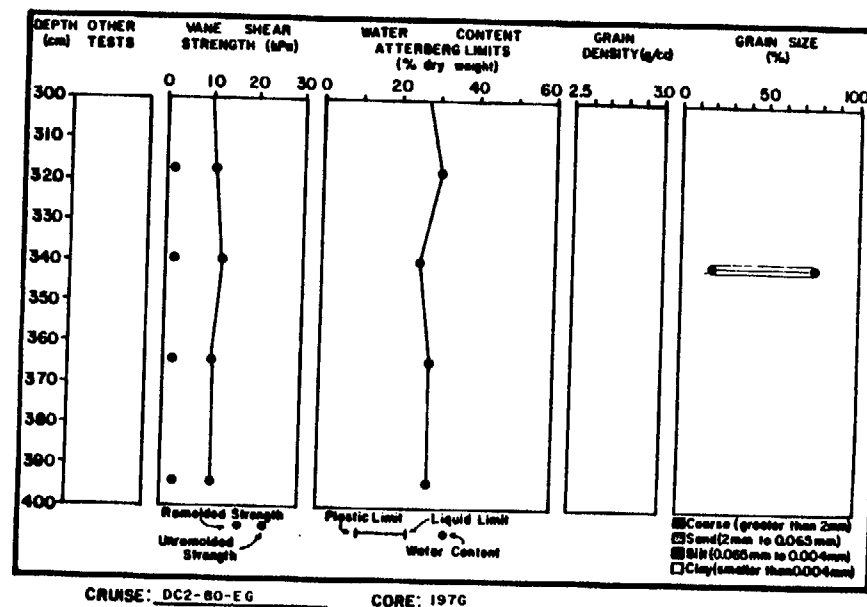
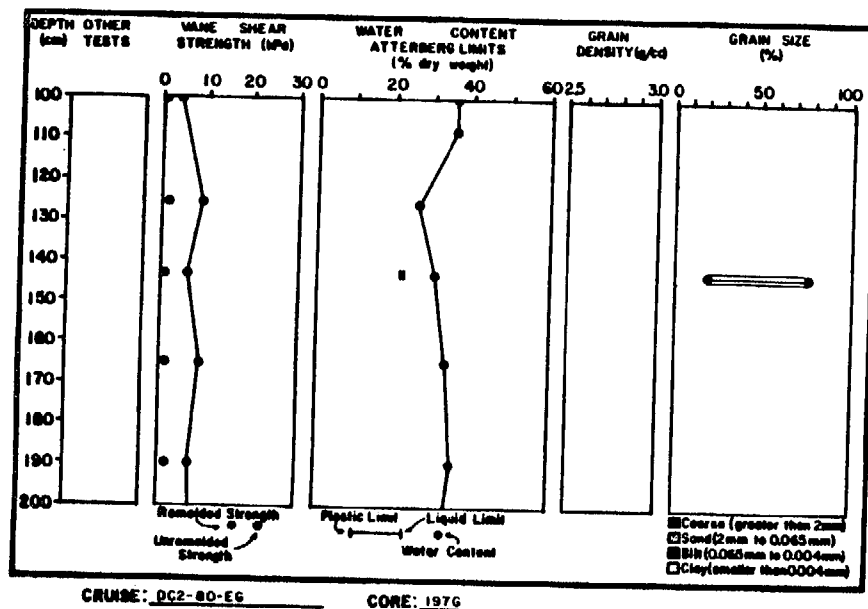
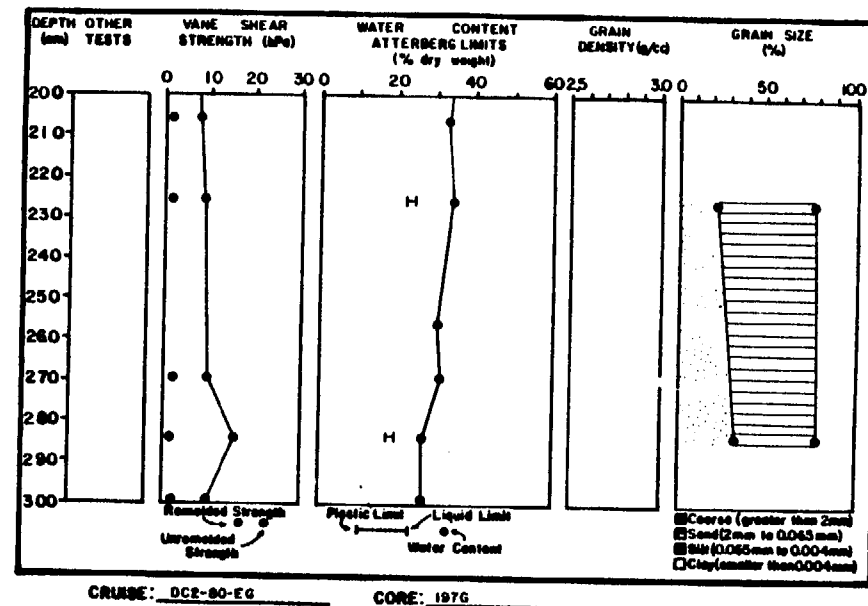
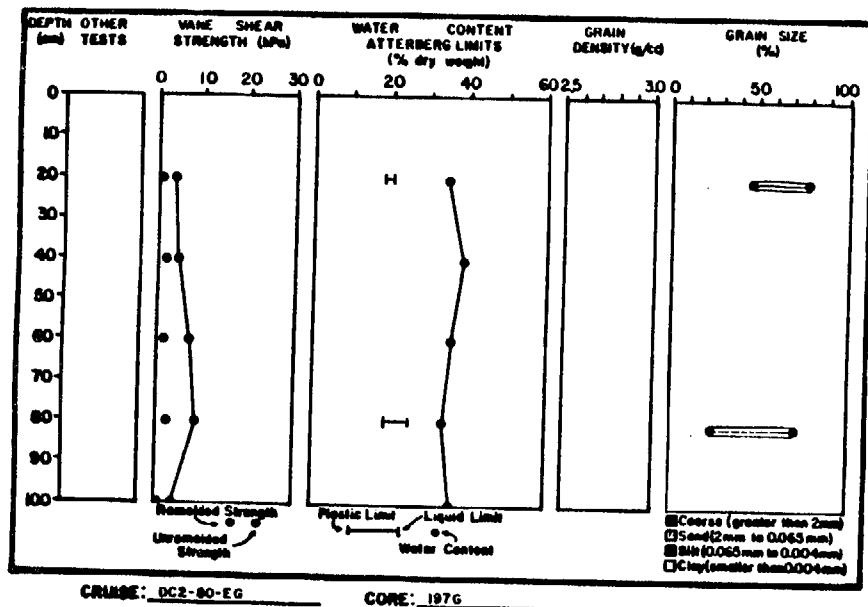
275

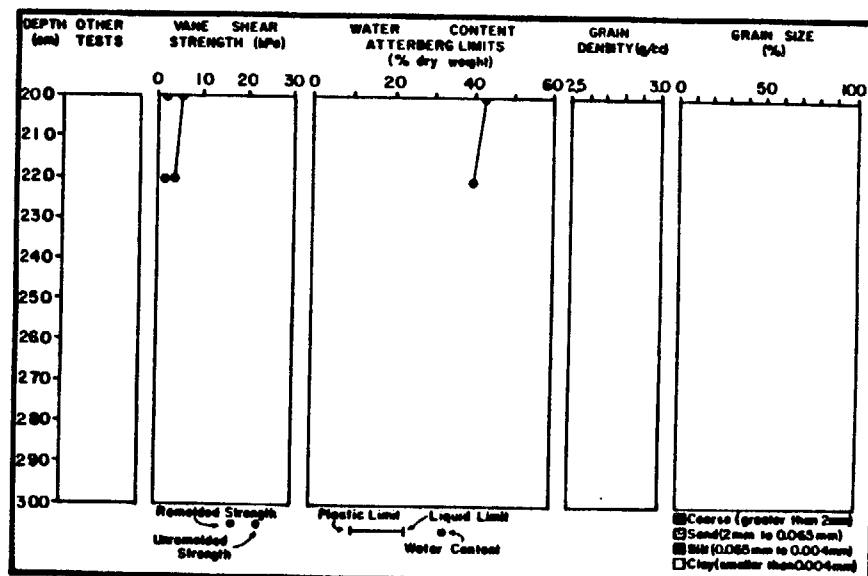
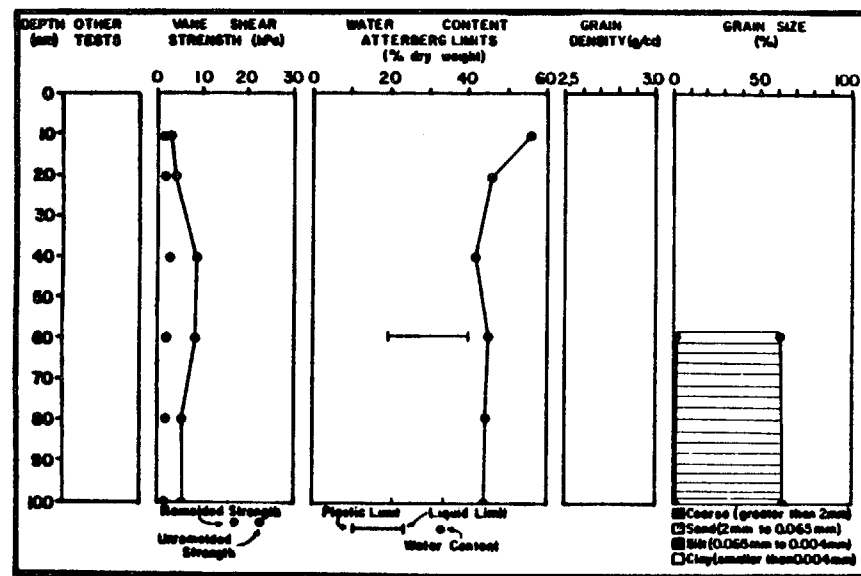
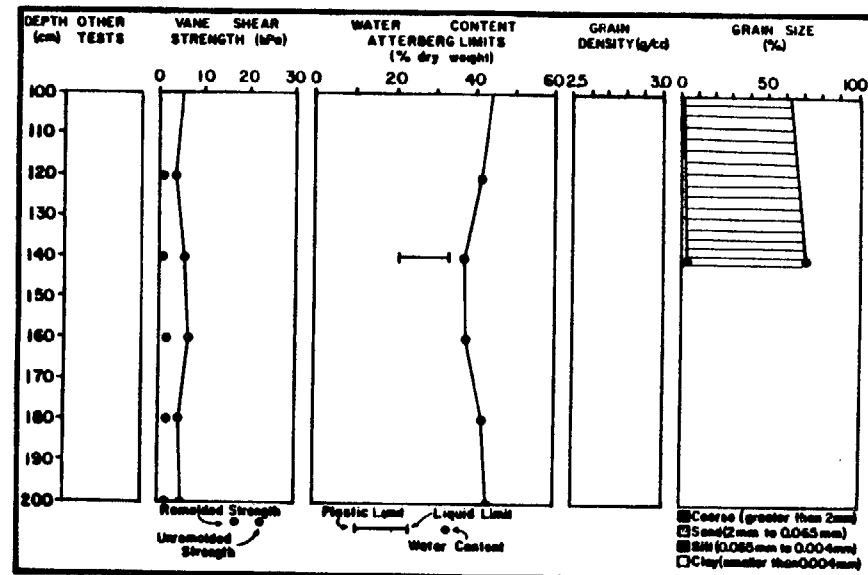
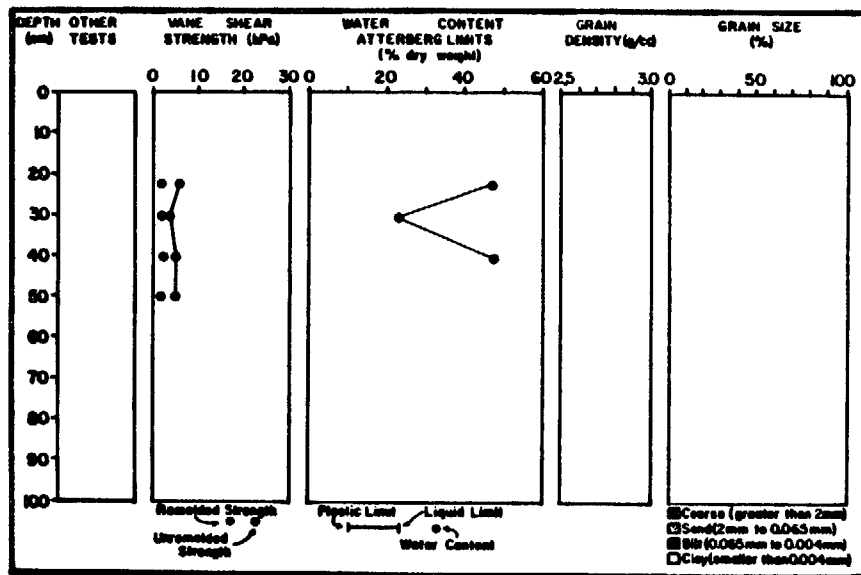


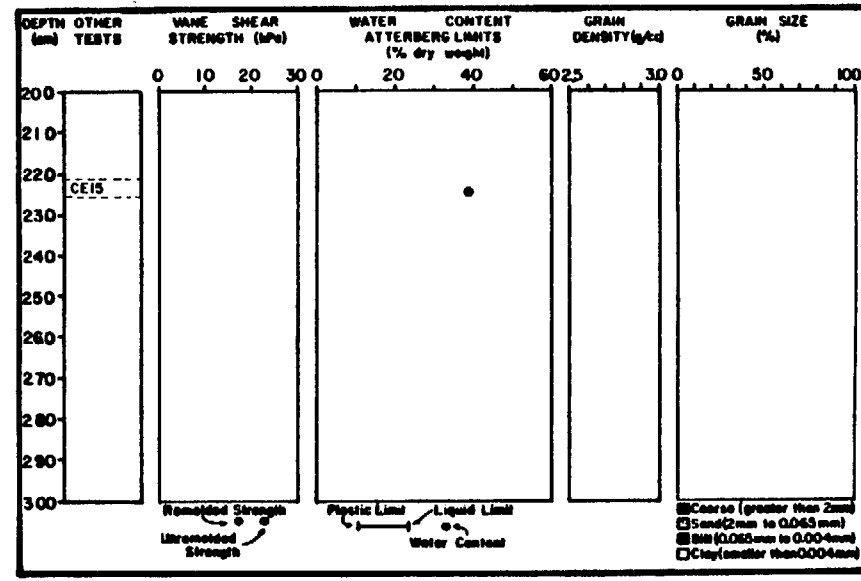
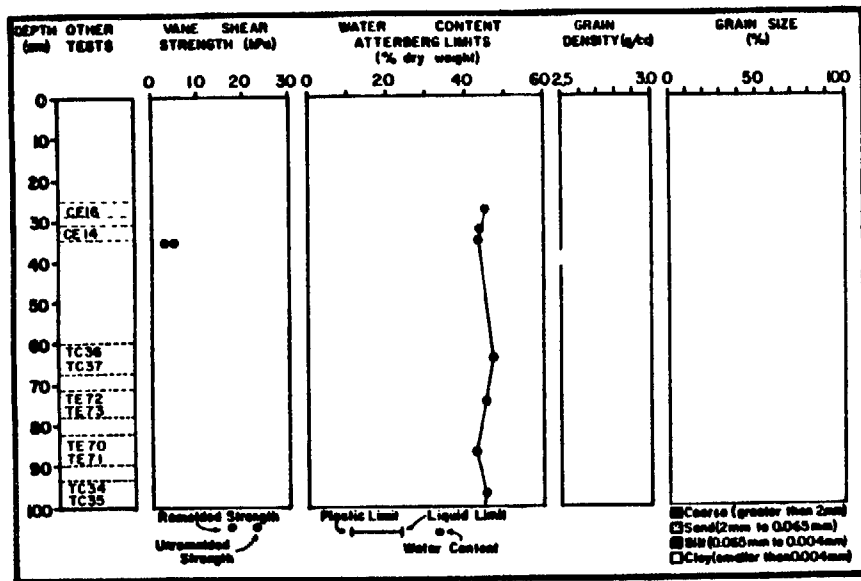


CRUISE: DC2-80-EG

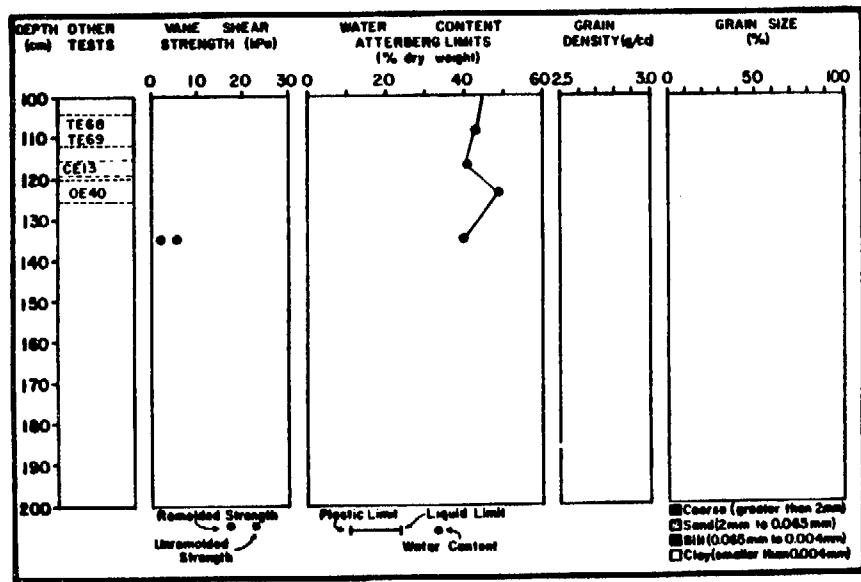
CORE: 1966

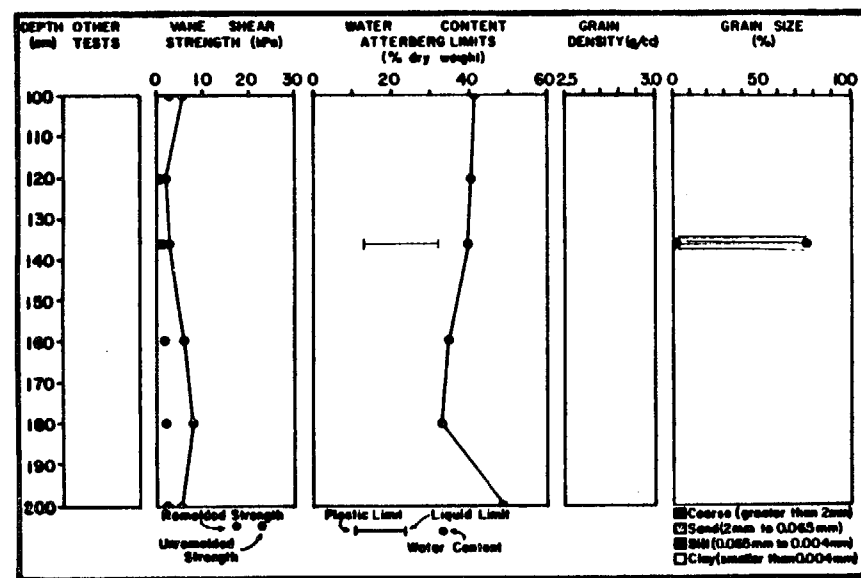
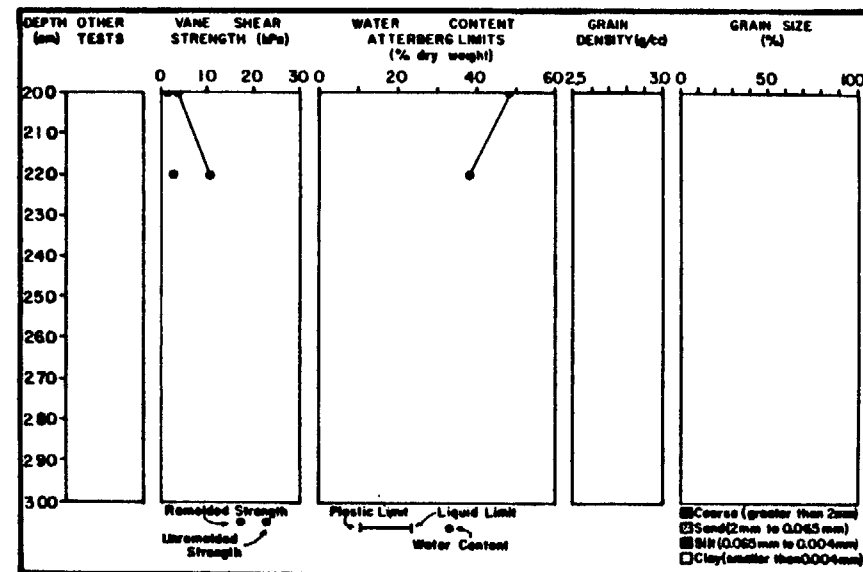
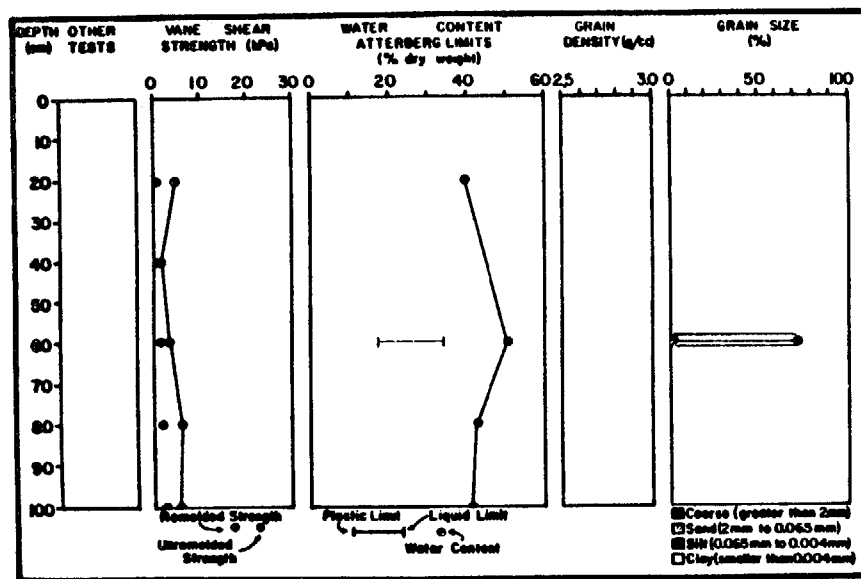


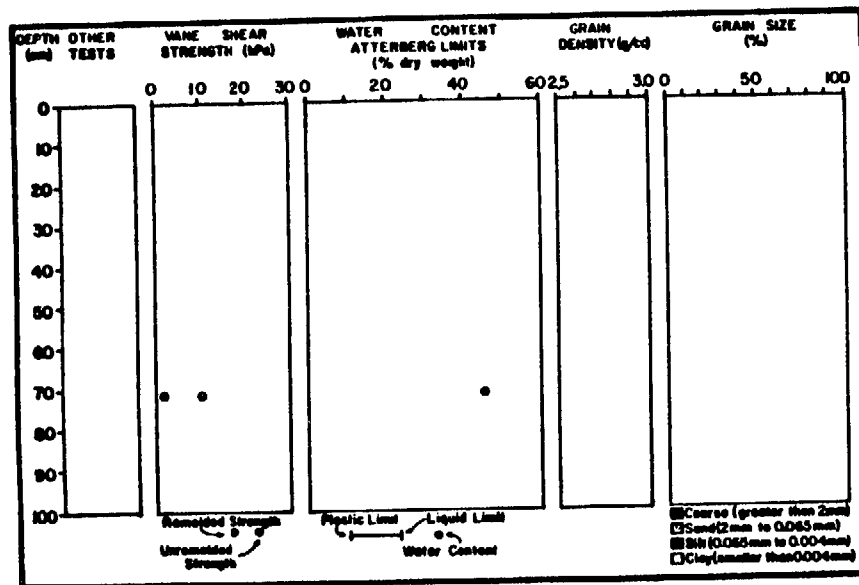




279

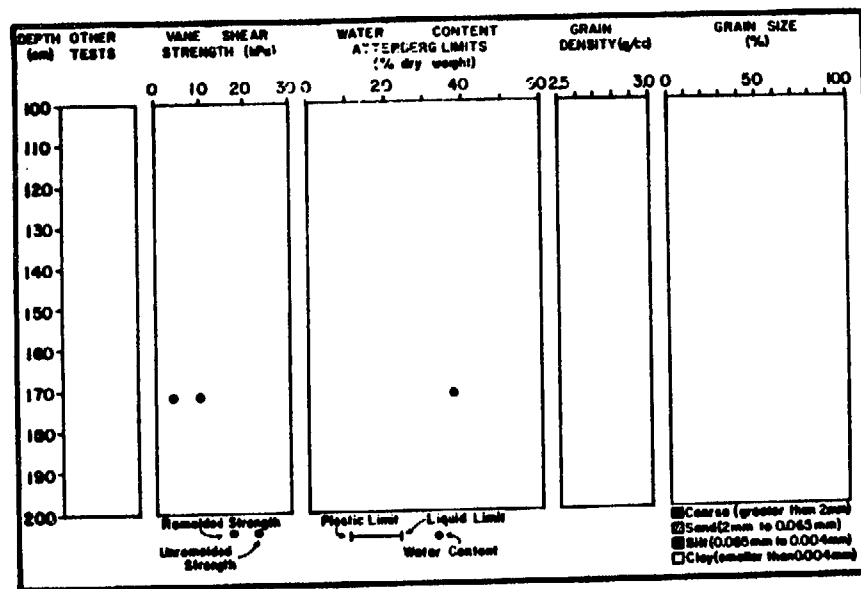






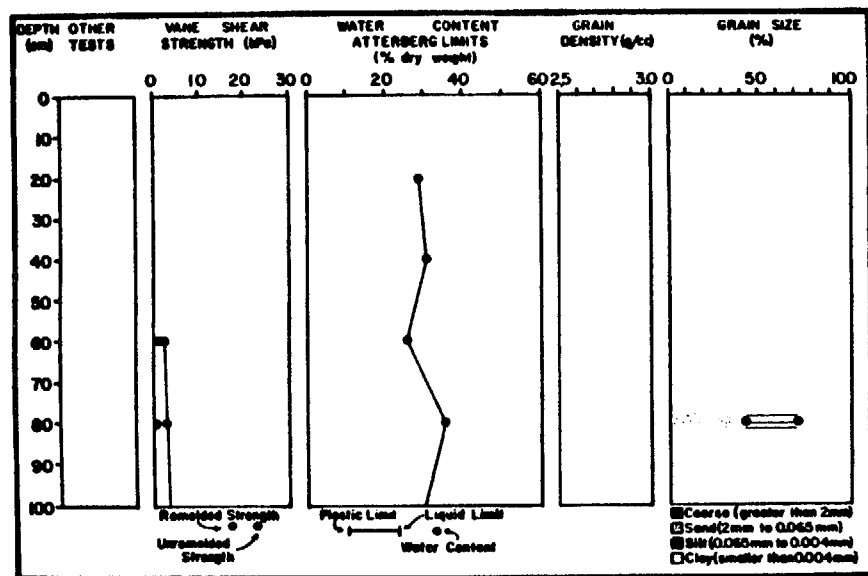
CRUISE: DCI-81-EG

CORE: 628G3

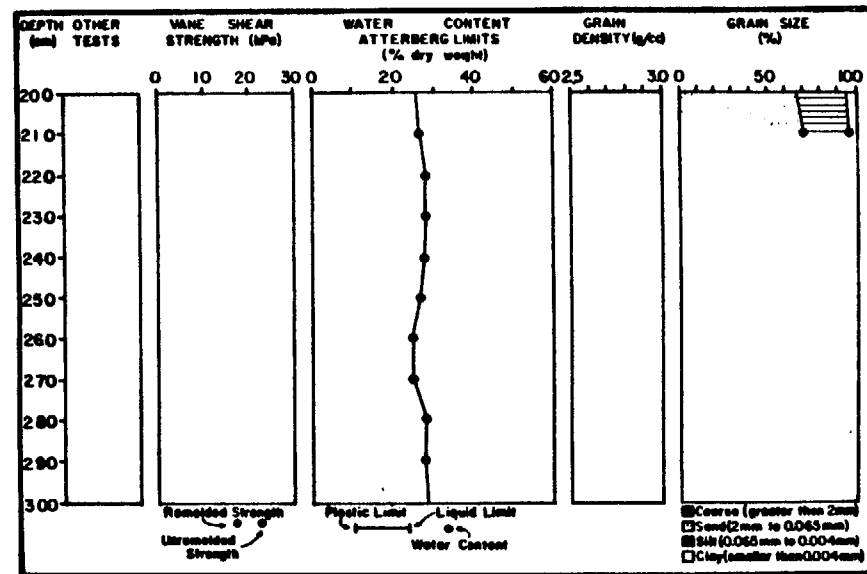


CRUISE: DCI-81-EG

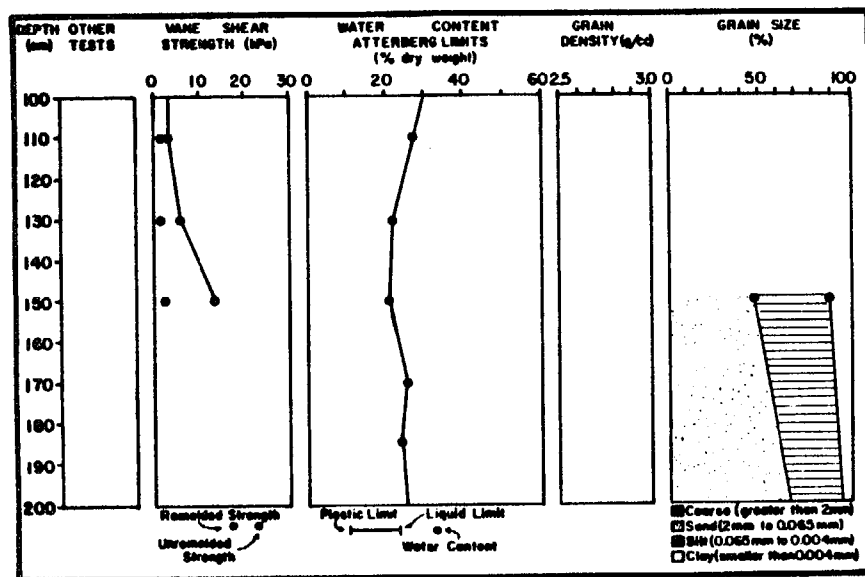
CORE: 628G3



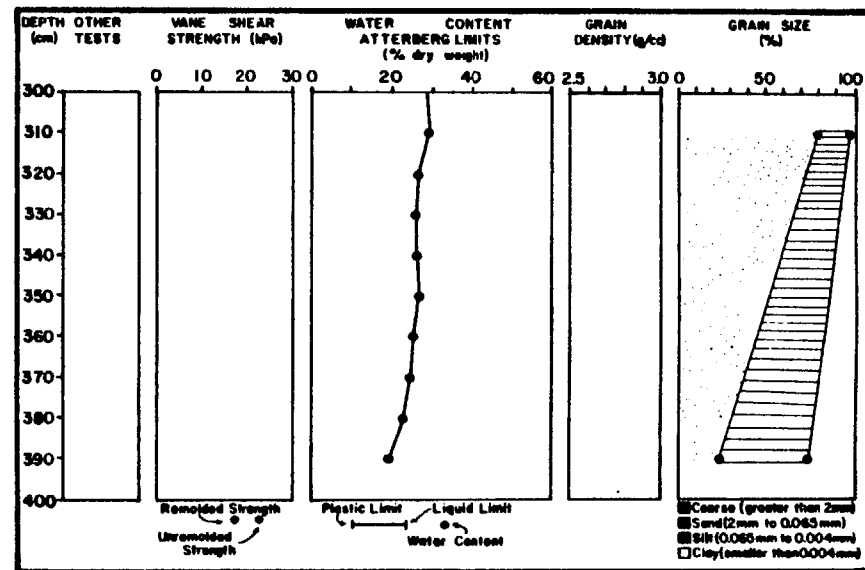
CRUISE: DCI-81-EG CORE: 630A1



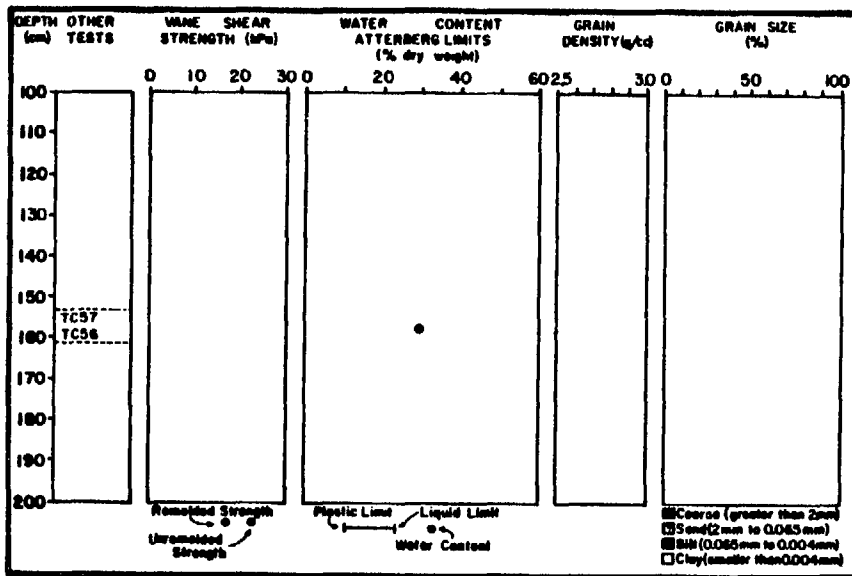
CRUISE: DCI-81-EG CORE: 630A1



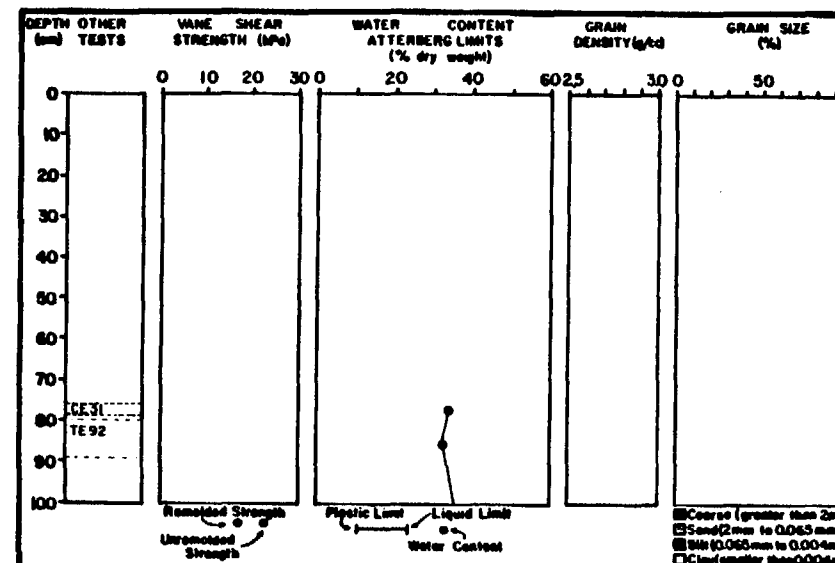
CRUISE: DCI-81-EG CORE: 630A1



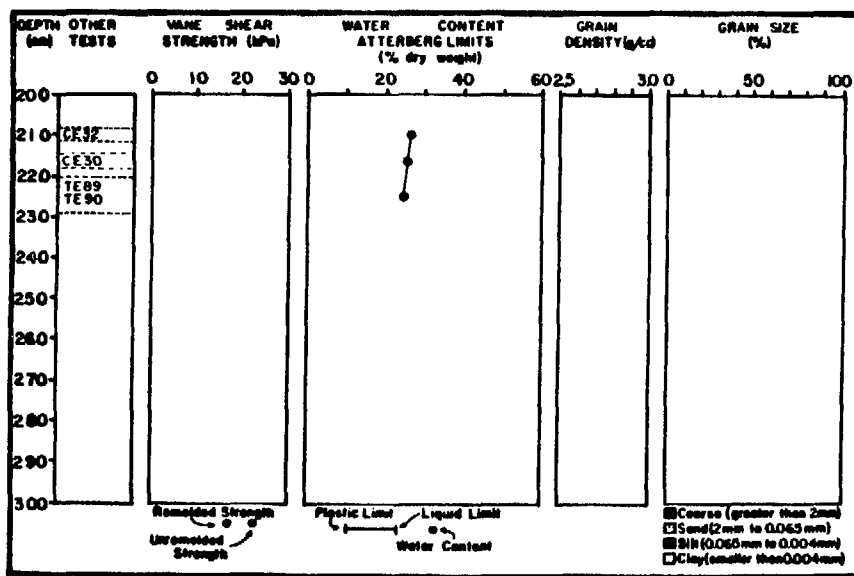
CRUISE: DCI-81-EG CORE: 630A1



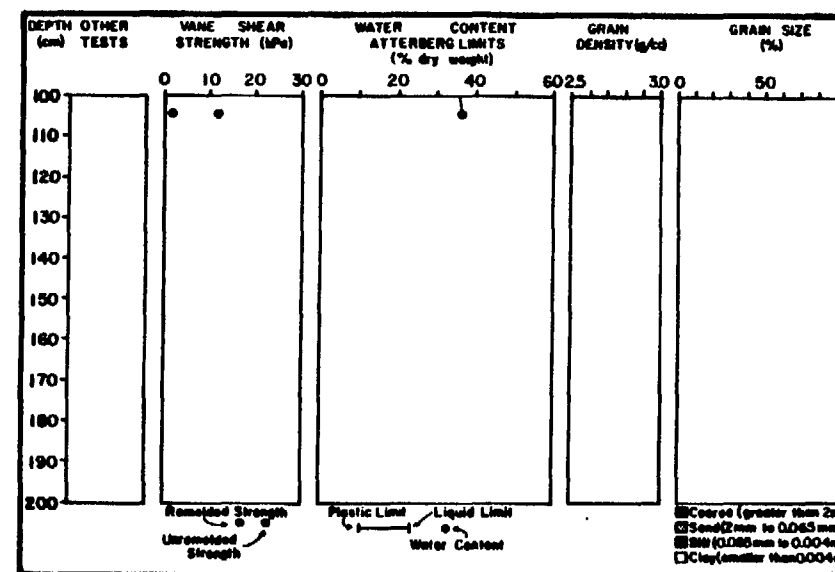
CRUISE: DCI-81-EG CORE: 630A2



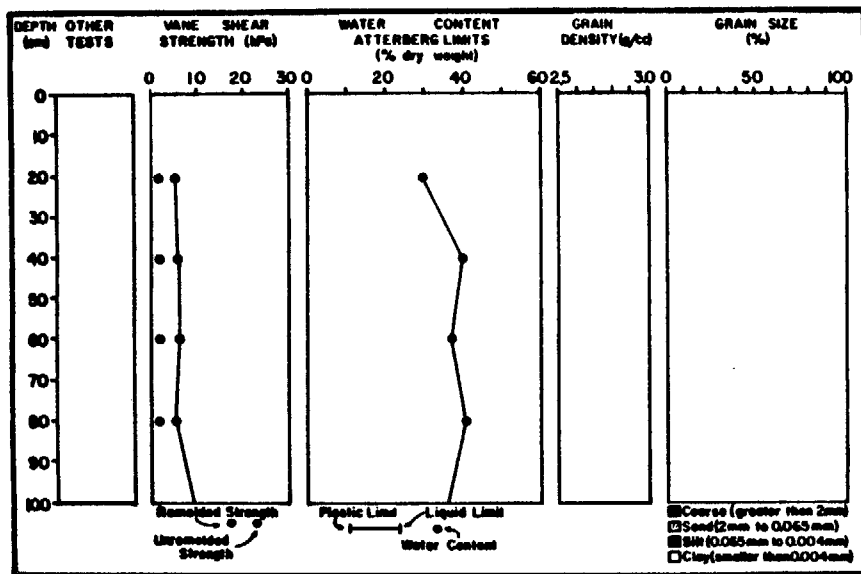
CRUISE: DCI-81-EG CORE: 632G1



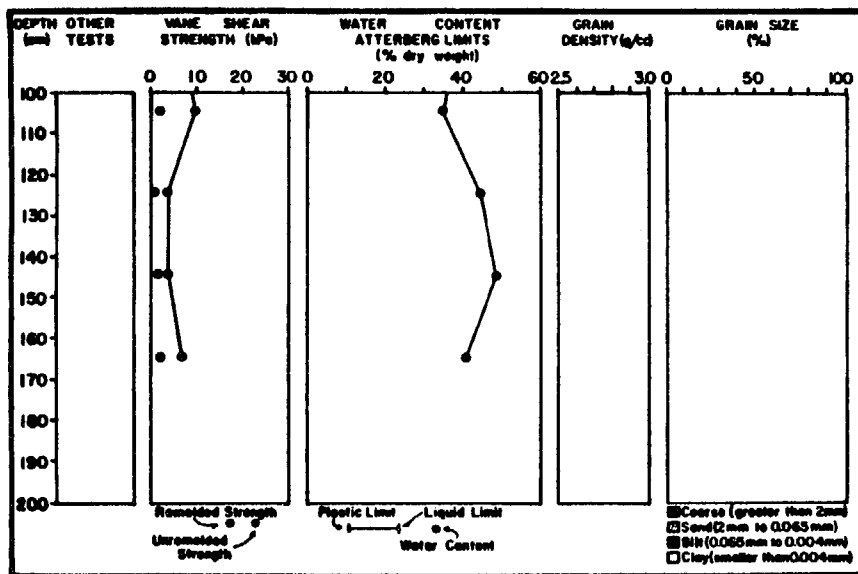
CRUISE: DCI-81-EG CORE: 630A2



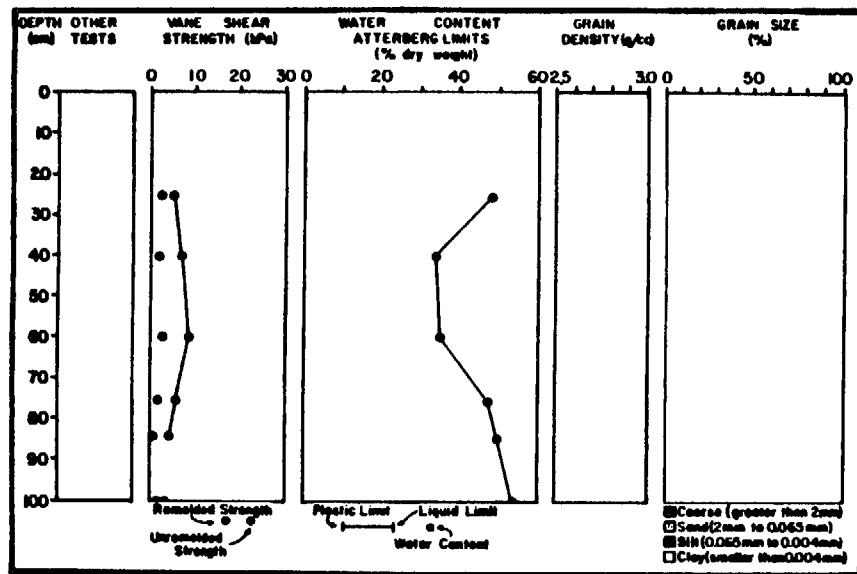
CRUISE: DCI-81-EG CORE: 632G1



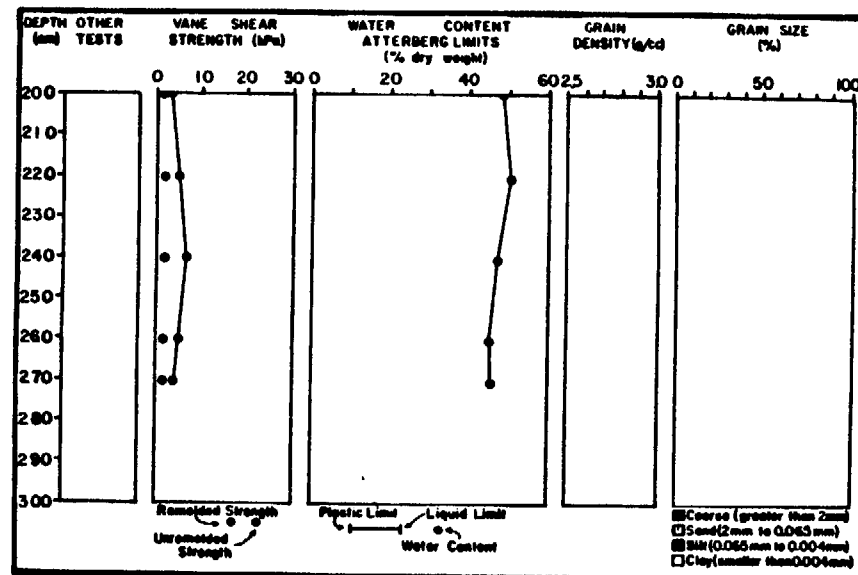
CRUISE: DCI-81-EG CORE: 63262



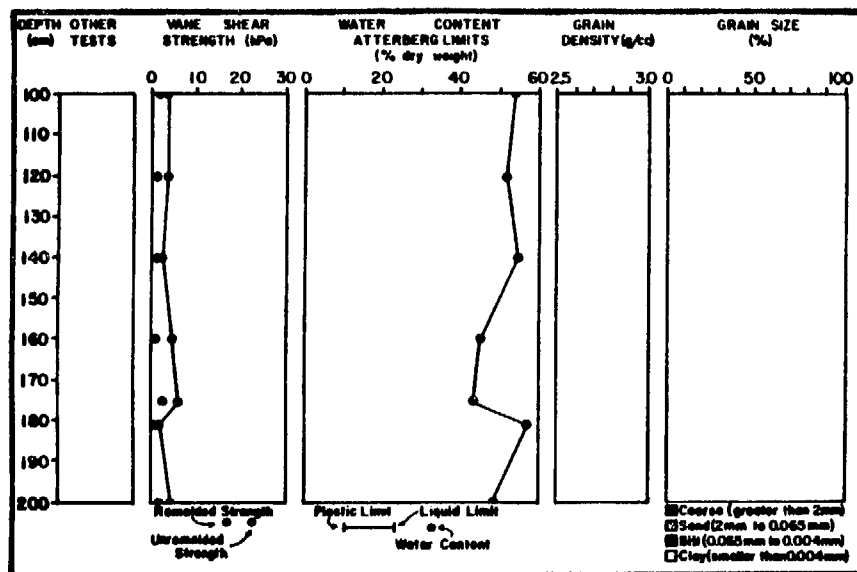
CRUISE: DCI-81-EG CORE: 63262



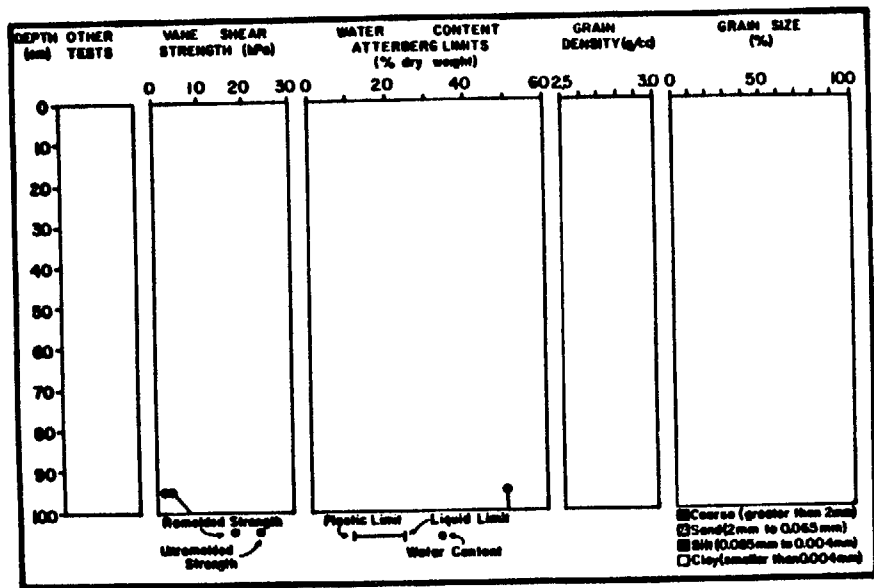
CRUISE: DCI-81-EG CORE: 633GI



CRUISE: DCI-81-EG CORE: 633GI

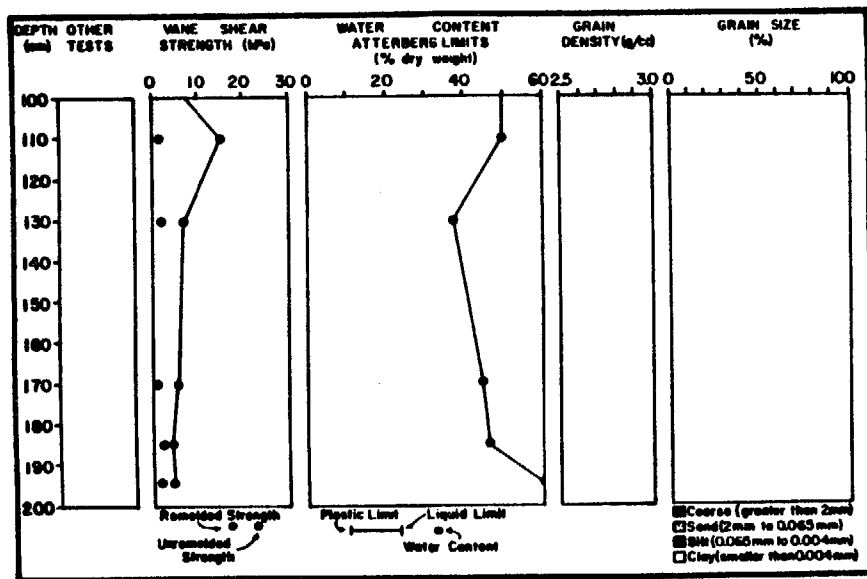


CRUISE: DCI-81-EG CORE: 633GI



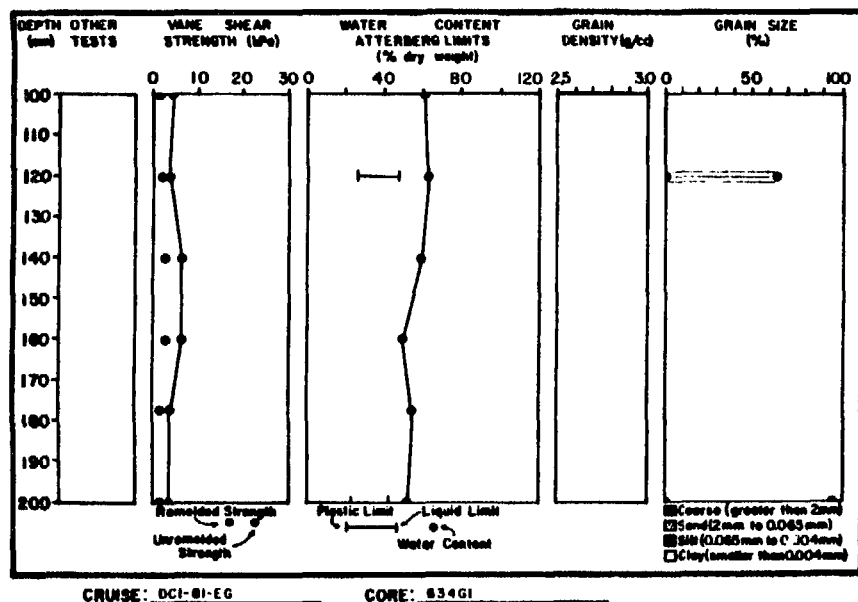
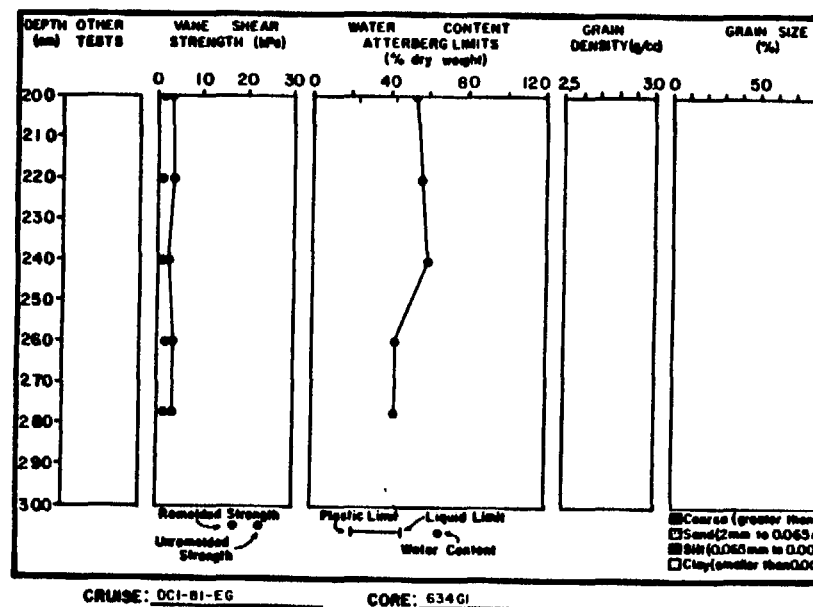
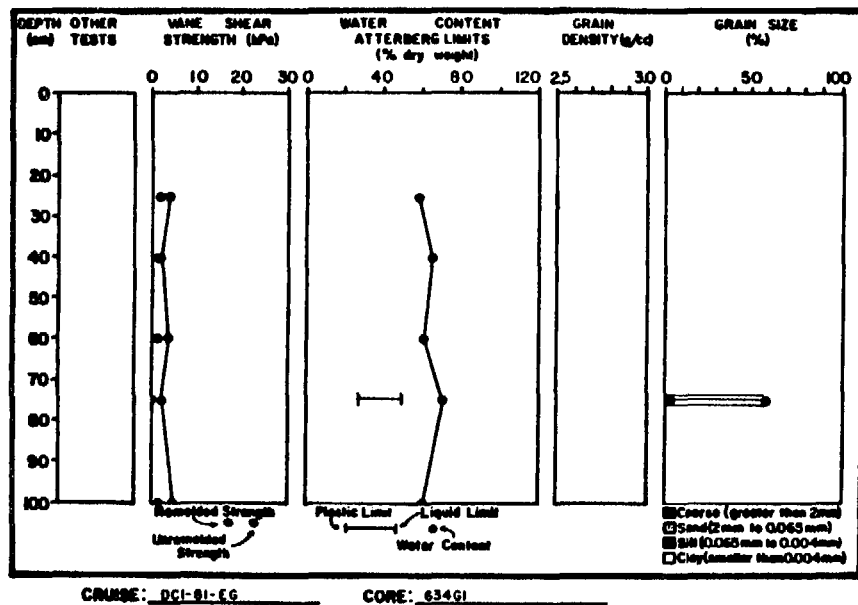
CRUISE: DCI-81-EG

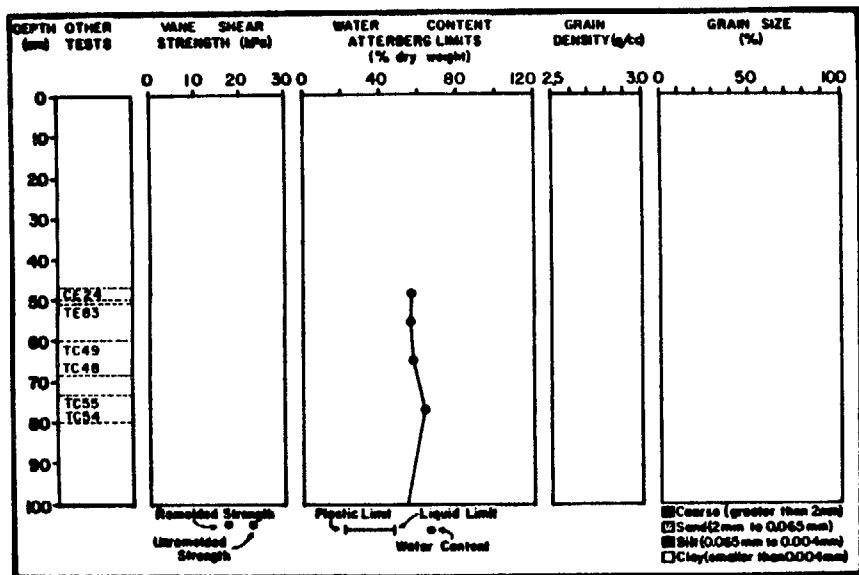
CORE: 633G2



CRUISE: DCI-81-EG

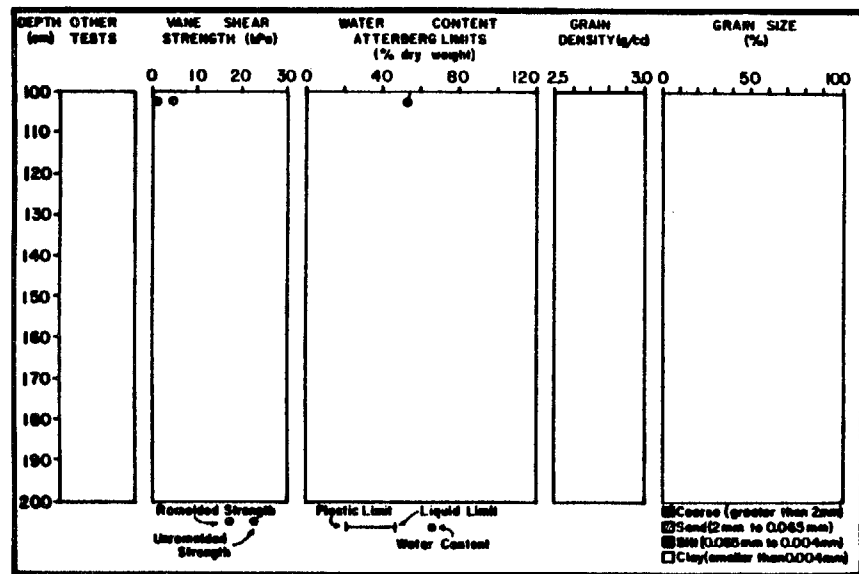
CORE: 633G2





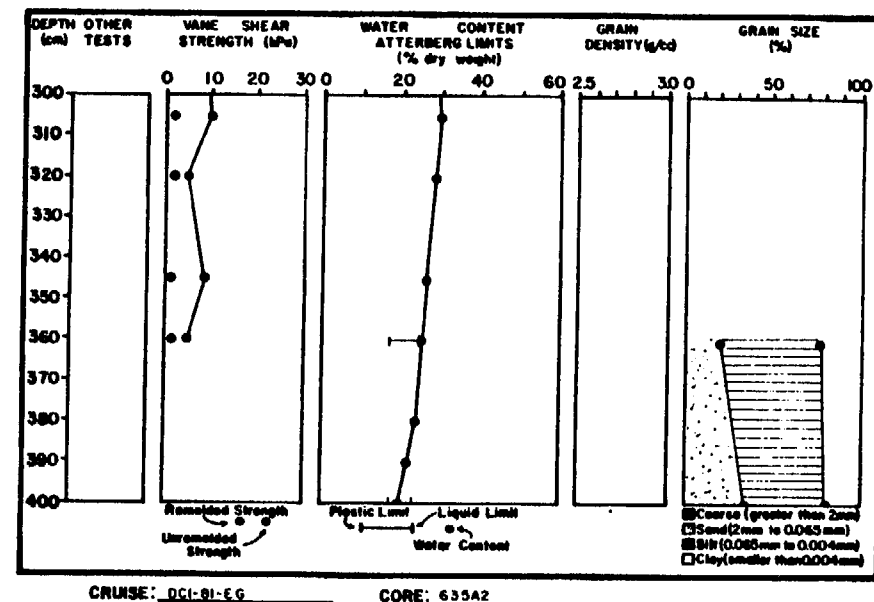
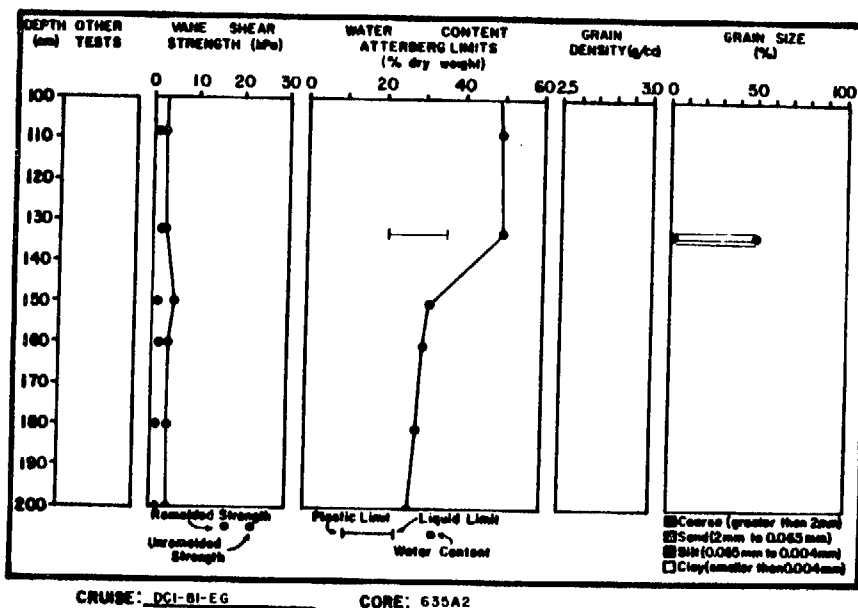
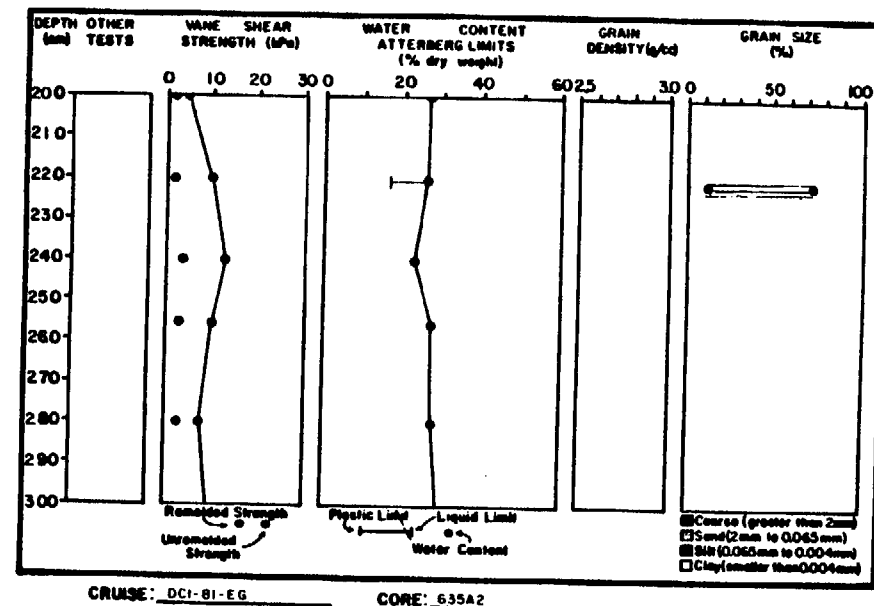
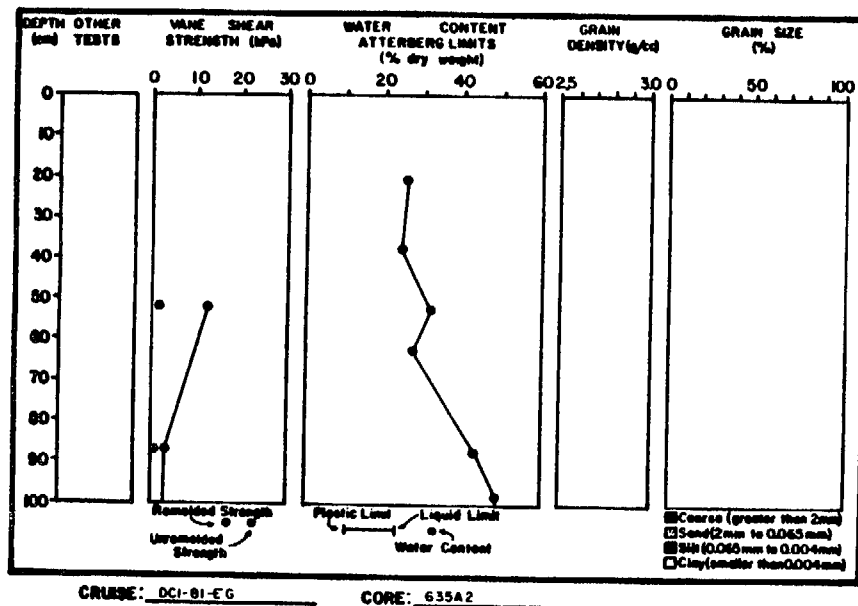
CRUISE: DCI-81-EG

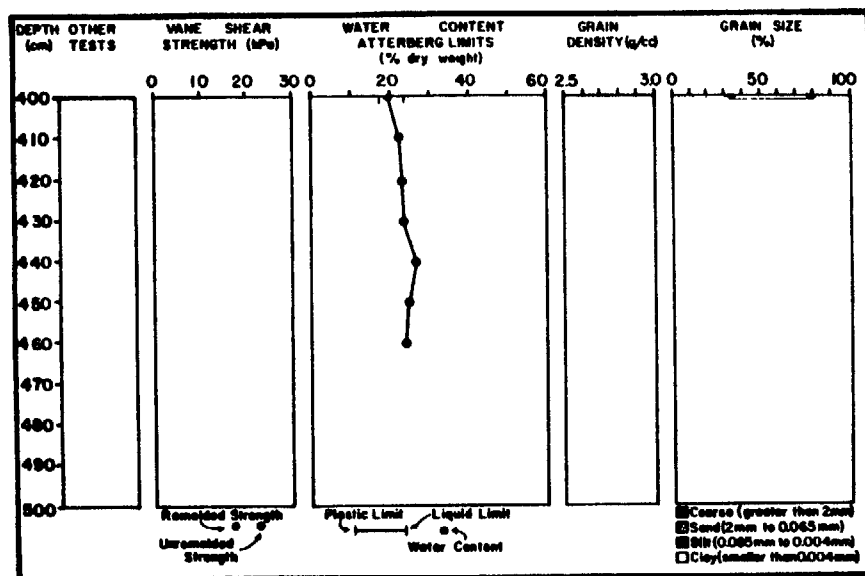
CORE: 63462



CRUISE: DCI-81-EG

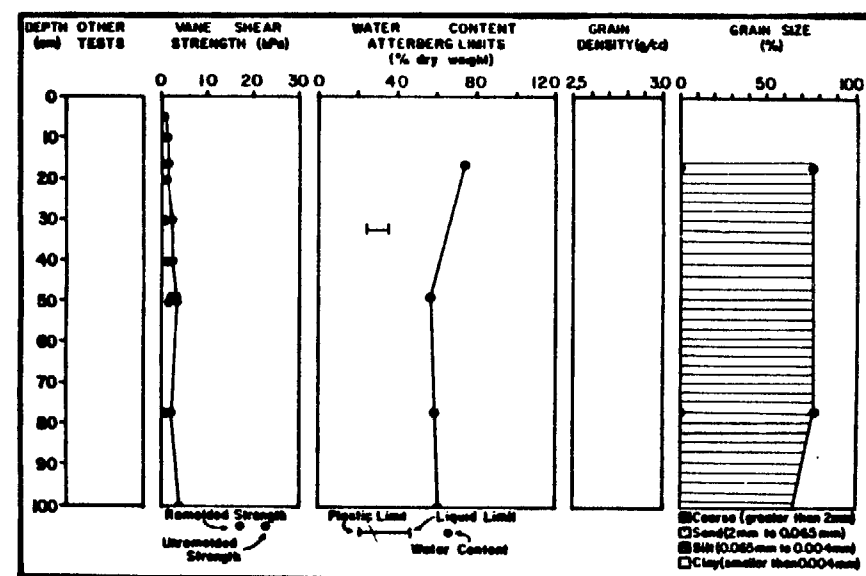
CORE: 63462





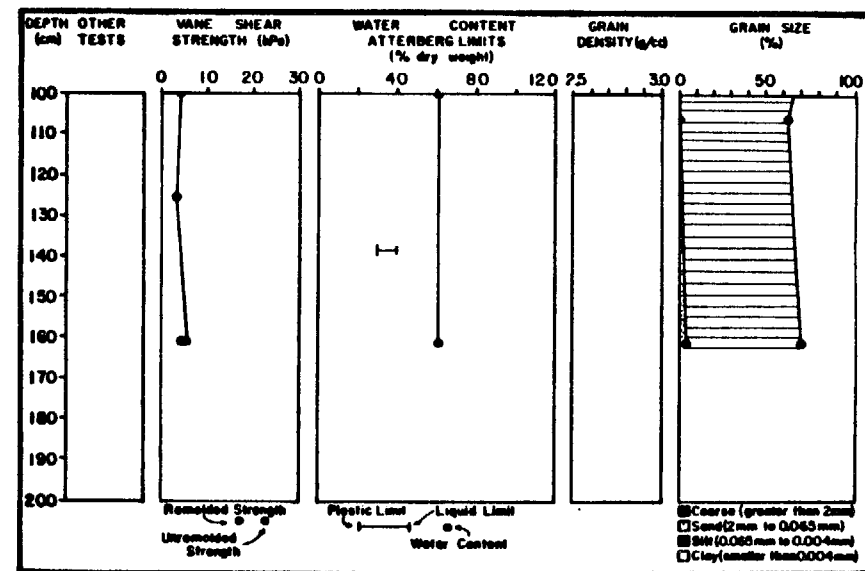
CRUISE: DCI-81-EG

CORE: 635A2



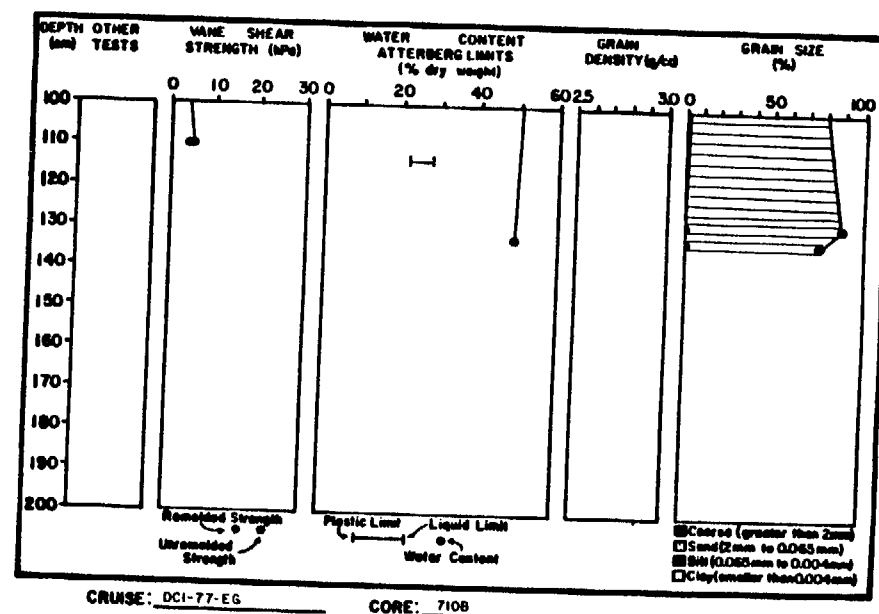
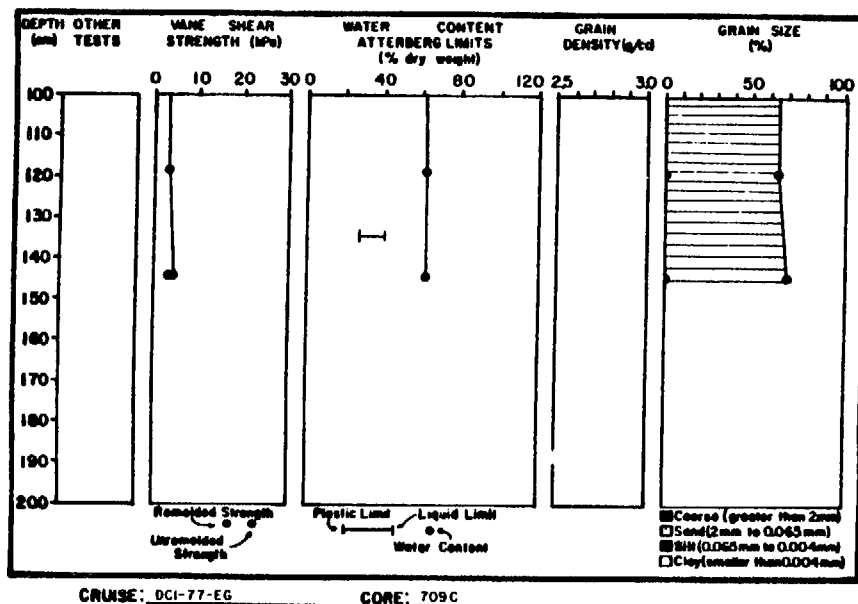
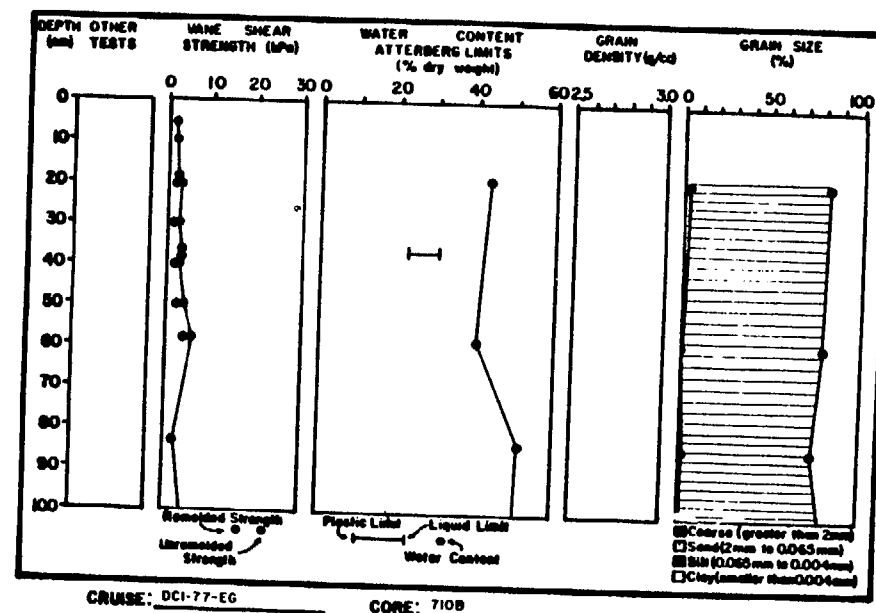
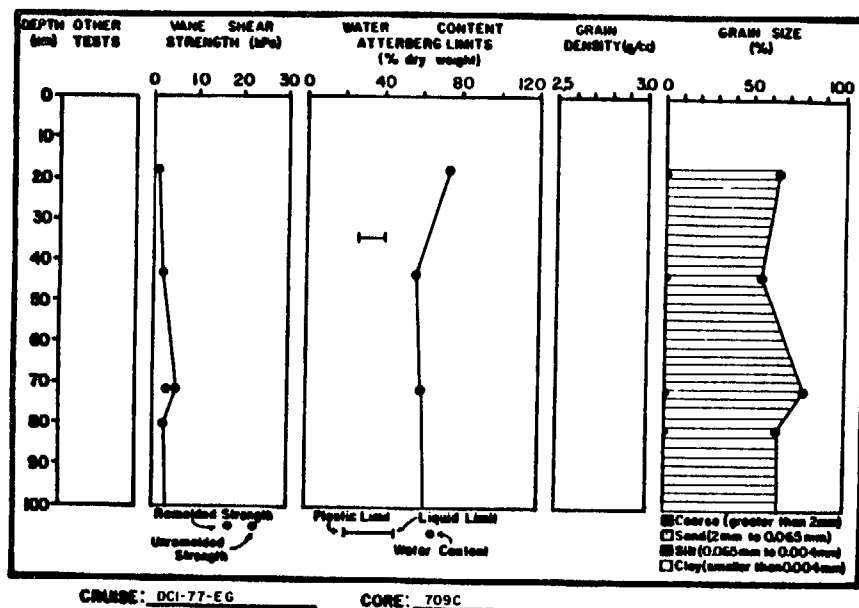
CRUISE: DCI-77-EG

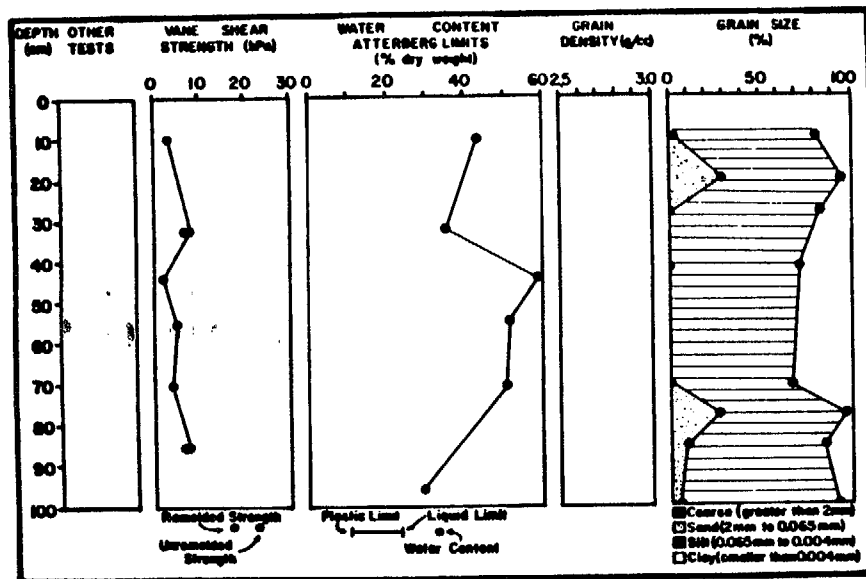
CORE: 709B



CRUISE: DCI-77-EG

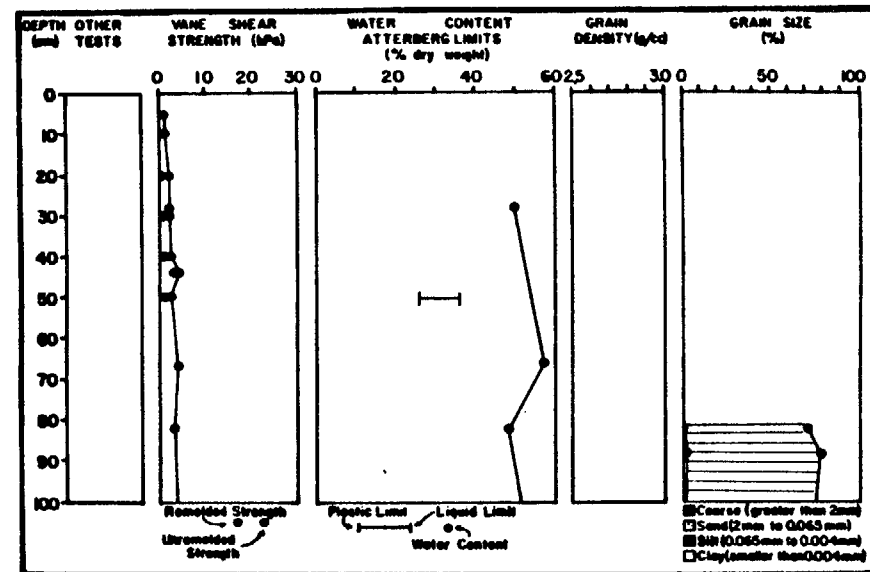
CORE: 709B





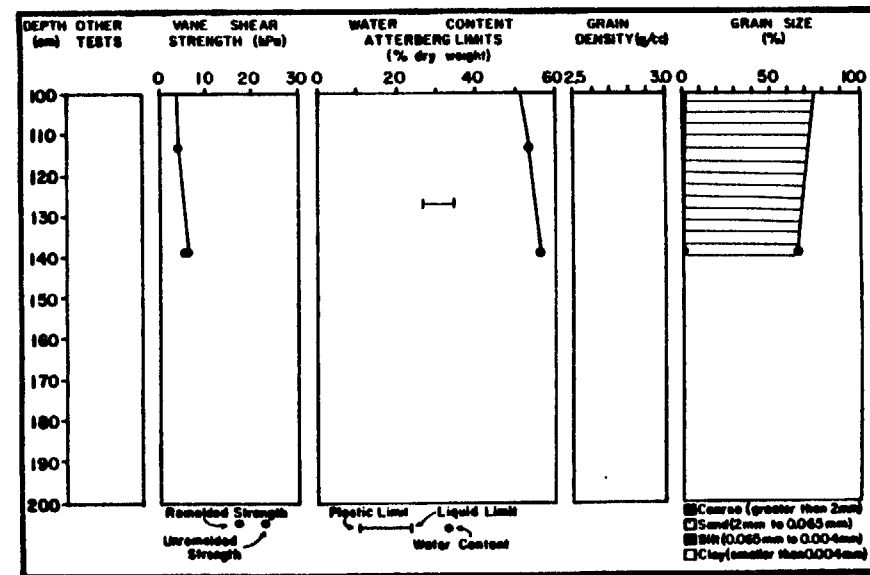
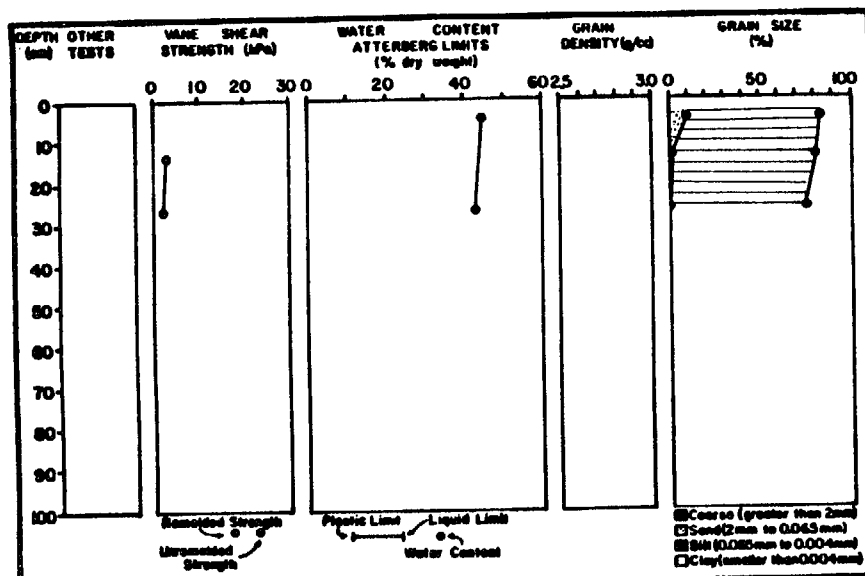
CRUISE: DCI-77-EG

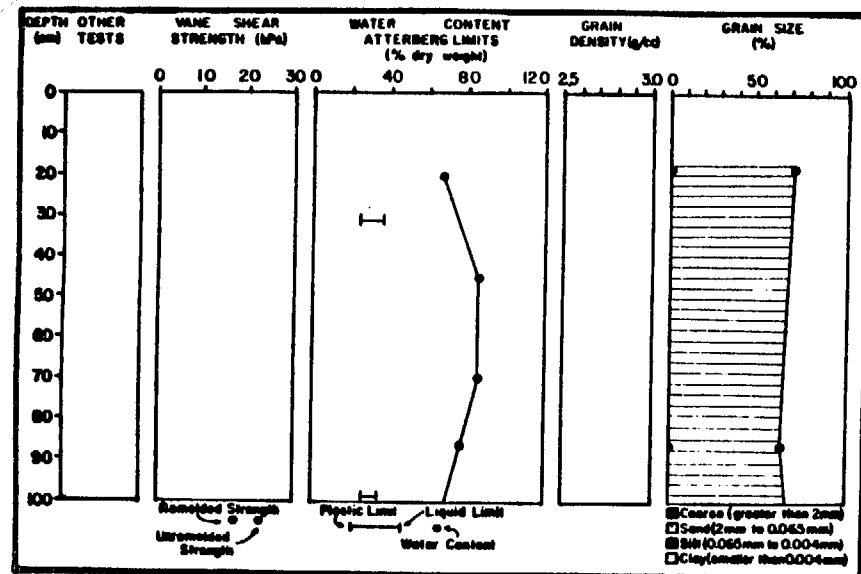
CORE: 710C



CRUISE: DCI-77-EG

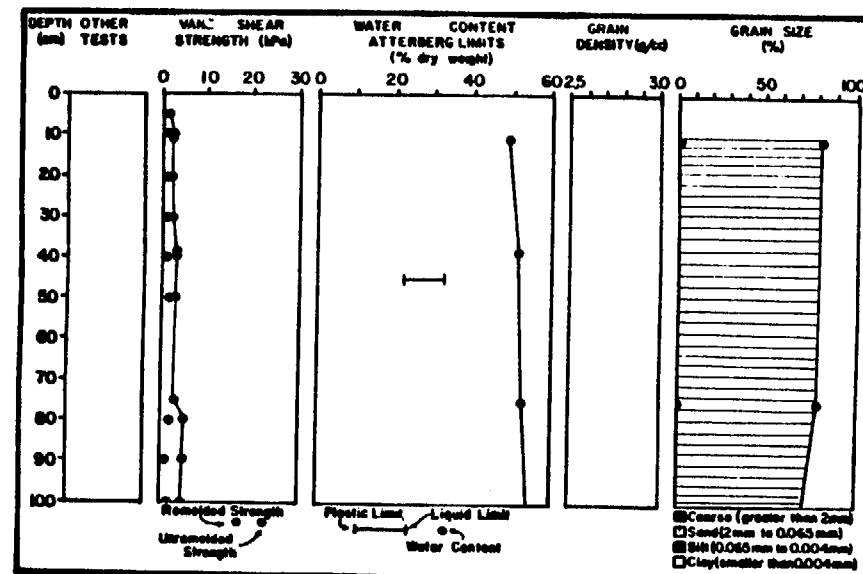
CORE: 715B





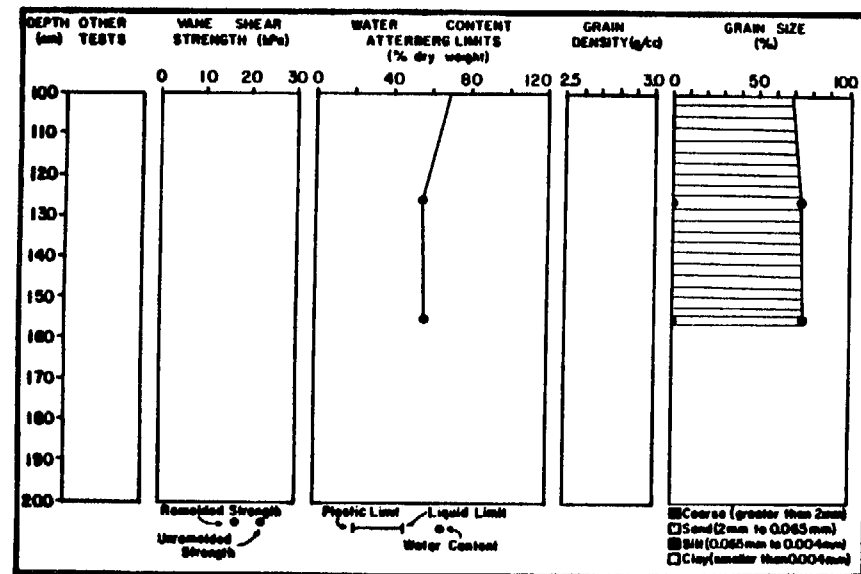
CRUISE: DCI-77-EG

CORE: 715C



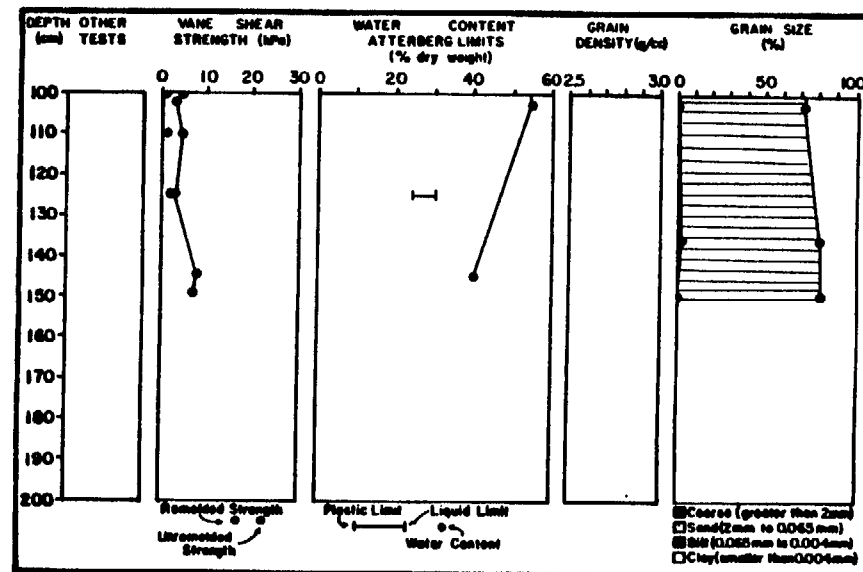
CRUISE: DCI-77-EG

CORE: 717B



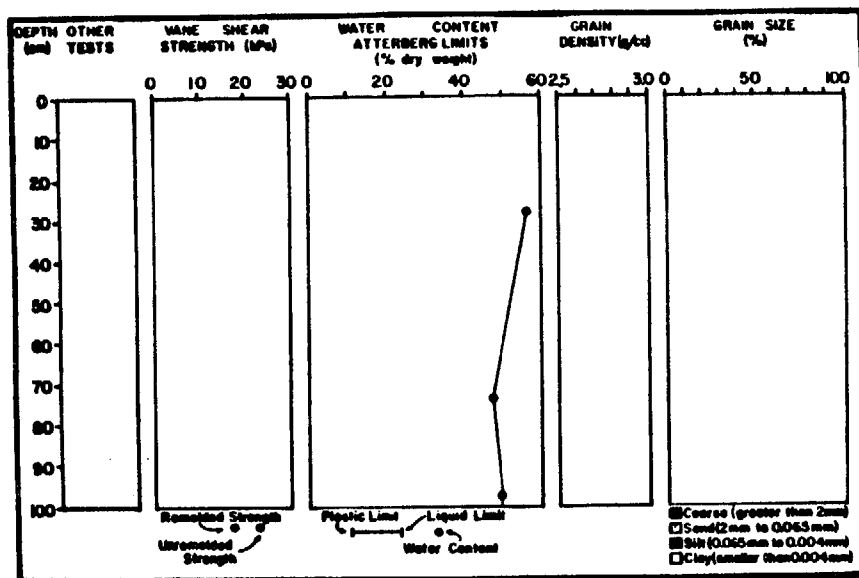
CRUISE: DCI-77-EG

CORE: 715C



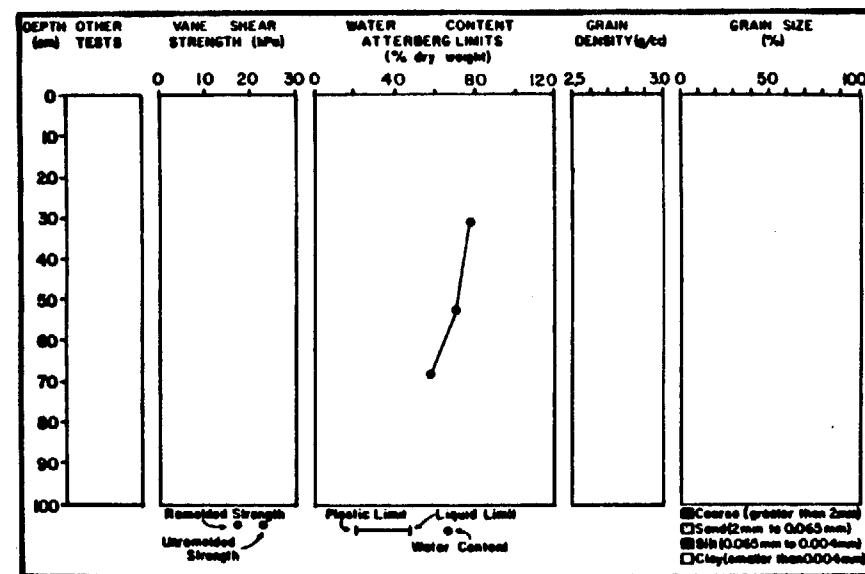
CRUISE: DCI-77-EG

CORE: 717B



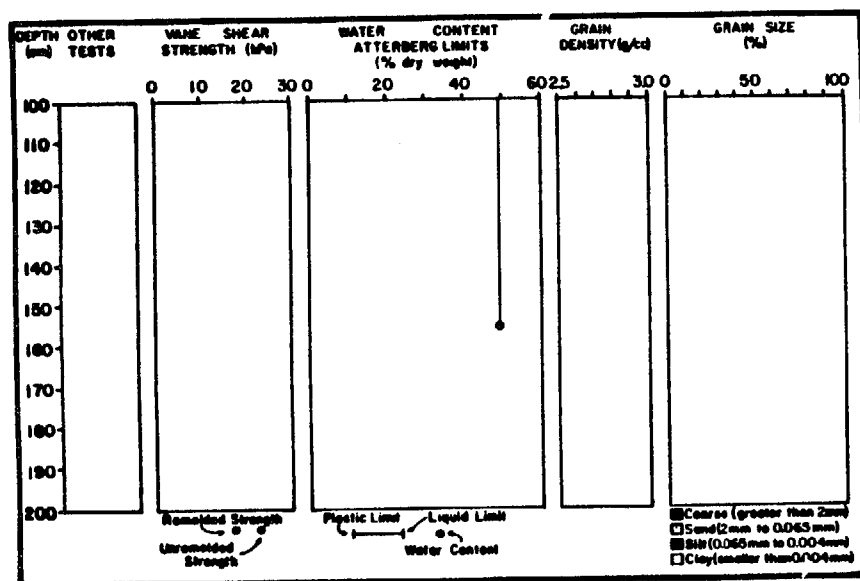
CRUISE: DCI-77-EG

CORE: 717C



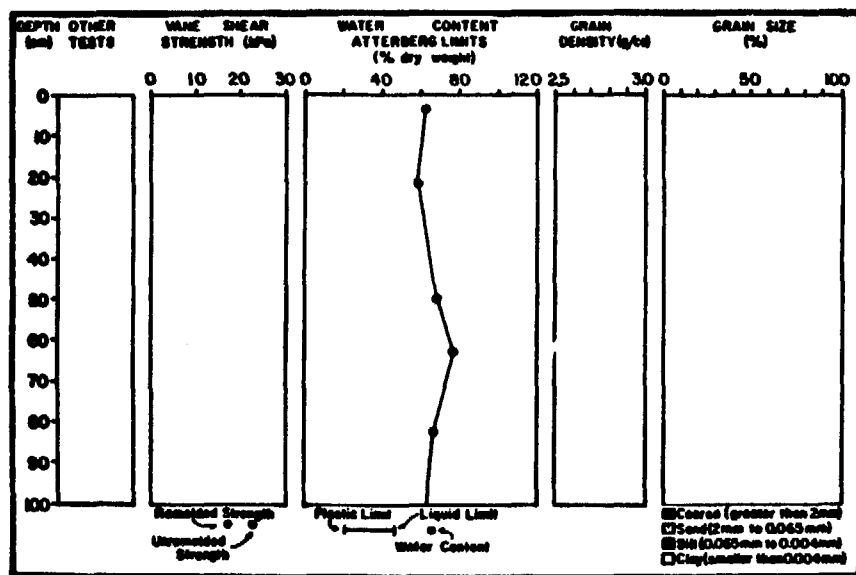
CRUISE: DCI-77-EG

CORE: 718B



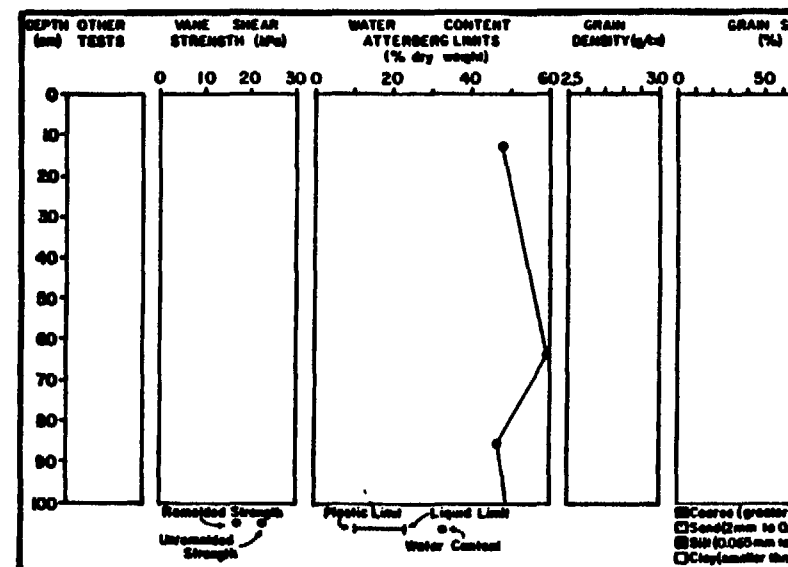
CRUISE: DCI-77-EG

CORE: 717C



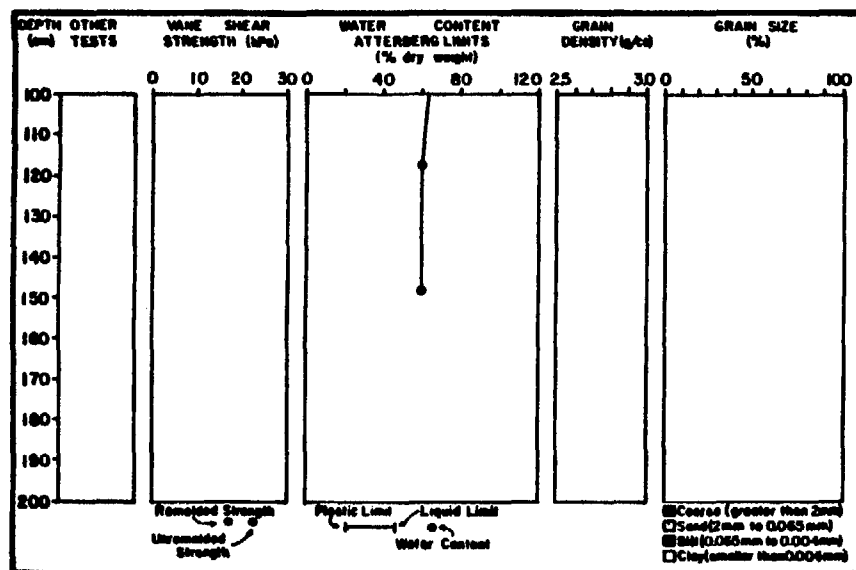
CRUISE: DCI-77-EG

CORE: 719B



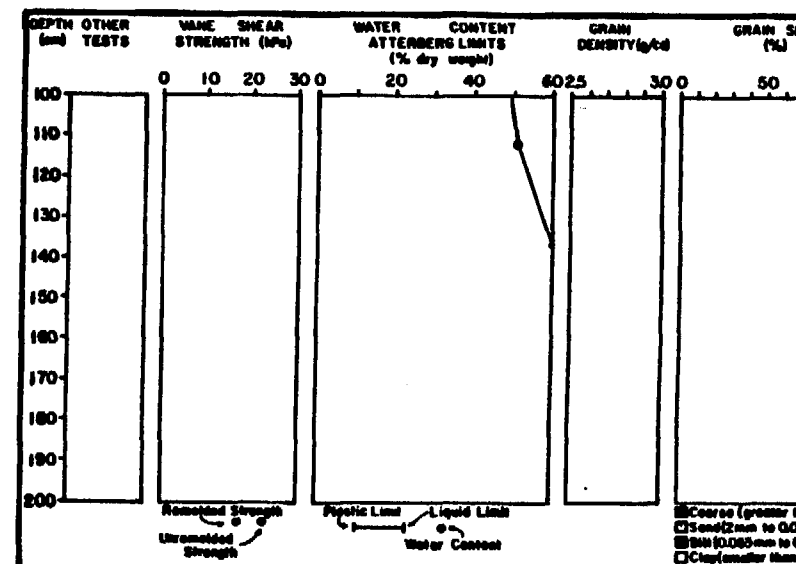
CRUISE: DCI-77-EG

CORE: 720B



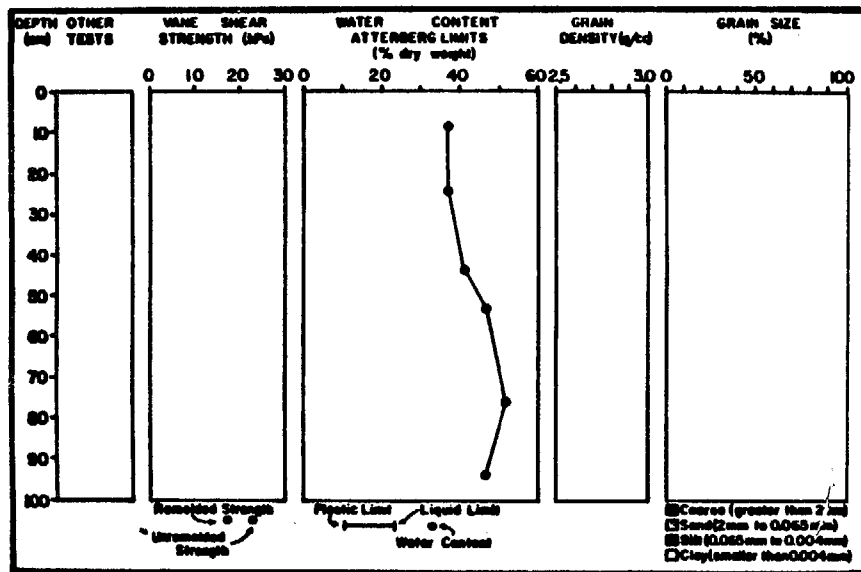
CRUISE: DCI-77-EG

CORE: 719B

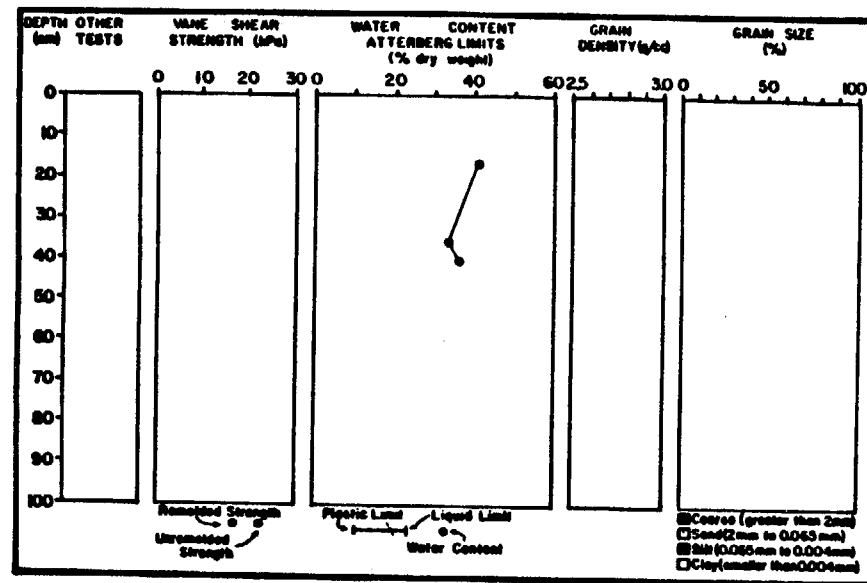


CRUISE: DCI-77-EG

CORE: 720B

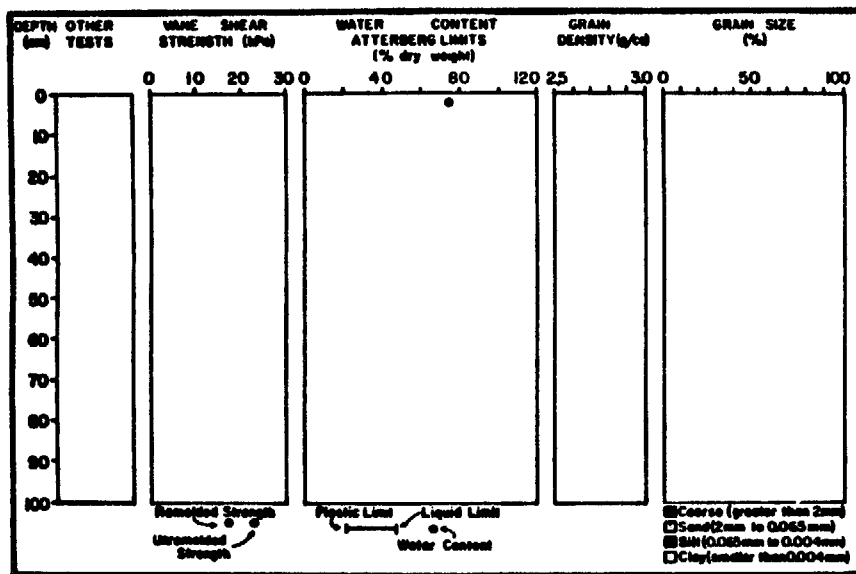


CRUISE: DCI-77-EG CORE: 721C



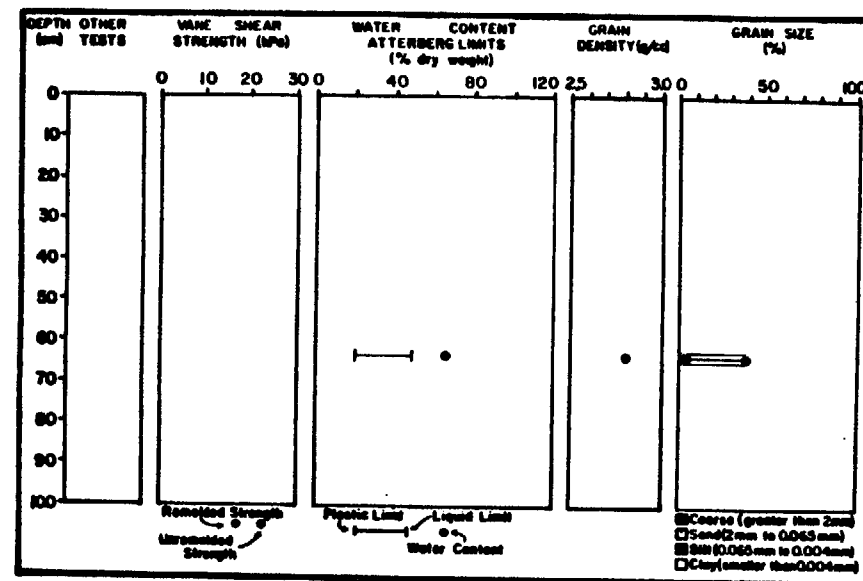
CRUISE: DCI-77-EG CORE: 721D

ICY BAY STUDY AREA



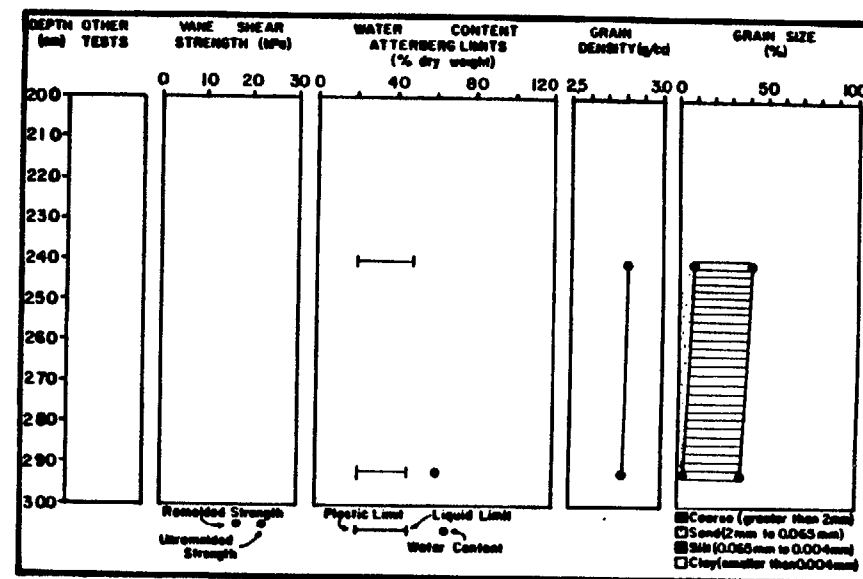
CRUISE: S8-77-EG

CORE: 39G



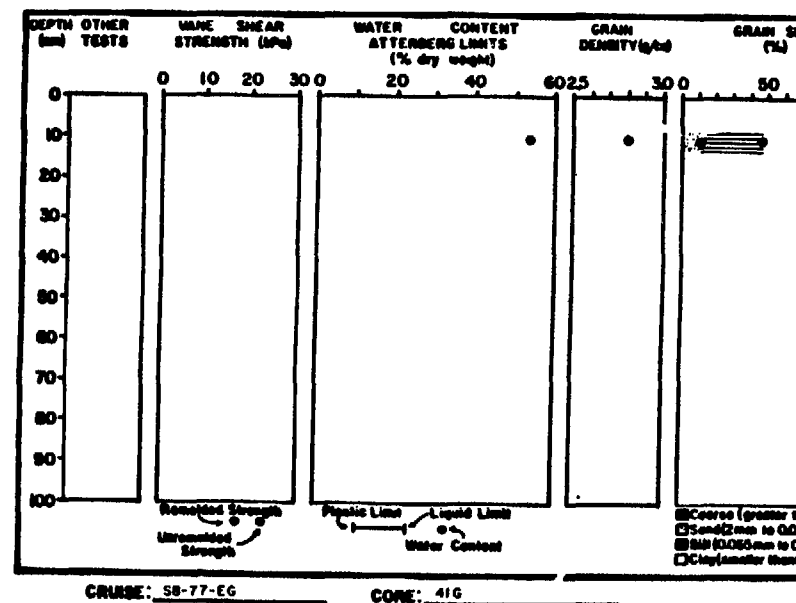
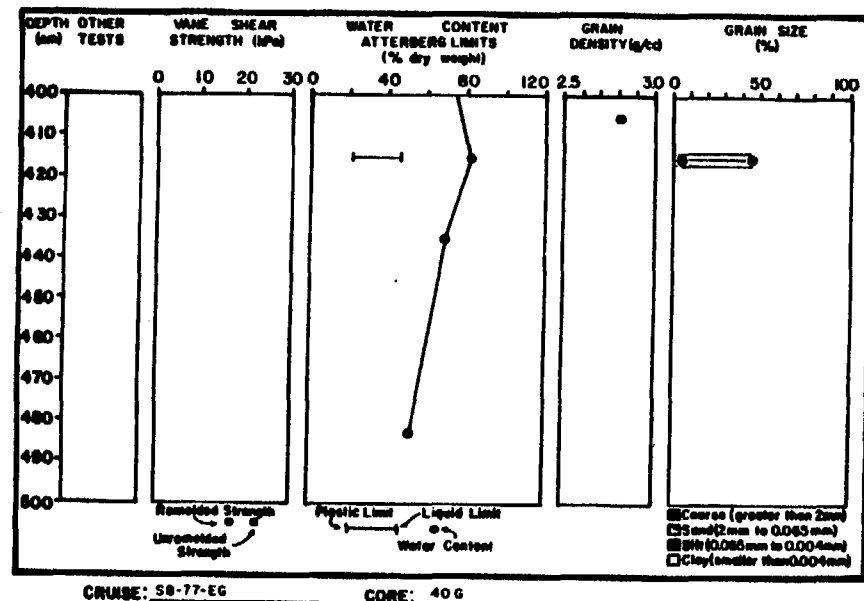
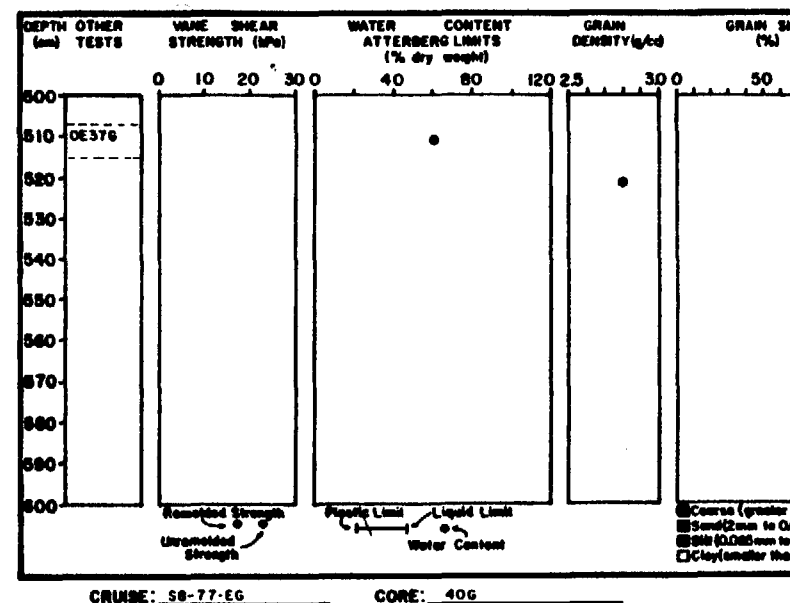
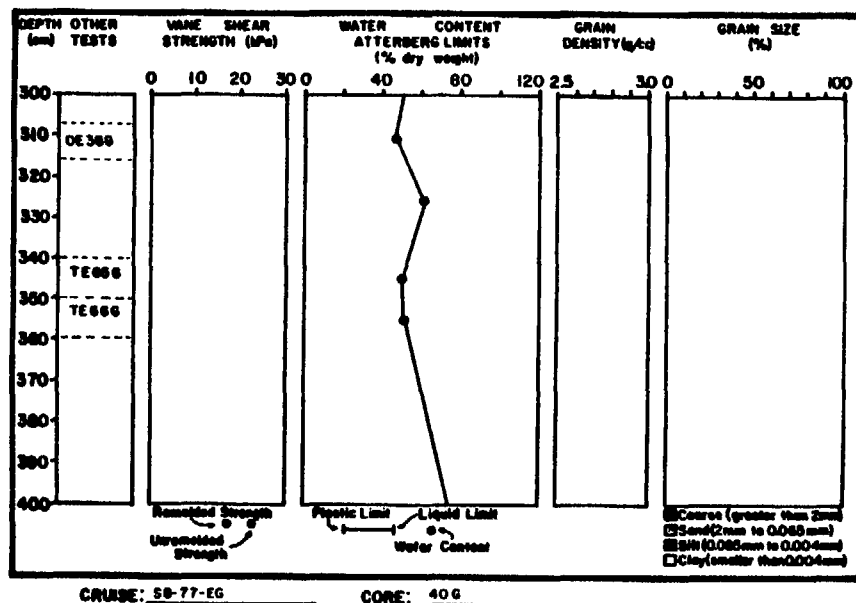
CRUISE: S8-77-EG

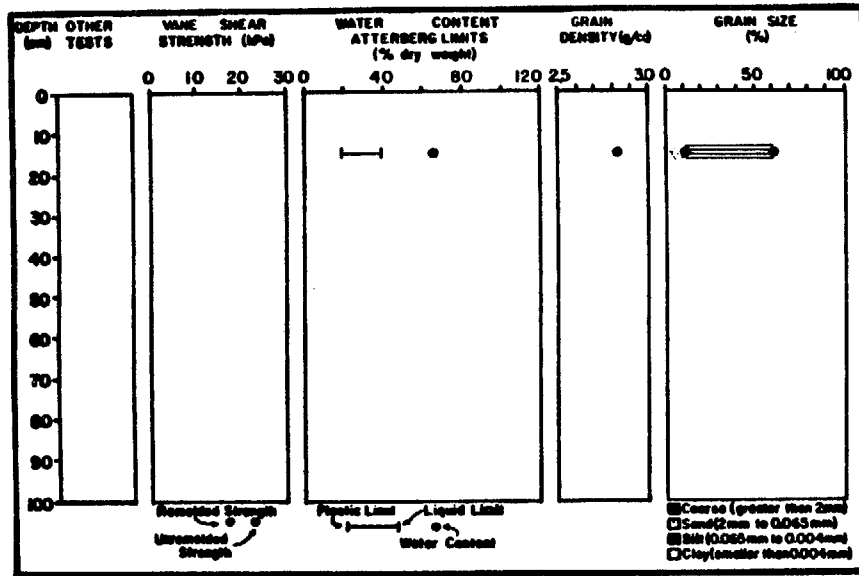
CORE: 40G



CRUISE: S8-77-EG

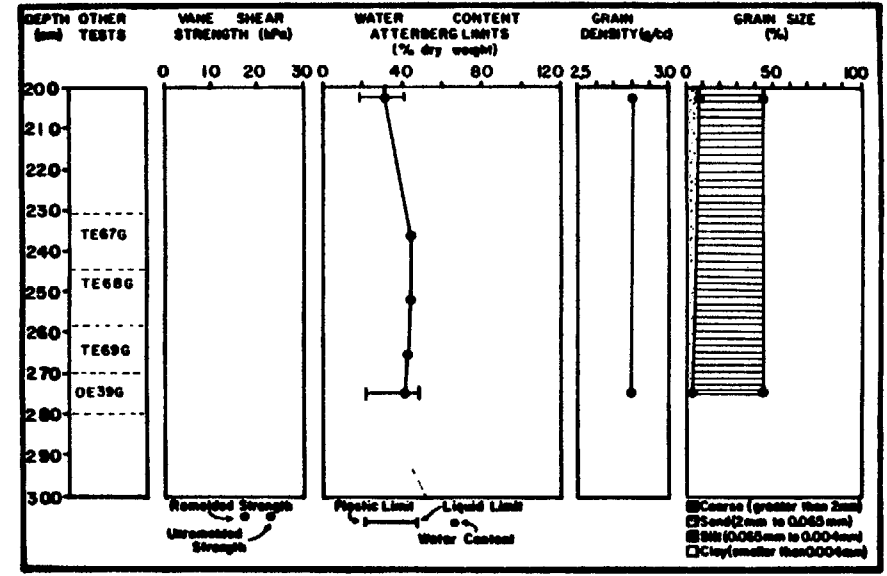
CORE: 40G





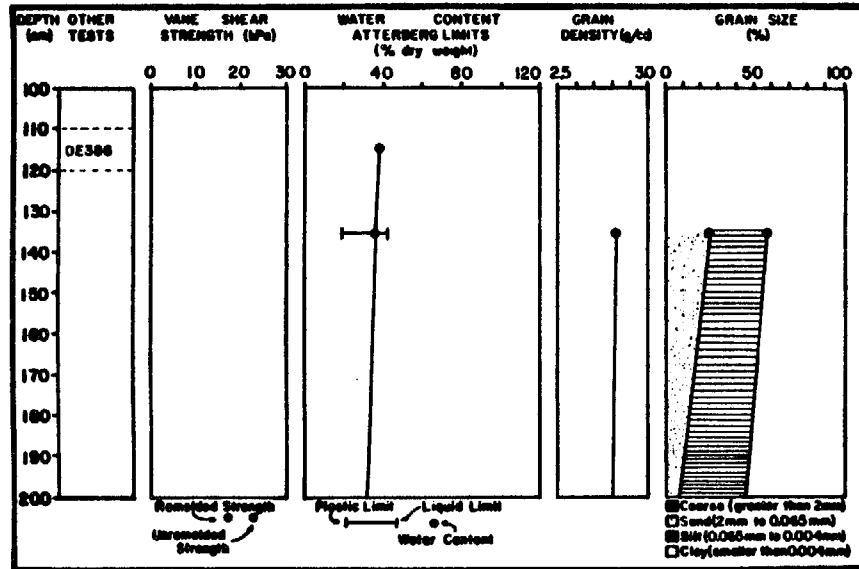
CRUISE: 58-77-EG

CORE: 42G



CRUISE: 58-77-EG

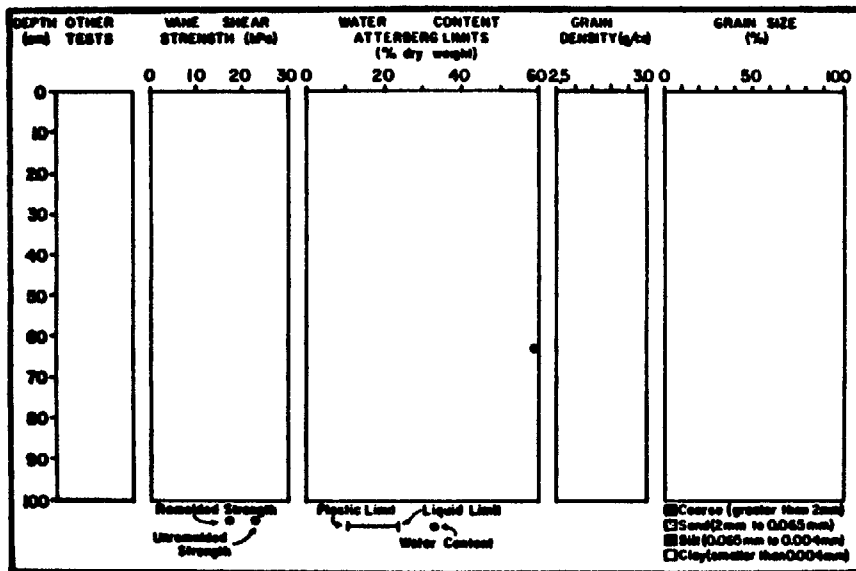
CORE: 42G



CRUISE: 58-77-EG

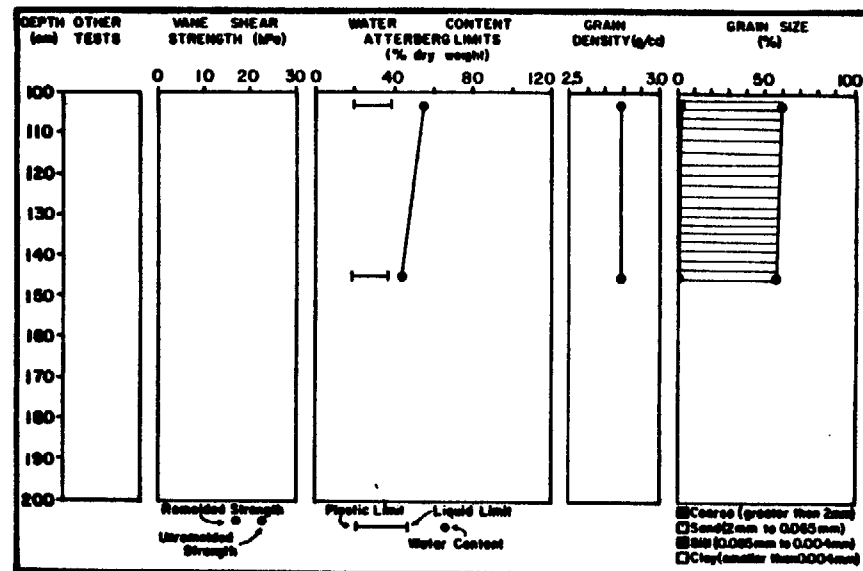
CORE: 42G

YAKUTAT BAY STUDY AREA



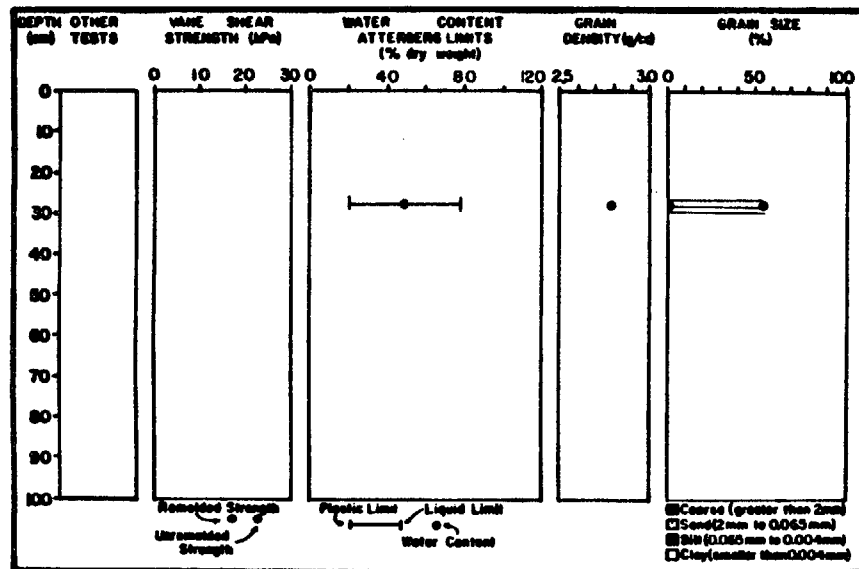
CRUISE: 58-77-EG

CORE: 456



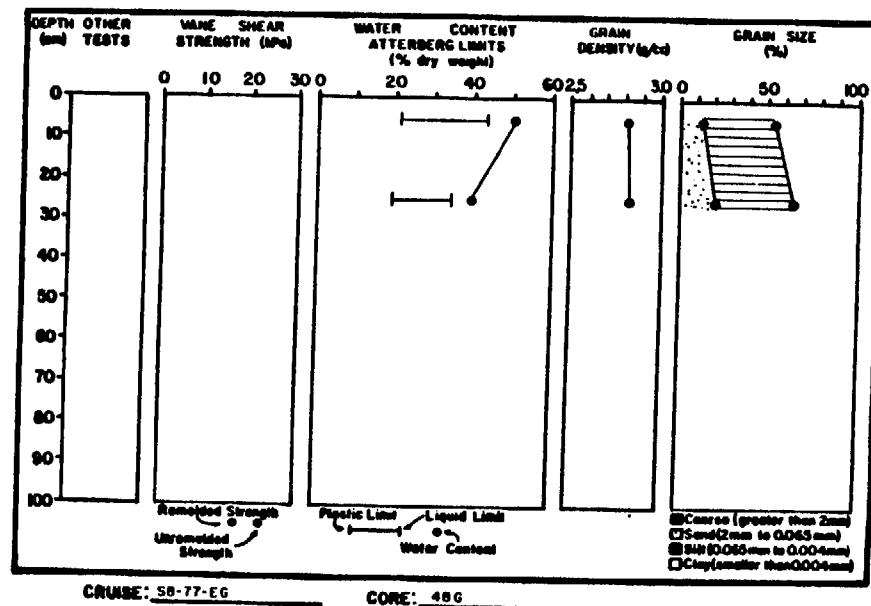
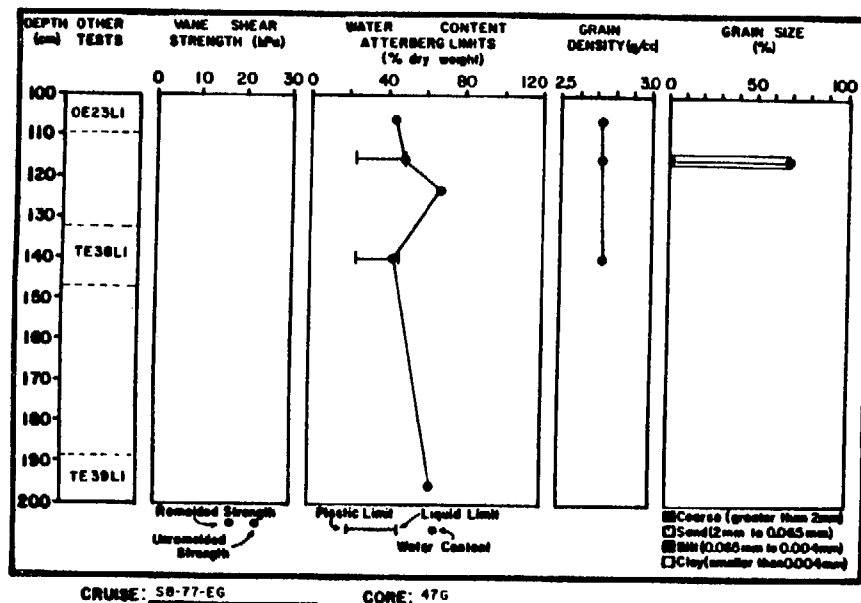
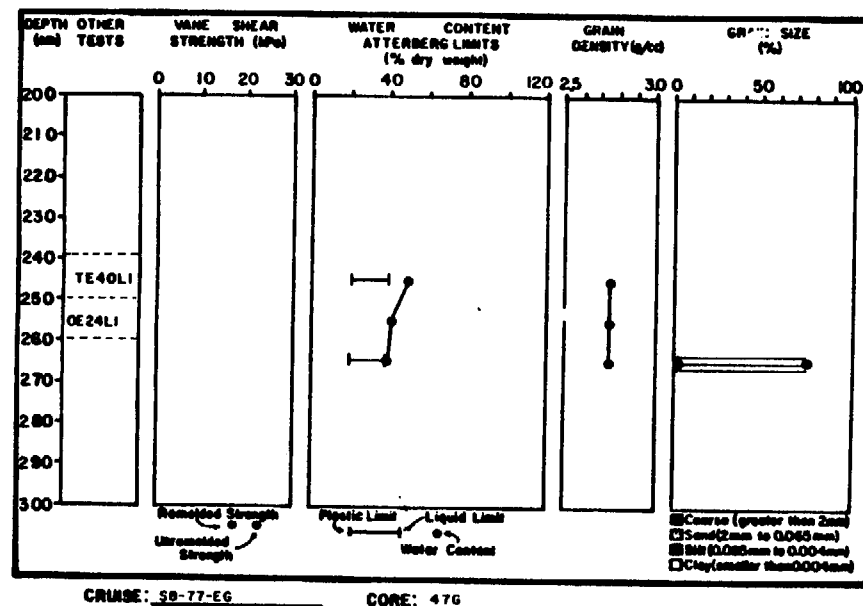
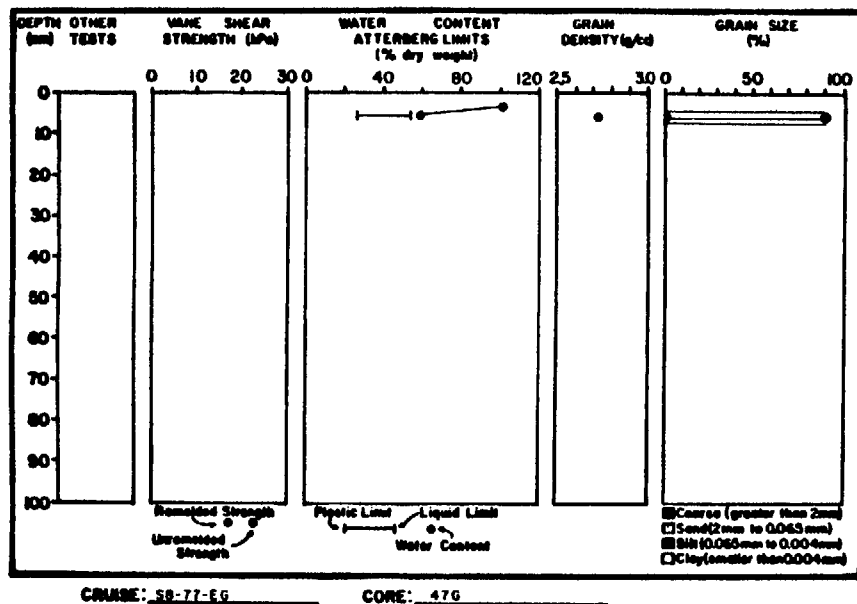
CRUISE: 58-77-EG

CORE: 456

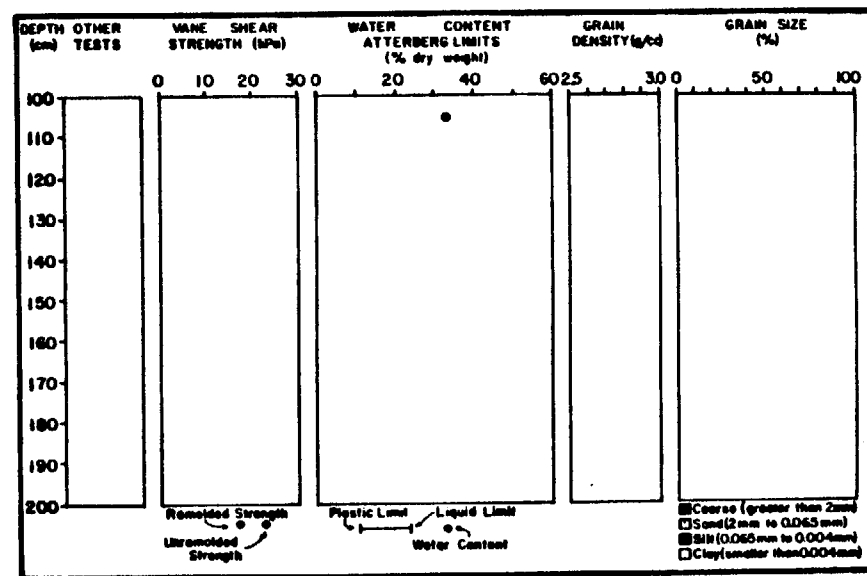
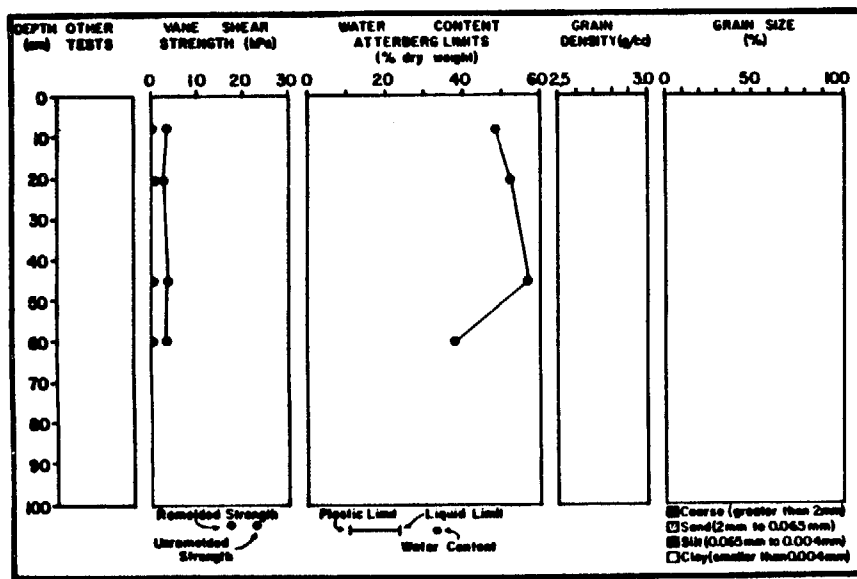
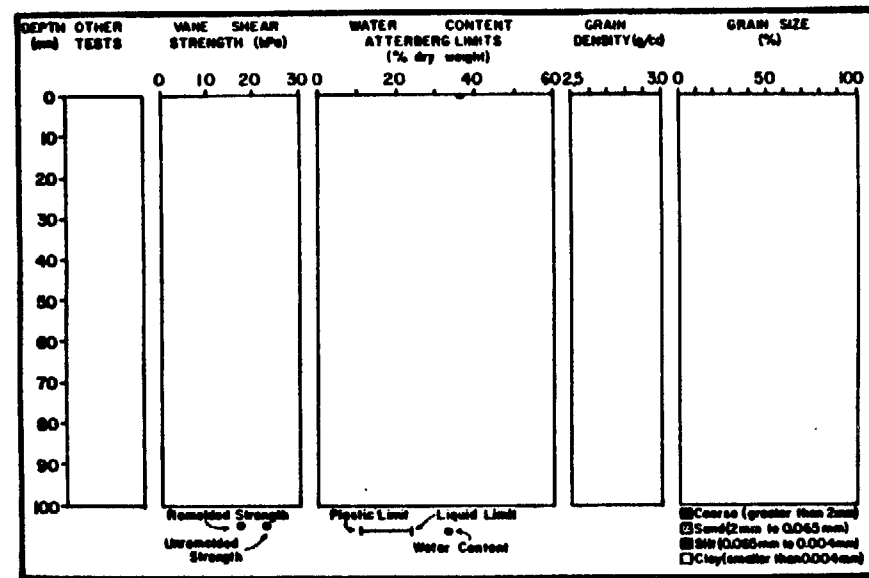
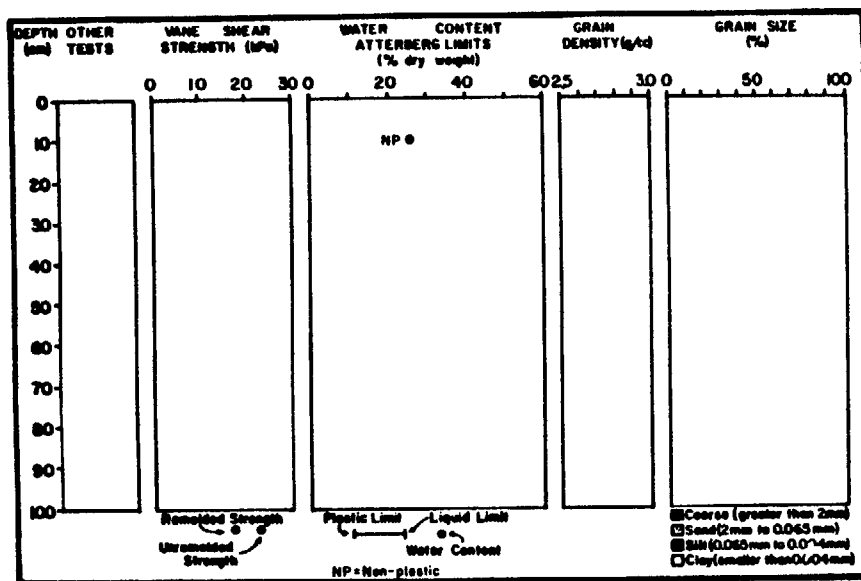


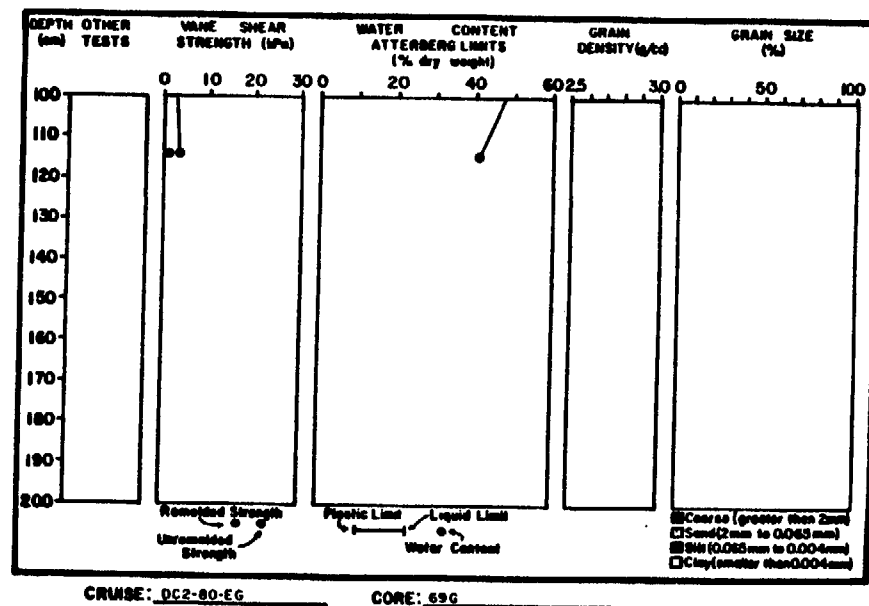
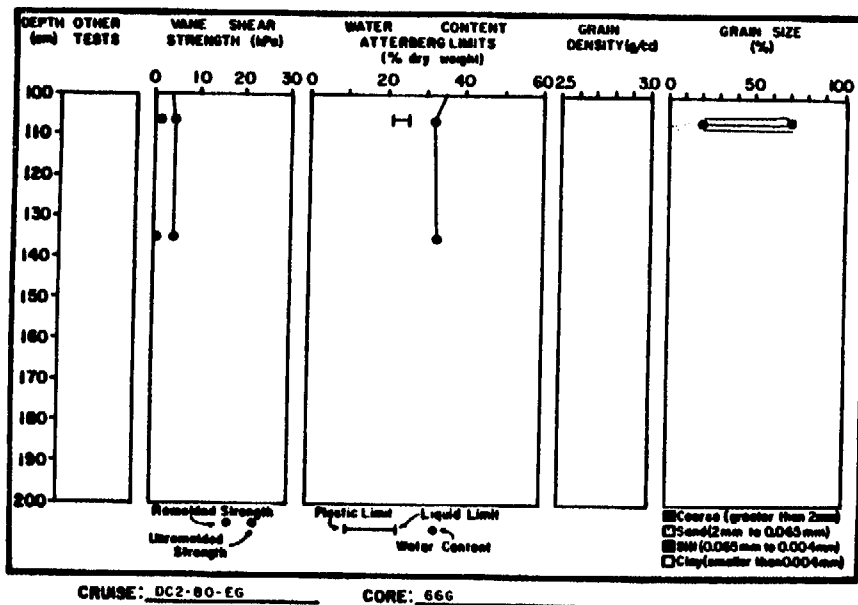
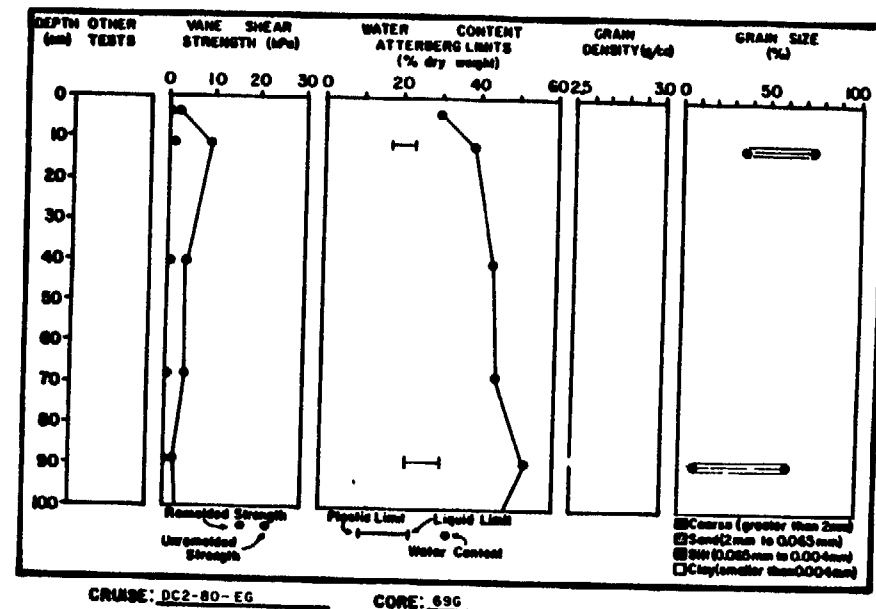
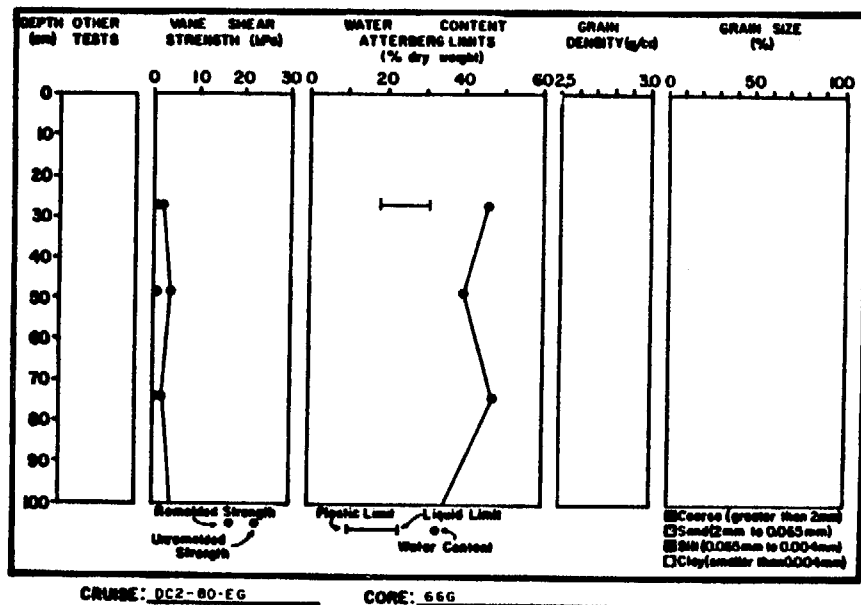
CRUISE: 58-77-EG

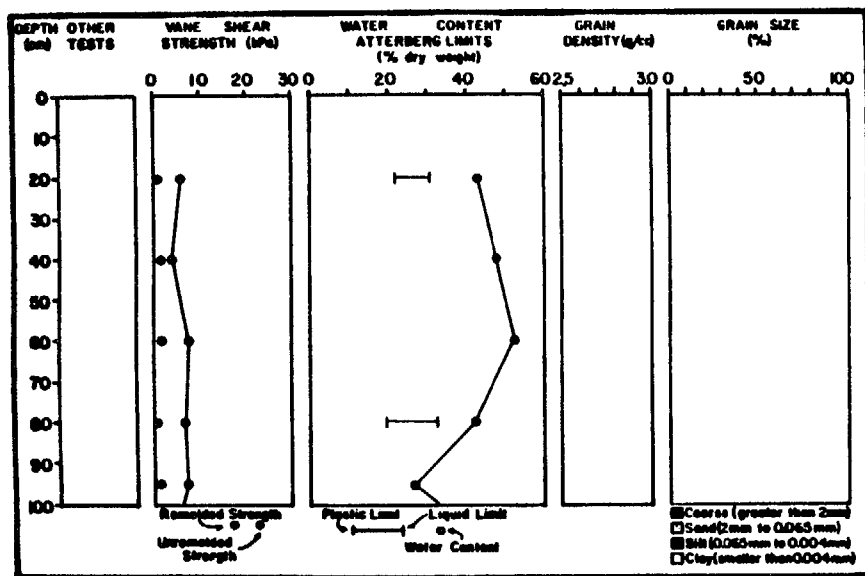
CORE: 466



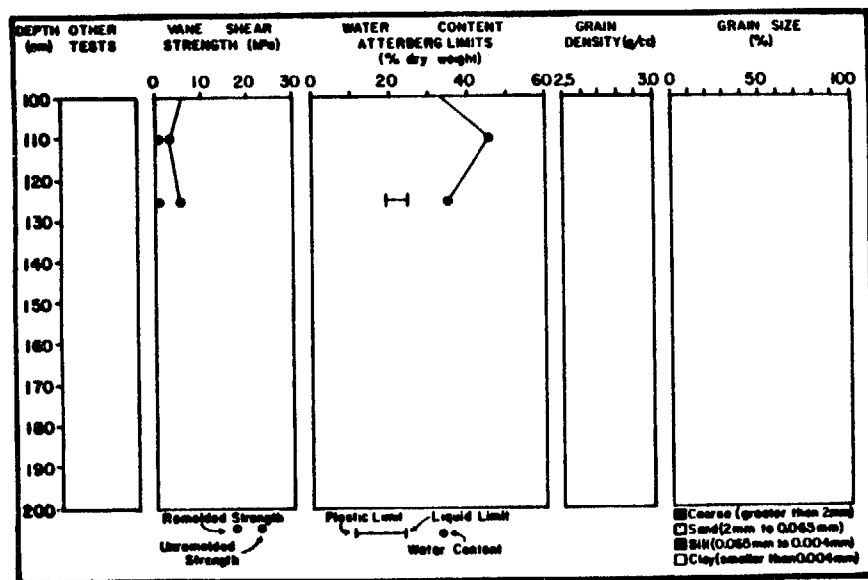
YAKUTAT STUDY AREA



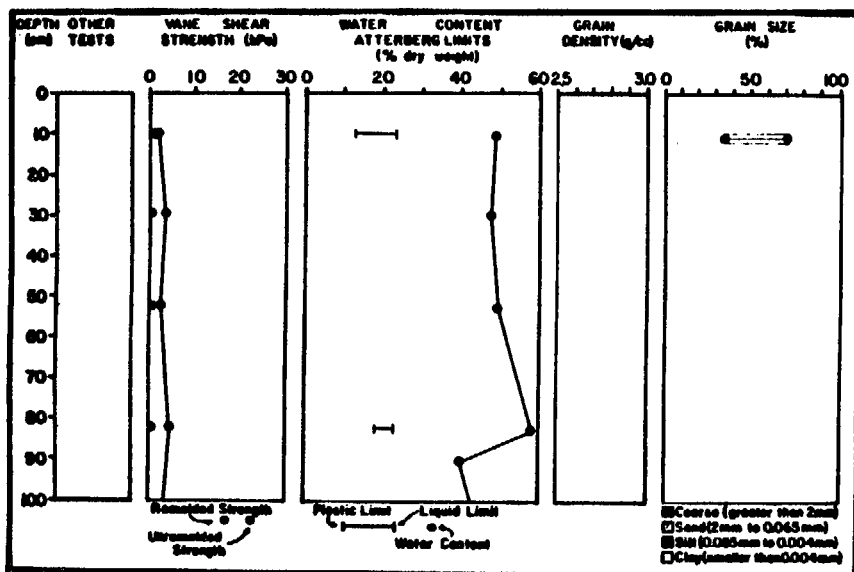




CRUISE: DC2-80-EG CORE: 72G

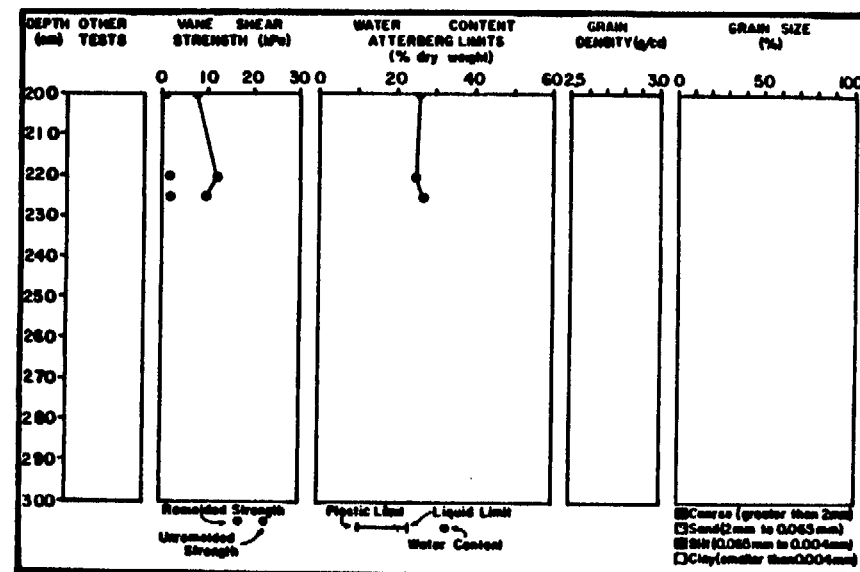


CRUISE: DC2-80-EG CORE: 72G



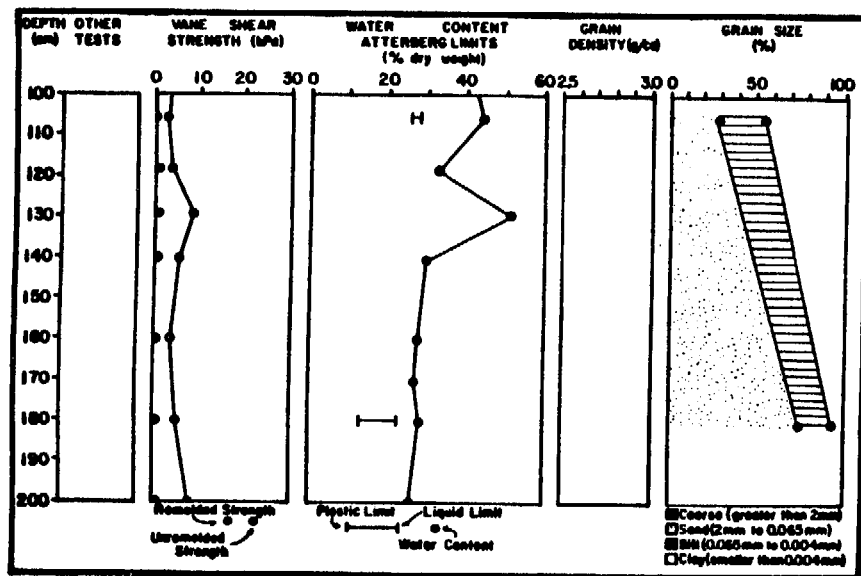
CRUISE: DC2-80-EG

CORE: 836



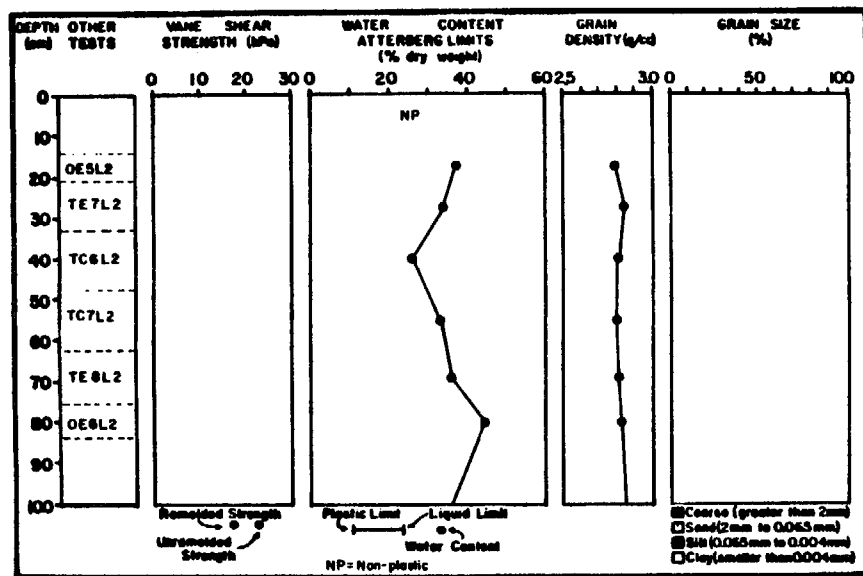
CRUISE: DC2-80-EG

CORE: 836



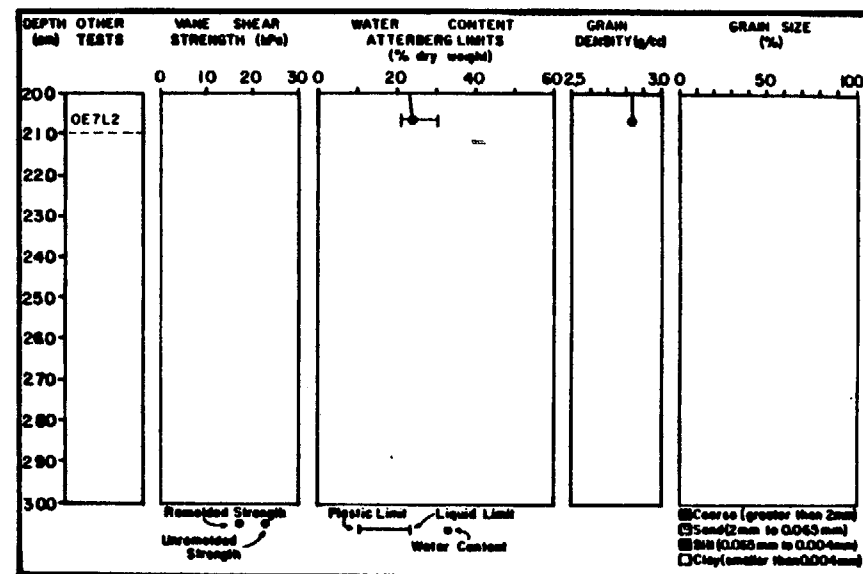
CRUISE: DC2-80-EG

CORE: 836



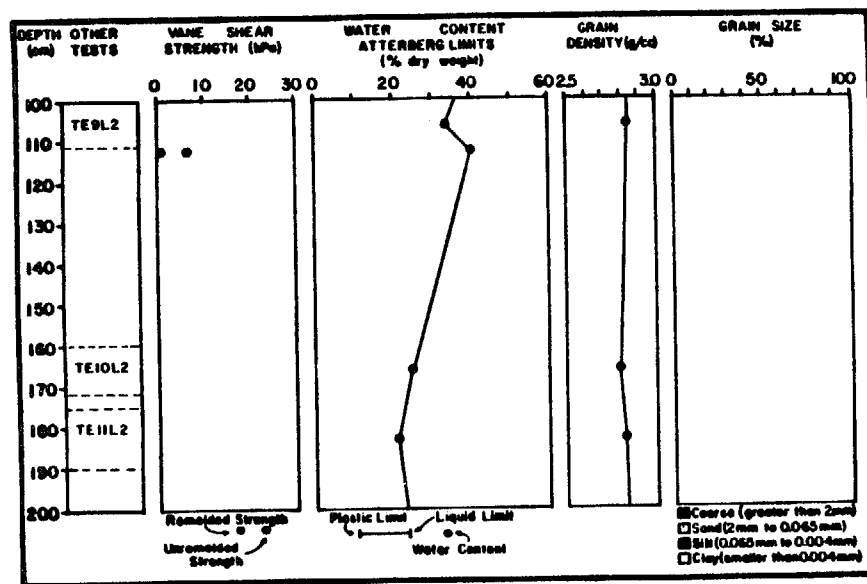
CRUISE: DC2-80-EG

CORE: 84G



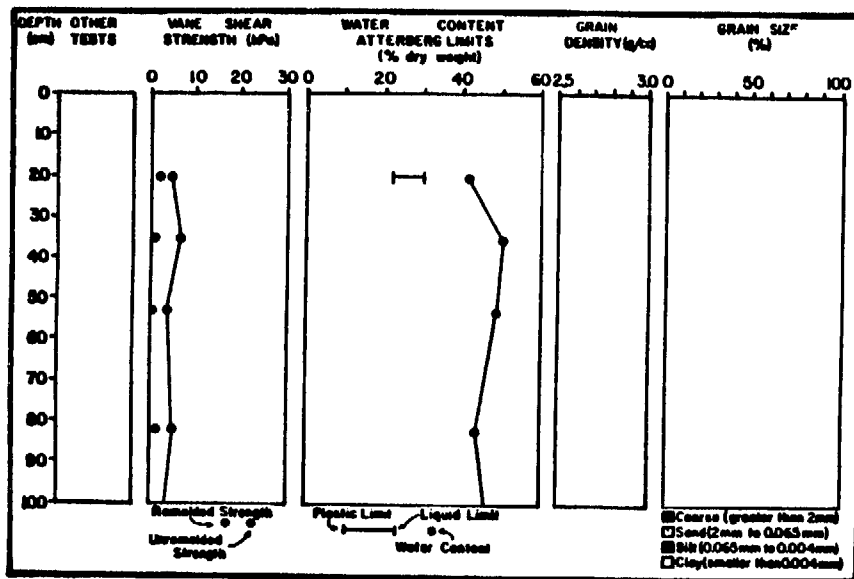
CRUISE: DC2-80-EG

CORE: 84G



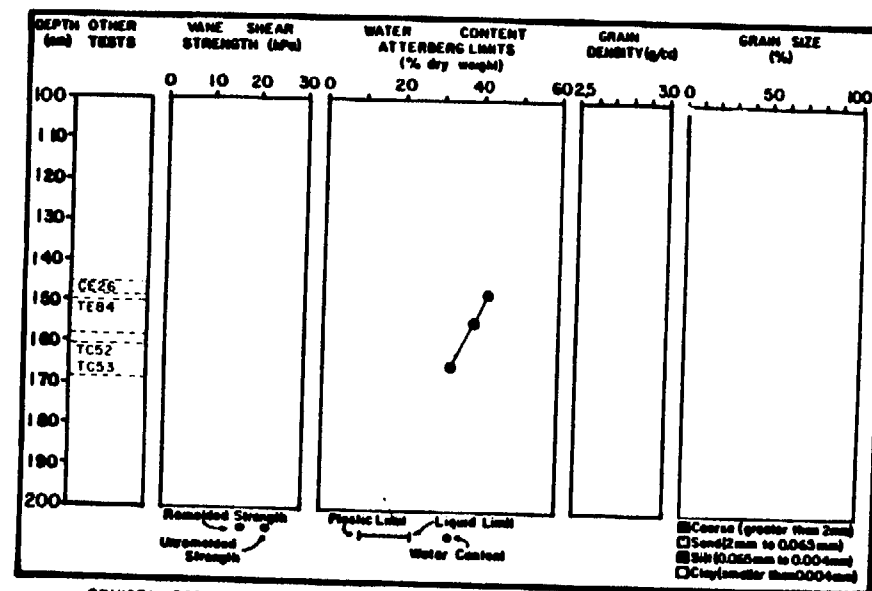
CRUISE: DC2-80-EG

CORE: 84G



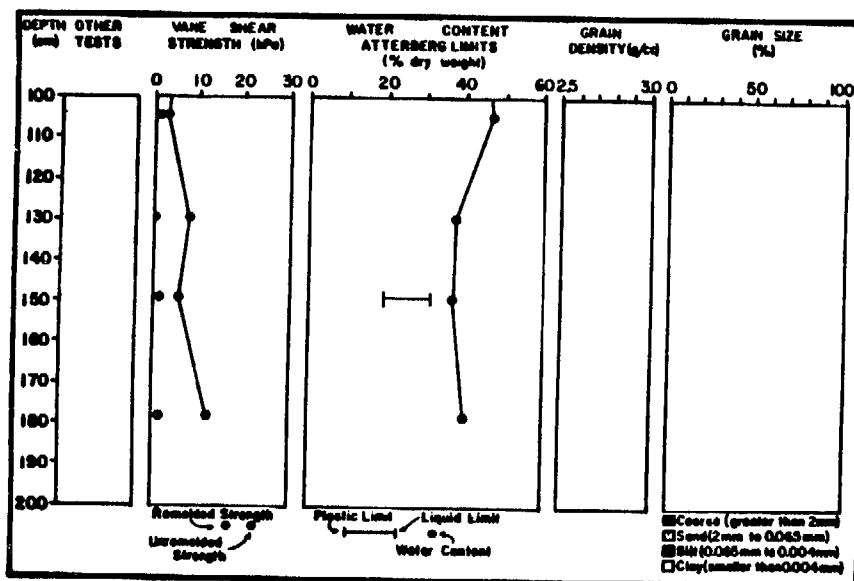
CRUISE: DC2-80-EG

CORE: 85G



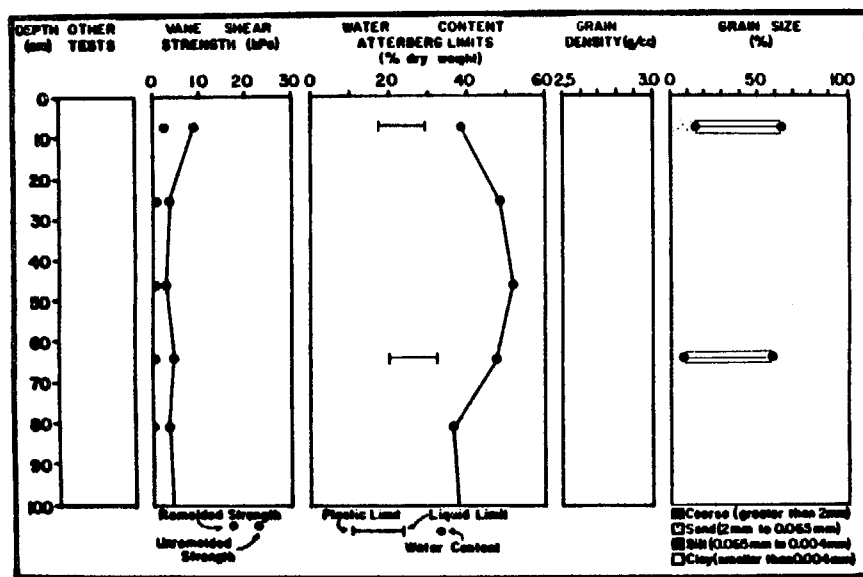
CRUISE: DC2-80-EG

CORE: 87G



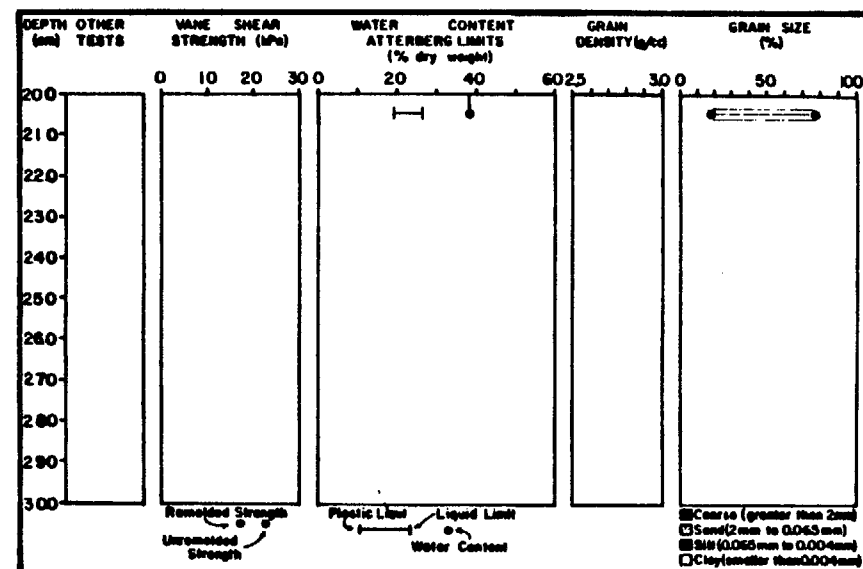
CRUISE: DC2-80-EG

CORE: 85G



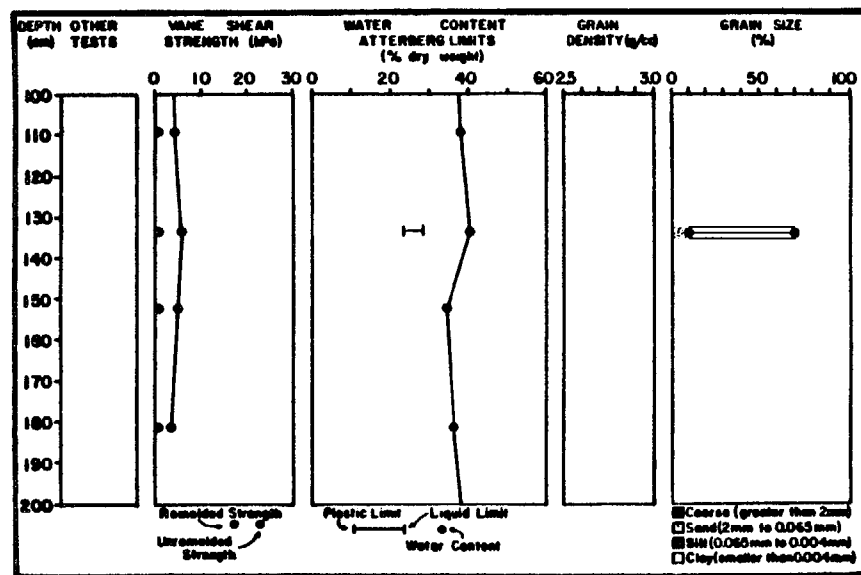
CRUISE: DC2-80-EG

CORE: 88G



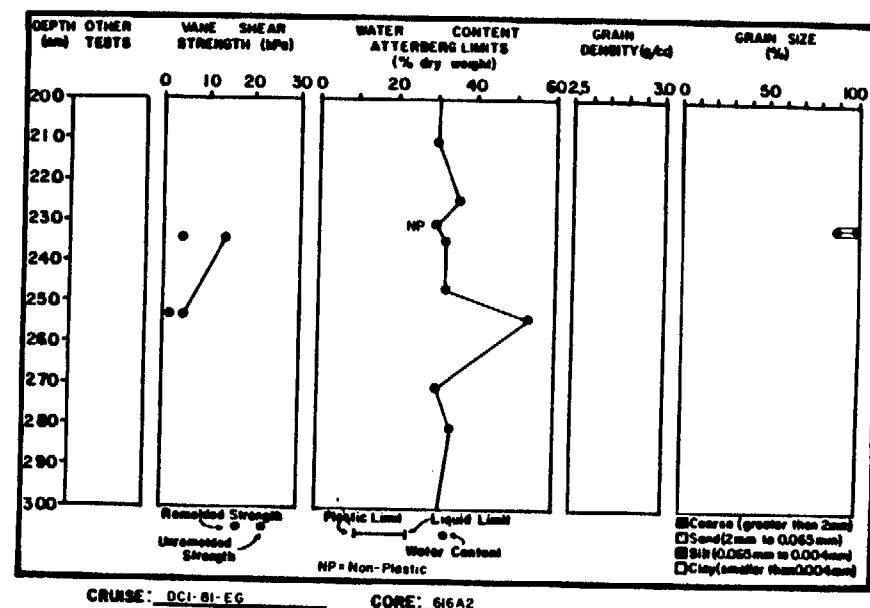
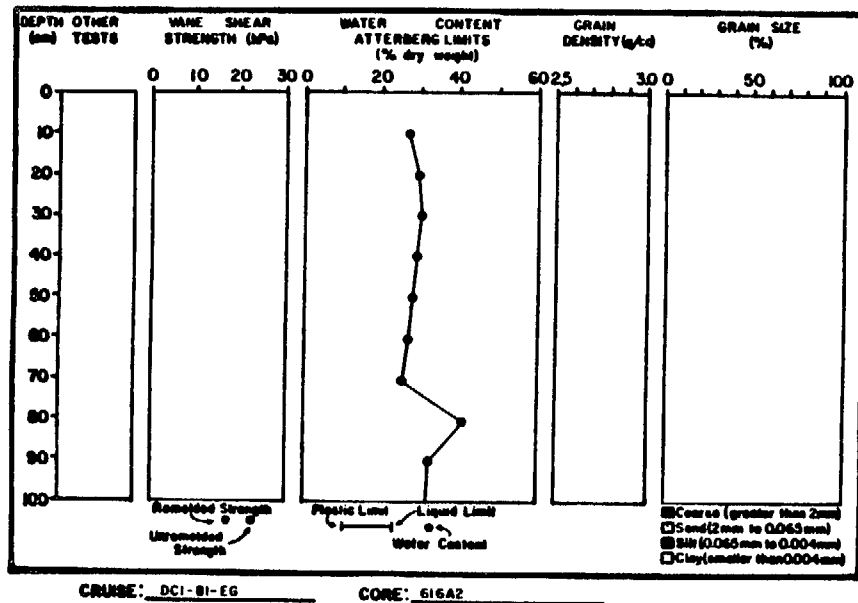
CRUISE: DC2-80-EG

CORE: 88G

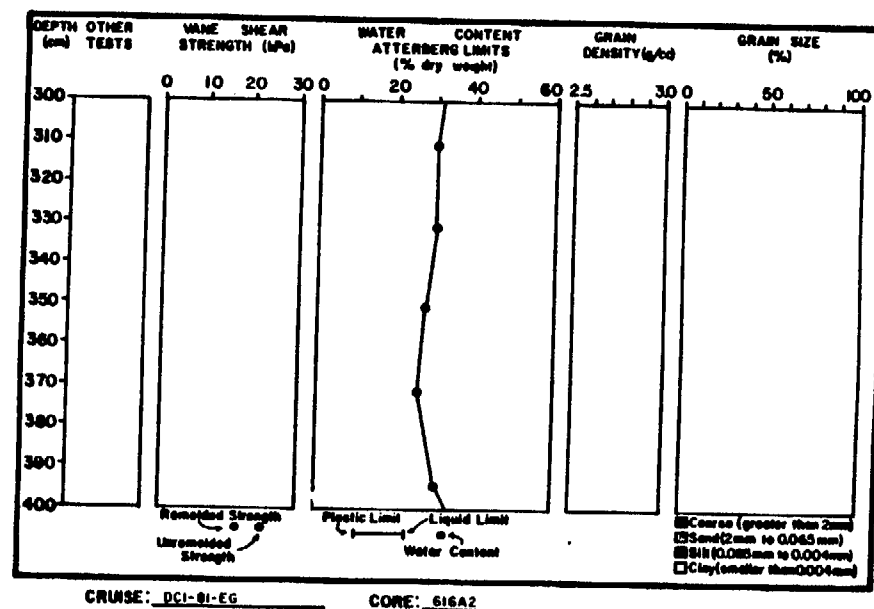
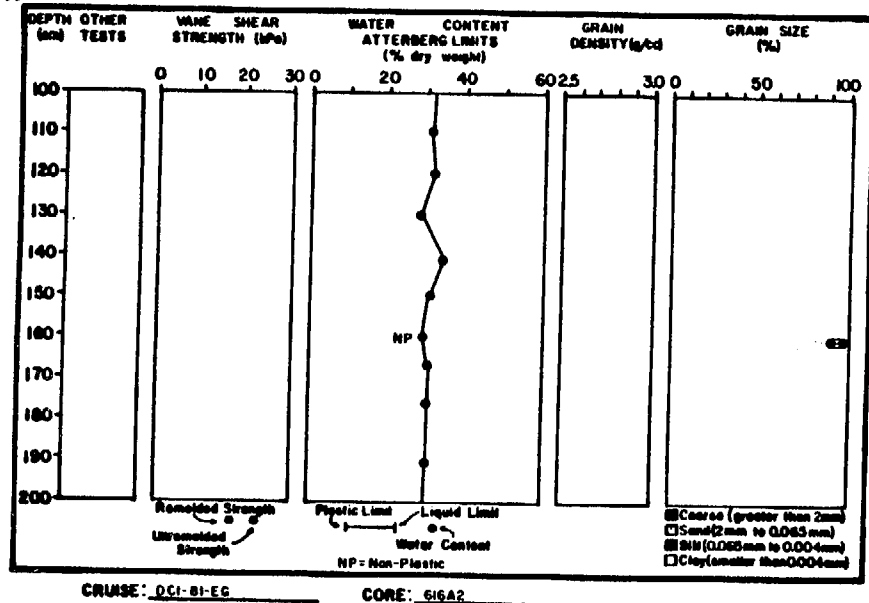


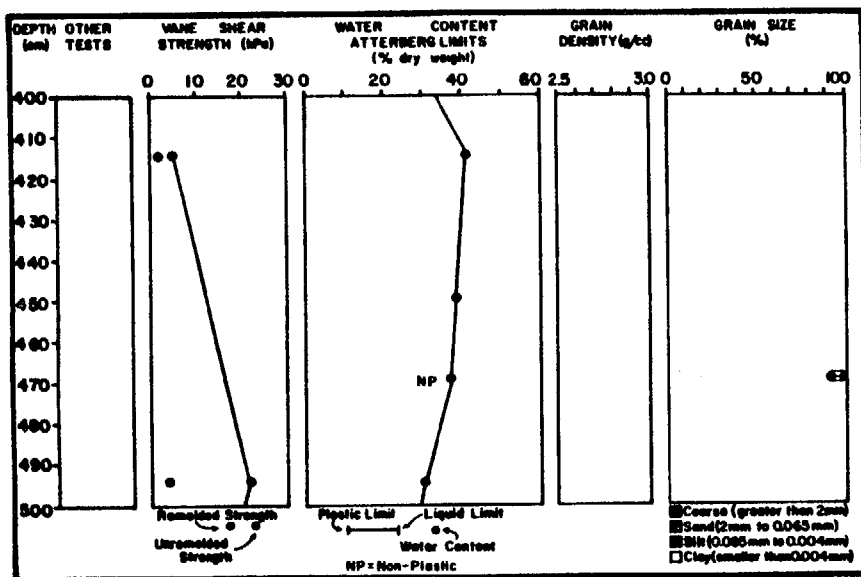
CRUISE: DC2-80-EG

CORE: 88G



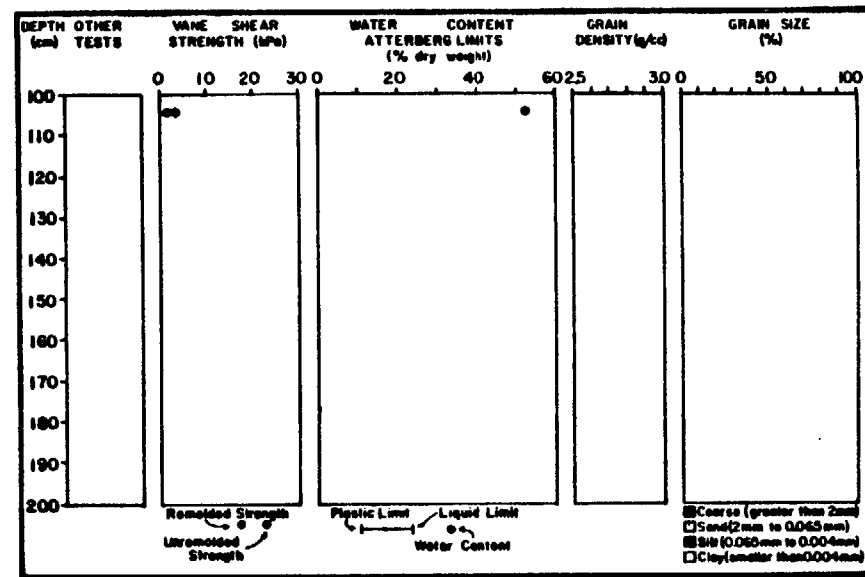
313





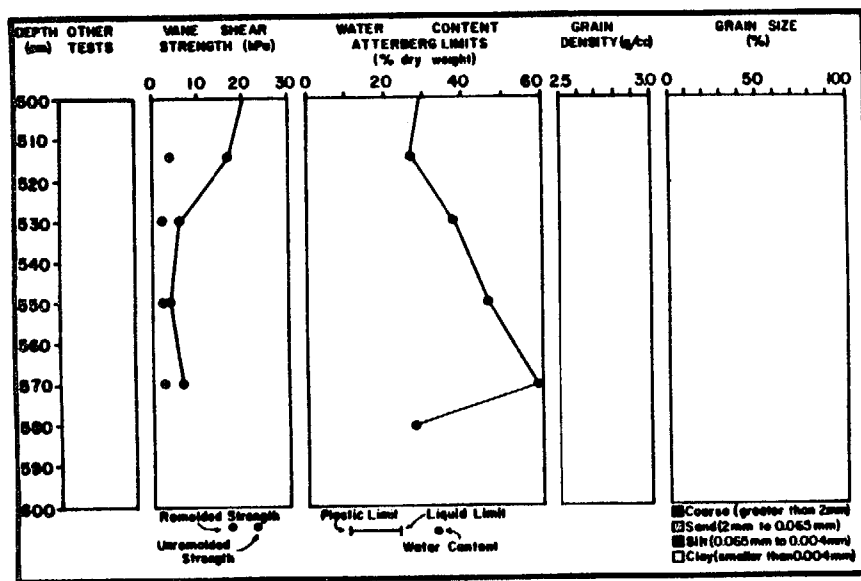
CRUISE: DCI-81-EG

CORE: 616A2



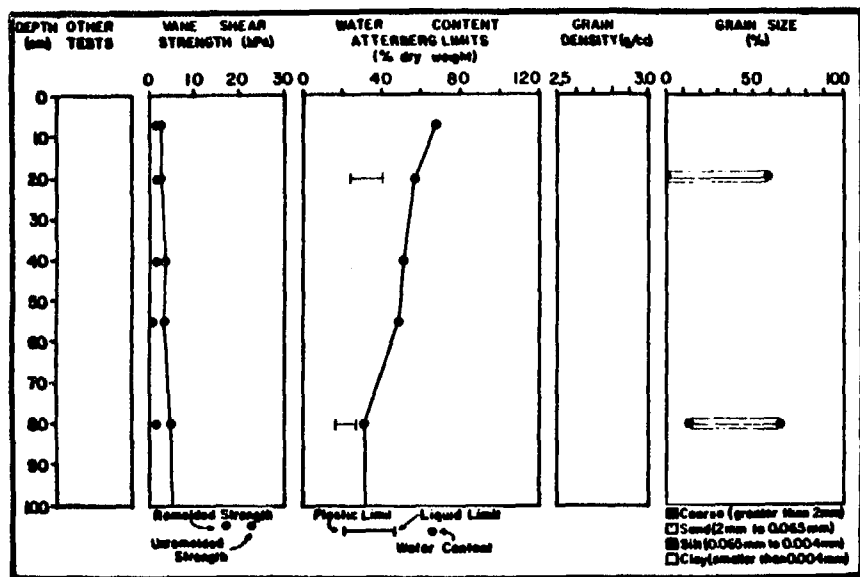
CRUISE: DCI-81-EG

CORE: 617G



CRUISE: DCI-81-EG

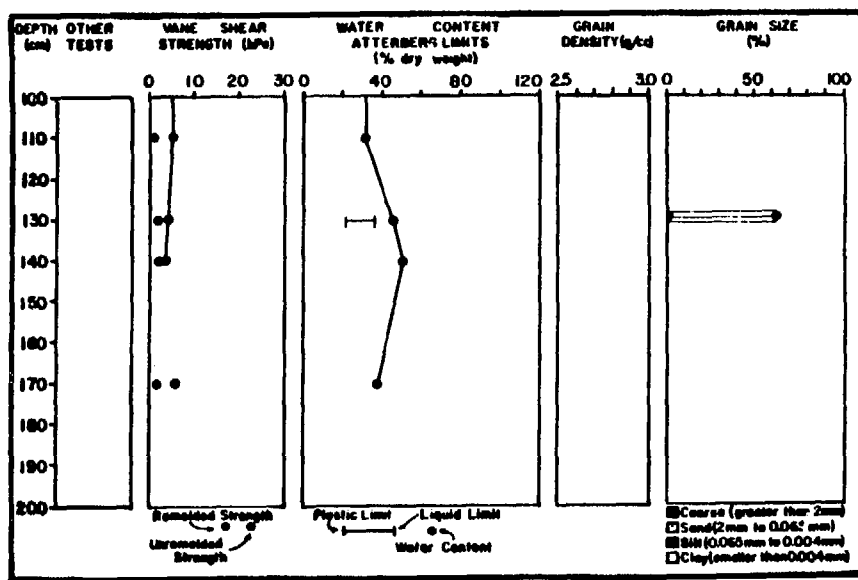
CORE: 616A2



CRUISE: DCI-81-EG

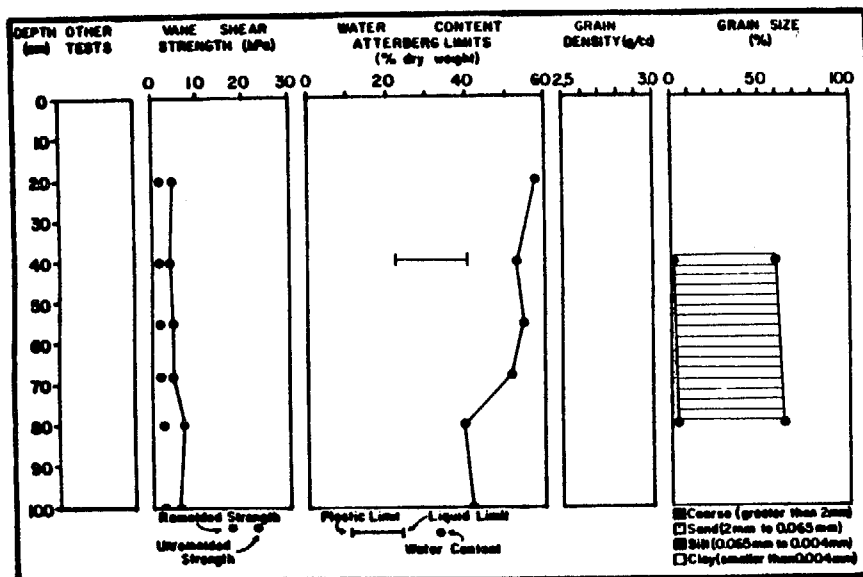
CORE: 61762

315

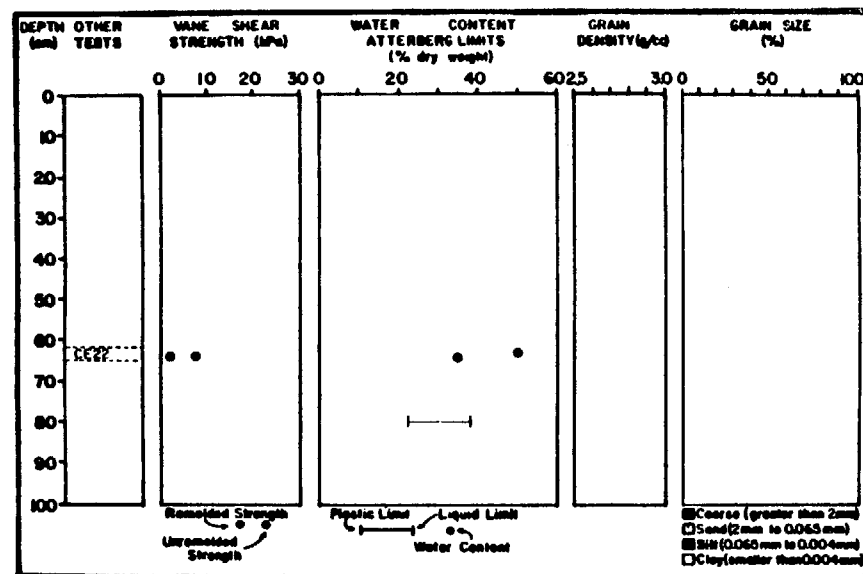


CRUISE: DCI-81-EG

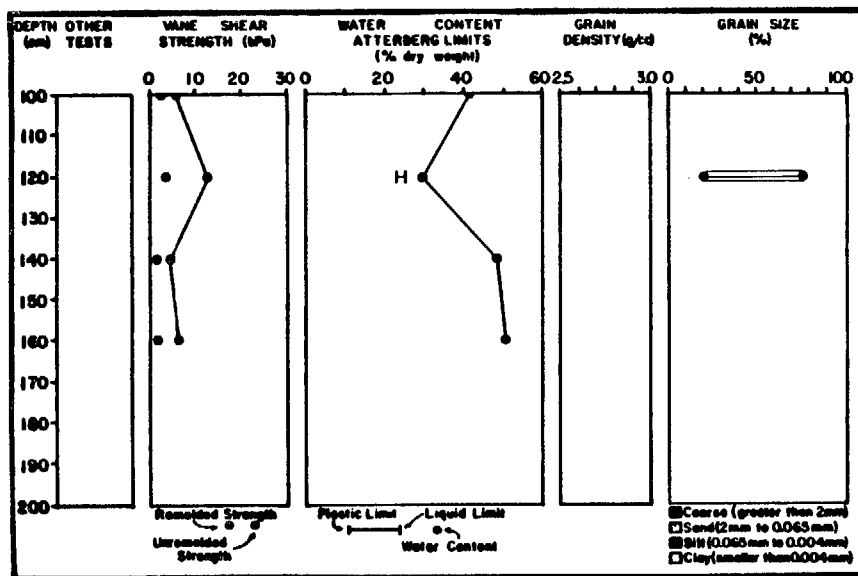
CORE: 61702



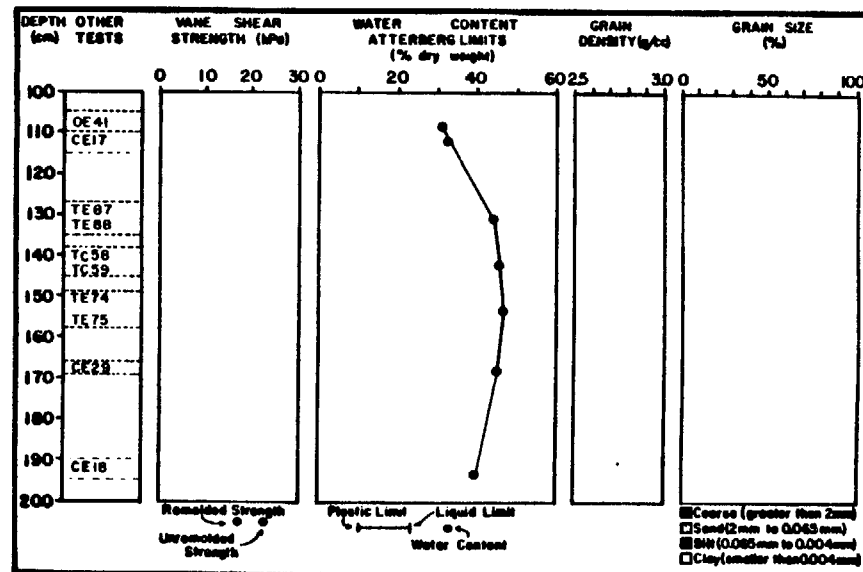
CRUISE: DCI-81-EG CORE: 618G1



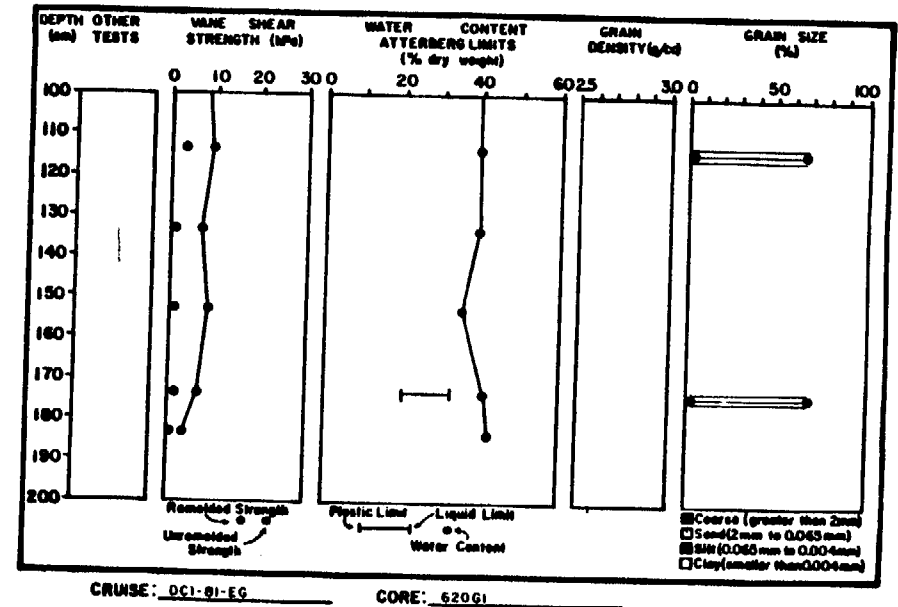
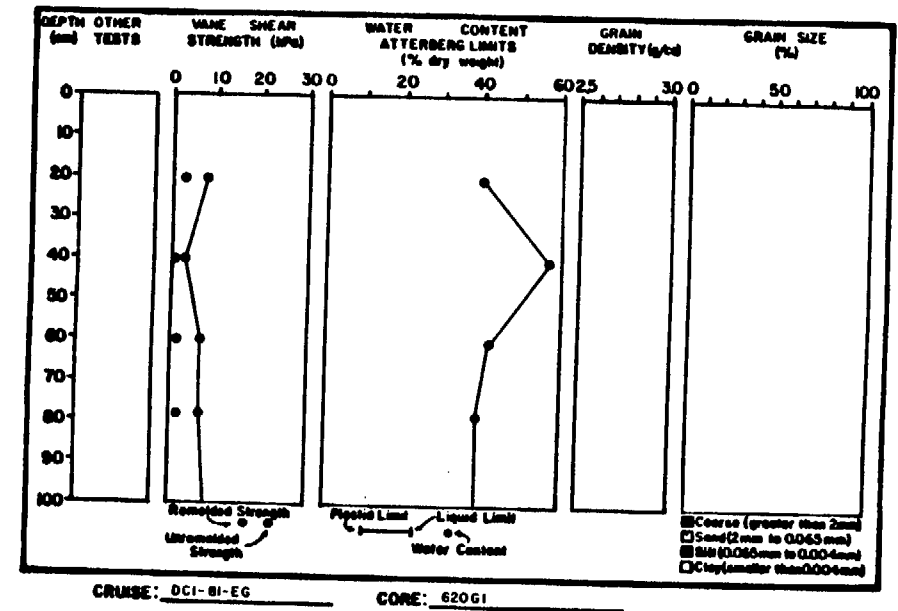
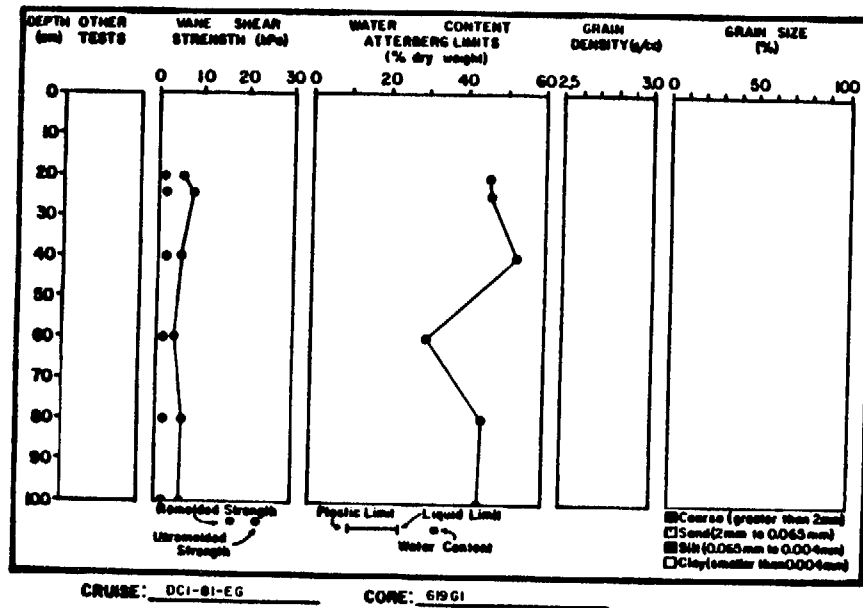
CRUISE: DCI-81-EG CORE: 618G2

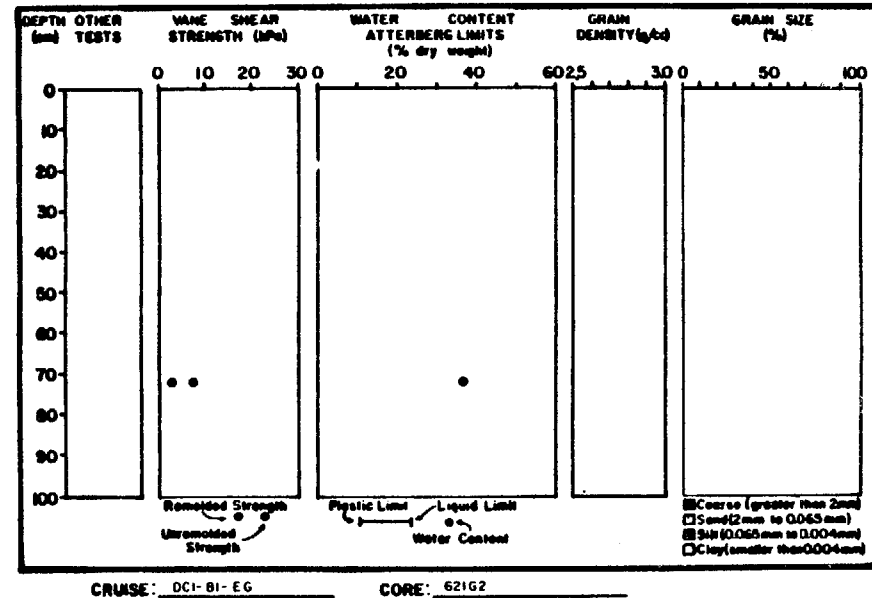
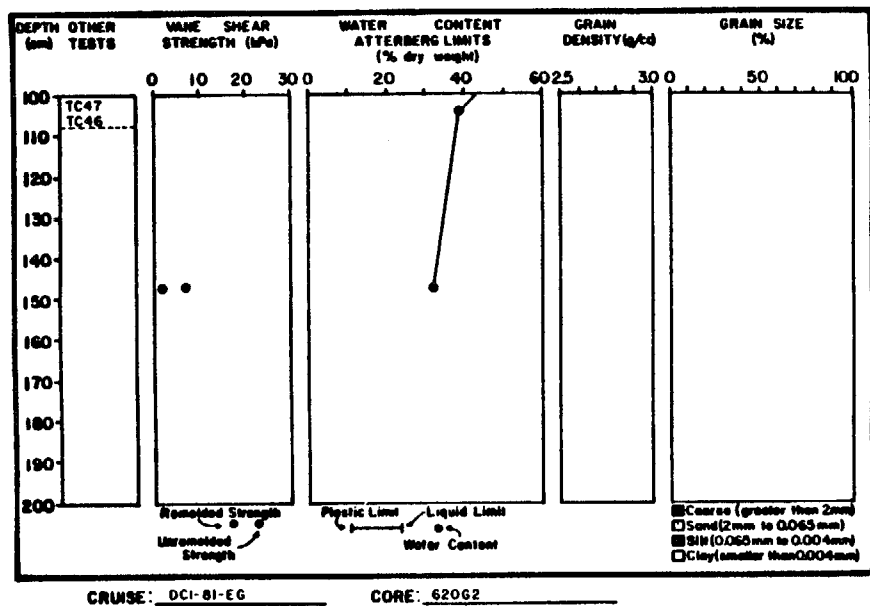
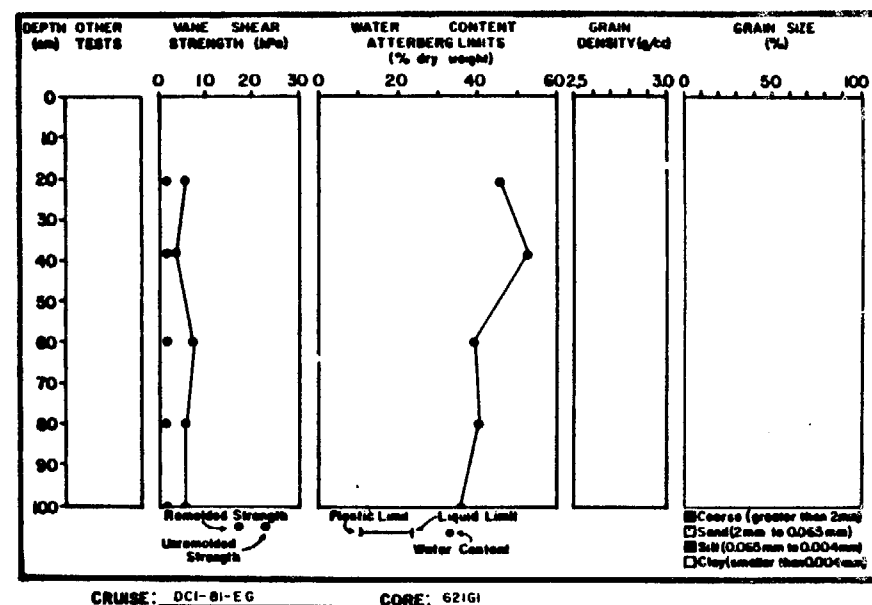
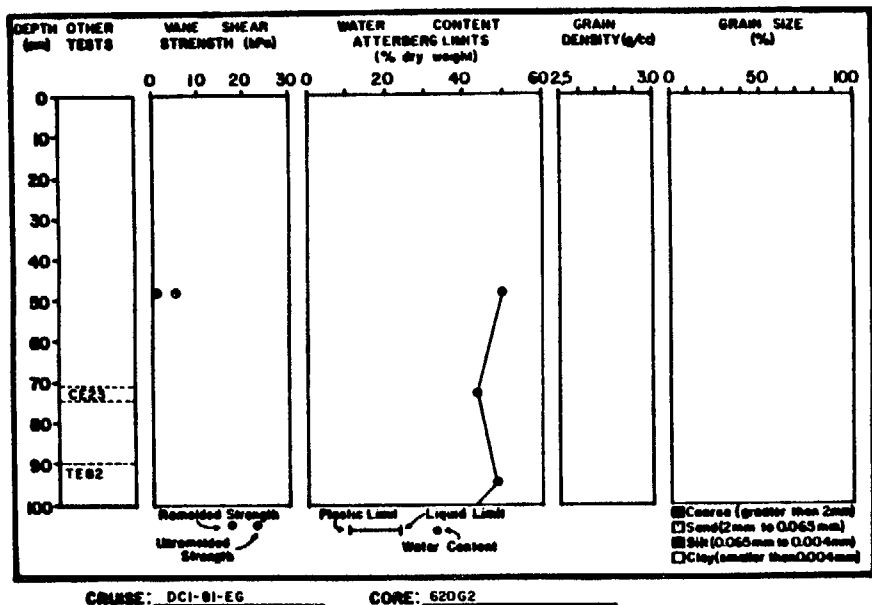


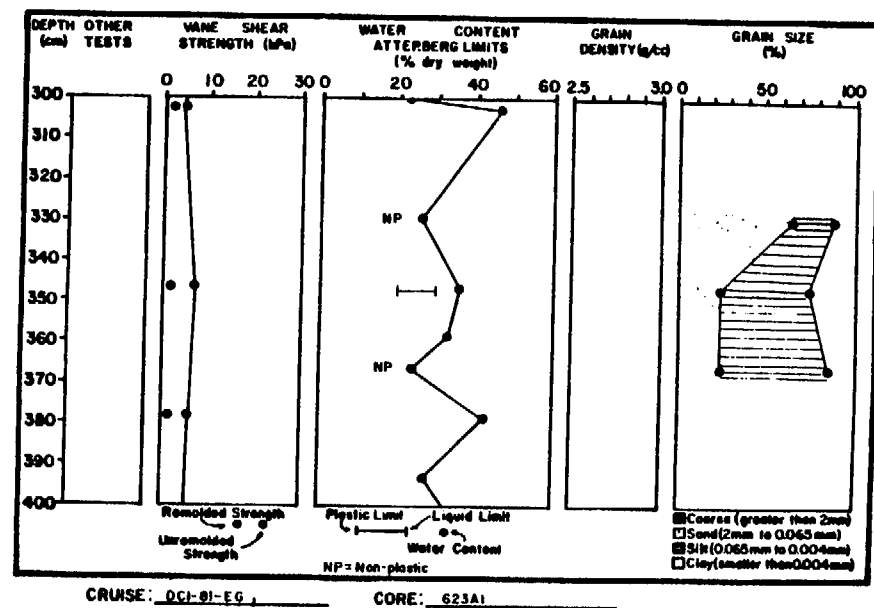
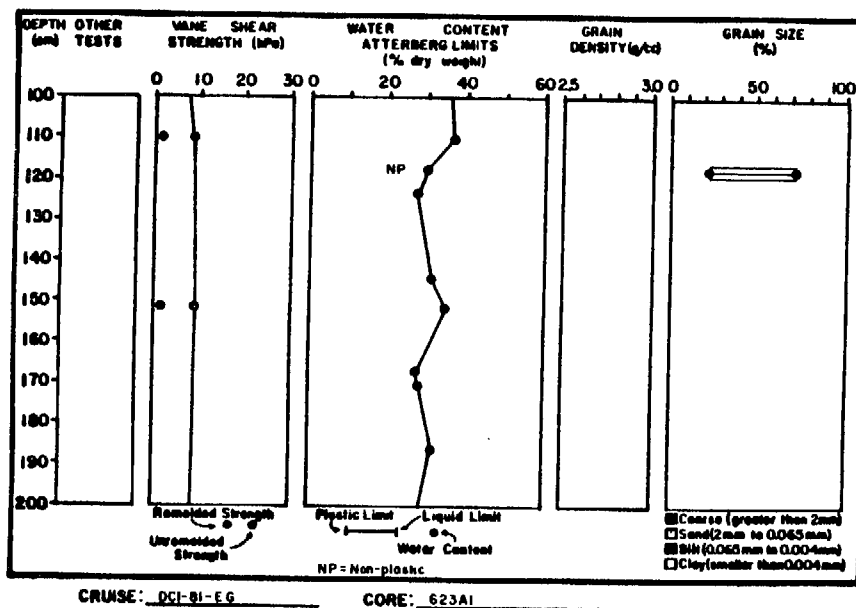
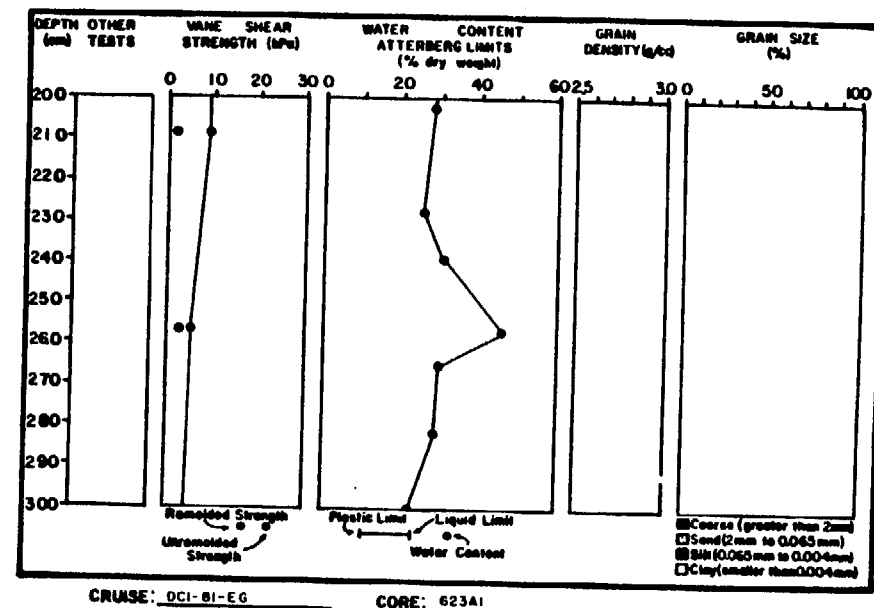
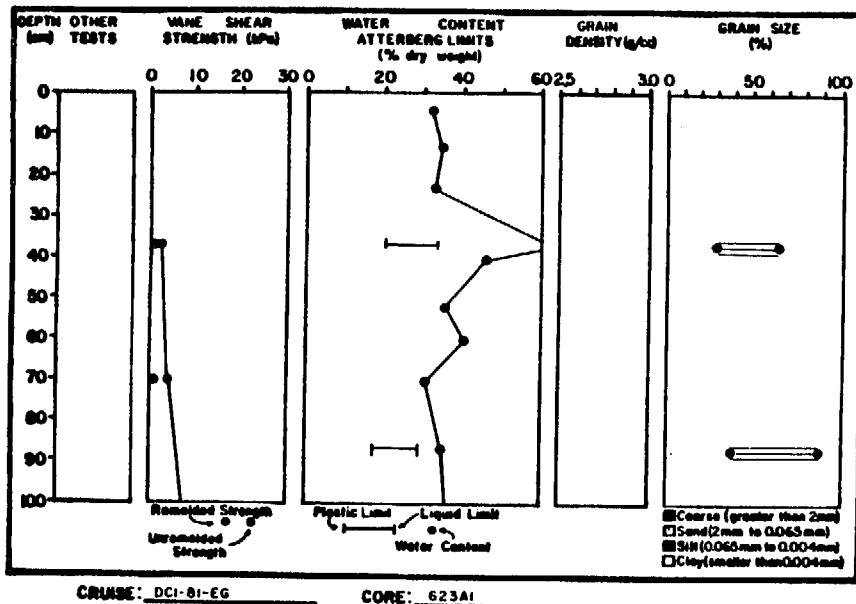
CRUISE: DCI-81-EG CORE: 618G1

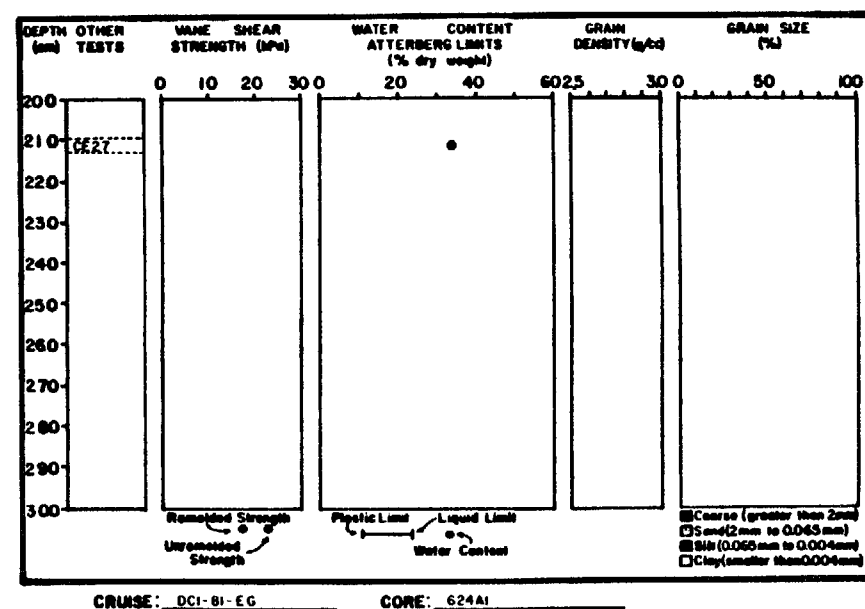
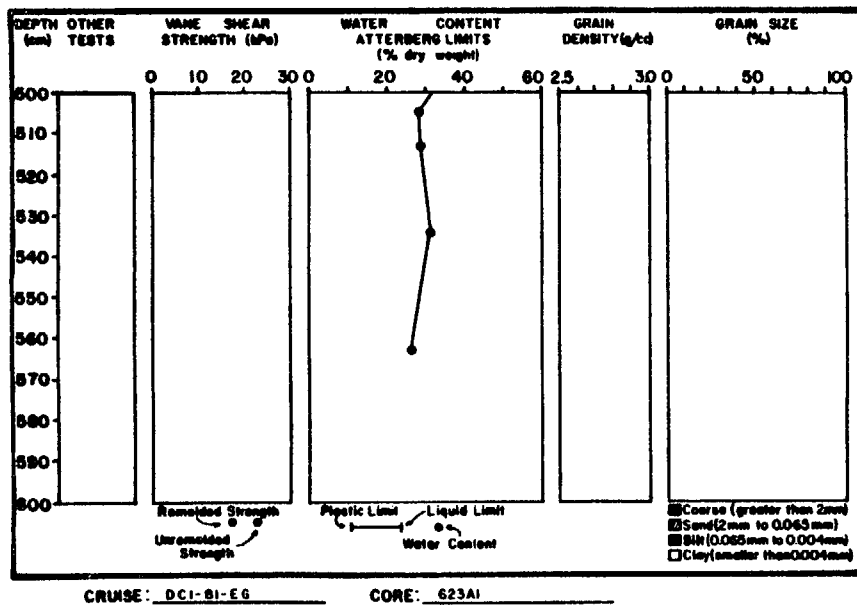
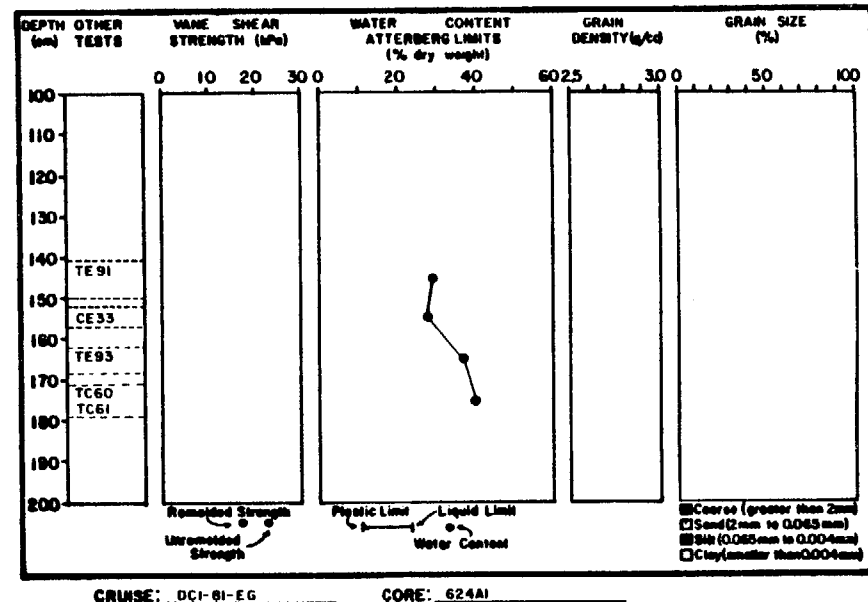
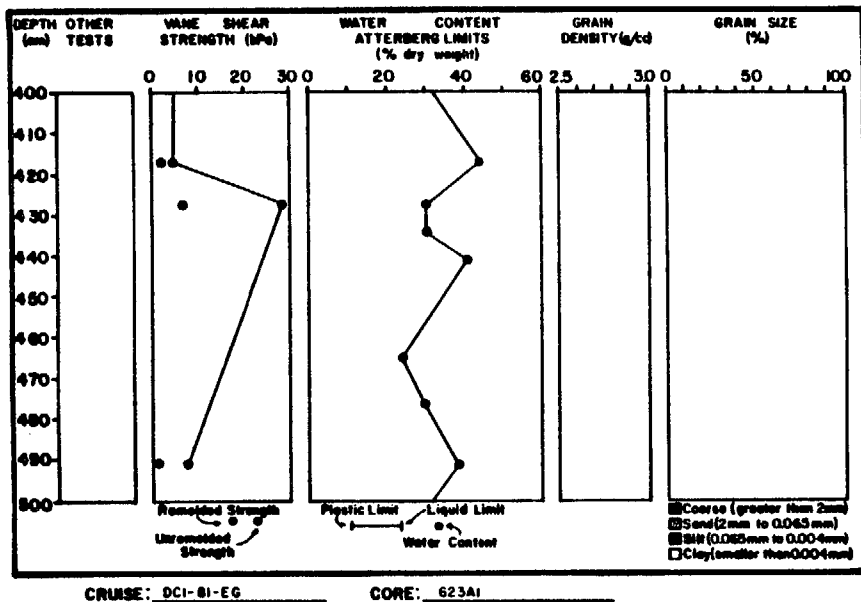


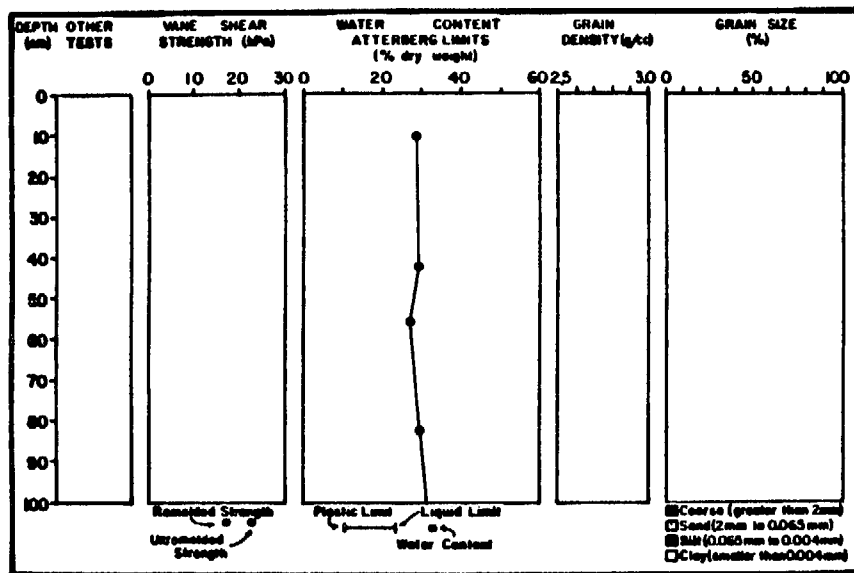
CRUISE: DCI-81-EG CORE: 618G2



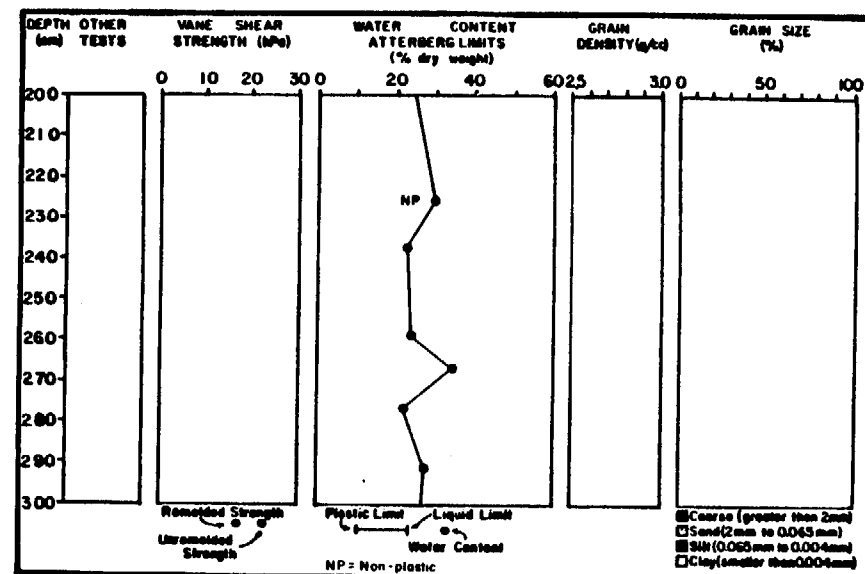




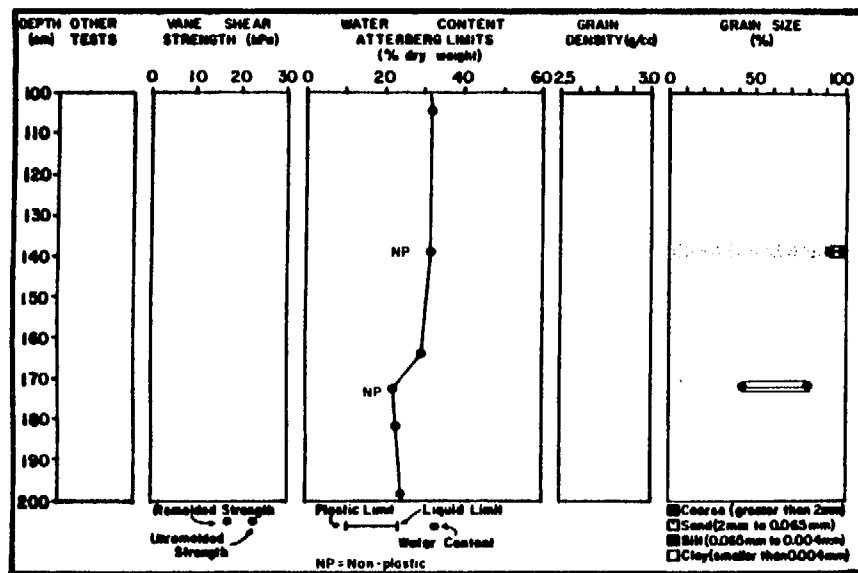




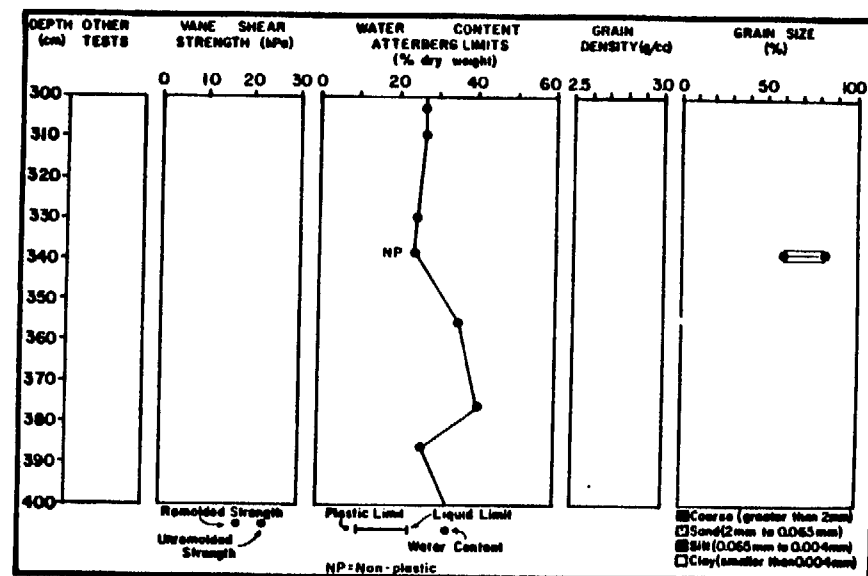
CRUISE: DCI-81-EG CORE: 624A2



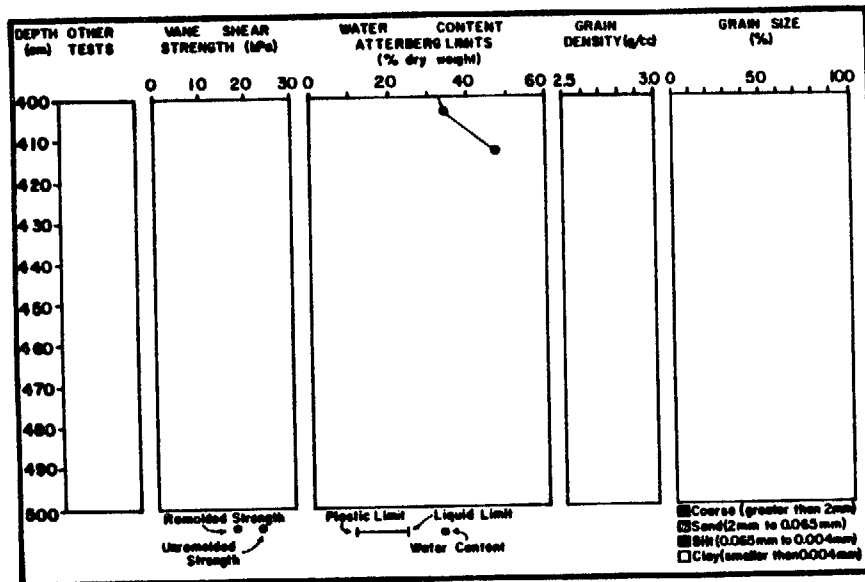
CRUISE: DCI-81-EG CORE: 624A2



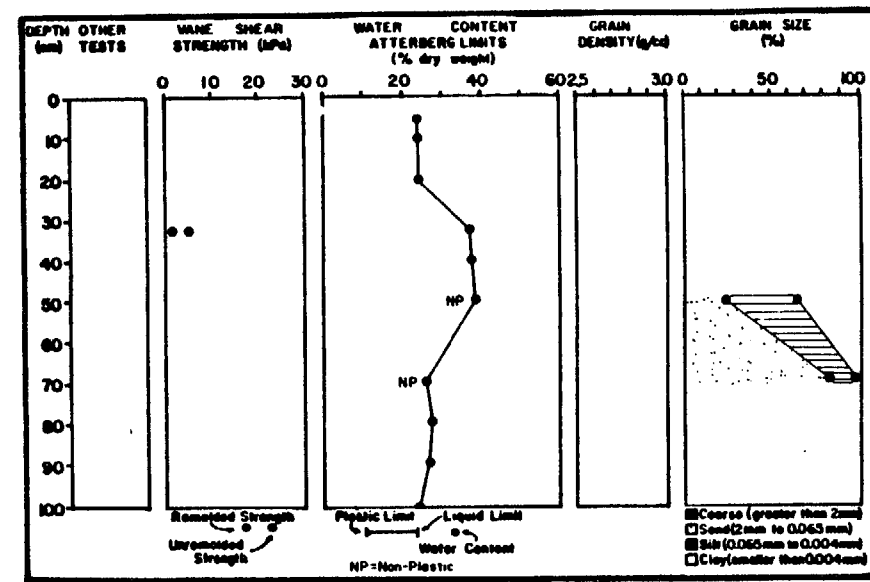
CRUISE: DCI-81-EG CORE: 624A2



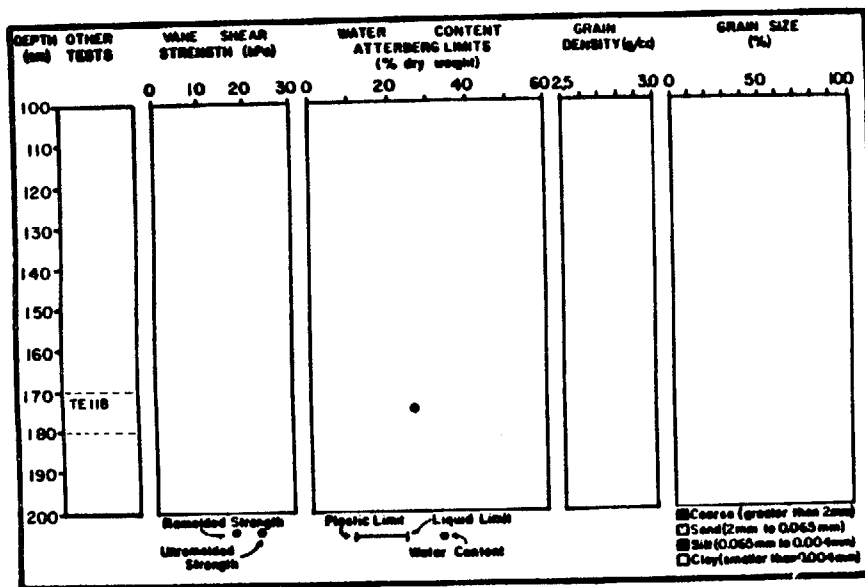
CRUISE: DCI-81-EG CORE: 624A2



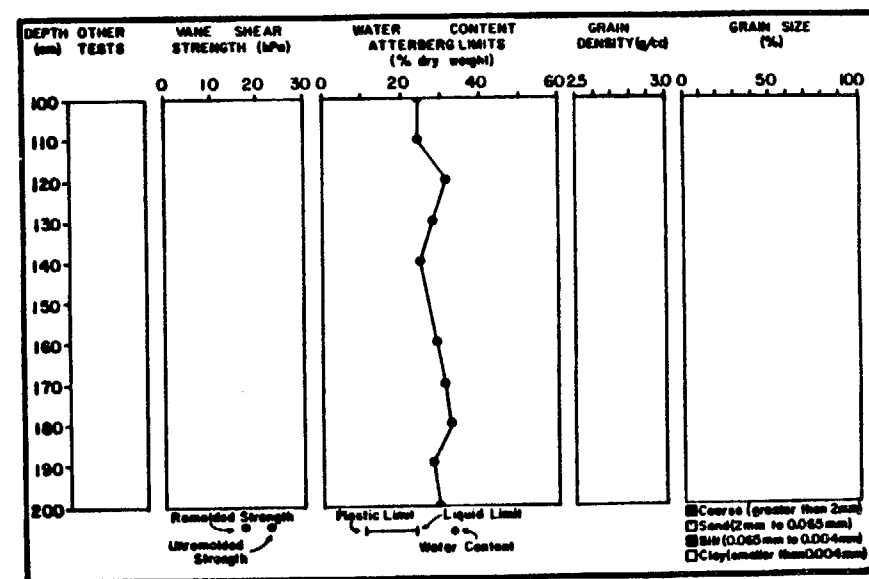
CRUISE: DCI-81-EG CORE: 624A2



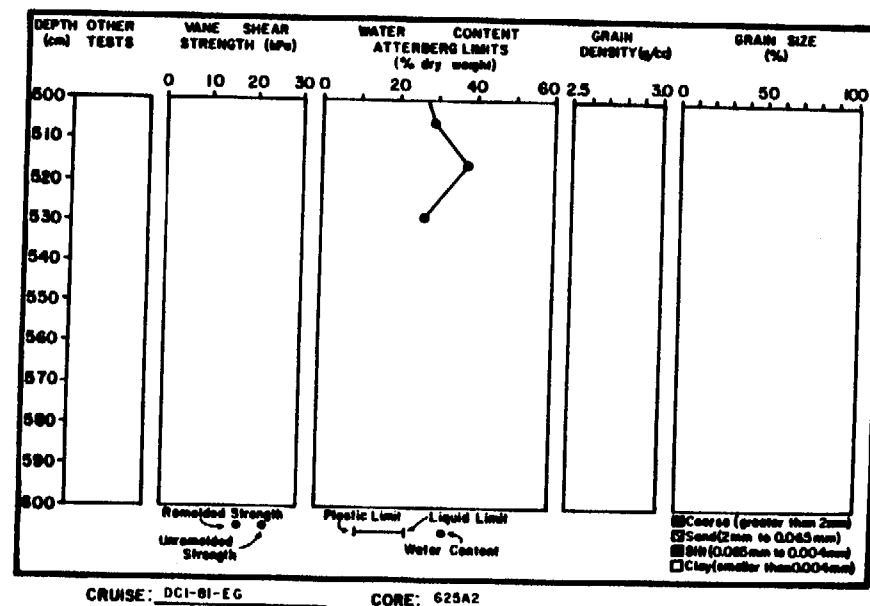
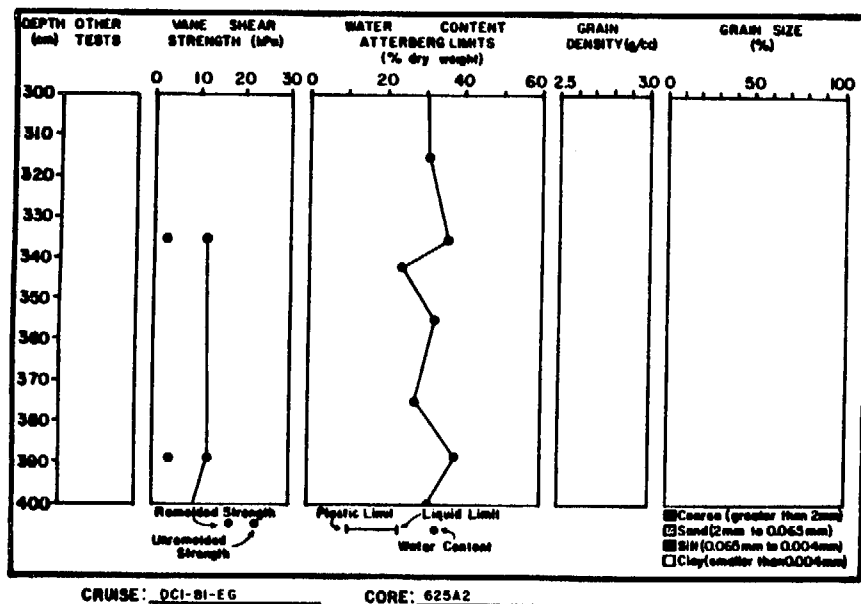
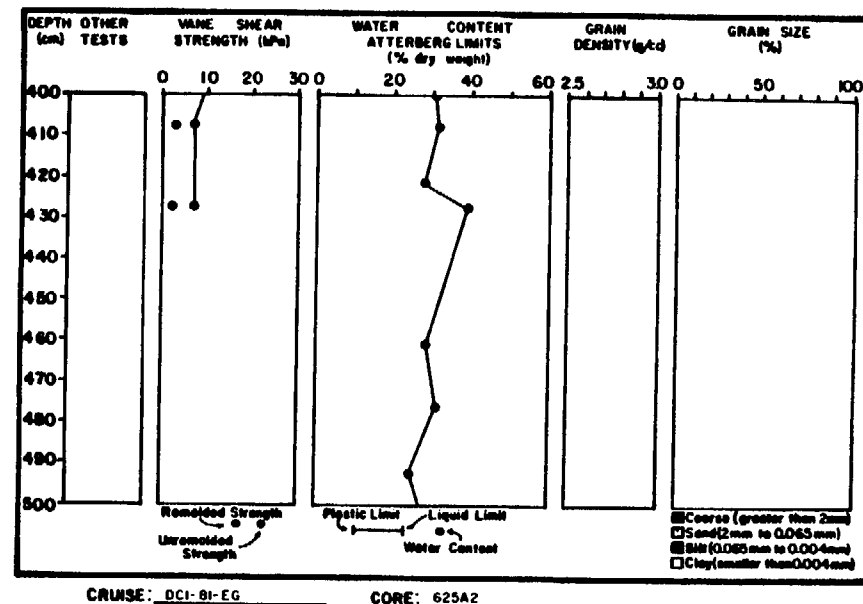
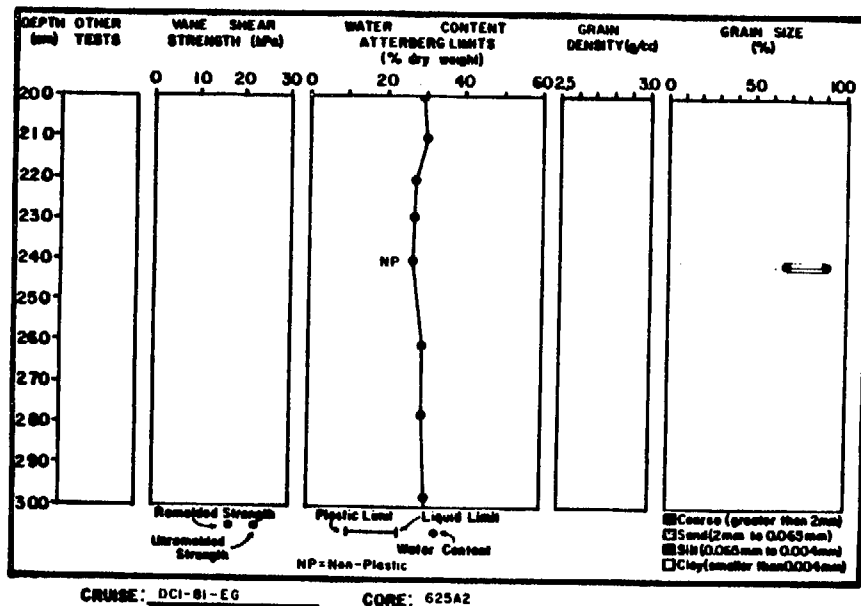
CRUISE: DCI-81-EG CORE: 625A2



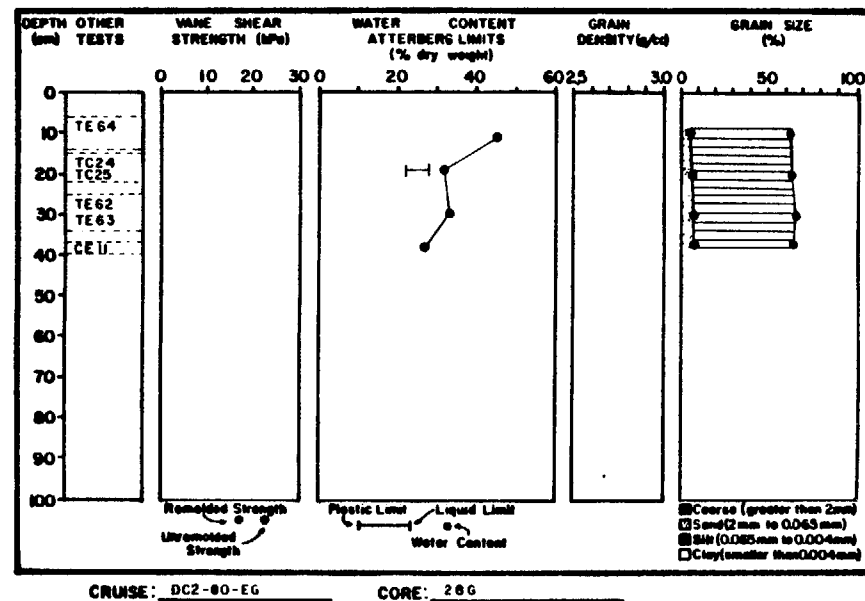
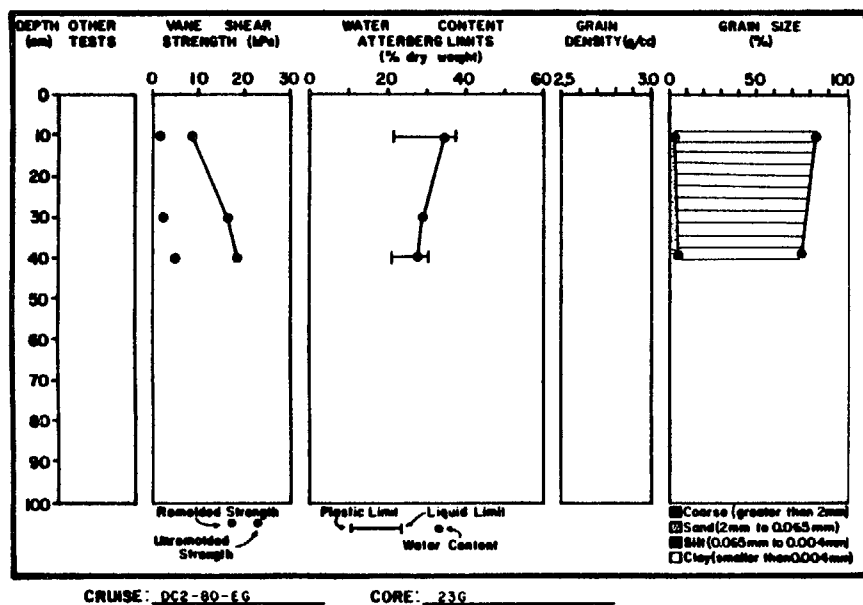
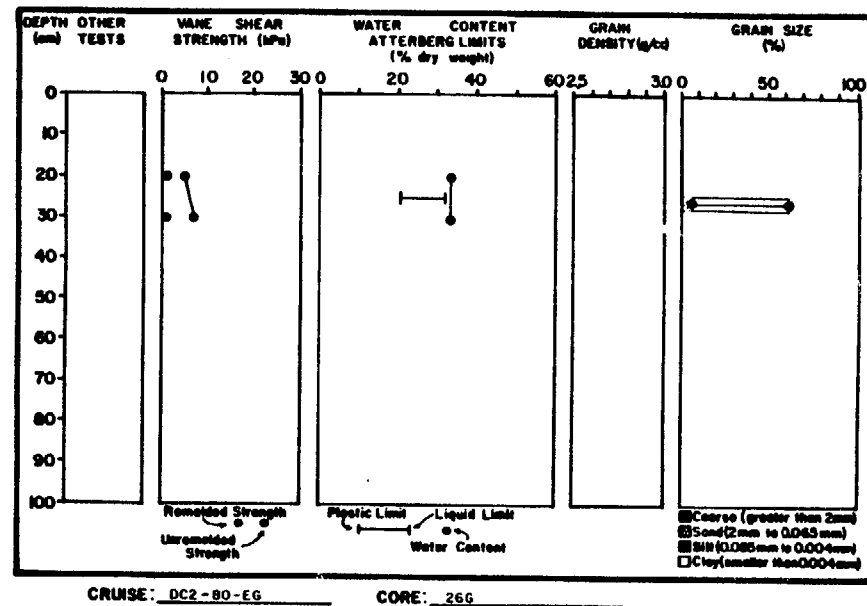
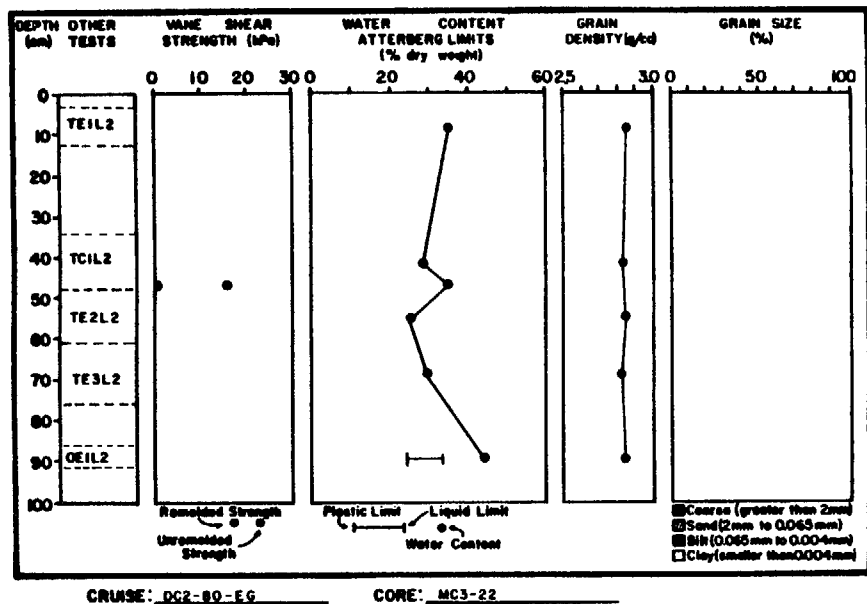
CRUISE: DCI-81-EG CORE: 625A1

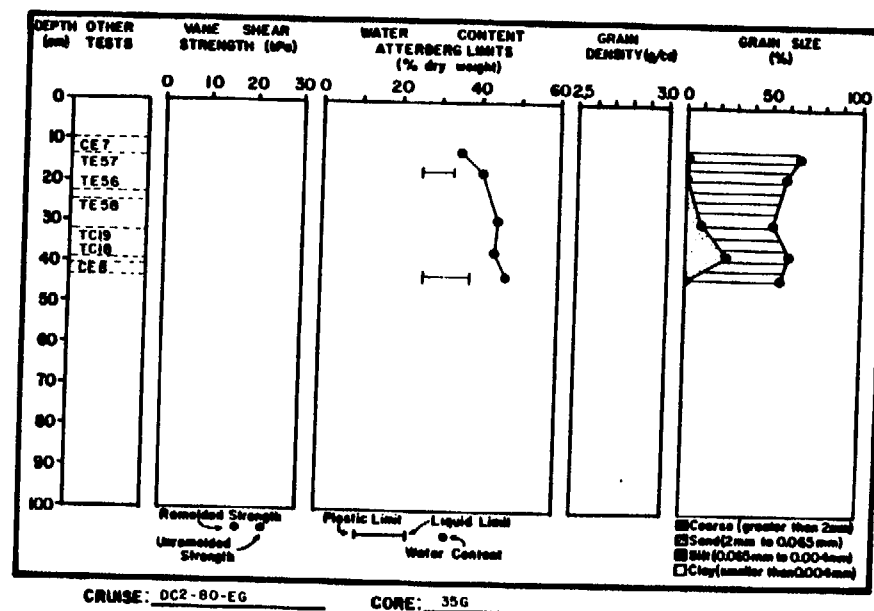
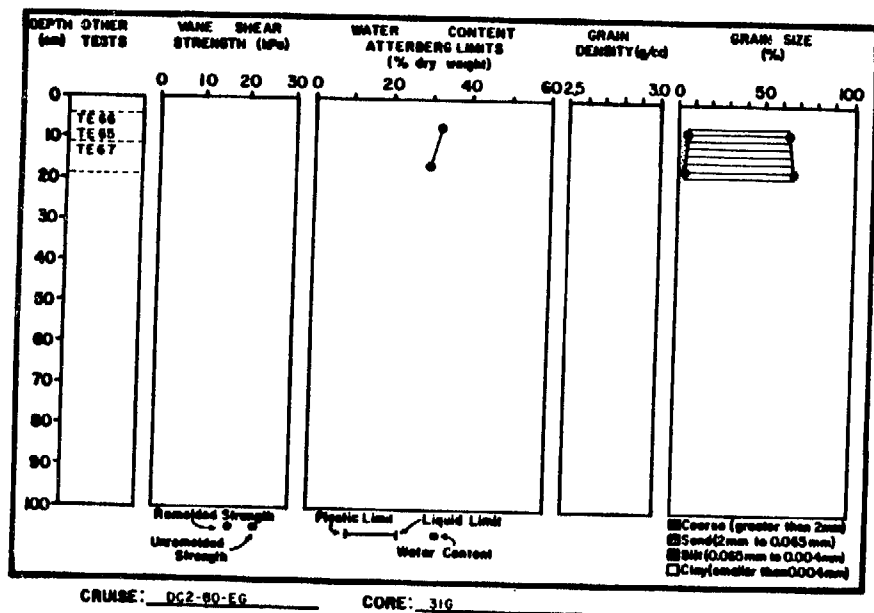
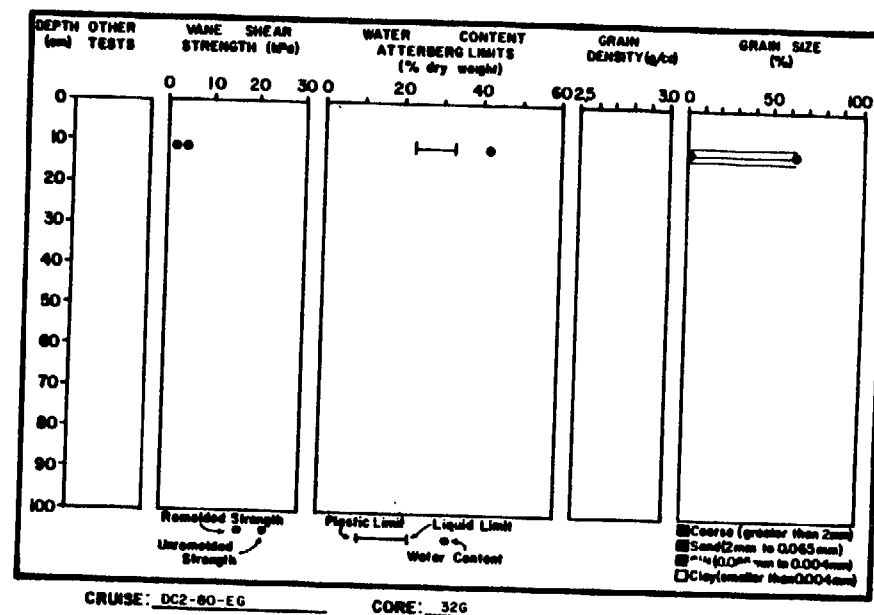
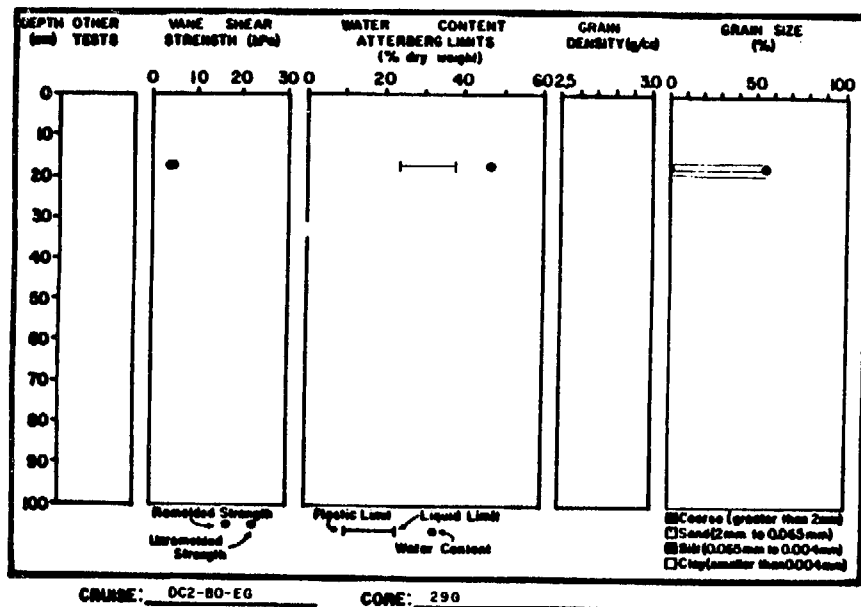


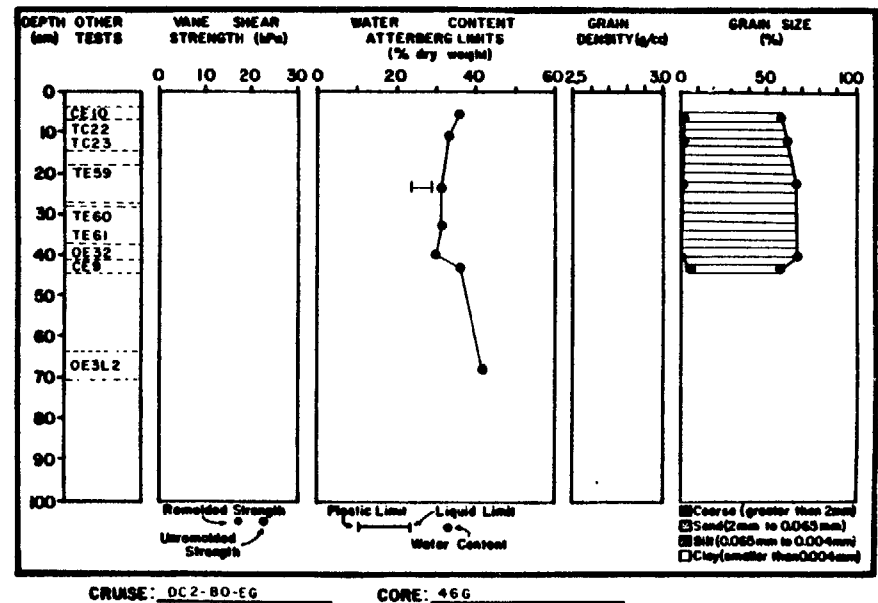
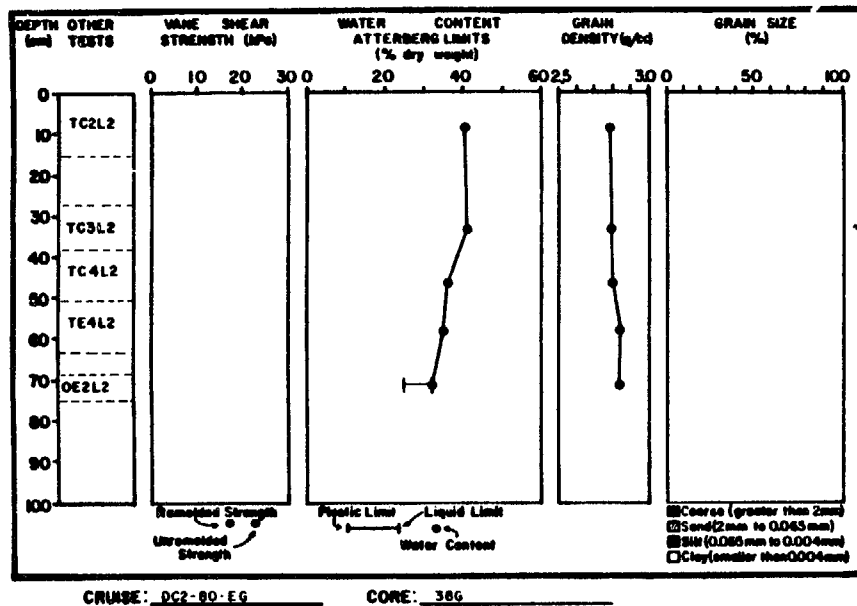
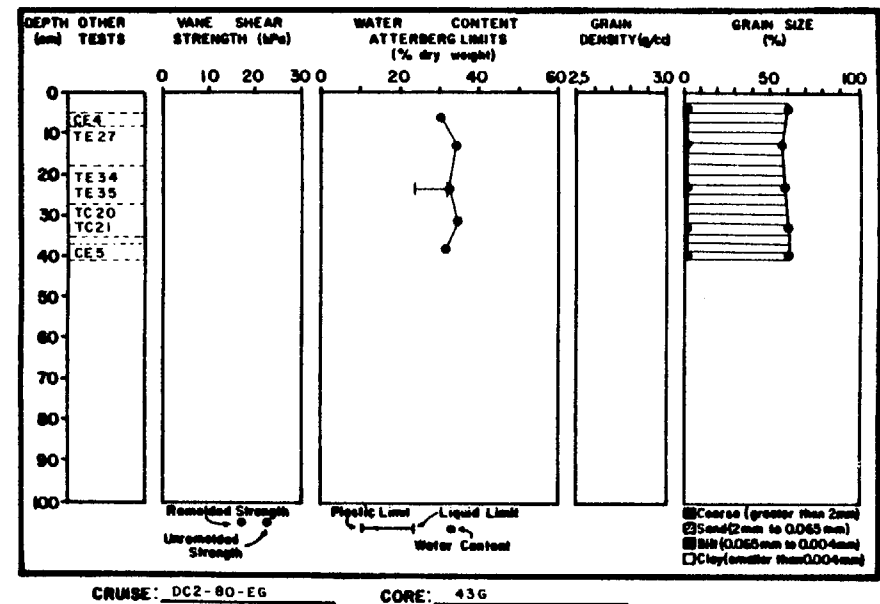
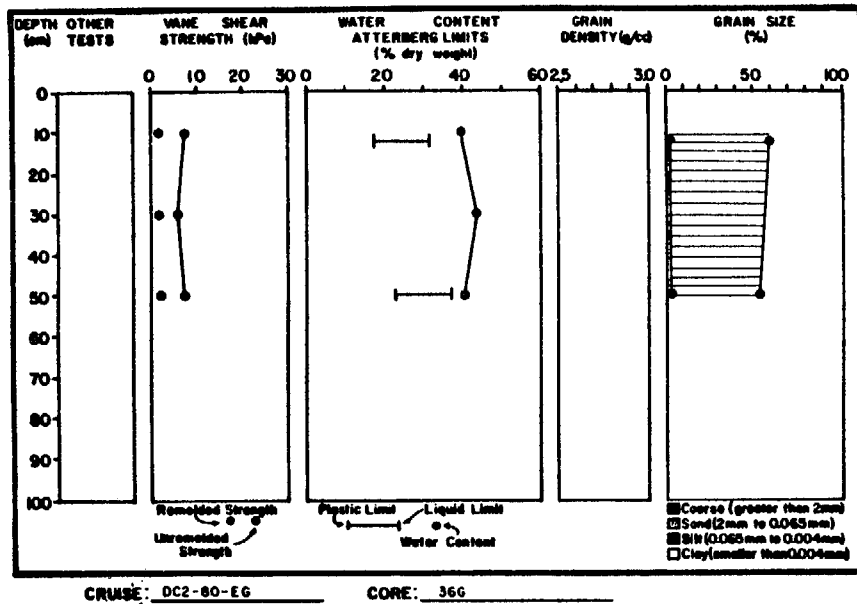
CRUISE: DCI-81-EG CORE: 625A2

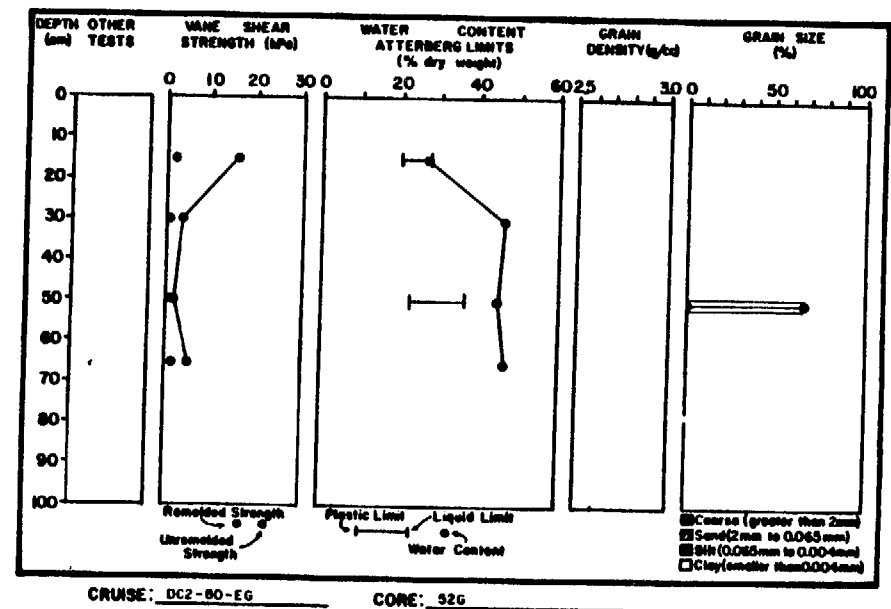
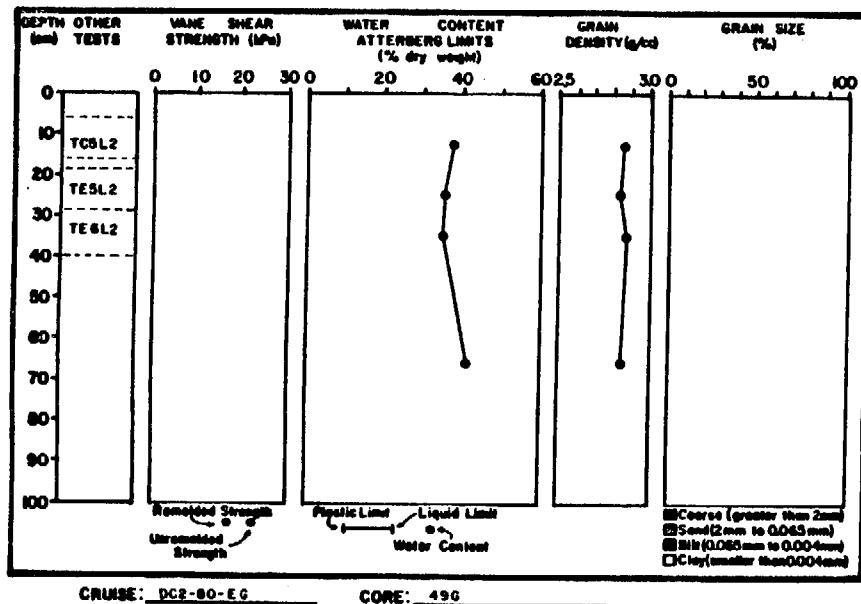
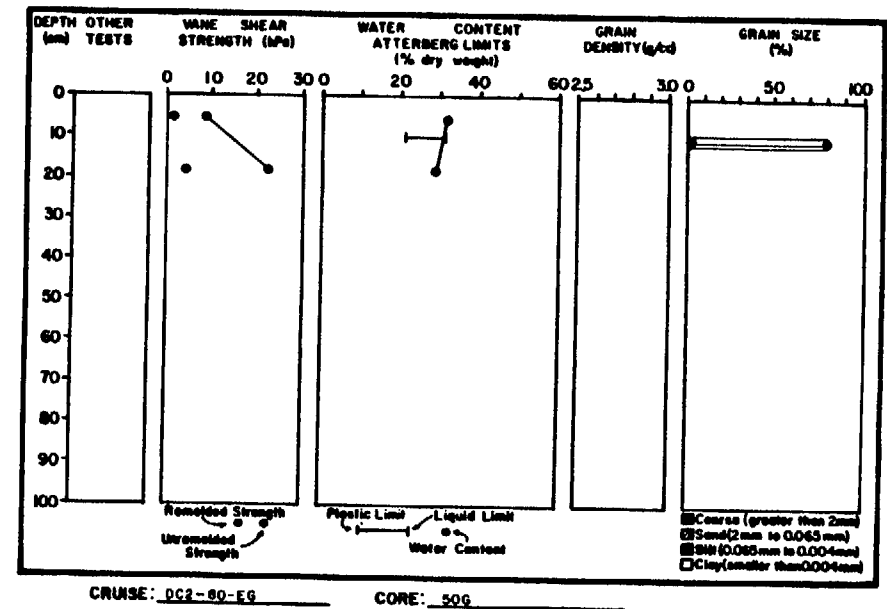
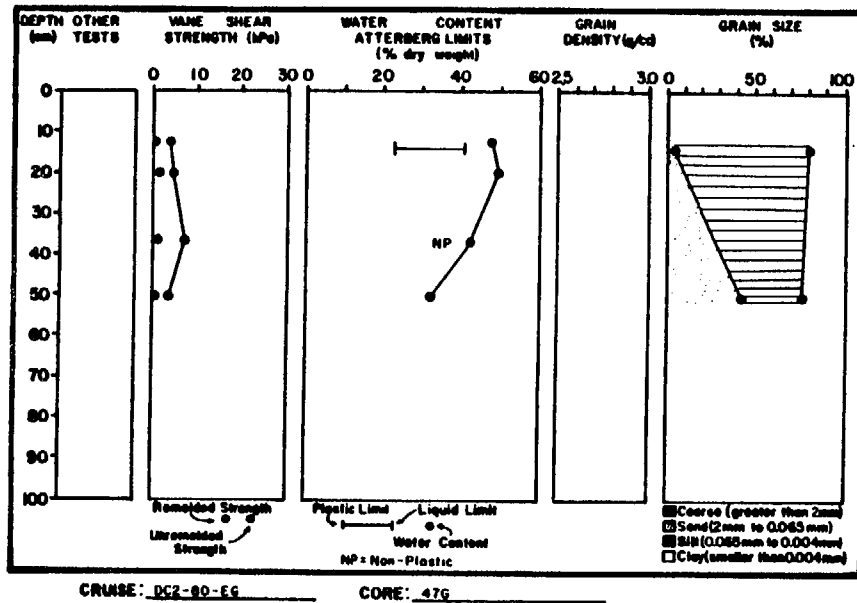


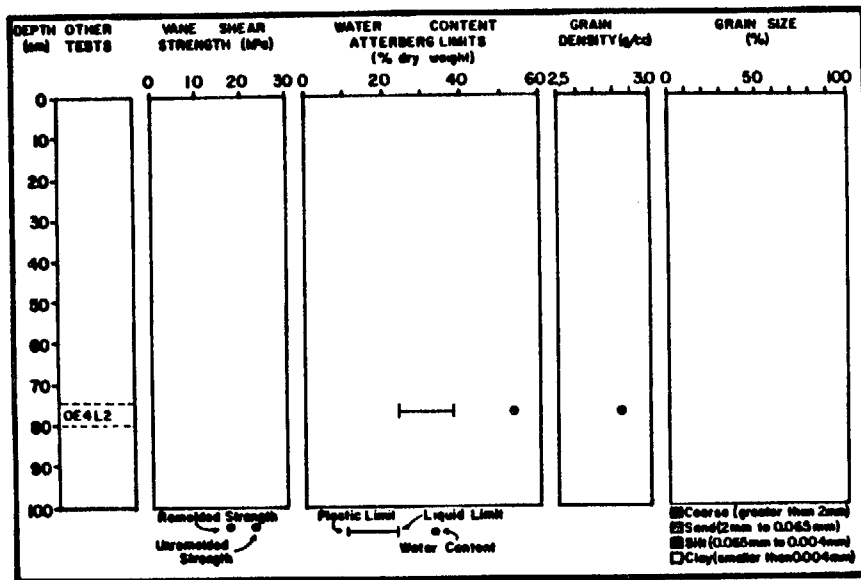
ALSEK RIVER STUDY AREA



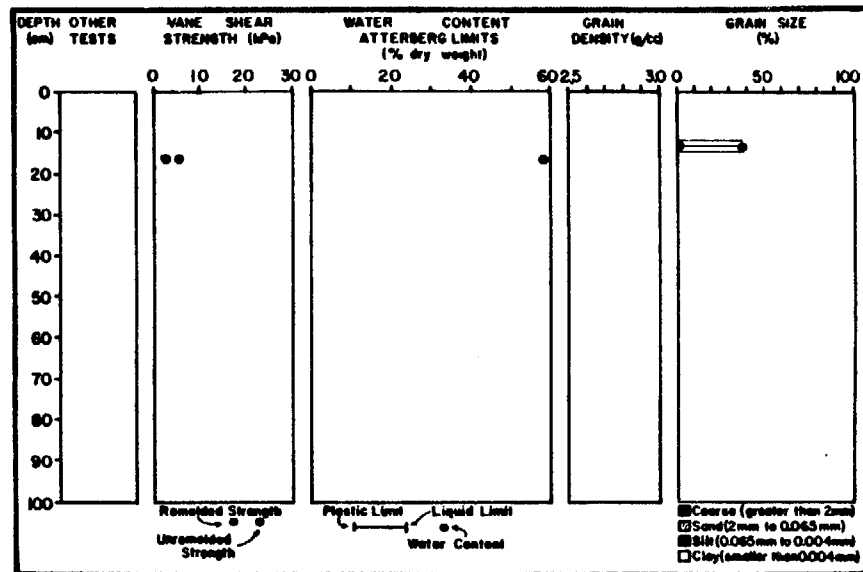




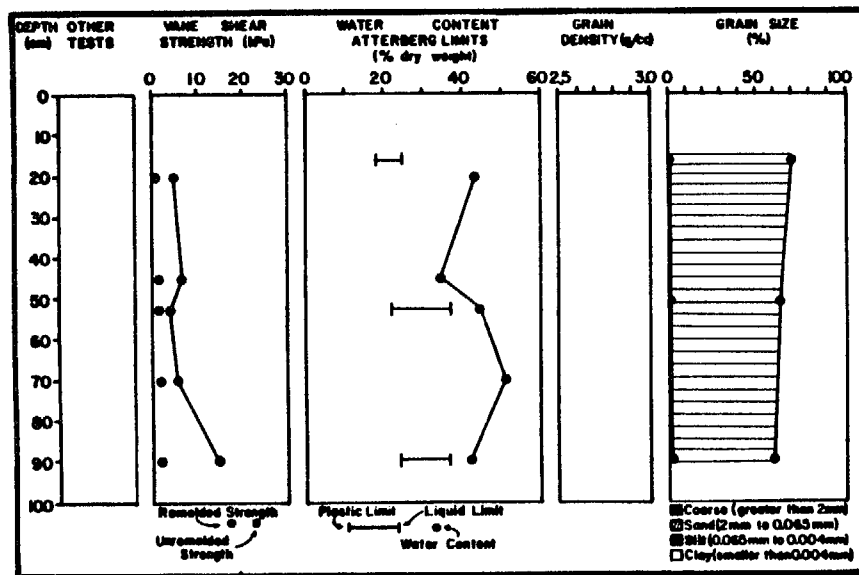




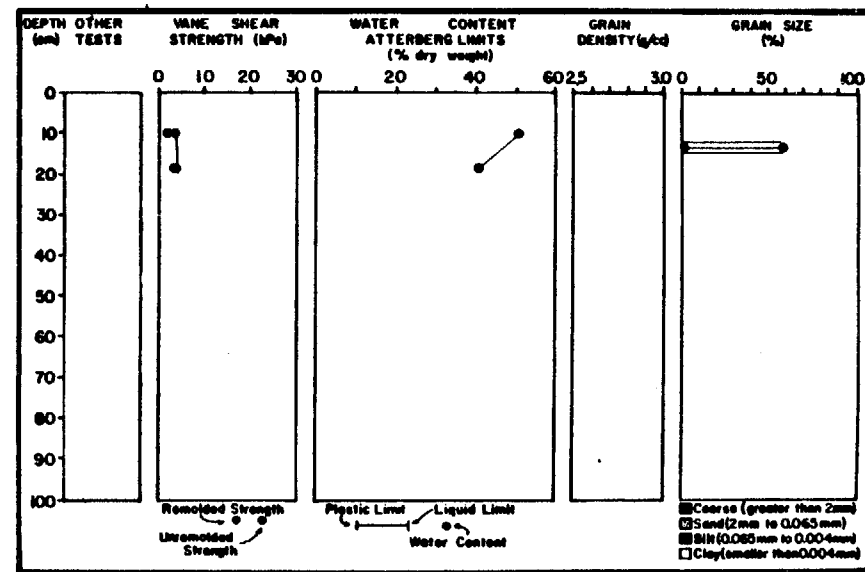
CRUISE: DC2-80-EG CORE: 55G



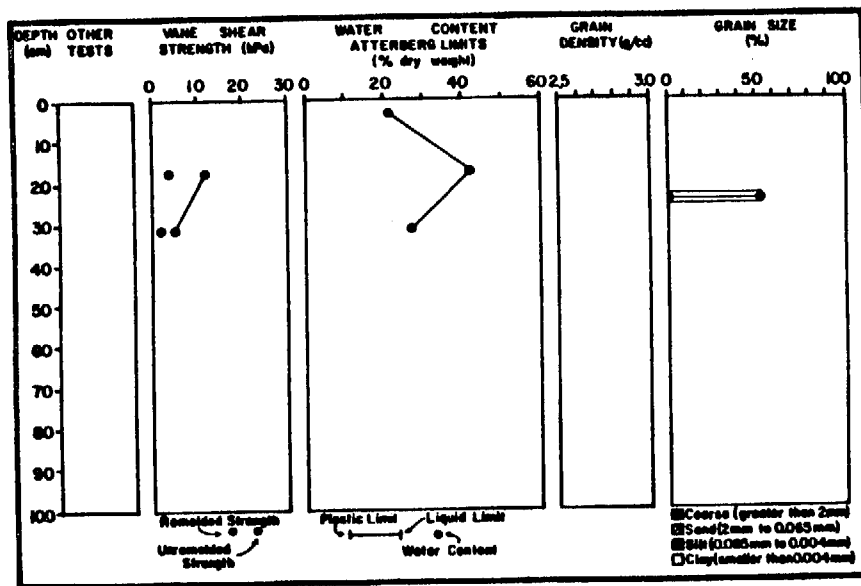
CRUISE: DC1-81-EG CORE: 601G2



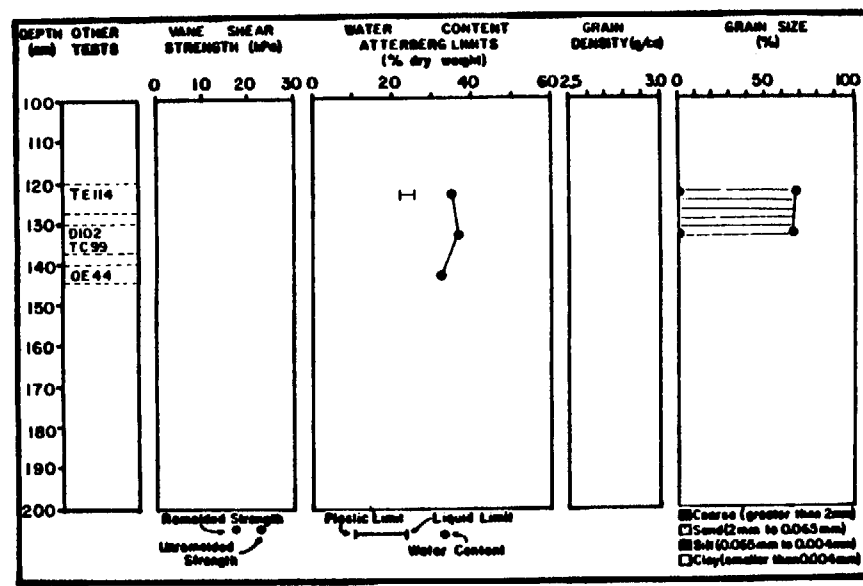
CRUISE: DC2-80-EG CORE: 56G



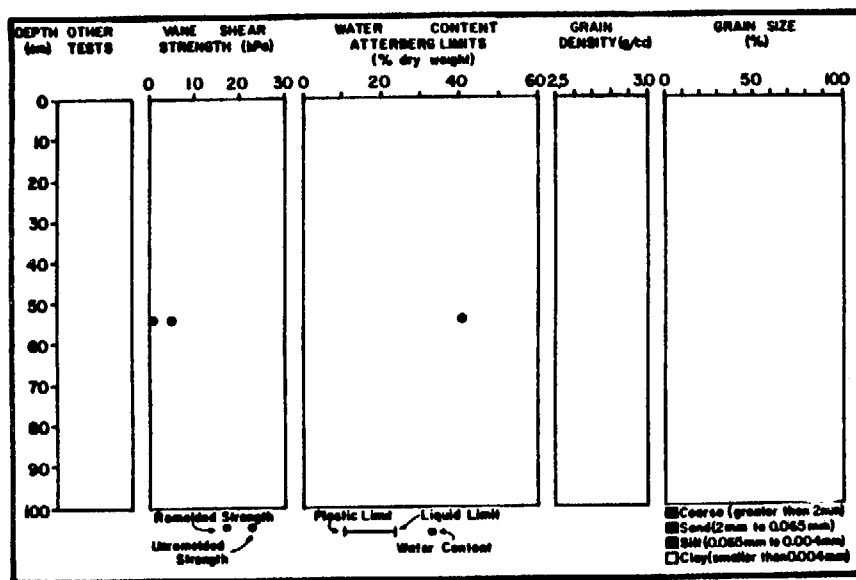
CRUISE: DC1-81-EG CORE: 602G3



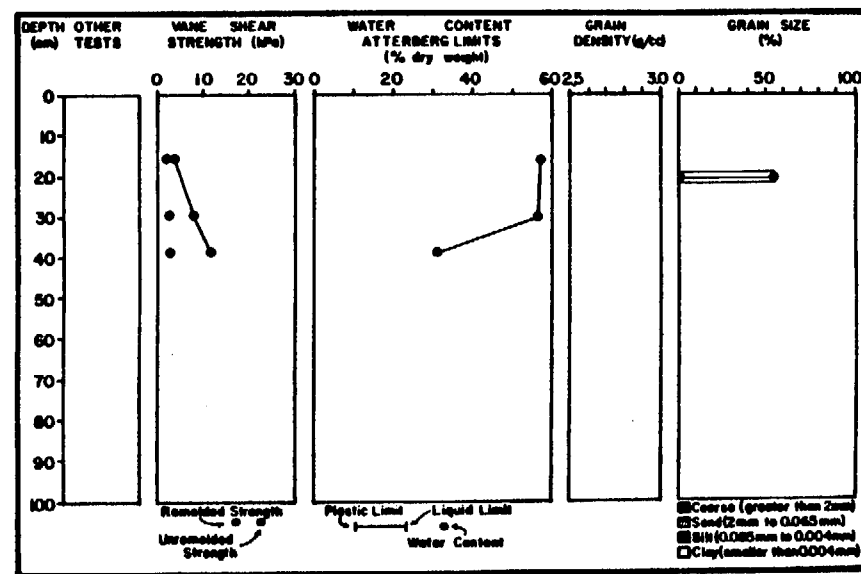
CRUISE: DCI-81-EG CORE: 60361



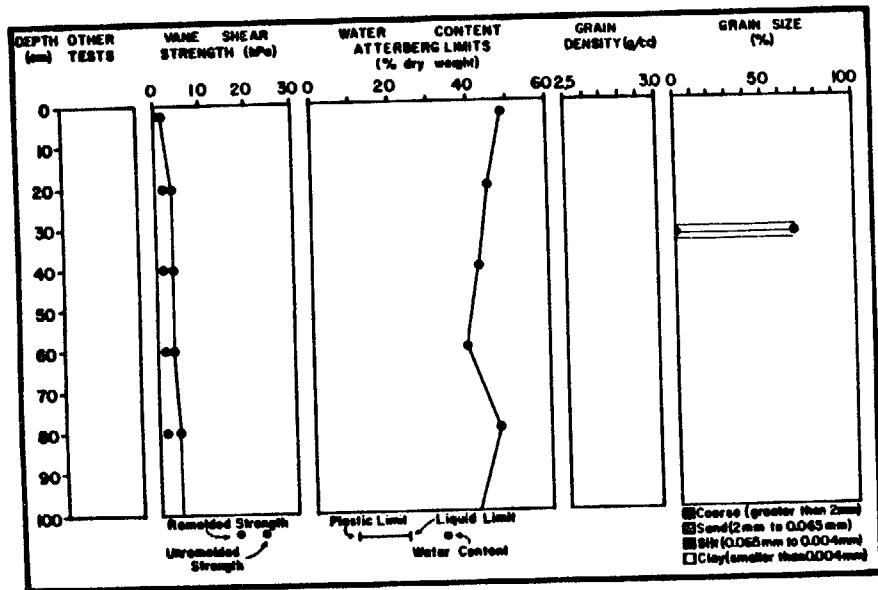
CRUISE: DCI-81-EG CORE: 60463



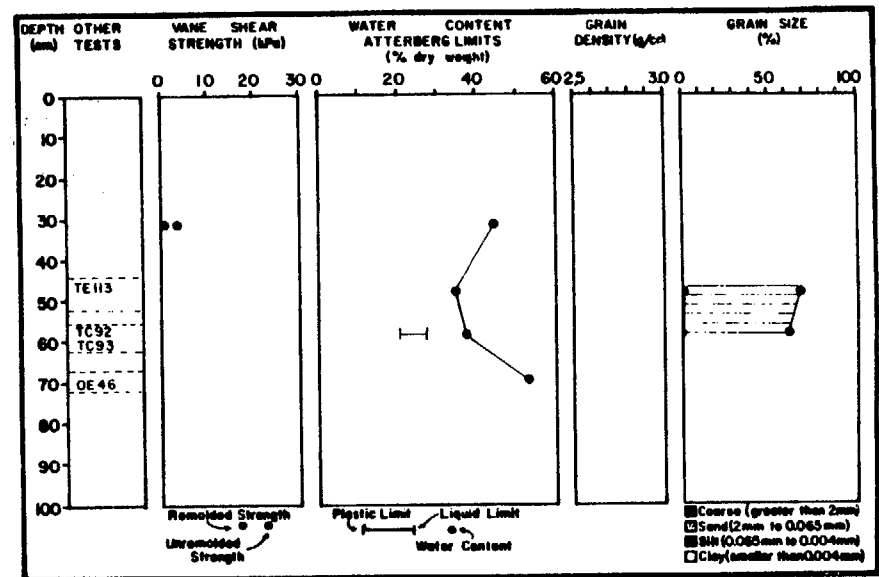
CRUISE: DCI-81-EG CORE: 60463



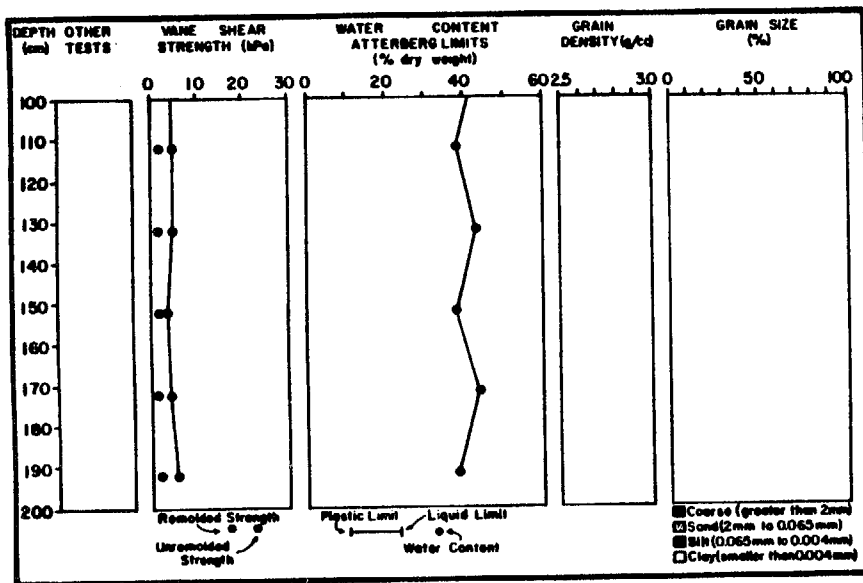
CRUISE: DCI-81-EG CORE: 60464



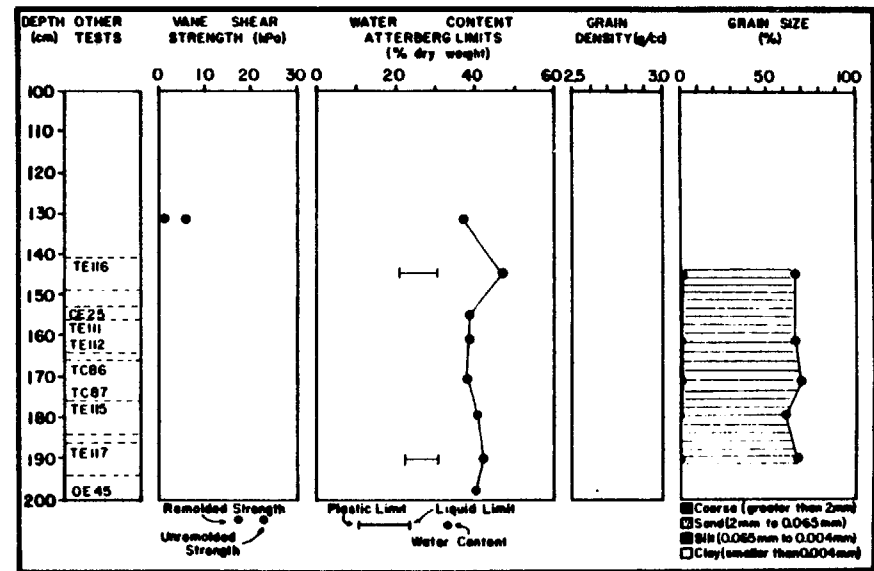
CRUISE: DCI-81-EG CORE: 605G1



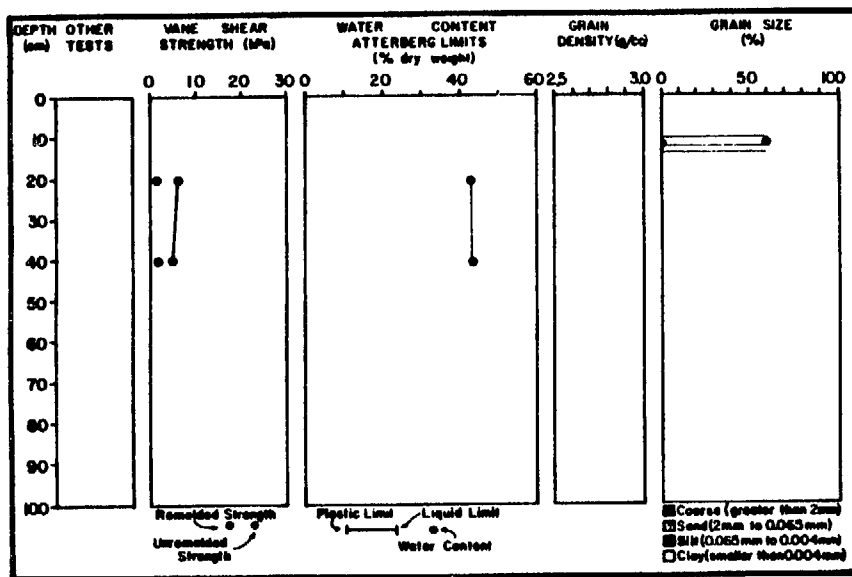
CRUISE: DCI-81-EG CORE: 605G2



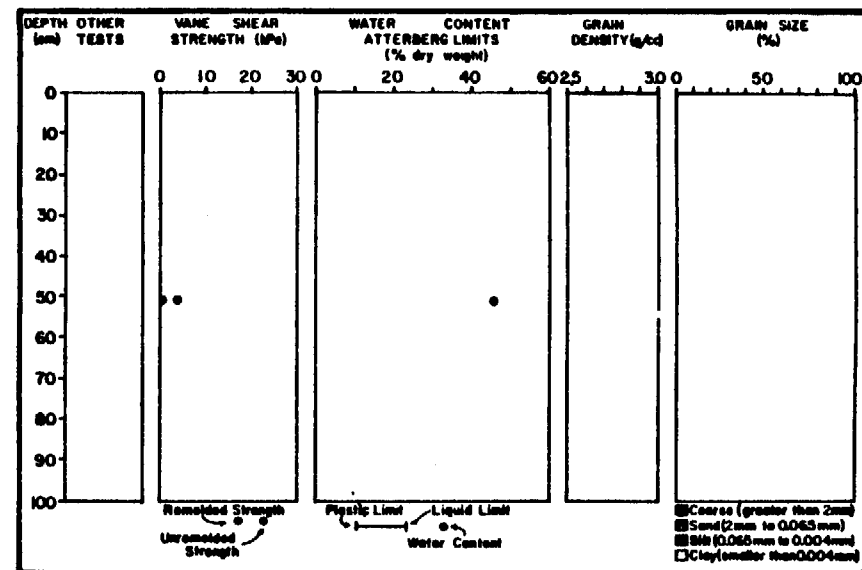
CRUISE: DCI-81-EG CORE: 605G1



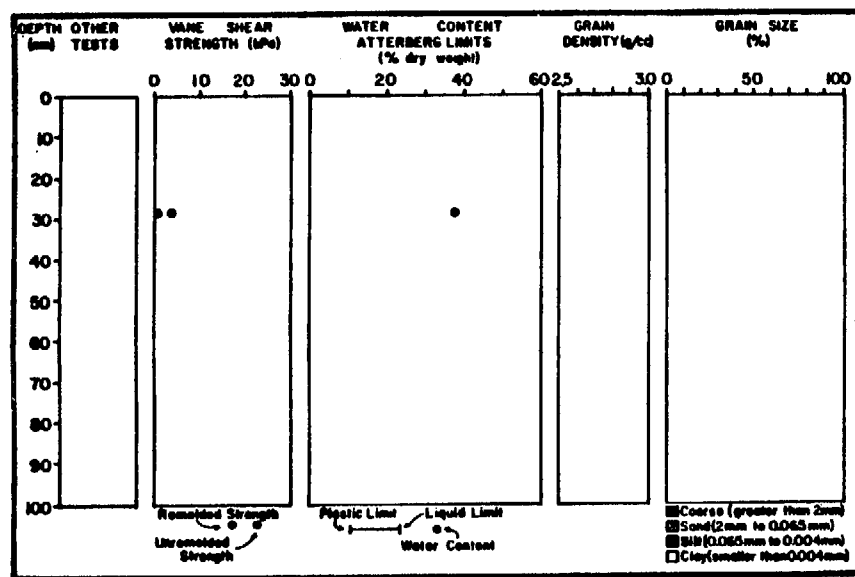
CRUISE: DCI-81-EG CORE: 605G2



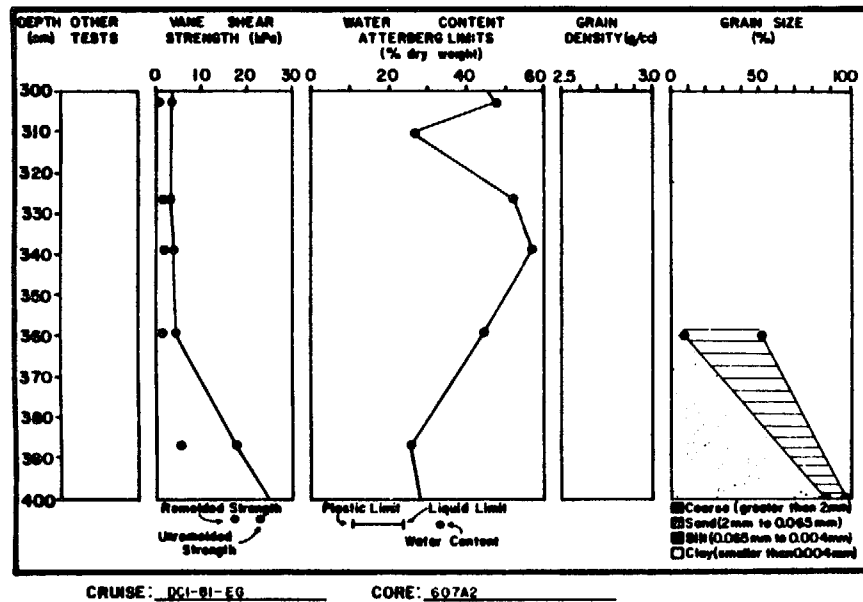
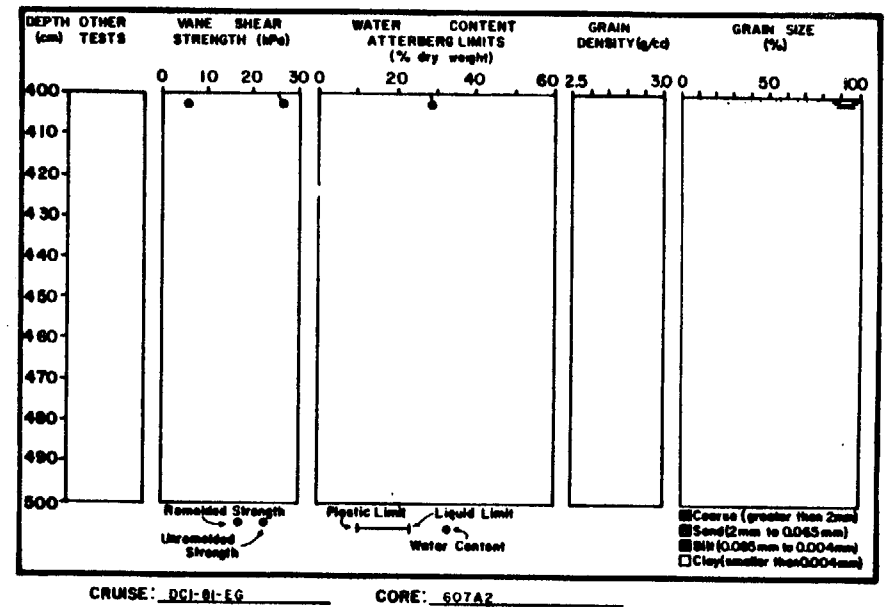
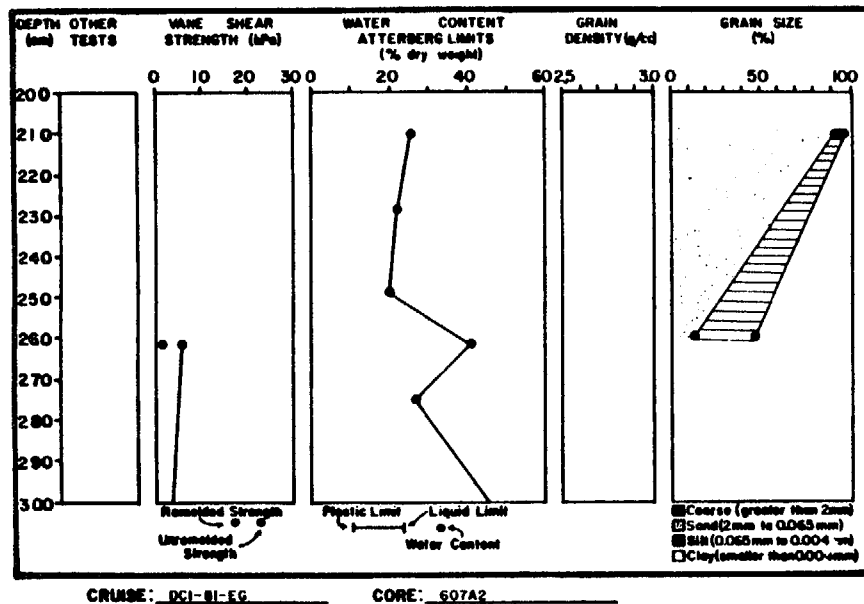
CRUISE: DCI-81-EG CORE: 60661

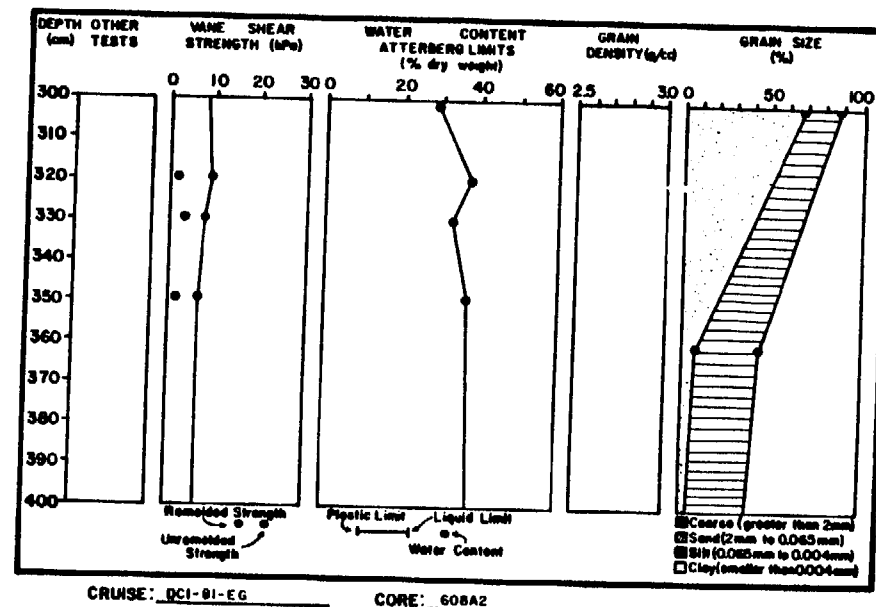
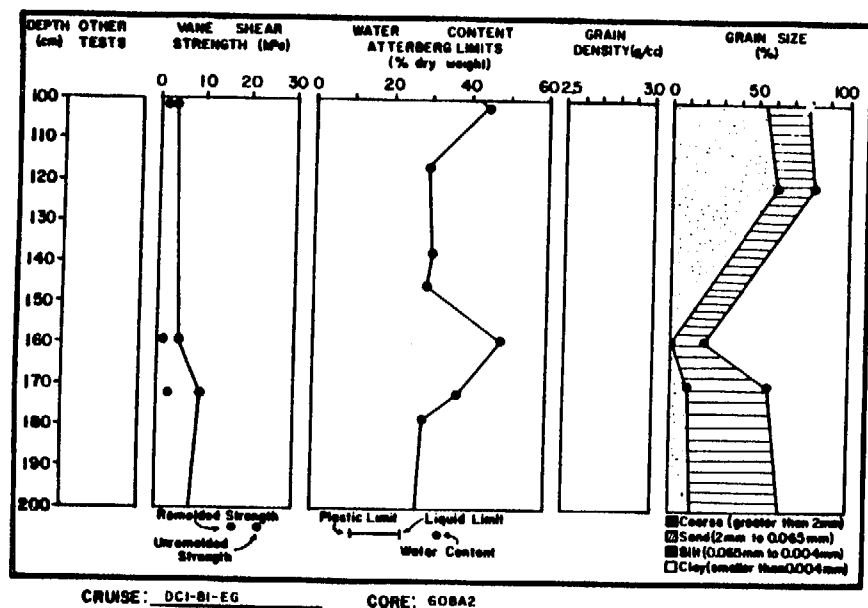
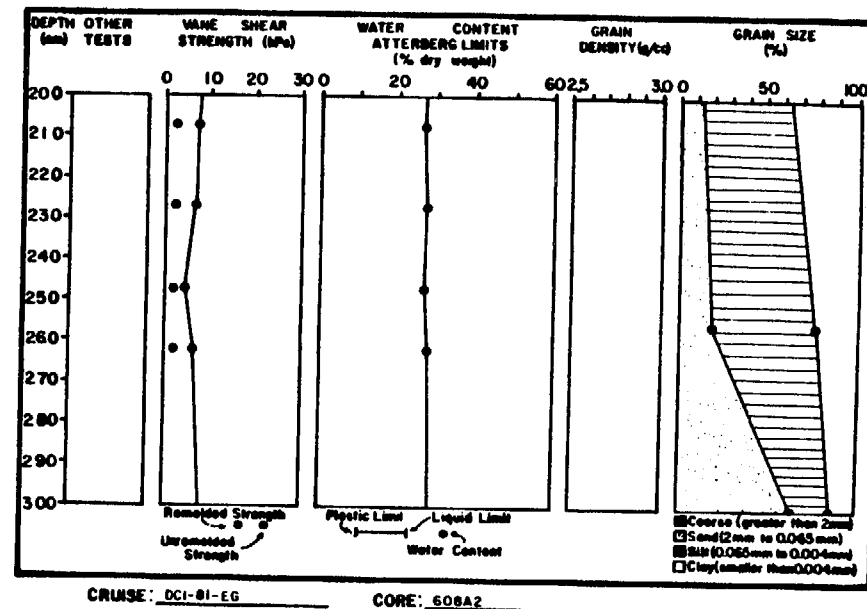
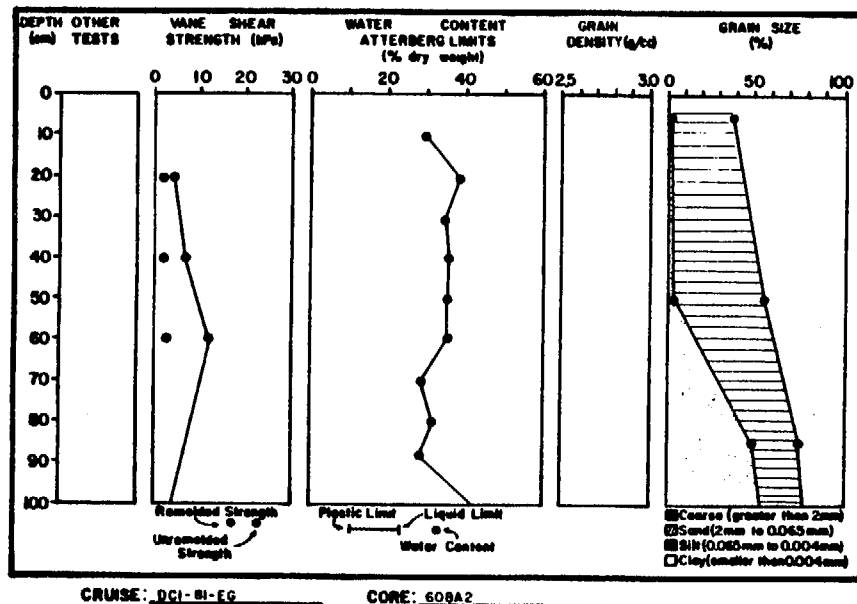


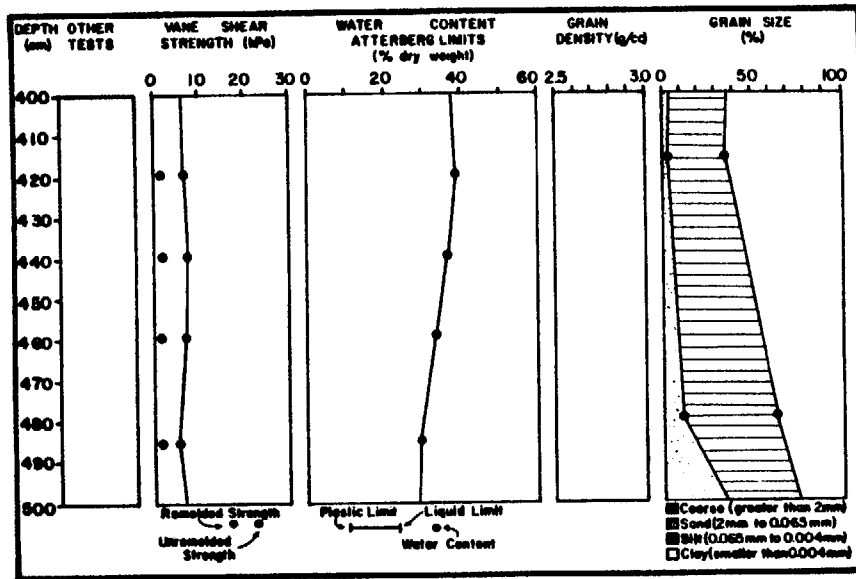
CRUISE: DCI-81-EG CORE: 607A1



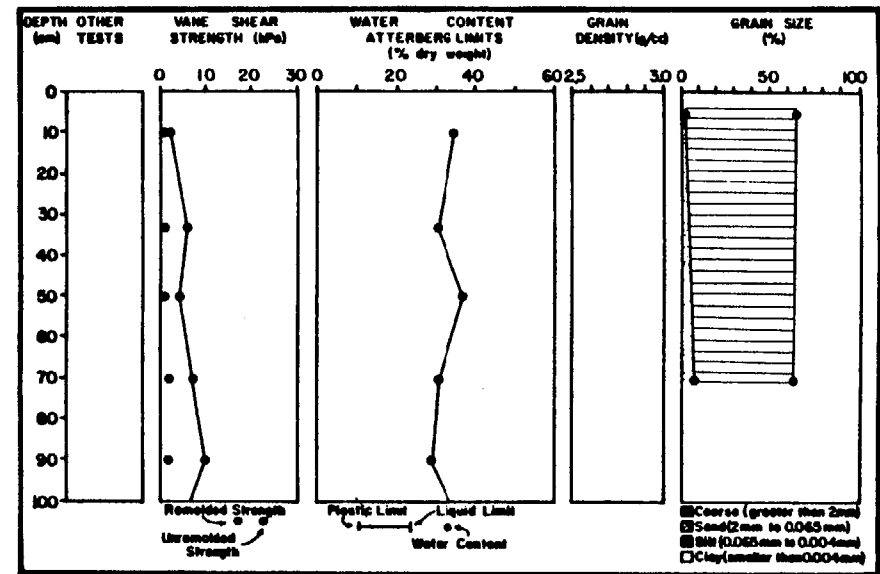
CRUISE: DCI-81-EG CORE: 60662



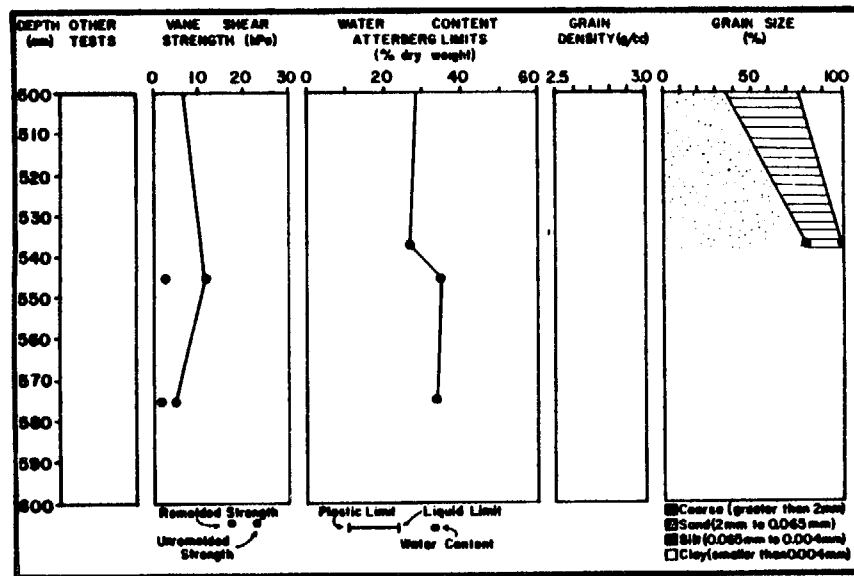




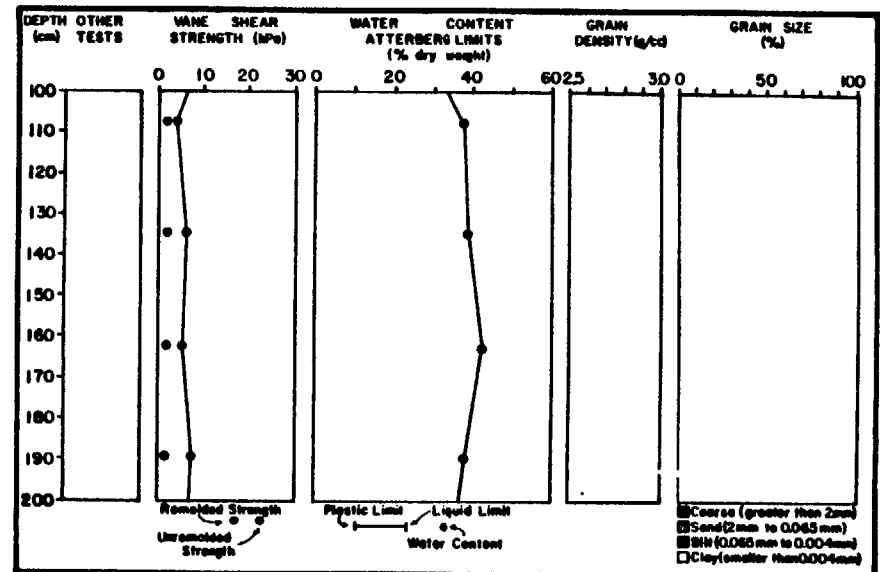
CRUISE: DCI-BI-EG CORE: 608A2



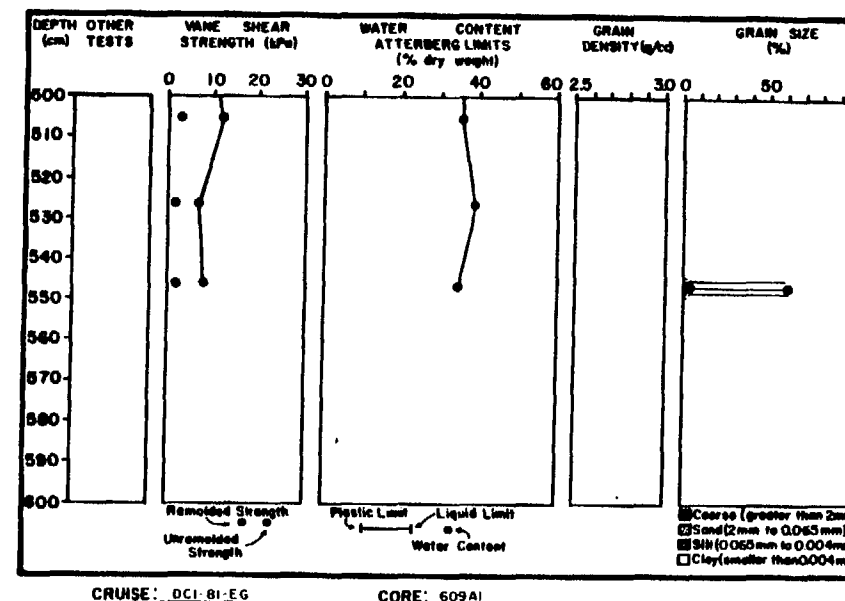
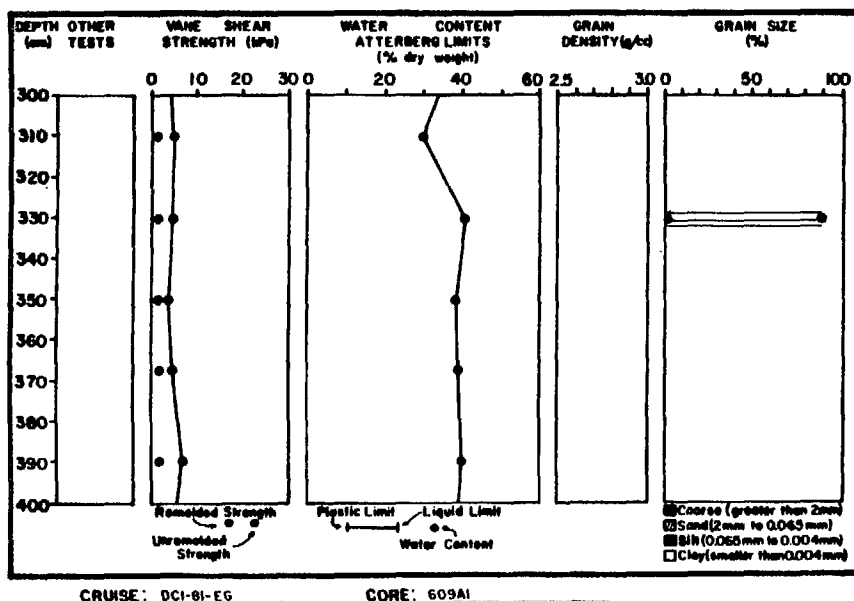
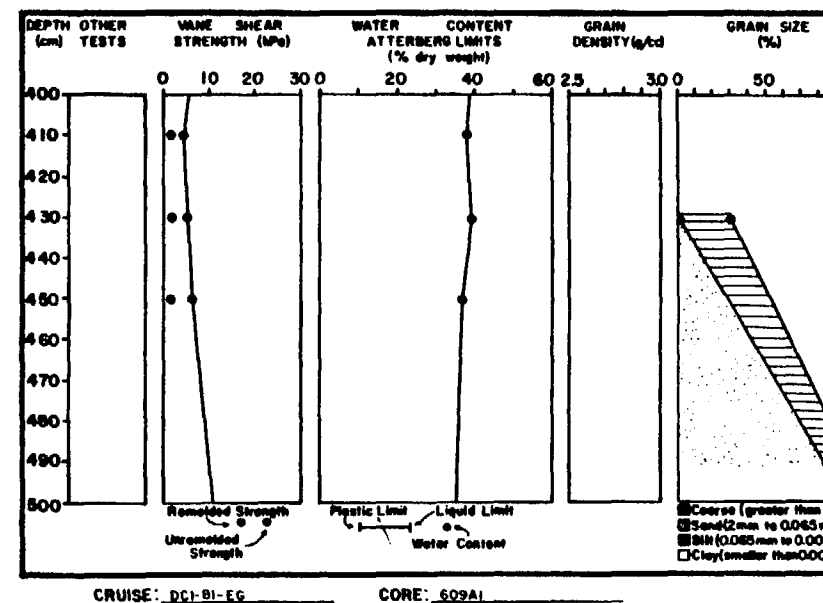
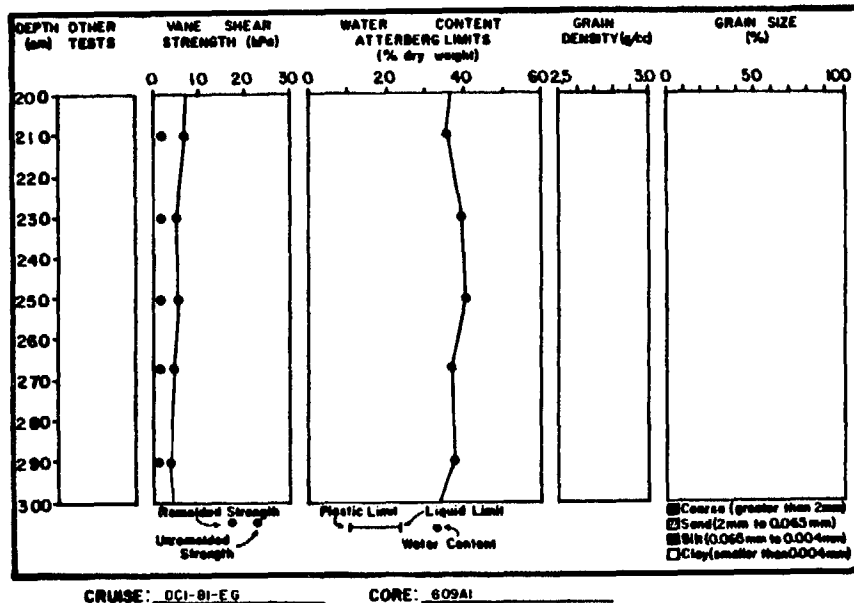
CRUISE: DCI-BI-EG CORE: 609A1

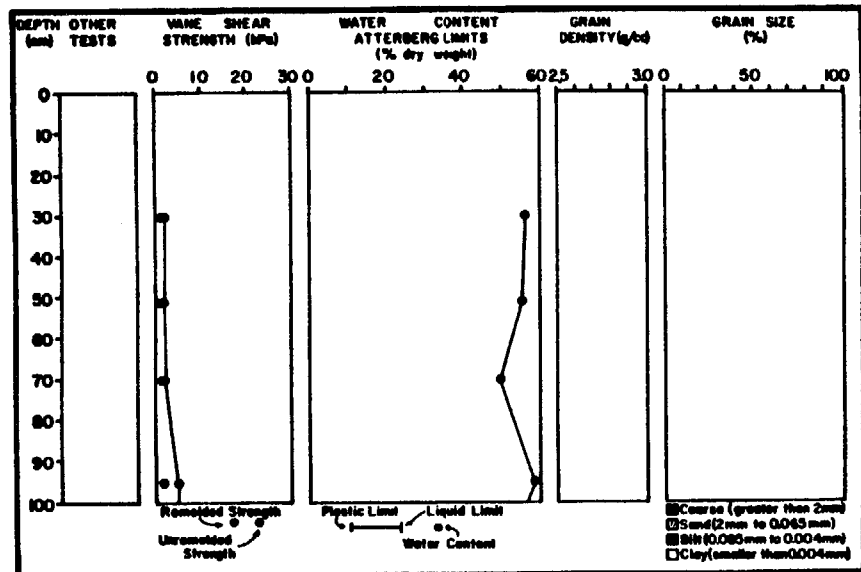


CRUISE: DCI-BI-EG CORE: 608A2



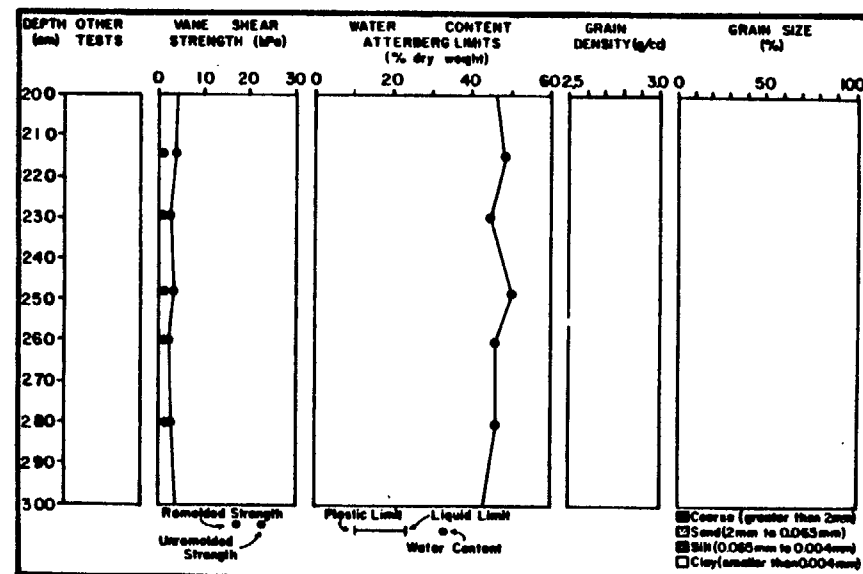
CRUISE: DCI-BI-EG CORE: 609A1





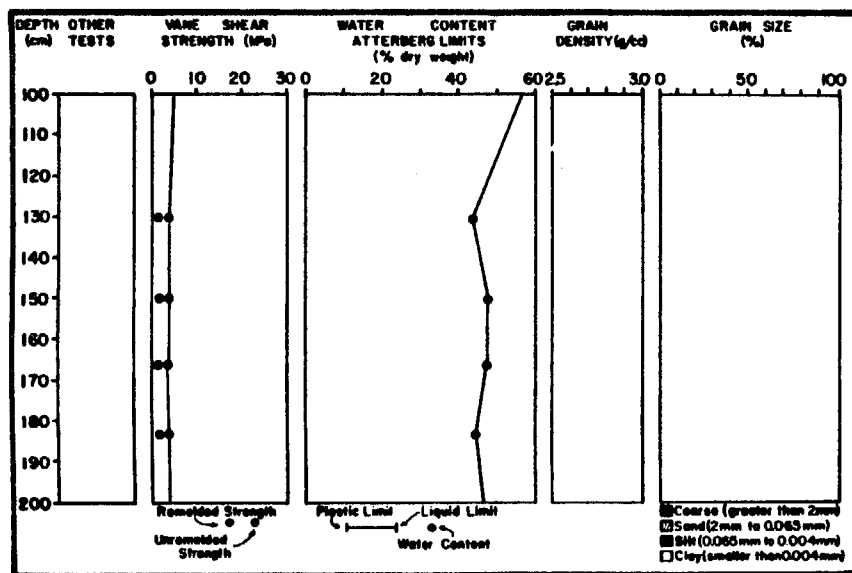
CRUISE: DCI-81-EG

CORE: 610A2



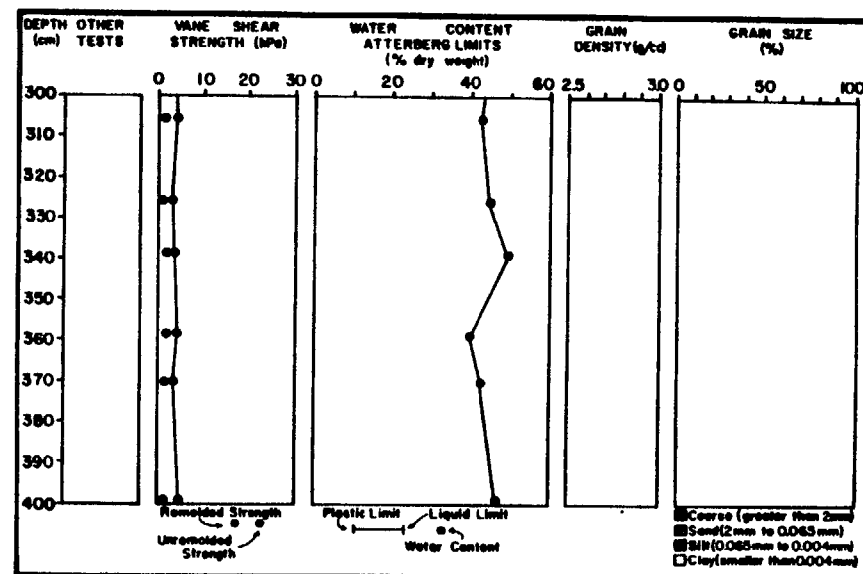
CRUISE: DCI-81-EG

CORE: 610A2



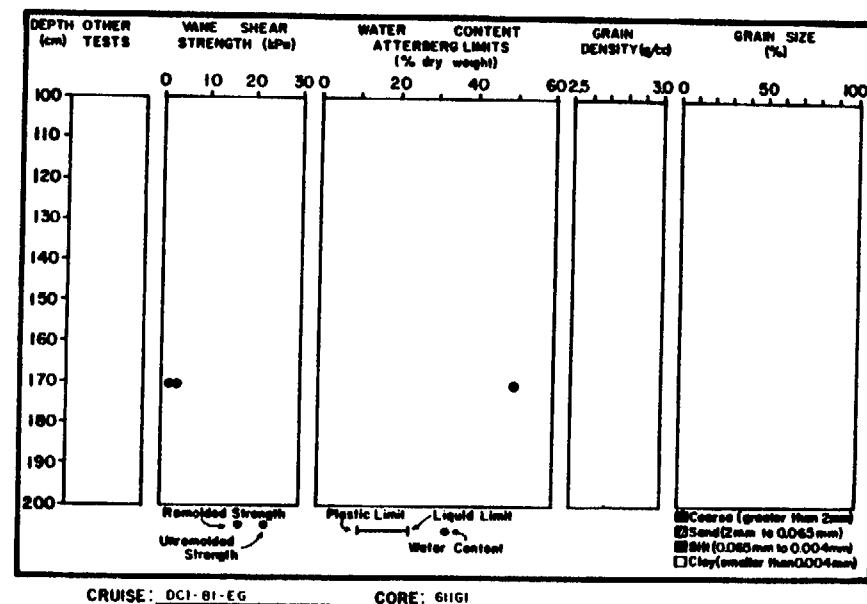
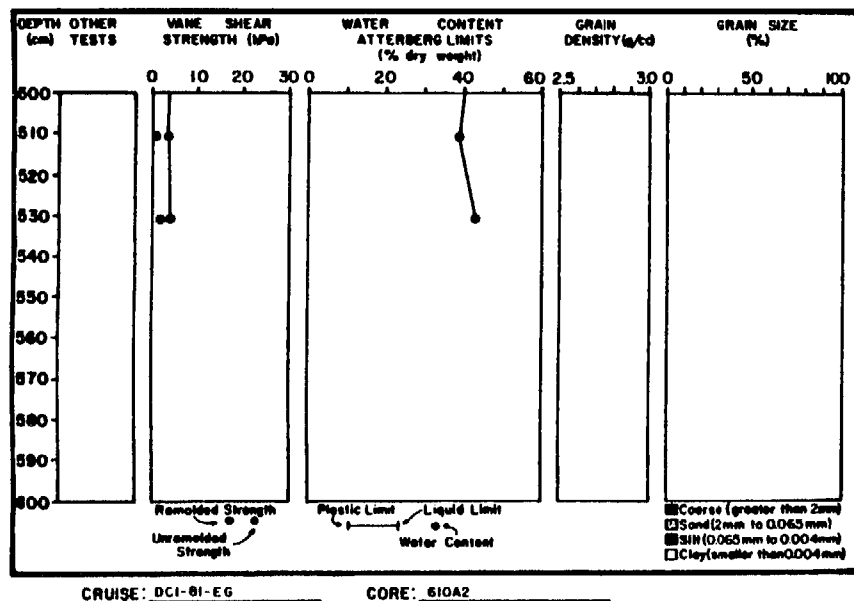
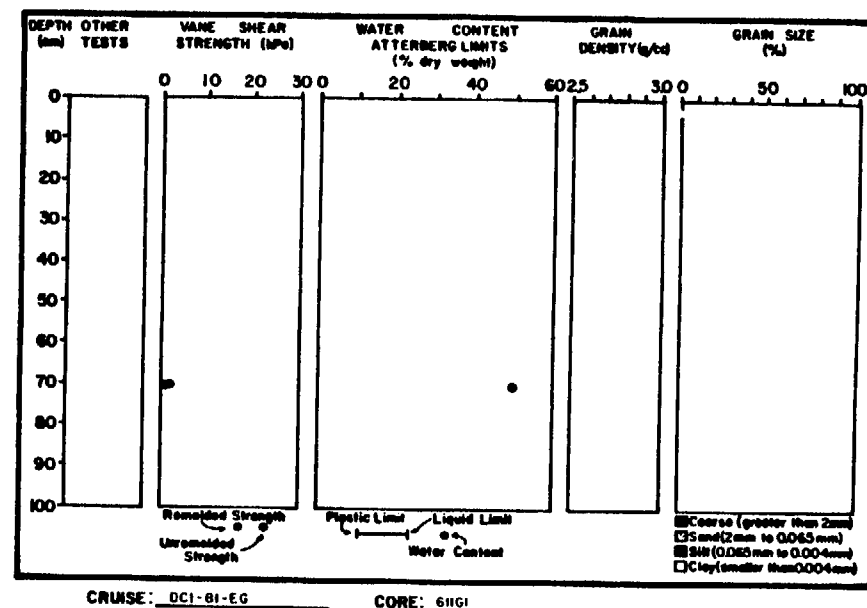
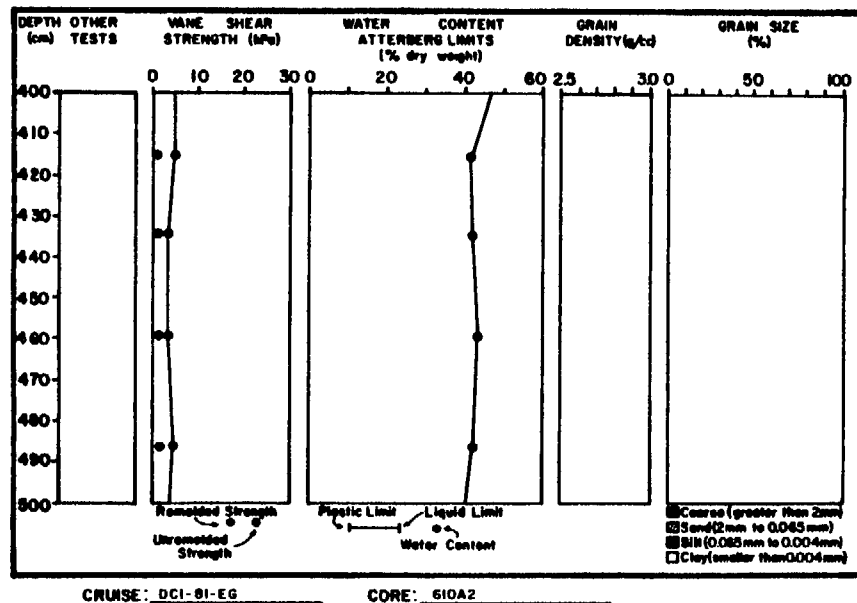
CRUISE: DCI-81-EG

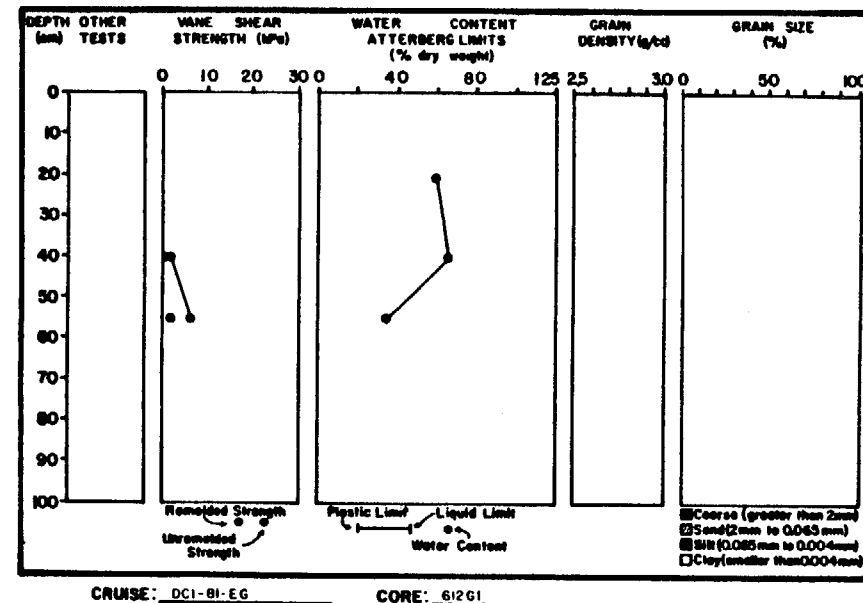
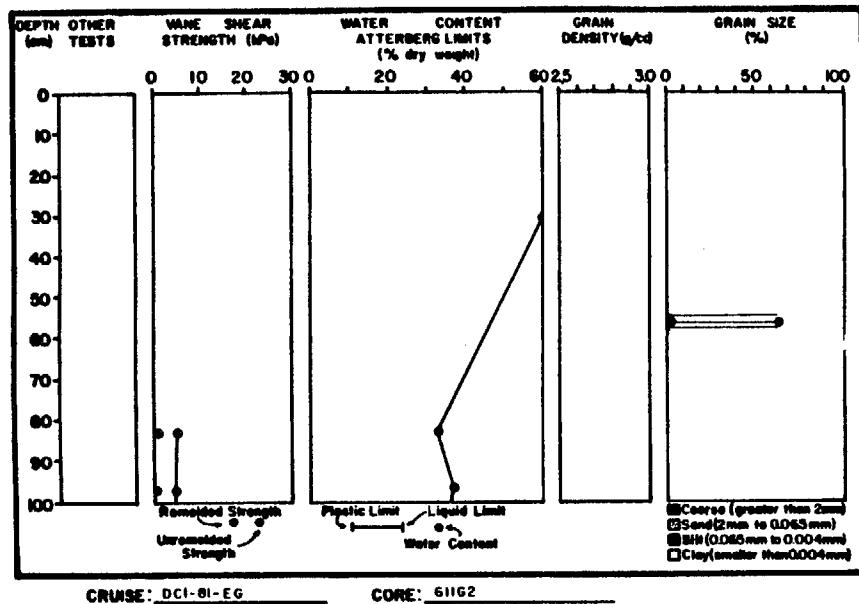
CORE: 610A2



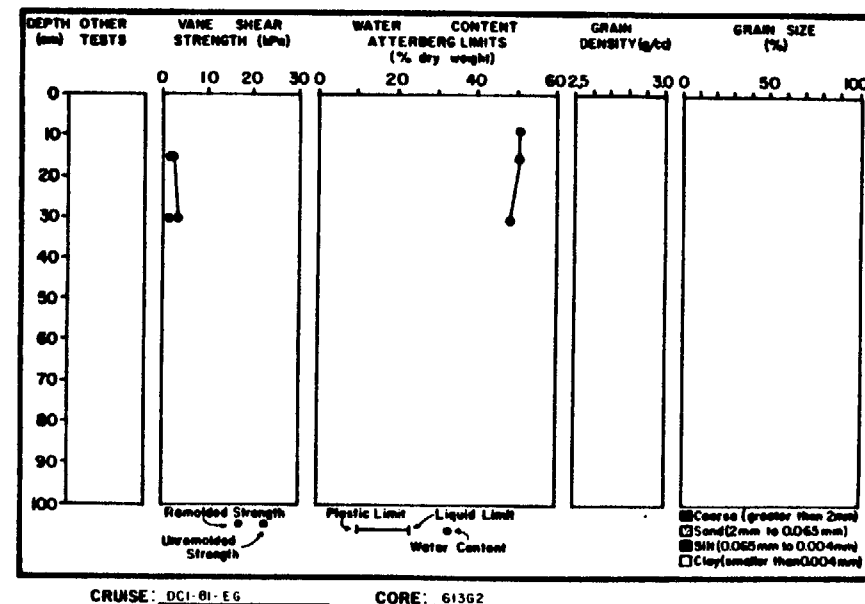
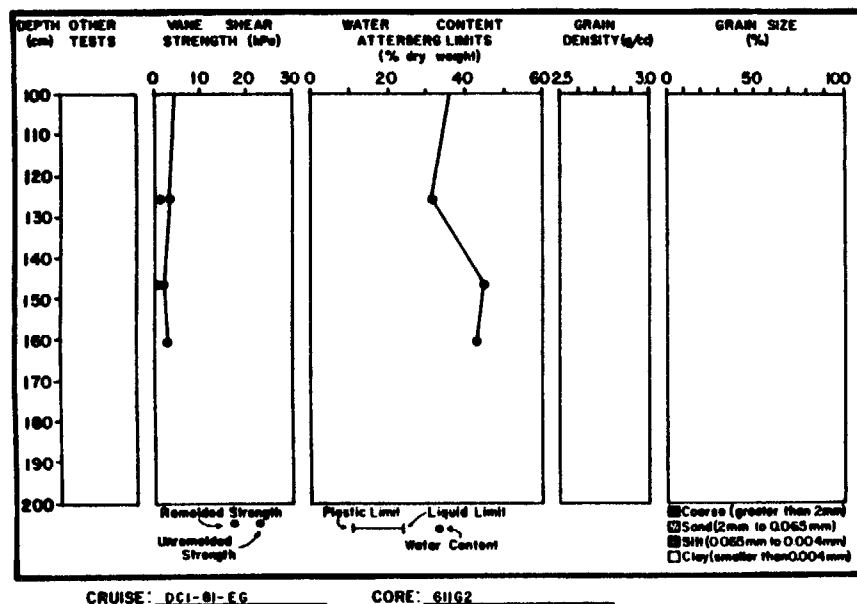
CRUISE: DCI-81-EG

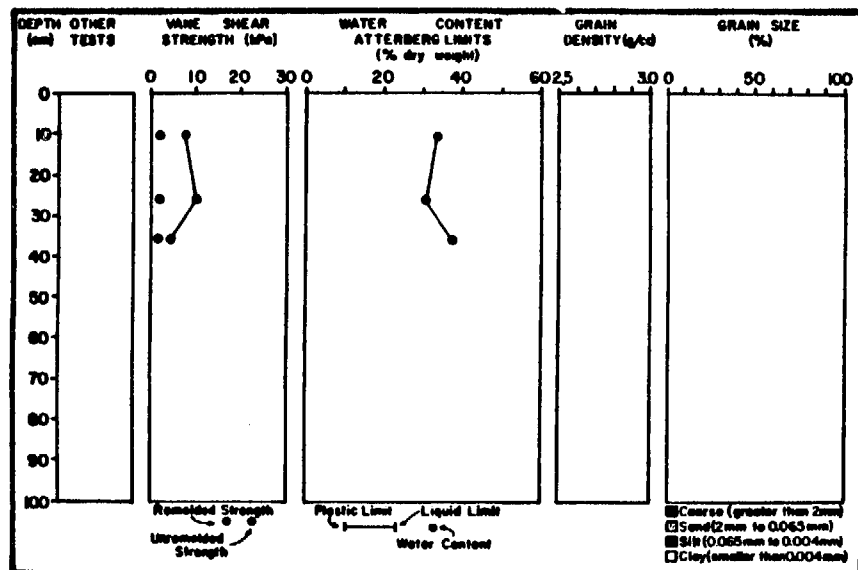
CORE: 610A2





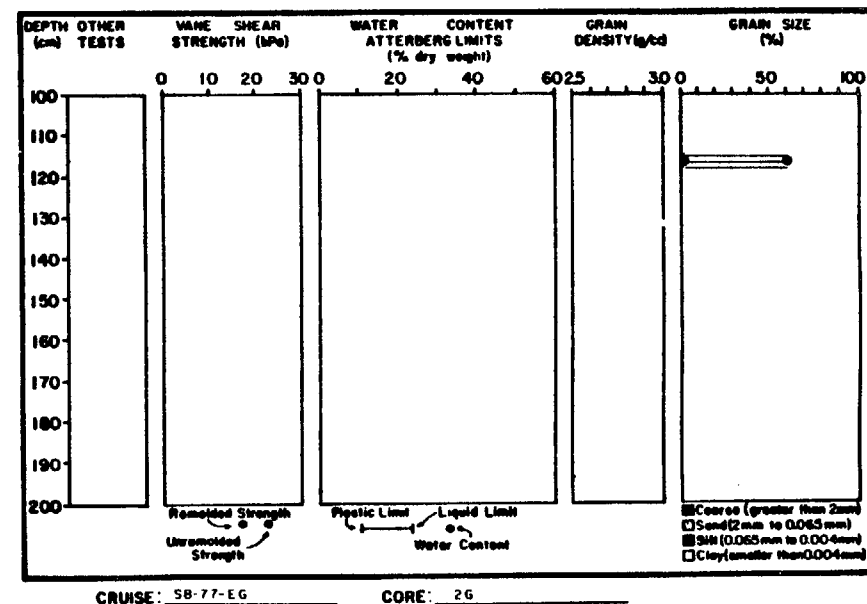
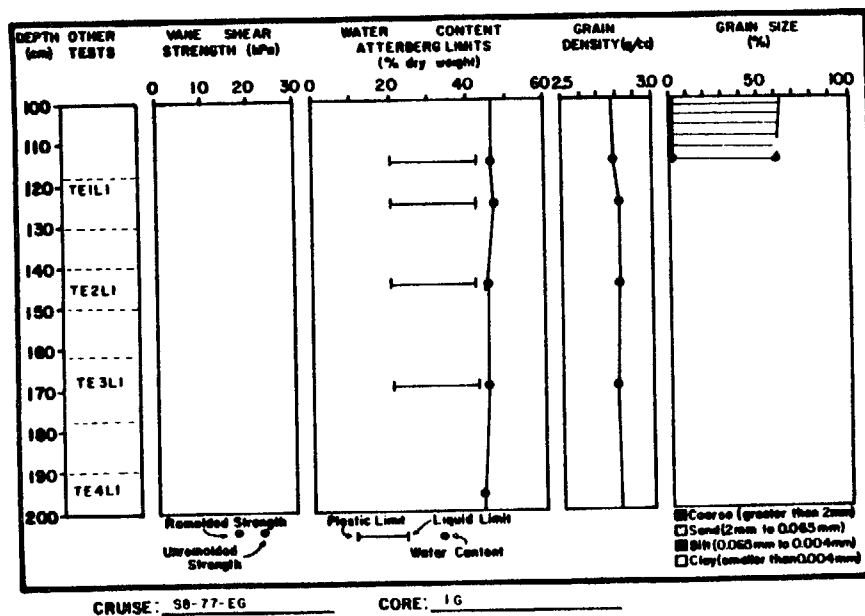
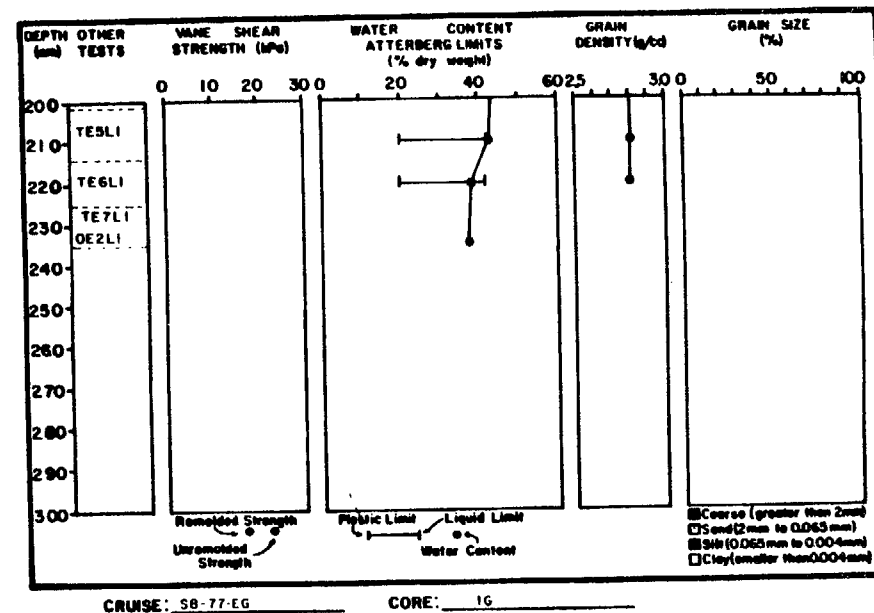
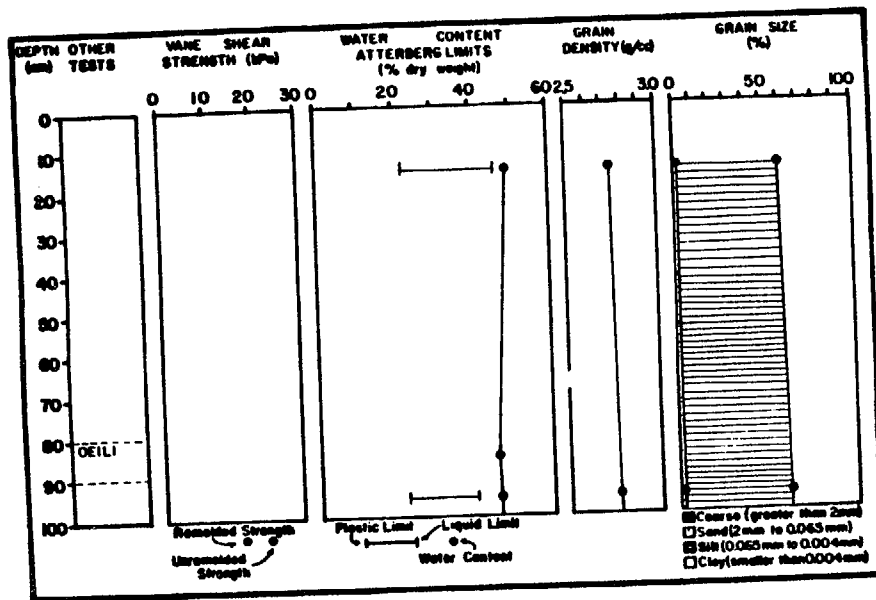
340

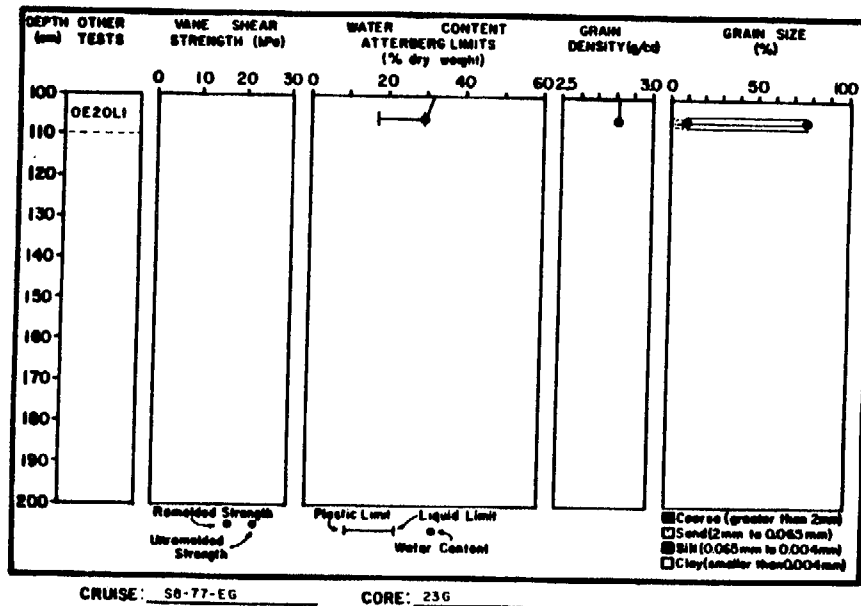
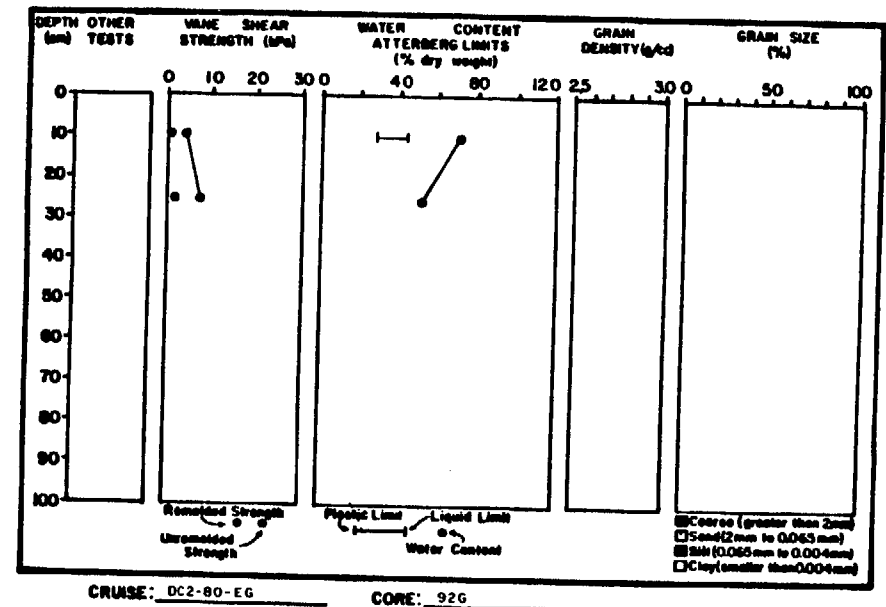
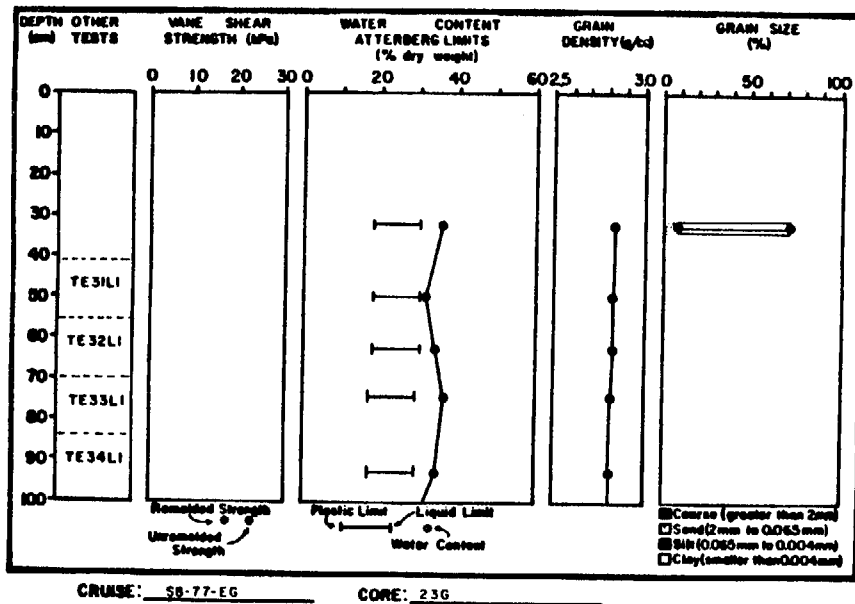


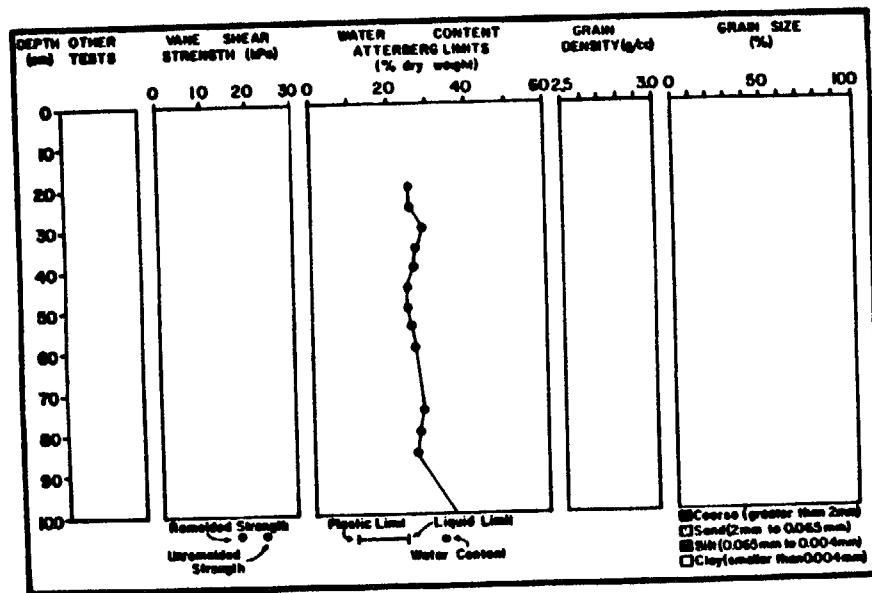


CRUISE: DCI-81-EG CORE: 614 G2

OTHER

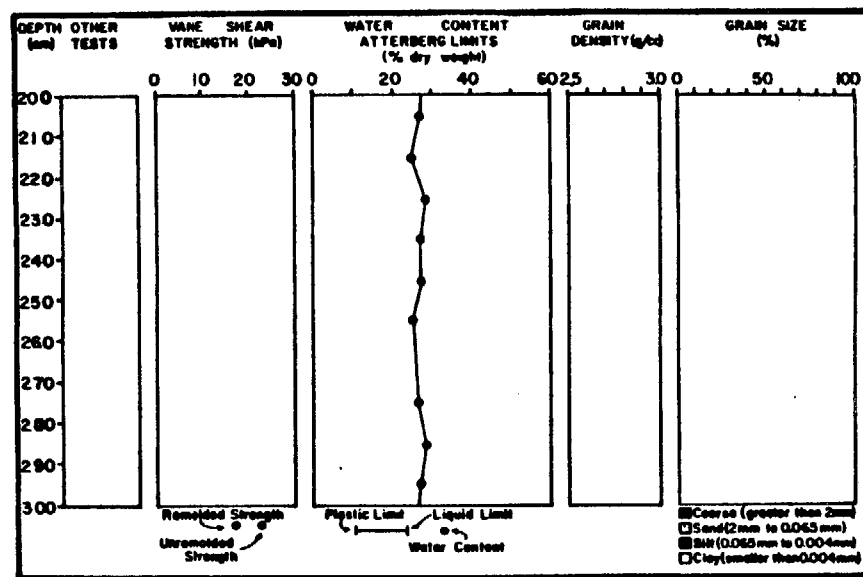






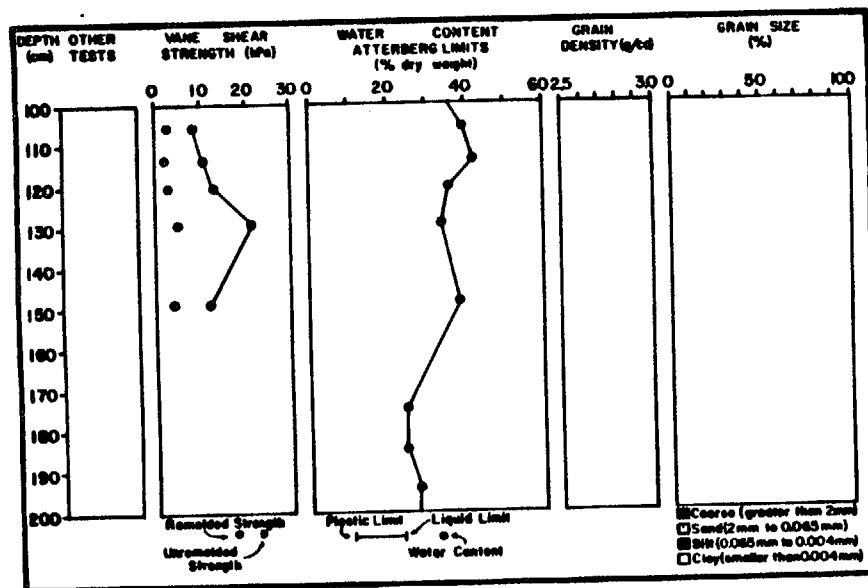
CRUISE: DCI-81-EG

CORE: 615A1



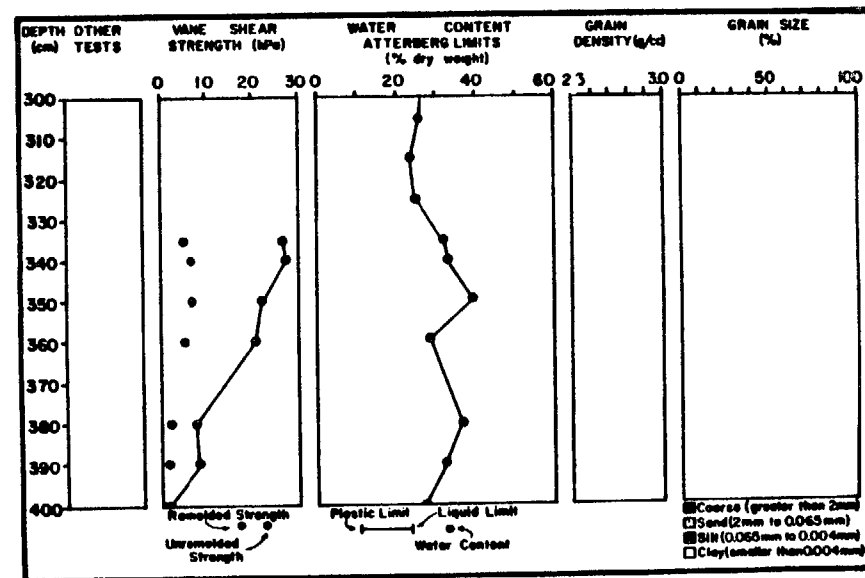
CRUISE: DCI-81-EG

CORE: 615A1



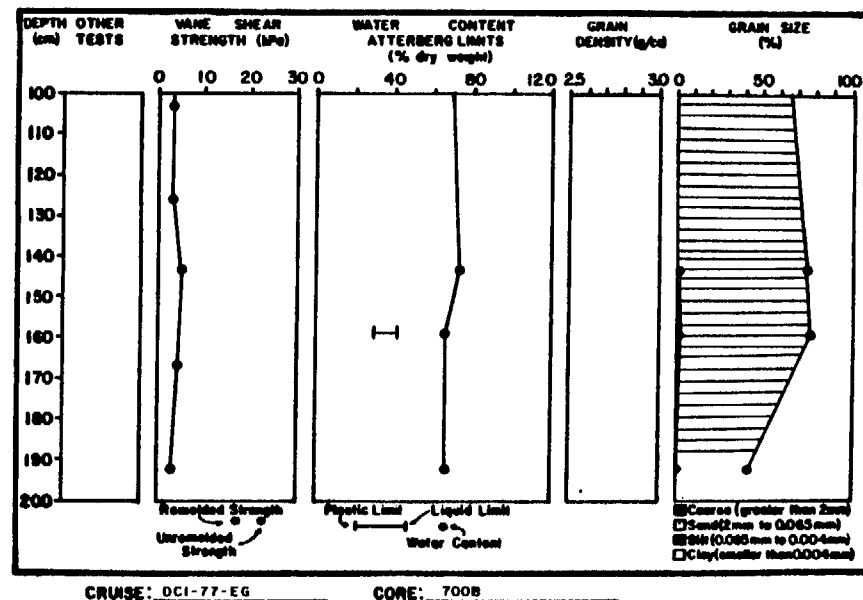
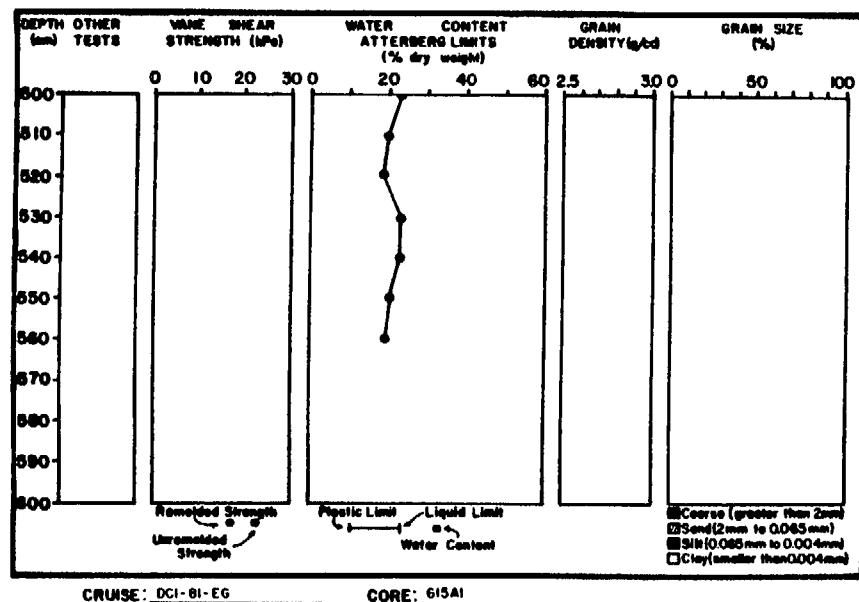
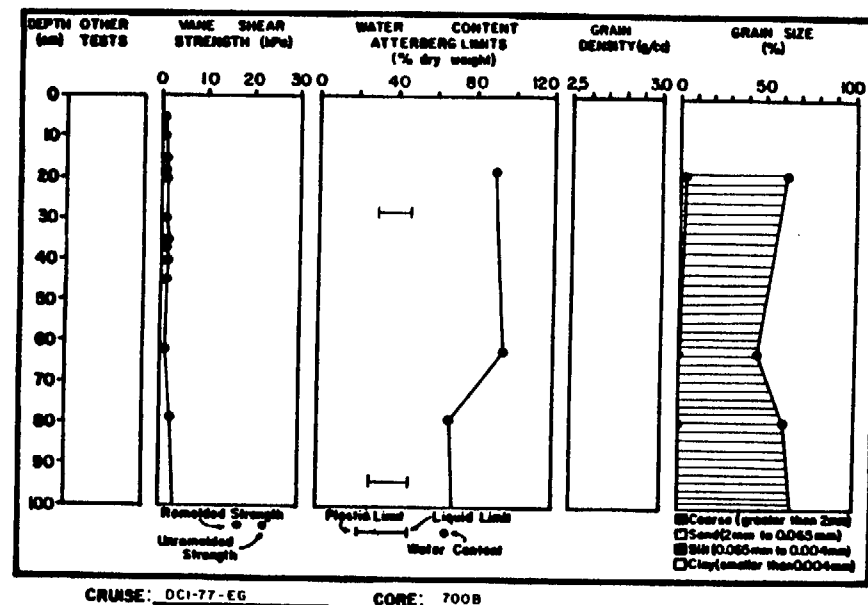
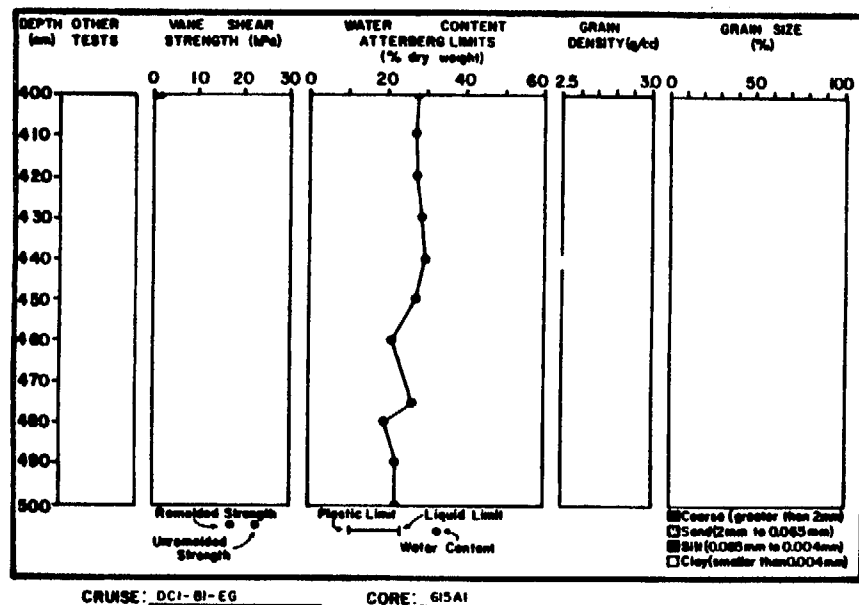
CRUISE: DCI-81-EG

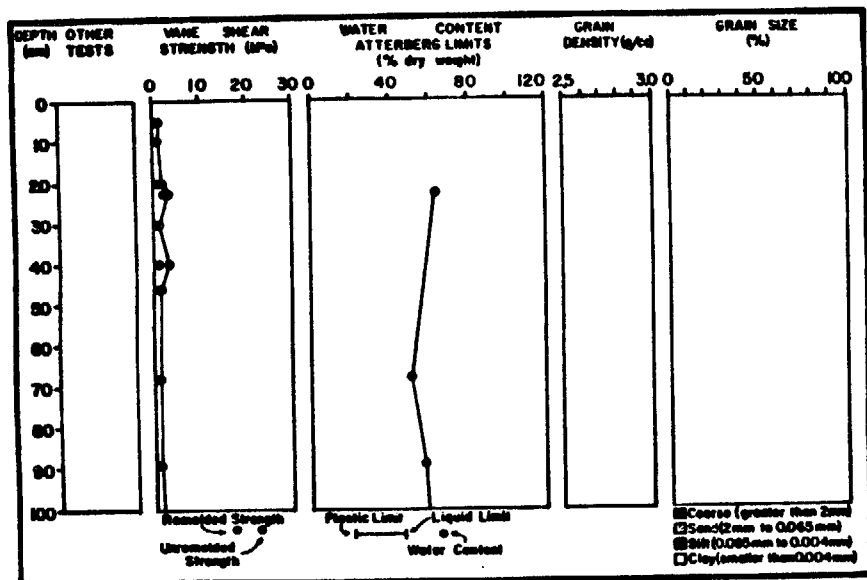
CORE: 615A1



CRUISE: DCI-77-EG

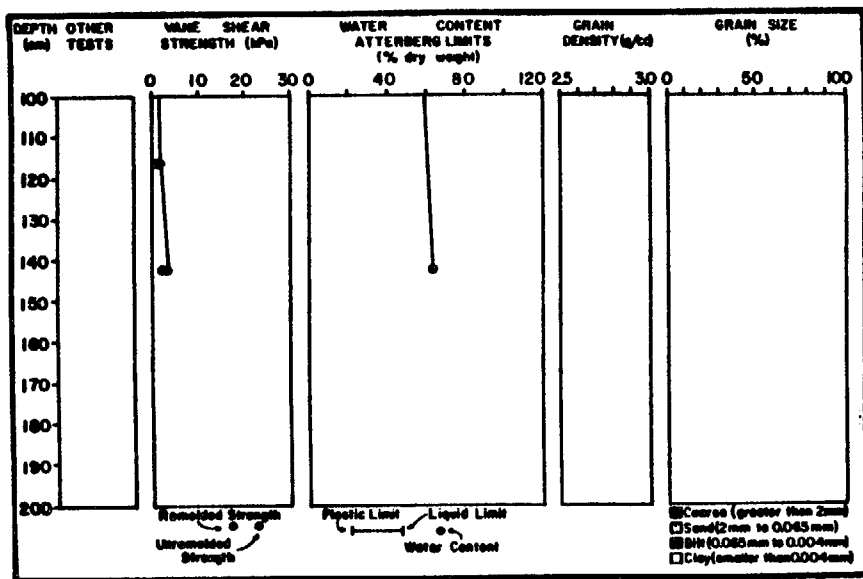
CORE: 615A1





CRUISE: DCI-77-EG

CORE: 704B



CRUISE: DCI-77-EG

CORE: 704B

APPENDIX D

CONSOLIDATION AND TRIAXIAL TEST RESULTS--

LAW ENGINEERING AND TESTING COMPANY (1977 cores)

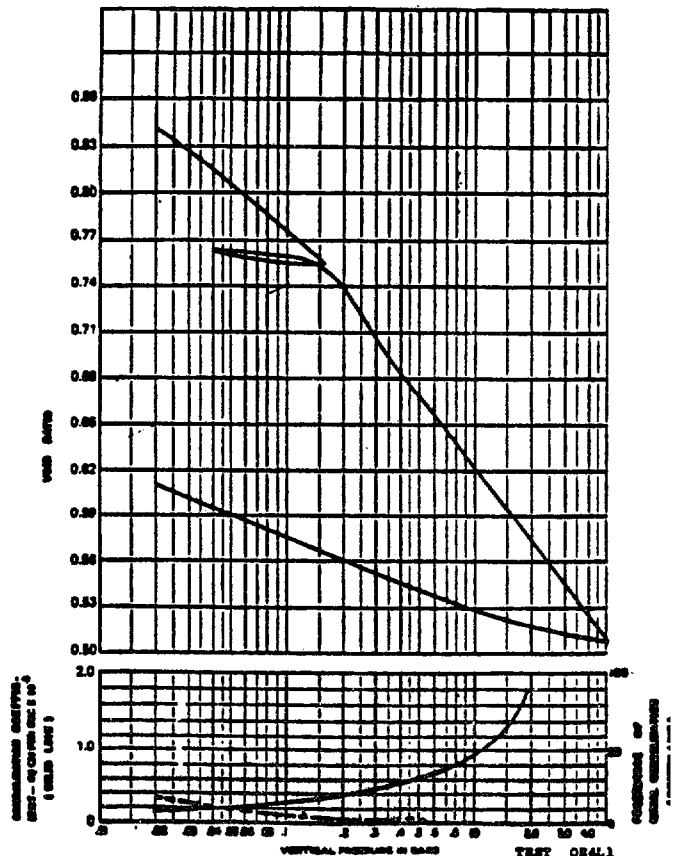
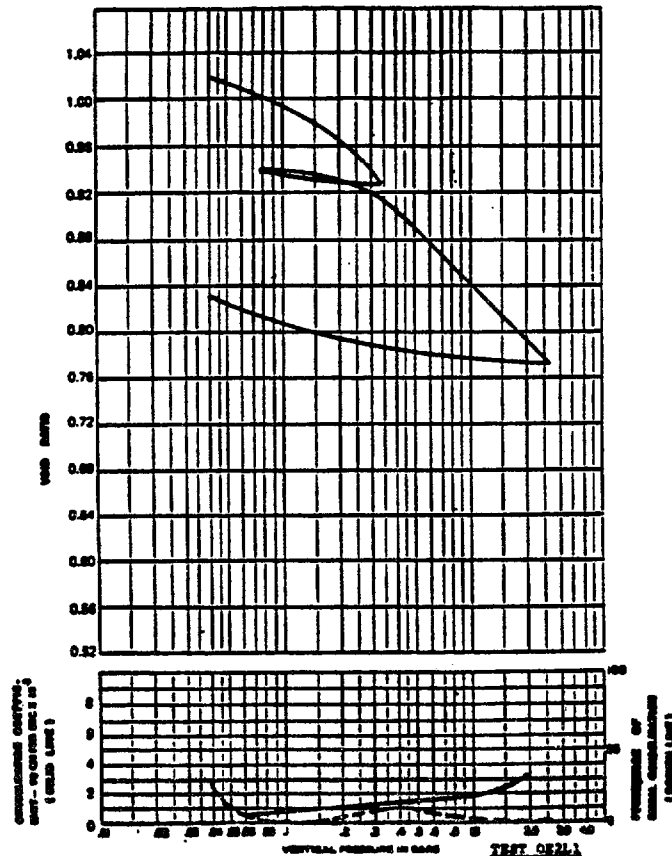
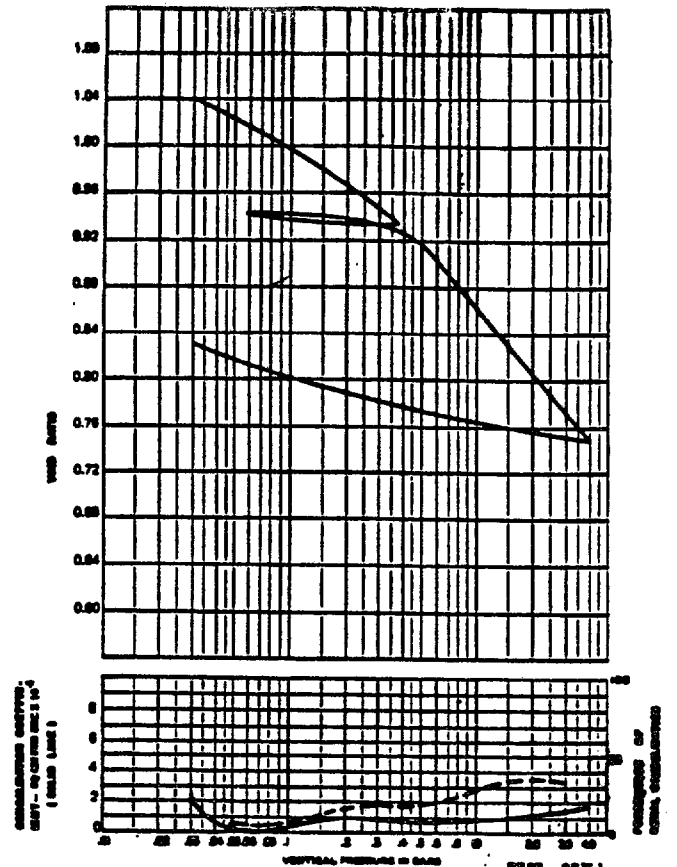
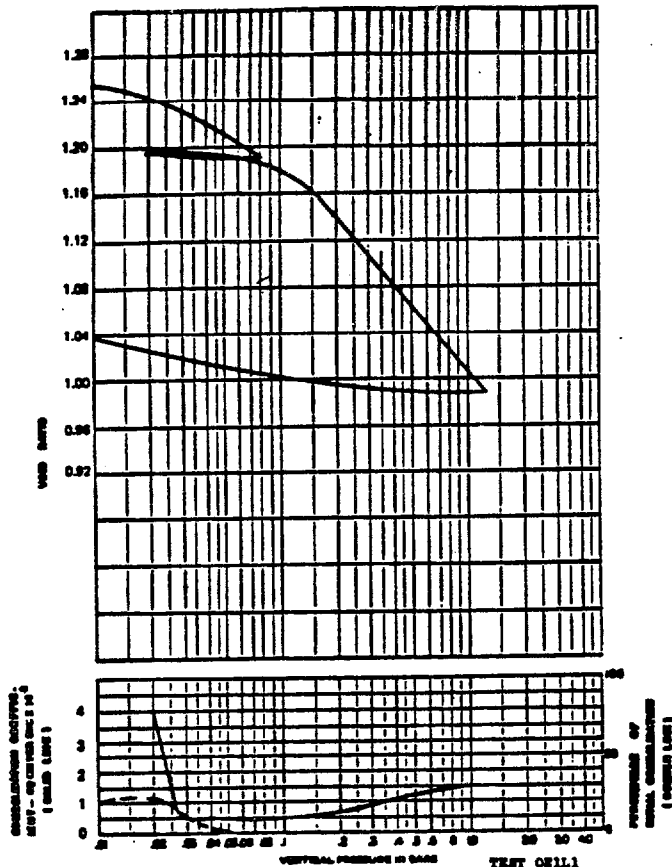
APPENDIX D. CONSOLIDATION AND TRIAXIAL TEST RESULTS-LAW ENGINEERING AND TESTING COMPANY (1977 cores)

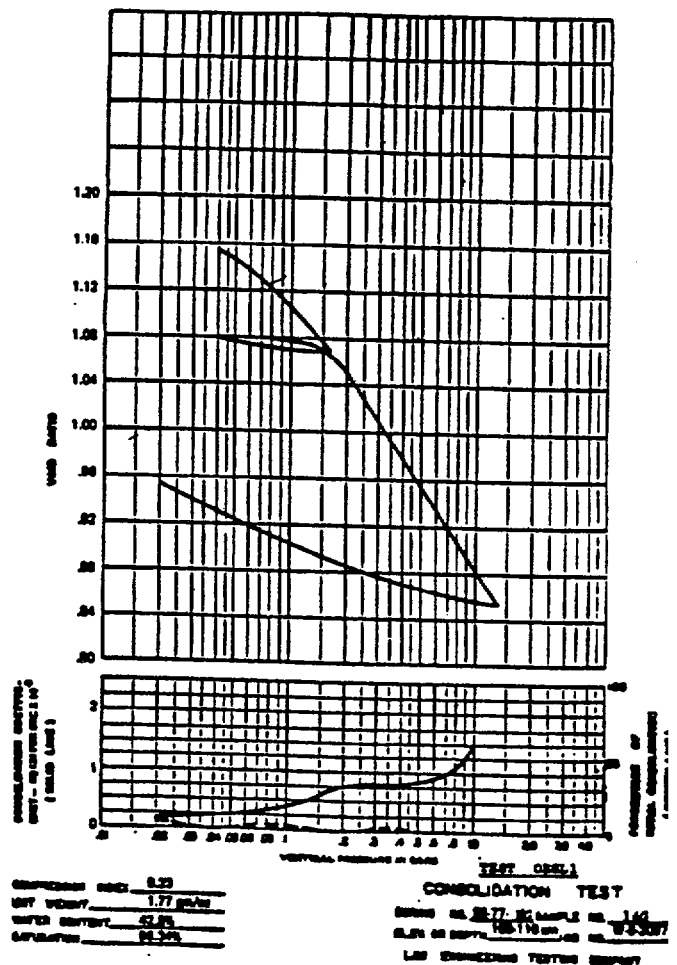
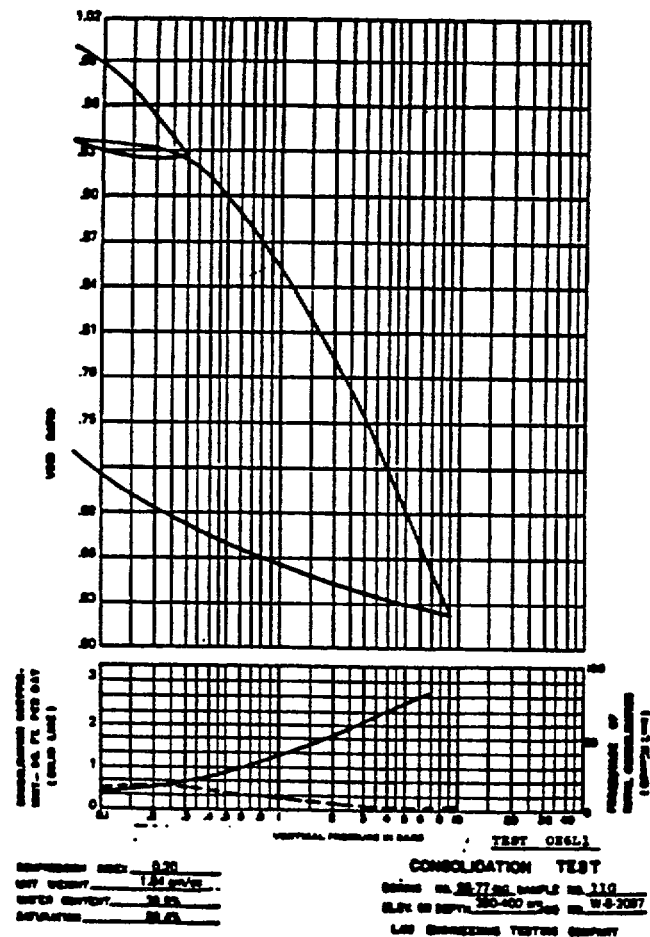
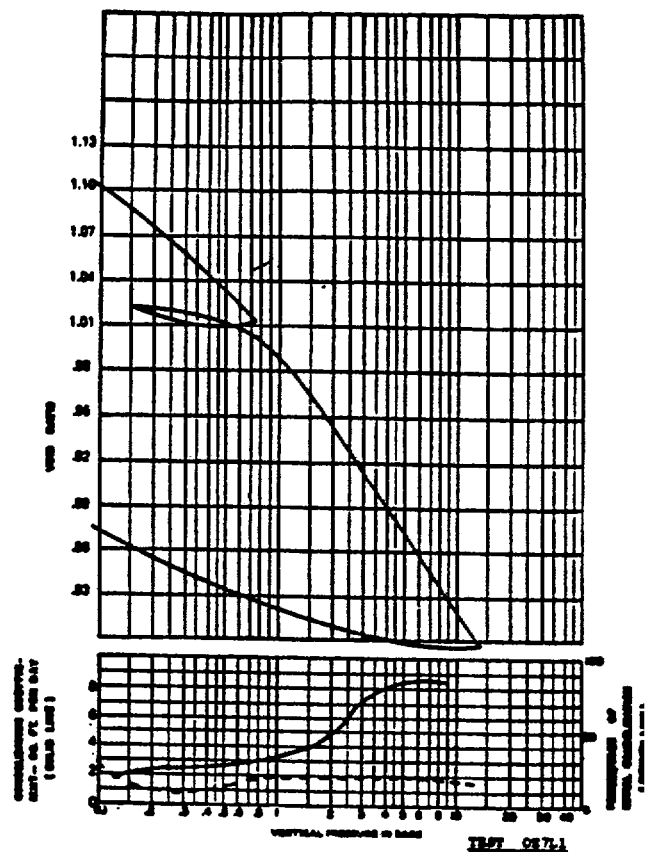
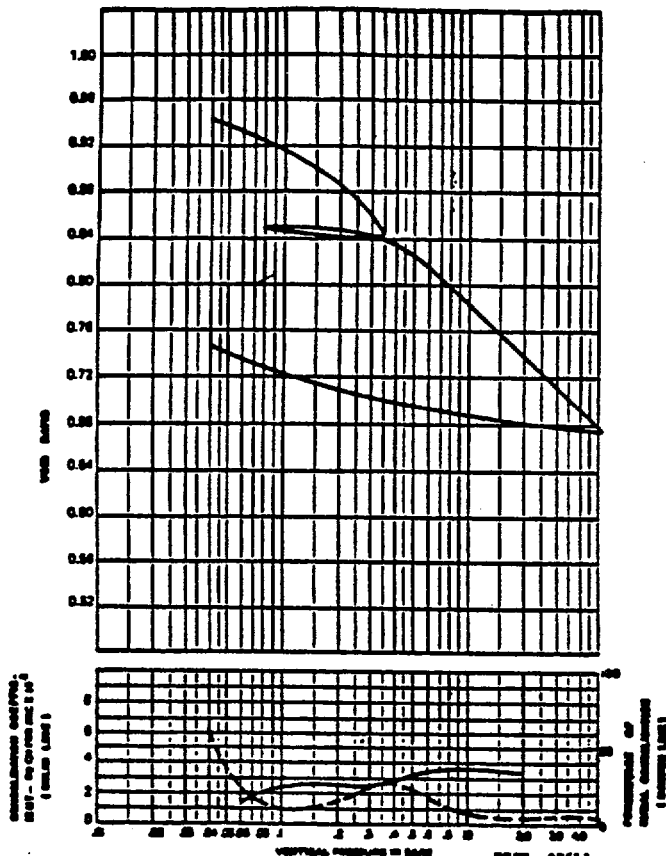
This appendix presents the results of consolidation and static triaxial testing performed by Law Engineering and Testing Company under Contract number 14-08-0001-17356 with the U.S. Geological Survey. Testing was performed under the direction of R.W. Sparrow, P.G. Swanson and R.E. Brown. Core samples were from Cruise S8-77-EG.

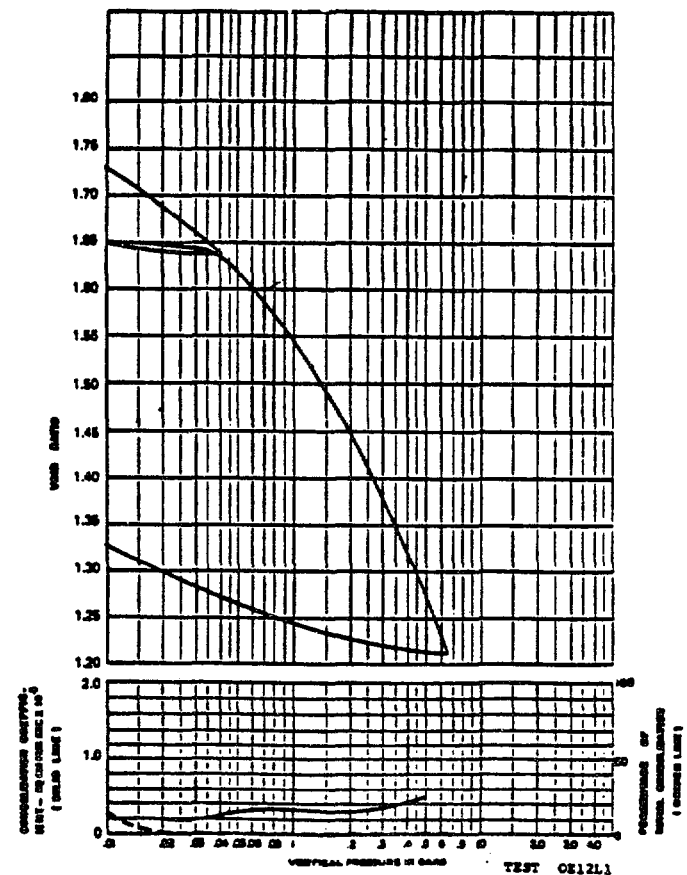
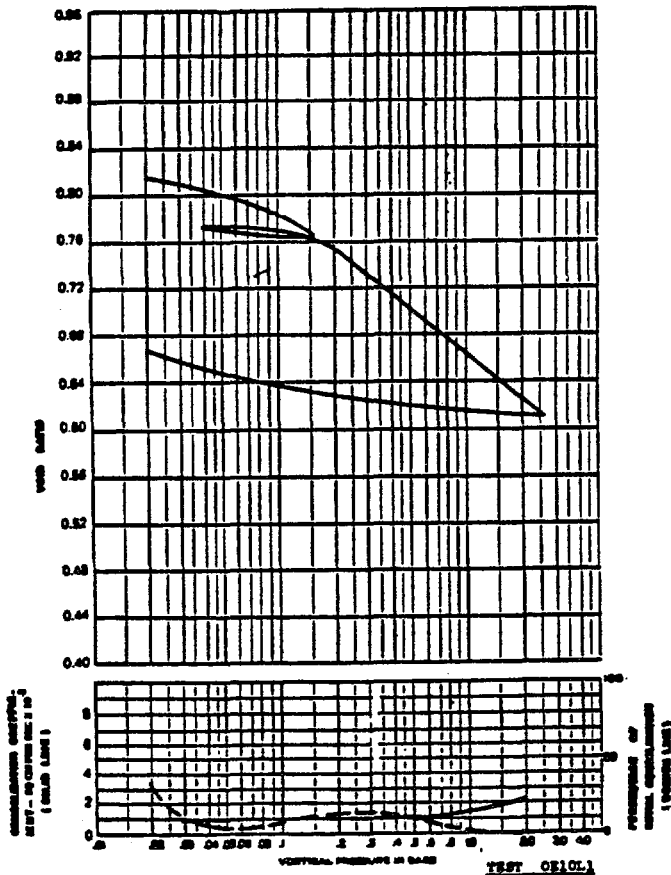
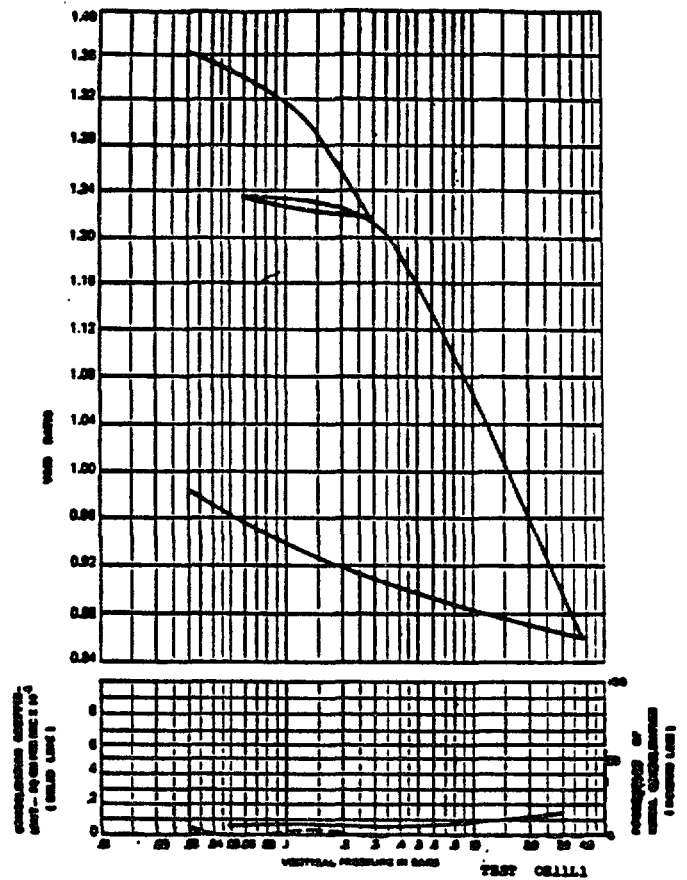
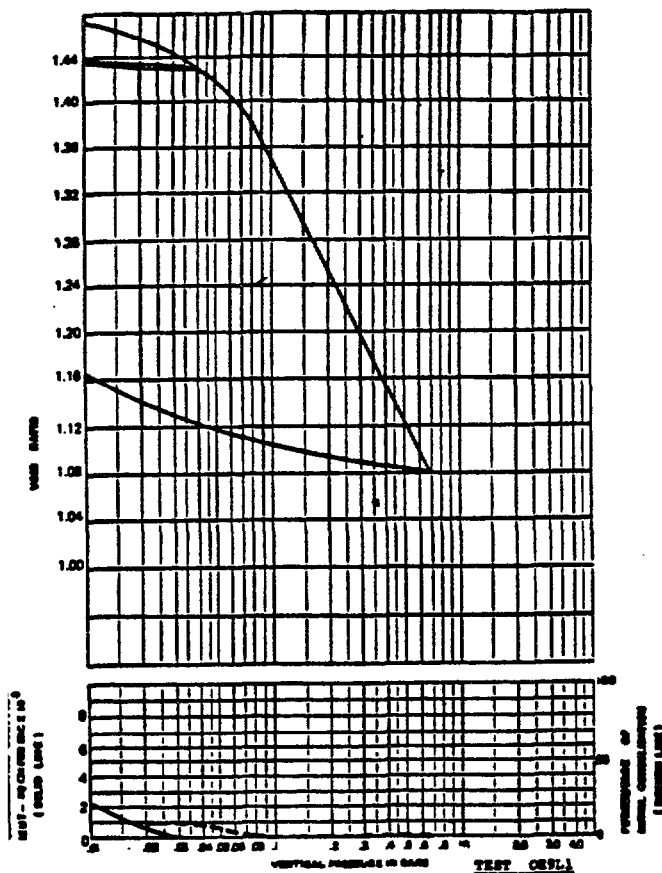
All tests in this group have been assigned a test number with LL as the last two characters. The consolidation tests (first two characters are OE) are presented first and are ordered by test number. Results from a single test are presented on a page in the form of void ratio and calculated coefficient of consolidation (c_v) versus the vertical effective stress given in bars (1 bar=101.3 kPa).

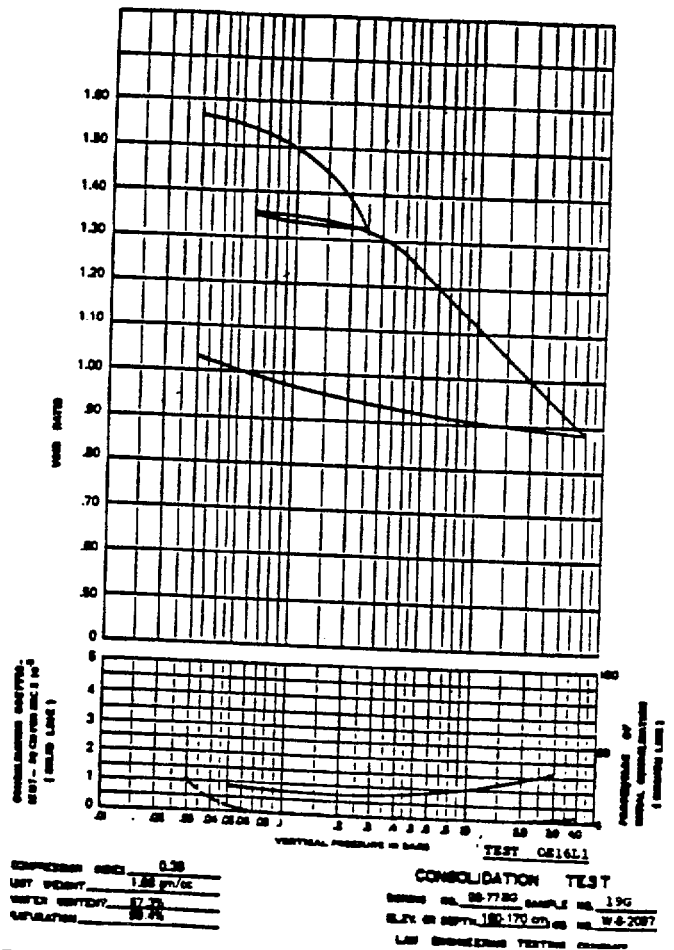
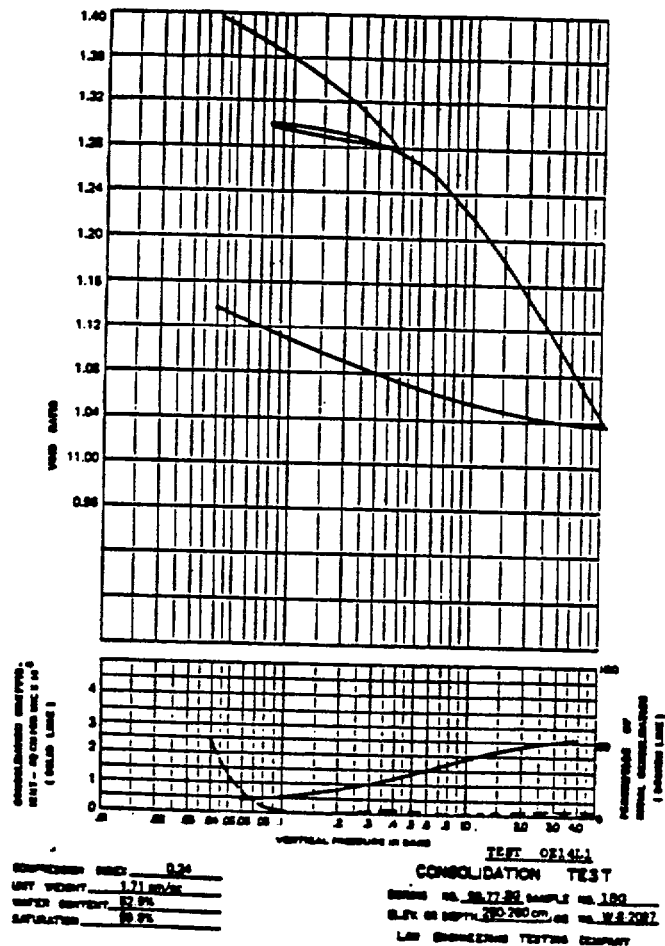
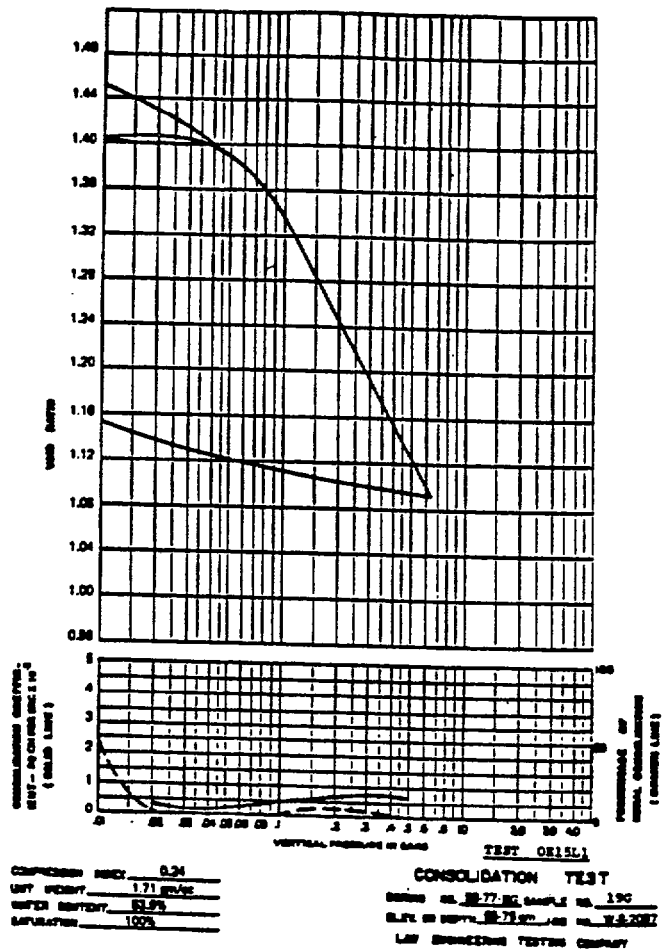
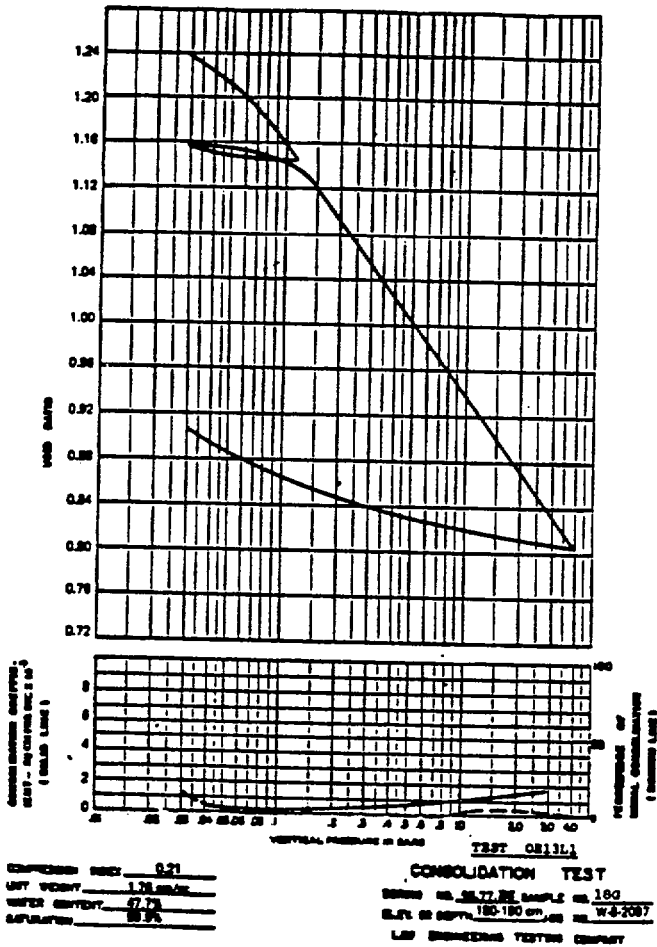
The static triaxial tests (first two characters are TE) are given second and ordered by test number. Results from one to as many as four tests are presented on the same sheet. The uppermost plot is a stress path presented as a plot of deviator stress versus mean normal effective stress. The deviator stress is the vertical effective stress (σ_v') minus the horizontal effective stress (σ_h'). The mean normal effective stress is $(\sigma_v' + 2\sigma_h')/3$. Note: This definition is not the same as that used in the stress paths given in Appendices E, F, and G.

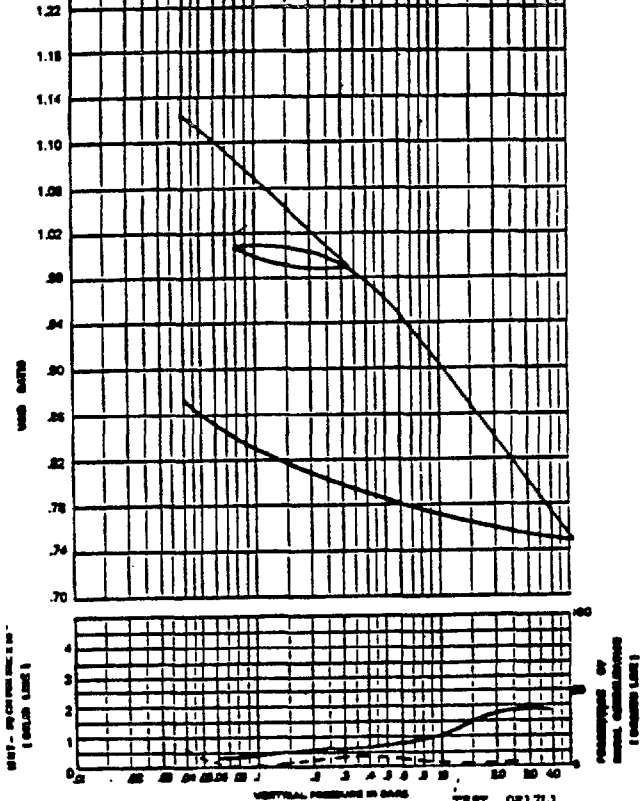
The middle graph is either the deviator stress or Q/U versus the axial strain. The parameter Q is the deviator stress while σ is the consolidation stress (or confining pressure). The last graph is the measured excess pore water pressure plotted versus axial strain.





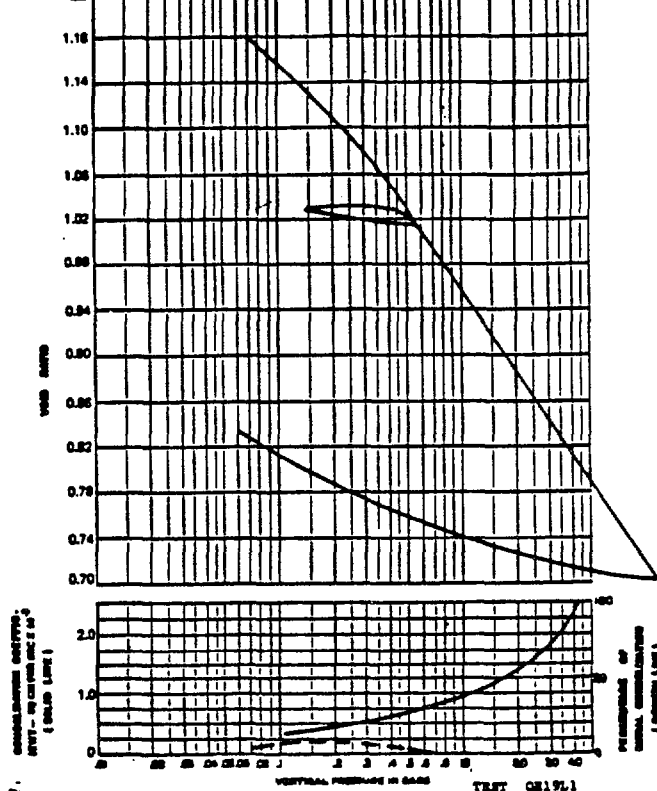






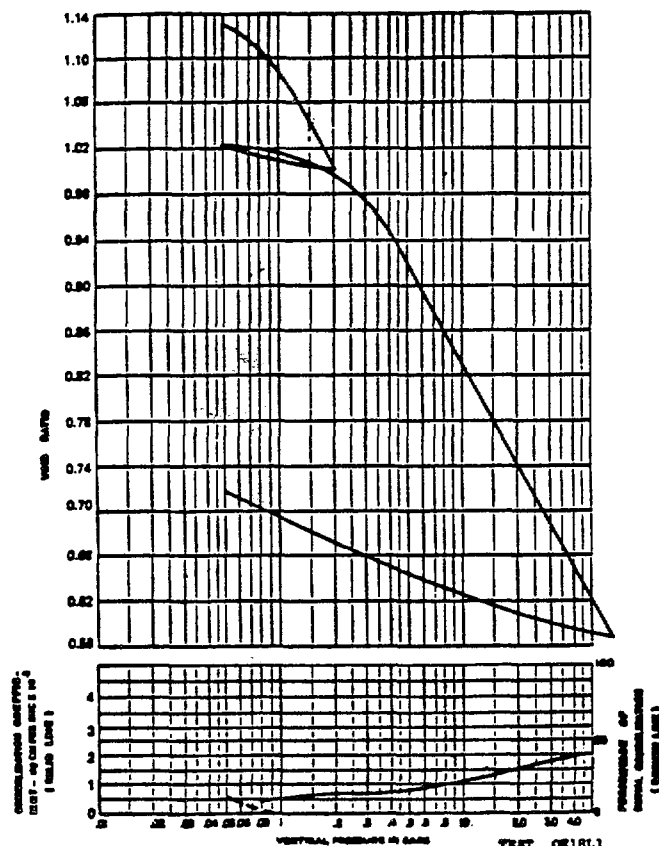
COMPRESSION INDEX: 0.20
 UNIT WEIGHT: 1.80 g/cm³
 WATER CONTENT: 62.2%
 SATURATION: 88.2%

TEST CB17L1
 CONSOLIDATION TEST
 SERIES NO. 28-77-16, SAMPLE NO. 120
 ELEV. OR DEPTH: 280-270 cm, NO. W-9-2087
 LAB. ENGINEERING TESTING COMPANY



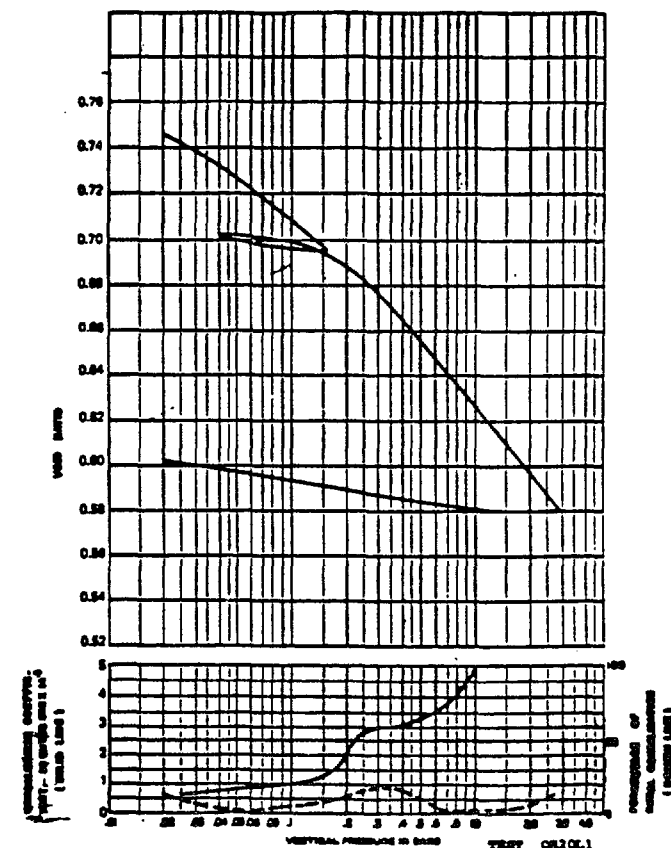
COMPRESSION INDEX: 0.25
 UNIT WEIGHT: 1.74 g/cm³
 WATER CONTENT: 69.7%
 SATURATION: 88.2%

TEST CB19L1
 CONSOLIDATION TEST
 SERIES NO. 28-77-20, SAMPLE NO. 210
 ELEV. OR DEPTH: 500-410 cm, NO. W-9-2087
 LAB. ENGINEERING TESTING COMPANY



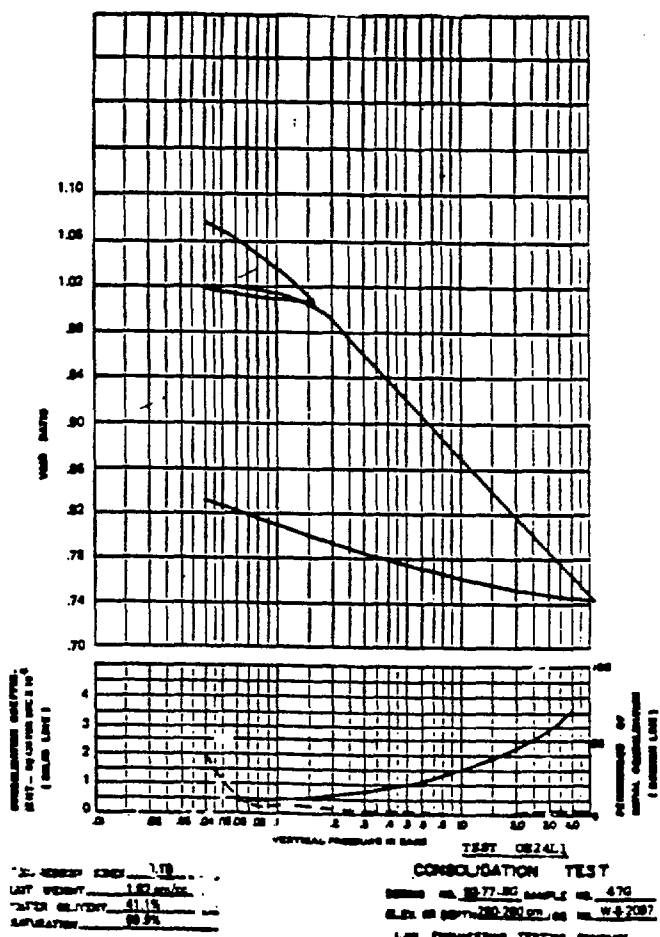
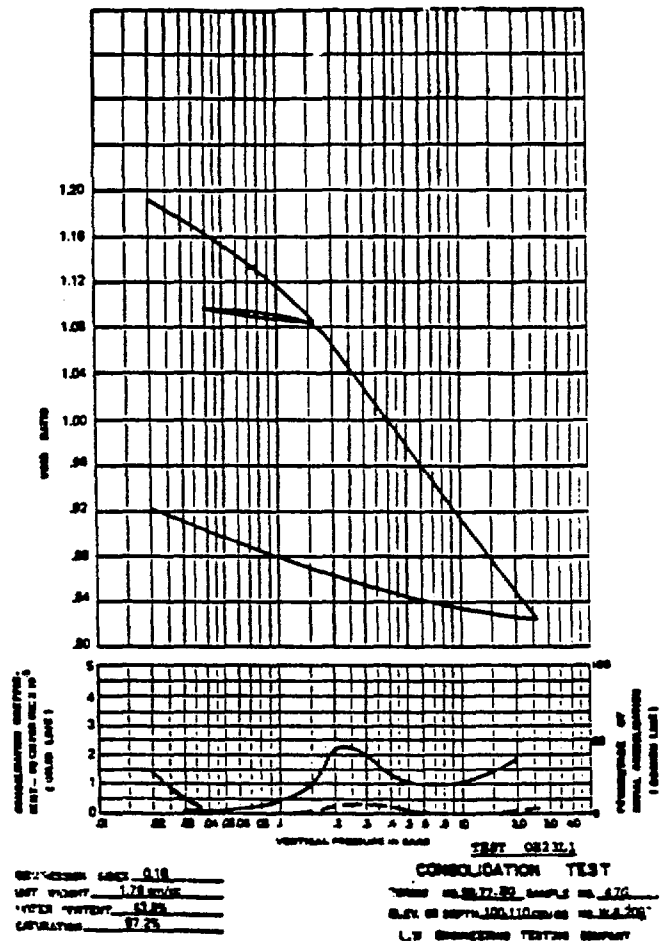
COMPRESSION INDEX: 0.20
 UNIT WEIGHT: 1.80 g/cm³
 WATER CONTENT: 62.2%
 SATURATION: 88.2%

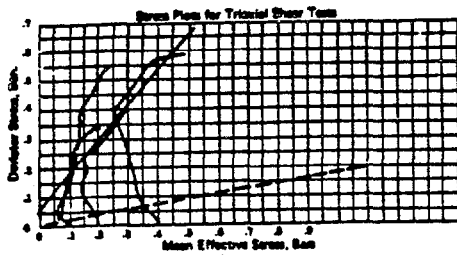
TEST CB18L1
 CONSOLIDATION TEST
 SERIES NO. 28-77-20, SAMPLE NO. 210
 ELEV. OR DEPTH: 280-300 cm, NO. W-9-2087
 LAB. ENGINEERING TESTING COMPANY



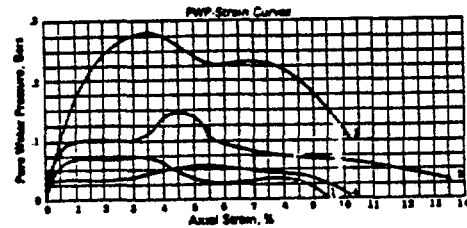
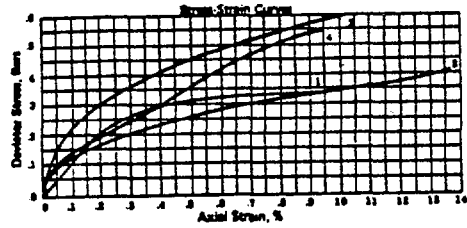
COMPRESSION INDEX: 0.50
 UNIT WEIGHT: 1.87 g/cm³
 WATER CONTENT: 29.0%
 SATURATION: 88.2%

TEST CB20L1
 CONSOLIDATION TEST
 SERIES NO. 28-77-20, SAMPLE NO. 230
 ELEV. OR DEPTH: 100-110 cm, NO. W-9-2087
 LAB. ENGINEERING TESTING COMPANY





Cohesion, C 200 BAR
Angle of Shear Resistance 31.1°



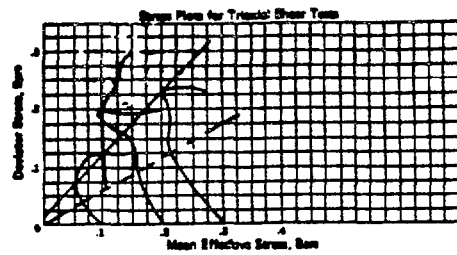
TESTS
(1) TE2L1
(2) TE2L1
(3) TE3L1
(4) TE4L1

* Stress Controlled Test

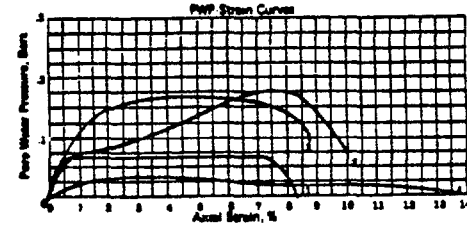
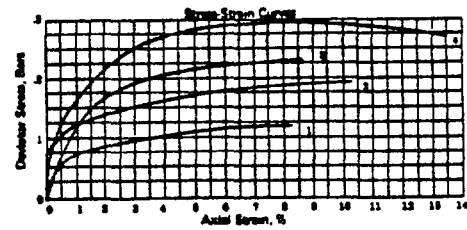
CURVE NO.	(1)	(2)	(3)	(4)
Confining Pressure Bars	1.0	2.0	3.0	4.0
Initial Length, cm	5.18	5.18	5.18	5.18
Initial Diameter, cm	1.77	1.77	1.77	1.77
Wet Unit Weight, gm/cc	17.68	17.68	17.68	17.68
Moisture Content, %	1.000	1.000	1.000	1.000
Initial Percent Saturation	88.75	88.75	88.75	88.75

Consolidated Undrained Triaxial Shear Test with Pore Pressure Measurements
COARSE 1G
CRUISE SS-77-BG
Date 8-18-78
Job No. W-0-0097

LAW ENGINEERING TESTING COMPANY



Cohesion, C 0.25 BAR
Angle of Shear Resistance 35.4°



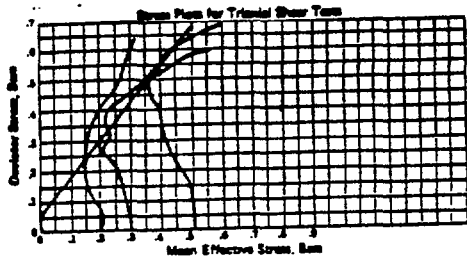
TESTS
(1) TE3L1
(2) TE3L1
(3) TE10L1
(4) TE11L1

* Stress Controlled Test

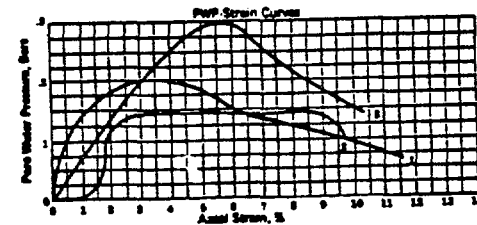
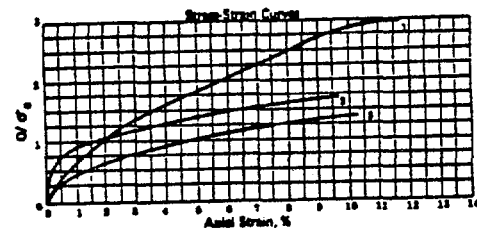
CURVE NO.	(1)	(2)	(3)	(4)
Confining Pressure Bars	1.0	2.0	3.0	4.0
Initial Length, cm	10.0	9.7	9.2	9.7
Initial Diameter, cm	0.97	0.98	0.98	0.98
Wet Unit Weight, gm/cc	1.71	1.54	1.54	1.71
Moisture Content, %	88.48	88.29	88.34	88.11
Initial Void Ratio	1.007	1.008	1.07	1.011
Initial Percent Saturation	88.81	88.88	87.68	88.88

Consolidated Undrained Triaxial Shear Test with Pore Pressure Measurements
COARSE 1G
CRUISE SS-77-BG
Date 8-18-78
Job No. W-0-0097

LAW ENGINEERING TESTING COMPANY



Cohesion, C 200 BAR
Angle of Shear Resistance 31.1°



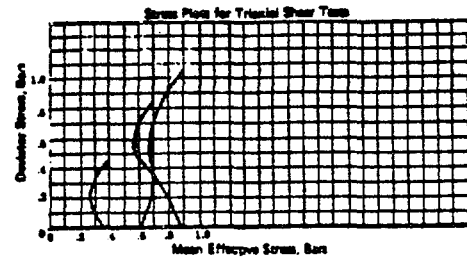
TESTS
(1) TE5L1
(2) TE5L1
(3) TE7L1

* Stress Controlled Test

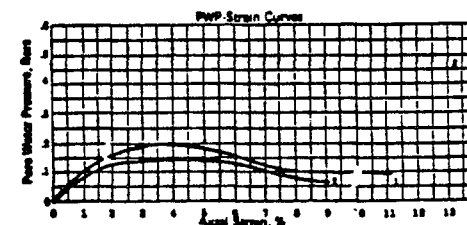
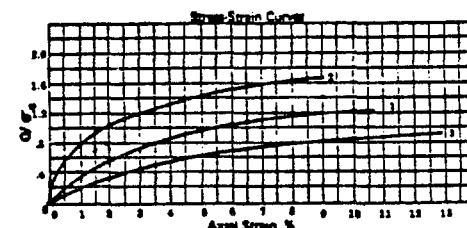
CURVE NO.	(1)	(2)	(3)	(4)
Confining Pressure Bars	1.0	2.0	3.0	4.0
Initial Length, cm	5.18	5.18	5.18	5.18
Initial Diameter, cm	1.77	1.77	1.77	1.77
Wet Unit Weight, gm/cc	17.68	17.68	17.68	17.68
Moisture Content, %	1.000	1.000	1.000	1.000
Initial Percent Saturation	88.75	88.75	88.75	88.75

Consolidated Undrained Triaxial Shear Test with Pore Pressure Measurements
COARSE 1G
CRUISE SS-77-BG
Date 8-18-78
Job No. W-0-0097

LAW ENGINEERING TESTING COMPANY



Cohesion, C 0
Angle of Shear Resistance 38.4°



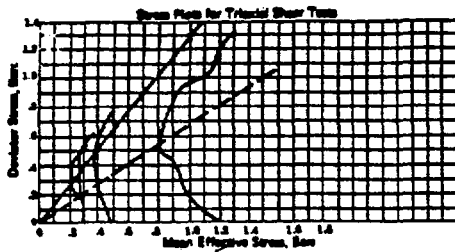
TESTS
(1) TE12L1
(2) TE13L1
(3) TE14L1

* Stress Controlled Test

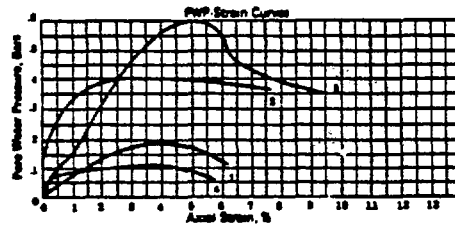
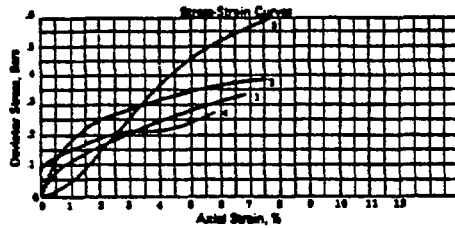
CURVE NO.	(1)	(2)	(3)	(4)
Confining Pressure Bars	1.0	2.0	3.0	4.0
Initial Length, cm	10.0	9.7	9.2	9.7
Initial Diameter, cm	0.97	0.98	0.98	0.98
Wet Unit Weight, gm/cc	1.71	1.54	1.54	1.71
Moisture Content, %	88.48	88.29	88.34	88.11
Initial Void Ratio	1.007	1.008	1.07	1.011
Initial Percent Saturation	88.81	88.88	87.68	88.88

Consolidated Undrained Triaxial Shear Test with Pore Pressure Measurements
COARSE 1G
CRUISE SS-77-BG
Date 8-18-78
Job No. W-0-0097

LAW ENGINEERING TESTING COMPANY



Cohesion, C 0
Angle of Shear Resistance 35.1°



TESTS
(1) TE15L1
(2) TE16L1
(3) TE17L1
(4) TE18L1

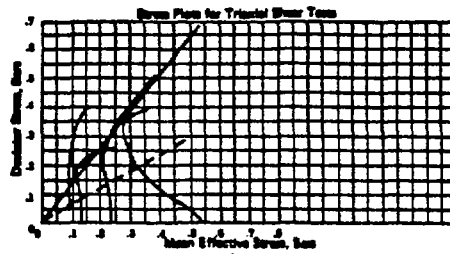
* Stress Controlled Test

CLPVE NO.	(1)	(2)	(3)	(4)
Confining Pressure Bar	30	30	30	30
Initial Length cm	10.5	10.5	10.5	10.5
Initial Diameter cm	4.00	4.00	4.00	4.00
Wet Unit Weight gm/cc	1.80	1.80	1.80	1.80
Moisture Content %	88.00	88.75	88.00	88.00
Initial Void Ratio	2.00	1.999	1.997	1.972
Initial Percent Saturation	95.44	97.80	96.50	95.80

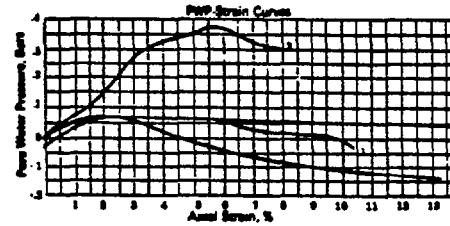
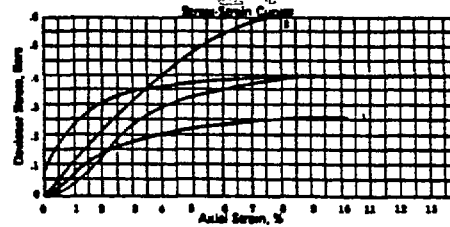
Consolidated Undrained
Triaxial Shear Test
with Pore Pressure Measurements

CORE 11G
CRUISE SS-77-BG
Date 6-17-78
Job No. W-6-0071

LAW ENGINEERING TESTING COMPANY



Cohesion, C 0
Angle of Shear Resistance 35.1°



TESTS
(1) TE22L1
(2) TE23L1
(3) TE24L1
(4) TE25L1

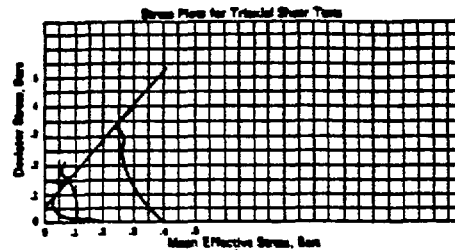
* Stress Controlled Test

CURVE NO.	(1)	(2)	(3)	(4)
Confining Pressure Bar	30	30	30	30
Initial Length cm	9.9	10.5	10.3	9.6
Initial Diameter cm	4.00	4.00	4.00	4.00
Wet Unit Weight gm/cc	1.80	1.80	1.80	1.79
Moisture Content %	88.00	88.00	88.00	88.0
Initial Void Ratio	2.00	2.00	2.00	1.980
Initial Percent Saturation	97.07	98.73	98.44	98.00

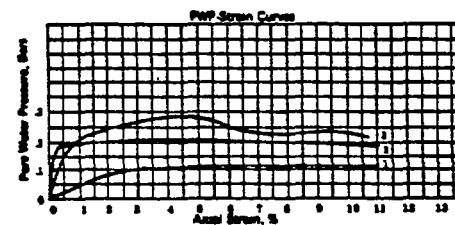
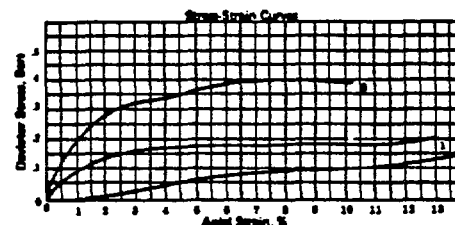
Consolidated Undrained
Triaxial Shear Test
with Pore Pressure Measurements

CORE 15G
CRUISE SS-77-BG
Date 6-6-78
Job No. W-6-1097

LAW ENGINEERING TESTING COMPANY



Cohesion, C 0.016 SA.33
Angle of Shear Resistance 35.1°



TESTS
(1) TE19L1
(2) TE20L1
(3) TE21L1

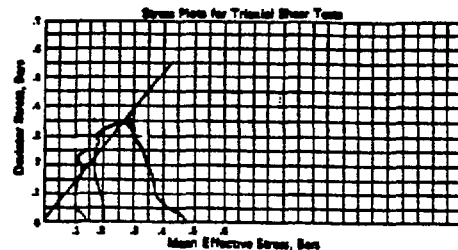
* Stress Controlled Test

CURVE NO.	(1)	(2)	(3)	(4)
Confining Pressure Bar	30	30	30	30
Initial Length cm	9.9	9.9	9.7	
Initial Diameter cm	4.00	4.00	4.00	
Wet Unit Weight gm/cc	1.80	1.80	1.80	
Moisture Content %	79.00	80.25	80.00	
Initial Void Ratio	1.800	1.800	1.807	
Initial Percent Saturation	95.47	95.50	95.50	

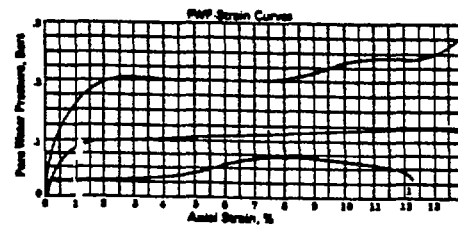
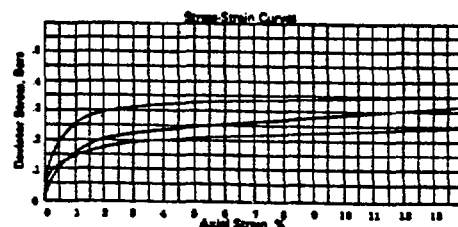
Consolidated Undrained
Triaxial Shear Test
with Pore Pressure Measurements

CORE 14G
CRUISE SS-77-BG
Date 6-1-78
Job No. W-6-1097

LAW ENGINEERING TESTING COMPANY



Cohesion, C 0
Angle of Shear Resistance 35.1°



TESTS
(1) TE26L1
(2) TE27L1
(3) TE28L1

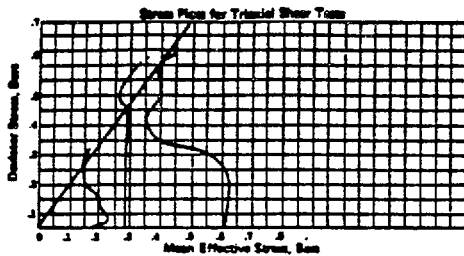
* Stress Controlled Test

CURVE NO.	(1)	(2)	(3)	(4)
Confining Pressure Bar	30	30	30	
Initial Length cm	9.9	10.5	10.4	
Initial Diameter cm	4.00	4.00	4.00	
Wet Unit Weight gm/cc	1.79	1.80	1.79	
Moisture Content %	88.00	88.00	88.00	
Initial Void Ratio	1.99	1.99	1.99	
Initial Percent Saturation	95.50	95.50	95.50	

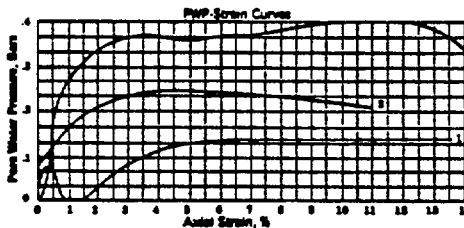
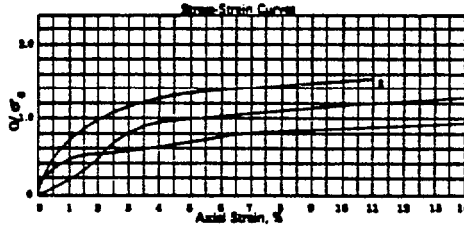
Consolidated Undrained
Triaxial Shear Test
with Pore Pressure Measurements

CORE 19G
CRUISE SS-77-BG
Date 6-6-78
Job No. W-6-1097

LAW ENGINEERING TESTING COMPANY



Cohesion, C _____
Angle of Shear Resistance _____ 35.0°



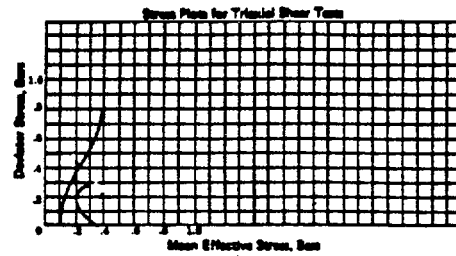
TESTS
(1) TE29L1
(2) TE30L1
(3) TE31L1

• Stress Controlled Test

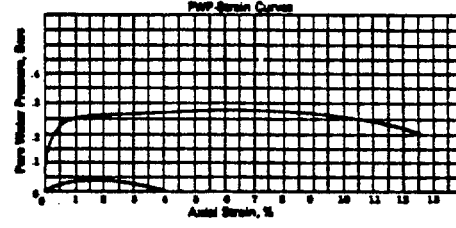
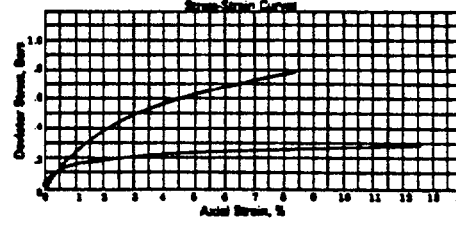
CURVE NO.	(1)	(2)	(3)	(4)
Confining Pressure, Bar	30	30	30	
Initial Length, cm	10.0	9.7	9.8	
Initial Diameter, cm	6.11	6.75	6.80	
Wet Unit Weight, gm/cc	1.88	1.73	1.77	
Moisture Content, %	66.60	65.30	66.00	
Initial Void Ratio	1.697	1.595	1.598	
Initial Percent Saturation	65.60	65.71	65.51	

Consolidated Undrained Triaxial Shear Test with Pore Pressure Measurements
CORR _____ 210
CRUISE SS-77-SG
Date 8-14-78
Job No. W-6-0097

LAW ENGINEERING TESTING COMPANY



Cohesion, C _____
Angle of Shear Resistance _____



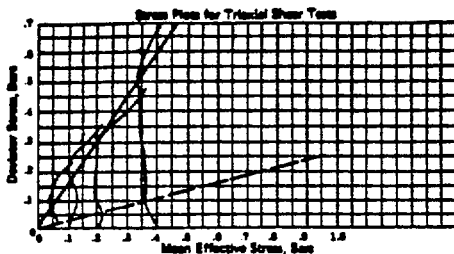
TESTS
(1) TE36L1
(2) TE37L1

• Stress Controlled Test

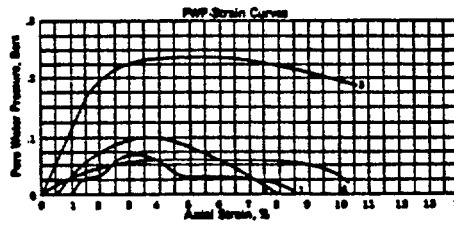
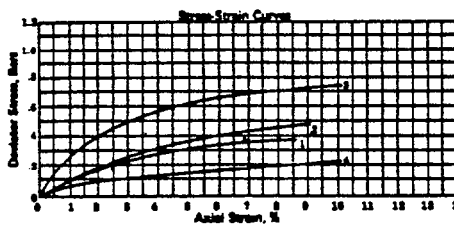
CURVE NO.	(1)	(2)	(3)	(4)
Confining Pressure, Bar	0.10	0.20		
Initial Length, cm	6.0	10.3		
Initial Diameter, cm	3.51	6.30		
Wet Unit Weight, gm/cc	1.80	1.80		
Moisture Content, %	55.8	55.8		
Initial Void Ratio	0.708	1.070		
Initial Percent Saturation	66.3	66.3		

Consolidated Undrained Triaxial Shear Test with Pore Pressure Measurements
CORR _____ 360
CRUISE SS-77-SG
Date 8-1-78
Job No. W-6-0097

LAW ENGINEERING TESTING COMPANY



Cohesion, C _____
Angle of Shear Resistance _____ 35.0°



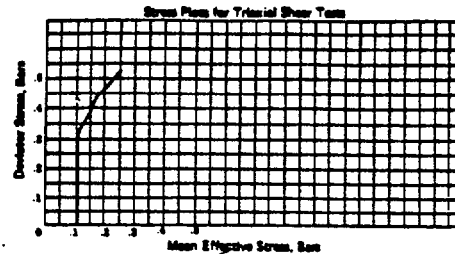
TESTS
(1) TE32L1
(2) TE33L1
(3) TE34L1
(4) TE35L1

• Stress Controlled Test

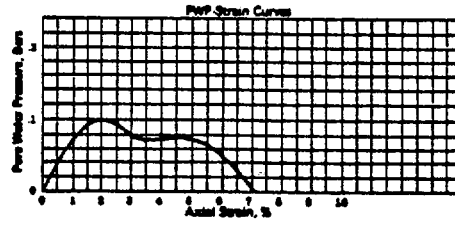
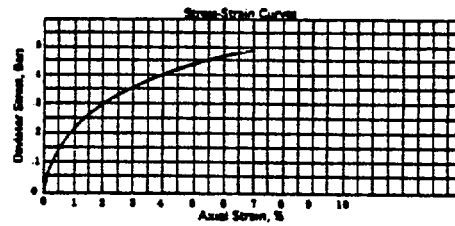
CURVE NO.	(1)	(2)	(3)	(4)
Confining Pressure, Bar	30	30	30	30
Initial Length, cm	10.0	10.3	10.3	9.8
Initial Diameter, cm	6.04	6.01	6.00	5.80
Wet Unit Weight, gm/cc	1.80	1.80	1.84	1.80
Moisture Content, %	66.30	65.40	65.50	65.50
Initial Void Ratio	1.692	1.692	1.694	1.690
Initial Percent Saturation	65.60	65.74	65.50	65.50

Consolidated Undrained Triaxial Shear Test with Pore Pressure Measurements
CORR _____ 330
CRUISE SS-77-SG
Date 8-10-78
Job No. W-6-0097

LAW ENGINEERING TESTING COMPANY



Cohesion, C _____
Angle of Shear Resistance _____



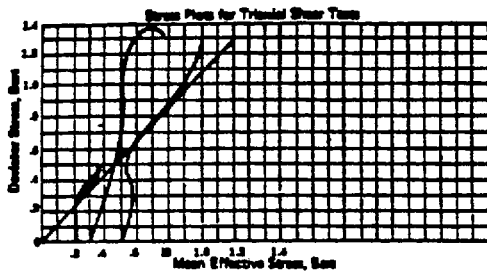
TEST TE36L1

• Stress Controlled Test

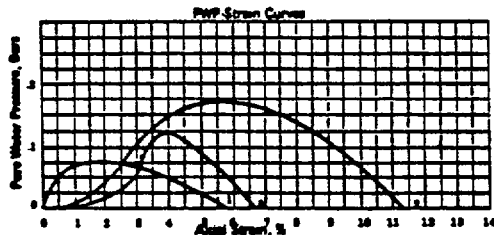
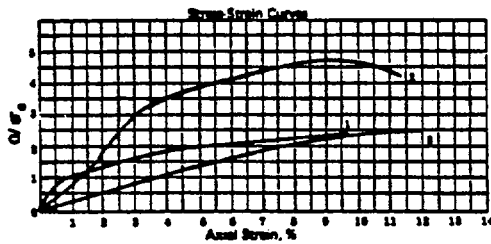
CURVE NO.	(1)	(2)	(3)	(4)
Confining Pressure, Bar	30			
Initial Length, cm	9.8			
Initial Diameter, cm	6.00			
Wet Unit Weight, gm/cc	1.87			
Moisture Content, %	65.00			
Initial Void Ratio	1.704			
Initial Percent Saturation	65.81			

Consolidated Undrained Triaxial Shear Test with Pore Pressure Measurements
CORR _____ 360
CRUISE SS-77-SG
Date 8-12-78
Job No. W-6-0097

LAW ENGINEERING TESTING COMPANY



Cohesion, C _____
 Angle of Shear
 Resistance ϕ _____



TESTS
 (1) TE39L1
 (2) TE40L1
 (3) TE41L1

• Stress Controlled Test

CUKVs	JO ₂	(1)	(2)	(3)	(4)
Confined Pressure Bars	30	30	30	30	
Initial Length, cm	7.3	8.7	10.1		
Initial Diameter, cm	5.00	5.00	5.10		
Wet Unit Weight, gm/cc	1.60	1.70	1.60		
Moisture Content, %	66.70	65.80	66.80		
Initial Void Ratio	1.170	1.097	1.080		
Initial Percent Saturation	100	85.40	89.80		

Consolidated Undrained
 Triaxial Shear Test
 with Pore Pressure Measurements

CODE 470
 CRUISE SS-77-30
 Date 8-0-78
 Job No. W-0-0097

LAW ENGINEERING TESTING COMPANY

APPENDIX **E**

CONSOLIDATION AND TRIAXIAL TEST **RESULTS--**

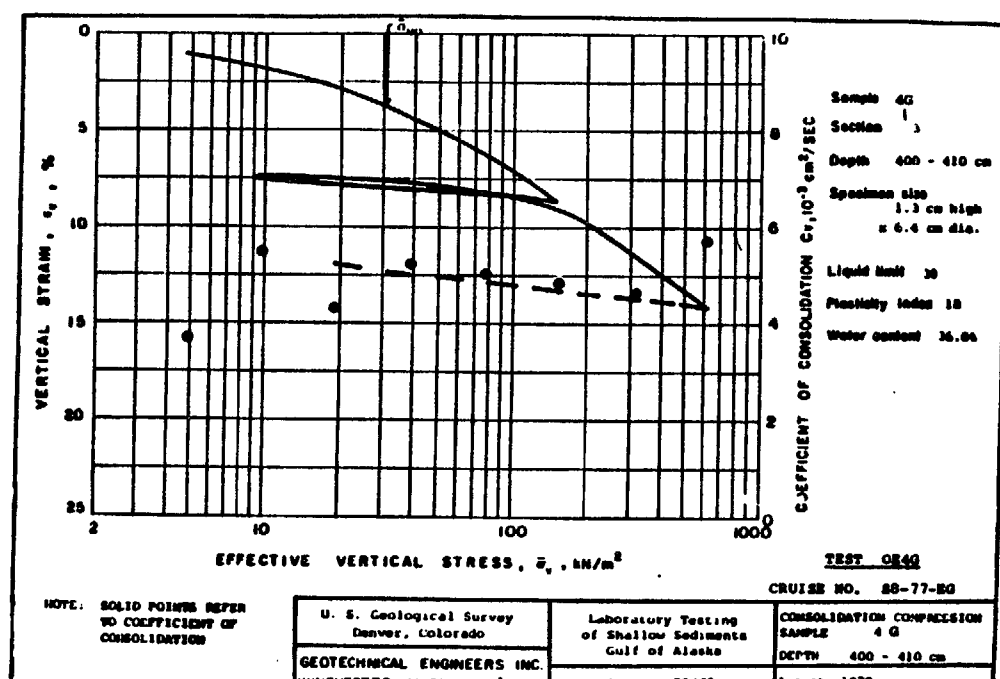
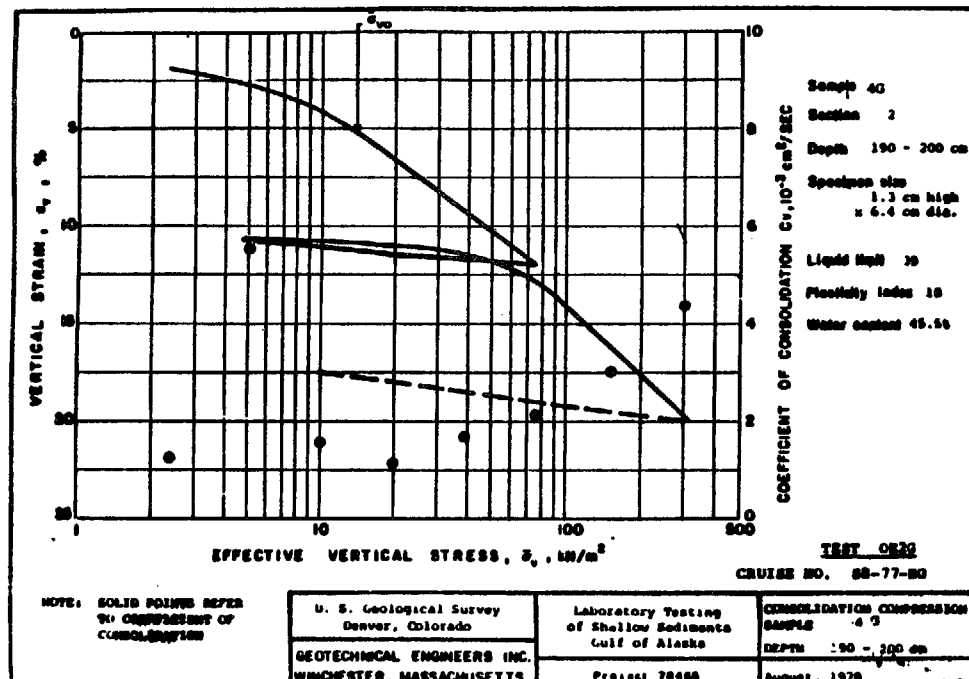
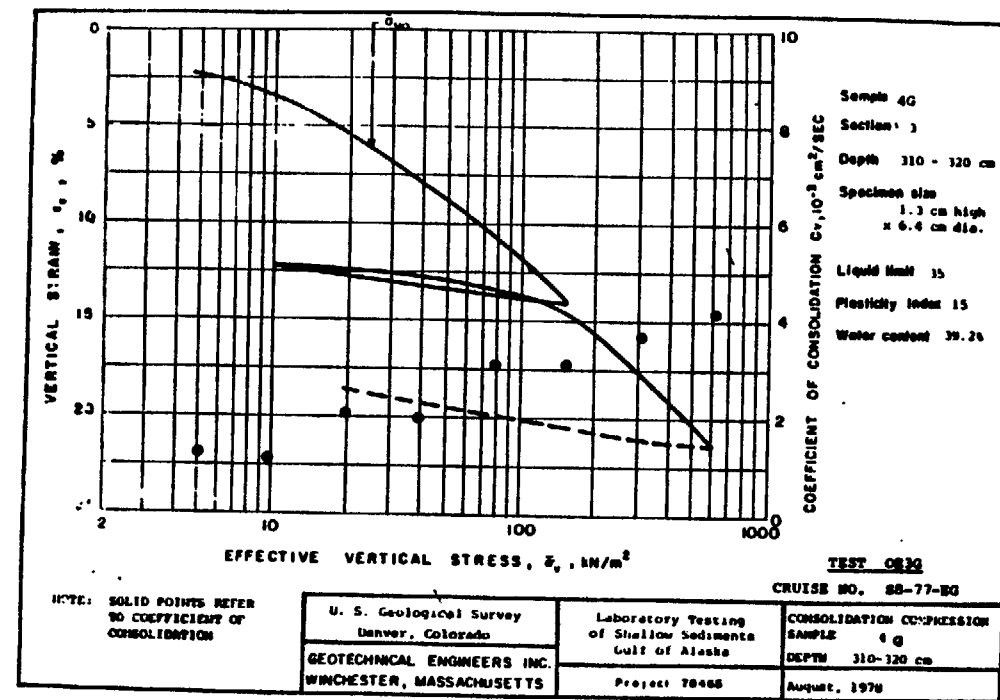
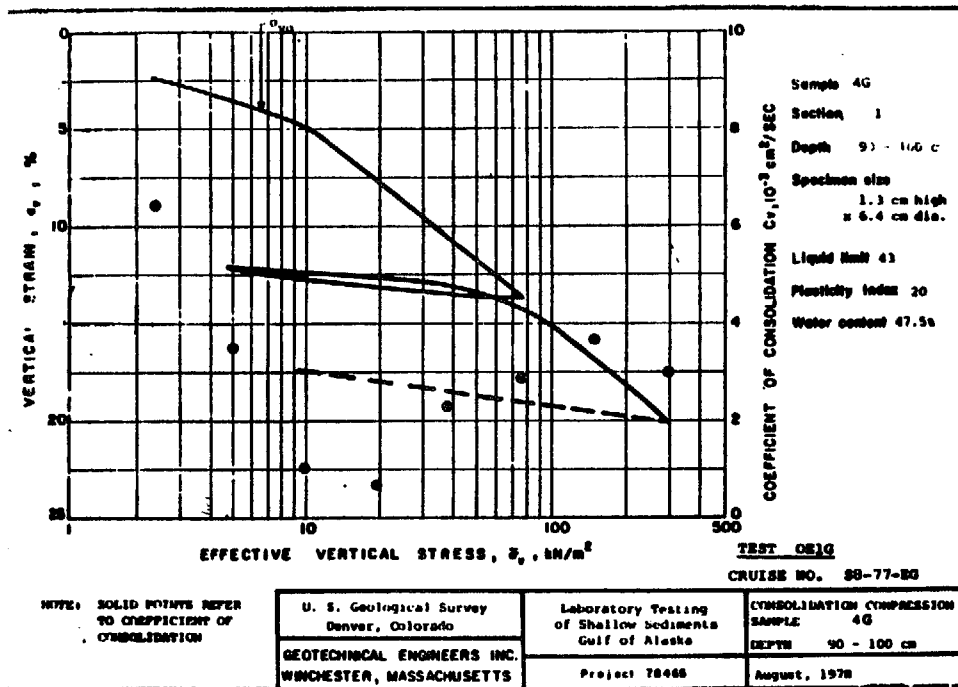
GEOTECHNICAL **ENGINEERS,** INCORPORATED (1977 cores)

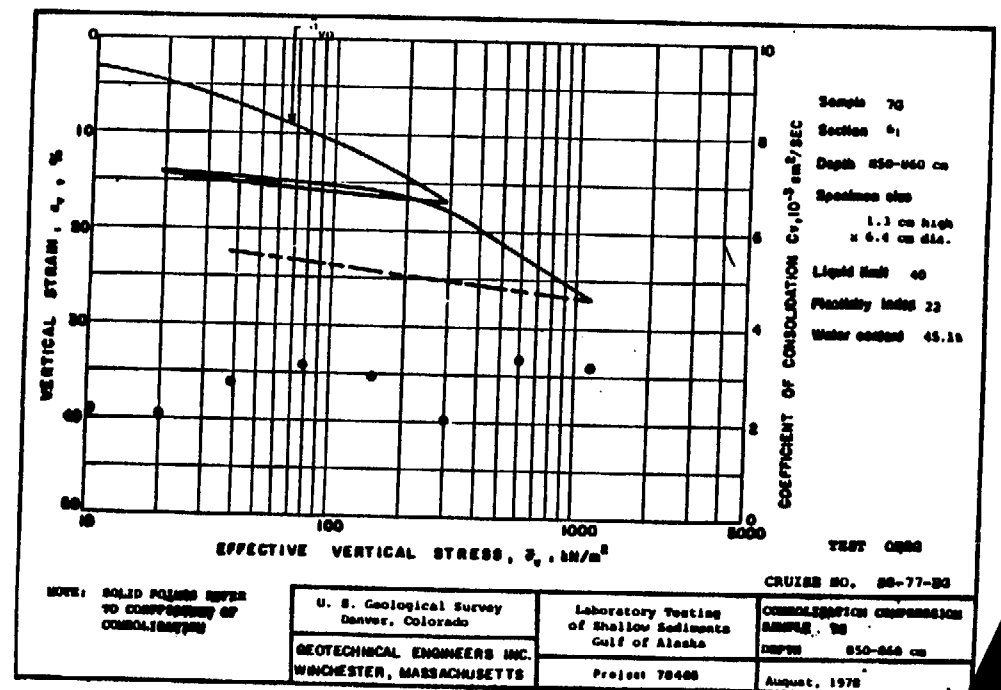
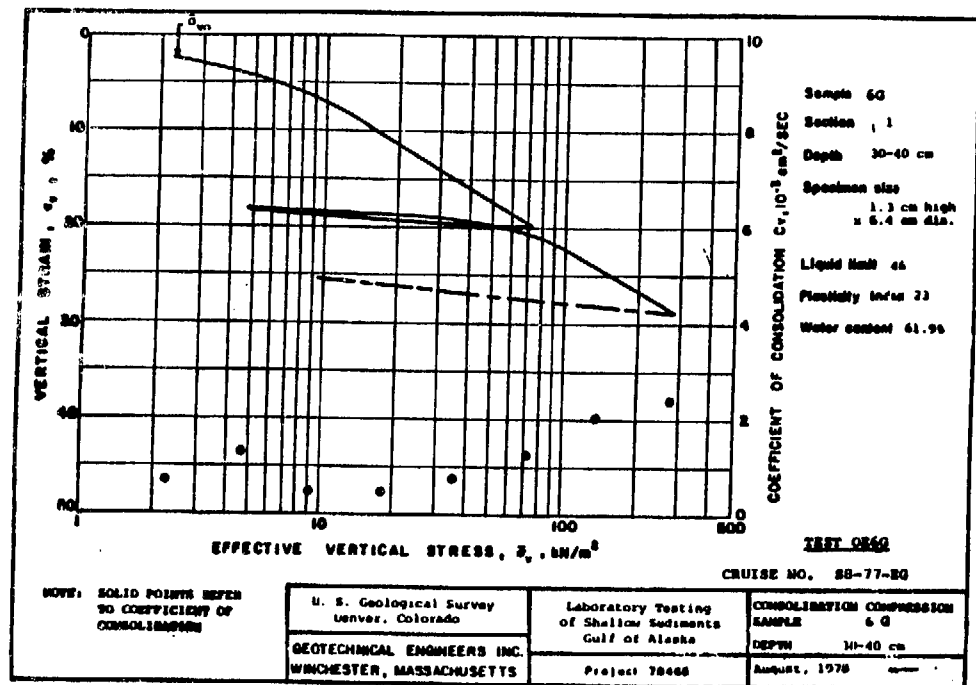
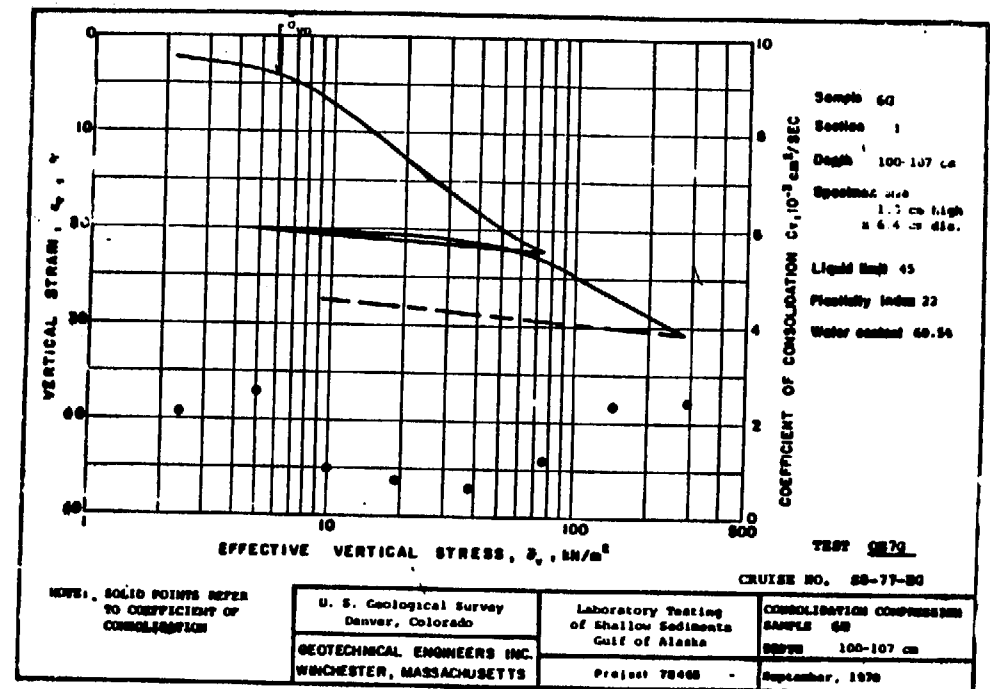
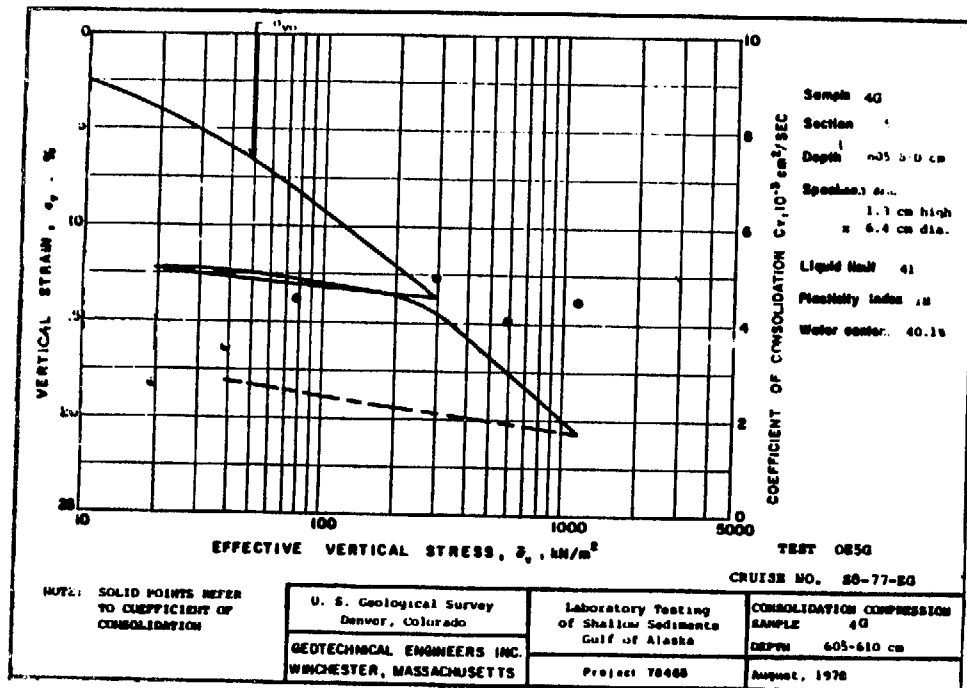
APPENDIX E. CONSOLIDATION AND TRIAXIAL TEST RESULTS-GEOTECHNICAL ENGINEERS,
INCORPORATED (1977 **cores**)

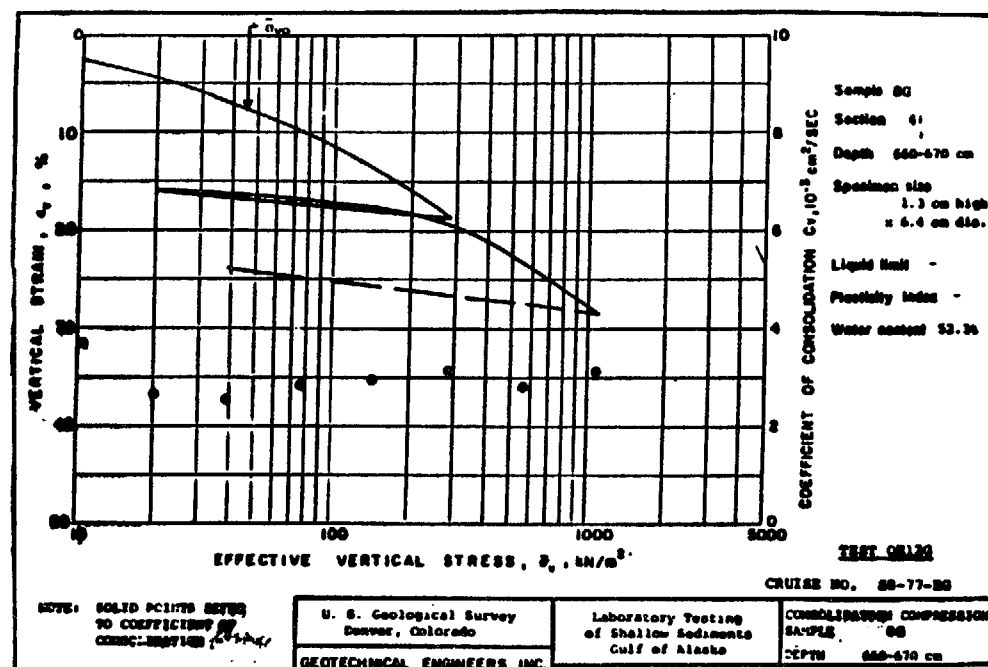
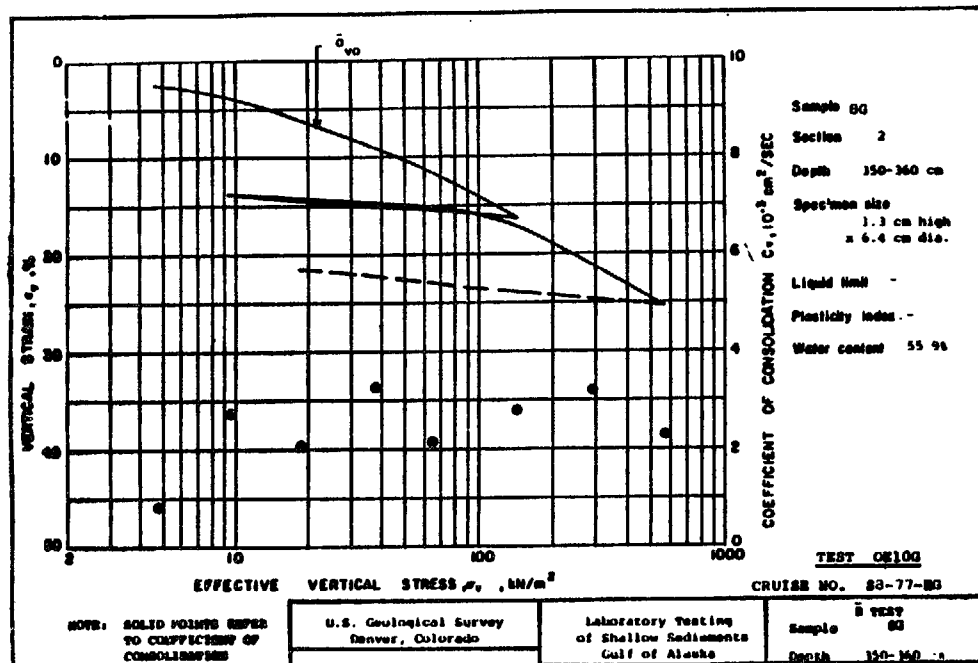
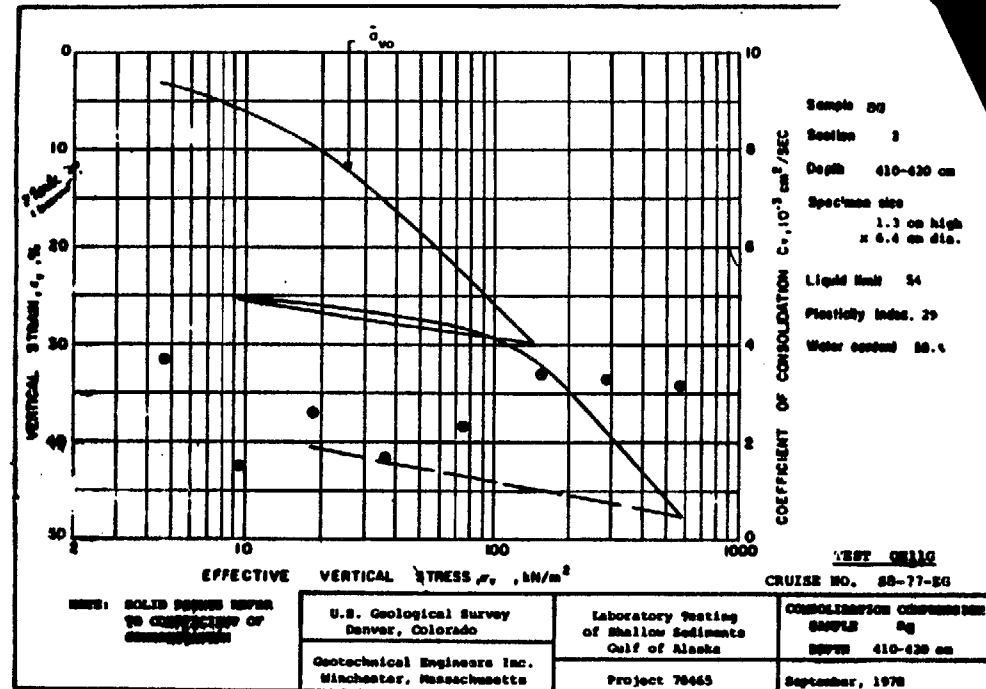
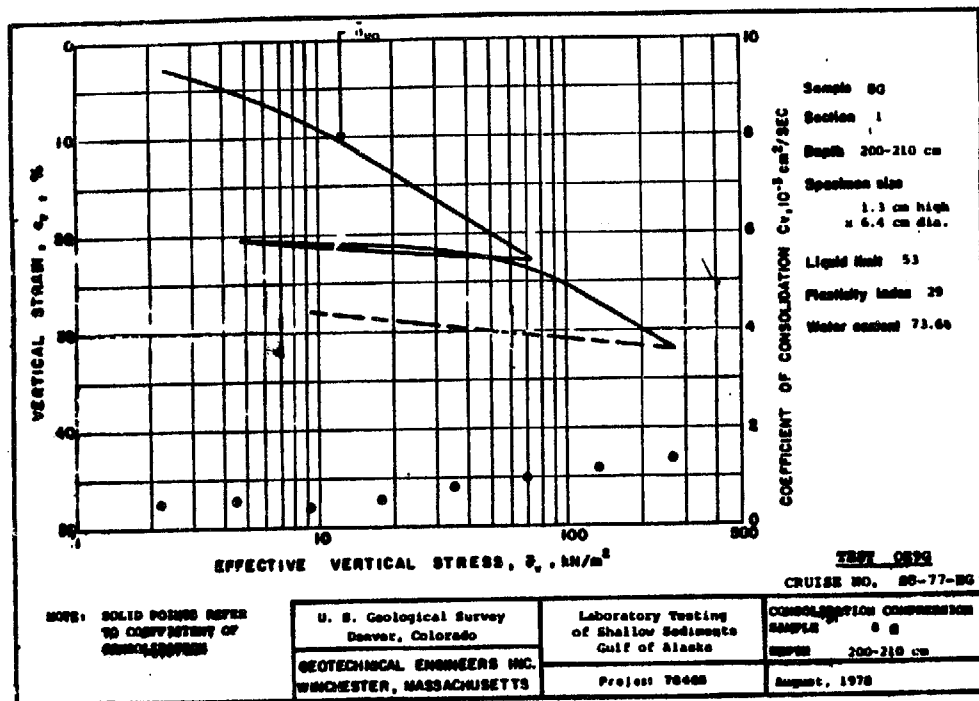
This appendix presents the results of consolidation and static triaxial tests performed by Geotechnical Engineers, Incorporated under Contract number 14-08-0001-17353 with the U.S. Geological Survey. Testing was performed under the direction of K. Dalenberg and D.P. LaGatta. Cores were from Cruise **S8-77-EG**.

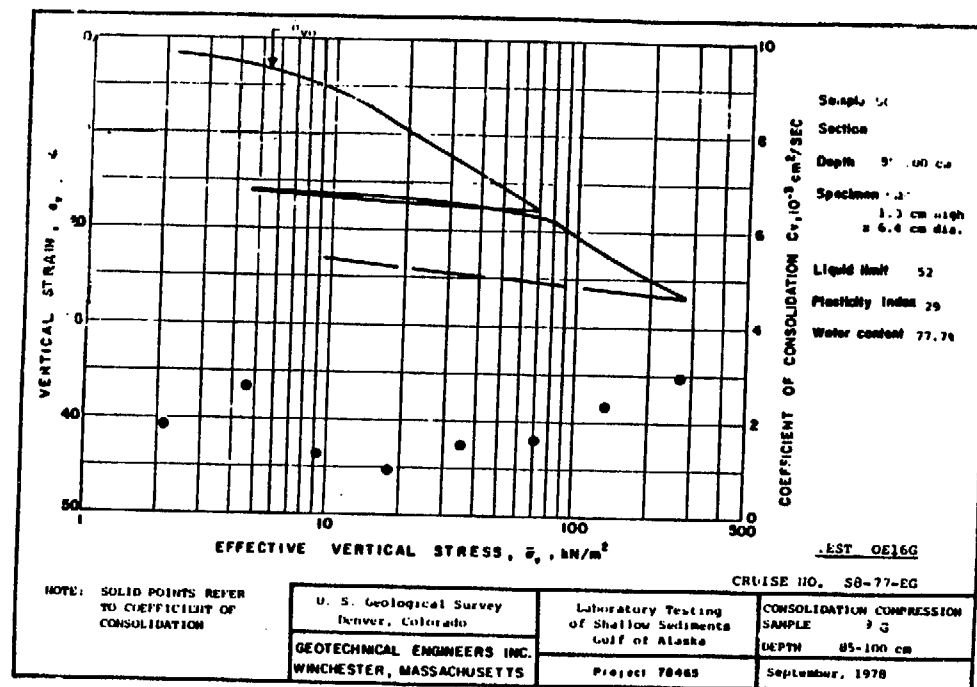
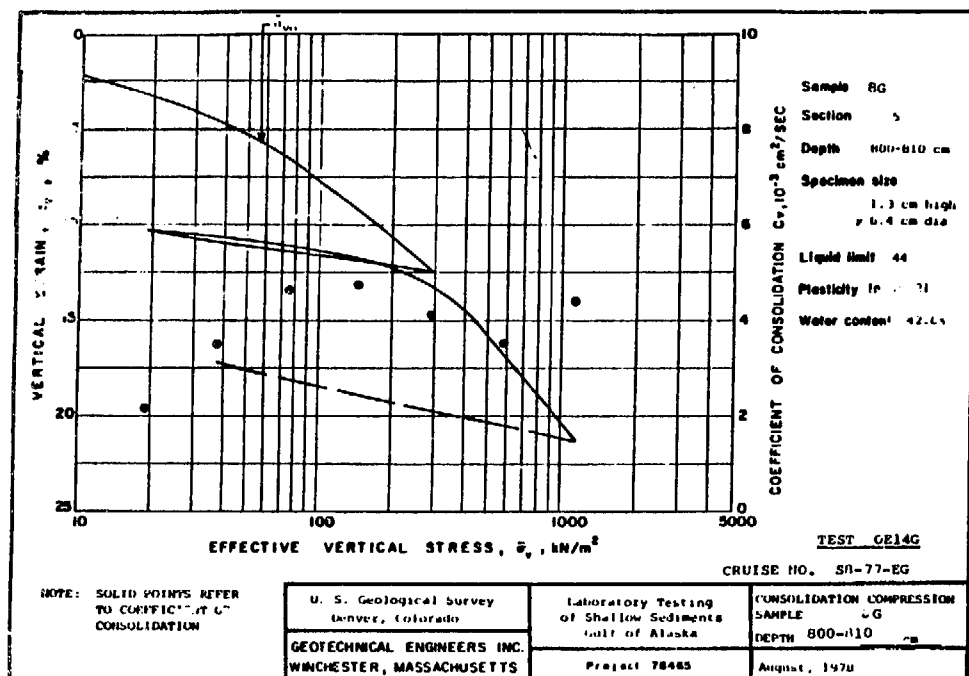
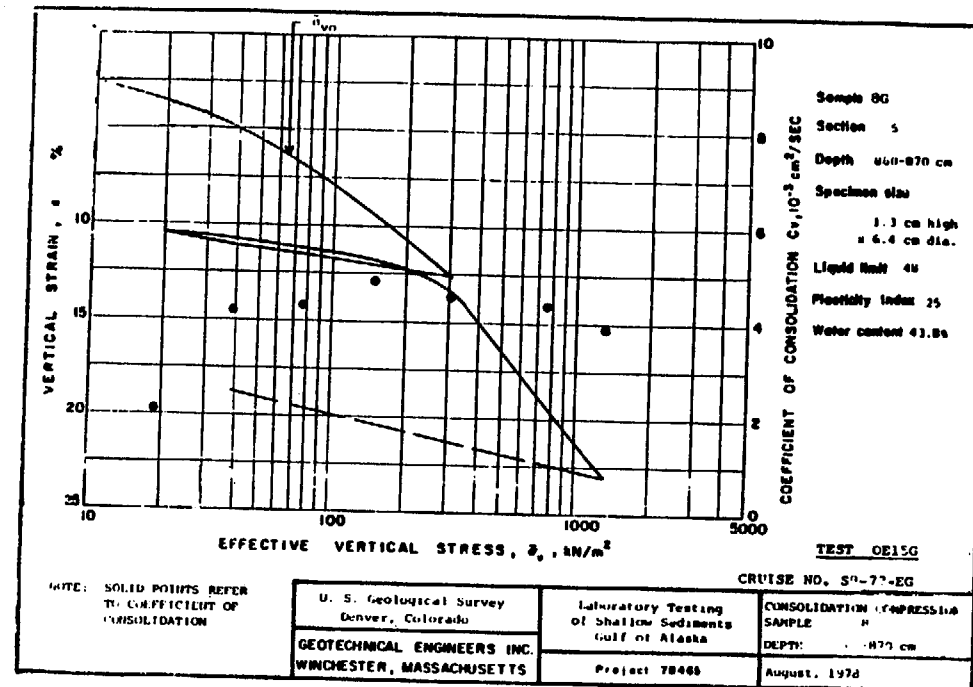
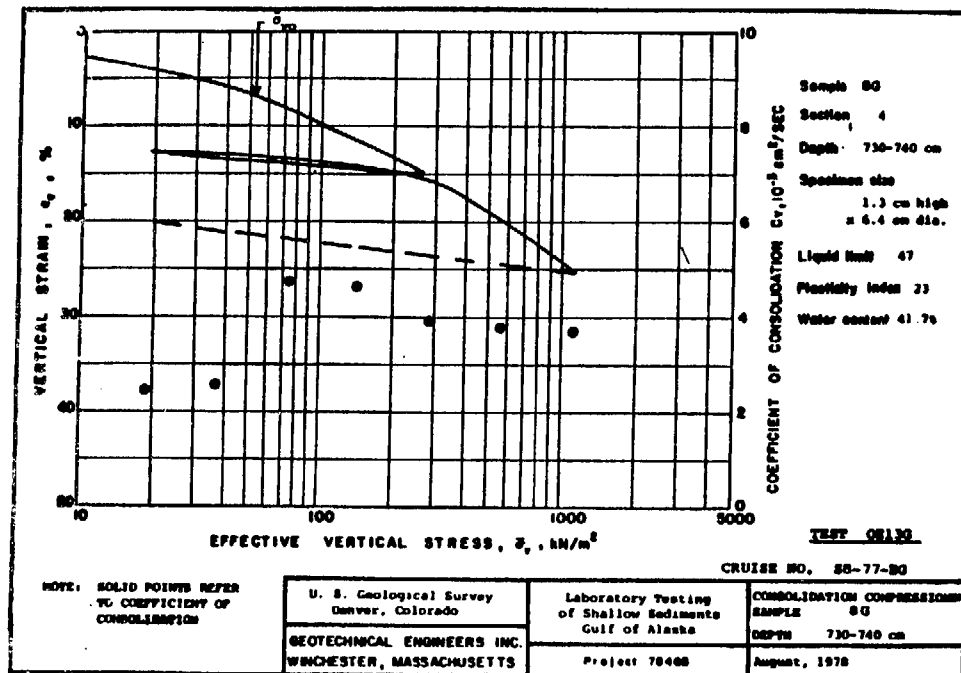
All tests in this group have been assigned a test number with G as the last character. The consolidation tests (first two characters are OE) are presented first and are ordered by test number. Results from a single test are presented on a page in the form of vertical strain and calculated coefficient of consolidation (c_v) versus the vertical effective stress in kPa (equivalent to kN/m^2).

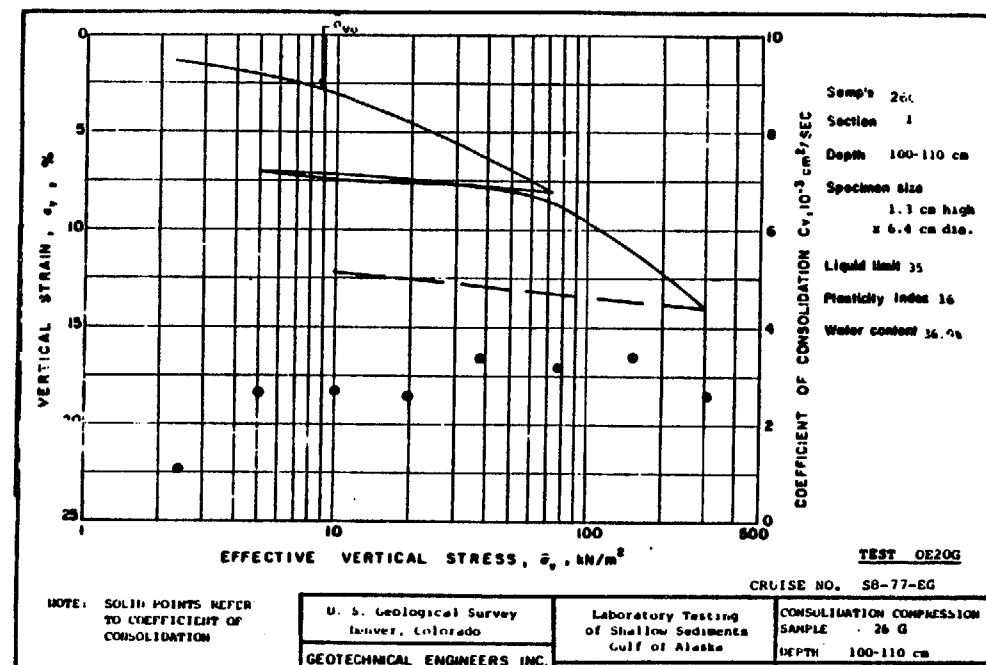
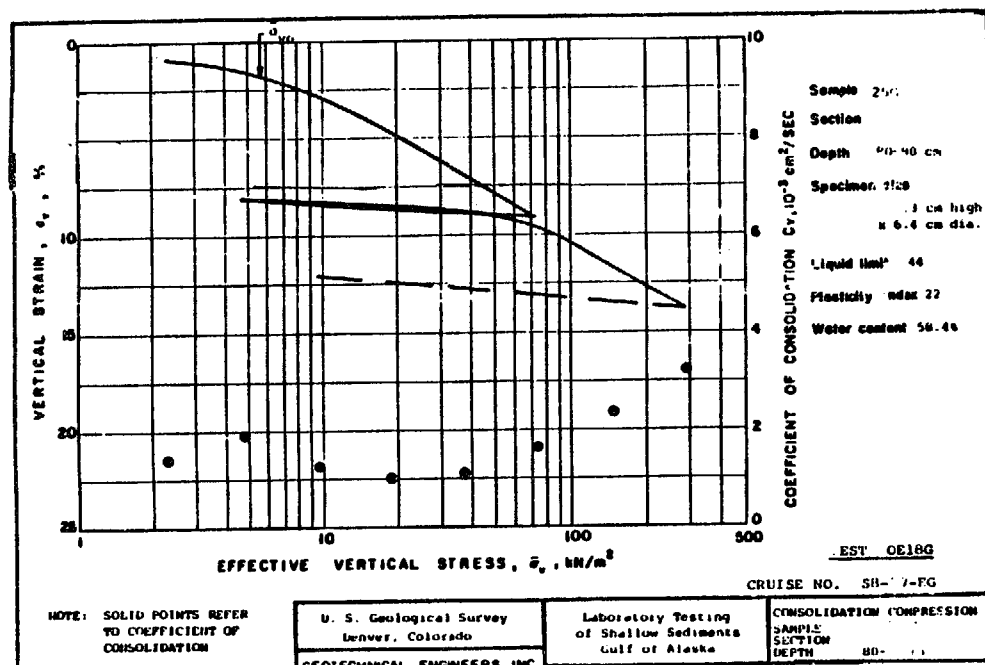
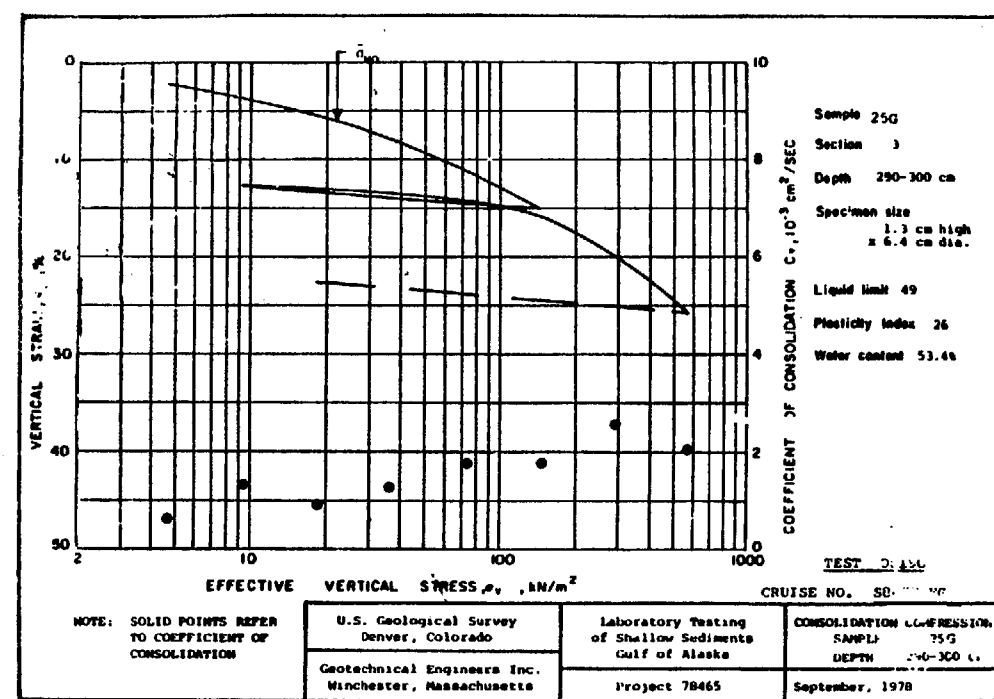
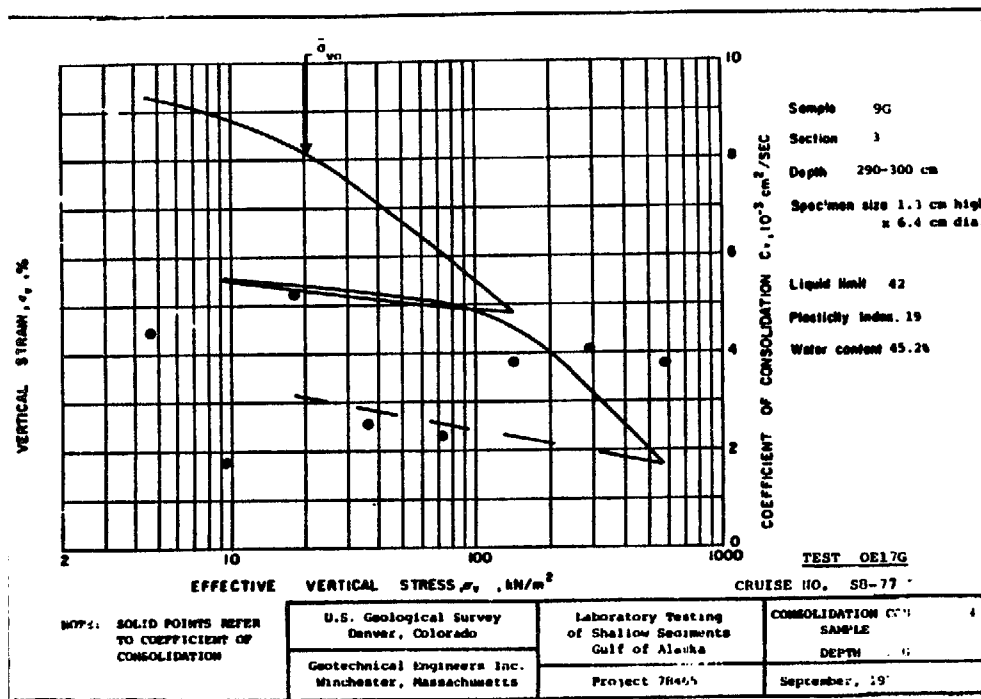
The static triaxial tests (first two characters are TE) are given second and ordered by test number. Results from a single test are given on a single **page**. The upper left plot is the maximum shearing stress or $(\sigma_1 - \sigma_3)/2$ versus the axial strain. The upper right plot is a stress path presenting the maximum shearing stress versus the normal effective stress on the plane of maximum shearing stress or $(\sigma_1' + \sigma_3')/2$. In Appendices F and G, the stress path plots are defined in the same way but identified as q versus p'. The stress path plots of Appendix D are defined differently. The lower left plot is the excess pore water pressure developed during shear ($u - u_0$) versus the axial strain.

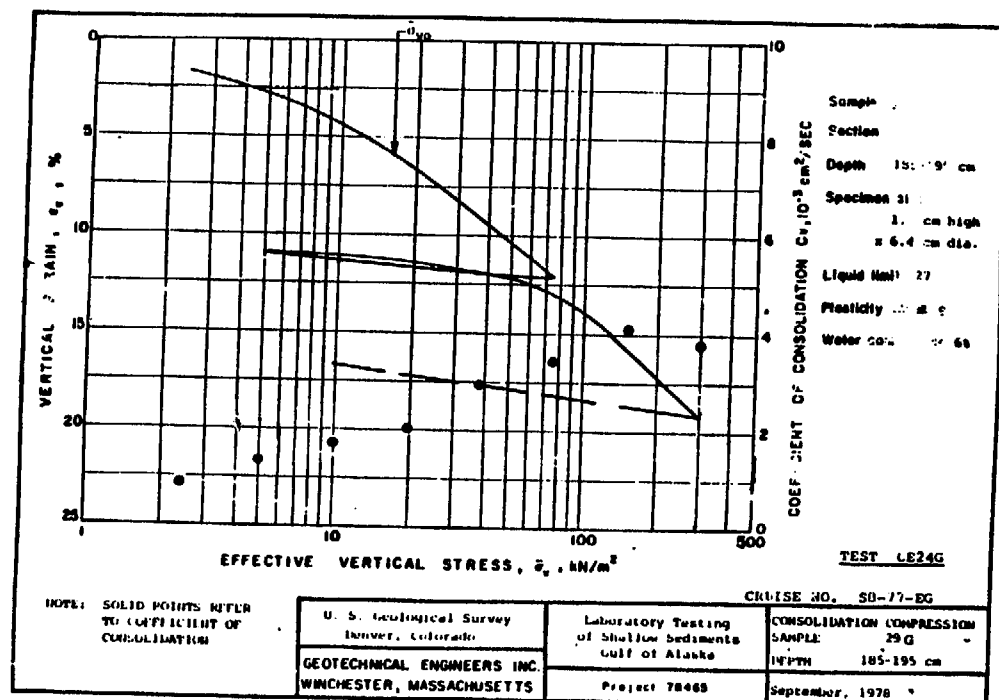
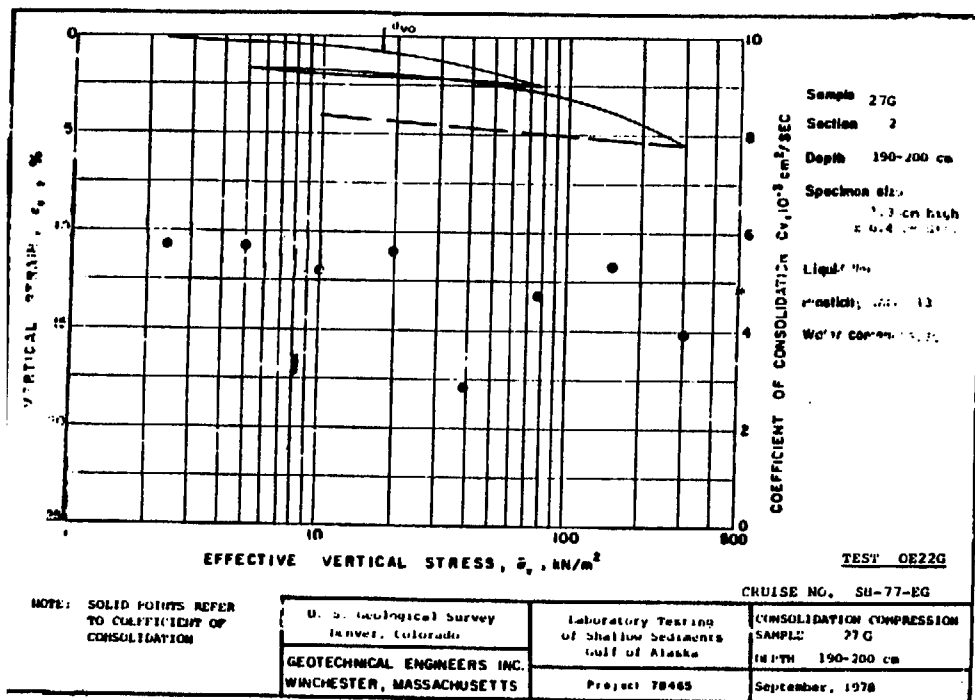
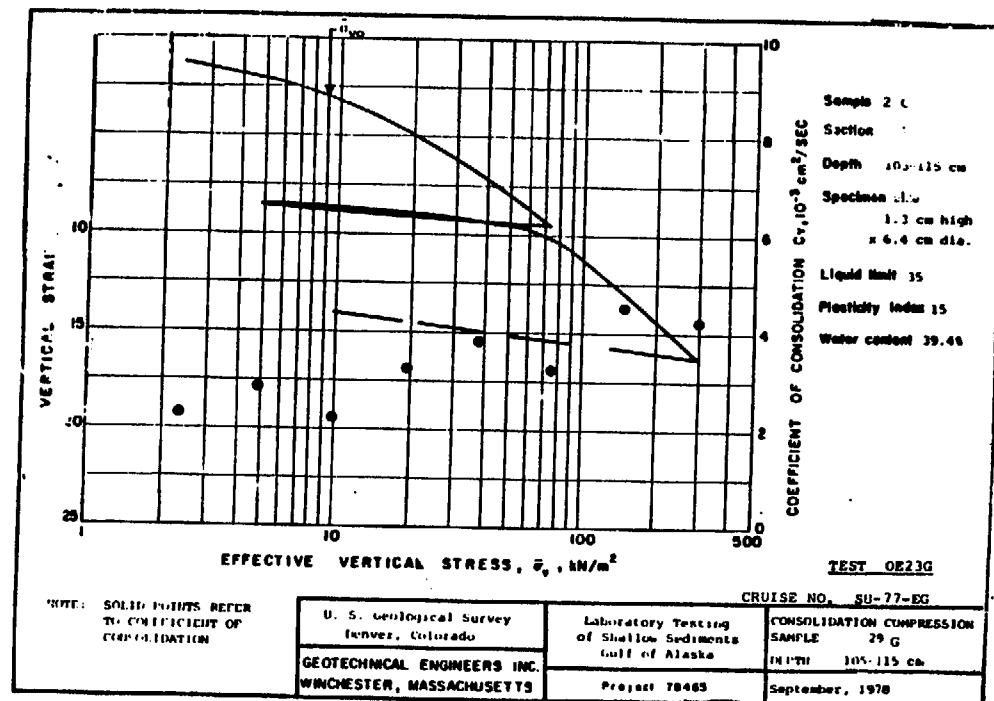
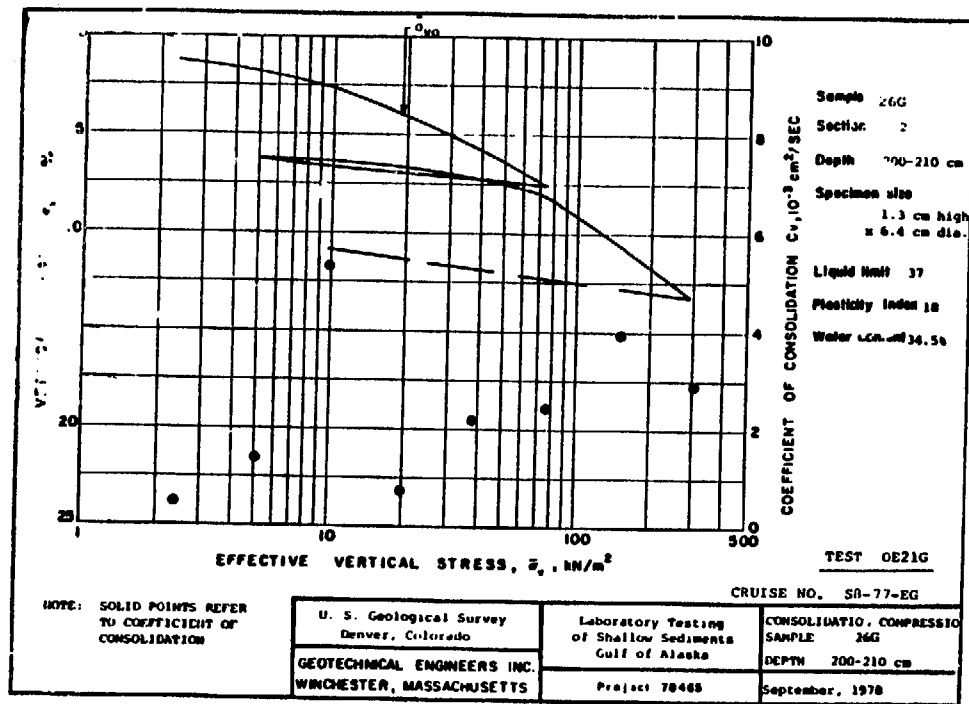


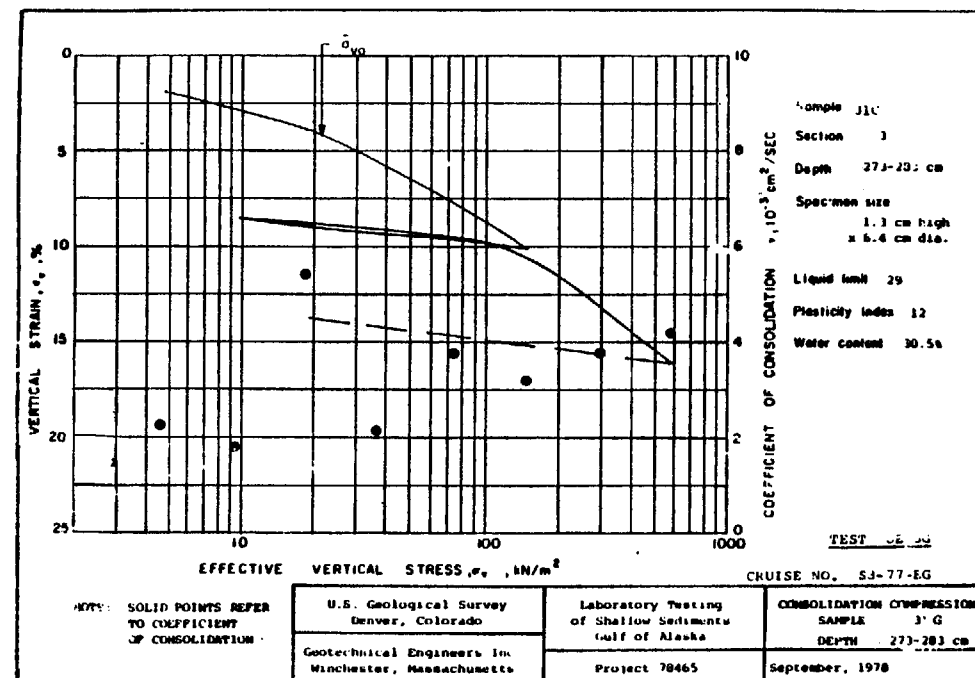
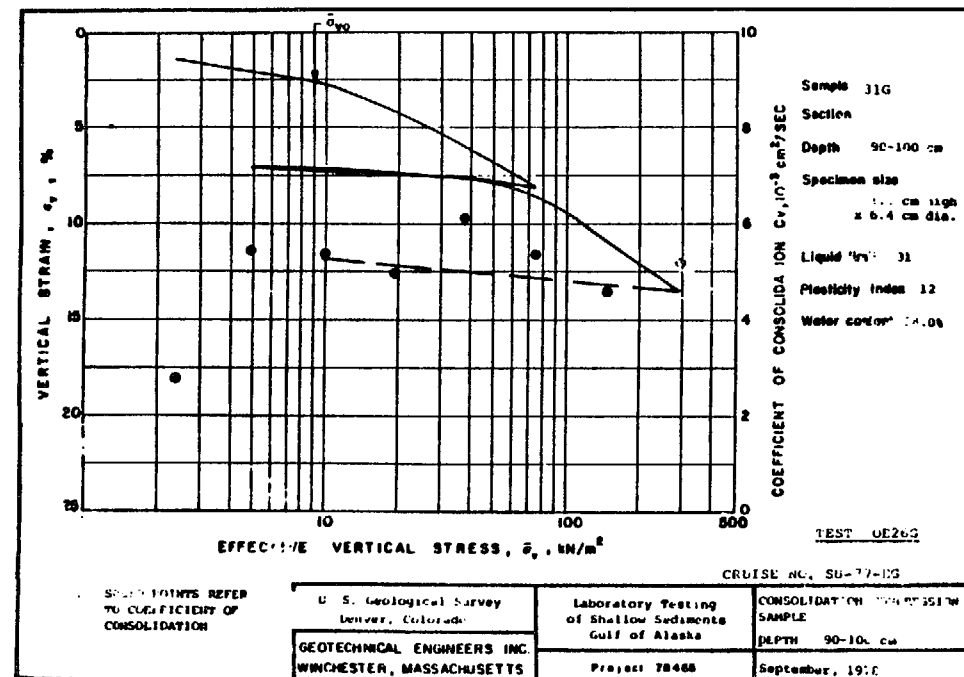
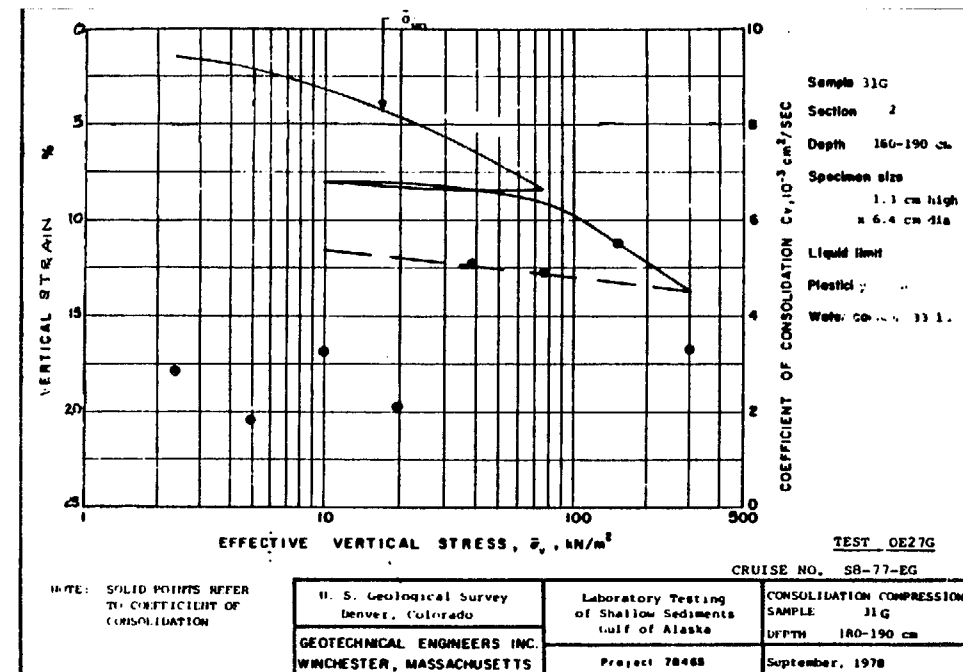
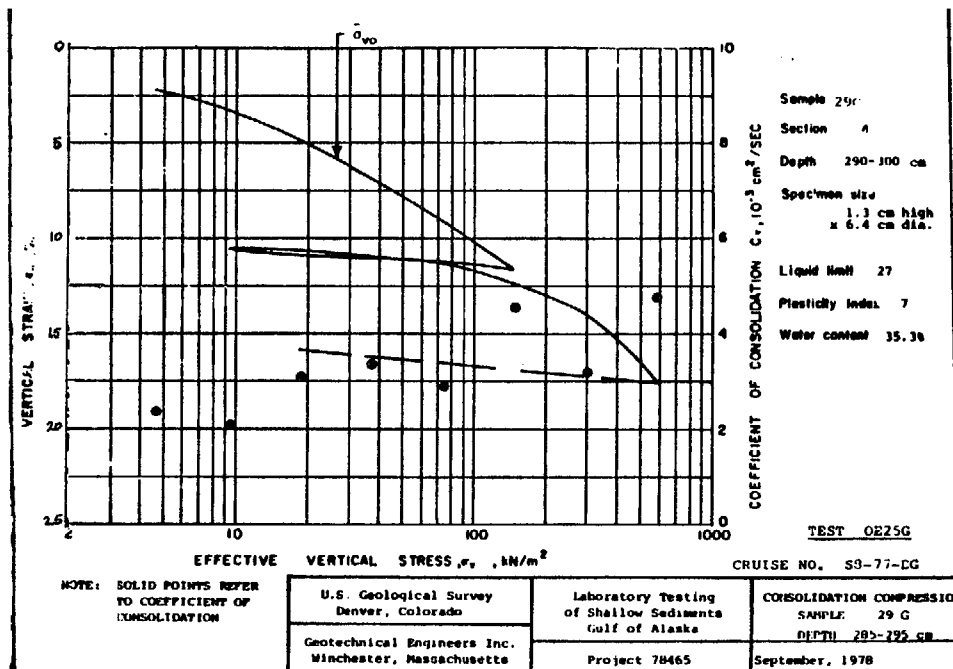


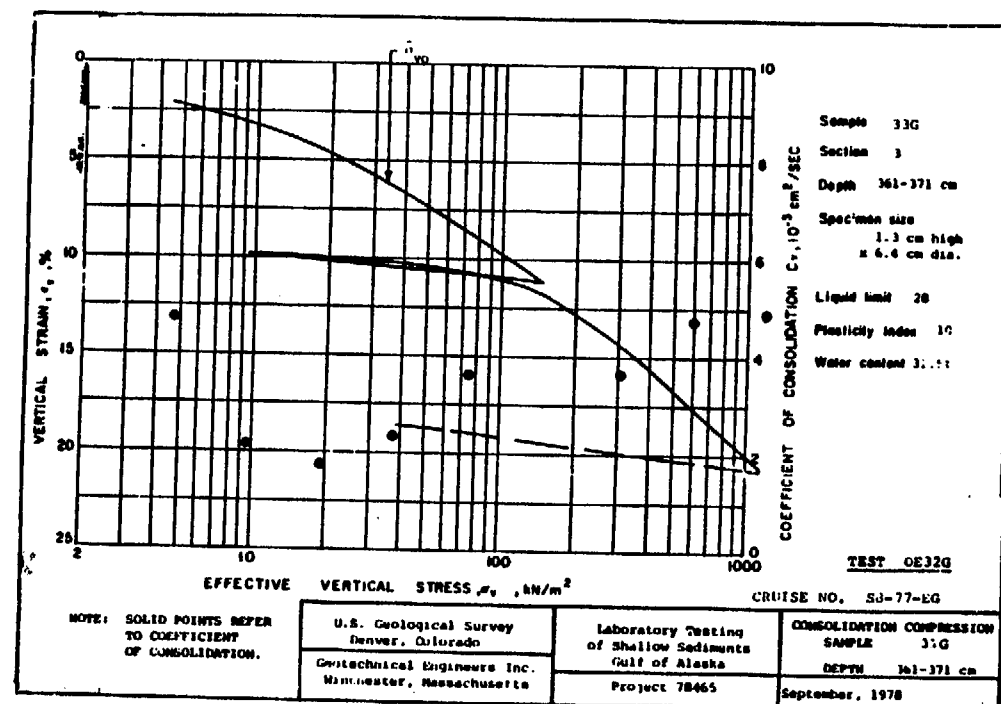
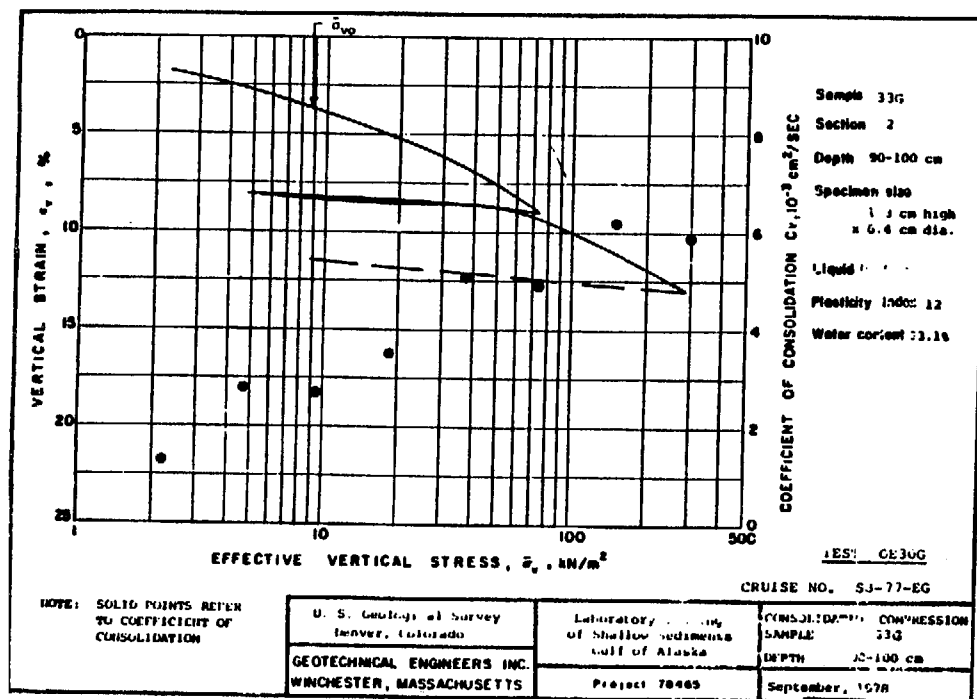
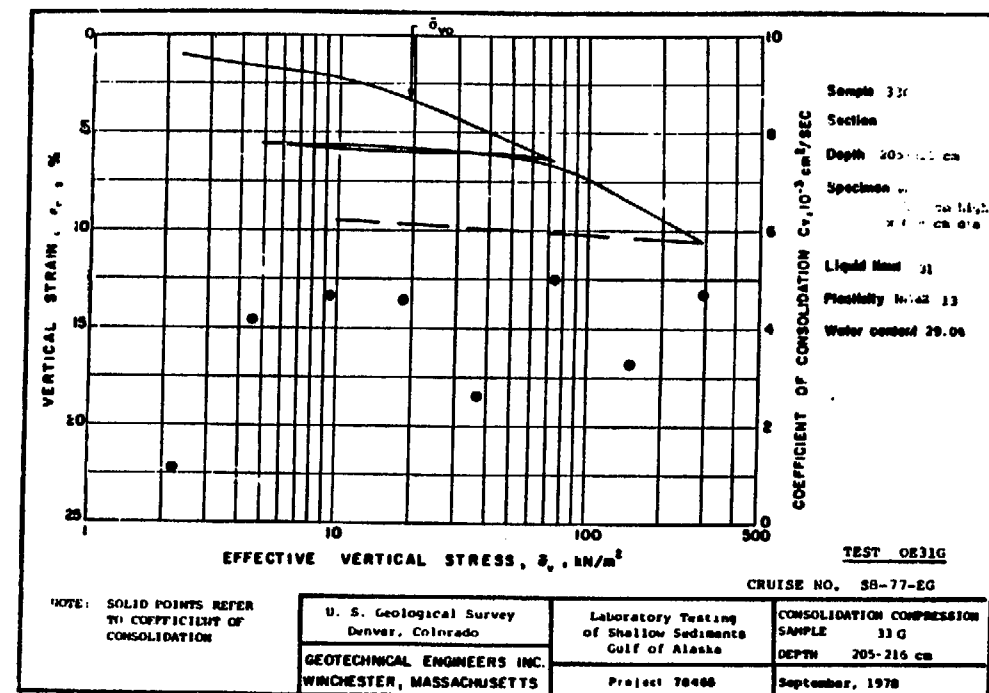
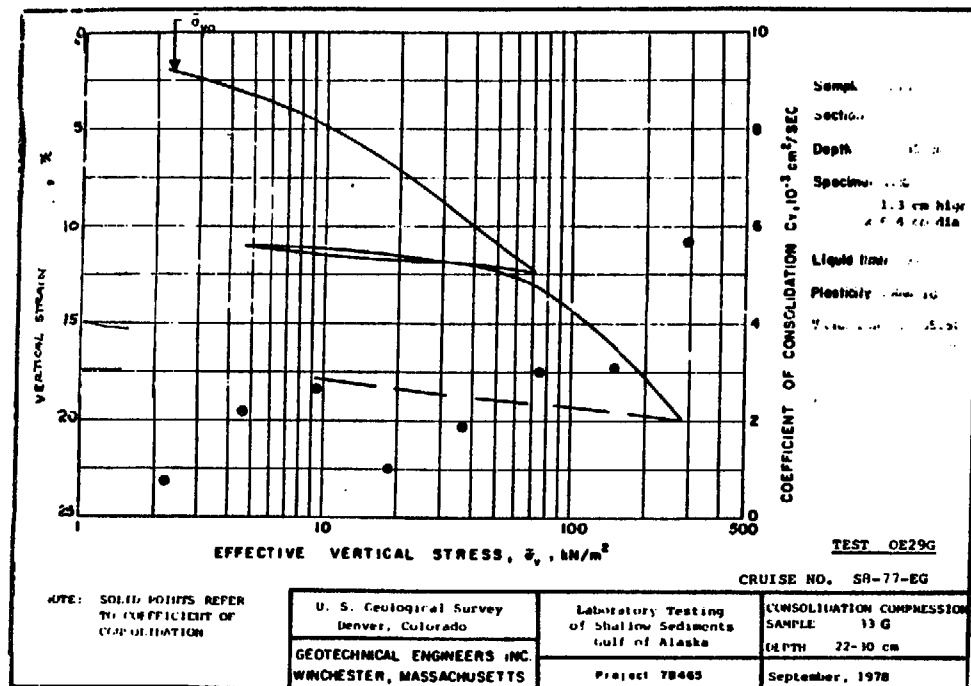


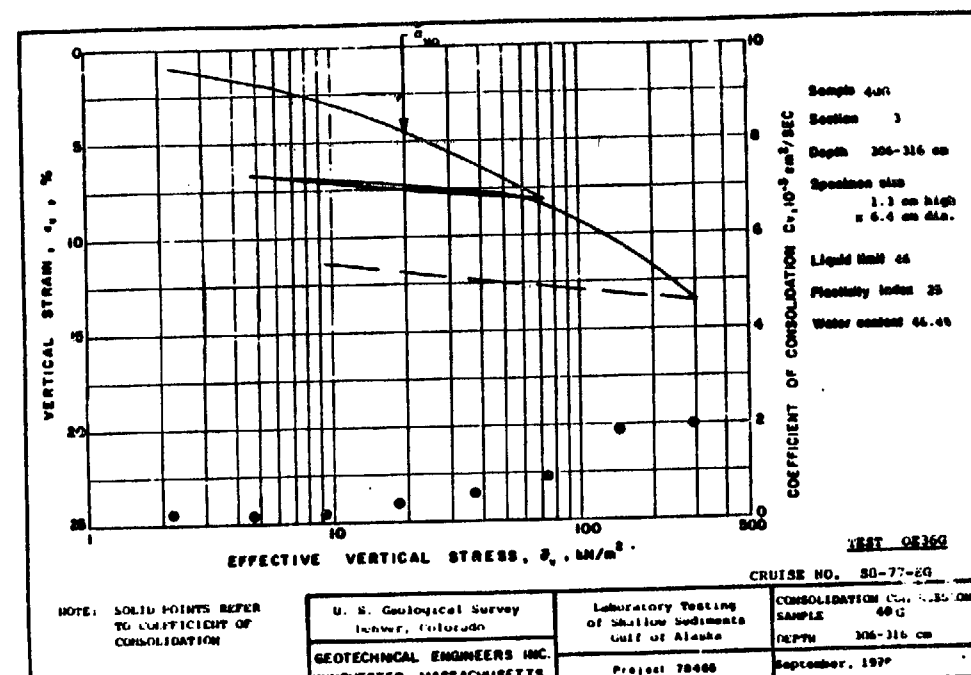
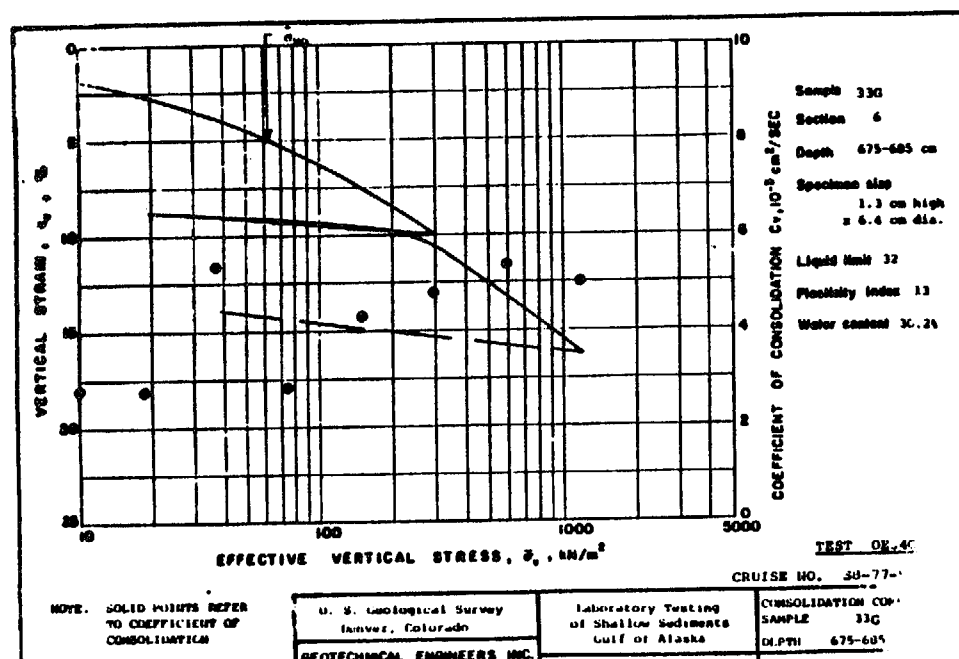
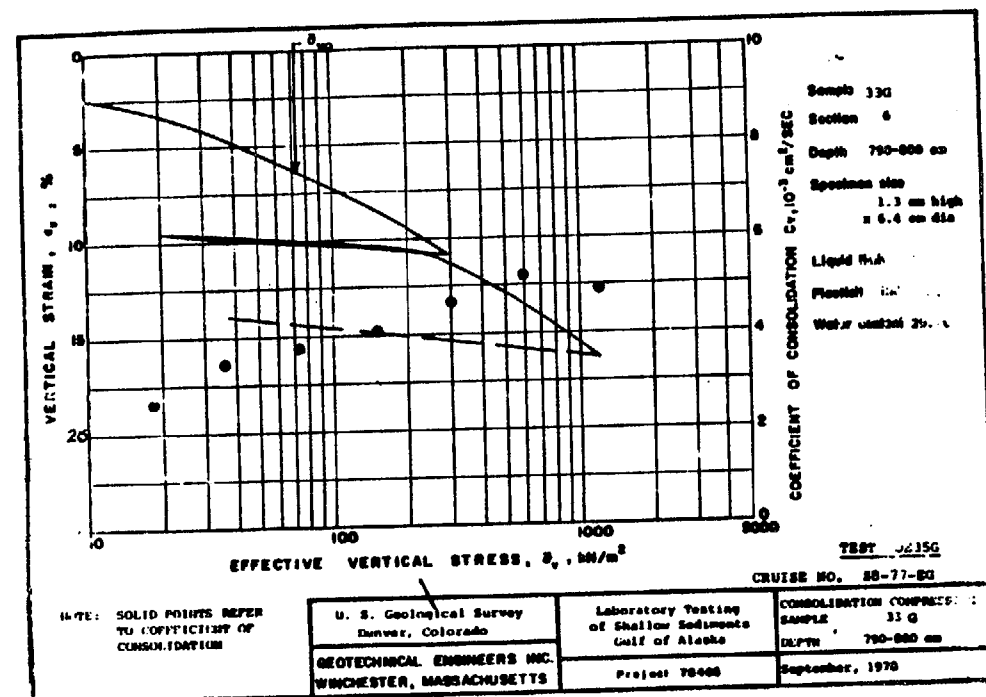
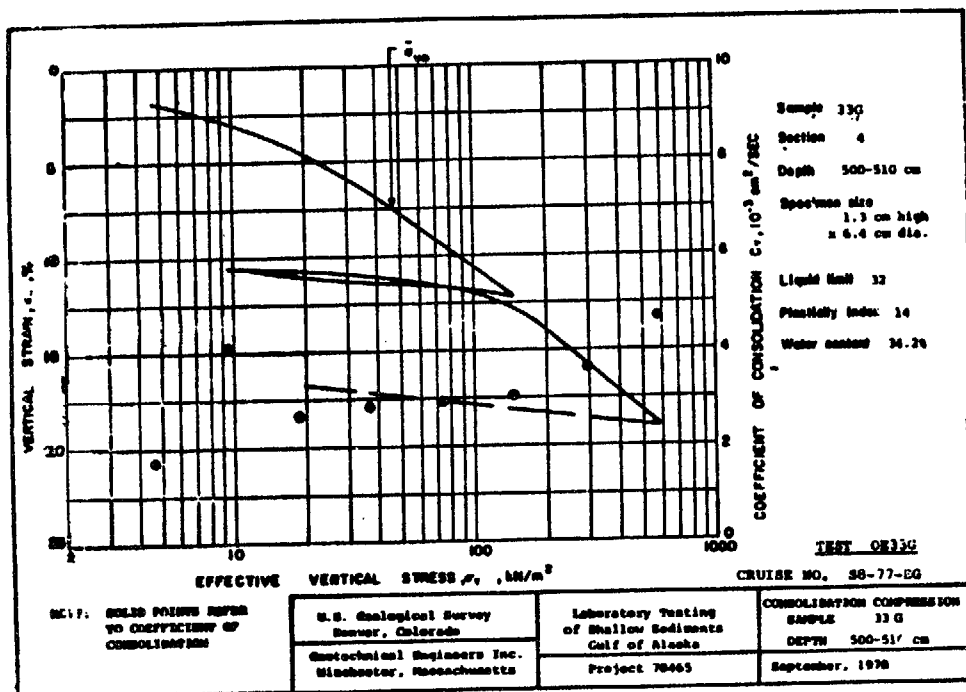


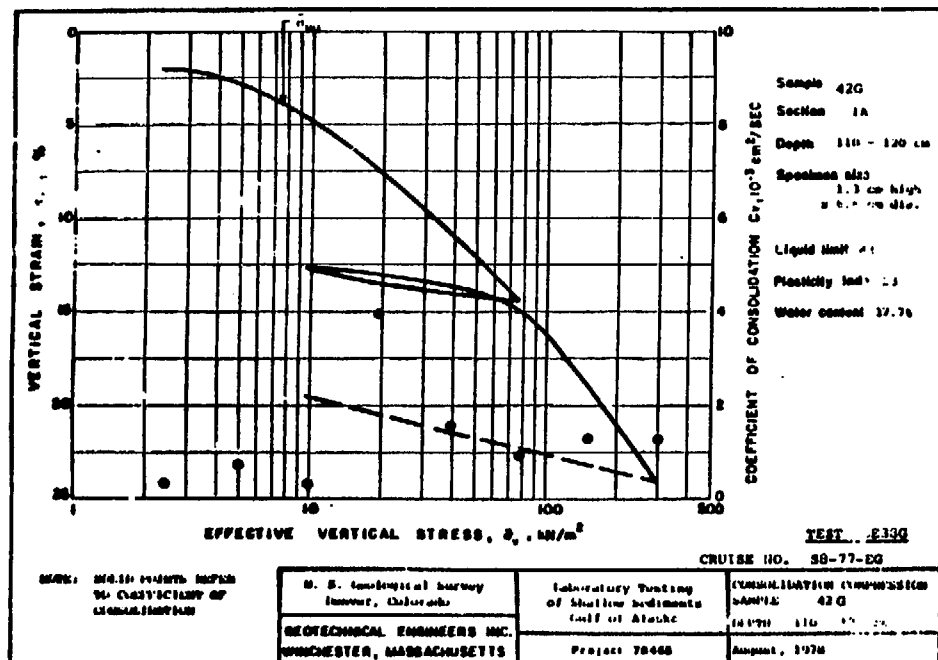
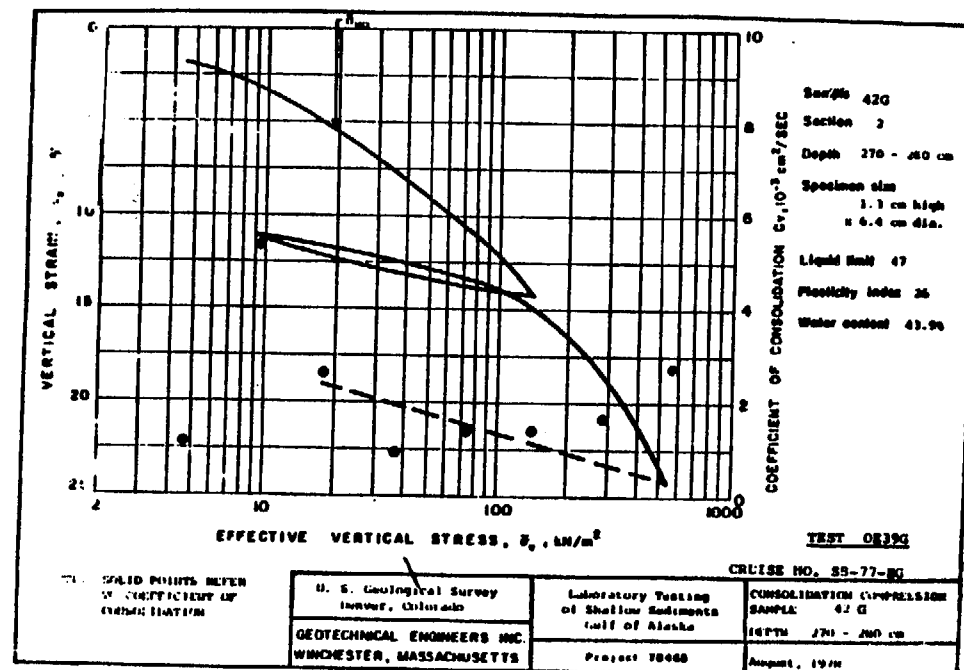
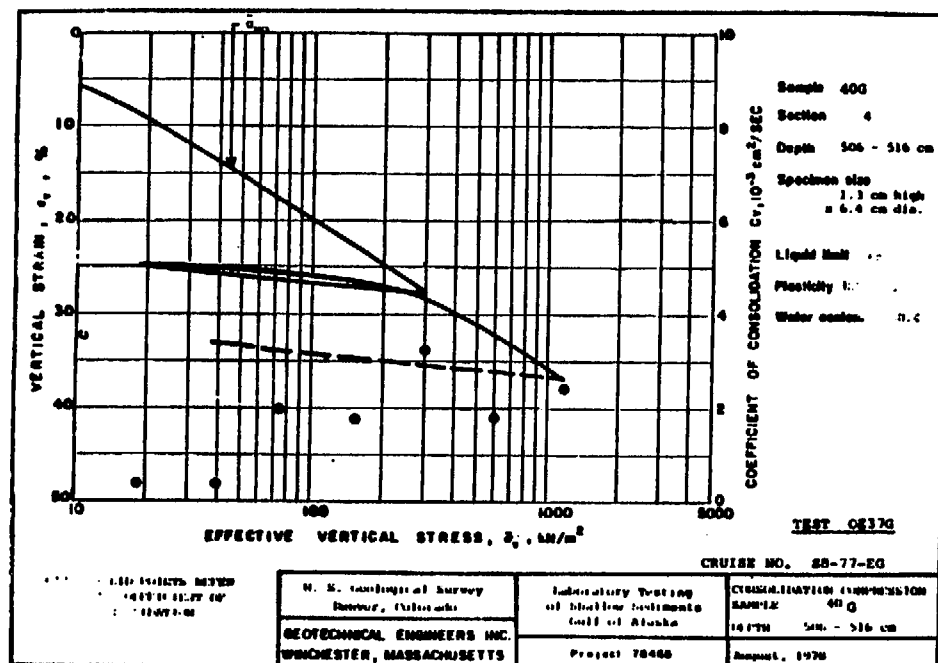


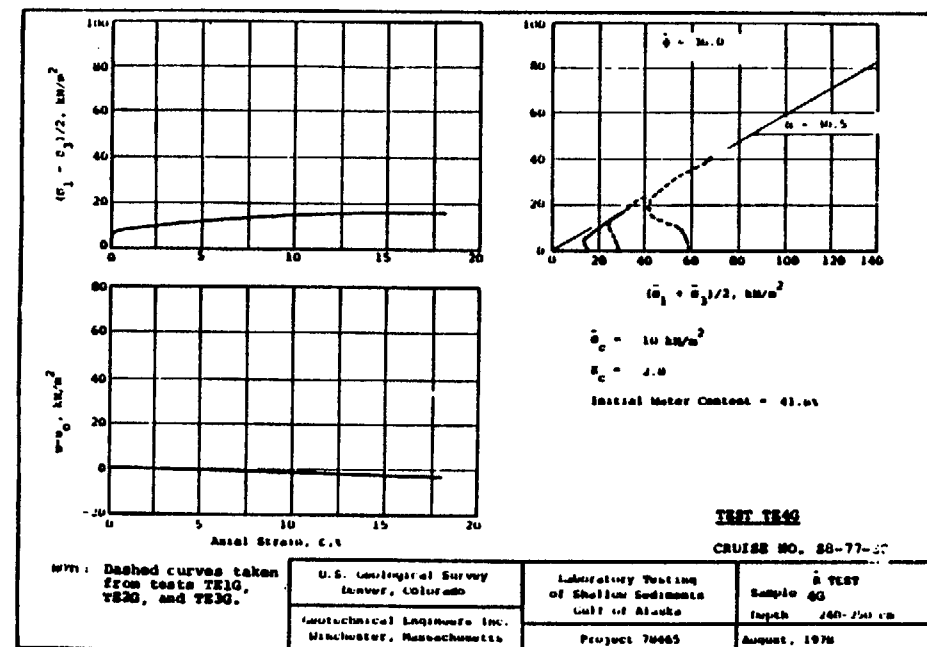
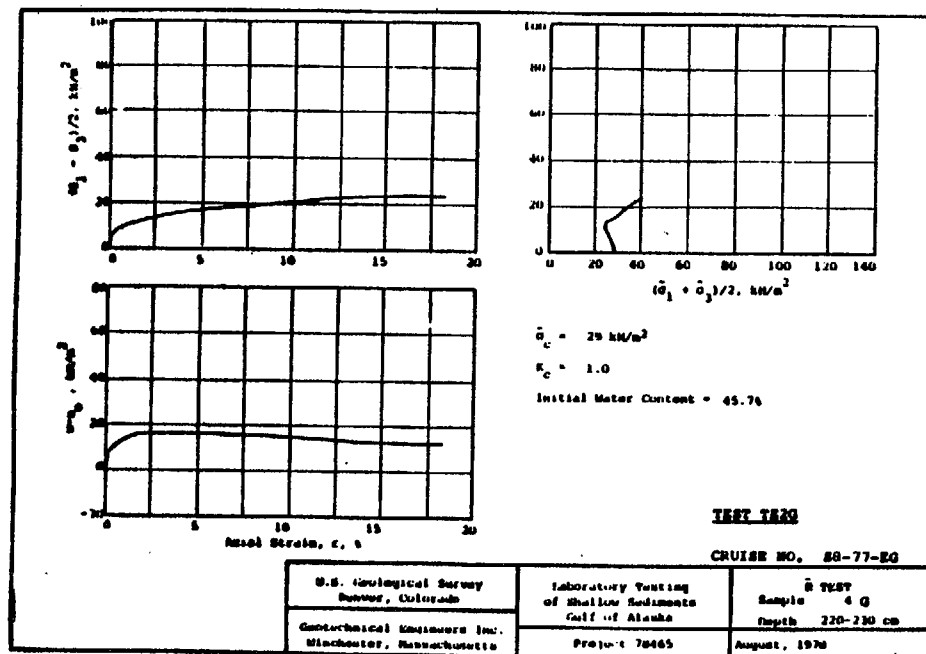
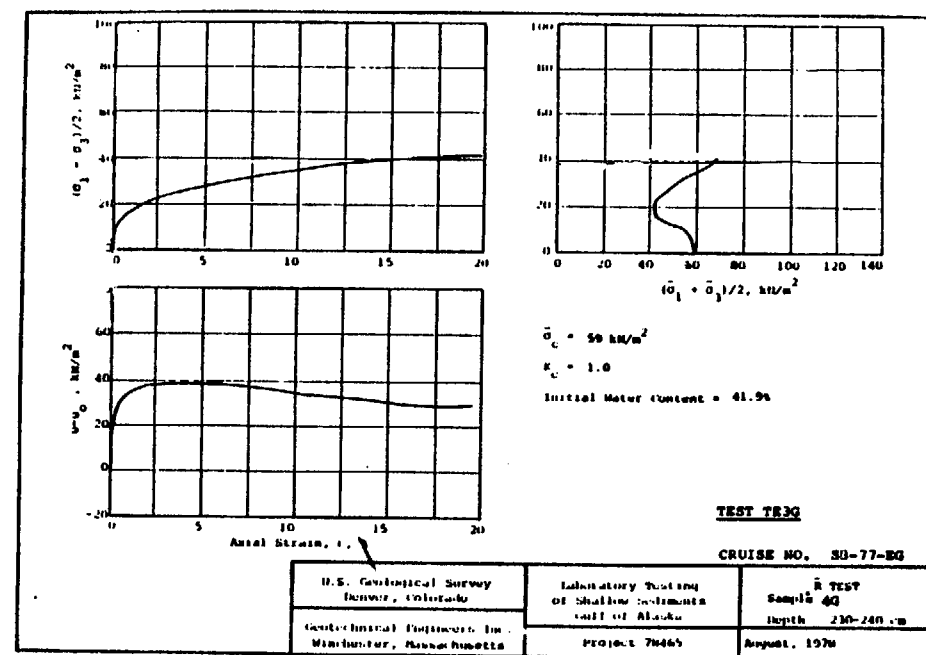
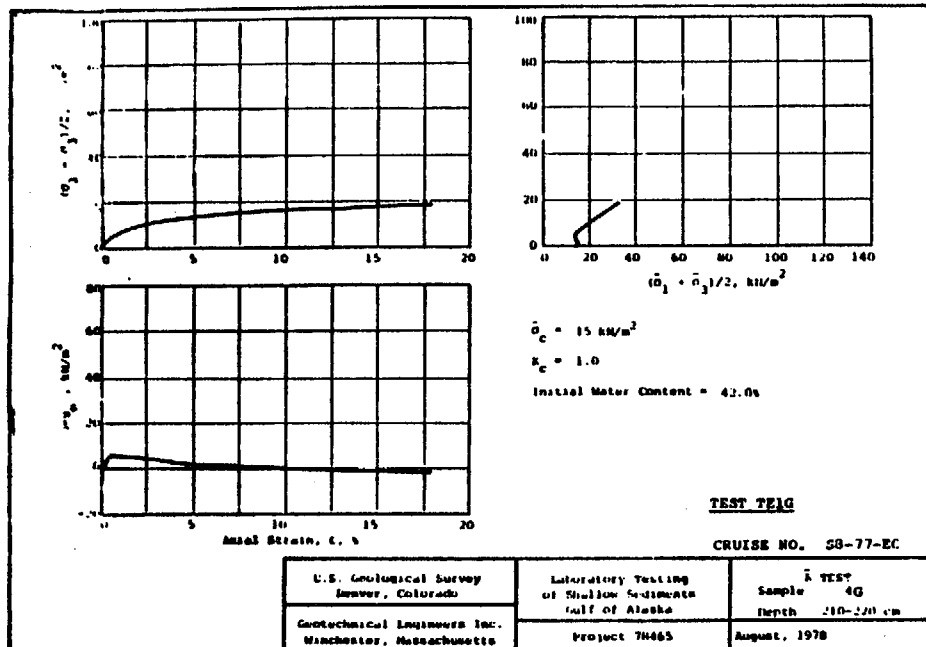


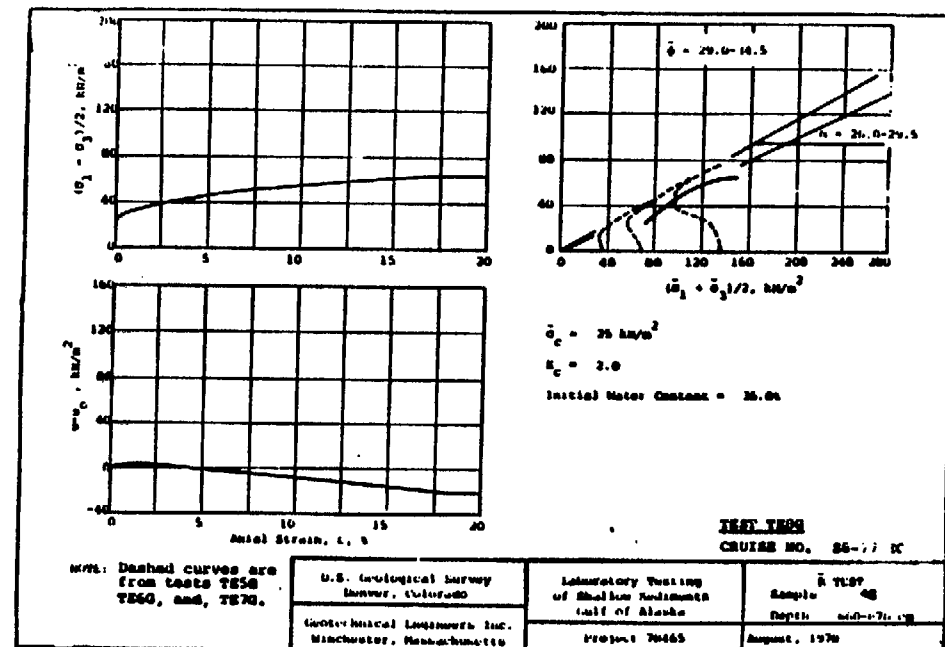
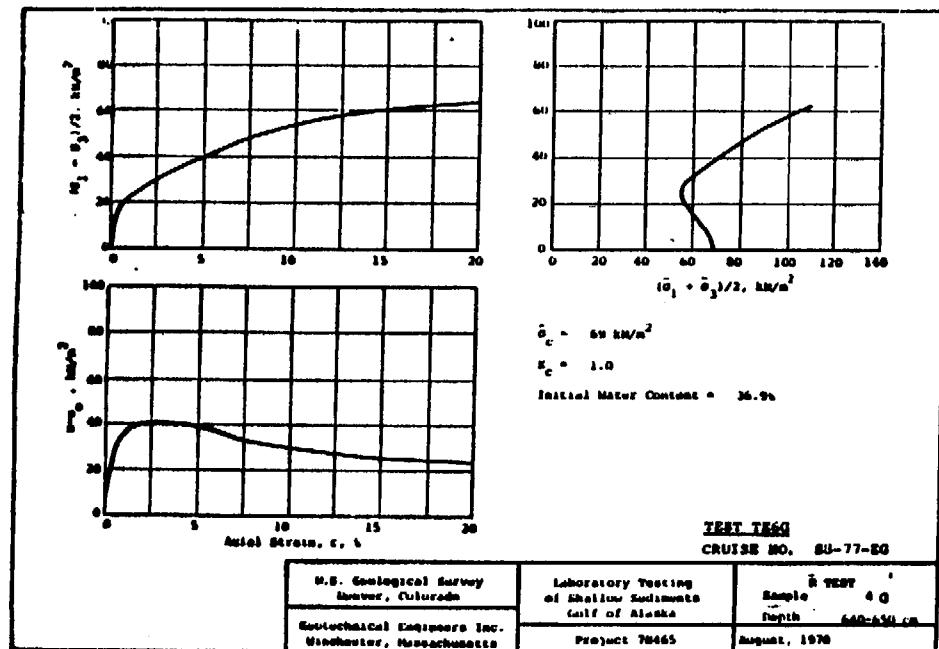
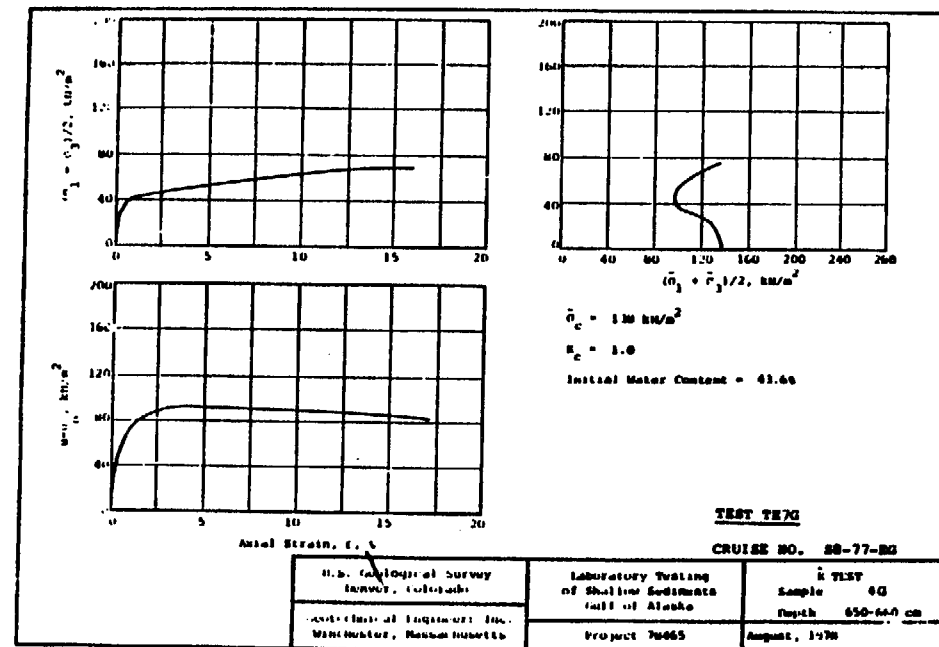
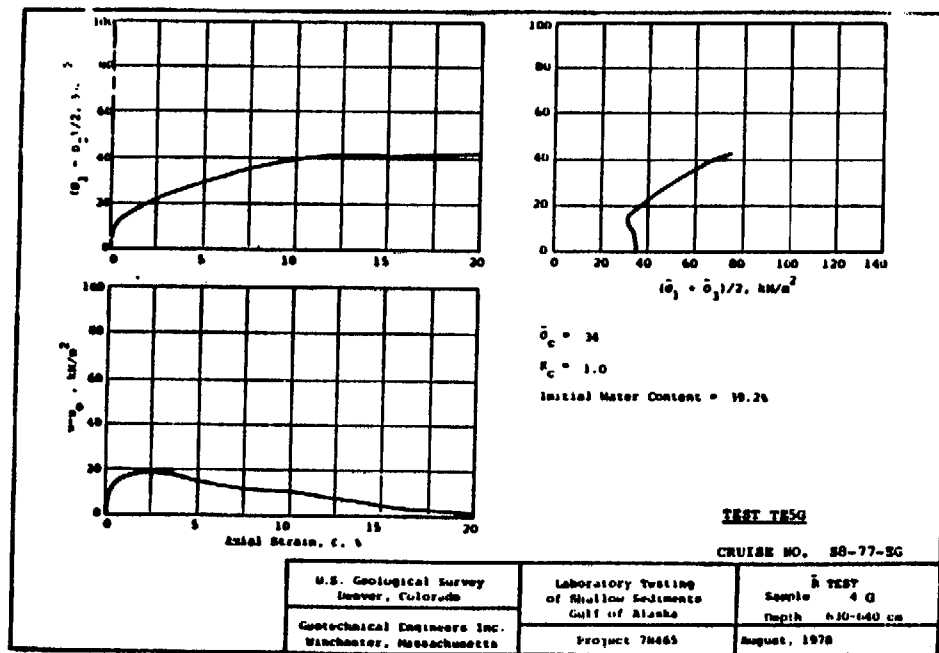


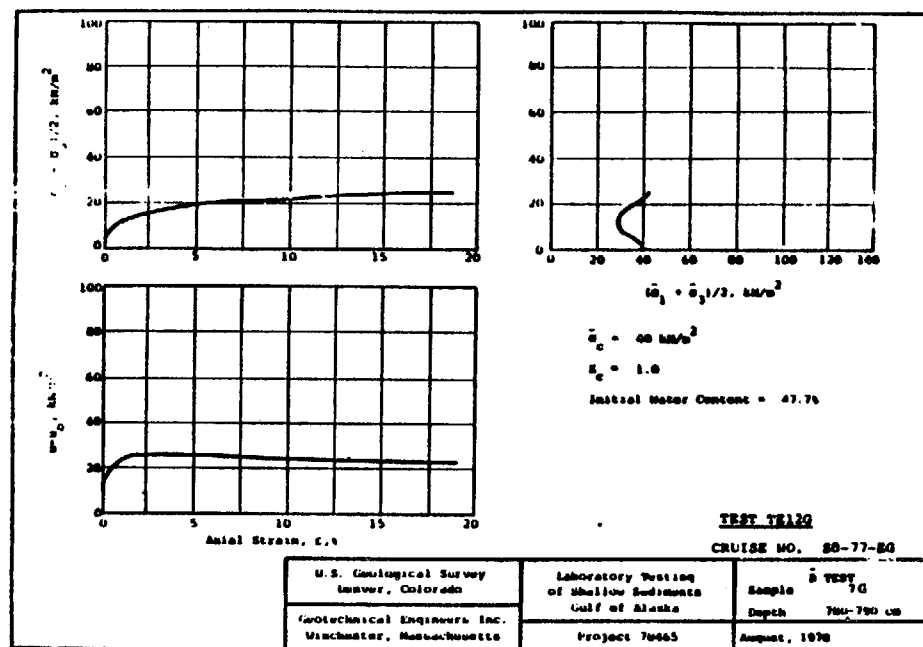
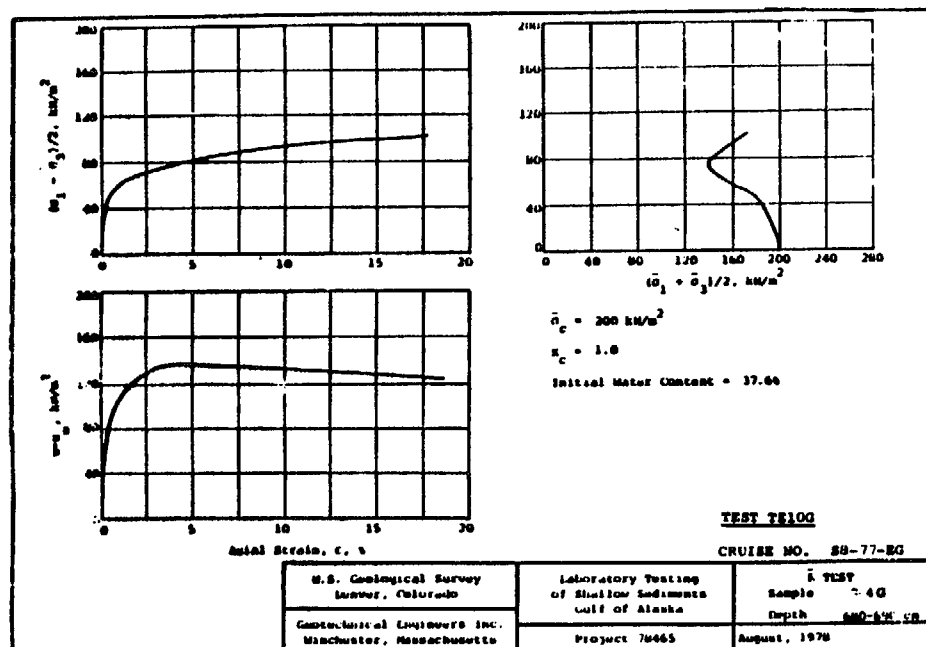
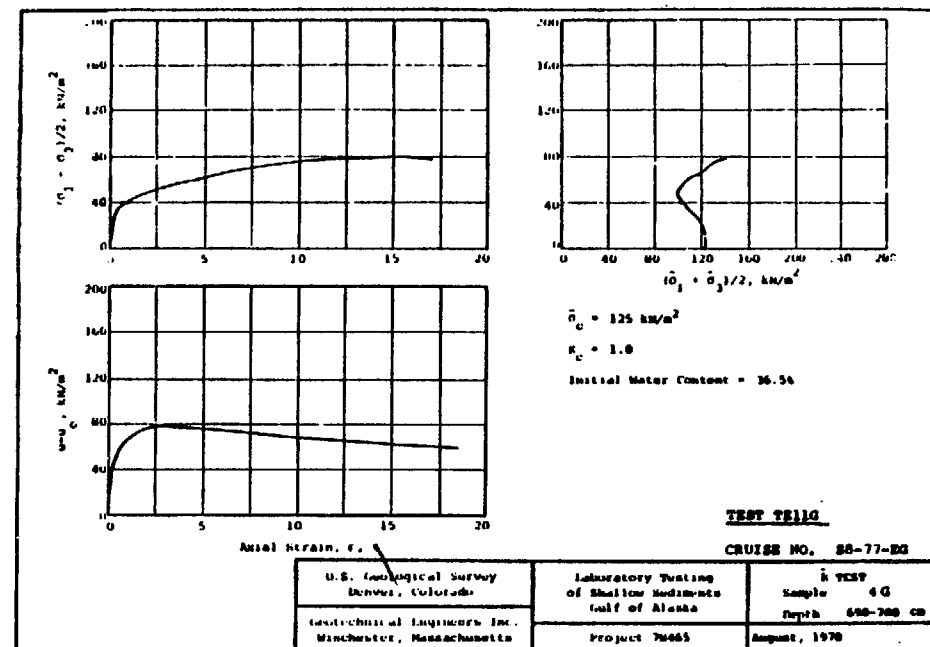
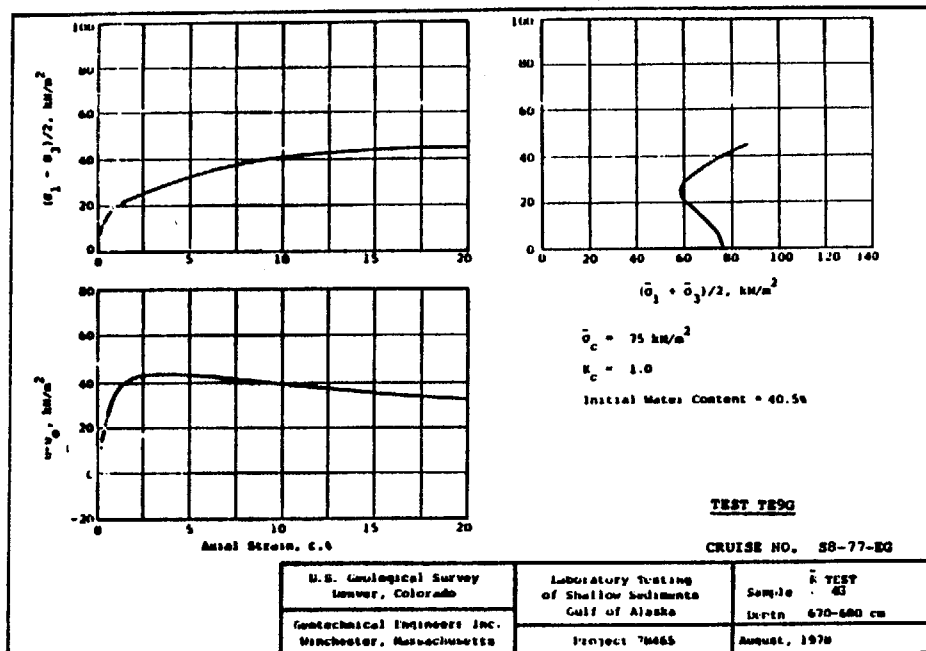


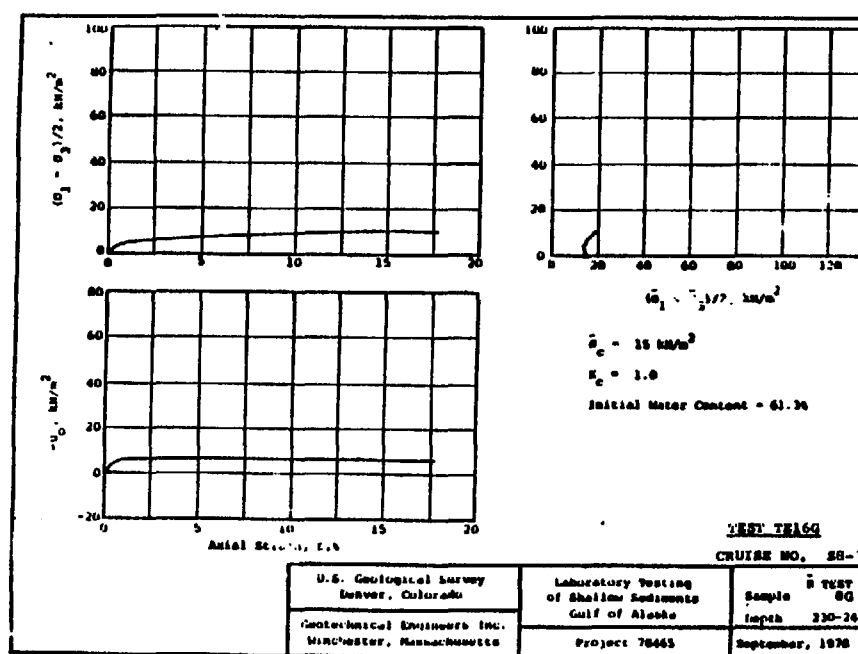
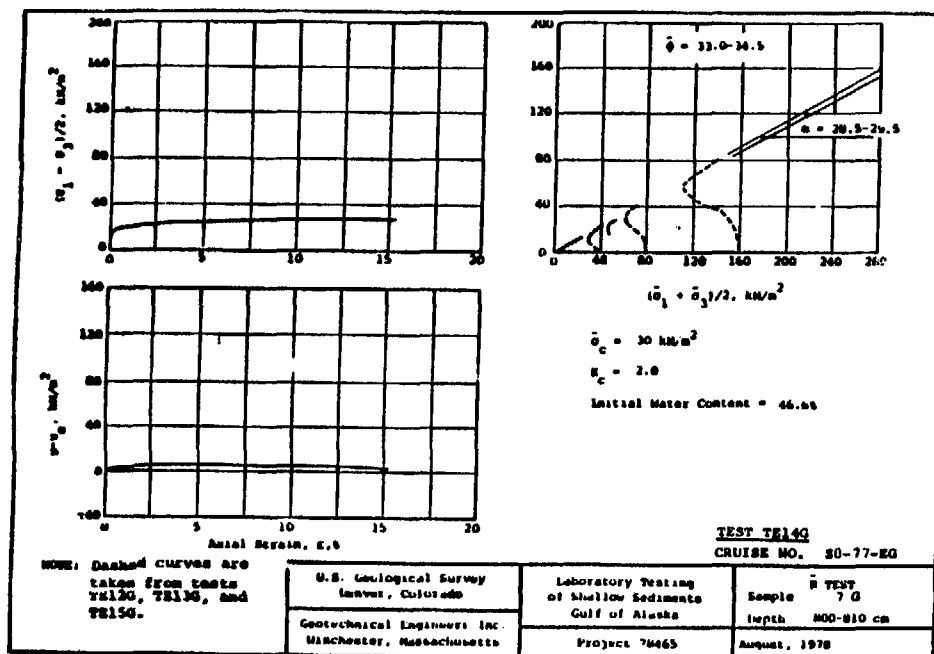
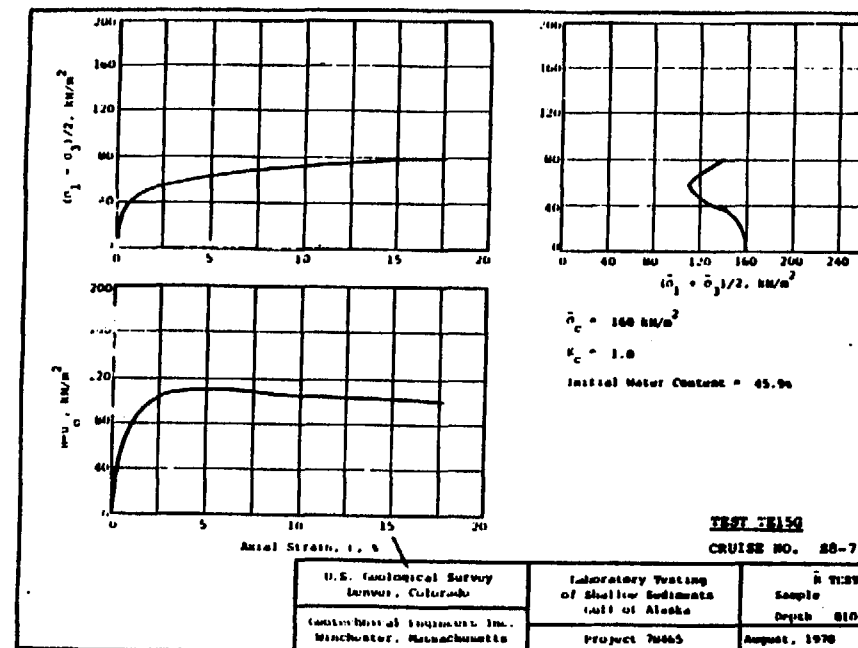
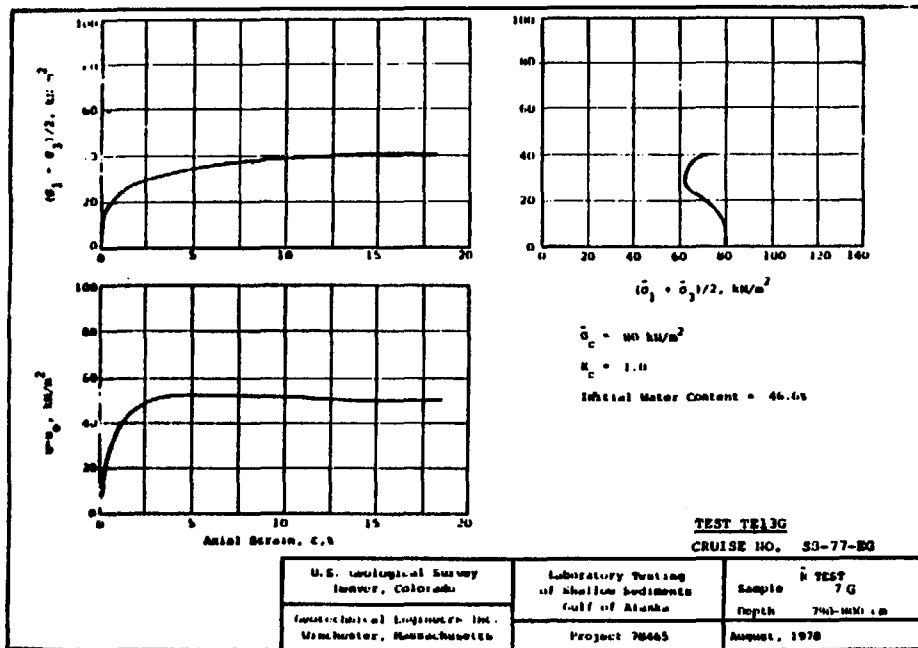


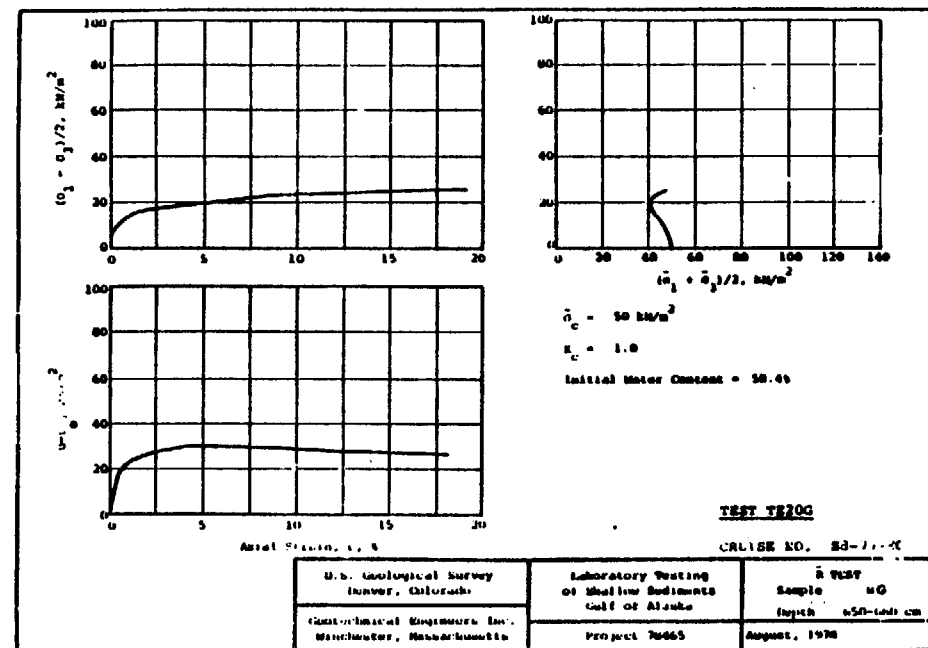
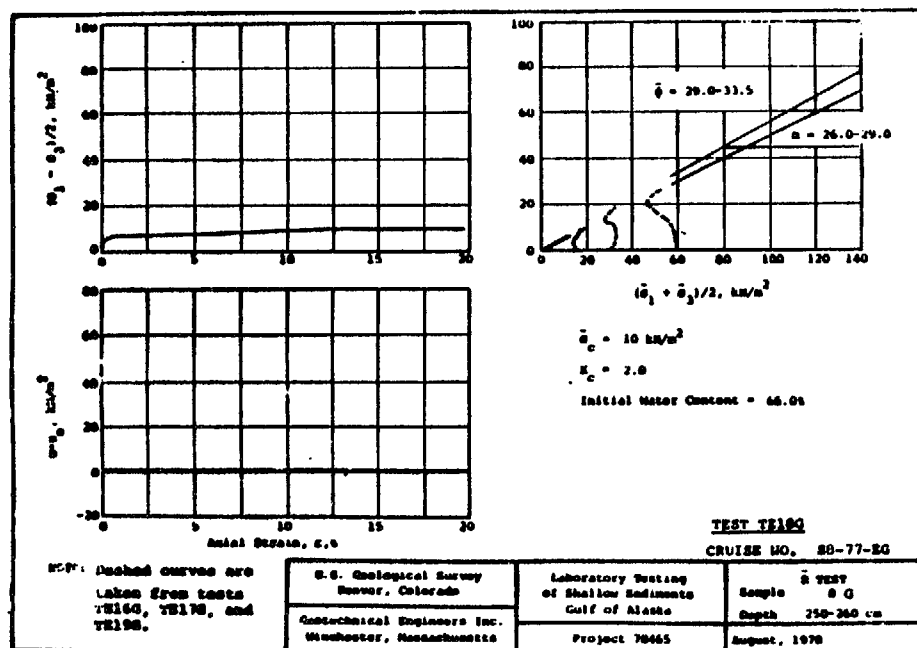
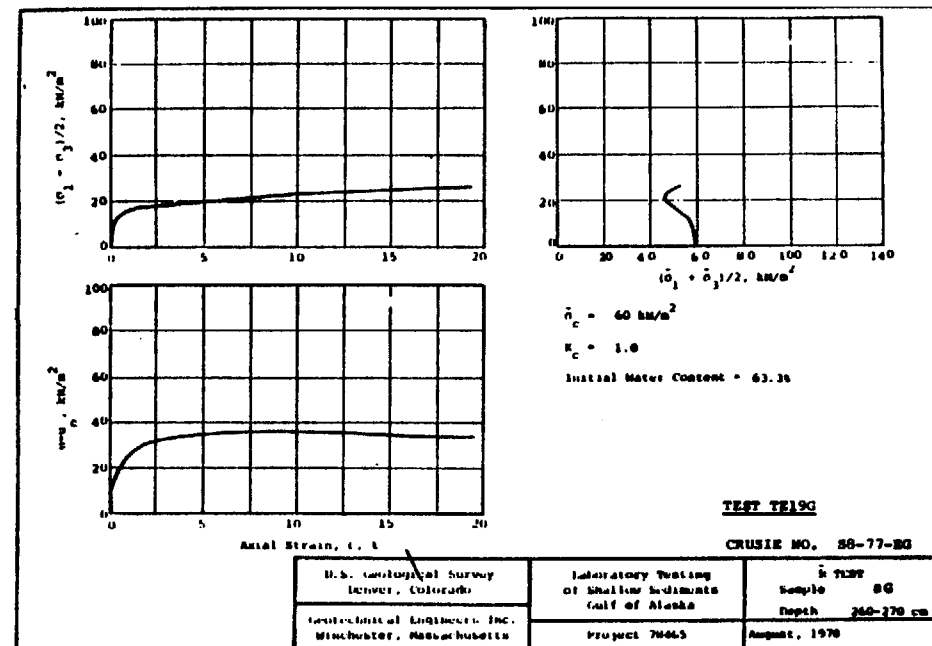
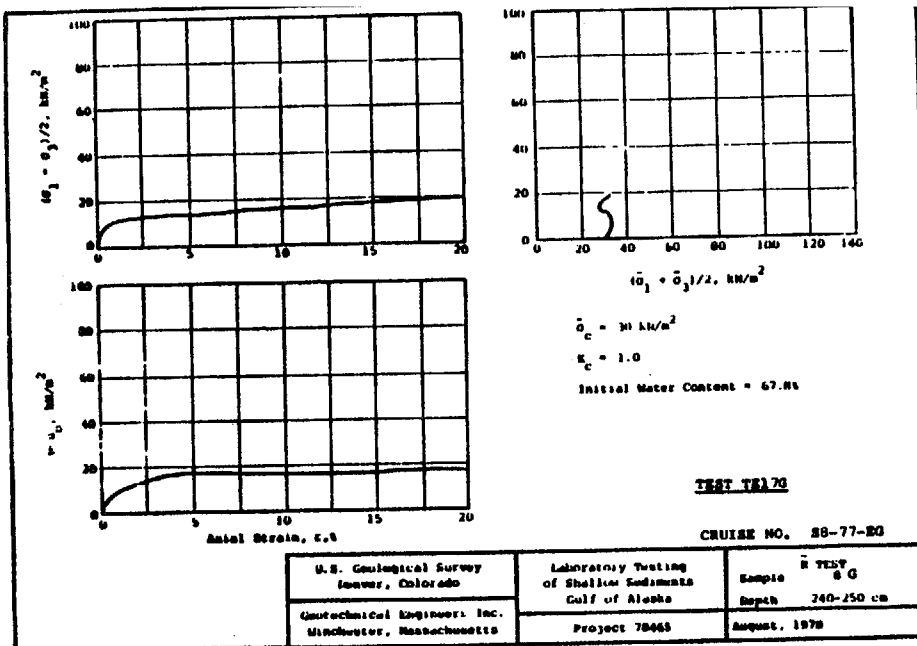


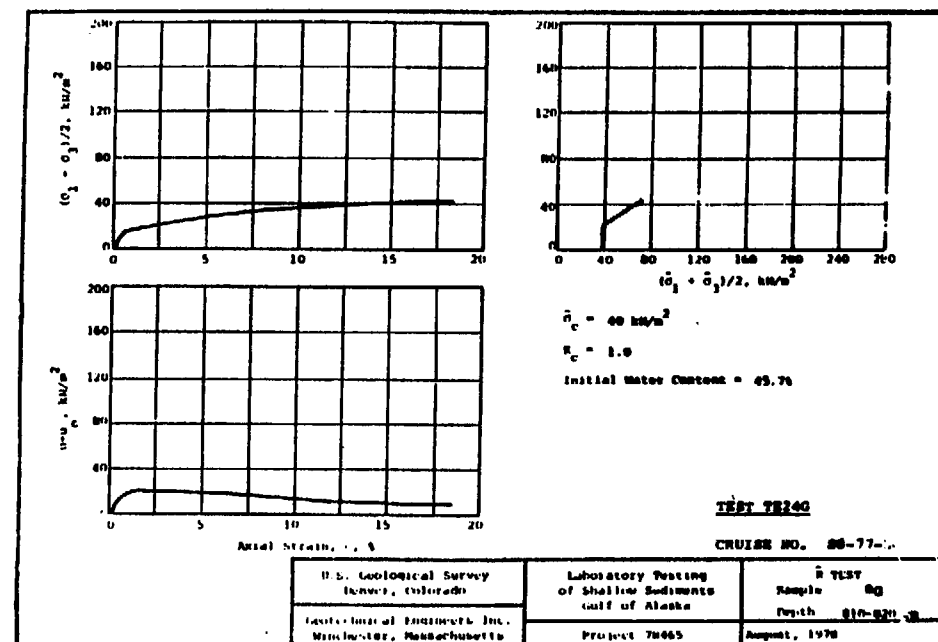
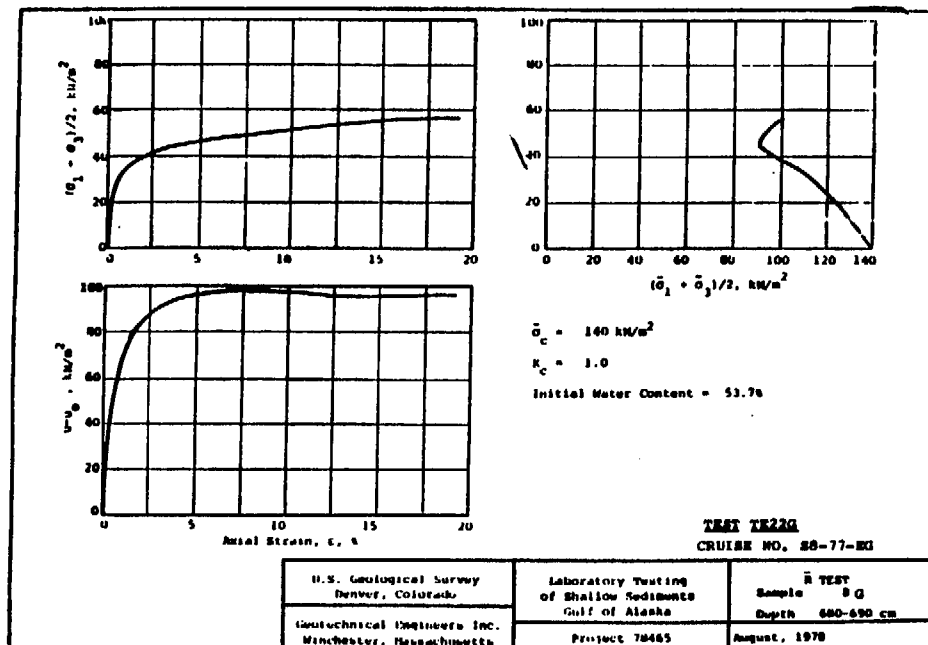
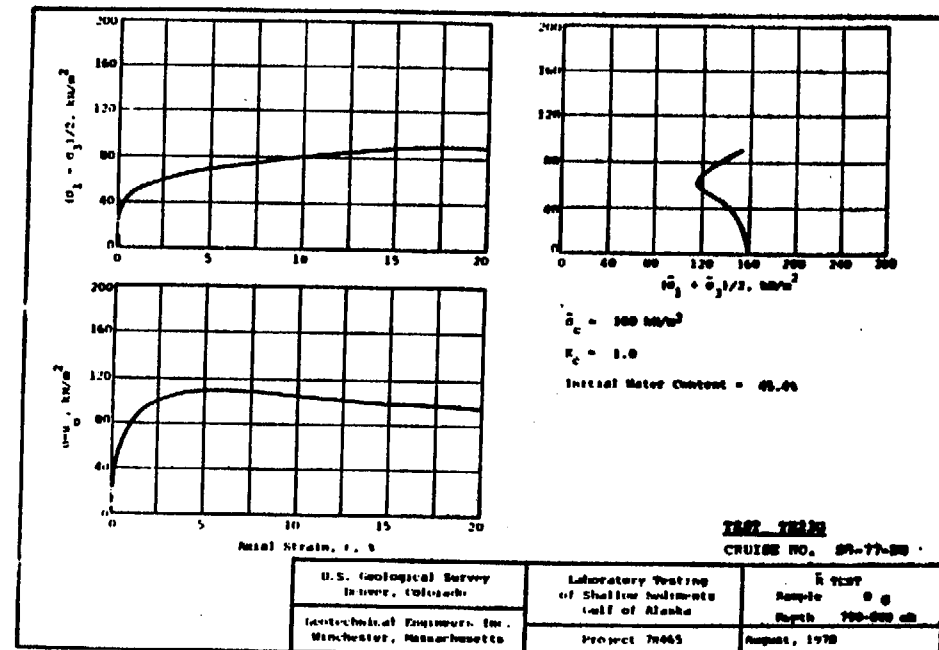
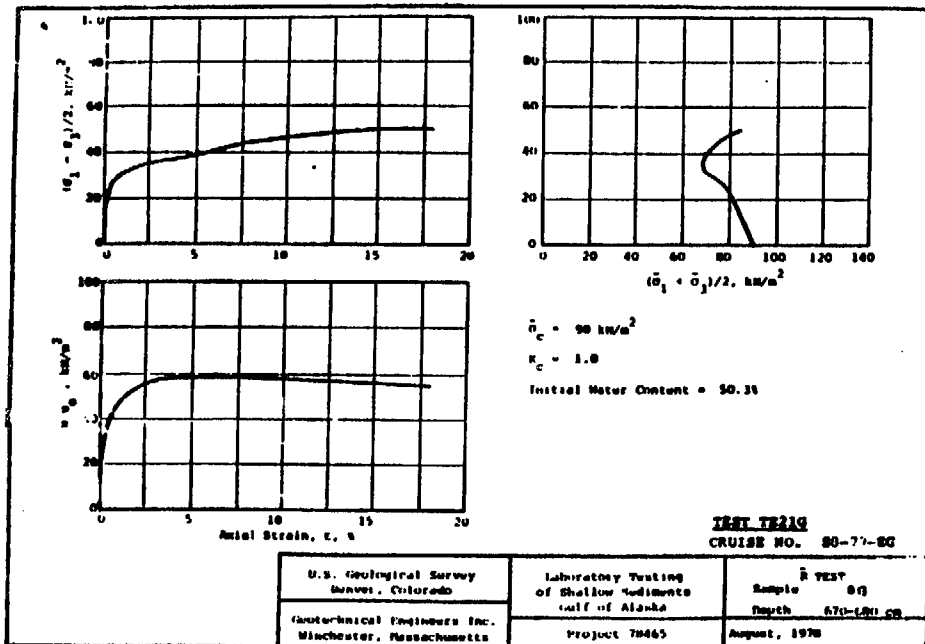


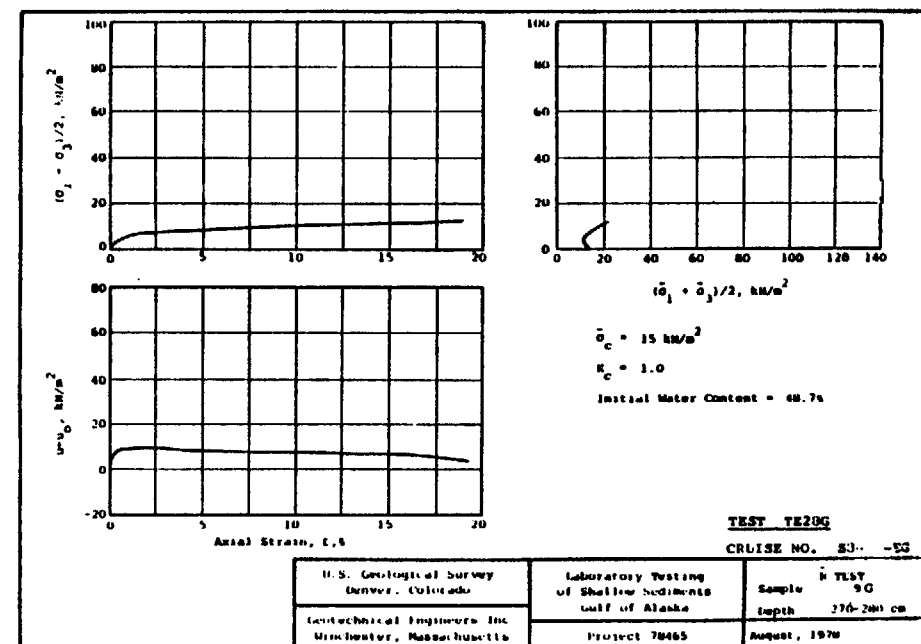
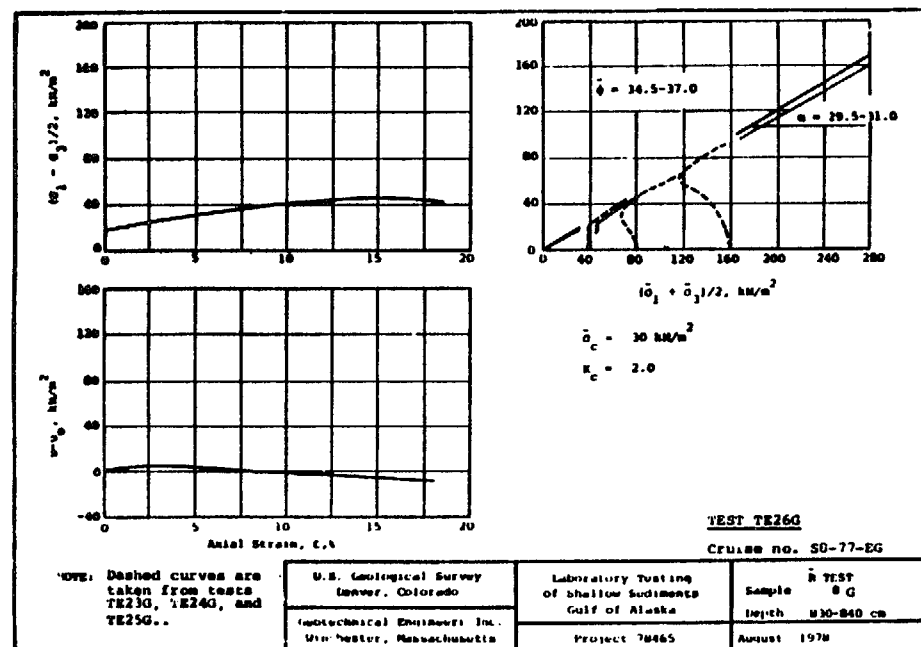
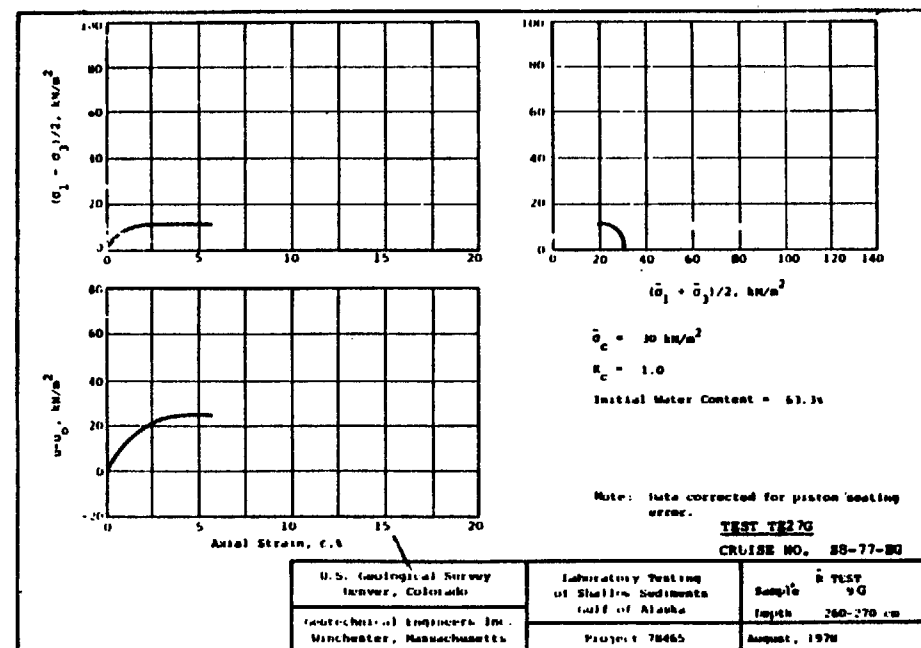
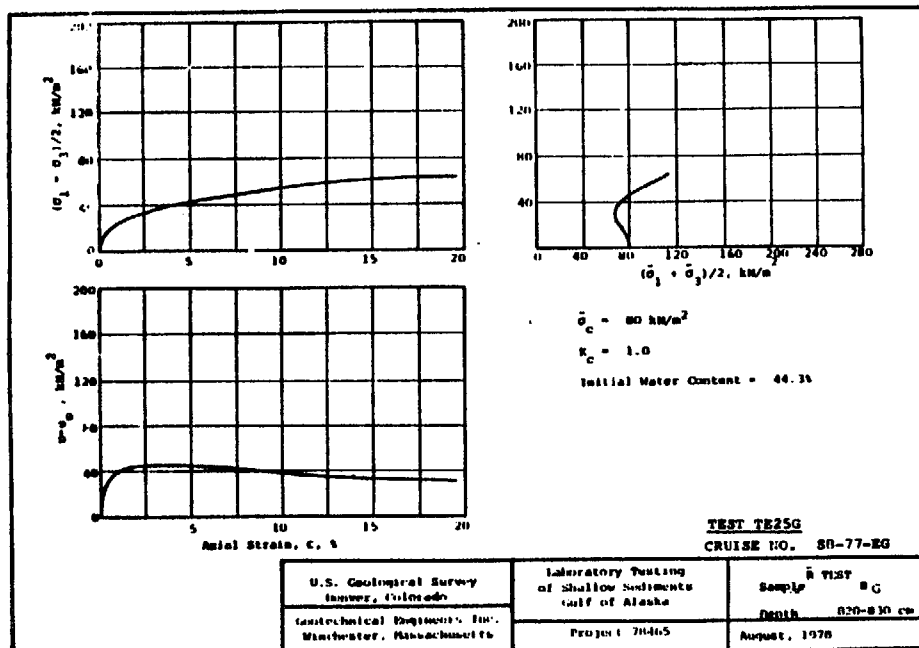


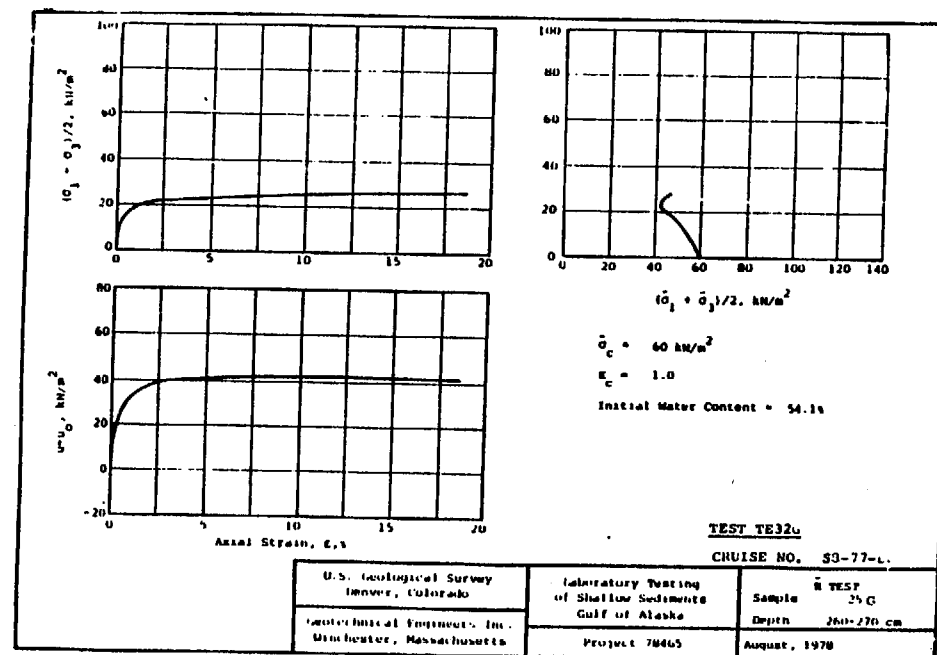
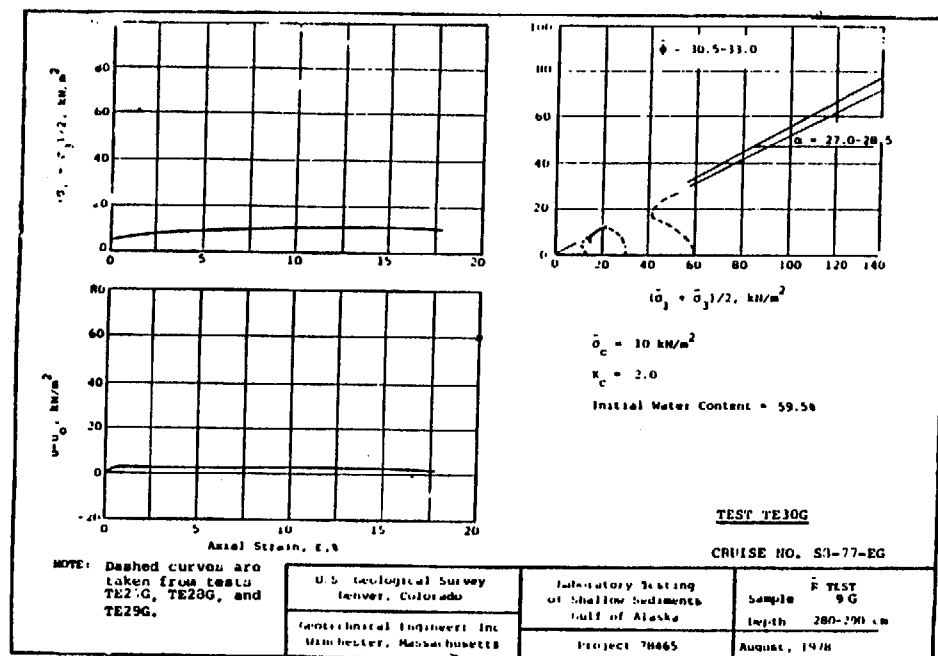
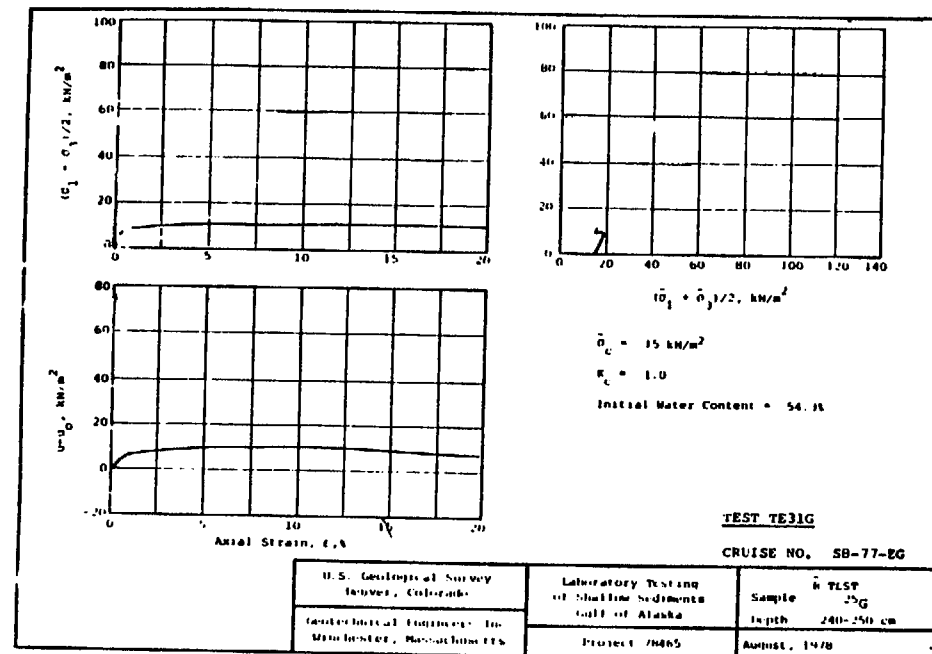
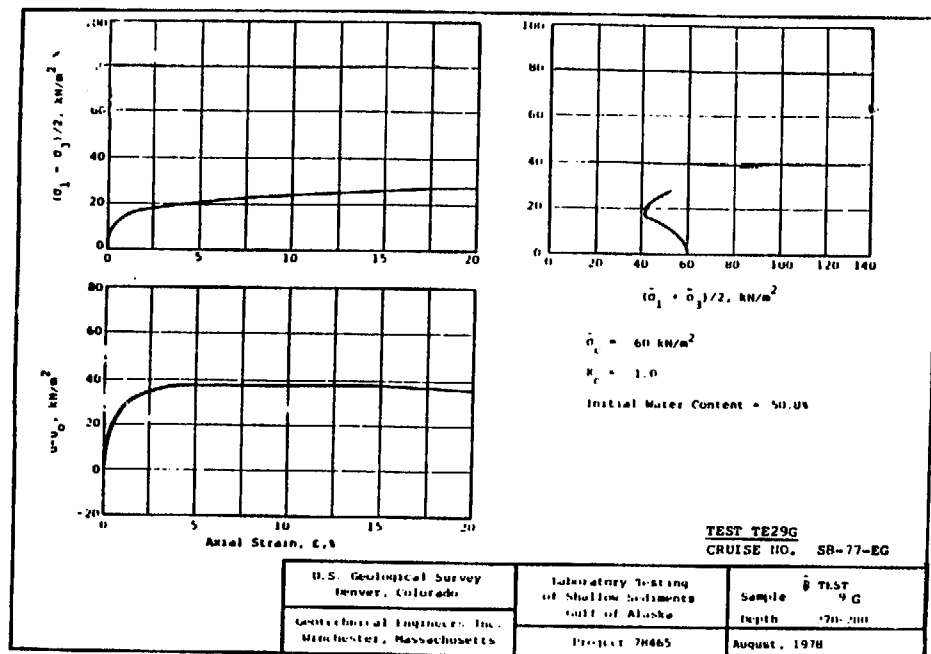


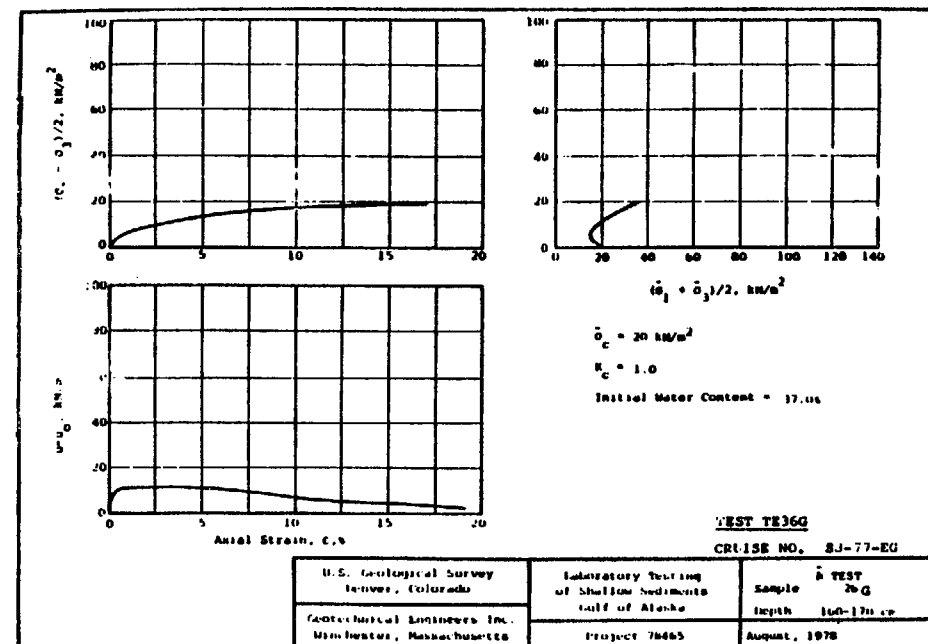
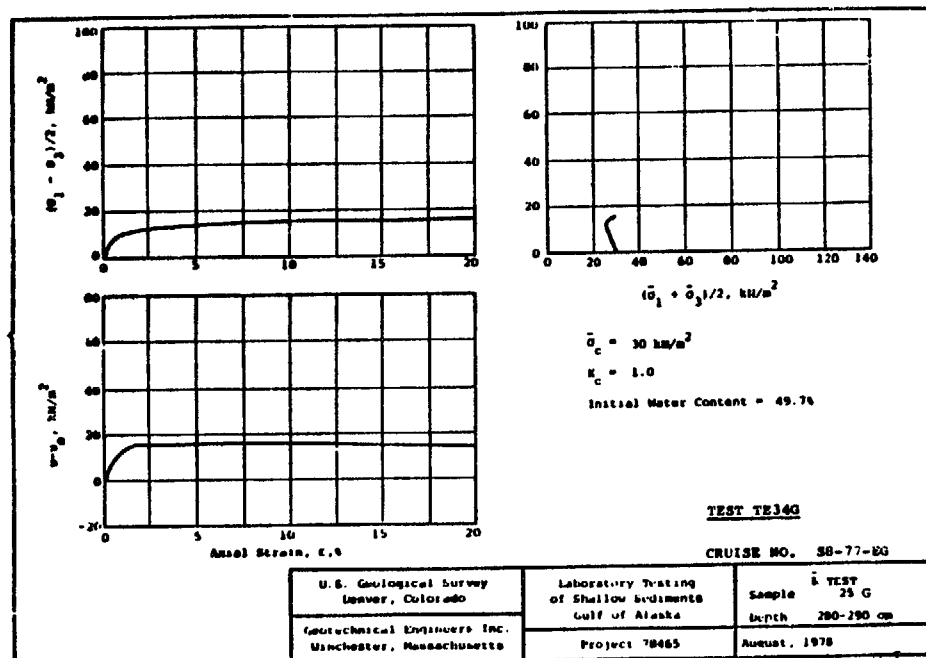
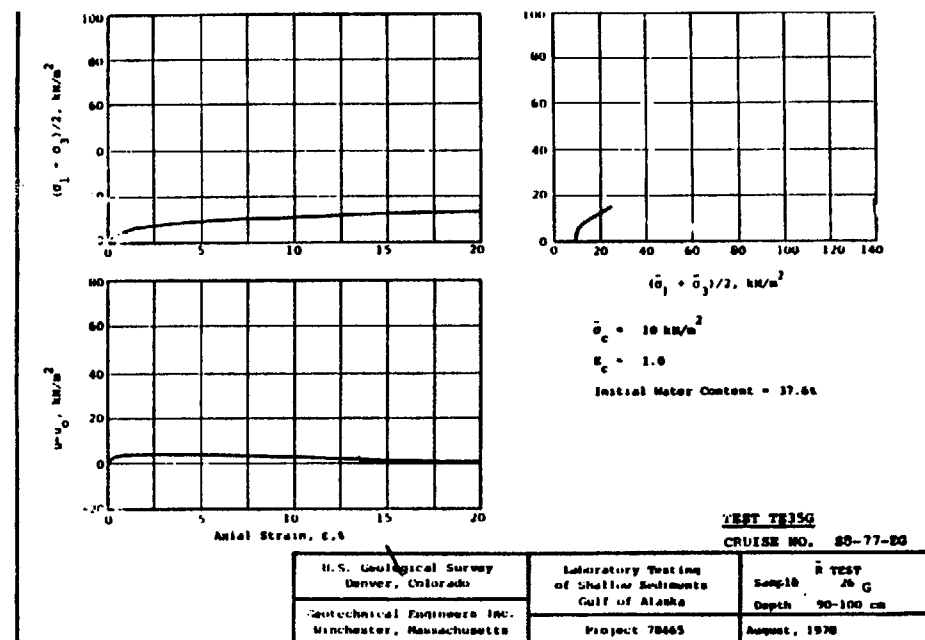
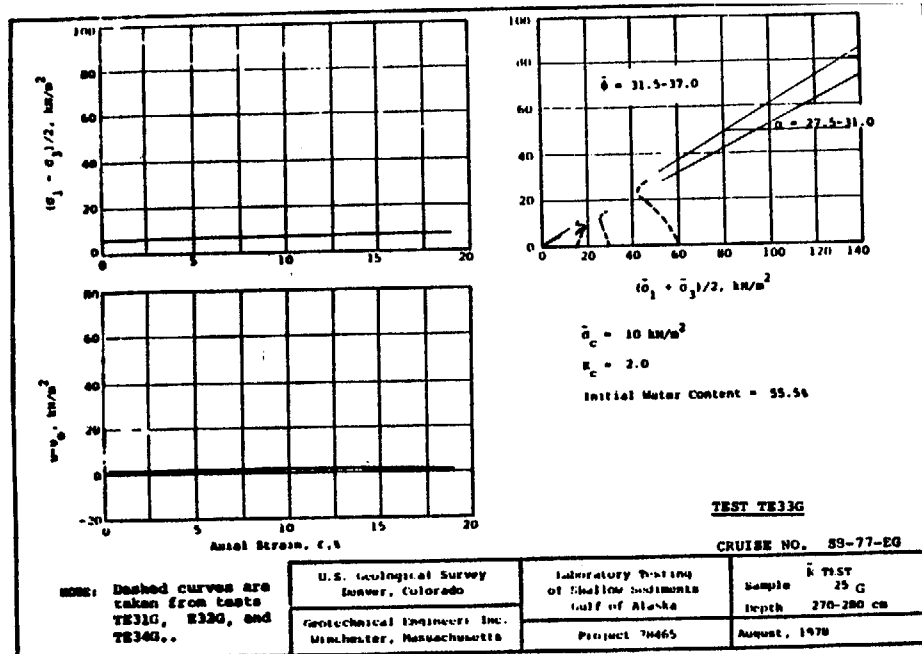


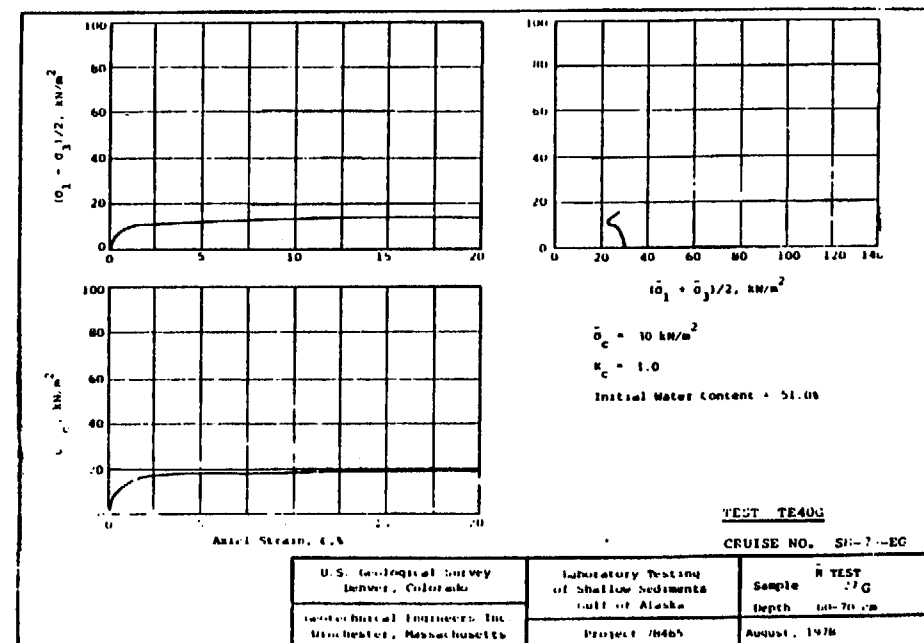
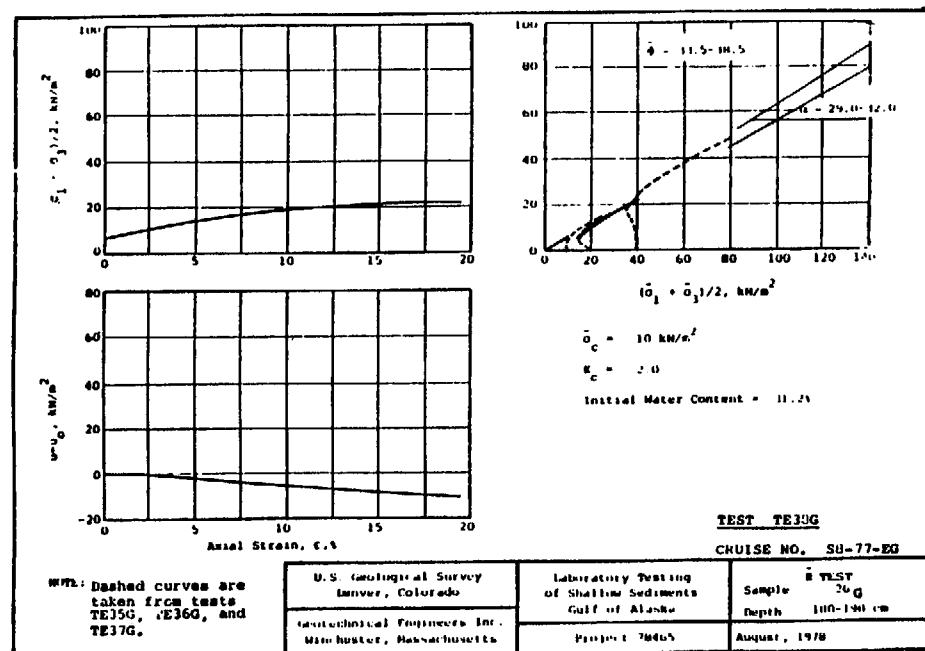
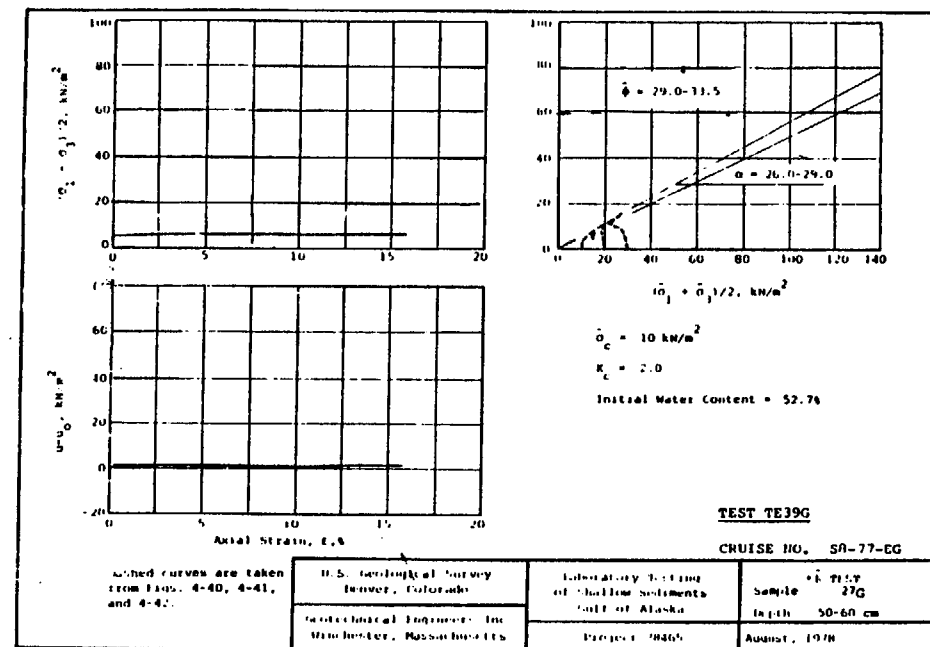
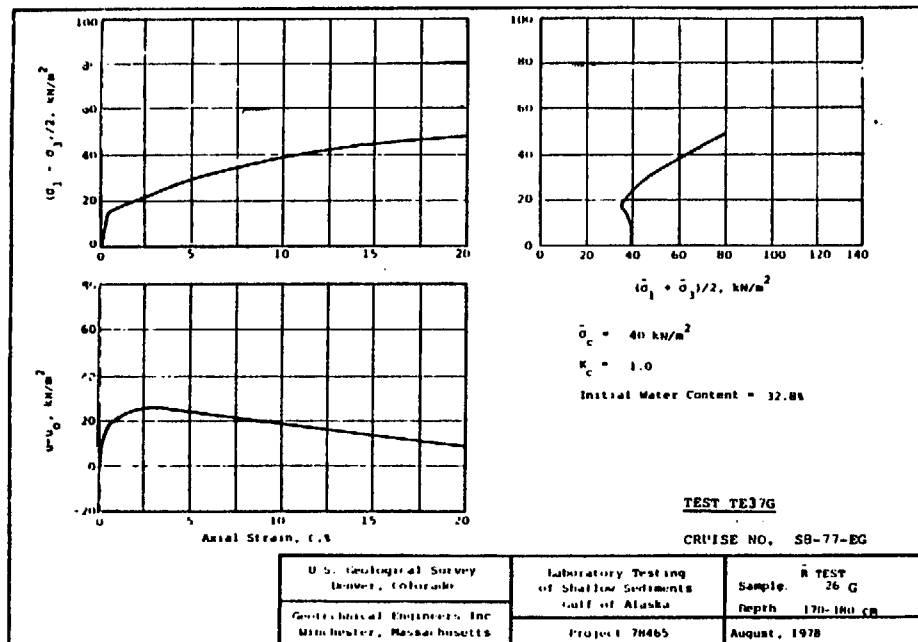


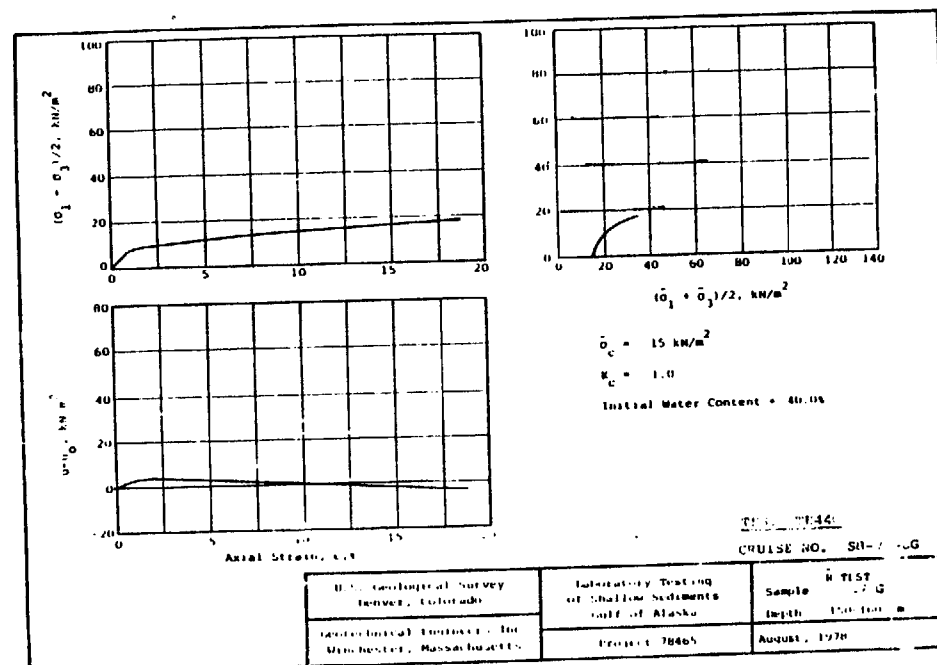
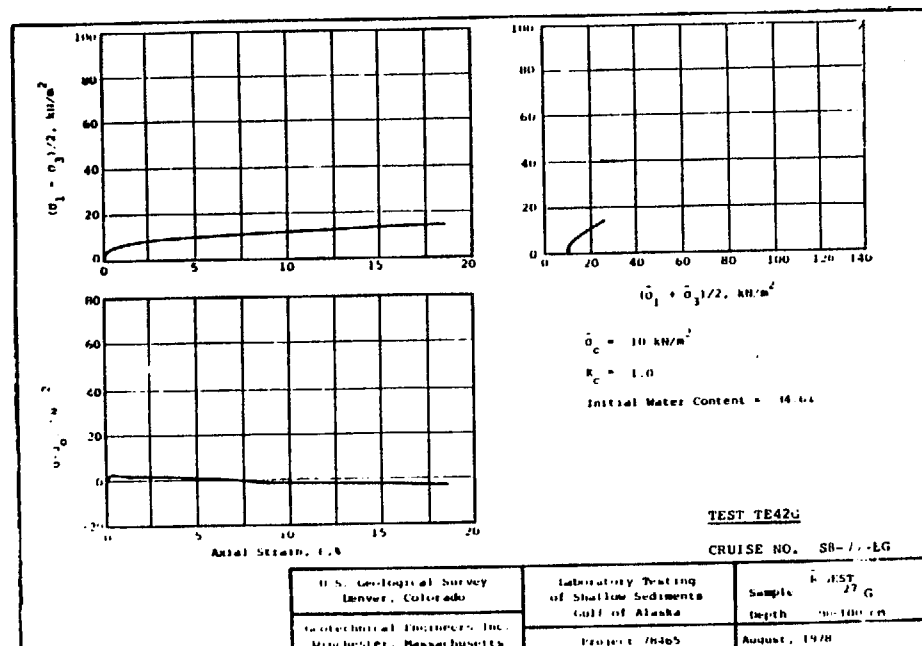
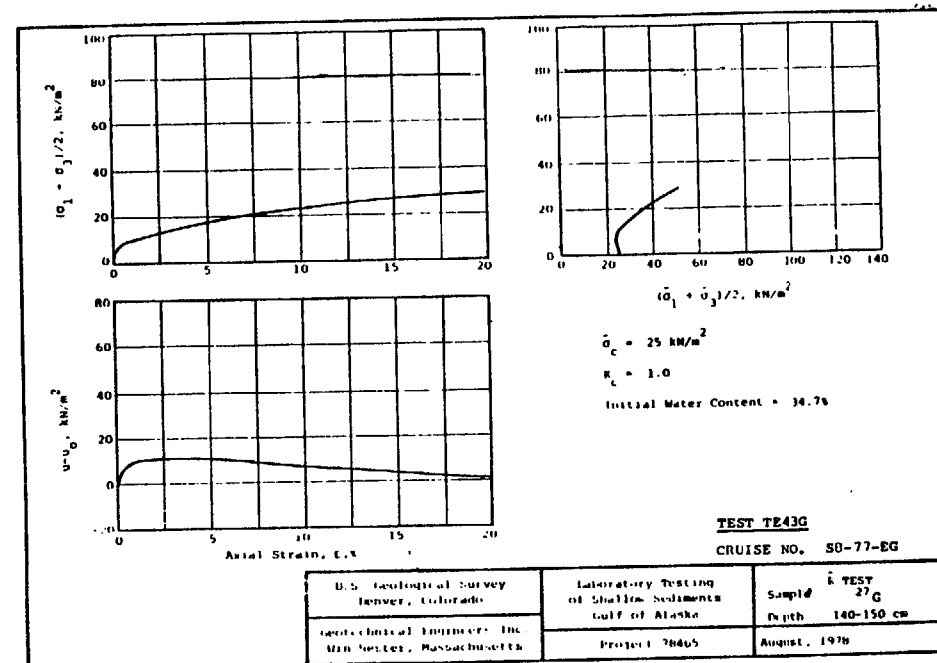
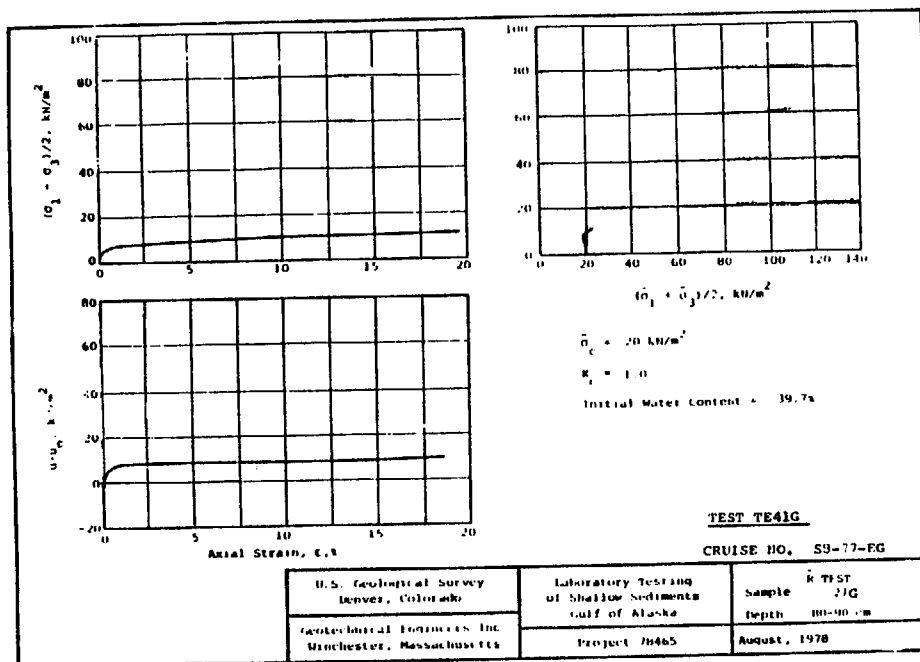


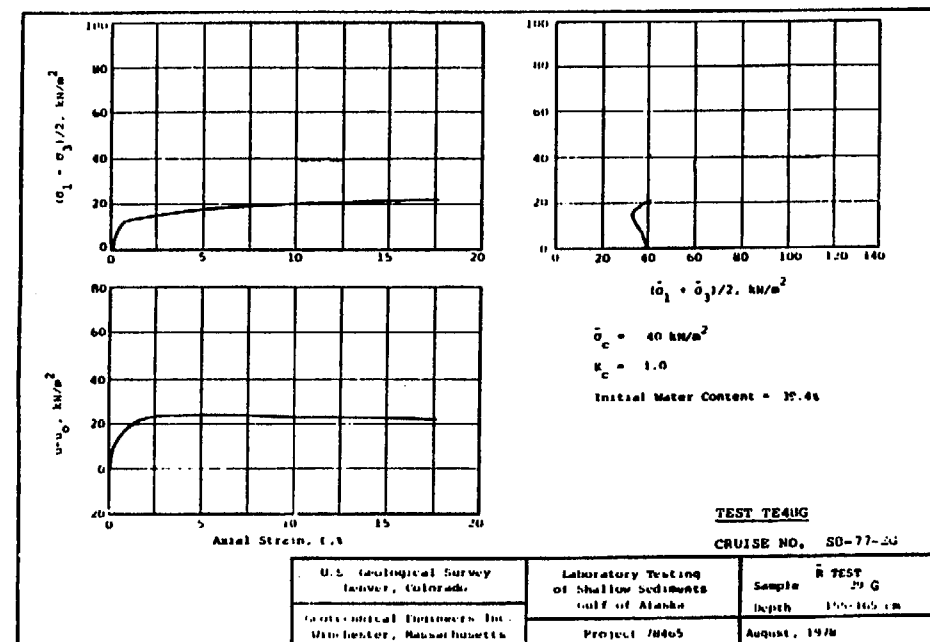
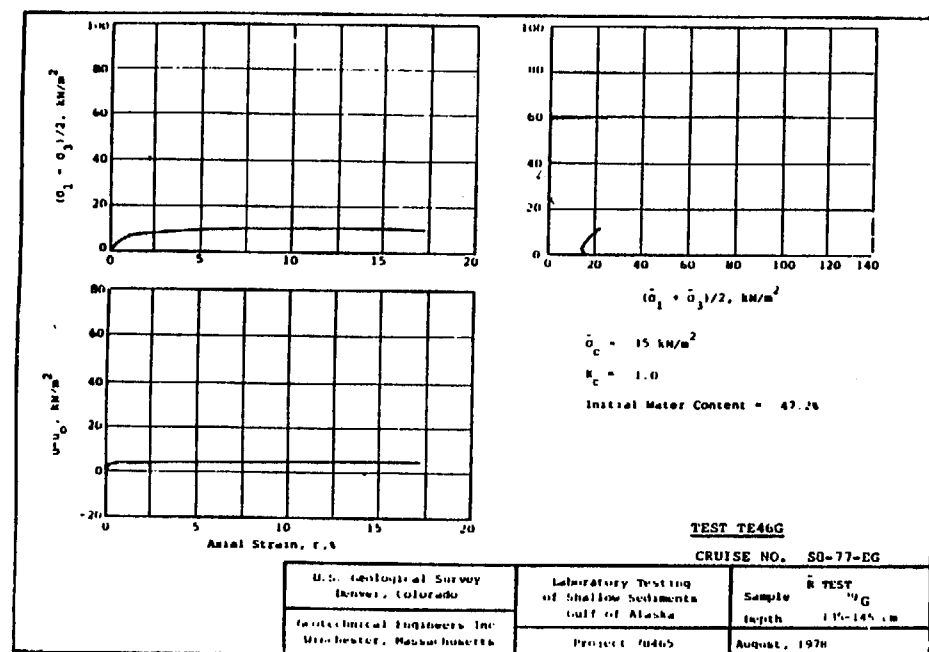
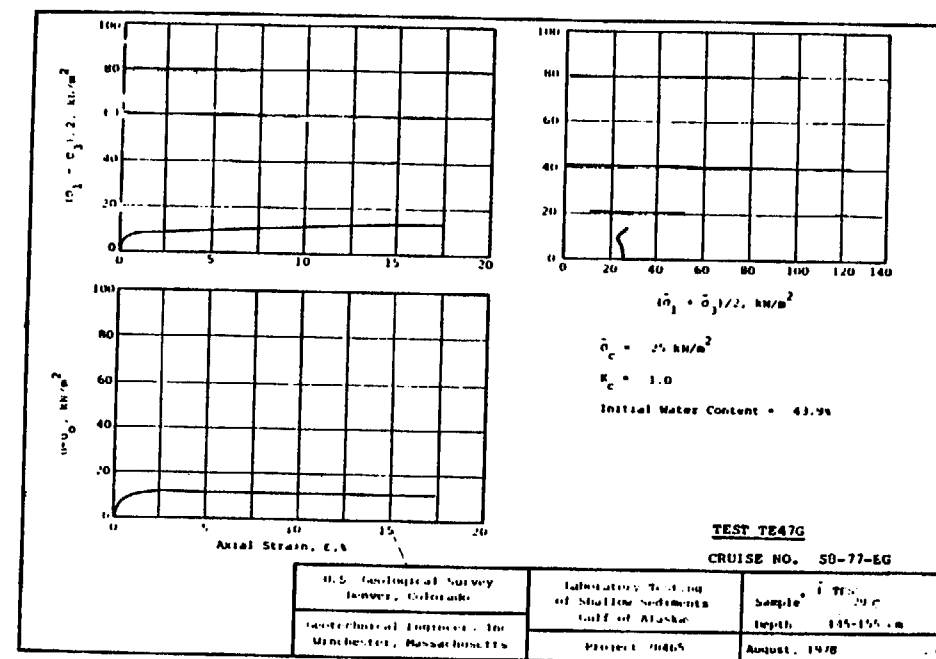
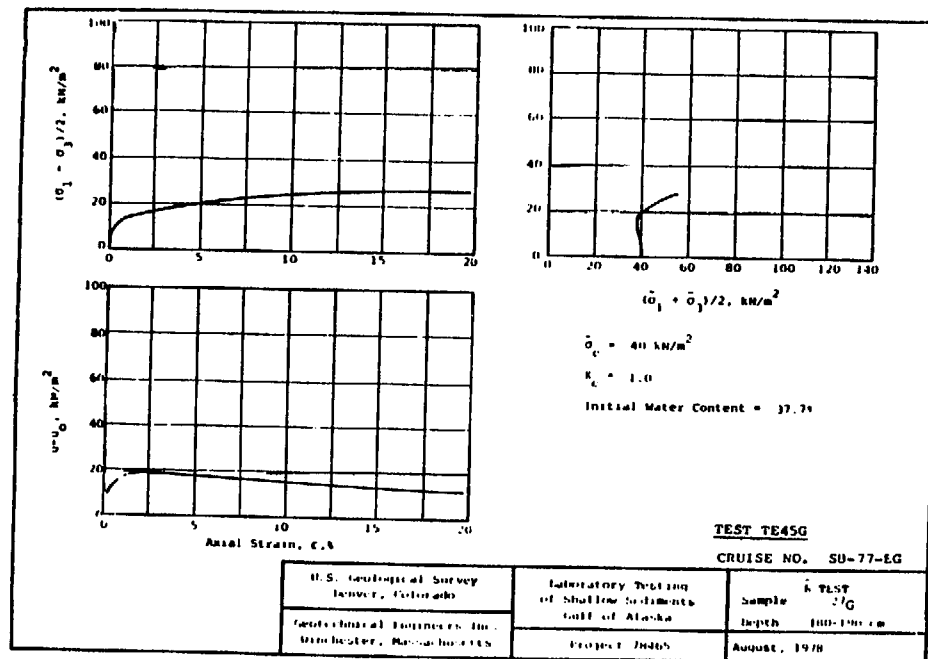


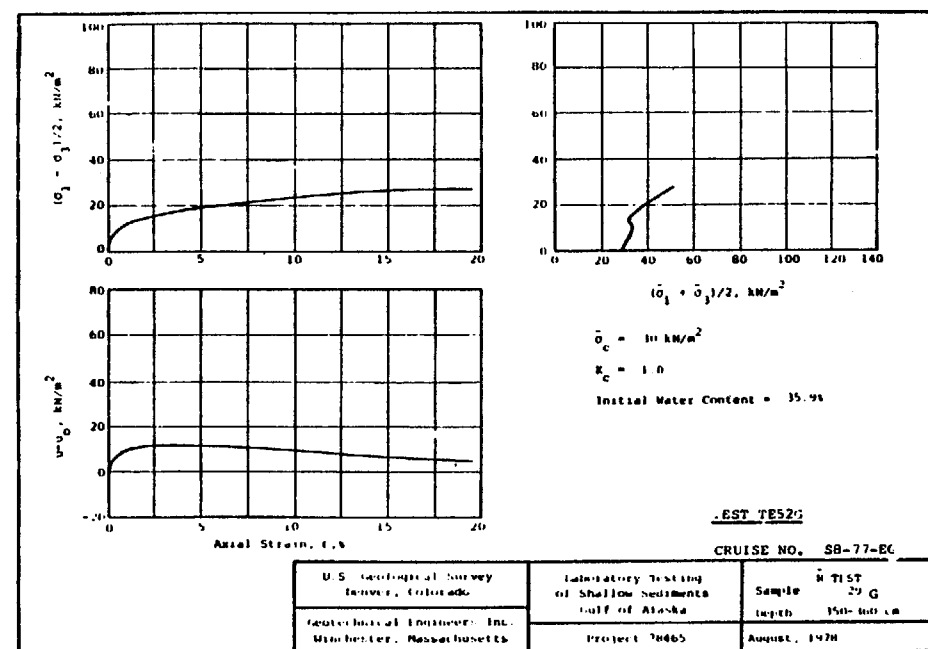
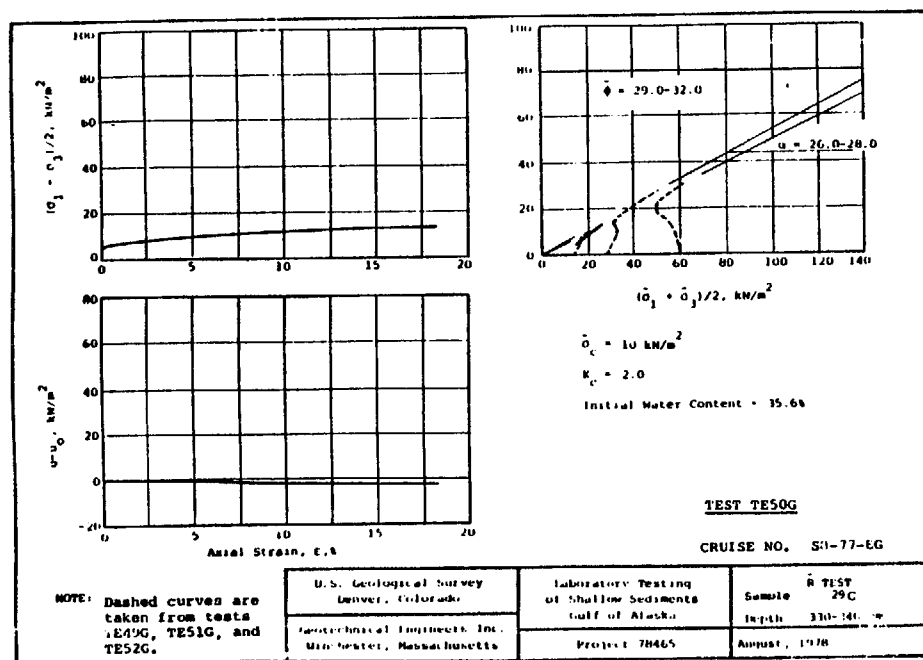
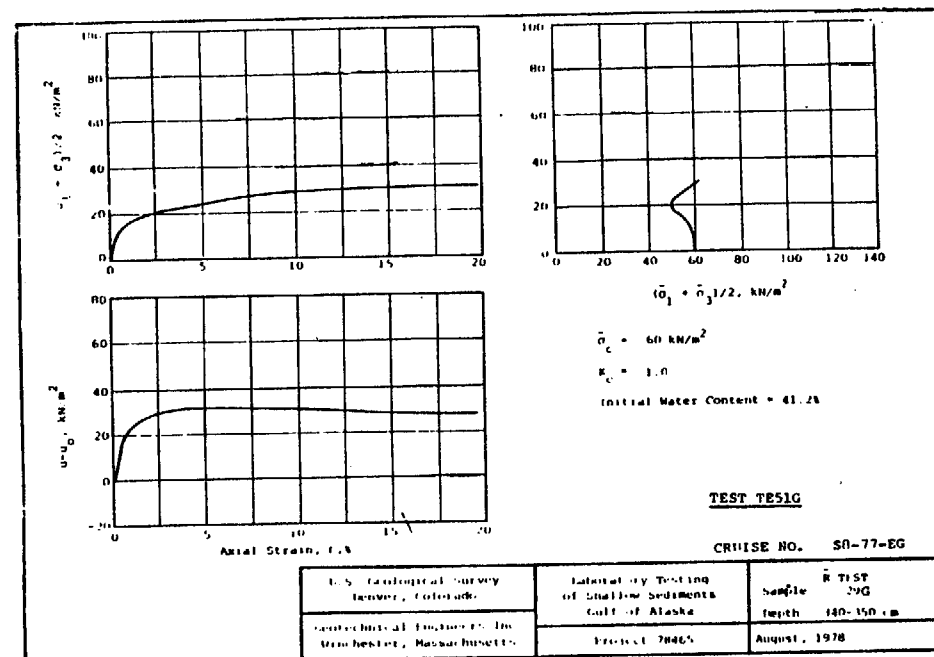
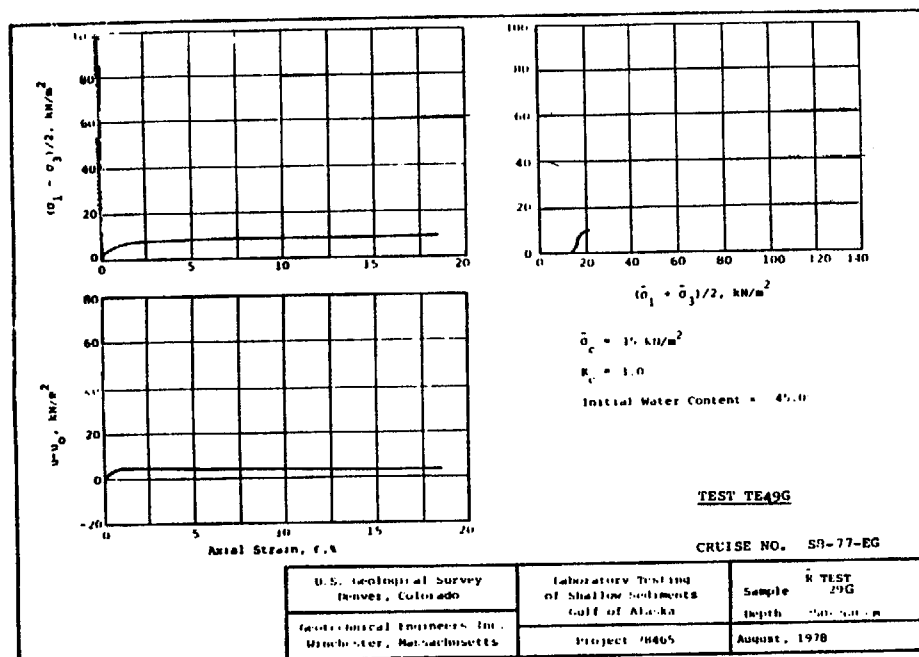


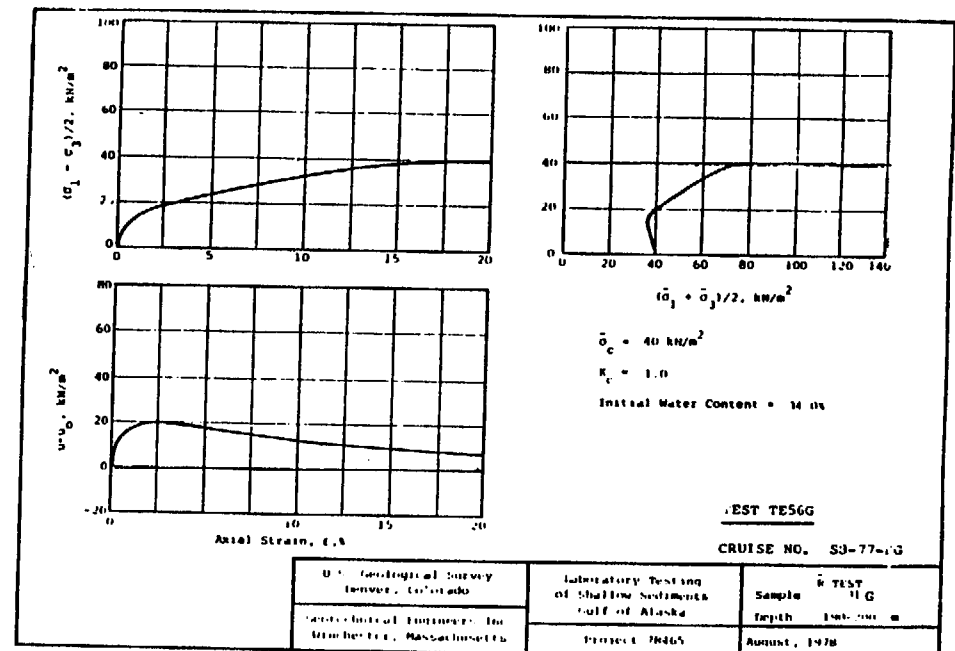
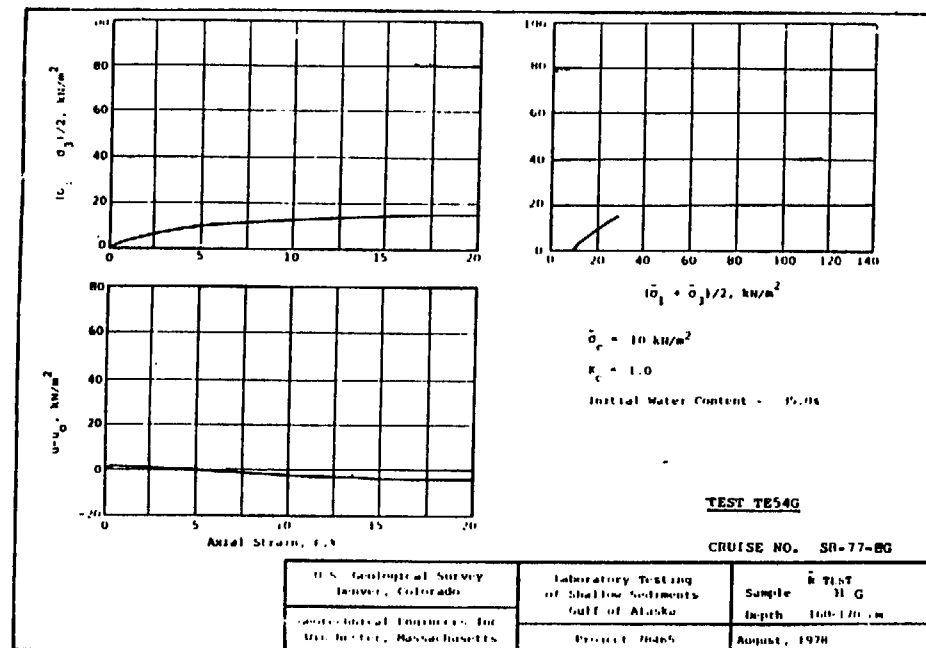
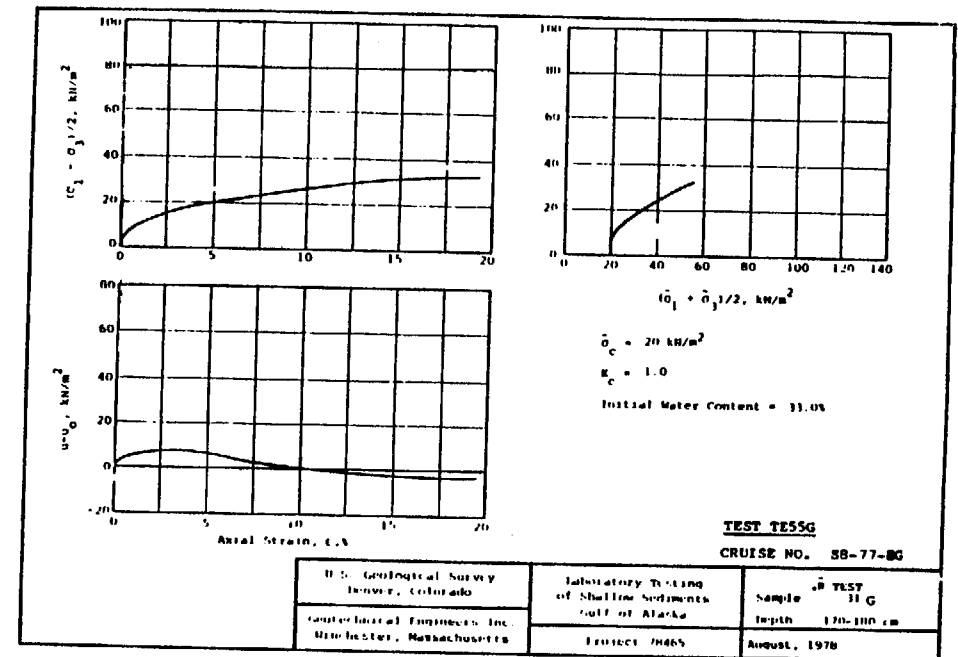
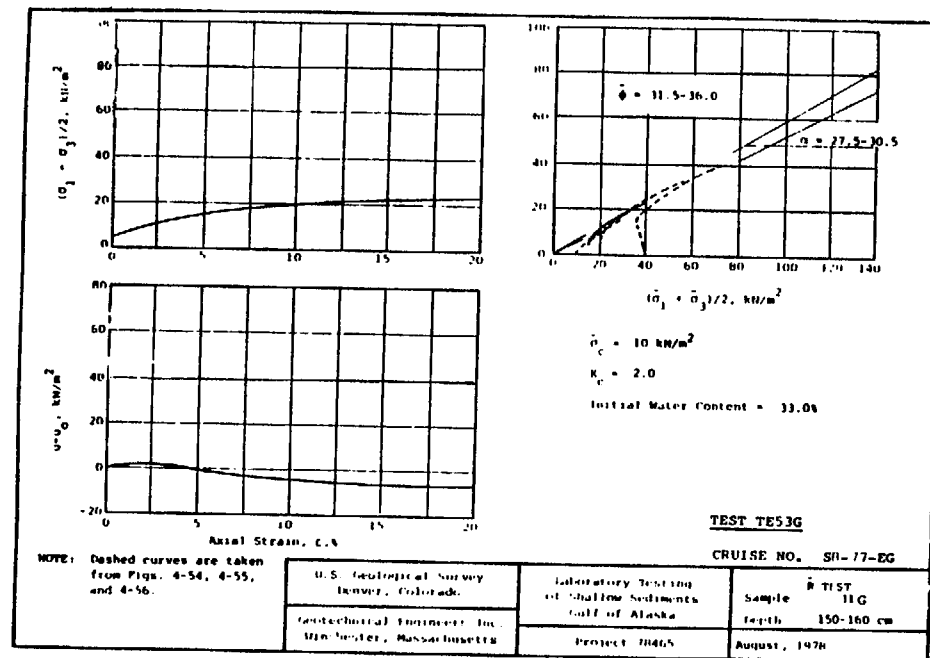


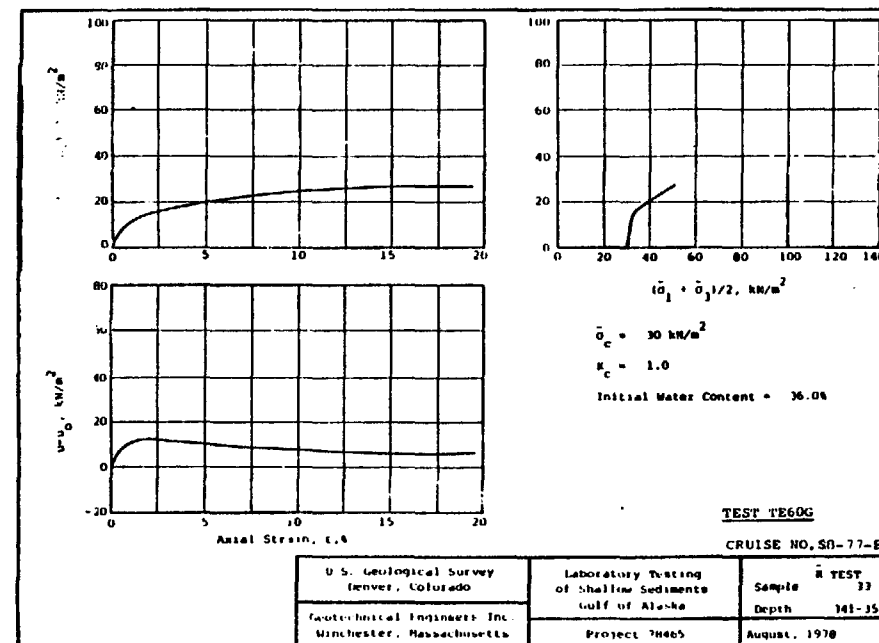
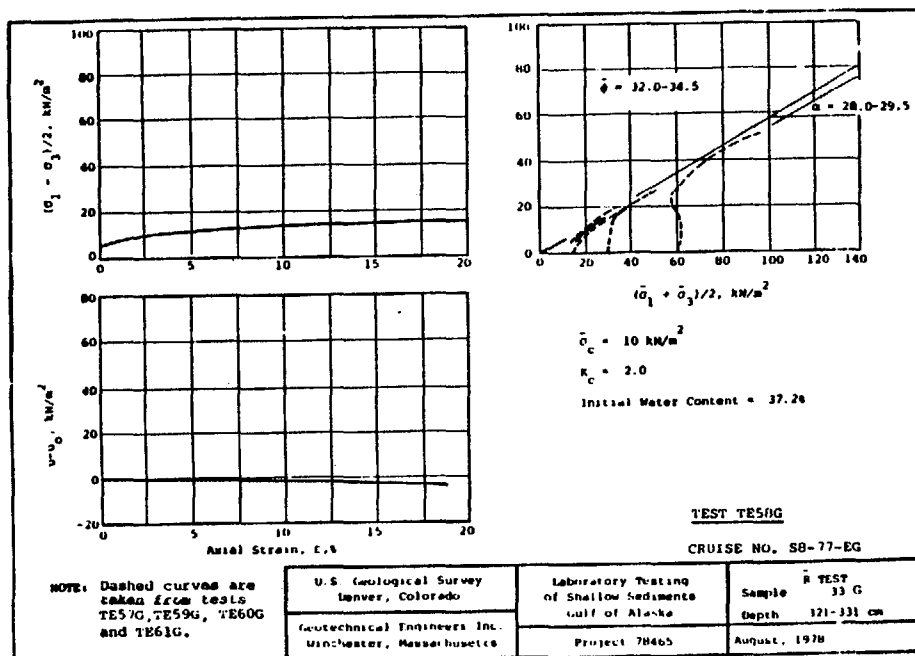
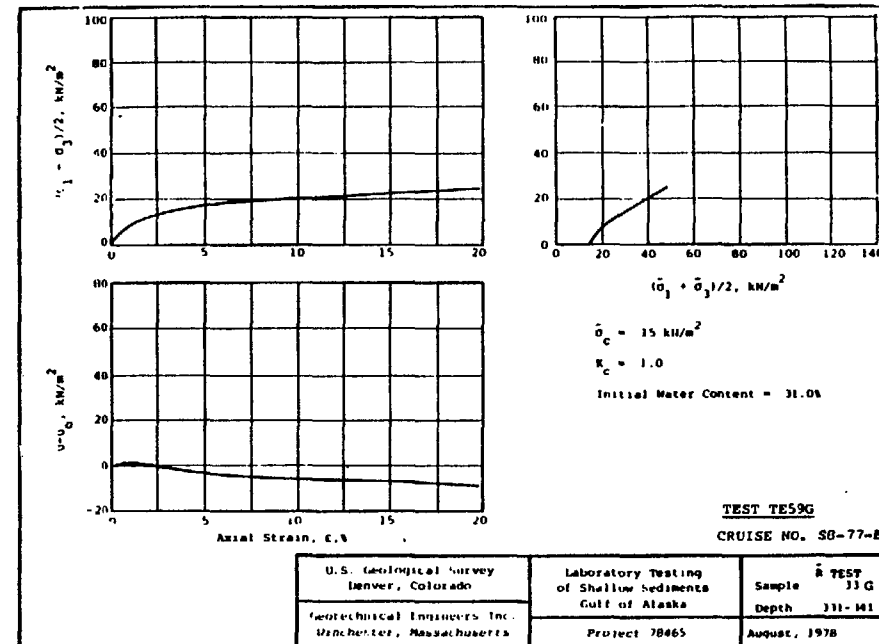
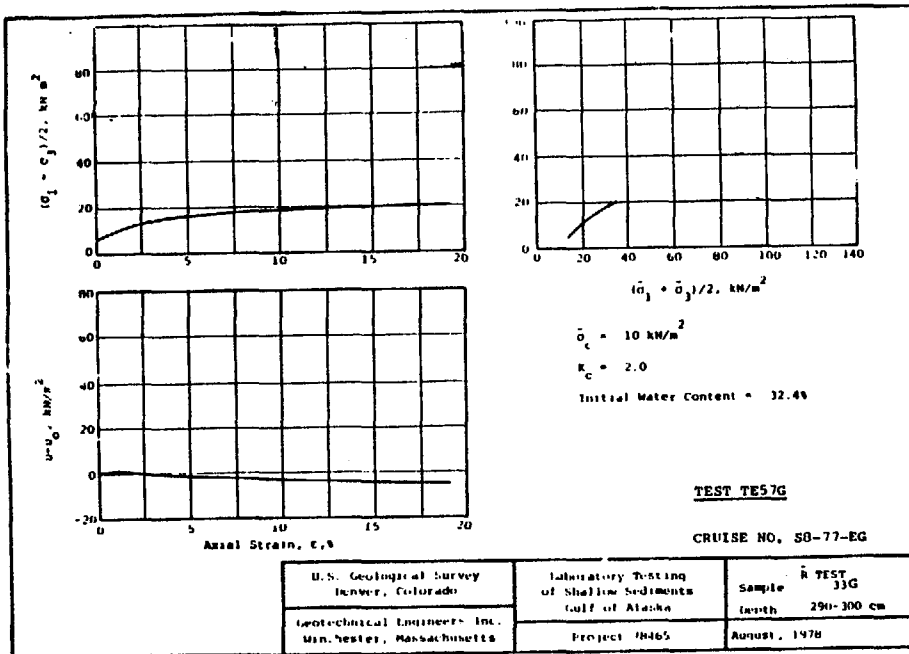


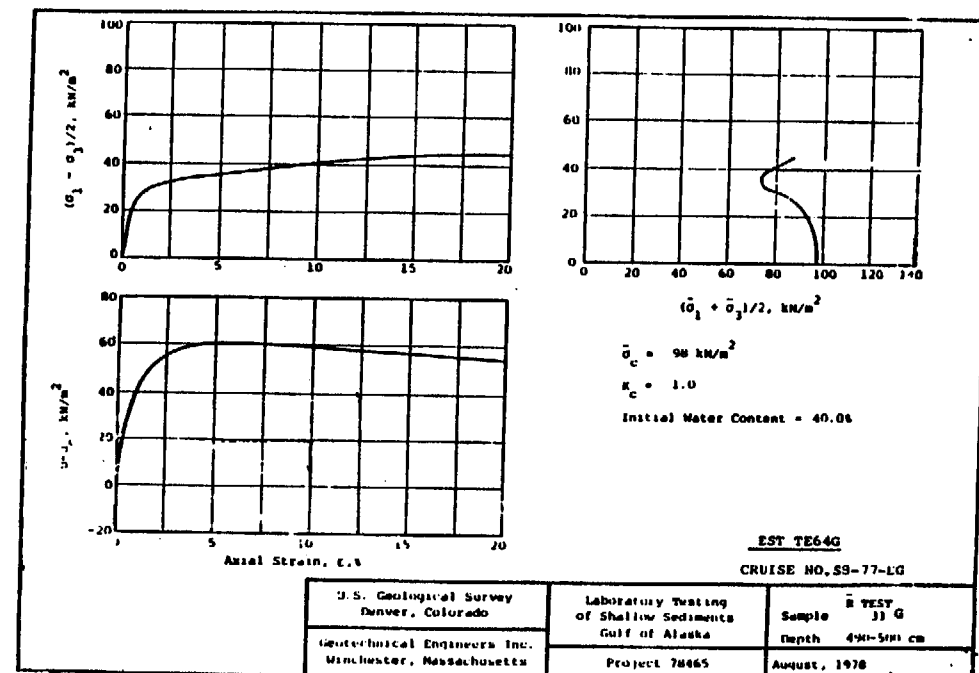
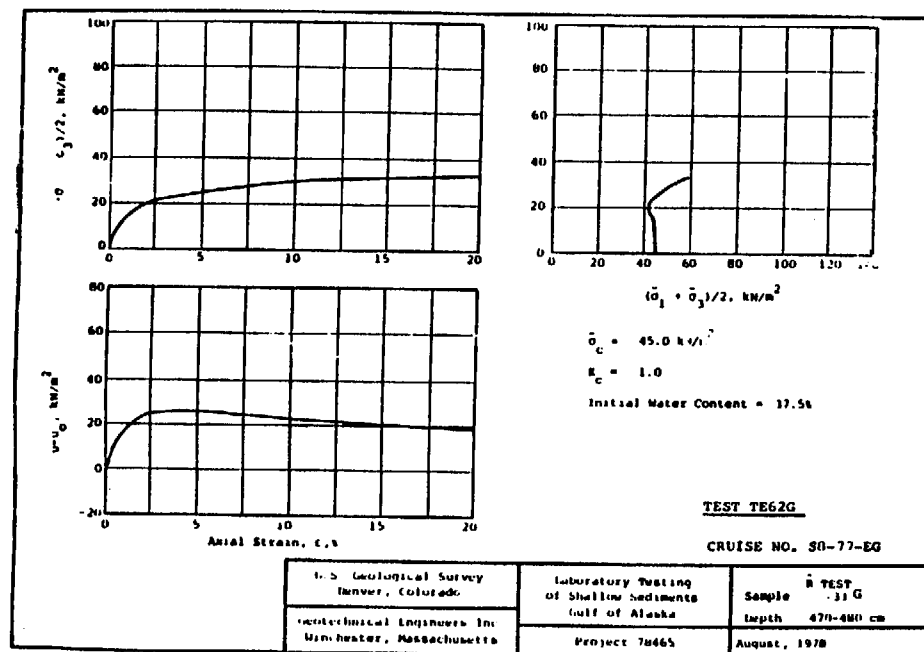
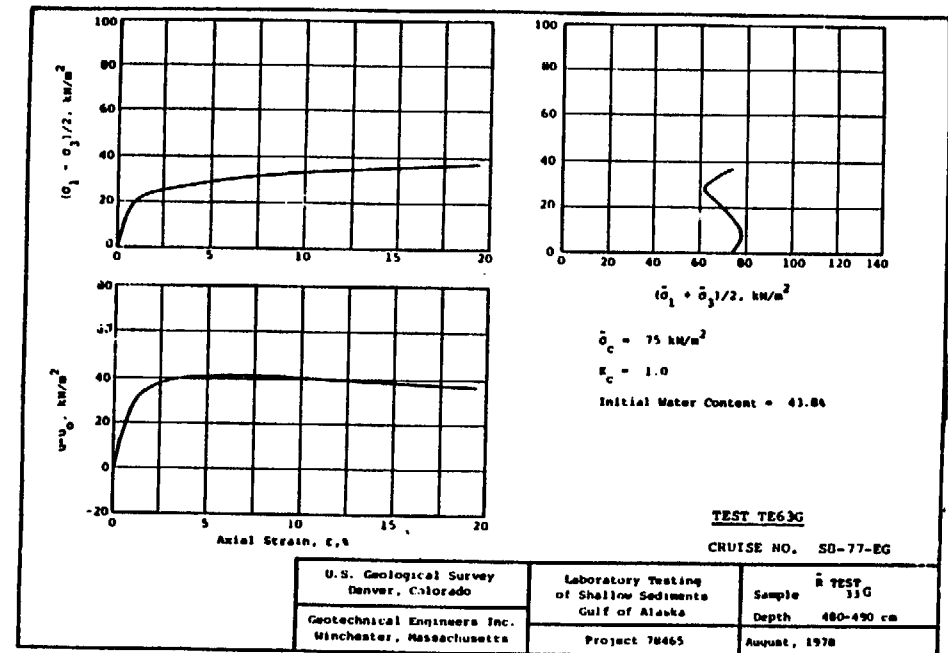
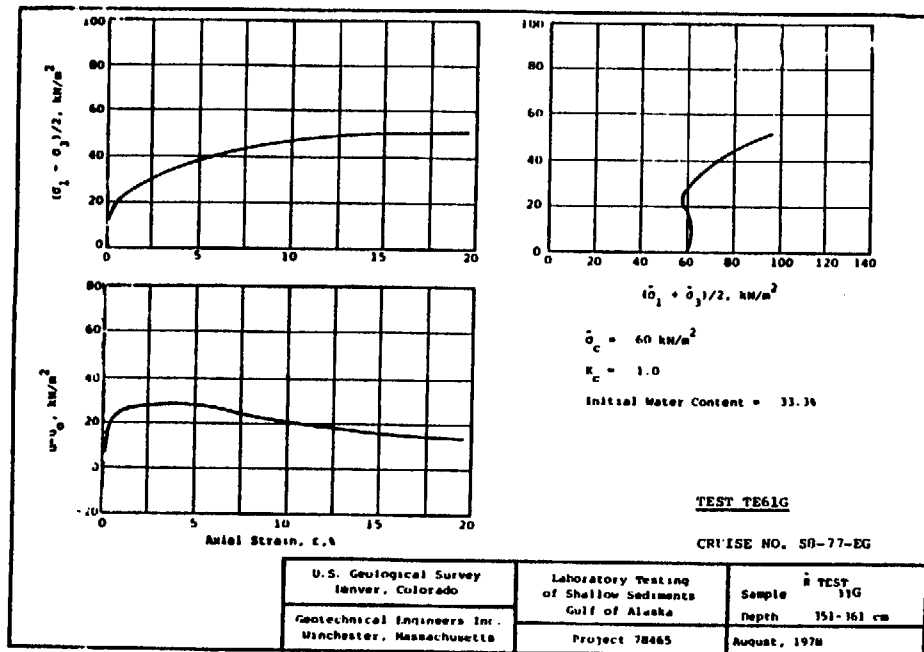


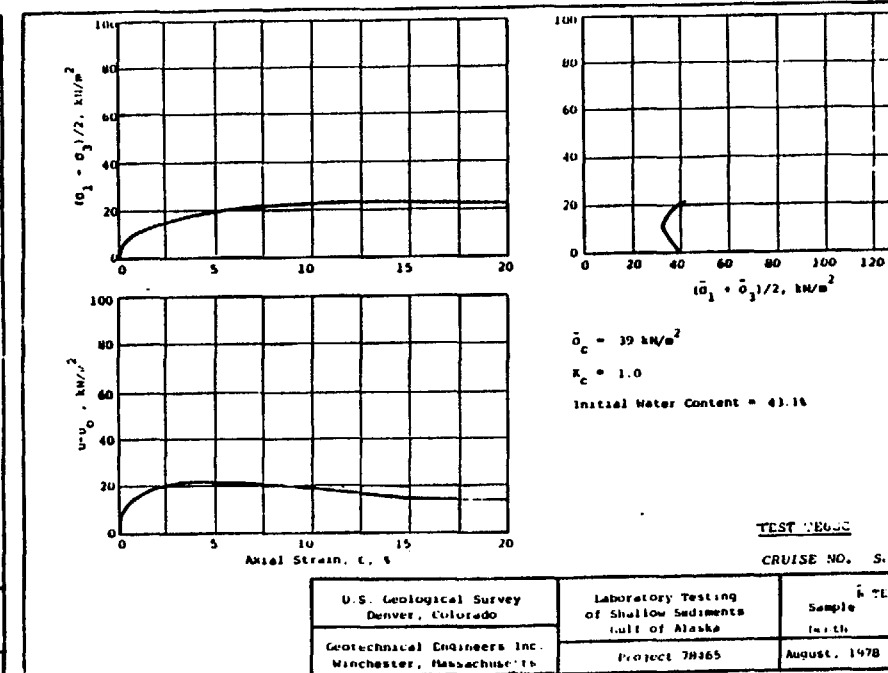
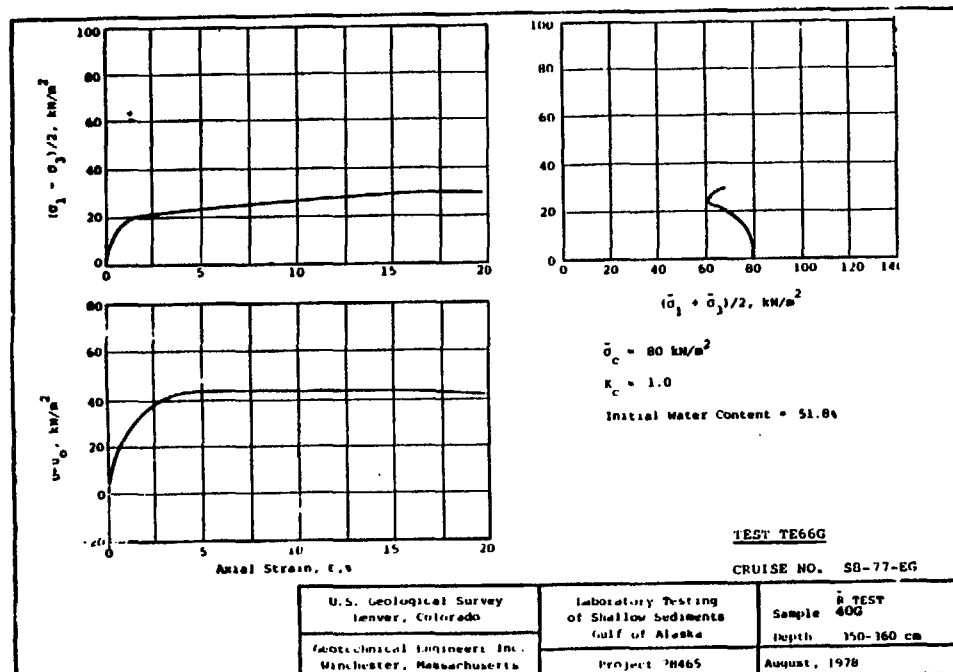
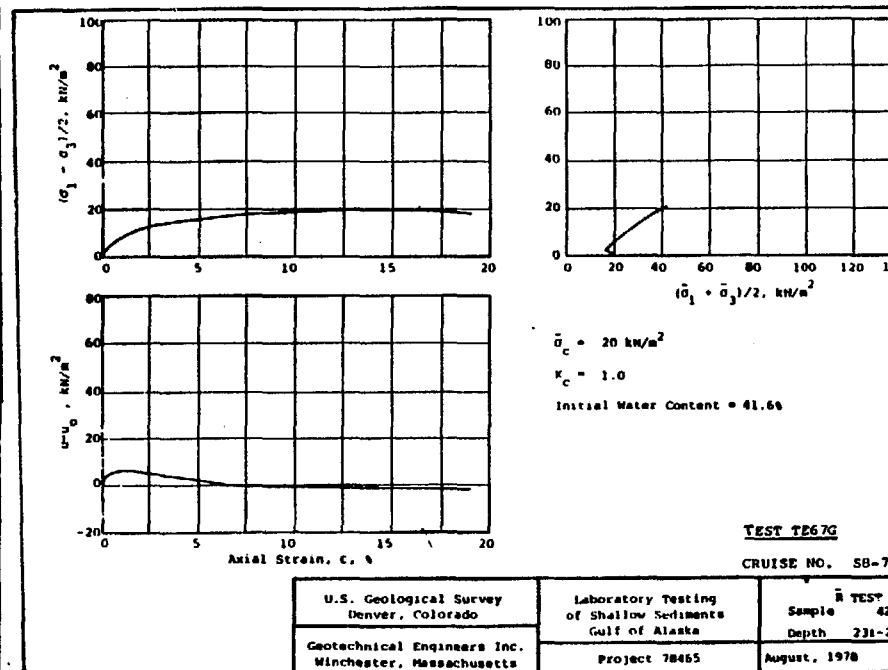
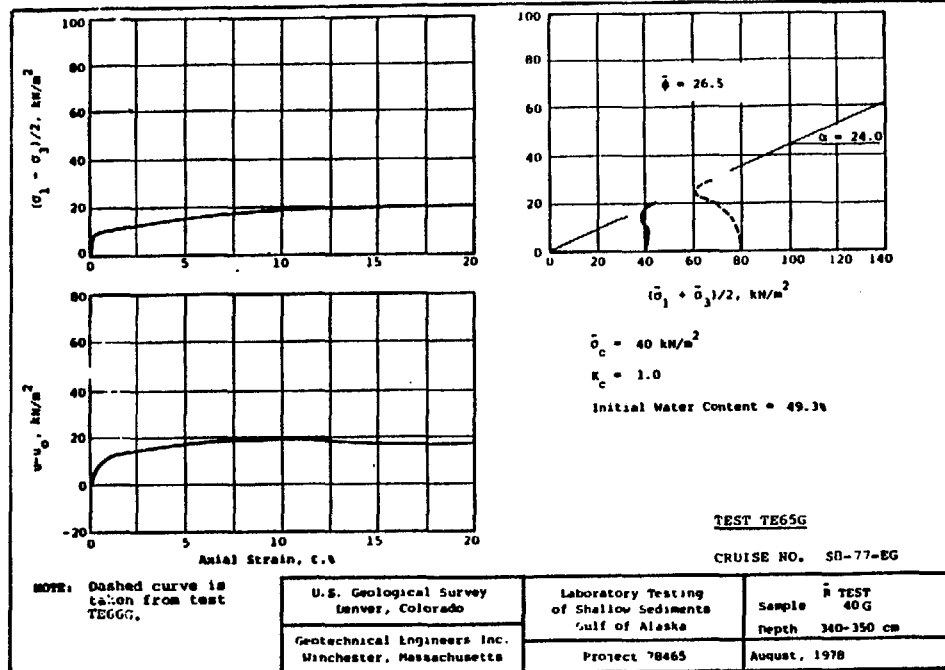


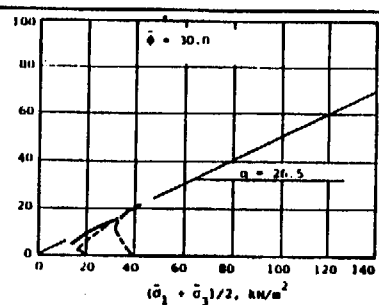
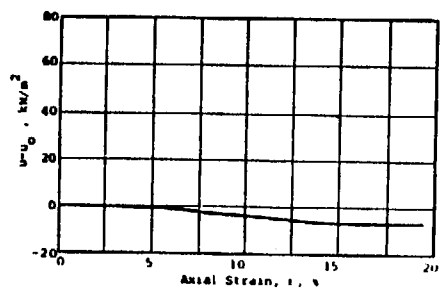
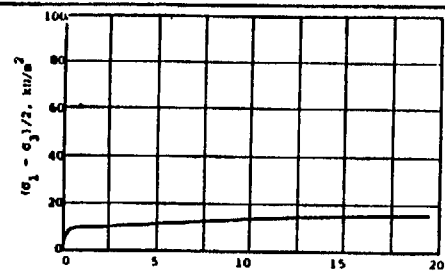












$\bar{\sigma}_c = 10 \text{ kN/m}^2$
 $K_L = 2$
 Initial Water Content = 42%

TEST TE69G

CRUISE NO. SH-7/-EG

NPL: Dashed curves are taken from tests TE67G and TE68G.

U.S. Geological Survey Denver, Colorado	Laboratory Testing of Shallow Sediments Gulf of Alaska	TEST Sample 42 G Depth 250-270 cm
Geotechnical Engineers, Inc. Winchester, Massachusetts	Project 70465	August, 1970

APPENDIX F

CONSOLIDATION AND TRIAXIAL TEST RESULTS--

LAW ENGINEERING AND TESTING COMPANY (1980 cores)

APPENDIX F. CONSOLIDATION AND TRIAXIAL TEST RESULTS-LAW ENGINEERING AND TESTING COMPANY (1980 Cores)

This appendix presents the results of consolidation and triaxial testing performed by Law Engineering and Testing Company under Contract number 4-08-0001-19241 with the U.S. Geological Survey. Testing was performed under the direction of R.G. Hamadock, P.G. Swanson and P.W. Mayne. Core samples were from DC2-80-EG.

All tests in this group have been assigned a test number with L2 as the last two characters. The consolidation tests (first two characters are OE) are presented first and are ordered by test number. Results from a single test are presented on a page in the form of void ratio versus the vertical effective stress.

The static triaxial tests (first two characters are TE) are given second and ordered by test number. Results from one to as many as four tests are presented on the same sheet. The upper left plot is a stress path presented as a plot of maximum shear stress (q) versus the normal effective stress on the plane of maximum shear (p'). The stress paths of Appendix D are defined differently. The upper right plot is the maximum shearing stress versus the axial strain. The lower left plot is the measured excess pore water pressure plotted versus axial strain.

The cyclic triaxial tests (first two characters are TC) are given third and ordered by test number. Results from one to three tests are presented on two sheets. The first sheet includes $p'-q$ stress path, shear stress-axial strain and excess pore pressure-axial strain plots that are analogous to the plots given for static triaxial tests. However, the plots are given for only a few selected cycles to illustrate how the response changes as the number of cycles increases. Numbers on the plots correspond to cycle number.

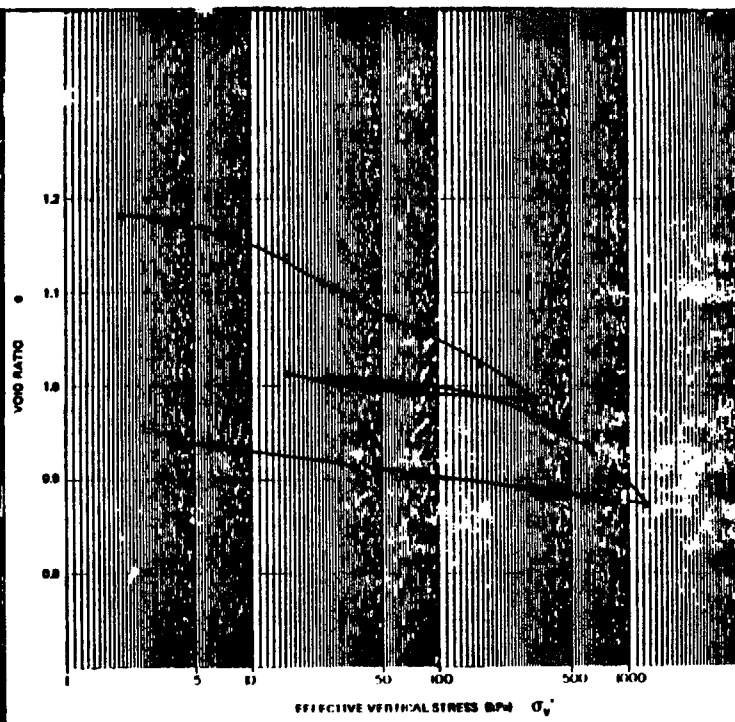
The second sheet shows several parameters plotted versus cycle number. The upper left graph shows the cyclic stress level normalized by the static strength (obtained from a nearby sample-Method I of the main text) versus the number of cycles to achieve a given double amplitude strain level. Lines are drawn connecting points corresponding to the same strain level. **The** upper right graph shows the excess pore pressure generated as a function of the cycle number. The lower right graph shows the double amplitude axial strain as a function of cycle number.

CONSOLIDATION TEST

TEST OE3L2

CLAMPING SPREAD INCH 0.197
 SWELLING SPREAD INCH 0.023
 MAXIMUM PRECONSOLIDATION STRESS 22
 INITIAL VOID RATIO 1.192
 INITIAL WATER CONTENT 43.8
 INITIAL SATURATION 100.0
 DENSITY (g/cm³) 18.27
 EFFECTIVE OVERBURDEN (PSF) 7.8
 SAMPLE IDENTIFICATION
 CRUISE NO. MC280 EG
 CORE NO. MC322
 DEPTH (m) 88.82

U.S.G.S. ALASKAN CORES
 CONTRACT NO. 14-00-0001 10041
 LEGAL PROJECT NO. W-0-7930



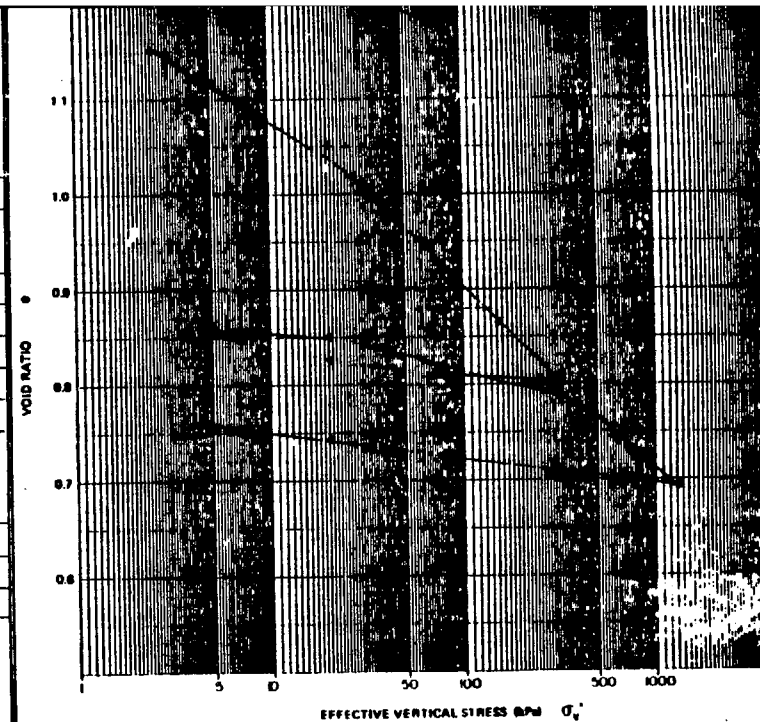
LAW ENGINEERING

CONSOLIDATION TEST

TEST OE3L2

CLAMPING SPREAD INCH 0.158
 SWELLING SPREAD INCH 0.037
 MAXIMUM PRECONSOLIDATION STRESS 30
 INITIAL VOID RATIO 1.104
 INITIAL WATER CONTENT 41.4
 INITIAL SATURATION 100.0
 DENSITY (g/cm³) 18.26
 EFFECTIVE OVERBURDEN (PSF) 5.6
 SAMPLE IDENTIFICATION
 CRUISE NO. DC180 EG
 CORE NO. 48 G
 DEPTH (m) 84.71

U.S.G.S. ALASKAN CORES
 CONTRACT NO. 14-00-0001 10041
 LEGAL PROJECT NO. W-0-7930



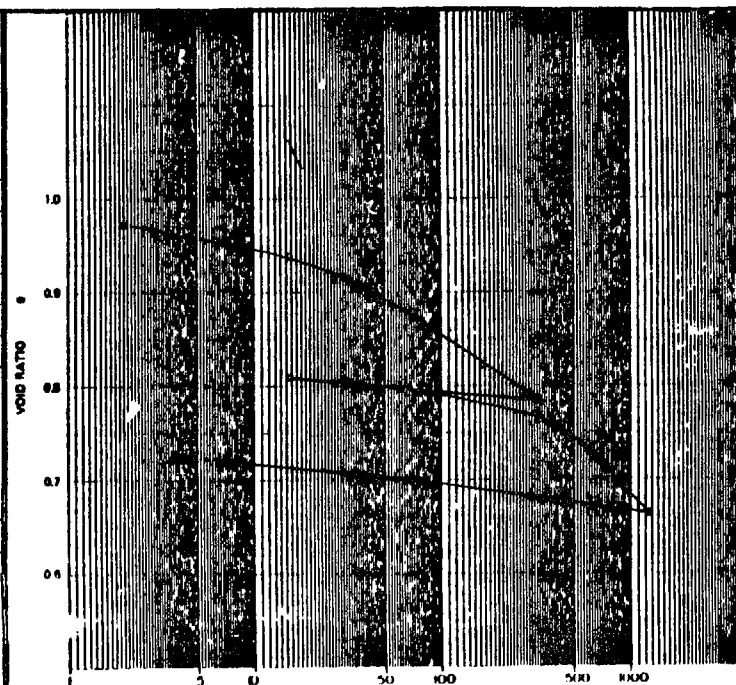
LAW ENGINEERING

CONSOLIDATION TEST

TEST OE2L2

CLAMPING SPREAD INCH 0.202
 SWELLING SPREAD INCH 0.021
 MAXIMUM PRECONSOLIDATION STRESS 22
 INITIAL VOID RATIO 0.998
 INITIAL WATER CONTENT 31.8
 INITIAL SATURATION 91.8
 DENSITY (g/cm³) 18.44
 EFFECTIVE OVERBURDEN (PSF) 8.0
 SAMPLE IDENTIFICATION
 CRUISE NO. DC280 EG
 CORE NO. 38 G
 DEPTH (m) 88.74

U.S.G.S. ALASKAN CORES
 CONTRACT NO. 14-00-0001 10041
 LEGAL PROJECT NO. W-0-7930

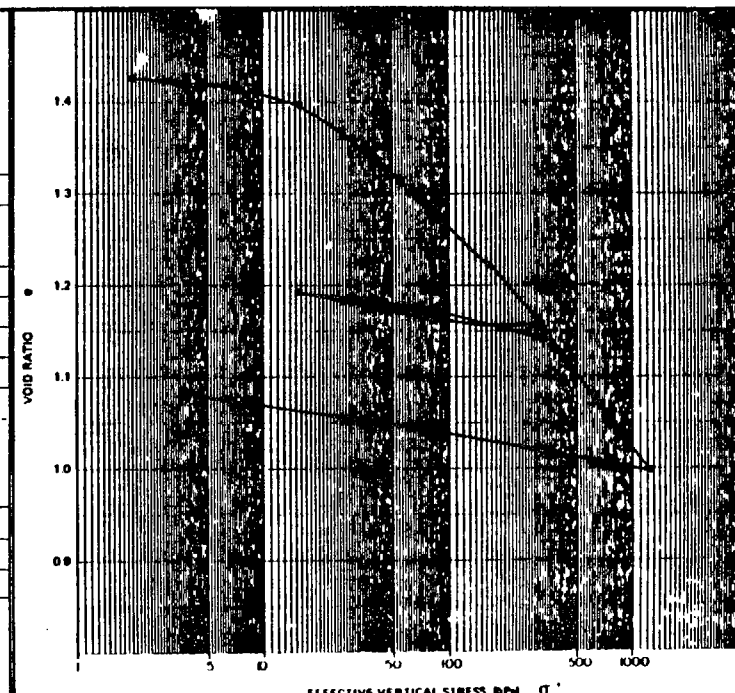


CONSOLIDATION TEST

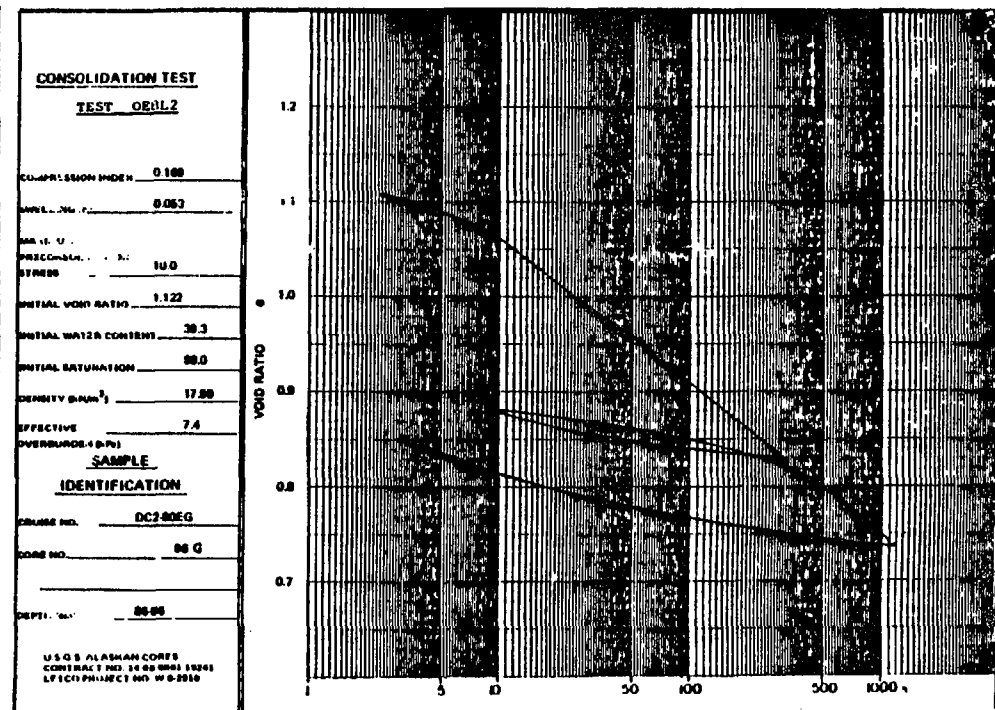
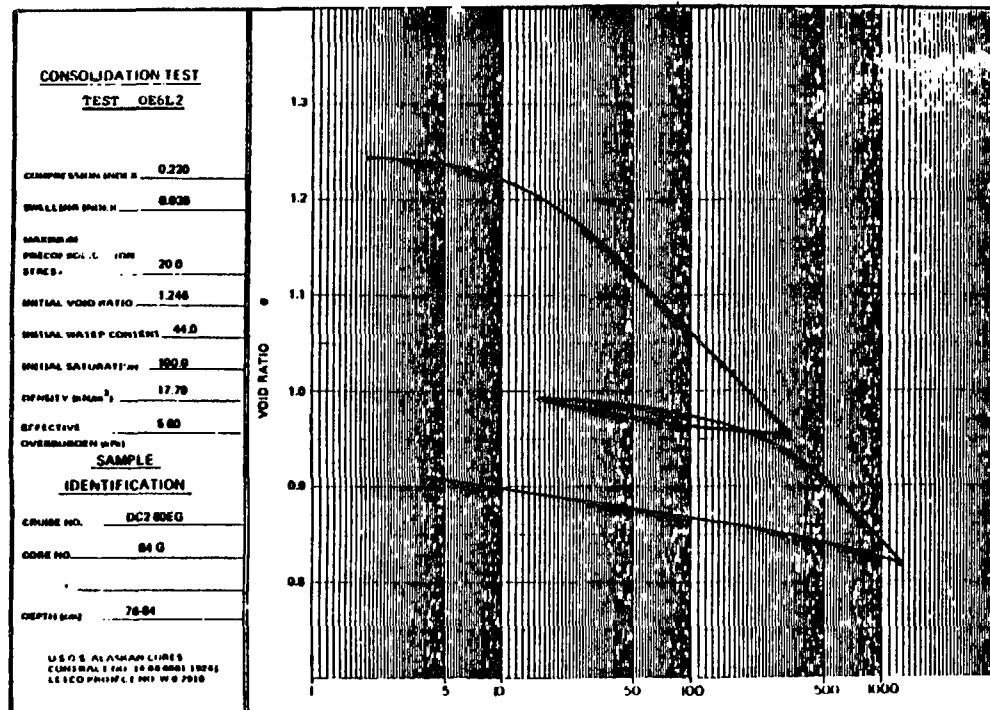
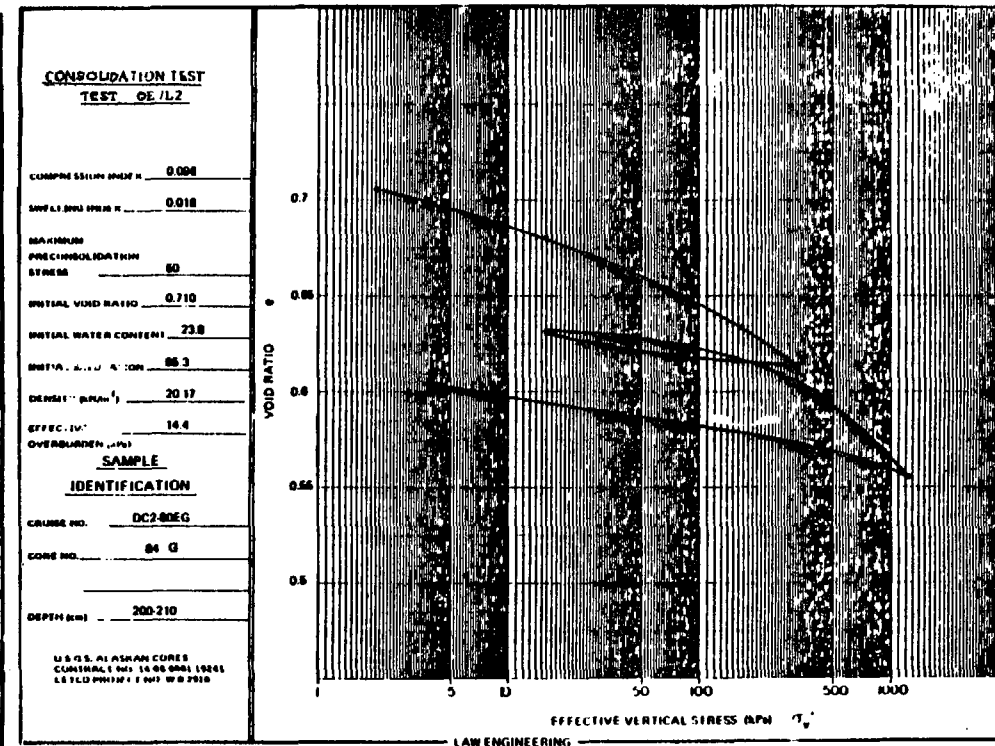
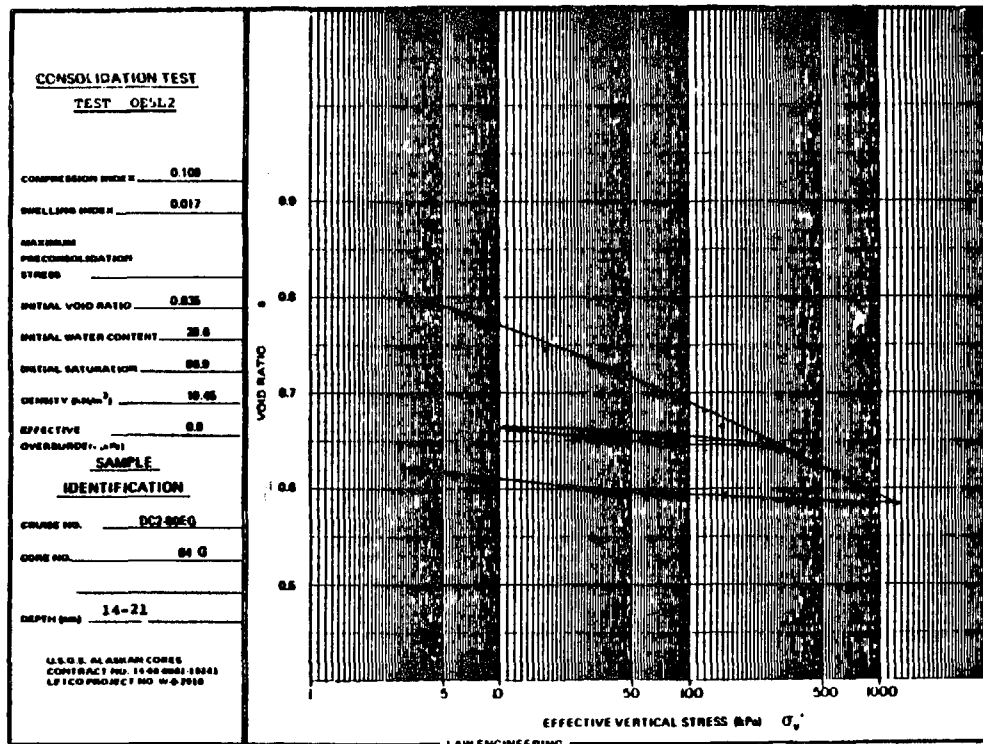
TEST OE4L2

CLAMPING SPREAD INCH 0.208
 SWELLING SPREAD INCH 0.028
 MAXIMUM PRECONSOLIDATION STRESS 20
 INITIAL VOID RATIO 1.434
 INITIAL WATER CONTENT 53.1
 INITIAL SATURATION 100.0
 DENSITY (g/cm³) 17.83
 EFFECTIVE OVERBURDEN (PSF) 6.2
 SAMPLE IDENTIFICATION
 CRUISE NO. DC280 EG
 CORE NO. 55 G
 DEPTH (m) 74.80

U.S.G.S. ALASKAN CORES
 CONTRACT NO. 14-00-0001 10041
 LEGAL PROJECT NO. W-0-7930



EFFECTIVE VERTICAL STRESS (psf) σ_v'



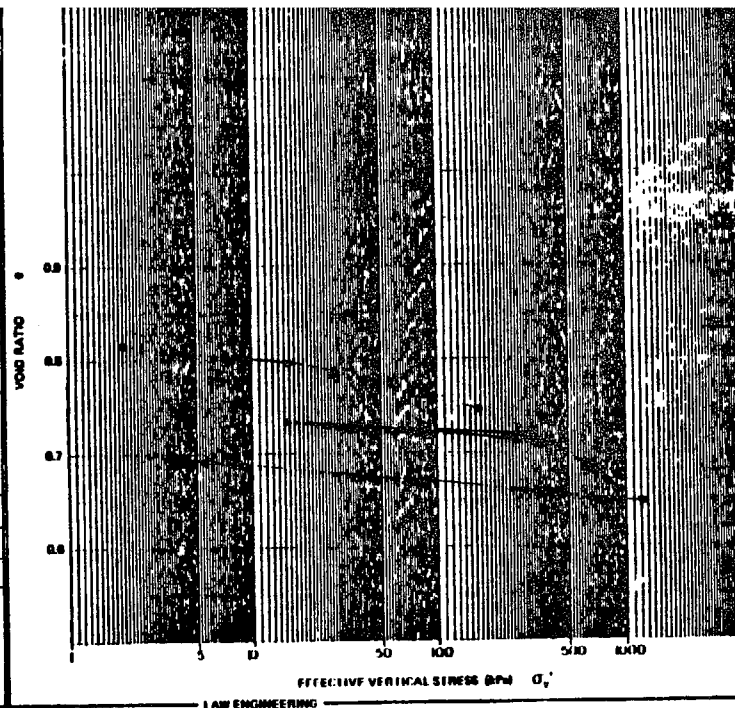
CONSOLIDATION TEST

TEST OE9L2

COMPRESSION INDEX 0.127
 SWELLING INDEX 0.016
 MAXIMUM PRECONSOLIDATION STRESS 120
 INITIAL VOID RATIO 0.810
 INITIAL WATER CONTENT 28.8
 INITIAL SATURATION 88.5
 DENSITY (g/cm³) 1.956
 EFFECTIVE OVERBURDEN (kPa) 27.8

SAMPLE IDENTIFICATION
 CRUSH NO. DC2-88 EG
 CORE NO. 88 G
 DEPTH (mm) 262.271

U.S.G. ALASKAN CORES
 CONTRACT NO. 14-00-0001 10241
 LECO PROJECT NO. W-0-2010



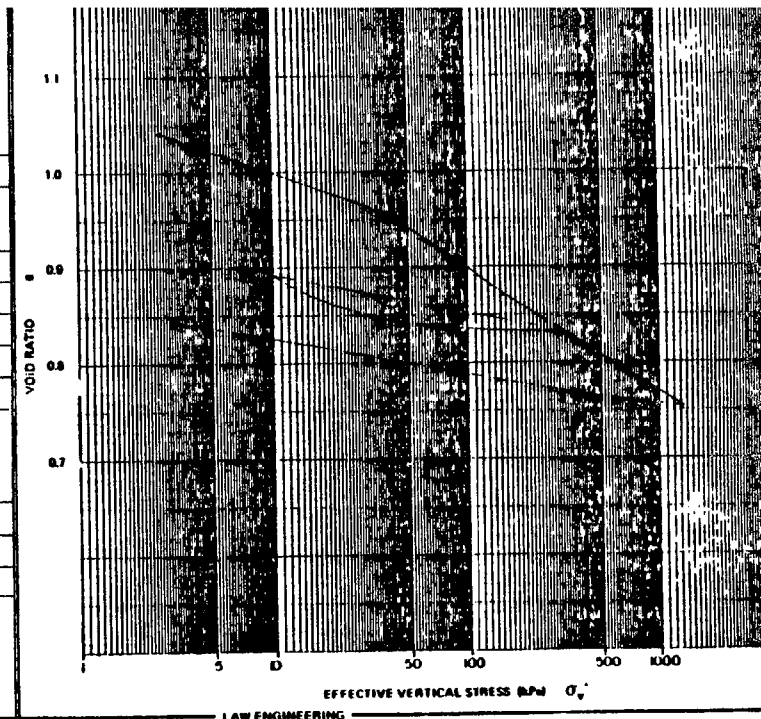
CONSOLIDATION TEST

TEST OE11L2

COMPRESSION INDEX 0.136
 SWELLING INDEX 0.037
 MAXIMUM PRECONSOLIDATION STRESS 40.0
 INITIAL VOID RATIO 1.047
 INITIAL WATER CONTENT 38.0
 INITIAL SATURATION 100.0
 DENSITY (g/cm³) 1.620
 EFFECTIVE OVERBURDEN (kPa) 20.4

SAMPLE IDENTIFICATION
 CRUSH NO. DC2-80 EG
 CORE NO. 88 G
 DEPTH (mm) 375.381

U.S.G. ALASKAN CORES
 CONTRACT NO. 14-00-0001 10241
 LECO PROJECT NO. W-0-2010



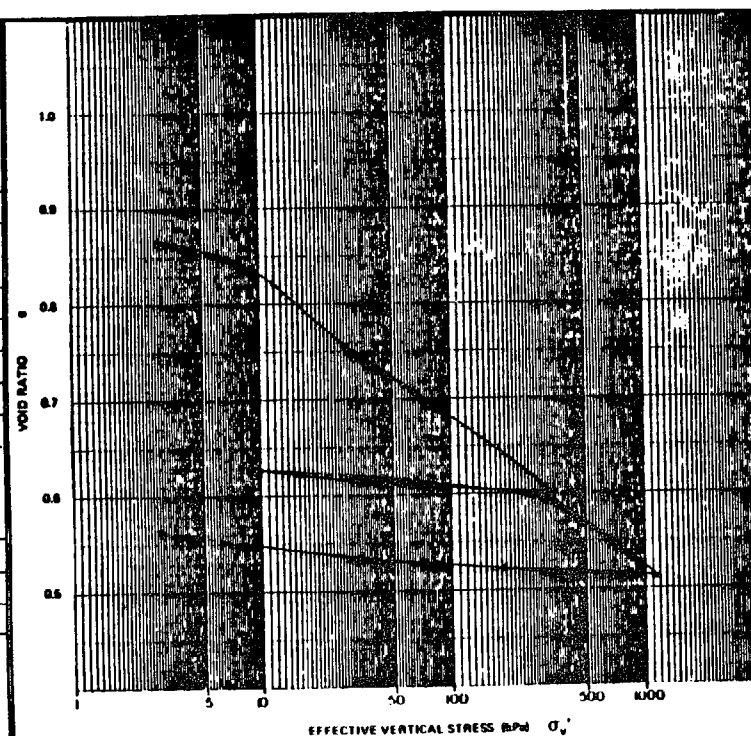
CONSOLIDATION TEST

TEST OE10L2

COMPRESSION INDEX 0.171
 SWELLING INDEX 0.022
 MAXIMUM PRECONSOLIDATION STRESS 31.0
 INITIAL VOID RATIO 0.954
 INITIAL WATER CONTENT 32.7
 INITIAL SATURATION 86.9
 DENSITY (g/cm³) 1.882
 EFFECTIVE OVERBURDEN (kPa) 29.8

SAMPLE IDENTIFICATION
 CRUSH NO. DC2-80 EG
 CORE NO. 88 G
 DEPTH (mm) 254.381

U.S.G. ALASKAN CORES
 CONTRACT NO. 14-00-0001 10241
 LECO PROJECT NO. W-0-2010



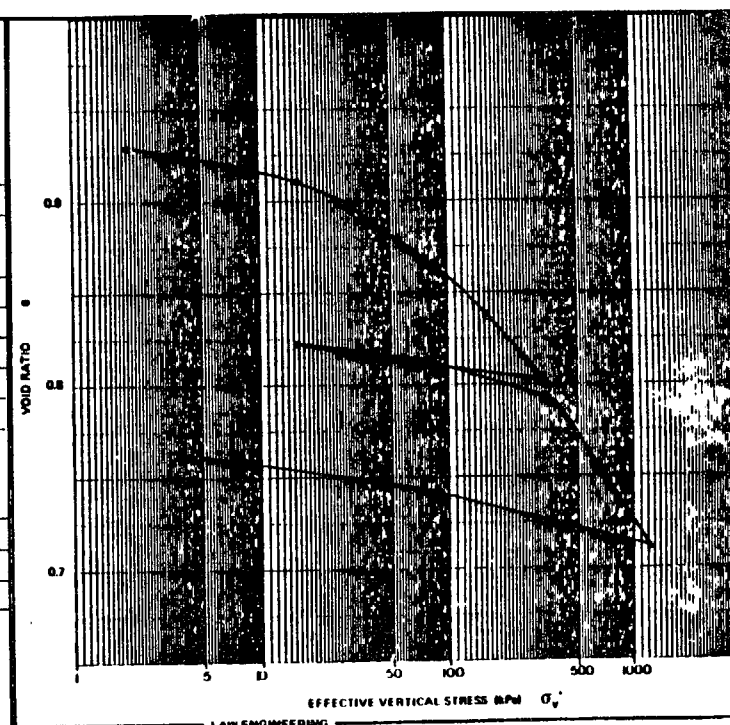
CONSOLIDATION TEST

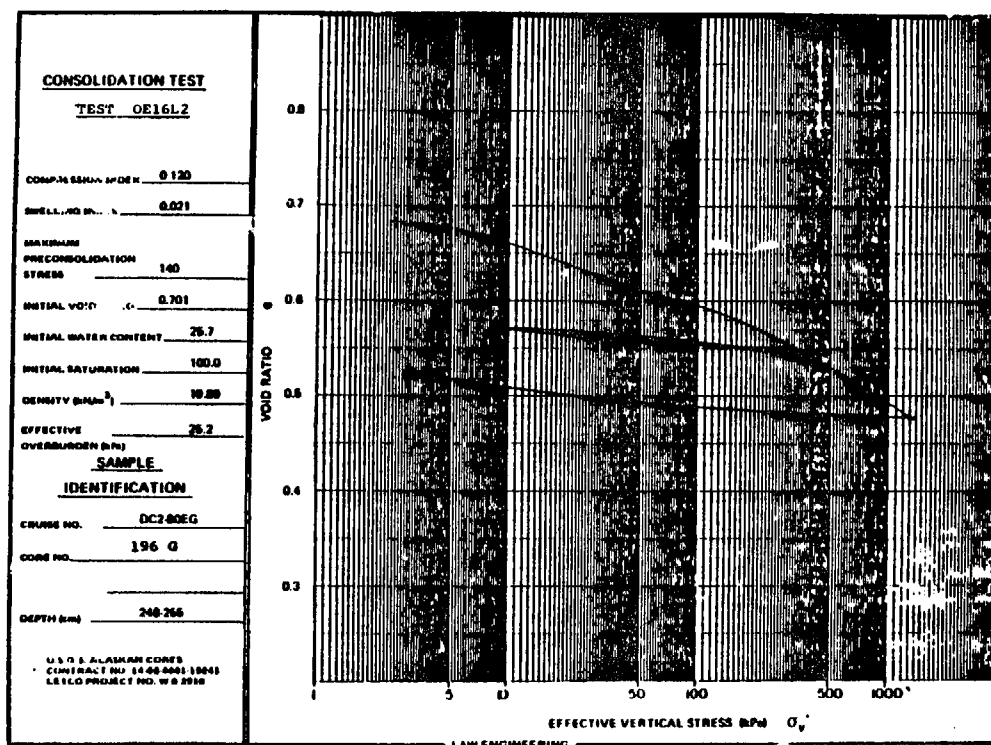
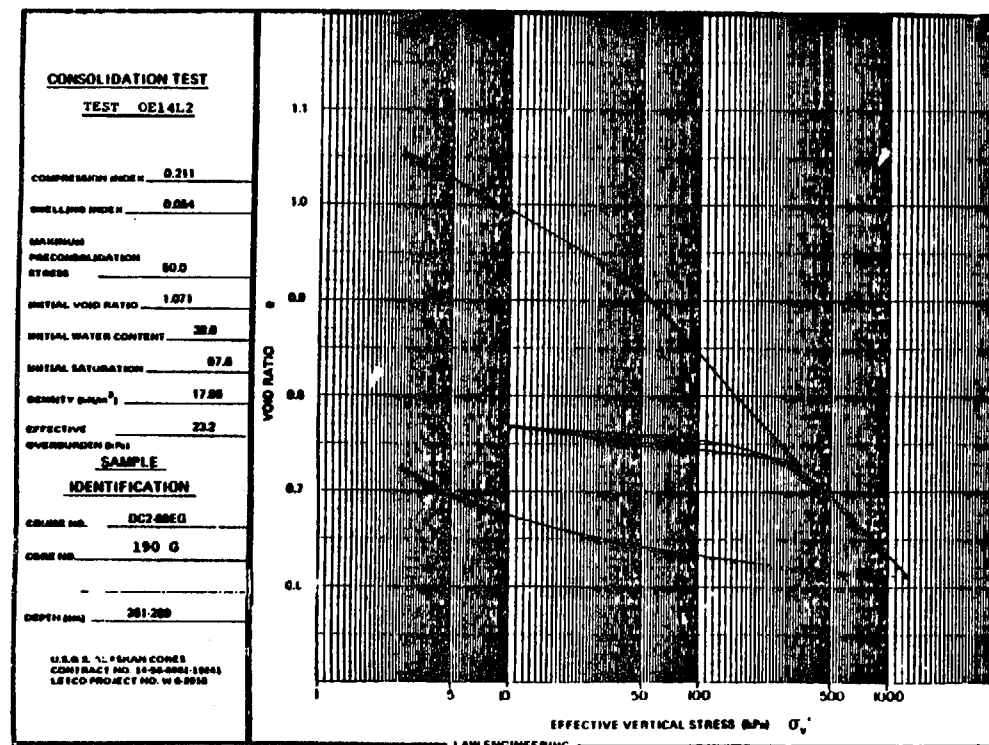
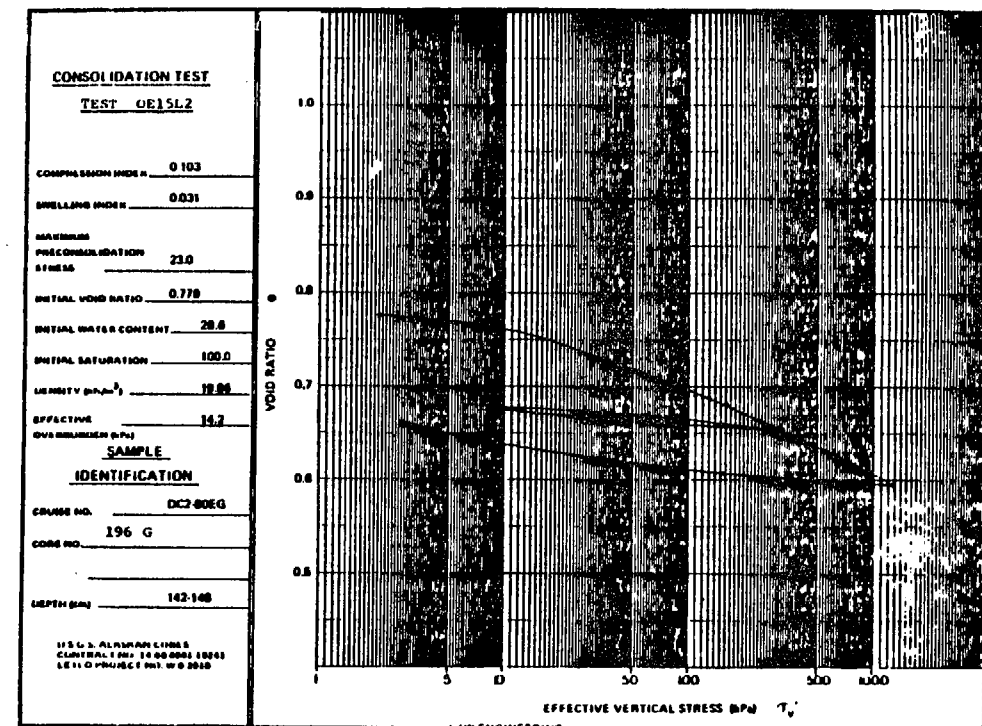
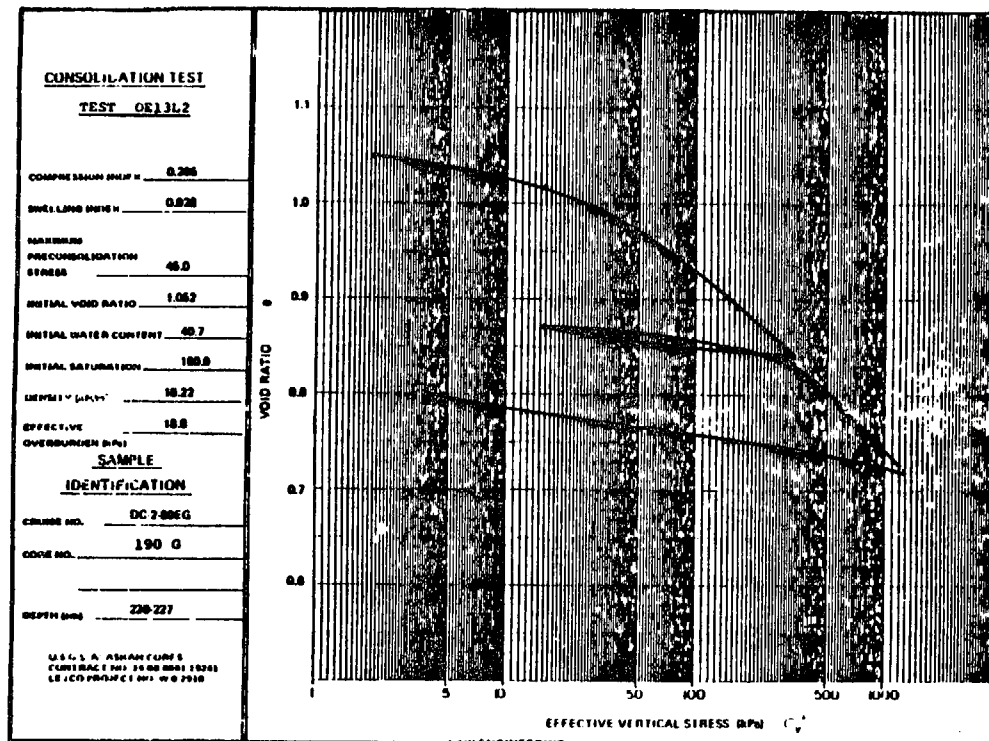
TEST OE12L2

COMPRESSION INDEX 0.156
 SWELLING INDEX 0.017
 MAXIMUM PRECONSOLIDATION STRESS 70
 INITIAL VOID RATIO 0.934
 INITIAL WATER CONTENT 31.48
 INITIAL SATURATION 86.3
 DENSITY (g/cm³) 1.886
 EFFECTIVE OVERBURDEN (kPa) 32

SAMPLE IDENTIFICATION
 CRUSH NO. DC2-80 EG
 CORE NO. 190 G
 DEPTH (mm) 30.38

U.S.G. ALASKAN CORES
 CONTRACT NO. 14-00-0001 10241
 LECO PROJECT NO. W-0-2010





CONSOLIDATION TEST

TEST OE17L2

COMPRESSION INDEX 0.108

SWELLING INDEX 0.027

MAXIMUM
PRECONSOLIDATION
STRESS 120.0

INITIAL VOID RATIO 0.882

INITIAL WATER CONTENT 21.8

INITIAL SATURATION 81.4

CHENE 20.20

EFFECTIVE
OVERBURDEN (psf) 46.8

SAMPLE

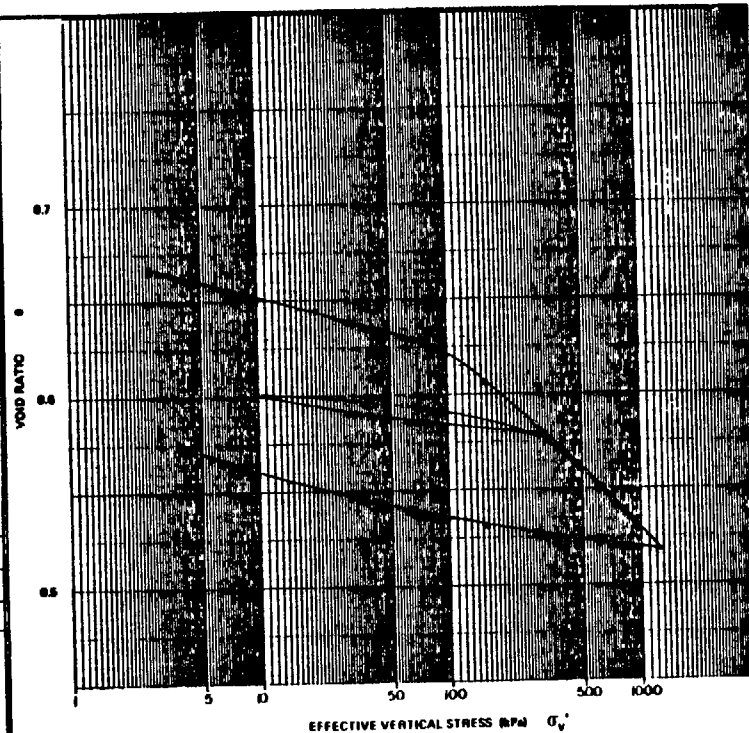
IDENTIFICATION

CRUISE NO. DC2-88EG

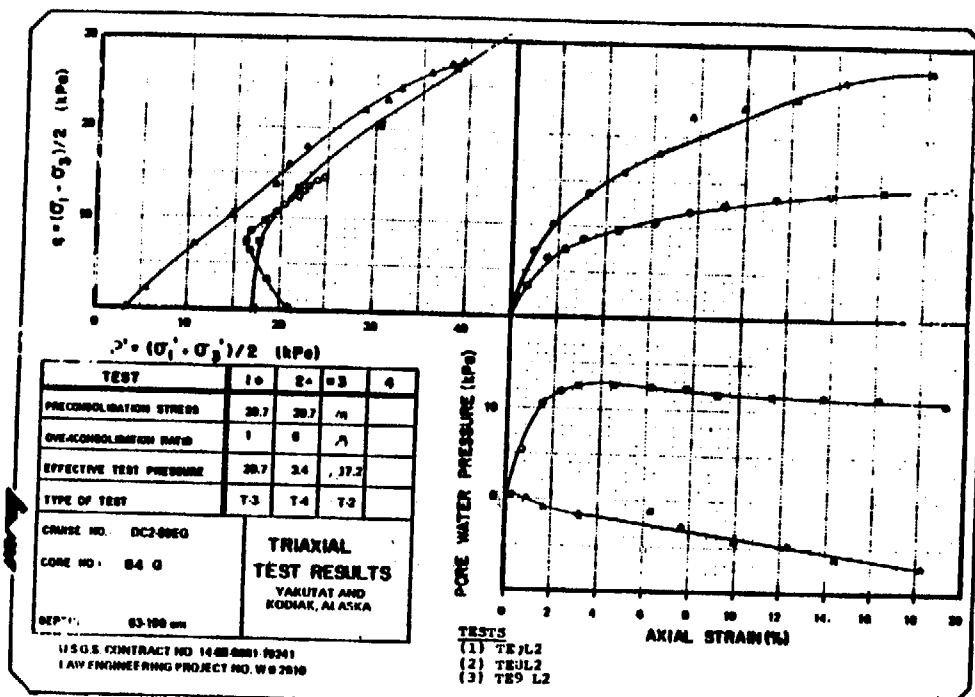
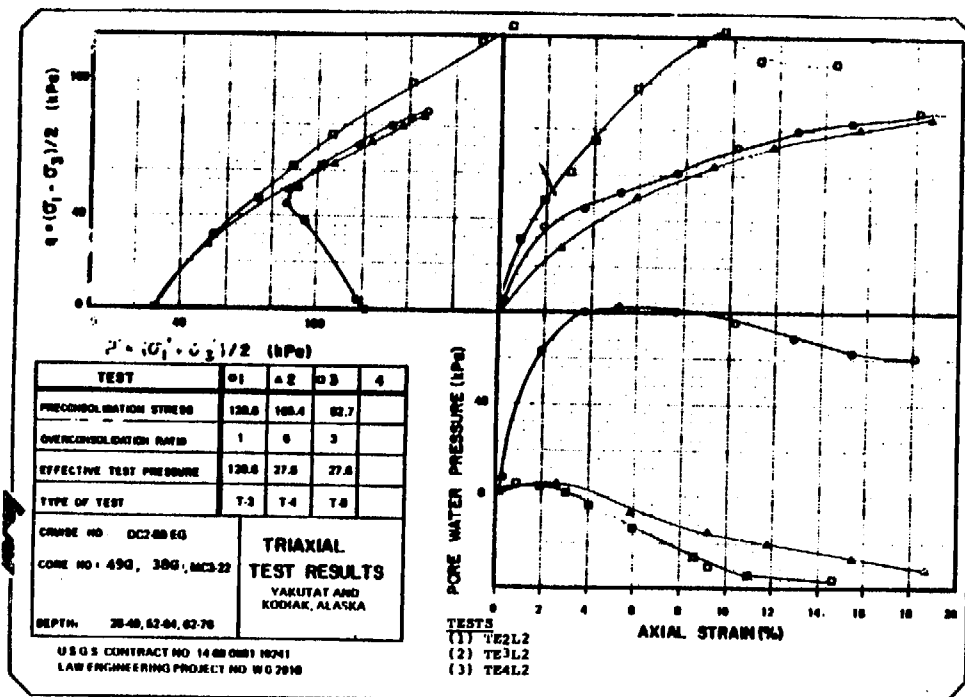
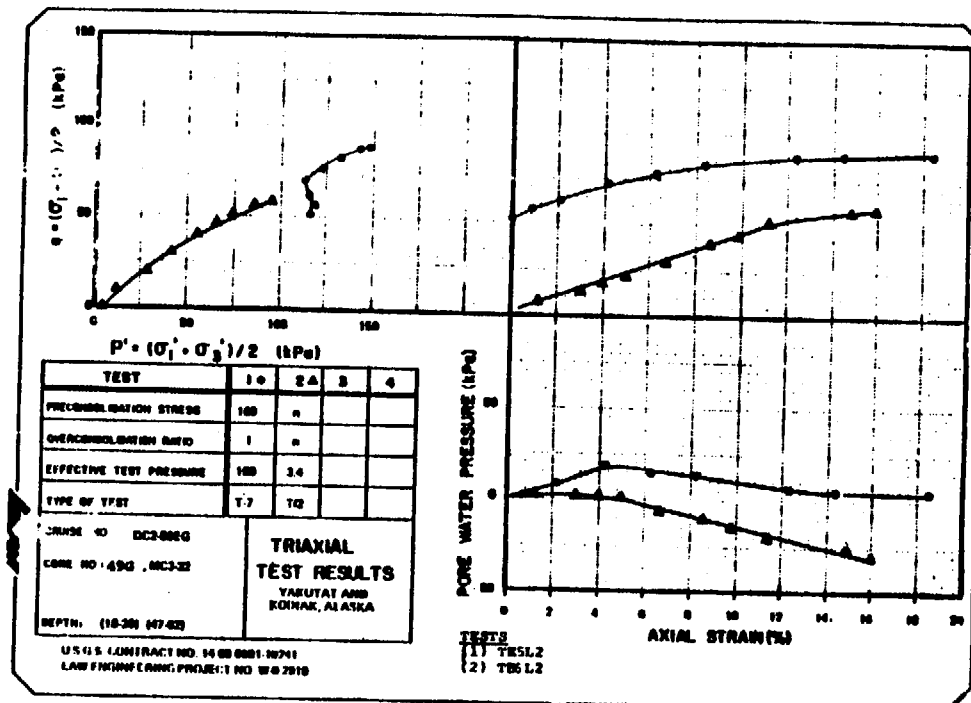
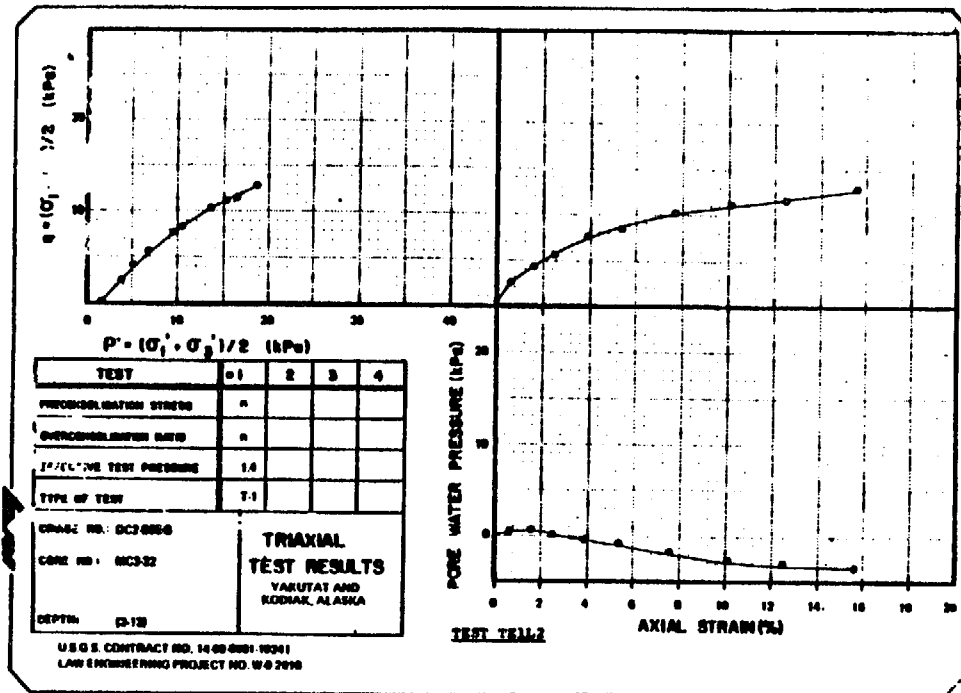
CODE NO. 196 G

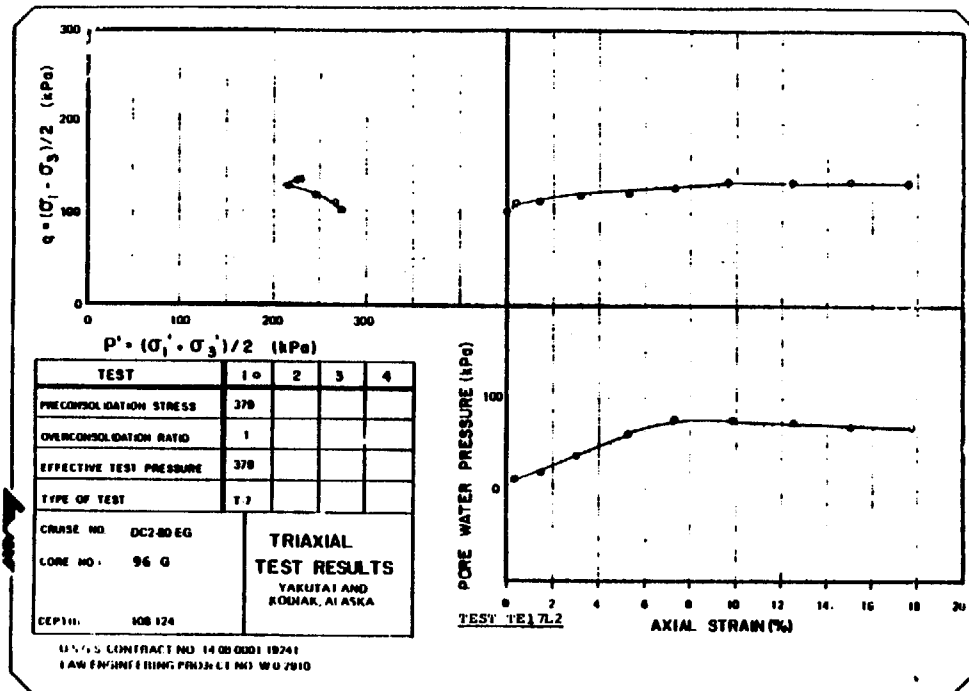
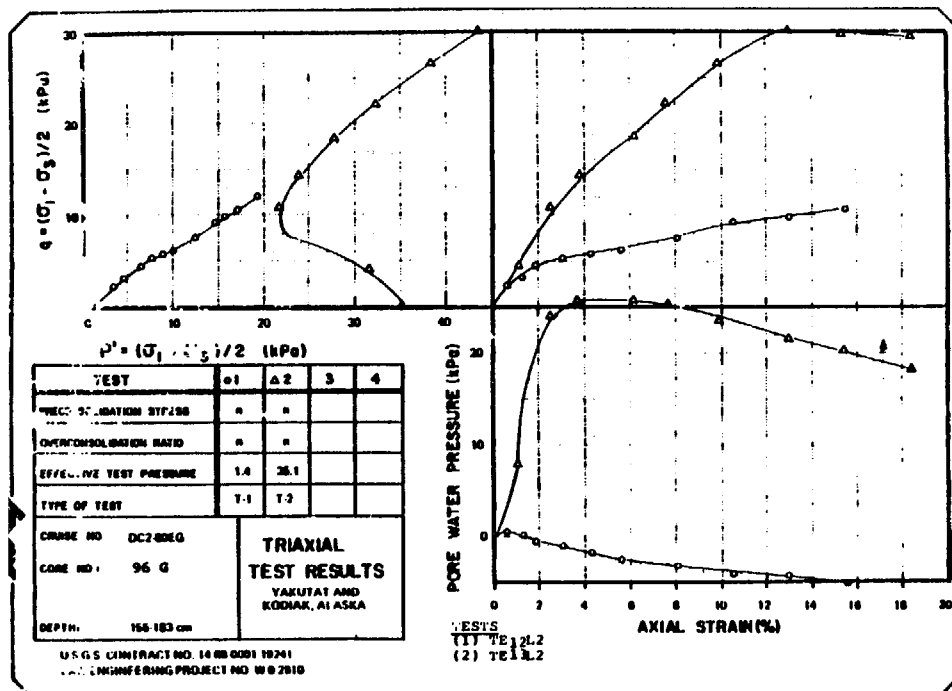
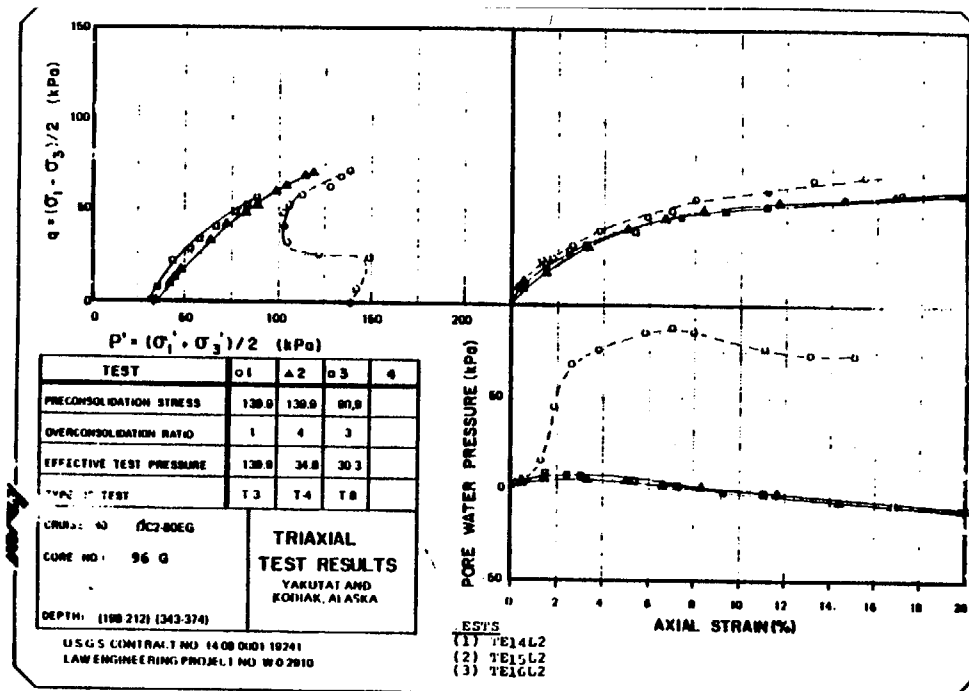
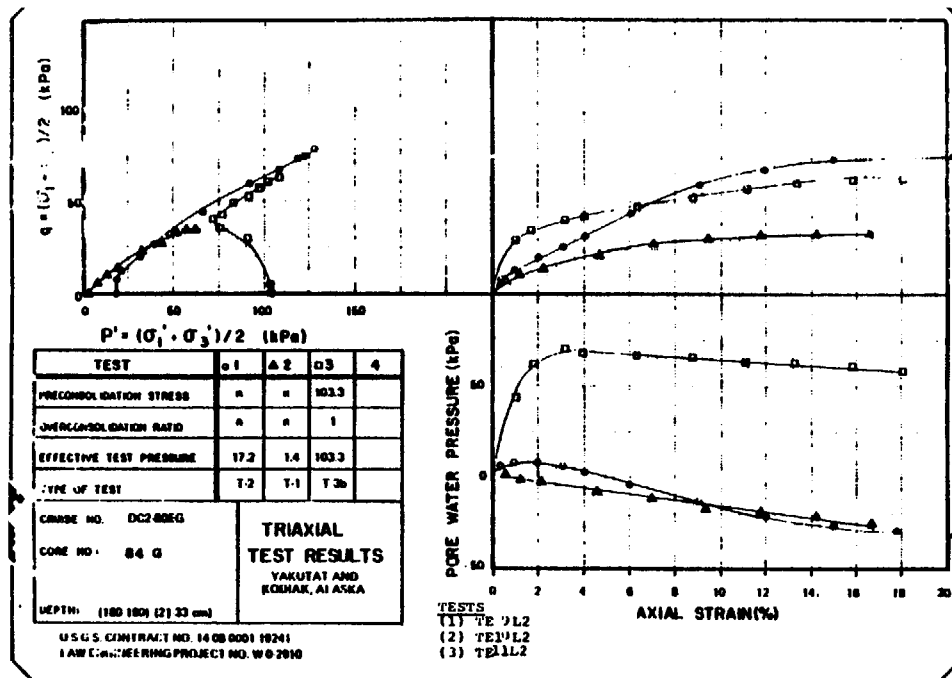
DEPTH (ft) 126-128

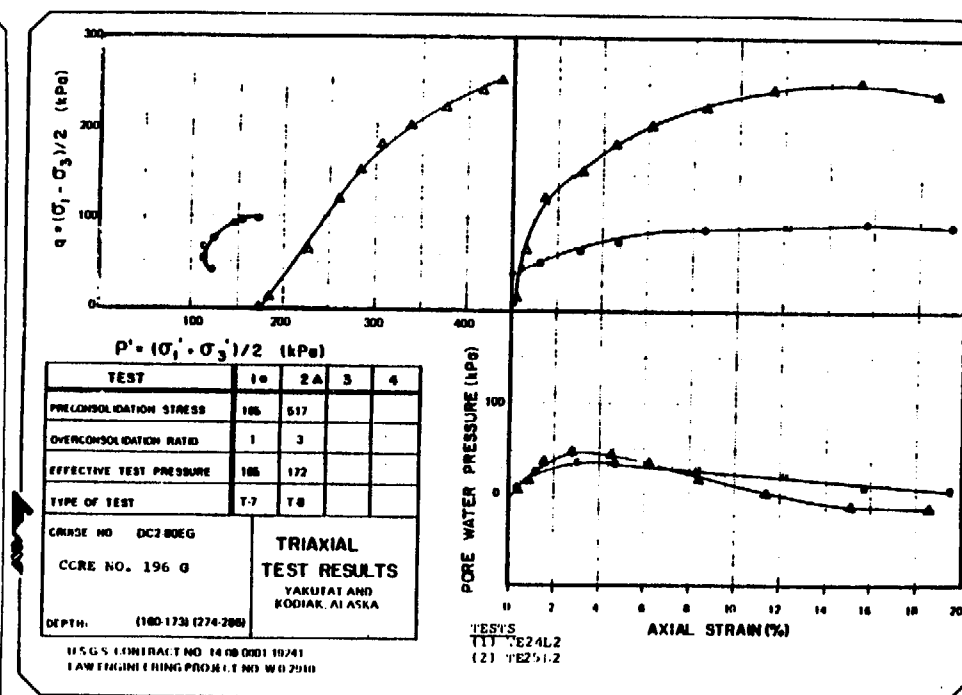
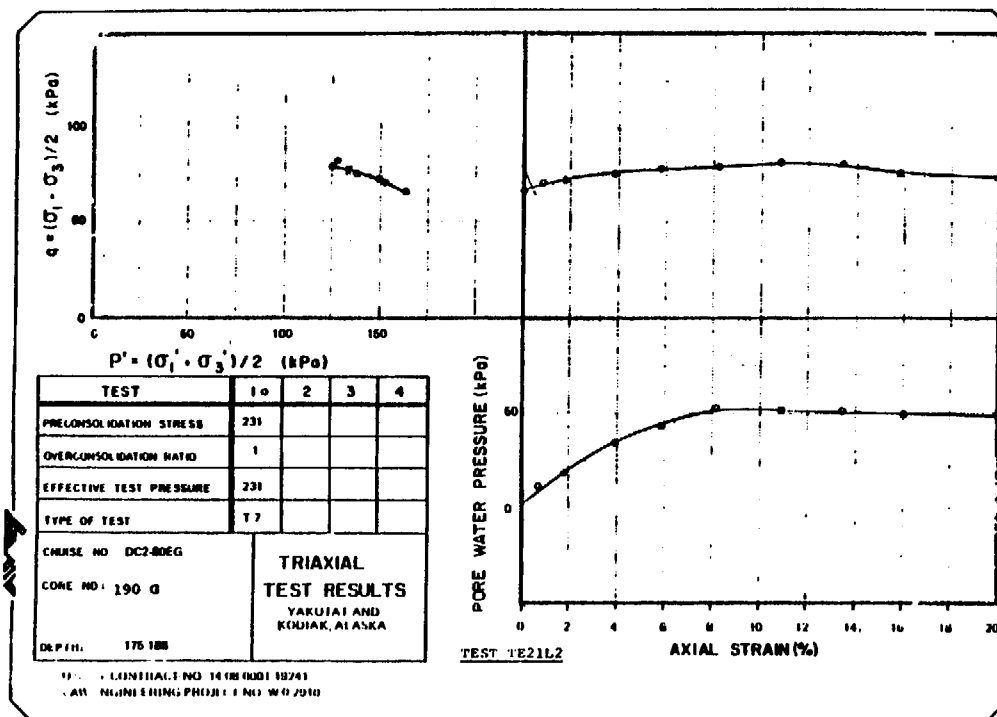
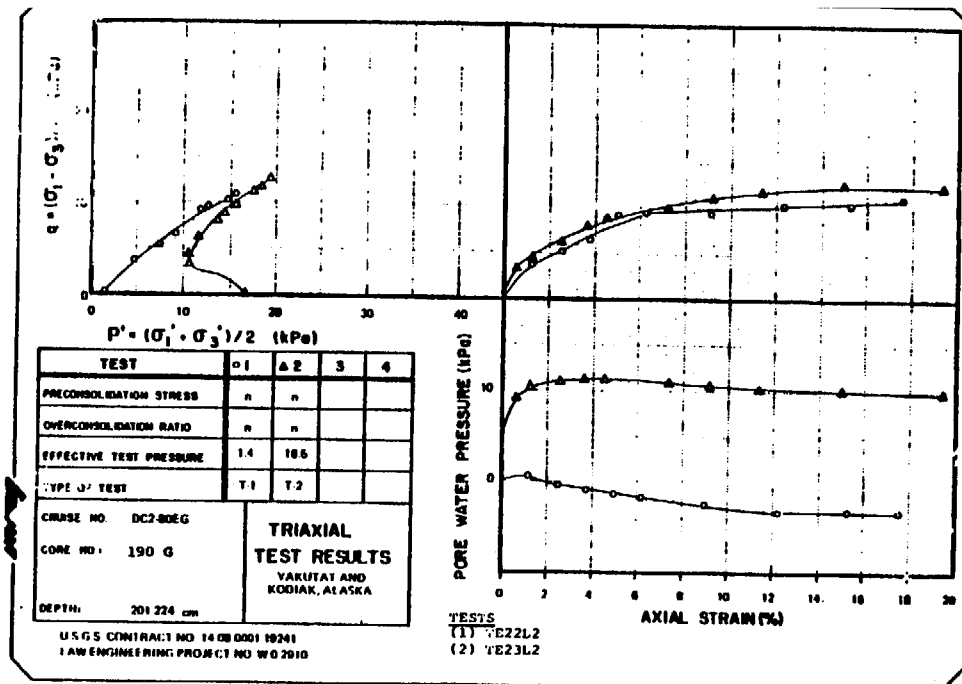
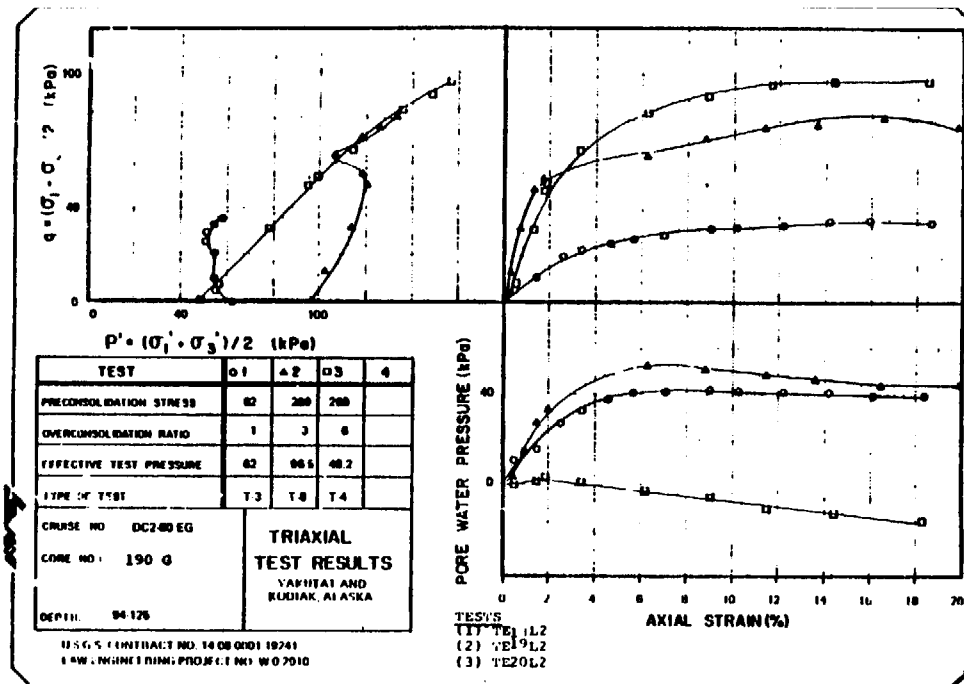
U.S.G.S. ALASKAN CORES
CONTRACT NO. 14-00-0002-10041
LETCO PROJECT NO. W-0-2010

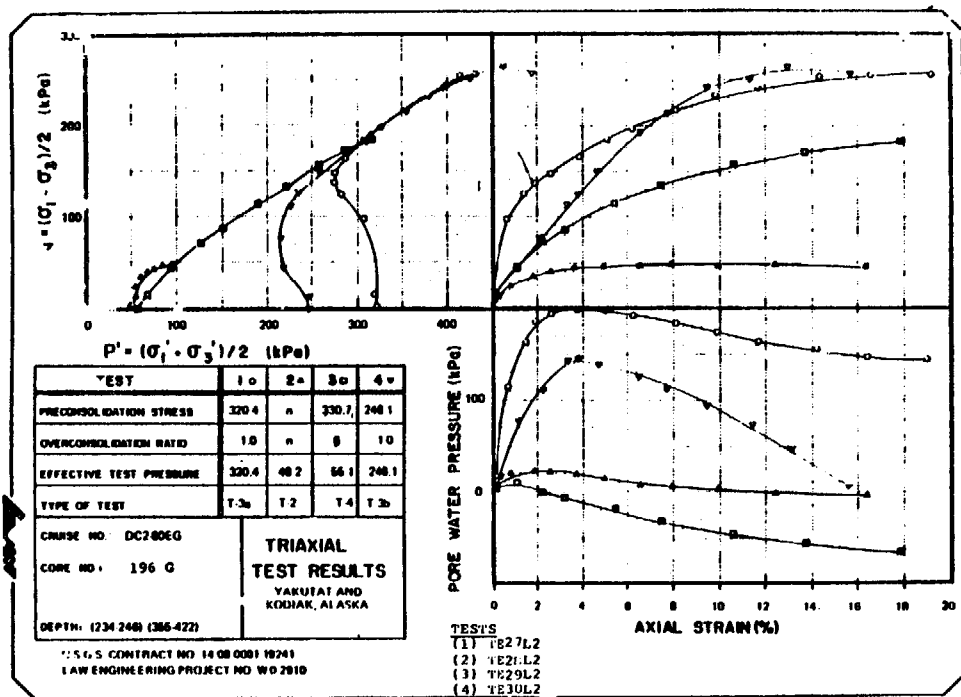
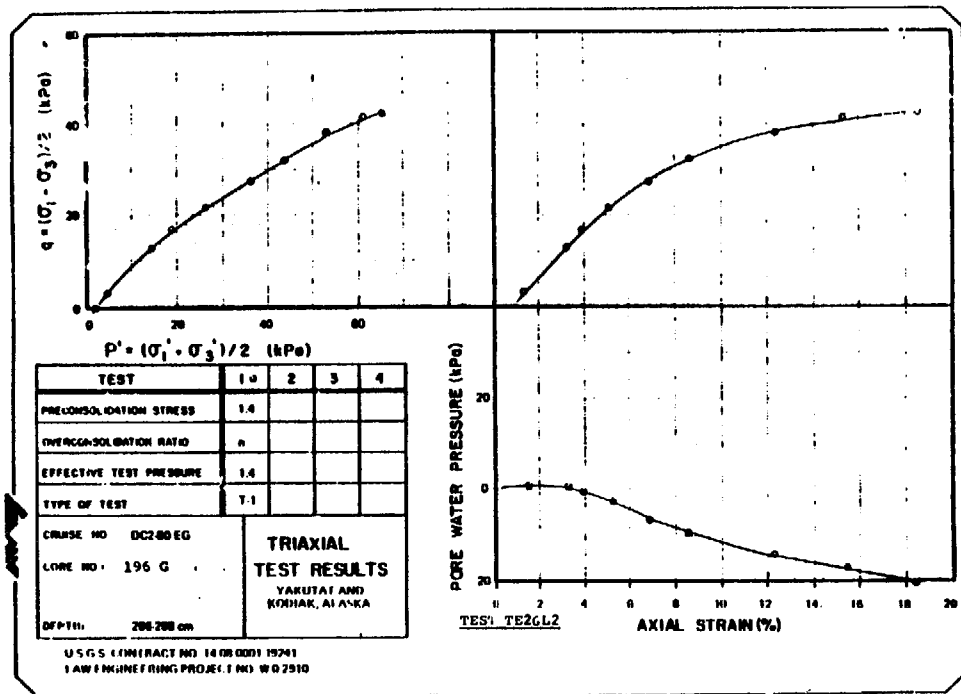


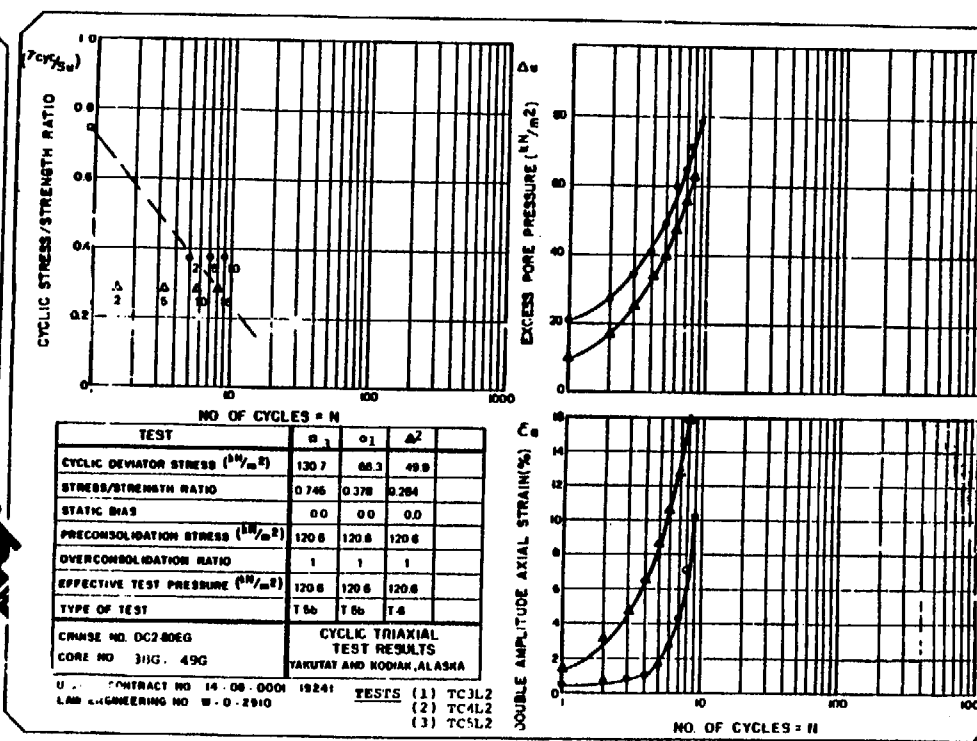
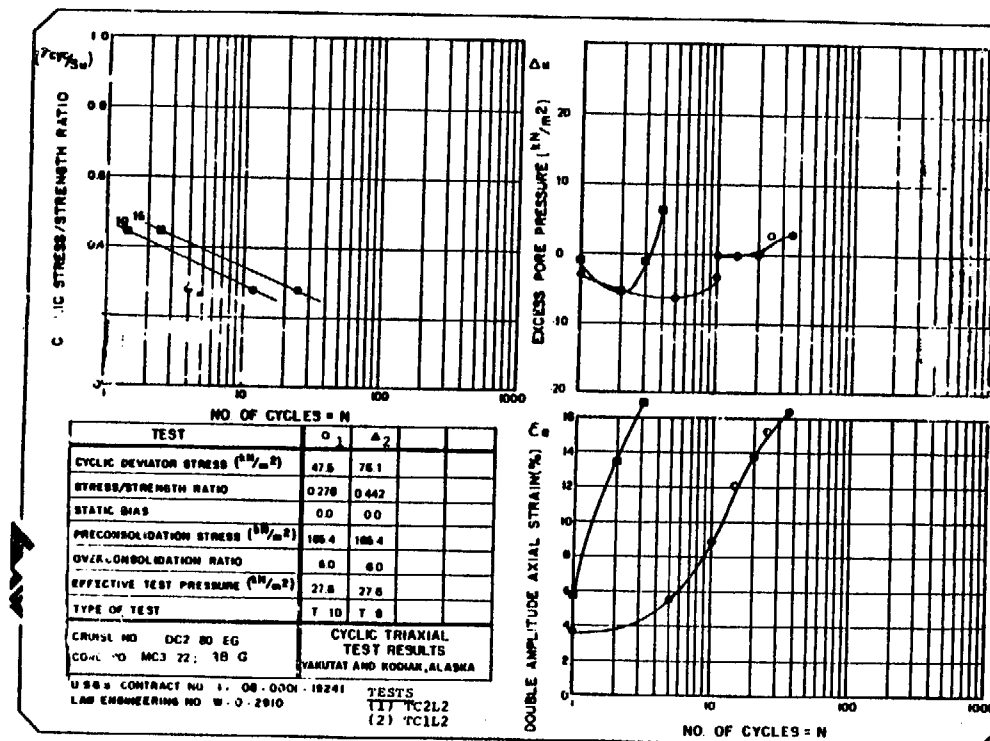
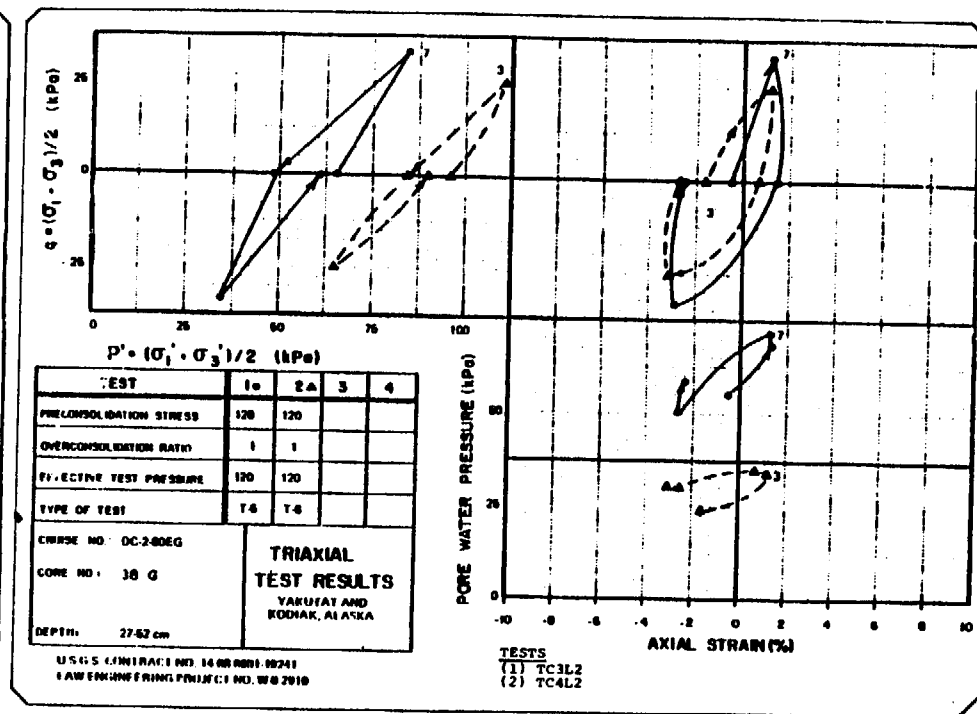
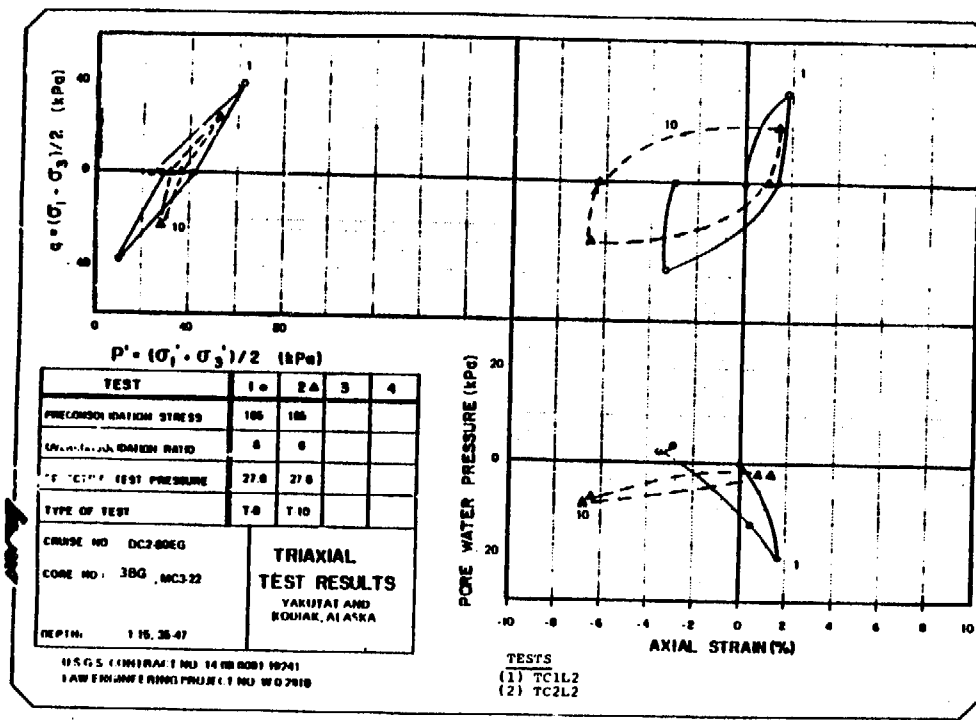
LAM ENGINEERING

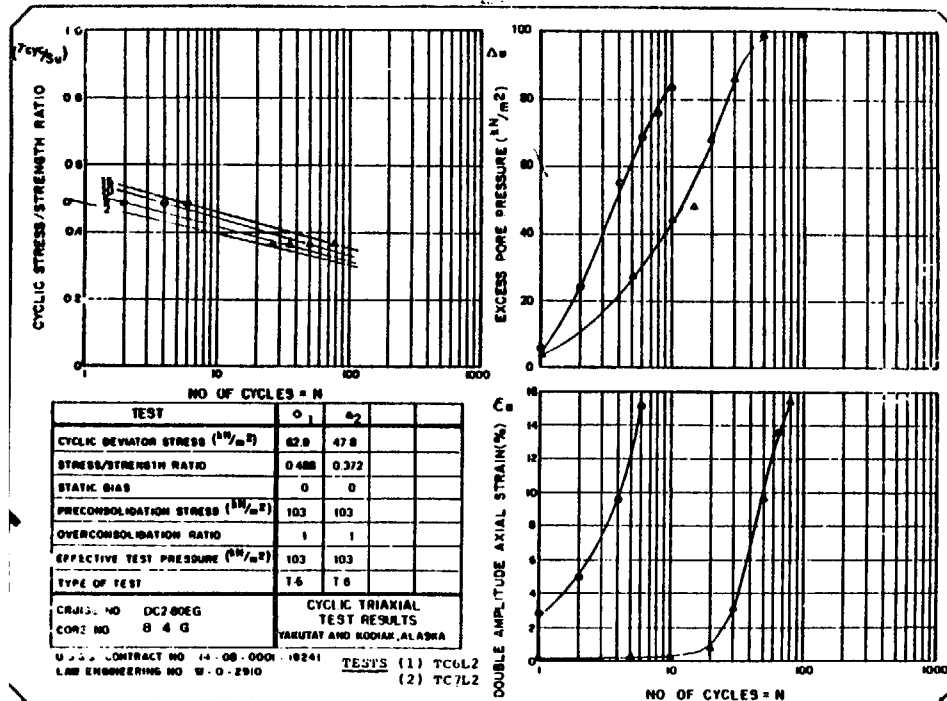
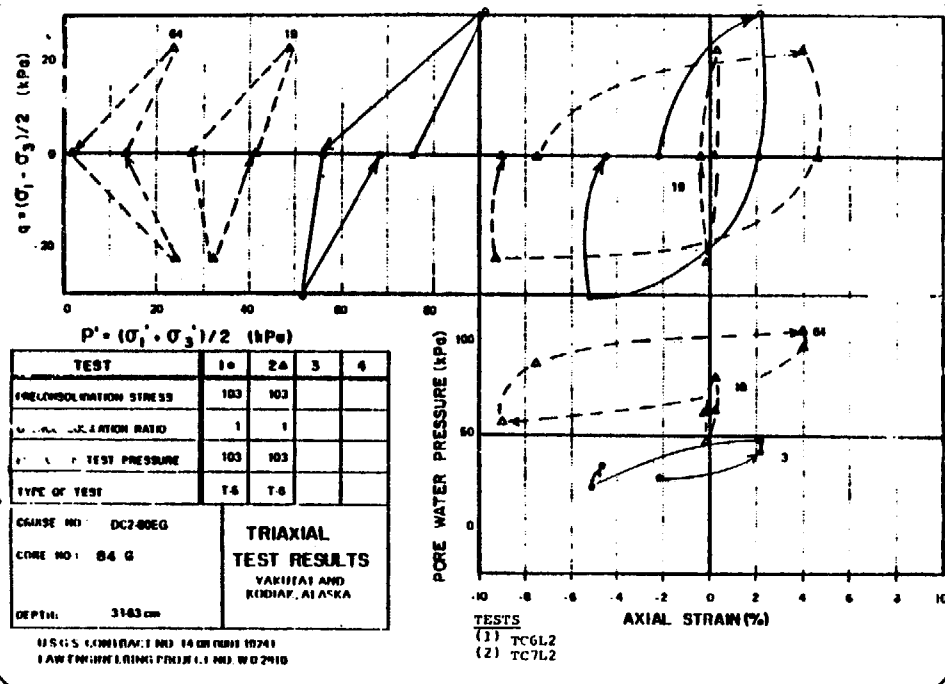


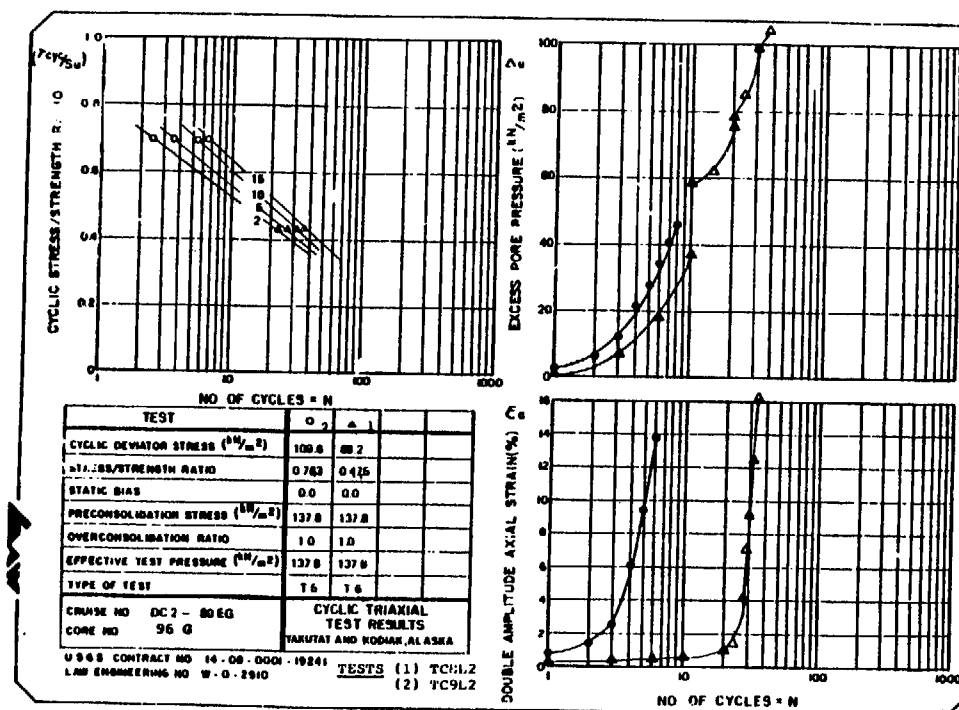
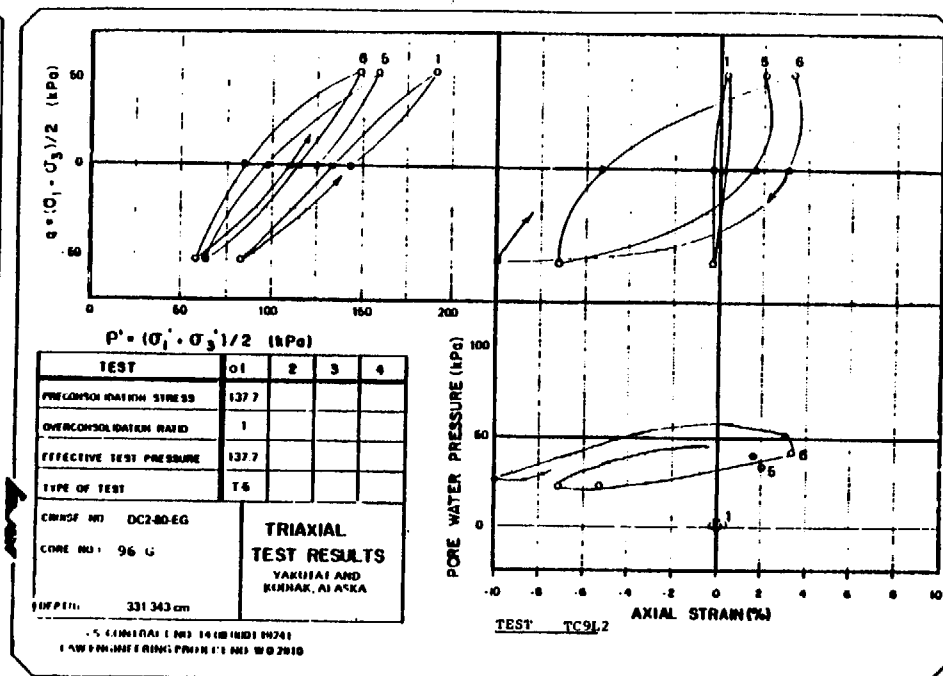
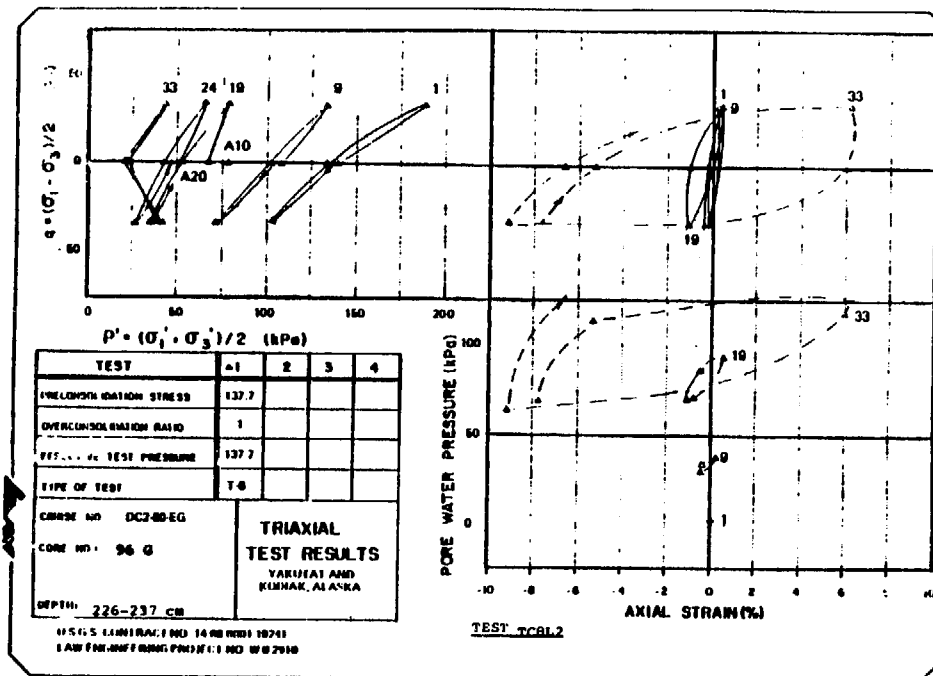


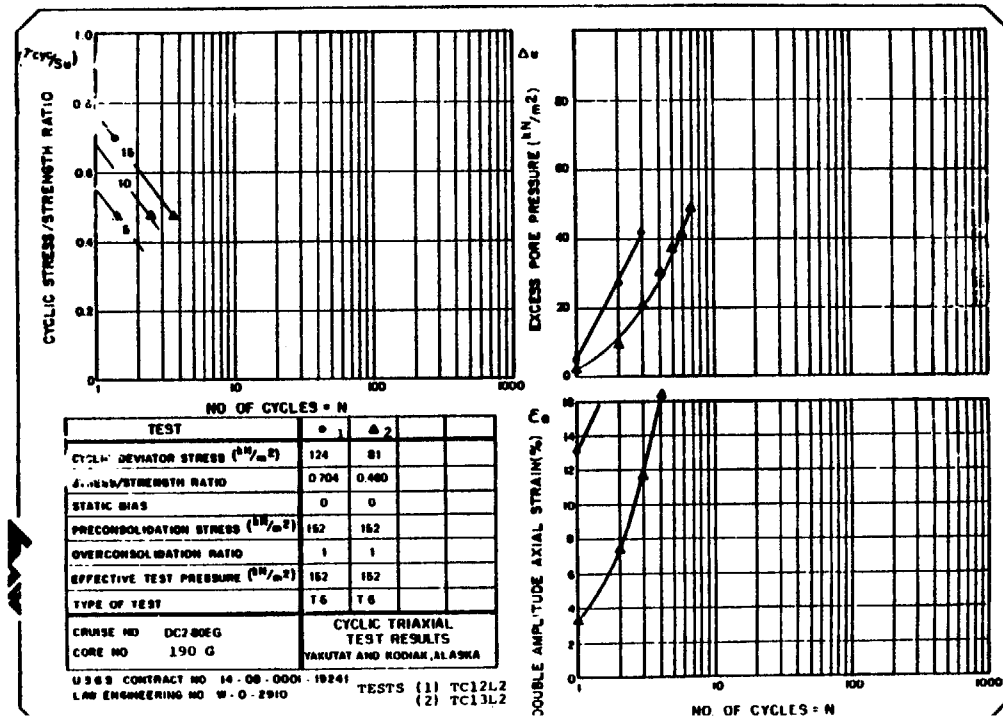
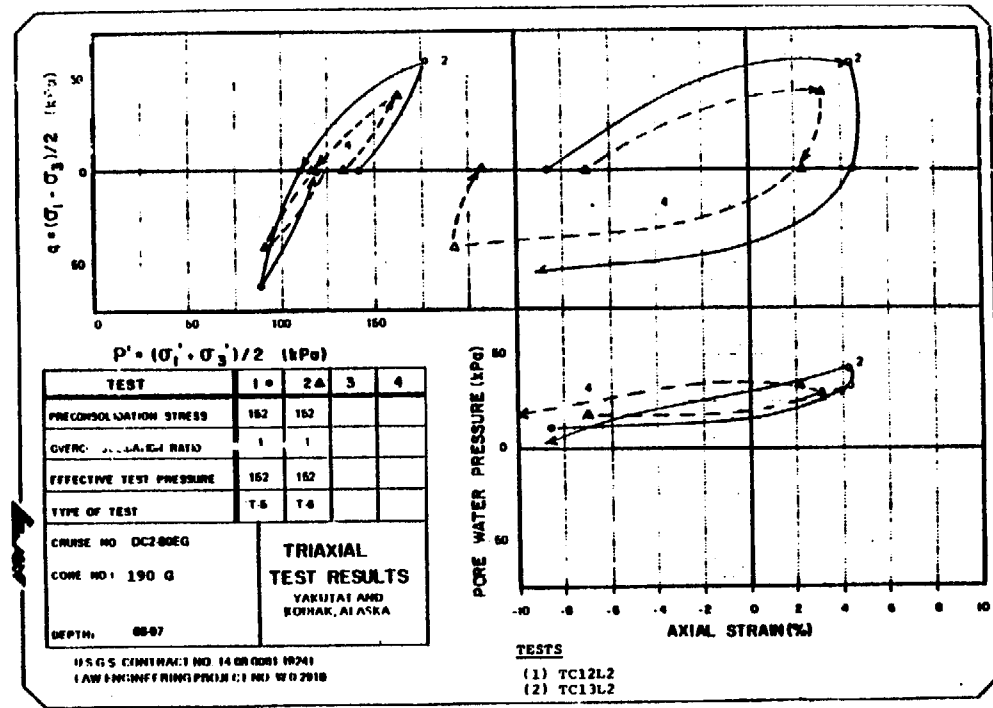
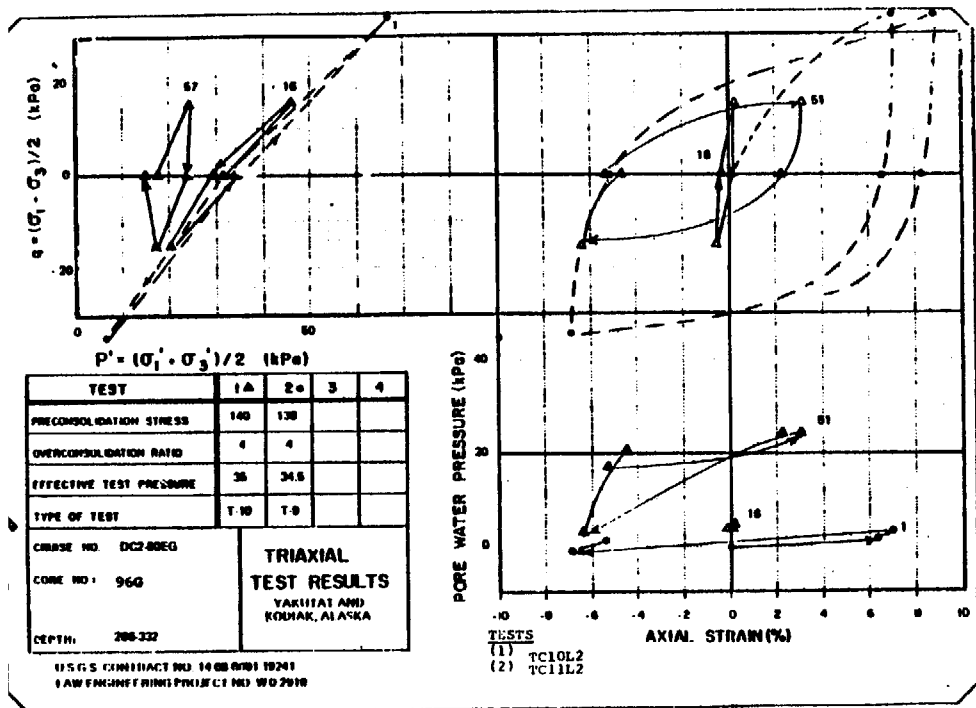


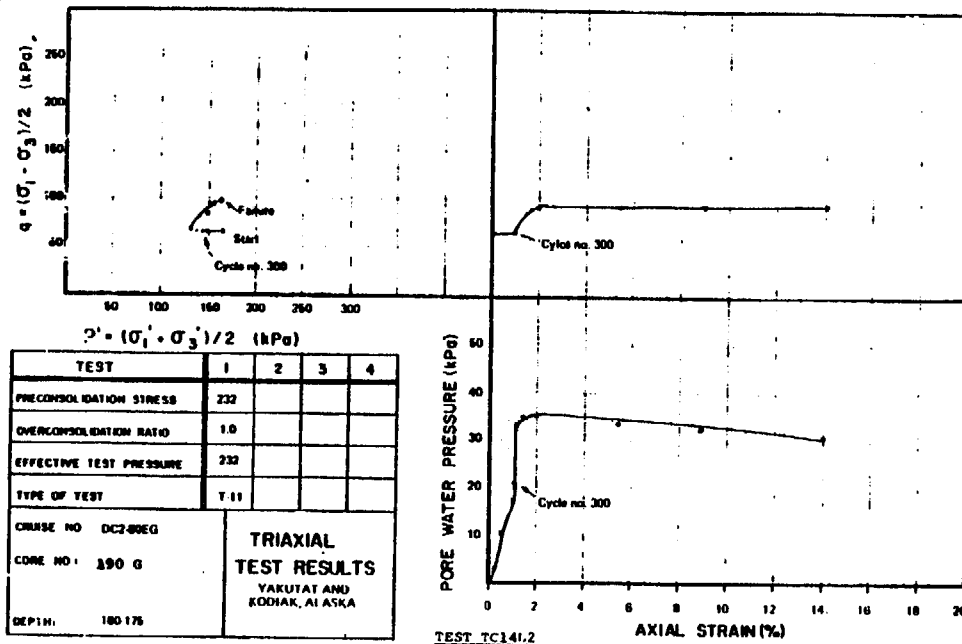










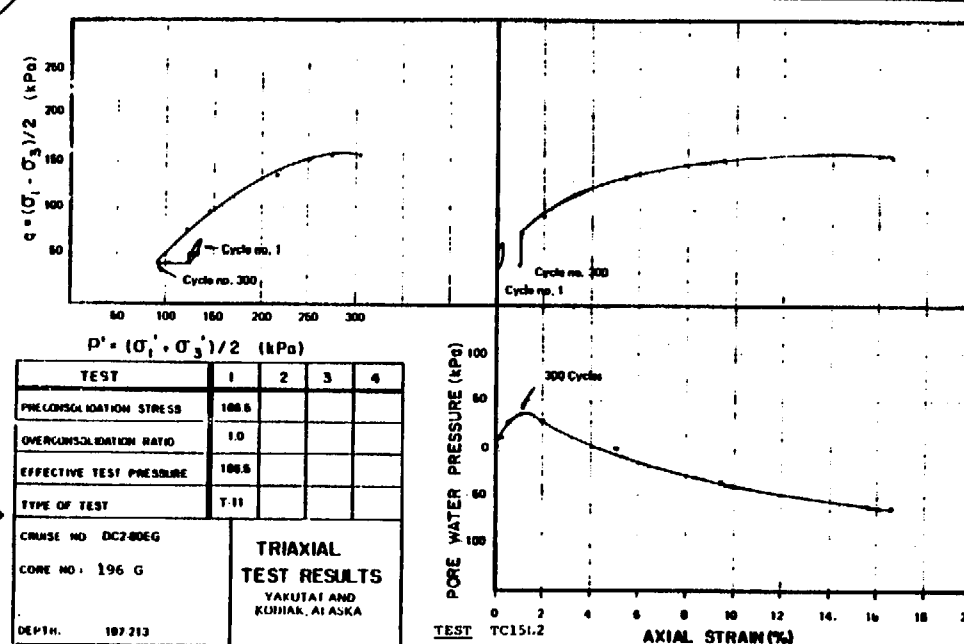


TEST	1	2	3	4
PRECONSOLIDATION STRESS	232			
OVERCONSOLIDATION RATIO	1.0			
EFFECTIVE TEST PRESSURE	232			
TYPE OF TEST	T-11			
COURSE NO. DC280EG				
CORE NO. 190 G				
DEPTH. 180.175				

TRIAXIAL TEST RESULTS
YAKUTAI AND KODIAK, ALASKA

TEST TC14L2

AXIAL STRAIN (%)

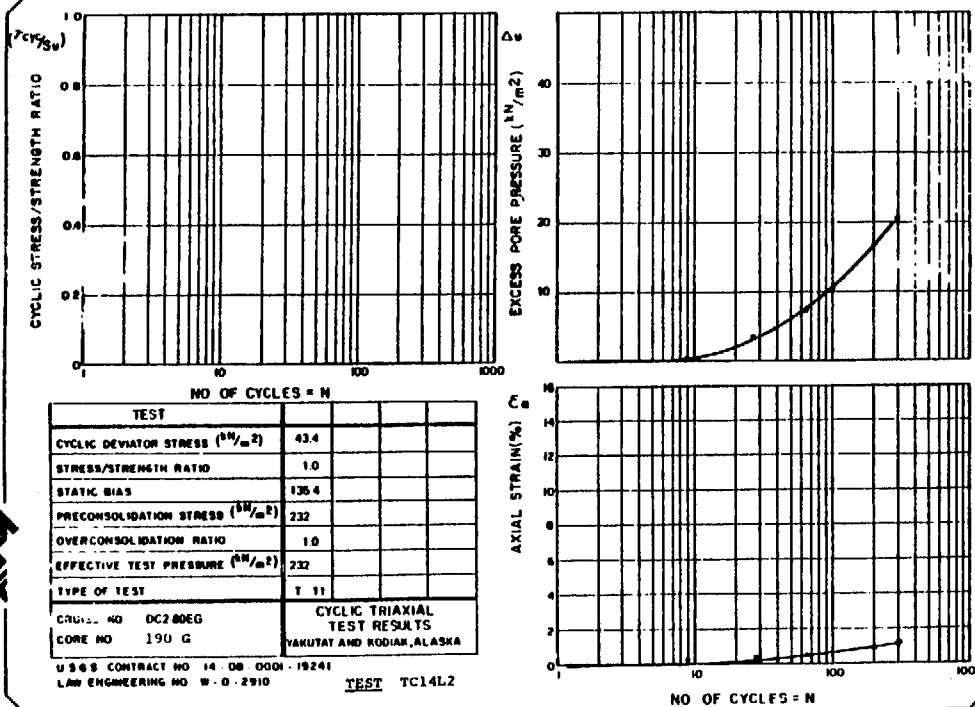


TEST	1	2	3	4
PRECONSOLIDATION STRESS	108.5			
OVERCONSOLIDATION RATIO	1.0			
EFFECTIVE TEST PRESSURE	108.5			
TYPE OF TEST	T-11			
COURSE NO. DC280EG				
CORE NO. 196 G				
DEPTH. 187.213				

TRIAXIAL TEST RESULTS
YAKUTAI AND KODIAK, ALASKA

TEST TC15L2

AXIAL STRAIN (%)

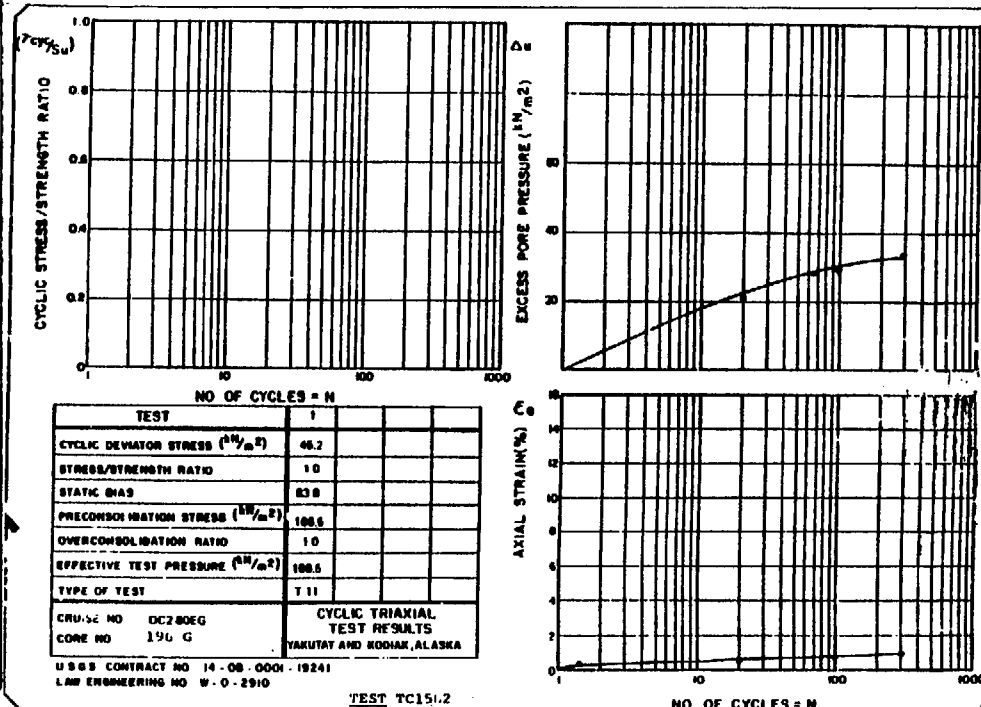


TEST	1	2	3	4
CYCLIC DEVIATOR STRESS (N/m^2)	43.4			
STRESS/STRENGTH RATIO	1.0			
STATIC BIAS	136.4			
PRECONSOLIDATION STRESS (N/m^2)	232			
OVERCONSOLIDATION RATIO	1.0			
EFFECTIVE TEST PRESSURE (N/m^2)	232			
TYPE OF TEST	T-11			
COURSE NO. DC280EG				
CORE NO. 190 G				

CYCLIC TRIAXIAL TEST RESULTS
YAKUTAI AND KODIAK, ALASKA

TEST TC14L2

NO OF CYCLES = N

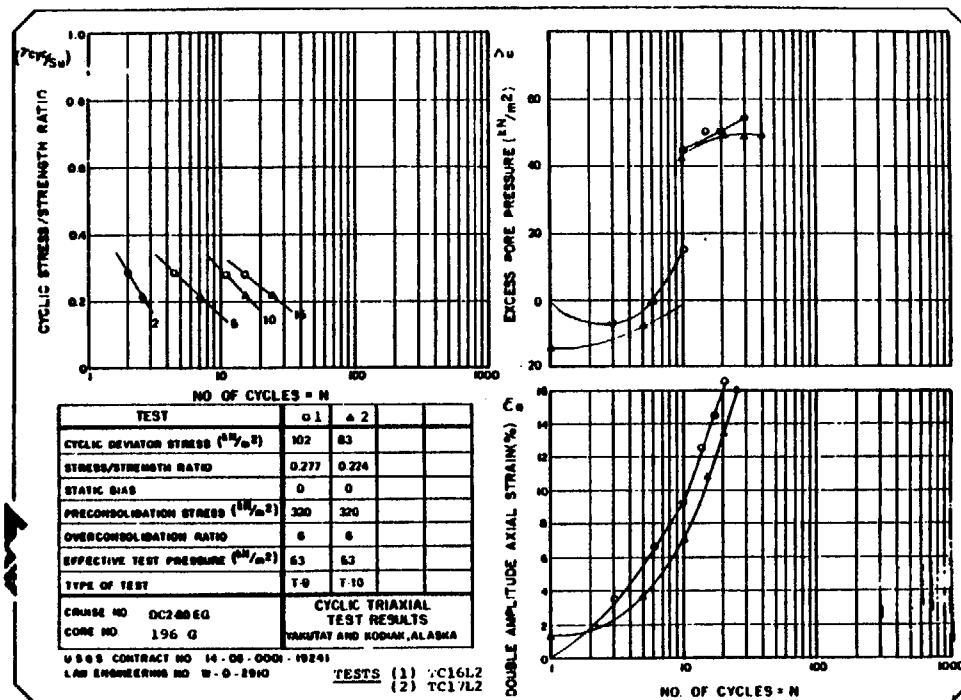
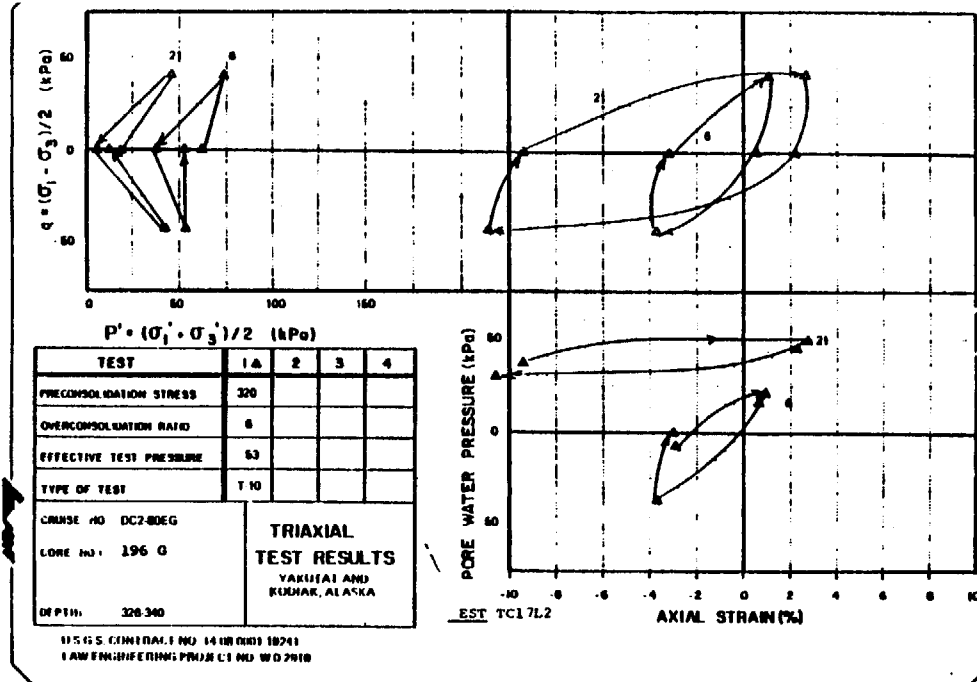
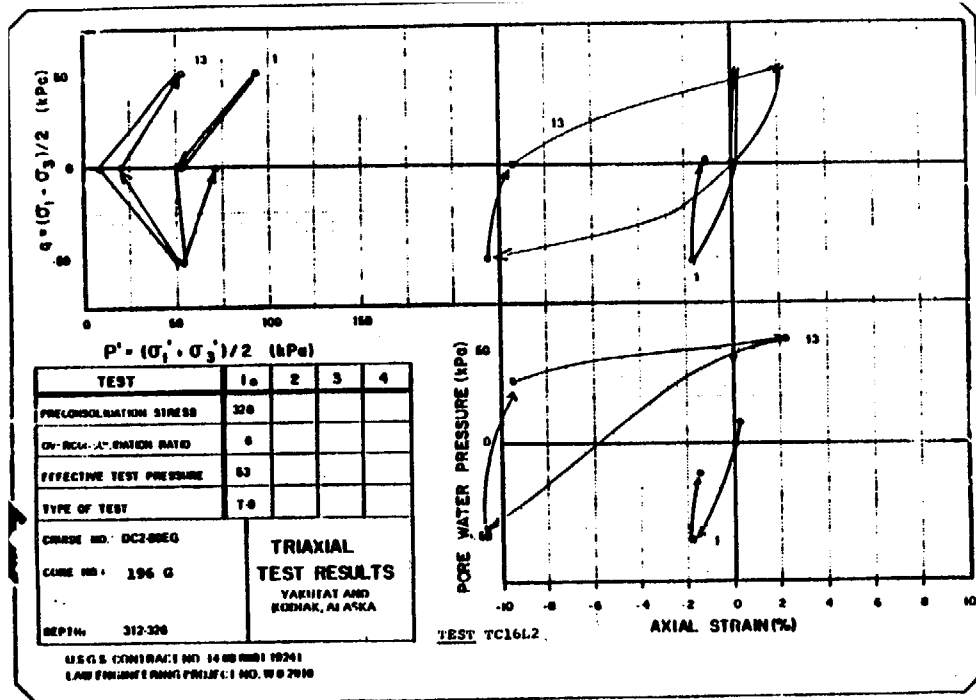


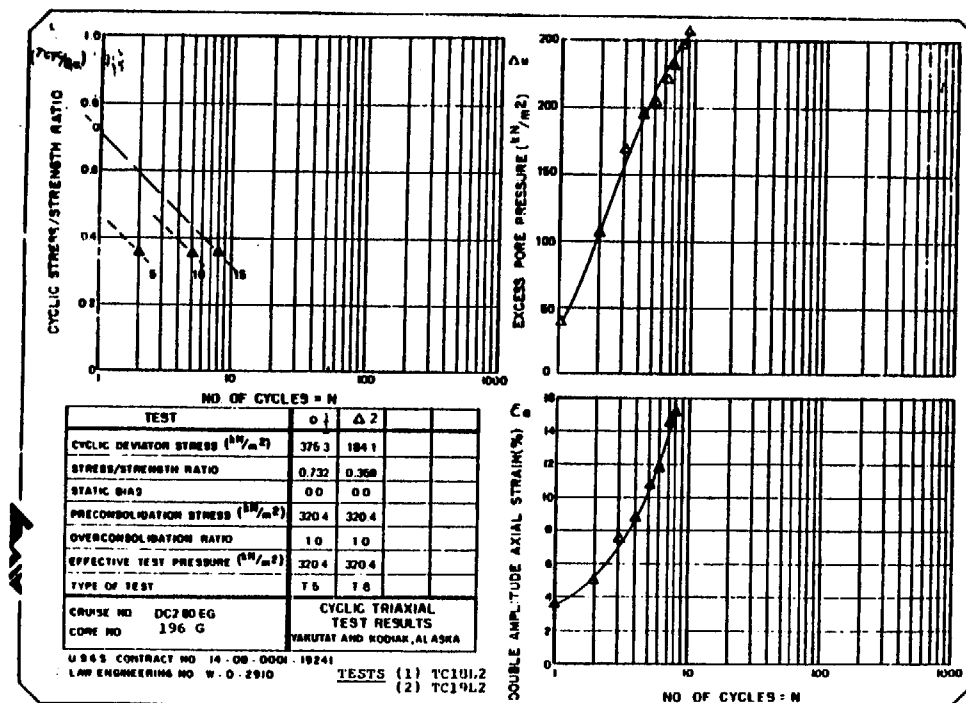
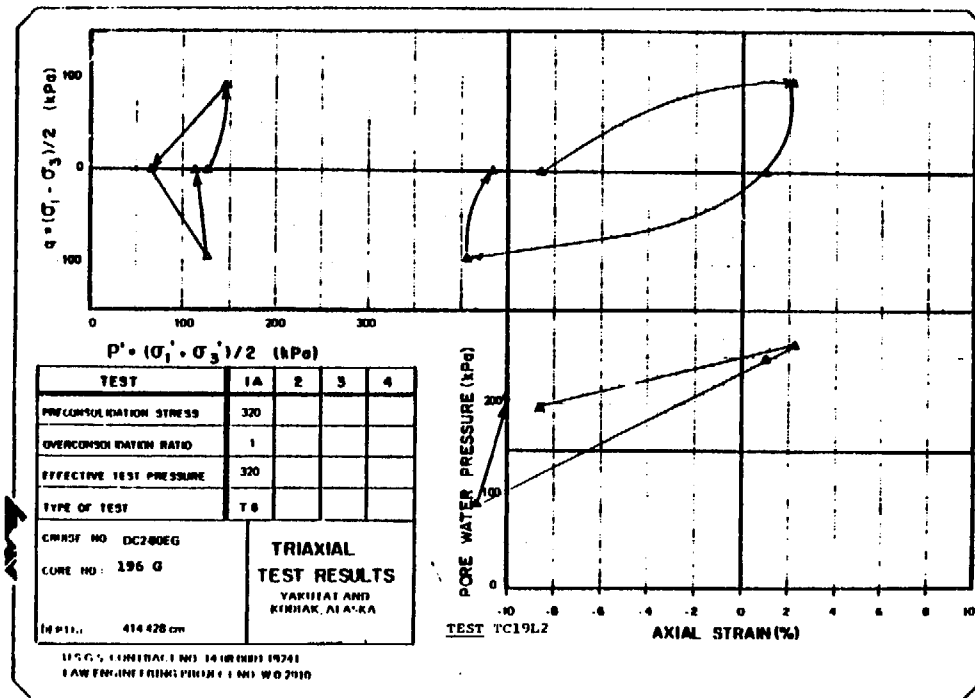
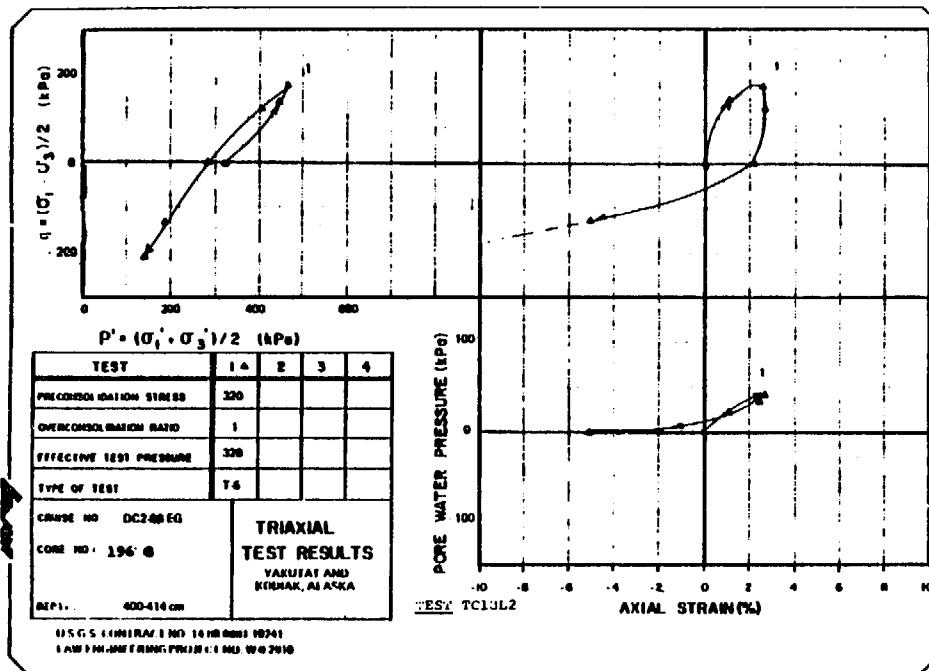
TEST	1	2	3	4
CYCLIC DEVIATOR STRESS (N/m^2)	46.2			
STRESS/STRENGTH RATIO	1.0			
STATIC BIAS	133.8			
PRECONSOLIDATION STRESS (N/m^2)	108.5			
OVERCONSOLIDATION RATIO	1.0			
EFFECTIVE TEST PRESSURE (N/m^2)	108.5			
TYPE OF TEST	T-11			
COURSE NO. DC280EG				
CORE NO. 196 G				

CYCLIC TRIAXIAL TEST RESULTS
YAKUTAI AND KODIAK, ALASKA

TEST TC15L2

NO OF CYCLES = N





APPENDIX G

CONSOLIDATION AND TRIAXIAL TEST RESULTS--

U.S. GEOLOGICAL SURVEY (1980 AND 1981 cores)

APPENDIX G. CONSOLIDATION AND TRIAXIAL TEST RESULTS-U.S. GEOLOGICAL SURVEY
(1980 and 1981 cores)

This appendix presents the results of consolidation and triaxial testing performed at the U.S. Geological Survey's marine geotechnical laboratory. Core samples were from cruises DC2-80-EG and DC1-81-EG. Results were automatically recorded, reduced and plotted.

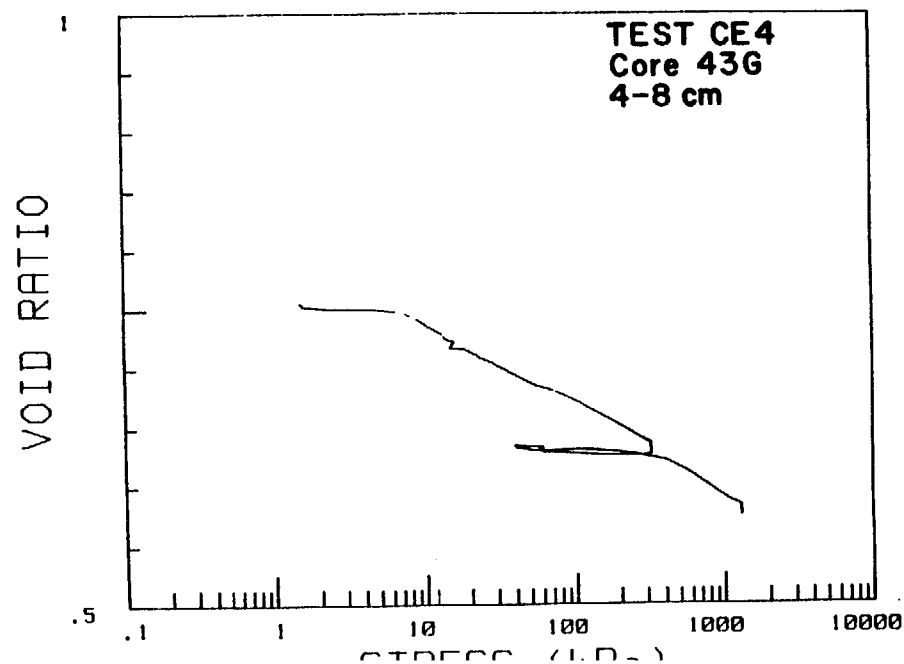
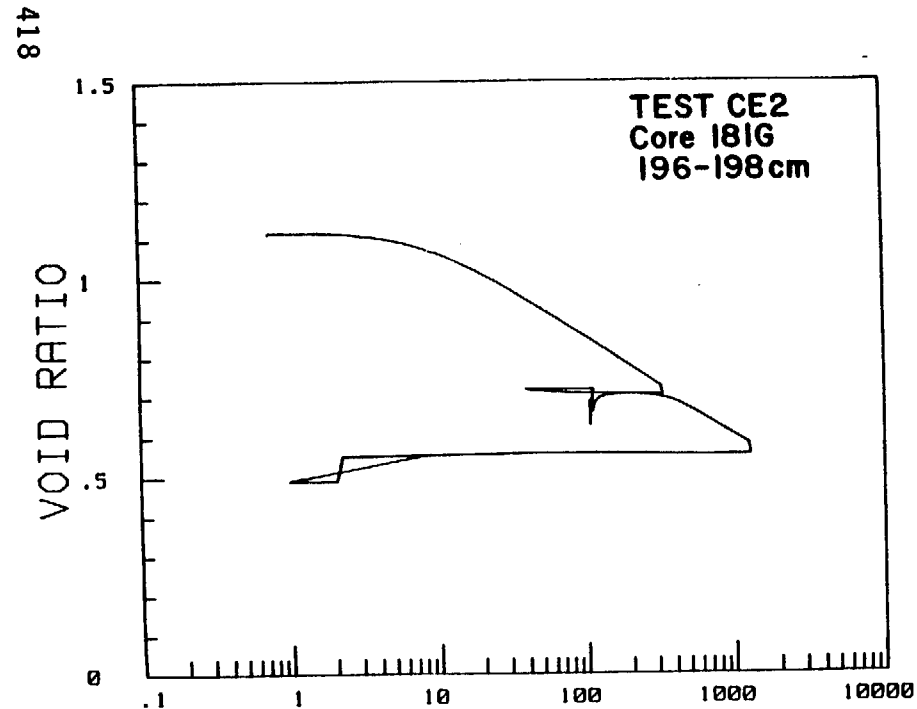
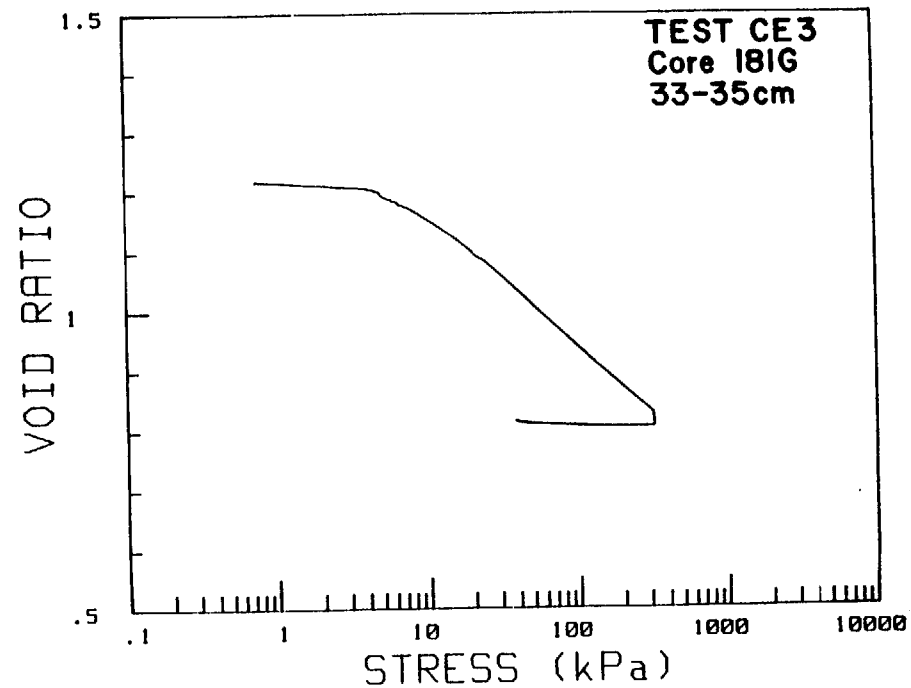
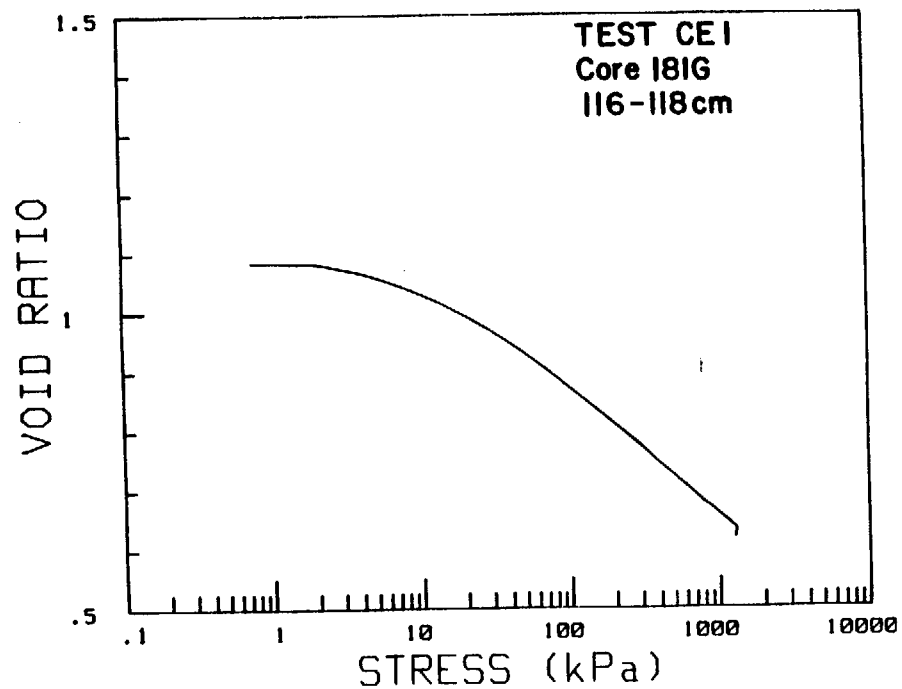
The tests in this group do not have trailing characters in their test numbers. The consolidation tests (first characters are CE for constant rate of strain, CRS, tests and OE for oedometer tests) are presented first and are ordered by test number. Results from a single test are presented on a single page in the form of void ratio and calculated coefficient of consolidation (c_v) versus the vertical effective stress (identified as STRESS). Some of the plots for CRS tests are irregular as a result of transducer drift.

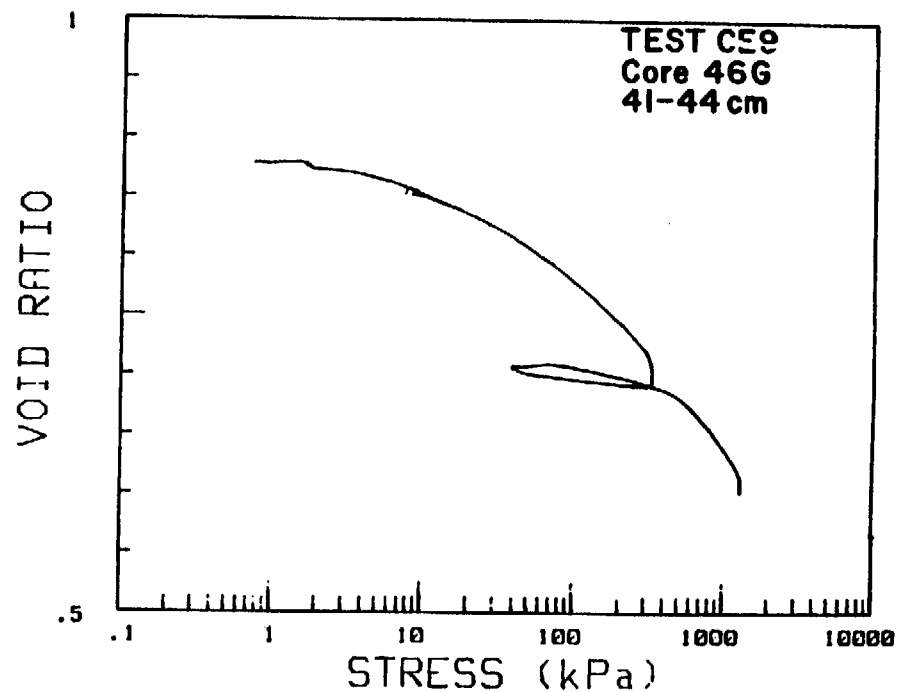
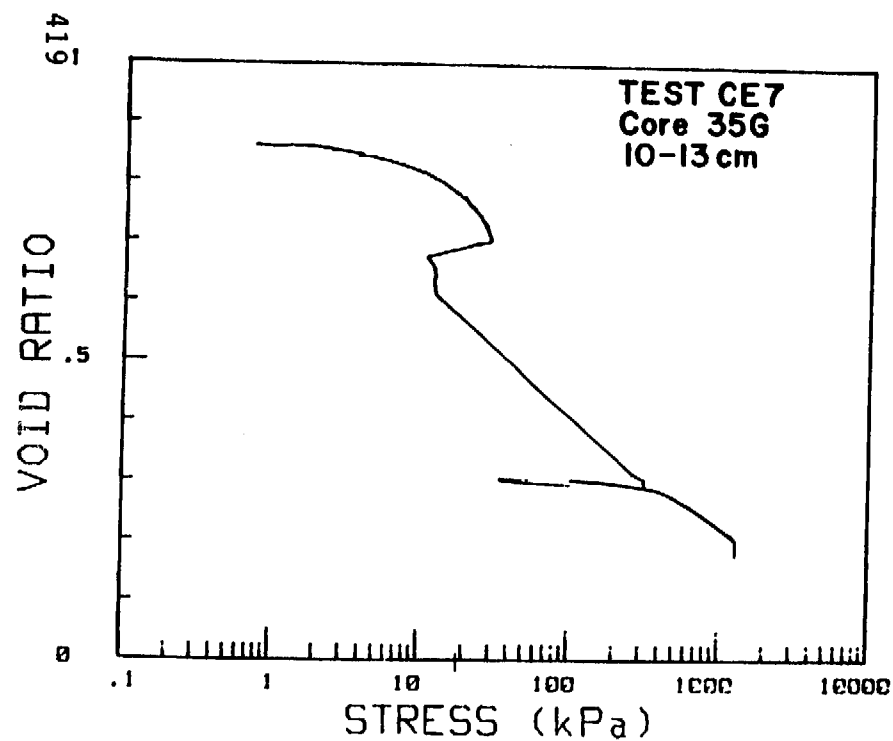
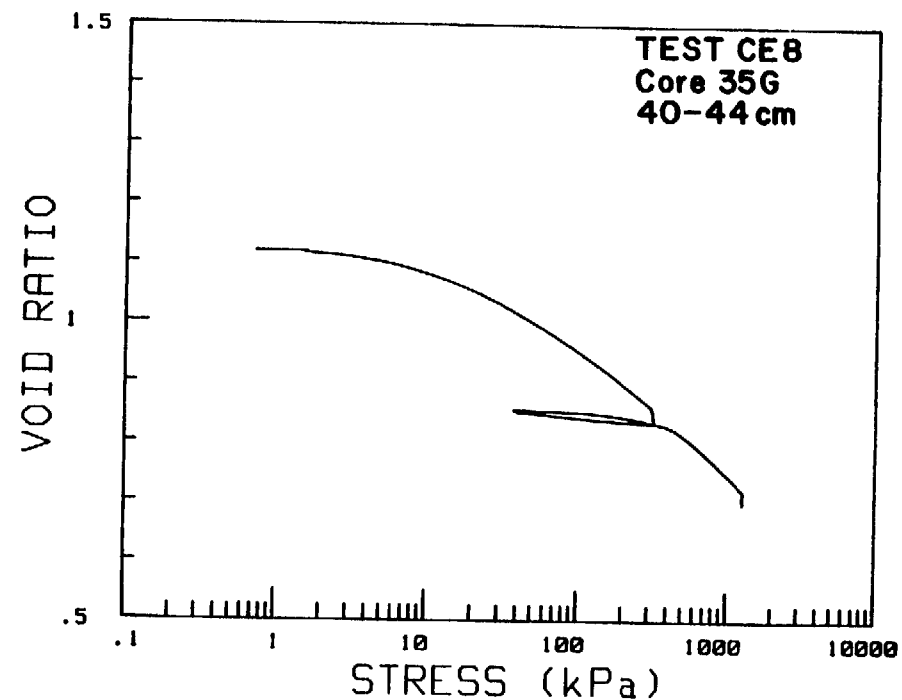
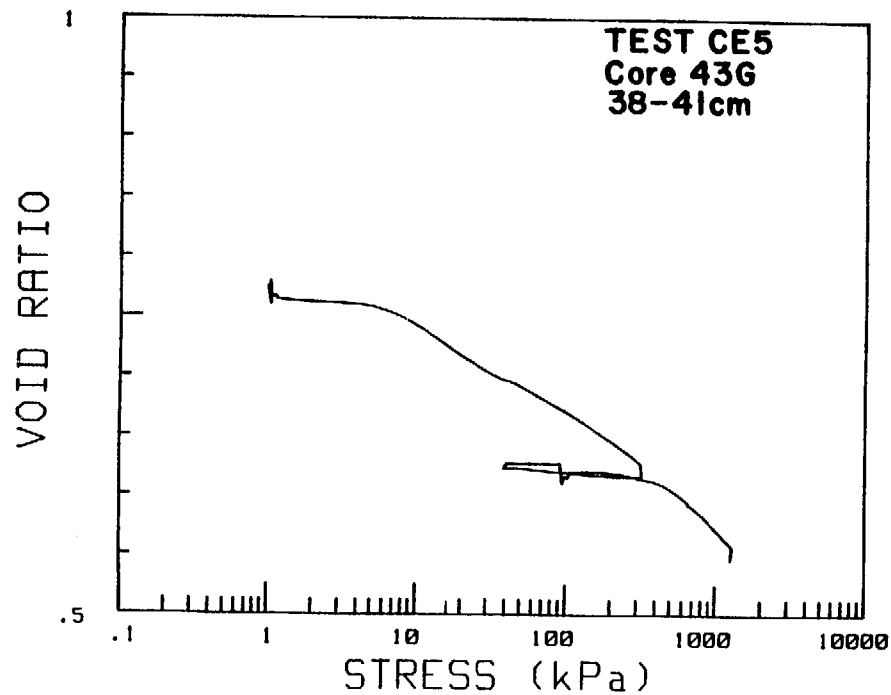
Static triaxial tests (first two characters are TE) are given second and ordered by test number. The upper left graph is a stress path presented as a plot of maximum shear stress (q) versus the normal effective stress on the plane of maximum shear (p'). The stress path plots of Appendix D are defined differently. The upper right plot is the maximum shearing stress versus strain. The lower right plot is the measured excess pore water pressure (Δu) versus axial strain. The title block gives $SIG1c'$ and $SIG3'$ which are the vertical and horizontal consolidation stresses, respectively. The induced OCR is the overconsolidation ratio forced on the sample in the triaxial cell. A value of 1.0 may **or** may not correspond to true overconsolidation because the triaxial cell consolidation stress may be less than the maximum past stress the sample experienced in place.

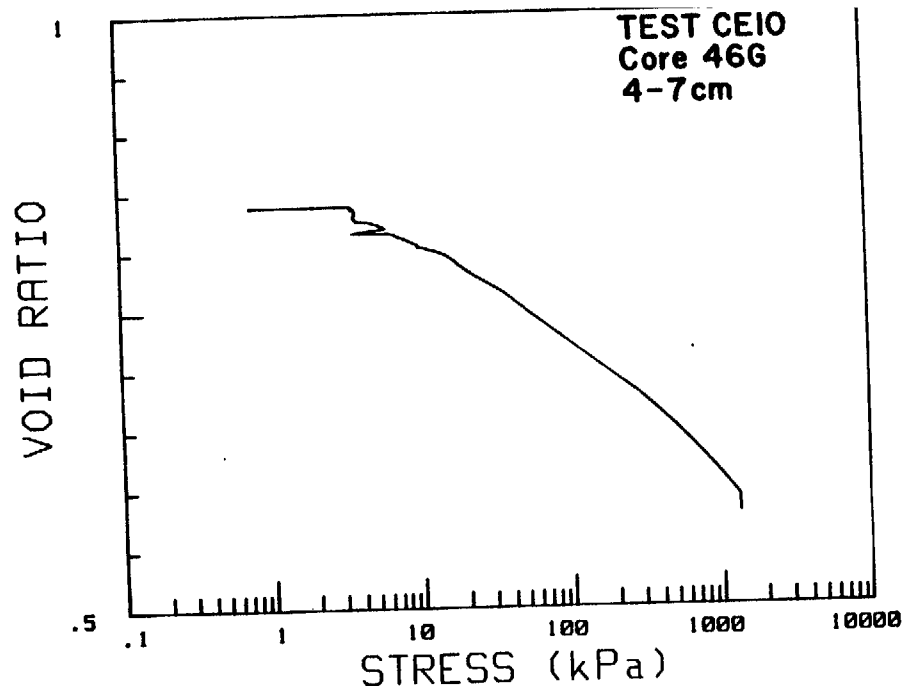
The cyclic triaxial tests (first two characters are TC) are given third and ordered by test number. Results from one test are presented on two sheets. The first sheet includes deviator stress (DEV STRESS or 2 times the shear stress)-axial strain and $p'-q$ stress paths that are analogous to the graphs given for static triaxial tests. However, the plots are given for only a few selected cycles of loading to illustrate how the response changes as the number of cycles increases. Numbers on the plots correspond to cycle number.

The second sheet shows several parameters plotted versus cycle number. The upper left plot shows peak single amplitude strain (positive in compression) versus cycle number. Lower left and lower right plots show calculated damping and Young's modulus (E) versus number of cycles, respectively. The upper right plot shows the minimum and maximum excess pore water pressure (Δu) measured during a cycle. In some plots a dashed line in both the strain and pore pressure plots shows an equilibrium value established between bursts of cyclic stress applications.

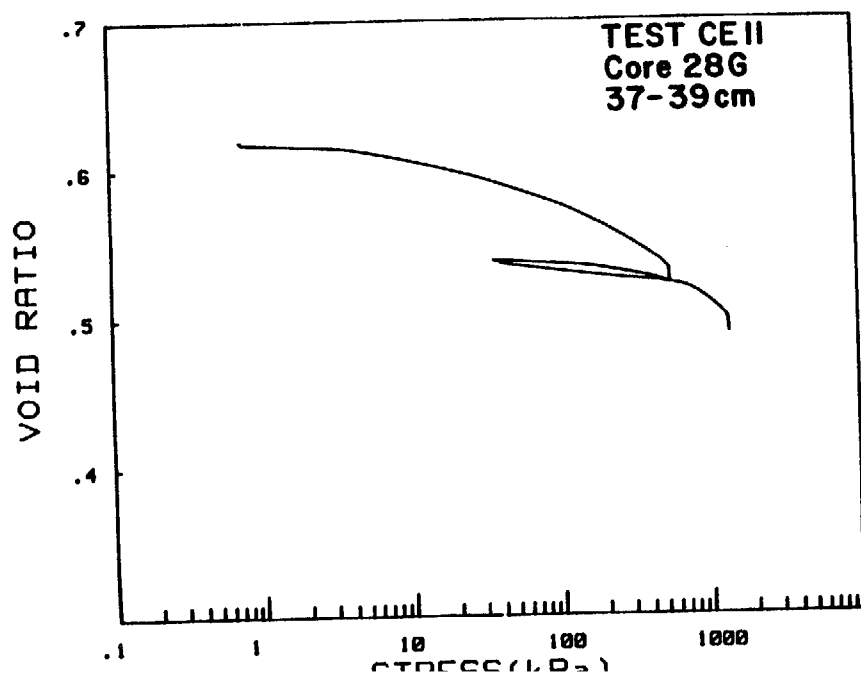
The title blocks for both figures show a static q_f or estimated static shearing strength. The value was obtained from a test on a nearby sample (Method I of the main text). The average maximum q (AVG MAX q) is the average peak compressive shearing stress for all of the cycles. The percentage value that follows in parentheses represents the percentage of the estimated (Method I) static shearing strength. The "AVG MIN q " is the same as the average maximum q except it represents values in tension.

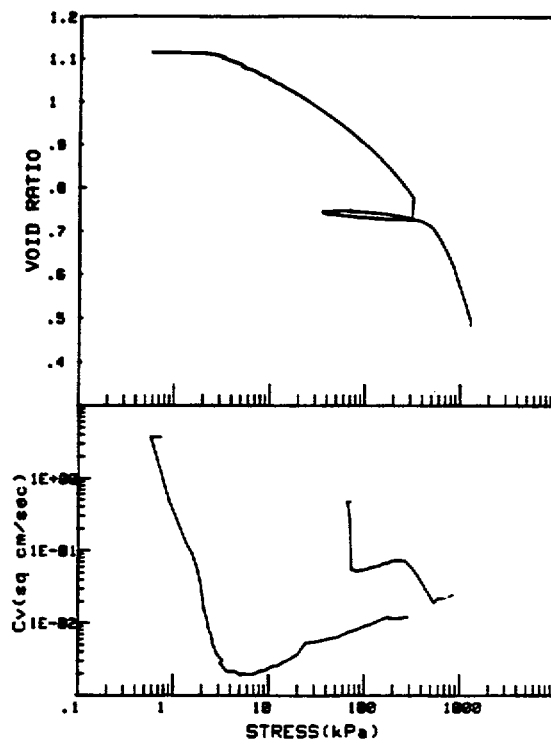




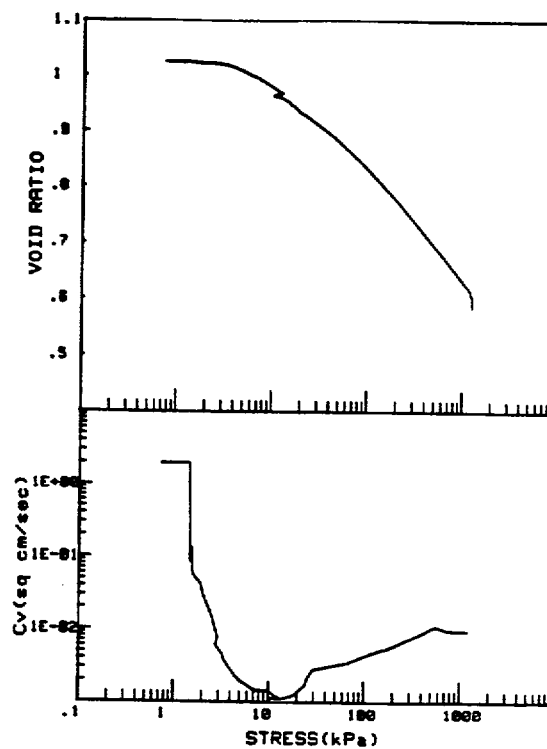


420

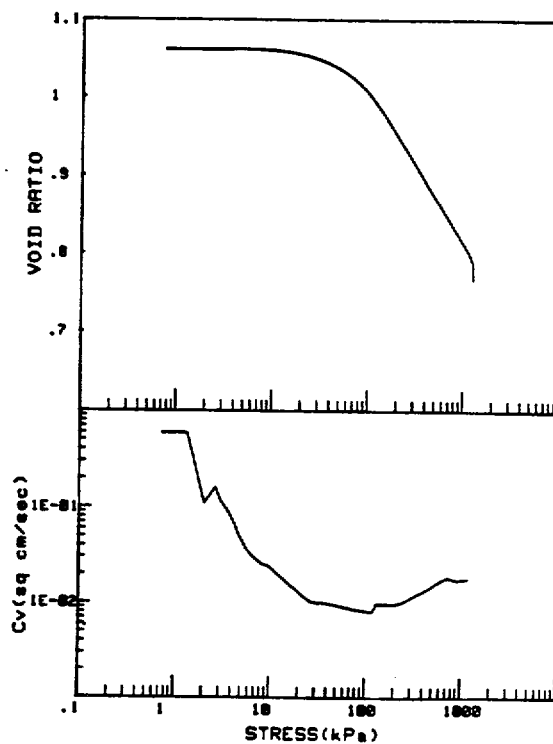




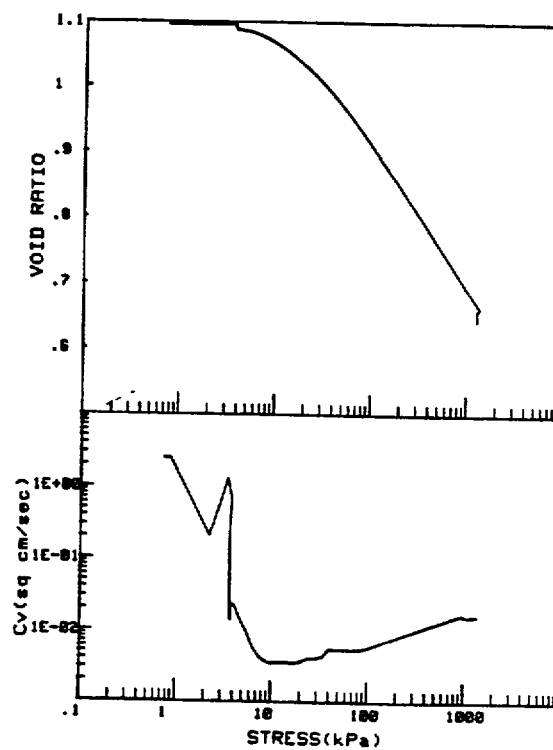
CRUISE DC1-81-EG	INCREMENT (cm)	116-118
CORE NO. 627G2	TEST NO.	CE13



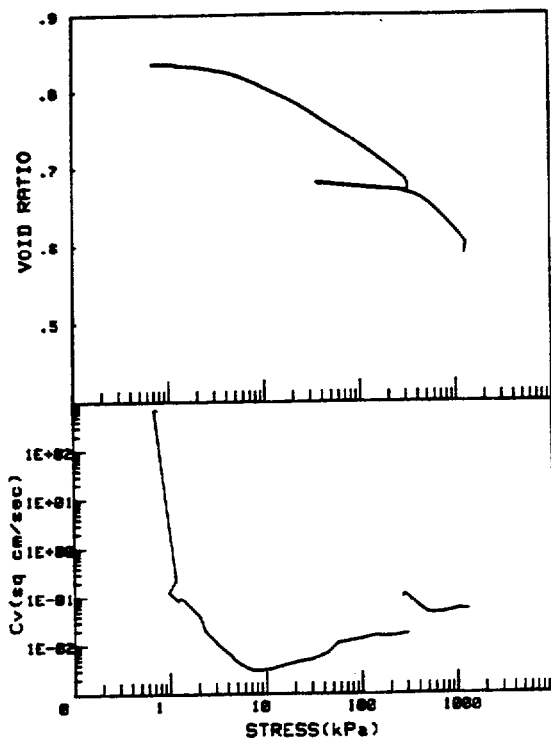
CRUISE DC1-81-EG	INCREMENT (cm)	222-224
CORE NO. 627G2	TEST NO.	CE15



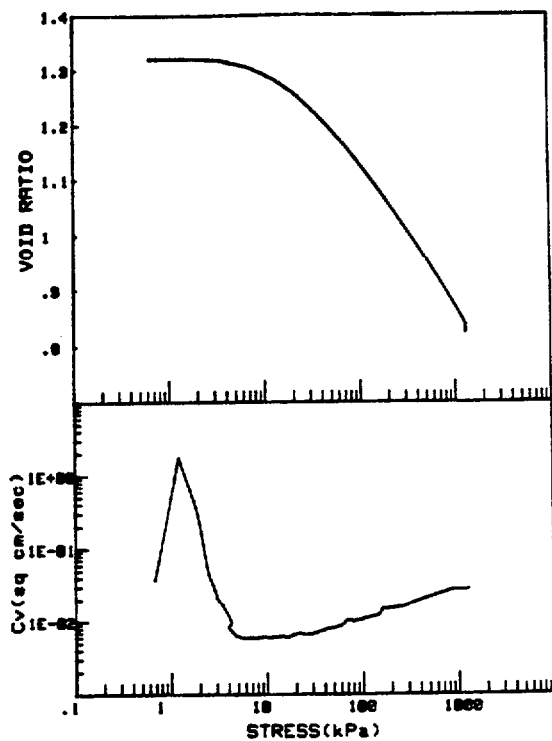
CRUISE DC1-81-EG	INCREMENT (cm)	32-34
CORE NO. 627G2	TEST NO.	CE14



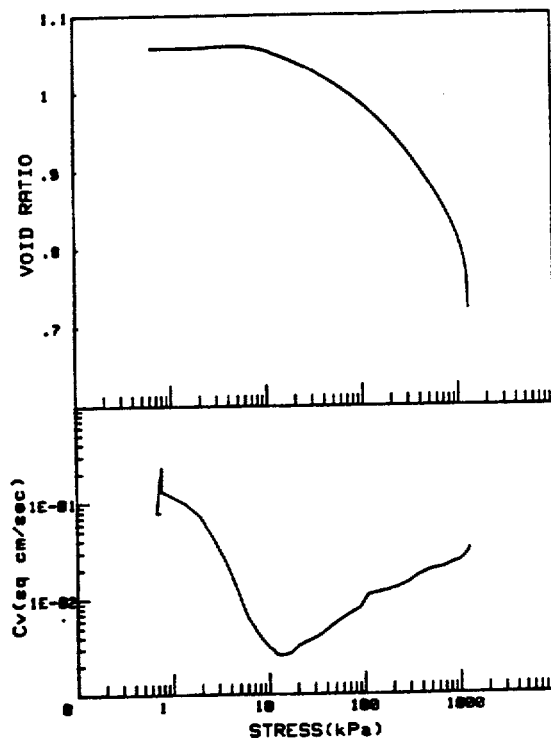
CRUISE DC1-81-EG	INCREMENT (cm)	26-28
CORE NO. 627G2	TEST NO.	CE16



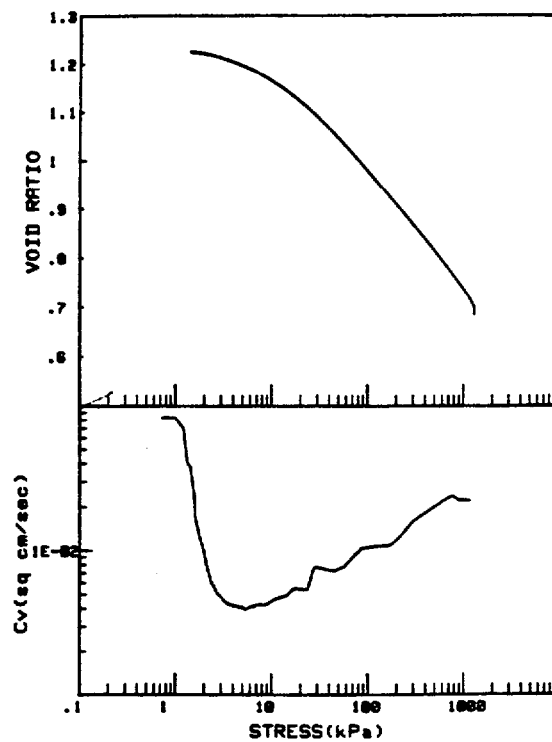
CRUISE DC1-81-EG	INCREMENT (cm)	110-115
CORE NO. 81062	TEST NO.	CE17



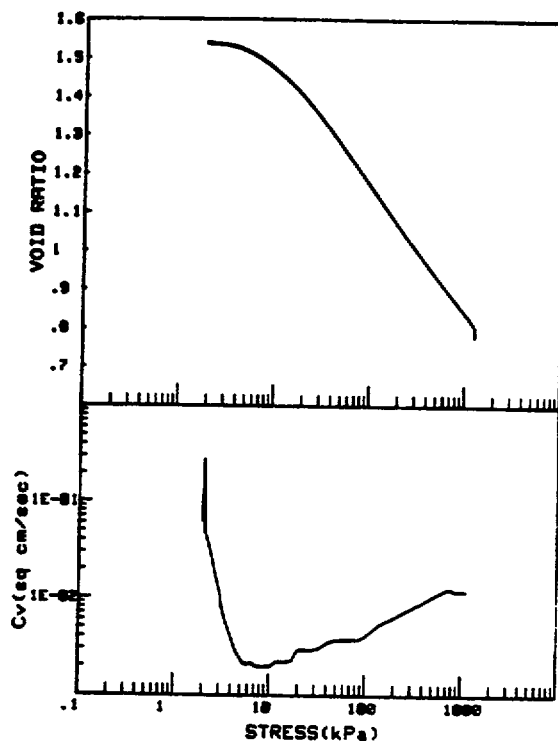
CRUISE DC1-81-EG	INCREMENT (cm)	82-84
CORE NO. 81062	TEST NO.	CE22



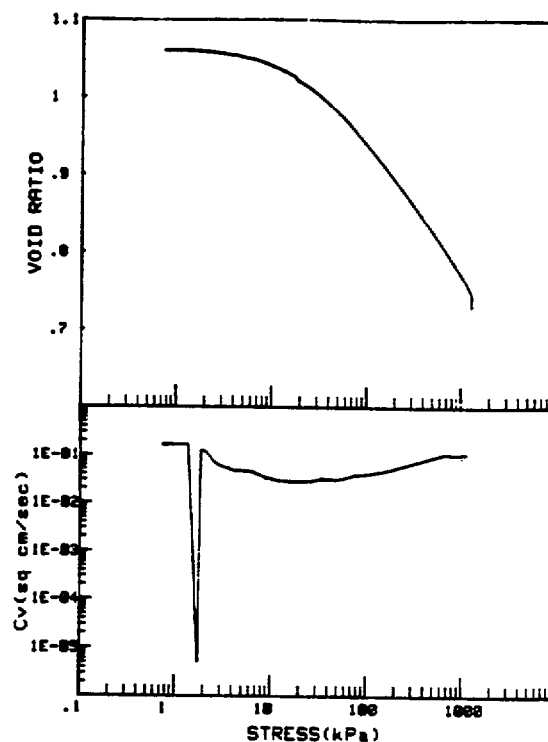
CRUISE DC1-81-EG	INCREMENT (cm)	180-185
CORE NO. 81062	TEST NO.	CE18



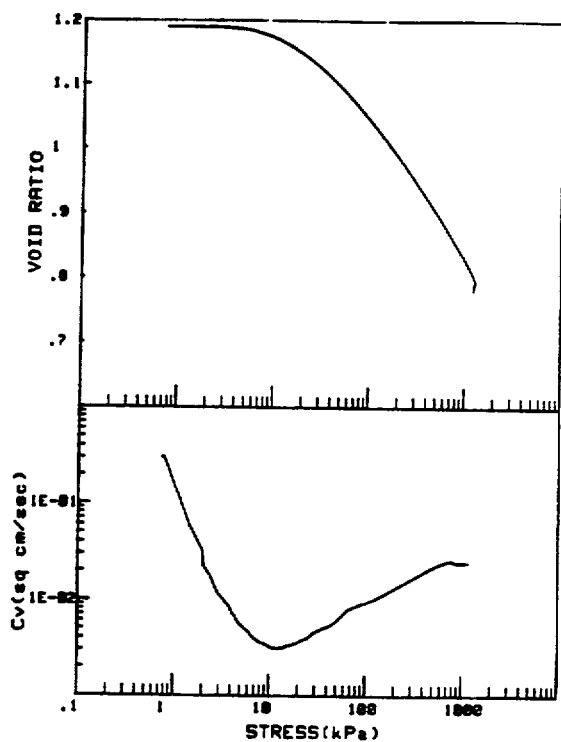
CRUISE DC1-81-EG	INCREMENT (cm)	71-73
CORE NO. 82062	TEST NO.	CE23



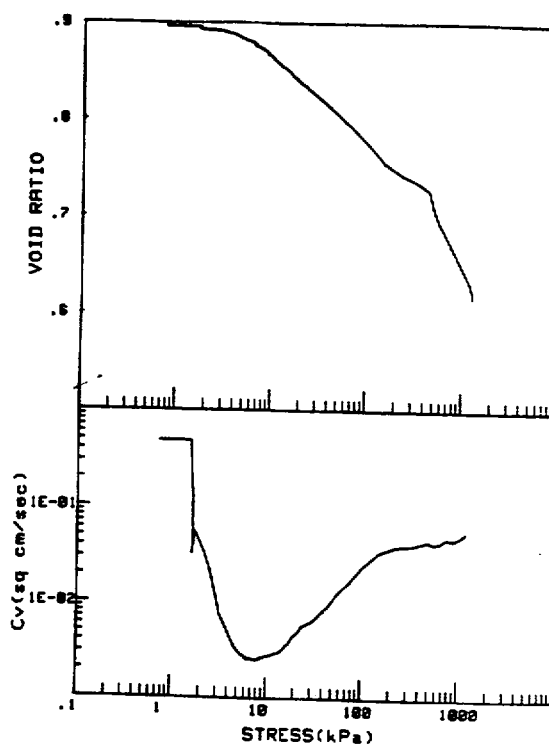
CRUISE DC1-81-EG	INCREMENT (cm)	47-48
CORE NO. 834G2	TEST NO.	CE24



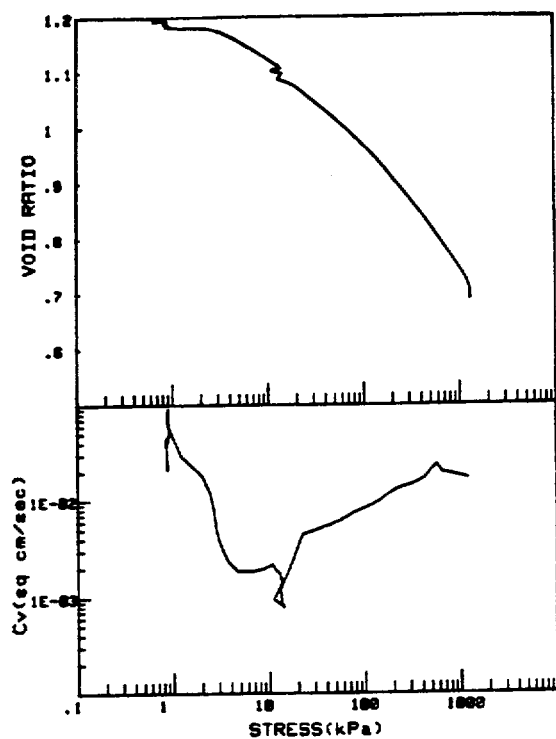
CRUISE DC2-88-EG	INCREMENT (cm)	146-148
CORE NO. 87G	TEST NO.	CE26



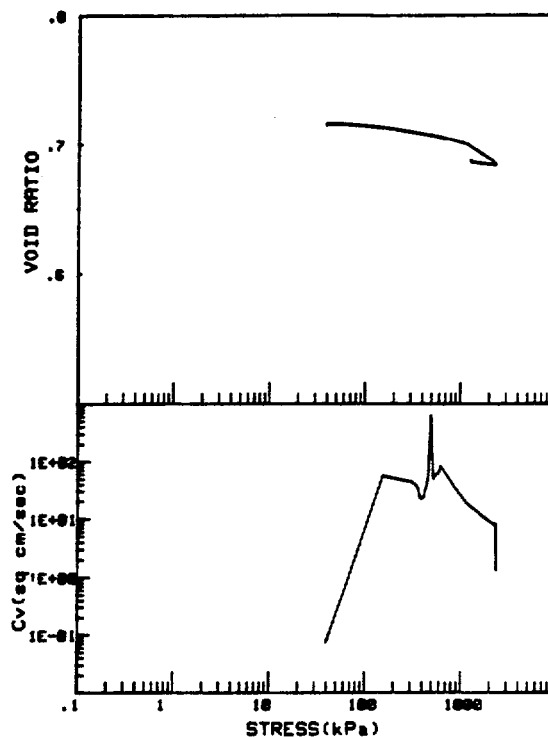
CRUISE DC1-81-EG	INCREMENT (cm)	193-195
CORE NO. 885G2	TEST NO.	CE25



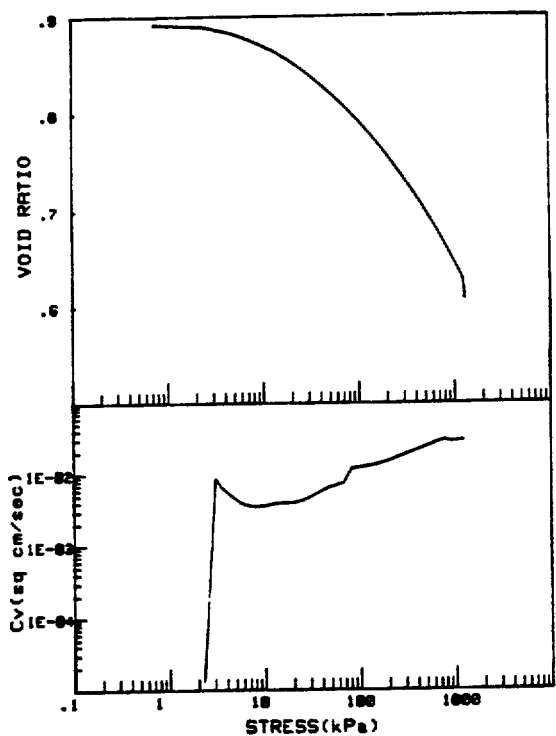
CRUISE DC1-81-EG	INCREMENT (cm)	218-212
CORE NO. 824A1	TEST NO.	CE27



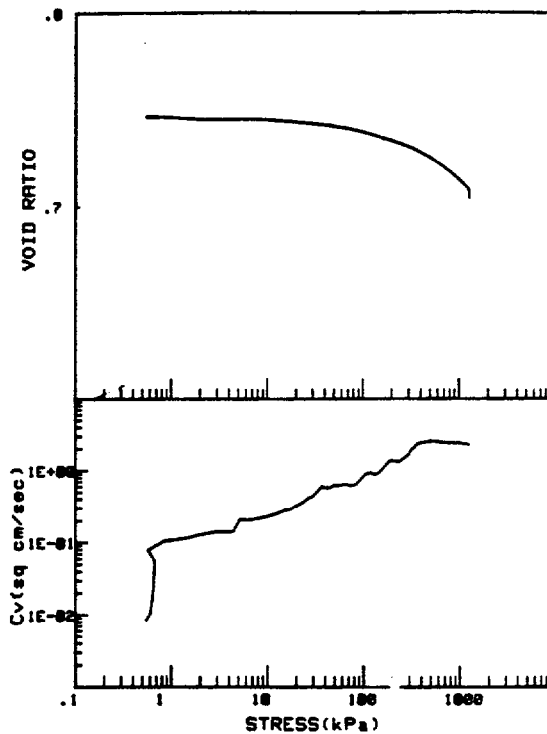
CRUISE DC1-81-EG	INCREMENT (cm)	188-188
CORE NO. 818G2	TEST NO.	CE28



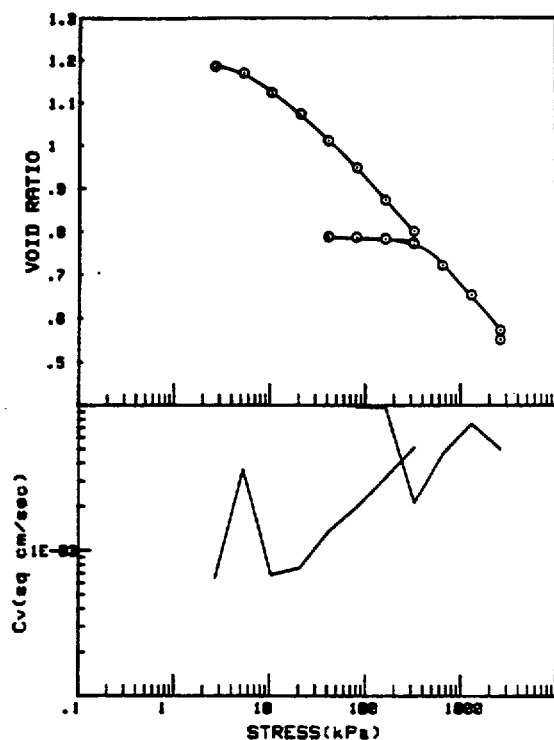
CRUISE DC1-81-EG	INCREMENT (cm)	209-211
CORE NO. 838P2	TEST NO.	CE32



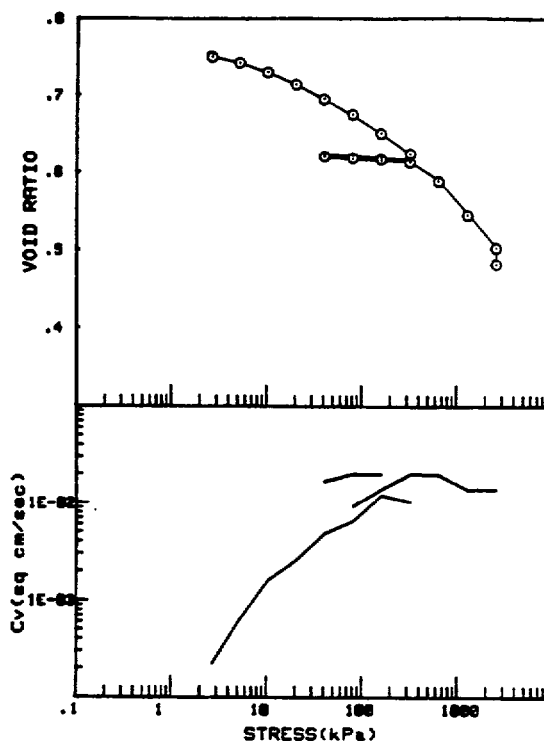
CRUISE DC1-81-EG	INCREMENT (cm)	76-78
CORE NO. 832G1	TEST NO.	CE31



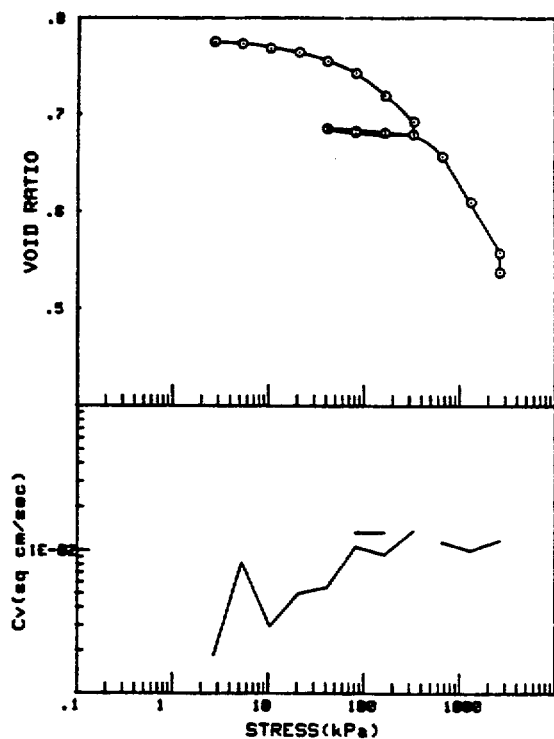
CRUISE DC1-81-EG	INCREMENT (cm)	152-157
CORE NO. 824R1	TEST NO.	CE33



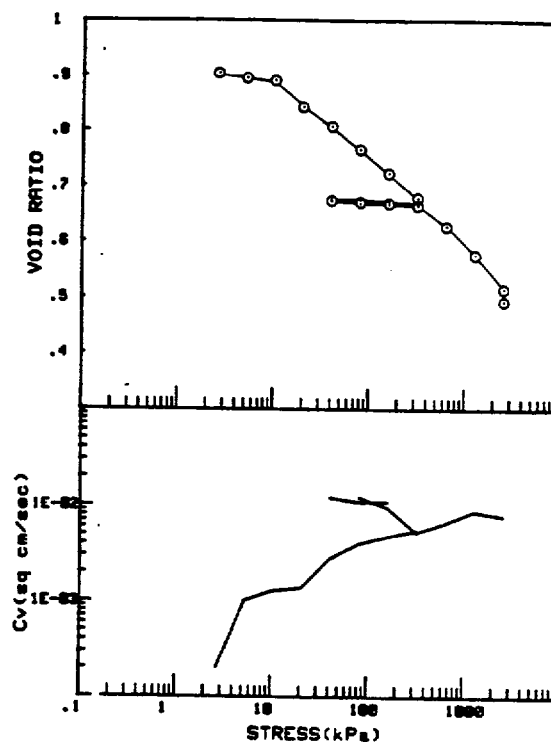
CRUISE DC1-81-EG	INCREMENT (cm)	122-124
CORE NO. 827G2	TEST NO.	OE48



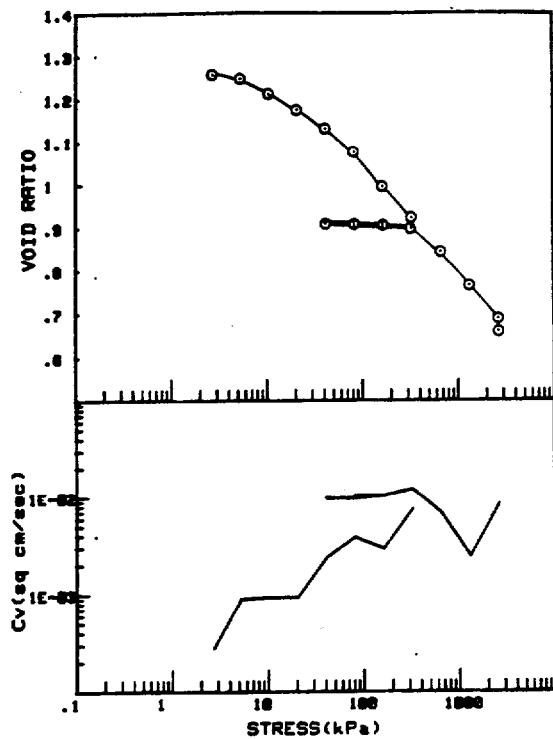
CRUISE DC1-81-EG	INCREMENT (cm)	148-144
CORE NO. 884G1	TEST NO.	OE44



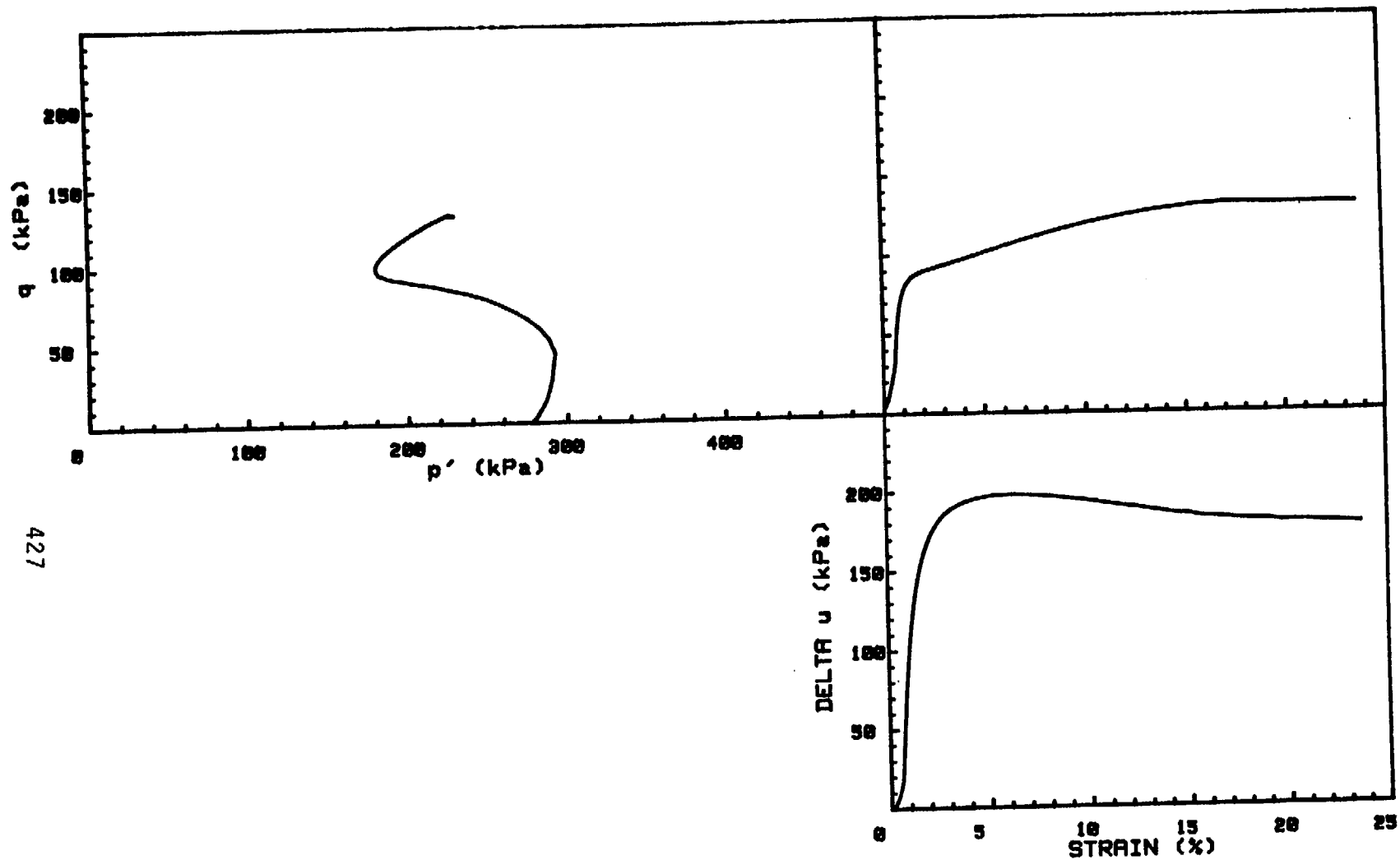
CRUISE DC1-81-EG	INCREMENT (cm)	185-188
CORE NO. 818G2	TEST NO.	OE41



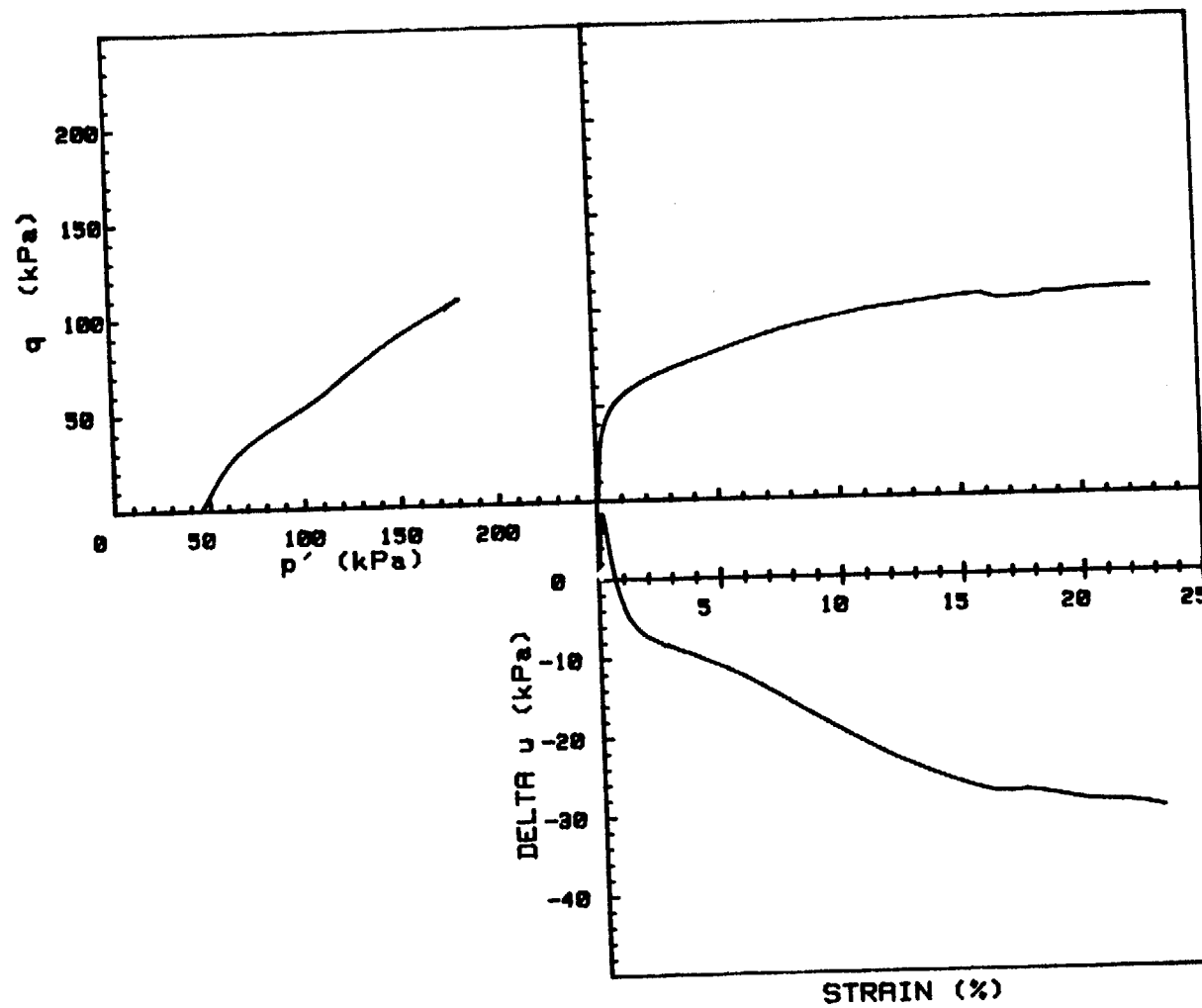
CRUISE DC1-81-EG	INCREMENT (cm)	196-200
CORE NO. 885G2	TEST NO.	OE45



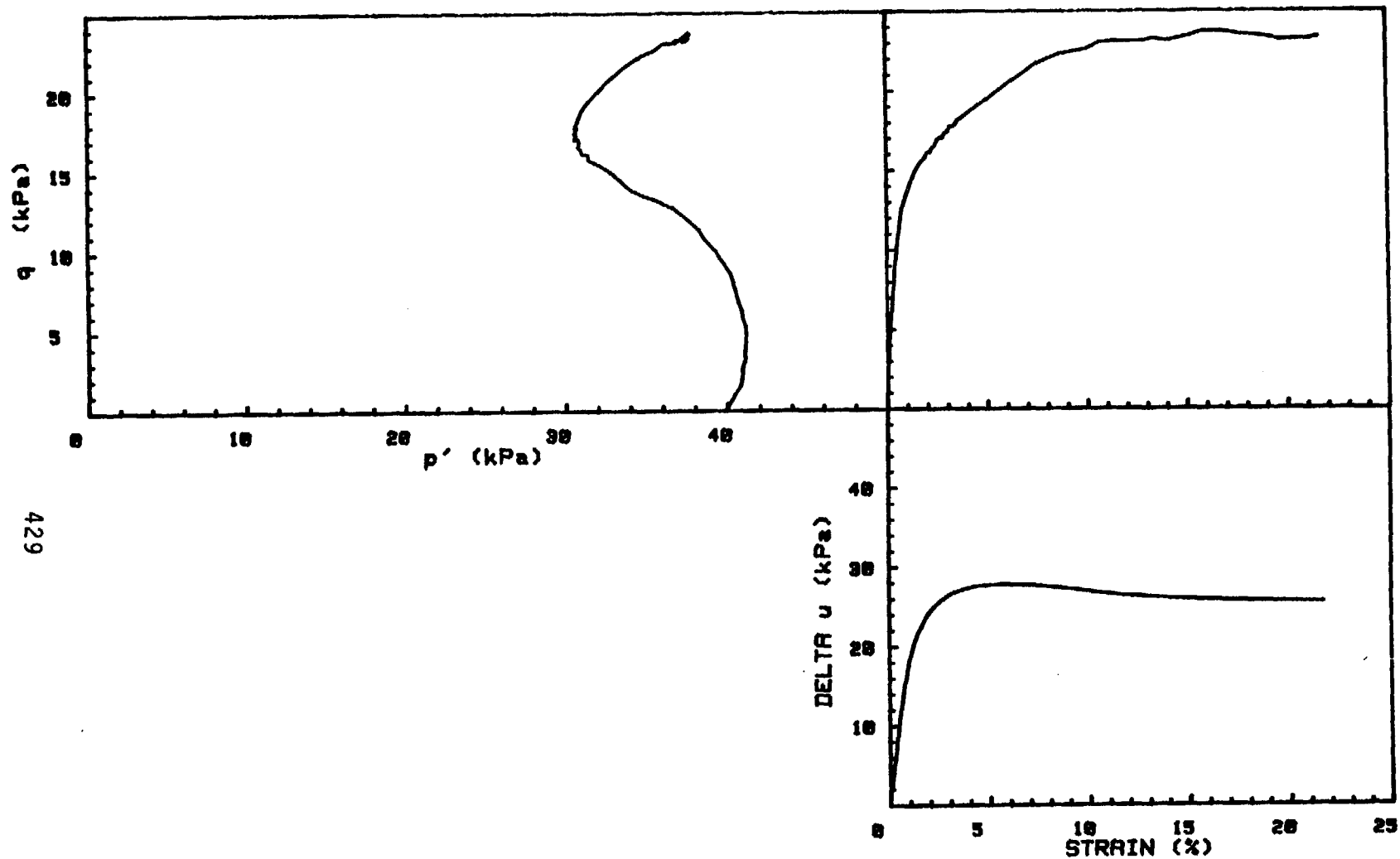
CRUISE DCI-01-EG	INCREMENT (cm)	07-72
CORE NO. 885G1	TEST NO.	0E46



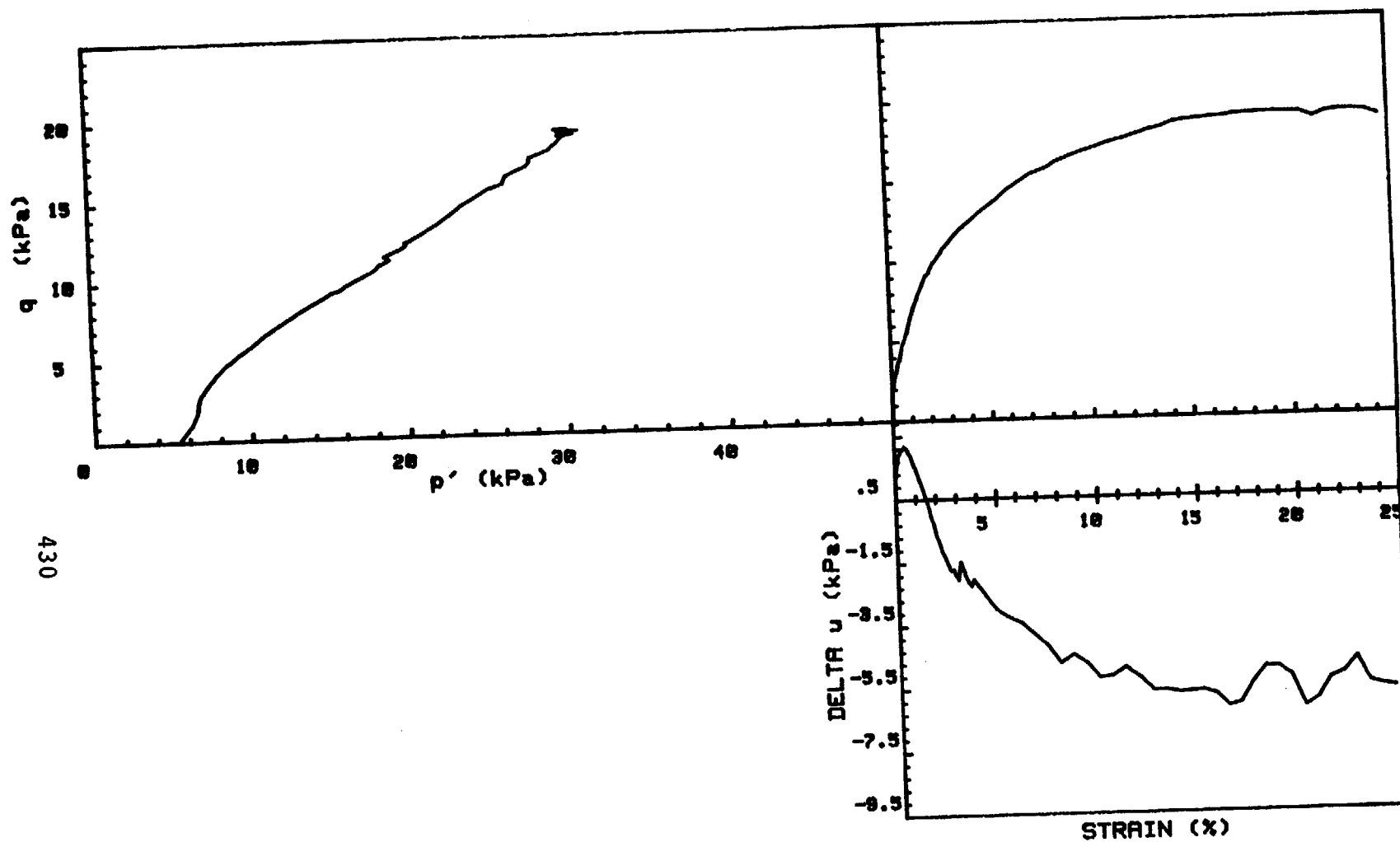
CRUISE DC2-80-EG	INCREMENT (cm)	5-15
CORE NO. G181	TEST NO.	TE15
SIG1c'(kPa)	277.7	
SIG3c'(kPa)	277.7	
INDUCED OCR	1.0	



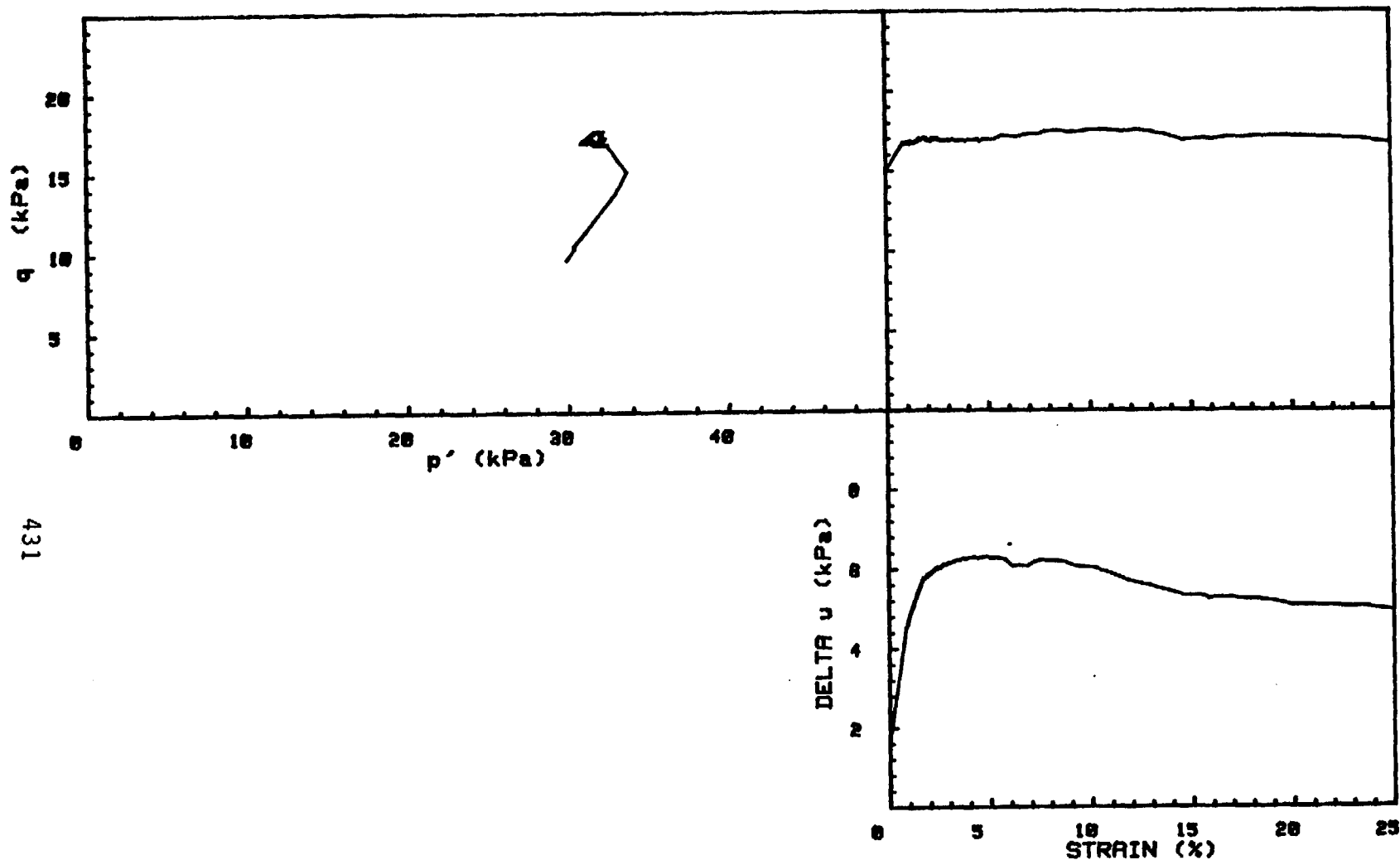
CRUISE DC2-80-EG	INCREMENT (cm)	5-14
CORE NO. G181	TEST NO.	TE16
SIG1c' (kPa)	45.0	
SIG3c' (kPa)	45.0	
INDUCED OCR	6.1	



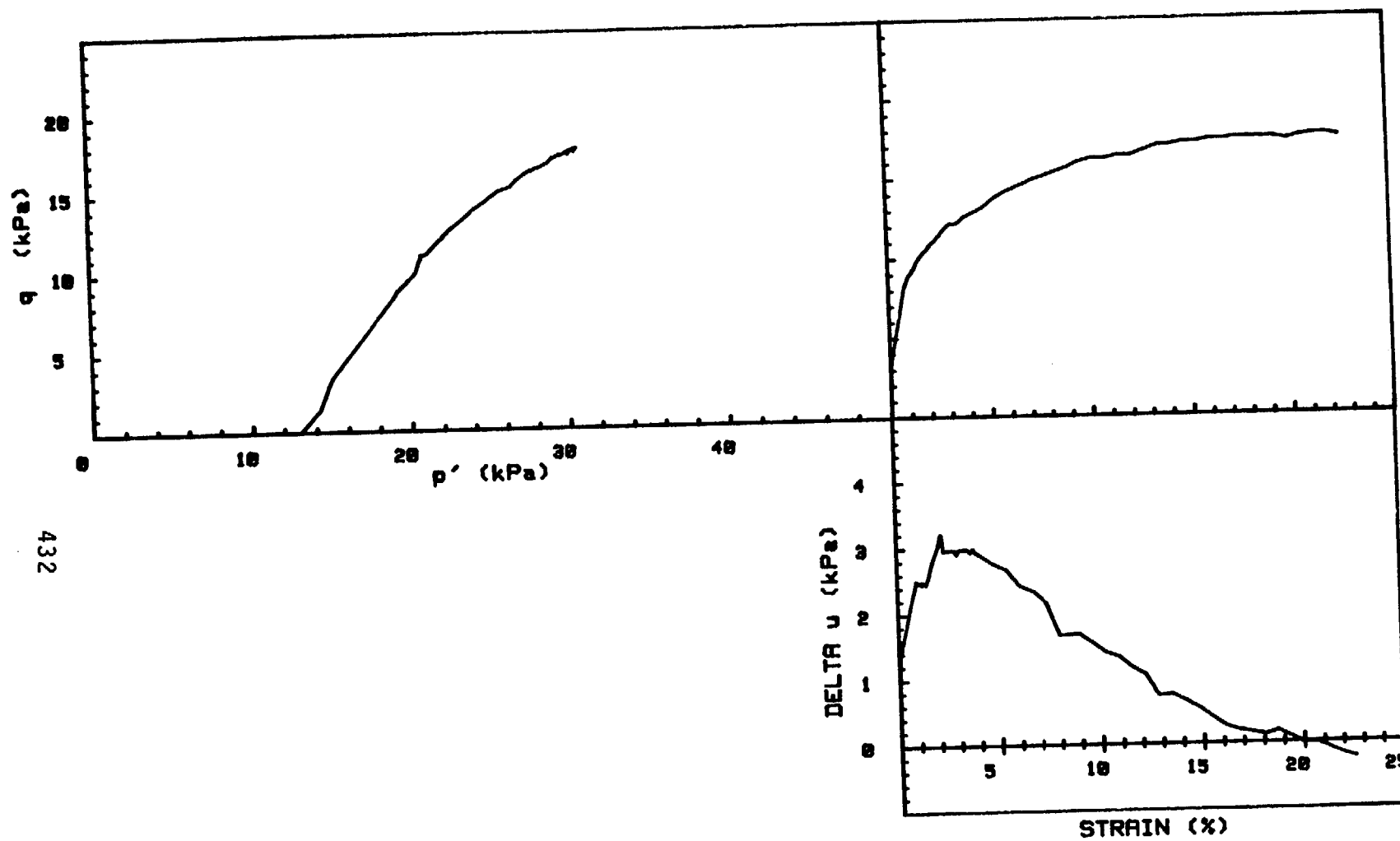
CRUISE DC2-80-EG	INCREMENT (cm)	71-81
CORE NO. G181	TEST NO.	TE18
SIG1c' (kPa)	39.9	
SIG3c' (kPa)	39.9	
INDUCED OCR	1.0	



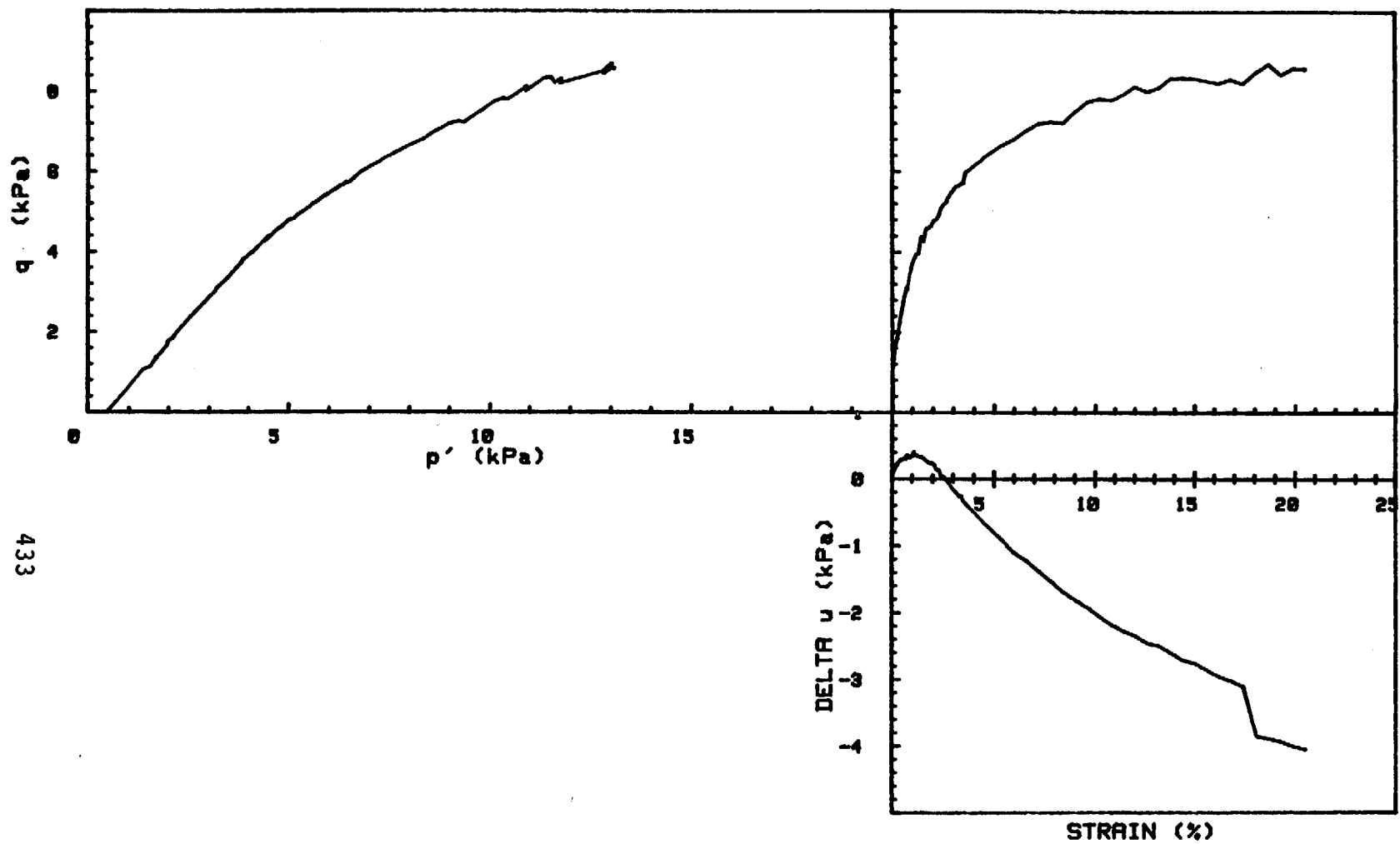
CRUISE DC2-80-EG	INCREMENT (cm)	71-80
CORE NO. G181	TEST NO.	TE19
SIG1c' (kPa)	5.3	
SIG3c' (kPa)	5.3	
INDUCED OCR	7.3	



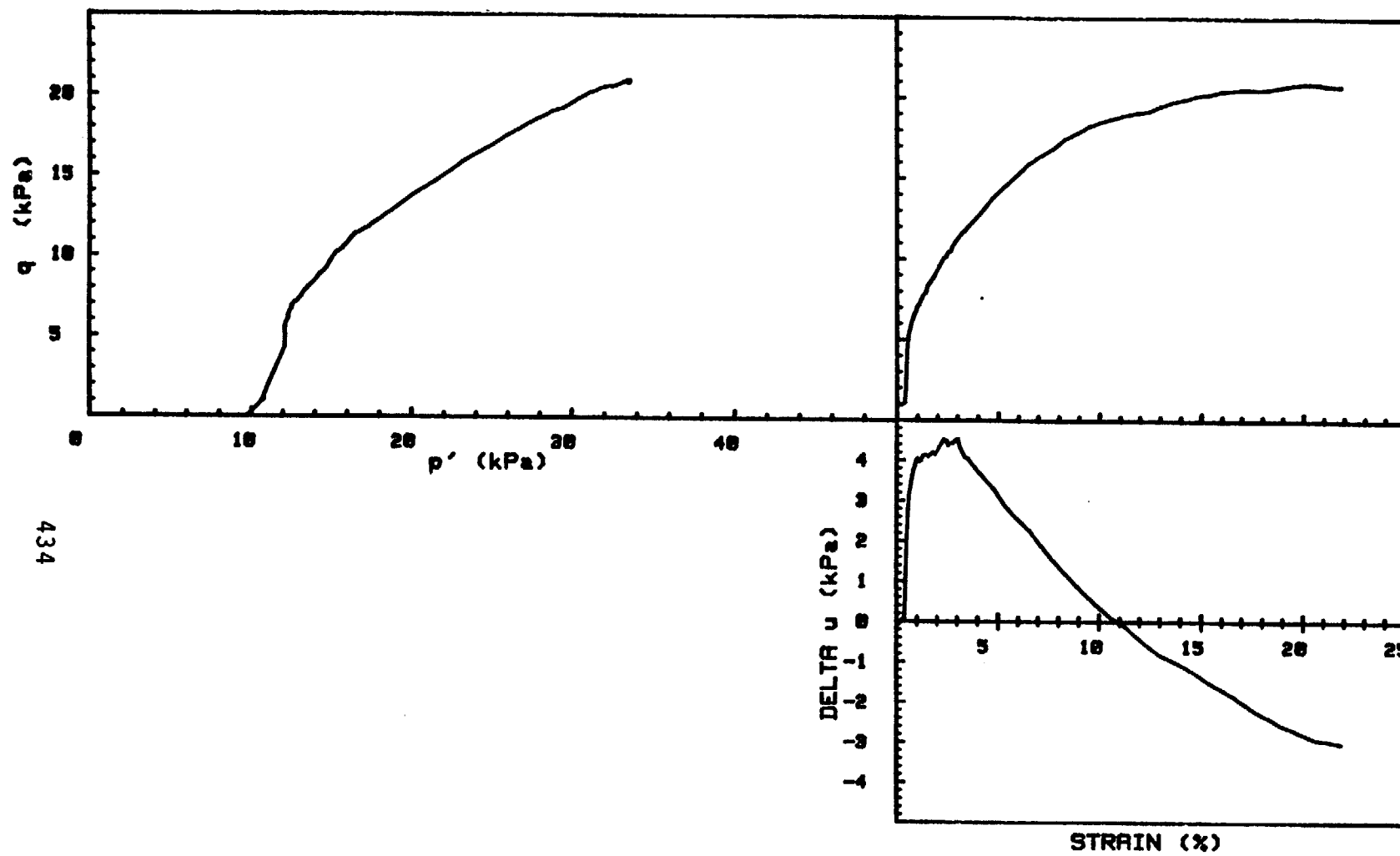
CRUISE DC2-80-EG	INCREMENT (cm)	100-109
CORE NO. G181	TEST NO.	TE20
SIG1c' (kPa)	39.4	
SIG3c' (kPa)	20.3	
INDUCED OCR	1.0	



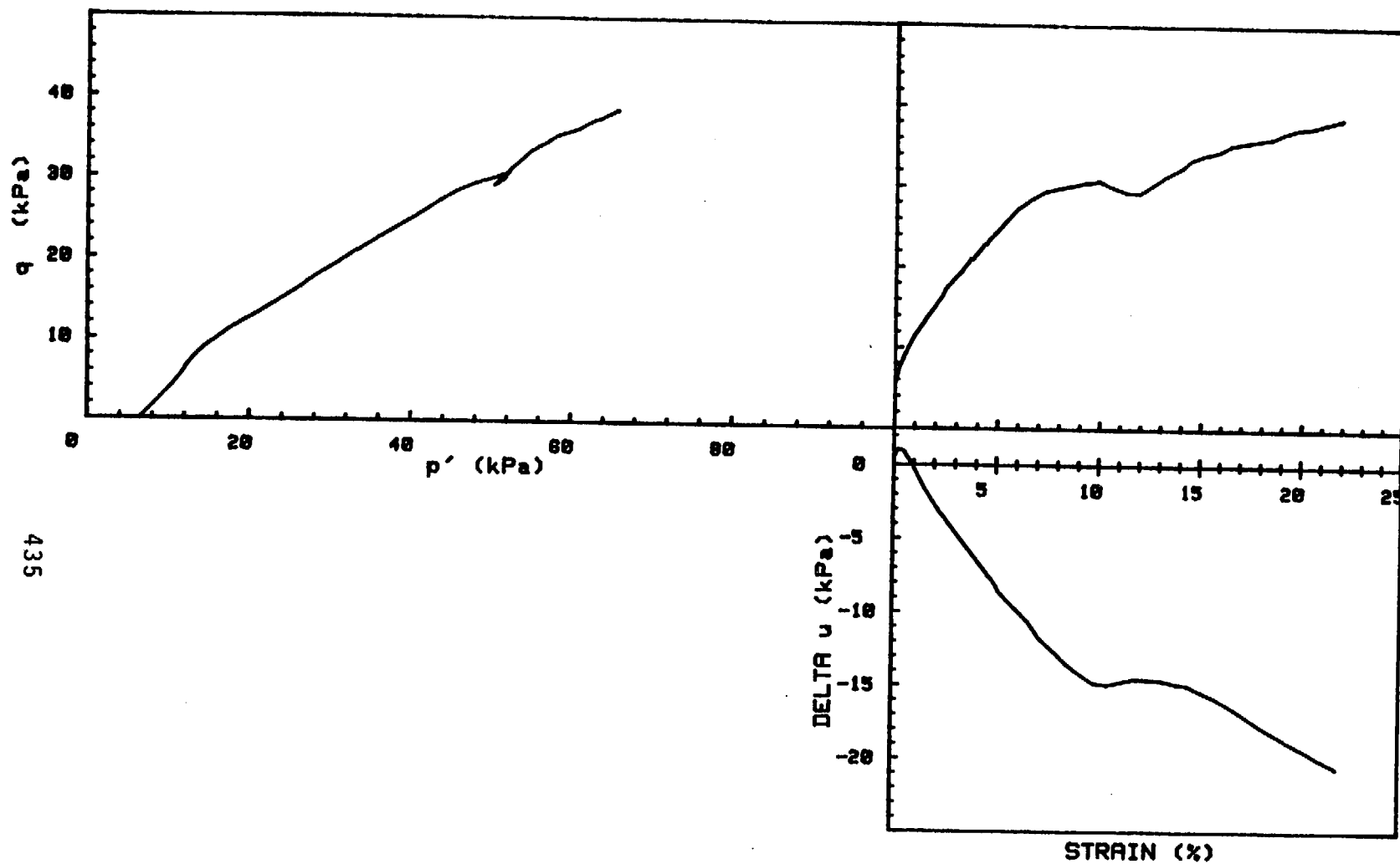
CRUISE DC2-80-EG	INCREMENT (cm)	100-110
CORE NO. G181	TEST NO.	TE21
SIG _{1c'} (kPa)	13.1	
SIG _{3c'} (kPa)	13.1	
INDUCED OCR	3.0	



CRUISE DC2-80-EG	INCREMENT (cm)	120-130
CORE NO. G101	TEST NO.	TE22
SIG1c'(kPa)	.5	
SIG3c'(kPa)	.5	
INDUCED OCR	1.0	

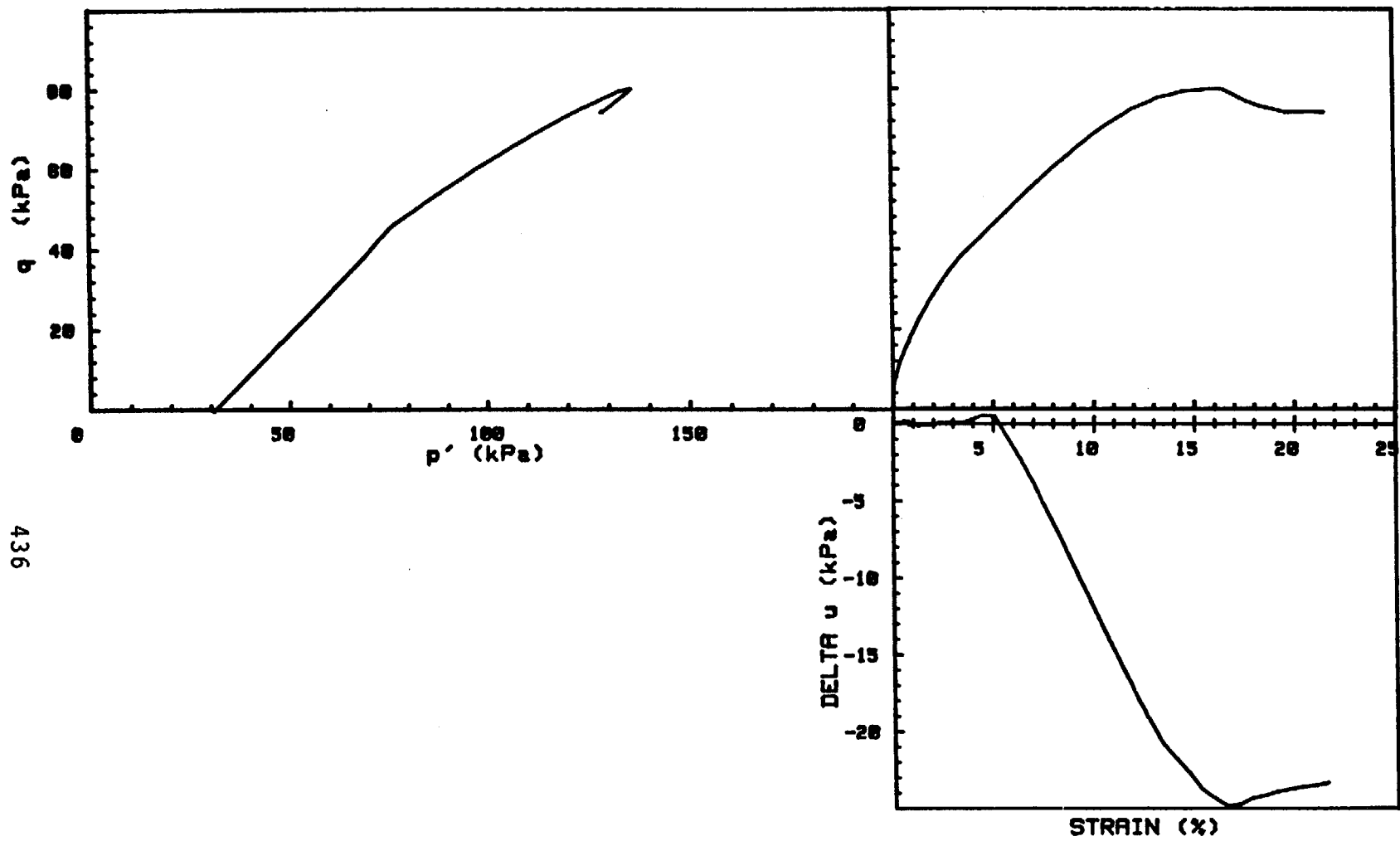


CRUISE DC2-00-EG	INCREMENT (cm)	120-130
CORE NO. G101	TEST NO.	TE23
SIG1c' (kPa)	9.7	
SIG3c' (kPa)	9.7	
INDUCED OCR	1.0	

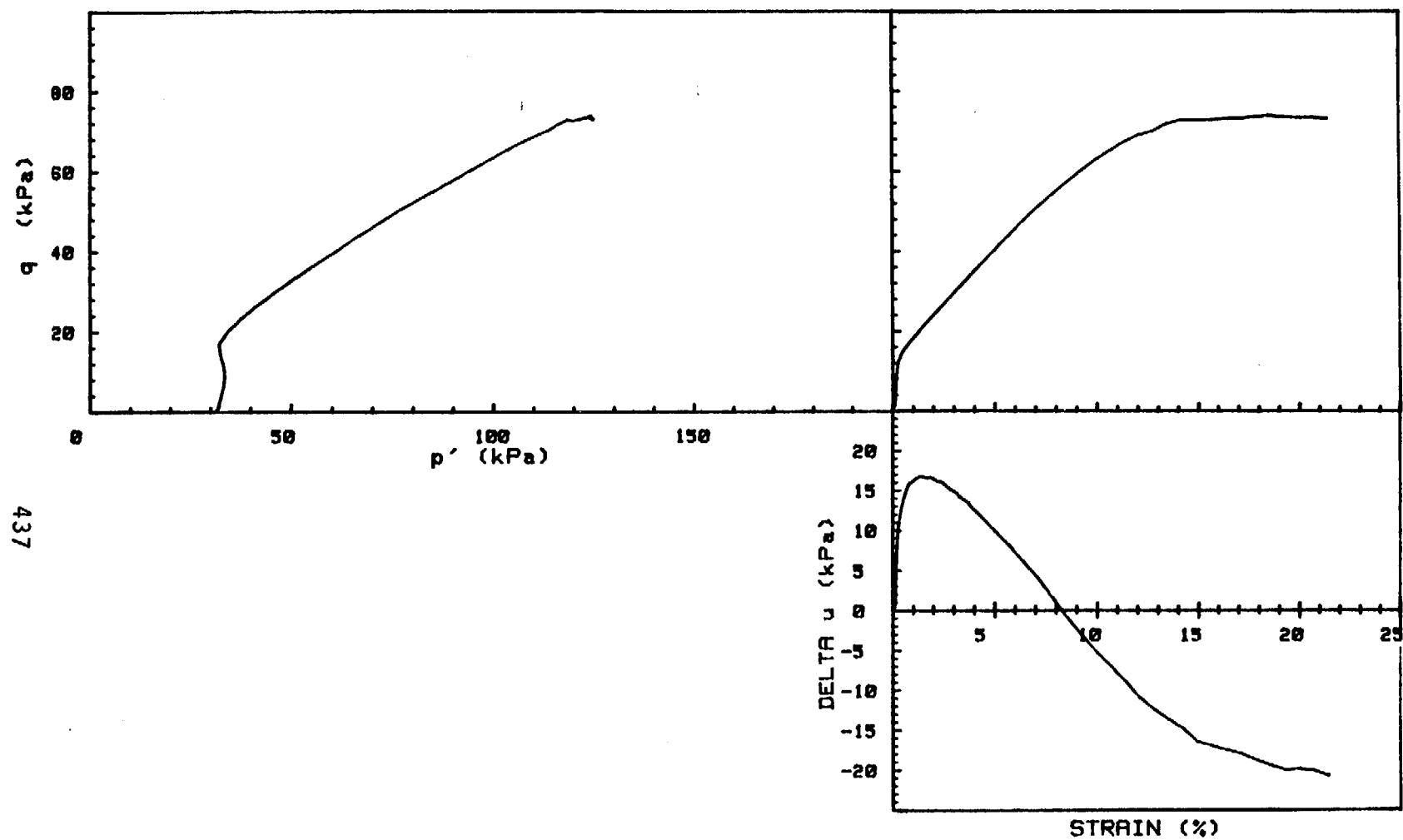


CRUISE DC2-80-EG	INCREMENT (cm)	8-17
CORE NO. 43G	TEST NO.	TE27
SIG1c'(kPa)	6.5	
SIG3c'(kPa)	6.5	
INDUCED OCR	5.0	

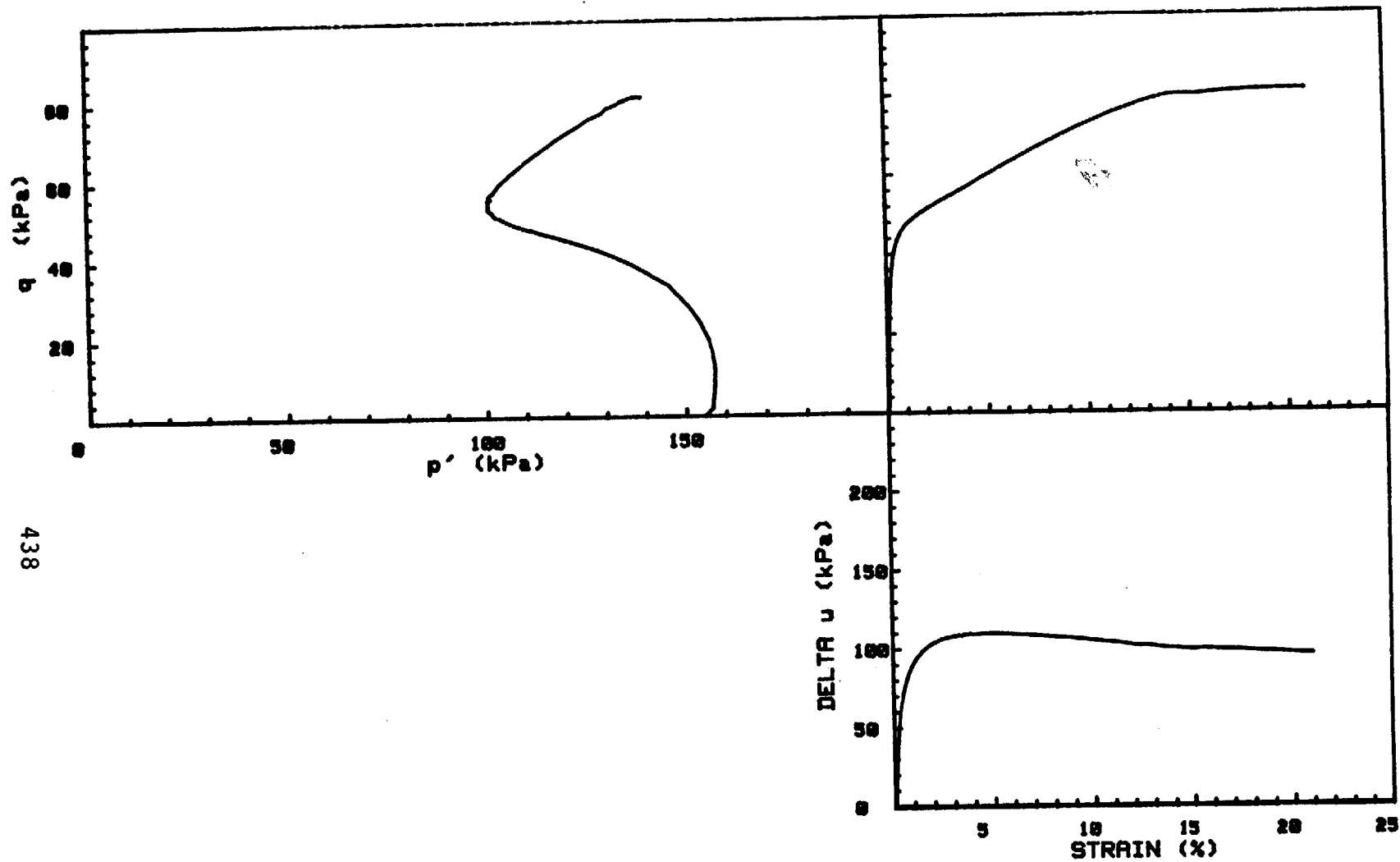
436



CRUISE DC2-80-EG	INCREMENT (cm)	18-27
CORE NO. 43G	TEST NO.	TE34
SIG1c' (kPa)	31.3	
SIG3c' (kPa)	31.3	
INDUCED OCR	1.0	

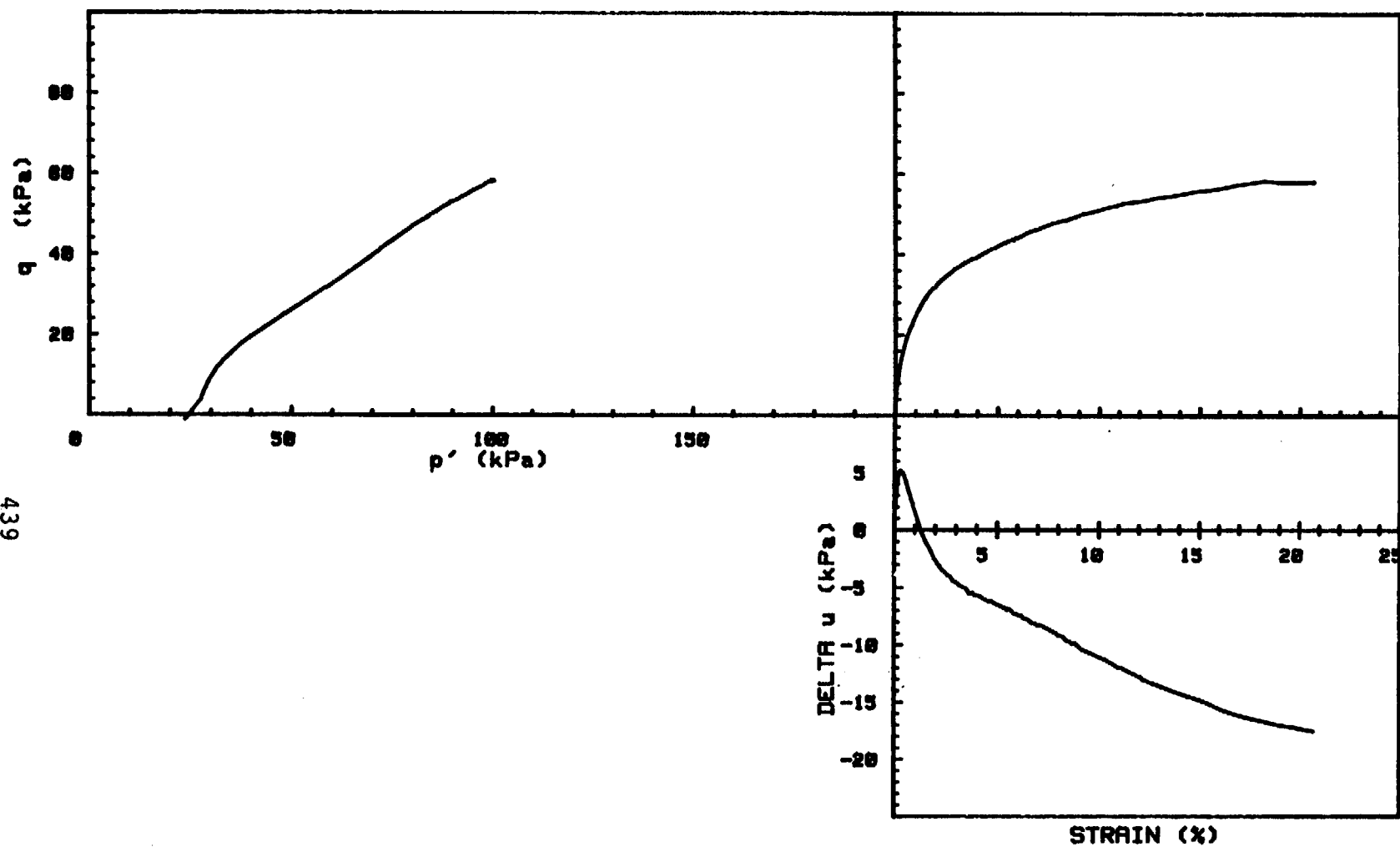


CRUISE DC2-80-EG	INCREMENT (cm)	18-27
CORE NO. 43G	TEST NO.	TE35
SIG1c'(kPa)	31.1	
SIG3c'(kPa)	31.1	
INDUCED OCR	1.0	

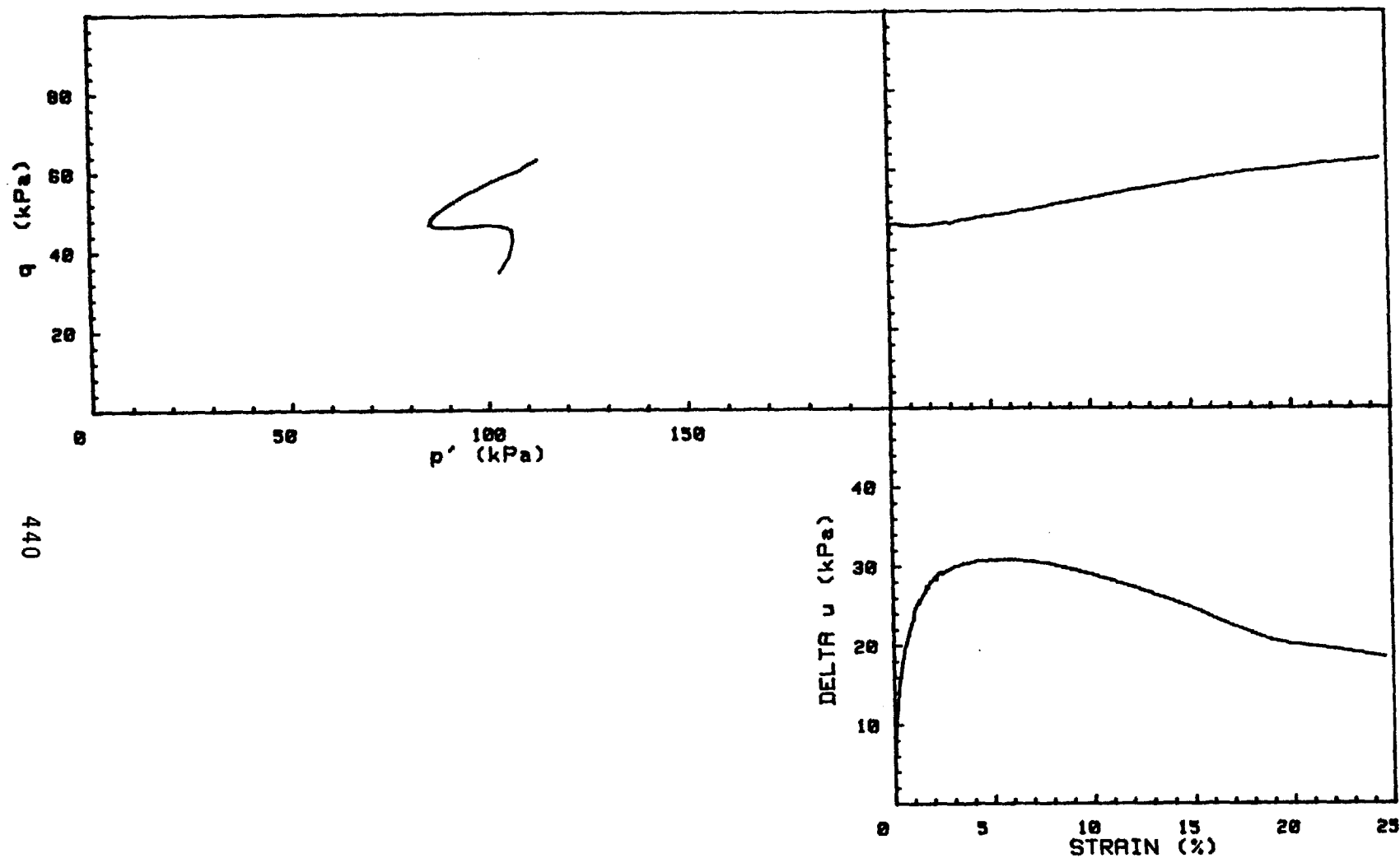


CRUISE DC2-80-EG	INCREMENT (cm)	13-22
CORE NO. 35G	TEST NO.	TE56
SIG1c'(kPa)	154.8	
SIG3c'(kPa)	154.8	
INDUCED OCR	1.0	

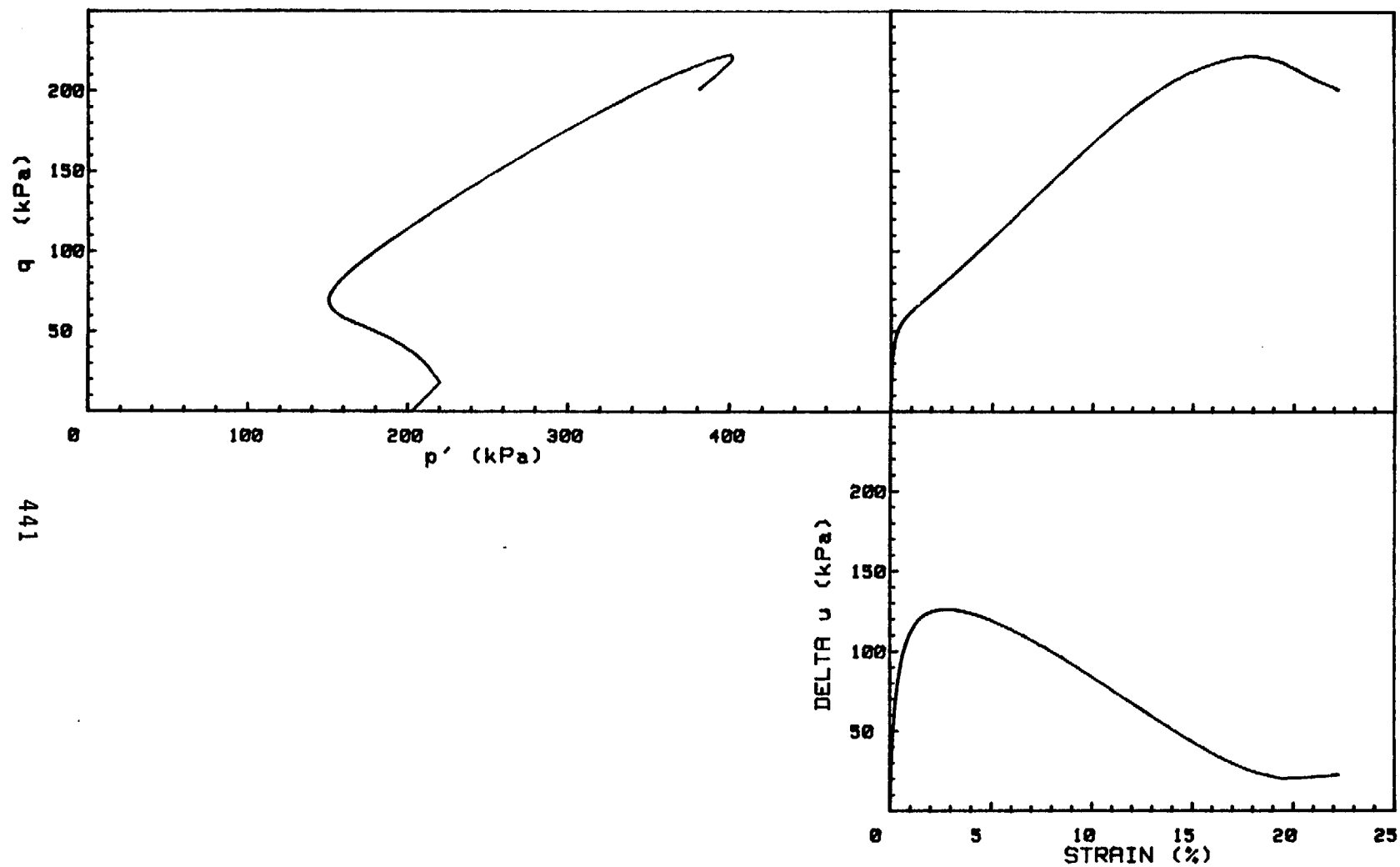
439



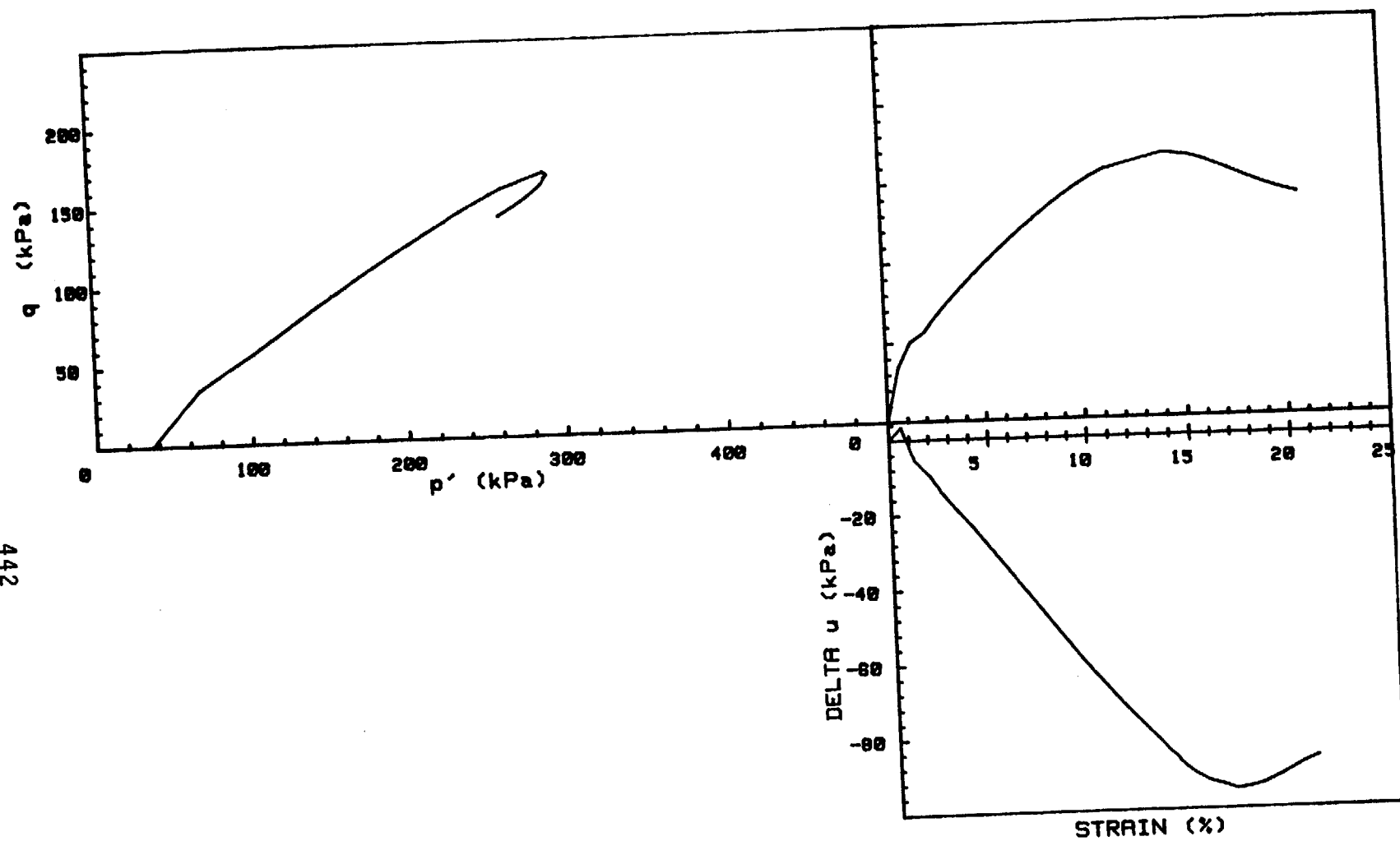
CRUISE DC2-80-EG	INCREMENT (cm)	13-25
CORE NO. 35G	TEST NO.	TE57
SIG _{1c'} (kPa) 24.7		
SIG _{3c'} (kPa) 24.7		
INDUCED OCR 6.0		



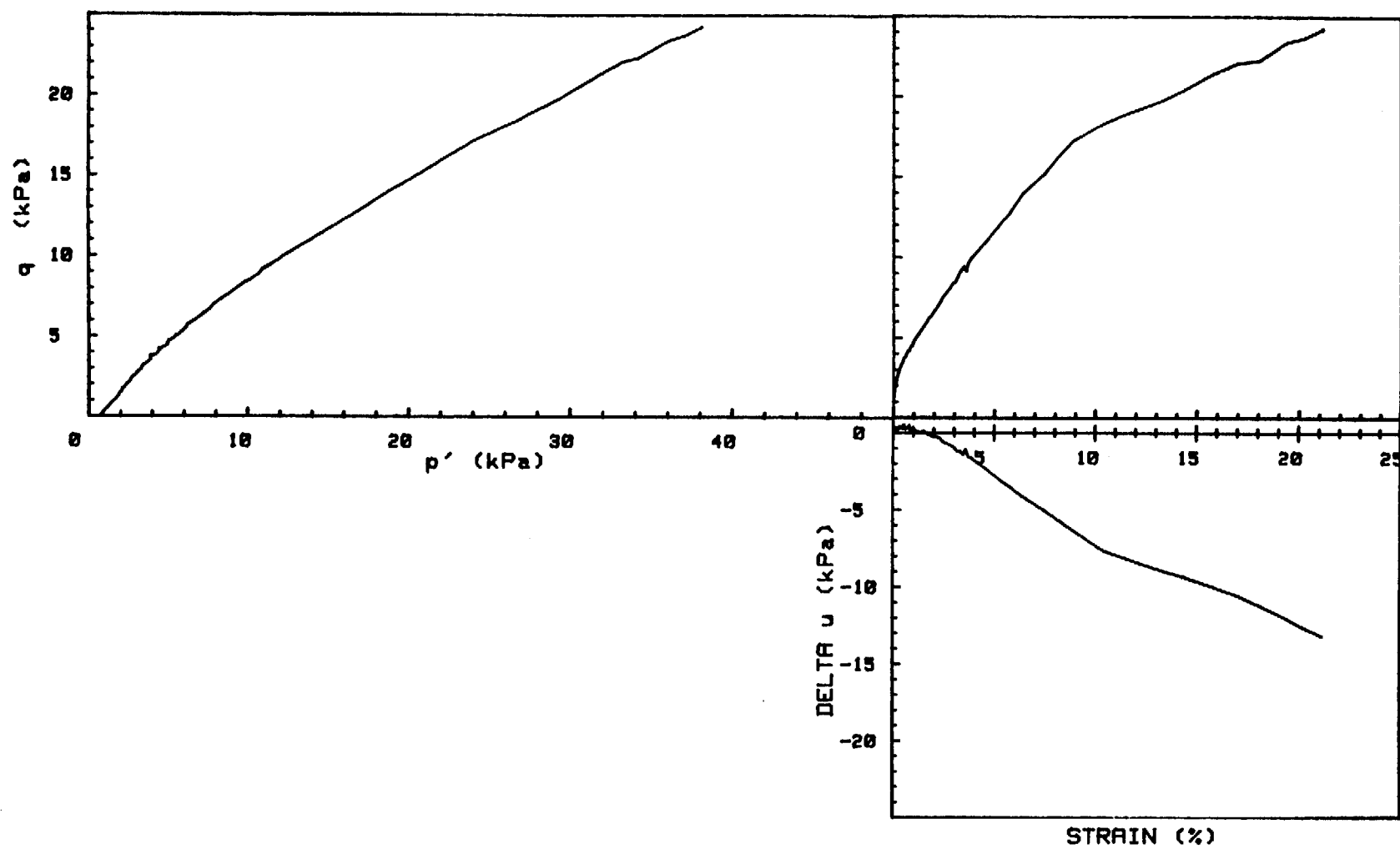
CRUISE DC2-80-EG	INCREMENT (cm)	25-32
CORE NO. 35G	TEST NO.	TE58
SIG1c' (kPa)	137.6	
SIG3c' (kPa)	68.5	
INDUCED OCR	1.0	



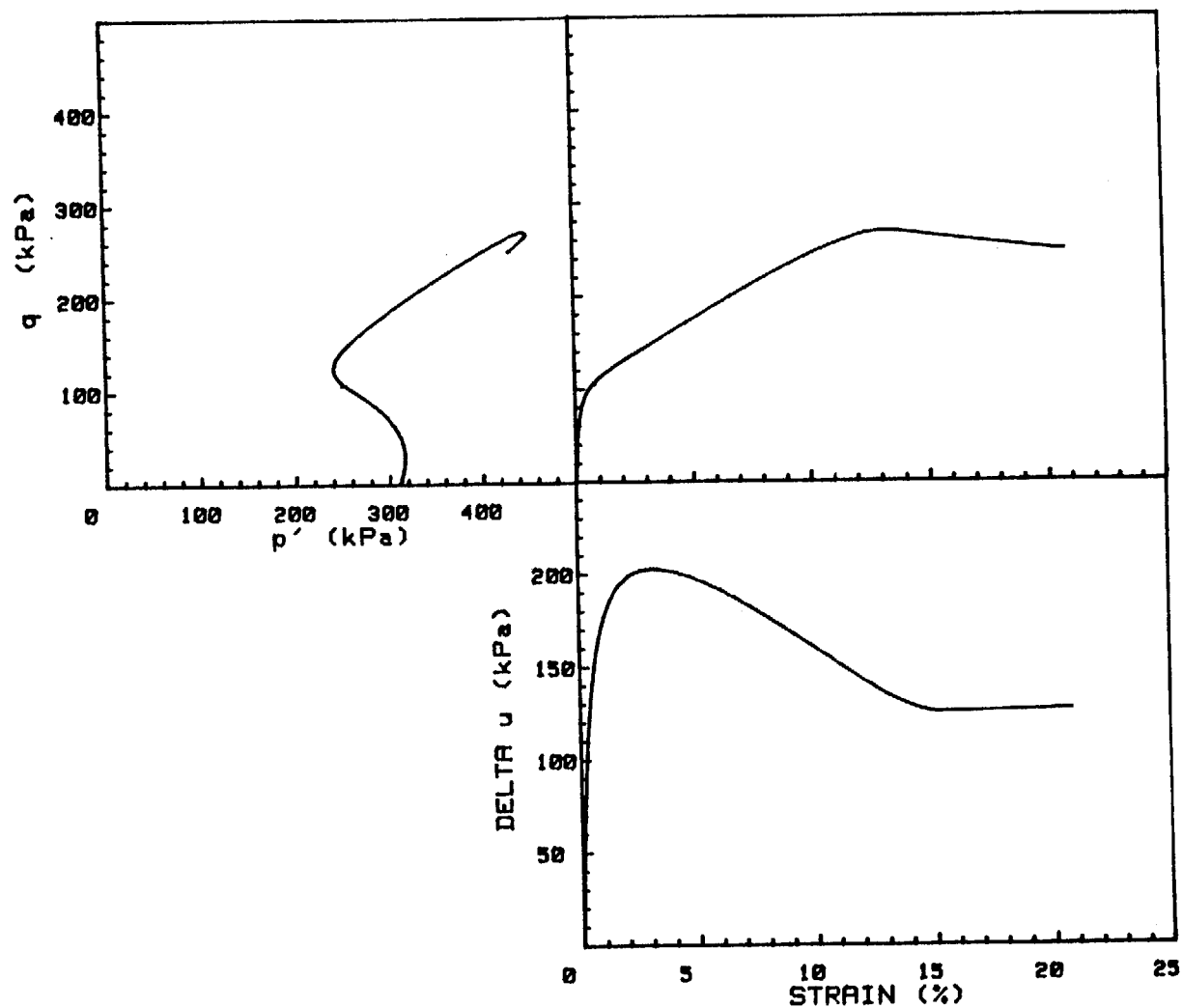
CRUISE DC2-80-EG	INCREMENT (cm)	17-28
CORE NO. 46G	TEST NO.	TE59
SIG1c' (kPa)	203.1	
SIG3c' (kPa)	203.1	
INDUCED OCR	1.0	



CRUISE DC2-80-EG	INCREMENT (cm)	28-37
CORE NO. 46G	TEST NO.	TE60
SIG1c' (kPa)	35.7	
SIG3c' (kPa)	35.7	
INDUCED OCR	6.0	

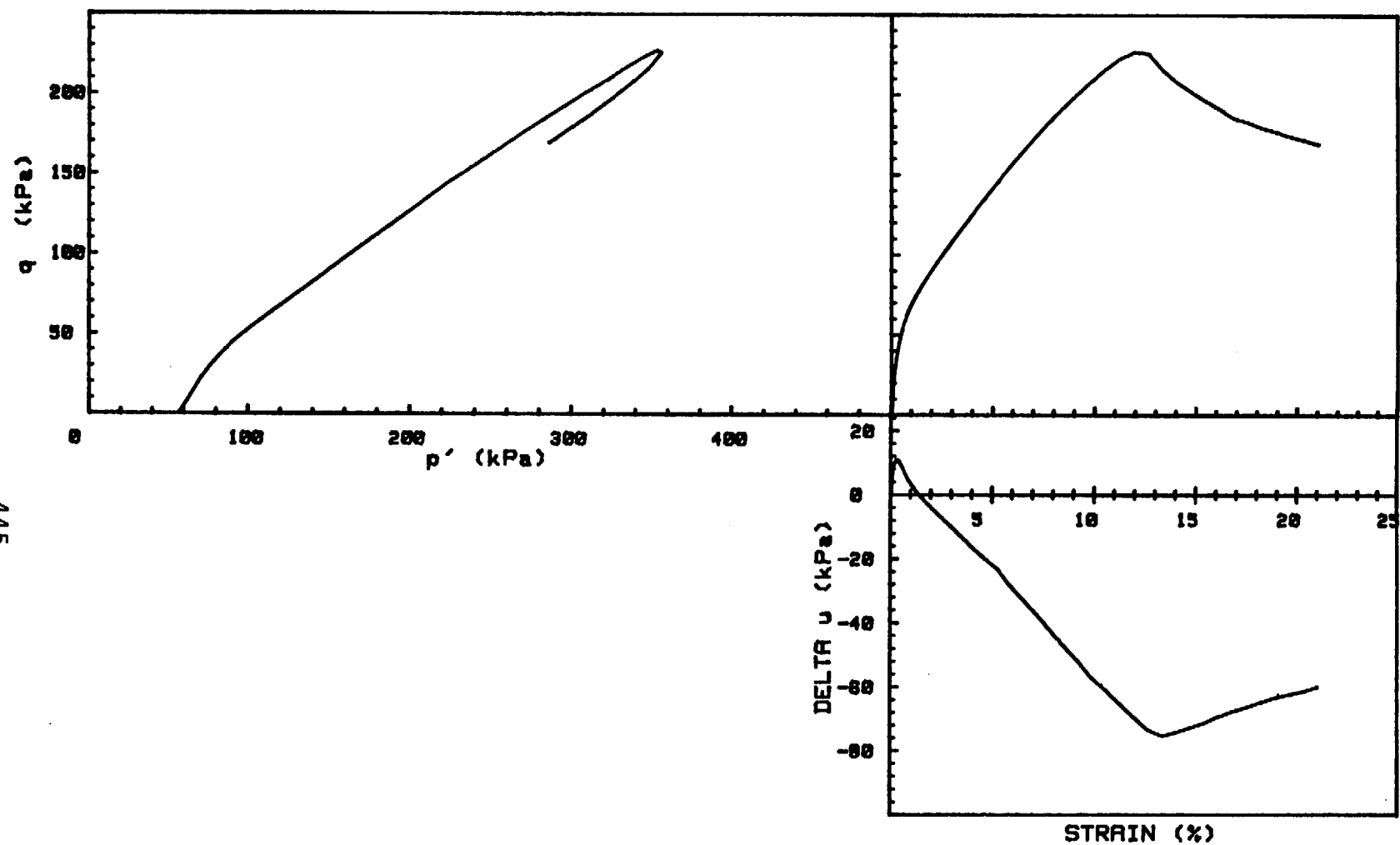


CRUISE DC2-80-EG	INCREMENT (cm)	28-37
CORE NO. 46G	TEST NO.	TE61
SIG1c' (kPa)	.7	
SIG3c' (kPa)	.7	
INDUCED OCR	1.0	

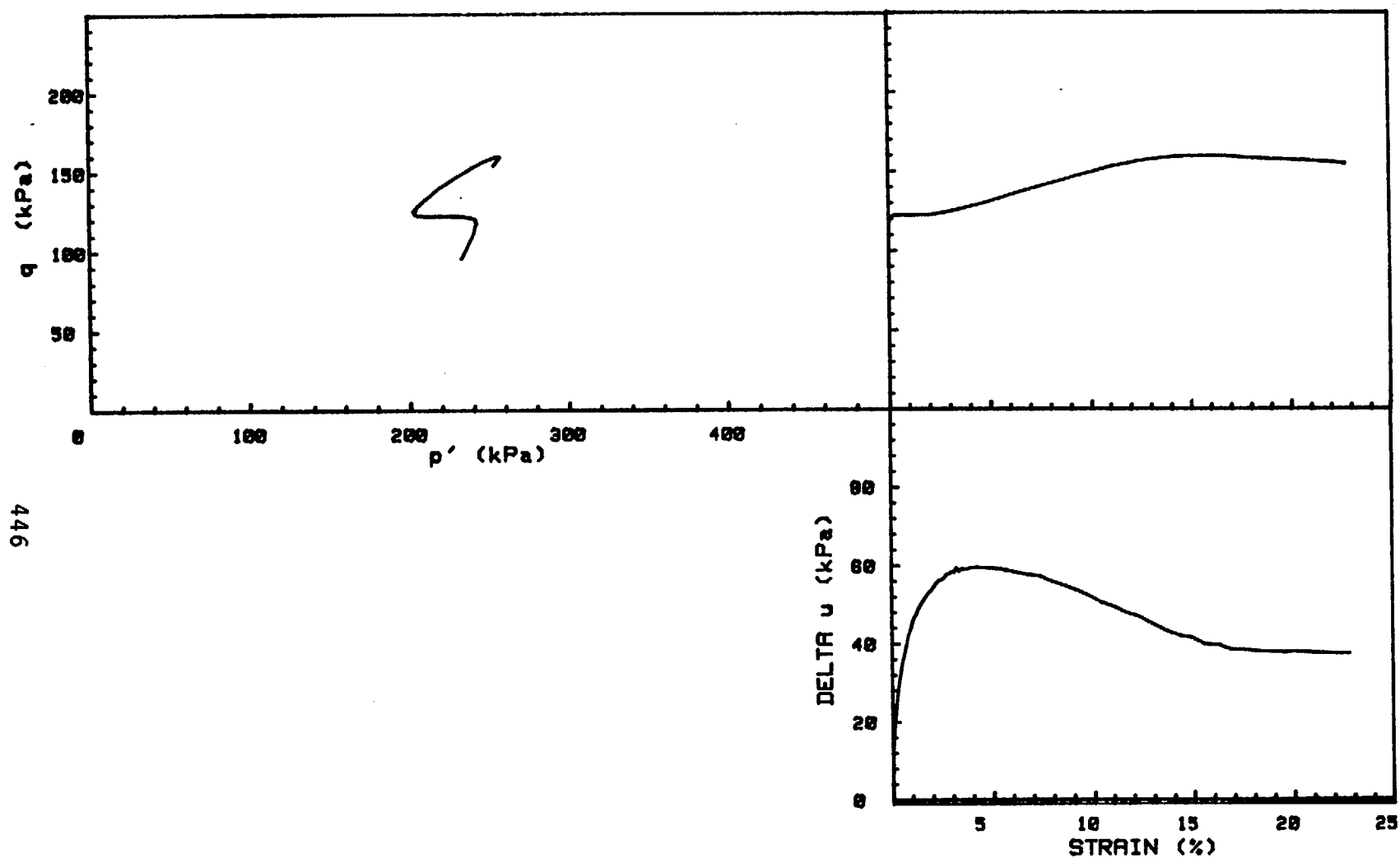


CRUISE DC2-80-EG	INCREMENT (cm)	26-35
CORE NO. 28G	TEST NO.	TE62
SIG1c'(kPa)	310.7	
SIG3c'(kPa)	310.7	
INDUCED OCR	1.0	

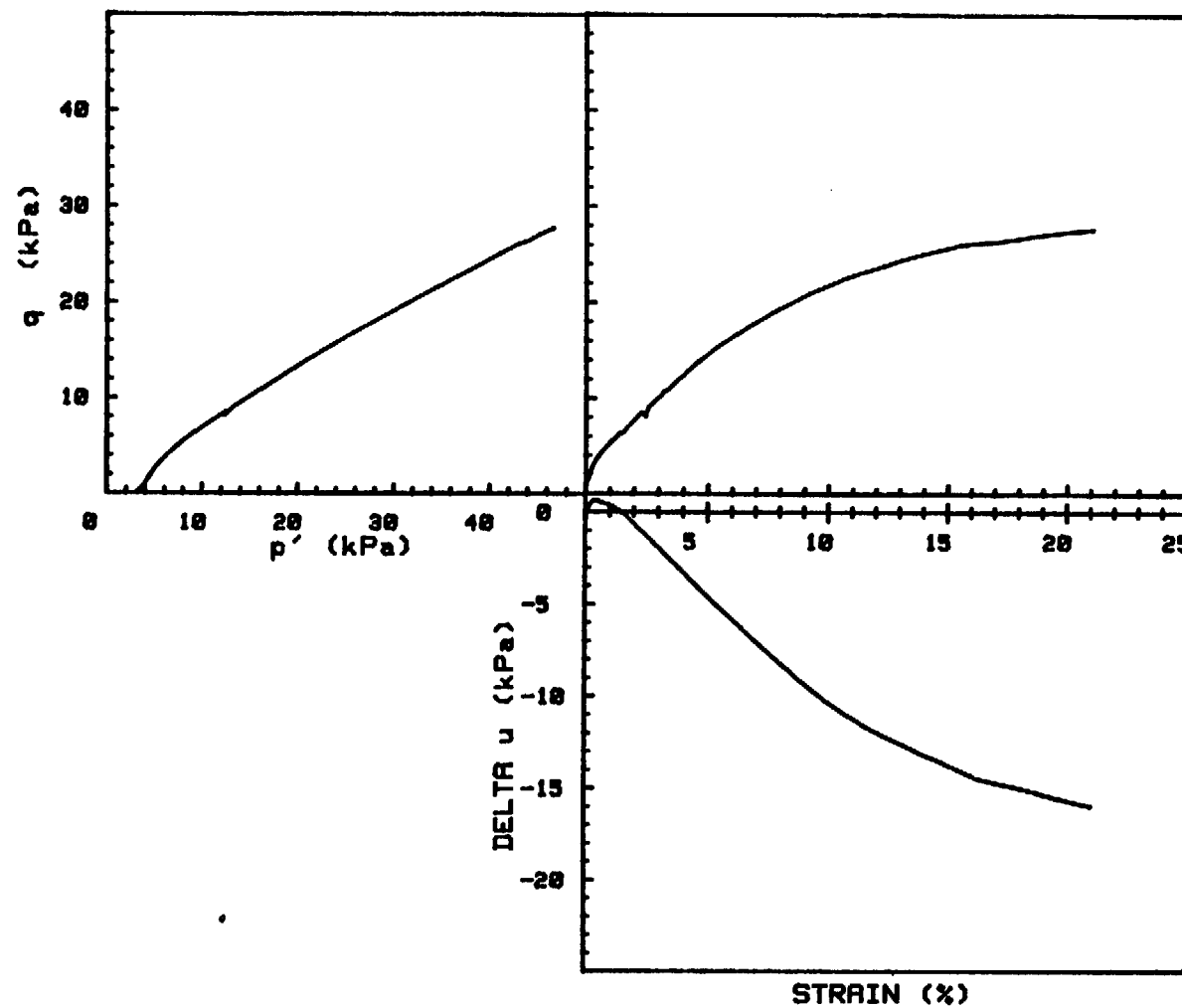
445



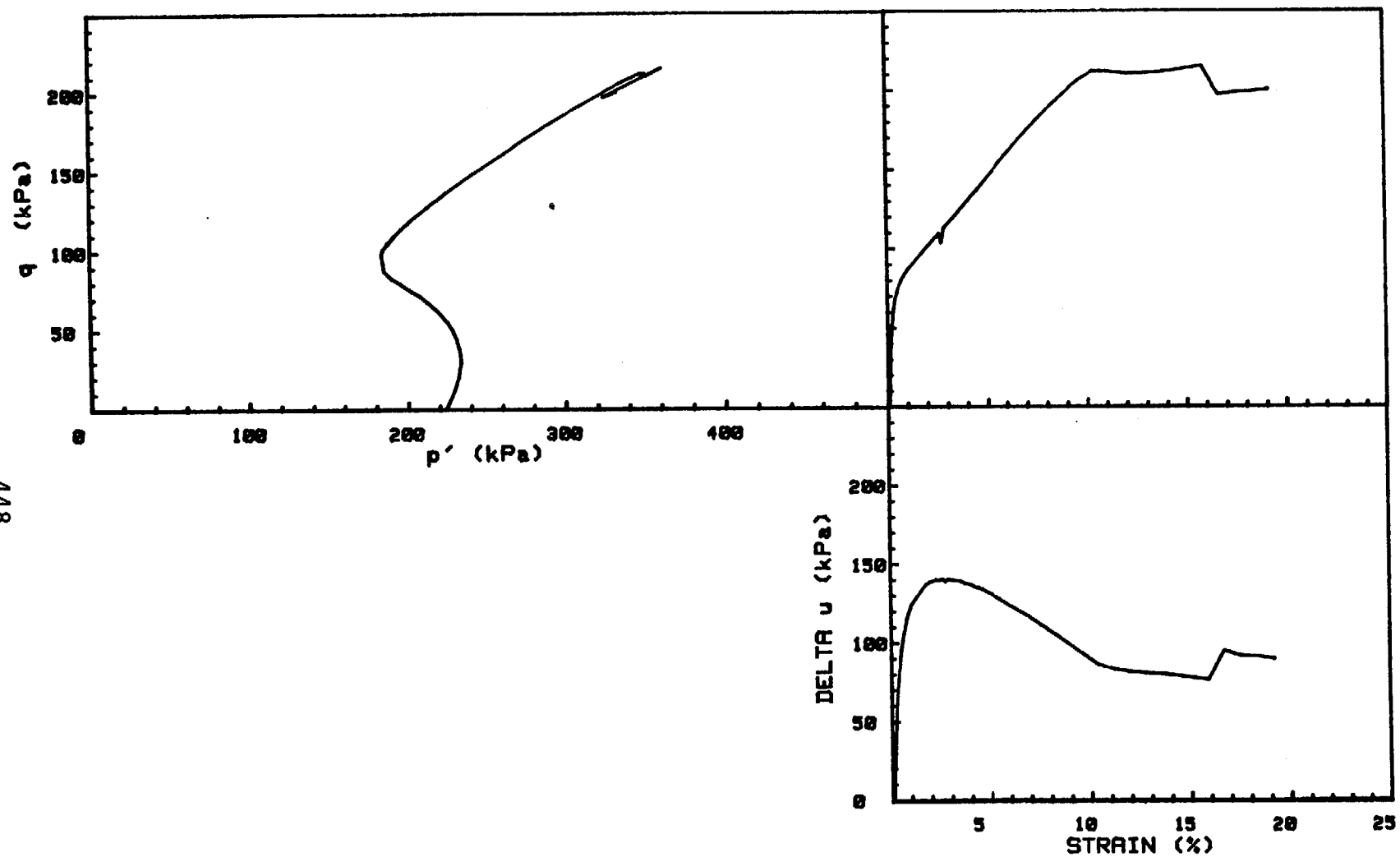
CRUISE DC-2-80 EG	INCREMENT (cm)	26.5-35.1
CORE NO. 28G	TEST NO.	TE63
SIG1c'(kPa)	56.9	
SIG3c'(kPa)	56.9	
INDUCED OCR	6.0	



CRUISE DC2-80-EG	INCREMENT (cm)	6.8-15.2
CORE NO. 28G	TEST NO.	TE64
SIG1c' (kPa)	328.5	
SIG3c' (kPa)	136.8	
INDUCED OCR	1.0	

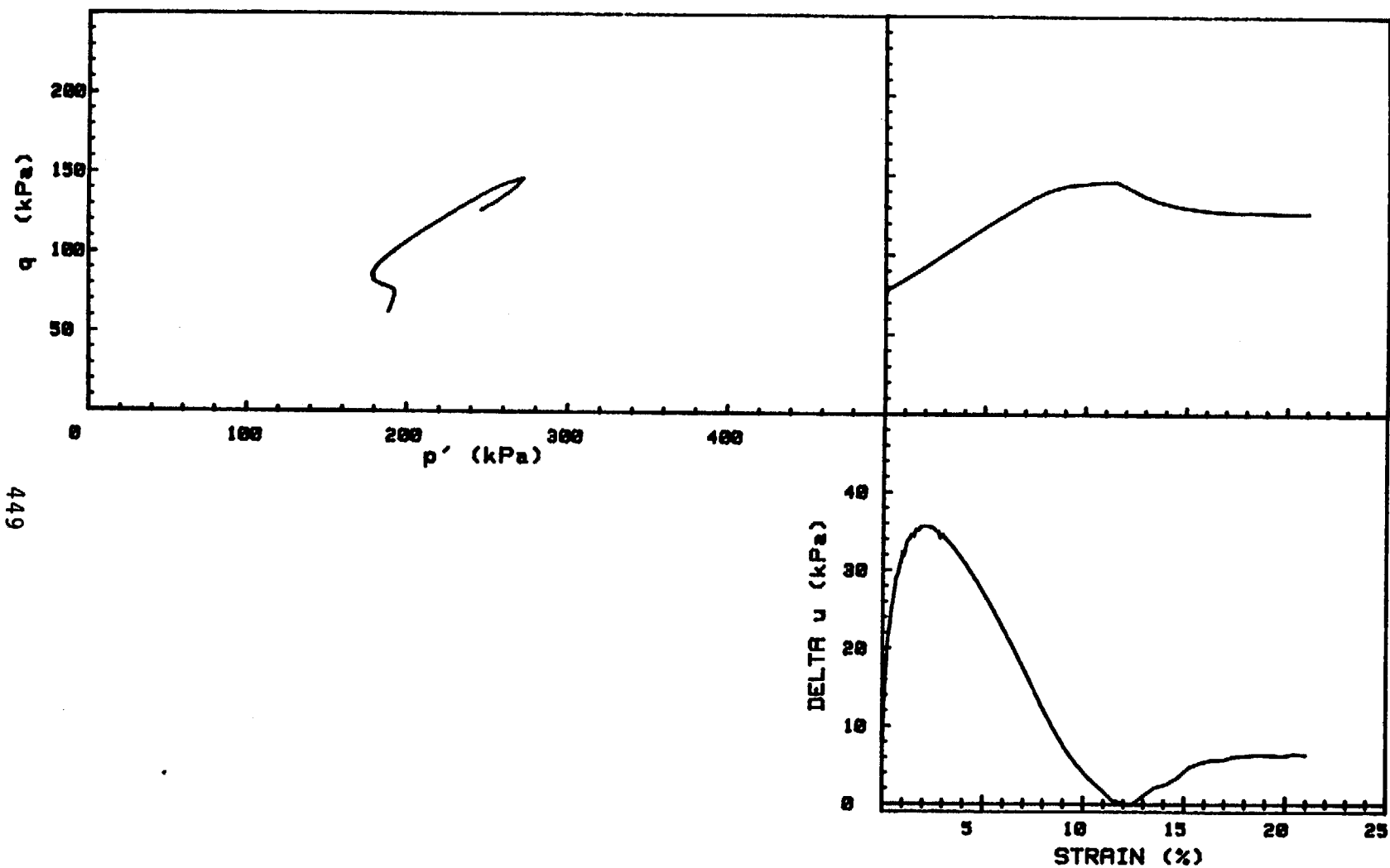


CRUISE DC2-80-EG	INCREMENT (cm)	4-11
CORE NO. 31G	TEST NO.	TE65
SIG1c' (kPa)	3.0	
SIG3c' (kPa)	3.0	
INDUCED OCR	1.0	

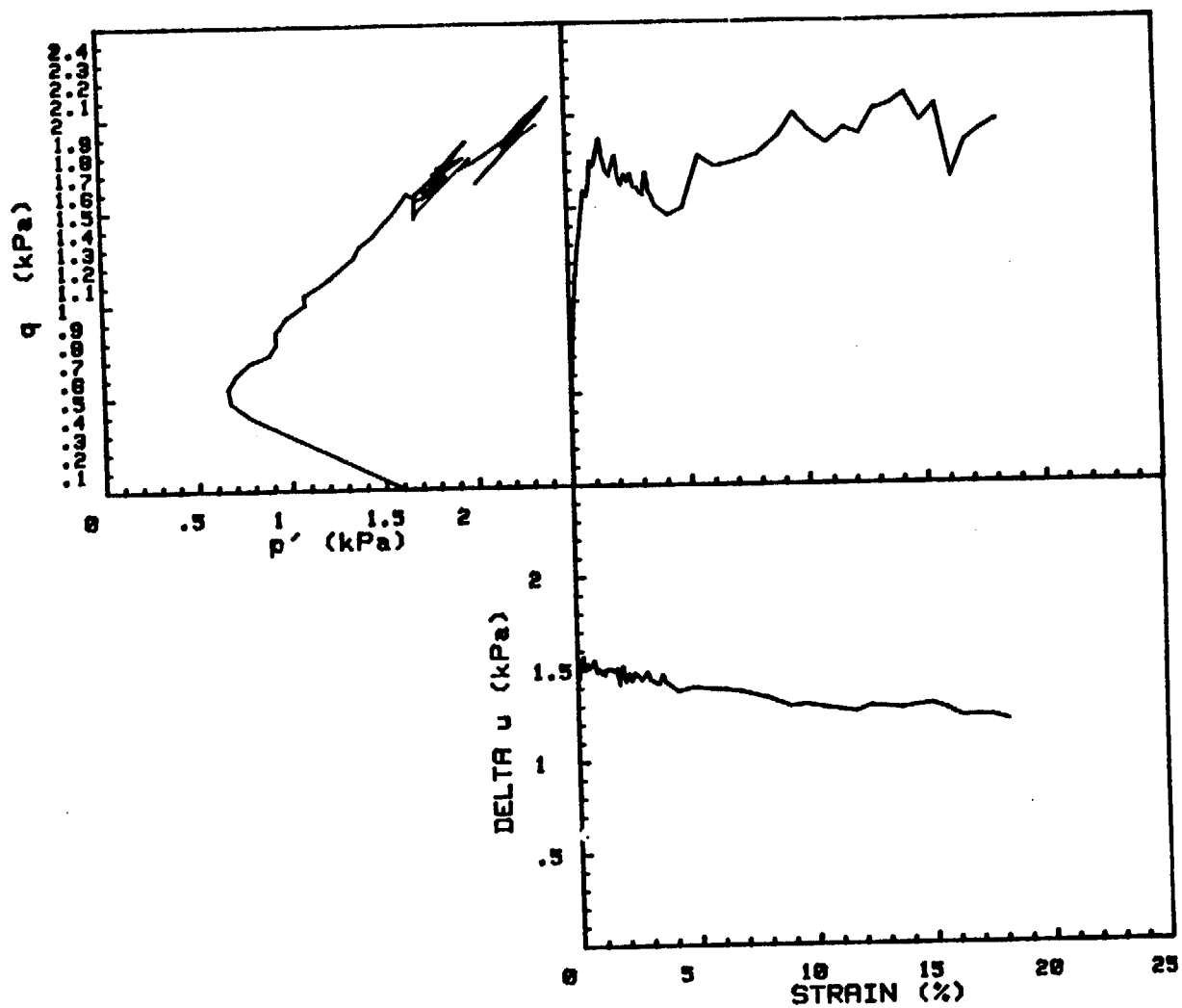


CRUISE DC2-80-EG	INCREMENT (cm)	4-11
CORE NO. 31G	TEST NO.	TE66

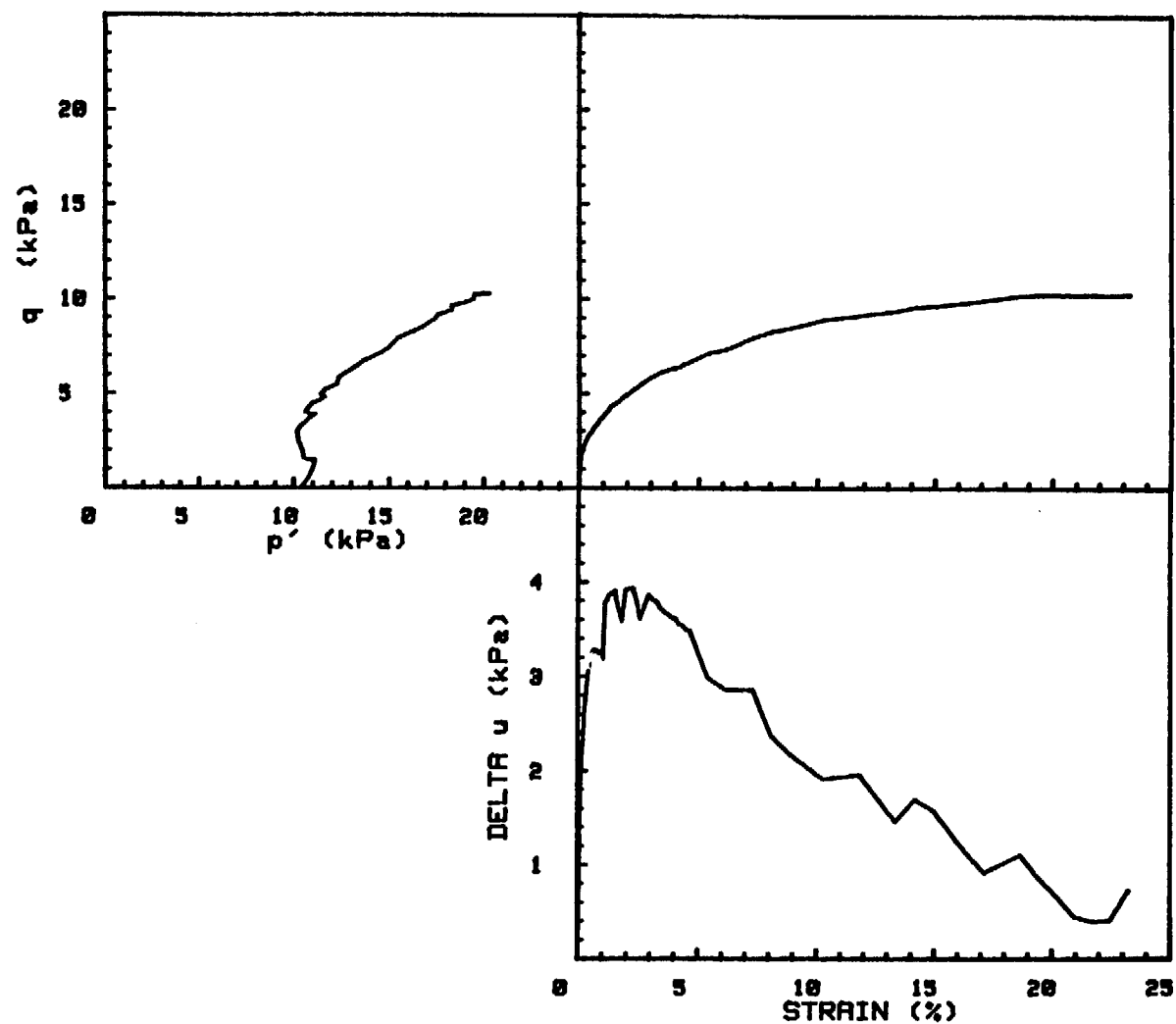
SIG1c' (kPa)	223.2
SIG3c' (kPa)	223.2
INDUCED OCR	1.0



CRUISE DC2-80-EG	INCREMENT (cm)	12.1-19.9
CORE NO. 31G	TEST NO.	TE67
SIG1c'(kPa)	251.2	
SIG3c'(kPa)	126.1	
INDUCED OCR	1.0	

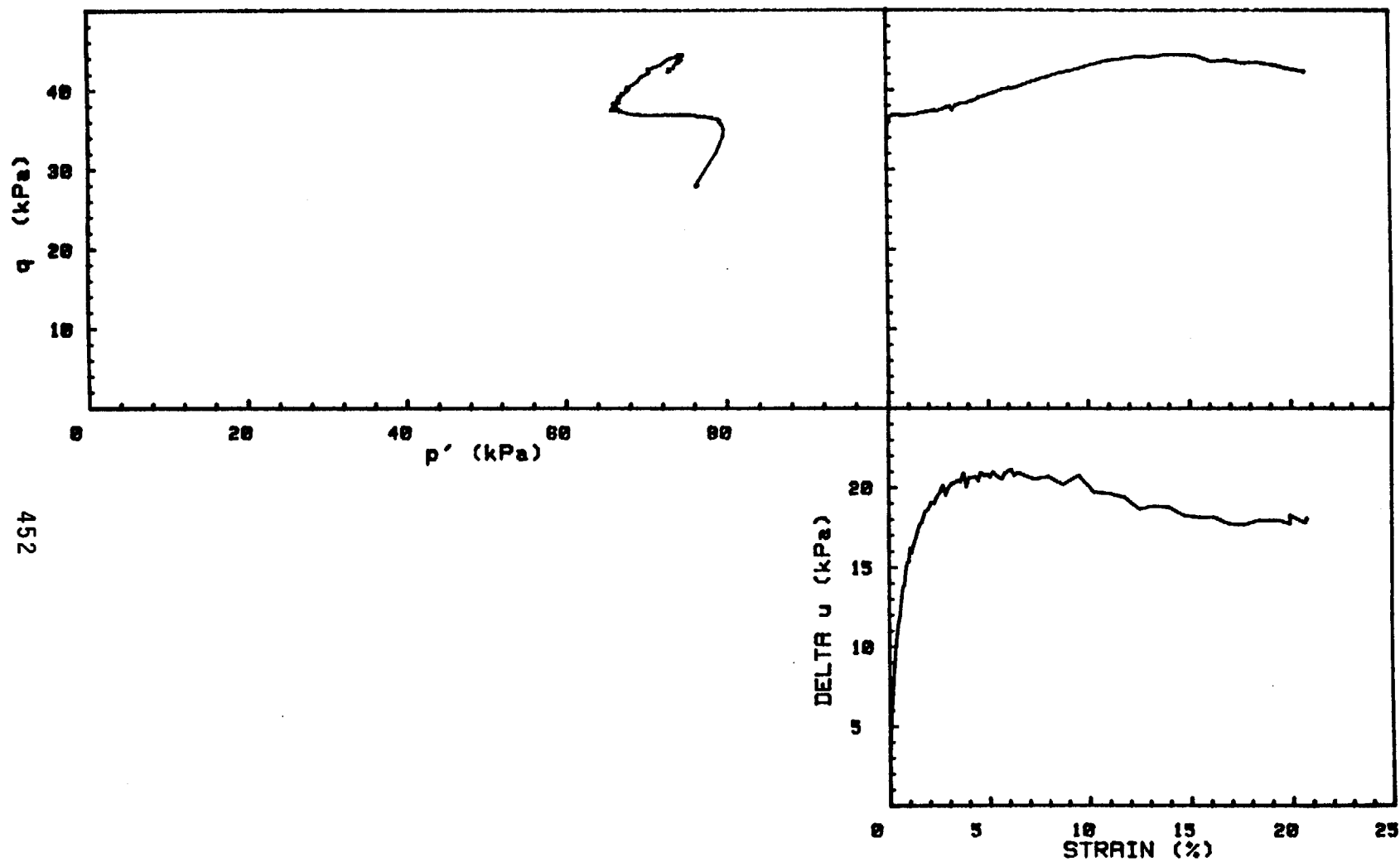


CRUISE DC1-81-EG	INCREMENT (cm)	105-113
CORE NO. 627G2	TEST NO.	TE68
SIG1c' (kPa)	1.6	
SIG3c' (kPa)	1.6	
INDUCED OCR	1.0	

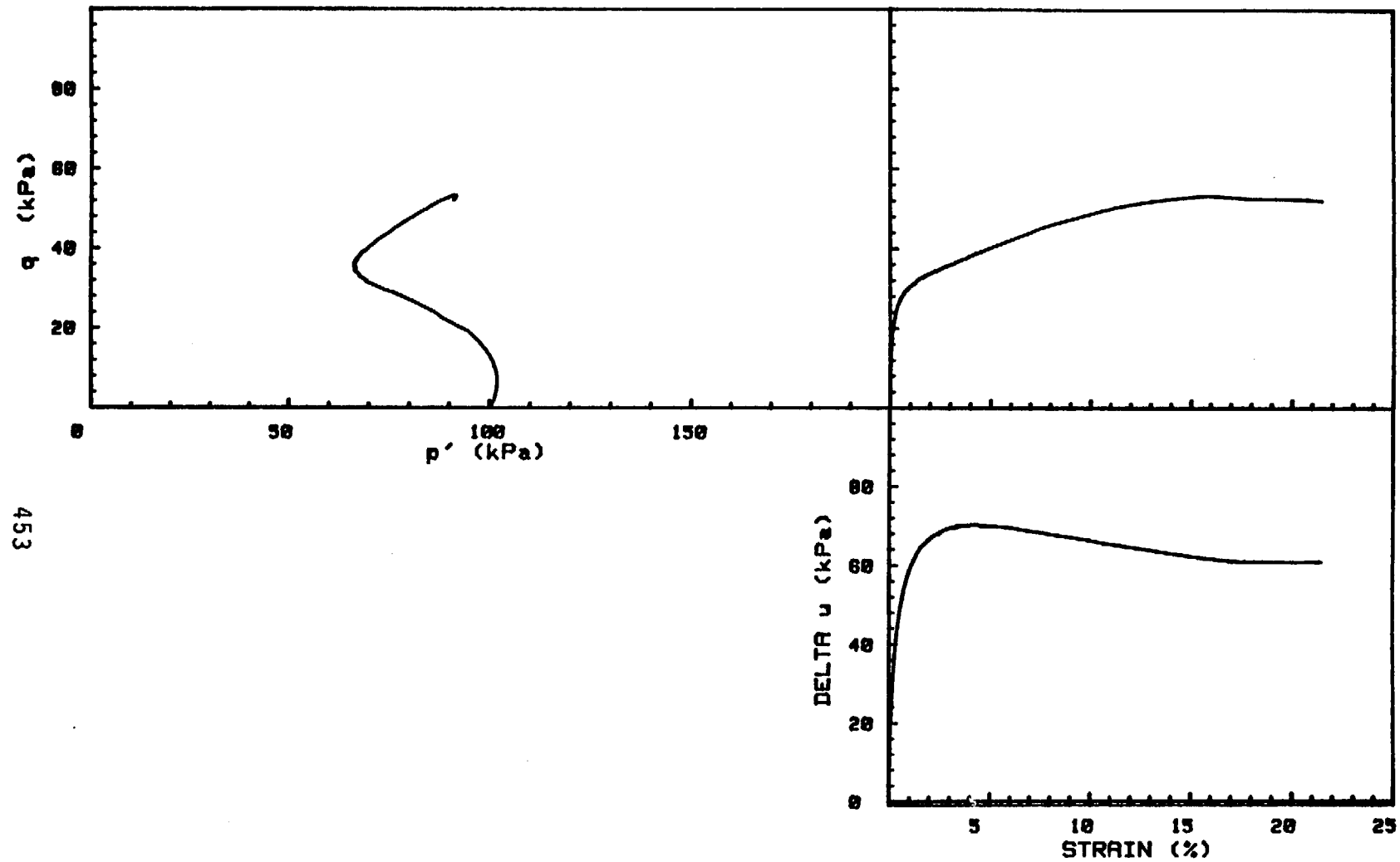


CRUISE DC1-81-EG	INCREMENT (cm)	105.5-113.7
CORE NO. 627G2	TEST NO.	TE69

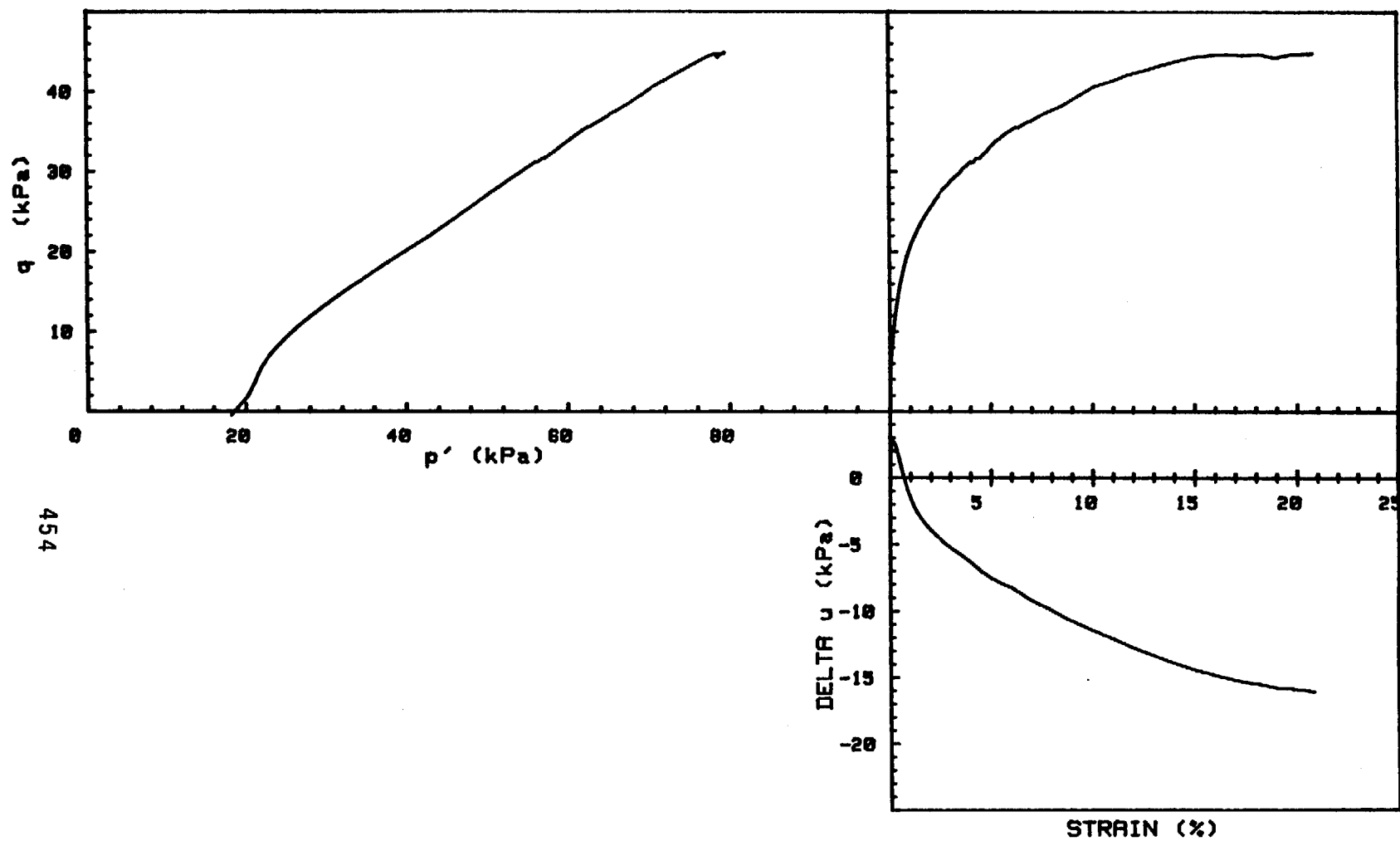
SIG1c' (kPa)	10.4
SIG3c' (kPa)	10.4
INDUCED OCR	1.0



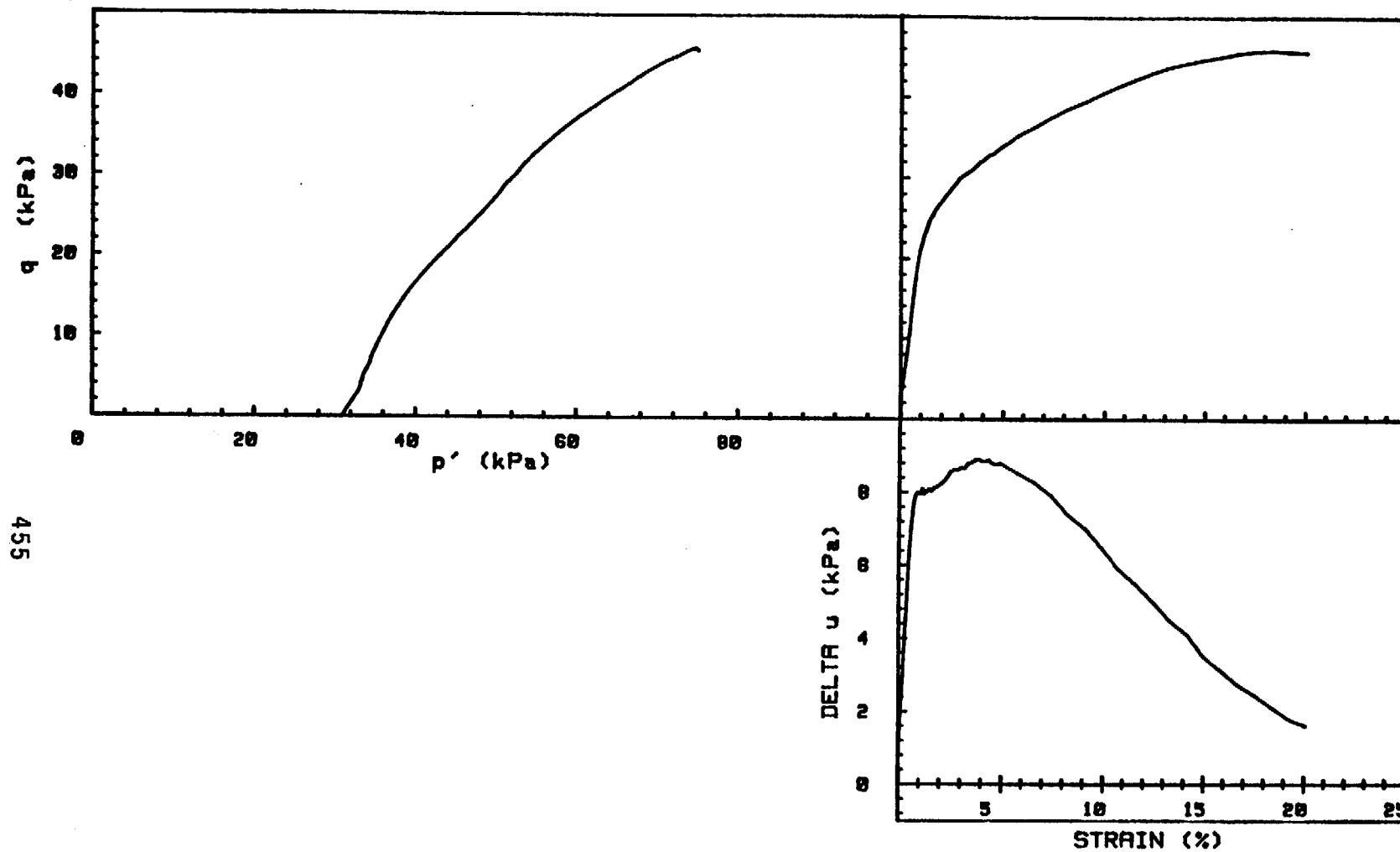
CRUISE DC1-81-EG	INCREMENT (cm)	82-93
CORE NO. 627G2	TEST NO.	TE70
SIG1c' (kPa)	104.7	
SIG3c' (kPa)	48.7	
INDUCED OCR	1.0	



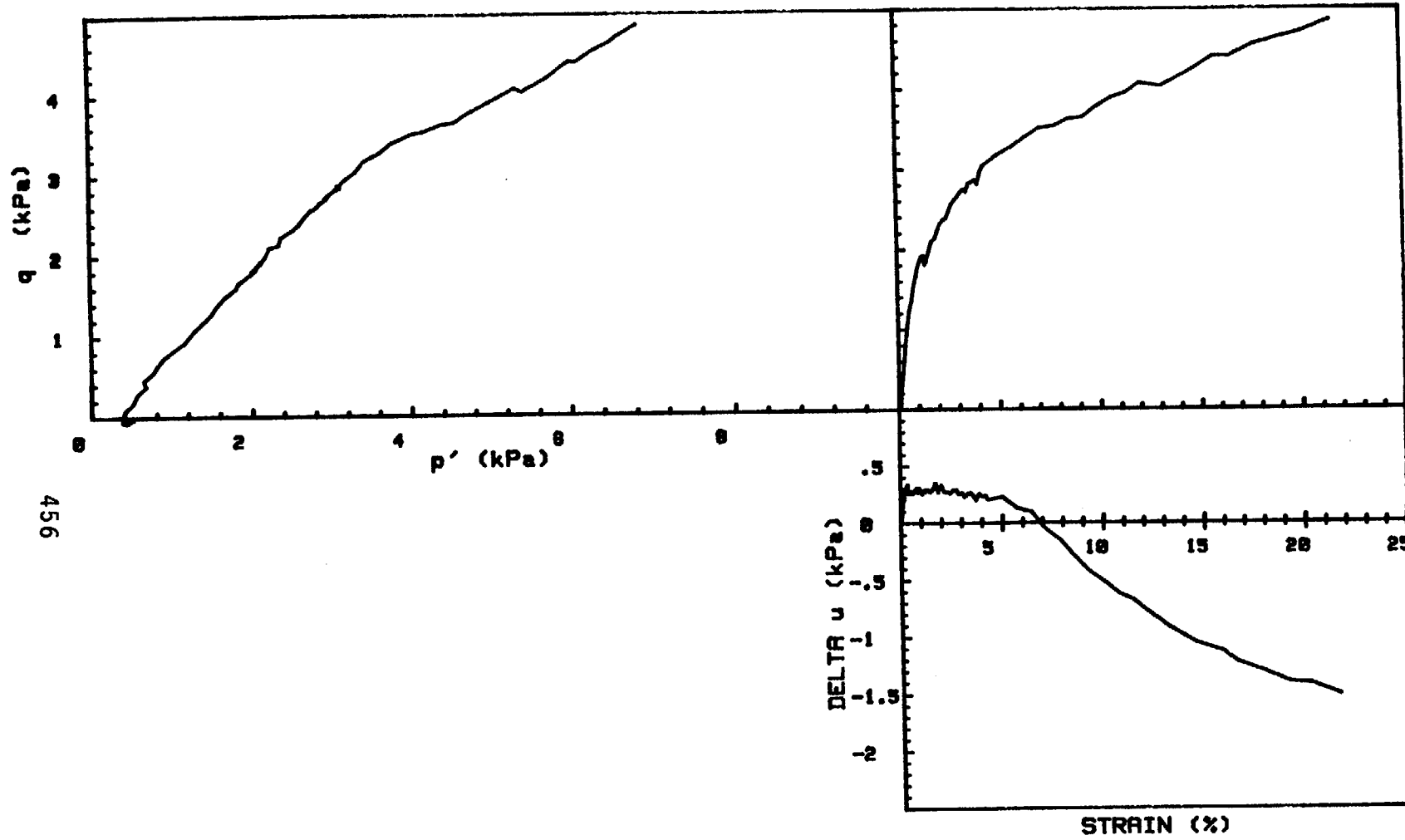
CRUISE DC1-01-EG	INCREMENT (cm)	02-93
CORE NO. 627G2	TEST NO.	TE71
SIG1 σ' (kPa)	100.1	
SIG3 σ' (kPa)	100.1	
INDUCED OCR	1.0	



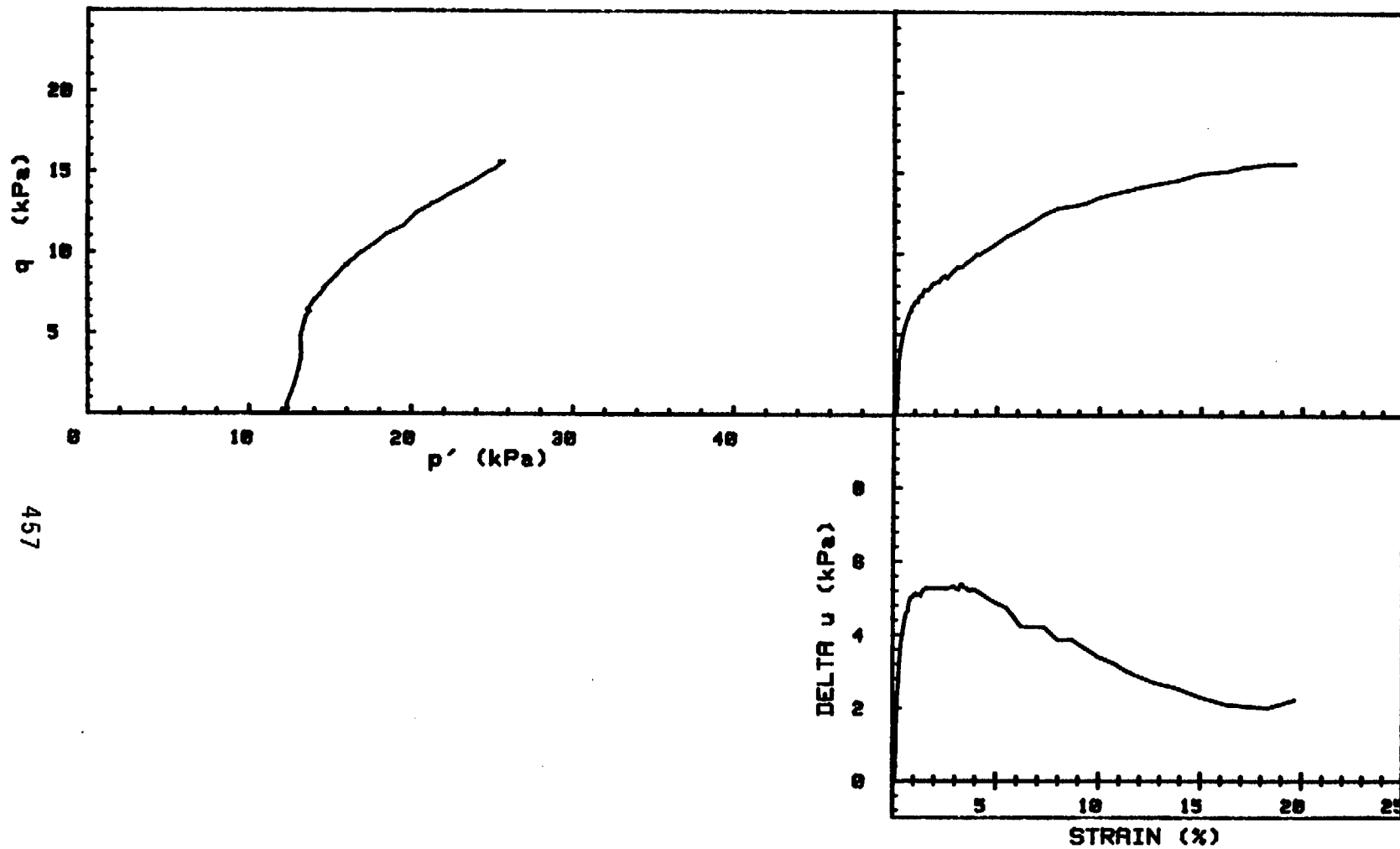
CRUISE DC1-81-EG	INCREMENT (cm)	71-82
CORE NO. 627G2	TEST NO.	TE72
SIG1c' (kPa)	18.6	
SIG3c' (kPa)	18.6	
INDUCED OCR	6.0	



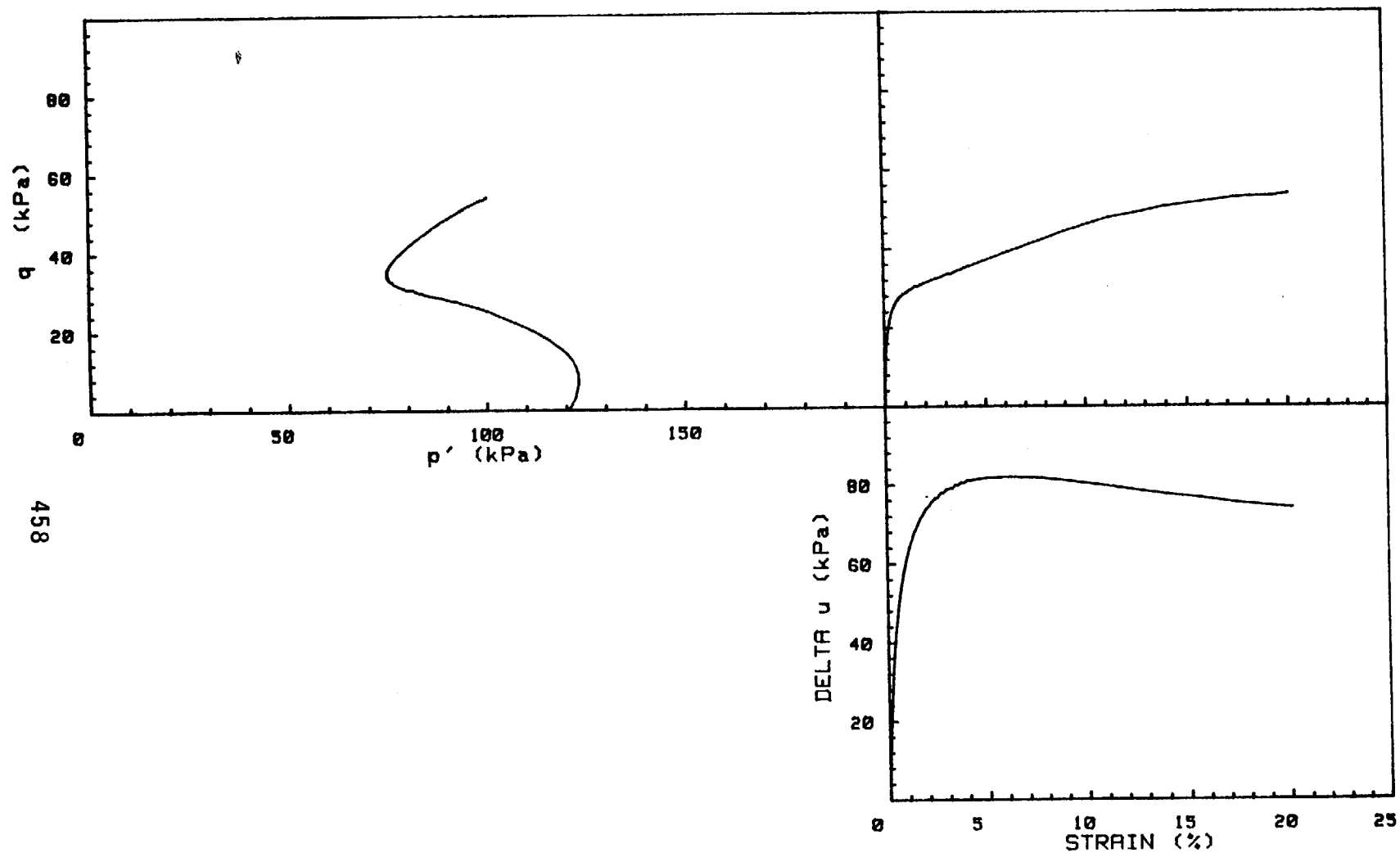
CRUISE DC1-01-EG	INCREMENT (cm)	71-02
CORE NO. 627G2	TEST NO.	TE73
SIG1c' (kPa)	31.0	
SIG3c' (kPa)	31.0	
INDUCED OCR	3.0	



CRUISE DC1-81-EG	INCREMENT (cm)	149-160
CORE NO. 618G2	TEST NO.	TE74
SIG1c'(kPa) .5 SIG3c'(kPa) .5 INDUCED OCR 1.0		

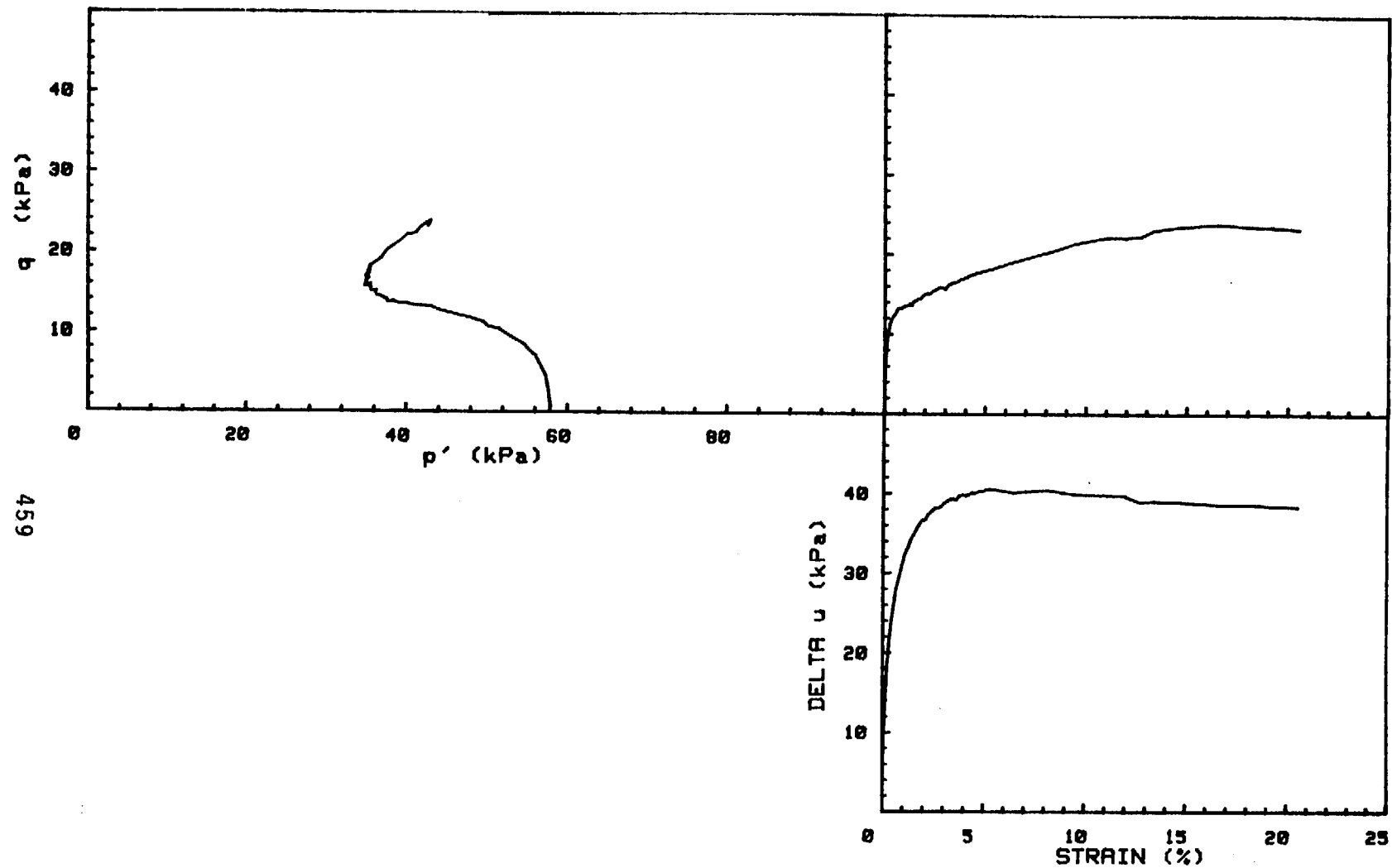


CRUISE DC1-81-EG	INCREMENT (cm)	149-160
CORE NO. 618G2	TEST NO.	TE75
SIG _{1c'} (kPa)	12.1	
SIG _{3c'} (kPa)	12.1	
INDUCED OCR	1.0	

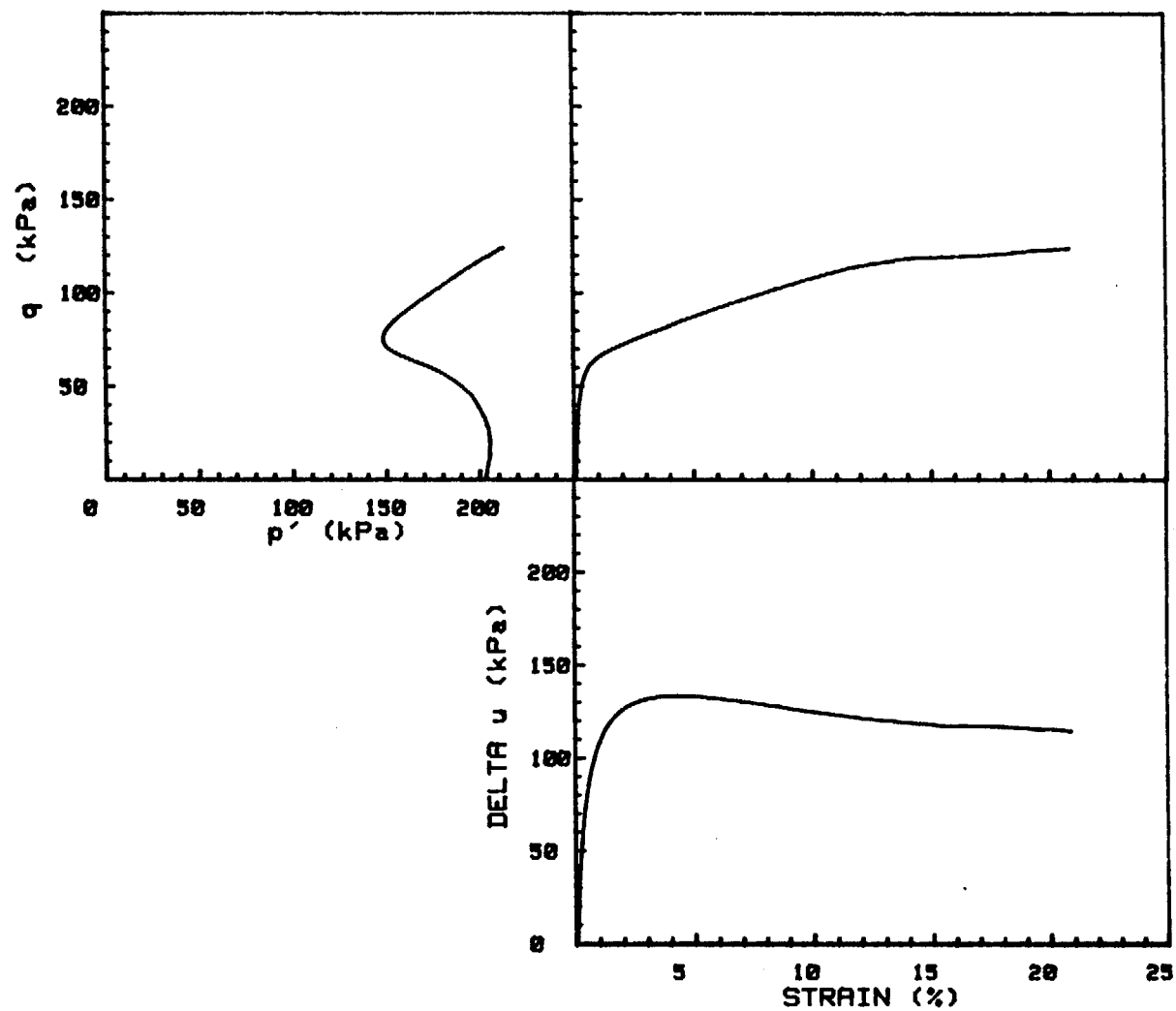


CRUISE DC1-81-EG	INCREMENT (cm)	90-99
CORE NO. 620G2	TEST NO.	TE82

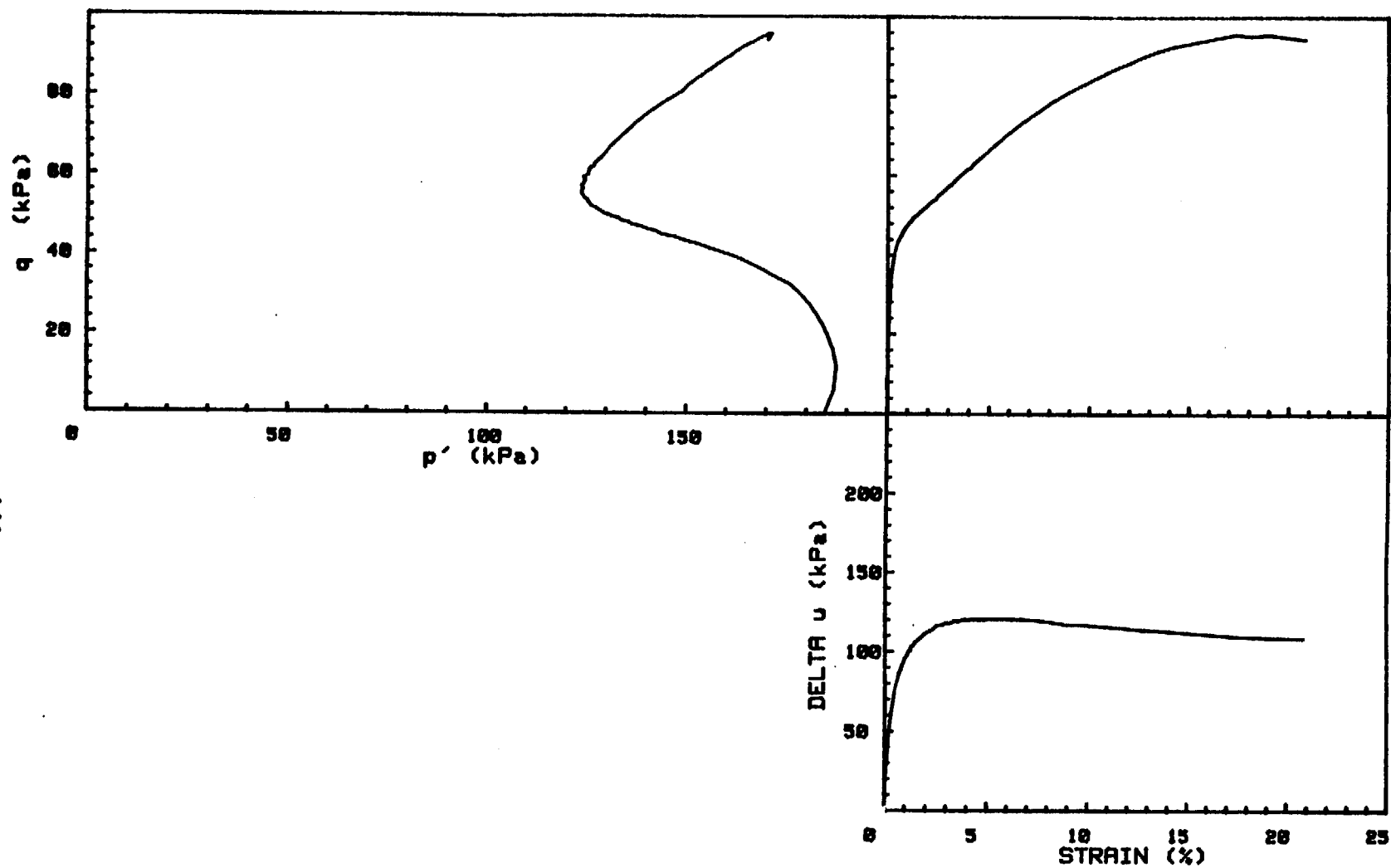
SIG1c' (kPa)	120.8
SIG3c' (kPa)	120.8
INDUCED OCR	1.0



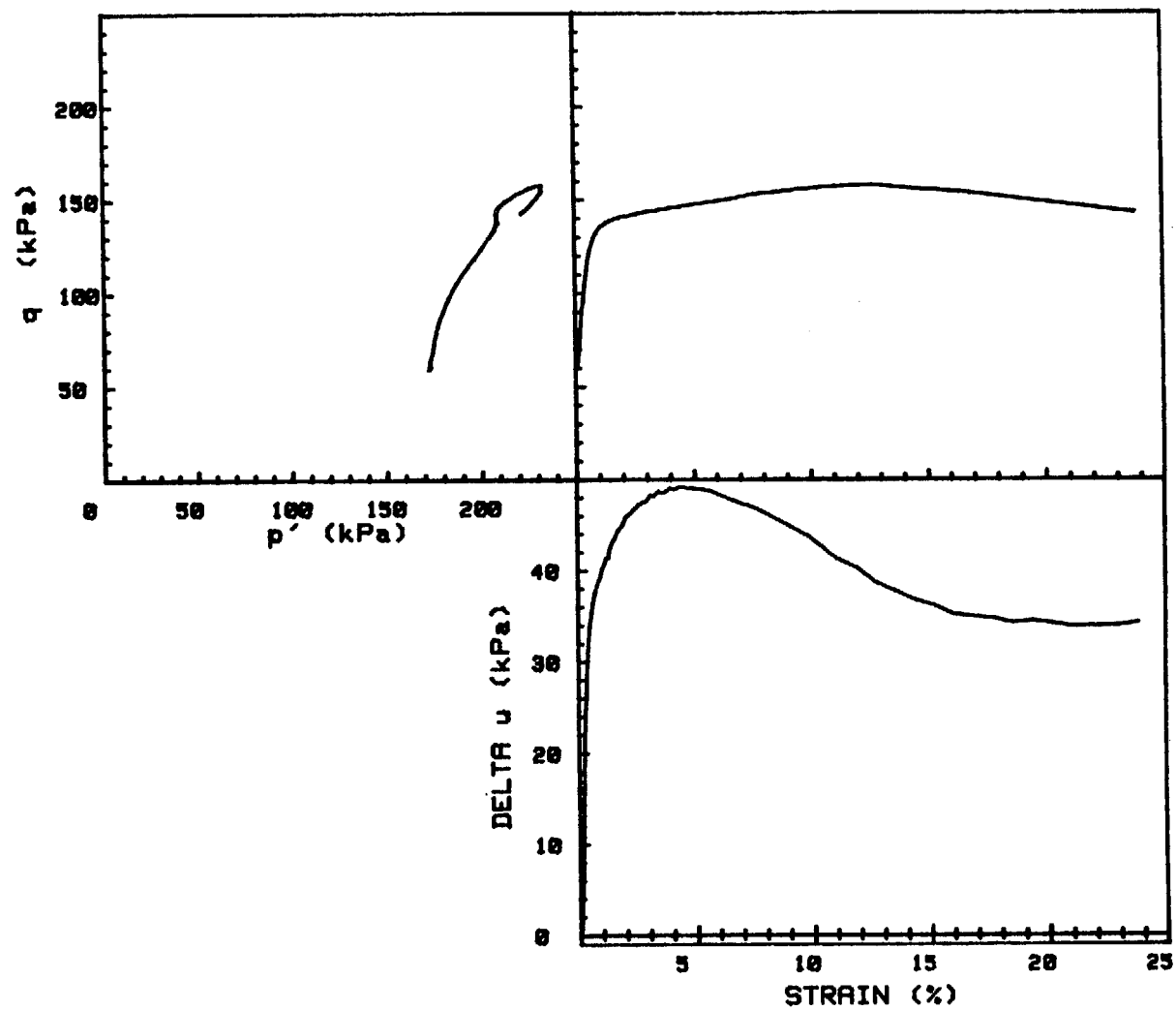
CRUISE DC1-81-EG	INCREMENT (cm)	51-60
CORE NO. 634G2	TEST NO.	TE83
SIG1c' (kPa)	57.9	
SIG3c' (kPa)	57.9	
INDUCED OCR	1.0	



CRUISE DC2-80-EG	INCREMENT (cm)	150-158
CORE NO. 87G	TEST NO.	TE84
SIG1c' (kPa)	203.1	
SIG3c' (kPa)	203.1	
INDUCED OCR	1.0	



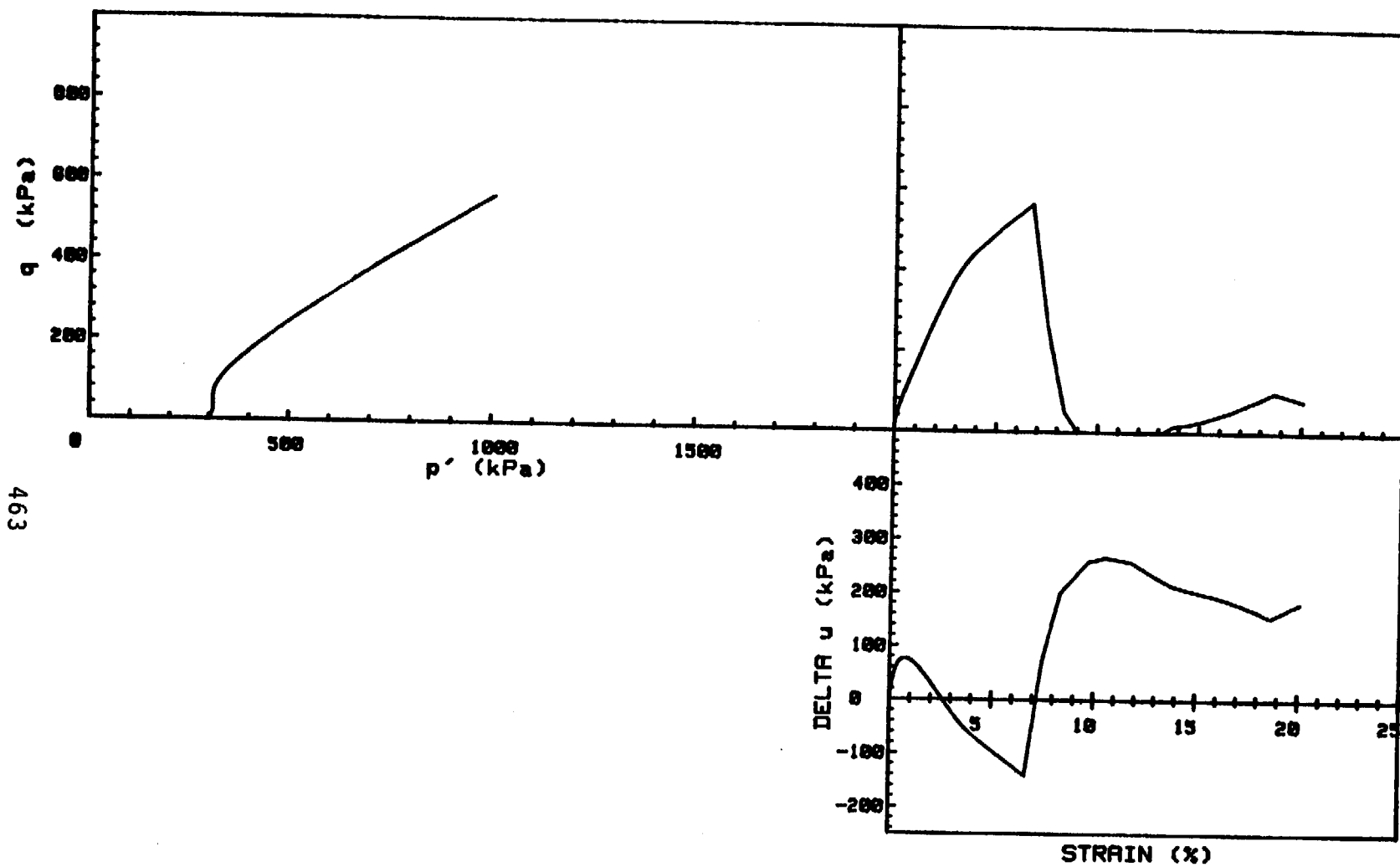
CRUISE DC1-81-EG	INCREMENT (cm)	127-138
CORE NO. 618G2	TEST NO.	TE87
SIG1c' (kPa)	184.7	
SIG3c' (kPa)	184.7	
INDUCED OCR	1.0	



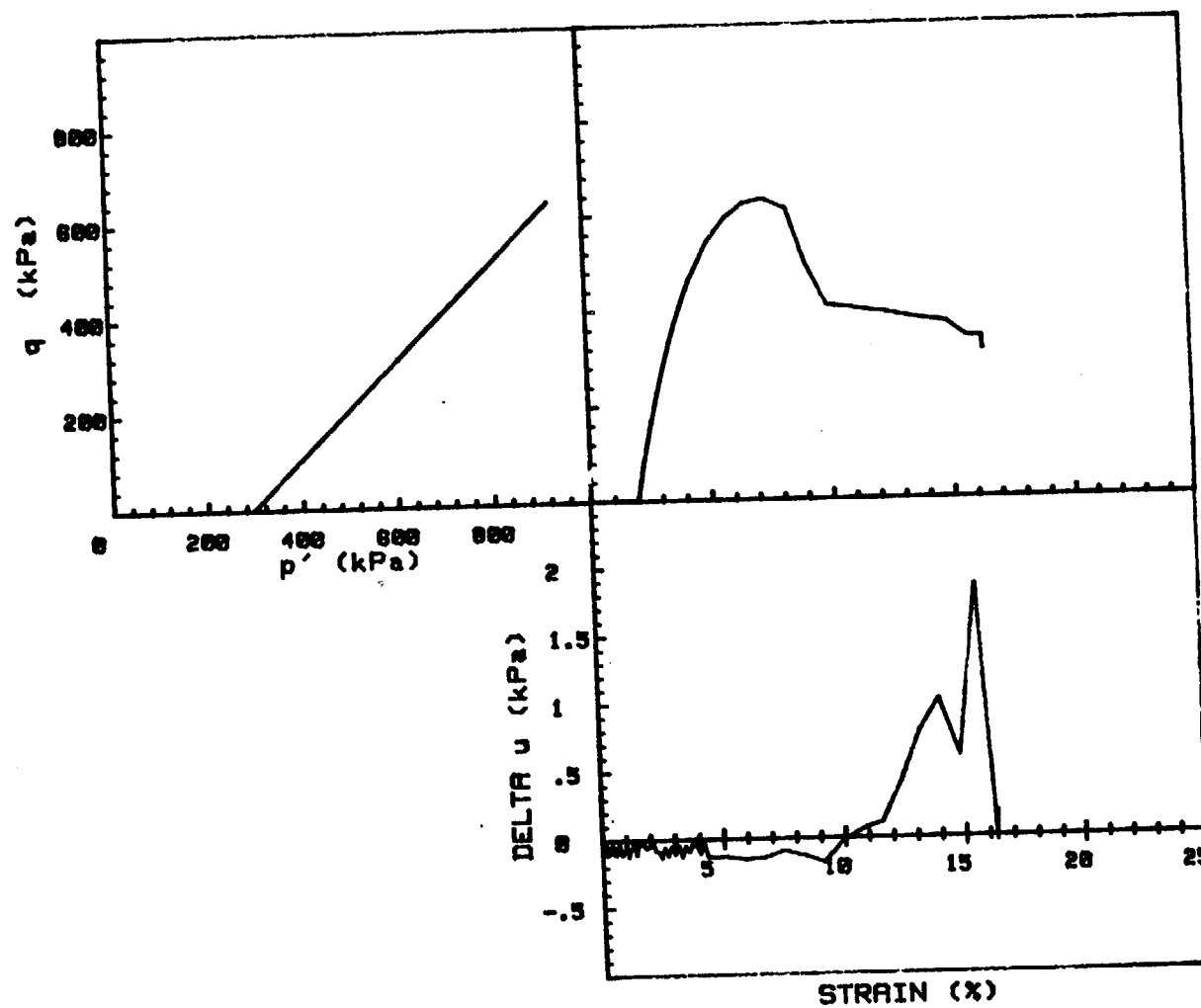
CRUISE DC1-81-EG	INCREMENT (cm)	127-138
CORE NO. 618G2	TEST NO.	TE88

SIG1c' (kPa)	231.5
SIG3c' (kPa)	113.6
INDUCED OCR	1.0

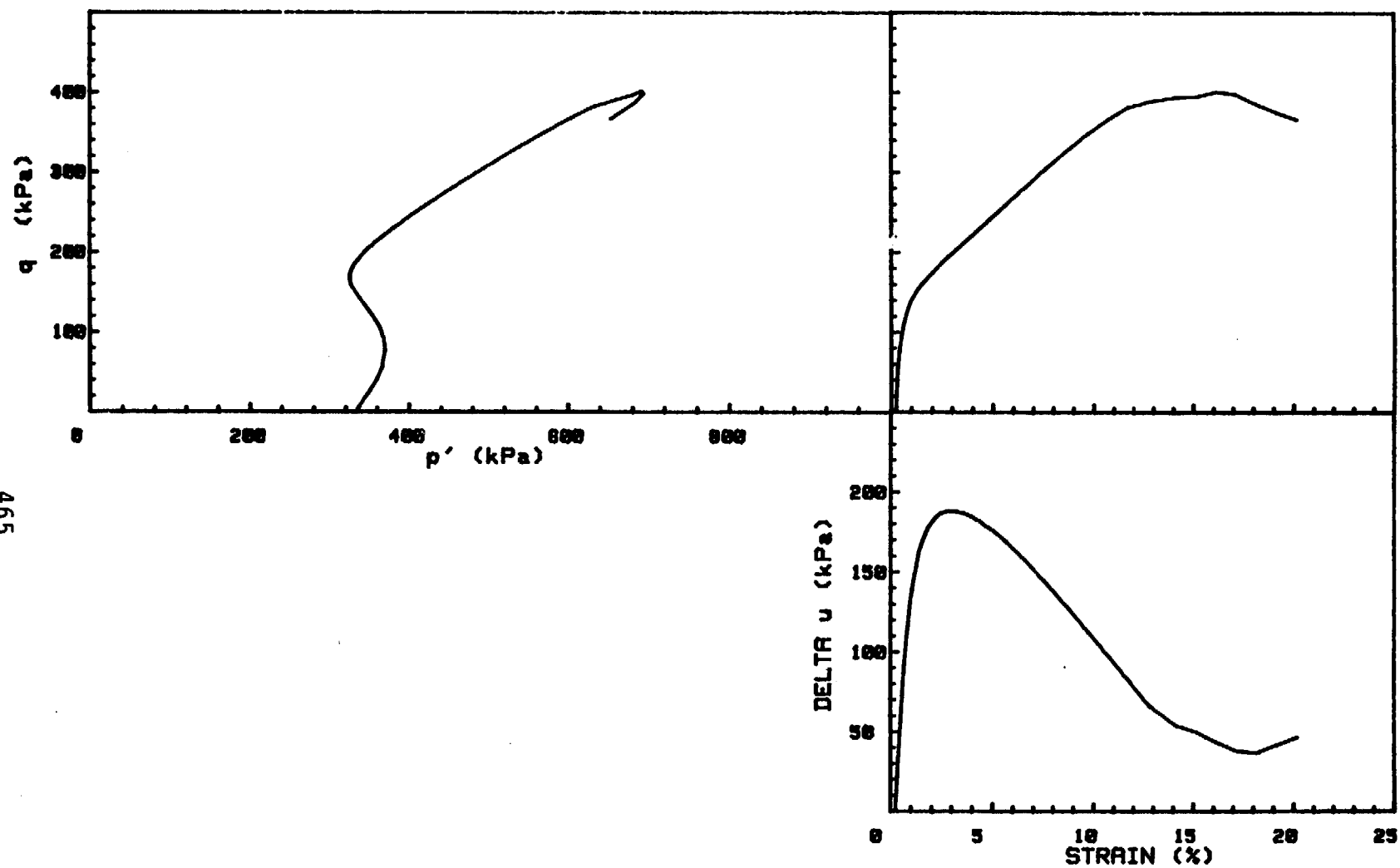
463



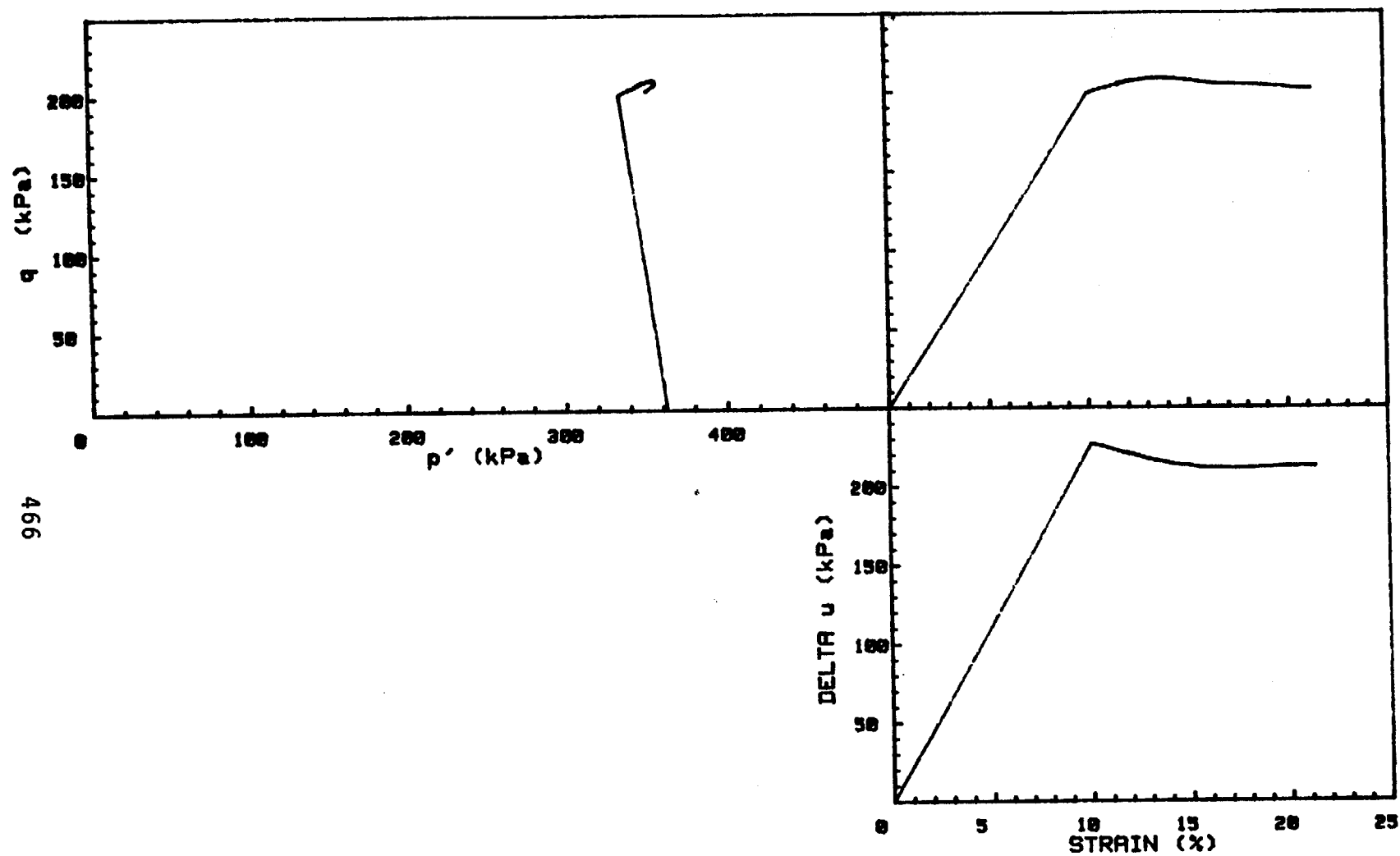
CRUISE DC1-81-EG	INCREMENT (cm)	220-230
CORE NO. 630A2	TEST NO.	TE09
SIG1c'(kPa)	299.9	
SIG3c'(kPa)	299.9	
INDUCED OCR	1.0	



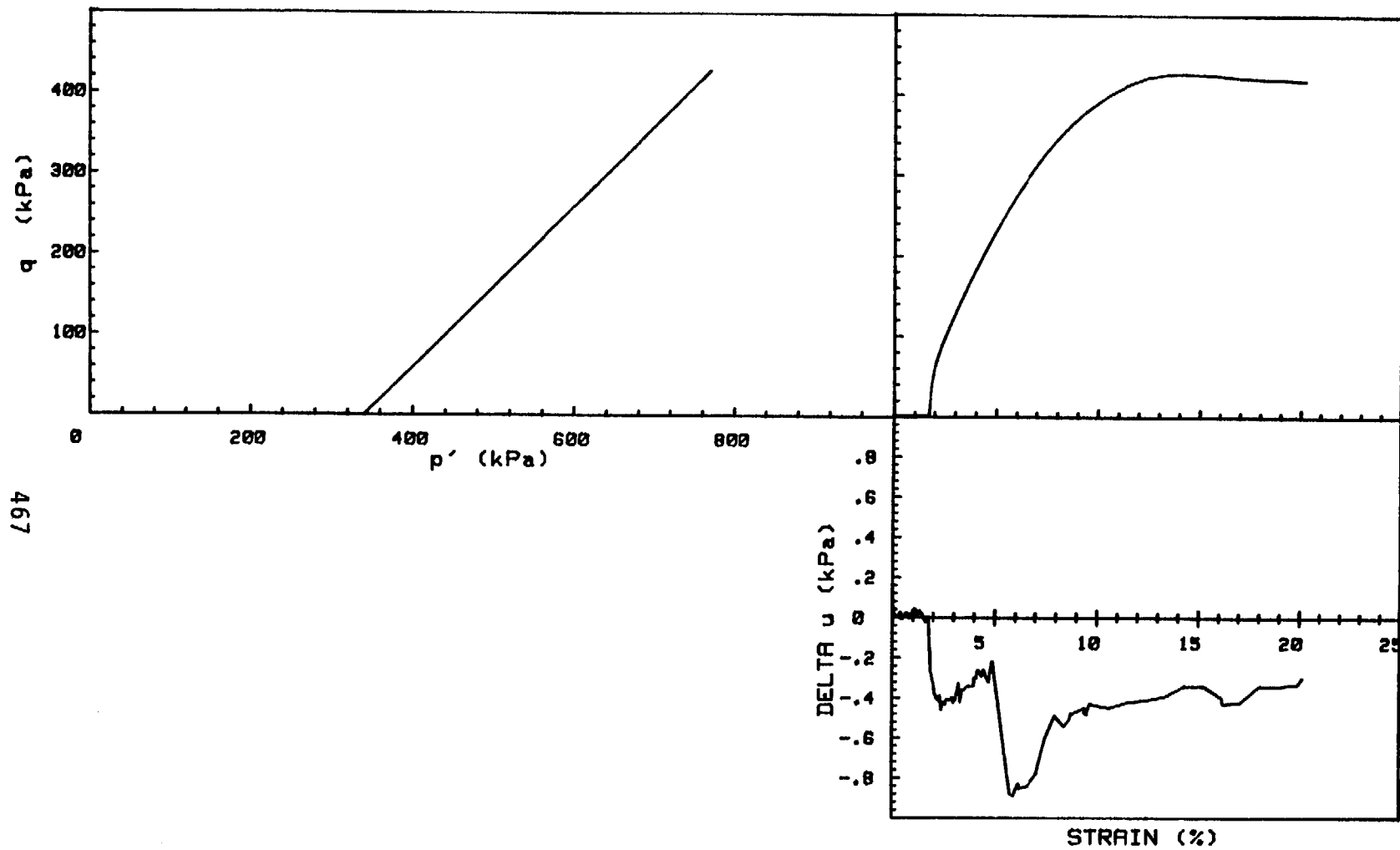
CRUISE DC1-01-EG	INCREMENT (cm)	220-229
CORE NO. 630A2	TEST NO.	TE90
SIG1c' (kPa)	295.5	
SIG3c' (kPa)	295.5	
INDUCED OCR	1.0	



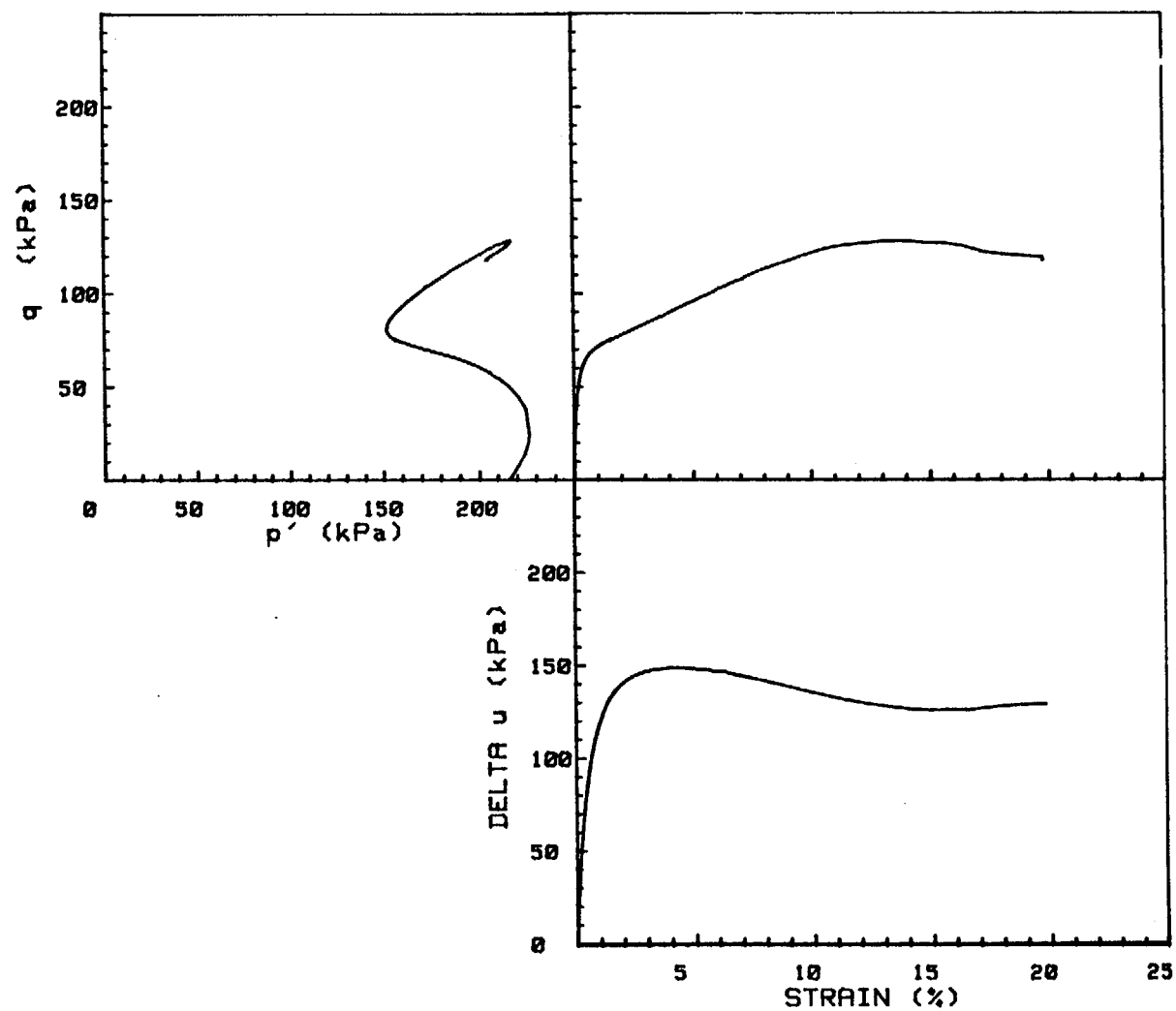
CRUISE DC1-01-EG	INCREMENT (cm)	141-150
CORE NO. 624A1	TEST NO.	TE91
SIG1c'(kPa)	333.1	
SIG3c'(kPa)	333.1	
INDUCED OCR	1.0	



CRUISE DC1-81-EG	INCREMENT (cm)	80-89
CORE NO. 632G1	TEST NO.	TE92
SIG1c'(kPa)	362.8	
SIG3c'(kPa)	362.8	
INDUCED OCR	1.0	

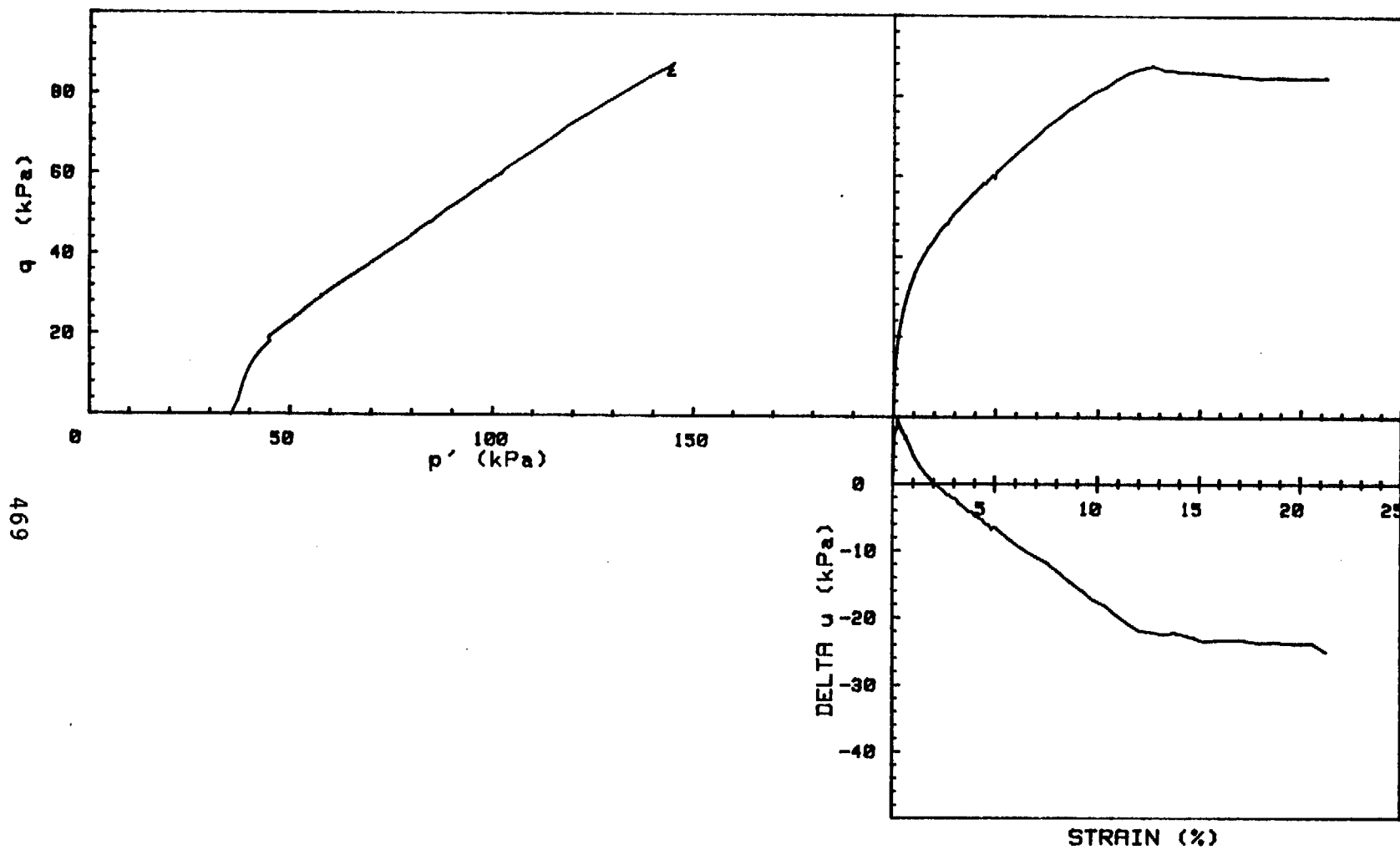


CRUISE DC1-81-EG	INCREMENT (cm)	162-168
CORE NO. 624R1	TEST NO.	TE93
SIG1c' (kPa)	341.5	
SIG3c' (kPa)	341.5	
INDUCED OCR	1.0	



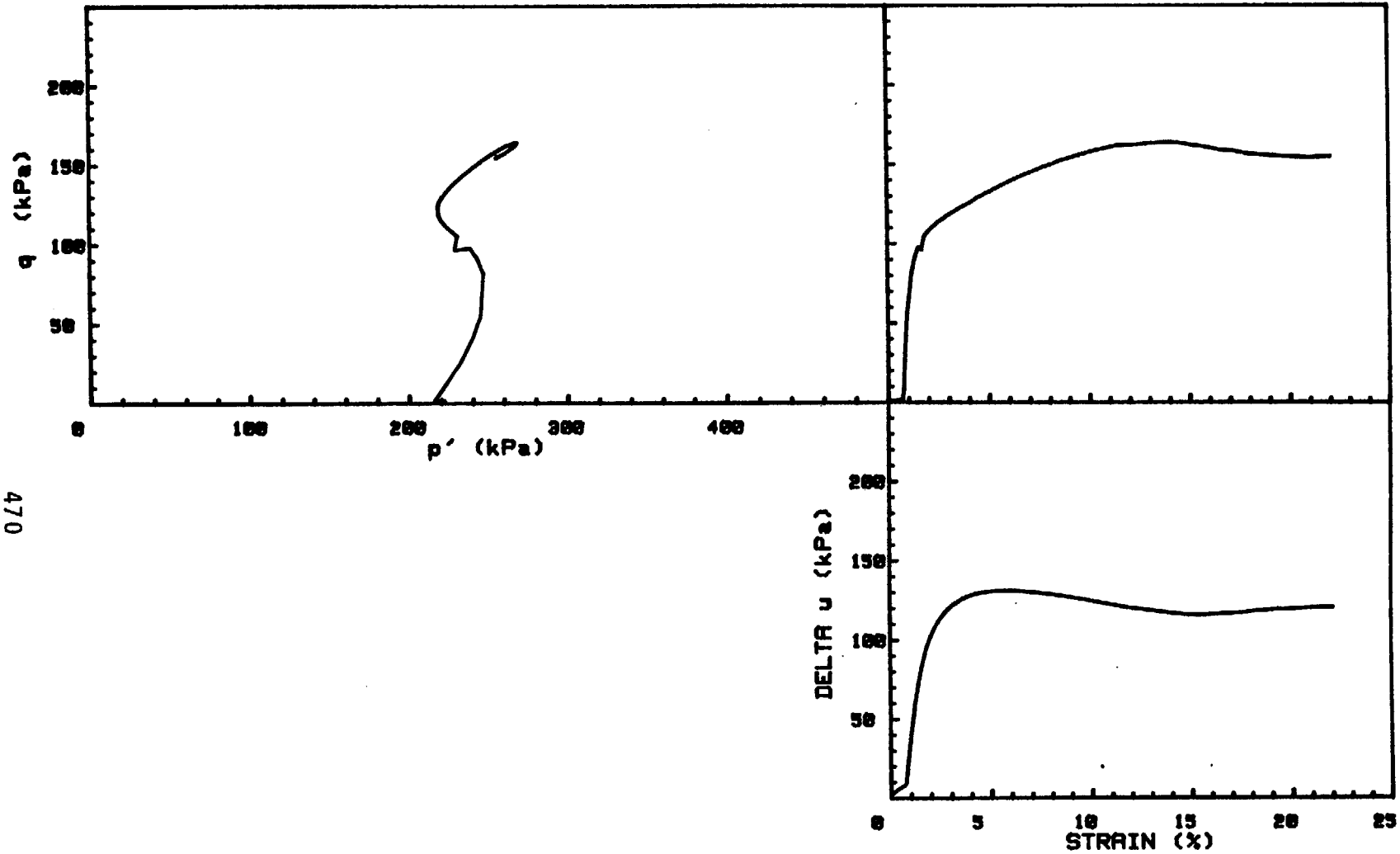
CRUISE DC1-81-EG	INCREMENT (cm)	157-165
CORE NO. 605G2	TEST NO.	TE111
SIG1c' (kPa)	216.1	
SIG3c' (kPa)	216.1	
INDUCED OCR	1.0	

469

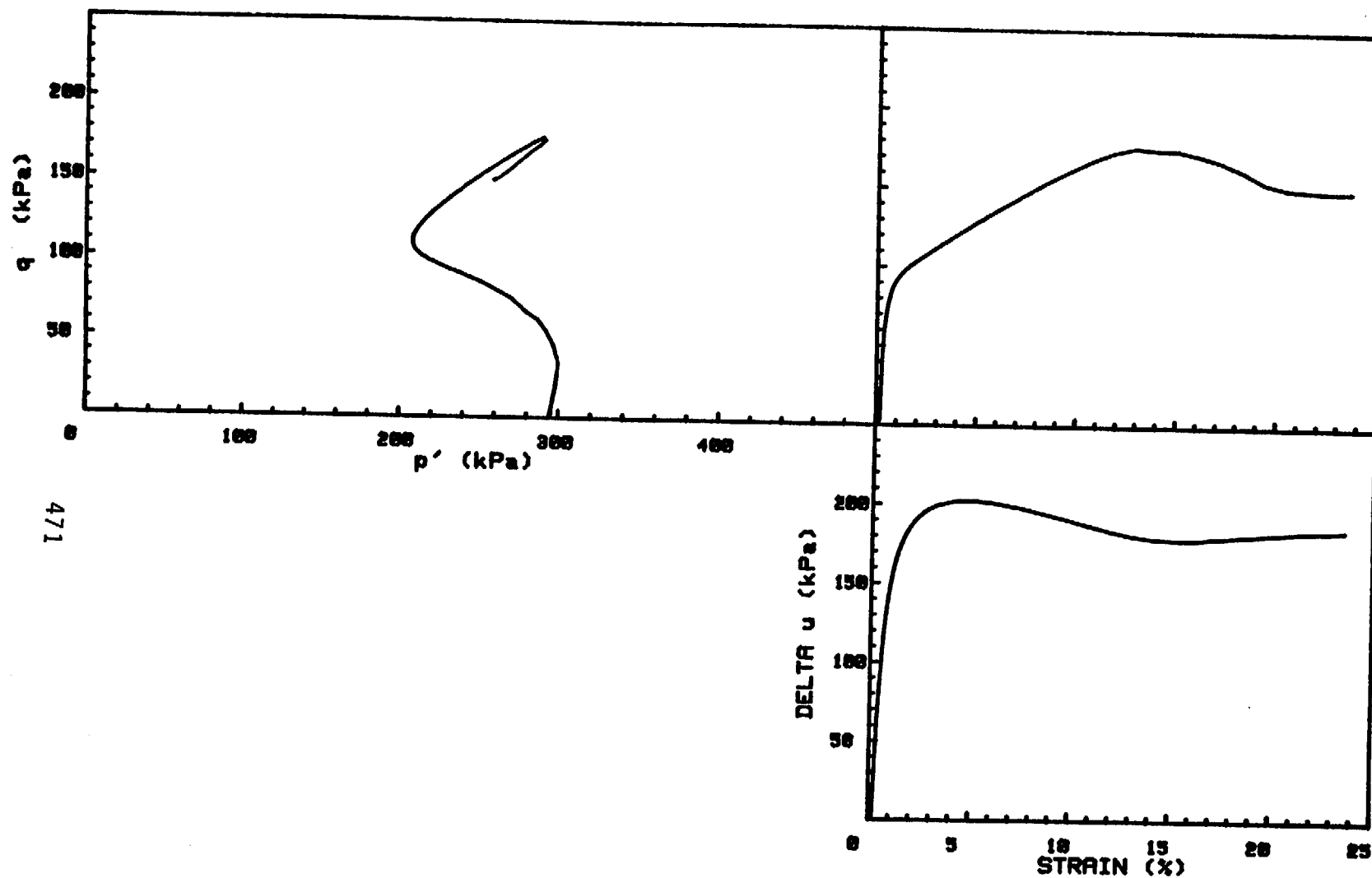


CRUISE DC1-81-EG	INCREMENT (cm)	156-164
CORE NO. 605G2	TEST NO.	TE112
SIG1c' (kPa)	35.3	
SIG3c' (kPa)	35.3	
INDUCED OCR	6.0	

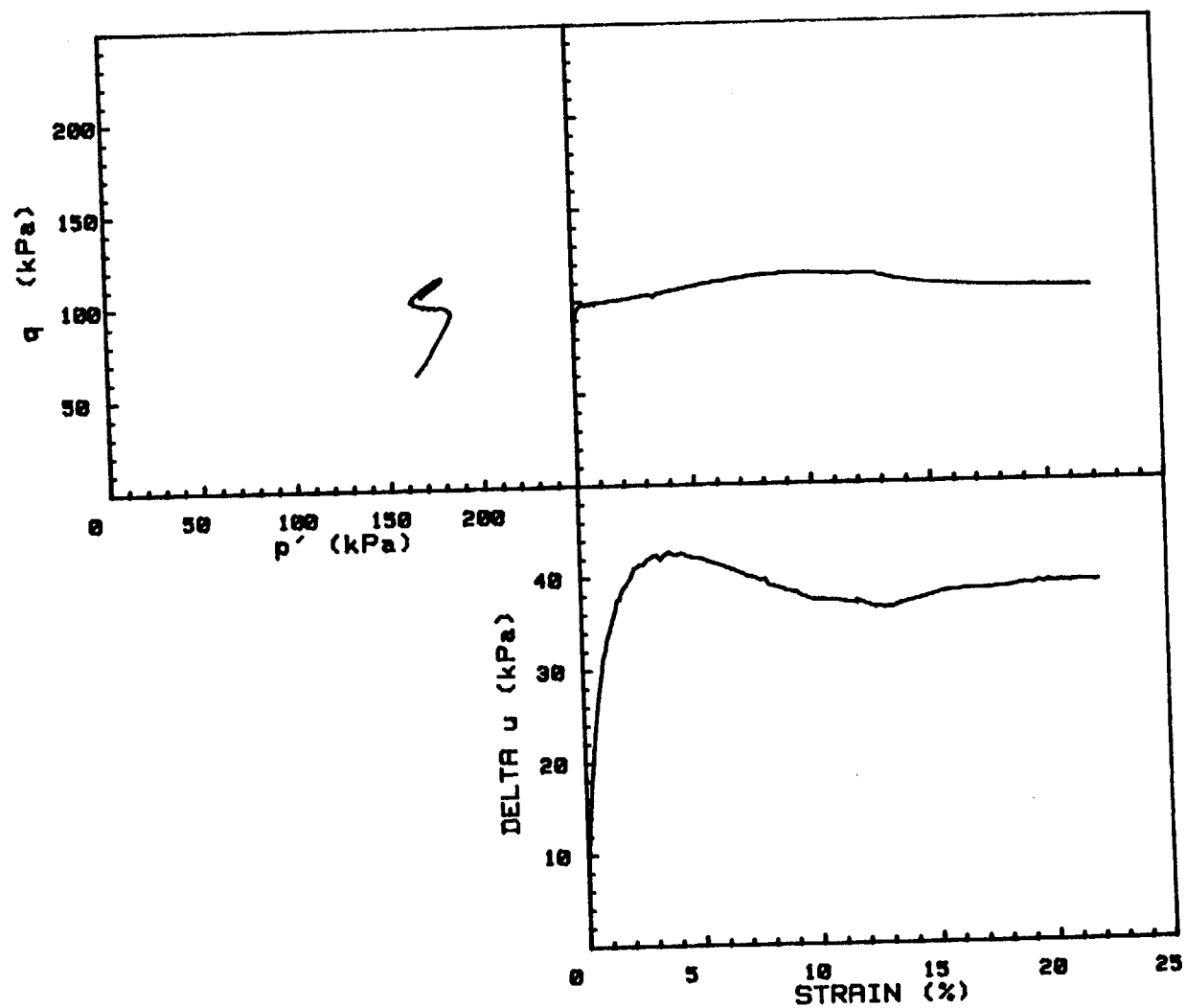
470



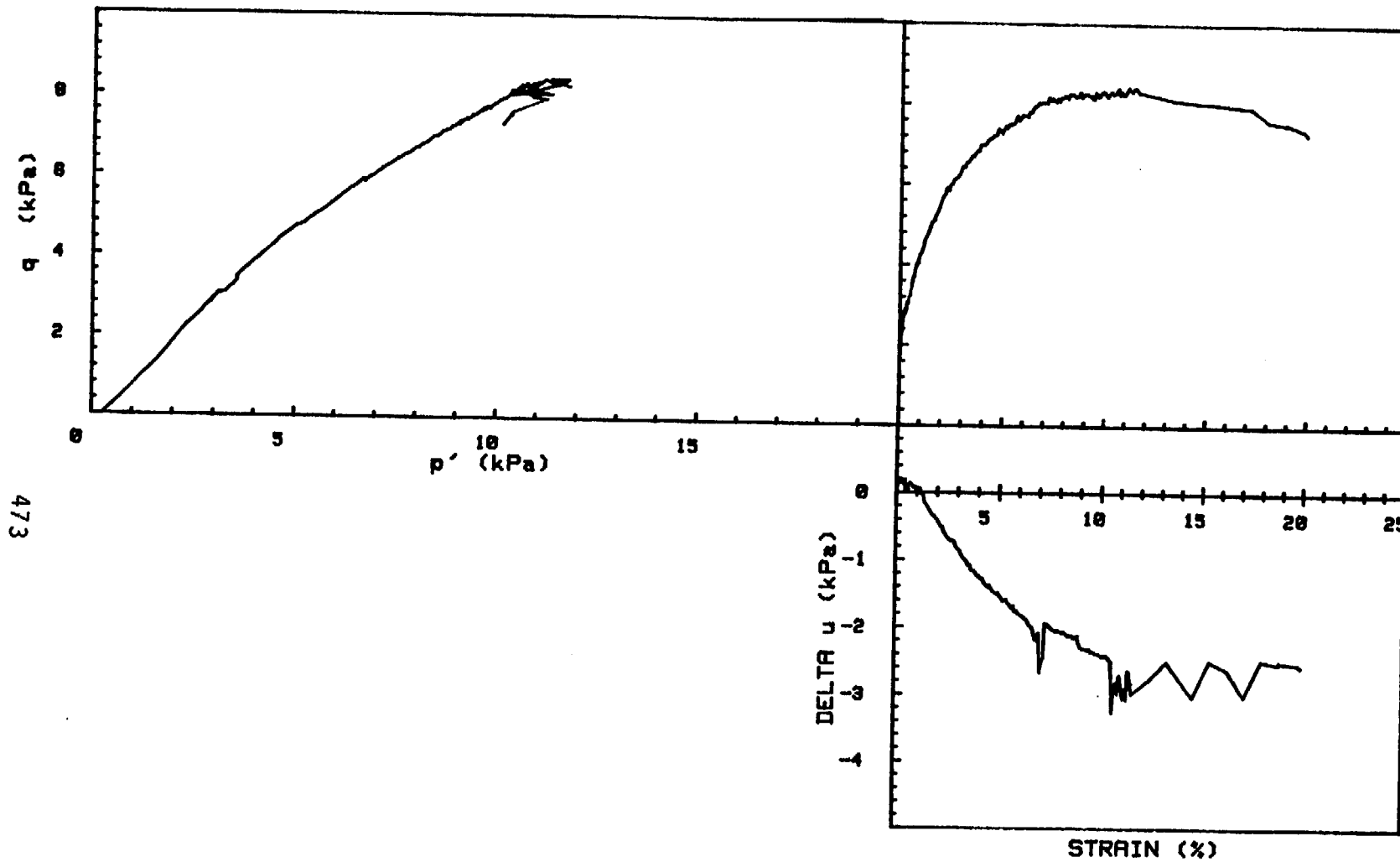
CRUISE DC1-81-EG	INCREMENT (cm)	45-53
CORE NO. 605G2	TEST NO.	TE113
SIG1c' (kPa)	222.2	
SIG3c' (kPa)	222.2	
INDUCED OCR	1.0	



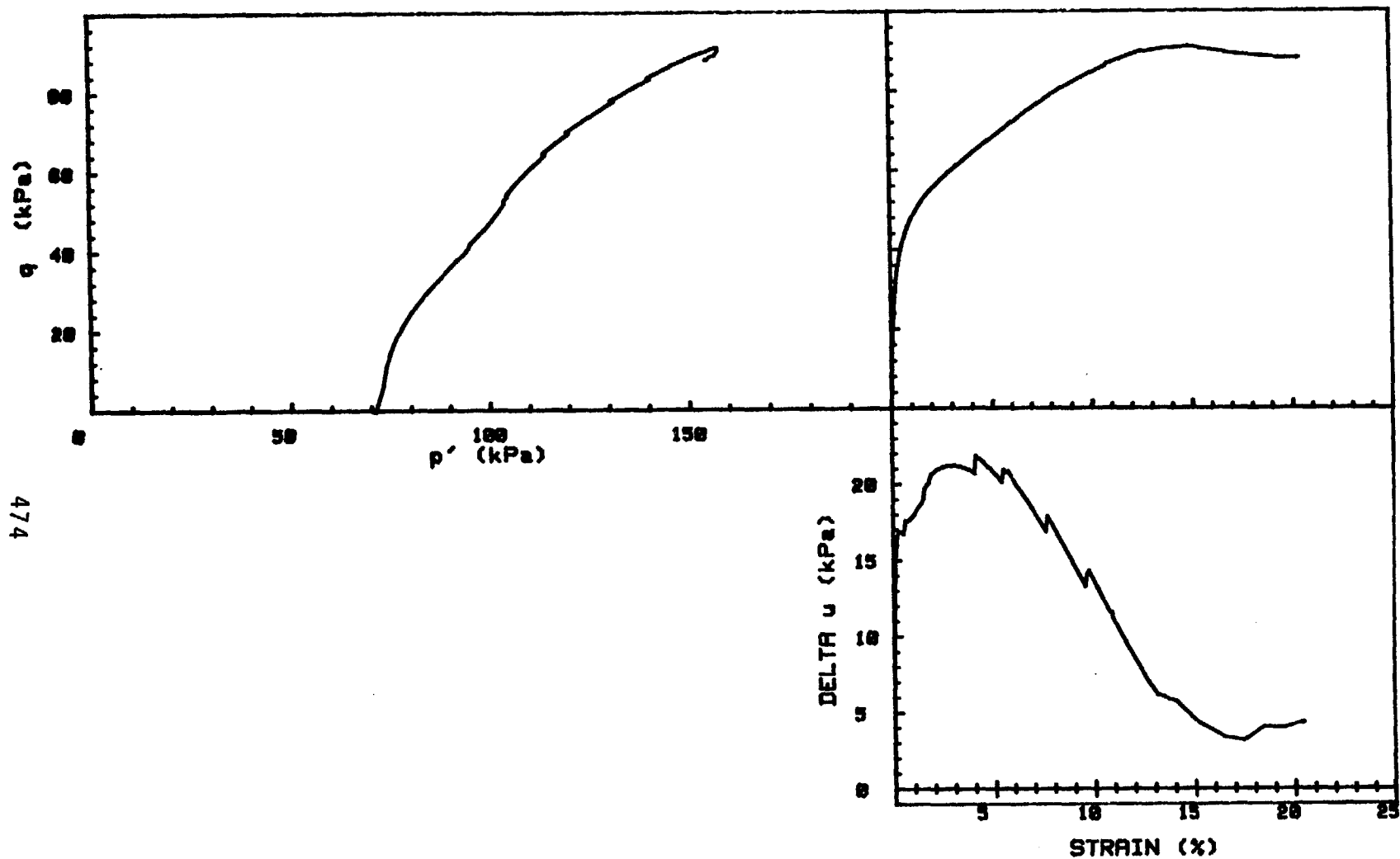
CRUISE DC1-81-EG	INCREMENT (cm)	121-129
CORE NO. 604G3	TEST NO.	TE114
SIG _{1o'} (kPa)	293.4	
SIG _{3o'} (kPa)	293.4	
INDUCED OCR	1.0	



CRUISE DC1-81-EG	INCREMENT (cm)	176-184
CORE NO. 605G2	TEST NO.	TE115
SIG1c' (kPa)	227.9	
SIG3c' (kPa)	102.9	
INDUCED OCR	1.0	

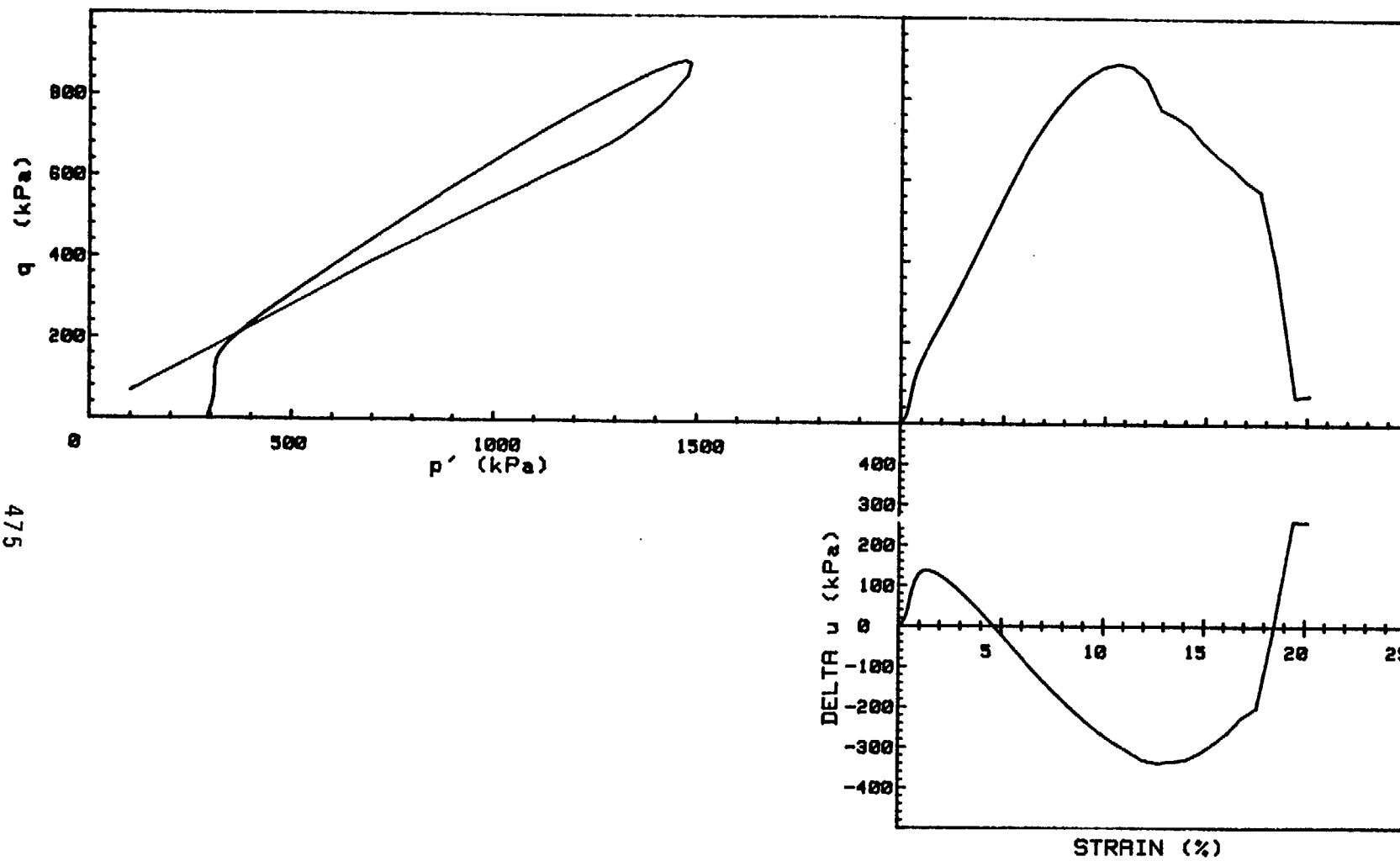


CRUISE DC1-81-EG	INCREMENT (cm)	141-149
CORE NO. 605G2	TEST NO.	TE116
SIG1c' (kPa)	.3	
SIG3c' (kPa)	.3	
INDUCED OCR	1.0	

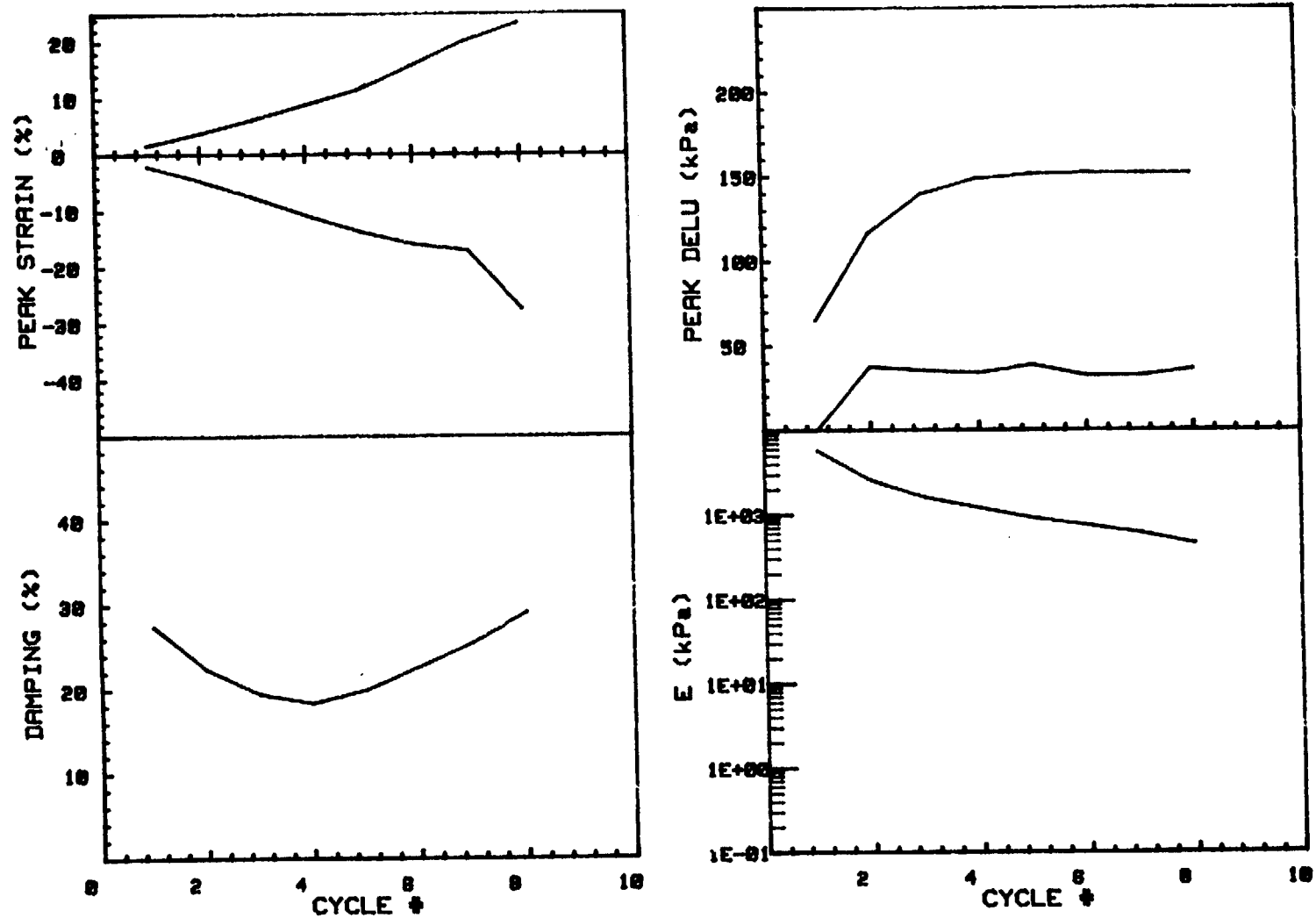


CRUISE DC1-81-EG	INCREMENT (cm)	186-194
CORE NO. 605G2	TEST NO.	TE117
SIG _{1o'} (kPa)	71.3	
SIG _{3o'} (kPa)	71.3	
INDUCED OCR	6.0	

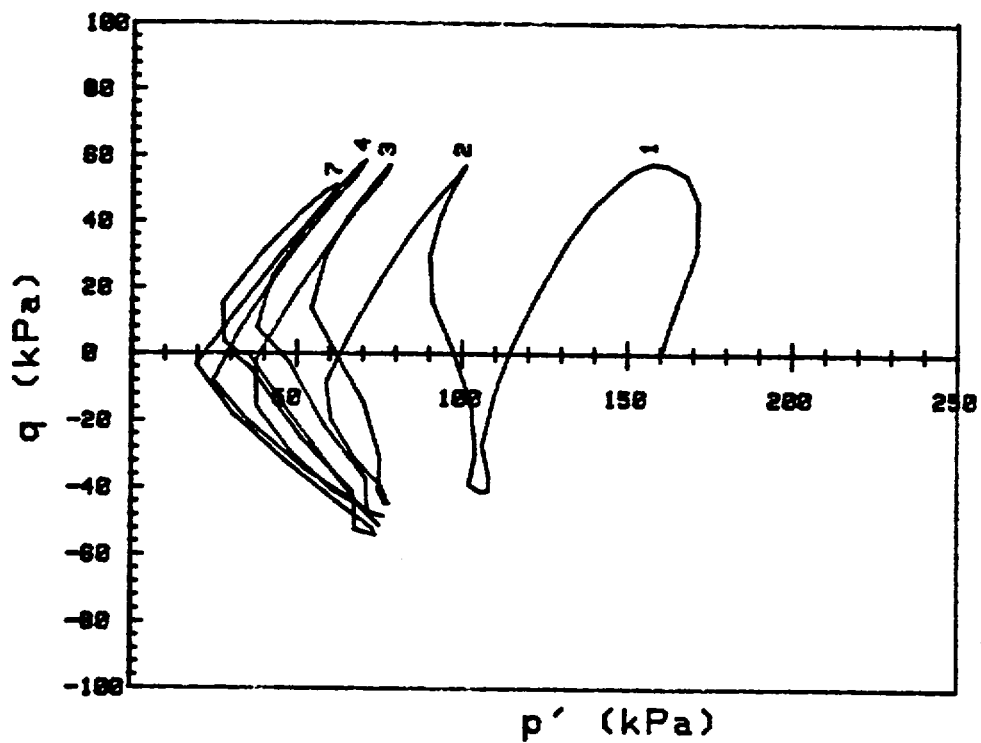
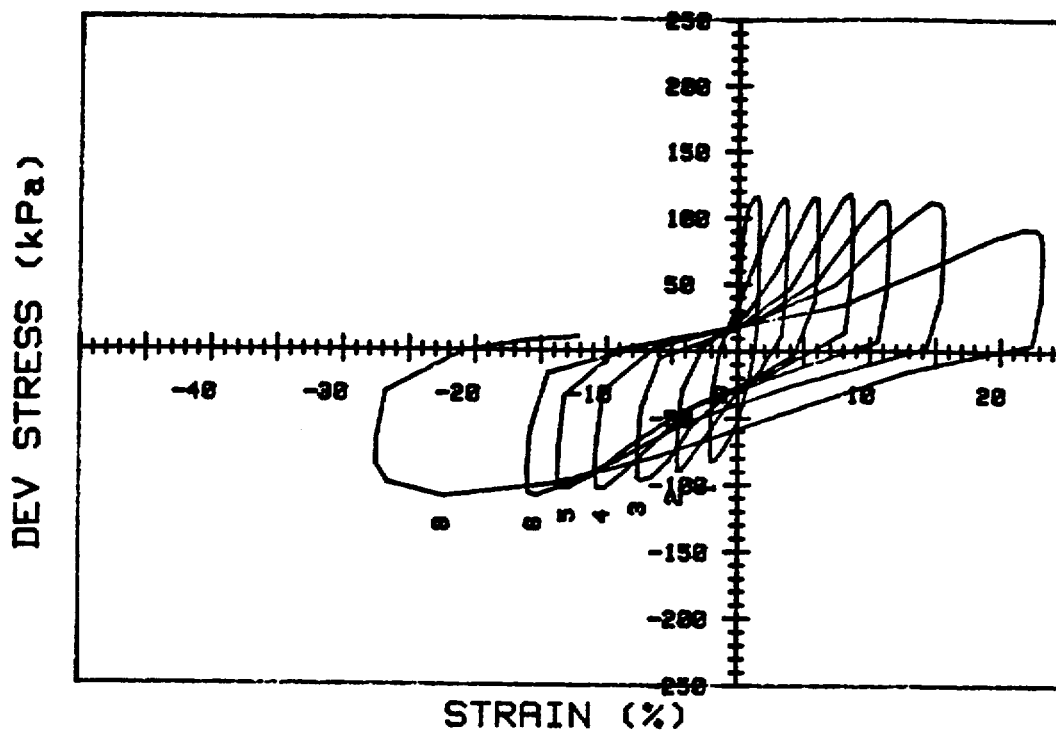
475



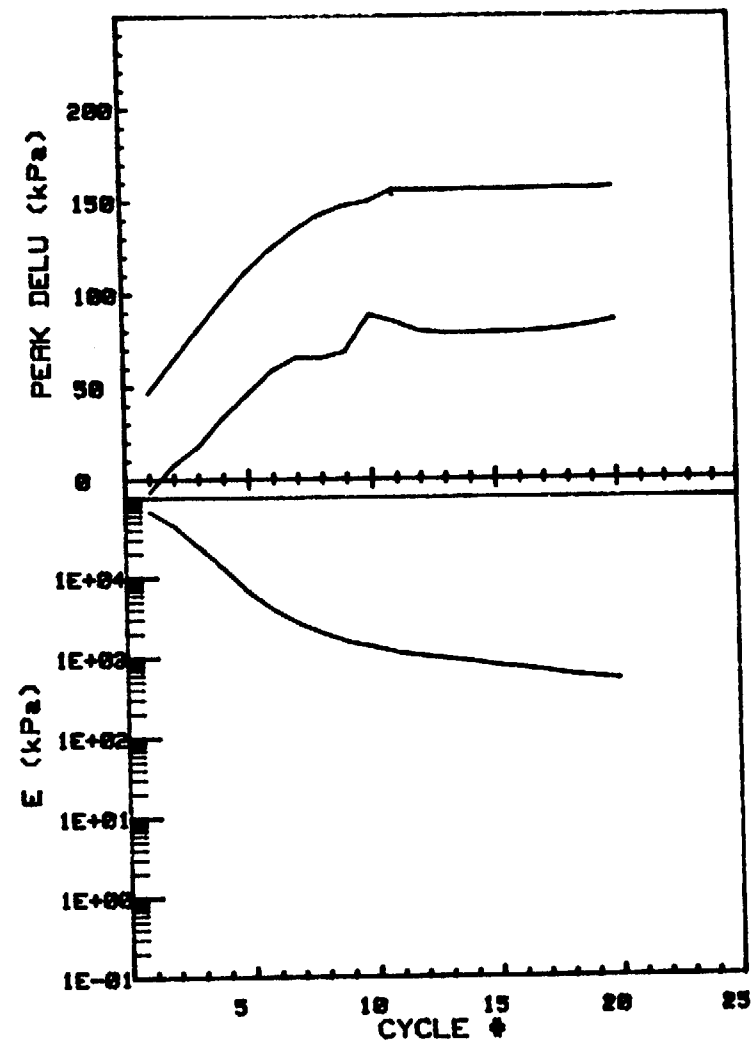
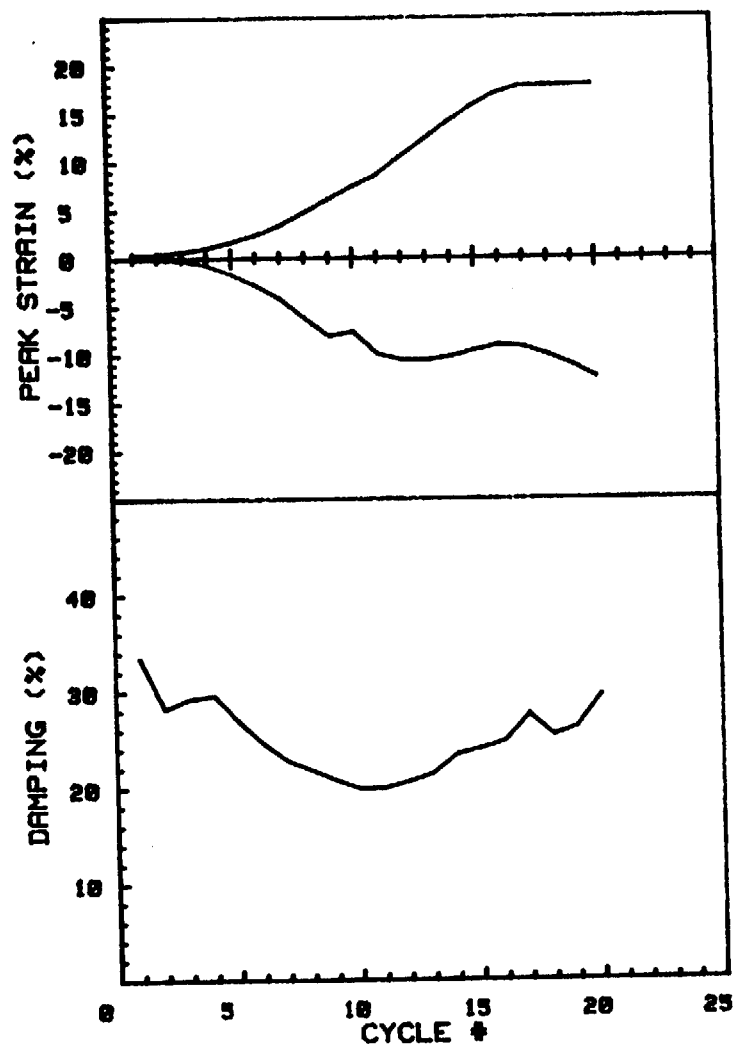
CRUISE DC1-81-EG	INCREMENT (cm)	170-180
CORE NO. 625A1	TEST NO.	TE118
SIG1c'(kPa)	293.3	
SIG3c'(kPa)	293.3	
INDUCED OCR	1.0	



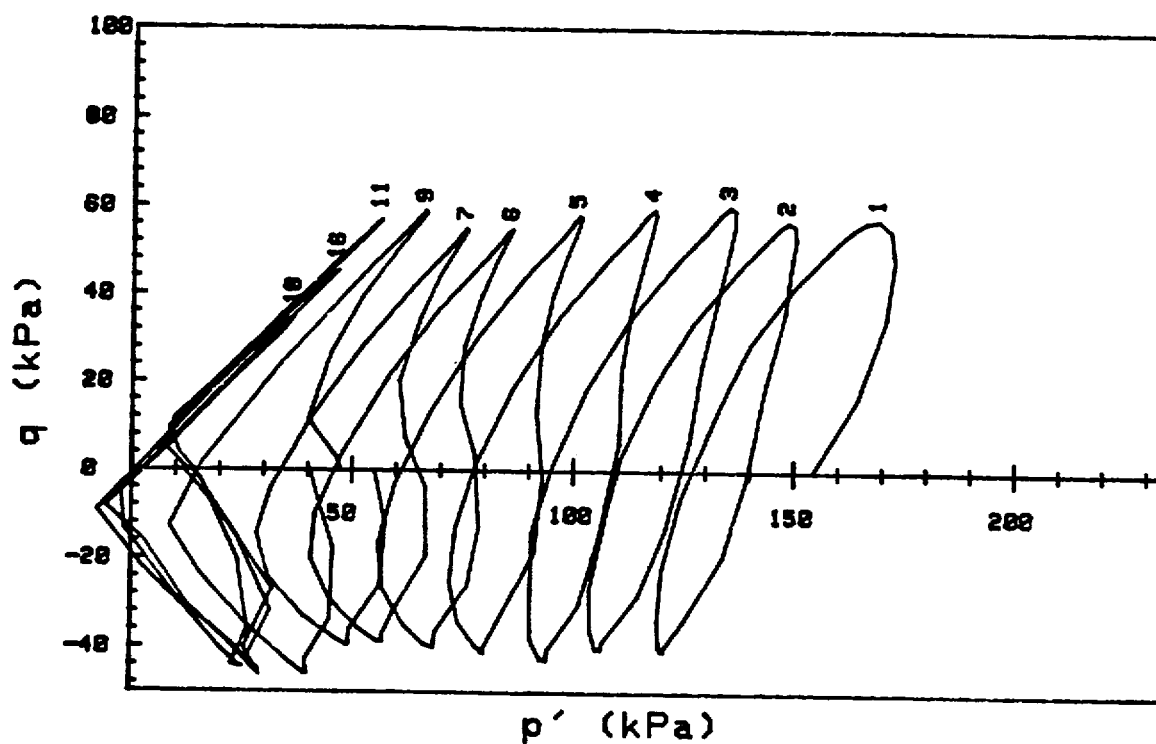
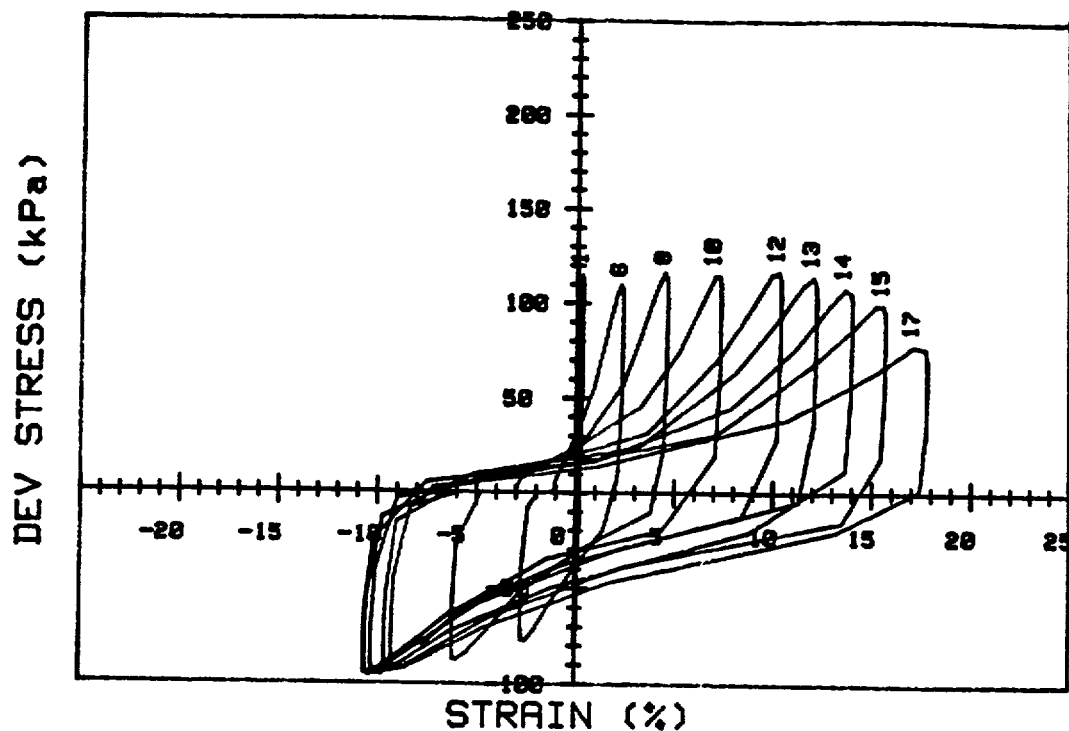
CRUISE DC2-80-EG		INCREMENT (cm)		32-39
CORE NO. 35G		TEST NO.		TC18
SIG1c'(kPa)	160.3	STATIC qf (kPa)	80.8	
SIG3c'(kPa)	160.3	AVG MAX q (kPa)	54.9 (67.9%)	
INDUCED OCR	1.0	AVG MIN q (kPa)	-49.9 (61.8%)	



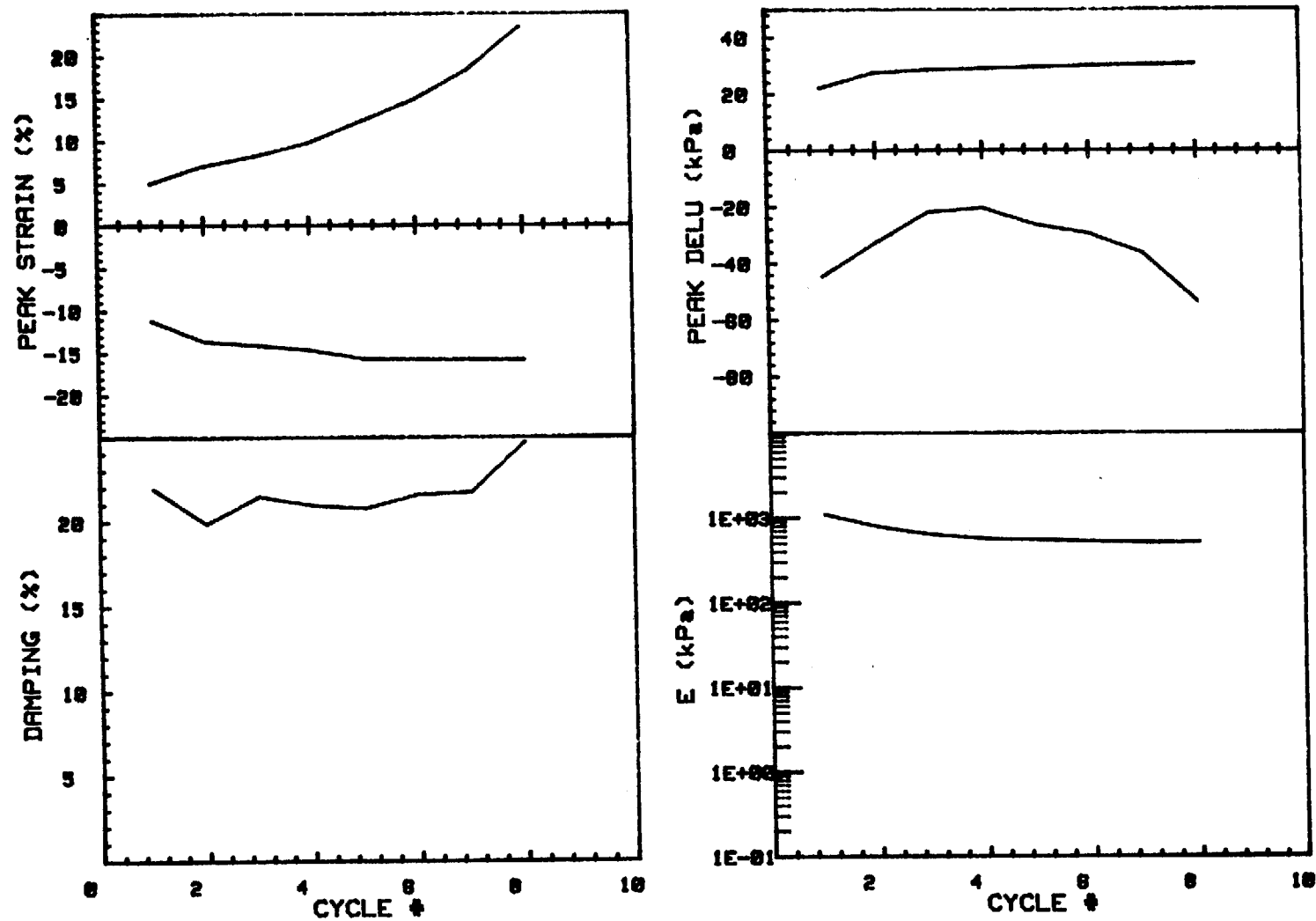
CRUISE DC2-88-EG	INCREMENT (cm)	32-39
CORE NO. 35G	TEST NO.	TC18
SIG1c' (kPa) 160.3	STATIC qf (kPa)	80.8
SIG3c' (kPa) 160.3	AVG MAX q (kPa)	54.9 (67.9%)
INDUCED OCR 1.0	AVG MIN q (kPa)	-49.9 (61.8%)



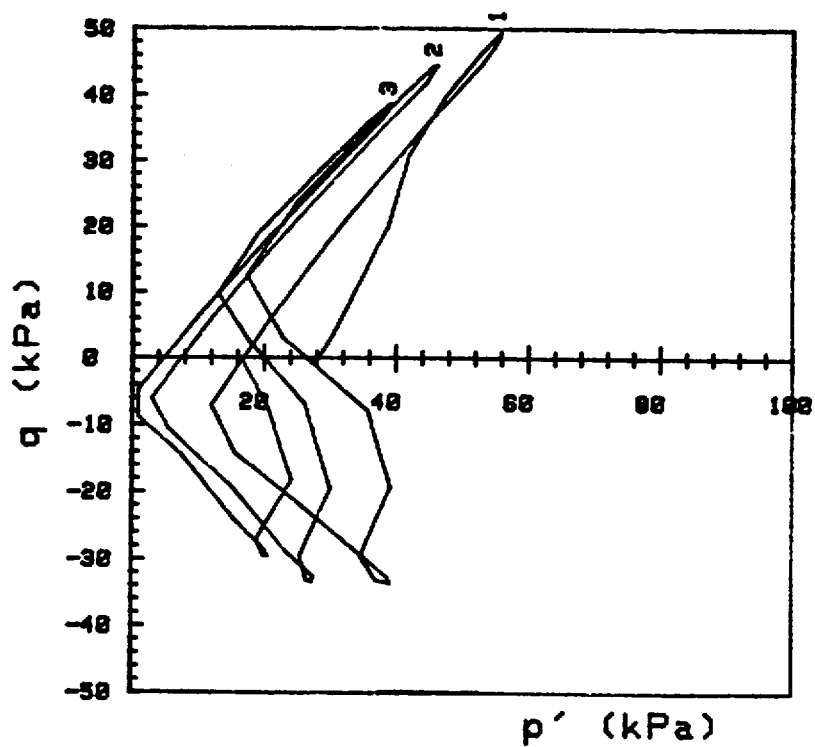
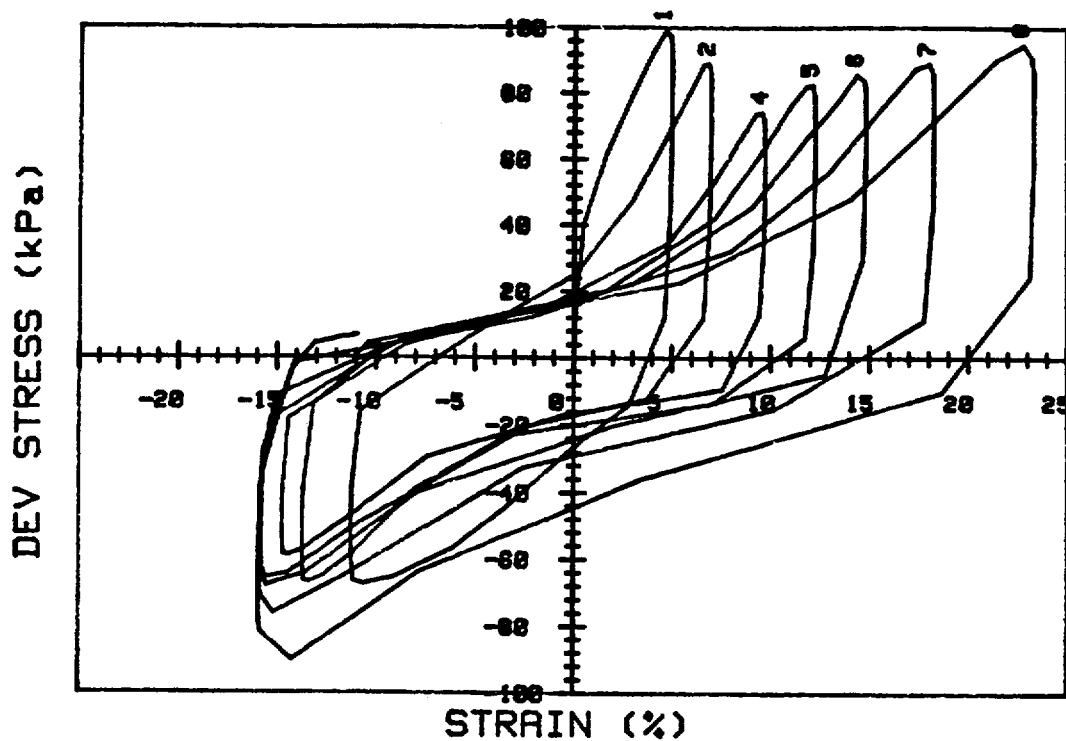
CRUISE DC2-80-EG		INCREMENT (cm)		32-39
CORE NO. 35G		TEST NO.		TC19
SIG1c' (kPa)	154.6	STATIC qf (kPa)	80.8	
SIG3c' (kPa)	154.6	AVG MAX q (kPa)	51.6 (63.9%)	
INDUCED OCR	1.0	AVG MIN q (kPa)	-43.5 (53.8%)	



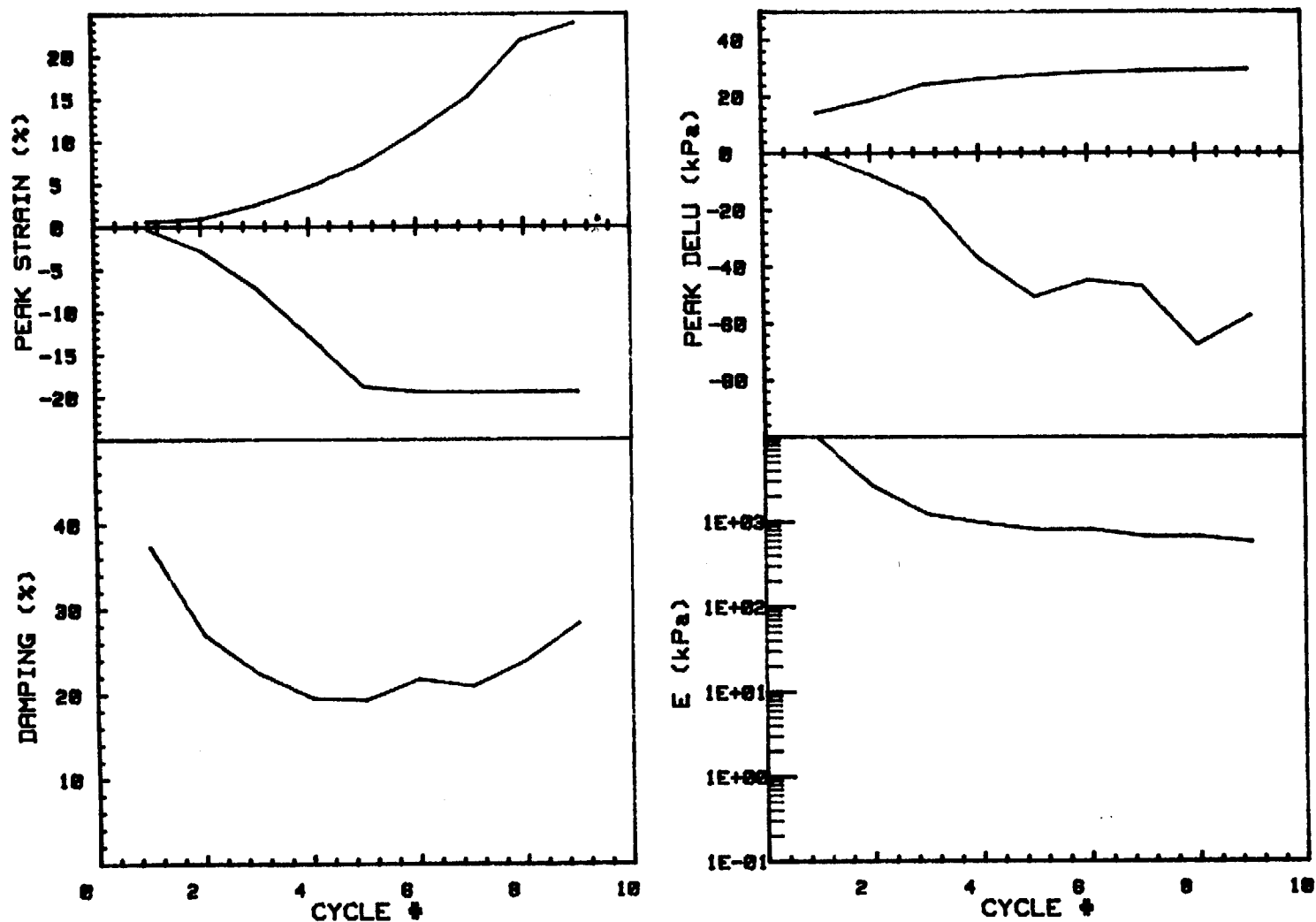
CRUISE DC2-80-EG	INCREMENT (cm)	32-39	
CORE NO. 35G	TEST NO.	TC19	
SIG1c' (kPa)	154.6	STATIC qf (kPa)	80.8
SIG3c' (kPa)	154.6	AVG MAX q (kPa)	51.6 (63.9%)
INDUCED OCR	1.0	AVG MIN q (kPa)	-43.5 (53.8%)



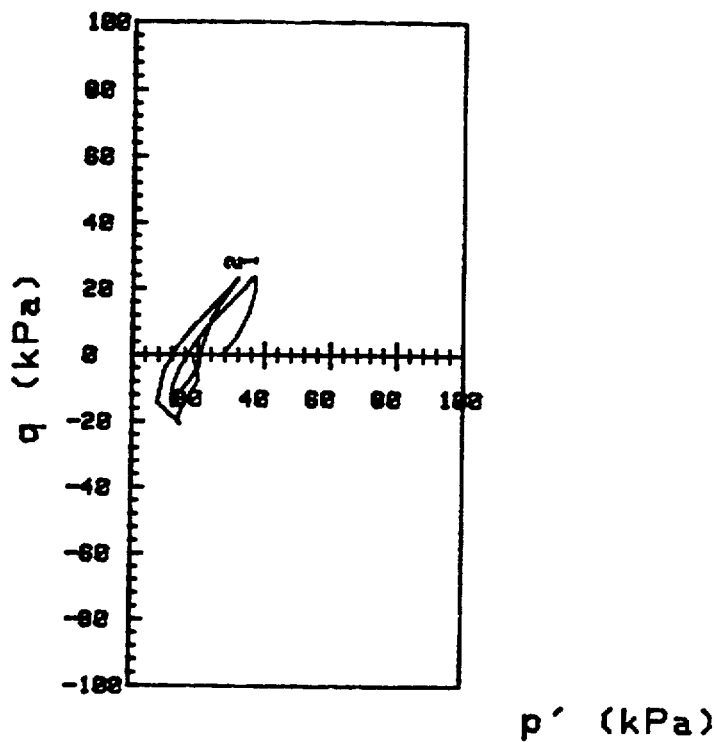
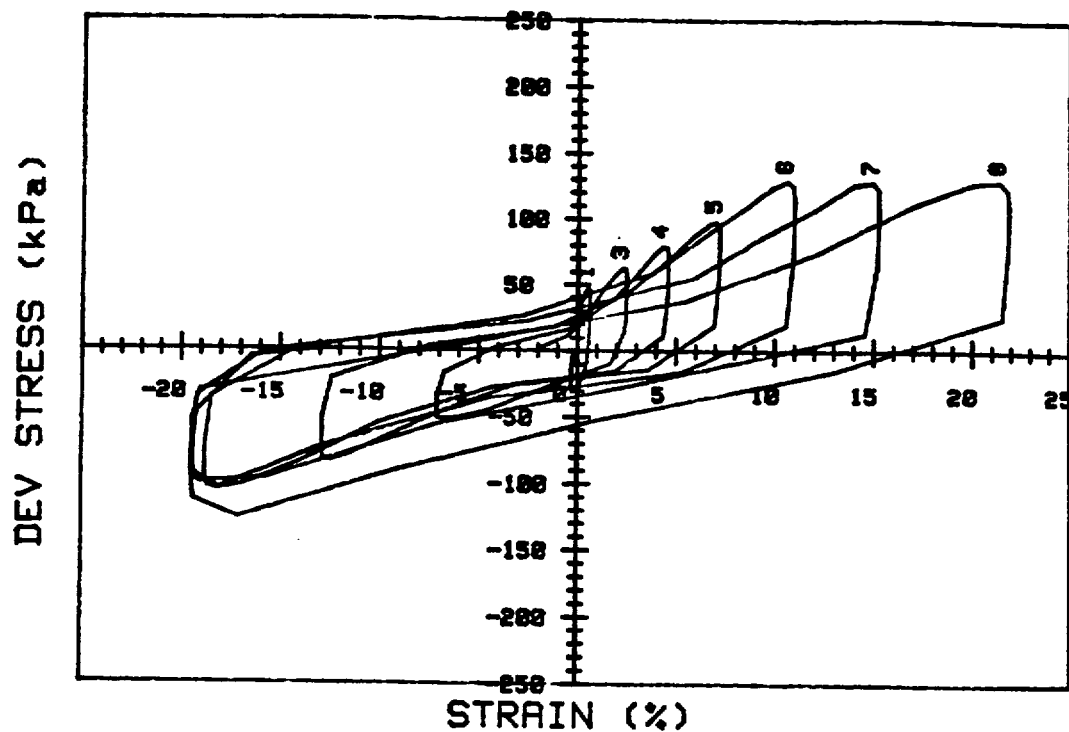
CRUISE DC2-80-EG	INCREMENT (cm)	27-35
CORE NO. 43G	TEST NO.	TC20
SIG1c' (kPa) 28.3	STATIC qf (kPa)	73.9
SIG3c' (kPa) 28.3	AVG MAX q (kPa)	43.2 (58.5%)
INDUCED OCR 1.0	AVG MIN q (kPa)	-34.5 (46.7%)



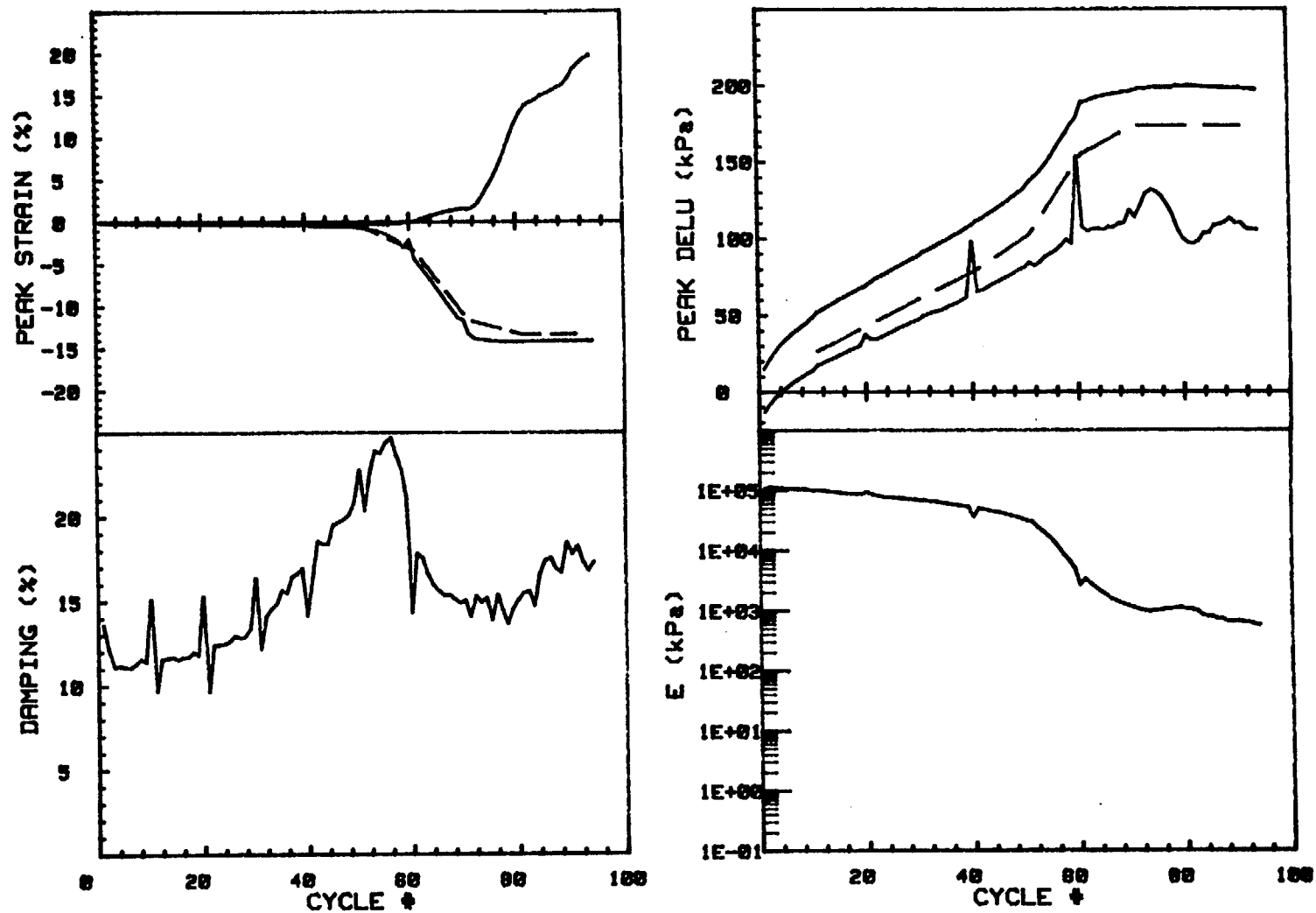
CRUISE DC2-80-EG		INCREMENT (cm)		27-35
CORE NO. 43G		TEST NO.		TC20
SIG1c' (kPa)	28.3	STATIC qf (kPa)	73.9	
SIG3c' (kPa)	28.3	AVG MAX q (kPa)	43.2 (58.5%)	
INDUCED OCR	1.0	AVG MIN q (kPa)	-34.5 (46.7%)	



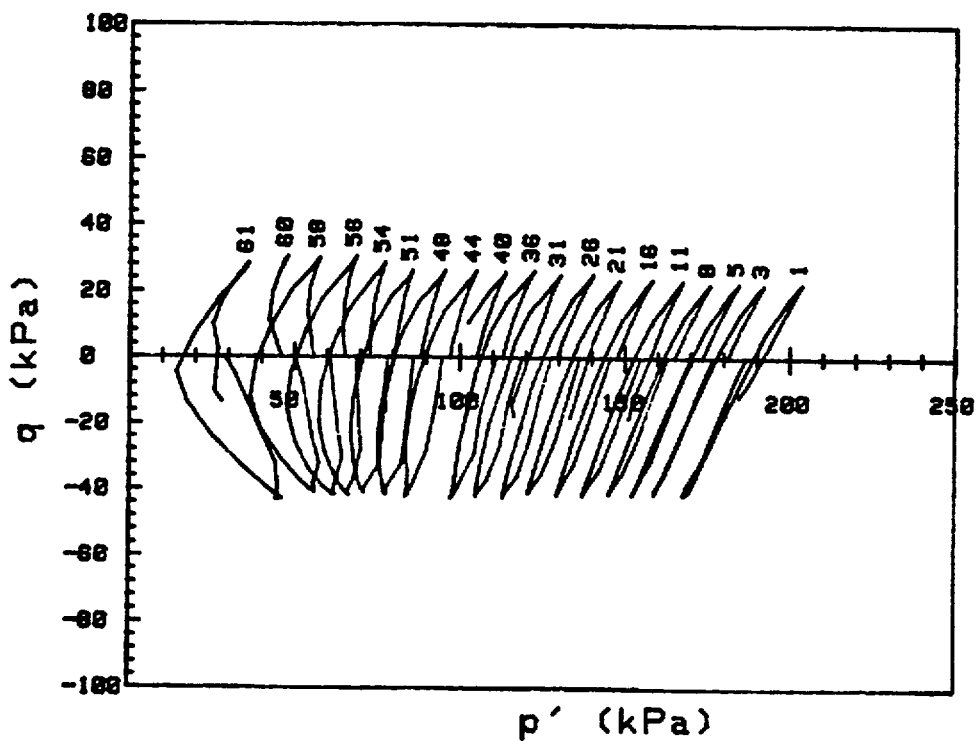
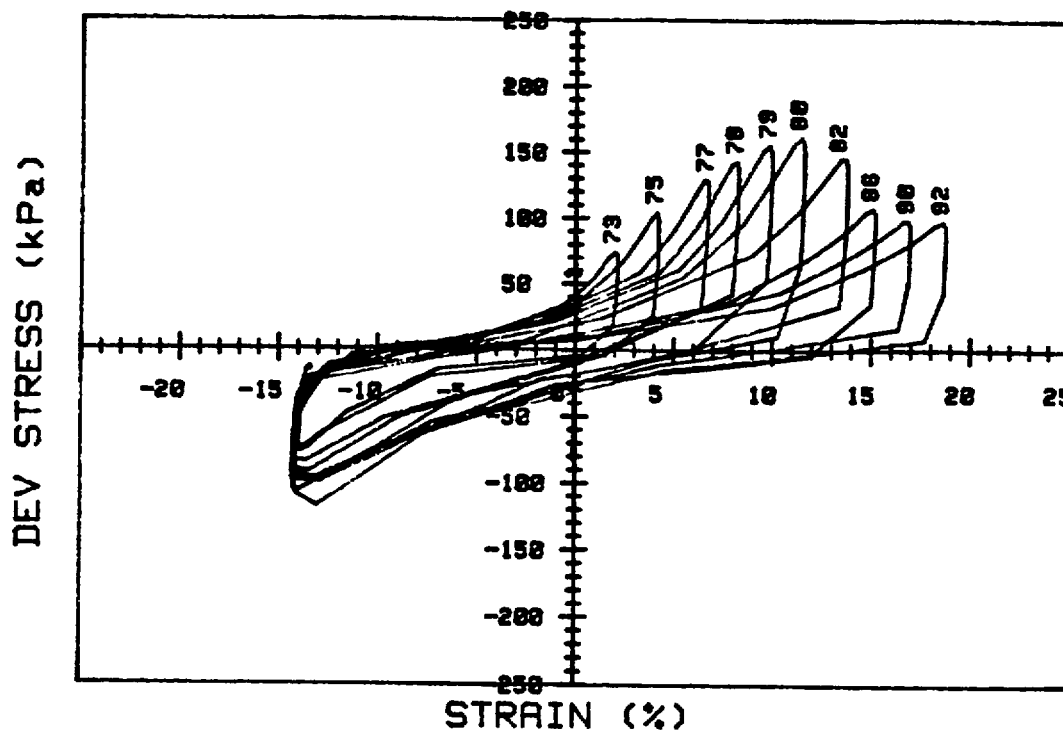
CRUISE DC2-80-EG		INCREMENT (cm) 27-35	
CORE NO. 43G		TEST NO. TC21	
SIG1c' (kPa)	27.2	STATIC qf (kPa)	73.9
SIG3c' (kPa)	27.2	AVG MAX q (kPa)	45.7 (61.8%)
INDUCED OCR	1.0	AVG MIN q (kPa)	-42.0 (56.8%)



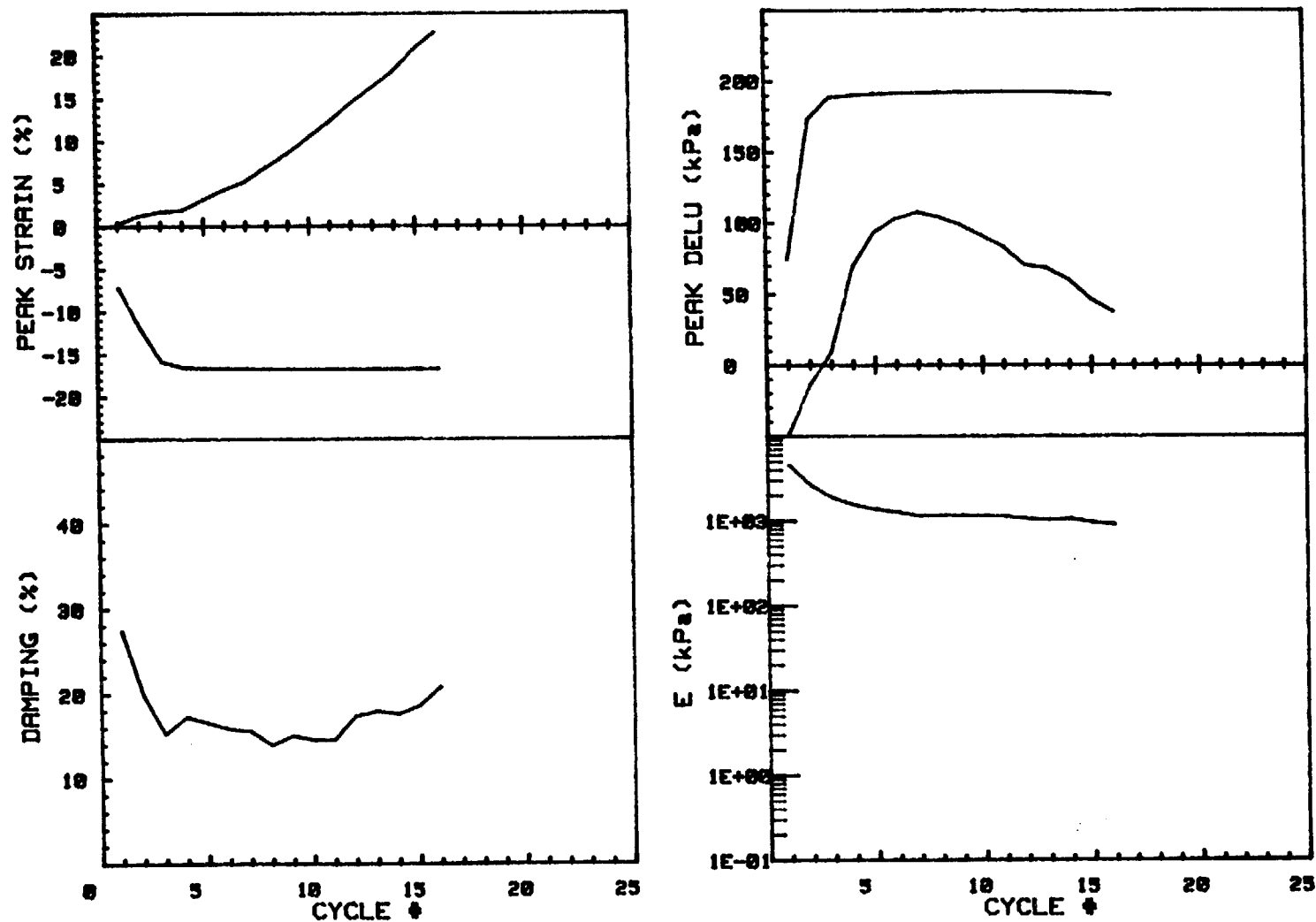
CRUISE DC2-80-EG	INCREMENT (cm)	27-35
CORE NO. 43G	TEST NO.	TC21
SIG1c' (kPa) 27.2	STATIC qf (kPa)	73.9
SIG3c' (kPa) 27.2	AVG MAX q (kPa)	45.7 (61.8%)
INDUCED OCR 1.0	AVG MIN q (kPa)	-42.0 (56.8%)



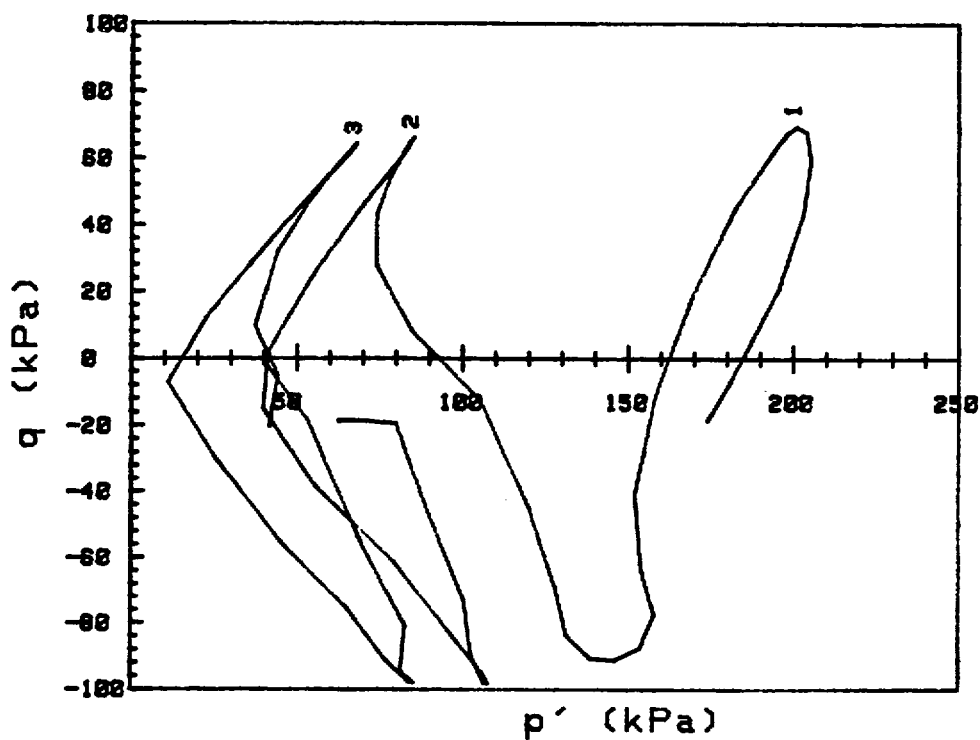
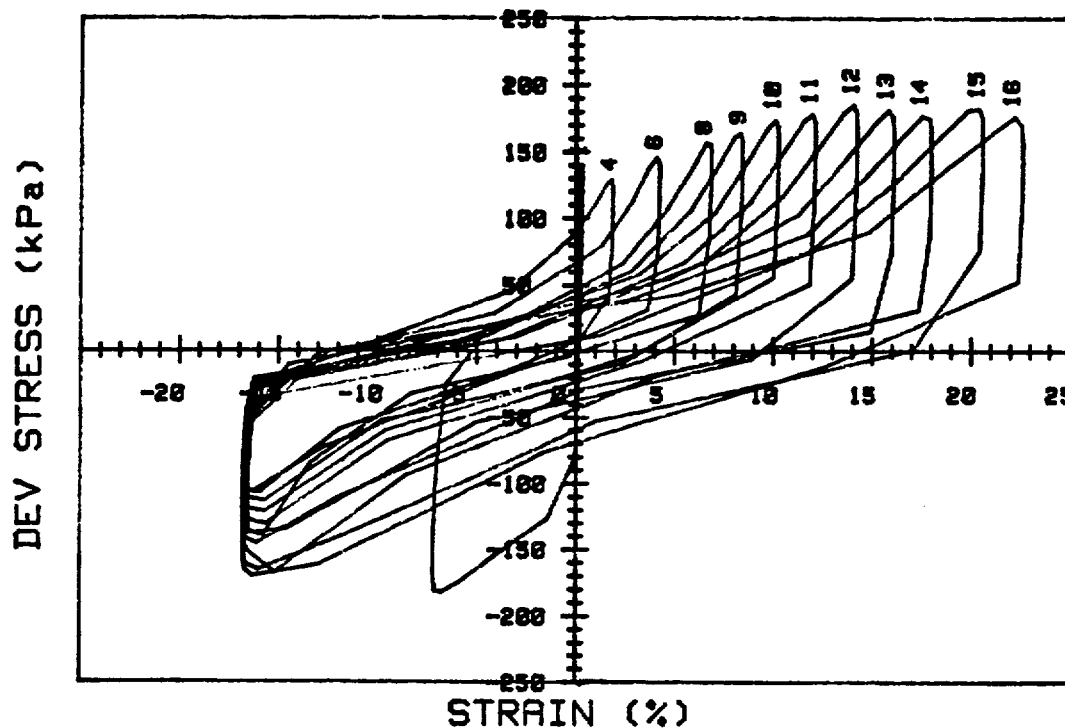
CRUISE DC2-80-EG		INCREMENT (cm) 7-15	
CORE NO. 46G		TEST NO. TC22	
SIG1c' (kPa)	196.2	STATIC qf (kPa)	222.4
SIG3c' (kPa)	196.2	AVG MAX q (kPa)	33.5 (15.1%)
INDUCED OCR	1.0	AVG MIN q (kPa)	-42.4 (19.1%)



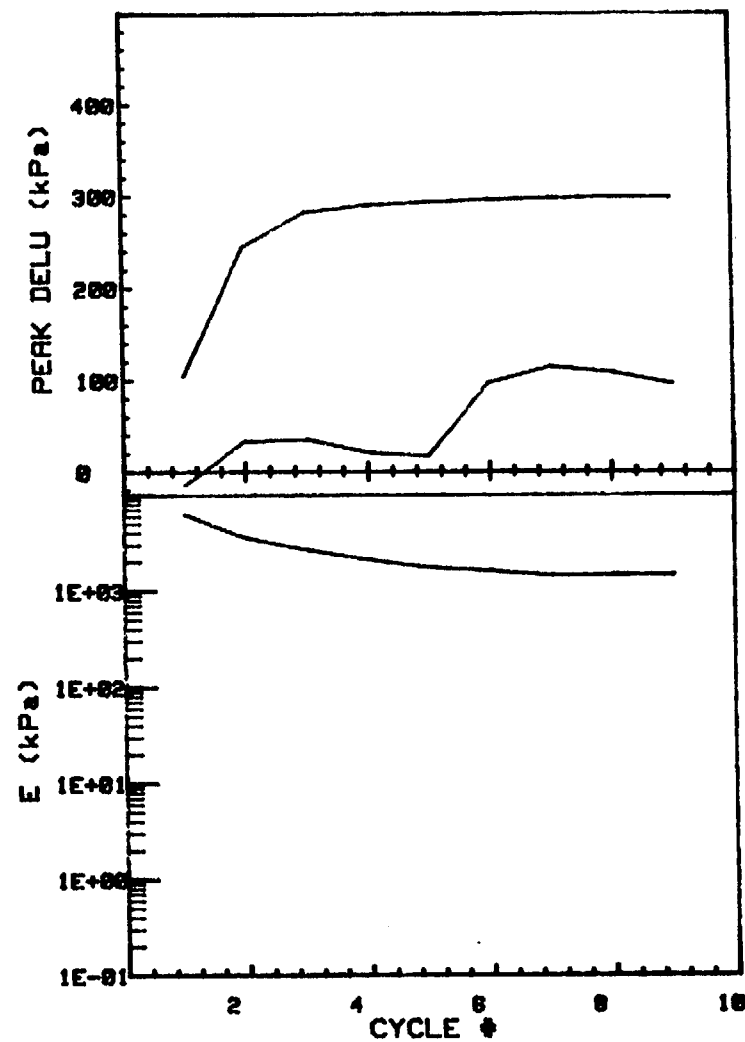
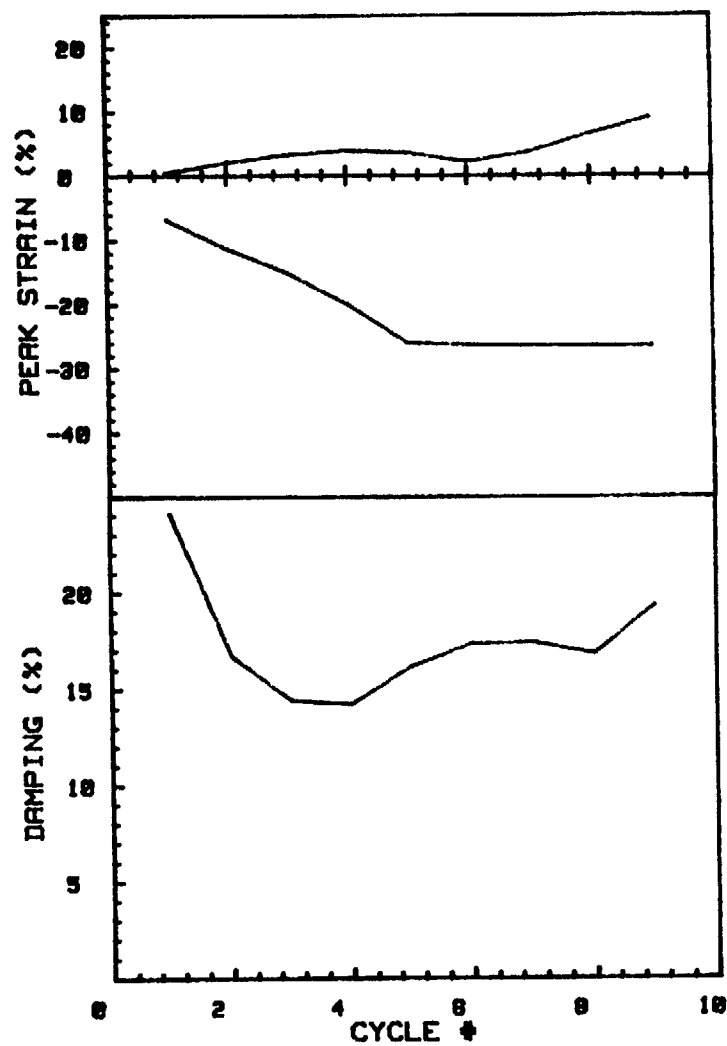
CRUISE DC2-88-EG		INCREMENT (cm)		7-15
CORE NO.	46G	TEST NO.		TC22
SIG1c' (kPa)	196.2	STATIC qf (kPa)	222.4	
SIG3c' (kPa)	196.2	AVG MAX q (kPa)	33.5 (15.1%)	
INDUCED OCR	1.0	AVG MIN q (kPa)	-42.4 (19.1%)	



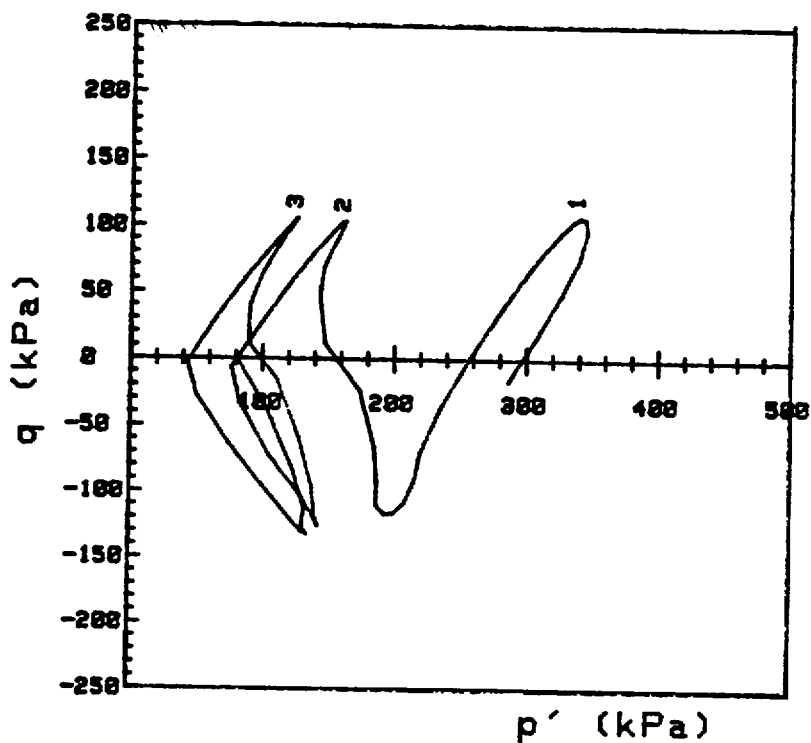
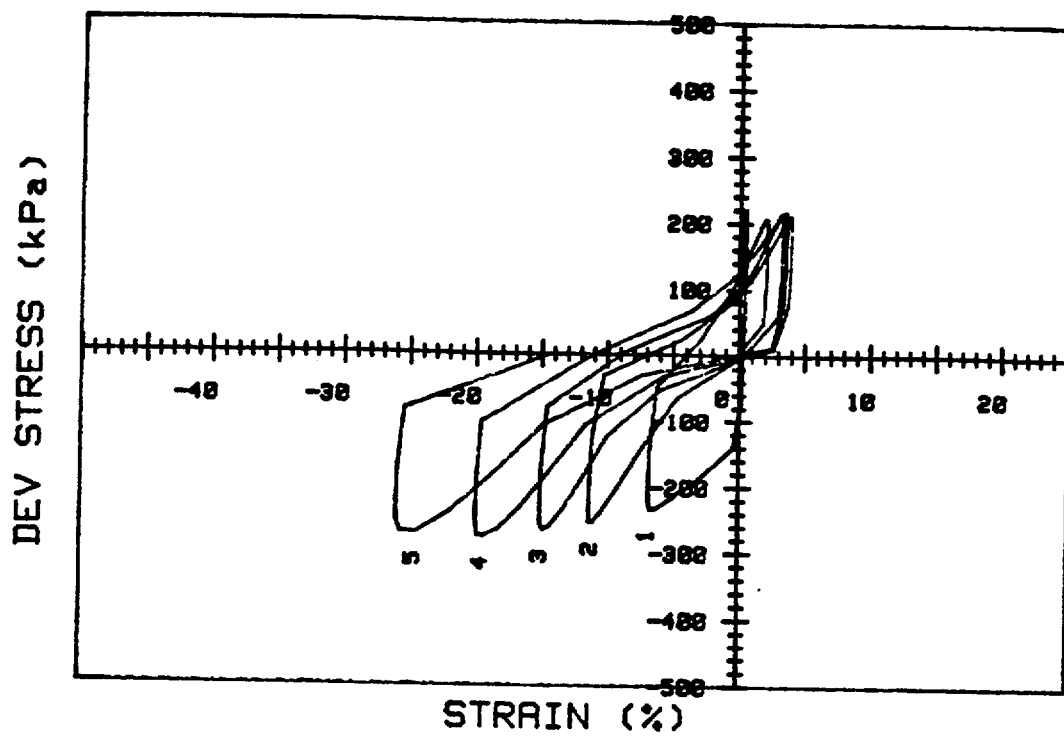
CRUISE DC2-80-EG		INCREMENT (cm)		7-15
CORE NO.	46G	TEST NO.	TC23	
SIG1c' (kPa)	192.6	STATIC qf (kPa)	222.4	
SIG3c' (kPa)	192.6	AVG MAX q (kPa)	79.0 (35.5%)	
INDUCED OCR	1.0	AVG MIN q (kPa)	-71.0 (32.3%)	



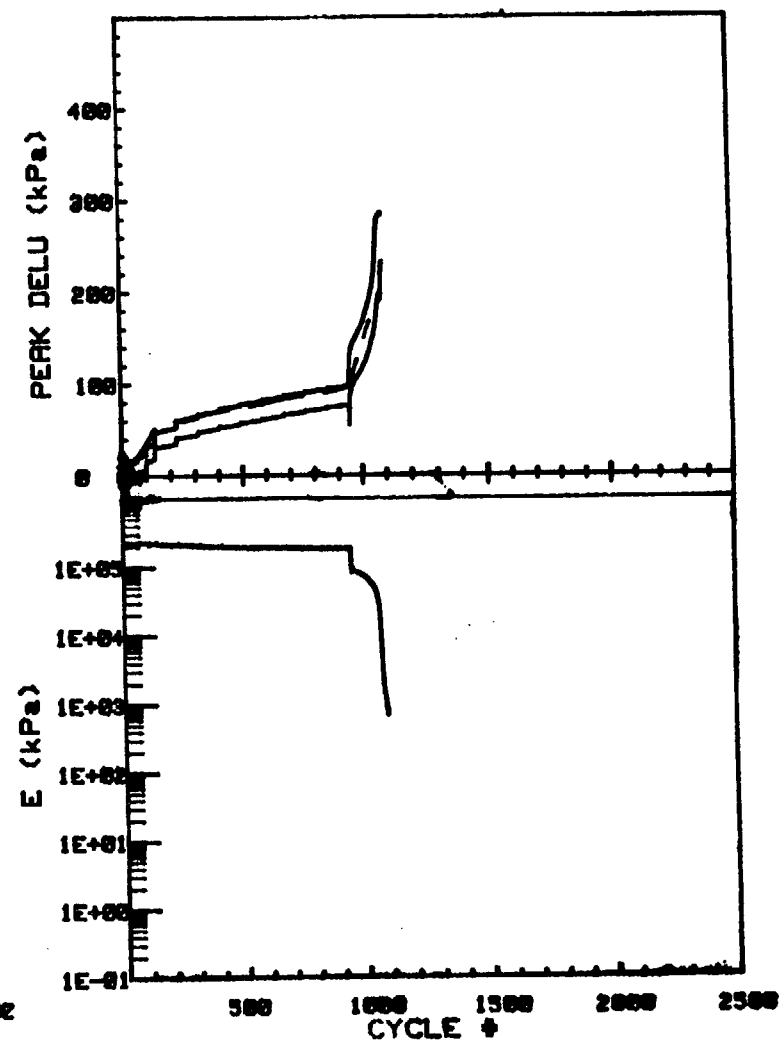
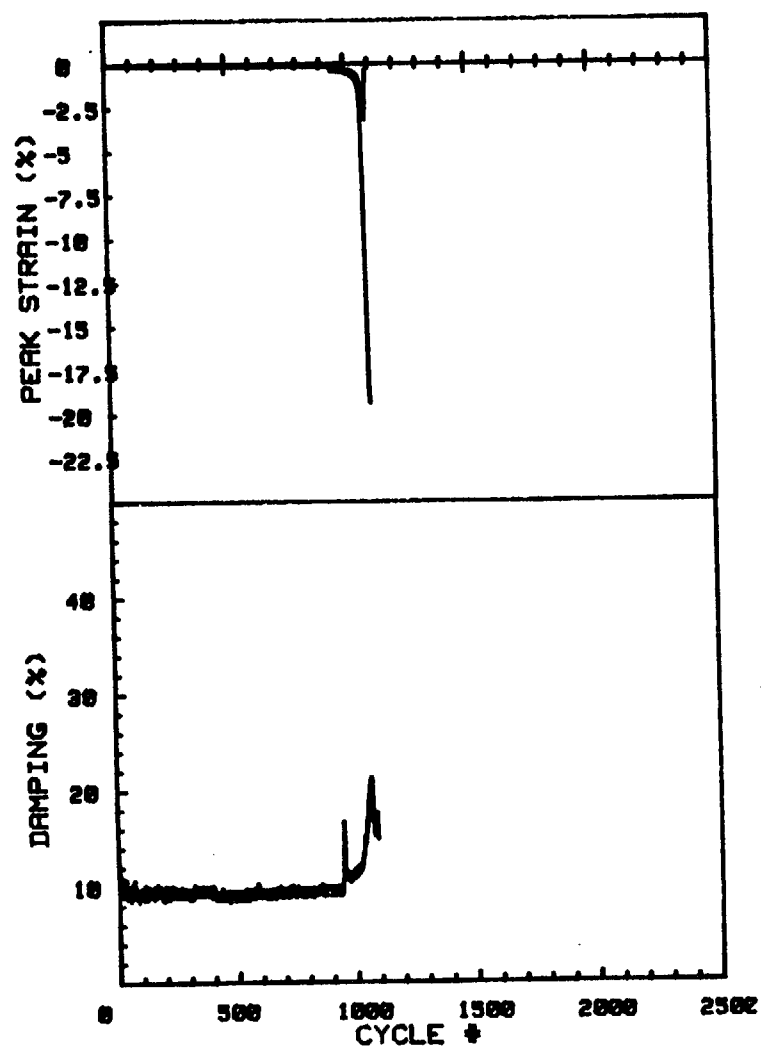
CRUISE DC2-80-EG		INCREMENT (cm)		7-15
CORE NO. 46G		TEST NO.		TC23
SIG1c' (kPa)	192.6	STATIC qf (kPa)	222.4	
SIG3c' (kPa)	192.6	AVG MAX q (kPa)	79.0 (35.5%)	
INDUCED OCR	1.0	AVG MIN q (kPa)	-71.8 (32.3%)	



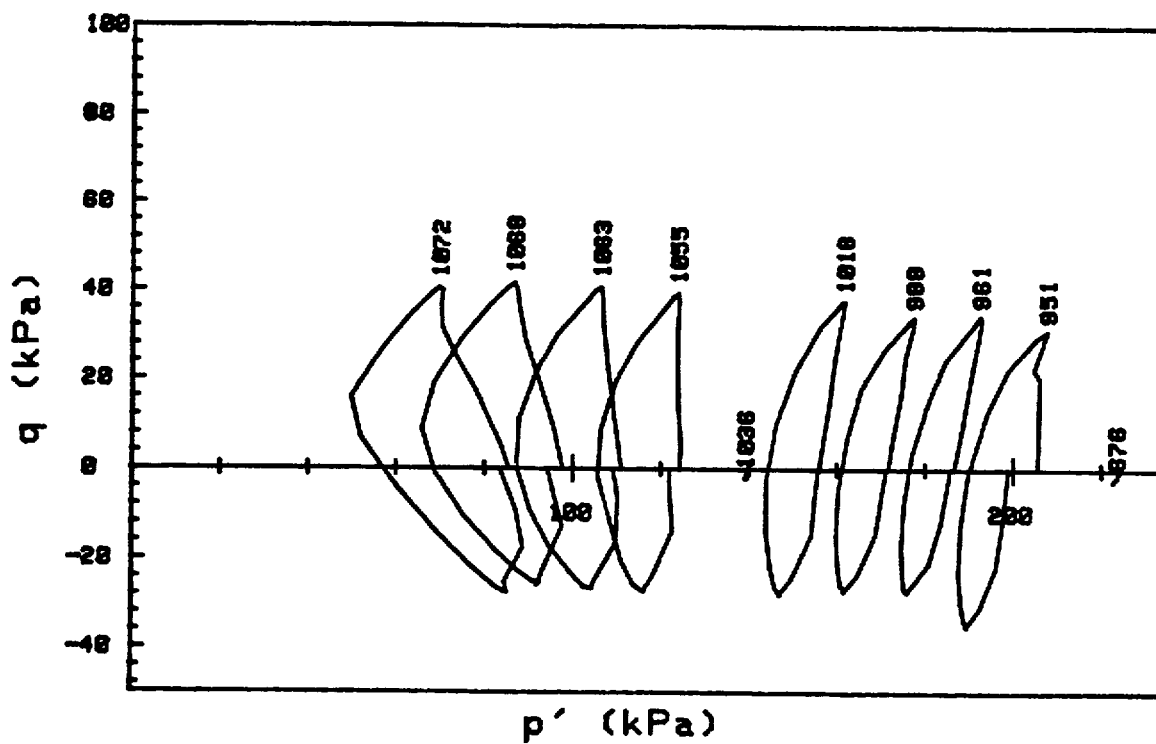
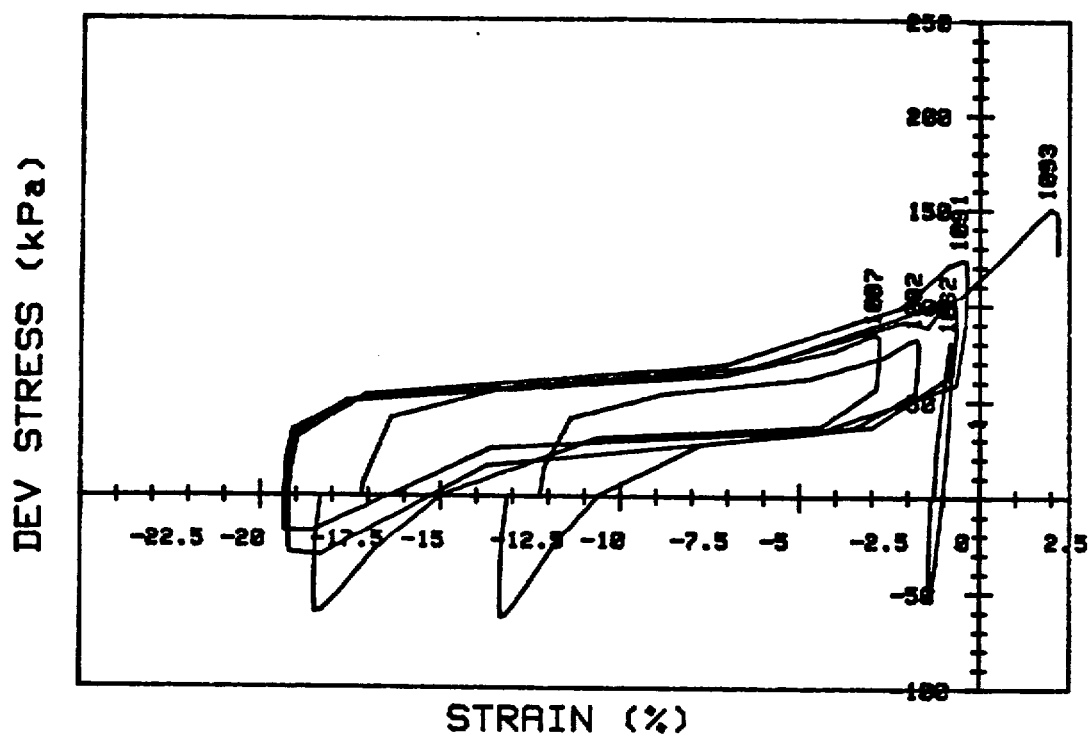
CRUISE DC2-80-EG	INCREMENT (cm)	15-22
CORE NO. 28G	TEST NO.	TC24
SIG1c' (kPa) 302.6	STATIC qf (kPa)	268.9
SIG3c' (kPa) 302.6	AVG MAX q (kPa)	115.6 (43.0%)
INDUCED OCR 1.0	AVG MIN q (kPa)	-100.5 (37.4%)



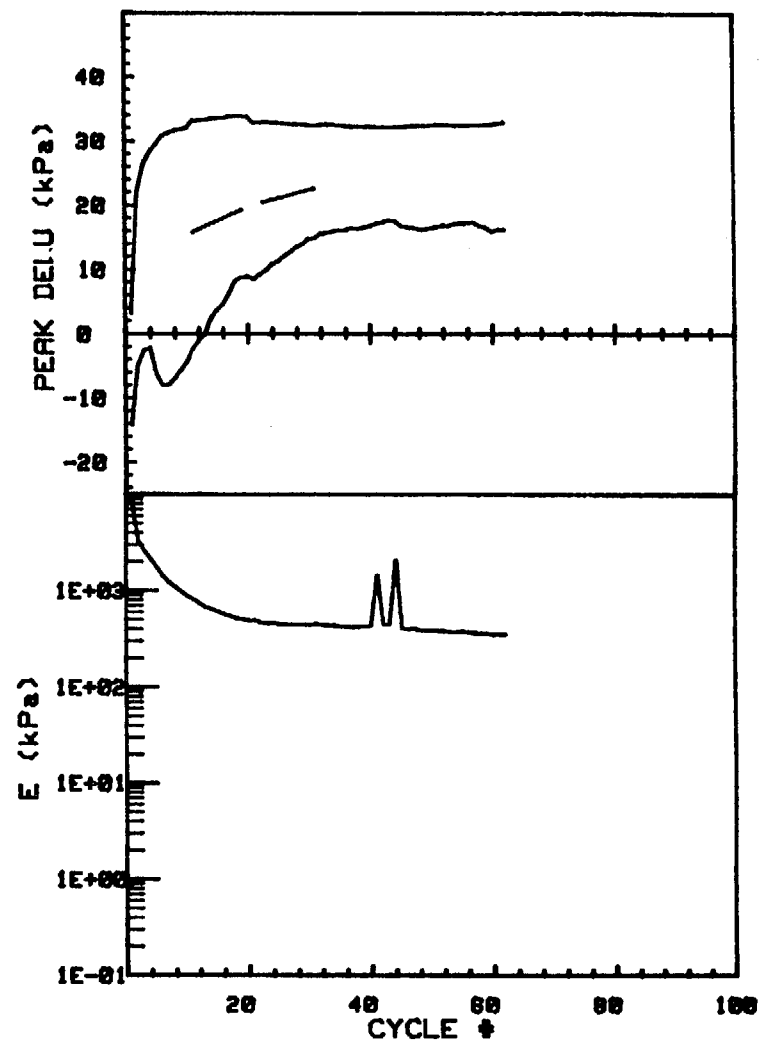
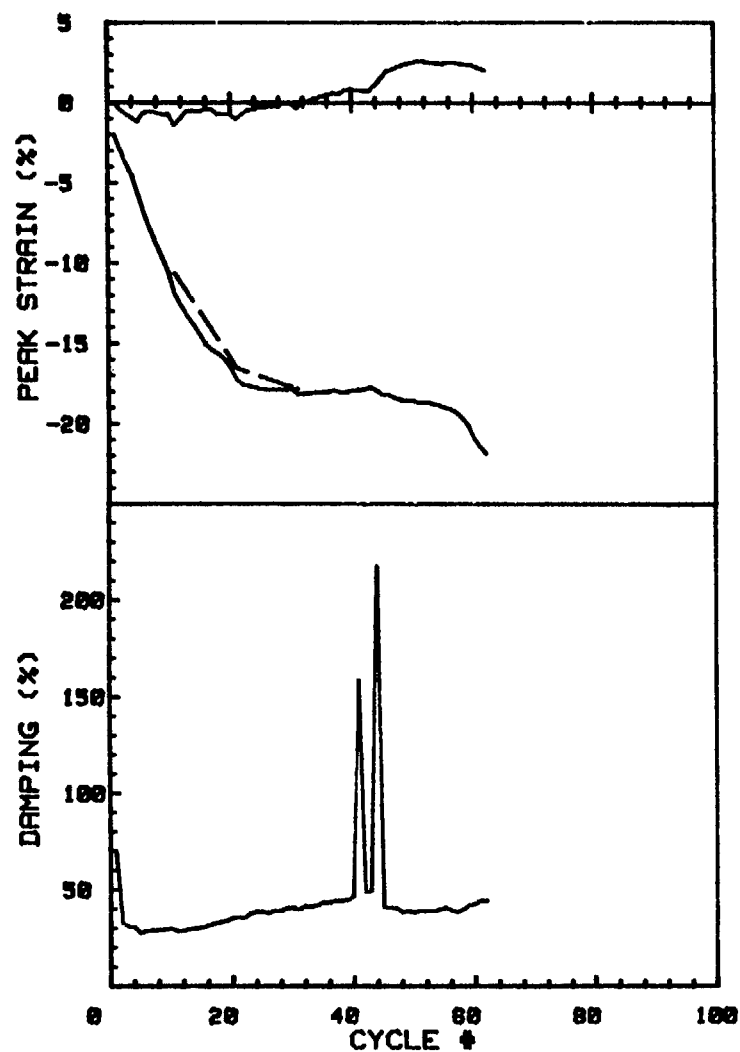
CRUISE DC2-80-EG		INCREMENT (cm)	
CORE NO.	28G	TEST NO.	15-22 TC24
SIG1c' (kPa)	302.6	STATIC qf (kPa)	268.9
SIG3c' (kPa)	302.6	AVG MAX q (kPa)	115.6 (43.0%)
INDUCED OCR	1.0	AVG MIN q (kPa)	-100.5 (37.4%)



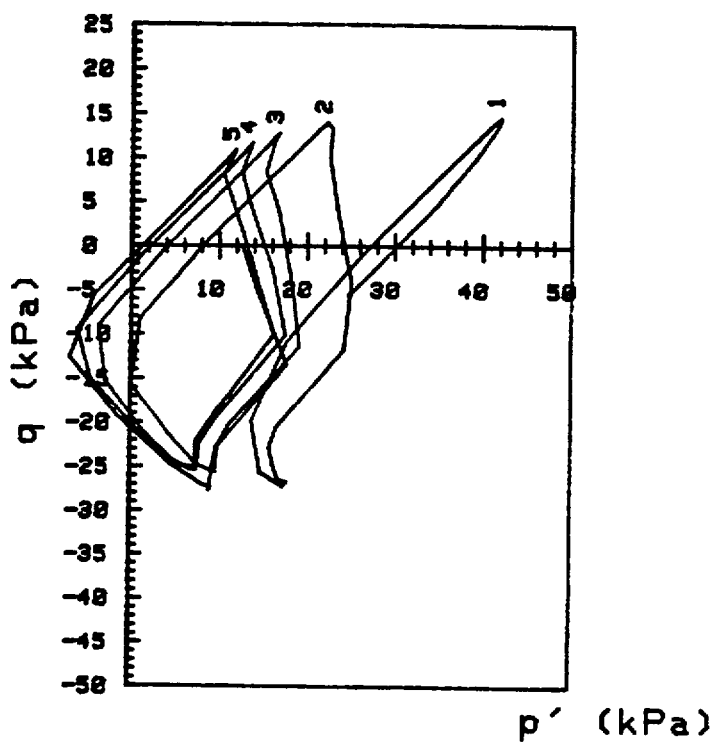
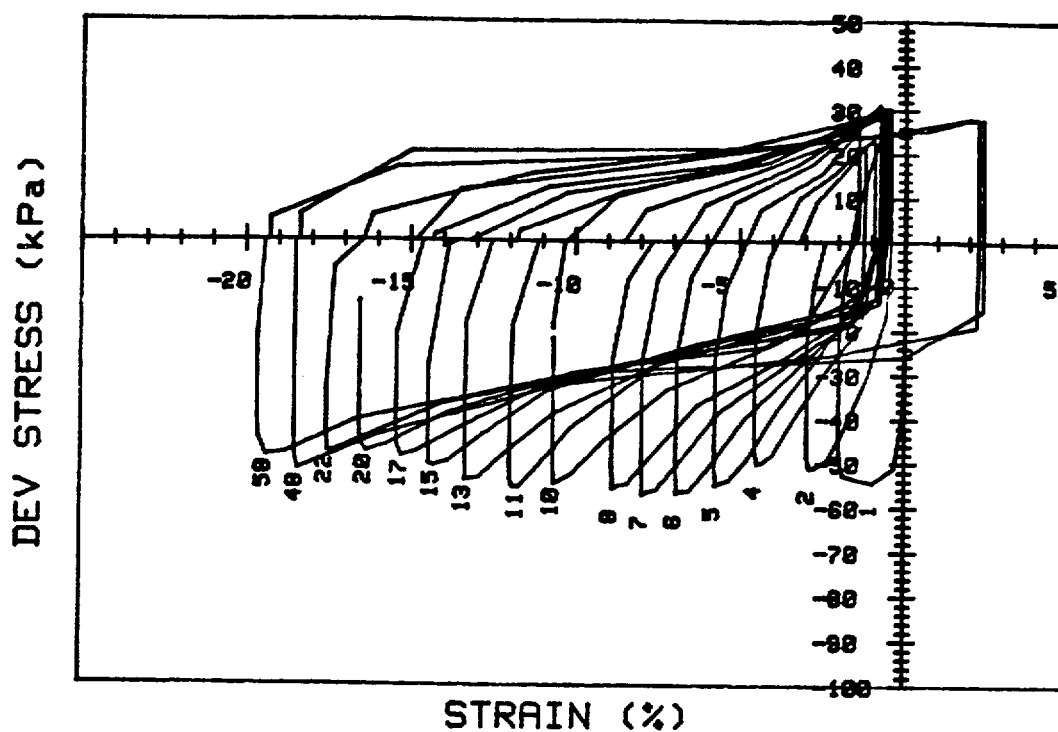
CRUISE DC2-80-EG	INCREMENT (cm)	15-22.4
CORE NO. 28G	TEST NO.	TC25
SIG1c' (kPa) 297.9	STATIC qf (kPa)	270.0
SIG3c' (kPa) 297.9	AVG MAX q (kPa)	21.1 (7.8%)
INDUCED OCR 1.0	AVG MIN q (kPa)	-16.6 (6.1%)



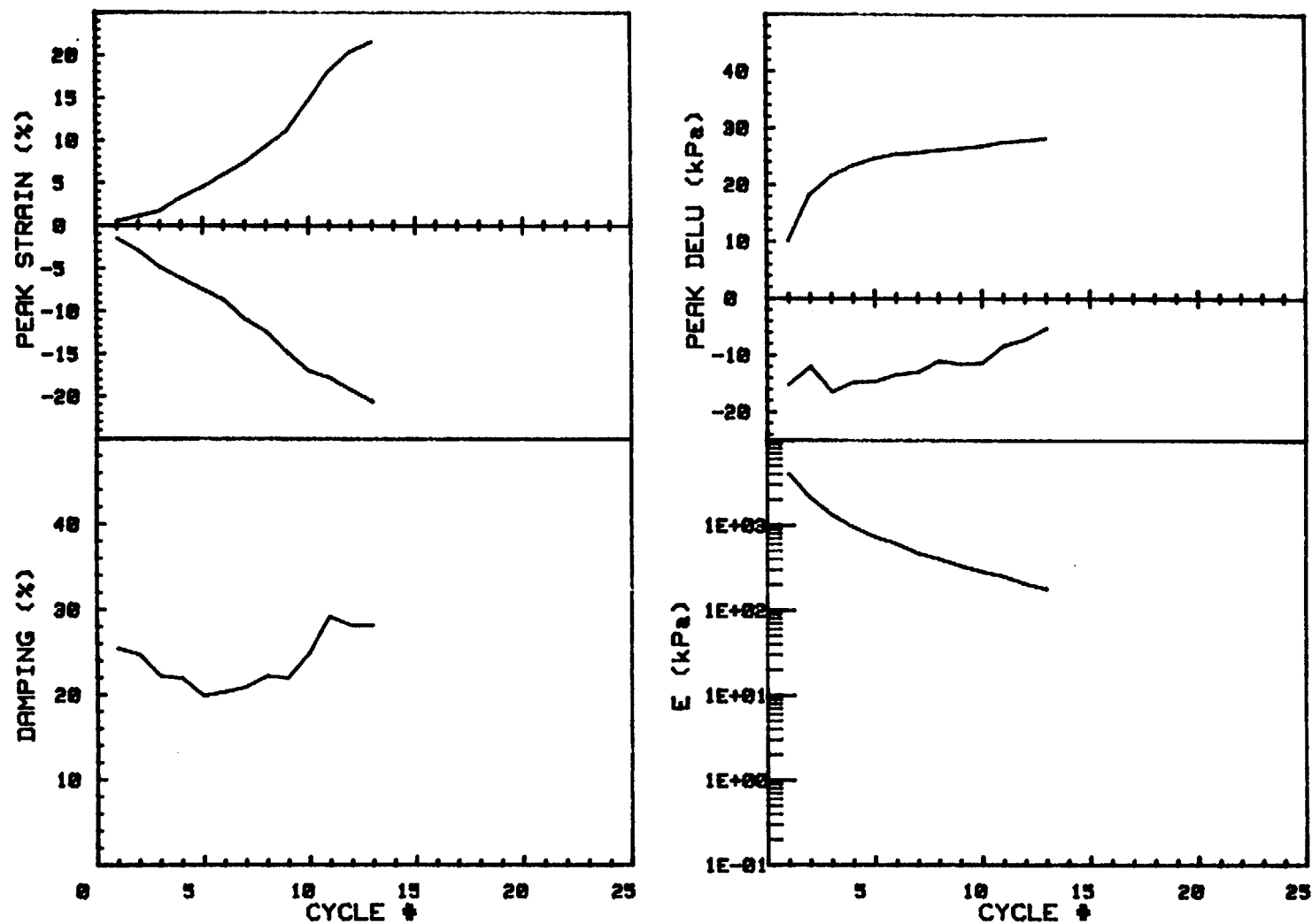
CRUISE DC2-80-EG	INCREMENT (cm)	15-22.4
CORE NO. 28G	TEST NO.	TC25
SIG1c' (kPa) 297.9	STATIC qf (kPa)	270.0
SIG3c' (kPa) 297.9	AVG MAX q (kPa)	21.1 (7.8%)
INDUCED OCR 1.0	AVG MIN q (kPa)	-16.6 (6.1%)



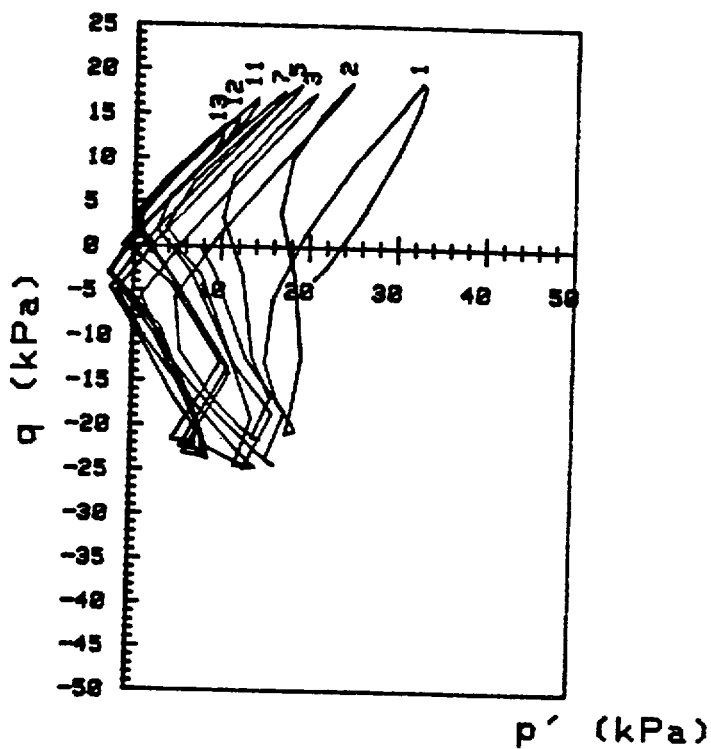
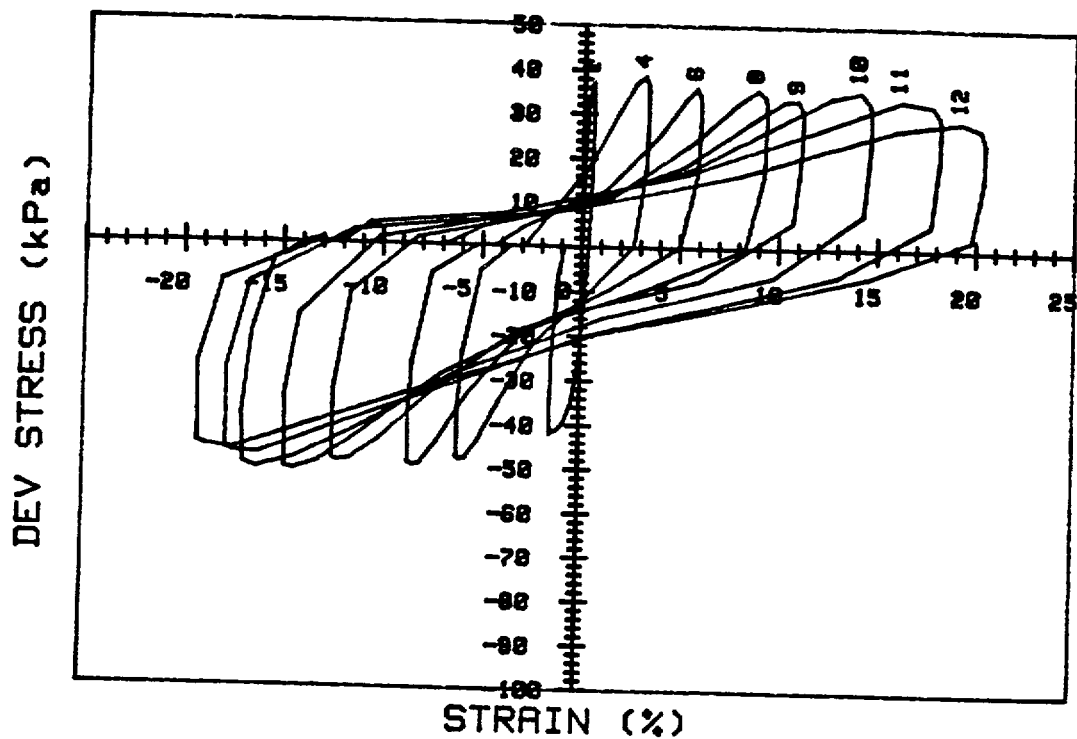
CRUISE DC2-80-EG		INCREMENT (cm) 61-71	
CORE NO.	181G	TEST NO.	TC30
SIG1c' (kPa)	30.3	STATIC qf (kPa)	23.7
SIG3c' (kPa)	30.3	AVG MAX q (kPa)	14.3 (60.3%)
INDUCED OCR	1.0	AVG MIN q (kPa)	-25.0 (105.5%)



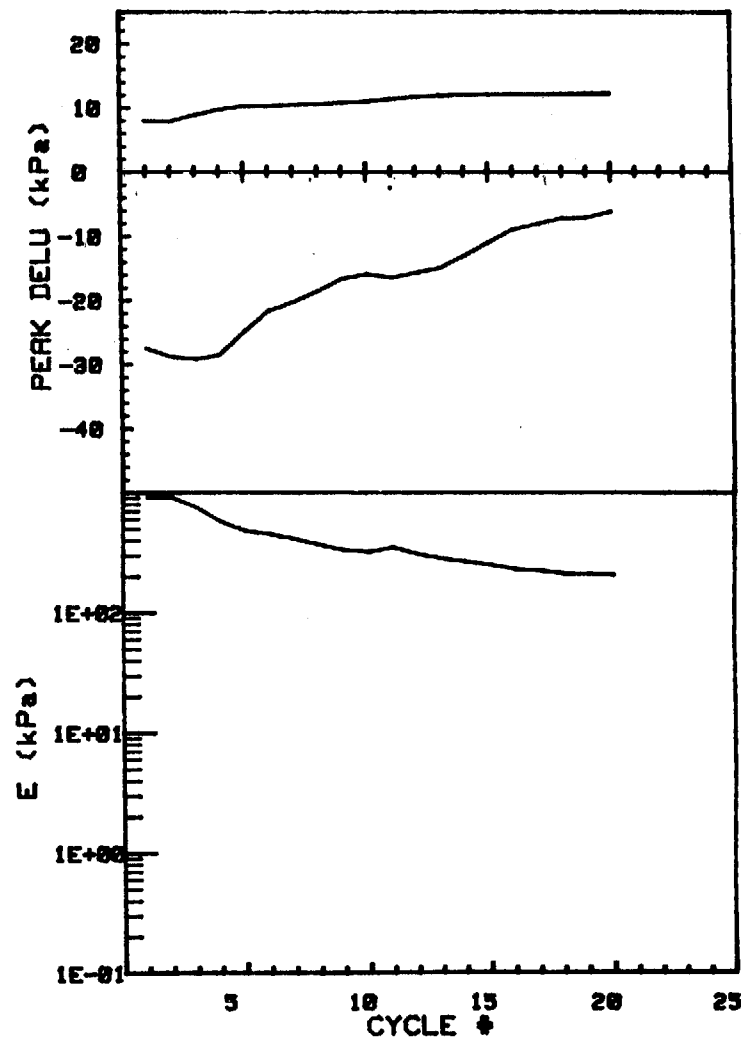
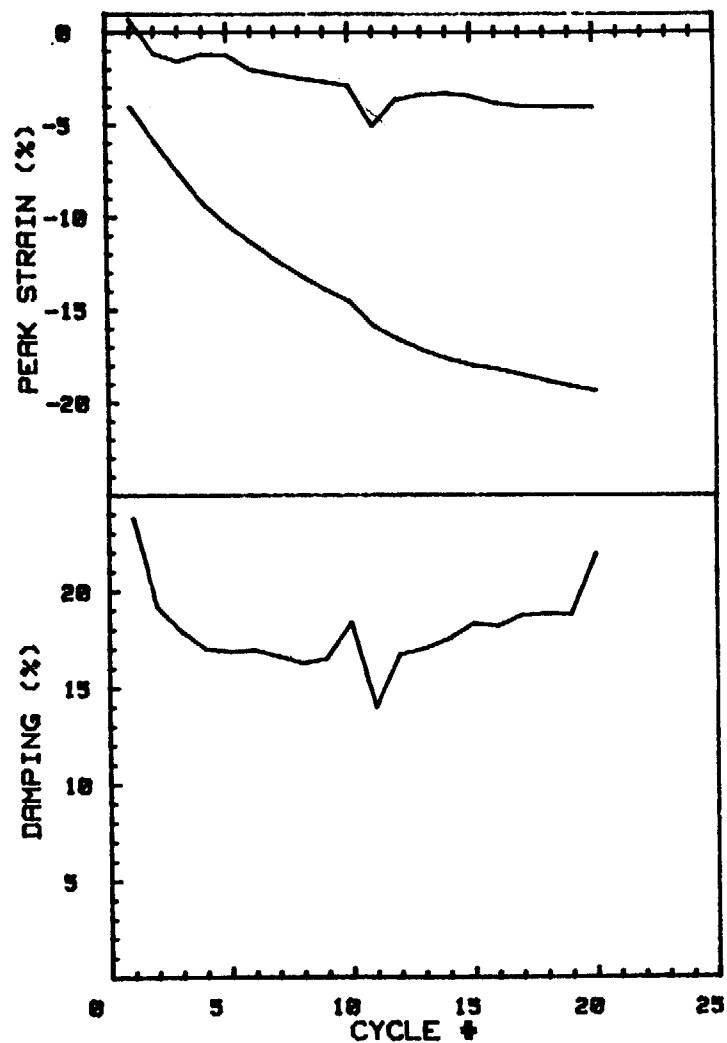
CRUISE DC2-80-EG	INCREMENT (cm)	61-71
CORE NO. 181G	TEST NO.	TC30
SIG1c' (kPa) 30.3	STATIC qf (kPa) 23.7	
SIG3c' (kPa) 30.3	AVG MAX q (kPa) 14.3 (60.3%)	
INDUCED OCR 1.0	AVG MIN q (kPa) -25.0 (105.5%)	



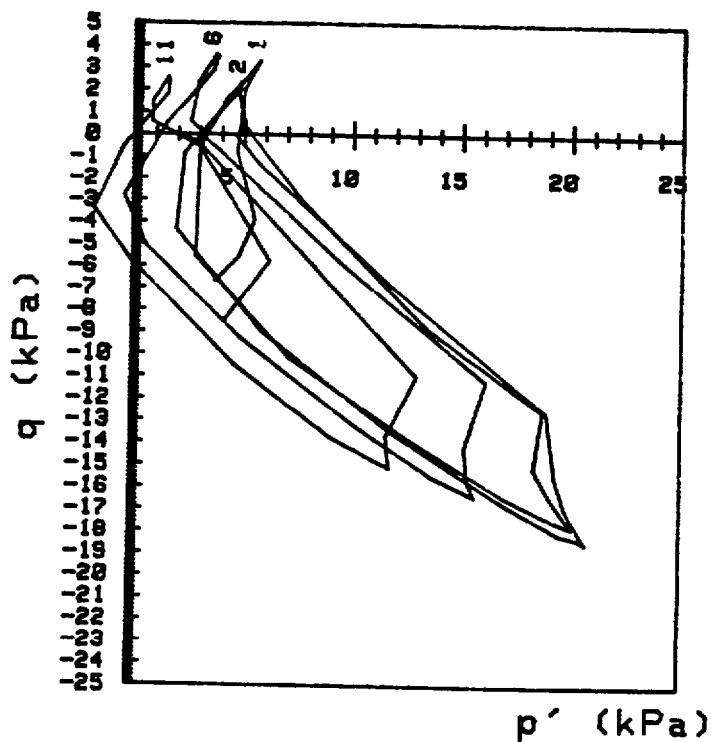
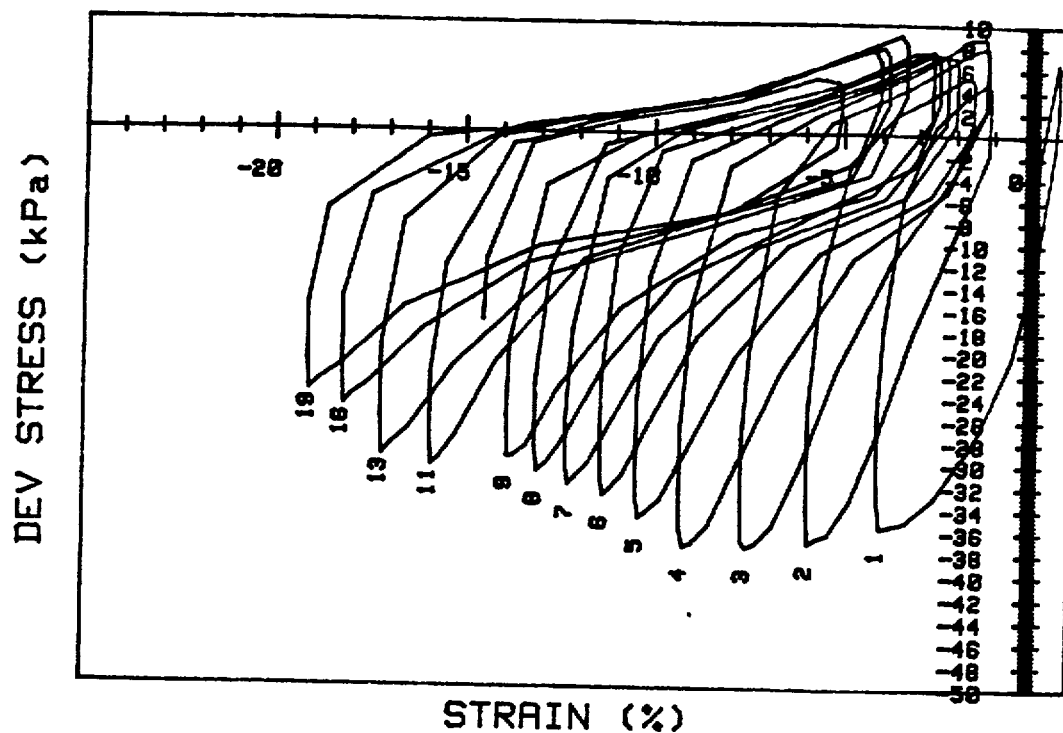
CRUISE DC2-80-EG		INCREMENT (cm) 61-71	
CORE NO. 181G		TEST NO. TC31	
SIG1c' (kPa)	24.2	STATIC qf (kPa)	23.7
SIG3c' (kPa)	24.2	AVG MAX q (kPa)	17.2 (72.6%)
INDUCED OCR	1.0	AVG MIN q (kPa)	-23.8 (100.4%)



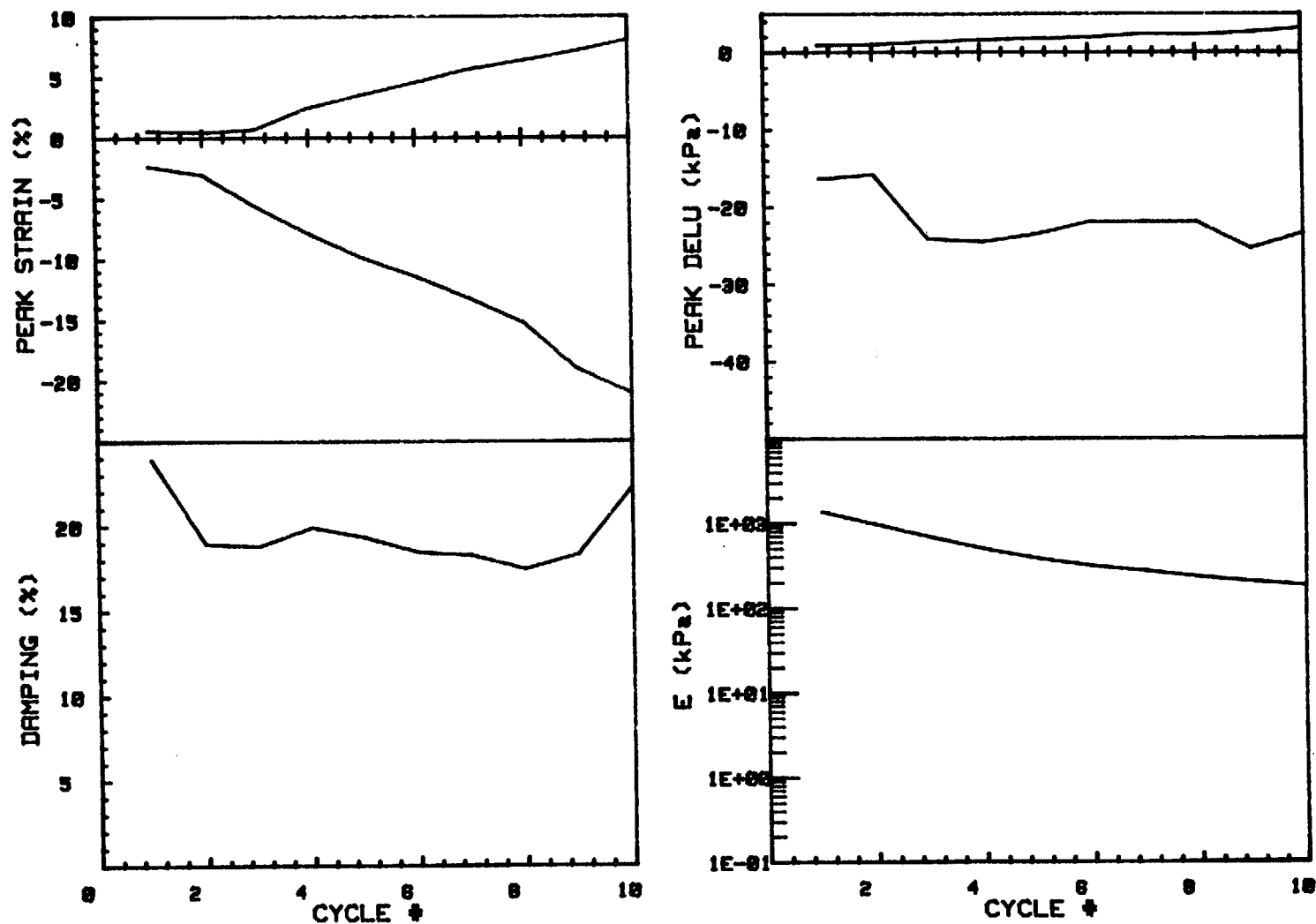
CRUISE DC2-80-EG		INCREMENT (cm)	
CORE NO.	181G	TEST NO.	61-71 TC31
SIG1c' (kPa)	24.2	STATIC qf (kPa)	23.7
SIG3c' (kPa)	24.2	AVG MAX q (kPa)	17.2 (72.6%)
INDUCED OCR	1.0	AVG MIN q (kPa)	-23.8 (100.4%)



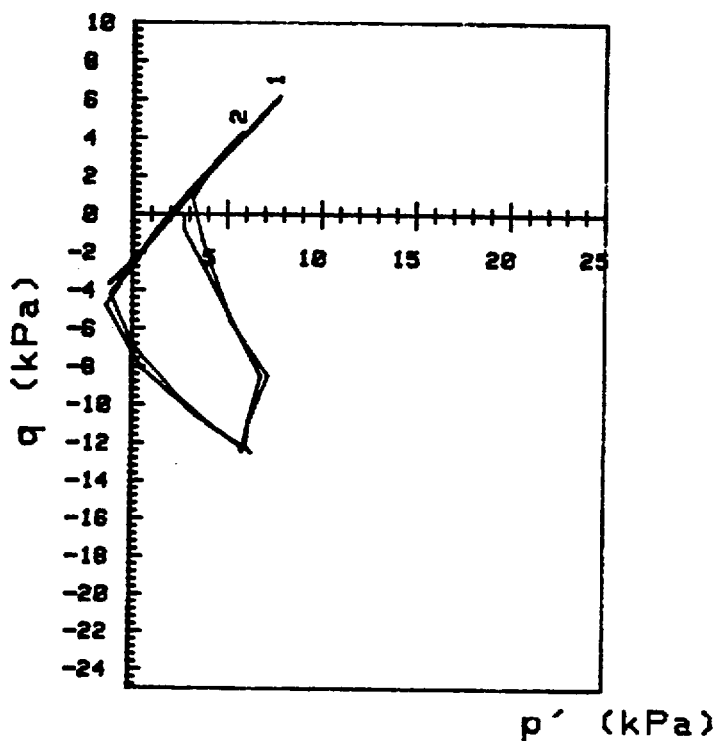
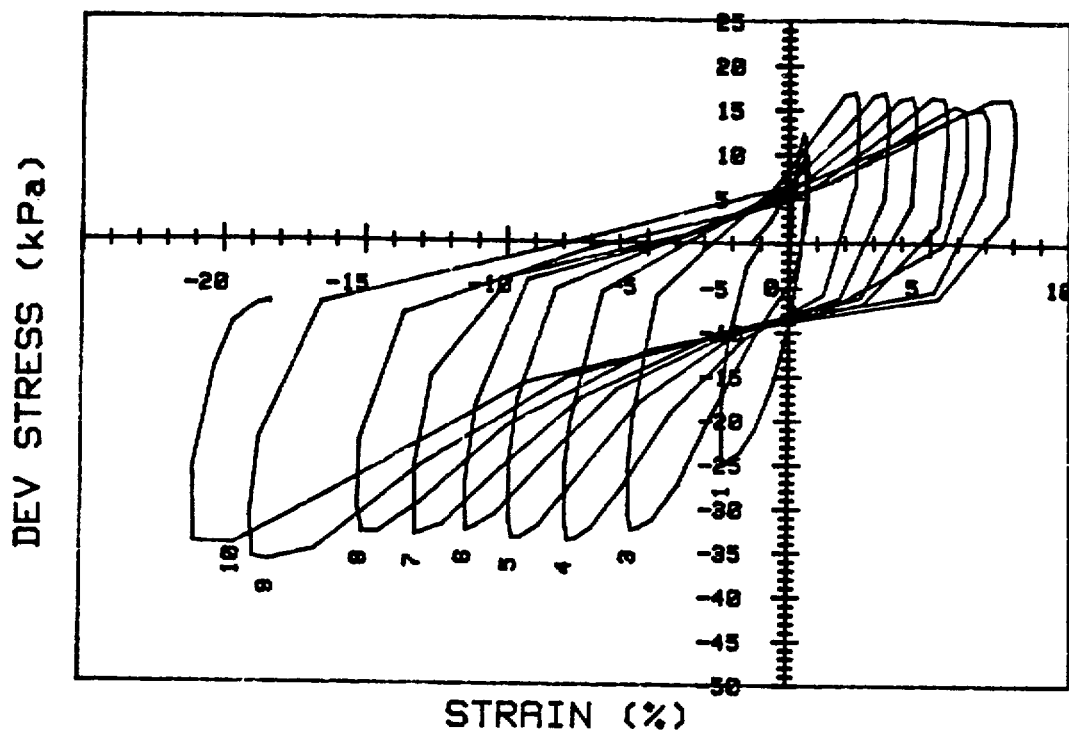
CRUISE DC2-80-EG		INCREMENT (cm) 85-95	
CORE NO. 181G		TEST NO. TC32	
SIG1c' (kPa) 10.4		STATIC qf (kPa) 19.0	
SIG3c' (kPa) 10.4		AVG MAX q (kPa) 3.7 (19.5%)	
INDUCED OCR 3.5		AVG MIN q (kPa) -15.0 (78.9%)	



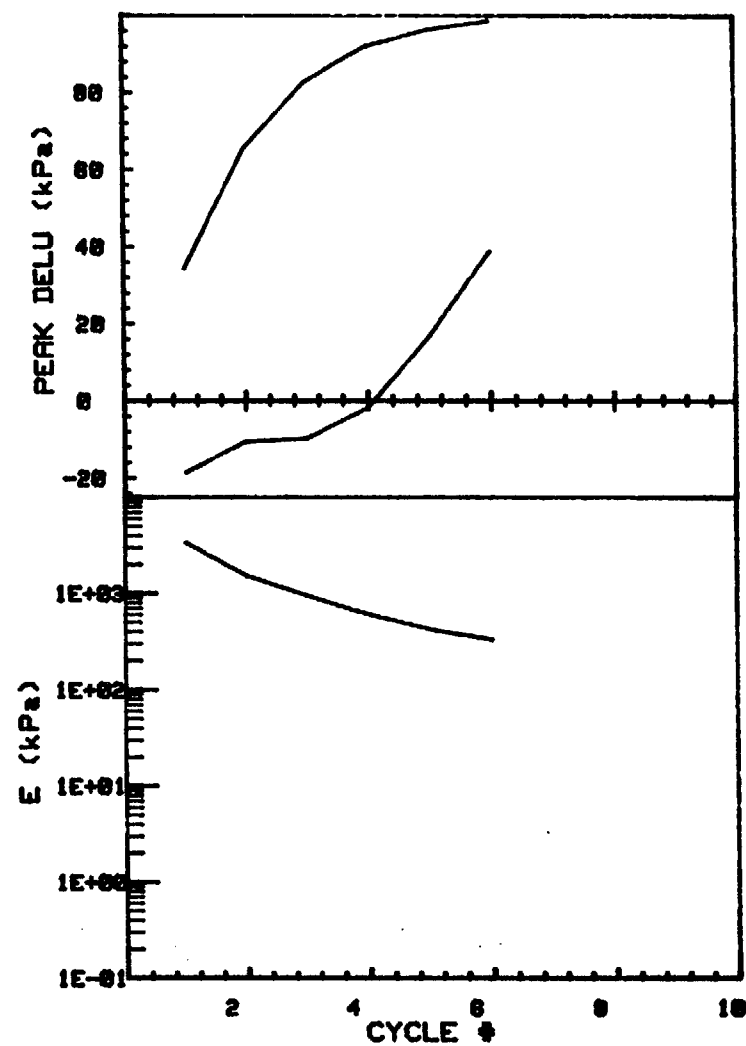
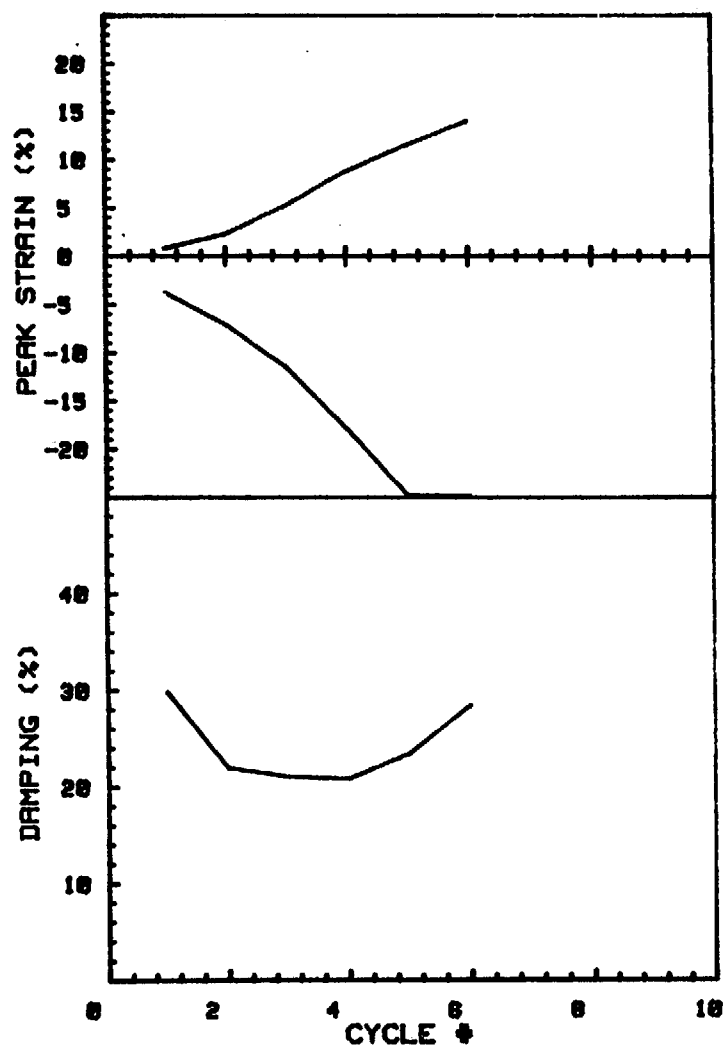
CRUISE DC2-80-EG	INCREMENT (cm)	85-95
CORE NO. 181G	TEST NO.	TC32
SIG1c' (kPa) 10.4	STATIC qf (kPa)	19.0
SIG3c' (kPa) 10.4	AVG MAX q (kPa)	3.7 (19.5%)
INDUCED OCR 3.5	AVG MIN q (kPa)	-15.0 (78.9%)



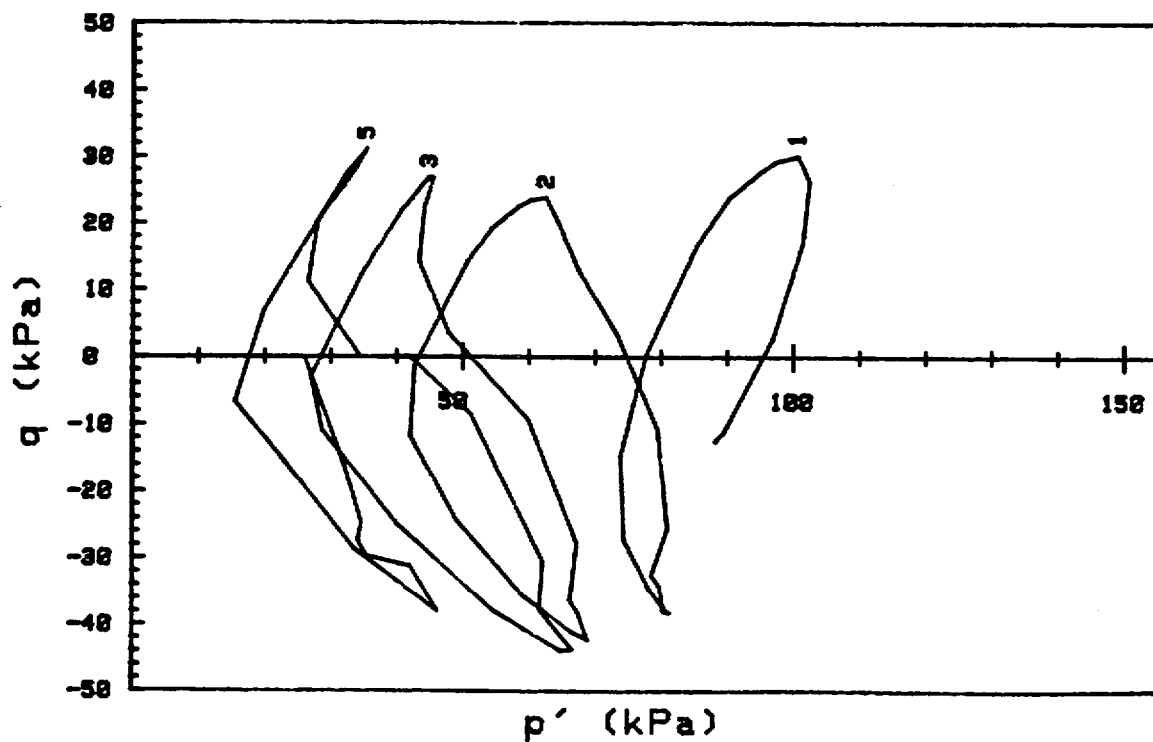
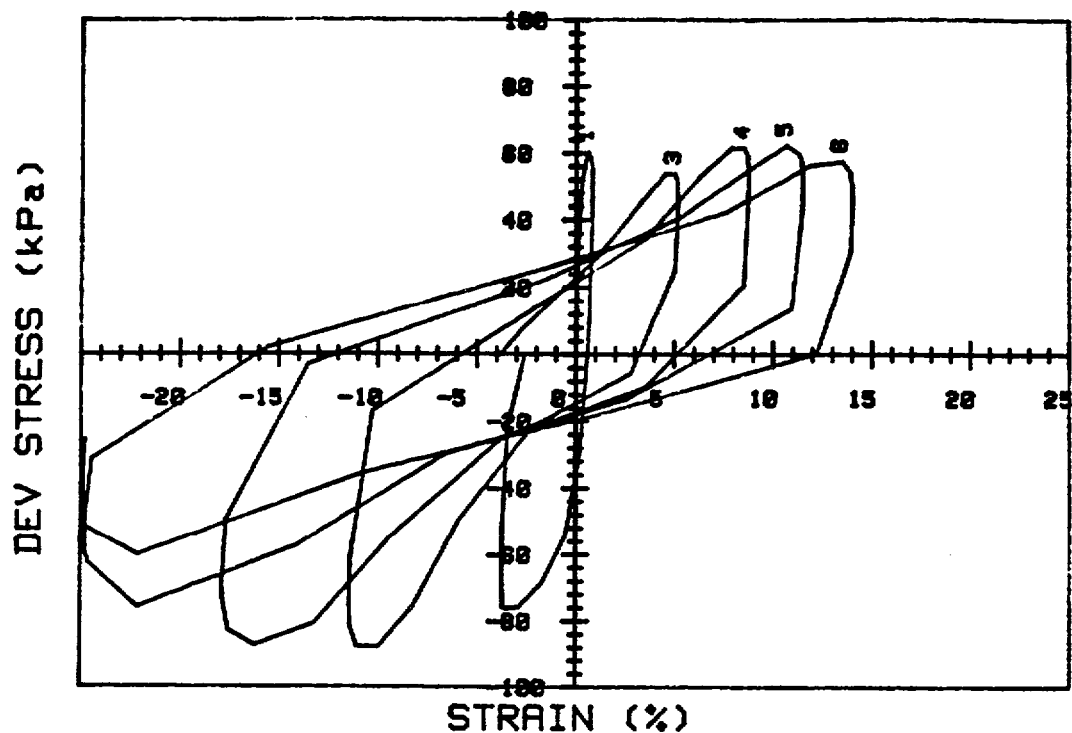
CRUISE DC2-80-EG	INCREMENT (cm)	85-95
CORE NO. 181G	TEST NO.	TC33
SIG1c' (kPa) 2.5	STATIC qf (kPa)	19.0
SIG3c' (kPa) 2.5	AVG MAX q (kPa)	7.2 (37.9%)
INDUCED OCR 14.4	AVG MIN q (kPa)	-15.9 (83.7%)



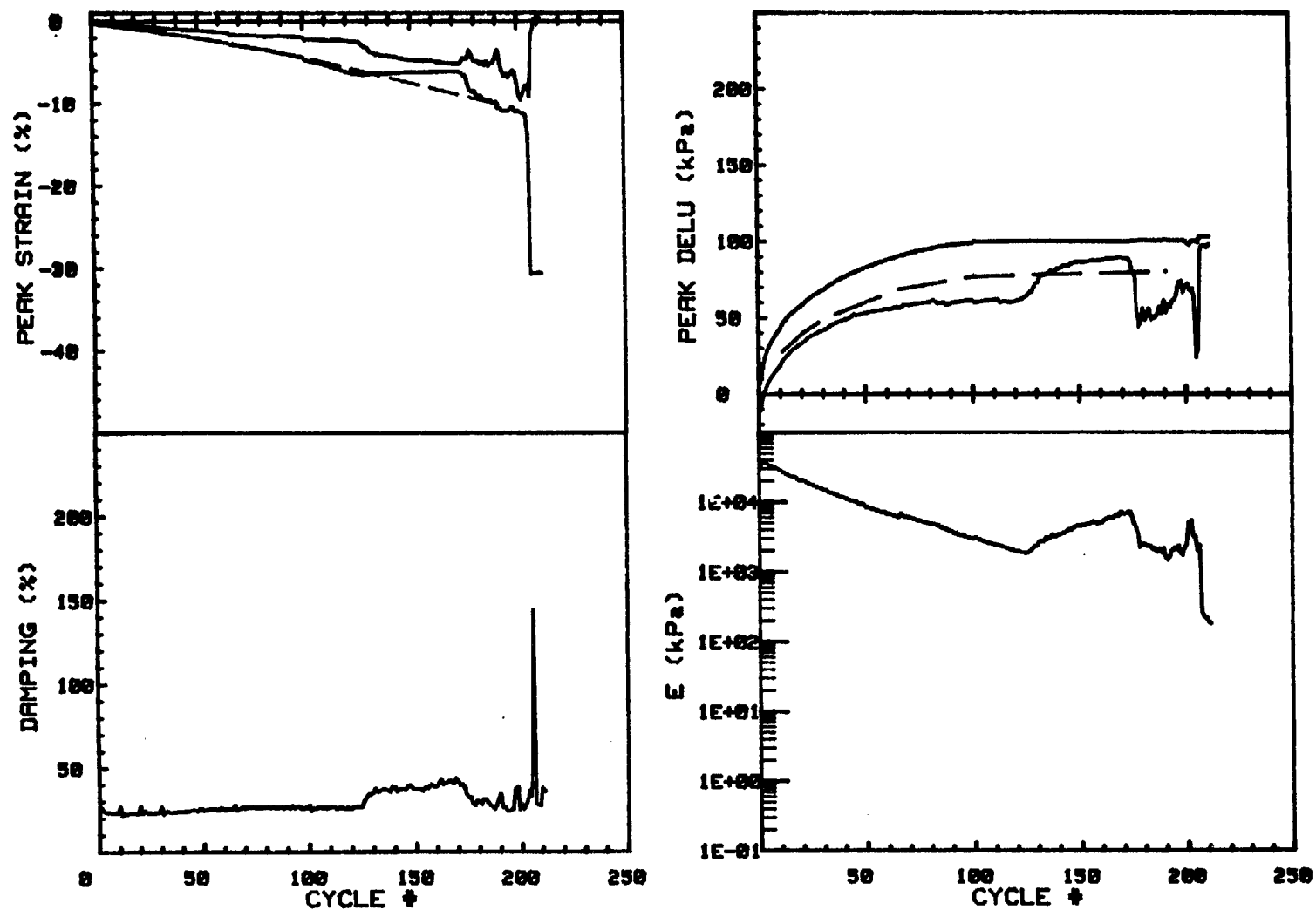
CRUISE DC2-80-EG	INCREMENT (cm)	85-95
CORE NO. 181G	TEST NO.	TC33
SIG1c' (kPa) 2.5	STATIC qf (kPa)	19.0
SIG3c' (kPa) 2.5	AVG MRX q (kPa)	7.2 (37.9%)
INDUCED OCR 14.4	AVG MIN q (kPa)	-15.9 (83.7%)



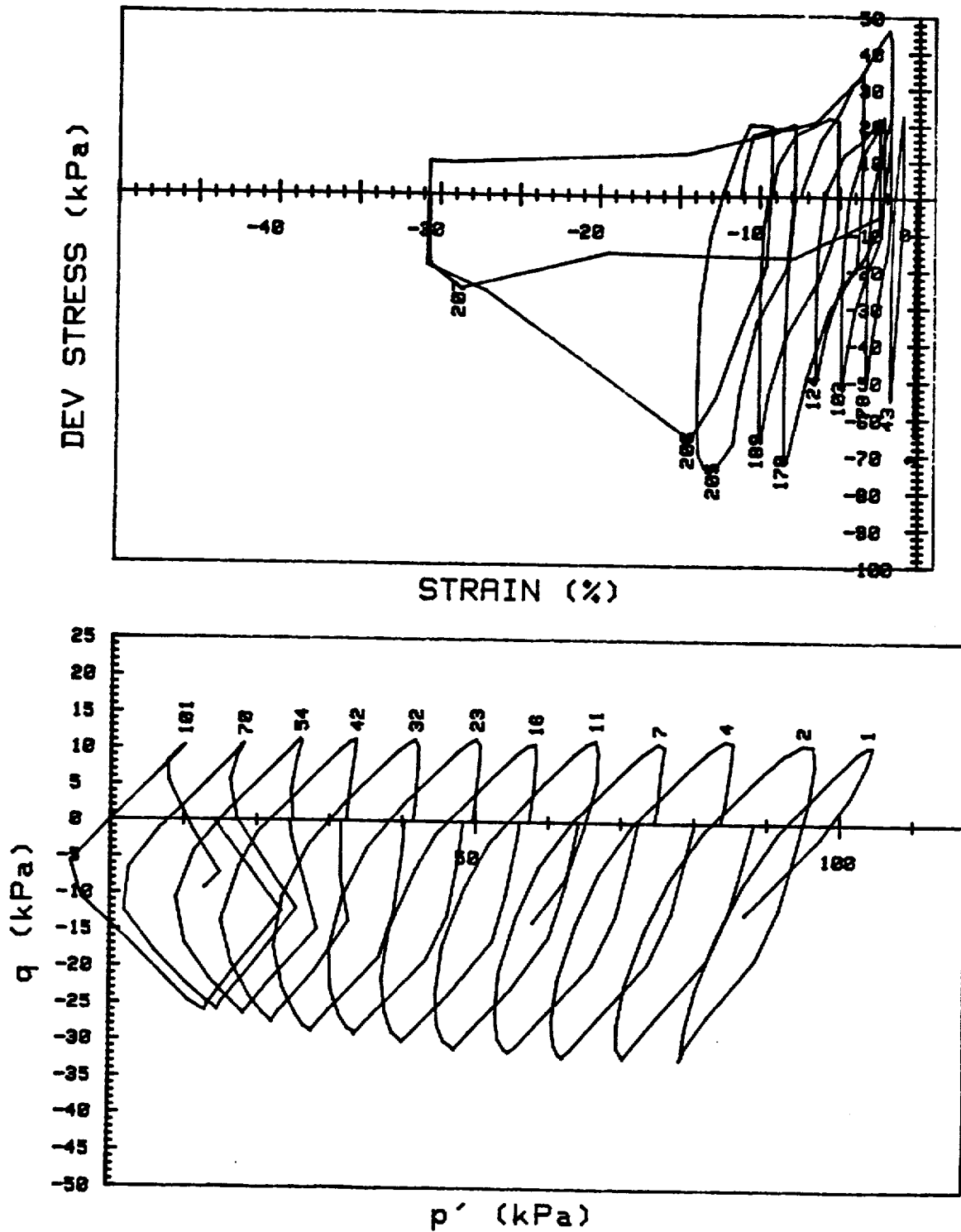
CRUISE DC1-81-EG		INCREMENT (cm)	93-104
CORE NO. 627G2		TEST NO.	TC34
SIG1c' (kPa)	100.7	STATIC qf (kPa)	53.2
SIG3c' (kPa)	100.7	AVG MAX q (kPa)	28.6 (53.8%)
INDUCED OCR	1.0	AVG MIN q (kPa)	-39.4 (74.1%)



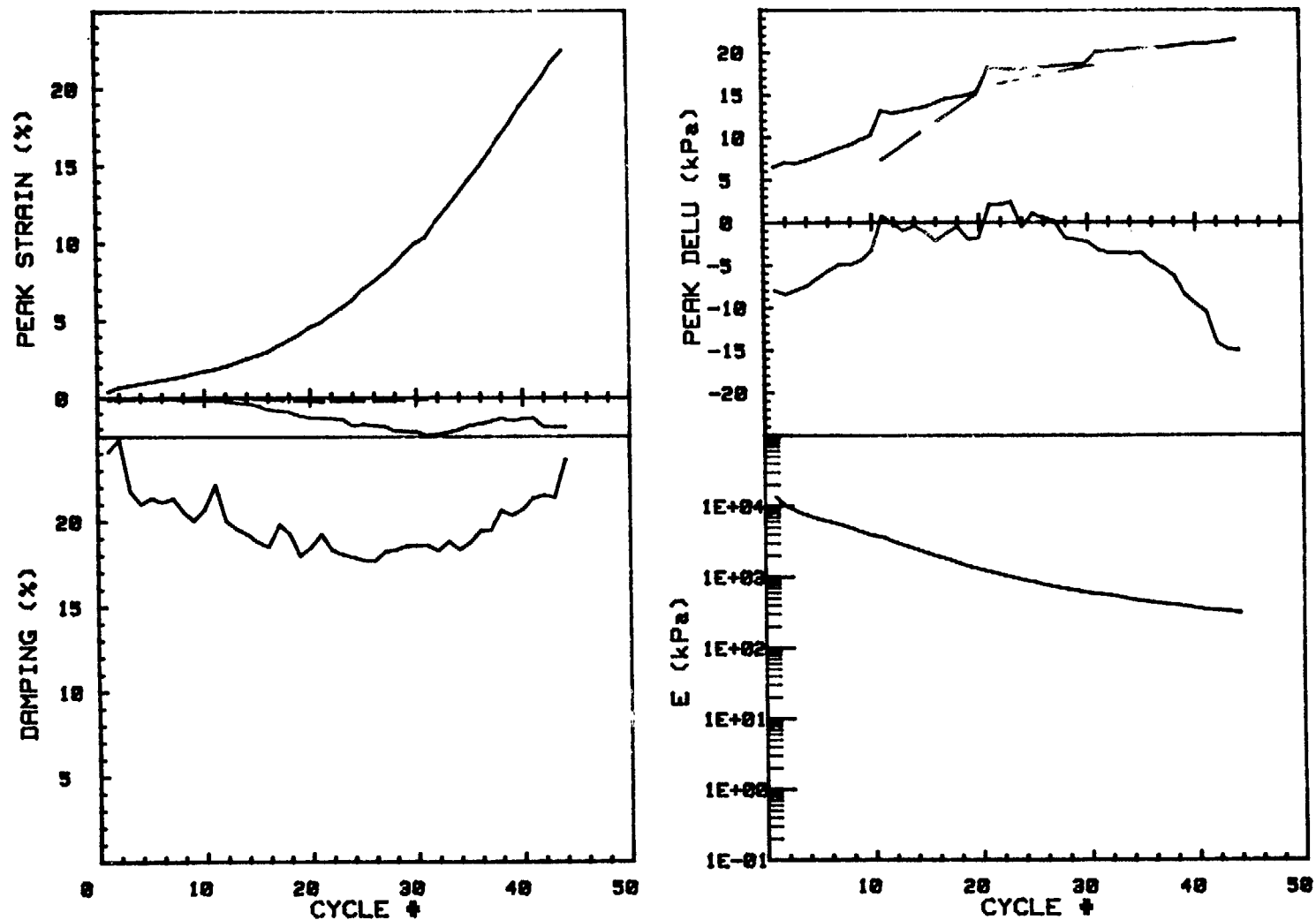
CRUISE DC1-B1-EG		INCREMENT (cm)		93-104
CORE NO.	627G2	TEST NO.		TC34
SIG1c' (kPa)	100.7	STATIC qf (kPa)	53.2	
SIG3c' (kPa)	100.7	AVG MAX q (kPa)	28.6 (53.8%)	
INDUCED OCR	1.0	AVG MIN q (kPa)	-39.4 (74.1%)	



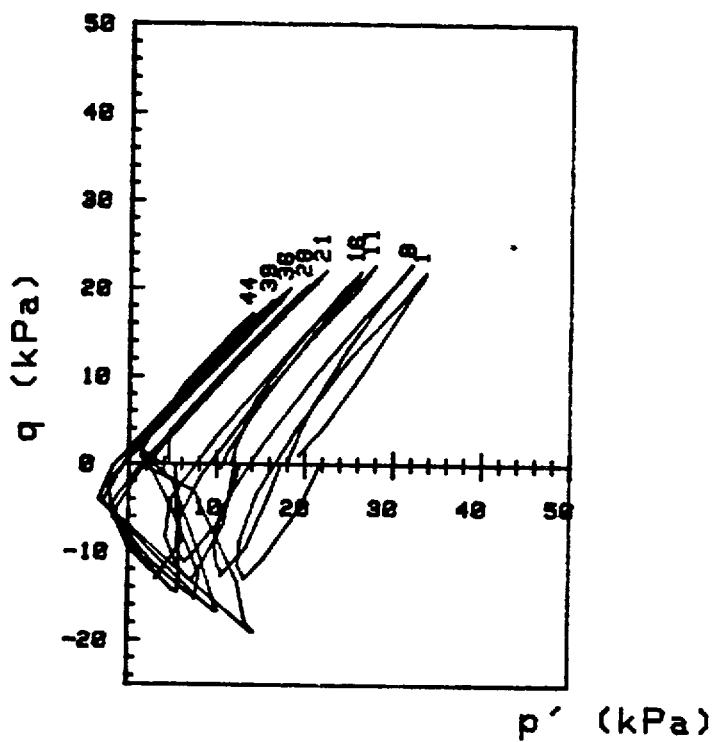
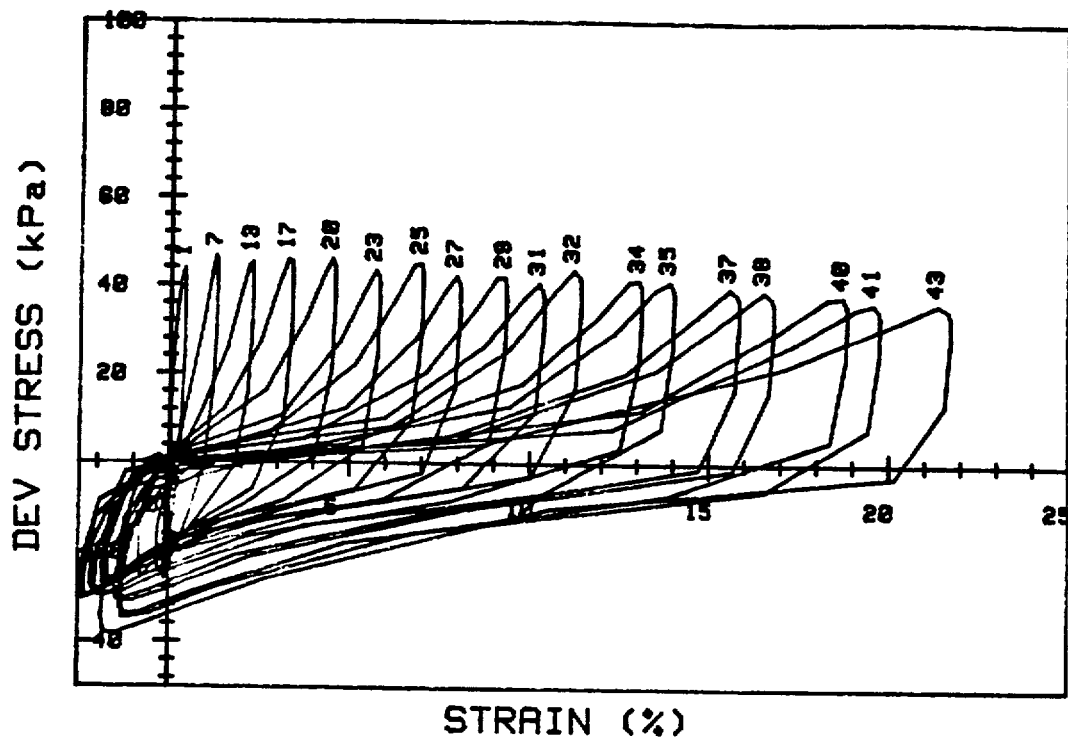
CRUISE DC1-B1-EG		INCREMENT (cm) 93-104	
CORE NO. 627G2		TEST NO. TC35	
SIG1c' (kPa)	99.5	STATIC qf (kPa)	53.2
SIG3c' (kPa)	99.5	AVG MAX q (kPa)	11.9 (22.4%)
INDUCED OCR	1.0	AVG MIN q (kPa)	-26.4 (49.6%)



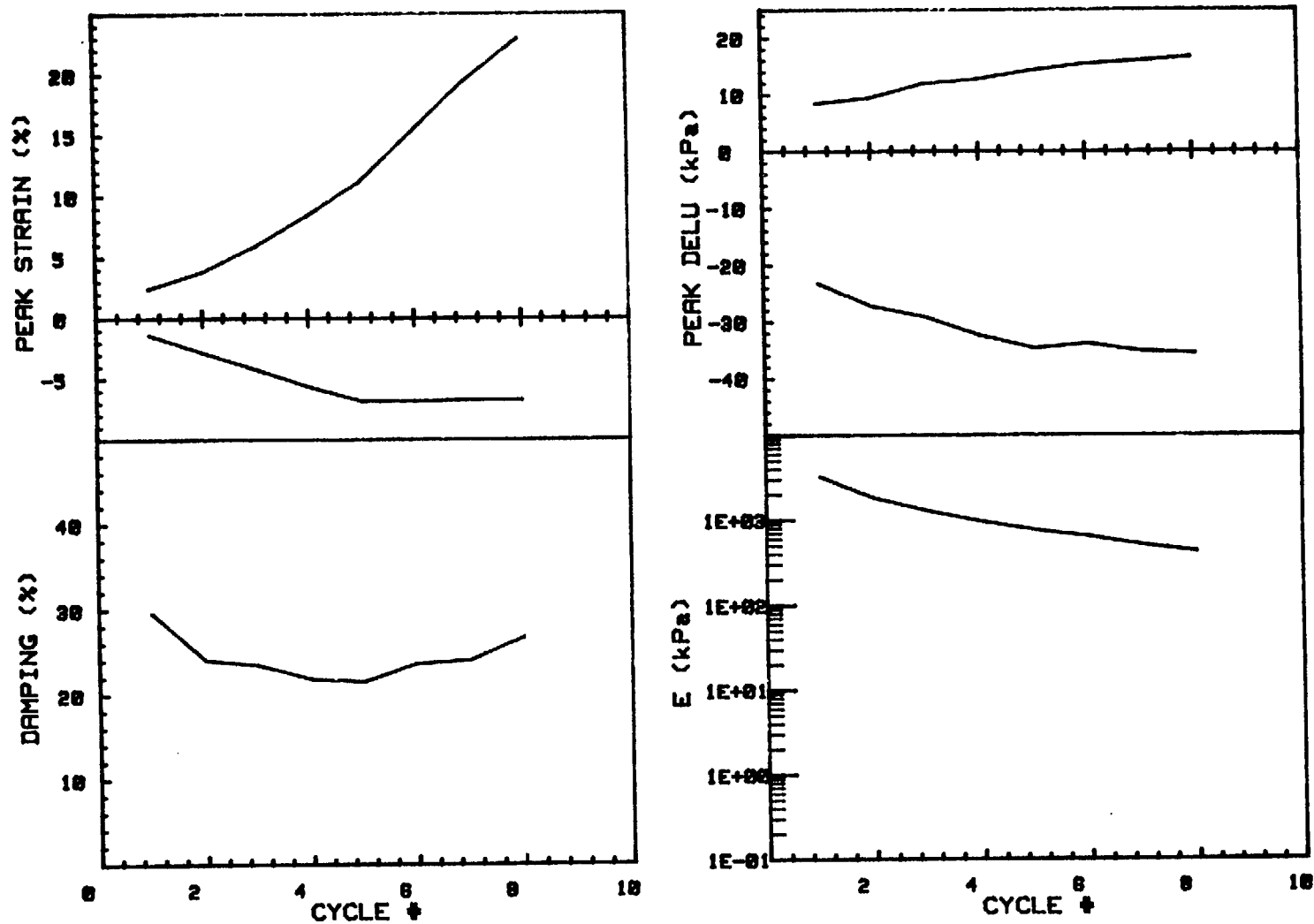
CRUISE DC1-81-EG		INCREMENT (cm)		93-104	
CORE NO.	627G2	TEST NO.		TC35	
SIG1c' (kPa)	99.5	STATIC q_f (kPa)		53.2	
SIG3c' (kPa)	99.5	AVG MAX q (kPa)		11.9 (22.4%)	
INDUCED OCR	1.0	AVG MIN q (kPa)		-26.4 (49.6%)	



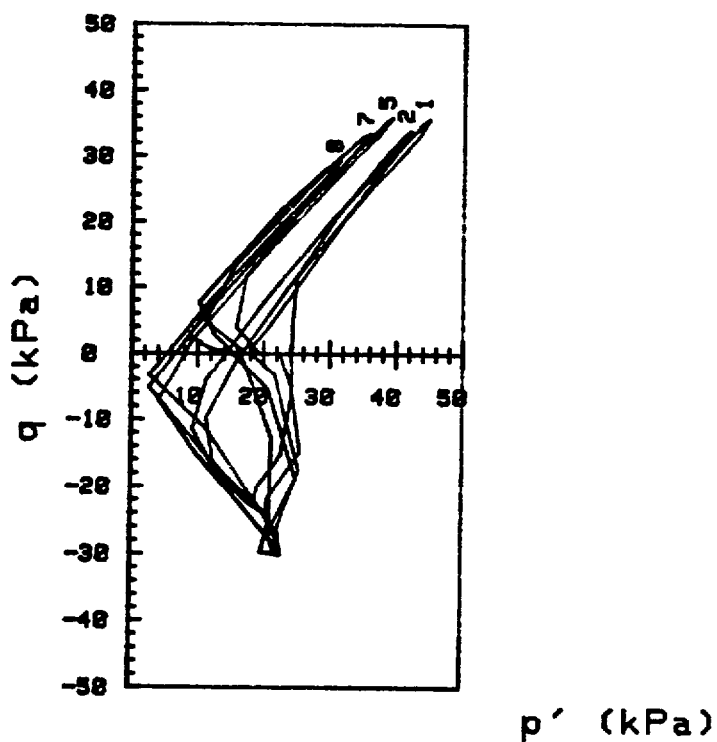
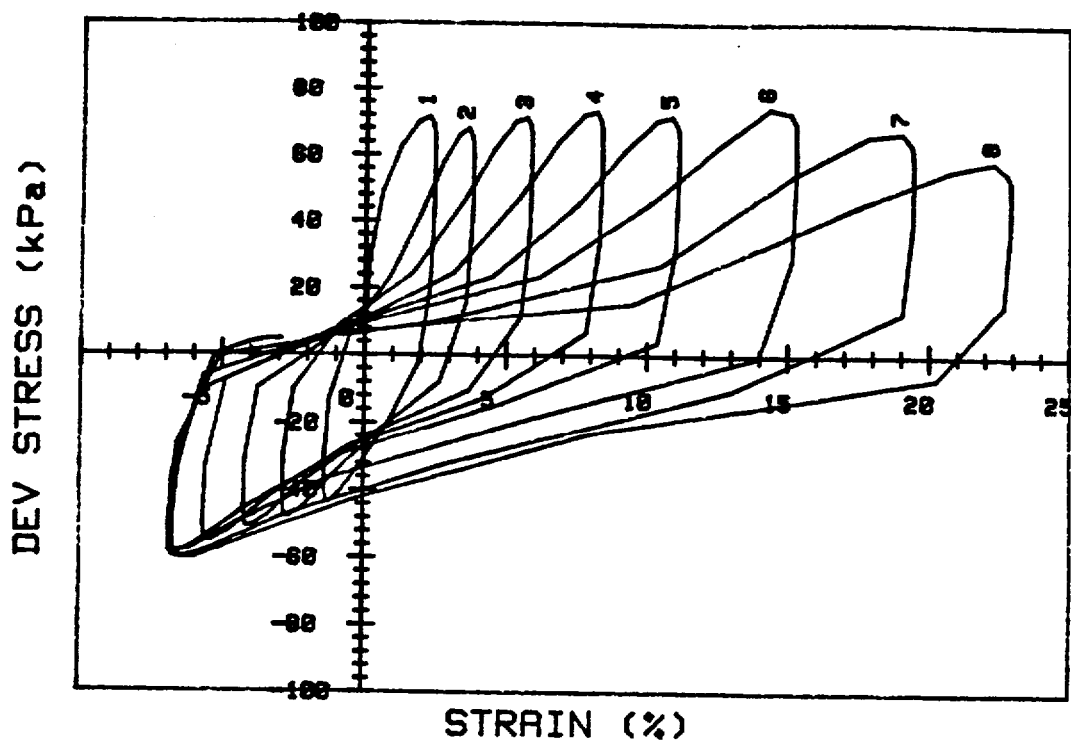
CRUISE DC1-81-EG		INCREMENT (cm)	60-71
CORE NO. 627G2		TEST NO.	TC36
SIG1c' (kPa)	18.3	STATIC qf (kPa)	44.7
SIG3c' (kPa)	18.3	AVG MAX q (kPa)	21.5 (48.1%)
INDUCED OCR	5.5	AVG MIN q (kPa)	-14.0 (31.3%)



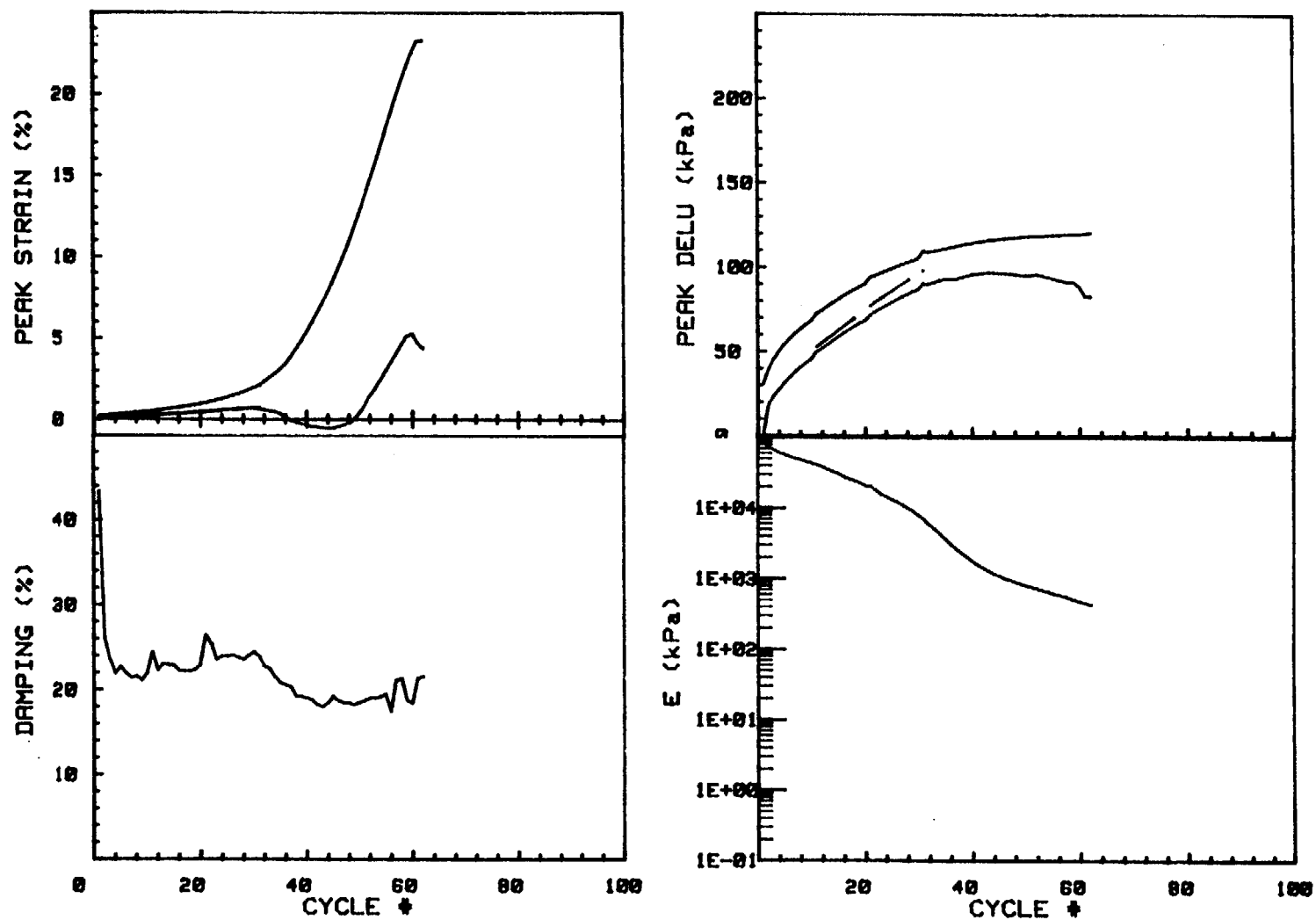
CRUISE DC1-81-EG		INCREMENT (cm)		60-71
CORE NO. 627G2		TEST NO.		TC36
SIG1c'(kPa)	18.3	STATIC qf (kPa)	44.7	
SIG3c'(kPa)	18.3	AVG MAX q (kPa)	21.5 (48.1%)	
INDUCED OCR	5.5	AVG MIN q (kPa)	-14.8 (31.3%)	



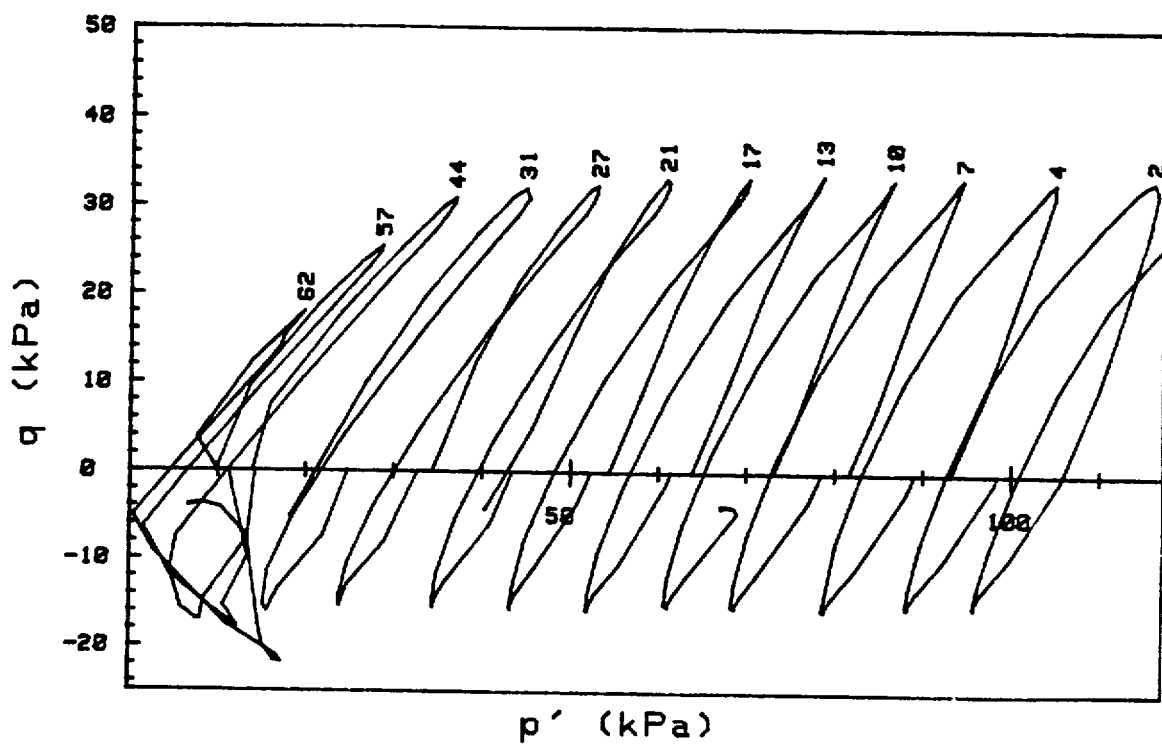
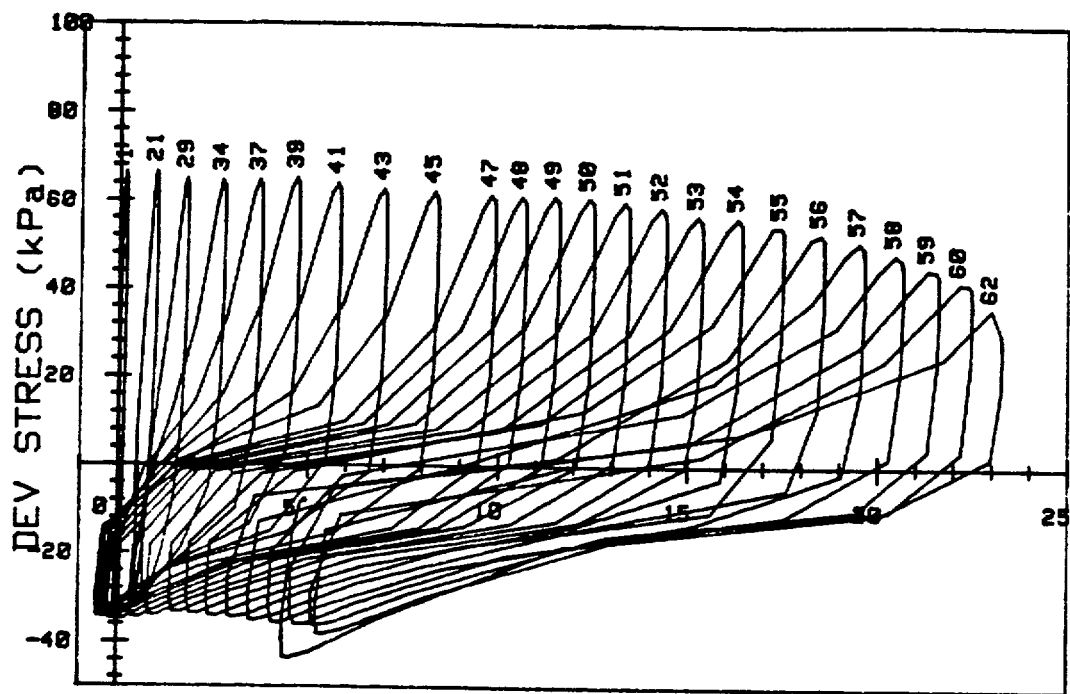
CRUISE DC1-81-EG		INCREMENT (cm)	60-71
CORE NO. 627G2		TEST NO.	TC37
SIG1c' (kPa)	17.3	STATIC qf (kPa)	44.7
SIG3c' (kPa)	17.3	AVG MAX q (kPa)	34.7 (77.6%)
INDUCED OCR	5.8	AVG MIN q (kPa)	-27.2 (60.9%)



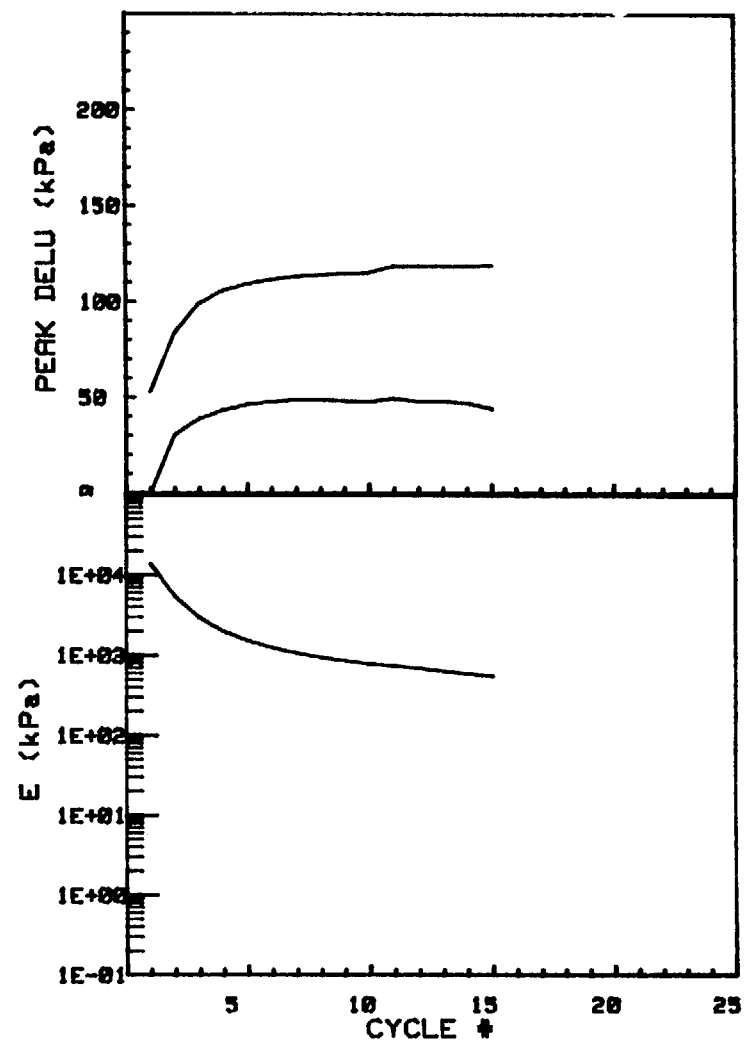
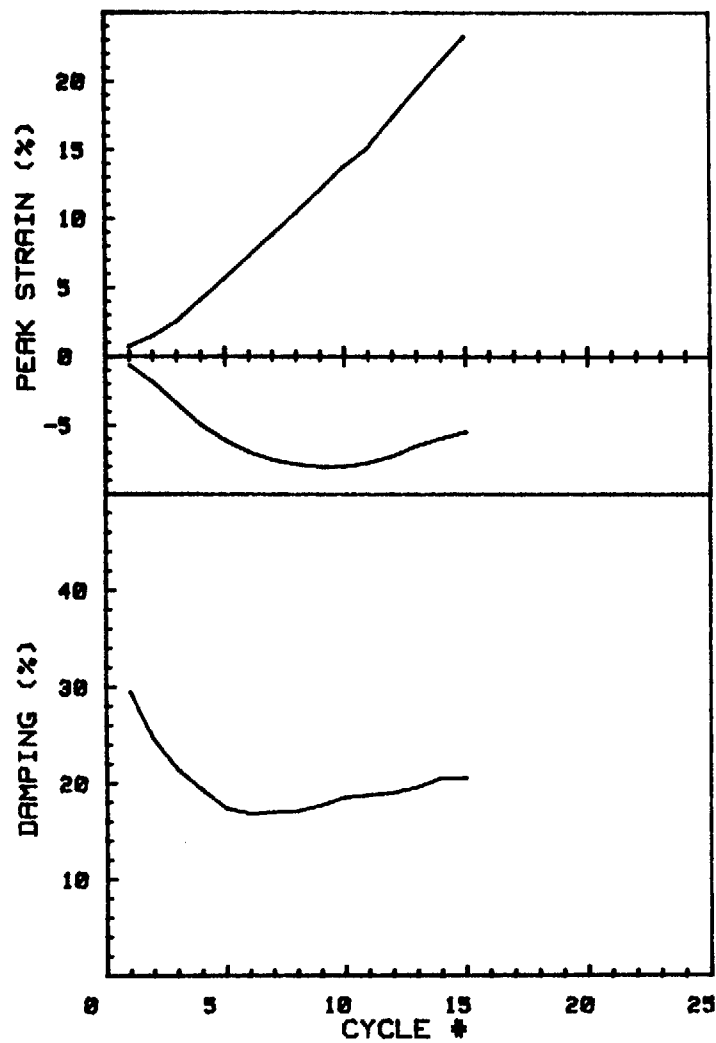
CRUISE DC1-81-EG	INCREMENT (cm)	60-71
CORE NO. 627G2	TEST NO.	TC37
SIG1c' (kPa) 17.3	STATIC qf (kPa)	44.7
SIG3c' (kPa) 17.3	AVG MAX q (kPa)	34.7 (77.6%)
INDUCED OCR 5.8	AVG MIN q (kPa)	-27.2 (60.9%)



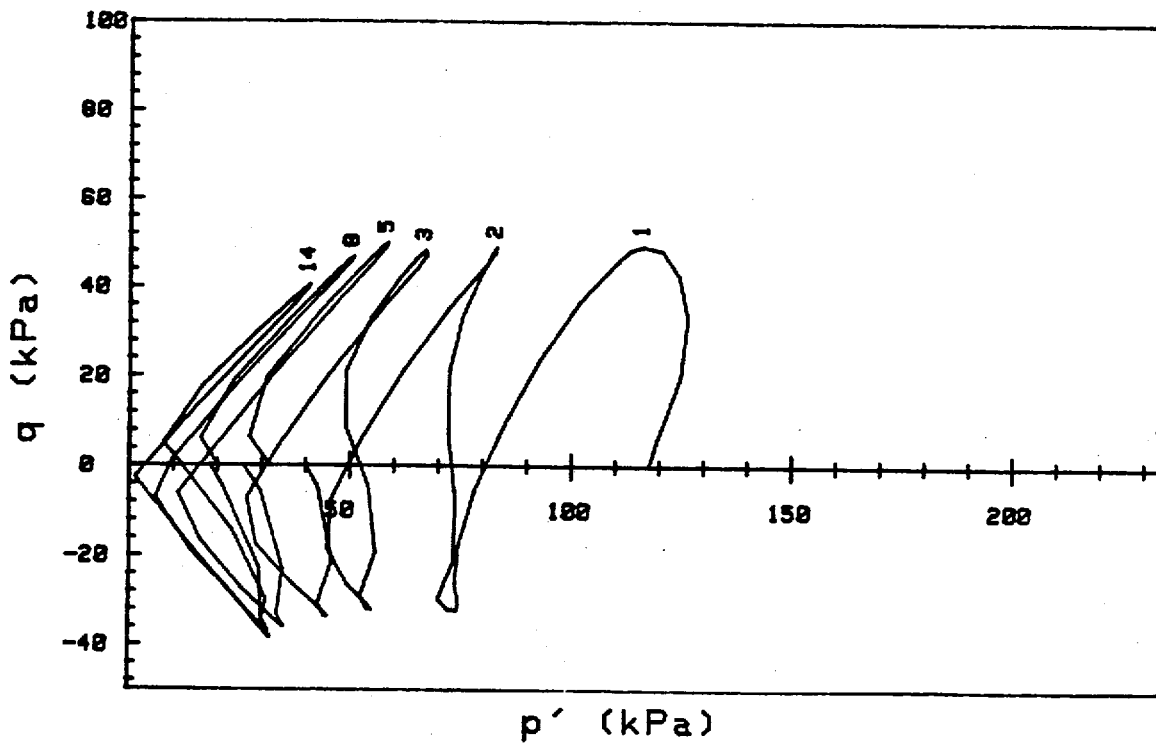
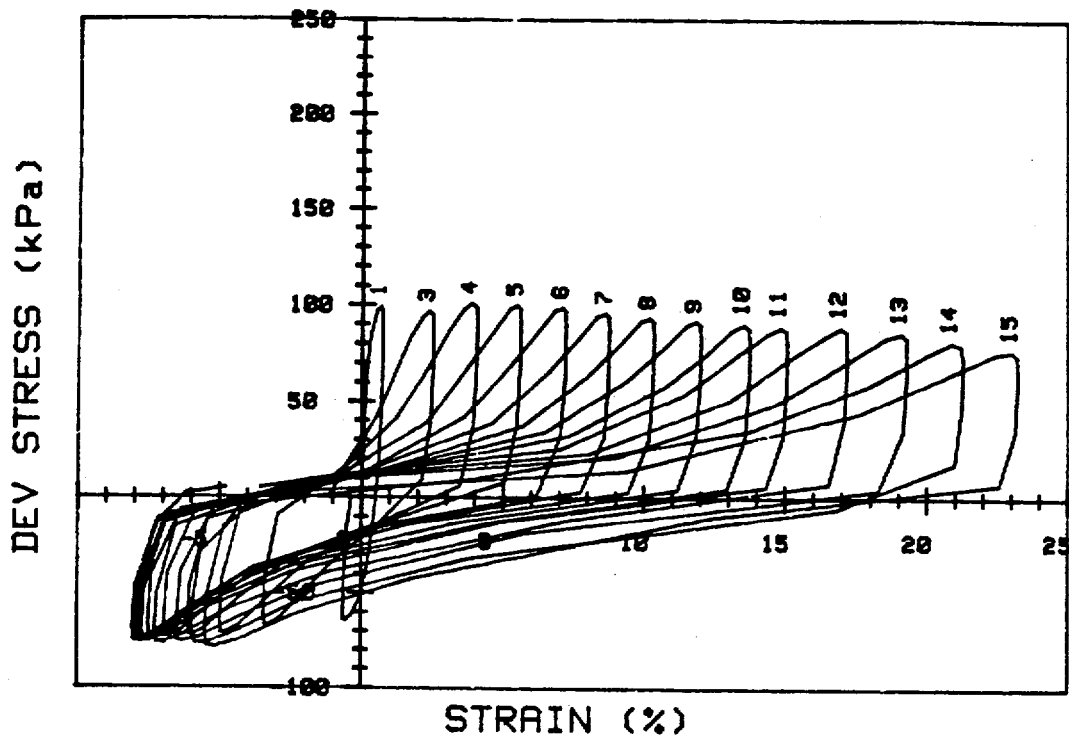
CRUISE DC1-81-EG		INCREMENT (cm)		100-108
CORE NO. 620G2		TEST NO.		TC46
SIG1c' (kPa)	121.8	STATIC qf (kPa)	53.2	
SIG3c' (kPa)	121.8	AVG MAX q (kPa)	31.0 (58.3%)	
INDUCED OCR	1.0	AVG MIN q (kPa)	-16.4 (30.8%)	



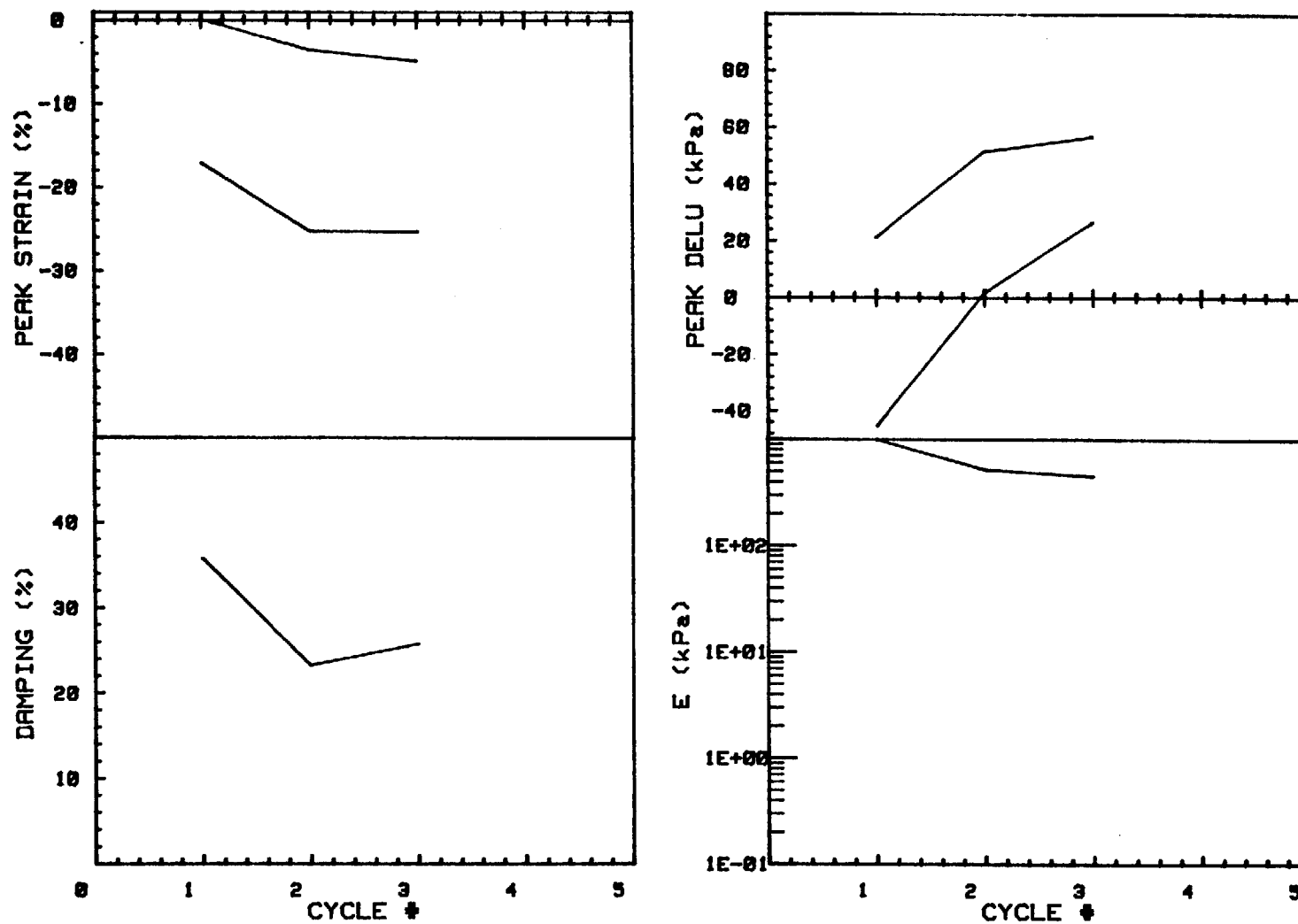
CRUISE DC1-81-EG	INCREMENT (cm)	100-108
CORE NO. 620G2	TEST NO.	TC46
SIG1c' (kPa) 121.8	STATIC qf (kPa) 53.2	
SIG3c' (kPa) 121.8	AVG MAX q (kPa) 31.0 (58.3%)	
INDUCED OCR 1.0	AVG MIN q (kPa) -16.4 (30.8%)	



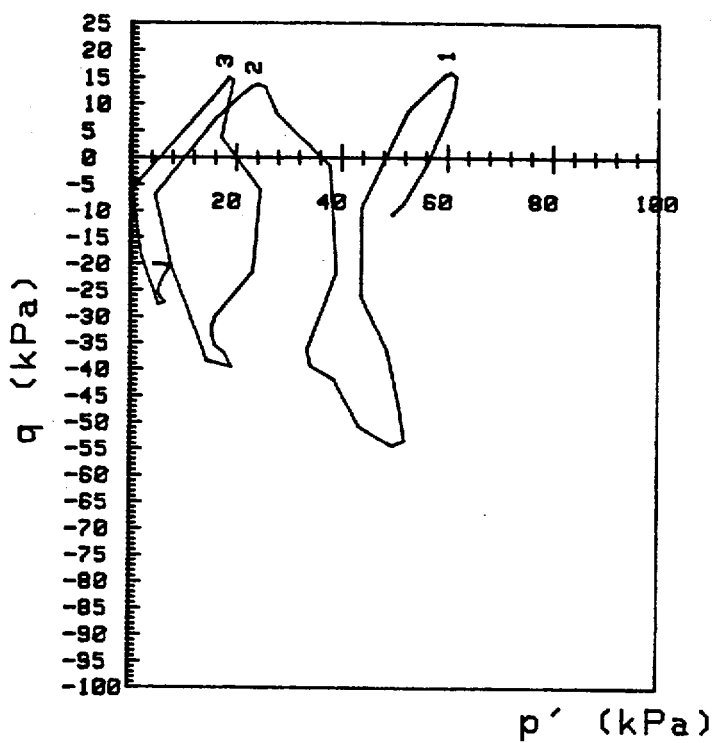
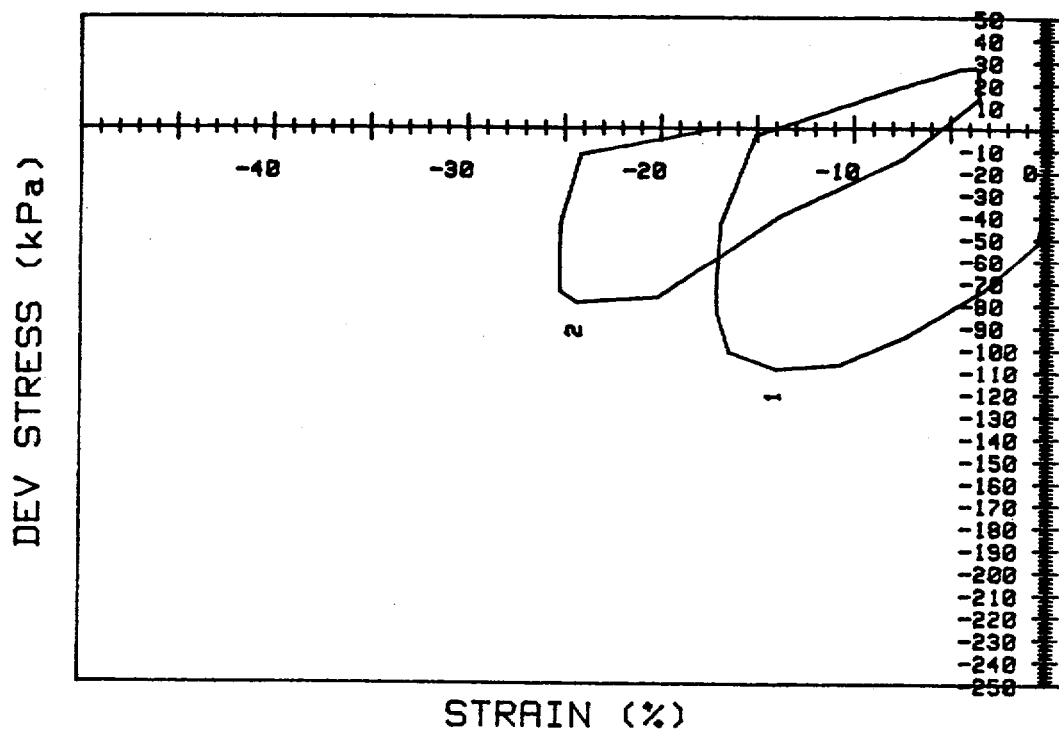
CRUISE DC1-01-EG	INCREMENT (cm)	100-108
CORE NO. 620G2	TEST NO.	TC47
SIG1c' (kPa) 117.6	STATIC qf (kPa)	53.2
SIG3c' (kPa) 117.6	AVG MAX q (kPa)	46.1 (86.7%)
INDUCED OCR 1.0	AVG MIN q (kPa)	-36.4 (68.4%)



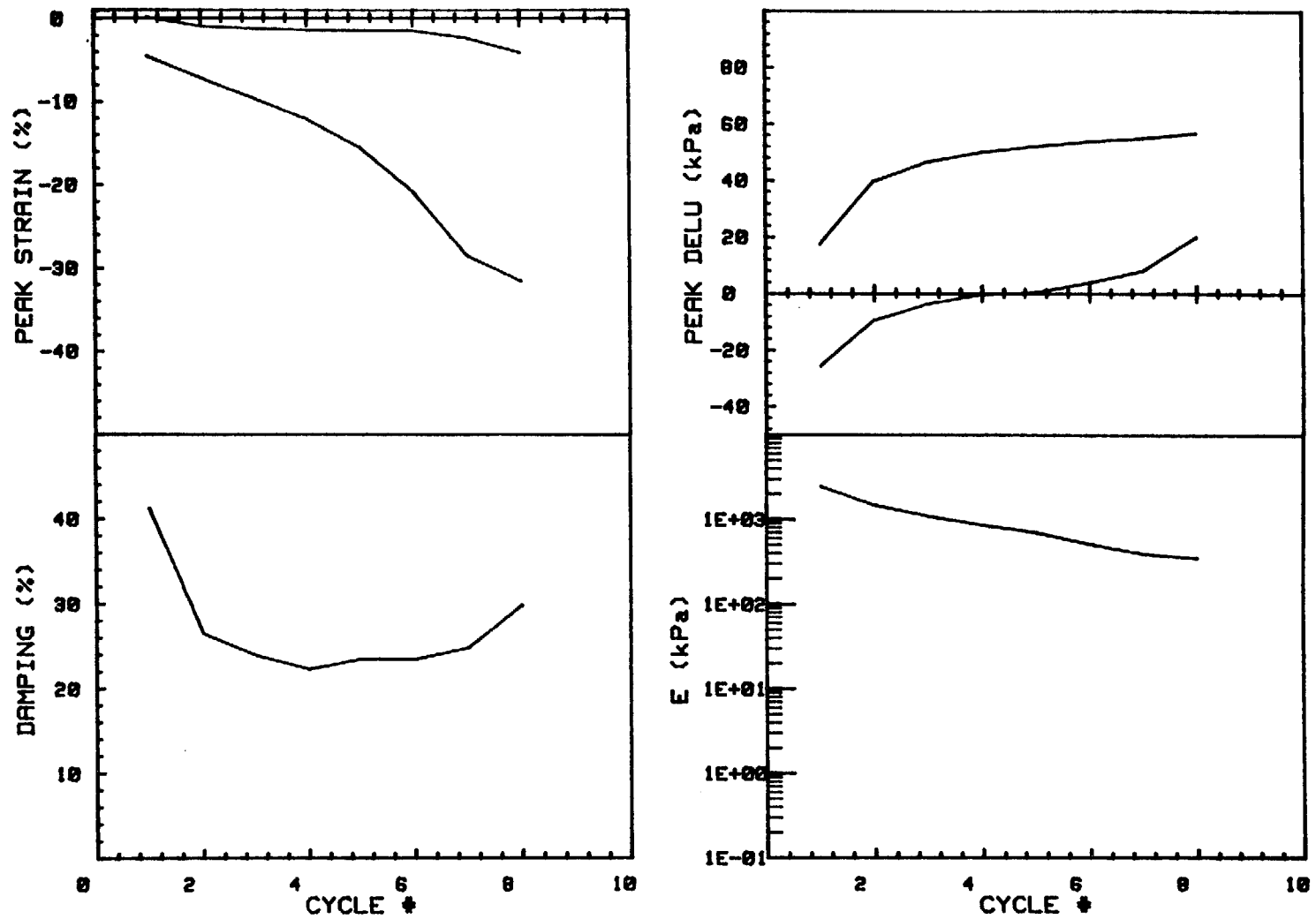
CRUISE DC1-81-EG		INCREMENT (cm)		100-108
CORE NO. 620G2		TEST NO.		TC47
SIG1c' (kPa)	117.6	STATIC qf (kPa)	53.2	
SIG3c' (kPa)	117.6	AVG MAX q (kPa)	46.1 (86.7%)	
INDUCED OCR	1.0	AVG MIN q (kPa)	-38.4 (68.4%)	



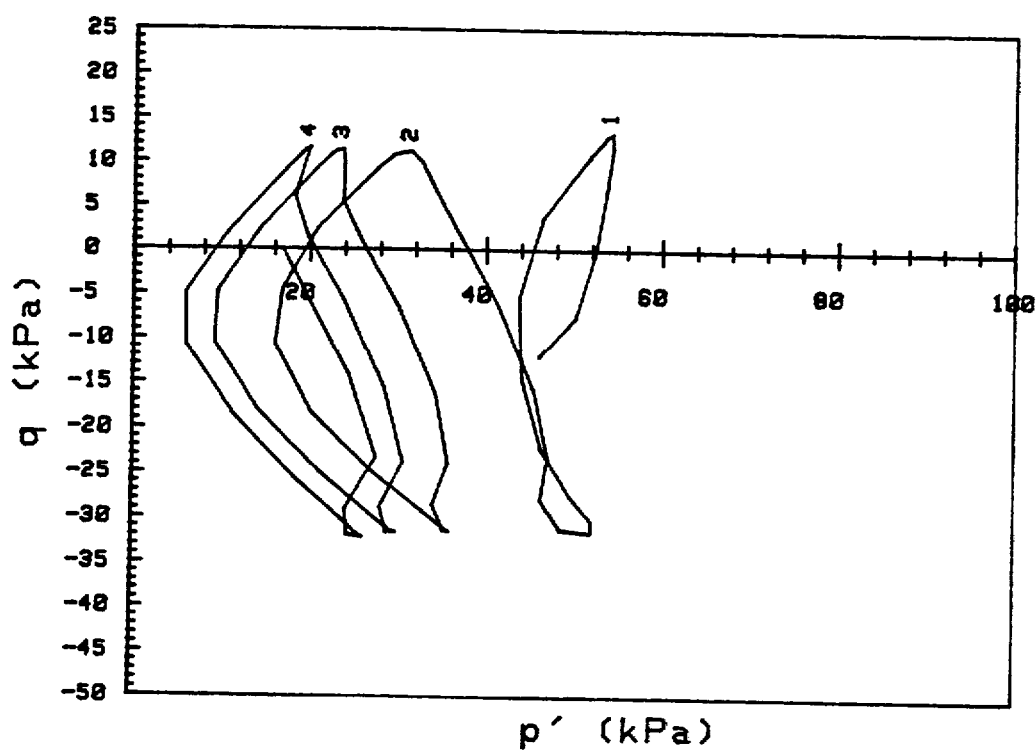
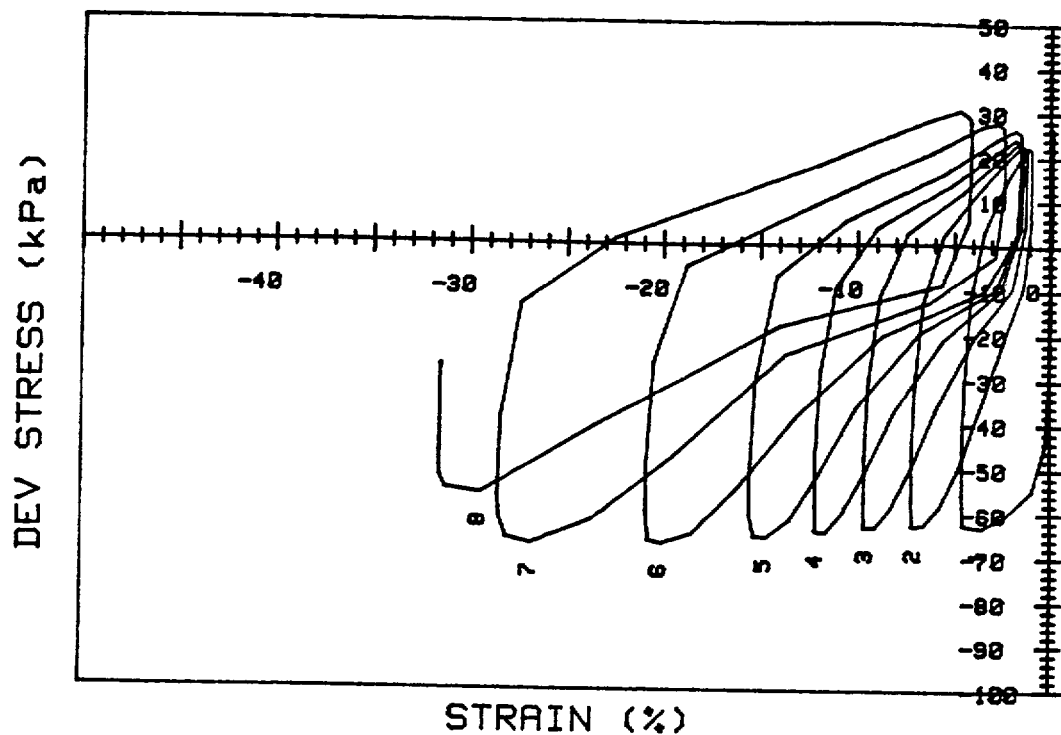
CRUISE DC1-81-EG	INCREMENT (cm)	61-69
CORE NO. 634G2	TEST NO.	TC48
SIG1c' (kPa) 60.3	STATIC qf (kPa)	23.9
SIG3c' (kPa) 60.3	AVG MAX q (kPa)	14.9 (62.3%)
INDUCED OCR 1.0	AVG MIN q (kPa)	-40.6 (169.9%)



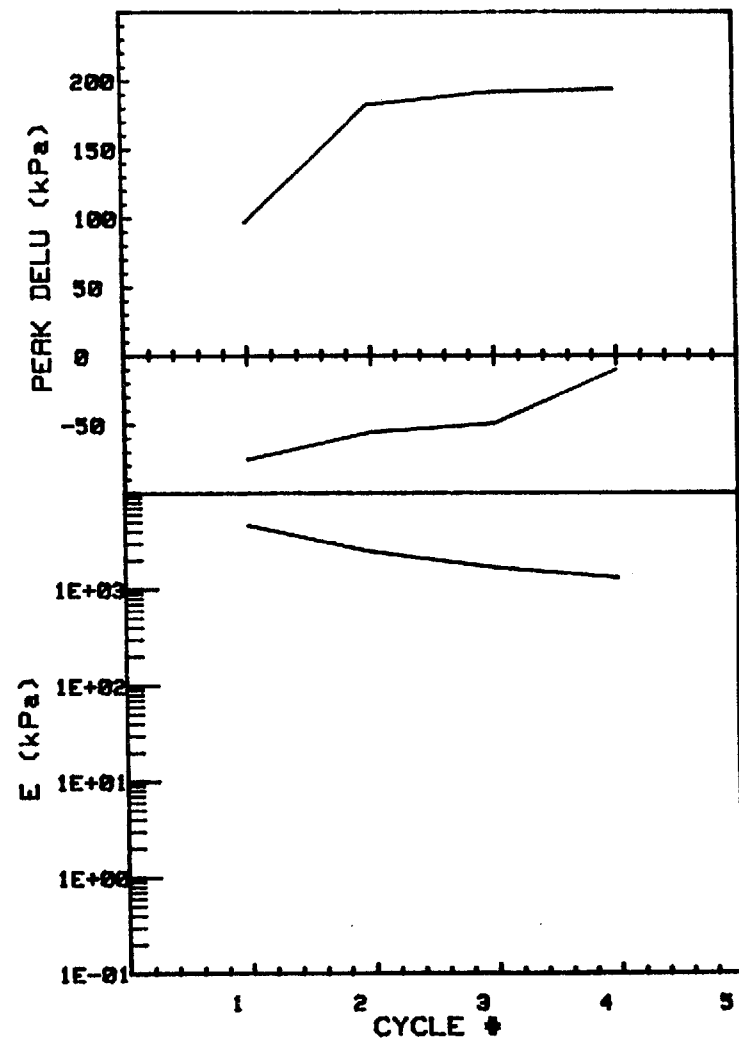
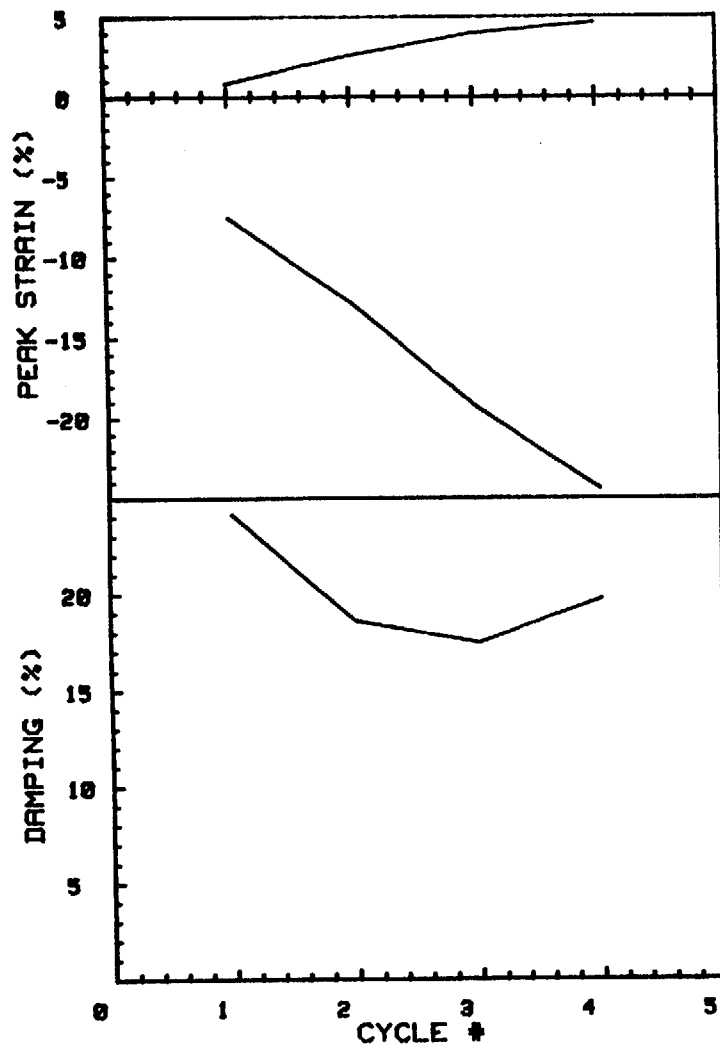
CRUISE DC1-81-EG		INCREMENT (cm)	
CORE NO.	634G2	TEST NO.	61-69 TC48
SIG1c' (kPa)	60.3	STATIC qf (kPa)	23.9
SIG3c' (kPa)	60.3	AVG MAX q (kPa)	14.9 (62.3%)
INDUCED OCR	1.0	AVG MIN q (kPa)	-40.6 (169.9%)



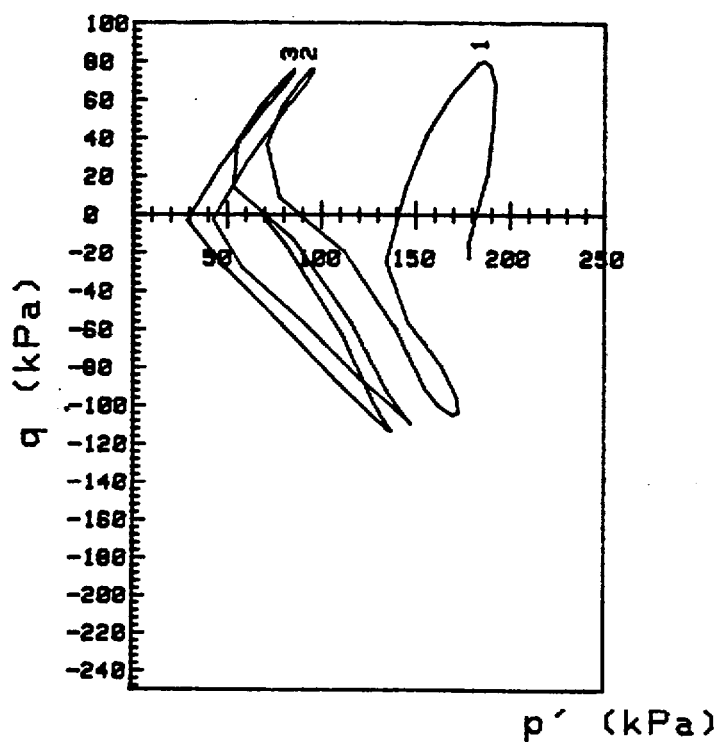
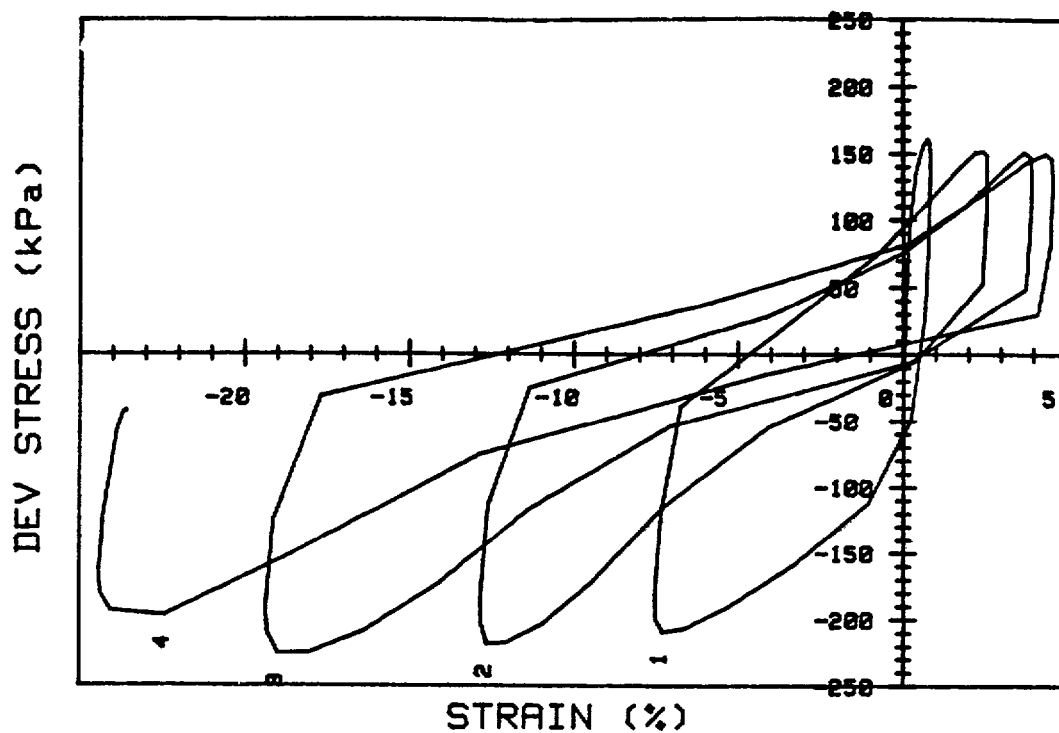
CRUISE DC1-81-EG		INCREMENT (cm)	61-68
CORE NO. 634G2		TEST NO.	TC49
SIG1c' (kPa)	58.1	STATIC qf (kPa)	23.9
SIG3c' (kPa)	58.1	AVG MAX q (kPa)	12.7 (53.1%)
INDUCED OCR	1.0	AVG MIN q (kPa)	-31.8 (133.1%)



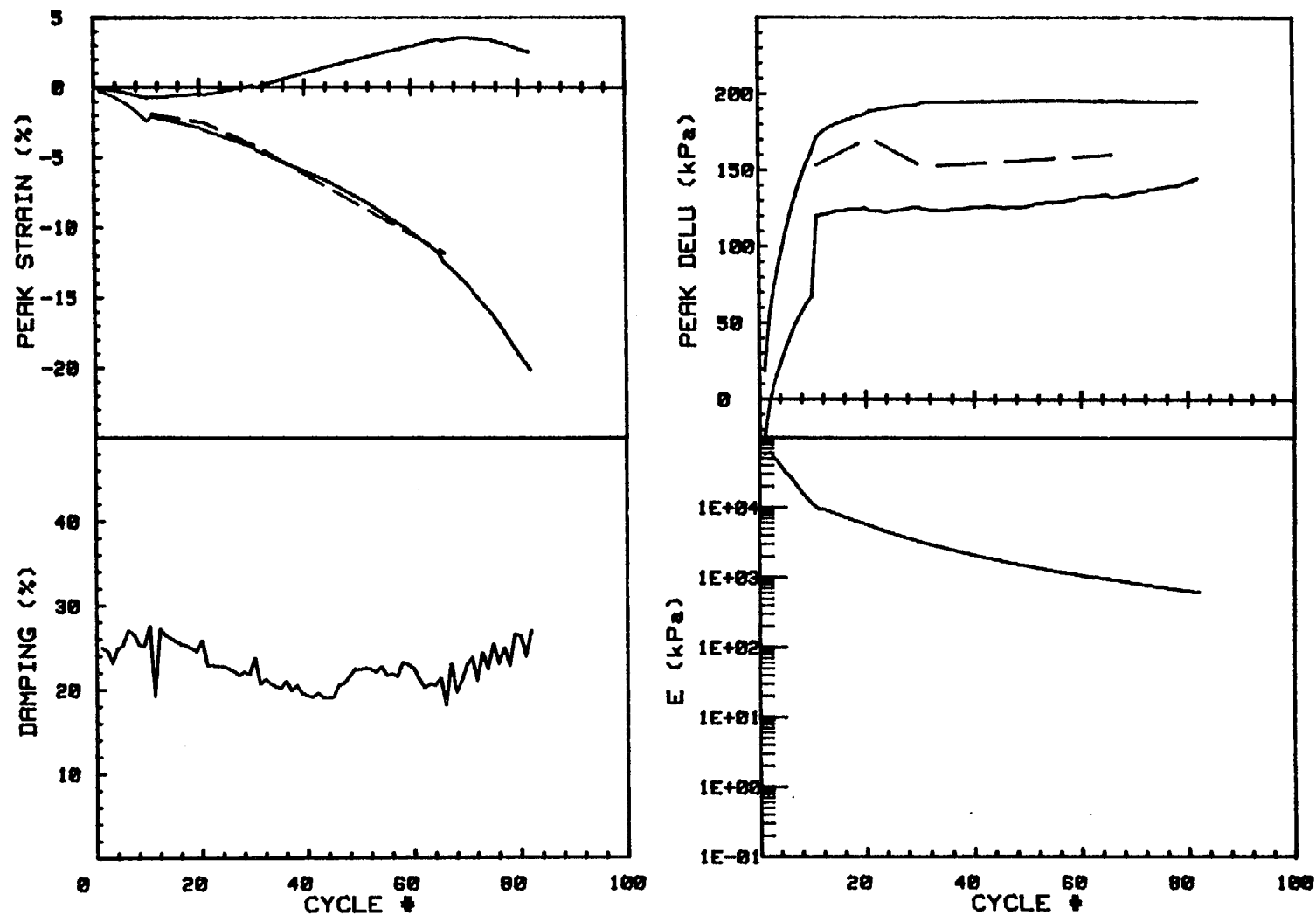
CRUISE DC1-81-EG	INCREMENT (cm)	61-68
CORE NO. 634G2	TEST NO.	TC49
SIG1c' (kPa) 58.1	STATIC qf (kPa)	23.9
SIG3c' (kPa) 58.1	AVG MAX q (kPa)	12.7 (53.1%)
INDUCED OCR 1.0	AVG MIN q (kPa)	-31.8 (133.1%)



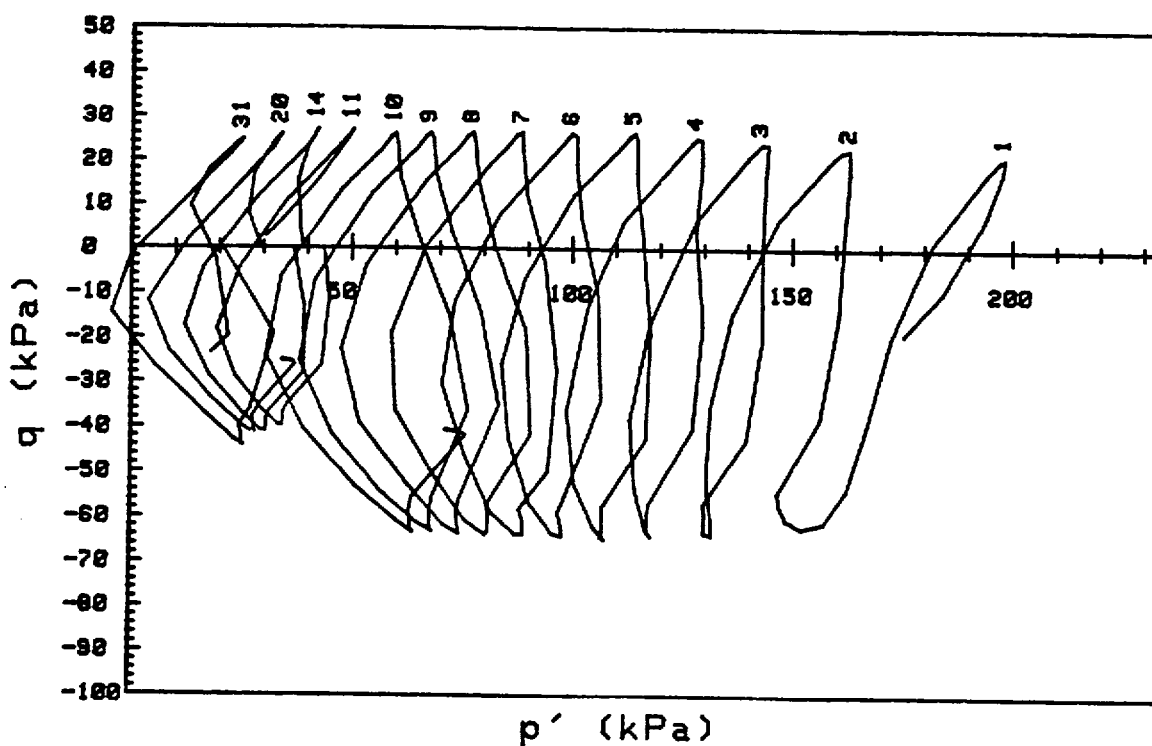
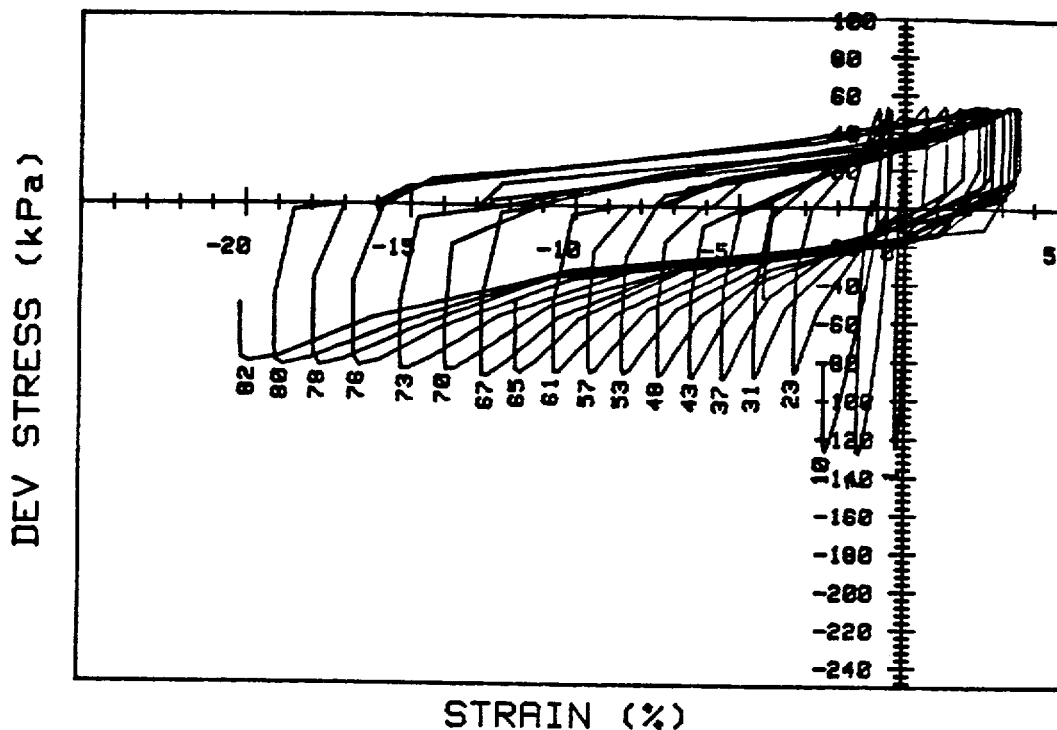
CRUISE DC2-80-EG		INCREMENT (cm) 161-172	
CORE NO. 87G		TEST NO. TC52	
SIG1c' (kPa)	200.9	STATIC qf (kPa)	122.8
SIG3c' (kPa)	200.9	AVG MAX q (kPa)	76.8 (62.5%)
INDUCED OCR	1.0	AVG MIN q (kPa)	-106.3 (86.6%)



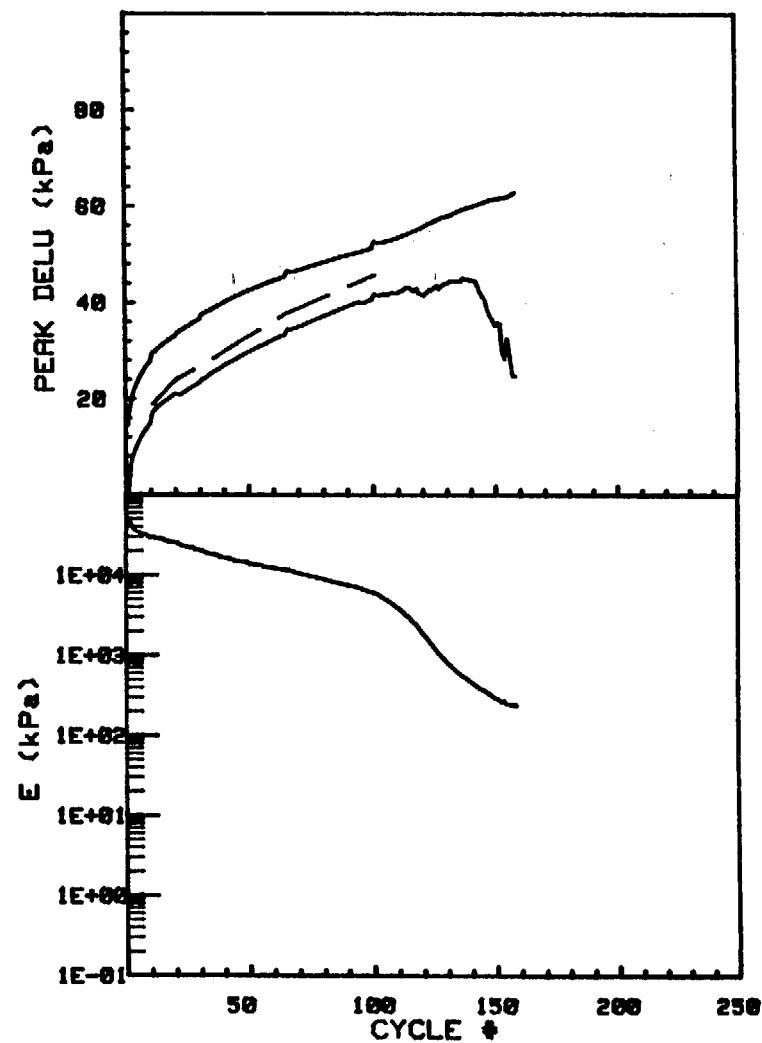
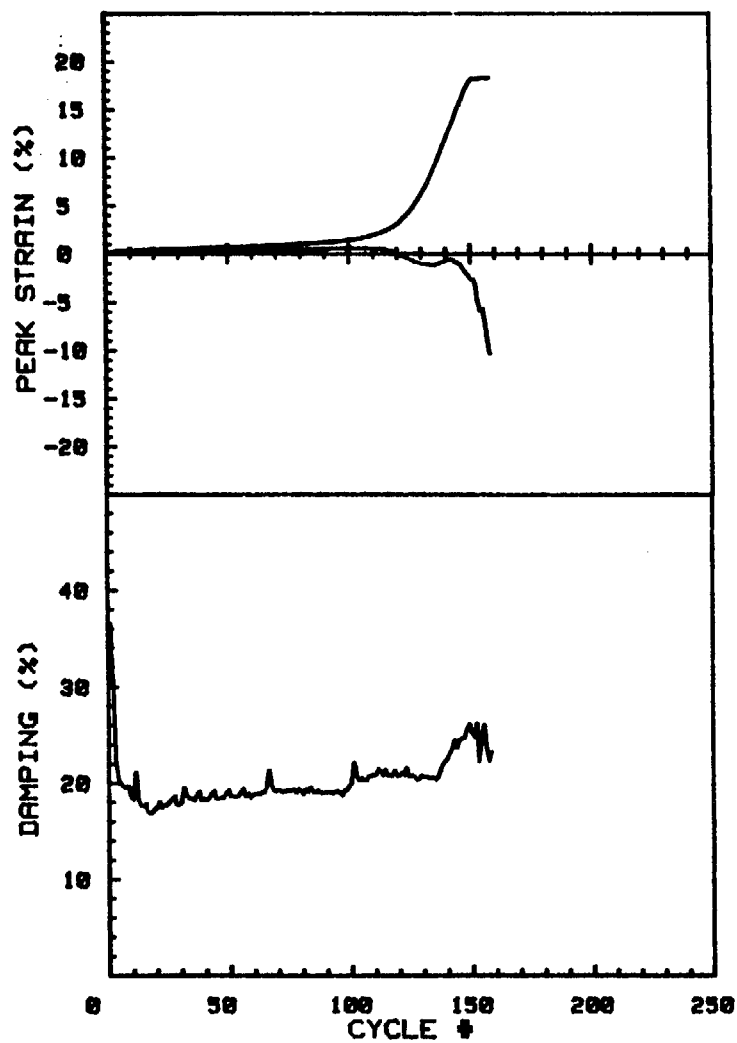
CRUISE DC2-80-EG	INCREMENT (cm)	161-172
CORE NO. 87G	TEST NO.	TC52
SIG1c' (kPa) 200.9	STATIC qf (kPa)	122.8
SIG3c' (kPa) 200.9	AVG MAX q (kPa)	76.8 (62.5%)
INDUCED OCR 1.0	AVG MIN q (kPa)	-106.3 (86.6%)



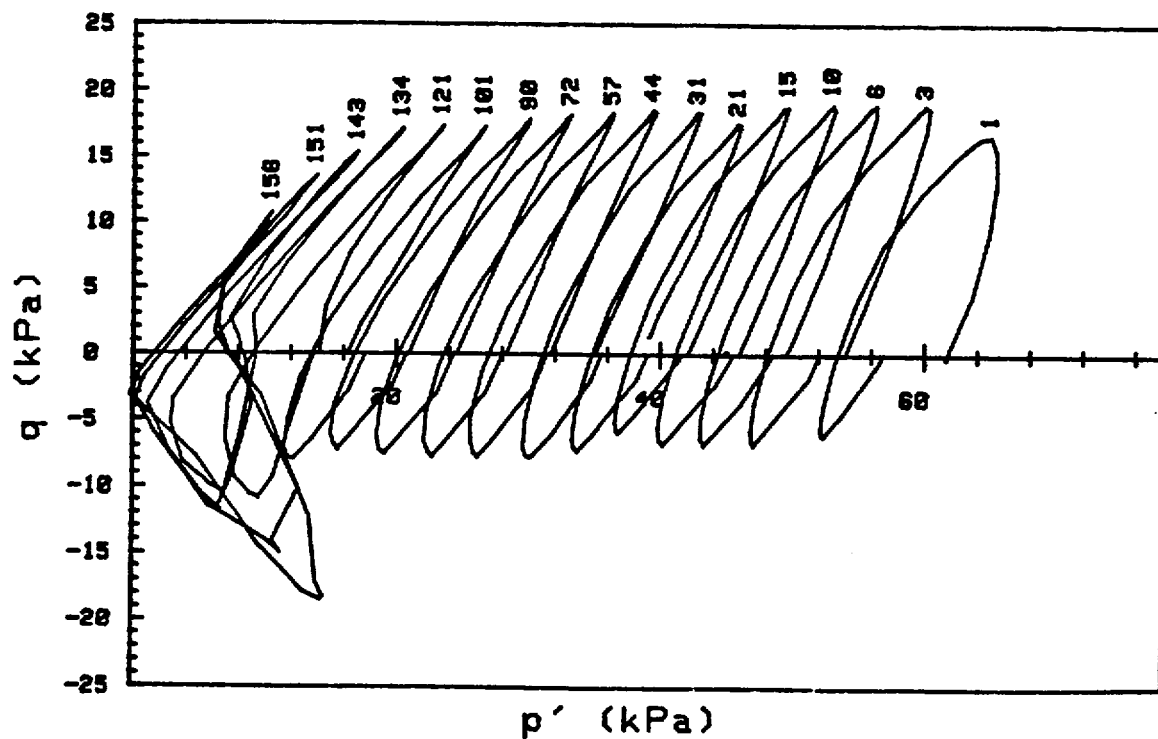
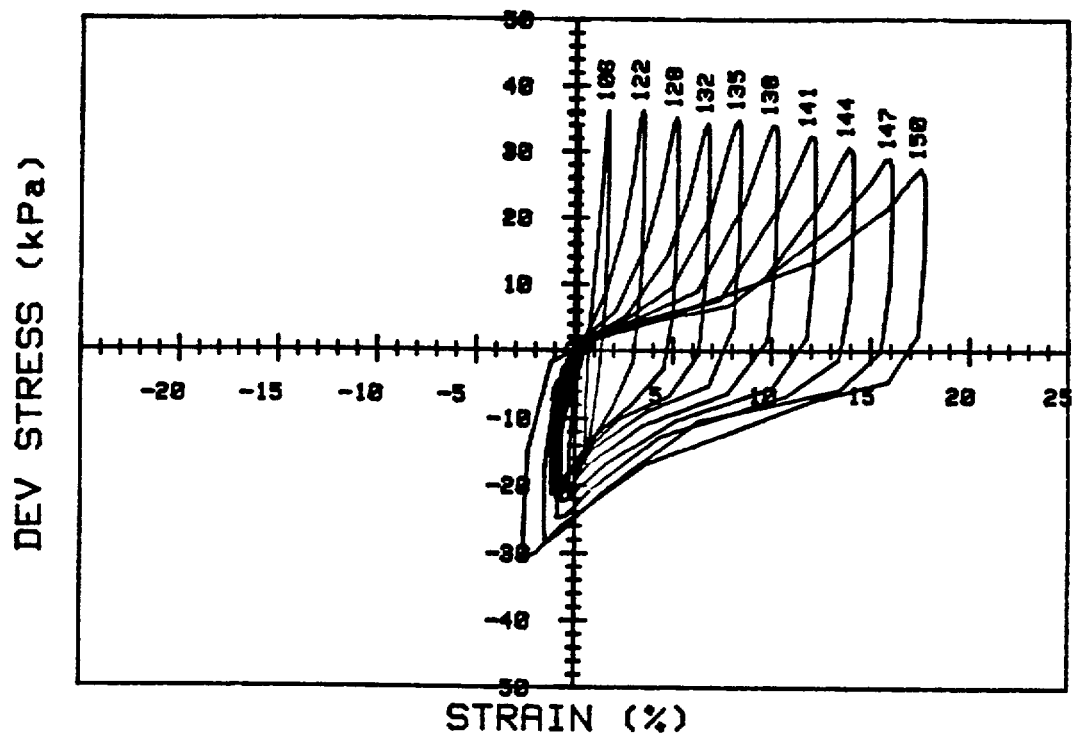
CRUISE DC2-80-EG		INCREMENT (cm) 161-172	
CORE NO. 87G		TEST NO. TC53	
SIG1c' (kPa)	194.3	STATIC qf (kPa)	122.8
SIG3c' (kPa)	194.3	AVG MAX q (kPa)	26.4 (21.5%)
INDUCED OCR	1.0	AVG MIN q (kPa)	-45.5 (37.1%)



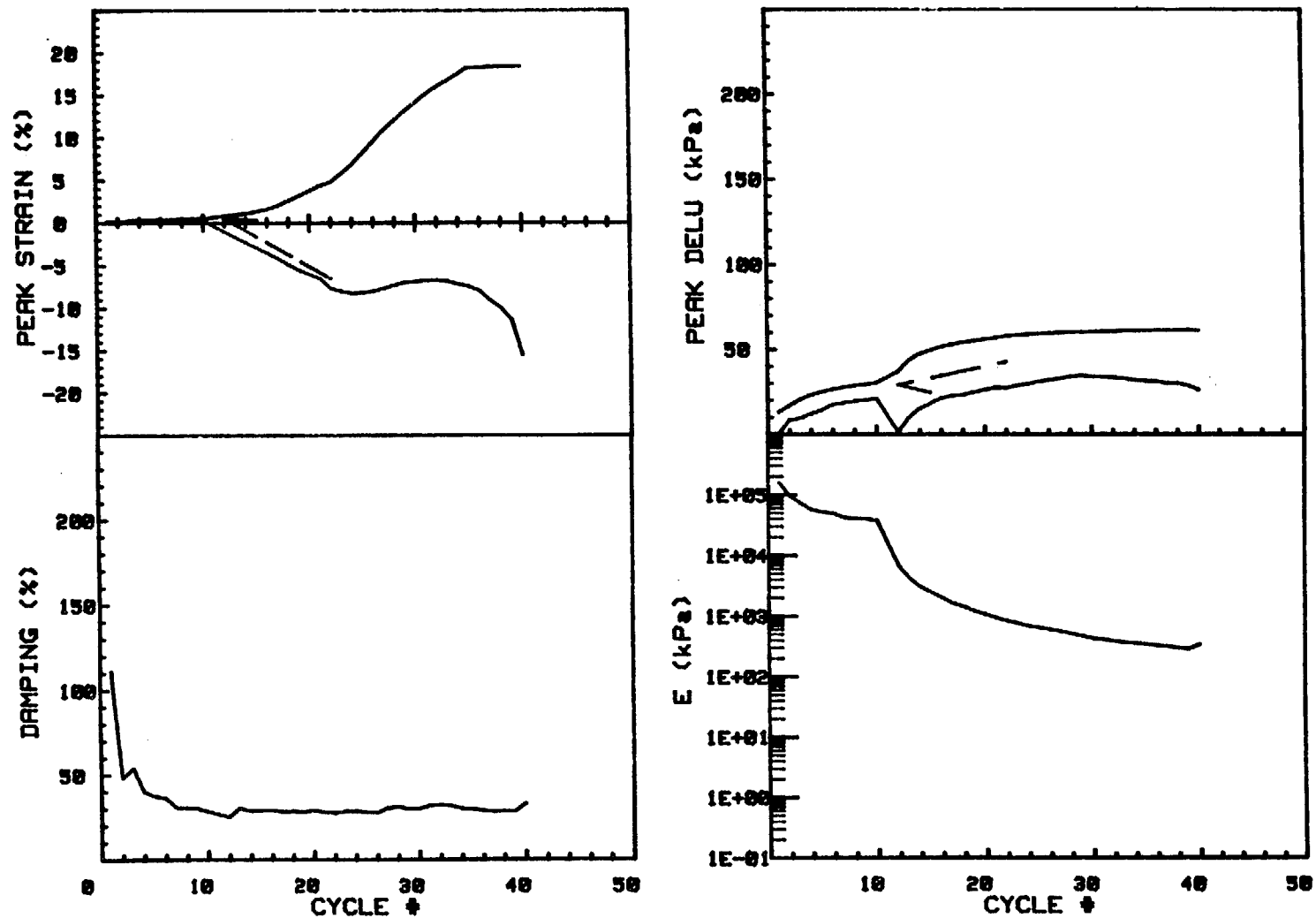
CRUISE DC2-80-EG		INCREMENT (cm)		161-172
CORE NO. 87G		TEST NO.		TC53
SIG1c' (kPa)	194.3	STATIC qf (kPa)	122.8	
SIG3c' (kPa)	194.3	AVG MAX q (kPa)	26.4 (21.5%)	
INDUCED OCR	1.0	AVG MIN q (kPa)	-45.5 (37.1%)	



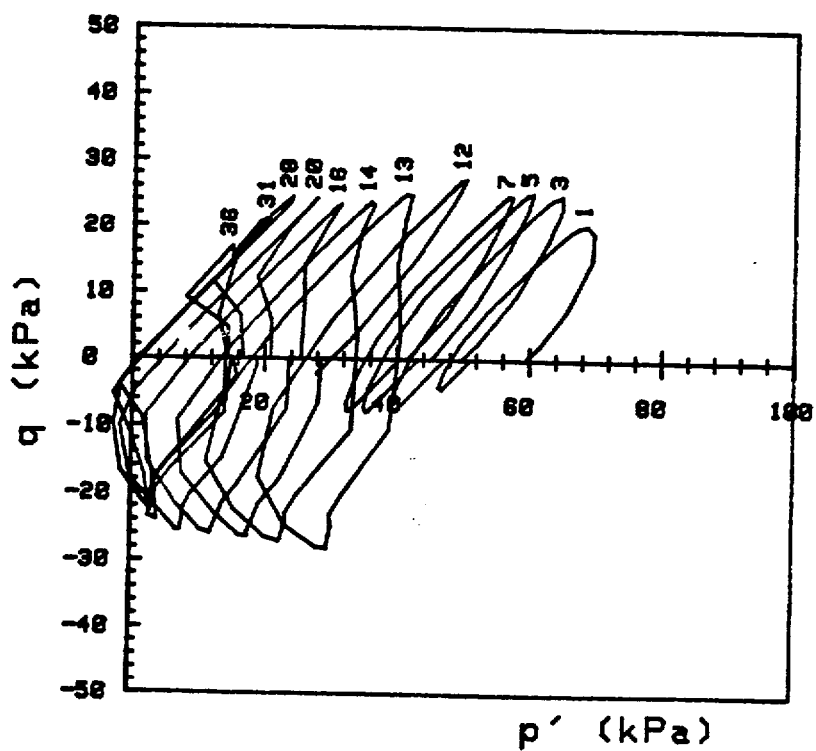
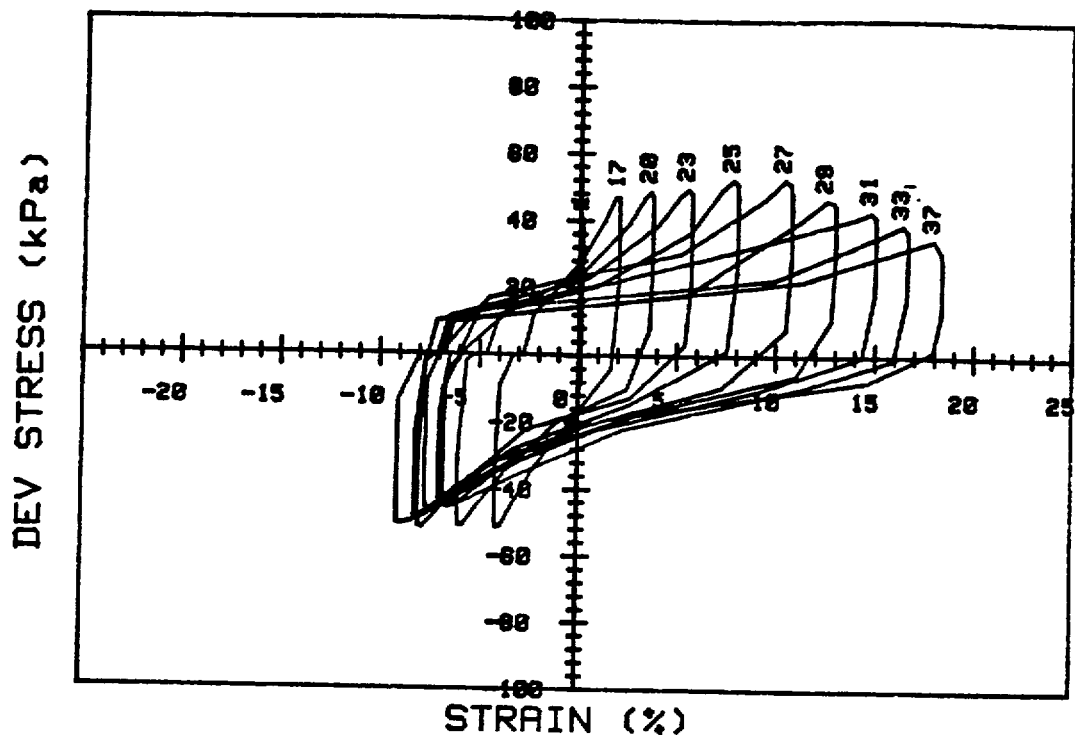
CRUISE DC1-81-EG	INCREMENT (cm)	72-82
CORE NO. 634G2	TEST NO.	TC54
SIG1c' (kPa) 61.9	STATIC qf (kPa)	23.9
SIG3c' (kPa) 61.9	AVG MAX q (kPa)	17.6 (73.6%)
INDUCED OCR 1.0	AVG MIN q (kPa)	-8.8 (36.8%)



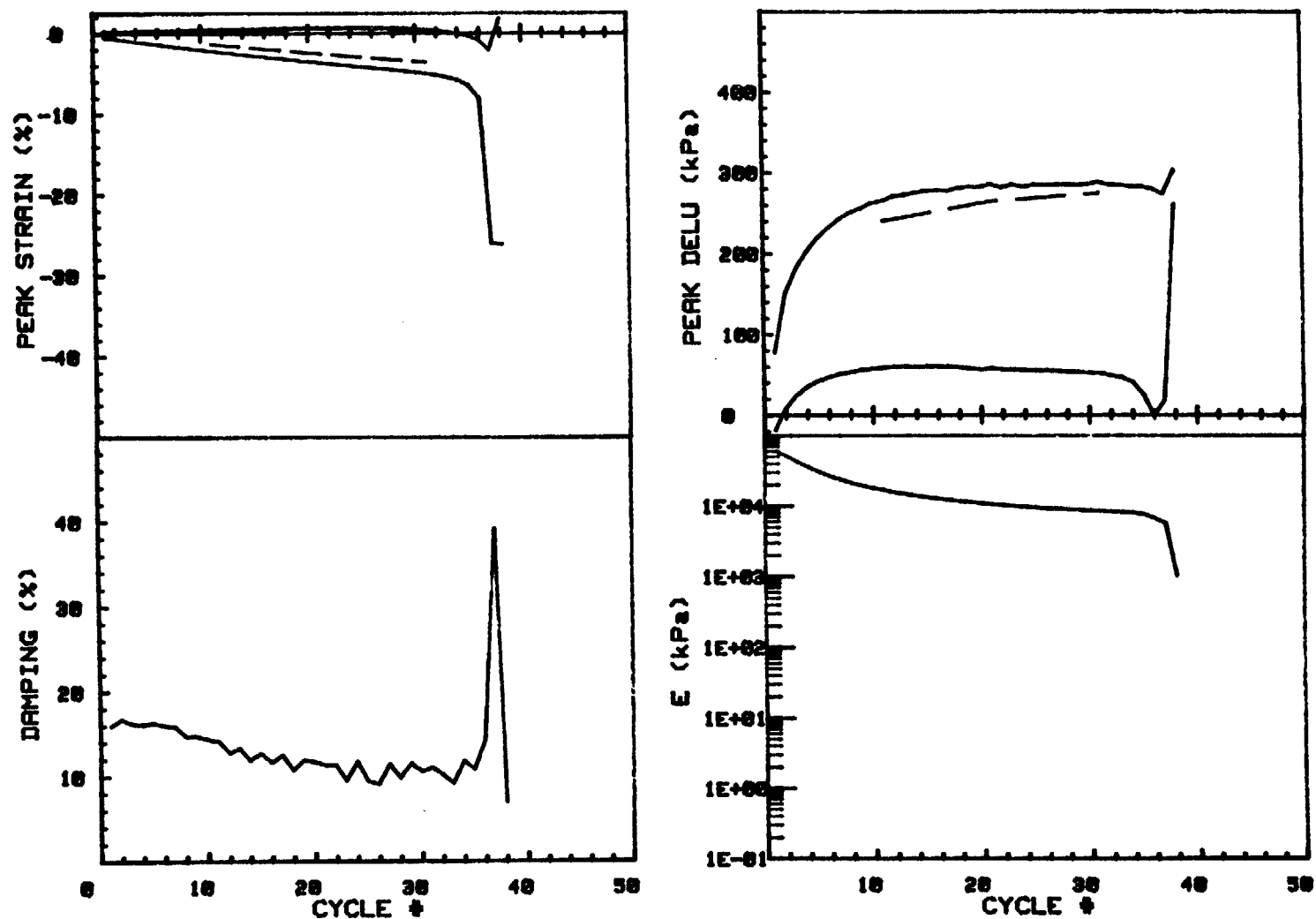
CRUISE DC1-81-EG		INCREMENT (cm)		72-82
CORE NO.	634G2	TEST NO.		TC54
SIG1c' (kPa)	61.9	STATIC qf (kPa)	23.9	
SIG3c' (kPa)	61.9	AVG MAX q (kPa)	17.6 (73.6%)	
INDUCED OCR	1.0	AVG MIN q (kPa)	-8.8 (36.8%)	



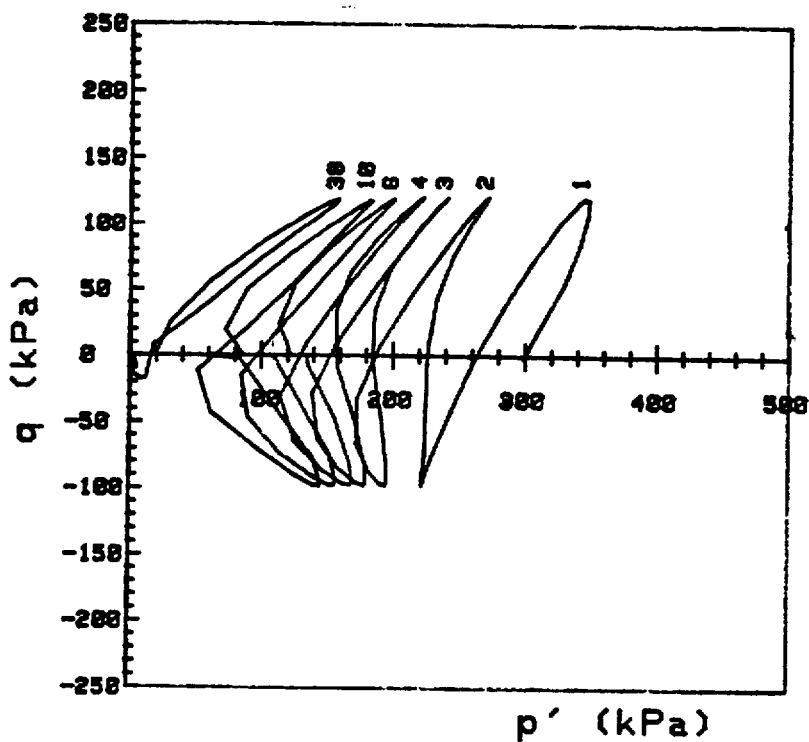
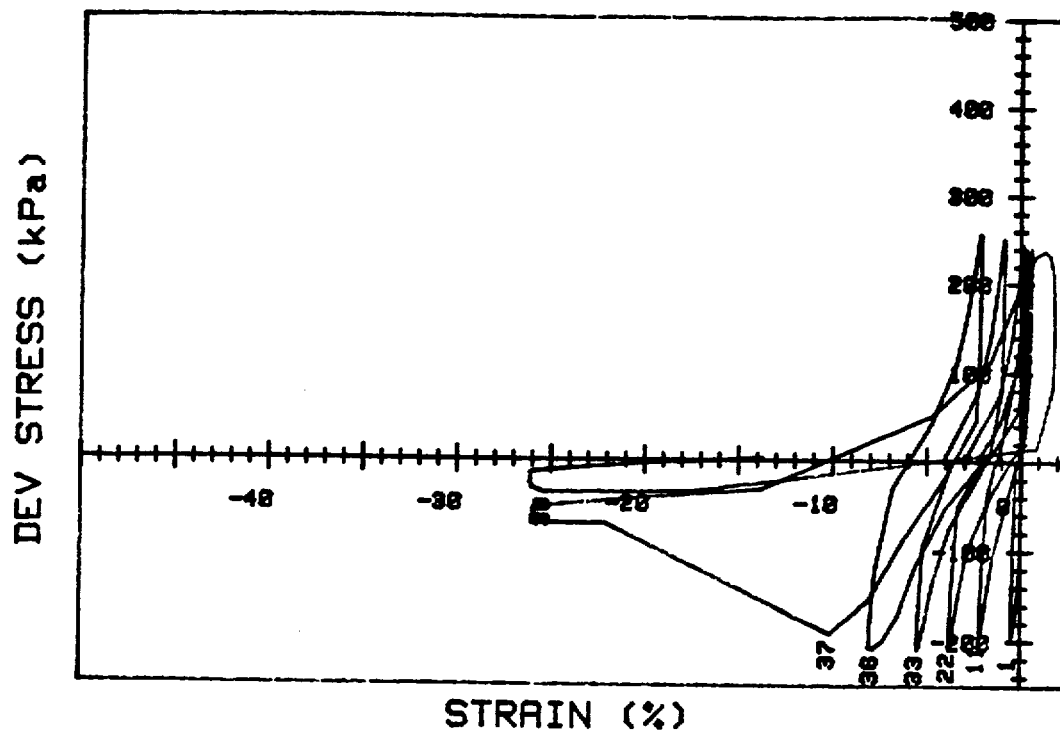
CRUISE DC1-81-EG		INCREMENT (cm) 72-82	
CORE NO. 634G2		TEST NO. TC55	
SIG1c'(kPa)	59.3	STATIC qf (kPa)	23.9
SIG3c'(kPa)	59.3	AVG MAX q (kPa)	22.2 (92.9%)
INDUCED OCR	1.0	AVG MIN q (kPa)	-19.9 (83.3%)



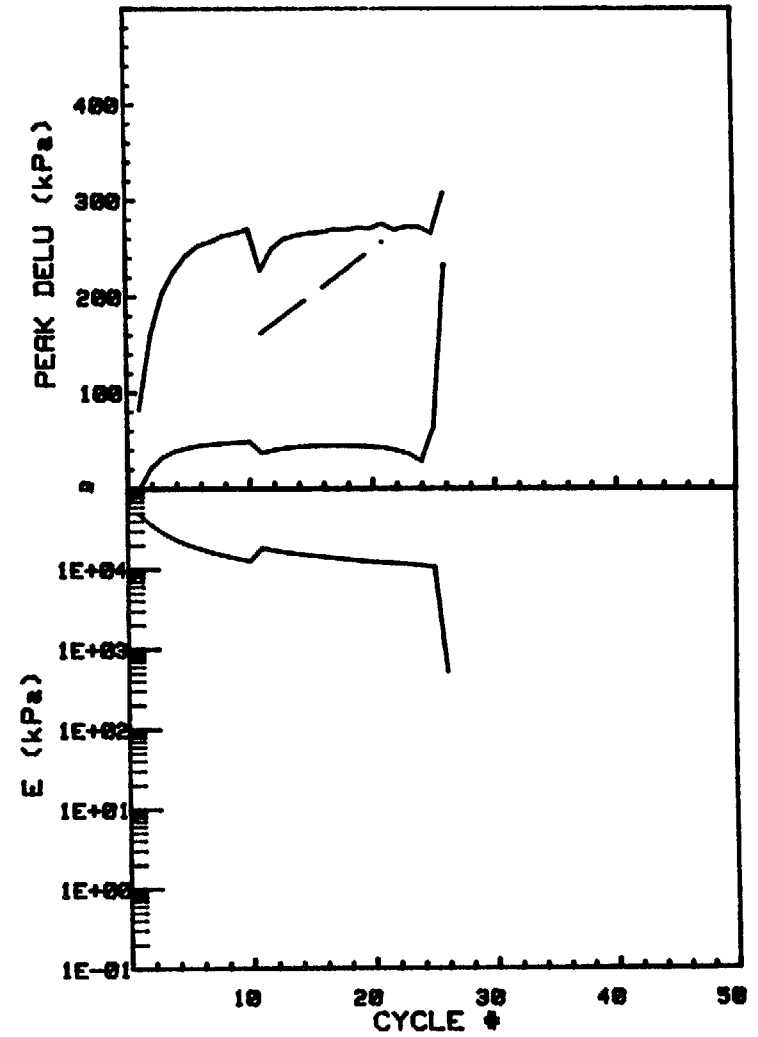
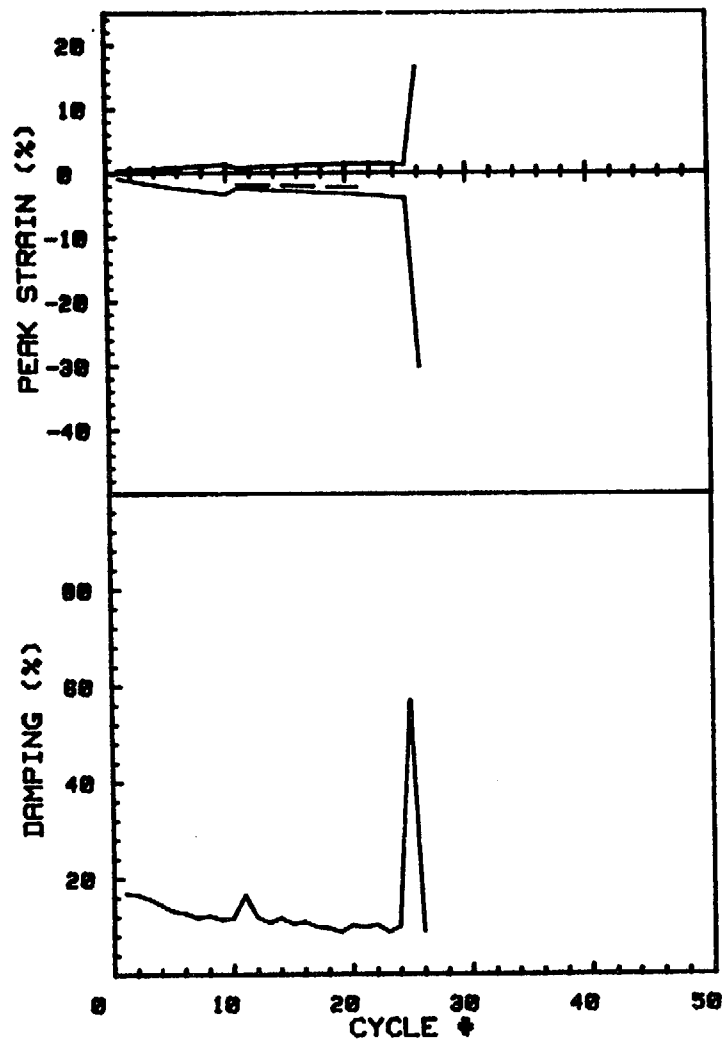
CRUISE DC1-81-EG	INCREMENT (cm)	72-82
CORE NO. 634G2	TEST NO.	TC55
SIG1c'(kPa) 59.3	STATIC qf (kPa)	23.9
SIG3c'(kPa) 59.3	AVG MAX q (kPa)	22.2 (92.9%)
INDUCED OCR 1.0	AVG MIN q (kPa)	-19.9 (83.3%)



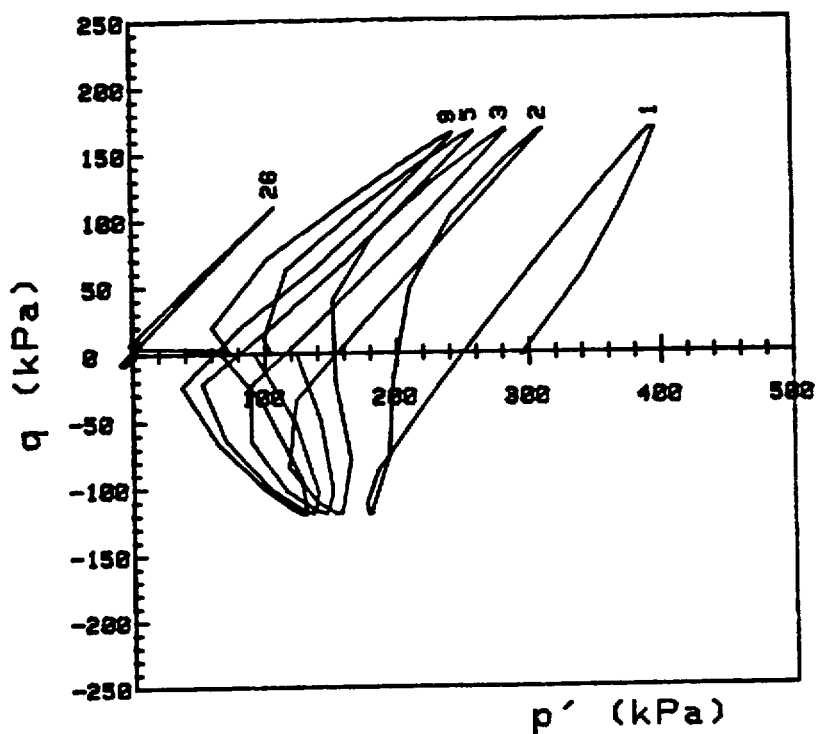
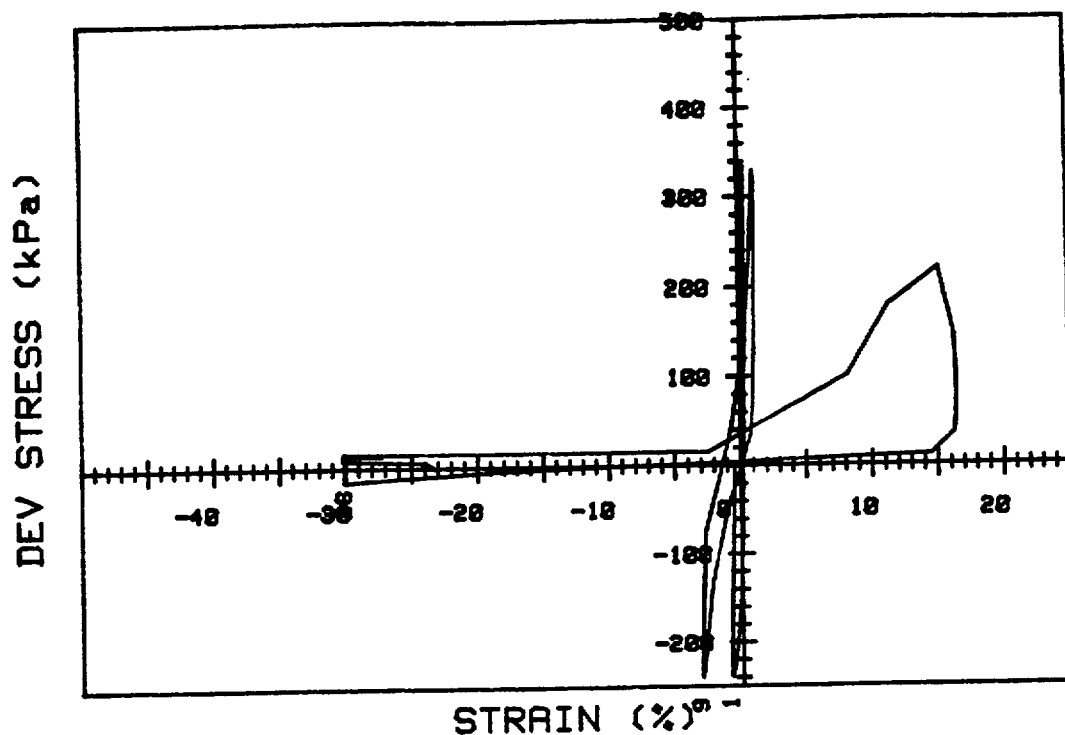
CRUISE DC1-01-EG		INCREMENT (cm) 153-161	
CORE NO. 630A2		TEST NO. TC56	
SIG1c' (kPa)	301.0	STATIC qf (kPa)	562.0
SIG3c' (kPa)	301.0	AVG MAX q (kPa)	120.2 (21.4%)
INDUCED OCR	1.0	AVG MIN q (kPa)	-98.8 (17.6%)



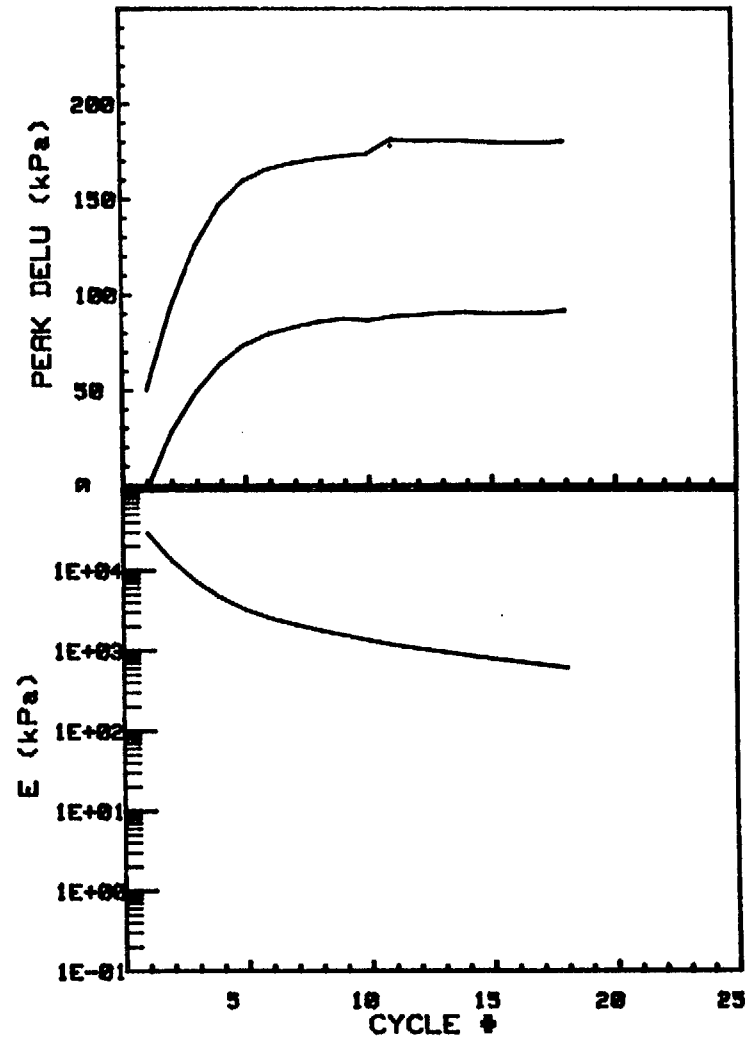
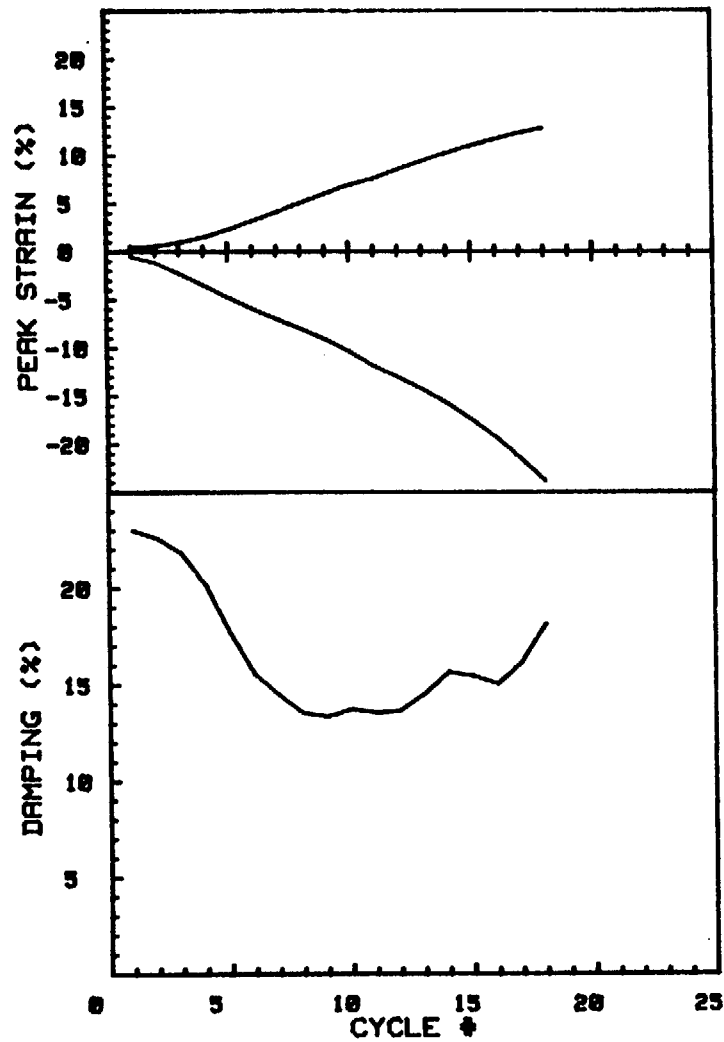
CRUISE DC1-81-EG	INCREMENT (cm)	153-161
CORE NO. 630A2	TEST NO.	TC56
SIG1c' (kPa) 301.0	STATIC qf (kPa)	562.0
SIG3c' (kPa) 301.0	AVG MAX q (kPa)	120.2 (21.4%)
INDUCED OCR 1.0	AVG MIN q (kPa)	-90.8 (17.6%)



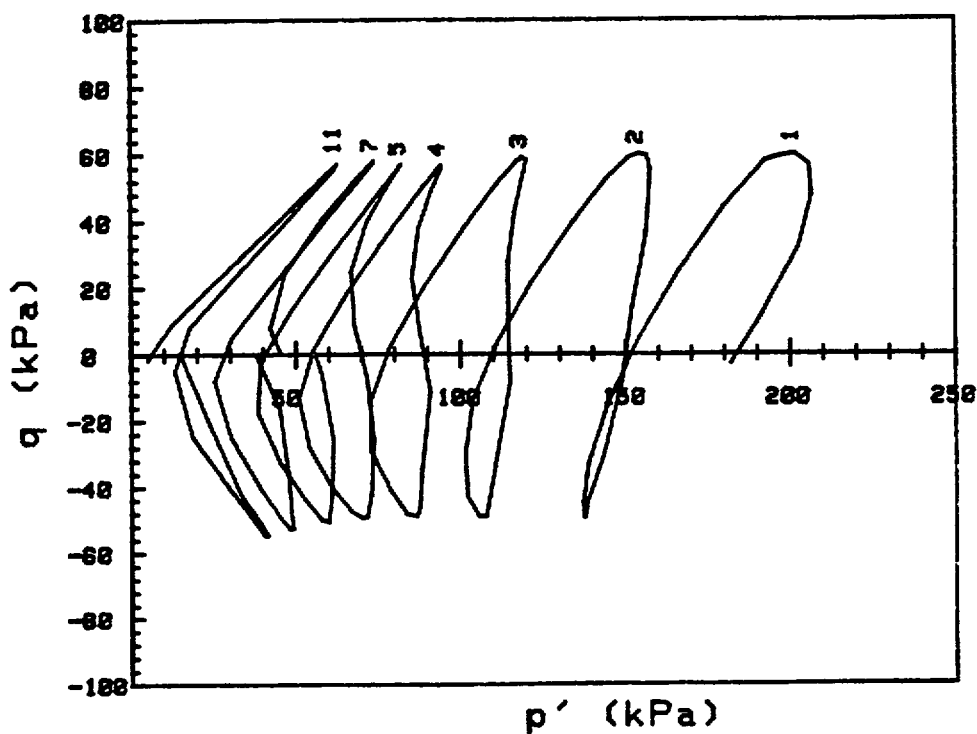
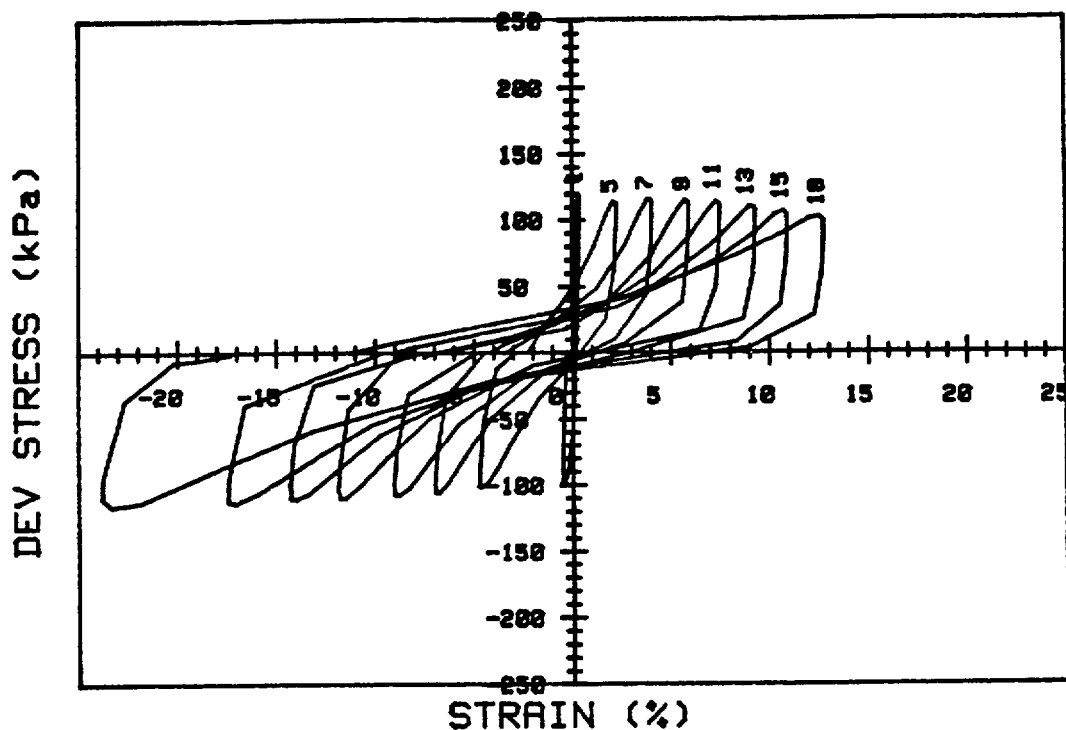
CRUISE DC1-81-EG		INCREMENT (cm)		153-160.5
CORE NO. 630A2		TEST NO.		TC57
SIG1c'(kPa)	297.9	STATIC qf (kPa)	562.0	
SIG3c'(kPa)	297.9	AVG MAX q (kPa)	162.9 (29.0%)	
INDUCED OCR	1.0	AVG MIN q (kPa)	-115.1 (20.5%)	



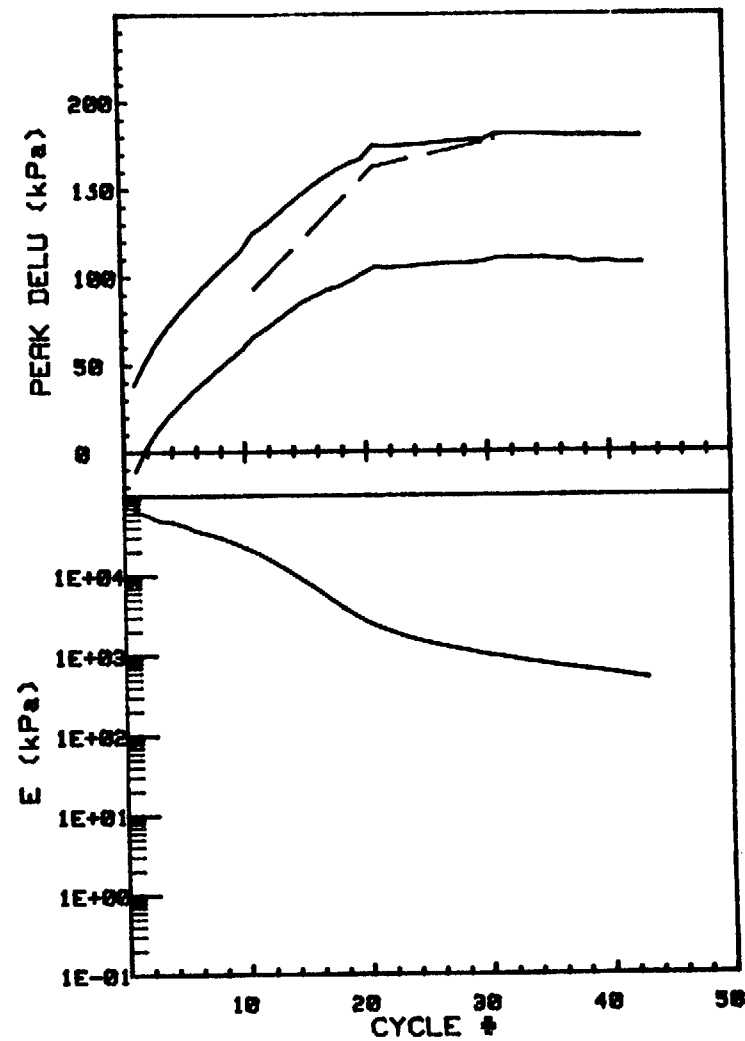
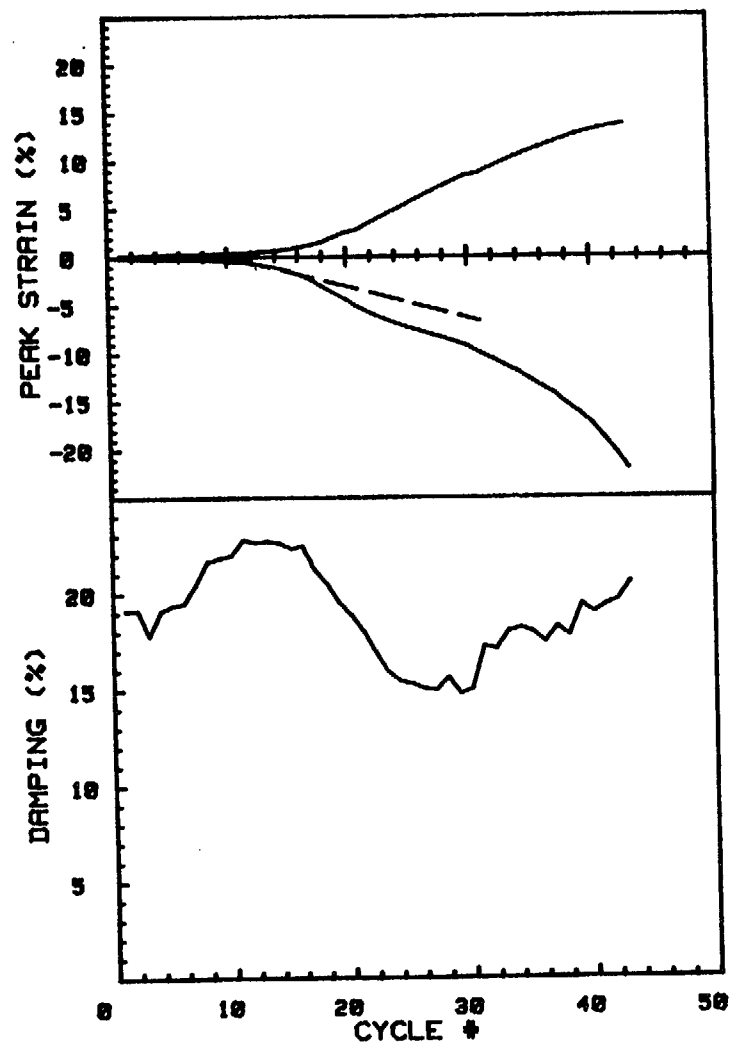
CRUISE DCI-81-EG	INCREMENT (cm)	153-160.5
CORE NO. 630A2	TEST NO.	TC57
SIG1c' (kPa) 297.9	STATIC qf (kPa)	562.0
SIG3c' (kPa) 297.9	AVG MAX q (kPa)	162.9 (29.0%)
INDUCED OCR 1.0	AVG MIN q (kPa)	-115.1 (20.5%)



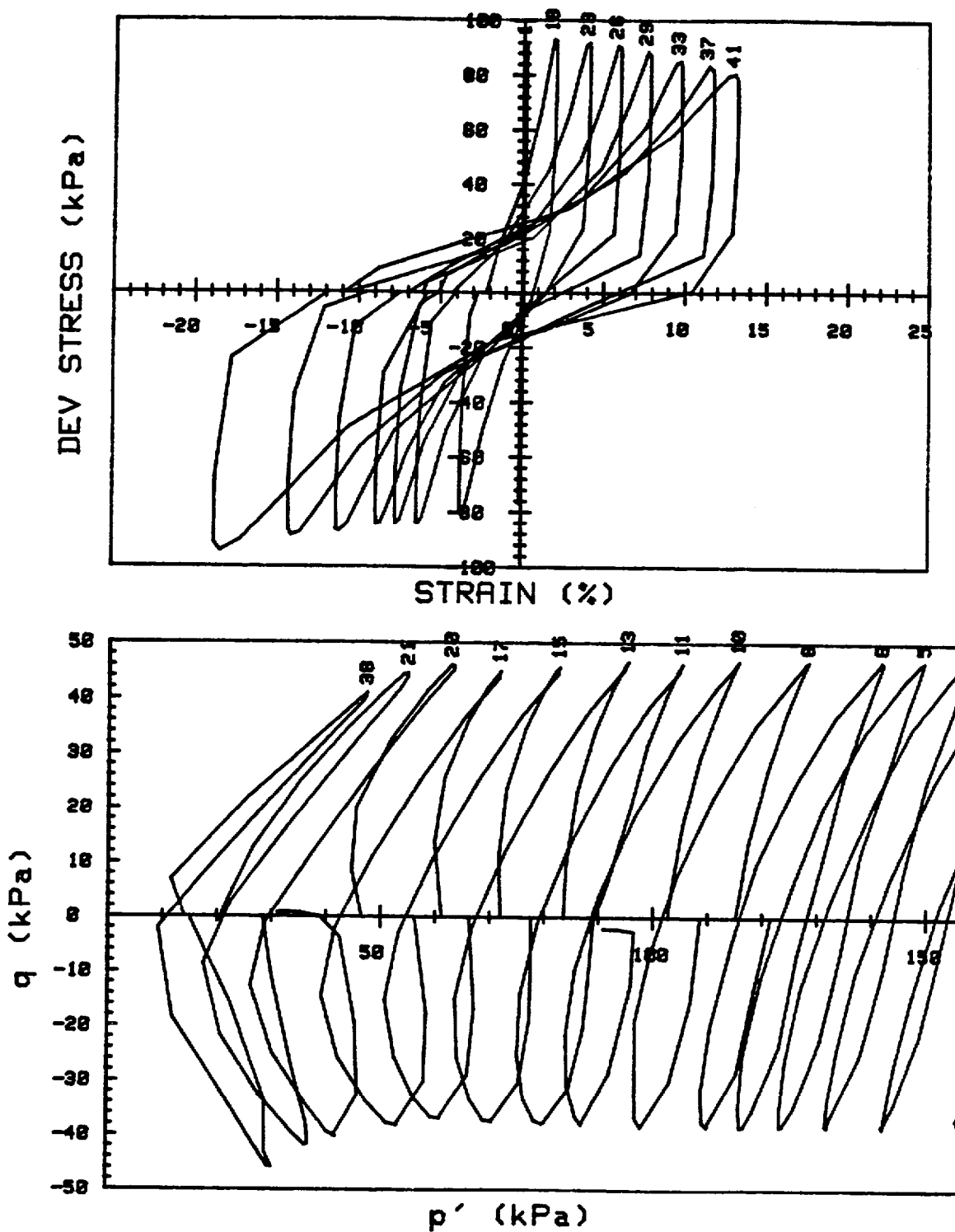
CRUISE DC1-81-EG		INCREMENT (cm)		138-149
CORE NO. 618G2		TEST NO.		TC58
SIG1c' (kPa)	184.8	STATIC qf (kPa)	95.6	
SIG3c' (kPa)	184.8	AVG MAX q (kPa)	56.2 (58.8%)	
INDUCED OCR	1.0	AVG MIN q (kPa)	-53.5 (56.0%)	



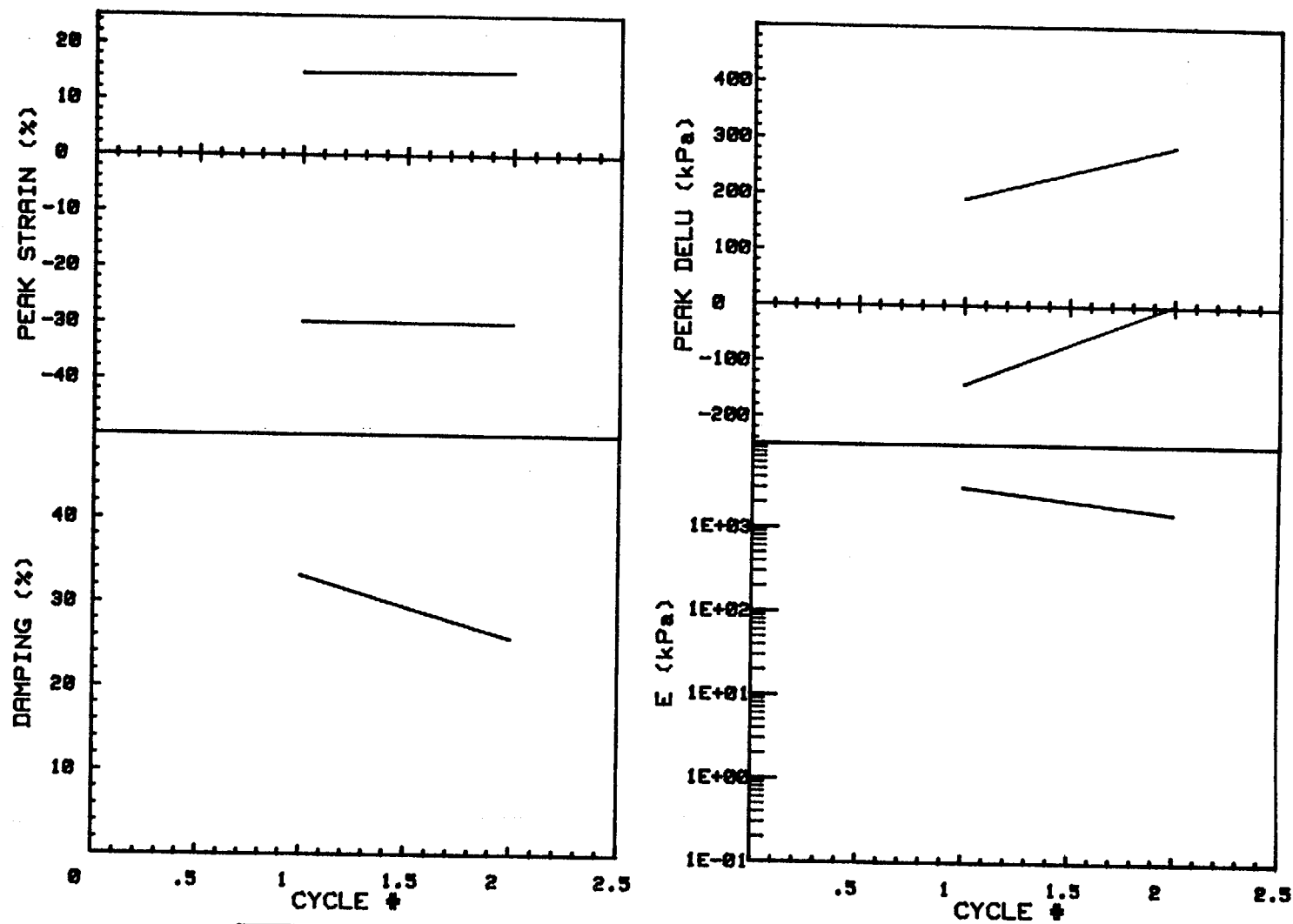
CRUISE DC1-81-EG		INCREMENT (cm)		138-149
CORE NO. 618G2		TEST NO.		TC58
SIG1c'(kPa)	184.8	STATIC qf (kPa)	95.6	
SIG3c'(kPa)	184.8	AVG MAX q (kPa)	56.2 (58.8%)	
INDUCED OCR	1.0	AVG MIN q (kPa)	-53.5 (56.0%)	



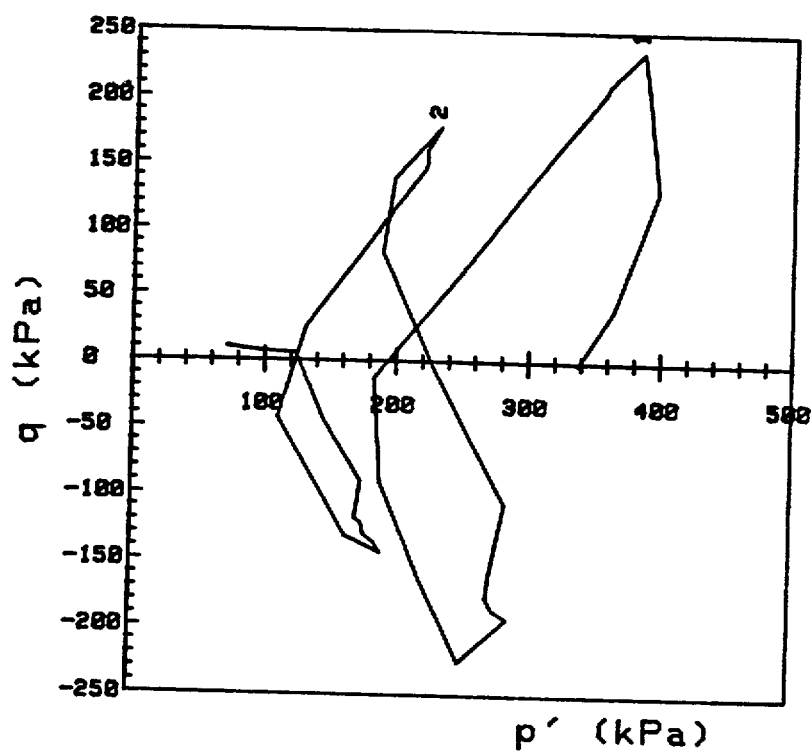
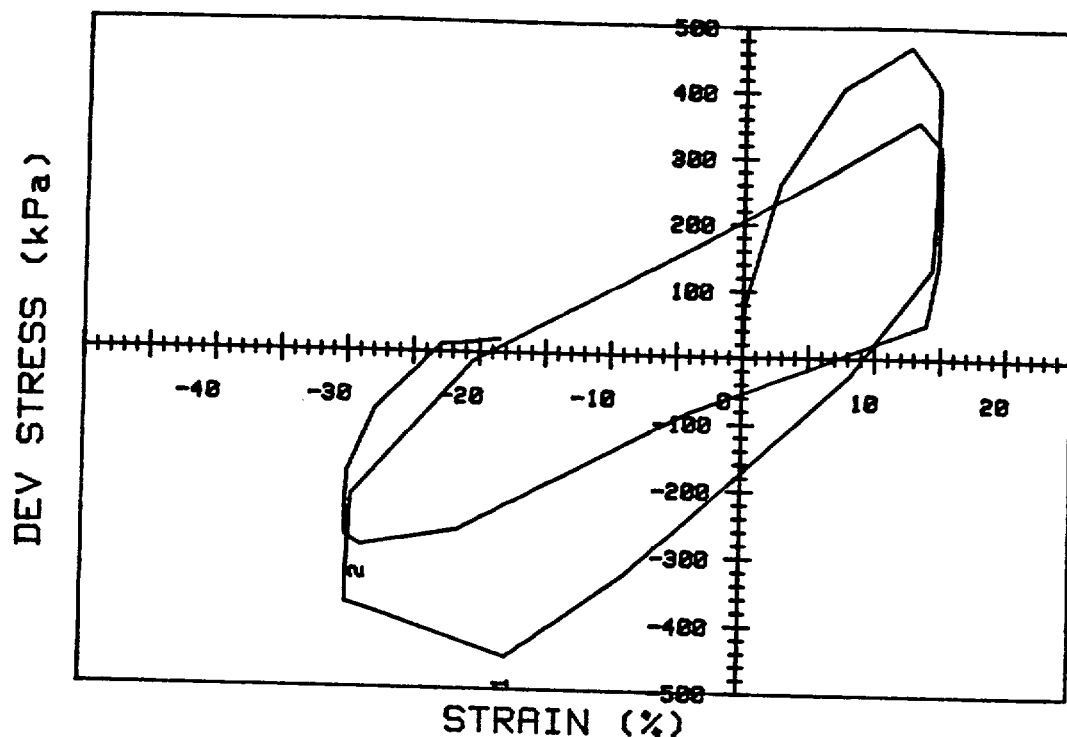
CRUISE DC1-81-EG		INCREMENT (cm)		138-149
CORE NO. 618G2		TEST NO.		TC59
SIG1c'(kPa)	183.9	STATIC qf (kPa)	95.6	
SIG3c'(kPa)	183.9	AVG MAX q (kPa)	44.6 (46.7%)	
INDUCED OCR	1.0	AVG MIN q (kPa)	-41.2 (43.1%)	



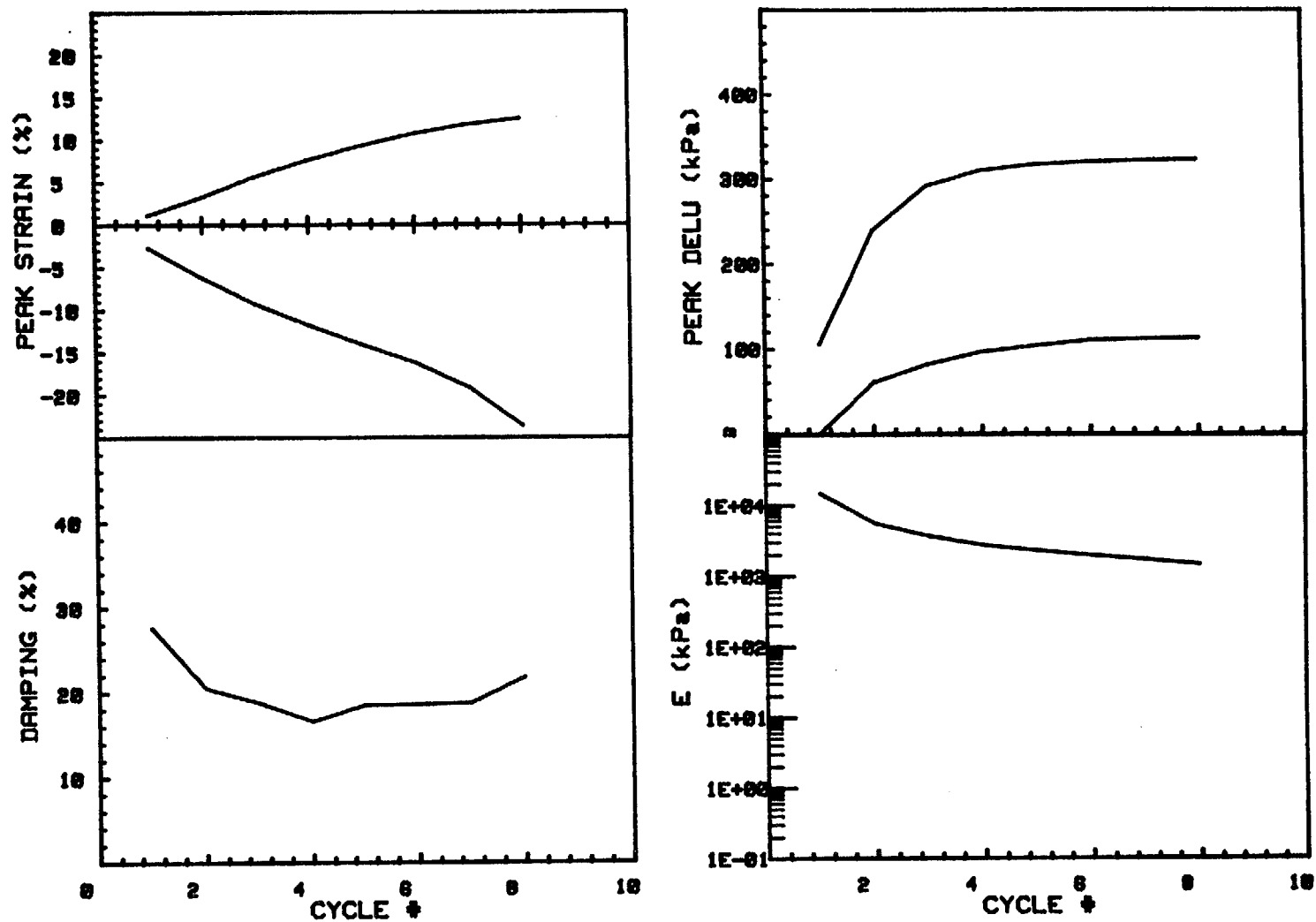
CRUISE DC1-81-EG		INCREMENT (cm)		138-149
CORE NO.	618G2	TEST NO.	TC59	
SIG1c'(kPa)	183.9	STATIC q_f (kPa)	95.6	
SIG3c'(kPa)	183.9	AVG MAX q (kPa)	44.6 (46.7%)	
INDUCED OCR	1.0	AVG MIN q (kPa)	-41.2 (43.1%)	



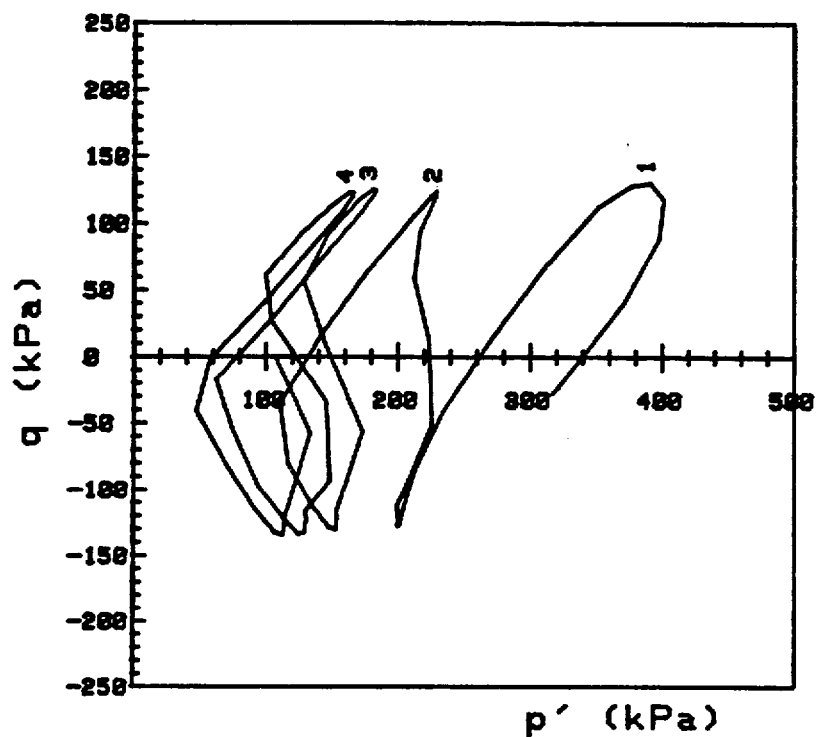
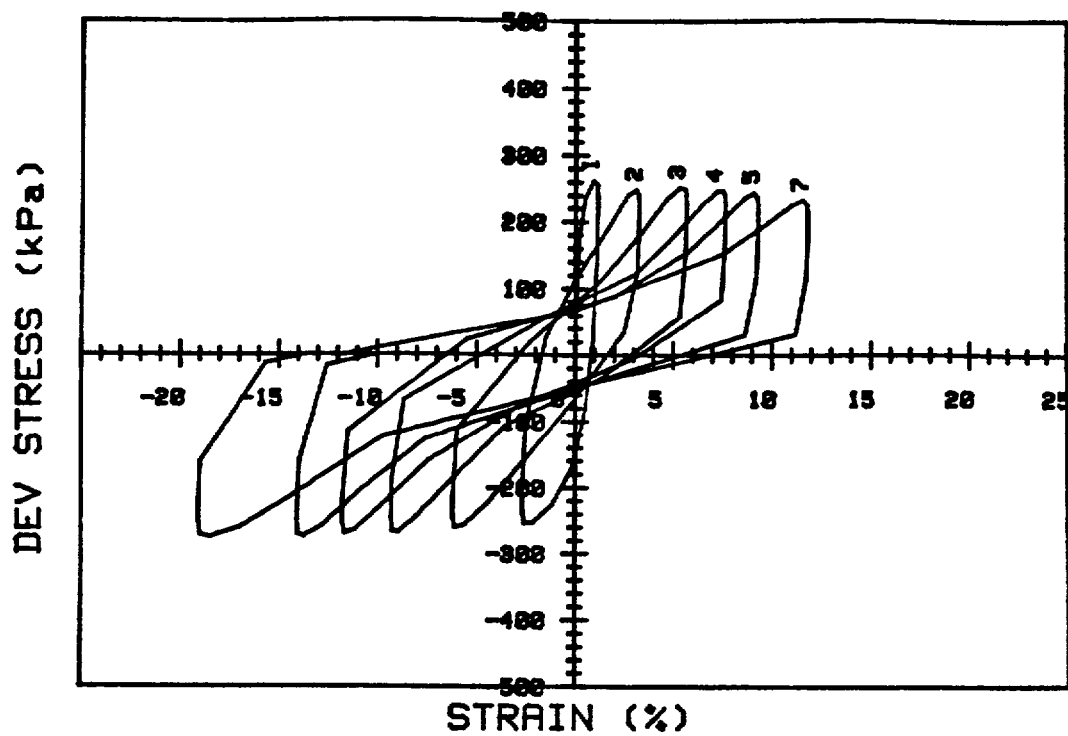
CRUISE DC1-81-EG		INCREMENT (cm)		174-181
CORE NO. 624A1		TEST NO.		TC60
SIG1c' (kPa)	338.9	STATIC qf (kPa)	401.3	
SIG3c' (kPa)	338.9	AVG MAX q (kPa)	206.6 (51.5%)	
INDUCED OCR	1.0	AVG MIN q (kPa)	-184.9 (46.1%)	



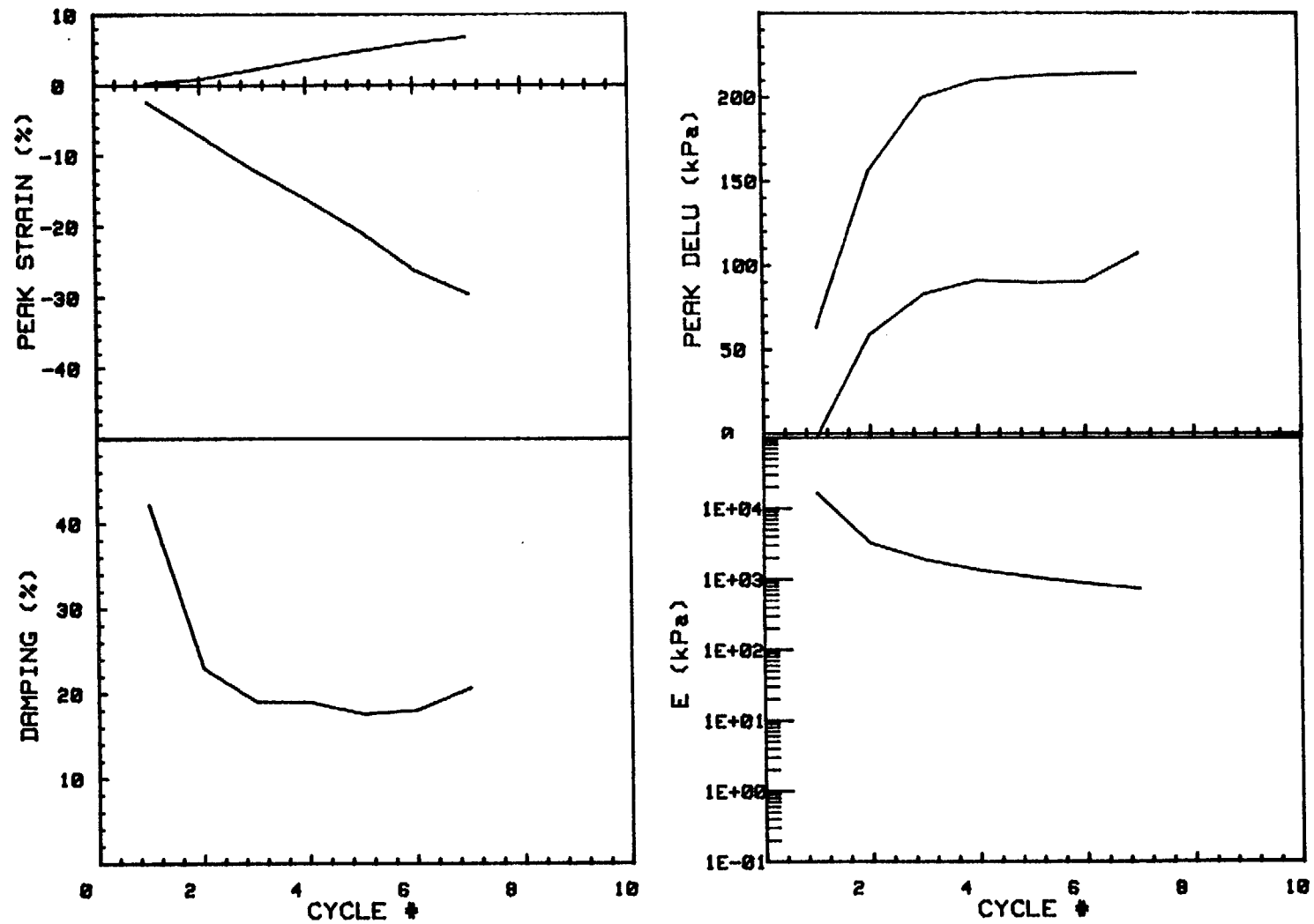
CRUISE DC1-81-EG	INCREMENT (cm)	174-181
CORE NO. 624R1	TEST NO.	TC60
SIG1c' (kPa) 338.9	STATIC qf (kPa)	401.3
SIG3c' (kPa) 338.9	AVG MAX q (kPa)	206.6 (51.5%)
INDUCED OCR 1.0	AVG MIN q (kPa)	-184.9 (46.1%)



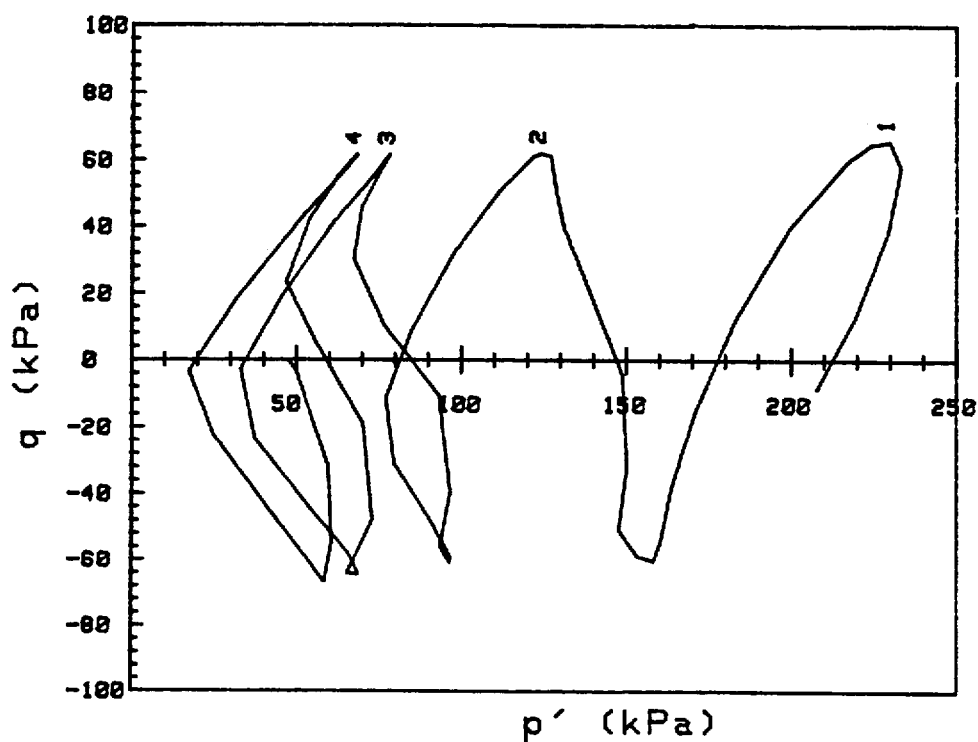
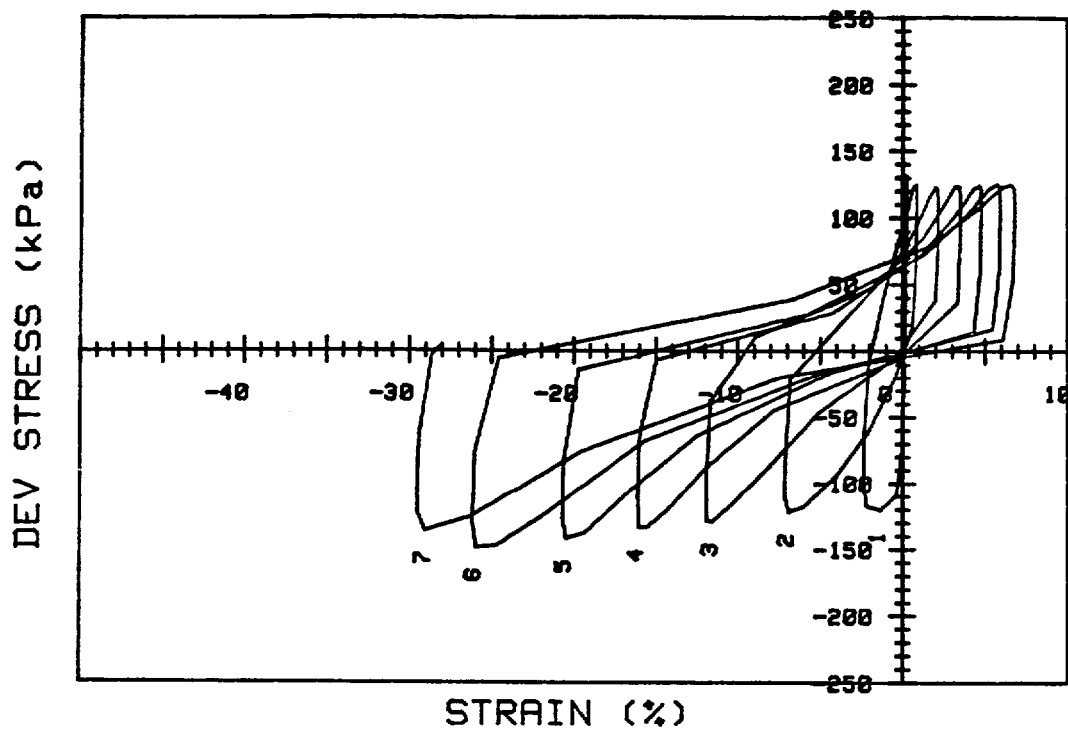
CRUISE DC1-81-EG		INCREMENT (cm) 174-181	
CORE NO. 624A1		TEST NO. TC61	
SIG _{1o'} (kPa)	344.7	STATIC q _f (kPa)	401.3
SIG _{3o'} (kPa)	344.7	AVG MAX q (kPa)	121.8 (30.4%)
INDUCED OCR	1.0	AVG MIN q (kPa)	-134.6 (33.5%)



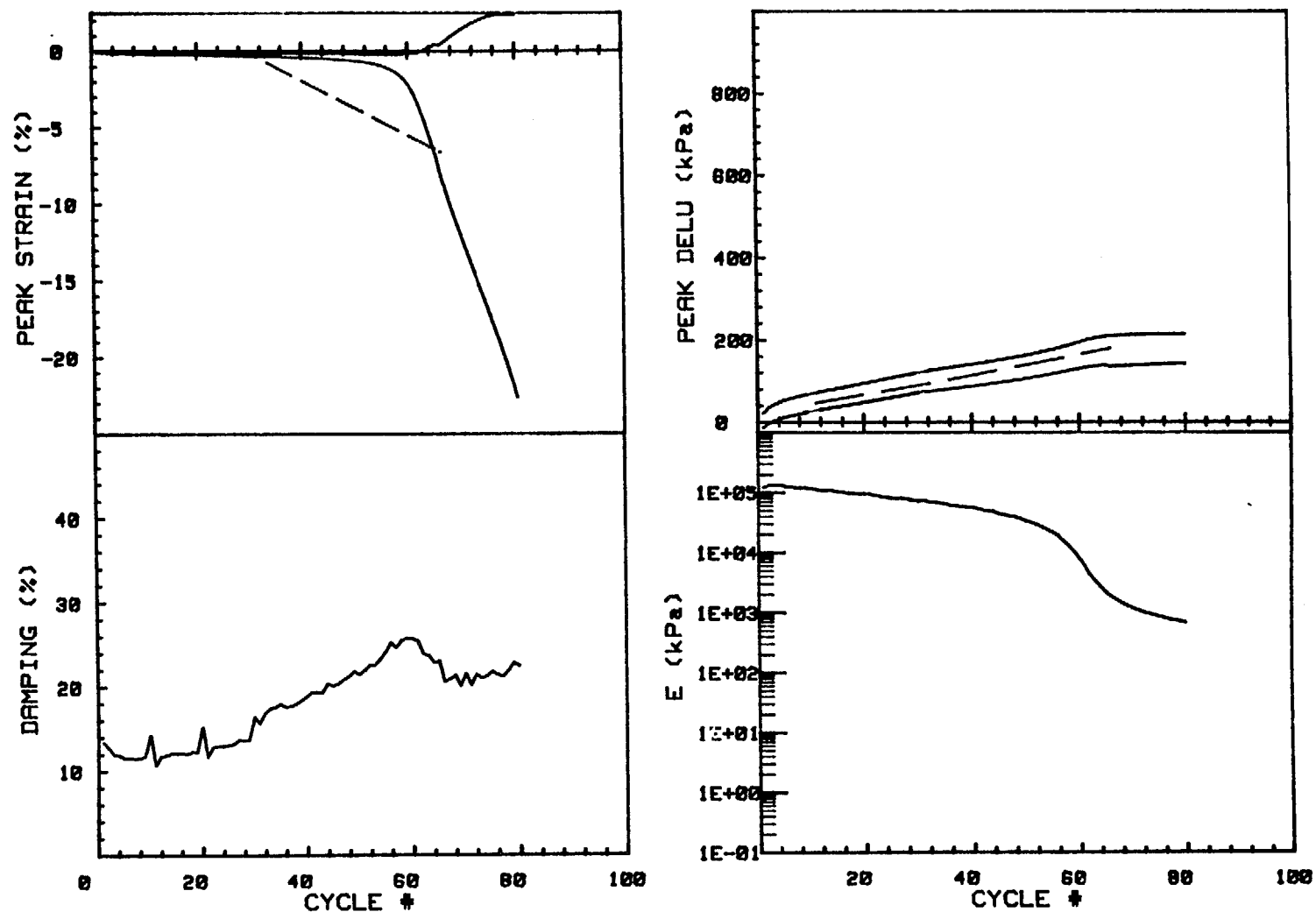
CRUISE DC1-81-EG	INCREMENT (cm)	174-181
CORE NO. 624A1	TEST NO.	TC61
SIG1c' (kPa) 344.7	STATIC q_f (kPa)	401.3
SIG3c' (kPa) 344.7	AVG MAX q (kPa)	121.8 (30.4%)
INDUCED OCR 1.0	AVG MIN q (kPa)	-134.6 (33.5%)



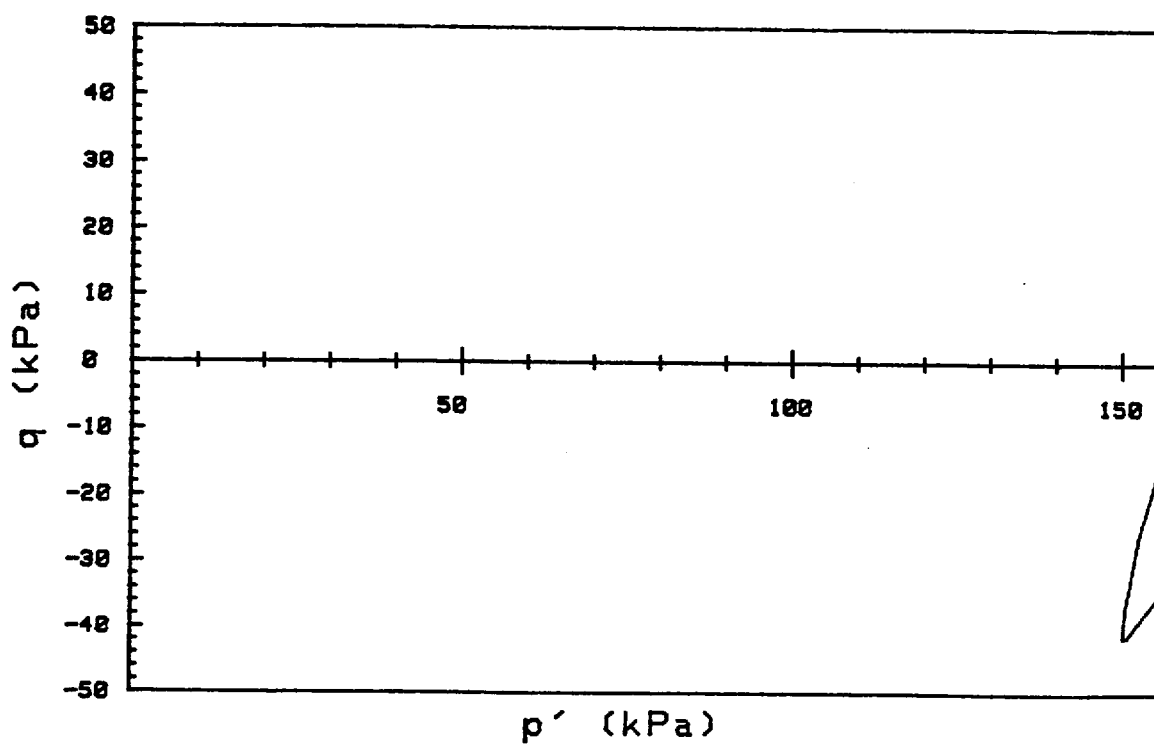
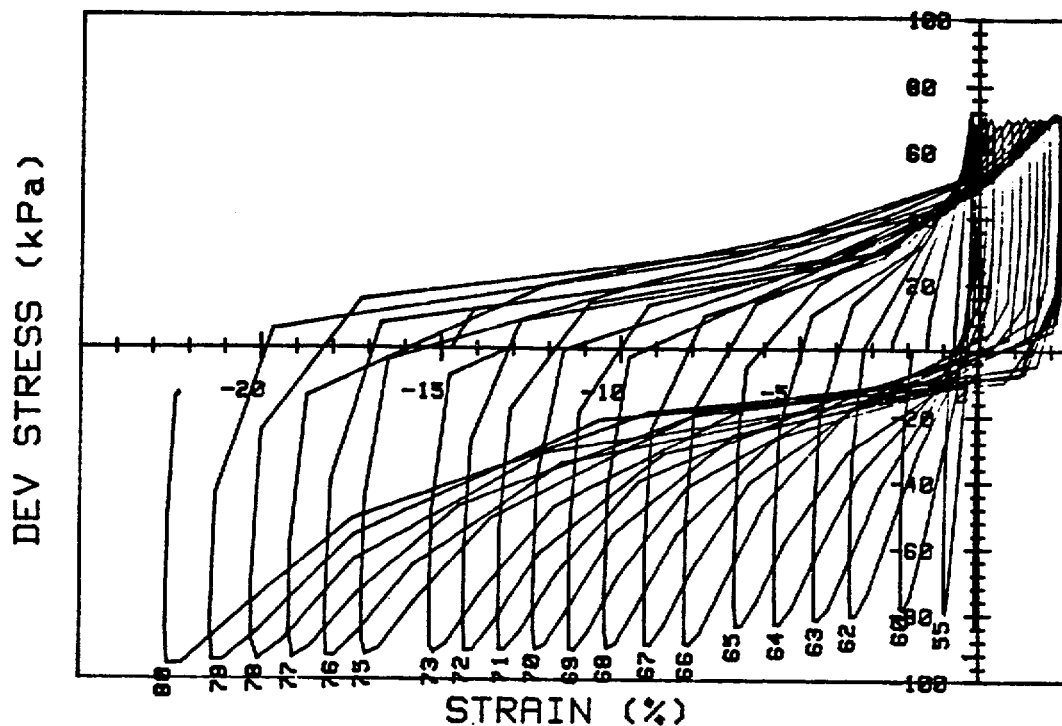
CRUISE DC1-81-EG		INCREMENT (cm) 166-173	
CORE NO. 605G2		TEST NO. TC86	
SIG1c' (kPa)	216.3	STATIC qf (kPa)	127.9
SIG3c' (kPa)	216.3	AVG MAX q (kPa)	62.6 (48.9%)
INDUCED OCR	1.0	AVG MIN q (kPa)	-66.5 (52.0%)



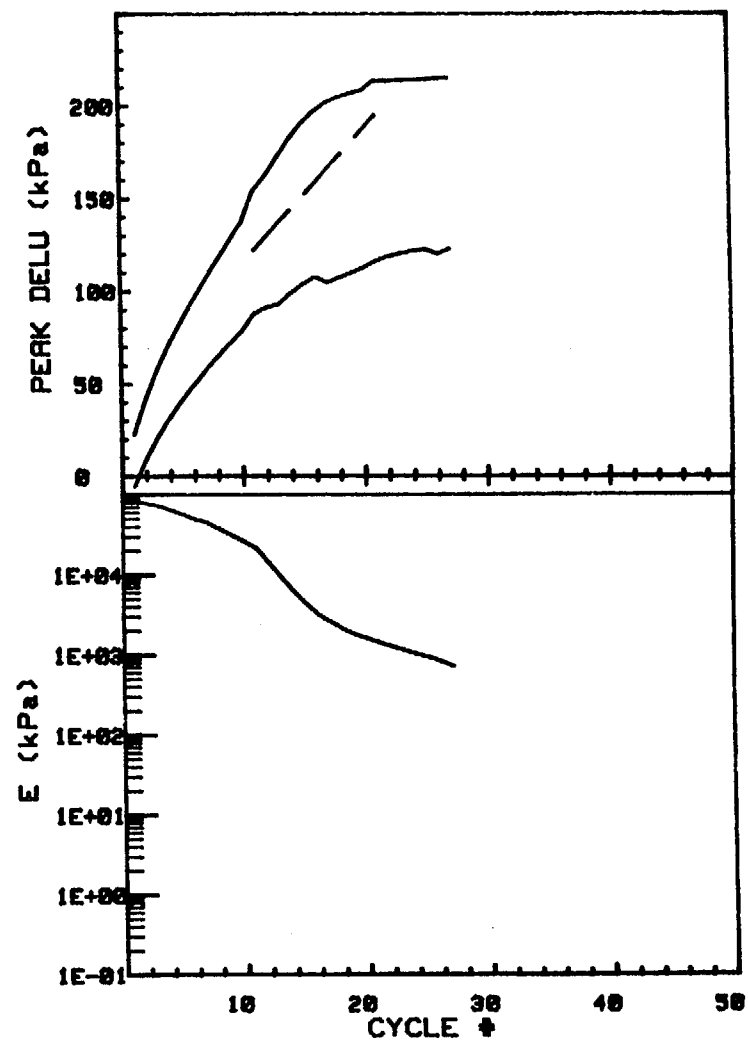
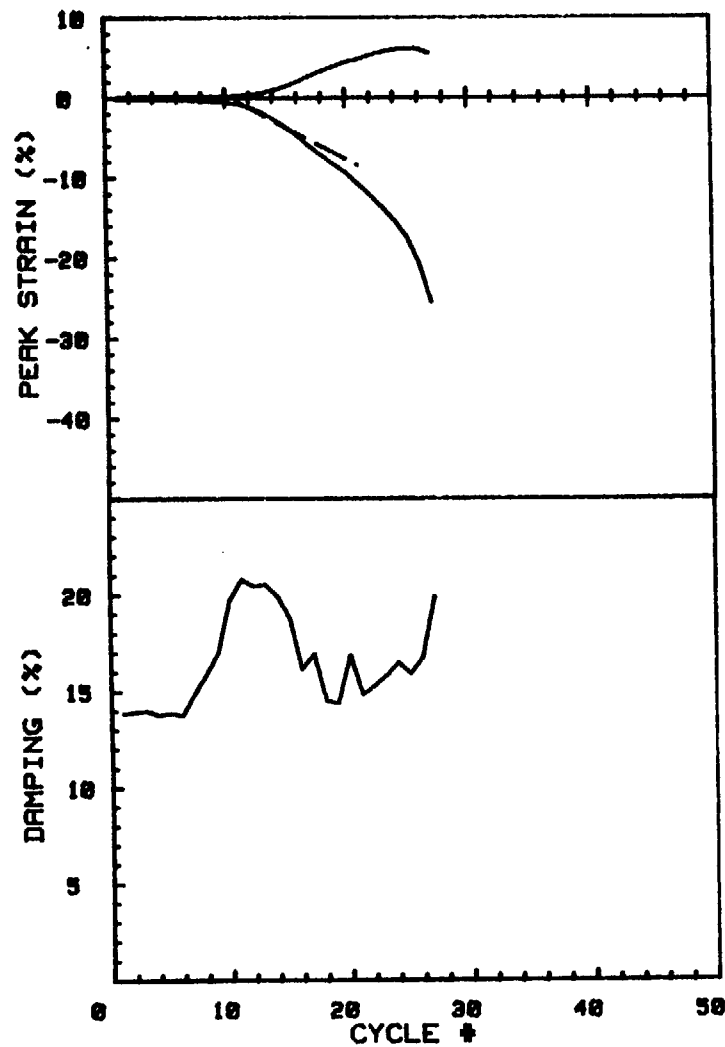
CRUISE DC1-81-EG	INCREMENT (cm)	166-173
CORE NO. 605G2	TEST NO.	TC86
SIG1c' (kPa) 216.3	STATIC qf (kPa)	127.9
SIG3c' (kPa) 216.3	AVG MAX q (kPa)	62.6 (48.9%)
INDUCED OCR 1.0	AVG MIN q (kPa)	-66.5 (52.0%)



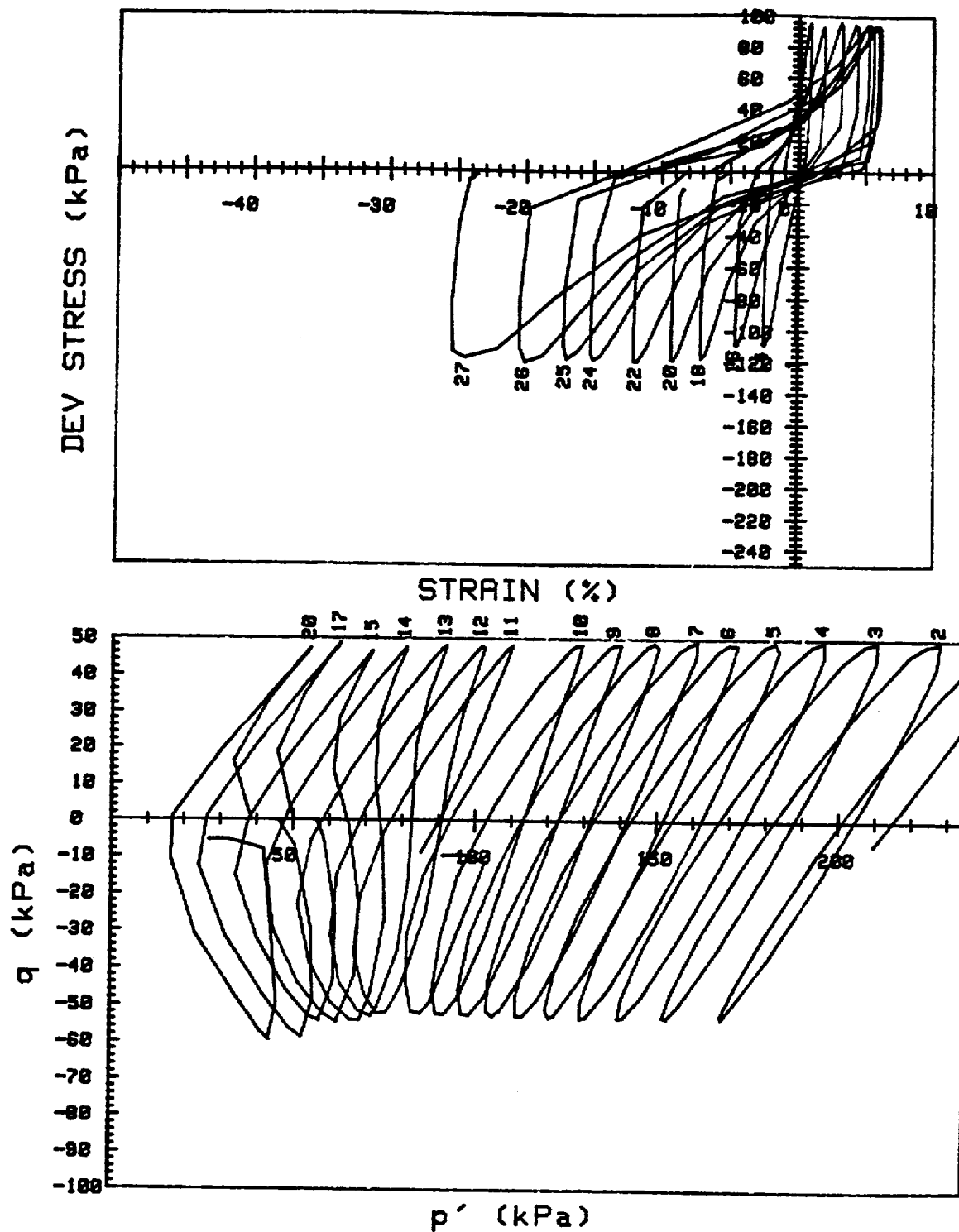
CRUISE DC1-81-EG	INCREMENT (cm)	166-173
CORE NO. 605G2	TEST NO.	TC87
SIG1c' (kPa) 215.1	STATIC qf (kPa)	127.9
SIG3c' (kPa) 215.1	AVG MAX q (kPa)	35.5 (27.8%)
INDUCED OCR 1.0	AVG MIN q (kPa)	-41.8 (32.7%)



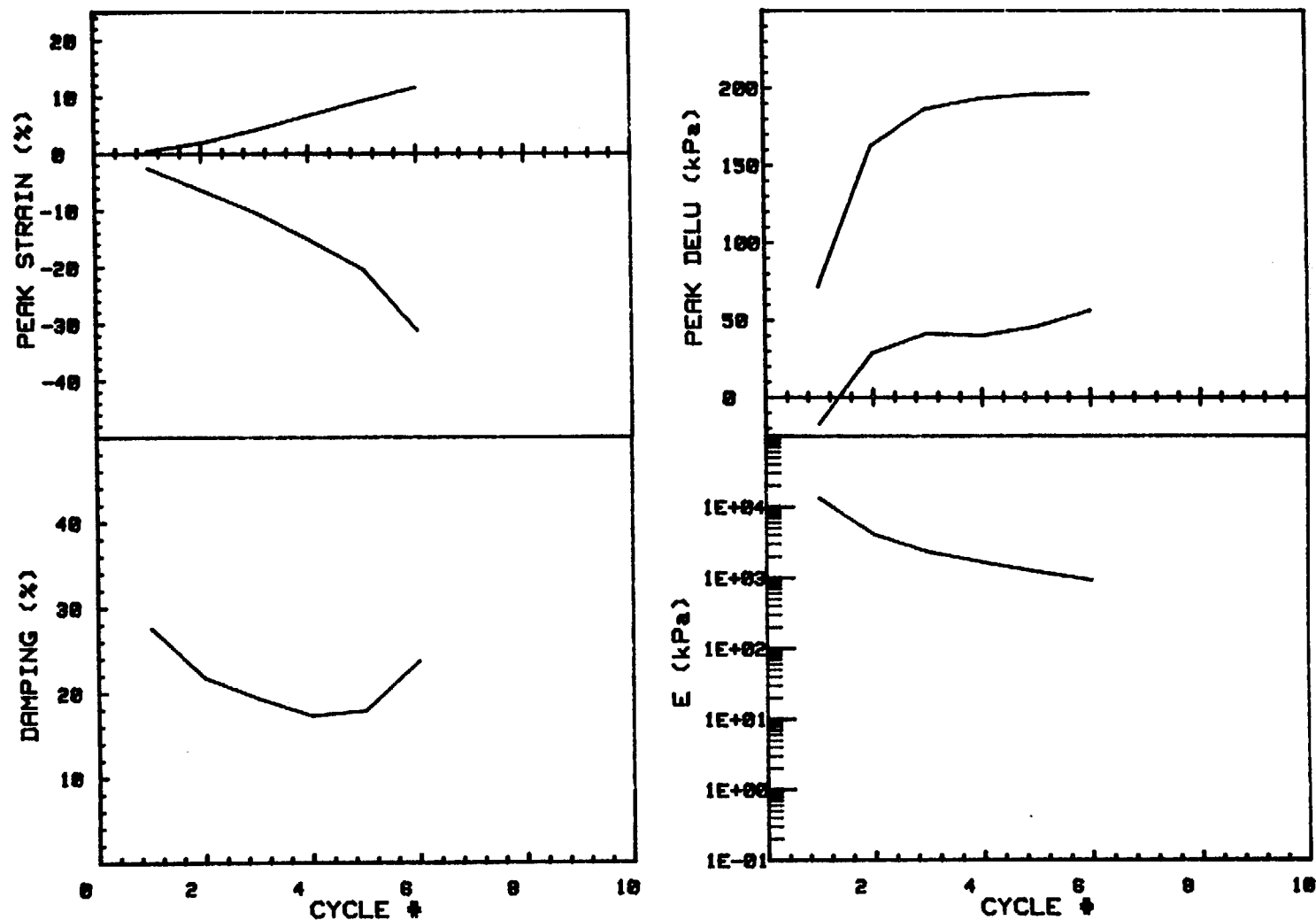
CRUISE DC1-81-EG		INCREMENT (cm)		166-173
CORE NO. 605G2		TEST NO.		TC87
SIG1c' (kPa)	215.1	STATIC qf (kPa)	127.9	
SIG3c' (kPa)	215.1	AVG MAX q (kPa)	35.5 (27.8%)	
INDUCED OCR	1.0	AVG MIN q (kPa)	-41.8 (32.7%)	



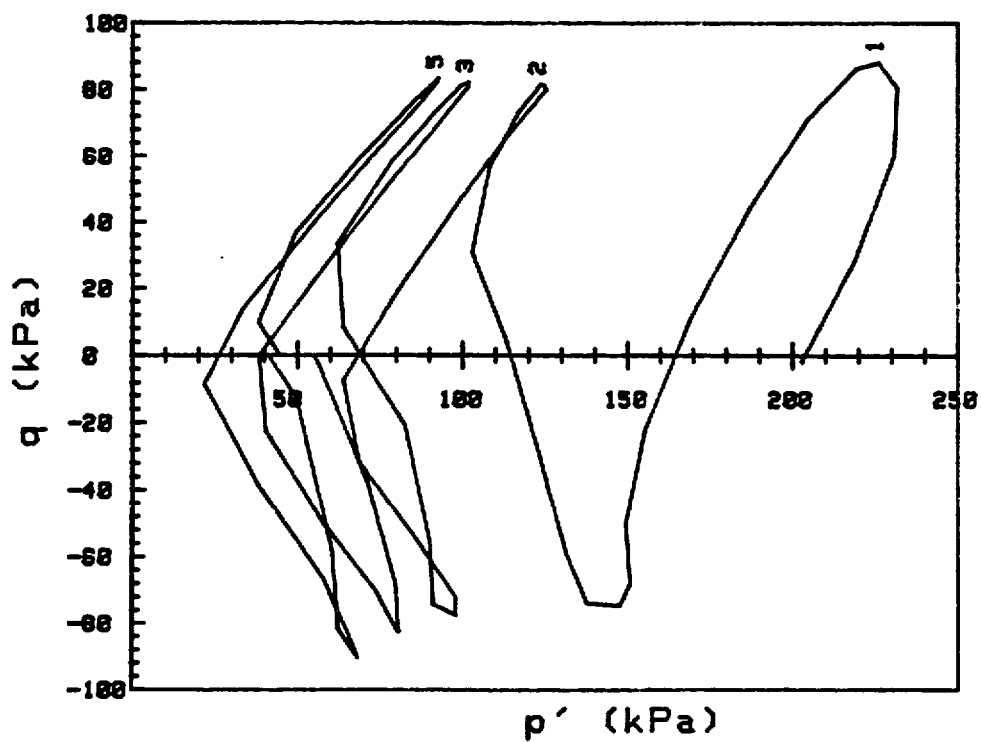
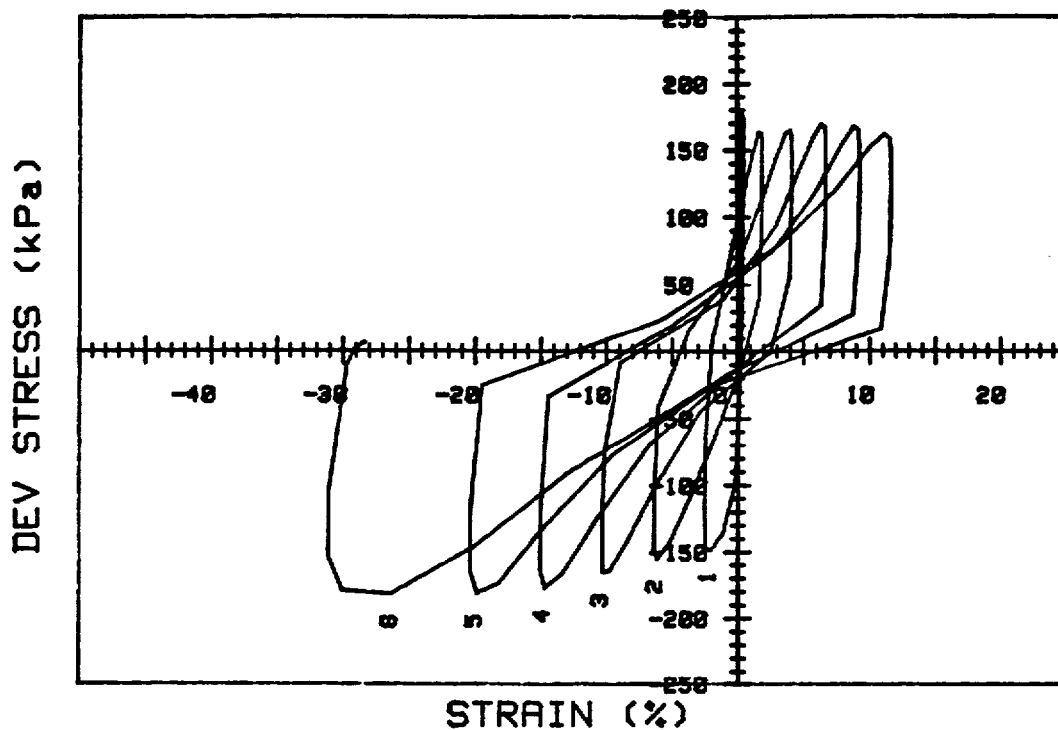
CRUISE DC1-81-EG	INCREMENT (cm)	54-61
CORE NO. 605G2	TEST NO.	TC92
SIG1c'(kPa) 215.9	STATIC qf (kPa)	163.8
SIG3c'(kPa) 215.9	AVG MAX q (kPa)	47.9 (29.2%)
INDUCED OCR 1.0	AVG MIN q (kPa)	-55.7 (34.0%)



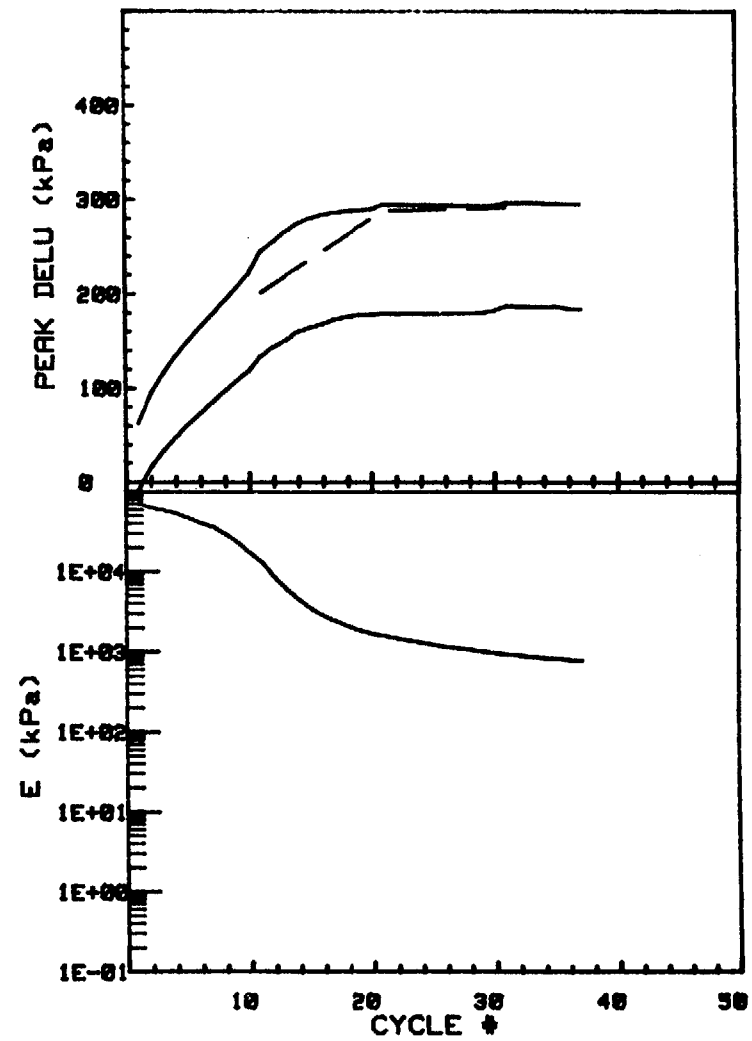
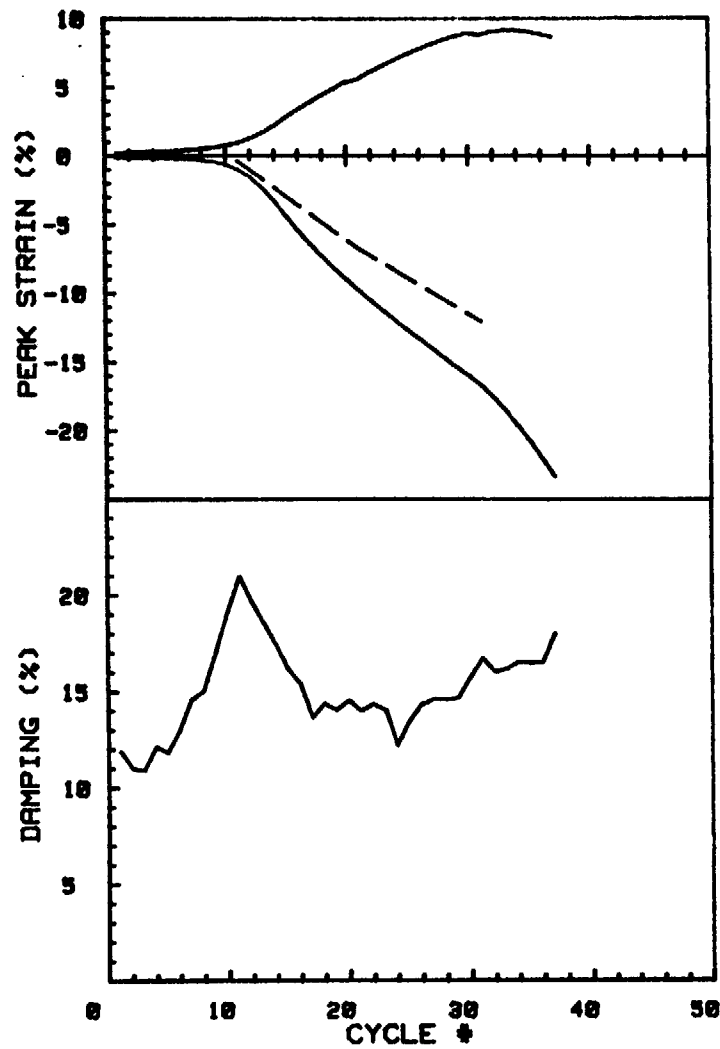
CRUISE DC1-81-EG	INCREMENT (cm)	54-61
CORE NO. 605G2	TEST NO.	TC92
SIG1c' (kPa) 215.9	STATIC qf (kPa)	163.8
SIG3c' (kPa) 215.9	AVG MAX q (kPa)	47.9 (29.2%)
INDUCED OCR 1.0	AVG MIN q (kPa)	-55.7 (34.0%)



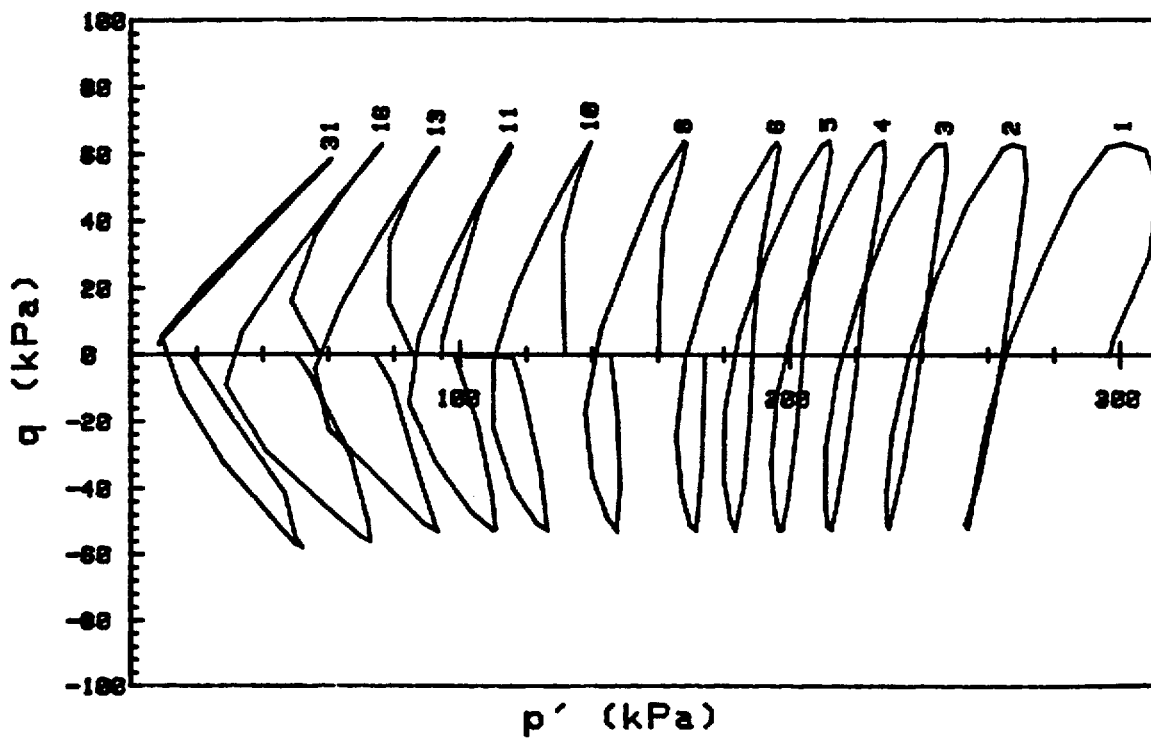
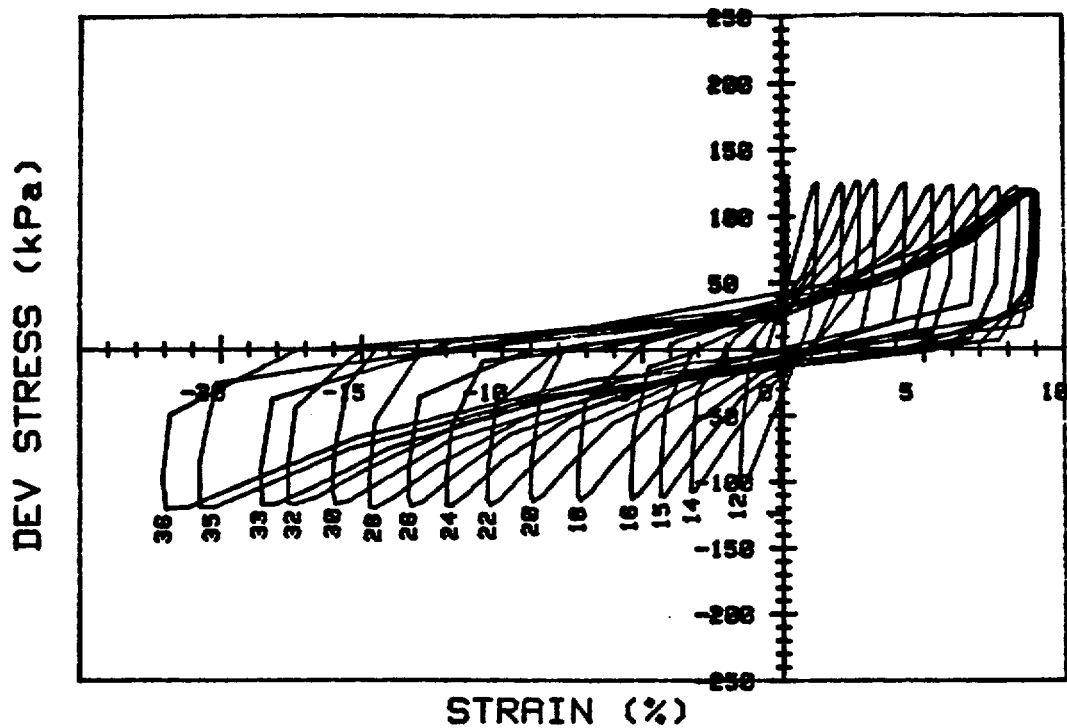
CRUISE DC1-81-EG		INCREMENT (cm)	54-60
CORE NO. 605G2		TEST NO.	TC93
SIG1c' (kPa)	204.8	STATIC qf (kPa)	163.8
SIG3c' (kPa)	204.8	AVG MAX q (kPa)	83.3 (50.9%)
INDUCED OCR	1.0	AVG MIN q (kPa)	-84.1 (51.3%)



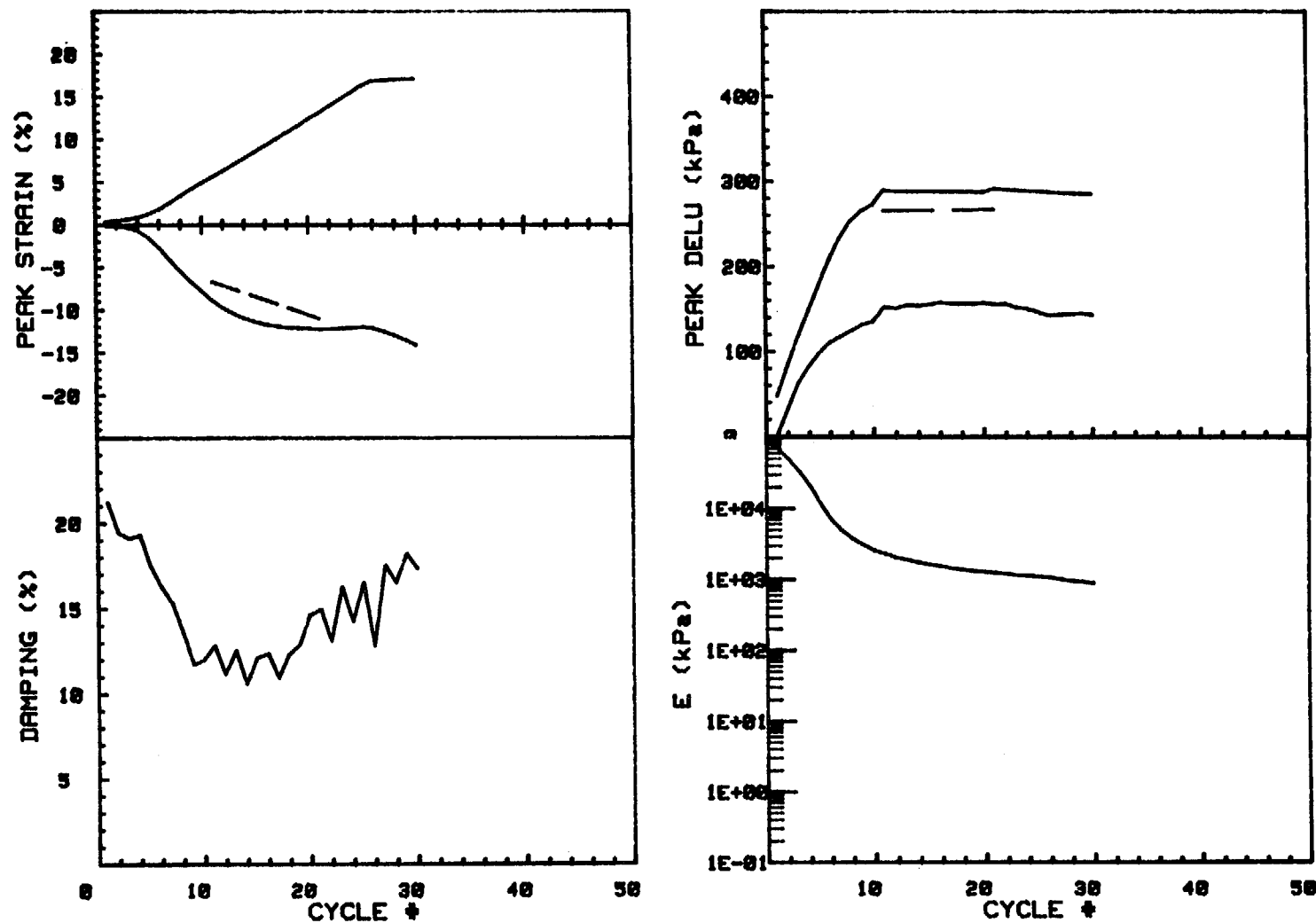
CRUISE DC1-81-EG	INCREMENT (cm)	54-60
CORE NO. 605G2	TEST NO.	TC93
SIG1c' (kPa) 204.8	STATIC qf (kPa)	163.8
SIG3c' (kPa) 204.8	AVG MAX q (kPa)	83.3 (50.9%)
INDUCED OCR 1.0	AVG MIN q (kPa)	-84.1 (51.3%)



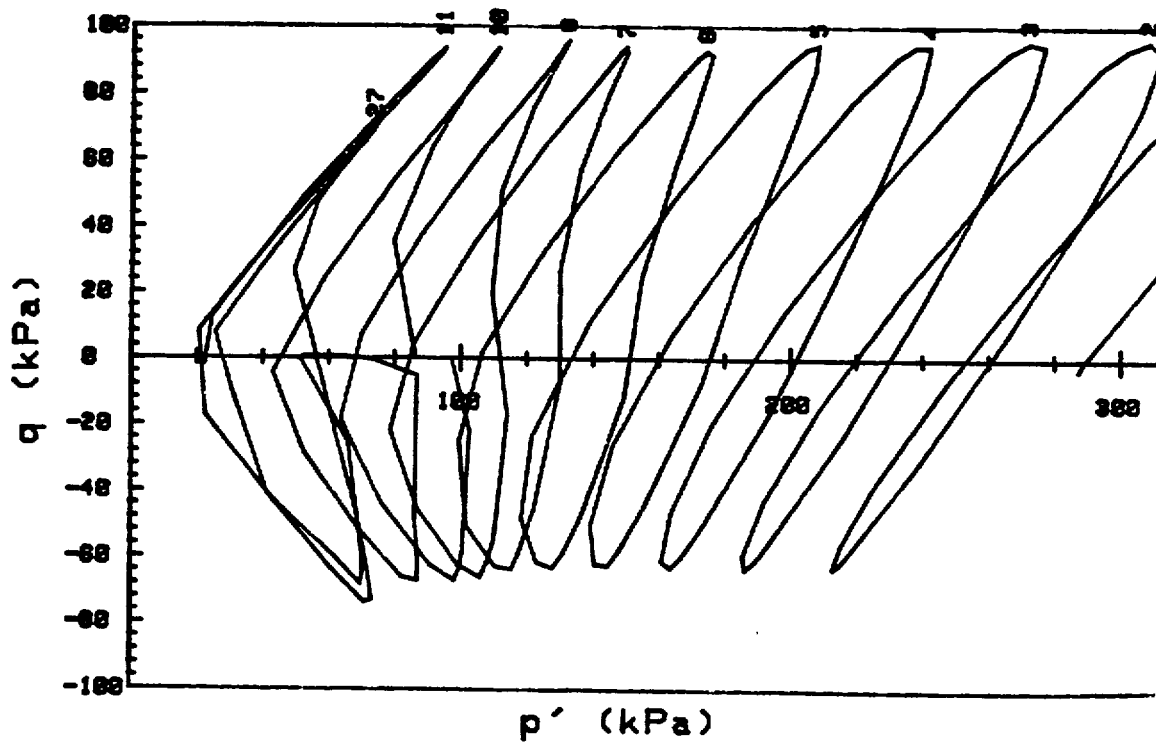
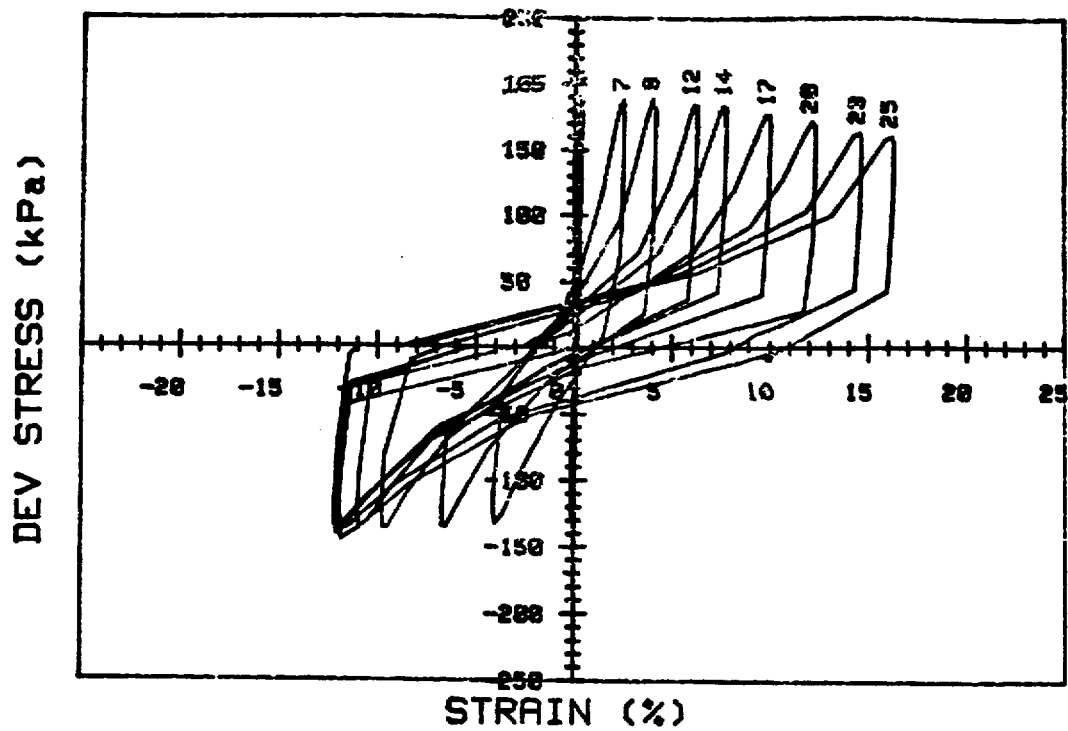
CRUISE DC1-81-EG	INCREMENT (cm)	130-137
CORE NO. 604G3	TEST NO.	TC99
SIG1c' (kPa) 297.1	STATIC qf (kPa) 176.6	
SIG3c' (kPa) 297.1	AVG MAX q (kPa) 61.5 (34.8%)	
INDUCED OCR 1.0	AVG MIN q (kPa) -56.2 (31.8%)	



CRUISE DC1-81-EG	INCREMENT (cm)	130-137
CORE NO. 604G3	TEST NO.	TC99
SIG1c' (kPa) 297.1	STATIC qf (kPa)	176.6
SIG3c' (kPa) 297.1	AVG MAX q (kPa)	61.5 (34.8%)
INDUCED OCR 1.0	AVG MIN q (kPa)	-56.2 (31.8%)



CRUISE DC1-81-EG		INCREMENT (cm) 130-137	
CORE NO. 604G3		TEST NO. D102	
SIG1c' (kPa)	290.4	STATIC qf (kPa)	176.6
SIG3c' (kPa)	290.4	AVG MAX q (kPa)	86.5 (49.0%)
INDUCED OCR	1.0	AVG MIN q (kPa)	-68.0 (38.5%)



CRUISE DC1-01-EG	INCREMENT (cm)	130-137
CORE NO. 604G3	TEST NO.	D102
SIG1c' (kPa) 290.4	STATIC qf (kPa)	176.6
SIG3c' (kPa) 290.4	AVG MAX q (kPa)	86.5 (49.0%)
INDUCED OCR 1.0	AVG MIN q (kPa)	-68.0 (38.5%)